

PROCEEDINGS

Study of Environmental Change using Isotope Techniques

International Conference held in Vienna, 23–27 April 2001

**Organized by the International Atomic Energy Agency
in co-operation with the
United Nations Educational, Scientific and Cultural Organization
and the Japan Science and Technology Corporation**



INTERNATIONAL ATOMIC ENERGY AGENCY

The originating Section of this publication in the IAEA was:

Isotope Hydrology Section
International Atomic Energy Agency
Wagramer Strasse 5
P.O. Box 100
A-1400 Vienna, Austria

STUDY OF ENVIRONMENTAL CHANGE USING ISOTOPE TECHNIQUES
IAEA, VIENNA, 2002
IAEA-CSP-13/P
ISBN 92-0-116402-5
ISSN 1563-0153

© IAEA, 2002

Printed by the IAEA in Austria
October 2002

FOREWORD

Global warming is acknowledged as a major crisis facing society today, principally due to anticipated impacts on the environment, and availability and distribution of water resources. Scientific understanding of recent human-induced climate change, as well as evaluation of potential mitigation strategies, is progressively being developed through studies of atmospheric greenhouse gases and modern water–energy–carbon cycling processes. These efforts have been advanced through study of past global climate changes to understand mechanisms that play a role in determining natural climate fluctuations observed in ice cores, lake and sea sediments, corals, paleo-groundwater, cave deposits, tree rings, and other archives. Predictive models incorporating natural and human-induced climate change processes contribute to a better appreciation for the sensitivity of climate to specific anthropogenic perturbations.

Increasingly, isotopes are being integrated in climate change studies. For example, isotope methodologies offer substantial improvements in the ability to label the origin and fate of greenhouse gases, and for studying the water and carbon cycle response to past climate changes, a high priority area for action identified by the Intergovernmental Panel on Climate Change (IPCC). Isotopes are also widely used as diagnostic variables for validation of models aimed at providing a prognosis of future environmental conditions.

The International Atomic Energy Agency (IAEA) has long supported research and development of isotope applications for climate studies. The joint IAEA/WMO Global Network for Isotopes in Precipitation managed by the IAEA has for the last four decades provided the basic isotope data necessary for integrating stable oxygen and hydrogen isotopes in climate models. The IAEA has also sponsored co-ordinated research projects on “Isotope Variations of Carbon Dioxide and other Trace Gases in the Atmosphere” and “Isotope-Aided Studies of Atmospheric Carbon Dioxide and other Greenhouse Gases”, has published technical documents on isotope measurement techniques for greenhouse gases (IAEA-TECDOC-1268 and 1269) and hosted international symposia on “Applications of Isotope Techniques in Studying Past and Current Environmental Changes in the Hydrosphere and the Atmosphere” in 1993 and on “Isotope Techniques in the Study of Environmental Change” in 1997. The International Conference on The Study of Environmental Change Using Isotope Techniques, held in Vienna in April 2001, was jointly co-ordinated by the Division of Physical and Chemical Sciences (NAPC) and the Marine Environment Laboratory (NAML) of the IAEA and co-sponsored by the United Nations Educational, Scientific, and Cultural Organization (UNESCO) and the Japanese Science and Technology Corporation. The conference was attended by experts from 39 Member States and international organizations. The major themes included isotope tracing of atmosphere–hydrosphere and atmosphere–ocean interactions, palaeoclimate archives, and development of new analytical techniques. These proceedings are anticipated to serve as a valuable resource for those involved in research on climate change and on the impact of climate change on water resources. P. Aggarwal and J.J. Gibson of the Division of Physical and Chemical Sciences and P. Povinec of the Marine Environment Laboratory were the IAEA officers responsible for the conference and for this publication.

EDITORIAL NOTE

This publication has been prepared from the original material as submitted by the authors. The views expressed do not necessarily reflect those of the IAEA, the governments of the nominating Member States or the nominating organizations.

The use of particular designations of countries or territories does not imply any judgement by the publisher, the IAEA, as to the legal status of such countries or territories, of their authorities and institutions or of the delimitation of their boundaries.

The mention of names of specific companies or products (whether or not indicated as registered) does not imply any intention to infringe proprietary rights, nor should it be construed as an endorsement or recommendation on the part of the IAEA.

The authors are responsible for having obtained the necessary permission for the IAEA to reproduce, translate or use material from sources already protected by copyrights.

CONTENTS

OPENING SESSION

Opening Statement.....	3
<i>W. Burkart</i>	

ISOTOPIC TRACERS OF HYDROSPHERE–ATMOSPHERE INTERACTIONS (Session 1)

Isotopes as validation tools for predictions of the impact of Amazonian deforestation on climate and regional hydrology (IAEA-CN-80/1)	7
<i>A. Henderson-Sellers, K. McGuffie, S. Chambers</i>	
Mass independent isotope effects and their observations in nature (IAEA-CN-80/25)	18
<i>M.H. Thiemens</i>	
Climate variability from isotope records in precipitation (IAEA-CN-80/71).....	24
<i>H. Grassl, M. Latif, U. Schotterer, L. Gourcy</i>	
Isotopic evidence for climatic conditions in Southeast Asia at the last glacial maximum (IAEA-CN-80/99)	28
<i>P.K. Aggarwal, J.J. Gibson, K. Fröhlich, K.M. Kulkarni</i>	
Inter- and intra-storm variability of the isotope composition of precipitation in southern Israel: Are local or large-scale factors responsible? (IAEA-CN-80/55).....	41
<i>J.R. Gat, E. Adar, P. Alpert</i>	
Deuterium excess in precipitation and its climatological significance (IAEA-CN-80/104)	54
<i>K. Fröhlich, J.J. Gibson, P.K. Aggarwal</i>	
Links between meteorological conditions and spatial/temporal variations in long-term isotope records from the Austrian precipitation network (IAEA-CN-80/63)	67
<i>A. Kaiser, H. Scheifinger, M. Kralik, W. Papesch, D. Rank, W. Stichler</i>	
Research on climate change and variability at the Abdus Salam International Centre for Theoretical Physics (IAEA-CN-80/87) (Abstract).....	77
<i>F. Giorgi, F. Molteni</i>	

PALAEOCLIMATE ARCHIVES I — GROUNDWATER (Session 2)

The palaeohydrology of coastal aquifers of Europe (IAEA-CN-80/103) (Abstract).....	81
<i>W.M. Edmunds</i>	
Paleogroundwaters of the Valréas Miocene aquifer (southeastern France) as archives of the LGM/Holocene climatic transition in the western Mediterranean region (IAEA-CN-80/24)	84
<i>F. Huneau, B. Blavoux, W. Aeschbach-Hertig, R. Kipfer</i>	
Oxygen isotope composition as late glacial palaeoclimate indicators of groundwater recharge in the Baltic Basin (IAEA-CN-80/5).....	91
<i>R. Mokrik, J. Mazeika</i>	
Paleoclimatic variations in Maknassy Basin (central Tunisia) during the Holocene period using multidisciplinary approaches (IAEA-CN-80/28)	100
<i>K. Zouari, N. Chkir, B. Ouda</i>	

ISOTOPE TRACERS FOR OCEAN–ATMOSPHERE INTERACTIONS (Session 3)

Does carbon isotope data help explain atmospheric CO ₂ concentrations during glacial periods? (IAEA-CN-80/102)	113
<i>K. Alverson, P. Le Grand</i>	
Isotopes as tracers of the oceanic circulation: Results from the World Ocean Circulation Experiment (IAEA-CN-80/98) (Abstract).....	129
<i>P. Schlosser, W.J. Jenkins, R. Key, J. Lupton</i>	

Biogeochemical proxies in Scleractinian corals used to reconstruct ocean circulation (IAEA-CN-80/81)	130
<i>T.P. Guilderson, M. Kashgarian, D.P. Schrag</i>	
Environmental change studies in the Caspian Sea and the north-east Atlantic Ocean (IAEA-CN-80/92)	140
<i>P. Povinec, B. Oregioni, J. Gastaud</i>	
The Kara Bogaz Gol Bay, Lake Issyk Kul and Aral Sea sediments as archives of climate change in the Aral–Caspian catchment basin (IAEA-CN-80/6)	144
<i>V.I. Ferronsky, V.S. Brezgunov, L.S. Vlasova, Y.A. Karpychev, V.A. Polyakov, A.F. Bobkov, V.V. Romanovsky, T. Johnson, D. Ricketts, K. Rasmussen</i>	
¹⁴ CO ₂ measurements in maritime air over the Northern Indian Ocean (IAEA-CN-80/9)	154
<i>K. Dutta, R. Bhushan, B.L.K. Somayajulu</i>	
An unexplored sedimentary record for the study of environmental change in Mediterranean coastal environments: <i>Posidonia oceanica</i> (L.) Delile peats (IAEA-CN-80/11)	163
<i>M.A. Mateo, P. Renom, R. Julia, J. Romero, R. Michener</i>	
Excess air in groundwater as a potential indicator of past environmental changes (IAEA-CN-80/29)	174
<i>W. Aeschbach-Hertig, U. Beyerle, J. Holocher, F. Peeters, R. Kipfer</i>	

PALAEOCLIMATE ARCHIVES II — LAKES AND TERRESTRIAL ENVIRONMENTS (Session 4)

Isotope tracers in global water and climate studies of the past and present (IAEA-CN-80/66)	187
<i>T.W.D. Edwards, S.J. Birks, J.J. Gibson</i>	
Palaeovegetation dynamics of an ecotone forest-savanna in the southern Brazilian Amazon during the late Pleistocene and Holocene based on carbon isotopes of soil organic matter (IAEA-CN-80/12)	195
<i>L.C.R. Pessenda, S.E.M. Gouveia, H.A. de Freitas, B.M. Gomes, R. Aravena, A.S. Ribeiro, R. Boulet, J.A. Bendassoli</i>	
Temporal variation in organic carbon stable isotope compositions of lacustrine sediments from sub-arid northern Tanzania (IAEA-CN-80/34) (<i>Abstract</i>)	205
<i>A.N.N. Muzuka, N. Nyandwi</i>	
Stable isotope composition of inorganic carbonates from Lake Abiyata (Ethiopia): Attempt of reconstructing $\delta^{18}\text{O}$ of lake surface water and implications for palaeohydrological changes during the Holocene (IAEA-CN-80/79)	207
<i>E. Gibert, Y. Travi, M. Massault, T. Chernet</i>	
$\delta^{15}\text{N}$, $\delta^{13}\text{C}$ and radiocarbon in dissolved organic carbon as indicators of environmental change (IAEA-CN-80/47)	219
<i>S. Geyer, K. Kalbitz</i>	
New estimates of oxygen isotope fractionation by plants and soils – Implications for the isotopic composition of the atmosphere (IAEA-CN-80/13)	222
<i>A. Angert, B. Luz</i>	
Hydrochemical and isotope study of Lake Titicaca (IAEA-CN-80/38)	231
<i>R. Gonfiantini, R. Cioni, M. Paredes, J. Campos, M. Collas, A. Gaita, R. Rojas, J. Quintanilla, L. Gourcy, M. Gröning, L.-F. Han, K. Rozanski, R. Kipfer</i>	
Climatic response of stable isotope variations in wood cellulose of pine (<i>Pinus sylvestris</i> L.) and their tree-ring width on the Kola Peninsula, north-western Russia (IAEA-CN-80/86)	243
<i>T. Boettger, A. Hiller, M. Gehre, M. Friedrich, C. Kremenetski</i>	
Paleoclimatic reconstruction in the Bolivian Andes from oxygen isotope analysis of lake sediment cellulose (IAEA-CN-80/69)	252
<i>B.B. Wolfe, R. Aravena, M.B. Abbott, G.O. Seltzer, J.J. Gibson</i>	

PALAEOCLIMATE ARCHIVES III — ICE CORES AND RELATED ENVIRONMENTS (Session 5)

Past climate changes derived from isotope measurements in polar ice cores (IAEA-CN-80/85)	265
<i>J. Beer, R. Muscheler, G. Wagner, P.K. Kubik</i>	
Stable isotopes and their relationship to temperature and precipitation as recorded in low latitude ice cores (IAEA-CN-80/97)	274
<i>L.G. Thompson, M.E. Davis, Pin-Nan Lin</i>	
Stable isotopes in speleothems as proxies of past environmental changes in the Alps (IAEA-CN-80/31)	286
<i>C. Spötl, S.J. Burns, A. Mangini</i>	
Stable isotopes in Alpine ice cores: Do they record climate variability? (IAEA-CN-80/83)	292
<i>U. Schotterer, W. Stichler, W. Graf, H.-U. Bärki, L. Goucy, P. Ginot, T. Huber</i>	
Climate history of the Tibetan Plateau for the last 1500 years as inferred from stable carbon isotopes in tree-rings (IAEA-CN-80/80)	301
<i>G. Helle, G.H. Schleser, A. Bräuning</i>	
Study of recent changes in sedimentation regime inside Cienfuegos Bay, Cuba using ²¹⁰ Pb and ¹³⁷ Cs as tracers (IAEA-CN-80/44)	312
<i>C. Alonso-Hernandez, R. Delfanti, M. Díaz-Asencio, C. Papucci, A. Munoz-Caravaca</i>	
New insights in postglacial paleoclimatic and paleoenvironmental changes in Central Europe derived from isotope analyses of laminated lake sediments and peat deposits (IAEA-CN-80/51)	319
<i>B. Mayer, L. Schwark, K.G. Zink, W.M. Buhay, J. Lechterbeck</i>	

ADVANCES IN ISOTOPE AND ANALYTICAL TECHNIQUES I (Session 6)

Accelerator mass spectrometry: An important tool for the geochronology of past climatic events (IAEA-CN-80/73) (<i>Abstract</i>)	329
<i>A.J.T. Jull, G.S. Burr, J.W. Beck, D.J. Donahue</i>	
Climatic changes at high altitudes from C-14 dating at the discovery site of the Iceman Oetzi (IAEA-CN-80/101) (<i>Abstract</i>)	331
<i>W. Kutschera, B. Jettmar, R. Golser, A. Priller, S. Puchegger, P. Steier, E.M. Wild, S. Bortenschlager, K. Oeggl, W. Rom</i>	
Clocks for Quaternary environments in Australia (IAEA-CN-80/70) (<i>Abstract</i>)	333
<i>C. Tuniz</i>	
Real time monitoring of isotopic CO ₂ in the atmosphere (IAEA-CN-80/100) (<i>Abstract</i>)	334
<i>J. Okil, T.J. McCarthy, D.E. Murnick</i>	
Iodine-129 as a long-lived tracer in the environment (IAEA-CN-80/27)	336
<i>R. Michel, T. Ernst, S. Szidat, C. Schnabel, H.-A. Synal</i>	
Portfolio of recent climate change studies utilizing AMS at ANTARES, ANSTO (IAEA-CN-80/90) (<i>Abstract</i>)	346
<i>D. Child, A. Smith, D. Fink, Q. Hua, G. Elliott, A. Williams, G. Jacobsen</i>	

ADVANCES IN ISOTOPE AND ANALYTICAL TECHNIQUES II (Session 7)

Mitigation of global warming and the role of identification of greenhouse gas sources (IAEA-CN-80/16)	351
<i>Y. Kaya</i>	
Isotopomer fractionation during photolysis of nitrous oxide by ultraviolet of 206 to 210 nm (IAEA-CN-80/18)	355
<i>S. Toyoda, N. Yoshida, T. Suzuki, K. Tsuji, K. Shibuya</i>	
Determination of isotopomers in pools of molecules with polyisotopic elements (IAEA-CN-80/74)	364
<i>A.M. Zyakun, C.A.M. Brenninkmeijer</i>	

Potential use of the non-random distribution of N ₂ and N ₂ O mole masses in the atmosphere as a tool for tracing atmospheric mixing and isotope fractionation processes (IAEA-CN-80/77)	376
<i>R. Well, R. Langel, A. Reineking</i>	
Use of lead-210 as a tracer to compensate climatological effects of airborne sulphate trends (IAEA-CN-80/8).....	384
<i>J.P. Paatero, T. Ruoho-Airola, J. Hatakka, Y. Viisanen</i>	
Stable isotope analysis of pollen as a palaeoindicator – methodological considerations and future challenges (IAEA-CN-80/33)	390
<i>N. J. Loader, D.L. Hemming</i>	
Can EC and UK national methane emission inventories be verified using high precision stable isotope data? (IAEA-CN-80/15).....	399
<i>D. Lowry, C.W. Holmes, E.G. Nisbet, N.D. Rata</i>	

POSTER SESSIONS

Climatic changes and isotopic content along the River Nile valley (IAEA-CN-80/1P).....	413
<i>A.A. Nada, M.F. Hassein, K. Fröhlich</i>	
Tropospheric CO ₂ in Romania: concentration and isotopic composition measurements (IAEA-CN-80/3P)	415
<i>A. Tenu, F. Davidescu, V. Cuculeanu</i>	
Use of ¹⁵ N/ ¹⁴ N ratio to evaluate the anthropogenic source of nitrates in surface and groundwaters in the Upper Orontes Basin (central Syria) (IAEA-CN-80/4P)	417
<i>Z. Kattan</i>	
Use of Cs-137 for the calibration of the circulation model of Lithuanian coastal waters (IAEA-CN-80/5P).....	420
<i>L. Davulienė, G. Trinkunas, V. Remeikis, L. Valkunas, S. Dick</i>	
Using isotopes for global warming observation (IAEA-CN-80/6P)	422
<i>K. Namata</i>	
Climatic significance of stable isotope characteristics of air-CO ₂ and rainfall in Delhi area water-plant-air system (IAEA-CN-80/7P).....	423
<i>P.S. Datta, S.K. Tyagi</i>	
Reconstruction of ¹³⁷ Cs signal in Cuba using ⁷ Be as a tracer of vertical transport processes in the atmosphere (IAEA-CN-80/8P).....	425
<i>C.M. Alonso-Hernandez, H. Cartas-Aguila, M. Diaz-Asencio, A. Munoz-Caravaca</i>	
The effect of climatic changes on Van Lake (IAEA-CN-80/10P)	428
<i>A. Dirican</i>	
Reconstruction of tritium time series in precipitation (IAEA-CN-80/11P)	430
<i>H. Celle-Jeanton, L. Gourcy, P.K. Aggarwal</i>	
Carbon isotopes confirm the competitive advantages of <i>Prosopis</i> over <i>Acacia Eriolo</i> (IAEA-CN-80/12P)	433
<i>I. Robertson, S. Woodborne</i>	
Use of K-40 standard source to measure beta-activity in environmental samples (IAEA-CN-80/13P)	435
<i>R.I. Mamatkulov, M.Z. Zakirov</i>	
Multi-collector ICP-MS for high precision isotope ratio measurements: application to isotopic dating methods (IAEA-CN-80/14P).....	437
<i>H. Hertle, S. Meffan-Main, Z. Palacz, P. Turner</i>	
Reconstruction of bomb ¹⁴ C time history recorded in the stalagmite from Postojna Cave (IAEA-CN-80/15P)	439
<i>B. Vokal, D. Genty, B. Obelić</i>	
Trace element records in high mountain lake sediments in north-western Slovenia dated by ²¹⁰ Pb (IAEA-CN-80/16P).....	441
<i>P. Vreča, Z. Jeran, S. Lojen, R. Jaćimović, T. Dolenec, A. Brancelj, G. Muri</i>	

Influence of local emissions on concentration and isotopic composition of trace gases (CO ₂ and CH ₄) under strong anthropopression: A case study from Kraków, southern Poland (IAEA-CN-80/17P)	444
<i>T. Florkowski, A. Korus, T. Kuc, J. Lasa, J.M. Necki, M. Zimnoch</i>	
Ecological policy, assessment and prediction of the fate of Chernobyl radionuclides in sediments of the Black Sea (IAEA-CN-80/19P)	445
<i>A.E. Kontar</i>	
Tree-ring stable oxygen isotope ratios indicating cooler and wetter climate conditions and high flood frequency periods in the Red River Basin, Manitoba, Canada (IAEA-CN-80/21P)	448
<i>W.M. Buhay, B. Mayer, S. St. George, E. Nielsen, P. Harms, D. Marcino</i>	
Preliminary data on dinosaurs habitat during the Upper Maastrichtian, Hateg Basin, Romania (IAEA-CN-80/22P)	450
<i>D. Grigorescu, A.-V. Bojar, L. Klarik</i>	
¹³ C analyses of CO ₂ in air using the Multiflow: Application for the monitoring of atmospheric ¹³ CO ₂ over hydro-electric reservoir in Quebec's boreal region – Canada (IAEA-CN-80/23P)	452
<i>G. Bilodeau, C. Hillaire-Marcel, J.-F. Hélie, F. Fourel, L. Varfalvy</i>	
A record of atmospheric ²¹⁰ Pb flux in Syria (IAEA-CN-80/24P)	454
<i>M.S. Al-Masri, H.S. Kalil</i>	
Simple environmental models for transport of natural radio-activity in aquatic systems (IAEA-CN-80/26P)	456
<i>A.A. El-Sayed</i>	
Geochemical and isotopic characterization of groundwater resources in El Hicha region, Gabes, southern Tunisia (IAEA-CN-80/27P)	457
<i>M.F. ben Hamouda, H. ben Kraiem, A. Mahjoub, B. Labidi, R. Ghoudi, H. Hamrouni, H. Nasr, K. Zouari, K. Fröhlich, M.I. Sajjad, E. Garcia-Agudo</i>	
Study of soil erosion dynamics on the arable lands of Lublin Upland using isotope techniques (¹³⁷ Cs) (IAEA-CN-80/28P)	460
<i>W. Zglobicki, M. Reszka</i>	
Some results of isotope studies of water exchange in boreal raised bogs (IAEA-CN-80/29P)	463
<i>A.A. Sirin, L.S. Vlasova, V.A. Polyakov, A.E. Trofimova</i>	
Developing insight into the isotope-climate of Canada and the isotopic expression of the 1997–98 ENSO (IAEA-CN-80/30P)	466
<i>S.J. Birks, T.W.D. Edwards, J.J. Gibson</i>	
Stable isotope characterization of pan-derived and directly sampled atmospheric water vapour (IAEA-CN-80/31P)	468
<i>R. Maric, N.A. St. Amour, J.J. Gibson, T.W.D. Edwards</i>	
The question of the renewal of groundwater resources in southwestern Burkina Faso (IAEA-CN-80/33P)	471
<i>D. Dakouré, G. de Marsily, M. Dray, H. Salvayre</i>	
Changes in thermal and mineral waters within the “Gölcük–İzmit August 17. 1999 earthquake area” as revealed by the ¹³ C and ³⁶ Cl isotopes (IAEA-CN-80/34P)	473
<i>W. Balderer, H.A. Synal, T. Yalcin, F. Leuenberger</i>	
Stable isotopes, δ ¹⁸ O and δ ² H, in the study of water balance of Lake Massoko, Tanzania: Investigation of the exchange between lake and underground water (IAEA-CN-80/35P)	475
<i>L. Bergonzini, E. Gibert, A. Winckel</i>	
Application of compound specific ¹³ C isotope investigations of chlorinated hydrocarbons in contaminated groundwaters (IAEA-CN-80/36P)	476
<i>K. Osenbrück, M. Heidinger, A. Voropaev, S. Ertl, L. Eichinger</i>	
Use of environmental isotopes for studying human induced change in groundwater environment in Lahore, Pakistan (IAEA-CN-80/37P)	478
<i>M. Ahmad, W. Akram, M.I. Sajjad, M. Rafiq, M. Azam Tasneem</i>	

Environmental radioactivity investigations in the Georgian subtropical region (IAEA-CN-80/38P)	480
<i>S. Pagava, P. Kakashvili, M. Avtandilashvili, G. Kharashvili, Z. Robakidze, V. Rusetski, G. Togonidze, D. Baratashvili</i>	
Using isotopes to improve impact and hydrological predictions of land-surface schemes in global climate models (IAEA-CN-80/39P)	482
<i>K. McGuffie, A. Henderson-Sellers</i>	
Long-term post-Chernobyl ⁹⁰ Sr and ¹³⁷ Cs profiles as the indicators of the large scale vertical water mixing in the Black Sea (IAEA-CN-80/41P)	484
<i>V.N. Egorov, N.A. Stokozov, N.Y. Mirzoyeva</i>	
River under anthropogenic stress: An isotope study of carbon cycling in the Vistula, Poland (IAEA-CN-80/42P)	487
<i>P. Wachniew, K. Rozanski</i>	
Rainfall-groundwater isotopic relationships in eastern Africa: The Addis Ababa anomaly (IAEA-CN-80/43P)	489
<i>G. Darling, B. Gizaw</i>	
Gas chromatographic isolation technique for compound-specific radiocarbon analysis (IAEA-CN-80/45P)	491
<i>M. Uchida, K. Kumamoto, Y. Shibata, M. Yoneda, M. Morita, K. Kawamura</i>	
New developments in radiometrics and mass spectrometry methods for radionuclide analysis of environmental samples (IAEA-CN-80/46P)	492
<i>P.P. Povinec, J.J. LaRosa, S.H. Lee, E. Wyse</i>	
Caspian Sea water balance and dynamics studies using anthropogenic radionuclides: Implications for environmental changes (IAEA-CN-80/47P)	494
<i>B. Oregioni, J. Gastaud, M.K. Pham, P.P. Povinec</i>	
Arabian Sea GEOSECS stations revisited: Tracer-depth profiles temporal variations? (IAEA-CN-80/48P)	496
<i>S. Mulsow, P.P. Povinec, B.L.K. Somayajulu</i>	
Temporal variations of radionuclides in the precipitation over Monaco (IAEA-CN-80/49P)	498
<i>S.H. Lee, M.K. Pham, P.P. Povinec</i>	
Water profile time series of ⁹⁰ Sr, ¹³⁷ Cs and ^{239,240} Pu in the NW Pacific Ocean (IAEA-CN-80/50P)	500
<i>T. Ito, H.D. Livingston, P.P. Povinec</i>	
Corals – Isotopic archives of marine environmental change (IAEA-CN-80/51P)	502
<i>P.P. Povinec, J. Gastaud, A. Sivo</i>	
Paleotemperature conditions for the southwest of Western Australia from the stable isotopic composition of deep, confined groundwater within the Perth Basin (IAEA-CN-80/52P)	504
<i>J.V. Turner, P.M. Thorpe</i>	
A high precision mass spectrometry method for measuring O ₂ /N ₂ ratios and CO ₂ concentrations in air (IAEA-CN-80/53P)	509
<i>A.D. Marca, P.F. Dennis, A. Etchells</i>	
Closing Remarks	511
<i>Jihui Qian</i>	
Chairpersons of Sessions and Secretariat of the Conference	513
List of Participants	515

OPENING SESSION

OPENING STATEMENT

W. Burkart

Deputy Director General,
Department of Nuclear Sciences and Applications,
International Atomic Energy Agency, Vienna

On behalf of the Director General of the International Atomic Energy Agency, and on my own behalf, I wish to extend a warm welcome to all participants of this International Conference on the Study of Environmental Change Using Isotope Techniques.

This is the 3rd international conference that the IAEA has convened on this subject, the previous two having been held in 1997 and 1993. The conference is particularly relevant this year as issues related to global warming and climate change are once again on top of the world's agenda. Unfortunately we have to be prepared to live with this topic for many decades to come. I am pleased to note that more than 39 countries and 7 international organizations are represented at this conference.

The IAEA has a broad interest and mandate in your area, particularly in those related to energy and water. A principal source of the greenhouse gases lies in the energy sector where fossil fuel burning releases large amounts of carbon dioxide to the atmosphere. Nuclear power produces virtually no greenhouse gas emissions and therefore could be an important consideration for strategies to reduce greenhouse gas emissions. We are not asking for more: careful consideration, a learned discussion.

While it is widely accepted that greenhouse gases in the atmosphere affect the Earth's radiation balance and temperature, uncertainty remains regarding the impacts of climate change on the Earth's water cycle. This aspect of climate change has great implications as it affects the very basic need for human existence. The Earth's freshwater resources are limited, with less than 0.01 percent of all water on earth being freshwater that is accessible for human consumption. As the world's population continues to increase, more than one billion people still lack access to safe drinking water.

The hydrological cycle on the Earth is deeply inter-twined with the climate system, which is linked not only with the atmosphere, but also with the oceans. In this context, I am happy to note that the conference will be addressing issues related to both the terrestrial and marine environments. The atmospheric heat engine is driven primarily by the energy exchange associated with the condensation of water. Water vapor is one of the most abundant and important greenhouse gases in the atmosphere, together with other trace gases that are influenced more directly by human activities. As a result of this close linkage, it is ironic that human efforts to respond to changes in the hydrological cycle may in fact contribute to further climate change. These linkages underscore the fact that the relationships between the hydrological cycle and climatic processes need to be studied and characterized to the best of our ability. Isotopes are indicators of climate related parameters like surface air temperature, relative humidity of the atmosphere, and amount of precipitation. In addition, the dynamics, transport and mixing processes in the atmosphere governing the climatic conditions and air-sea interactions can be investigated through measurements of radioisotopes. The input of isotope data can thus strengthen the modeling efforts aimed at providing a prognosis of future environmental conditions.

The IAEA's programme on Water Resources continues to play a major role in developing and facilitating the use of isotope techniques in climate and climate change studies. For the last forty years, the global network of isotopes in precipitation has provided researchers worldwide with isotope data that have been used for studying relationships between precipitation

and climate parameters, and for evaluating the validity of climate models. This network, that has been operating in collaboration with the World Meteorology Organization (WMO), has been recognized by the scientific community as an invaluable source of data for isotope applications in climate studies. It is only fitting that the first paper in the Conference aims to discuss this very aspect of the use of isotope data in precipitation.

A further extension of the use of isotope data for studying the link between the hydrological cycle and the climate is being pursued through isotope monitoring of large rivers of the world. River water is a repository of the climate and hydrologic processes. Isotope measurements in river water provide integrated information on watershed-scale phenomena, as well as on the impacts of climate and land use changes on the hydrologic system. A new co-ordinated research project will soon be launched to develop a network of river stations where isotope monitoring would be initiated and data made available to the scientific community.

I should note that climate change is an integral part of the Earth's history. Severe changes in climate have occurred in the past, and are likely to occur in the future. While the climatic cycles of the Earth may vary over a much larger time scale, our instrumental records of climate parameters span only a century or so. Understanding the causes of past climate changes in the Earth's history allows us to better evaluate the present and future effects of human activities on climatic conditions. The isotopic compositions of precipitation preserved in such archives as groundwater, ice cores, marine sediments, etc., provide valuable tools for studying the relationships between climatic conditions and the hydrological cycle in the past. I am pleased that isotope proxy records in different terrestrial and marine archives will be presented and discussed at the Conference.

Environmental changes and climate variability occur at global or continental scales, and their impacts on the hydrological cycle will also be felt over a similar scale. As a result, co-ordinated international efforts are necessary to study these processes and their impacts. On our part, we have taken several steps to facilitate greater international co-operation. A memorandum of understanding was recently signed between the IAEA and the WMO to provide stronger organizational support to the global network of isotopes in precipitation. A joint international programme on isotopes in hydrology is being formulated with UNESCO. This programme is likely to strengthen the long-standing collaboration between IAEA and UNESCO and to open additional avenues for joint activities. I am glad that representatives of UNESCO and its programmes are present in this conference. In addition to sister UN agencies, national institutions are important partners for international co-operation. I am pleased that this conference is being co-sponsored by the Japanese Science and Technology Corporation and that their representatives are here. This will undoubtedly help to widen the impact of our activities and to involve more scientists in the relevant projects.

The Conference will cover a range of issues and isotope applications, particularly those related to atmosphere-hydrosphere interactions, past climatic and environmental changes, and advances in isotope and other analytical techniques. A round-table discussion is also planned where you will have an opportunity to present your thoughts and suggestions on trends and additional needs for integrating isotope applications into environmental change studies.

I know that all of you are, as I am, eagerly waiting to listen to your colleagues and discuss the scientific issues at length. I am confident that with over 39 Member States and 7 international organizations represented, the conference will achieve a critical review of the state of the art and develop a clear vision for the future. The Agency is looking forward to the outcome of this important conference.

Once again, I wish you a successful conference and a pleasant stay in this beautiful city of Vienna.

**ISOTOPIC TRACERS OF
HYDROSPHERE-ATMOSPHERE INTERACTIONS**

(Session 1)

Chairpersons

D.D. SOOD

IAEA

H.D. LIVINGSTON

IAEA

ISOTOPES AS VALIDATION TOOLS FOR PREDICTIONS OF THE IMPACT OF AMAZONIAN DEFORESTATION ON CLIMATE AND REGIONAL HYDROLOGY

A. HENDERSON-SELLERS

Australian Nuclear Science and Technology Organisation,
Lucas Heights, New South Wales, Australia

K. McGUFFIE

Department of Applied Physics, University of Technology,
Sydney, New South Wales, Australia

S. CHAMBERS

Australian Nuclear Science and Technology Organisation,
Lucas Heights, New South Wales, Australia

Abstract. Isotopic analysis and modelling of the Amazon Basin have both been reported for about thirty years. Isotopic data have been used to explain important characteristics of Amazonian hydrologic cycling by means of simple models. To date there has been no attempt to use isotopic data to evaluate global climate models employed to predict the possible impacts of Amazonian deforestation. This paper reviews the history of isotopic analysis and simulations of deforestation in the Amazon and initiates isotopic evaluation of GCMs. It is shown that one widely reported simulation set gives seasonal transpiration and re-evaporated canopy interception budgets different from those derived from isotopic analysis. It is found that temporal changes (1965 to 1990) in wet season deuterium excess differences between Belem and Manaus are consistent with GCM results only if there has been a relative increase in evaporation from non-fractionating water sources over this period. We propose synergistic future interactions among the climate/hydrological modelling and isotopic analysis communities in order to improve confidence in simulations of Amazonian deforestation.

1. HISTORY OF ISOTOPE ANALYSIS FOR THE AMAZON

The simple topography of the extensive basin and the single water source, the Atlantic Ocean, makes the Amazon Basin unique as a study region of isotopic fractionation processes. Salati *et al.* [1] used one year's isotope data from precipitation and river samples and results from a sector box model to reinforce Molion's [2] conclusion that about half the Amazon Basin's water is recycled. On the basis of 13 months data (October 1972 to October 1973) they were able to identify that the gradient inland of $\delta^{18}\text{O}$ is surprisingly weak, compared to other continental areas, which shows that a proportion of the hydrologic recycling is from non-fractionating sources i.e. transpiration and canopy re-evaporation. This recycling within the Amazon Basin leads to a smaller 'continental' gradient in $\delta^{18}\text{O}$ going inland on an east to west transect with seasonally averaged gradients of only 1.5‰ per 1000 km cf. 2.0‰ in Europe [3] (Fig. 1).

In 1981, Leopoldo [4] reported values of the stable isotopes of oxygen and hydrogen as measured in samples of stemflow and throughflow at the Duke Reserve, near Manaus. Although his results were somewhat contradictory, they seem to point to isotope heterogeneity in originating air masses as the most likely source of observed differences. These results have been cited by more recent researchers (e.g. Ref. [5]) because the fate of water intercepted by the canopy is crucially important to a complete understanding of forest hydrology.

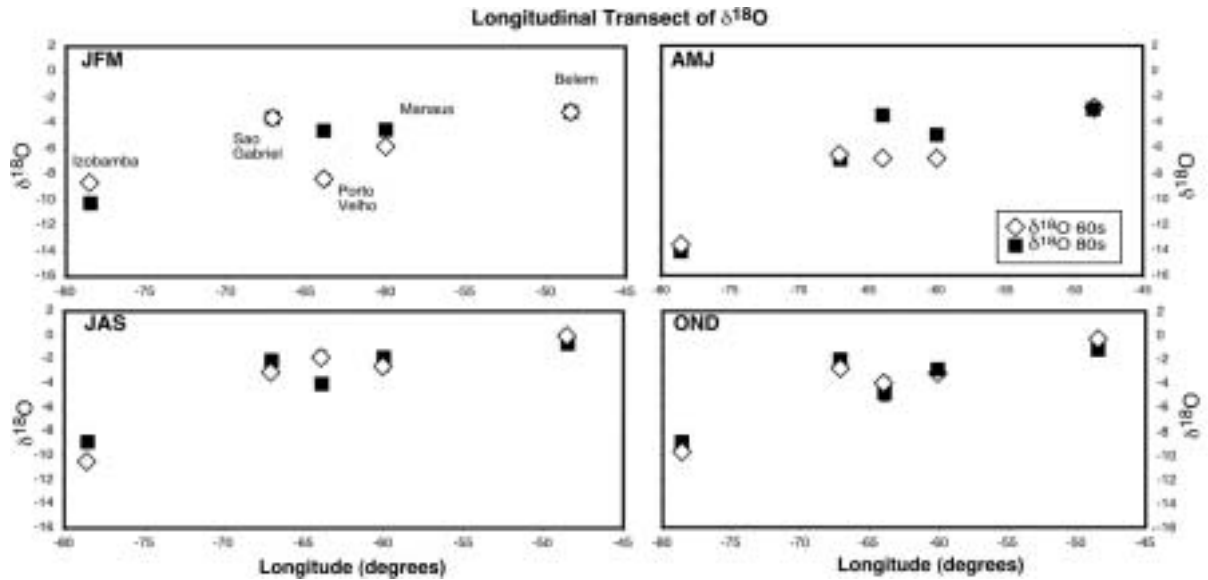


FIG. 1. Isotopic signature ($\delta^{18}O$) across a longitudinal transect of the Amazon from Belem on the coast and at the river mouth to Izobamba in the Andes for each of four seasons. The solid diamonds are the 1960s values (similar to those analyzed by [1]) while the open squares are for the 1980s.

An important review of Amazonian isotopic and other data was published by Salati and Vose in 1984 [6]. This paper was influential because its publication coincided with the first reports of a simulation using a Global Climate Model (GCM) to assess the possible impact of deforestation of the Amazon. Indeed, Salati and Vose [6] quote preliminary (1983) results from the work of Henderson-Sellers and Gornitz [7]. Although the Salati and Vose [6] paper was primarily a collection of their, and others', previous work with isotopic analysis, it underlined to the newly emerging global climate modelling community that the Amazon recycles about half its water within its basin (Fig. 2(a)).

Two papers were published in 1991 on the subject of isotopic analysis of Amazonian precipitation and its implications for regional hydrology and climate. Gat and Matsui [5] employed a simple box model of the central Amazon Basin to demonstrate that some of the water recycling is from fractionating sources. Using data from the International Atomic Energy Agency/World Meteorological Organization (IAEA/WMO) global station network up to 1981, they interpreted a +3‰ deviation from the World Meteoric Line as indicative of 20-40% of the recycled moisture within the basin being derived from fractionating sources such as lakes, the river or standing water. The paper by Victoria *et al.* [8] also used IAEA/WMO data; they analysed isotopic results from Belem and Manaus over the fourteen year period from 1972 to 1986. Using the box/sector model of Dall'Olio [9] also described in Ref. [1] these researchers were able to employ isotopic data to show that wet season recycling is by means of transpiration while dry season recycling in the Amazon is primarily by re-evaporation of precipitation intercepted on the canopy. Since the mid 1990s, there have been relatively few reports on Amazonian isotopes. However, Gat [10] reviews some work and reports that an updated model of the Amazon's water balance, which uses isotopic input, improves earlier predictions.

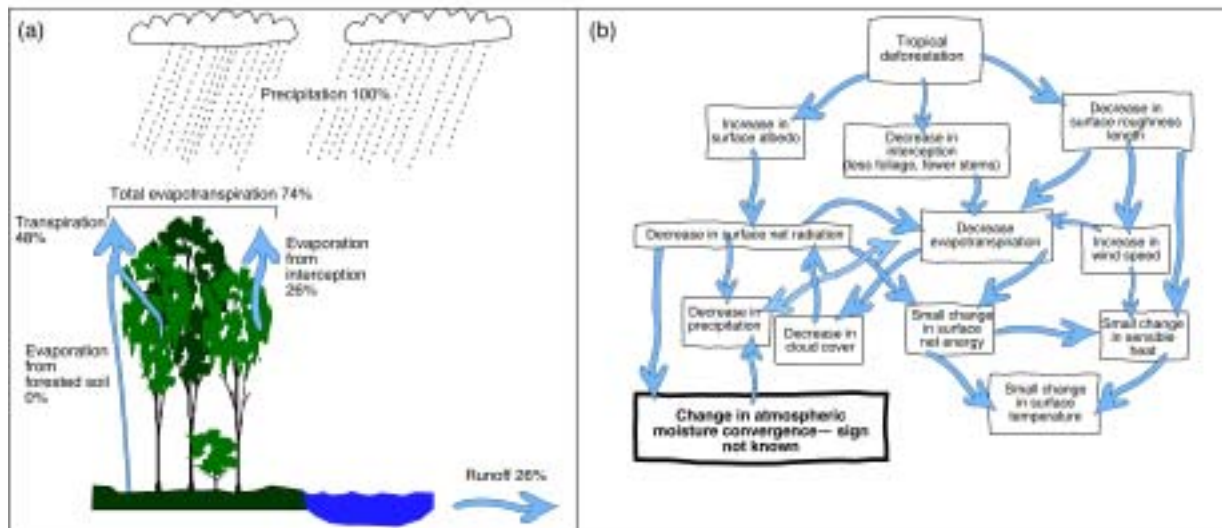


FIG. 2. (a) Schematic of the Amazonian Basin water cycle; and (b) schematic illustration of processes simulated in a global climate model (GCM) predicting changes following deforestation.

2. EVALUATION OF GCMS' SIMULATION OF AMAZONIA USING ISOTOPIC DATA

As mentioned above, the first global climate model (GCM) simulation of the impact of Amazonian deforestation was published by Henderson-Sellers and Gornitz in 1984. Since then, there have been rather a large number of simulations (Table I). McGuffie *et al.* [11] review the problems associated with correctly specifying climate model parameters in both control (present day) and deforested simulations. Some of the differences in the outcomes of predictions in Table I are due to the imposed differences in surface albedo, surface roughness, density and mix of original and replacing vegetation, soil type and state and so on (Fig. 2(b)). Almost all models predict increased surface temperatures (ΔT) following deforestation. There is also general agreement that both precipitation and evaporation decrease but less consensus on the sign of the change in atmospheric moisture convergence (Table I).

As far as we are aware, no GCM simulations of the impact of Amazonian deforestation have yet been tested against the available isotopic data. This is partly the result, we suspect, of the relevant research communities' ignorance of one another. It is also because very few GCMs have, as yet, included isotopic composition as a computed variable. Notable exceptions include work by Jouzel *et al.* [33,34] but neither of these studies include consideration of deforestation impacts. The wide dispersion in the results shown in Table I indicate that GCM evaluation by any available means can only be beneficial.

One means of assessing GCM performance in this area is to utilize the results of Gat and Matsui [5] regarding the relative amounts of water recycled in the Amazon from fractionating and non-fractionating sources. They deduced by comparing deuterium and oxygen isotopic observations with results from their box model of the central Amazon Basin that of the input precipitation 10%-20% is re-evaporated from fractionating sources (e.g. lakes and rivers), 30%-40% from non-fractionating sources (e.g. transpiring plants and complete re-evaporation of canopy-intercepted water), with about half of the total hydrological budget going to runoff. These values can be used to evaluate GCMs.

Table I. Annually-averaged regional changes predicted in response to Amazon tropical deforestation for surface temperature, T, precipitation, P, evaporation, E, and moisture convergence from various GCM studies since 1984 (N/A means the information is not available)

Study	Albedo change	Roughness change	ΔT (°C)	ΔP (mm)	ΔE (mm)	Moisture convergence change
Henderson-Sellers and Gornitz [7]	0.11/0.19	2.0/0.09	0	-220	-164	+
Dickinson and Henderson-Sellers [12]	0.12/0.19	2.00/0.05	+3.0	0	-200	+
Lean and Warrilow [13]	0.136/0.188	0.79/0.04	+2.4	-490	-310	-
Nobre <i>et al.</i> [14]	0.13/0.20	2.65/0.08	+2.5	-643	-496	-
Dickinson and Kennedy [15]	0.12/0.19	2.00/0.05	+0.6	-511	-256	-
Mylne and Rowntree [16]	0.135/0.200	No change	-0.1	-335	-176	-
Dirmeyer [17]	+0.03	2.65/0.08	N/A	+33	-146	+
Lean and Rowntree [18]	0.136/0.188	0.79/0.04	+2.1	-296	-201	-
Henderson-Sellers <i>et al.</i> [19]	0.12/0.19	2.0/0.2	+0.6	-588	-232	-
Pitman <i>et al.</i> [20]	0.12/0.19	2.00/0.05	+0.7	-603	-207	-
Manzi [21]	0.13/0.20	2.00/0.06	+1.3	-15	-113	+
Polcher and Laval [22]	0.098/0.177	2.30/0.06	+3.8	+394	-985	-
Polcher and Laval [23]	0.135/0.216	2.30/0.06	-0.1	-186	-128	-
Sud <i>et al.</i> [24]	0.092/0.142	2.65/0.08	+2.0	-540	-445	-
McGuffie <i>et al.</i> [25]	0.12/0.19	2.0/0.2	+0.3	-437	-231	-
Manzi and Planton [26]	0.13/0.20	2.00/0.06	-0.5	-146	-113	-
Zhang <i>et al.</i> [27]	0.12/0.19	2.0/0.2	+0.3	-402	-222	-
Lean and Rowntree [28]	0.13/0.18	2.10/0.03	+2.3	-157	-296	+
Hahman and Dickinson [29]	0.12/0.19	2.00/0.05	+1.0	-363	-149	-
Zhang <i>et al.</i> [30]	0.15/0.21	1.1/0.1	+0.9	+445	+248	+
Costa & Foley [31]	0.135/0.173	0.151/0.05	+1.4	-266	-223	-
Zhang <i>et al.</i> [32]	0.12/0.19	2.0/0.2	+0.3	-403	-221	-

McGuffie *et al.* [11] report on a series of GCM experiments conducted using the USA's National Center for Atmospheric Research's Community Climate Model (CCM1-Oz). Fig. 3 illustrates the components of the Amazonian water budget derived from these CCM1-Oz simulations for the annual and two 3-month seasonal means. While the amount of water recycled via transpiration does not vary all that greatly through the year, its percentage contribution to the total ranges from 38% in the wet season to 73% in the dry season.

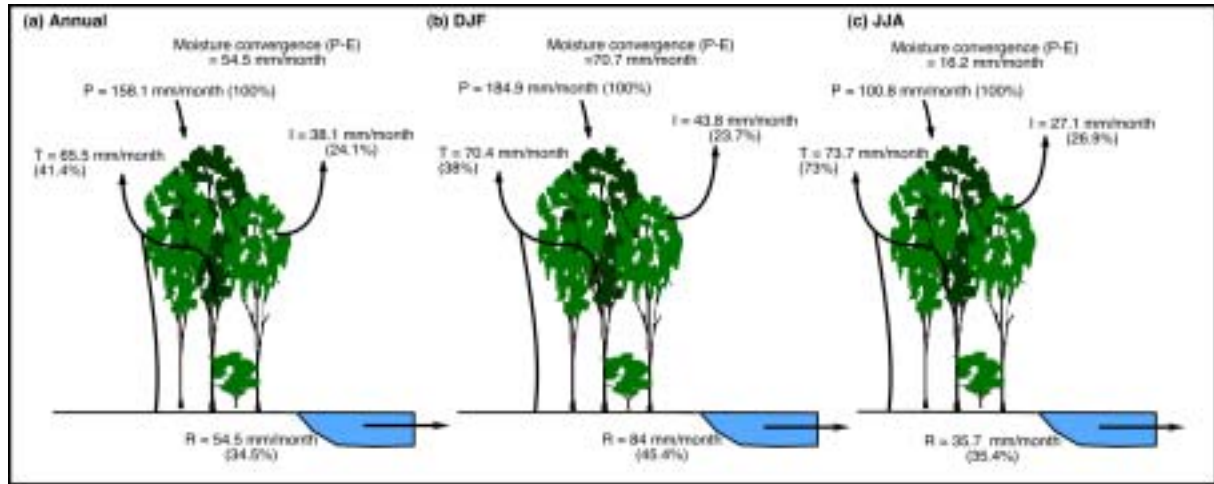


FIG. 3. One GCM (CCM1-Oz) simulation of the water budget of the Amazon for (a) annual means, (b) wet season (DJF) and (c) dry season (JJA) all given in mm month^{-1} and as percentages of the total precipitation.

Although the land surface scheme (BATS – the Biosphere Atmosphere Transfer Scheme) used in the CCM1-Oz simulations does permit inclusion of lakes, this option was not used in these GCM experiments. It is therefore not possible to examine the Gat and Matsui [5] conclusion regarding the fraction of recycled moisture from lakes directly in terms of this GCM. However, the results in Fig. 3 are in contrast with those of Victoria *et al.* [8]. The latter claimed on the basis of isotope analysis that transpiration is the major source of recycled water in the wet season while Fig. 3(c) shows that at least one GCM simulates transpiration as being very much more significant in the Amazon forest's dry season budget of recycled water.

Thus it appears that there are grounds for suspecting that a more thorough examination of the components of the Amazonian water cycle using isotopic data could both reveal inadequacies in current simulations and, hopefully, indicate how simulations by GCMs could be improved to more completely and correctly capture the moisture exchanges. This is an important issue because it has been shown that tropical deforestation has the potential to excite large-scale Rossby waves in the atmosphere. These waves can propagate from the source of their initiating disturbance into the middle and high latitudes of both hemispheres and, hence, prompt impacts far distant from deforestation in the Amazon [35].

3. RECENT ISOTOPIC ANALYSIS IN THE AMAZON

The data used in this study were obtained from the Global Network for Isotopes in Precipitation database [36], jointly maintained by the World Meteorological Organization (WMO) and the International Atomic Energy Agency (IAEA) since 1961. From each Amazon station, monthly average values of temperature, humidity, precipitation, precipitation type, deuterium, oxygen-18 and tritium are available. As part of our investigation of the possible synergies between isotopic and global climate modelling studies of Amazonian deforestation,

we have examined these IAEA/WMO station records in the Amazon Basin for temporal trends. We find noticeable changes in the wet season, which extends from about December to May (e.g. Fig. 4). The continental gradient of $\delta^{18}\text{O}$, already the weakest in the world, has been further weakened over the last three decades in the wet months from December to May (Fig. 1).

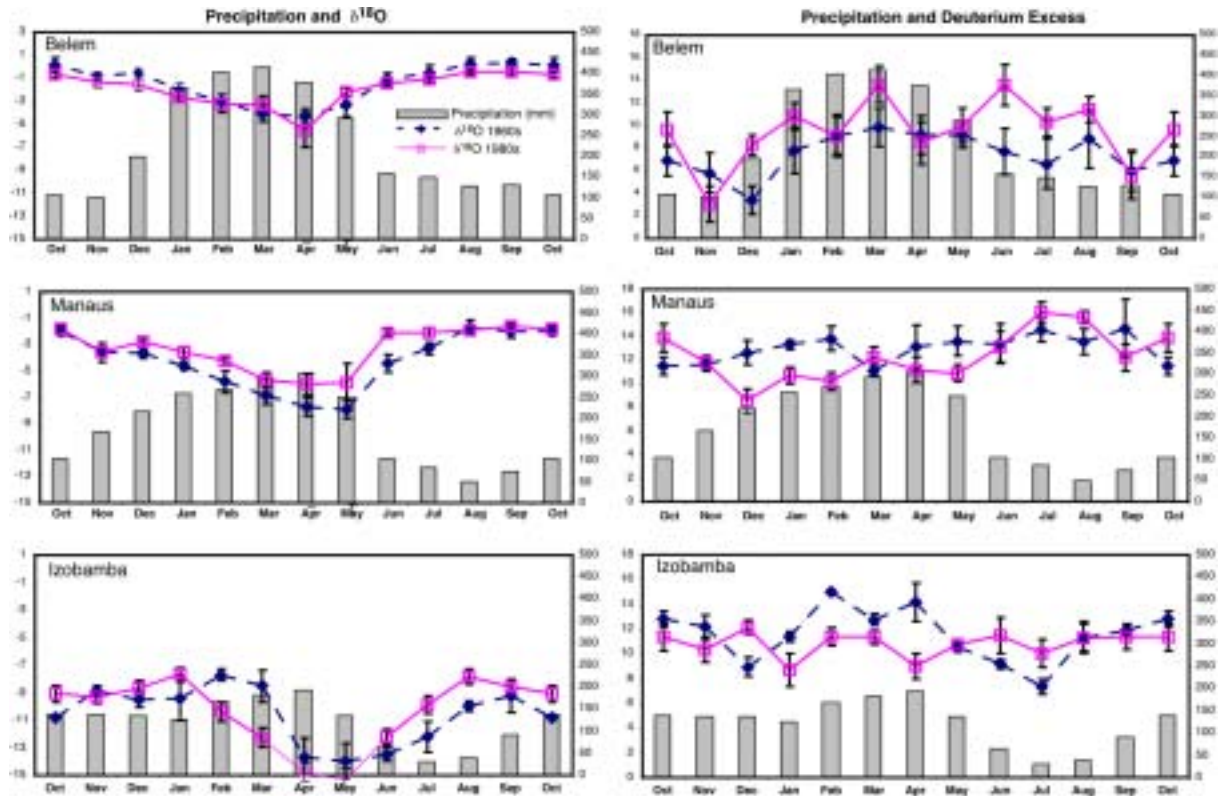


FIG. 4. Monthly mean values of $\delta^{18}\text{O}$ and deuterium excess at Belem, Manaus and Izobamba for the 1960s and the 1980s running from October to October. Mean monthly precipitation (mm) for the whole period is also shown as a histogram.

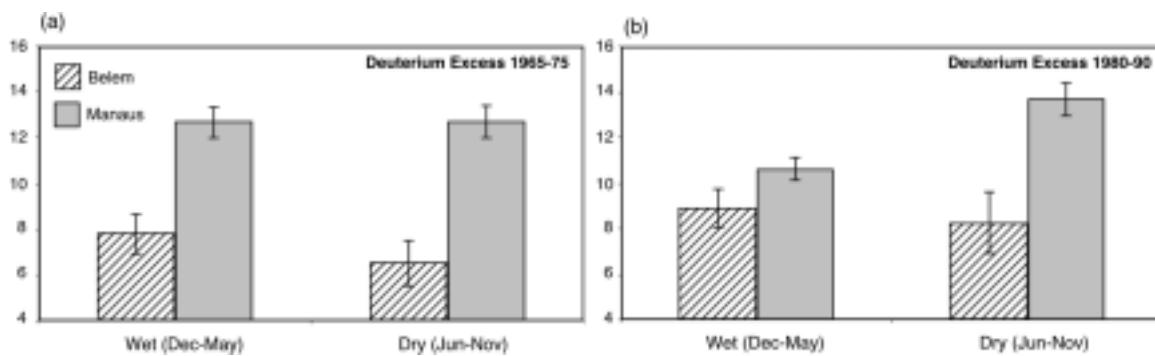


FIG. 5. Wet (Dec-May) and dry (Jun-Nov) half-year deuterium excess comparisons for Manaus and Belem at (a) the earliest decade of IAEA/WMO data (1965-1975) and (b) the most recent decade (1980-1990). Error bars show ± 1 standard error.

In the 1960s, when the collection of isotopic data began in the Amazon Basin, monthly average values of the deuterium excess at Manaus were significantly greater than at Belem for both the wet and dry seasons (Fig. 5(a)). Furthermore, there was no significant difference between the mean monthly deuterium excess values from the wet to the dry season at either the coastal or interior sites. By the 1980s, the Belem mean monthly deuterium excess for both the wet and dry seasons have increased slightly compared to the values in the 1960s, but the difference is not statistically significant. In contrast, large changes are observed in the seasonal deuterium excess inside the basin at Manaus. Although the annual mean deuterium excess at Manaus in the 1980s ($11.83 \pm 0.44\text{‰}$) is not significantly different to that in the 1960s ($12.62 \pm 0.48\text{‰}$), results now show a significant difference between the wet and dry season values (Fig. 5(b)). In particular, the deuterium excess has decreased in the wet season and increased in the dry season. The difference in deuterium excess between Belem and Manaus is also much reduced in the wet season and Manaus' wet season value is significantly decreased in the 1980s.

Plausible explanations of the wet season deuterium excess decrease involve either more non-fractionating (e.g. transpiration) or less fractionating (e.g. lake) recycling, or both. Thus the observed temporal shift in isotope data (1960s to 1980s) requires a change in the recycling behaviour in the Amazon. These isotopic results are consistent with the GCM deforestation predictions, which show less overall transpiration (Fig. 6) only if there has been a relative decrease in the evaporation of water from lakes and other fractionating sources over this period.

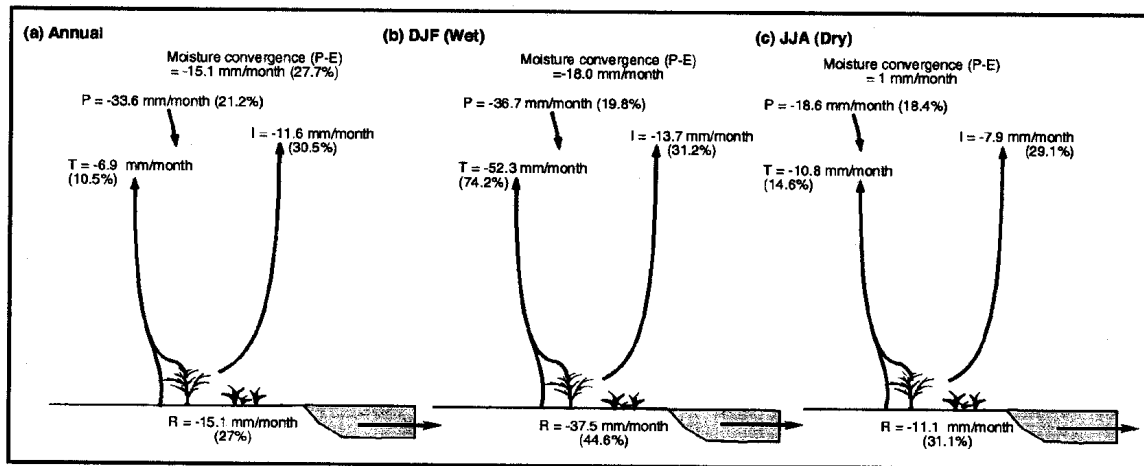


FIG. 6. Changes simulated by CCM1-Oz to the Amazon water budget following deforestation. Differences and percentages are all from the forested case in Fig. 3 for the same periods.

This isotope-GCM "missing link" warrants further detailed study. One possibility is that the temporal isotopic records are illustrative of the impact of Amazonian deforestation. At present, the available GCM studies are unable to demonstrate or deny the validity of this conclusion. Another possibility that deserves some consideration is that the disturbances in the isotopic record over time have not been caused solely by forest removal. Although the regional extent of deforestation in the Amazon is great, there are other effects which may also be contributing to the observed temporal shifts in the isotopic signatures. These could include both the direct and indirect effects of greenhouse gas increases.

4. RECENT GCM STUDIES OF THE AMAZON

There have been very few GCM studies so far which have attempted to assess the impact of deforestation and greenhouse gas increases in the Amazon. Table II lists the imposed changes and predicted outcomes for the three available studies. The paper by Henderson-Sellers *et al.* [37] was not focussed on deforestation but did consider plant physiological responses to increased atmospheric CO₂ levels which includes stomatal closure. Costa and Foley's [31] study is a much more sophisticated evaluation of the independent and combined effects of stomatal closure in response to an enriched CO₂ atmosphere, deforestation and greenhouse warming. Zhang *et al.* [32] consider the latter two effects but not the plant physiological responses. The challenge for future use of isotopic signatures for GCM evaluation is to know which of these representations most closely fit "present-day" isotopic measurements.

Table II. Annually-averaged regional response to Amazon tropical deforestation for surface temperature, T, precipitation, P, evaporation, E, and moisture convergence from recent GCM studies which have included the effects of greenhouse gas increases. (N/A means information is not available)

Study	Albedo change	Roughness change	ΔT (°C)	ΔP (mm)	ΔE (mm)	Moisture convergence change
Henderson-Sellers <i>et al.</i> [37]) Doubled stomatal resistance and warming no deforestation	No change	No change	+	N/A	-	+
Costa & Foley [31] Doubled CO ₂ & deforestation with plant physiological response	0.135/0.173	0.151/0.05	+3.5	-153	-146	-
Zhang <i>et al.</i> [32] Doubled CO ₂ & deforestation	0.12/0.19	2.0/0.2	+0.4	-424	-215	-

Tables I and II emphasize an outstanding disagreement among GCM representations of the impact of Amazonian deforestation: the sign of the change in moisture convergence (Fig. 2(b)). The challenges associated with predicting this are illustrated in [35] which shows the changes in the vertically-integrated water flux across the north, south, east and west boundaries of the Amazon Basin as derived from one set of GCM simulations of deforestation. We have examined the possibility of determining at least the sign of this important change by reverting to the isotopically-derived central basin box model of Gat and Matsui [5]. Since the total runoff equals the atmospheric moisture convergence, changes in either indicate a change in the other. We have employed values of parameters derived by Gat and Matsui [5] and investigated the effects of modelling runoff larger and smaller than their values. Our results suggest that it is necessary to decrease the runoff fraction by 10% in order to match the changed isotopic signature at Manaus between the periods 1965-75 and 1980-90. This result is consistent with the (larger number of) GCMs in Tables I and II that find a decrease in moisture convergence.

5. FUTURE USE OF ISOTOPES IN EVALUATING MODELS OF THE AMAZON'S CLIMATE AND HYDROLOGY AND THE POSSIBLE IMPACTS OF DEFORESTATION

Isotopic analysis and modelling studies relating to the Amazon date back to the early 1970s and estimates of the likely impacts of deforestation begin around 1984. Results from isotopic research have influenced climate and hydrological modelling but the two communities have rarely worked closely. The potential importance of the impact of Amazonian deforestation to distant locations has been suggested recently. Such results increase the importance of using all available data in the evaluation and, hopefully, validation of global climate models used to predict these impacts.

In this paper, we have shown that results derived from isotopic data from the IAEA/WMO network can be compared with outputs from GCMs. We find that water recycling in the central Amazon has changed over the last thirty years, significantly so in the wet season. While GCM results may be consistent with this conclusion, they are not, so far, correctly simulating the relative components of transpiration and re-evaporated canopy interception for the complementary dry season. These results warrant further detailed analysis and extension to the very large number of GCMs already predicting the impacts of Amazonian deforestation.

Furthermore, there is potential to explore isotopic modification by Amazonian deforestation by utilizing state of the art land surface schemes combined with one of the current 'isotope' GCMs (e.g. Ref. 38]). Finally, the great need for new validation data for GCMs, and the obvious and beneficial synergy, seems to demand that new observational programmes, such as the Large Scale Biosphere Atmosphere Experiment in Amazonia (LBA), embrace isotopic studies as a potentially very valuable tool for model validation. Ideas include: (a) moisture convergence estimates; (b) partitioning among transpiration, free evaporation and canopy evaporation; and (c) detection of the impacts of forest change and greenhouse signals.

REFERENCES

- [1] SALATI, E., et al., Recycling of water in the Amazon Basin: An isotopic study, *Wat. Res. Res.* **15**(5): (1979) 1250-1258.
- [2] MOLION, L.C.B., A climatonic study of the energy and moisture fluxes of the Amazonas basin with considerations of deforestation effects, PhD. Thesis, Univ. of Wis., Madison (1975).
- [3] ROZANSKI, K., et al., Isotopic patterns in modern global precipitation, *Climate Change in Continental Isotopic Records. Geophysical Monographs* **78**: (1993) 1-36.
- [4] LEOPOLDO, R.R., Aspetos hidrologicos at florista amazonica denga na regio de Manaus, PhD thesis, University National Estado San Paolo, Botucato SP Brasil (1981).
- [5] GAT, J.R., MATSUI, E., Atmospheric water balance in the Amazon Basin: an isotopic evapotranspiration model, *J. Geophys. Res.* **96**(D7): (1991) 13,179-13,188.
- [6] SALATI, E. VOSE, P.B., Amazon Basin: a system in equilibrium, *Science* **225**: (1984) 129-137.
- [7] HENDERSON-SELLERS, A., GORNITZ, V., Possible climatic impacts of land cover transformations, with particular emphasis on tropical deforestation, *Clim. Change* **6**: (1984) 231-258.
- [8] VICTORIA, R.L., et al., Mechanisms of water recycling in the Amazon Basin: Isotopic insights, *Ambio* **20**(8): (1991) 384-387.

- [9] DALL'OLIO, A., A composicao isotopica das precipitacoes do Brasil: modelos isotermicos e a influencia de evapo-transpiracao na Bacia amazonica, MS thesis, University of Sao Paulo, Piracicaba, Brasil (1976).
- [10] GAT, J.R., Atmospheric water balance – the isotopic perspective, *Hydrological Processes* **14**: (2000) 1357-1369.
- [11] MCGUFFIE, K., et al., Modelling climatic impacts of future rainforest destruction, in B.K. Maloney (eds), *Human Activities and the Tropical Rainforest*, Kluwer, Netherlands (1998) 169-193.
- [12] DICKINSON, R.E., HENDERSON-SELLERS, A., Modelling tropical deforestation: a study of GCM land surface parameterisations. *Quarterly Journal of the Royal Meteorological Society* **114**: (1988) 439–462.
- [13] LEAN, J., WARRILOW, D.A., Simulation of the regional climatic impact of Amazon deforestation, *Nature* **342**: (1989) 411–413.
- [14] NOBRE, C.A., et al., Amazonian deforestation and regional climatic change. *Journal of Climate* **4**: (1991) 957–988.
- [15] DICKINSON, R.E., KENNEDY, P.J., Impacts on regional climate of Amazon deforestation. *Geophysical Research Letters* **19**: (1992) 1947–1950.
- [16] MYLNE, M.F., ROWNTREE, P.R., Modelling the effects of albedo change associated with tropical deforestation, *Climatic Change* **21**: (1992) 317-343.
- [17] DIRMEYER, P.A., GCM studies of the influence of vegetation on the general circulation: the role of albedo in modulating climate change, unpublished PhD thesis, Department of Meteorology, University of Maryland (1992).
- [18] LEAN, J., ROWNTREE, P.R., A GCM simulation of the impacts of Amazonian deforestation on climate using an improved canopy representation. *Climate Research Technical Note No26*, Hadley Centre for Climate Prediction and Research, Meteorological Office, Bracknell, UK (1992).
- [19] HENDERSON-SELLERS, A., et al., Tropical deforestation: modelling local to regional-scale climate change. *Journal of Geophysical Research* **98**: (1993) 7289–7315.
- [20] PITMAN, A.J., et al., Assessing climate model sensitivity to prescribed deforested landscapes, *International Journal of Climatology* **13**: (1993) 879–898.
- [21] MANZI, AO, Introduction d'un schema des transfert sol-vegetation-atmosphere duns un modèle de circulation general et application a la deforestation Amazonienne, PhD Thesis, Université Paul Sabatier, Toulouse (1993).
- [22] POLCHER, J., LAVAL, C., The impact of African and Amazonian deforestation on tropical climate. *Journal of Hydrology* **155**: (1994) 389–405.
- [23] POLCHER, J., LAVAL, C., A statistical study of the regional impact of deforestation on climate in the LMD GCM. *Climate Dynamics* **10**: (1994) 205-219.
- [24] SUD. Y.C., et al., Biogeophysical effects of a tropical deforestation scenario: a GCM simulation study. *Journal of Climate* **9**: (1996) 3225–3247.
- [25] MCGUFFIE, K., et al., Global climate sensitivity to tropical deforestation, *Global and Planetary Change* **10**: (1995) 97–128.
- [26] MANZI, O., PLANTON, S., Calibration of a GCM using ABRACOS and ARME data and simulation of Amazonian deforestation, *Amazonian Deforestation and Climate* (eds. J.H.C. Gash, et al.), John Wiley and Sons (1996) 505-530.
- [27] ZHANG, H., et al., Impacts of tropical deforestation .1. Process analysis of local climatic change. *Journal of Climate* **9**: (1996) 1497-1517.
- [28] LEAN, J., ROWNTREE, P.R., Understanding the sensitivity of a GCM simulation of Amazonian deforestation to the specification of vegetation and soil characteristics. *Journal of Climate* **10**: (1997) 1216-1235.

- [29] HAHMANN, A.N., DICKINSON, R.E., RCM2-BATS model over Tropical South America: Applications to tropical deforestation. *Journal of Climate* **10**: (1997) 1944–1964.
- [30] ZHANG, H., et al., Uncertainties in GCM evaluations of tropical deforestation: a comparison of two model simulations, in W. Howe and A. Henderson-Sellers (eds), *Assessing Climate Change: results from the Model Evaluation Consortium for Climate Assessment*, Gordon and Breach, Sydney, Australia (1997) 323-355.
- [31] COSTA, M.H., FOLEY, J.A., Combined effects of deforestation and doubled atmospheric CO₂ concentrations on the climate of Amazonia, *Journal of Climate* **13**: (2000) 18-34.
- [32] ZHANG, H., et al., The compounding effects of tropical deforestation and greenhouse warming, *Clim. Change* (2001) in press.
- [33] JOUZEL, J., et al., Simulations of the HDO and H₂¹⁸O atmospheric cycles using the NASA GISS general circulation model: sensitivity experiments for present-day conditions, *J. Geophys. Res.* **96**(D4): (1991) 7495-7507.
- [34] JOUZEL, J., et al., Water isotopes in precipitation: data/model comparison for present-day and past climates, *Quaternary Science Reviews* **19**: (2000) 363-379.
- [35] ZHANG, H., et al., Impacts of tropical deforestation II: the role of large-scale dynamics, *J. Clim.* **9**: (1996) 2498-2521.
- [36] IAEA/WMO, Global Network for Isotopes in Precipitation. The GNIP Database. Release 3, Oct. 1999 (1999) URL: <http://www.iaea.org/programs/ri/gnip/gnipmain.htm>
- [37] HENDERSON-SELLERS, A., et al., Sensitivity of global climate model simulations to increased stomatal resistance and CO₂ increases, *J. Clim.* **8** (7): (1995) 1738-1756.
- [38] HOFFMANN, G., et al., Stable isotopes in atmospheric general circulation models, *Hydrological Processes* **14**: (2000) 1385-1406.

MASS INDEPENDENT ISOTOPE EFFECTS AND THEIR OBSERVATIONS IN NATURE

M.H. THIEMENS

Department of Chemistry and Biochemistry, University of California,
La Jolla, California, United States of America

Abstract. In 1983, Thiemens and Heidenreich reported the first chemically produced mass independent isotope effect. A significant feature of the fractionation was that it identically produced the isotopic relation observed in the calcium-aluminum inclusions in the Allende meteorite. This $\delta^{17}\text{O}=\delta^{18}\text{O}$ composition had previously been thought to represent a nucleosynthetic component as no chemical process was capable of producing a mass independent isotopic composition. It now appears nearly certain that the meteoritic oxygen isotopic anomalies were produced by chemical, rather than nuclear, processes. Since oxygen is the major element in stony planets this represents a major event in the formation of the solar system. In a recent review (Thiemens, 1999), it has been shown that mass independent isotopic compositions are pervasive in the Earth's atmosphere. Molecules which have been demonstrated to possess mass independent isotopic compositions include: O_2 , O_3 , CO_2 , CO , and N_2O . In each case, the specific nature of the mass independent isotopic composition has provided details of their atmospheric chemistry that could not have been obtained by any other measurement technique. Most recently, solid materials have been observed to possess mass independent isotopic composition. In this paper, these observations are briefly discussed. These solid reservoirs include: 1) carbonates and sulphates from Mars, 2) terrestrial aerosol sulphate, 3) sulphides and sulphates from the Earth, ranging in time from 3.8 to 2.2 billion years before present, 4) sulphates from the Namibian desert and 5) the Antarctic Dry Valleys. The information obtained from these measurements is extraordinarily wide ranging, extending from understanding the history of Martian atmosphere-regolith interaction to the evolution of the oxygen in the Earth's earliest atmosphere. As was the case for gas phase species, this information and insight could not have been obtained by any other measurement technique.

1. INTRODUCTION

Alteration of stable isotope ratios in nature has permitted significant discoveries in an enormous range of scientific endeavours. Insight into the origin and evolution of the solar system and pervasive applications in biologic, geologic, oceanographic and atmospheric sciences have been developed based upon precise interpretation of stable isotope ratio compositions. The first quantitative model which was capable of determining how temperature influences the position of chemical equilibrium in an isotope exchange reaction was by Urey [1] and Bigeleisen and Mayer [2]. This groundbreaking work essentially opened the fields of geo- and paleo-thermometry. By careful, precise measurements of, for example, oxygen isotope ratios, and with knowledge of the temperature dependency of the equilibrium constant for the isotope exchange reaction, the temperature during the exchange reaction may be precisely determined. The actual physical-chemical dependency of the equilibrium upon temperature arises from the variation of the molecular vibrational frequency with temperature.

Alteration of isotope ratios by other processes such as diffusion, evaporation/condensation, kinetics, velocity, and gravitational escape are well known and quantified. Though these isotope effects all vary, they have one common feature; they all ultimately depend in one fashion or another upon mass. In general, the change in isotope ratio is small, and they are generally reported in the conventional δ notation. For oxygen, this is given by:

$$\delta^{18}\text{O} = (R_{\text{sa}}^{18}/R_{\text{std}}^{18} - 1) \times 1000 \quad (1)$$

and

$$\delta^{17}\text{O} = (R_{\text{sa}}^{17}/R_{\text{std}}^{17} - 1) \times 1000 \quad (2)$$

where $R^{17} = {}^{17}\text{O}/{}^{16}\text{O}$, $R^{18} = {}^{18}\text{O}/{}^{16}\text{O}$.

For oxygen, STD refers to the standard, which is standard mean ocean water. The mass dependency for isotope effects produces a correlation between $\delta^{17}\text{O}$ and $\delta^{18}\text{O}$. The relation for O_2 is:

$$\delta^{17}\text{O}/\delta^{18}\text{O} = (1/32 - 1/33)/(1/32 - 1/34) \quad (3)$$

which yields the mass dependent relation:

$$\delta^{17}\text{O} = 0.5 \delta^{18}\text{O} \quad (4)$$

In the field of cosmochemistry, the observation that calcium-aluminum inclusions in the chondritic meteorite Allende possess an isotopic composition $\delta^{17}\text{O} = \delta^{18}\text{O}$, rather than $\delta^{17}\text{O} \cong 0.5 \delta^{18}\text{O}$ was reasoned at the time that, since no chemical process may produce a mass independent isotopic fractionation this observation must reflect exotic nuclear material, e.g. the injection of pure ${}^{16}\text{O}$ into the proto-solar nebula. This has major consequences as the deserved effect is large and occurs in the most abundant element (in stony planets), oxygen. This observation catalyzed an enormous number of measurements and searches for nucleosynthetic anomalies in other elements.

In 1983, Thiemens and Heidenreich [3] were the first to demonstrate that a mass independent isotopic composition may be produced by a simple chemical process. During the process of ozone formation it is observed that it is enriched in the heavy isotopes with respect to the precursor oxygen with $\delta^{17}\text{O} = \delta^{18}\text{O}$, precisely the same as in the meteoritic inclusions. Since those measurements a large body of experimental data has accumulated directed towards resolving the physical chemical mechanism responsible for generation of the mass independent effect. The purpose of this paper is directed towards the application of this effect in nature. Reviews by Thiemens [5] and Weston [6] summarize the physical chemistry.

There now exists a wide range of environments in space and time, where mass independent isotopic compositions are observed. In each instance, the characteristic isotopic compositions permits new information to be obtained on the particular natural environment. This paper briefly highlights some of these examples.

2. ATMOSPHERIC SPECIES

It was demonstrated that stratospheric ozone possesses a strikingly large ${}^{18}\text{O}$ enrichment [7]. Subsequently, it was demonstrated that stratospheric ozone possesses the same mass independent isotopic composition observed in laboratory experiments [8]. A review of the many existing ozone isotopic measurements is given in [5,6]. It is now known that tropospheric ozone possesses a mass independent composition that is slightly variable with location and season [9, 10]. From these measurements it appears that the variation may be of utility in tracking source, stratosphere-troposphere mixing, and chemical heritage.

It was first observed by Thiemens et al. [11] that stratospheric CO₂ possesses a large mass independent isotopic composition. Models by Yung et al. [12, 13] have shown that this arises from the exchange of atomic oxygen, derived from ozone photolysis, with CO₂ via :



This was later confirmed by measurement of CO₂ stratospheric and mesospheric samples obtained with a rocket-borne cryogenic air sampler [14]. The observed isotopic anomaly still has unexplained features. However, there are two significant applications of the isotopic effect. First, since the anomaly arises from isotopic exchange with electronically excited atomic oxygen, the magnitude is a direct reflection of the steady state concentration of oxygen. The concentration of atomic oxygen is a significant parameter in stratospheric chemistry, it is the concentration of O(¹D) that determines the lifetime of many molecular species, however, given its low concentrations it is nearly impossible to measure. The mass independent isotopic signature therefore provides an independent means by which the concentration of atomic oxygen may be determined. A second application of the observed isotopic anomaly is as a tracer of stratosphere-troposphere mixing. Since tropospheric CO₂ is strictly mass dependent, due to its exchange with H₂O, and stratospheric CO₂ is mass independent, any mass independent CO₂ observed in the troposphere must be stratospherically derived. Thus, $\delta^{17}\text{O} = \delta^{18}\text{O}$ measurements of atmospheric CO₂ provides a new means by which stratosphere-troposphere mixing may be evaluated.

2.1. Atmospheric O₂

Recently, it has been observed that atmospheric O₂ possesses a slight mass independent isotopic composition. Since stratospheric O₃ is enriched in ¹⁷O and ¹⁸O, the parent, O₂ must be depleted [15]. Though slight, the depletion is measurable. The isotopic anomaly is removed when it crosses the air-sea interface and is removed by photosynthesis and respiration, both mass dependent. This rate of removal of the isotopic anomaly is a direct measure of biospheric productivity. As shown by Luz et al. [15] the columnar measurement of $\delta^{17}\text{O}$, $\delta^{18}\text{O}$ in the oceans has provided a new and unique means by which oceanic primary productivity may be determined. In addition, measurement of the oxygen isotopes in O₂ trapped in polar ice provides a means by which global biospheric productivity over the past 80,000 years may be determined.

2.2. Other atmospheric molecules

Several atmospheric molecules have been observed to possess mass independent isotopic compositions. In each instance, the measurements have provided information unattainable by either concentration or single isotope ratio measurements. Mass independent isotopic compositions have been observed in atmospheric carbon monoxide [16, 17]. It is well known that carbon monoxide controls the OH budget of the troposphere and consequently its oxidative capacity. The result is that the lifetime of species such as H₂S, SO₂ and CH₄ is indirectly mediated by carbon monoxide. Laboratory experiments have shown that the source of the mass independent isotopic composition is the OH + CO reaction [18]. Since the source of the mass independent anomaly is derived from the OH reaction, the magnitude of the $\Delta^{17}\text{O}$ anomaly is a measure of the OH number density. These measurements have provided a new means by which OH number densities may be evaluated. At present, the physical-chemical mechanism by which the $\Delta^{17}\text{O}$ (the deviation from mass fractionation) anomaly arises is unknown.

2.3 Nitrous oxide

Atmospheric nitrous oxide is the catalytic destruction agent of stratospheric ozone. In addition, it is a significant greenhouse agent. In spite of decades of high precision concentration measurements and modelling efforts, the budget is inadequately resolved. Cliff and Thiemens [19] have shown that atmospheric nitrous oxide possesses a large and variable mass independent isotopic composition. This work has the potential to provide new a new outlook on the atmospheric cycle of N_2O . In addition, this work has catalysed several investigations into the complete isotopic structural arrangements of N_2O . This new work is presented elsewhere in this volume.

2.4 Mars

The atmosphere of Mars is primarily composed of carbon dioxide. It is well known that the Martian atmosphere possesses ozone, thus, with its photolysis, $\text{O}(^1\text{D})$ is generated and as occurs in the Earth's atmosphere, a mass independent anomaly is inscribed in the CO_2 . Farquhar, Jackson, and Thiemens [20] have measured carbonate in the Martian meteorite ALH84001 and demonstrated that it possesses a mass independent isotopic composition. This measurement has been suggested as arising from Martian atmospheric CO_2 , which undergoes exchange with the Martian Regolith and water, with subsequent formation of the carbonate minerals. Thus, the carbonate measurements provide a new means by which Martian atmosphere-regolith interactions may be investigated. In a subsequent work it was shown that carbonate and sulphate in the Martian meteorite possess a large $\Delta^{17}\text{O}$ [21]. The observation of an anomaly in another secondary mineral, sulphate, adds another view into Martian weathering processes. Most recently, it has been shown that sulphate sulphur in Martian meteorites possesses a mass independent isotopic composition [22]. Based upon laboratory experiments, it has been shown that the mass independent isotopic composition arises from the photolysis of SO_2 in the Martian atmosphere. These results have opened the possibility that with further quantification of the isotope effect coupled with additional Martian meteorite measurements may provide a means by which the photochemical history of Mars may be established.

2.5 Atmospheric aerosol sulphate

For decades, a means by which the oxidation pathways of sulphur may be quantified has been sought. Specifically, the relative proportions of homogenous (gas phase) vs. heterogeneous (liquid phase) is an important parameter. It has recently been observed that atmospheric aerosol sulphate possesses a large and variable mass independent isotopic composition [23-25]. Based upon laboratory experiments by Savarino et al [26], the source of the mass independent composition has been determined. It has been shown that the anomaly arises from transfer of the oxygen isotopes from ozone and hydrogen peroxide. Since the isotopic composition of both of these atmospheric species is known, as are all relevant rate constants, the $^{17}\Delta$ anomaly provides a quantitative measure of the relevant oxidation pathways [27]. The measurement of $\delta^{17}\text{O}$, $\delta^{18}\text{O}$ in aerosol sulphate has provided a completely new means by which the atmospheric cycle of sulphur may be investigated. Most recently, it has been shown that $\delta^{17}\text{O}$, $\delta^{18}\text{O}$ measurements of sulphate in polar ice samples provides a means by which the past oxidation capacity of the atmosphere may be studied (Alexander, Savarino and Thiemens, 2000).

2.6 Paleo-applications

Recently, sulphur isotope ratio measurements of sulphides and sulphates from sedimentary and metasedimentary rocks older than 2090 MA (million years ago) have revealed a mass independent isotopic composition [28]. The sulphur isotopic data appear to be global, as the isotopic anomaly is observed in a wide variety of different hydrothermal and sedimentary rocks between 2.5 and 3.9×10^9 years ago. Sulphate samples record the dissolved oceanic sulphate reservoir, and the reduced samples likely record an insoluble reduced reservoir. Based upon laboratory observations it is apparent that the sulphur isotopic composition arises from the UV photolysis of SO_2 in the earth's early atmosphere. The photolytic reaction does not occur in the present atmosphere due to screening out of the relevant wavelengths by ozone. In the early ozone-oxygen free environment this wavelength of light penetrates to ground level. With the evolution of photosynthesis the build up of oxygen and ozone screens the short wavelength light such that by $\leq 2.0 \times 10^9$ years ago UV is optically shielded and this photochemistry no longer occurs. The measurement of these sulphur isotopic anomalies therefore has provided an entirely new means by which the evolution of oxygen in the Earth's early atmosphere may be followed.

Recent studies of sulphates from arid environments have demonstrated mass independent oxygen isotopic compositions [29,30]. Gypsum from the central Namib Dessert possesses a large and variable $\Delta^{17}\text{O}$. It has been suggested that this reflects enhanced dimethyl sulphite emissions from the nearby oceans [29,30]. Similar isotopic compositions have been observed in sulphates from the Antarctic Dry valleys [29,30], and these samples also record atmospheric and oceanic processes on ancient time scales.

3. SUMMARY

Mass independent isotopic compositions in natural samples have been observed in a wide variety of environments on Earth and Mars. Numerous atmospheric molecules and aerosols possess mass independent isotopic compositions. Chemical transformation processes, sources, and transport information is uniquely obtained from these measurements. Atmosphere-regolith interactions on Mars are studied from the mass independent isotopic compositions of carbonates and sulphates. The evolution of life from 3.9×10^9 to 2.0×10^9 years ago is visualized from mass independent sulphur isotopic compositions in ancient sulphides and sulphates. Oceanic productivity tens of millions years ago have been studied from oxygen isotopic compositions. In sum the use of chemically produced mass independent isotopic effects as first discovered in 1983 by Thiemens and Heidenreich has been found to have applications in a broad range of environments. In each instance this new tool has provided information which could not be obtained by any other technique.

REFERENCES

- [1] UREY, H. C., J. Chem. Soc. **1947** (1947) 561.
- [2] BIGELEISEN, J. and MAYER, M., J. Chem. Phys. **15** (1947) 261.
- [3] CLAYTON, P. N., GROSSMAN, L, MAYEDA, T.K. Science **182** (1973) 485.
- [4] THIEMENS, M. H. and HEIDEREICH III, J. E., Science **219** (1983) 1073 .
- [5] THIEMENS, M. H., Science **283** (1999) 341.
- [6] WESTON, R. E., Chem. Rev. **99** (1999) 2115.
- [7] MAUERSBERGER, K. Geophys. Res. Lett. **8** (1981) 935.
- [8] MAUERSBERGER, K. Geophys. Res. Lett. **14** (1987) 80.
- [9] KRANKOWSKI, D. Geophys. Res. Lett. **22** (1995) 1713 .

- [10] JOHNSTON, J. C. and THIEMENS, M. H. J. *Geophys. Res.* **102** (1997) 25395.
- [11] THIEMENS, M. H., JACKSON, T., MAUERSBERGER, K., SCHUELER, B., MORTON, J. *Geophys. Res. Lett.* **18** (1991) 669 .
- [12] YUNG, Y. L., DEMORE, W. B., PINTO, J. P., *Geophys. Res. Lett.* **18** (1991) 13 .
- [13] YUNG, Y. L., LEE, A.Y. T., IRION, F. W., DEMORE, W. B., WEN, J. J. *Geophys. Res.* **102** (1997) 10857.
- [14] THIEMENS, M. H., JACKSON, T., E. ZIPF, C., ERDMAN, P. W., VAN EGMOND, C., *Science* **270** (1995) 969.
- [15] LUZ, B., BARCAN, E., BENDER, M. L., THIEMENS, M. H., BOERING, K. *Nature* **400** (1999) 547.
- [16] A. K. Huff and M. H. Thiemens, *Geophys. Res. Lett.* **25** (1998) 3509.
- [17] RÖCKMANN, T., BRENNINKMEIJER, C. A. M., NEEB, P., CRUTZEN, P. J. J. *Geophys. Res.* **103** (1998) 1463 .
- [18] CLIFF, S. S. and THIEMENS, M. H. *Science* **278** (1997) 1779 .
- [19] RÖCKMANN, T., BRENNINKMEIJER, C. A. M., NEEB, P., CRUTZEN, P. J. *Science* **281** (1998) 544.
- [20] J. Farquhar and M. H. Thiemens, *Science* **280** 1580 (1998).
- [21] FARQUHAR, J. and THIEMENS, M. H. J. *Geophys. Res. - Planets* **105** (2000) 11991.
- [22] FARQUHAR, J., SAVARINO, J., JACKSON, T. L., THIEMENS, M. H. *Nature* **404** (2000) 50.
- [23] LEE, C. W. and THIEMENS, M. H. in AGU Fall Meeting, A.G. U.; Supplement Transaction: San Francisco, 1997; Vol. 78, p F111.
- [24] LEE, C. W., SAVARINO, J., THIEMENS, M. H. In AGU Fall Meeting; Supplement E., Ed.: San Francisco, 1998, Vol. 79; pp F91.
- [25] LEE, C. W., and THIEMENS, M. H. J. *Geophys. Res.* Accepted (2001).
- [26] SAVARINO, J. and THIEMENS, M. H. *Atmos. Envir.* **33** (1999) 3683 .
- [27] SAVARINO, J., LEE, C. W., THIEMENS, M. H. J. *Geophys. Res.* (2001). In press.
- [28] FARQUHAR, J., BAO, H., THIEMENS, M. H. *Science* **289** (2000) 756.
- [29] BAO, H., CAMPBELL, D. A., BOCKHEIM, J. G., THIEMENS, M. H. *Nature* **406** (2000) 176.
- [30] BAO, H. D., CAMPBELL, A., BOCKHEIM, J. G., THIEMENS, M. H. *Nature* **407** (2000) 499.

CLIMATE VARIABILITY FROM ISOTOPE RECORDS IN PRECIPITATION

H. GRASSL

Max-Planck-Institut für Meteorologie und Meteorologisches Institut, Universität Hamburg,
Hamburg, Germany

M. LATIF

Meteorologisches Institut, Universität Hamburg,
Hamburg, Germany

U. SCHOTTERER

Physics Institute and Department of Chemistry, University of Bern,
Berne, Switzerland

L. GOURCY

Isotope Hydrology Section,
International Atomic Energy Agency,
Vienna

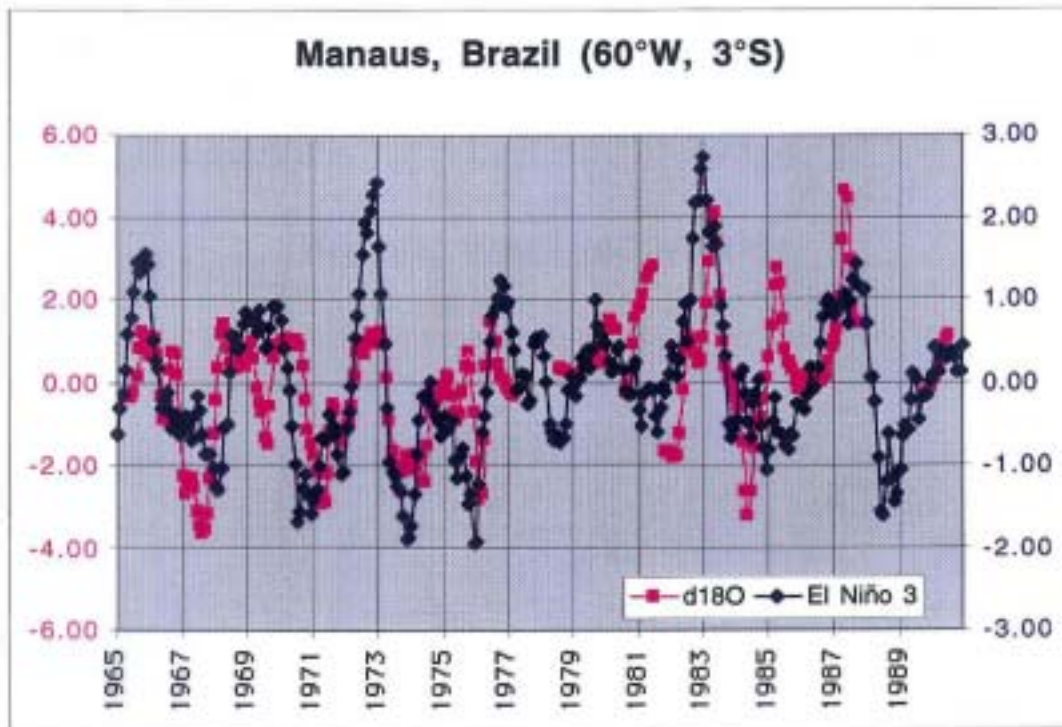
Abstract. Selected time series from the Global Network for Isotopes in Precipitation (GNIP) revealed a close relationship to climate variability phenomena like El Niño – Southern Oscillation (ENSO) or the North Atlantic Oscillation (NAO) although the precipitation anomaly in the case studies of Manaus (Brazil) and Groningen (The Netherlands) is rather weak. For a sound understanding of this relationship especially in the case of Manaus, the data should include major events like the 1997/98 El Niño, however, the time series are interrupted frequently or important stations are even closed. Improvements are only possible if existing key stations and new ones (placed at “hot spots” derived from model experiments) are supported continuously. A close link of GNIP to important scientific programmes like CLIVAR, the Climate Variability and Predictability Programme seems to be indispensable for a successful continuation.

1. MOTIVATION

The quantitative reconstruction climate history became possible largely by the measurement of isotopic composition in layered deposits. For example, the high correlation between greenhouse gas concentration in the atmosphere and atmospheric temperature from gas bubbles in ice cores and the ice itself is one of the pillars of the anthropogenic climate change debate and it is relying totally on isotopic composition records. The close relationship between atmospheric temperature and the composition of stable isotopes of the water molecule in precipitation (hence in ice) was one of the major earlier findings of the Global Network for Isotopes in Precipitation (GNIP), as reviewed in the 1960s by Dansgaard [1].

On the other hand, the understanding of climate variability on interannual to decadal time scales is a prerequisite for the separation of natural and anthropogenic climate change. As GNIP is now operating since four decades it should be possible to look for climate variability signals in its longest station records. In other words: Do isotopes in precipitation show strong climate variability phenomena like El Niño or the North Atlantic Oscillation (NAO)? A first attempt to answer this question was started some years ago by Hans Oeschger's Isotopes in the Hydrological Cycle (ISOHYC) Initiative.

Observations:



ECHAM-4:

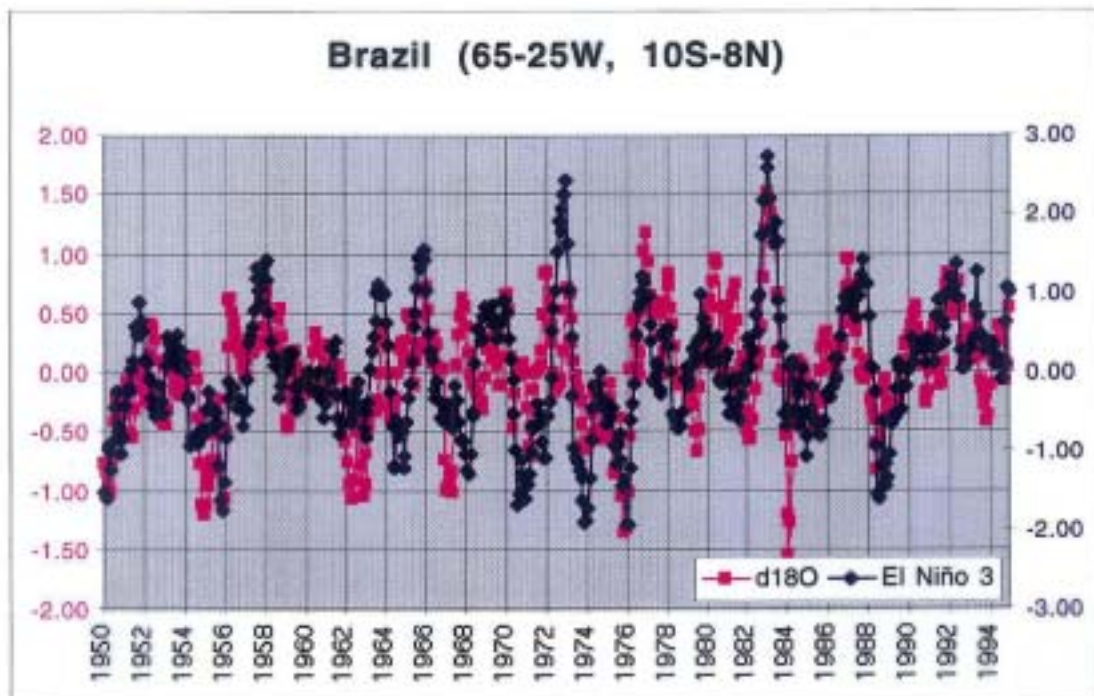


FIG. 1. Correlation of $\delta^{18}\text{O}$ from monthly composites of precipitation in Manaus with sea surface temperatures from the Niño 3 area; upper panel: observations, lower panel: modelling result.

2. FIRST RESULTS

As GNIP was not meant for climate variability studies, there exist only very few continuous records in areas sensitive to El Niño. Although the station Manaus, in the Amazon basin, Brazil, does not represent a key area of ENSO-related precipitation anomalies due to the intensive water recycling [2], which may overprint this anomaly a first statistical treatment of the available isotope data between 1965 and 1989 [3] shows a close correlation to SST anomalies in the central Pacific Ocean (Fig. 1).

Unfortunately, the data collection stopped in 1989 and the major 1997/98 El Niño was not included. However, a reconstruction of El Niño events in natural archives (ice cores, tree rings, corals, lake deposits) close to strong impacts of El Niño (hot spots) seems feasible.

The denser isotope network in Europe opens a much better opportunity to look for even weaker climate anomalies like the NAO. For example, despite the weak precipitation anomaly related to NAO in Groningen (The Netherlands) the isotope anomaly is significantly correlated to NAO (Fig. 2).

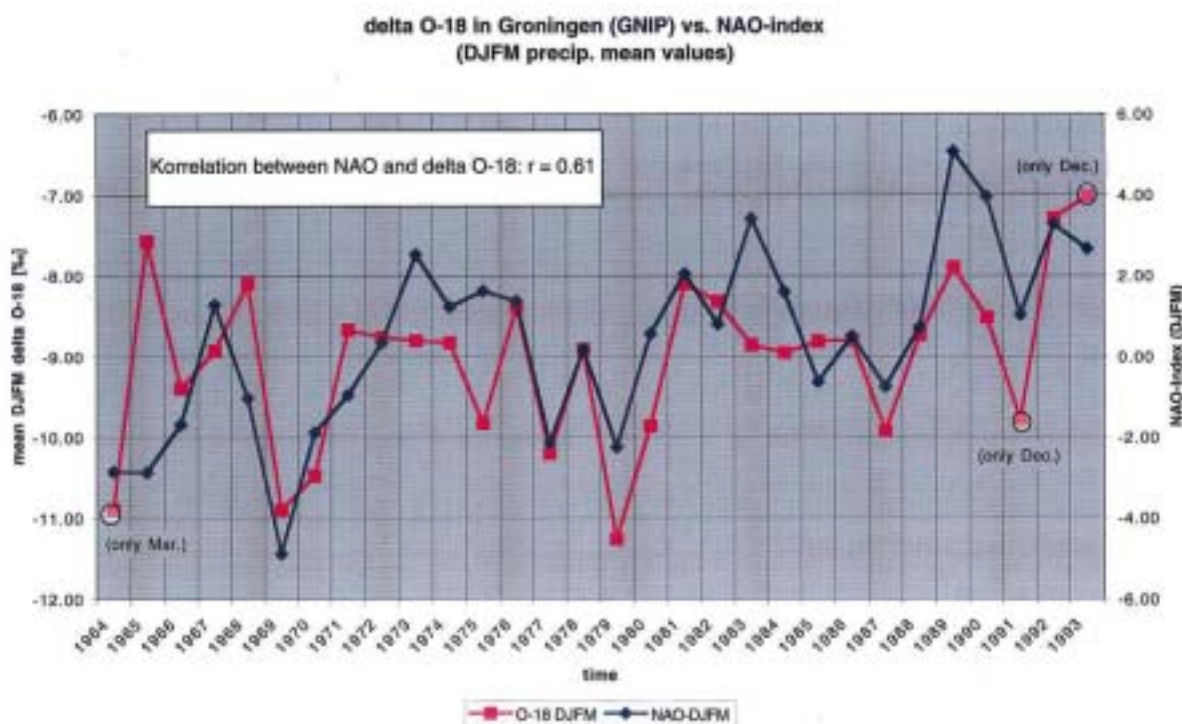


FIG. 2. Time series of winter (DJFM) North Atlantic Oscillation (NAO) index (blue) and the $\delta^{18}\text{O}$ measurements at Groningen. Both time series are highly correlated.

The high correlation of $\delta^{18}\text{O}$ may be addressed to ocean-atmosphere interactions within the source area of atmospheric moisture during a specific NAO situation and the rain-out history of the air masses precipitating at Groningen. Improvements in the connection between isotopic composition and changes in the atmosphere/ocean-interaction, on which they are based, can be achieved by model experiments. These models have to contain balance equations for the stable isotopes oxygen-18 and deuterium as well.

These improvements will remain wishful thinking if no new data from stations in "hot spot" areas are initiated, continuously supported and evaluated (extended GNIP).

3. FURTHER INITIATIVES NEEDED

The science initiative ISOHYC, together with the GNIP sponsoring agencies IAEA and WMO, already could halt the further decay of the GNIP. A memorandum of understanding between IAEA and WMO led to:

- Scientific Steering committee of the GNIP,
- revival of stations
- event-based sampling at a few stations in order to follow climate anomalies
- stronger integration of national networks, and
- the strengthening of the open-access GNIP database.

Although this has strengthened GNIP as a whole, it is, however, still not suited to fulfil its role in an isotope climatology as envisaged by Hans Oeschger, when he - together with the Beatenberg Group- started the ISOHYC Initiative in 1997.

A prominent example, where a science initiative has led to intergovernmental support is the World Climate Research Programme's (WCRP) study on Climate Variability and Predictability (CLIVAR [4]), that now has started to implement a global upper ocean observing system called ARGO, jointly with another science initiative GODAE (Global Ocean Data Assimilation Experiment) with the financial support of most OECD countries.

If a CLIVAR question like "Do we intensify El Niño events or influence monsoonal variability by an enhanced greenhouse effect?" has to be answered convincingly, we need to extend the instrumental record into the recent past by isotope-based quantitative reconstruction of the relevant climate parameters. An Isotope Climatology, therefore, would be a proper module within CLIVAR. This would then give the push for a further strengthening of GNIP by the synergy of scientific and intergovernmental support.

REFERENCES

- [1] DANSGAARD, W. Stable isotopes in precipitation, *Tellus* **16** (1964) 436-468.
- [2] GAT, J.R., MATSUI, E. Atmospheric water balance in the Amazon Basin: an isotopic evapotranspiration model, *J. Geophys. Res.*, **96 (D7)** (1991) 13179-13188.
- [3] WERNER, M. Private Communication.
- [4] CLIVAR EXCHANGES No. **19, 20, 21** (2001) <http://www.clivar.org/>

ISOTOPIC EVIDENCE FOR CLIMATIC CONDITIONS IN SOUTHEAST ASIA AT THE LAST GLACIAL MAXIMUM

P.K. AGGARWAL, J.J. GIBSON
International Atomic Energy Agency,
Vienna

K. FRÖHLICH
Vienna, Austria

K.M. KULKARNI
Isotope Hydrology Section, Bhabha Atomic Research Centre,
Trombay, Mumbai, India

Abstract. Stable isotope composition of dated groundwater archives from the Philippines, Vietnam, Thailand and Bangladesh trace changes in monsoon conditions, primarily rainout processes between the Last Glacial Maximum (LGM) and present day in southeast Asia. Today, isotope-climate relations are well established by the IAEA/WMO Global Network of Isotopes in Precipitation survey which reveals more depleted $\delta^{18}\text{O}$ and $\delta^2\text{H}$ for the Pacific Ocean monsoon regime than for the Indian Ocean monsoon regime, primarily due to proximal ocean sources and subdued continental moisture recycling for the latter region. Groundwater archives, reflecting past isotopic composition of precipitation, strongly suggest that this distinction was preserved or slightly enhanced at the time of the LGM, despite an apparent weakening of the summer monsoon and associated rainout processes. Overall, precipitation and moisture recycling, and enhanced continental effects are inferred to be the primary controls on $\delta^{18}\text{O}$ signals in groundwater in southeast Asia. Comparison of groundwater isotope signatures and an ECHAM4 model simulation of the isotopic distribution in precipitation at 21ka reveal similar patterns, but the impacts of increased air mass contributions from high latitudes and reduced Eurasian moisture recycling at the LGM are shown to be potentially greater for the Pacific region than predicted by the model.

1. INTRODUCTION

The wind circulations of northern and southern hemispheres are separated by the *Intertropical Convergence Zone (ITCZ)*, where the northeast and southeast trade winds flow together. Air circulation patterns within the ITCZ, dominated by air rising at the equator and descending at about 30 degrees north and south latitudes, result in heavy monsoonal rainfall in the tropics. The Asian summer monsoon, covering the Indian subcontinent and South East Asia, is one of the most conspicuous features of the monsoonal climate and is a major climate system of the world, reflecting complex interactions between land surface, atmosphere, and oceans [1]. It has been suggested that Eurasian snow cover, the Indian monsoon, and the El Niño/Southern Oscillation (ENSO) are inter-connected. Anomalously high winter Eurasian snow has been linked to weak rainfall in the following summer Indian monsoon. Major droughts (floods) have been correlated with warmer (cooler) than normal equatorial Eastern Pacific sea surface temperatures (SST) [1]. An understanding of the causes and patterns of the Asian Monsoon variability in the present as well as in the past has attracted much research attention, as rainfall variability in this monsoon system directly impacts nearly one third of the world's population.

Rainfall variability in monsoon regions results from differences in moisture sources, circulation patterns, and temperature fields. Information on these climate factors can be deduced from isotopic evidence provided by coastal aquifers [2]. Climatic conditions in the past can be evaluated from the isotopic composition of groundwater that may have infiltrated under previous climate regimes. Groundwater inherits the stable isotope signature of recharge sources, predominantly precipitation, although aquifers usually act as low pass filters, smoothing out high-frequency variability by mixing and dispersion at a range of scales [3].

Despite this, such archives have been shown to provide adequate time resolution for distinguishing pervasive shifts in climate, such as differences between climate conditions today and at the time of the last glacial maximum (LGM). In this paper we examine systematic temporal trends in $\delta^{18}\text{O}$ and $\delta^2\text{H}$ in groundwaters of this age range that were sampled at coastal areas in southeast Asia. Importantly, trends in $\delta^{18}\text{O}$ and $\delta^2\text{H}$ provide a proxy record of changes in the precipitation isotope signals between the LGM (21ka) and today.

2. PRESENT DAY ISOTOPE VARIATIONS IN THE ASIAN MONSOON REGION

The climate of the Asian monsoon region is dependant on the interactions of polar, continental, and oceanic (both Pacific- and Indian-maritime) air masses. Precipitation in this region is controlled primarily by two large scale, low level circulation systems that are modulated by sea surface temperatures (SSTs) in the Indian and Pacific oceans, and the presence of the Tibetan Plateau [1]. The western system produces the South Asian or Indian monsoon roughly between 70-100°E and 10-30°N, covering the Indian subcontinent and the Bay of Bengal. This circulation system is related to the easterlies over the southern Indian Ocean, connected through the Somali jet to westerlies over the Indian subcontinent. The eastern circulation pattern produces the Southeast Asian monsoon roughly between 100-130°E and 5-25°N, covering South China Sea, western Pacific and Indo-China. Air circulation in this area is related to the easterlies in the tropical western Pacific, northerlies from the South China Sea, and southwesterlies across the Korean Peninsula and Japan [1; see their Fig. 20]. Origin and transport calculations using an atmospheric general circulation model (AGCM) suggest that the mean age of precipitation water since its origin, and mean recycling count between the atmosphere and the continental surface, are typically several times greater for the Pacific monsoon regime than for the Indian regime due to the larger role of the Eurasian *versus* Indian land mass [4].

These differences in circulation patterns are reflected in the isotopic composition of precipitation [5]. Notably, Pacific-maritime air masses are found to be depleted in $\delta^{18}\text{O}$ and $\delta^2\text{H}$ compared to Indian-maritime air masses (FIG. 1). The distinct isotopic labeling of Pacific verses Indian Ocean regimes is evident in both the summer monsoon signals and also in the mean annual amount-weighted isotope values, which are heavily biased toward the wet season conditions due to high summer rainfall (FIGS. 1 & 2a). Precipitation in the wet season is characterized by more negative isotope values than for the dry season, which has been attributed mainly to amount effects for both regimes [5].

Isotopic differences in precipitation across the boundary which separates the two air circulation patterns at about 100°E longitude, result from different moisture sources in the two precipitation regimes. Moisture in the South Asian or Indian monsoon is derived from the southern Indian Ocean and the Bay of Bengal with only minimal transport (and rainout/recycling) over the continental areas. In the South-East Asian monsoon, the moisture source appears to be a mixture from low and high latitudes. The high latitude moisture is transported over northeast China to the South China Sea and the Pacific and consequently has more negative isotope values due to rainout over continental areas. The proportion of continentally recycled moisture in southeastern Eurasia is estimated to be as high as 20% annually [4]. The Pacific circulation is also more negative due to a longer circulation pathway.

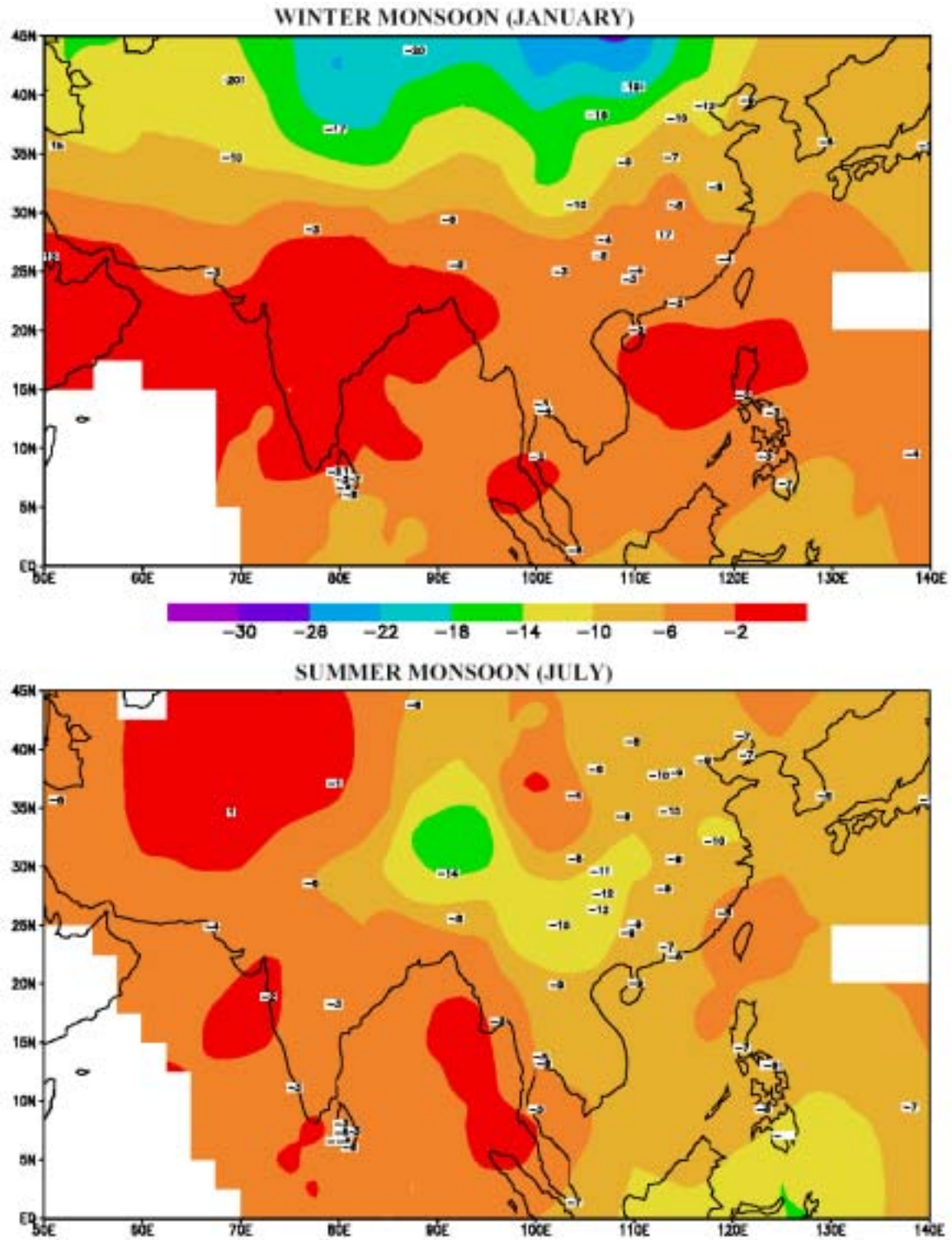


FIG. 1. (a) January amount-weighted $\delta^8\text{O}$ (‰), typical of precipitation patterns during the winter monsoon. Note that surface winds are predominantly from the northeast. Moisture originates from continental high-pressure centres, with typically drier air masses and reduced precipitation during this period. (b) July amount-weighted $\delta^8\text{O}$ (‰), typical of precipitation patterns during the summer monsoon. Note that surface winds are predominantly from the southwest. Moisture originates from Indian Ocean and Pacific Ocean sources, with typically wet air masses and heavy precipitation during this period. Note that heavy isotope content is greater (less negative $\delta^8\text{O}$ values) in winter than in summer.

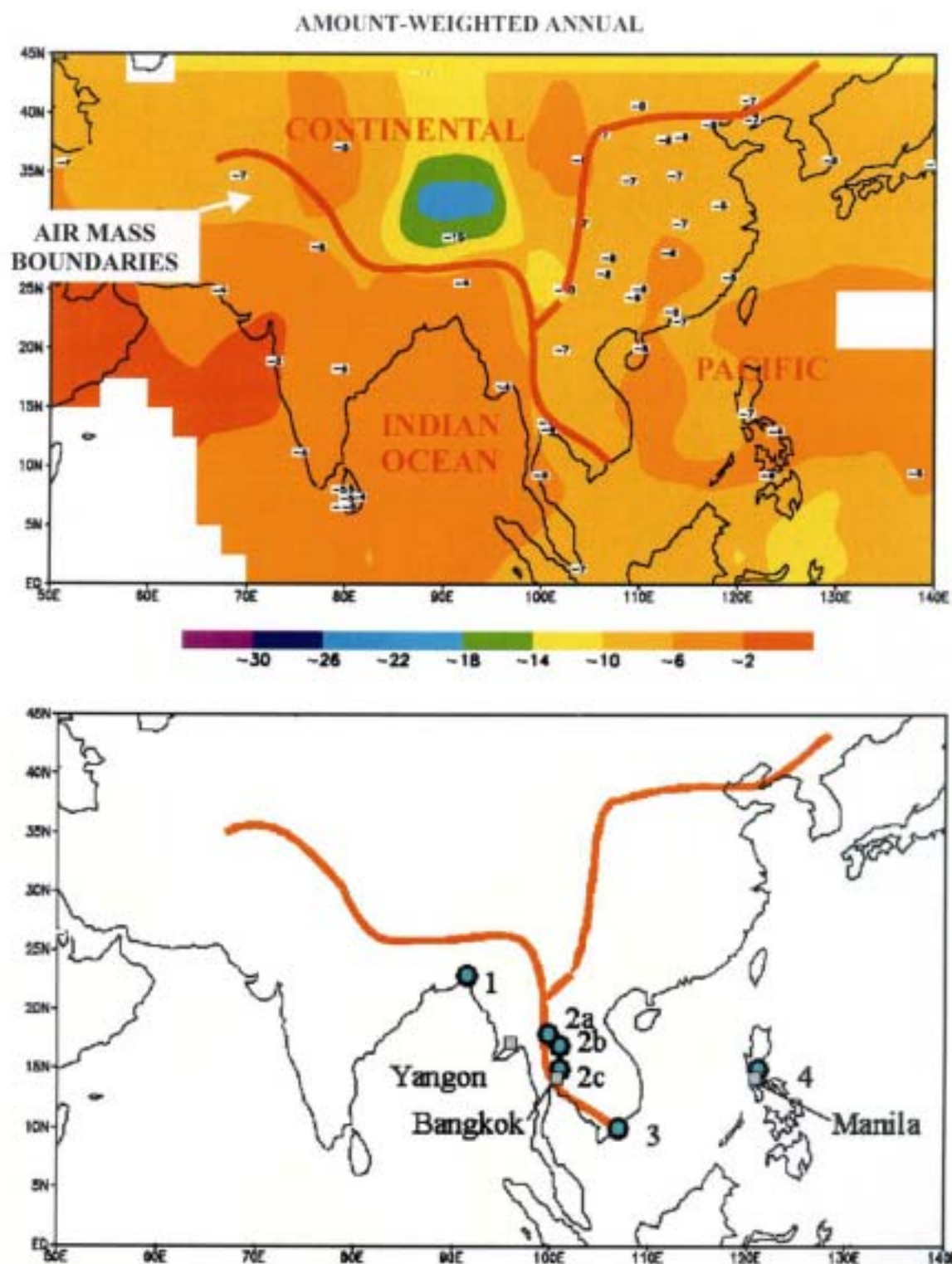


FIG. 2. (a) Mean annual amount-weighted $\delta^{18}O$ (‰) for the Asian Monsoon region. The long-term boundaries of the Asian continental, Pacific, and Indian circulation zones, are defined by the position of wind streamlines in the NCEP/NCAR (National Centers for Environmental Prediction/National Center for Atmospheric Research) global reanalysis climatology dataset. The Pacific Ocean regime is shown to exhibit more depleted $\delta^{18}O$ in precipitation. In both regimes, isotopic composition generally decreases along the monsoon track (i.e. toward the continent) as a function of the degree of rainout from the air masses, as noted previously [4]. (b) Map showing study sites described in TABLE I.

Table I. Study site characteristics

<p>1. Bangladesh aquifer type: deltaic, floodplain, unconfined to semi-confined transmissivity: 820 to 3200 m²/day sampling: ¹⁸O, ²H, ³H, ¹³C and ¹⁴C (1979, 1999) depth range: 0-340 m characteristics: TDS up to 1800 mg/L ¹⁴C TDIC ages modern to 23,000 years reference: [14]</p>	<p>Altitude Range: ~2-30m.a.s.l. Precipitation: 2500 mm MAT: 25°C δ¹⁸O: -4.8 ‰</p>
<p>2a. Chaing May Basin, N. Thailand aquifer type: alluvial intermontane, confined transmissivity: 40-3500 m²/day sampling: ¹⁸O, ²H, ³H, and ¹⁴C (1991) depth range: 18-180 m characteristics: TDS up to 790 mg/L ¹⁴C TDIC ages modern to 30,000 years reference: [10]</p>	<p>Mean Altitude: ~300 m.a.s.l. Precipitation: 1253 mm MAT: 28°C δ¹⁸O: ~-6.6 ‰</p>
<p>2b. Khon Kaen Area, N.E. Thailand aquifer type: intermontane, confined transmissivity: 0.45-1050 m²/day sampling: ¹⁸O, ²H, ³H, and ¹⁴C (1996-97) depth range: 20-250 m characteristics: TDS up to 15000 mg/L uncorrected ¹⁴C TDIC ages modern to 20,00 years reference: [11]</p>	<p>Altitude Range: ~150-300 m.a.s.l. Precipitation: ~1112 mm MAT: 28°C δ¹⁸O ~-6.6 ‰</p>
<p>2c. Lower Chao Phraya Basin, S. Thailand aquifer type: multi-layered alluvial deposits, confined transmissivity: 0-2400 m²/day sampling: ¹⁸O, ²H, ³H, ¹³C, and ¹⁴C (1987-90) depth range: 57-254 m characteristics: TDS up to 15000 mg/L ¹⁴C TDIC ages modern to 38,000 years reference: [12,13]</p>	<p>Altitude Range: ~0-150m Precipitation: 1452 mm MAT: 28°C δ¹⁸O: -6.6 ‰</p>
<p>3. Mekong Delta, Vietnam aquifer type: graben fill, unconfined to confined transmissivity: N/A, velocity 2.5 to 5.7 m/a sampling: ¹⁸O, ²H, ³H, ¹³C and ¹⁴C (1982-1986) depth range: 0-470 m characteristics: TDS up to 1800 mg/L ¹⁴C TDIC ages modern to 40,000 years reference: [9]</p>	<p>Altitude Range: ~2-100 m.a.s.l Precipitation: ~2000 mm MAT: 27°C δ¹⁸O =-6.4 ‰</p>
<p>4. Manila, Philippines aquifer type: complex, semi-confined transmissivity: 250 to 1000 m²/day sampling: ¹⁸O, ²H, ³H, ¹³C and ¹⁴C (1986-1988) depth range: 0-305 m characteristics: TDS mostly <250 mg/L ¹⁴C TDIC ages modern to 35,000 years reference: [8]</p>	<p>Altitude Range: 2 to 300 m.a.s.l Precipitation: 1957 mm MAT: 27°C δ¹⁸O =-6.7 ‰</p>

Recent atmospheric general circulation model (AGCM) reconstructions suggest that similar patterns persisted at in the Asian monsoon region at the LGM with reduced temperatures in the range of 2-4°C below present, and decreased continental recycling. Positive isotope anomalies in precipitation at this time are attributed to weaker rainout/recycling associated with a weaker summer monsoon [see 6,7].

3. STUDY SITES

In this paper, groundwater archives of $\delta^{18}\text{O}$ and $\delta^2\text{H}$ from Philippines [8], Vietnam [9], Thailand [10-13] and Bangladesh [14] are used as a proxy record of paleo-precipitation dating back to between 20,000 and 38,000 years at selected sites in the region (Fig. 2b). Comparison of the isotope signal of climate changes at sites located in the Asian monsoon region. One site (No.1, Fig.2b) is situated in the Indian Monsoon region, whereas the others are situated in the South-East Asian monsoon region. An overview of basic characteristics of each site and investigations are provided in TABLE I. These studies were primarily sponsored by the International Atomic Energy Agency to address the hydrodynamics, sustainability, and contamination of regional groundwater supplies in Philippines, Vietnam, Thailand, and Bangladesh.

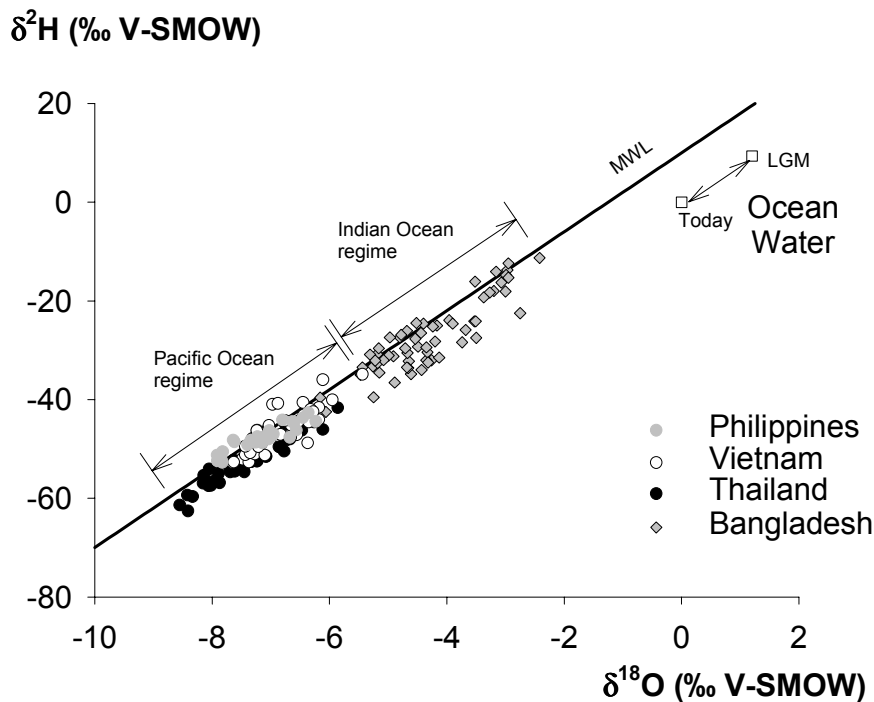


FIG. 3. Deuterium versus oxygen-18 plot for groundwaters at various sites in southeast Asia dating back to 35 ka. Also shown is ocean water isotopic compositions assumed to maintain a d-excess of 10 at the time of the LGM. Overall, water samples plot on or close to the MWL (meteoric water line) and shifts occur primarily parallel to the MWL suggesting predominance of input (precipitation) rather than evaporative signals. Distinct ranges are observed for Pacific and Indian Ocean regimes.

Although the groundwaters were analyzed for ^{14}C , $\delta^{13}\text{C}$, ^3H , ^2H , and ^{18}O , no previous analysis of climate signals preserved in the records has been undertaken. To obtain better control on the groundwater ages, ^{14}C corrections were applied to the reported data (a few exceptions are noted in TABLE I) to account for carbonate dissolution and for methanogenesis [15], the latter process being noted in the Bangladesh aquifer. Overall, corrections resulted in minor shifts to slightly younger apparent ages in all locations. Data were also screened to eliminate

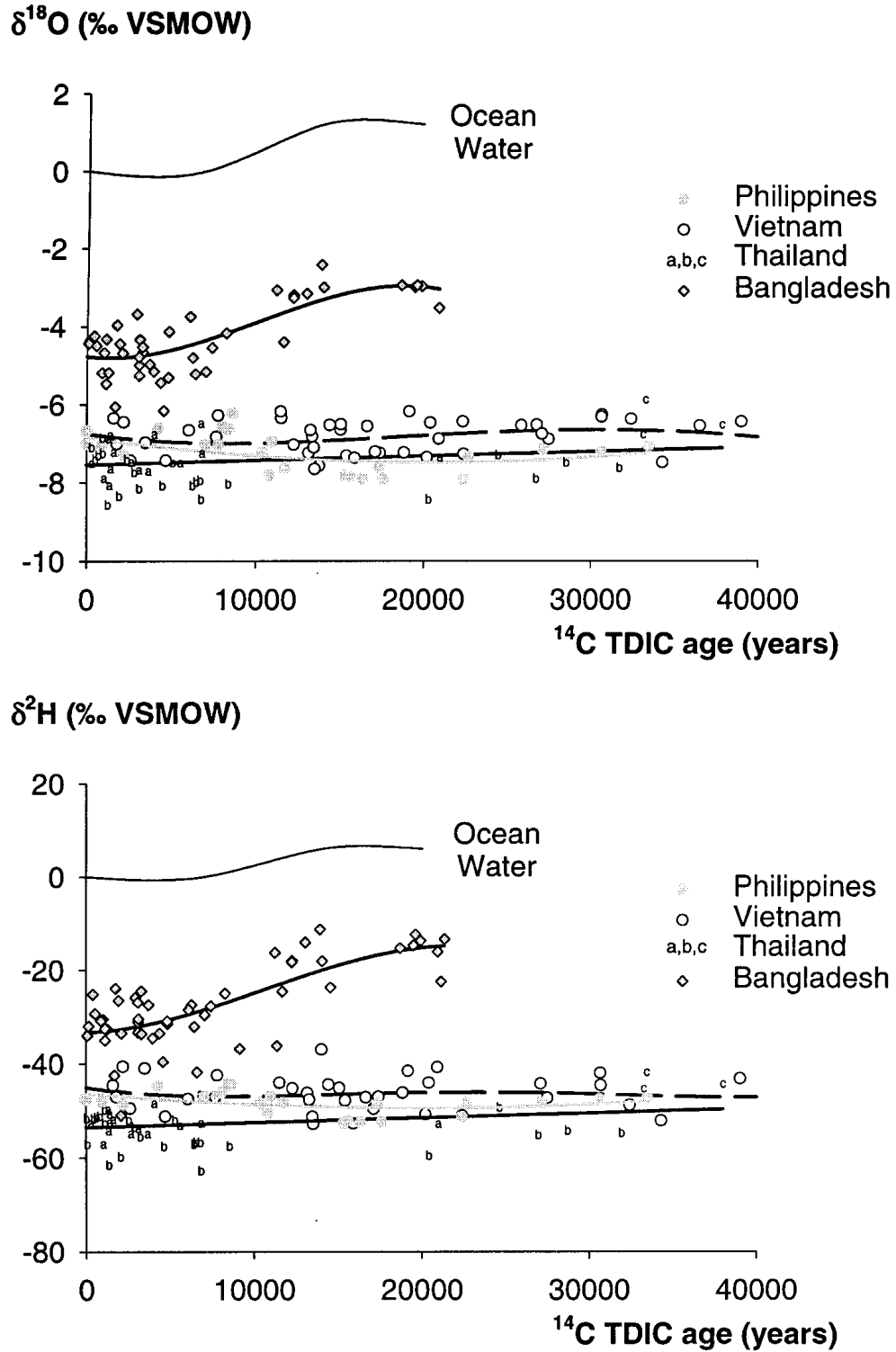


FIG. 4. (a) Plot of $\delta^{18}\text{O}$ versus corrected ^{14}C TDIC age years (‰ V-SMOW); (b) $\delta^2\text{H}$ versus corrected ^{14}C TDIC age years (‰ V-SMOW), illustrating temporal trends in precipitation as inferred from groundwater archives at various sites as indicated. Note that generalized trends in $\delta^{18}\text{O}$ of ocean water for LGM to present are based on planktonic foram. and interstitial water records [16]. Similar trends in deuterium for ocean water assume $\delta^2\text{H}=8\delta^{18}\text{O}$.

waters which were suspected of containing non-precipitation sources such as seawater intrusion and river infiltration. In a $\delta^2\text{H}$ versus $\delta^{18}\text{O}$ diagram (FIG. 3), groundwaters from the study sites, ranging in age from 38 000 years to the present, plot on or close to the MWL (meteoric water line) and shifts occur primarily parallel to the MWL suggesting that modification of the precipitation signal by evaporation effects are negligibly small. Also shown are LGM-modern shifts in the isotopic composition of ocean water which are assumed to maintain a d-excess of close to 0 ‰ at the LGM. Distinct ranges are observed for Pacific and Indian Ocean regimes, which is similar to conditions observed today.

4. RESULTS

A plot of $\delta^{18}\text{O}$ versus corrected ^{14}C TDIC age (FIG. 4a) shows a comparison between paleo-precipitation records obtained in Bangladesh, a site dominated by the Indian monsoon, and sites dominated by the Pacific monsoon (Manila, Vietnam, Thailand). Similar trends are observed for $\delta^2\text{H}$ (FIG. 4b). Regression lines are also shown to depict long-term shifts. Short-term variability (or local scatter) in each record is comparable, limited to about 1‰ in $\delta^{18}\text{O}$ and 8‰ in $\delta^2\text{H}$. A summary of $\delta^{18}\text{O}$ in precipitation, ocean water and calculated ocean-precipitation isotopic separations ($\Delta^{18}\text{O}$) are given in TABLE II. Similar calculations can be produced for $\delta^2\text{H}$, although independent information on its concentration in the oceans at the time of the LGM is scarce, and conversion of $\delta^{18}\text{O}$ records requires assumptions regarding the shift of the d-excess in ocean water. For this reason only $\delta^{18}\text{O}$ is used for assessing LGM-today shifts. Note that only uncorrected ^{14}C TDIC ages are available for the NE Thailand site (see Thailand symbol “b”; FIG. 4).

Table II. Summary of precipitation and seawater $\delta^{18}\text{O}$ and $\Delta^{18}\text{O}$ characteristics today and inferred at LGM

Characteristics	<u>Indian Ocean</u>	<u>Pacific Ocean Regime</u>		
	<u>Regime</u> Bangladesh	Philippines	Vietnam	Thailand
Today Precip.	-4.8 ^(a)	-6.7 ^(b)	-6.4 ^(c)	-6.6 ^(d)
Today Ocean	0.0 ^(e)	0.0 ^(e)	0.0 ^(e)	0.0 ^(e)
$\Delta \text{Today} = \delta^{18}\text{O}_{\text{OCEAN}} - \delta^{18}\text{O}_{\text{PRECIP}}$	+4.8 ‰	+6.7 ‰	+6.4 ‰	+6.6 ‰
LGM Precip.	-3.0 ^(f)	-7.7 ^(f)	-6.5 ^(f)	-7.6 ^(f)
LGM Ocean	+1.2 ^(g)	+1.2 ^(g)	+1.2 ^(g)	+1.2 ^(g)
$\Delta \text{LGM} = \delta^{18}\text{O}_{\text{OCEAN}} - \delta^{18}\text{O}_{\text{PRECIP}}$	+4.2 ‰	+8.9 ‰	+7.7 ‰	+8.8 ‰
$\Delta \text{Today} - \Delta \text{LGM}$	+0.6 ‰	-2.2 ‰	-1.3 ‰	-2.2 ‰
(or net shift from LGM to present)				

a- value based on Yangon precipitation and shallow groundwaters in Bangladesh, Fig. 4a

b- value inferred from shallow groundwaters in Mekong delta, Fig. 4a

c- GNIP data, Manila, Philippines

d- GNIP data, Bangkok, Thailand

e- V-SMOW

f- inferred from respective paleogroundwater archives, Fig. 4a.

g- [16]

Relatively little change in $\delta^{18}\text{O}$ and $\delta^2\text{H}$ in precipitation is inferred since the LGM based on the groundwater archives for Vietnam and Thailand, sites dominated by Pacific-maritime air masses. Nevertheless, note that few groundwaters in the 10000 to 20000 year age range are available in Thailand. Lack of long-term changes in $\delta^{18}\text{O}$ and $\delta^2\text{H}$ imply an alteration in the rainout signal as isotopic composition of the ocean is known to have been enriched in $\delta^{18}\text{O}$ and $\delta^2\text{H}$ at the LGM due to ice volume effects [16]. This suggests that the isotopic separation between the ocean water and precipitation must have been greater by about $1.2 \pm 0.5\%$ in $\delta^{18}\text{O}$ at the LGM for both sites. For Philippines, situated well within the Pacific-maritime regime, small gradual shifts in $\delta^{18}\text{O}$ and $\delta^2\text{H}$ are noted from 20 ka to present, with a net 1‰ shift in $\delta^{18}\text{O}$ to more enriched values for precipitation from LGM to the present. In contrast, the isotopic composition of precipitation in Bangladesh was appreciably enriched in $\delta^{18}\text{O}$ at the time of the LGM relative to today. This shift roughly parallels the changes that occurred in ocean water. A summary of $\delta^{18}\text{O}$ values and ocean-precipitation isotope separations for the various stations, referred to as $\Delta^{18}\text{O}$, are provided for the present day and for the LGM (TABLE II). Most important to the evaluation of rainout effects are changes in the $\Delta^{18}\text{O}$, which is found to be enhanced in the Indian Ocean regime (Bangladesh) and reduced in the Pacific Ocean regime (Thailand, Vietnam, Philippines). The present day distinction in $\delta^{18}\text{O}$ between the Indian and Pacific air masses was maintained at the LGM, and differences in $\Delta^{18}\text{O}$ appear to have been enhanced (FIG. 5). Discussion of these trends and probable causes are presented below.

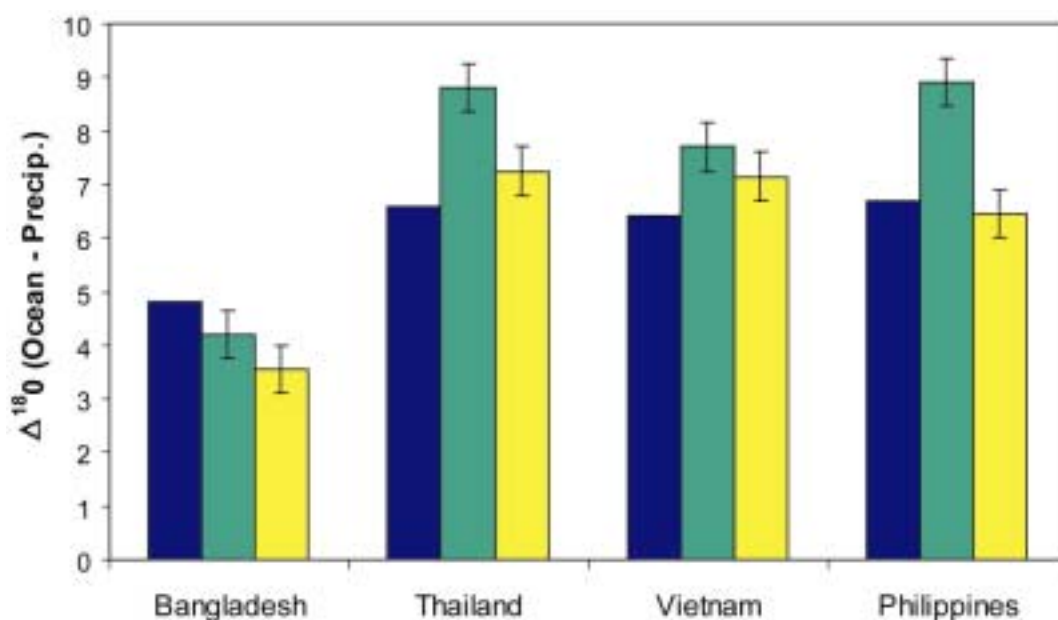


FIG. 5. Bar graph showing oxygen-18 isotopic separation between ocean water and precipitation ($\Delta^{18}\text{O}$) for today (solid bars), inferred from groundwater archives at the time of the LGM (dark grey bars), and (iii) based on LGM-control anomalies in an ECHAM4 simulation (light grey bars) [7]. Error bars denote uncertainty associated with the isotopic composition of the ocean at the LGM. Note that isotopic separation for Bangladesh, which is in the Indian Ocean monsoon regime is distinct from sites in the Pacific Ocean regime. (See this effect also in FIG. 3).

5. DISCUSSION

Changes in the isotopic composition of precipitation reflects climatic processes, including: (i) isotopic composition of the ocean, and factors noted in [17] including (ii) meteorological conditions in the source area (i.e. humidity, wind regime, sea surface temperature (SST) and their impact on kinetic isotope fractionation during evaporation from the oceans), (iii) rainout mechanisms (i.e. fraction of precipitable water and continental recycling), (iv) air mass mixing and interaction, and (iv) second-order kinetic effects, such as those that occur during snow formation and during evaporation from raindrops.

Of the first order factors, the impact of shifting isotopic composition of ocean water is reasonably quantified from the marine isotope record [16] and this factor is explicitly accounted for in the present analysis by considering the ocean-precipitation separation rather than the isotopic composition of the precipitation alone. Humidity and wind regime are considered to be unlikely sources of pervasive long-term changes due to similar vapour characteristics observed over the oceans from 40°N to 40°S for the present day, reflecting low variability of kinetic isotope effects during evaporation of seawater. Observed isotope shifts may have been influenced by changes in the SST, but are not likely a product of changes in SST alone as $\delta^{18}\text{O-T}$ and $\delta^2\text{H-T}$ gradients are also generally subdued in tropical (monsoon) regions [5,6]. Temperature-related changes may have indirectly played a larger role in the Pacific monsoon regime due to interaction with polar/continental air masses with larger isotope-temperature signals, particularly in areas above 35°N which exhibit pronounced $\delta^{18}\text{O-T}$ relationships [5]. Continental moisture recycling (re-evaporation of precipitated water) is an important process in the region [4] and is likewise expected to affect the isotope composition of precipitation. In general, subdued inland isotope gradients are observed along precipitation trajectories where recycling is significant, as in the case of the Amazon Basin [18]. In the present setting, reduced recycling at the LGM (expected under lower ambient temperatures) may have contributed to an increase in the isotopic separation between the ocean and inland precipitation. Enhancement of the continental effect during the LGM may also have contributed to an increase in this isotopic separation. In [5], the modern $\delta^{18}\text{O}$ continental effect during the rainy (monsoon) season is characterized by gradients of about 0.25 ‰ per 100 km from Hong Kong to Guiyan. During the LGM, emergence of the continental shelf in the Gulf of Thailand and South China Sea during the low sea level stand is likely to have increased the distance from the coast by several hundred kilometers [19], thereby causing additional depletion of $\delta^{18}\text{O}$ values in precipitation on the order of 1 ‰.

Of the second order factors, evaporation from raindrops is a process which may be widespread in monsoon climates, although it is more common in the dry season when rainfall accounts for only a negligible contribution to the overall annual precipitation and recharge. For this reason, it is not expected to account for the observed signals. The role of snow formation as a secondary modifier is unknown but is assumed in the present analysis to play a negligible role in defining long-term shifts in the isotope content of precipitation.

On the whole, rainout processes, polar/Pacific air mass mixing, moisture recycling and enhanced continental effects are the most likely causes of the shifts in the isotopic composition of precipitation for the LGM-present. Lower SSTs at the LGM are expected to have produced a weaker monsoon, characterized by reduced precipitation amounts in the wet season and reduced evaporation and recycling. Reduced monsoon strength would have produced precipitation enriched in heavy isotopes compared to that of today, as observed for precipitation archives in Bangladesh. More negative $\delta^{18}\text{O}$ values observed for the Pacific

regime during the LGM may in part reflect enhancement of air mass contributions from high latitude sources due to weaker Hadley circulation, and decreased moisture recycling (due to decreased evaporation) and/or enhanced continental effect on the Eurasian continent at that time. In contrast, the south Asian region would have been more effectively isolated from such interaction by the Tibetan moisture barrier and a smaller continental effect. Overall, the contrasting behaviour of the two precipitation regimes manifested in the observed decoupling of the isotope signals of these two monsoon regimes during the LGM can be attributed to differences in large-scale circulation patterns arising mainly from the presence of Tibet as a barrier for moisture transport to the Indian subcontinent.

6. ECHAM4 MODEL COMPARISONS

The scenario of climatic conditions inferred from groundwater isotope data is broadly consistent with an AGCM simulation of LGM climate and isotopic composition in the southeast Asian monsoon region [7]. Comparison of predicted values of $\Delta^{18}\text{O}$ based on the groundwater archives and an AGCM run (FIG. 5) reveal consistent trends at all sites except for the Philippines. Similarly, the model tends to predict heavier isotope values (and perhaps a weaker Indian monsoon) than is inferred from the Bangladesh groundwater archives. In general, the structure of the isotope distributions predicted by the model appears similar to that of the groundwater archives, although the impact of the rainout effect on the isotope signatures is apparently muted in the model representation.

7. CONCLUDING REMARKS

Due to the 2 to 3‰ difference in $\delta^{18}\text{O}$ of annual precipitation in Pacific-dominated *versus* Indian-dominated regimes, it is expected that any substantial, long-term shifts in this circulation boundary should be recorded in the isotopic composition of groundwater at these sites. Given that drastic shifts in isotopic composition of groundwater in Vietnam and Thailand are not observed, it appears that this boundary has remained relatively stable over the period of record. Although short-term shifts in the $\delta^{18}\text{O}$ of groundwater may be masked by aquifer mixing and dispersion, short-duration fluctuations in the boundary could possibly account for some of the observed noise or scatter in the records. However, there is no clear indication of long-term shifts or oscillations in the boundary between Pacific and Indian dominated systems from the observed groundwater records.

The analysis of groundwater isotope data to infer the LGM climatic conditions has been strongly aided by the availability of the GNIP database, in addition to physical data and climate model output that provides the basis for interpreting isotope data. Without an integrated climate-isotope analysis, the isotope data have only limited utility.

ACKNOWLEDGEMENTS

Special thanks to Jean Birks for providing the custom maps showing isotope distribution in precipitation in the monsoon region. Similar maps for Asia and other regions are available from IAEA/University of Waterloo “GNIP Maps and Animations” [20].

REFERENCES

- [1] LAU, K.-M., KIM, K.-M., YANG, S. Dynamical and boundary layer forcing characteristics of regional components of the Asian summer monsoon. *Journal of Climate* **13(14)** (2000) 2461-2482.
- [2] PLUMMER, L. N. Stable Isotope Enrichment in Paleowaters of the Southeast Atlantic Coastal Plain, United States. *Science* **262** (1993) 2016-2020
- [3] STUTE, M., TALMA, A.S., Glacial temperatures and moisture transport regimes reconstructed from noble gases and $\delta^{18}\text{O}$, Stampriet Aquifer, Namibia. In: *Isotope Techniques in the Study of Environmental Change*, IAEA, Vienna, IAEA-SM-349/53 (1997) 307-317 .
- [4] NUMAGUTI, A., Origin and recycling of precipitating water over the Eurasian continent: experiments using an atmospheric general circulation model. *J. Geophys. Res.* **104 (D2)** (1999) 1957-1972.
- [5] ARAGUÁS-ARAGUÁS, L., FROEHLICH, K., ROZANSKI, K. Stable isotope composition of precipitation over southeast Asia. *J. Geophys. Res.* **103(D22)** (1998) 28721-28742.
- [6] HOFFMANN, G., HEIMANN, M., Water isotope modeling in the Asian monsoon region. *Quaternary International* **37** (1997) 115-128 .
- [7] HOFFMANN, G. et al., in press. 2001
- [8] IAEA. Origin and dynamics of saltwater and groundwater in Manila, Bulacan, Pampanga, and Cebu. IAEA TC Project Report PHI/8/011 (1990).
- [9] LOUVAT, D., DUNG, H.H. Environmental isotope study of Mekong Delta groundwater (Vietnam), IAEA TC Report, VIE/8/003 (1989) 37pp.
- [10] BUAPENG, S., SANGKHABUN, S.-N., LO-PENSRI, O., Environmental isotope study of groundwater in Chiang Mai Basin, northern Thailand, Final Report. IAEA Research Contract No. 6233/R1/RB, Department of Mineral Resources, Bangkok (1993) 47pp.
- [11] BUAPHAN, C., YANGME, W., WANNAKAO, L., SRIBOONLUE, V., TASSANASORN, A., BUAPENG, S. Groundwater origin investigation with isotopic compositions for evaluation of high productive deep aquifers in Khon Kaen area, northeast Thailand. *Isotope Techniques in Water Resources Development and Management*. 10-14 May 1999, IAEA, Vienna (1999).
- [12] YURTSEVER, Y., BUAPENG, S. Compartmental modeling approach for simulation of spatial isotopic variations in the study of groundwater dynamics: A case study of a multi-aquifer system in the Bangkok Basin, Thailand. *Isotope Techniques in Water Resources Development 1991, Proceedings*. IAEA –SM-319/29 (1992) 291-308.
- [13] SANDFORD, W.E., BUAPENG, S. A comparison of groundwater ages based on ^{14}C data and three dimensional advective transport modeling of the lower Chao Phraya Basin: paleohydrology and implications for water resources development in Thailand. *Isotopes in Water Resources Management, Proceedings IAEA-SM-336/37* (1996) 383-394.
- [14] AGGARWAL, P. BASU, A.R., POREDA, R.J., KULKARNI, K.M., FROEHLICH, K., TARAFDAR, S.A., ALI, M., AHMED, N., HUSSAIN, A., RAHMAN, M., AHMED, S.R., Isotope hydrology of groundwater in Bangladesh: Implications for characterization and mitigation of arsenic in groundwater. IAEA TC Project Report (BGD/8/016) (2000) 61pp.
- [15] CLARK, I, FRITZ, P., Age Dating Old Groundwaters, Chapter 8 in *Environmental Isotopes in Hydrogeology*, Lewis Publishers Inc., (2000) 352p.
- [16] SCHRAG, D.P., HAMPT, G., MURRAY, D.W. Oxygen isotopic composition of interstitial waters from Leg 154: determination of the temperature and isotopic composition of the glacial ocean, In: Shackleton, N.J., Curry, W.B., Richeter, C., and Bralower, T.J., (Eds.) *Proceedings of the Ocean Drilling Program, Scientific Results* **154** (1997) 201-206.

- [17] ARAGUÁS-ARAGUÁS, L., FROEHLICH, K., ROZANSKI, K. Deuterium and oxygen-18 isotope composition of precipitation and atmospheric moisture, *Hydrol. Process.* **14** (2000) 1341-1355.
- [18] HENDERSON-SELLERS, A., MCGUFFIE, K., CHAMBER, S., Isotopes as validation tools for predictions of the impact of Amazon deforestation on climate and regional hydrology, IAEA-CN-80/1, this volume (2002).
- [19] PELEJERO, C., KIENAST, M., WANG, L., GRIMALT, J.O., The flooding of Sundaland during the last deglaciation: imprints in hemipelagic sediments from the South China Sea, *Earth and Planetary Science Letters* **171** (1999) 661-671.
- [20] IAEA/University of Waterloo. GNIP Maps and Animations, developed by S.J. Birks et al., International Atomic Energy Agency, Vienna and University of Waterloo, Ontario, Canada. Accessible at <http://isohis.iaea.org>. (2001).

INTER- AND INTRA-STORM VARIABILITY OF THE ISOTOPE COMPOSITION OF PRECIPITATION IN SOUTHERN ISRAEL: ARE LOCAL OR LARGE-SCALE FACTORS RESPONSIBLE?

J.R. GAT

Department of Environmental Sciences and Energy Research,
The Weizmann Institute of Science, Rehovot, Israel

and

Center for Water Science and Technology, Ben-Gurion University of the Negev, Israel

E. ADAR

Department of Environmental Hydrology and Microbiology,
Blaustein Institute of Desert Research, Ben-Gurion University of the Negev, Sde-Boker, Israel

P. ALPERT

Department of Geophysics and Planetary Sciences, Tel-Aviv University, Israel

Abstract. A detailed sequential rain sampling of rainstorms was carried out during the 1989/90 and 1990/91 rainy season in the coastal plain of Israel with an annual average of 530 mm of rain and in the western Negev where the average annual rainfall is 93 mm. On four occasions, rain was concurrently available at both stations. The variability of the isotope composition within a rainy spell is quite considerable but falls short of the range of isotopic values encountered during the total season. Different rainy episodes show distinguishable isotope compositions, which evidently are characteristic of a larger time/space niche than that of the momentary, local, rain event. This is confirmed by the good correlation between the mean isotope composition of concurrently sampled events at both stations. A “rain amount effect” is not apparent when the amount-weighted data for each complete rain episode are compared, because any possible effect is masked by the inter-storm variability. However by singling out the data within each storm sequence separately, a moderate effect is seen. On the whole, the results seem to support the notion that the isotope data are determined by the large, synoptic scale, situation. However within the range of values characteristic of the origin of the air masses there is a pronounced dependence of the isotope composition on the extent of the cloud field associated with each event, which is interpreted as a measure of the degree of rainout from the air mass, i.e. a typical Rayleigh effect. Local effects related to momentary rain intensity contribute only to a residual modulation of the above-mentioned effects.

1. INTRODUCTION

The isotope composition of precipitation (^{18}O and ^2H abundance) is herein being applied in hydrological and hydro-meteorological investigations in Israel. Monthly or annual averages, as well as shorter term temporal variations, have been measured. Moreover, it is being attempted to use long term records of the isotopic composition of precipitation (as measured directly in ice cores or paleowaters, or as inferred from measurements on proxy materials such as lake deposits, tree rings or speleothems) as indicators of climatic change.

Average monthly or annual values are generally correlated with the mean local temperatures [1]. At Bet-Dagan station (the GNIP station in Israel) such a correlation is less pronounced however than in mid-continental locations. An amount effect, i.e. lower δ values during months with large rain amounts, was found to apply to monthly data at Bet-Dagan with a rather low coefficient of correlation; an exception are the enriched values when rain amounts are less than about 10 mm/month, in which case the enrichment of the heavy isotopic species in residual raindrops exposed to evaporative water loss becomes the dominant factor [2].

The isotopic composition of individual rainy spells in Israel were shown to be related primarily to the origin and pathways of the precipitating air masses [3,4,5]. On the other hand, the in-storm changes in the isotope composition appeared to be controlled by more local parameters and especially the rain intensity [6]. This apparent paradox was addressed in the study of Rindsberger et al. [7] who concluded that the intra-storm variations in the isotopic composition were also, to a large extent, the result of the synoptic scale history of the different air masses which transverse the station during the course of a storm.

An understanding of what determines the isotopic composition of an individual precipitation event and how the “climatic” average is synthesized from the individual events is necessary in order to solve the inverse problem of relating changes of the isotope composition to changes in climatic parameters and to climate change, in general.

The present study was undertaken in order to relate the progression of the isotopic composition during a rain-shower to the synoptic pattern on the one hand, and to local parameters such as rain intensity, location within the regional cloud pattern, etc. Detailed rain sampling was thus undertaken at two stations with different rain amounts in the southern coastal plain and in the northern Negev during the 1989/90 and 1990/91 rainy seasons.

2. RAIN COLLECTION AND METHODOLOGY

Sampling was carried out during the 1989/90 and 1990/91 rainy season at Rishon-Lezion in the southern Coastal plain of Israel and at Sde-Boker and Retamim in the arid Negev.

The Rishon-Lezion site is situated just 5 kms south of the local GNIP station of Bet-Dagan (where the mean annual precipitation is 531 mm, the rainy season extending from September to April only) and is about the same distance from the seashore (about 5 kms). Samples were changed manually during the course of each shower and the accumulated water depth for each sample was recorded. A tipping-bucket recording pluviometer was available during the second sampling season.

The Sde-Boker site is situated at the Blaustein Desert Research Institute in the central Negev, with a mean annual rainfall of 93 mm. Retamim in the western Negev is closer to the seashore. A mechanical sequential rain sampler was used [8] whereby rain samples corresponding to 1.62 cm of rainfall are obtained.

Mass-spectrometric analysis for stable isotopes of oxygen and hydrogen was carried out at the Rehovot Isotope Laboratory at the Weizmann Institute of Science and at the Niedersächsische Landesanstalt fuer Forschung in Hannover, Germany. The average reproducibility is ± 0.1 ‰ for $\delta^{18}\text{O}$ and ± 1 ‰ for $\delta^2\text{H}$.

Printout of cloud-radar echoes at 30-minute intervals during the rainspells were provided by courtesy of Shoham (EMS-Mekorot) Co. from their weather radar situated at Ben-Gurion airport, close to the Bet-Dagan and Rishon-Lezion stations. In these printouts, the area in the vicinity of the radar site is blanketed out in view of spurious topographical reflections. These radar echoes are calibrated in terms of rain intensities in units of mm/hr.

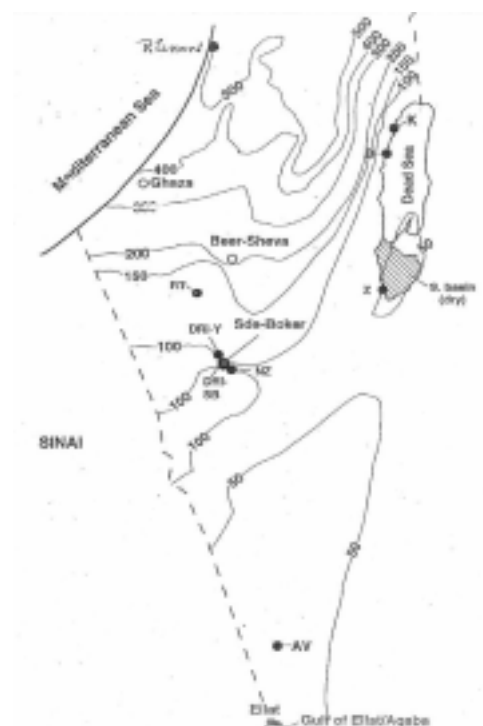


FIG. 1. Rain map of southern Israel, showing isohyets of the mean annual rainfall in mm. Location of sampling sites are indicated.

3. RESULTS

3.1 Results from the Rishon-Lezion station

The 1989/90 season was a good rain-year with slightly above average rain amounts. In particular, anomalously high rain amounts were recorded in November. The average isotope composition at Bet-Dagan stations was $\delta^{18}\text{O} = -5.7\text{‰}$ (-5.80‰ for the mid-winter months of December to February only). These values are slightly depleted compared to the long-term average of -4.70‰ and -5.15‰ , respectively, for the total annual rainfall and the mid-winter months.

Ten rain spells were sampled during January-March 1990, accounting for 50% of the total rain during that period. During the 1990/91 seasons four rain events were sampled in February and March 1991. The two last ones were very heavy storms, with precipitation amounts of 35-40 mm during a 24-hour period. This sampling was accompanied by pluviometric measurements. The data are shown in Table I.

The range of the isotope composition within a rainy spell was quite considerable, amounting to differences of up to 6‰ in $\delta^{18}\text{O}$ in one extreme case. The total range of the measured isotope compositions throughout the season was only about twice that number. However it is apparent that the different rainy episodes have an individuality of isotope compositions which can be distinguished. The comparison between individual rain data and the averaged value for the whole storm, shown in Fig. 2, suggests that the individual characteristic isotopic compositions apply to a larger time-space niche than the momentary rain event, even when the latter constitutes only a small fraction of the total rainfall.

Table I. Rishon Lezion station

Date & Time	Precipitation (mm)	Delta ¹⁸ O	Description of event
15-01-90: 0000-0700	4.90	1.00	shower
15-01-90: 0700-0815	0.60	-1.51	scattered showers
15-01-90: 1500-1700	1.60	-1.81	scattered showers
16-01-90: 0000-0600	4.60	-3.64	strong shower
16-01-90: 0830-1230	4.80	-4.81	
16-01-90: 1230-1630	2.40	-2.44	one strong shower
17-01-90: 2100-0630	5.30	-3.97	
17-01-90: 0800-1230	3.40	-2.86	isolated shower
(15-17)-01-90	Sum 27.6	w. av. -2.73	
21-01-90: 0730-0830	4.80	-3.90	Continuous showers
21-01-90: 0830-1235	0.80	0.25	
22-01-90: 0000-0600	3.00	-2.63	
(21-22)-01-90	Sum 8.6	w. av. -3.34	
26-01-90: 1500-1715	4.10	-10.18	continuous rains
26-01-90: 1715-1930	5.50	-11.39	
26-01-90: 1930-2230	2.80	-8.94	
1990-01-26	Sum 12.4	w. av. -10.45	
01-02-90: 0000-0645	7.60	-5.56	Thunder storm
01-02-90: 0655-1300	1.10	-3.75	
01-02-90: 1300-1545	6.00	-5.30	Thunder storm
1990-02-01	Sum 14.7	w. av. -5.31	
06-02-90: 1800-1915	6.90	-6.56	Day long showers thunder storms.
06-02-90: 1915-2130	8.00	-6.05	
1990-02-06	Sum 14.9	w. av. -6.29	
09-02-90: 1900-2100	2.30	-6.43	
10-02-90: 0600-0700	1.60	-6.35	
10-02-90: 0700-0900	2.80	-8.12	Strong showers
10-02-90: 1100-2100	9.70	-4.95	Scattered rain
10/11-02-90: 2100-0300	3.70	-4.32	Continuing rain
11-02-90: 0300-0700	2.40	-4.80	
(9-11)-02-90	Sum 22.5	w. av. -5.47	
14-02-90: 1500-1620	3.00	-4.94	Thunders
14-02-90: 1620-1845	4.00	-6.17	Thunders + hail
14/15-02-90: -0700	2.30	-1.96	

Table I. Rishon Lezion station

Date & Time	Precipitation (mm)	Delta ¹⁸ O	Description of event
(14-15)-02-90	Sum 9.3	w. av. -4.75	
24-02-90: 1800-1915	1.85	-4.48	
24-02-90: 1915-2200	1.60	-3.08	
1990-02-24	Sum 3.45	w. av. -3.85	
01-03-90: 0000-0815	5.70	-5.13	
01-03-90: 0815-1000	2.50	-3.78	
01-03-90: 1000-1700	7.70	-4.37	
1990-03-01	Sum 15.9	w. av. -4.32	
11-03-90: -0750	0.50	-4.18	
12-03-90: 0000-0600	6.70	-4.19	
12/13-03-90: 1800-0630	20.20	-3.86	
13-03-90: 0630-1800	2.05	-2.65	
(11-13)-03-90	Sum 29.45	w. av. -3.86	

07-02-91: 0400-0530	2.95	-4.30	Thunder storm
07-02-91: 0530-0700	0.95	-2.62	
07-02-91: 1630-1815	1.60	-4.12	Thunder storm
7/8-02-91:1815-0515	1.20	-3.28	Intermittent
08-02-91: 0530-0730	5.80	-7.11	Thunder storm
08-02-91: 0845-0910	2.60	-5.18	Renewed shower
08-02-91: 0915-1100	1.75	-4.37	Cont. rain
(7-8)-02-91	Sum 16.85	w. av. -5.22	
16-02-91: 1300-1600	0.80	1.21	light rain
16-02-91: 1600-1710	1.40	0.05	Cont. light rain
16-02-91: 1730-2100	1.80	0.36	intermittent
1991-02-16	Sum 4.0	w. av. 0.56	
26-02-91: -0545	2.00	-8.47	
26-02-91: 0545-0615	2.05	-7.16	Thunder storm
26-02-91: 0615-0825	2.95	-6.03	Very intense rain
26-02-91: 0825-1320	14.50	-6.65	Very intense rain + hail
26/27-02-91:1320 -0730	7.40	-7.78	Intense rain
27-02-91: 0730-1215	7.40	-10.50	Intense rain
(26-27)-02-91	Sum 36.3	w. av. -7.74	

Table I. Rishon Lezion station

Date & Time	Precipitation (mm)	Delta ¹⁸ O	Description of event
05-03-91: 0400-0510	10.30	-5.97	Intermittent
05-03-91: 0615-1300	1.05	-6.69	One hour shower
05-03-91: 1300-1400	3.00	-10.00	Intermittent
05-03-91: 1400-1645	4.30	-12.15	Very strong
05-03-91: 1930-2030	9.30	12.51	Continuous strong
05-03-91: 2030-2100	1.25	-11.81	Continuous strong
06-03-91: 2100-0100	1.45	-10.09	
06-03-91: 0100-0430	5.15	-8.11	Intermittent
06-03-91: 0430-0600	2.85	-6.51	Thunder storm
(5-6)-03-91	Sum 39.30	w. av -8.38	

The progression of the isotopic composition within the different rainy episodes was quite varied and the regularity of the V or W shaped time curve, described both by Rindsberger et al. [7] and others, applied only to one third of all cases. It is further notable that there is no consistent trend of the 'd-excess' parameter throughout the rainstorms.

A rain amount effect, i.e. a change in the isotopic composition of a shower as a function of the water yield of the rain event, is not apparent in the data (Fig. 3). However by singling out the data from each rain sequence separately, as shown in Fig. 4, a moderate amount effect can be recognized in about half of the cases, ranging up to 2‰ ($\delta^{18}\text{O}/\text{mm}$). The picture is further cleared up to a considerable extent when the first sample of each rain event is left out, for example during the rain spells of Jan. 1-17, 1990 and March 5-6, 1991. It is further notable that the correlation of the amount effect is not improved when the momentary rain intensity, rather than the average water yield, is considered.

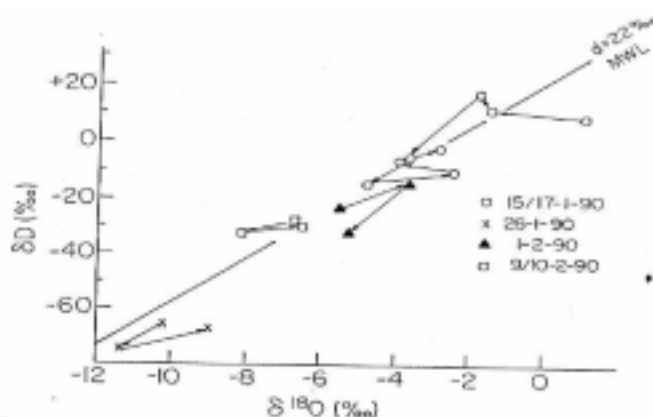


FIG. 2. Intra-storm variation of the isotopic composition of precipitation samples from Rishon-Lezion station. Arrows show the sequential order of samples within each rainy spell.

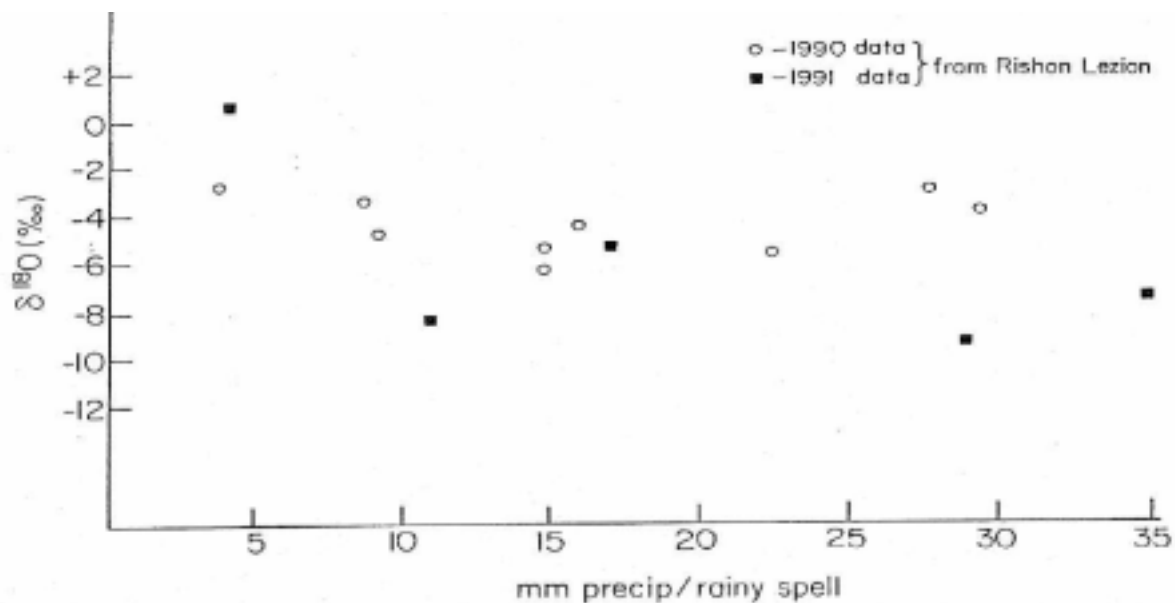


FIG. 3. The isotope composition vs. the total rain amounts in each rain event. Data from the Rishon-Lezion station.

3.2 Results from the Negev stations

The rainy season of 1989/90 started in the Negev in November and ended in April 1990, with the total rainfall amounting to 73.3 mm which is below the annual average for Sde-Boker. Out of the 14 recorded rainspells, only three had rain amounts exceeding 10 mm, the largest being 20.4 mm. Rainfall intensities were quite low, and intensities of more than 10 mm/hr were recorded only twice. Another notable characteristic was the intermittency of the rainfall where distinct short showers were separated by dry intervals.

During the rainy season of 1990/1991 rainfall started in October 1990 and ended in March 1991, with a total amount of 139.4 mm which is considerably higher than the long term average and almost twice as much as of the previous year. Of the seven recorded rainstorms two were extreme. In particular the rain event of January 24-26, 1991, with rain amounts of 51.5 mm, deserves special mention as it is the strongest rainstorm recorded since the beginning of rainfall monitoring in the area in 1951. Rain intensities were also high during the season and unlike the previous year, many of the rain showers lasted for hours. Selected values of the data have been published [9].

On four occasions during the two rainy seasons, rain was sampled concurrently both at the Rishon Lezion station and in the Negev. Figure 5 summarizes the data during these periods. With but one exception, it is to be noted that the evolution of isotope compositions is rather similar, with the Negev data lagging a few hours behind the Rishon-Lezion pattern, and with a tendency of somewhat less enriched values (by about 2‰) in the Negev. This pattern applies even though the rain amounts and intensities differ considerably. This trend is in confirmation of the good spatial correlations established by Rindsberger et al. [7] for other stations in Israel.

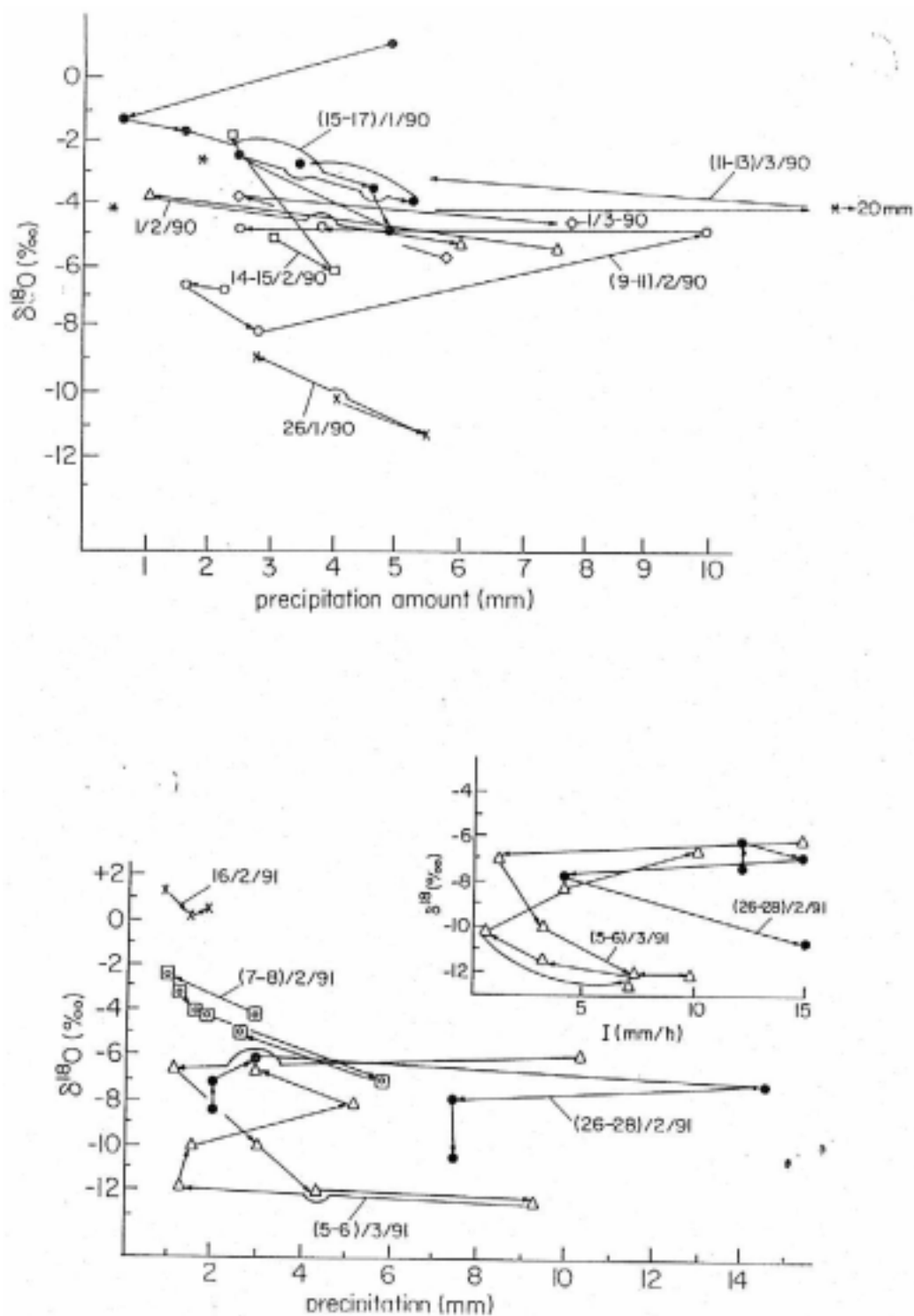


FIG. 4. The isotope composition vs. the rain yield in portions of each rainy spell, during the 1990 (top drawing) and the 1991 season (bottom drawing). In the inset, the isotope data are plotted as a function of the maximal rain intensity during each collection period.

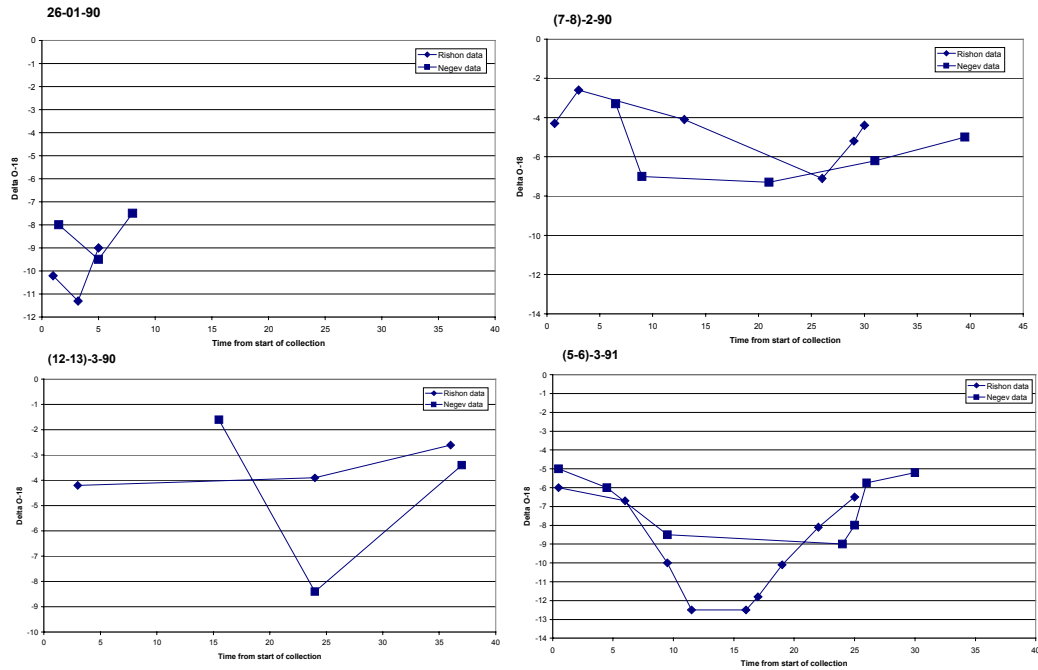


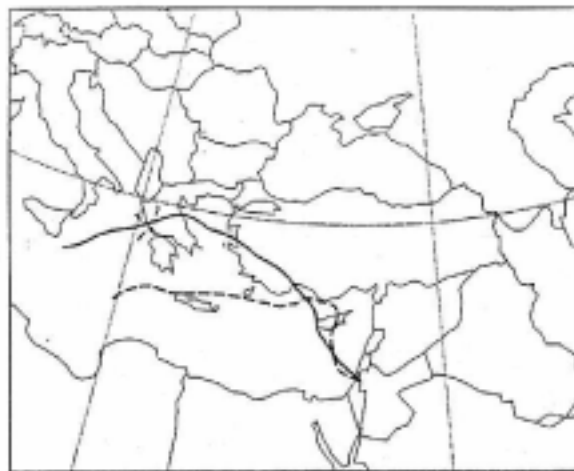
FIG.5.(a-d) Comparison of the evolution of the isotope composition during the rainy period at the Rishon-Lezion and Negev stations.

4. METEOROLOGICAL BACKGROUND

The overriding effect of the origin of the air masses on the isotopic composition of the precipitation can be exemplified by the backtracking of surface and upper air during the rain event of March 5, 1991 (Fig. 6). From the morning to the afternoon of that day, the air mass trajectory veered from a course originating in the central Mediterranean basin and moving across the northern shores of the eastern Mediterranean, to one originating in Russia and moving directly across the very eastern extremity of the sea. This change expressed itself by a depletion from about -6‰ to -12‰ in $\delta^{18}\text{O}$ (see Fig. 5).

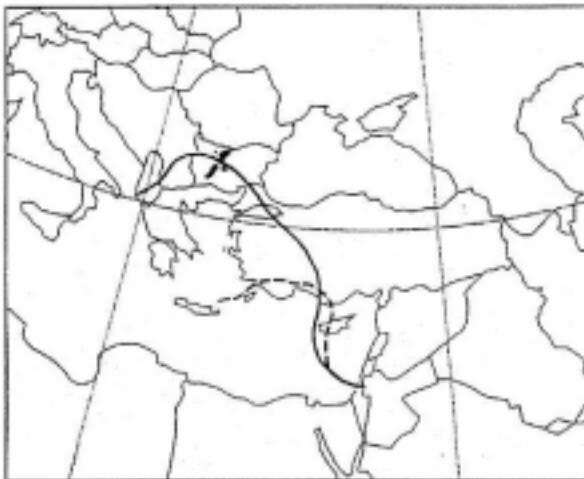
The processes at play can be further clarified in the light of the cloud radar echoes associated with these rain events. A selected suite of data are given in Figs 7(a-c). One sees very different patterns of the cloud field, ranging from well focused bands of clouds moving over the area to cases when a large part of the eastern Mediterranean lies under a precipitating cloud cover. If one attempts to quantify this aspect by specifying the percentage of the total area covered by the cloud field (parameter PCQ) and then plots this parameter against the amount-weighted stable isotope content of the precipitation (Fig. 8), one notices a distinct correlation. The extreme example is that of January 26, 1990, when a very large and widespread cloud field covered the whole of the region, characterized by rain intensities up to 5 mm/hr. However, the location of the storm center relative to the target area has also to be taken into account, as is exemplified during the period of March 11-13, 1990, when the southern station which was located along the storm path showed a much more depleted isotopic composition than the Rishon Lezion station. In contrast, on February 16, 1990, an extremely widespread but not very intense cloud field developed over the northern half of the eastern Mediterranean with the Rishon station situated on the southern and weakened fringes of the system. A detailed analysis of the results is given in the appendix to the report to the IAEA for contract No 4793/RB [10].

BACK TRAJECTORIES: 32N, 35E

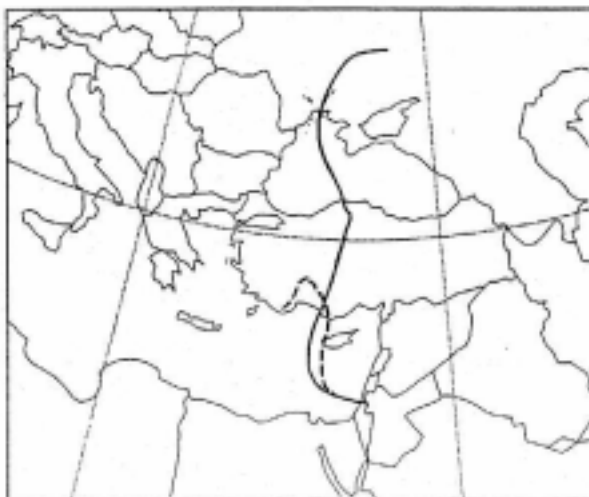


—— 900 mb
----- 1000 mb

5 March 1991 06 UTC
-120 hours



5 March 1991 12 UTC
-120 hours



5 March 1991 18 UTC
-120 hours

FIG. 6. Backtracking of the trajectory of the precipitating air masses during the rain spell of March 5, 1991.

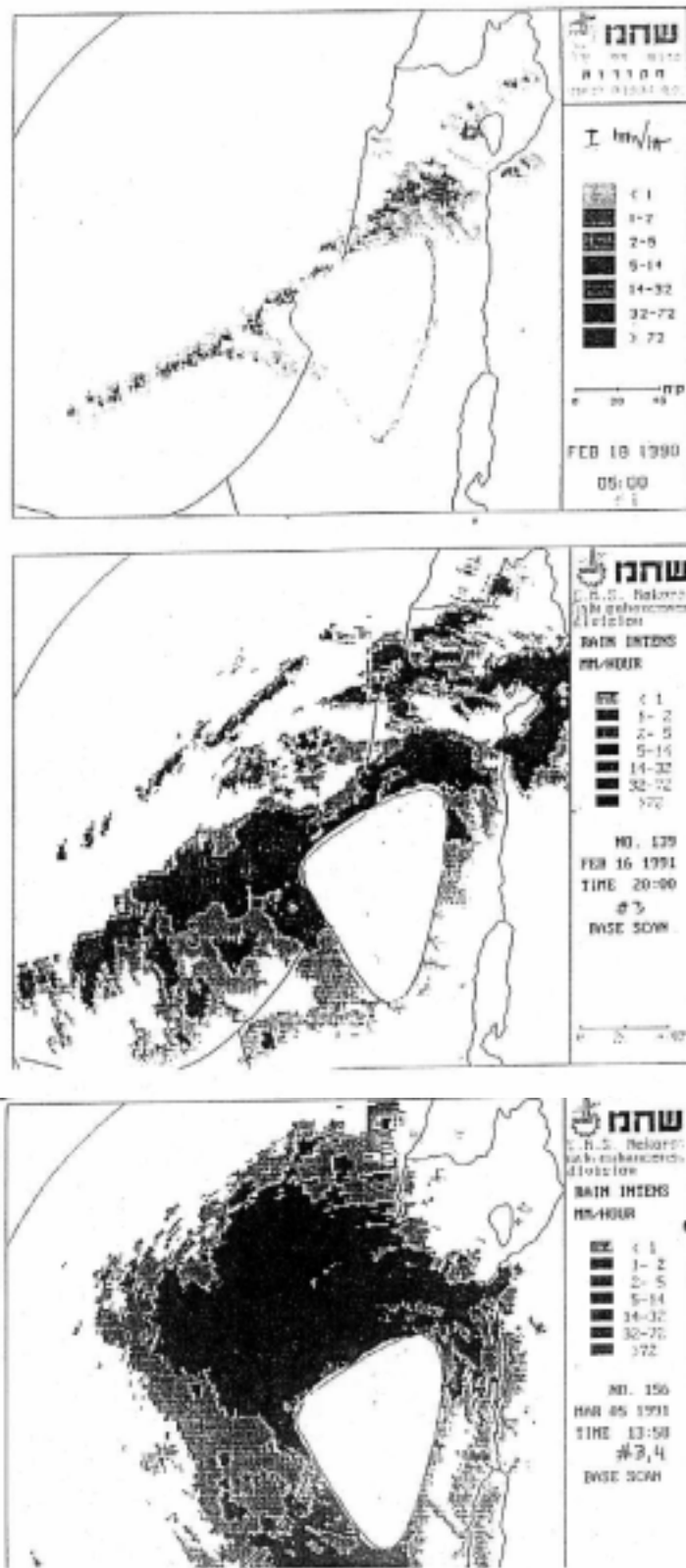


FIG. 7. (a-c) Maps of cloud-radar echoes for selected rain events (see text for discussion).

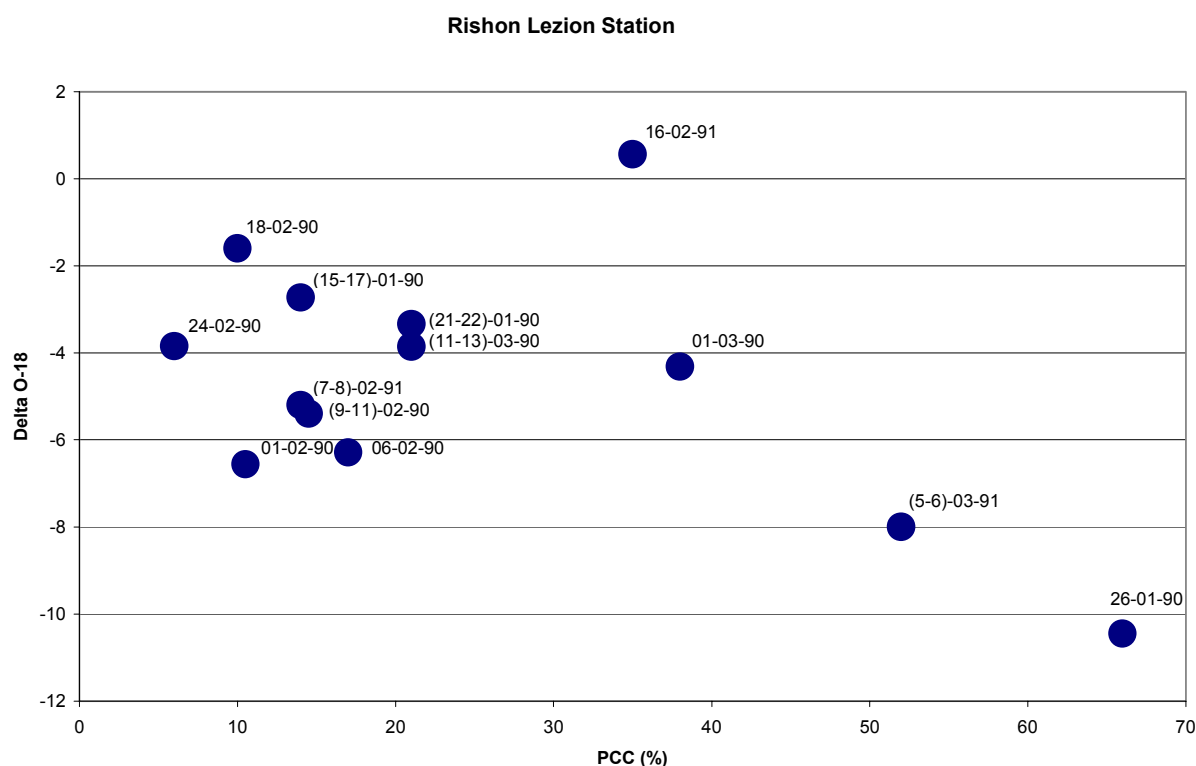


FIG. 8. The isotope composition during rain events as a function of the percent of cloud cover over the eastern Mediterranean area

These interesting correlations are interpreted in terms of a “Rayleigh” depletion of the air masses by rainout being an important factor determining the isotopic composition.

5. DISCUSSION AND CONCLUSIONS

On the whole, the results obtained seem to support the notion that the isotope data are determined foremost by the large, synoptic scale, situation. Within the range of values characterized by the origin of the air mass, there is a pronounced dependence of the isotope composition on the extent of the cloud field associated with each event, which is interpreted as a measure of the degree of rainout from the air mass prior to its arrival on the coast. This intermediate scale effect is thus a typical Rayleigh effect. Obviously a combined analysis, whereby the degree of rainout along the actual trajectory of the precipitating system is estimated, would further sharpen the correlation.

Less depleted δ -values at the beginning of some rainy spells are not, in most cases the result of an evaporation effect, since the d-excess parameter does not decrease as would be expected. Rather the effect is explained by the pristine nature of the air masses at that time. Some residual variability in the data after taking into account the synoptic scale signature are most probably related to the strong vertical mixing in the vicinity of a cold front, i.e. a more local effect. Often such samples represent also higher rain intensities and thus contribute to the residual amount effect in this data set.

ACKNOWLEDGEMENTS

The data from the Rishon-Lezion station were obtained under Research Contract 4793/RB of the IAEA; the Negev study was supported by GIF project No. 1-017/87.

REFERENCES

- [1] YURTSEVER, Y., Worldwide survey of stable isotopes in precipitation, Report, Section of Isotope Hydrology, IAEA (1975) 40pp.
- [2] GAT, JR. et al., The isotopic composition of precipitation at Bet-Dagan, Israel: the climatic record (1961-1990), Israel Meteorological Research Papers **5** (1994) 10-19.
- [3] LEGUY, C., et al., The relation between the $\delta^{18}\text{O}$ and deuterium contents of rainwater in the Negev desert and air-mass trajectories, Isotope Geoscience **1** (1983) 205-218.
- [4] RINDSBERGER, M., et al., The relation between air mass trajectories and the water isotope composition of rain in the Mediterranean Sea area, Geophys. Research Letters **10** (1983) 43-46.
- [5] GAT, J.R. and RINDSBERGER, M., The isotopic signature of precipitation originating in the Mediterranean Sea area: a possible monitor of climate modification?, Israel J. Earth Sci. **34** (1985)
- [6] LEVIN, M., et al., Precipitation, flood and groundwater of the Negev highlands, an isotopic study of desert hydrology, Arid zone hydrology investigation with isotope techniques, IAEA, Vienna (1980) 3-22.
- [7] RINDSBERGER, M., et al., Patterns of the isotopic composition of precipitation in time and space: data from the Israeli storm water collection program, Tellus **42B** (1990) 263-271.
- [8] ADAR, E., et al., A mechanical sequential rain sampler for isotopic and chemical analysis, Final report, contract no.5542/RO/RB, IAEA, Vienna (1991) 32 p.
- [9] ADAR, E.M., et al., Distribution of stable isotopes in and around storms: I. Relation between the distribution of isotopic composition in rainfall and in the consequent runoff, Hydrogeology Journal **6** (1998) 50-65.
- [10] Final report to the IAEA on research entitled "The detailed Isotope Anatomy of a Rainshower" conducted at the Isotope Dept. of the Weizmann Institute of Science, Rehovot, under contract 4793/RB (1991).

DEUTERIUM EXCESS IN PRECIPITATION AND ITS CLIMATOLOGICAL SIGNIFICANCE

K. FRÖHLICH
Vienna, Austria

J.J. GIBSON, P.K. AGGARWAL
International Atomic Energy Agency, Vienna

Abstract. The climatological significance of the deuterium excess parameter for tracing precipitation processes is discussed with reference to data collected within the IAEA/WMO Global Network for Isotopes in Precipitation (GNIP) programme. Annual and monthly variations in deuterium excess, and their primary relationships with $\delta^{18}\text{O}$, temperature, vapour pressure and relative humidity are used to demonstrate fundamental controls on deuterium excess for selected climate stations and transects. The importance of deuterium excess signals arising from ocean sources *versus* signals arising from air mass modification during transport over the continents is reviewed and relevant theoretical development is presented. While deuterium excess shows considerable promise as a quantitative index of precipitation processes, the effectiveness of current applications using GNIP is largely dependent on analytical uncertainty ($\sim 2.1\text{‰}$), which could be improved to better than 1‰ through basic upgrades in routine measurement procedures for deuterium analysis.

1. INTRODUCTION

The deuterium excess (or d-excess), defined by $d(\text{‰}) \equiv \delta^2\text{H} - 8 \cdot \delta^{18}\text{O}$ [1], where $\delta^2\text{H}$ and $\delta^{18}\text{O}$ are deuterium and oxygen-18 composition of water¹, respectively, has shown specific potential in climate studies for tracing past and present precipitation processes. D-excess is a measure of the relative proportions of ^{18}O and ^2H contained in water, and can be visually depicted as an index of deviation from the global meteoric water line (MWL; $d=10$) in $\delta^{18}\text{O}$ *versus* $\delta^2\text{H}$ space (Fig. 1). While oxygen-18 ($\delta^{18}\text{O}$) and deuterium ($\delta^2\text{H}$) at moderate and high latitude continental areas are well correlated with the surface air temperature at precipitation site, the d-excess is correlated with the physical conditions (humidity, air temperature and sea surface temperature) of the oceanic source area of the precipitation [2]. In addition, d-excess reflects the prevailing conditions during evolution and interaction or mixing of air masses *en route* to the precipitation site. Recently, the d-excess was demonstrated to be a useful, independent climatic parameter to calibrate atmospheric general circulation models [3-6] and to characterize atmospheric circulation in polar regions [7].

Despite these demonstrated advantages, the use of d-excess has some current drawbacks. Compared with the application of the individual isotopes of oxygen-18 or deuterium, d-excess variations can be complicated, and theoretical understanding of d-excess and related climatic controls has not yet been fully explored. Because changes in the d-excess depend on changes in both oxygen-18 and deuterium, the analytical uncertainty of this parameter can be relatively high in comparison with its natural variability. To date, the most definitive applications of the d-excess in climatological studies were achieved in studies of polar and high mountain glacier ice wherein analyses were performed in specialized laboratories capable of measuring d-excess with an uncertainty below one per mille [10].

¹ δ values express isotopic ratios as deviations in per mil (‰) from the Vienna-SMOW (Standard Mean Ocean Water), such that $\delta_{\text{SAMPLE}} = 1000((R_{\text{SAMPLE}}/R_{\text{SMOW}})-1)$, where R is $^{18}\text{O}/^{16}\text{O}$ or $^2\text{H}/^1\text{H}$. Values cited herein are normalized on the SMOW-SLAP scale so that SLAP (Standard Light Arctic Precipitation) has a value of -55.5‰ in $\delta^{18}\text{O}$ and -428‰ in $\delta^2\text{H}$ [8].

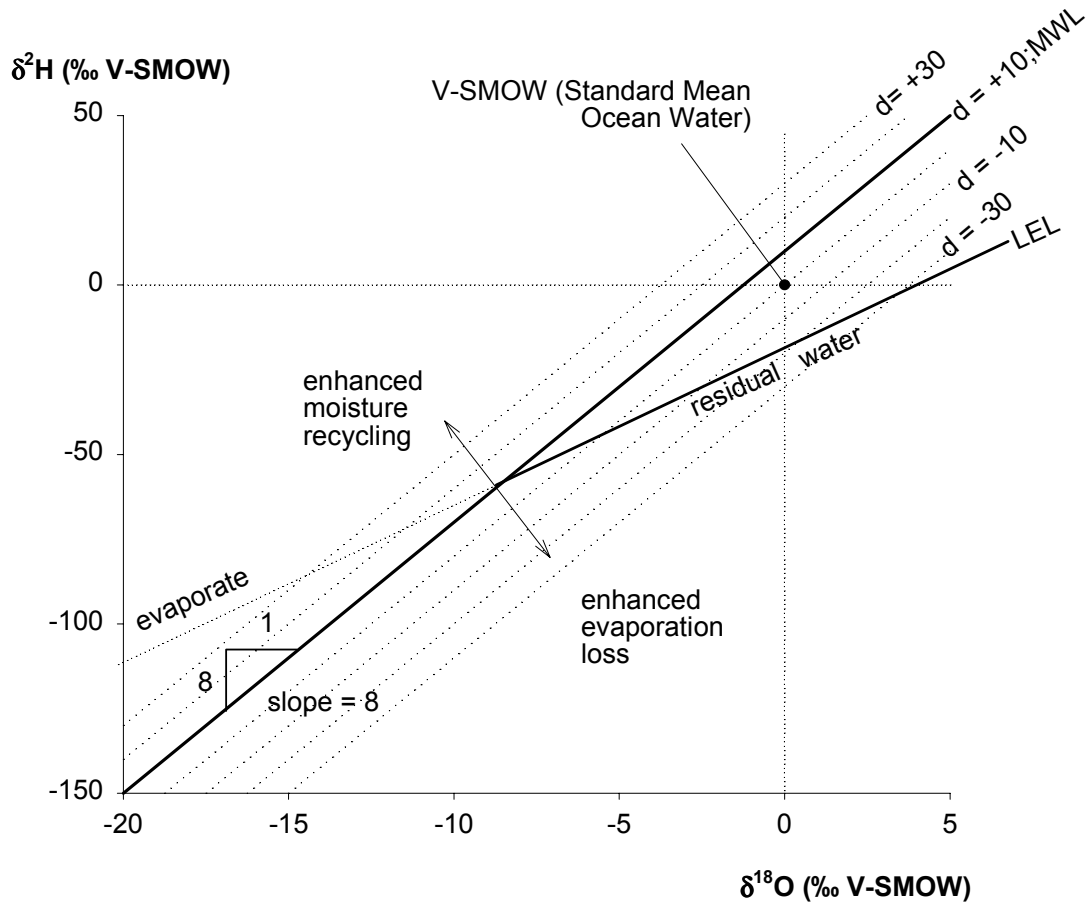


FIG. 1. Schematic plot of $\delta^{18}\text{O}$ versus $\delta^2\text{H}$ showing the global meteoric water line (MWL; $d = 10$, slope = 8) of Craig [9], local evaporation line (LEL; slope < 8), ocean water (SMOW) and relative changes in the d -excess (d). D -excess in precipitation increases in response to enhanced moisture recycling as a result of increased evaporate content. D -excess is reduced in the case where water is lost by evaporation.

One prerequisite for widespread application of d -excess in climatology is improvement in routine analytical precision, primarily of deuterium measurements. Another prerequisite, which is the focus of this paper, is the development of an improved understanding of spatial and temporal variations in d -excess and their controls in present day precipitation. To demonstrate fundamental local, regional, and global patterns in the d -excess and its correlation with other climate parameters, namely $\delta^{18}\text{O}$, air temperature, and vapour pressure, we present a synthesis of long-term monthly and annual patterns observed for selected stations within the IAEA/WMO Global Network for Isotopes in Precipitation (GNIP) database. The synthesis, which also provides relevant theoretical development, underlines the nature of d -excess variations in modern precipitation and its climatic controls. As shown, the potential of the tracer justifies the need to improve basic analytical precision so that it can be fully exploited in future isotope-based climate research.

2. ANNUAL PATTERNS

The GNIP database comprises oxygen-18, deuterium and tritium values of monthly composite precipitation samples collected during 1961 to present from a network of 550 meteorological

stations which are irregularly distributed over the globe [11,12]. It also includes monthly mean values of air temperature, atmospheric vapour pressure and monthly precipitation amount. Maximum reported analytical uncertainty in oxygen-18 and deuterium measurements is 0.2 ‰ and 2 ‰, respectively although some laboratories (and therefore some stations or years) report lower values. Analytical uncertainty in d-excess for routine measurements is currently estimated at $u(d) = \sqrt{(u\delta^2H)^2 + 8 \cdot (u\delta^{18}O)^2} \approx 2.08 \text{ ‰}$, which is strongly dependent on the uncertainty in deuterium (2 ‰). Current uncertainty leaves obvious room for future improvement.

The annual averages of air temperature, vapour pressure, $\delta^{18}O$, δ^2H and deuterium excess of the GNIP stations are presented in Fig. 2. Although there is a considerable scatter of the data, the plots reveal statistical correlations between some of these parameters, such as a curvilinear dependency between temperature (vapour pressure) and oxygen-18 and a linear dependency between the oxygen-18 and deuterium values. These statistical relationships have been extensively discussed in various reviews of the GNIP database [1,11,13,14].

Herein, special consideration is given to the d-excess (Fig. 2E and 2F). Despite the considerable scatter in the data presented in Fig. 2F, a slight increase of the d-excess is visible between the cluster at 30 mbar and the one at about 15 mbar, and a notable decrease in d-excess is visible for vapour pressures below about 15 mbars. (It should be noted that there is certain equivalence in the dependency of the temperature and the vapour pressure, respectively, for the temperature range below 15°C. This “equivalence” is seen in the oxygen-18 plots of Fig. 2C and D, and it is founded on the apparent vapour pressure - temperature relationship manifested by Fig.2A). Fig.2F also illustrates the exceptionally high d-excess values recorded at stations receiving precipitation from the eastern Mediterranean, e.g. ISR (Israel), SAU (Saudi Arabia), and CYP (Cyprus). These high d-excess values reflect the specific conditions of the vapour formation over the eastern Mediterranean [12]. Annual average d-excess values below zero per mil are observed at stations with high temperature and/or low vapour pressure (e.g. VEN – Venezuela, MAL – Mali, CHA – Chad), where kinetic isotope fractionation processes, connected with the partial evaporation of the falling raindrops [16], affect the d-excess of the collected precipitation.

Partial evaporation of the precipitation sample during the storage in the rain gauge under warm and dry atmospheric conditions may also be accountable for a portion of the observed decrease of the d-excess.

Three distinct data clusters are discernible on a plot of deuterium excess versus oxygen-18 (Fig. 2E). The first cluster includes stations with high oxygen-18 values and d-excess values ranging from about 5‰ to 15‰. These stations, with latitudes from 45 °S to 45 °N, mainly receive precipitation from tropical and subtropical oceanic source areas. A second cluster, characterized by about 3‰ lower oxygen-18 values and a d-excess ranging from about 5‰ to 12‰ is also discernible. This cluster is represented by stations located in the latitude band from 45° to 60° both of the northern and the southern hemisphere. The depletion in oxygen-18 relative to the first cluster points to the rainout effect of water vapour (Rayleigh distillation model) during poleward air mass movement. Mixing with water vapour evaporated from more northern (southern) oceanic areas may account for the observed slight depletion of the d-excess values. Stations receiving precipitation from the Mediterranean Sea region form the third cluster with deuterium excess values above 15‰ (Fig. 2E).

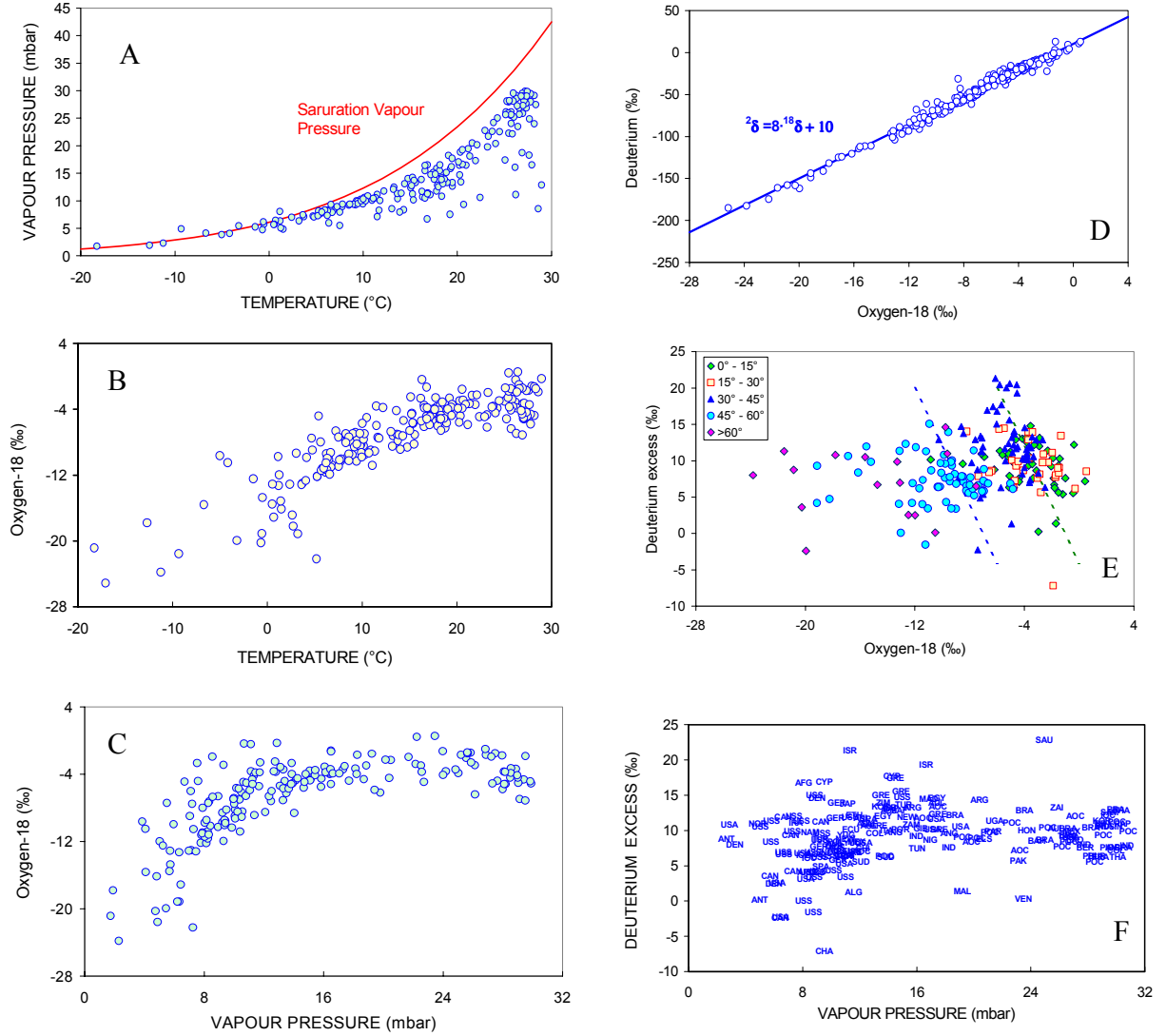


FIG. 2. Compilation of long-term annual averages of isotopic and climatic variables of the GNIP database.

Two dashed lines with a slope of -4 have been plotted in Fig.2E. This value has been chosen because it corresponds to the estimated ratio between the change of d-excess and the change of oxygen-18 due to evaporation of falling raindrops (see below). As shown in Fig. 2E, clusters appear to be stretched along lines with this slope, indicating that sub-cloud evaporation is one of the major processes responsible for the observed spread of the d-excess.

Despite the considerable scatter in the global d-excess values, Fig. 2E suggests a slight overall increase of the d-excess with oxygen-18 of about $\frac{dd}{d^{18}\delta} = 0.1$ to 0.2 . With the relationship

$\frac{dd}{d^{18}\delta} = \frac{d^2\delta}{d^{18}\delta} - 8$, which follows from the definition of the d-excess, the value of the slope $\frac{d^2\delta}{d^{18}\delta}$ in the $\delta^{18}O$ vs δ^2H plot would be between 8.1 and 8.2 . This estimate is in good agreement with the value 8.2 ± 0.07 , which followed from a statistical evaluation of the GNIP data [14].

3. MONTHLY PATTERNS

While the spatial distribution of the long-term annual averages of the d-excess is characterized by a considerable statistical spread, the long-term monthly averages generally show a well-defined and systematic seasonal variation. For the northern hemisphere, the average d-excess over all stations usually reaches its maximum in December/January and its minimum in June/July (Fig. 3). In the southern hemisphere the seasonal variation of the d-excess shows a 6-month phase-shift. Fig. 3 also indicates that the amplitude of the seasonal variation is higher in the northern than in the southern hemisphere. This asymmetry seems to reflect the irregular distribution of land and sea at the two hemispheres. In summer, the relative humidity can reach lower values on land than on sea. Thus, on average, sub-cloud evaporation and consequently decrease of the d-excess is of stronger influence in the northern hemisphere.

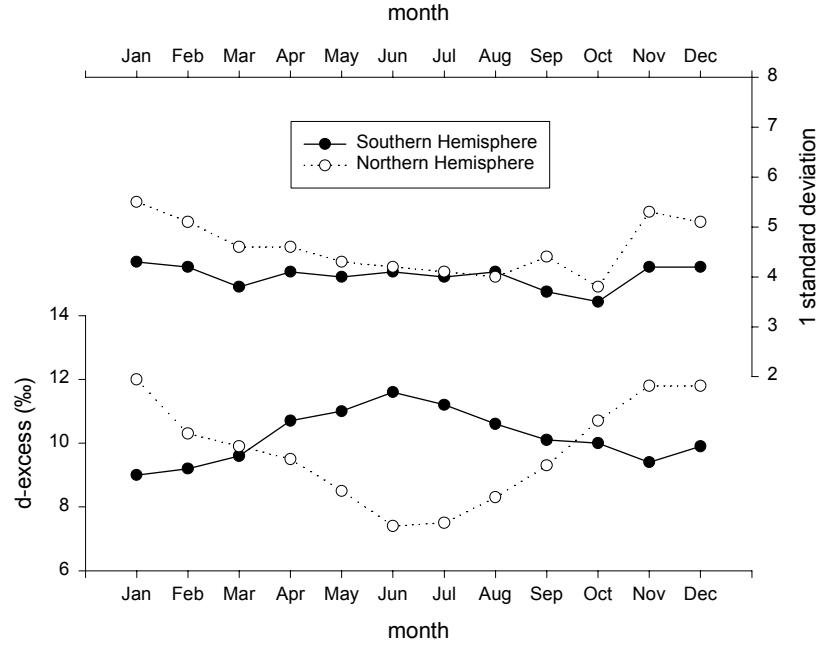


FIG. 3. Seasonal variation of deuterium excess in precipitation estimated from long-term mean monthly values of the stations included in the GNIP database.

The model of Merlivat and Jouzel [2] allows a more quantitative description of the seasonal variation of the d-excess. It is based on the following relationship between the isotopic composition of the water vapour evaporating from the sea surface (δ_E) and the one of the atmospheric moisture above the sea (δ_{V0}):

$$\delta_E = (1 - k) \frac{1/\alpha_e - h(1 + \delta_{V0})}{1 - h} - 1 \quad (1)$$

For $\delta_E = \delta_{V0}$, the isotopic composition of the first-fraction precipitation in the oceanic source area, $1 + \delta_{P0} = \alpha_e(T_c) (1 + \delta_V)$ becomes:

$$\delta_{P0} = \frac{\alpha_e(T_c)}{\alpha_e(T_s)} \frac{1 - k}{1 - kh} - 1 \quad (2)$$

where $\alpha_e(T_c)$ and $\alpha_e(T_s)$ are the equilibrium fractionation factors at condensation temperature (T_c) and sea surface temperature (T_s), respectively, h is the relative humidity related to the sea

surface temperature, and k is a factor characterizing the kinetic isotope fractionation of the evaporation process. Merlivat and Jouzel obtained for a smooth regime $^{18}k = 6\text{‰}$ (for oxygen-18), and the ratio is $^{2}k/^{18}k = 0.88$. It should be noted that the condition $\delta_E = \delta_{v0}$ applies for a steady-state regime of the *whole* water cycle [2]. For following it is also applied, since it is considered as a reasonable approximation for oceanic source areas with high evaporation flux and smooth wind regime (e.g. in tropical and sub-tropical regions).

Using eq. (2), the annual average d-excess values of first-fraction precipitation has been calculated for oceanic stations at which long-term measurements of the humidity, air temperature and sea surface temperature have been carried out [17]. Figure 4 shows the calculated values as a function of the latitude of the corresponding marine observation stations. The wide spread of the values, especially for the North Pacific, is probably due to the large distance between the stations, and thus the different climatic conditions, even at comparable latitudes. It is also possible that the assumption on which eq. (2) is based, does not fully describe the complexity of the evaporation-condensation processes at the various stations. As far as the Indian Ocean is concerned, the data suggest lower d-excess values in equatorial regions and higher values in sub-tropical areas. Maximum values seem to be reached at latitude of around 30° , both in the southern and the northern hemisphere.

The same approach has been used to calculate the monthly mean d-excess of first-fraction precipitation at various stations in the North Atlantic, for which the long-term monthly averages of the required parameters are available. Fig. 5 demonstrates that the calculated d-excess values reach at all stations a maximum in winter and a minimum in summer. This result is in good agreement with the GNIP data (Fig. 3, curve for the northern hemisphere). Fig. 5 also indicates the strong influence of the relative humidity on the d-excess. At the stations 30°N and 40°N , the relative humidity is lower and the d-excess accordingly higher than at the more northern stations (55°N and 56°N). Finally, Fig. 5 reveals an important feature of these isotopic and climatological parameters, namely the phase shift between their seasonal variations. The maximum of the air temperature appears a few months later than the one of the relative humidity.

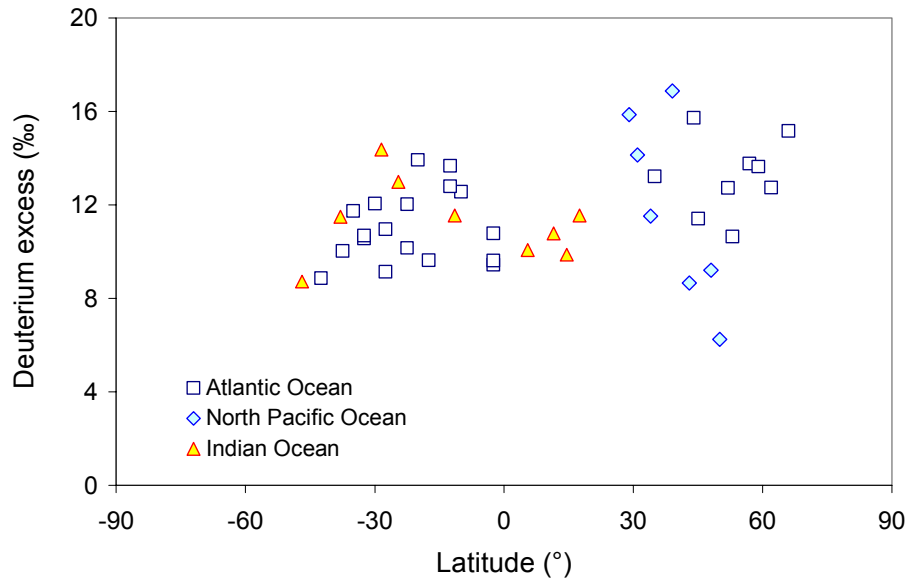


FIG. 4. Plot of annual average deuterium excess in first-fraction precipitation versus latitude of maritime stations. The climatic variables used for calculating the deuterium excess by eq.(2) are taken from van Loon [17].

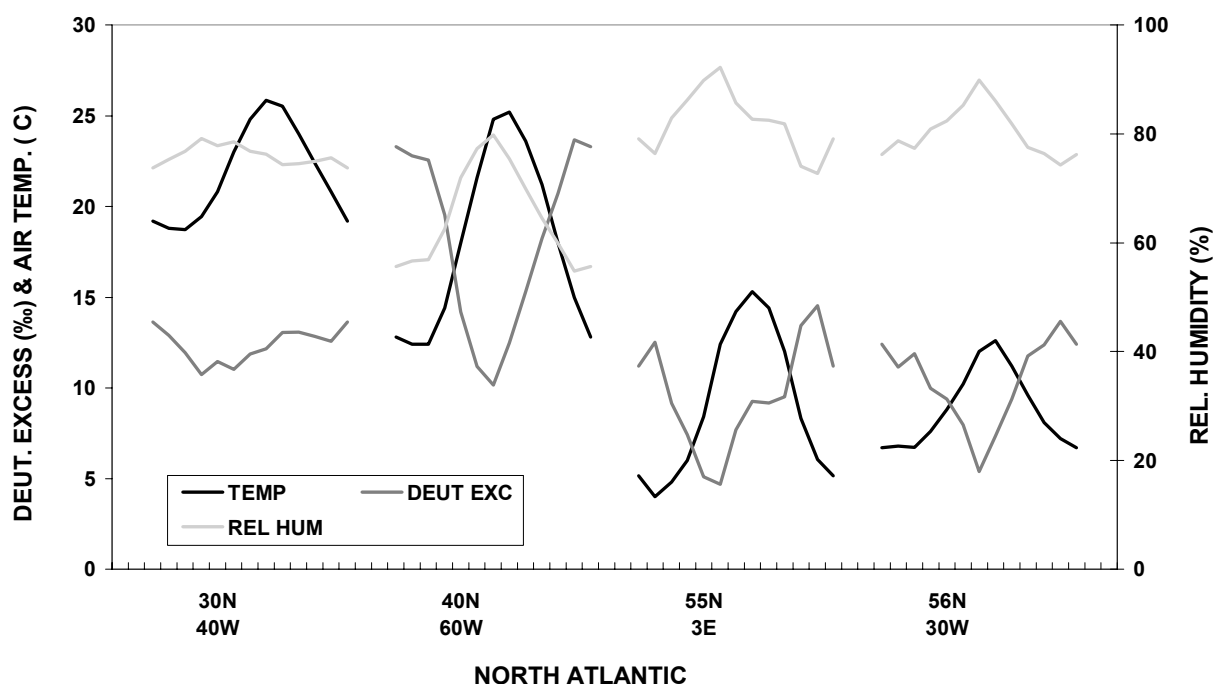


FIG. 5. Long-term monthly averages of climatic variables (air temperature and relative humidity related to sea surface temperature) taken from van Loon [17] for selected observation stations in the North Atlantic, and deuterium excess derived from these variables using Eq. (2).

The phase shift between the seasonal variations of the various parameters gives rise to the hysteresis effect observed in the temperature *versus* relative humidity, $\delta^{18}\text{O}$ and d-excess relationships (Fig. 6). It should be noted that such hysteresis curves indicate that the observed isotopic pattern is dependent on the thermodynamic conditions in the atmosphere in the preceding months. While the phase shift between air temperature and relative humidity as well as oxygen-18 is only a couple of months, the d-excess is nearly in anti-phase to the air temperature. It should be noted that the hysteresis curves in this figure would “degenerate” to straight lines, if the phase shifts were exactly zero months, for the relative humidity and for oxygen-18, or six months, for the d-excess. In fact, the phase shift between oxygen-18 and deuterium excess of first-fraction precipitation in the considered oceanic areas appears to be exactly 6 months, as shown by Fig. 7. This plot also demonstrates that in oceanic areas the seasonal variation of oxygen-18 is rather small.

Considering the Rayleigh distillation model [1], it is expected that the average oxygen-18 values become lower and the amplitude of the seasonal variation of oxygen-18 higher, when water vapour partially rains out at lower temperatures during the moisture transport away from the oceanic source area. This trend is verified by the GNIP data, as shown in Fig. 8 for the example of a transect from the Atlantic Ocean to the continental station in Vienna, Austria. It is interesting to note that over the large distance from the Azores to Gibraltar there is a rather small change in the isotopic composition of the precipitation compared to the short travel over continental regions up to Vienna. Furthermore, Fig. 8 indicates that there is a lower decrease of the d-excess maximum (winter season) with decreasing oxygen-18 than of the d-excess minimum (summer season). This trend, and particularly the very low d-excess in summer at Gibraltar indicate the effect of kinetic isotope fractionation due to partial evaporation of the falling raindrops. Stewart [16] studied this process and provided a

theoretical description. Assuming that the partial evaporation of the falling raindrop is not higher than about 20%, the following relationship can be derived from Stewart's theory:

$$\frac{\Delta d}{\Delta^{18}\delta} \approx \frac{1 - 1/2 \alpha_k}{1 - 1/18 \alpha_k} - 8 \quad (3)$$

where $\alpha_k = \alpha_e (D/D')^{0.58}$, α_e is the equilibrium fractionation factor, and D/D' the ratio of the diffusion coefficients for the light and heavy isotope of oxygen and hydrogen, respectively. Using the values given by Stewart, the ratio of the change of the d-excess and the one of the oxygen-18 due to evaporation of falling raindrops is approximately:

$$\frac{\Delta d}{\Delta^{18}\delta} \approx -4. \quad (3a)$$

An example of the air mass evolution in North America and the distinctive imprints of $\delta^{18}\text{O}$ and d-excess is shown in Fig. 9 for a transect extending from Bermuda, located in the Atlantic Ocean, to Gimli Manitoba, and traversing the Great Lakes region. The progression in “continentality” of the air masses coming from the Bermudas is clearly labeled by the relationship of the long-term monthly means of $\delta^{18}\text{O}$ and temperature. In maritime areas (Bermuda and Hatteras), $\delta^{18}\text{O}$ is controlled by the rain amount compared to continental areas where it is strongly controlled by temperature effects (oxygen-18-temperature coefficient increases to about $0.5\text{‰}/^\circ\text{C}$). This behaviour, also observed in other regions [18], agrees with conclusions from measurements of vertical moisture and temperature profiles [19], namely

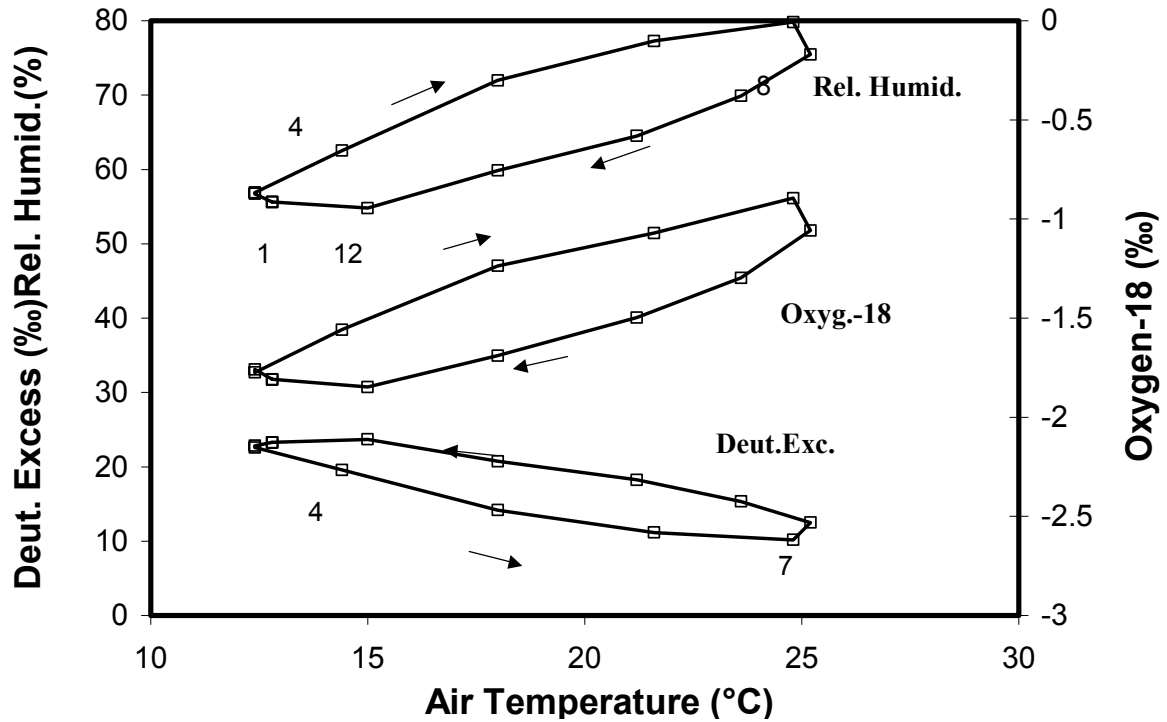


FIG. 6. Hysteresis curves of monthly deuterium excess and oxygen-18 values calculated for first fraction precipitation and climatic variables for the observation station in the North Atlantic at 40°N and 60°W .

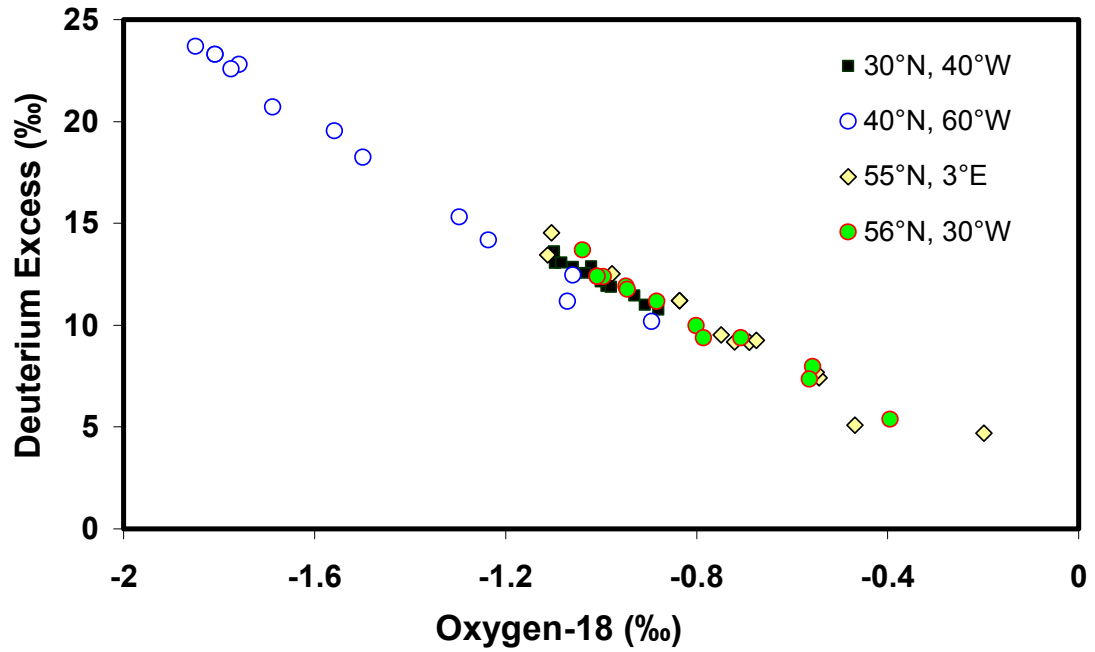


FIG. 7. Monthly deuterium excess versus monthly $\delta^{18}\text{O}$ in first-fraction precipitation at selected maritime stations in the North Atlantic. The values are calculated by eq.(2) and using data published by van Loon [17].

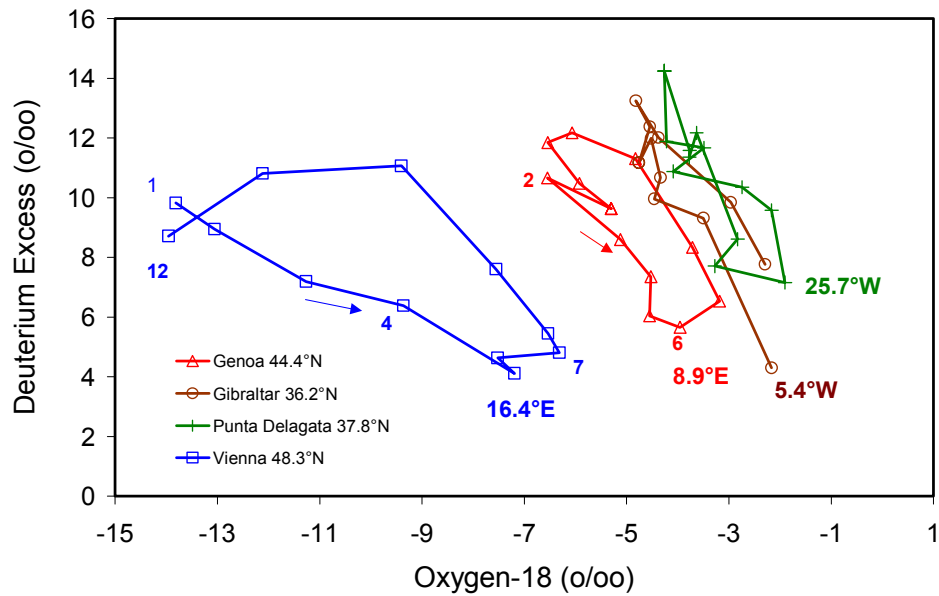


FIG. 8. Plot of monthly deuterium excess versus monthly $\delta^{18}\text{O}$ for precipitation collected at GNIP stations along a transect from the Punta Delgada, Azores, to Vienna, Austria.

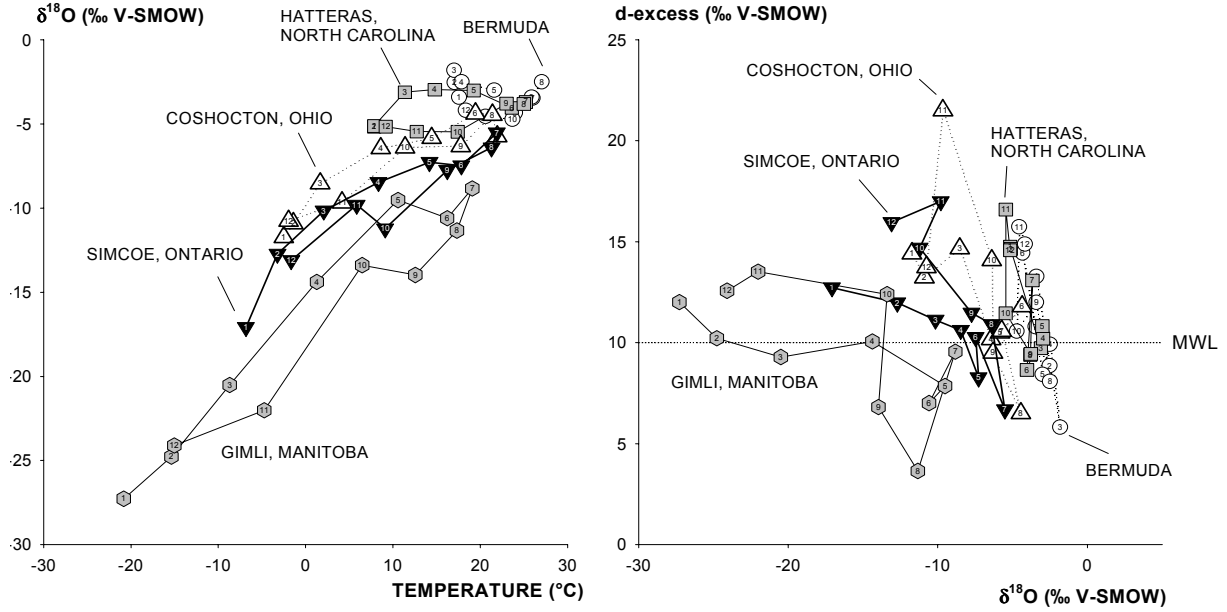


FIG. 9. Plot of monthly $\delta^{18}\text{O}$ versus temperature (a) and monthly deuterium excess versus $\delta^{18}\text{O}$ for precipitation collected at GNIP stations along a transect from the Atlantic Ocean at Bermuda to Gimli, Manitoba and crossing the Great Lakes region. MWL refers to the meteoric water line. Numbers denote months of year.

that in tropical (and subtropical) areas the precipitable water is not a strong function of temperature but of vertical convection, whereas in humid (and continental) regions the precipitable water is controlled by horizontal advection and temperature.

The maritime character of the air mass over the Bermudas is also represented by the steep trend of d-excess versus oxygen-18 (Fig. 9b). The “degeneration” of the hysteresis at this station indicates that there is just a 6-month phase shift between oxygen-18 and d-excess. The deformation of the systematic transformation of the hysteresis curves at continental stations of the transect (Fig. 9b) suggests mixing of air masses of different origin. Principally, there are 4 sources of air moisture moving into the Great Lakes region. These are from Gulf of Mexico (dominating in summer), Pacific Ocean, Arctic region and the Atlantic Coast.

A striking feature of Fig. 9b is the increase of the d-excess by up to 5‰ at stations in the Great Lakes region, particularly in the fall (months 9 through 12) at Coshocton and Simcoe. This suggests enhanced continental water recycling [20], i.e., return of land surface evaporation water to the land surface as precipitation [21]. A simple relationship between the change in d-excess, Δd , due to recycling and the recycling ratio, R (= relative amount of vapour evaporated from open water surfaces in the precipitation), can be derived as follows. Considering the isotopic composition of vapour evaporating from open water surfaces (e.g. [22], assuming that the isotopic composition of the surface water corresponds with the one of the preceding precipitation, then a simple mass balance yields:

$$\Delta d = R(8^{18}C_k - 2C_k). \quad (4)$$

With the values of the kinetic fractionation coefficients $^2C_k = 14.3\text{‰}$ and $^{18}C_k = 12.4\text{‰}$ [22], the recycling ratio becomes $R = \Delta d/100$ (Δd in ‰). Thus, an increase of the deuterium excess by about 5‰ would correspond with a recycling from open water surfaces of about 5%. It should be noted that for the Great Lakes region the assumption made in deriving eq. (4) (isotopic composition of the surface water equal to the isotopic composition of the preceding precipitation) is not exactly realized. Nevertheless, the value of the recycling ratio estimated here for a d-excess increase of 5‰ is in good agreement with a more specific evaluation for the Great Lake region by Gat et al. [20]. Similarly, d-excess in the range of +20‰ for the Mediterranean indicates a recycling ratio close to 20%.

The GNIP data enable selecting numerous such transects across Europe, Africa and other continental regions. As demonstrated here, these transects provide insight into the long-term isotopic signals of the continental effect as atmospheric moisture evolves by progressive rainout and mixing processes over the continents. Transects crossing Germany and transects in mountainous regions can also be useful to study the evolution of the d-excess with increasing altitude [23,24]. The systematic relationships between $\delta^{18}\text{O}$, d-excess and climatic parameters are useful for labeling and quantifying important air-mass regimes and seasonal fluctuations. These transects provide further information on the natural variability of the deuterium excess relevant for enhancing its use in climatic studies.

4. CONCLUSIONS

The database of the Global Network for Isotopes in Precipitation can be used to study the long-term annual and monthly averages of the deuterium excess in relation to oxygen-18 of precipitation and other climatic variables. Despite that uncertainty in the reported deuterium excess is currently quite high, variations both in the long-term annual and monthly averages of the deuterium excess are robust and systematic, suggesting significant potential of this parameter in climatic studies. The deuterium excess can be used as fingerprint of (1) the oceanic source area of the precipitation collected at a given station and (2) mixing of air masses of different source, in particular, recycled air moisture. Relationships for estimating these effects are given in the paper. This also includes the effect on the deuterium excess of partial evaporation of falling raindrops under warm and dry conditions below the cloud base. The model of Merlivat and Jouzel of the formation of the isotopic composition of water vapour in the oceanic source area has been used to estimate the monthly variation of the isotopic composition and the deuterium excess in first-fraction precipitation at selected maritime observation stations. The results are in good agreement with data derived from the GNIP database and contribute to better understand the seasonal variations of the deuterium excess in precipitation. In the paper, advantage has been taken of deuterium excess versus oxygen-18 plots, which proved to be complementary and sometimes more “sensitive” (with regard to identification deuterium excess changes) than conventional deuterium versus oxygen-18 plots. Furthermore, hysteresis curves have been plotted to better demonstrate phase shifts between the seasonal variation of the deuterium excess and oxygen-18 and/or other climatic variables. Some regions with pronounced variations/phase shifts should be selected for further studies of long-term seasonal variations. With the advancement in using AGCMs for climate studies, experimental data on long-term seasonal variations of the isotopic composition and, thus, the deuterium excess in precipitation will be very useful for model validation.

ACKNOWLEDGEMENTS

The authors wish to thank Mr. L. Araguás-Araguás, former staff of the IAEA, for his efforts in extending and improving the quality of the GNIP database. Ms. L. Gourcy, IAEA, continues these efforts, and her initiatives in this regard are acknowledged. Thanks is also extended to K. Rozanski, Poland, U. Schotterer, Switzerland, and W. Stichler, Germany, for valuable discussions related to the deuterium excess.

REFERENCES

- [1] DANSGAARD, W., Stable isotopes in precipitation. *Tellus* **16** (1964) 436-468.
- [2] MERLIVAT, L., JOUZEL, J., Global climatic interpretation of the deuterium-oxygen 18 relationship for precipitation. *J. Geophys. Res.* **84** (1979) 5029-5033.
- [3] JOUZEL, J., KOSTER, R.D., SUOZZO, R.J., RUSSEL, G.L., WHITE, J.W.C., BROECKER, W.S., Simulations of the HDO and H₂¹⁸O atmospheric cycles using the NASA GISS General Circulation Model: Sensitivity experiments for present-day conditions. *J. Geophys. Res.* **96** (1991) 7495-7507.
- [4] JOUZEL, J., KOSTER, R.D., SUOZZO, R.J., RUSSEL, G.L., Stable water isotope behaviour during the last glacial maximum: a general circulation model analysis. *J. Geophys. Res.* **99**: (1994) 25791-25801.
- [5] CIAIS, P., White, W.W.C. Jouzel, J., Petit, J.R., The origin of present-day Antarctic precipitation from surface snow deuterium excess data. *J. Geophys. Res.* **100**: (1985) 18917-18927.
- [6] HOFFMANN, G., JOUZEL, J., MASON, V., Stable water isotopes in atmospheric general circulation models, *Hydrological Processes* **14** (2000) 1385-1406.
- [7] PETIT, J.R., WHITE, J.W.C., YOUNG, N.W., JOUZEL, J., KOROTKEVICH, Y.S., Deuterium excess in recent Antarctic snow. *J. Geophys. Res.* **96** (1991) 5113-5122
- [8] COPLEN, T.B., New guidelines for reporting stable hydrogen, carbon, and oxygen isotope-ratio data, *Geochim. Cosmochim. Acta* **60** (1996) 3359-3360.
- [9] CRAIG, H., Isotopic variations in meteoric waters, *Science* **133** (1961) 1702-1703.
- [10] JOHNSON, S.J., DANSGAARD, W., WHITE, J.W.C., The origin of Arctic precipitation under present and glacial conditions. *Tellus* **41B** (1989) 452-468.
- [11] ROZANSKI, K., ARAGUÁS-ARAGUÁS, L., GONFIANTINI, R., Isotopic patterns in modern global precipitation. In : Swart, P.K., Lohmann, K.C., McKenzie, J., Savin, S. (eds), *Climate Change in Continental Isotopic Records*, American Geophysical Union, Washington. *Geophysical Monograph* **78** (1993) 1-36.
- [12] PANARELLO, H.O., ARAGUÁS-ARAGUÁS, L., GERARDO-ABAYA, J., GIBERT, E., The role of the Global Network for Isotopes in Precipitation (GNIP) in hydrological and hydroclimatic studies. In: *Isotope Techniques in the Study of Environmental Change. Proc. Of a Symposium*, IAEA, Vienna, 14-18 April 1997, (1998) 79-91.
- [13] YURTSEVER, Y., GAT, J., Atmospheric waters. In: *Stable Isotope Hydrology: Deuterium and Oxygen-18 in the Water Cycle*, International Atomic Energy Agency, Vienna. *Technical Report Series* **210** (1981) 103-142.
- [14] ARAGUÁS-ARAGUÁS, L., FROEHLICH, K., ROZANSKI, K. 2000. Deuterium and oxygen-18 isotope composition of precipitation and atmospheric moisture. *Hydrol. Process.* **14** (2000) 1341-1355.
- [15] GAT, J.R., CARMI, I., Evolution of the isotopic composition of atmospheric waters in the Mediterranean Sea area. *J. Geophys. Res.* **75** (1970) 3039-3048.
- [16] STEWART, M.K., Stable isotope fractionation due to evaporation and isotope exchange of falling water drops: application to atmospheric processes and evaporation of lakes. *J. Geophys. Res.* **80** (1975) 1133-1146.

- [17] VAN LOON, H., *Climates of the Oceans*, *World Survey of Climatology* **15** (1984) 453-458.
- [18] ARAGUÁS-ARAGUÁS, L., FROEHLICH, K., ROZANSKI, K. 1998. Stable isotope composition of precipitation over Southeast Asia. *J. Geophys. Res.* **103** (1998) 28721-28742
- [19] GAFFEN, D.J., ROBOCK, A., ELLIOTT, W.P., Annual Cycles of Tropospheric Water Vapor. *J. Geophys. Res.* **97** (1992) 18185-18193.
- [20] GAT, J.R., BROWSER, C.J., KENDALL, C., The contribution of evaporation from the Great Lakes to the continental atmosphere: estimate based on stable isotope data. *Geophys. Res. Letters* **21** (1994) 557-560.
- [21] Koster, R.D., PERRY DE VALPINE, D., JOUZEL, J., Continental water recycling and ¹⁸O concentrations, *Geophys. Res. Lett.* **20** (20) 2215-2218.
- [22] FROEHLICH, K., Evaluating the water balance of inland seas using isotopic tracers: the Caspian Sea experience. *Hydrol. Process.* **14** (2000) 1371-1383.
- [23] FROEHLICH, K. 1996. Deuterium excess and its variation in precipitation. *Glaciers from the Alps*. *Climate and Environmental Archives*. Proc. Workshop 21-23 October 1996, Wengen Switzerland. Paul Scherrer Institut, Villingen, Switzerland, (1996) 45-47.
- [24] GONFIANTINI, R., ROCHE, M.A., OLIVRY, J.C., ZUPPI, G.M., The altitude effect on the isotopic composition of tropical rains. *Chem. Geol.* (2001 in press).

LINKS BETWEEN METEOROLOGICAL CONDITIONS AND SPATIAL/TEMPORAL VARIATIONS IN LONG-TERM ISOTOPE RECORDS FROM THE AUSTRIAN PRECIPITATION NETWORK

A. KAISER, H. SCHEIFINGER

Central Institute for Meteorology and Geodynamics, Vienna, Austria

M. KRALIK

Environment Agency, Vienna, Austria

W. PAPESCH, D. RANK

Arsenal Research, Vienna, Austria

W. STICHLER

GSF Institute of Hydrology, Neuherberg, Germany

Abstract. The isotope records from the Austrian Network for Isotopes in Precipitation (ANIP) show significant but not uniform long-term trends. While the 10-year running means of some mountain stations exhibit a pronounced increase in $\delta^{18}\text{O}$ of about 1 ‰ since 1975, the change of $\delta^{18}\text{O}$ at the valley stations is much lower. There are also differences in the time behaviour. The differences in the $\delta^{18}\text{O}$ -values of sampling stations at similar altitudes can be explained by different origins of the air moisture (Atlantic or Mediterranean influence). Furthermore, a significant difference in the behaviour of the deuterium excess at neighbouring mountain and valley stations has been observed. There is a slight increase of the yearly mean of the deuterium excess with increasing altitude of the sampling station. But moreover, the seasonal pattern of the deuterium excess is quite different. While the valley stations exhibit the expected minimum in summer, the mountain stations show a distinct maximum between June and October. As a first step into a comprehensive analysis of the meteorological effects on the isotope patterns, the role of advection of different air masses is studied by trajectory statistics. Back trajectories, based on the three dimensional wind fields of the ECMWF model, are calculated for each hour within each precipitation event. Thus, the frequency of the origin of air masses and their contribution to the isotope patterns of the monthly precipitation samples are studied for two selected mountain stations north and south of the main ridge of the Alps.

1. INTRODUCTION

The Austrian Network for Isotopes in Precipitation (ANIP) started in 1972. At some stations samples have already been taken since the 1960s. 71 stations ranging from 120 to 2250 m in altitude are presently in operation all over Austria with some preference given to the Karst areas north and south of the Alpine mountain range (Fig. 1 shows a map of the stations mentioned in this paper). The precipitation water is collected on a daily basis in ombrometers (500 cm²) and mixed to monthly samples. All samples not measured immediately have been stored in 1L bottles in a specially dedicated cellar (16000 samples) in Vienna and are available for analysis in the future. The aim of ANIP is to provide input data for hydrological and hydrogeological investigations and a data-base for climatological research. The amount of precipitation in Austria is highly influenced by the Alpine mountain range (400-3000 mm/a). The amount of annual precipitation increases towards the mountain ranges, in particular at the high altitude regions. However, strong regional differences exist between the windward and the lee side of the Alpine ranges. Precipitation time series from 1901 to 1990 show no continuous trend. Periods of precipitation above and below the long-term trend are recorded with peculiarities in some geographical regions. Wet periods are supposed to represent maritime phases, but there are so far no detailed studies about the origin of the precipitating air masses

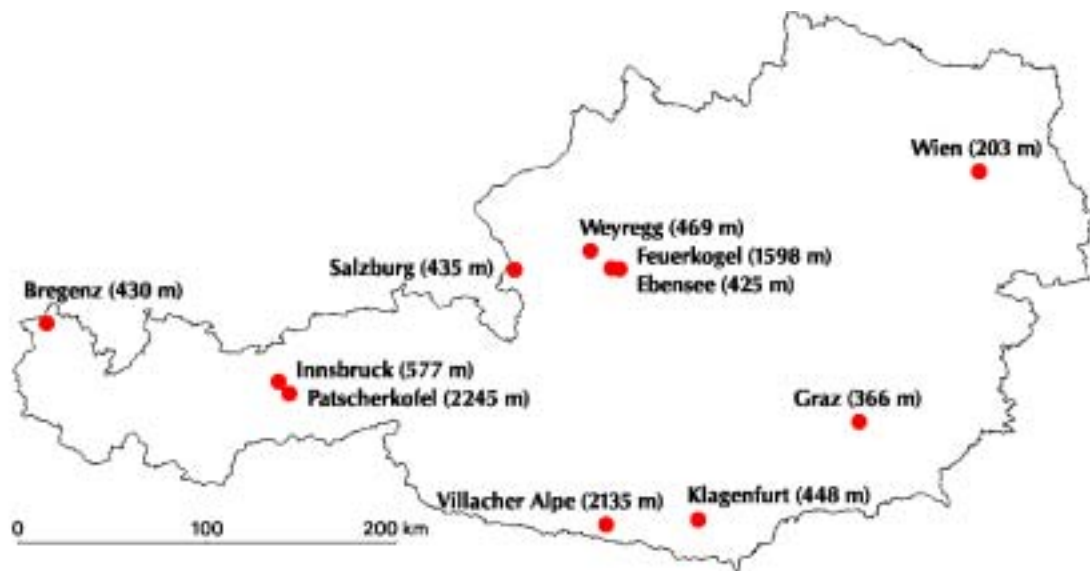


FIG. 1. Selected sampling stations of the Austrian precipitation network.

in Austria. However, the Alps as a weather divide sharply distinguish precipitation events caused by different air flow directions. They are therefore a unique platform to study the origin of precipitating air masses and possible trends in air flow and precipitation patterns.

2. LONG-TERM RECORDS

The isotope time series of the stations of the Austrian precipitation network show significant but not uniform long-term trends [1, 2]. While the 10-year running mean of some mountain stations exhibits a pronounced increase in $\delta^{18}\text{O}$ of about 1 ‰ since 1975, the change of $\delta^{18}\text{O}$ at the valley stations is much lower (Fig. 2). There are also differences in the time behaviour. The differences in the $\delta^{18}\text{O}$ -values of sampling stations at similar altitudes can be explained by the origin of the air moisture. An Atlantic influence (moisture from NW) causes lower $\delta^{18}\text{O}$ -values (e.g. Patscherkofel and Bregenz) than a Mediterranean one (e.g. Villacher Alpe and Graz). The main reason for this different ^{18}O -content is the longer way of the Atlantic air masses over the continent along which the moisture becomes stepwise depleted in heavy isotopes by successive rainout (continental effect).

The stable isotope variations in precipitation are a consequence of the isotope effects accompanying each step of the water cycle. Temperature is the most influencing parameter (Fig. 3), but there are also other influences like changes in the origin of air masses or in rain formation mechanisms [2, 3, 4]. The fluctuations of the ^{18}O -content of precipitation correlate also to a large extent with those of the North Atlantic Oscillation (NAO) index, except during some years where the influence of the amount of precipitation probably dominates (Fig. 4). The NAO has strong impacts on the weather and the climate in North Atlantic region and surrounding continents, especially Europe [6]. Since the NAO is particularly dominant in winter, average values of the November to March period are shown in Fig. 4. The time series were normalized by the standard deviation over the whole observation period and a Gaussian filter (5 years) was applied to smooth the curves.

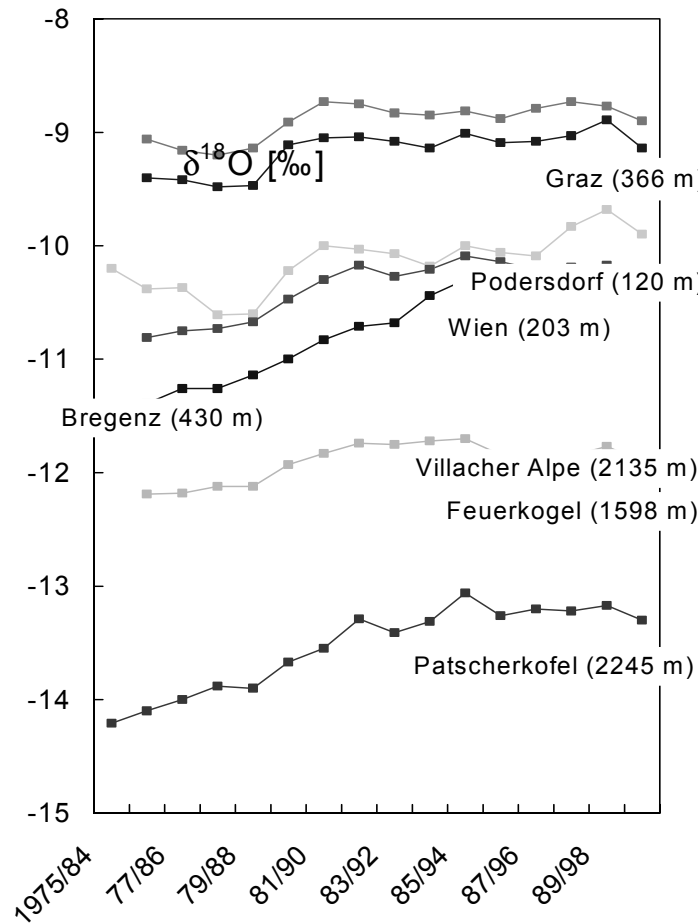


FIG. 2. Long-term $\delta^{18}\text{O}$ variations (10-year running means) at several stations of the Austrian precipitation network [1, 2].

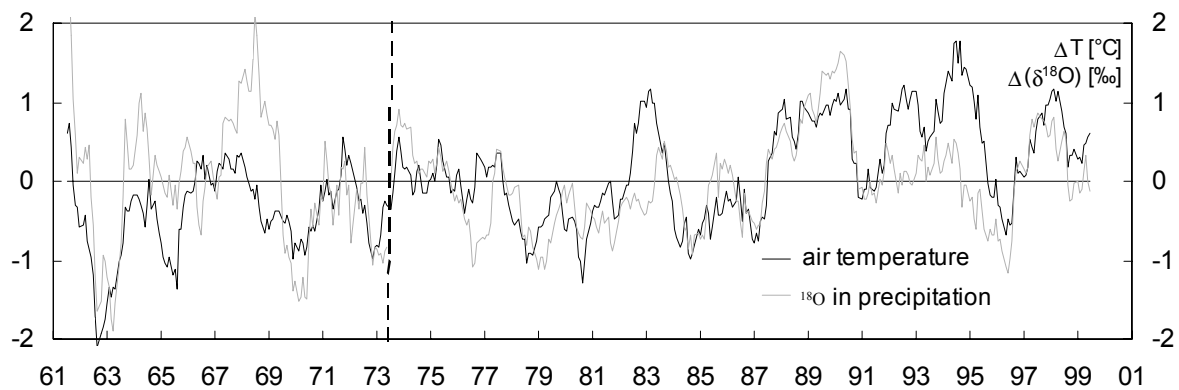


FIG. 3. Long-term fluctuations of isotope composition ($\delta^{18}\text{O}$) of precipitation and surface air temperature in Austria. Running 12-month mean of seven meteorological stations ($\delta^{18}\text{O}$ up to 1973: data of Vienna) [2, 5].

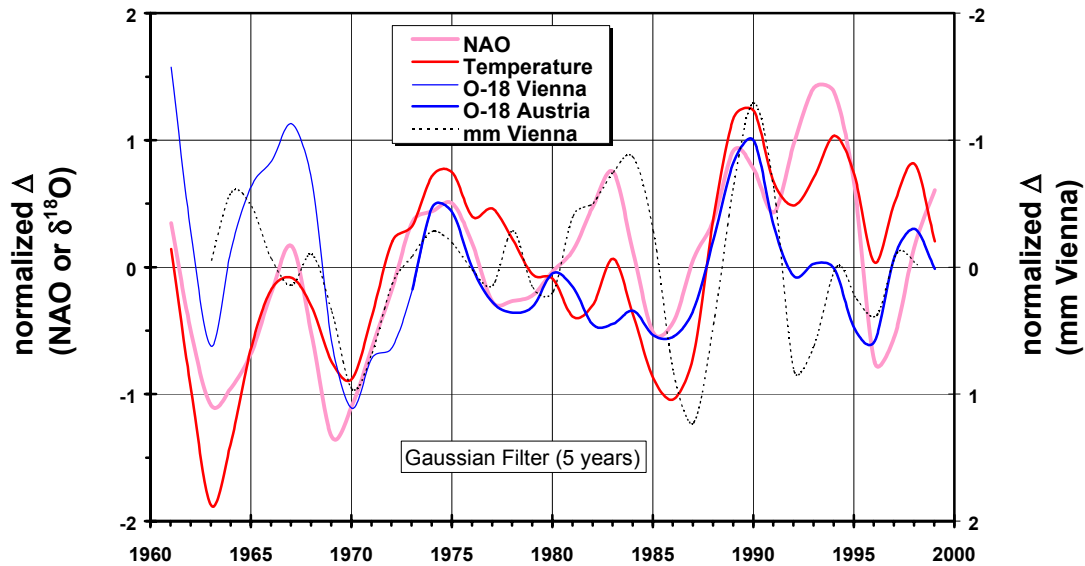


FIG. 4. Long-term fluctuations of $\delta^{18}\text{O}$ in precipitation, surface air temperature and NAO index.

Deuterium excess has widely been used as an additional parameter to identify the source region of water vapour. However, it turns out that a simple relationship cannot be established due to secondary fractionation processes, like snow formation or partial evaporation of raindrops below the cloud base. From the isotope time series a significant difference in the behaviour of the deuterium excess at neighbouring mountain and valley stations has been observed (Fig. 5a) [2]. There is a slight increase of the yearly mean of the deuterium excess with increasing altitude of the sampling station [7]. But moreover, the seasonal pattern of the deuterium excess is quite different. While the valley stations (e.g. Innsbruck) exhibit the expected minimum in summer, the mountain stations show a distinct maximum (ca. 15 ‰) between June and October. This is also the period with the seasonal maximum of precipitation.

In contradiction to these findings, the deuterium excess from a valley station at the northern border of the Alps showed a similar time dependence like that of the mountain stations (d-maximum in summer), but at a lower level (Fig. 5b, Weyregg and Feuerkogel). From this it was supposed that there might be a difference in the d-excess between the weather and the lee side of mountains. To prove this, old samples from a former observation station nearby in the shadow of the mountains were analyzed (Ebensee, Fig. 6). The values differ significantly from those of Feuerkogel and Weyregg, there is no summer maximum. There is a difference of about 3 ‰ between the average d-excess at Feuerkogel and at Ebensee, although the horizontal distance between these two stations is only three kilometers. Evaporation and isotopic exchange during the falling of the raindrops has obviously an important influence on the d-excess. Whereas the transport of air moisture on the weather side of the mountains takes place also in lower air layers, the humid air masses ascend when reaching the foot hills of the mountains (Fig. 6). On the lee side of the mountains, the humid air masses proceed in a higher altitude. Both, the ascent of the moisture at the slope of the mountains as well as the bigger height of fall of the raindrops in the shadow of the mountains lead to an “altitude” effect of the d-excess. Investigations of single events will help to understand the observed variability.

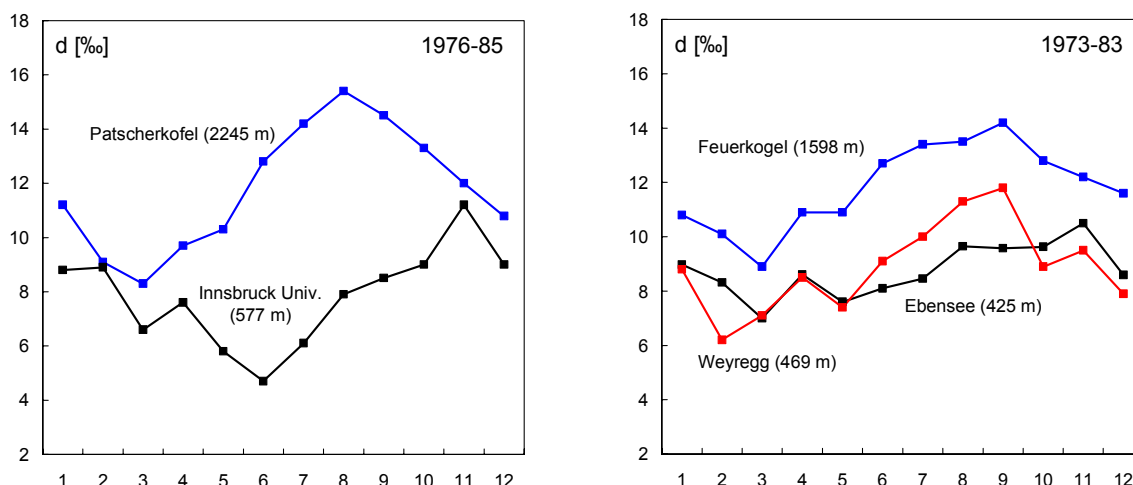


FIG. 5. a) Seasonal variations of deuterium excess in precipitation at a mountain station (Patscherkofel, 2245 m a.s.l.) and a valley station nearby (Innsbruck, 577 m a.s.l.) in the Eastern Alps [2]. b) Seasonal variations of deuterium excess in precipitation at Weyregg (469 m a.s.l.), Feuerkogel (1598 m a.s.l.) and Ebensee (425 m a.s.l.) (see profile Fig. 6).



FIG. 6. Orographic position of the sampling stations Weyregg, Feuerkogel and Ebensee (profile NW-SE).

3. STATISTICAL ANALYSIS OF BACK TRAJECTORIES AT PATSCHERKOFEL AND VILLACHER ALPE DURING JULY AND AUGUST 1998

As a first step into a comprehensive analysis of the meteorological effects on the isotope patterns, the differences in the isotope content of precipitation water during July and August 1998 between the stations Patscherkofel and Villacher Alpe were studied with help of trajectory statistics. While in July the $\delta^2\text{H}$ - and $\delta^{18}\text{O}$ -values at Villacher Alpe are much higher than at Patscherkofel, in August both stations show similar values (Table I). The high $\delta^2\text{H}$ - and $\delta^{18}\text{O}$ -values at Villacher Alpe in July are attributed to a strong Mediterranean influence. This interpretation is also supported by the low ^3H -content. Both sites are elevated points in the Alps. Patscherkofel is north of the main Alpine ridge and Villacher Alpe south of it (Fig. 1).

The trajectory model FLEXTRA uses 3-dimensional wind fields (including the vertical component of the wind) from the ECMWF in Reading [8, 9]. Trajectories are calculated -240 h (= 10 days) backwards and are released each hour at 3 levels, 100 m above model topography, 700 hPa (approx. 3000 m) and 500 hPa (approx. 5000 m). For statistical analysis 24*31 trajectories are compiled for each month and end point. The area for which the analysis is done spans 24°W to 25°E and 31°N to 65°N.

Table I. Isotopic composition of precipitation water at Patscherkofel and Villacher Alpe, summer 1998

	Precipitation sum [mm]	$\delta^2\text{H}$ [‰]	$\delta^{18}\text{O}$ [‰]	d [‰]	^3H [TU]
Villacher Alpe, July	171	-14,8	-2,30	3,6	9,7
Villacher Alpe, August	132	-51,9	-8,25	14,1	15,3
Patscherkofel, July	116	-59,7	-9,11	13,2	19,3
Patscherkofel, August	116	-54,3	-8,41	13,0	18,0

The isotope data are based on monthly precipitation amounts. Therefore, the contribution of each precipitation event to the total monthly amount has to be considered. This is done by weighting each trajectory with the hourly precipitation sum at the each station (= end point of the trajectory). Only trajectories connected with precipitation events at their end points are of interest, therefore trajectories without precipitation are not considered (weight = 0). For statistical trajectory analysis a grid is used with horizontal resolution of 0.5° degrees and the vertical column is divided in 500 m intervals.

- The time (hours) the trajectories spend in each grid square is added up to analyse the geographical origin of the air masses and
- the time the trajectories spend in each height interval gives a vertical cross section along the path of the trajectories to the stations.

Both variables are presented as relative variables, divided by the total sum of hours over the total area and, in case of the vertical cross section, the total sum of hours at each time step.

Table II gives an overview about some precipitation characteristics for July and August 1998. These simple parameters provide a first idea concerning the possible causes of the differences in isotope ratios: During both months precipitation amounts and intensities are higher at Villacher Alpe, but the differences between the two stations are much more pronounced in July. In July, hourly precipitation sums less than 1 mm are observed at Patscherkofel in 85 hours, at Villacher Alpe only in 44 hours, but strong precipitation events are found more often at Villacher Alpe. The strong differences of the precipitation characteristics between the two stations in July are due to a high portion of convective precipitation events at Villacher Alpe, e.g. thunderstorms, connected with strong upward motion of air. At Patscherkofel, convective precipitation events are much less dominant. In August, precipitation sums, intensities and frequency distributions are much more similar at both stations.

Table II: Precipitation characteristics for Patscherkofel and Villacher Alpe, summer 1998

	Precipitation sum [mm]	Hours of precipita- tion	Precipitation inten- sity [mm/h]
Villacher Alpe, July	171	87	1.96
Villacher Alpe, August	132	75	1.76
Patscherkofel, July	116	128	0.90

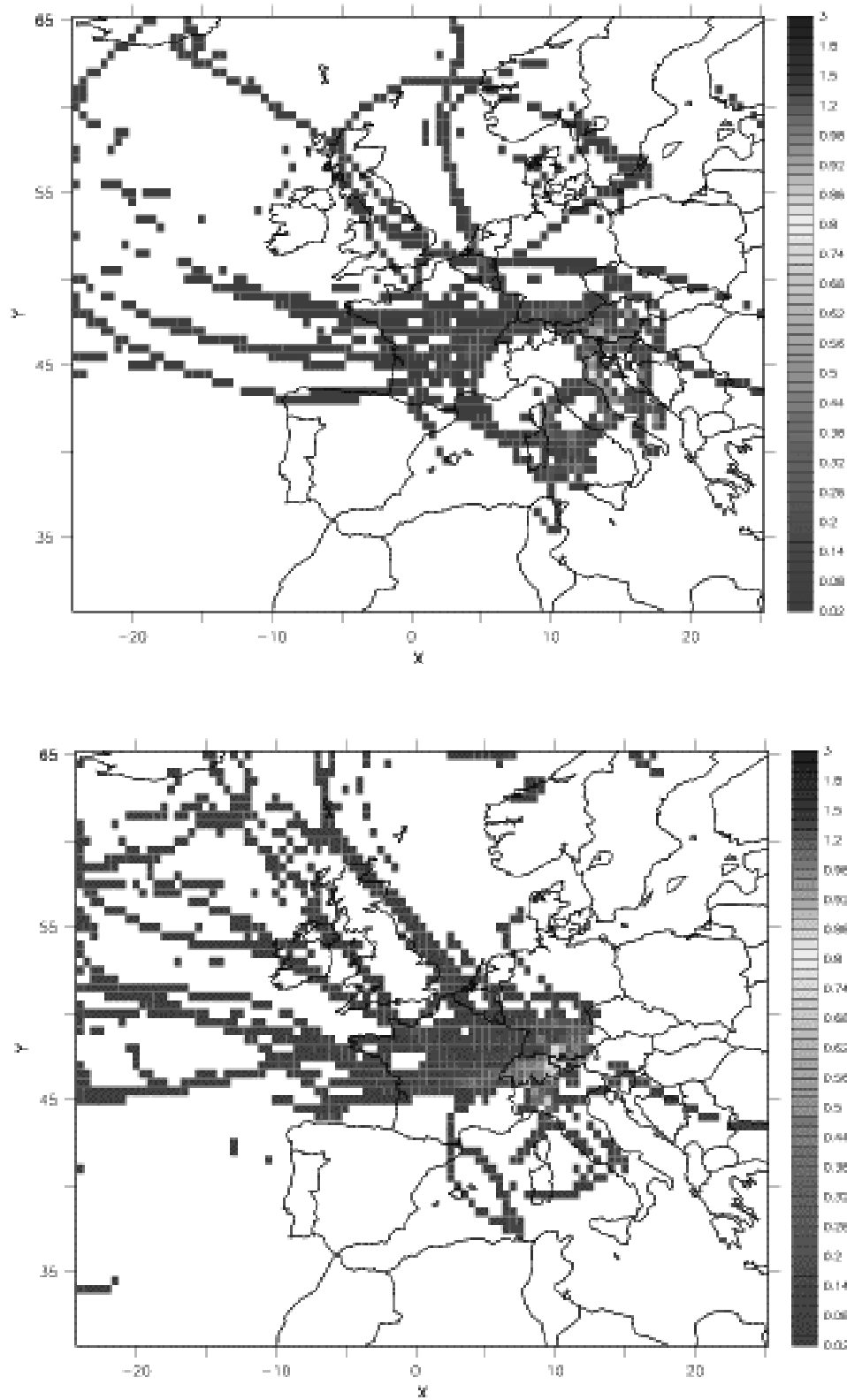


FIG. 7. Relative 700 hPa trajectory residence times in each of the $0,5 \times 0,5$ degree squares for Patscherkofel (upper panel) and Villacher Alpe (lower panel) during July 1998.

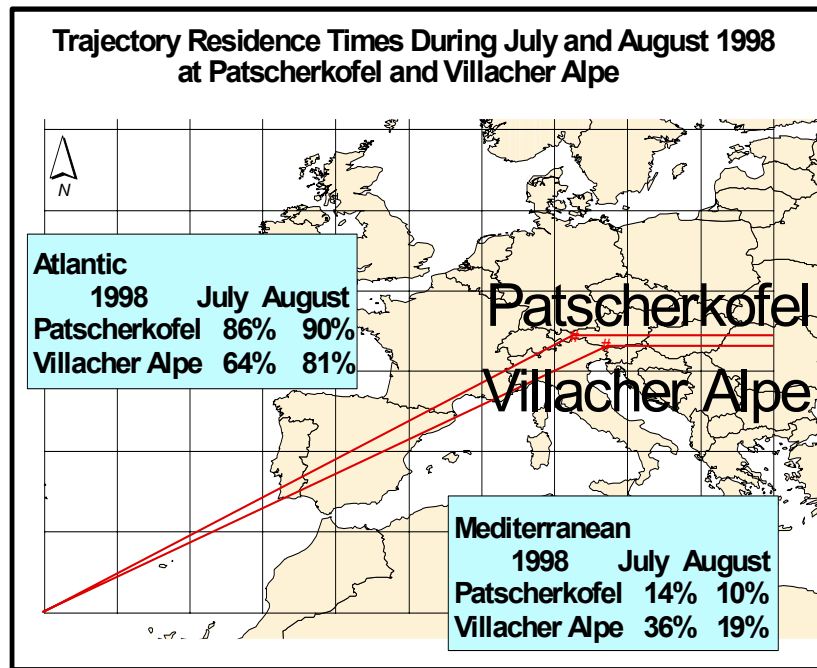


FIG. 8. Residence times of 700 hPa back trajectories ending at Patscherkofel and Villacher Alpe during July and August 1998 added up over the 'Mediterranean' and the 'Atlantic'. The red lines separate both subregions.

The number of precipitation hours (Table II) is equal to the number of trajectories for the specific month. Fig. 7 shows an example of the calculated relative residence times of the trajectories for both stations in July 1998. The arrival height of the trajectory is 700 hPa, a height, where it can be assumed that most of the precipitation is formed. Of course, the relevant height, where most of the precipitation is produced, may vary for different precipitation events and will depend on the season too, but this will be an objective for further investigations. Fig. 7 shows that in July Villacher Alpe is highly influenced by air masses originating in the Mediterranean, whereas Patscherkofel is nearly free from such influence. Due to the little spatial extension of each grid square ($0,5 \times 0,5$ degrees), the relative residence times are very small (only up to 3% of the air masses are transported over a special grid element). To give an overview, we summarised the residence times for two regions of origin, the Atlantic and Mediterranean (Fig. 8). In both months, 10% - 14% of the air masses connected with precipitation at Patscherkofel originate in the Mediterranean. The remaining precipitation events arrive at Patscherkofel from west or north, originating over the Atlantic. In general, the portion of precipitation events with origin in the Mediterranean is higher at Villacher Alpe compared to Patscherkofel, but note the strong differences between July and August due to strong influence from the Mediterranean in July at Villacher Alpe.

Vertical distribution of the trajectory residence times (Fig. 9) shows that the majority of trajectories ascends to the end point. This is to be expected with trajectories which are connected with precipitation at the end points. Moist air masses cool while ascending and release their moisture as precipitation. In July even the very high 500 hPa trajectories ascend from low levels at Villacher Alpe due to the high portion of convective precipitation events, whereas at Patscherkofel only a minority of these trajectories ascends.

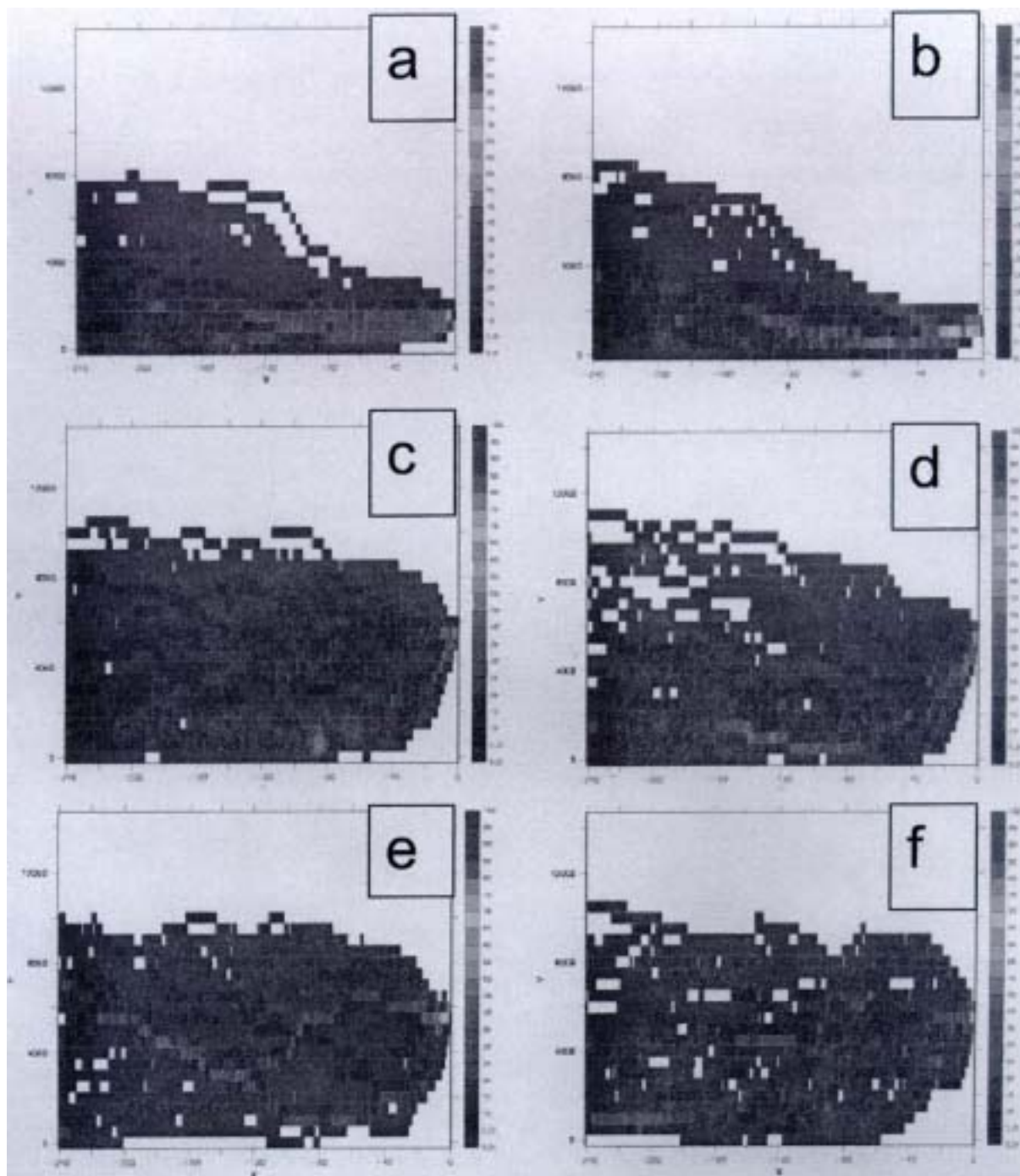


FIG. 9. Vertical distribution of trajectory residence times for trajectories arriving at 100 m above model topography in July 1998 (a and b) and for trajectories arriving at 500 hPa in July (c and d) and August 1998 (e and f) at Patscherkofel (left) and Villacher Alpe (right).

The trajectories arriving 100 m above model topography at Patscherkofel in July 1998 are frequently moving close to the surface throughout the 240 hours. Uptake of moisture can happen all the way to the trajectory end point. In contrast, at Villacher Alpe the majority of trajectories moves along the lowest grid boxes only during the last 80 to 120 hours prior arrival at the trajectory end point. From 240 to 120 hours they descend from higher levels. One can conclude that the moisture source area is different at both trajectory end points in July 1998. Villacher Alpe might receive a certain fraction of moisture originating in the Mediterranean, which Patscherkofel does not receive during July 1998. In August 1998 both end points might receive moisture from both moisture sources, the Atlantic and the Mediterranean.

4. CONCLUSIONS

- The stored samples of the close-meshed Austrian Network for Isotopes in Precipitation turned out to be an excellent material for isotope-climatological investigations. This applies for long-term trends as well as for local variations of isotope parameters.
- The long-term records show a good correlation between fluctuations of isotope ratios in precipitation and surface air temperature, but also other influences like changes in precipitation mechanisms are reflected. This finding applies also for the correlation with the NAO index.
- Local variations of the deuterium excess were found in the Alpine region, obviously a consequence of secondary fractionation processes and depending on the morphology of the investigation area.
- The statistical analysis of back trajectories promises to become a valuable instrument to trace the path and the isotopic evolution of a humid air mass. Precipitation sampling for isotope measurements on a monthly base will not be sufficient for such work, the samples should be taken on an event base.

REFERENCES

- [1] RANK, D., Das österreichische Niederschlagsisotopenmeßnetz, Mitteilungsblatt des Hydrographischen Dienstes in Österreich, Heft 70, Wien (1993) 72-76.
- [2] RANK, D., PAPESCH, W., Isotopenverhältnisse im natürlichen Wasserkreislauf – Indikatoren für Klimaänderungen, Barbara-Gespräche Payerbach 1998, Geoschule Payerbach, Wien (2001) 241-255.
- [3] ROZANSKI, K., GONFIANTINI, R., Isotopes in climatological studies, IAEA Bulletin 32, No. 4, Vienna (1990) 9-15.
- [4] GNIP (Global Network for Isotopes in Precipitation), IAEA, Vienna (1996).
- [5] AUER, I., BÖHM, R., SCHÖNER, W., Austrian long-term climate: Multiple instrumental climate time series in central Europe (1767-2000), Österreichische Beiträge zu Meteorologie und Geophysik, Wien (2001) in press.
- [6] CLIMATIC RESEARCH UNIT, <ftp://ftp.cru.uea.ac.uk/data/> (2001).
- [7] ROCHE, M.A., GONFIANTINI, R., FONTES, J.C., ABASTO, N., NORIEGA, L., The Isotopic Composition of Precipitation on the Andes and Amazon of Bolivia, Symposium on Isotope Techniques in Water Resources Development and Management, IAEA, Vienna (1999).
- [8] STOHL, A., WOTAWA, G., A method for computing single trajectories representing boundary layer transport, Atmos. Environ. **29** (1995) 3235-3239.
- [9] STOHL, A., WOTAWA, G., SEIBERT, P., KROMP-KOLB, H., Interpolation errors in wind fields as a function of spatial and temporal resolution and their impact on different types of kinematic trajectories, J. Appl. Meteor. **34** (1995) 2149-2165.

**RESEARCH ON CLIMATE CHANGE AND VARIABILITY AT THE
ABDUS SALAM INTERNATIONAL CENTRE FOR THEORETICAL PHYSICS***
(Abstract)

F. GIORGI, F. MOLTENI

Abdus Salam International Centre for Theoretical Physics,
Trieste, Italy

The Physics of Weather and Climate Section at the Abdus Salam International Centre for Theoretical Physics, established in 1998, is currently performing research on different aspects of climate variability, dealing with both natural and anthropogenic aspects of climate changes. In addition to performing diagnostic work on multi-decadal observational datasets and climate simulations carried out in major research centres, the PWC section has been developing its own climate modeling capability, which is focused on three main areas:

- a) modeling of regional climate change;
- b) seasonal forecasting at global and regional scale;
- c) development of simplified models of the general circulation.

On topic a), research on different aspects of anthropogenic climate change is being carried out using the Regional Climate (RegCM) developed by Giorgi and collaborators at the National Centre for Atmospheric Research. Time-slice experiments with a high-resolution atmospheric GCM, comparing current climate conditions with future climate scenarios in selected decades, are also planned for the near future.

On topic b), a strategy based on ensembles of high-resolution simulations with atmospheric GCM's, using sea surface temperature anomalies predicted by lower-resolution coupled models from other institutions, is currently under experimentation. A one-way nesting of RegCM into the GCM simulations will also be tested.

On item c), a 5-layer atmospheric GCM with simplified physical parameterizations has been developed. This model has a very small computational cost compared with state-of-the-art GCMs, and is suitable for studies of natural climate variability on inter-decadal and inter-centennial time scales. It is planned to couple this model to simplified ocean models of different complexity, from a simple, static mixed layer model, to simplified models of the tropical Pacific circulation suited to the simulation of the El Niño phenomenon. A joint project with the IAEA-MEL Laboratory in Monaco has been established, to validate the statistics of such a coupled model against multi-decadal records of oceanic temperatures deduced from isotopic analysis of coral samples in the Pacific.

* Only an abstract is given here as the full paper was not available.

**PALAEOCLIMATE ARCHIVES I
GROUNDWATER**

(Session 2)

Chairpersons

R. GONFIANTINI
Italy

W.M. EDMUNDS
United Kingdom

THE PALAEOHYDROLOGY OF COASTAL AQUIFERS OF EUROPE**(Abstract)*

W.M. EDMUNDS

British Geological Survey, Wallingford, Oxon, United Kingdom

The PALAEAUX project, funded by the European Community, has brought together geochemical, isotopic and hydrogeological information on coastal groundwaters across Europe in a transect from the Baltic to the Canary Islands. These data have been interpreted in relation to past climatic and environmental conditions as well as extending and challenging concepts about the evolution of groundwater near the present day coastlines. Freshwater of high quality originating from different climatic conditions to the present day and when the sea level was much lower is found at depth beneath the present coast in several countries. The implications of the scientific results for management of aquifers in European regions are considered.

Results show that information on palaeotemperature, past precipitation and recharge regimes as well as air mass circulation can be deduced from the geochemical and isotopic evidence contained in European coastal aquifers. An age gap can be recognized in some aquifers which indicates that no recharge took place at the time of the last glacial maximum (LGM), for example in UK and Belgium. This indicates that these areas were free of ice cover but sealing due to permafrost was effective. Groundwaters from Estonia have $\delta^{18}\text{O}$ values of approximately 22‰ which demonstrates that recharge took place directly beneath the Scandinavian ice sheet during the LGM. Noble gas recharge temperatures supported by stable isotopic data provide convincing evidence in aquifers from northern Europe (UK, Denmark, Belgium, Switzerland) that recharge occurred during the cooler climates prior to the LGM and that recharge temperatures (soil air temperatures) were some 6°C colder than at the present day.

In southern Europe the radiocarbon ages indicate continuity of recharge through the LGM. Noble gas recharge in the Aveiro Cretaceous aquifer also indicate as elsewhere, that atmospheric cooling of 5–6°C occurred before and during the LGM. However in contrast to northern Europe, an enrichment in $\delta^{18}\text{O}$ of around 0.6‰ is found in the late Pleistocene recharge waters, and is considered to reflect the enrichment in the Pleistocene ocean water as well as the constancy in the source of moisture from the Azores region of the Atlantic as at the present day. The overall results emphasize that the stable isotope signal in palaeowaters may either reflect the source or the temperature of the precipitation.

For most of the past 100 000 a sea levels considerably below those of the present day provided an opportunity for recharge and movement of groundwater beyond the present coastline as well as emplacement on shore to greater depths than allowed by the present day flow regime. The greatest recorded depth of palaeo-fresh water (to about –500 m) is found in the UK East Midlands aquifer. The timescale of this groundwater movement, shown by radiocarbon data which have been calibrated and extended using chemical tracers, probably represents a continuous sequence of recharge over 100 000 a, supporting the evidence from speleothem growth for infiltration of groundwater through the Devensian glacial period. In Estonia, movement of colder palaeowaters took place to depths of –250 m and excess dissolved gases found in these waters indicate recharge beneath the ice sheet. The model, proposed by Boulton et al., for deep groundwater circulation due to high heads imposed by

*Only an abstract is given here as the full paper was not available.

the ice sheets has been closely examined in the present programme but no evidence can be found from geochemical and isotopic data together with local modelling.

In several regions waters of Holocene age have been recorded at the coast (as in the Dogger aquifer of the Caen and Atlantic coast regions of northern France) which represents recharge of marine or estuarine water during the Flandrian (Holocene) transgression. The use of borehole hydrogeophysical logging has helped to confirm the complex stratification that may exist beneath present day coastlines. Freshwater and saline water (of modern or ancient origins) may be found side by side (as in the south coast of UK) related to structural and palaeohydrogeological controls. Direct as well as indirect evidence is found from the present study that fresh or brackish water, recharged during the late Pleistocene, is found in aquifers currently offshore (off the North Sea coast of Denmark, the Channel coast of UK and Portugal, for example). This is consistent with results from the drilling off the eastern seaboard of the USA where fresh/brackish waters were proven to depths of 300 m to a distance of 100 km from the modern coasts. The results of modelling show that such features may take tens of thousands of years to erase.

The main attribute of palaeowaters in terms of water quality is their high bacterial purity, total mineralization often less than that of modern waters and being demonstrably free of man-made chemicals. As a result of long residence times, some palaeowaters may be enriched in some beneficial trace elements whilst others especially in reducing environments may have high iron or other species requiring treatment.

In Estonia and in the UK freshwaters found at depths up to 300 m in aquifers of Mesozoic to Palaeozoic age, are of lower salinity than the present day recharge. Very low Cl in the East Midlands aquifer is almost entirely the result of pre-industrial atmospheric inputs and the lack of increasing salinity with depth is strong evidence for a lack of cross-formational flow from adjacent formations containing more mineralized waters. Modern waters usually have additional solutes resulting from human impacts. In the Mediterranean coastal areas lower recharge leads to higher salinity conditions in both palaeo and modern waters.

The development of aquifers in Europe during the past 50–100 years by abstraction from boreholes has generally disturbed flow systems that have evolved over varying geological timescales and especially those derived from the late Pleistocene and Holocene. Hydrogeophysical logging has demonstrated time and quality-stratified aquifers resulting in mixed waters which are produced on pumping. A range of specific indicators including ^3H , $^3\text{H}/^3\text{He}$, ^{85}Kr , CFCs, as well as pollutants have been used to recognize the extent to which waters from the modern (industrial) era have penetrated into the aquifers, often replacing the natural palaeogroundwaters.

In the coastal regions where development pressures are already severe, many problems for management come together including issues relating to quantity and quality of water, seasonal demand, pollution risks and ecosystem damage. The water balance in many coastal areas may not be fully understood and wells are drilled or deepened without the awareness that palaeowaters belonging to a former recharge regime are being intercepted. In many areas there is induced replenishment as modern (often polluted) waters are drawn in. However in some aquifers the rates of withdrawal exceed the natural recharge and in effect a part of the resource is being mined.

In these areas there is a need for careful drilling to establish the age and quality layering as well as proper well completion. Proper monitoring networks and strategies need to be set up

to follow the position of interfaces in both the vertical and lateral planes. Correct management is needed often for seasonal demands: this may be beneficial, allowing winter recovery of water levels. The palaeowater however is a high quality resource and should be treated as a strategic reserve. It should receive priority for potable use and not be wasted for agricultural or industrial purposes which do not require waters of such high purity. Conservation targets are needed to allow for sustainability including ecosystem preservation. Changes may be needed in the administrative and legal framework to safeguard the use of the palaeowater reserves.

PALEOGROUNDWATERS OF THE VALRÉAS MIOCENE AQUIFER (SOUTHEASTERN FRANCE) AS ARCHIVES OF THE LGM/HOLOCENE TRANSITION IN THE WESTERN MEDITERRANEAN REGION

F. HUNEAU, B. BLAVOUX
Laboratoire d'Hydrogéologie,
Université d'Avignon,
Avignon, France

W. AESCHBACH-HERTIG, R. KIPFER
Swiss Federal Institute of Technology (ETH),
Swiss Federal Institute of Environmental Science and Technology (EAWAG),
Dübendorf, Switzerland

Abstract. An isotopic survey, including ^{18}O , ^2H , ^{13}C , ^{14}C , ^3H and noble gases, has been carried out since 1998 on groundwaters of the Valréas Miocene aquifer. This aquifer is situated in the South of France, close to the Rhône valley. It consists of calcareous cemented sandstones interbedded with marl and sand lenses. A major paleo-ria, resulting from the drastic Messinian crisis, cuts the Miocene sediments. During the Pliocene, it was infilled with marl and clays. This Pliocene cover keeps the aquifer confined in the South of the study area. A strong isotopic contrast is found between unconfined and confined aquifer. The depletion in the water molecule stable isotopes occurs around 20 000 years BP and points out the transition from the Last-Glacial to Holocene. The constant value of deuterium excess suggests persistence of the atmospheric circulation pattern over the South of Europe since the end of the Pleistocene. The isotopic signature of the Miocene aquifer groundwaters indicates the perfect integration of Southern France palaeoprecipitation into the present-day regional atmospheric frame. A reliable estimate of the warming during the Pleistocene-Holocene transition could only be derived from stable isotopes by calibrating them against noble gas temperatures.

1. INTRODUCTION

Climatic change during the Late Quaternary has been inferred from isotopic composition of groundwater in various places all over the world, in Africa [1, 2, 3], North America [4, 5], Asia [6, 7], Australia [8] and Europe [9, 10, 11]. Only a few of these studies concern Mediterranean regions [12, 13, 14] and none of them the Northern part of the Western Mediterranean basin. Comparison of isotopic composition of dated groundwater in confined and unconfined aquifers can supplement paleoclimatic inferences based on pollen and other currently used paleoclimatic indicators. Stable isotopes analyses of groundwater ($\delta^{18}\text{O}$ and $\delta^2\text{H}$) yield additional information on the Late Pleistocene moisture sources and regional atmospheric circulation.

The understanding of paleoclimatic conditions prevailing during the recharge of groundwaters is obviously an important parameter which contributes to the understanding of complex aquifer systems. Such suitable aquifers are sparse and mainly located in large sedimentary basins (Paris-London basin, Great Artesian basin of Australia, Hungarian plain, etc ...), this paper is devoted to a small sedimentary basin from Southeastern France.

The Valreas Miocene Aquifer is an important resource for both domestic and agricultural water supplies in Provence. Declining potentiometric levels are of concern for the long term sustainability of the resource. An isotope study aimed at the estimation of groundwater residence time and paleorecharge conditions has been carried out from 1997 to 2000 in order to contribute to the definition of the system and to set up the basis of a proper managing of the aquifer.

2. HYDROGEOLOGICAL SETTING

The Valreas Miocene Aquifer is located close to the Rhône Valley, within a small sedimentary basin of almost 500 km² (Fig. 1). It is formed of multilayered sands, sandstone, clays and marls, with a maximum thickness of 600 m and an average permeability around 10⁶ m.s⁻¹ [15, 16]. A major paleo-ria resulting from the drastic Messinian crisis cuts the Miocene sediments. During the Pliocene, it was infilled with poorly permeable sediments, mainly marls and clays interbedded with some sand lenses. In the Southern part of the basin, the Pliocene cover keeps the Miocene aquifer confined and most of the boreholes tap the Miocene aquifer through a marlaceous layer of 100 to 300 m thickness. The recharge area is located in the Northern part of the basin where Miocene sediments out crop, at an elevation of about 240 m. The general direction of groundwater flow is oriented from the NE to the SW of the basin and then in direction of the Rhône Valley through the Lez River Valley.

Samples from boreholes tapping the unconfined and the confined Miocene aquifer were collected by means of submersed pumps pre-existing on these irrigation wells. Hydrochemistry, radionuclides (³H, ¹⁴C) and stable isotopes ratios ($\delta^{13}\text{C}$, $\delta^2\text{H}$ and $\delta^{18}\text{O}$) were measured.

3. RESULTS

A strong isotopic contrast is found between the unconfined and the confined parts of the aquifer. This suggests the existence of long residence time waters in the confined aquifer. Radiocarbon activities close to the detection limit and the enrichment in $\delta^{13}\text{C}$ imply isotope exchange between groundwater and the aquifer matrix. Radiocarbon ages have been corrected by means of the Fontes & Garnier model [17] which accounts for such phenomena. This provides ages up to 30-35 ka within the confined aquifer. Note that the record covers the entire period rather uniformly, there is no indication of an “infiltration gap” at the Last Glacial Maximum as observed in other European aquifers [18, 19].

An isotopic shift is observed (Fig. 2) between recent groundwaters from the recharge area ($\delta^{18}\text{O} \approx -7\text{‰}$; $\delta^2\text{H} \approx -45\text{‰}$) and old groundwaters confined under Pliocene sediments ($\delta^{18}\text{O} \approx -9\text{‰}$; $\delta^2\text{H} \approx -60\text{‰}$).

The isotopic signature of modern recharge groundwaters is consistent with local precipitation [20] whereas old groundwaters are depleted by up to 2‰ in $\delta^{18}\text{O}$ and 15‰ in $\delta^2\text{H}$. This indicates that old groundwaters have been recharged under colder climatic conditions than at present time. The depletion in stable isotopes occurs around 18-20 ka and points out the transition from the Late-Glacial to Holocene [21].

All the data match the World Meteoric Water Line and show a good agreement with the regional meteoric water line defined by Celle-Jeanton *et al.* [22] for the Western Mediterranean area ($\delta^2\text{H}=8\delta^{18}\text{O}+13.7$). The deuterium excess ($d=\delta^2\text{H}-8\delta^{18}\text{O}$) does not show any strong variations from the Pleistocene to the Holocene and remains close to its present-day value (Fig. 3). 85% of the data set show a deuterium excess between 10‰ and 14‰ that is to say between Atlantic ($d \approx 10\text{‰}$) and Western Mediterranean influences ($d \approx 14\text{‰}$). This is in good agreement with the observations made by Celle [20] on the atmospheric circulation affecting the study area.

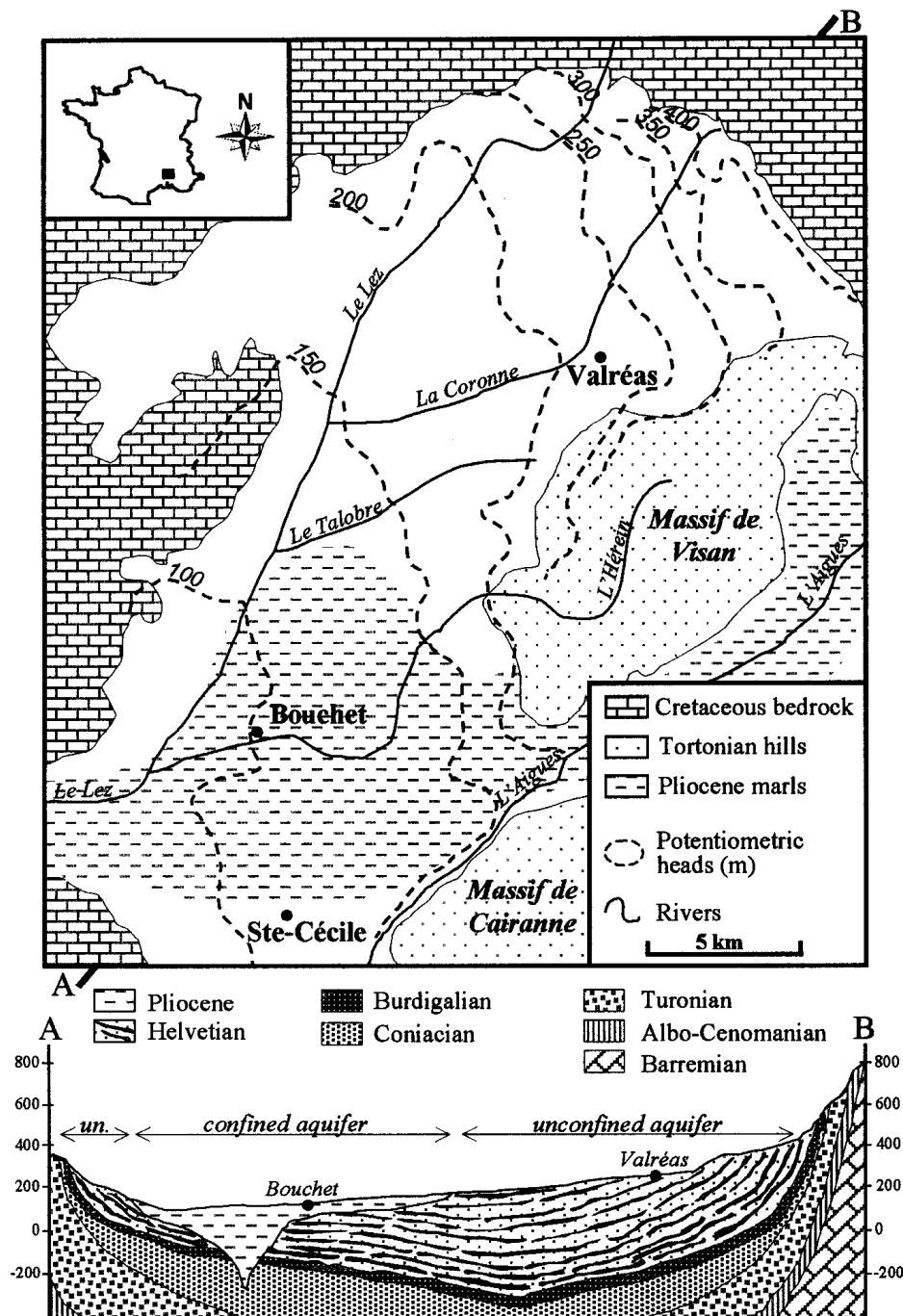


FIG. 1 : Study area, location of the sampled boreholes and geological cross-section of the Valréas Miocene basin.

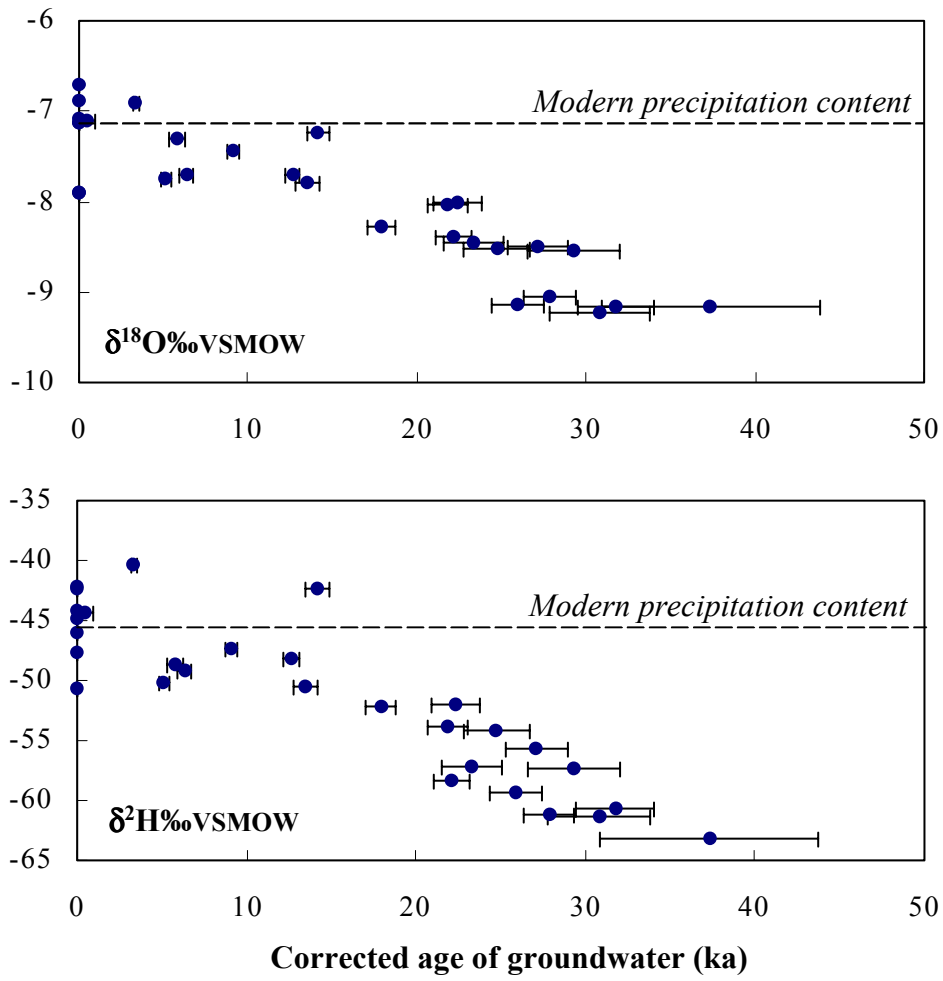


FIG. 2. Evolution of the stable isotopic signature of groundwaters with residence time within the Miocene aquifer.

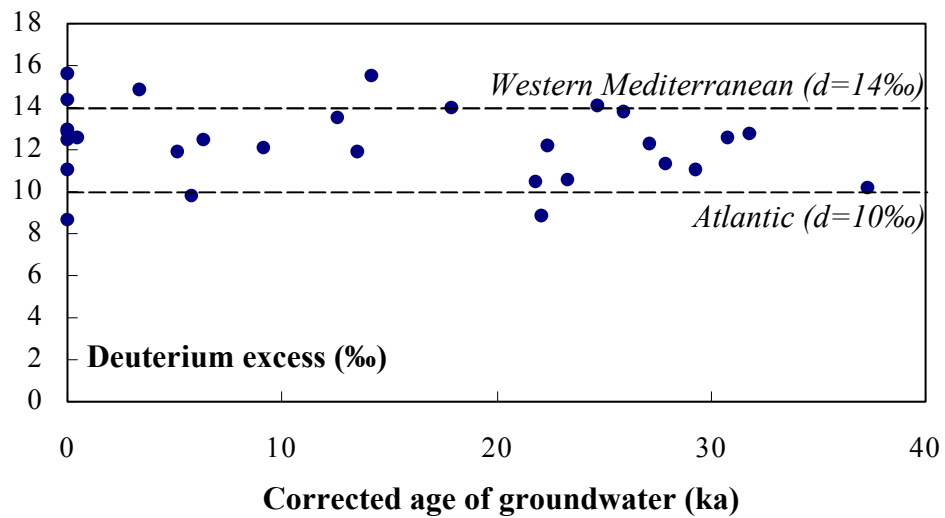


FIG. 3. Deuterium excess (d) against groundwater residence time.

4. DISCUSSION

The deuterium excess in precipitation is usually interpreted as an isotope signal depending on climate conditions during evaporation. So, from a palaeoclimatic point of view, our results suggest that the circulation pattern of the atmosphere over the South of Europe remained unchanged since the Last-Glacial Maximum and confirm the observations made in Western and Central Europe [9].

This study provides strong evidence that deuterium excess in Mediterranean precipitation has remained constant for more than 30 ka. Thus, it suggests a constant relative humidity over the Atlantic Ocean and the Western Mediterranean from the last glacial period up to the present time.

Estimation of the magnitude of the warming that occurred at the Pleistocene-Holocene transition on the basis of the stable isotope data is difficult, because slopes of the $\delta^{18}\text{O}$ /temperature relationship derived from modern data may not be appropriate for long-term climate changes. Thus, noble gas measurements on 25 boreholes were used to quantify the climate signal recorded in the Valréas Miocene aquifer. Palaeorecharge temperatures indicate an increase of about 7°C during the Pleistocene-Holocene transition. The good correlation between noble gas temperatures and ^{18}O data provides a slope of the $\delta^{18}\text{O}$ /temperature relationship close to 0.22‰/°C (Fig. 4), clearly lower than present day seasonal or spatial slopes. This highlights the inadequacy of modern analogues [23, 24] to interpret stable isotopes in term of Pleistocene palaeotemperatures, and the need to locally calibrate the long-term $\delta^{18}\text{O}$ /temperature relationship.

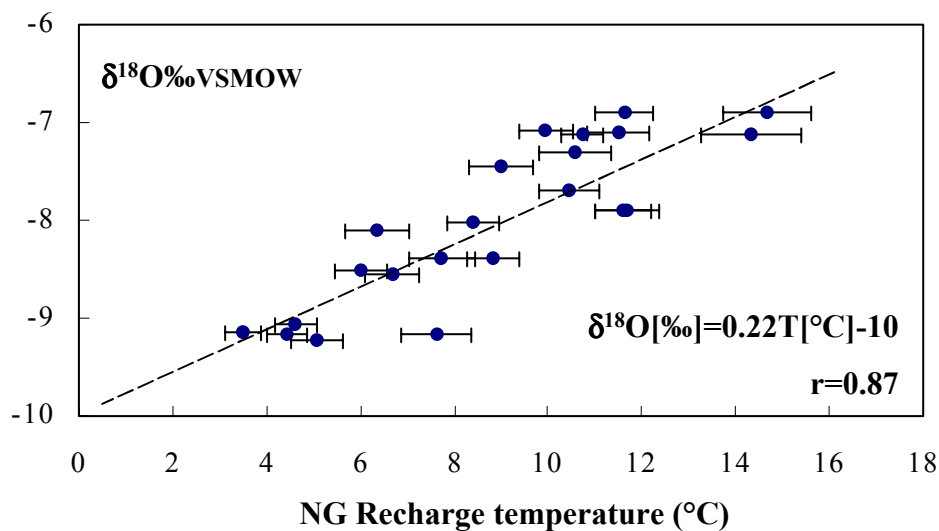


FIG. 4 : $\delta^{18}\text{O}$ /Noble Gas recharge temperature in Valreas Miocene aquifer groundwaters.

5. CONCLUSIONS

This isotopic study demonstrates the continuous recharge of the Miocene aquifer from the Last Glacial to present time. The depletion in heavy isotopes of the groundwaters with ^{14}C

ages of about 20 ka and higher in comparison to more recently recharged waters clearly marks the climatic transition from the Pleistocene to the Holocene.

In contrast, the deuterium excess remains uniform throughout the record, suggesting that the general cooling during the Late Pleistocene was not accompanied by a major change in source of water vapour recharging the aquifer.

Our data point out that the long term $\delta^{18}\text{O}$ /temperature relationship has to be locally calibrated in order to reconstruct palaeotemperatures from stable isotope data. This can be done by the noble gas results.

REFERENCES

- [1] FONTES, J.C, ANDREWS, J.N., EDMUNDS, W.M., GUERRE, A., TRAVI, Y., Paleorecharge by the Niger river (Mali) deduced from groundwater geochemistry, *Water Resources Research* **27** (1991) 199-214.
- [2] ANDREWS, J.N., FONTES, J.C., ARANYOSSY, J.F., DODO, A., EDMUNDS, W.M., JOSEPH, A., TRAVI, Y., The evolution of alkaline groundwater in the Continental Intercalaire aquifer of the Irhazer Plain, Niger, *Water Resources Research* **30** (1994) 45-61.
- [3] EDMUNDS, W.M., FELLMAN, E., GONI, I.B., Lakes, groundwater and palaeohydrology in the Sahel or NE Nigeria : evidence from hydrogeochemistry, *Journal of the Geological Society, London* **156** (1999) 345-355.
- [4] STUTE, M., SCHLOSSER, P., CLARK, J.F., BROECKER, W.S., Paleotemperatures in the Southwestern United States from noble gases in ground water, *Science* **256** (1992) 1000-1003.
- [5] DUTTON, A.R., Groundwater isotopic evidence for paleorecharge in U.S. High Plains aquifers, *Quaternary Research* **43** (1995) 221-231.
- [6] SHI, D., YIN, X., YIN, Z., A simulation study on the evolution of groundwater circulation systems in Cenozoic basins of Northern China, *Acta Geologica Sinica* **72** (1998) 100-107.
- [7] SUKHIJA, B.S., REDDY, D.V., NAGABHUSHANAM, P., Isotopic fingerprints of paleoclimates during the last 30,000 years in deep confined groundwaters of Southern India, *Quaternary Research* **50** (1998) 252-260.
- [8] LOVE, A.J., HERCZEG, A.L., LEANEY, F.W., STADTER, M.F., DIGHTON, J.C., ARMSTRONG, D., Groundwater residence time and palaeohydrology in the Otway Basin, South Australia : ^2H , ^{18}O and ^{14}C data, *Journal of Hydrology* **153** (1994) 157-187.
- [9] ROZANSKI, K., Deuterium and Oxygen-18 in European groundwaters – links to atmospheric circulation in the past, *Chemical Geology* **52** (1985) 349-363.
- [10] DARLING, W.G., EDMUNDS, W.M., SMEDLEY, P.L., Isotopic evidence for palaeowaters in the British Isles, *Applied Geochemistry* **12** (1997) 813-829.
- [11] WALRAEVEENS, K., Natural isotopes and noble gases in groundwater of the Tertiary Ledo-Paniselian aquifer in East and West Flanders, *Natuurwet. Tijdschr.* **78** (1998) 246-260.
- [12] SULTAN, M., STURCHIO, N., HASSAN, F.A., HAMDAN, M.A.R., MAHMOOD, A.M., EL ALFY, Z., STEIN, T., Precipitation source inferred from stable isotopic composition of Pleistocene groundwater and carbonate deposits in the Western desert of Egypt, *Quaternary Research* **48** (1997) 29-37.
- [13] MALIKI, M.A., KRIMISSA, M., MICHELOT, J.L., ZOUARI, K., Relationship between shallow and deep aquifers in the Sfax basin (Tunisia), *C. R. Acad. Sci. Paris, Earth and Planetary Sciences* **331** (2000) 1-6.

- [14] BAJJALI, W., ABU-JABER, N., Climatological signals of the paleogroundwater in Jordan, *Journal of Hydrology* **243** (2001) 133-147.
- [15] HUNEAU, F., Fonctionnement hydrogéologique et archives paléoclimatiques d'un aquifère profond méditerranéen, Etude géochimique et isotopique du bassin miocène de Valréas, Sud-Est de la France, PhD Thesis, University of Avignon, France (2000).
- [16] HUNEAU, F., BLAVOUX, B., Isotopic hydrogeology within the Miocene basin of Carpentras-Valreas (Southeastern France), In : Dassargues A. (Ed), Tracers and Modelling in Hydrogeology, Proceedings of the TraM'2000 Conference held at Liège, Belgium, May 2000, IAHS Publ. **262** (2000) 433-438.
- [17] FONTES, J.C., GARNIER, J.M., Determination of the initial ^{14}C activity of the total dissolved carbon : a review of the existing models and a new approach, *Water Resour. Res.* **15** (1979) 399-413.
- [18] ANDREWS, J.N., LEE D.J., Inert gases in groundwater from the Bunter Sandstones of England as indicators of age and palaeoclimatic trends, *Journal of Hydrology* **41** (1979) 233-252.
- [19] BEYERLE, U., PURTSCHERT, R., AESCHBACH-HERTIG, W., IMBODEN, D.M., LOOSLI, H.H., WIELER, R., KIPFER R., Climate and groundwater recharge during the last glaciation in an ice-covered region, *Science* **282** (1998) 731-734.
- [20] CELLE, H., Caractérisation des précipitations sur le pourtour de la Méditerranée occidentale, approche isotopique et chimique, PhD Thesis, University of Avignon, France (2000).
- [21] ROZANSKI, K., JOHNSEN, S.J., SCHOTTERER, U., THOMPSON, L.G., Reconstruction of past climates from stable isotope records of palaeo-precipitation preserved in continental archives, *Hydrol. Sciences J.* **42** (1997) 725-745.
- [22] CELLE-JEANTON, H., TRAVI, Y., BLAVOUX B., Isotopic typology of precipitation in the Western Mediterranean region at three different time scales, *Geophysical Research Letters* (accepted).
- [23] ROZANSKI, K., ARAGUAS-ARAGUAS, L., GONFIANTINI, R., Relation between long-term trends of oxygen-18 isotope composition of precipitation and climate, *Science* **258** (1992) 981-985.
- [24] FRICKE, H.C., O'NEIL J.R., The correlation between $^{18}\text{O}/^{16}\text{O}$ ratios of meteoric water and surface temperature : its use in investigating terrestrial climate change over geologic time, *Earth and Planetary Science Letters* **170** (1999) 181-196.

OXYGEN ISOTOPE COMPOSITION AS LATE GLACIAL PALAEOCLIMATE INDICATORS OF GROUNDWATER RECHARGE IN THE BALTIC BASIN

R. MOKRIK

Vilnius University and Institute of Geology, Vilnius, Lithuania

J. MAZEIKA

Institute of Geology, Vilnius, Lithuania

Abstract. Several hypotheses were established to explain low $\delta^{18}\text{O}$ values of groundwater which have been found in the Estonian Homocline. Traces of depleted groundwater were found also in other parts of the Baltic Basin near the shoreline. From data collected in this and previous studies, the $\delta^{18}\text{O}$ values of groundwater in most aquifers are known to range from -7.7 to -13.9‰. However, the groundwater in Estonia in the Cambrian-Vendian aquifer system has significantly lower $\delta^{18}\text{O}$ values, which vary mainly from -18 to -22.5‰. The overlying Ordovician-Cambrian aquifer is also depleted in ^{18}O , but, as a rule, the degree of depletion is several per mille less than in case of the Cambrian-Vendian aquifer. The thickness of the depleted water in Estonia reaches 450 m. At similar depths beneath Gotland Island (Sweden Homocline), groundwater has significantly higher $\delta^{18}\text{O}$ values (from -5.7 to -6.1‰). A hydrogeologic model, depicting conditions during the pre Late Glacial, and accounting for hydraulic connections between the lake and river systems through taliks in permafrost, was developed to explain the observed groundwater isotope data. According to the adopted model, penetration of isotopically depleted surface waters could have reached depths of up to 500 m, with subsequent mixing between subglacial meltwater and old groundwater of Huneborg-Denekamp time. Traces of this penetration were discovered only near the shoreline, where $\delta^{18}\text{O}$ values vary from -12 to -13.9‰ and ^{14}C is below 4%. In the territory of the Estonian Homocline, the hydraulically close connection via the Cambrian-Vendian aquifer between talik systems of the Gulf of Riga and the Gulf of Finland existed through permafrost before the Late Glacial. This was due to subglacial recharge during the recessional Pandivere (12 ka BP) and Palivere (11.2 ka BP) phases, which is also associated with recharge of isotopically depleted groundwater.

1. INTRODUCTION

The Quaternary glacial history on formation of groundwater recharge of the Baltic Basin is still uncertain. Several hypotheses were built up because very low $\delta^{18}\text{O}$ values of groundwater have been found in Estonian Homocline. The first of them was related with the aquaglacial recharge from Baltic Ice Lake (BIL) [8] and the second with cryogenic metamorphization in the presence of permafrost during the Pleistocene [4]. In the first case the problem of the mechanism of the penetration of glacial meltwater of BIL into the Cambrian-Vendian aquifer remained unclear. It was supposed that it became possible owing to the existence of lowered pressures in the aquifer during the glacial period, what further caused the instant penetration of surface water from BIL through the aquitard clays of the Lontova Regional Stage [8]. However, taking into consideration the quite good screening properties of clays of the Lontova Regional Stage (k_0/m_0 ranges within the interval from 10^{-7} to $5 \times 10^{-6} \text{ d}^{-1}$), the more intensive areal penetration of the BIL water from above is hardly real. Besides, in the opposite case, it is difficult to imagine in the large scale the mechanism of full exclusion of the “older” groundwater from the Cambrian-Vendian aquifer. The low ^{14}C concentrations below 3-4 pmC could suggest that the age of the groundwater was about 26-34 ka BP, which indicated, that the recharge by cold climate condition took place much earlier, at the time when the Estonian territory was not covered by Late Glacial ice sheet. The model of paleo-recharge of the Cambrian-Vendian groundwater formed during the epoch of Denekamp Interstadial in the

western part of the Estonian Homocline, where aquitard clays of the Lontova Regional Stage are replaced in facies by the terrigenous complex of the Voosi Formation deposits, was proposed by R. Mokrik [4]. It follows from the aforesaid that the model of groundwater forming in Cambrian-Vendian aquifer is complicated and requires further elaboration. In this work there is considered more extended model on possibilities of subpermafrost communication of aquifers with the isotopically depleted surface waters through the talik zones before the Last Glacial period taking into account also later effects as subglacial recharge after glacier degradation, BIL influence, modern water intrusion from the Baltic Sea, modern recharge in terrestrial part of Baltic artesian Basin. This model firstly was analyzed in [5, 6].

The Quaternary period in the Baltic region is characterized by a number of repeated glaciations related with isostatic movements of the Earth's crust caused by the load of glaciers. In the epochs before the Menapian, Elsterian, Saalian and Late Weichselian Glacial, there formed the permafrost zones, the depth of which could reach 450 m in the Estonian Homocline. The surface permafrost before Late Weichselian Glacier froze the discharge areas of the Ordovician-Cambrian and Silurian-Ordovician shallow aquifers. This freezing increased the hydrostatic pressure of shallow groundwater and caused a squeezing depleted by the isotopic composition of groundwater via taliks downwards to the Cambrian-Vendian aquifer. The best conditions for groundwater to penetrate into the Cambrian-Vendian aquifer existed only on the territory of the West Estonian Homocline and on the present Gulf of Finland domain. During the Huneborg Stadial time (34–35 ka BP) the Cambrian-Vendian aquifer could be recharged by arctic meteoric water. The Denekamp subsequent permafrost (26 ka BP) initiated percolation into the Cambrian-Vendian aquifer above the layered subsurface groundwater and the deeper underground freezing. The manifestation of such a process is observed at present in the West Siberian Platform [3]: between underground ice and freezing water the redistribution of salts occurred simultaneously with the forming of underground ice, calcium carbonates and calcium sulphates, which have reached the limit of saturation at low temperatures come out from the solutions. The calcium and bicarbonate contents in the Cambrian-Vendian groundwater are decreased very much in comparison with groundwater from the above layered zone of active water exchange. If the mean content of bicarbonates varies in the interval of 380–500 mg/l in the zone of distribution of fresh groundwater of the Baltic basin, in the Estonian Homocline it reaches 165–220 mg/l only. The calcium content also decreases by 5-10 times in the Cambrian-Vendian aquifer, if to compare it with non-cryogenic conditions. Calculation of the solubility indices by thermodynamic reaction constants shows that calcite is undersaturated and could be precipitated during the Pleistocene. A sharp increase of calcium content in groundwater is observed under the conditions of shallow occurrence of aquifers near buried paleovalleys, where during the Holocene due to atmospheric influence water was enriched with calcium, as well as during the mixing with the basement calcium chlorides under conditions of intensive development, a cone of depression arose as a result of operation of coastal water intakes. Besides, the calcium content is increased at a depth of about 500 m in the mixing zone with saline water advancing from the south.

2. ISOTOPE EVIDENCE IN THE BALTIC BASIN

The process of data collection on isotopes in groundwater of Baltic Basin was not very purposeful, however many researchers worked here during two decades of years. On the basis of results obtained by them and considering new data it is possible to characterize the isotope

significance for study of groundwater origin and forming in Baltic Basin. In diverse territories of the Baltic Basin (in Estonia, Latvia, Lithuania, Russia, Poland) groundwater by different isotope methods in the period 1972-1997 was studied by R. Mokrik [4]; M. Yezhova, V. Polyakov [8]; G. Bondarenko [1]; J. Banys, V. Juodkazis, J. Mazeika, R. Petrosius [2]; and others [7, 9]. Unfortunately, in recent years extension of isotope studies due to economical and other related changes, including groundwater resources usage and management, in independent Baltic states began to decrease.

According to available data and relevant publications, changes on $\delta^{18}\text{O}$ in groundwater of the Baltic Basin for main aquifers of active water exchange zone (up to 450 m depth) are presented in Fig. 1.

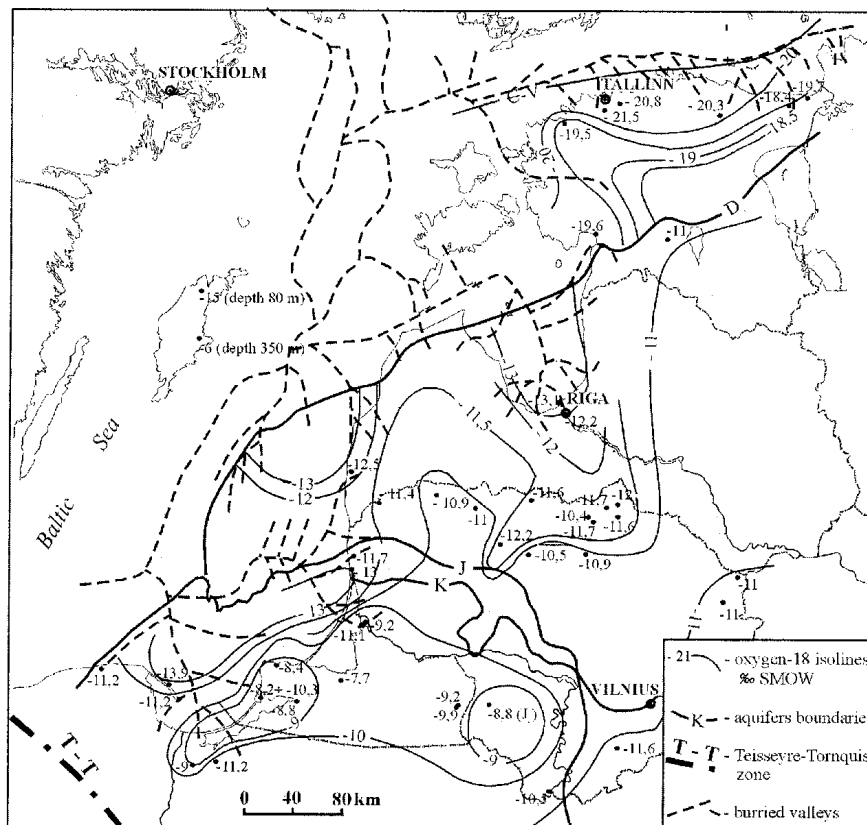


FIG. 1. Oxygen-18 distribution (% SMOW) in the fresh groundwater of the Baltic Basin.

Conventional radiocarbon dating of groundwater in scale of Baltic Basin is quite controversial due to complicated evolution of DIC system and mixing of groundwater originated from different sources in regional flow systems during paleoclimatic changes, which have taken place in Pleistocene and Holocene. Radiocarbon content in groundwater of active exchange zone varies in wide range from almost 0 to 80-90 pmC. Radiocarbon content data plotted depending on sampling depth show complicated and irregular view (Fig. 2).

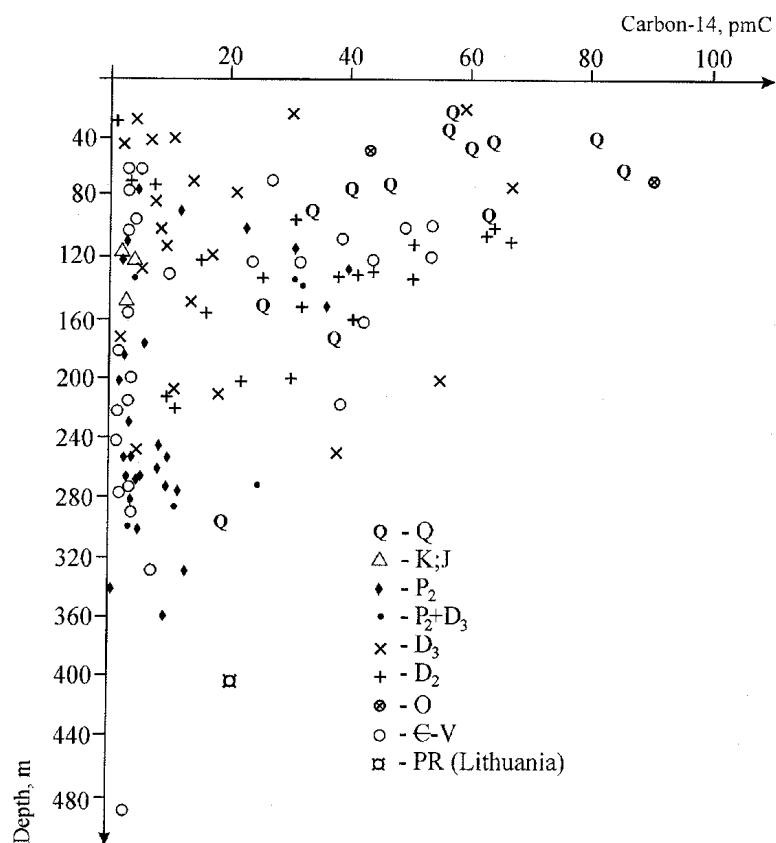


FIG. 2. Radiocarbon content (pmC) vs. sampling depth in the fresh groundwater of the Baltic Basin.

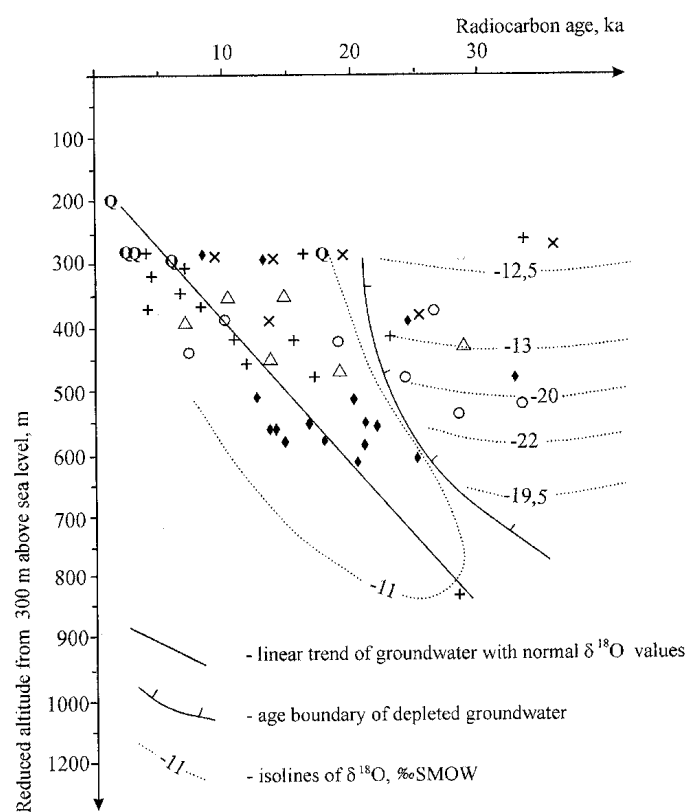
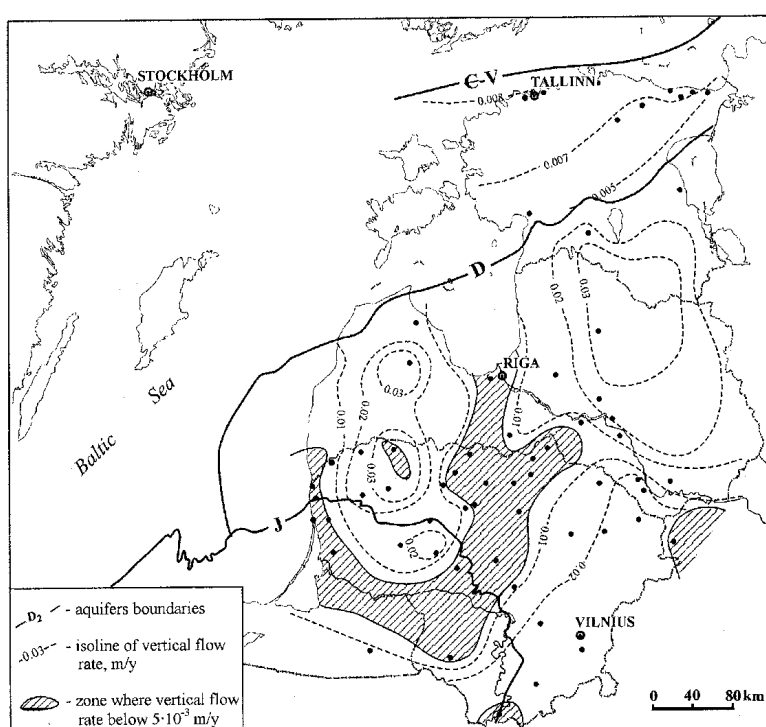


FIG. 3. Radiocarbon age (ka BP) vs. reduced altitude in the fresh groundwater of the Baltic Basin.

If to plot corrected (according to statistical and carbonate dilution approaches) radiocarbon age of groundwater depending on reduced altitude from 300 m above sea level, two type of isotopically different groundwater could be distinguished (Fig. 3). They are: groundwater with quite normal $\delta^{18}\text{O}$ values and with radiocarbon age changing from modern to 18 ka BP depending on reduced altitude according to linear relationship characterizing regional flow system; and groundwater with $\delta^{18}\text{O}$ values ranging from -12.5 to -22.5‰ and with radiocarbon age 20-35 ka BP.

Using distribution of ^{14}C content in groundwater in regional flow system apparent vertical flow rate (sampling depth difference/radiocarbon age difference) was calculated (Fig. 4). The highest vertical flow rate values are peculiar to modern watersheds. The lowest flow rate values were observed in lowlands, where traces of depleted by ^{18}O water were fixed many times.



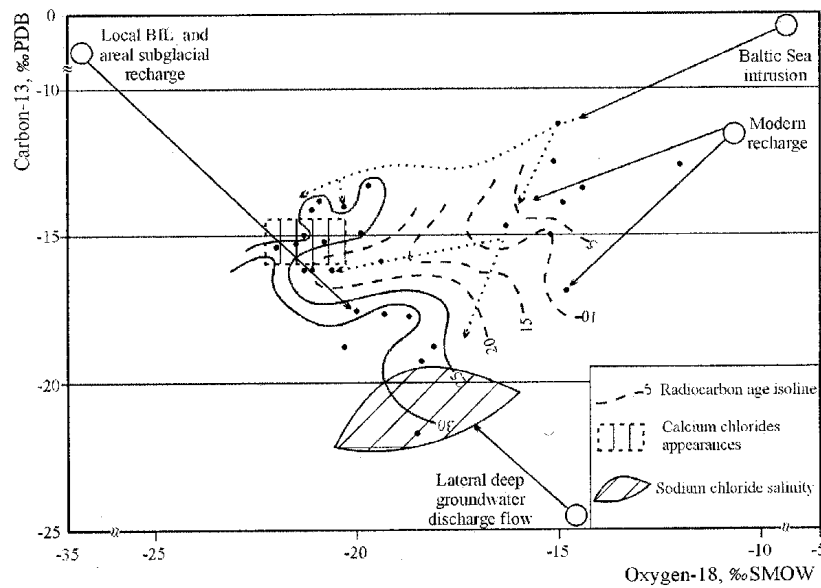


FIG. 5. Different mixed sources of groundwater projected onto $\delta^{18}\text{O}$ - $\delta^{13}\text{C}$ plot for fresh groundwater of the Baltic Basin.

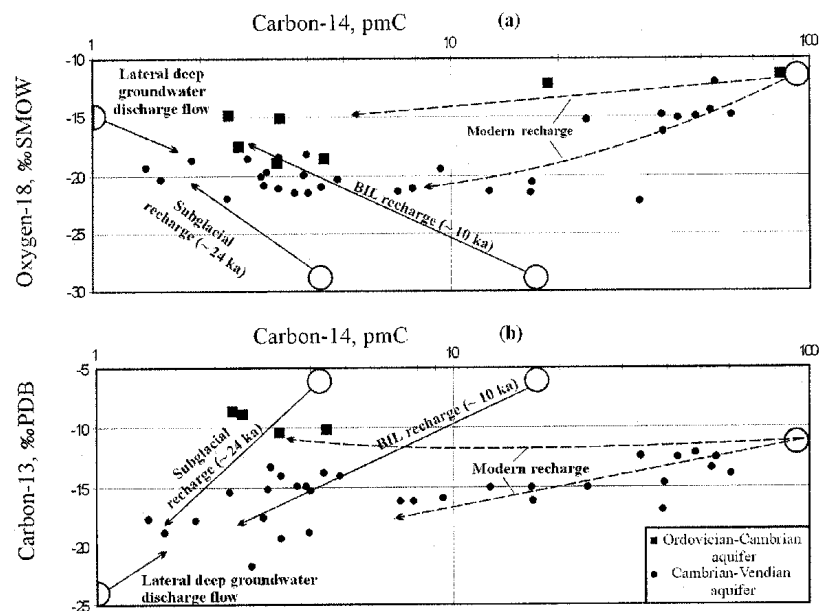


FIG. 6. Different mixed sources of groundwater projected onto ^{14}C - $\delta^{18}\text{O}$ (a) and ^{14}C - $\delta^{13}\text{C}$ (b) plots for fresh groundwater of the Baltic Basin.

In first zone with higher water exchange rate groundwater recharged in Holocene by meteoric water with $\delta^{18}\text{O}$ values close to those of modern precipitation prevails. Glacial meltwater has been drained from this zone by hydrographic systems (see Fig. 1).

In second zone with relatively slow water exchange in the lower part of section (especially, in Southern Baltic) groundwater excluded from northern area southwards by penetrated subglacial meltwater according to plug-flow mechanism during recessional Middle-North Lithuanian phases (13-14 Ka BP) prevails. This water originated from lower part of section has more positive $\delta^{18}\text{O}$ values.

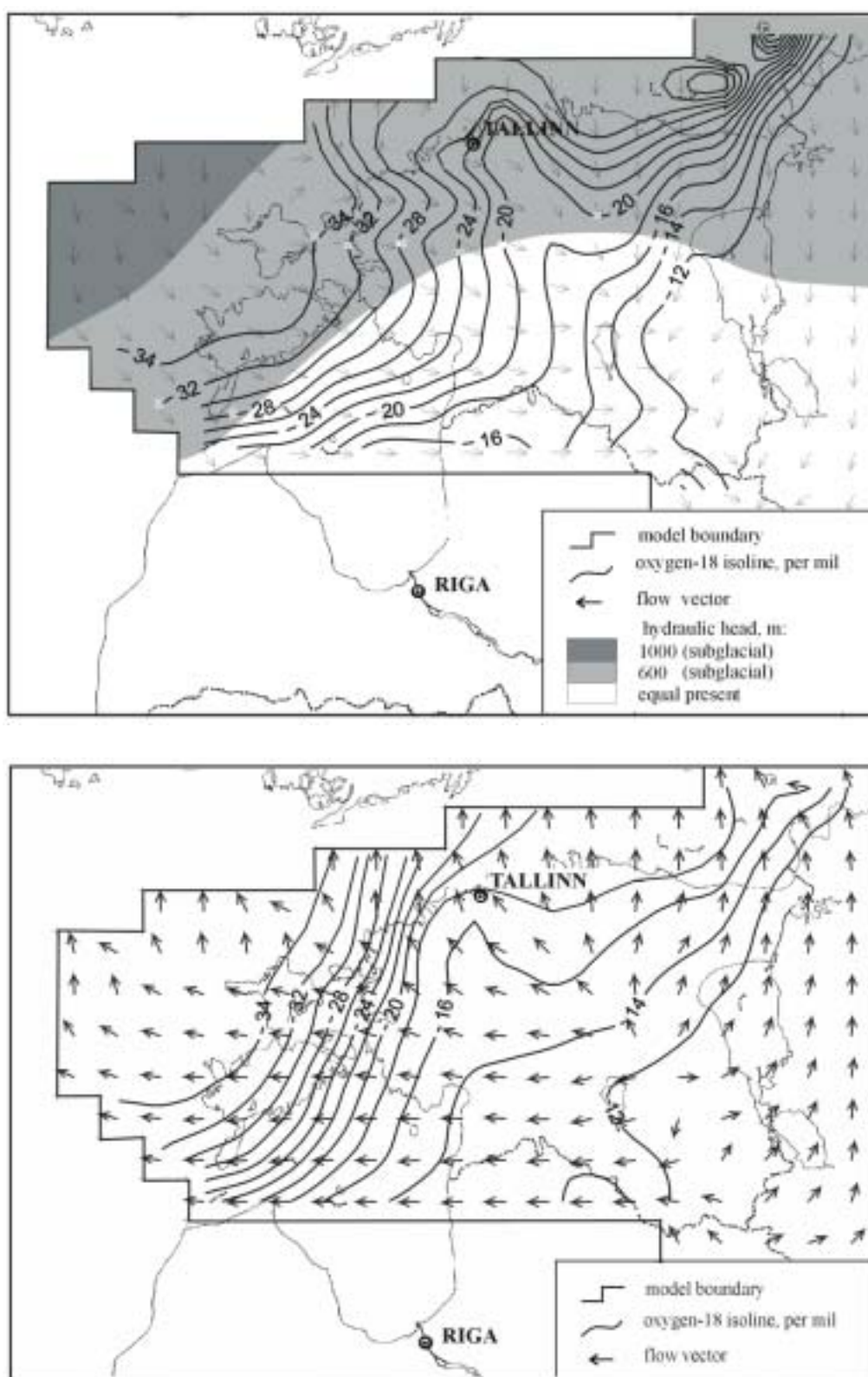


FIG. 7. MT3D models of oxygen-18 distribution in the Cambrian-Vendian aquifer (a) at time of maximum subglacial recharge, and (b) at present.

In third zone with negative $\delta^{18}\text{O}$ values of groundwater in mouths of river basins close to shoreline due to mixing of Holocene water with one or another type of paleo-recharged water depleted isotope composition ($\delta^{18}\text{O}$ values range from -12 to -13.9‰) of groundwater has remained. Most significant traces of mixed different recharge portions (Denekamp-Huneborg paleorecharge; subglacial recharge; paleorecharge from Baltic Ice Lake close to northern shoreline of Estonia; Holocene modern recharge, regional lateral flow of groundwater with sodium chloride salinity from south) have remained in Estonian Homocline (Fig. 6).

It is assumed that during Denekamp-Huneborg time in pre Late Glacial permafrost environments (26-34 ka BP) the groundwater in aquifers of cryolite zone could be hydraulically communicated with the lake and river systems through taliks and could be recharged by surface water depleted by ^{18}O and ^{13}C . The $\delta^{18}\text{O}$ values could vary from -18.5 to -22.2‰ and the $\delta^{13}\text{C}$ values - from -18.8 to -21.7‰. The Cambrian-Vendian aquifer could be also palaeorecharged in several different paleoenvironments later on: by subglacial meltwater with age also close to ~26 ka BP, or from Baltic Ice Lake (~10 ka BP). Depleted $\delta^{13}\text{C}$ values of old groundwater (-19 to -21‰) in Eastern Estonia most likely depend on methanogenesis in pre-Huneborg time. Paleorecharge of aquifer from Baltic Ice Lake became evident only locally near buried valleys on the coastal area of the Gulf of Finland, while ice meltwater $\delta^{18}\text{O}$ values extend up to -25 or -35‰ and $\delta^{13}\text{C}$ values were about -7‰. Most likely, that on the territory of Estonian Homocline the hydraulically close connection via Cambrian-Vendian aquifer between talik systems of the Gulf of Riga and the Gulf of Finland existed what had an influence on groundwater recharge by isotopically depleted water. This northward flow direction could be favourable because the surface falls towards ice sheet in Bothnia area.

The degradation of permafrost zones, which began since retreating of Late Weichselian Ice sheet in Baltic region, led to further mixing of different recharge portions and to discharge of aquifers with isotopically traced groundwater. During Pandivere recessional phase beneath the ice formed high pressed meltwater flow determined the maximum subglacial recharge to an aquifer. Preliminary simulations using MODFLOW and MT3D codes confirm this glacial forcing. The unsteady state simulations model comprise all hydrogeological units of sedimentary cover in Estonia (10 aquifers and aquitards). In model case meltwater driven out from beneath the ice sheet continues to flow through all aquifers to the depth 450 m under potential gradient. Discharge zone was found to be in southern Estonia. Simulated maximum retreating ice pressure on the western and northern boundaries of Estonian Homocline was presented from 1 to 0.6 km and at ice margins close the southern Estonia sub-surface pressure was distributed to be as similar as existing today. The integrated groundwater velocities driven by the heads in the aquifer are shown in Fig. 7.

In Cambrian-Vendian aquifer diffusion-dispersion and mixing of subglacially recharged and residual groundwater of cryogenic metamorphism and laterally transported old deep groundwater with sodium chloride salinity could be expressed also. These changes were still active in Holocene period, when isostatic rise of territory continued, resulting in a stadial evolution of the Baltic Sea to present contour of its extension.

Presented approach has begun to consider and will be examined in future by reconstruction of groundwater flow in aquifers overpressured by the last ice sheet and undergone consequences of deglaciation (isostatic rise, changes in hydraulic gradients and flow rates, reversal regional flow directions, etc.) in detail basing on numerical modeling.

4. CONCLUSION

The Late Glacial permafrost environments and ice cover retreating in the Baltic territory had important influence to formation of the groundwater isotope composition. Much evidence support the hypothesis that permafrost phenomenon which led to water circulation processes into aquifers from surface water and from subglacial meltwater through talik zones as well as areal paleorecharge during retreating phases here took place.

In future detailed modeling studies are still needed to establish the formation model of groundwater in the Baltic region in the Late Pleistocene and Holocene.

ACKNOWLEDGEMENTS

Much of this work carried out as part of a Lithuanian Scientific Programme “Lithosphere” and the new Visby Programme “Crustal permeability and groundwater discharge in the Baltic Sea Basin: a new interdisciplinary approach”.

REFERENCES

- [1] BONDARENKO, G.N., GUDZENKO, V.V., KOVALYUKH, N.N., Forming of the front of radioactive and stable isotope in discharge zone of the artesian basin. In: Investigation of Natural Water by Isotope Methods. Moscow. Publishing house “NAUKA” (1981). 157-164 (in Russian).
- [2] JUODKAZIS, V., MAZEIKA, J., PETROSIUS R., Radioisotope Methods in Environmental Hydrogeology. Vilnius. Geologija **18**: (1995) 1-132 (in Lithuanian).
- [3] KONONOVA, R.S., Hydrochemical regularities of groundwater as one of the indicators of permafrost conditions. In: Groundwater in the Cryolithozone.
- [4] MOKRIK, R., The Palaeohydrogeology of the Baltic Basin. Vendian & Cambrian. Tartu. Tartu University Press (1997) 138 p.
- [5] MOKRIK, R., MONKEVICIUS, A., FLODEN, T., PUURA, V., ZUZEVICIUS. A. The Pleistocene icings evidences and their influence on the erosion of the ground water discharge areas in the Baltic Basin. In: Geophysics in the Baltic Region: Problems and Prospects for the New Millennium. Tallinn. Institute of Geology (2000) 45-46.
- [6] MOKRIK, R. Groundwater formation model of the Cambrian-Vendian aquifer during Quaternary in the Baltic Basin. Vilnius. Litosfera **4**: (2000) 134-136.
- [7] ROZANSKI, K. ZUBER, A. Glacial infiltration in Europe – myth or reality. Prz. Geol., **48**: (2000) 796-803.
- [8] YEZHOVA, M., POLYAKOV, V., TKACHENKO, A., Palaeowaters of North Estonia and their influence on changes of resources and the quality of fresh groundwater of large coastal water supplies. Vilnius. Geologija **19**: (1996) 37-40.
- [9] VAIKMÄE, R., VALLNER, L., LOOSLI, H. H., BLASER, P.C., JUILLARD, M., Palaeogroundwater of glacial origin in the Cambrian-Vendian aquifer of northern Estonia. In: W.M. Edmunds, C. Milne (Eds.), PALAEWAUX. Management of Coastal Aquifers in Europe. Palaeowaters, natural controls and human influence: Final Report, June 1999. Keyworth, Nottingham. British Geological Survey Technical Report. 11-18, Hydrogeology Series, WD/99/35. KT 1.10 0330357s98, CT-96 (1999).

PALEOCLIMATIC VARIATIONS IN MAKNASSY BASIN (CENTRAL TUNISIA) DURING THE HOLOCENE PERIOD USING MULTIDISCIPLINARY APPROACHES

K. ZOUARI, N. CHKIR, B. OUDA

Laboratoire de Radio-Analyses et Environnement,
Ecole nationale d'ingénieurs de Sfax (ENIS), Tunis, Tunisia

Abstract. The signature of humid climatic episodes in the Holocene paleoclimatic history of Tunisia are evident in outcroppings along riverbanks almost all over the Tunisian drainage network. Previous multidisciplinary studies have already identified some sites where these remnants can contribute valuable information for reconstruction of paleoenvironmental and paleoclimatic variations in the presently hyper-arid zone of the Northern Sahara. Sedimentary deposits outcropping on Wadi Leben and Wadi Ben Sellam banks, in the Maknassy Basin (Central Tunisia), have been sampled. Multidisciplinary studies, including prehistory, sedimentology, mineralogy, ecology and radiochronology have been conducted to improve palaeoenvironmental interpretations and to determine a precise chronological history of humid episodes during the Holocene in Tunisia. This paper deals with the interpretation of results obtained from the Maknassy Basin in comparison with some other Tunisian sites in order to highlight Holocene humid episodes. Establishment of a precise chronological framework is prerequisite to exploring potential relationships between the occurrence of humid phases and recharge of aquifers located in this area.

1. MAKNASSY BASIN (SITE 1)

The Maknassy Basin, located in Central Tunisia (Figure 1), is characterized by a semi-arid climate. Mean annual precipitation ranges between 180 and 200 mm/y and mean annual temperatures are about 19°C. A mean annual flow deficit, calculated by the Turk formula, is estimated at about 190 mm/y. However, groundwater reserves are important, and more than 7 springs and 15 boreholes supply approximately 20 million m³ of variable salinity water for domestic use and irrigation [1,2]. Wadi Leben and its major tributary Wadi Sellam are the principal channels of surface flow. Stream flow is permanent in several places due to springs situated along the riverbank.

Quaternary deposits have been sampled along Wadi Leben and Wadi Ben Sellam riverbanks over ten sections (Figure 1). The sedimentology is complex, characterized by lacustrine, paludal, fluvial and even eolian material. Three terraces (T1, T2 and T3), generally nested and occasionally superposed [3], constitute the classical geomorphological configuration of riverbanks. An abundant fauna, relatively varied, demonstrates various ecological conditions. The same species are present with distinct ratios, underlining different environments.

Terrace T3 is the largest one, especially in the centre of the basin. Three sections were studied for this terrace (Figure 3): Aïn el Guettar Section (C1), at the major spring of the wadi, and C2 Section and the Meander Section (C3), respectively, located at 200 m and 2500 m downstream of C1. According to radiochronological data, the oldest sediments of this terrace are Pleistocene deposits [4].

Terrace T2, is characterized by smaller surface and thickness (11 to 12 m) was studied along three sections (Figure 1): C4, on the left riverbank at 200 m upstream of C1, C5a and C5b,

separated by 100 m, on the right riverbank of wadi Ben Sellam at 1000 m upstream of wadi Leben confluence. Deposits are clayish blackish at the bottom, covered with poorly sandy silts, and finally by a silted-gypsum level. No prehistoric remnants have been found in these sediments. Two apparent ages (7 and 10 ka BP) for *Helix* samples of the terrace T2 (Table I), in correct stratigraphic correlation, probably initially equilibrated with atmospheric carbon, may be regarded as reliable (Figure 2). All sedimentology, mineralogy, bioremnants, geochemical and isotopic results tend toward the same conclusions, i.e. a humid period dated around 7-10 ka BP [4].

FIG.1. Location map of Maknassy basin (central Tunisia) and location of cross section on riverbanks of Wadi Leben and Ben Sellam wadis (CI- C10) [4].

Section	Elevation (m)	Material	¹⁴ C ages (y. B.P.)	Activity (%)
C4	2,4	<i>Helix melanostoma</i>	7130±130	41,20±0,70
C5a	2,1	<i>Helix melanostoma</i>	10440±170	27,30±0,60

charophytes (<10%). The upper part, made of eolian (and/or fluvial) sands, is azoic. Palaeoecology shows a great diversity of species, it is noticeable that species representative of brackish waters are more abundant than those living in fresh waters. This is in agreement with former observations reported for Chotts area [5] and wadi el Akarit [6]. Sites of historical interest, have been recognized at the top of the terrace T1, along the wadi Ben Sellam including innumerable potsherds, which may be attributed to Vth and VIth centuries AD [3]. With regard to the Terrace 1, analysed gastropods, including *Helix*, have given youngest ages (Table II), between 2 and 4.1 ka BP (Figure 3). Even if their stratigraphic correlations are good, it is noticeable that samples including aquatic species always yielded older ages than the strictly terrestrial ones (*Helix*). This suggests a slight disequilibria of water carbon compared to atmospheric carbon probably due to contribution of fossil water. Radiocarbon dating allows for identification of a second humid period between 2-4 ka BP.

These humid periods have already been identified in Northern Sahara but have been considered as a single episode ranging in age between 3 and 10 ka BP (see [7], [8] and [9]).

Table II. Radiocarbon dating of carbonate sampled on C6, C7, C8, C9 section of Terrace 1

Section	Elevation (m)	Material	^{14}C ages (y. BP)	Activity (%)
C6	2	<i>Gastéropodes</i>	4020 \pm 126	60,62 \pm 0,96
C7	3,5	<i>Helix melanostomma</i>	3020 \pm 108	68,7 \pm 0,9
	1,2-1,4	<i>Gastéropodes</i>	4116 \pm 100	59,9 \pm 0,75
C8	3,58-3,78	<i>Helix melanostomma</i>	1992 \pm 200	78,04 \pm 1,95
	1,4	<i>Gastéropodes</i>	3105 \pm 198	67,94 \pm 1,68
C9	2,2	<i>Helix melanostomma</i>	3270 \pm 100	66 \pm 0,80

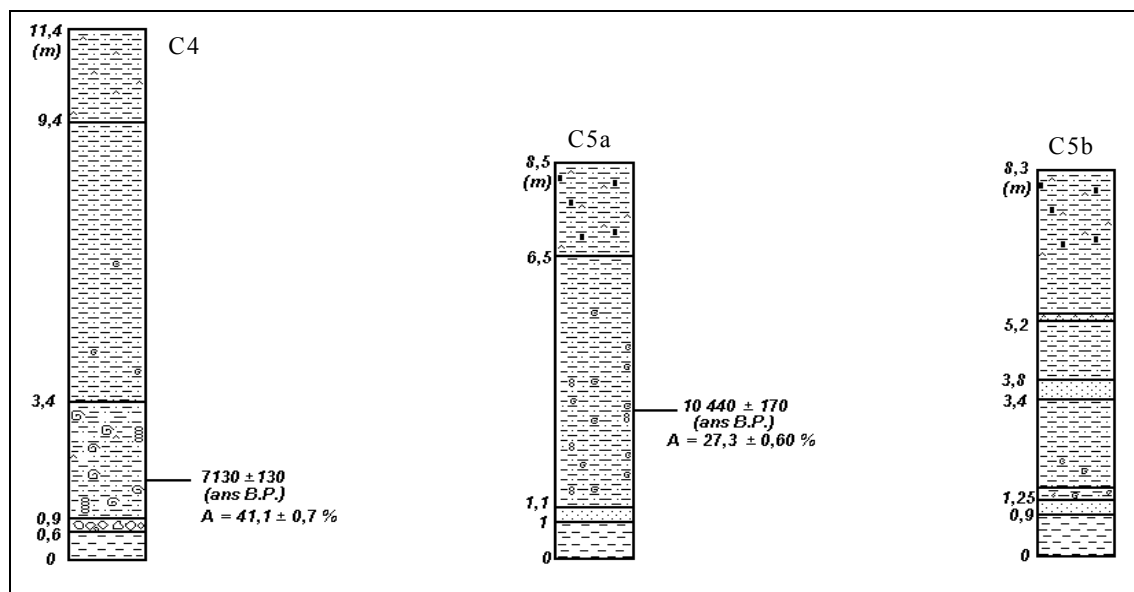


FIG.2. Radiocarbon dating of C4 and C5 section of Terrace 2 [4].

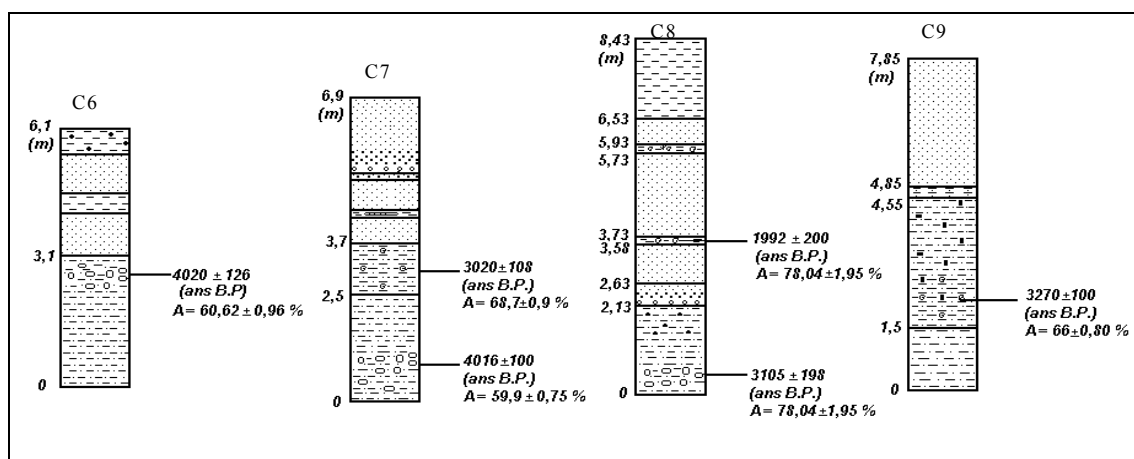


FIG.3. Radiocarbon dating of C6, C7, C8 and C9 section of Terrace 1 [4].

2. OTHER SITES OVER TUNISIA

Geomorphological structures of almost all sites presented in this comparison (Table III: site Nos 1 to 9, Figure 4) show great similarity in architectural aspects of the basins. Sedimentological studies completed with ^{14}C -dating applied to main stratigraphic chronosequences have facilitated the investigation of humid periods during the last 12 000 years.

2.1. Wadi Mejerdha valley (Site 2)

The medjerda basin, mainly composed of early and mid quaternary loamy sediments has been partly eroded by incision and meandering of the river. This area of incision has been refilled during Holocene in several sedimentation phases. The main stratigraphic sequences of wadi Medjerda flood plain within Ghardimaou basin allows to distinguish incision periods from those of accumulation during the last 10 000 y BP [10]. Holocene period is marked by the accumulation of thick fluvial deposits. In these, different soil horizons can be distinguished from sedimented layers. ^{14}C -dating, pottery fragments and field study allow to establish a morphodynamic sequence with different phases focused on Holocene:

- Transition into Holocene is marked by fine accumulation of floodplain sediments. A big number of snail shells indicate in situ remnant of an ancient settlement, ^{14}C -dating yield an age of 11160 and 11440 y. BP.
- Period of morphodynamic stability permitted soil formation under more humid conditions. Thick clayey layers with weak humic contents prove slow accumulation conditions which end at about 2680 y. BP.

Sedimentology analysis of layers stratified between the two dates can not be attributed clearly to arid phases. But it shows decreases of incision and a regression of the wadi flood plain.

This study allows to identify a humid period ranging between 3000-11000 y. BP but it does not distinguish the two humid periods investigated in wadi Leben site.

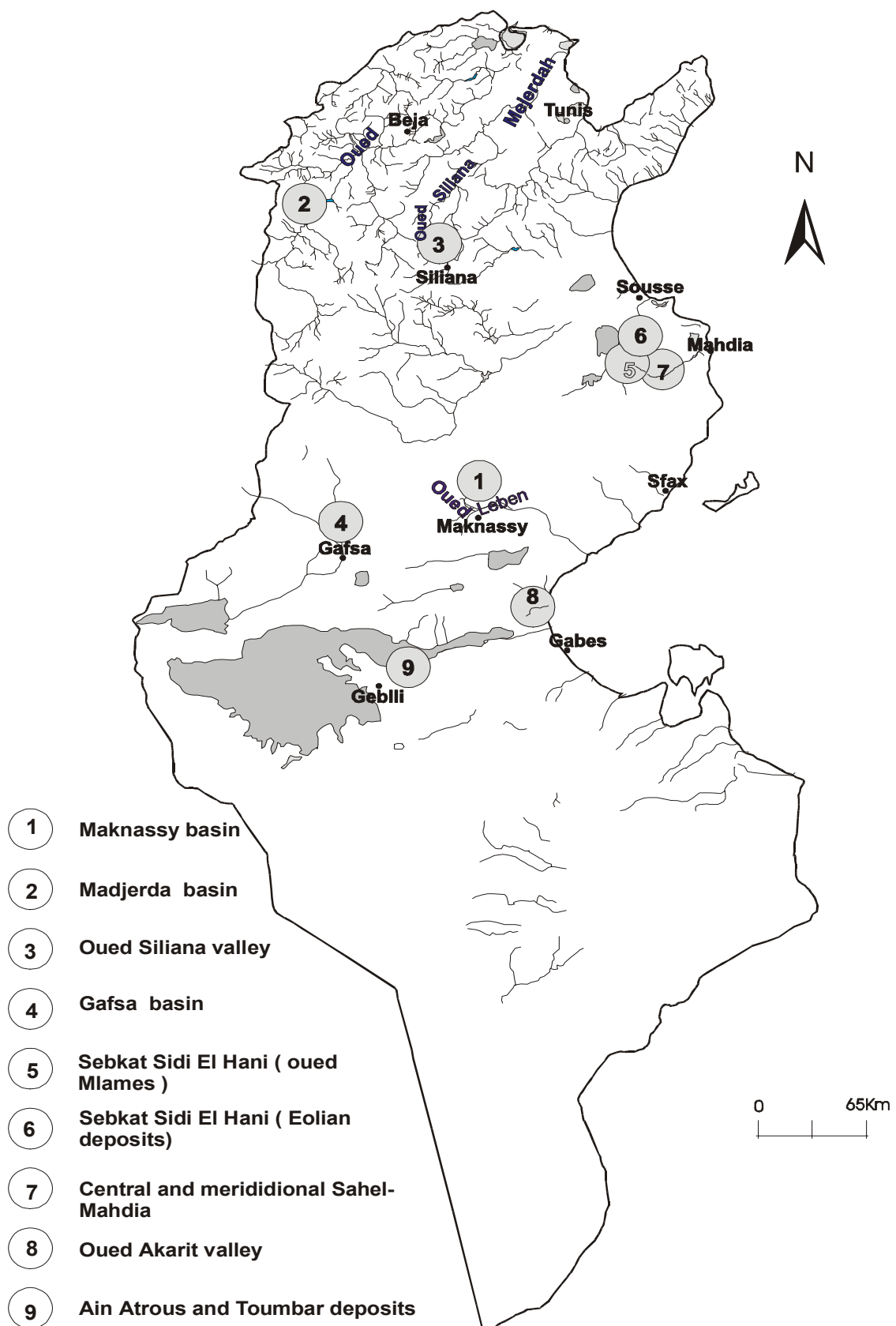


FIG 4. Holocene sites over Tunisia.

Table III. Radiocarbon dating of holocene deposits all over Tunisia

n°	Localisation		Deposits	¹⁴ C dating	Prehistoric remnants	References
1	Wadi leben and wadi ben sallem – Maknassy		High Terrace (T2)	Top: 7130 ± 130 y.BP Base: 10440 ± 170 y.BP	typical of aterian industry innumerable potsherds, attributed to Vth and VIth centuries AD	[4]
			Low Terrace (T1)	Top: 1992 ± 200 y.BP Inter: 3020 ± 108 y.BP Base: 3270 ± 100 y.BP		
2	Wadi Medjerdha - Ghardimaou		Holocene terrace	Top: 2680 y.BP Base: 11440 y.BP	pottery fragments	[10]
3	Wadi Siliana		Holocene terrace	Top: 7980 y.BP Base: 9830 y.BP	flint fragments of epipaleolithic and neolithic age	[11]
4	Meridional part of Tunisian steppe – Gafsa	- Wadi bouzayene	Terraces	Top: 4180 ± 240 y.BP Inter: 5900 ± 170 y.BP Base: 8380 ± 695 y.BP	-	[3]
		- Wadi Nebch	Terraces	: 6910 ± 250 y.BP		
		- Wadi Khsaf	Terraces	Top: 7540 ± 230 y.BP Inter: 9400 ± 190 y.BP Base: 9600 ± 160 y.BP		
5	Sbekhat Sidi El hani - Wadi Mlamès		High Terrace	Top: 2750 ± 130 y.BP Base: 7130 ± 250 y.BP	Pottery, ruins,...	[12]
			Low Terrace	4620 ± 130 y.BP		
6	Sebkhat Sidi El Hani - Eolian deposit		Basin deposits on the tableland	6585 ± 195 y.BP	Byzantine and roman pottery fragment	[12]
7	Central and Meridional Sahel – Mahdia	- Wadi Guelet	High terrace	Bottom: 3520 ± 105 y.BP		[13]
		- Wadi Zrata	High terrace	Base : 5765 ± 200 y.BP		
8	Wadi Akarit - Gabès		Levelled stratigraphic profile	Top: 3600± 40 y.BP : 5595 ± 500 y.BP : 6700 ± 600 y.BP Base: 8700 ± 200 y.BP	Mousterian site	[6]
9	Aïn El Atrous and Toumbar – Chott Fejej and Jerid		Dead spring deposits	9000 and 8500 y.BP		[6]

2.2. Wadi Siliana valley (Site 3)

Holocene deposits constitute the most important morphology structures observed on Wadi Siliana valley [11]. These deposits are cut on terraces with variable thickness and facies from the upstream to the down stream of the basin. Several Holocene terraces are fossilised on snail nests containing prehistoric remnants

- In wadi Oussafa section (one of the tributary of wadi Siliana), three snail settlements concealed by colluviums have been identified in the Holocene terrace. One of them contains prehistoric remnants of epipaeolithic and neolithic age
- In Gaafour site (left riverbank of wadi Siliana), several snail nests fossilised in surface deposits. One of them contains some flint fragments, well identified as epipaleolithic and neolithic age

Therefore, prehistoric remnants indicate that Holocene terraces could be older than 6 000/7 000 year BP.

Some *Helix* shells have been sampled and ¹⁴C-dated in order to determine with precision deposits ages.

- The first sample was taken from the basal layer of Holocene terrace. It indicates an age of $9\,830 \pm 230$ y. BP.
- Two other samples were taken from a nearby Holocene terrace. The first one, taken from a basal layer, indicates an age of 9630 ± 180 y. BP which is in agreement with the first sample. The second one, taken from the upper layer of the Terrace, indicates an age of 7980 ± 250 y BP.

Radiocarbon dating has provided a more precise chronology than prehistoric remnants. A humid episode has occurred in Wadi Siliana valley around 8000-10000 y. BP.

2.3. Meridional part of Tunisian steppe – Gafsa (Site 4)

Septentrional Sahara margin is marked by quaternary eolian deposits. This deposition has various sedimentological characteristics and it has a great importance to reconstitute paleoenvironmental conditions in desertic margins. Dune ranges are located on the northern limb of mountains, near valley of great wadis that have brought abundant alluvium. Eolian deposits on meridional part of Tunisian steppe have been studied in order to establish a chronological stratigraphy [3]. This pluridisciplinary approach (sedimentology, archeology,...) has been supported by radiocarbon dating. Fluvial deposits presented on wadi terraces can be dated through fossilised shells whereas eolian deposits can be dated through prehistoric sites that crowned them. Radiocarbon dating is summarised as follow:

- Deposits on wadi Bouzayene (northern piedmont of Gafsa link) present several beds of *Helicoides* that have been dated at the base $8\,380 \pm 695$ y. BP, in the middle $5\,900 \pm 170$ y. BP, and at the top $4\,180 \pm 240$ y. BP. This radiocarbon dates are coherent and allow to attribute this terrace to Holocene period

- Wadi Nebch (meridional piedmont of Gafsa link): Some shells sampled on hydromorphic bed situated in the middle part of a terrace yield a date of $6\,910 \pm 250$ y. BP which is in agreement with dates obtained on wadi Bouzayene. Eolian deposits, dated through a snail settlement, have a 14-C age of $7\,780$ y. BP.
- Wadi Khsaf (septentrional piedmont of Gafsa link): A terrace, characterised by three superposed capsian sites, has been dated: base layer has a date of $9\,600 \pm 160$ y. BP, middle layer has a date of $9\,400 \pm 190$ y. BP and the upper layer has a date of $7\,540 \pm 230$ y. BP. Like the wadi Bouzayene terrace, this terrace has been deposit on Holocene period during 2 000 years. Eolian deposits facing this terrace have been dated to $8\,360 \pm 360$ y. BP.

These radiocarbon dates indicate that a first terrace can be attributed to a humid period ranging from 8000 to 10000 y. BP while a second terrace deposits range between 4000 and 8000 y. BP. These two period, following each other without a discontinuity, are included in the humid period ranging from 4000 to 10000 y. BP.

2.4. Sebkhath Sidi el Hani – Wadi Mlames basin (Site 5)

This wadi is located on the low steppe of Sahel region (Eastern Tunisia). The high terrace is constituted by alluvium valley containing several remnants of animals (bones, ostrich eggs, shells), vegetation and anthropic presence (pottery, ruins,...) [12]. All these remnants witness a sedimentation that occurred in a calm environment. This terrace has been dated through helix shells samples. 14-C age is of 7130 ± 250 y. BP. The low terrace dominates the landscape. It is nested on the high terraces or on eolian deposits. Deposits that constitute this terrace are rich in Helix fragment. From upstream to downstream of wadi, these deposits become thicker and more stretched. Sampled helix indicate an age of 4620 ± 130 y. BP. These dates are not sufficient evidence to suggest the deposit period of these terraces but they confirm that humid conditions have occurred in this valley around 4000 y. BP and around 7000 y. BP.

2.5. Sebkhath Sidi el Hani – Eolian deposits (Site 6)

The development of an eolian accumulation south-eastern Sidi Hani Sebkhath (eastern Tunisia) has been studied [12]. This accumulation is structured in a long cordon of 20 kilometres and is called El Meslen lunette. It is crowned by a rich gypsum peat deposit giving an age of 6585 ± 195 y. BP or by a nested high terrace of wadi Mlames and El guettar containing pottery fragments and dated to roman period of IV-V centuries (2750 ± 150 y. BP) and Byzantine period of VI century (7130 ± 250 y. BP).

These results may be considered as resumption of humid conditions around 7000 y. BP and around 3000 y. BP. These humid periods followed arid periods favourable to eolian deposits and similar to present conditions.

2.6. Central and Meridional Sahel – Mahdia (Site 7)

The central and meridional part of sahel is a low and weakly uneven region. A complete geomorphological study of this region has been done [13]. Radiocarbon analysis has been used on some helix shells sampled from a little wadi crossing this region to the sea or to some little sebkhat (endoreic depression):

- Wadi Guelet: 14-C age obtained on Helix shells sampled on the base of the terrace is $3\,520 \pm 105$ y. BP. It indicates that deposits have taken place during Holocene period.
- Wadi Zrata: 14-C date is obtained for a historic site situated on the surface of the terrace. The 14-C date confirm that the Holocene terrace has ended its deposit before $7\,765 \pm 200$ y. BP.

These two wadis are contemporary and allow to identify a humid period ranging from 3500 to 8000 y. BP.

2.7. Wadi Akarit (Site 8)

Wadi Akarit is a perennial watercourse supplied by artesian springs from the deep aquifer of the Complexe Terminal [14]. This wadi runs through its own quaternary deposits that have been eroded to a depth of about 15 m. It has been known for a long time for its Mousterian and Caspian artefacts and for the quality of the section suitable for quaternary investigations (Figure 5) [15]. Two common cores were investigated [6]. Major results concerning Holocene period can be summarised as follows [8]:

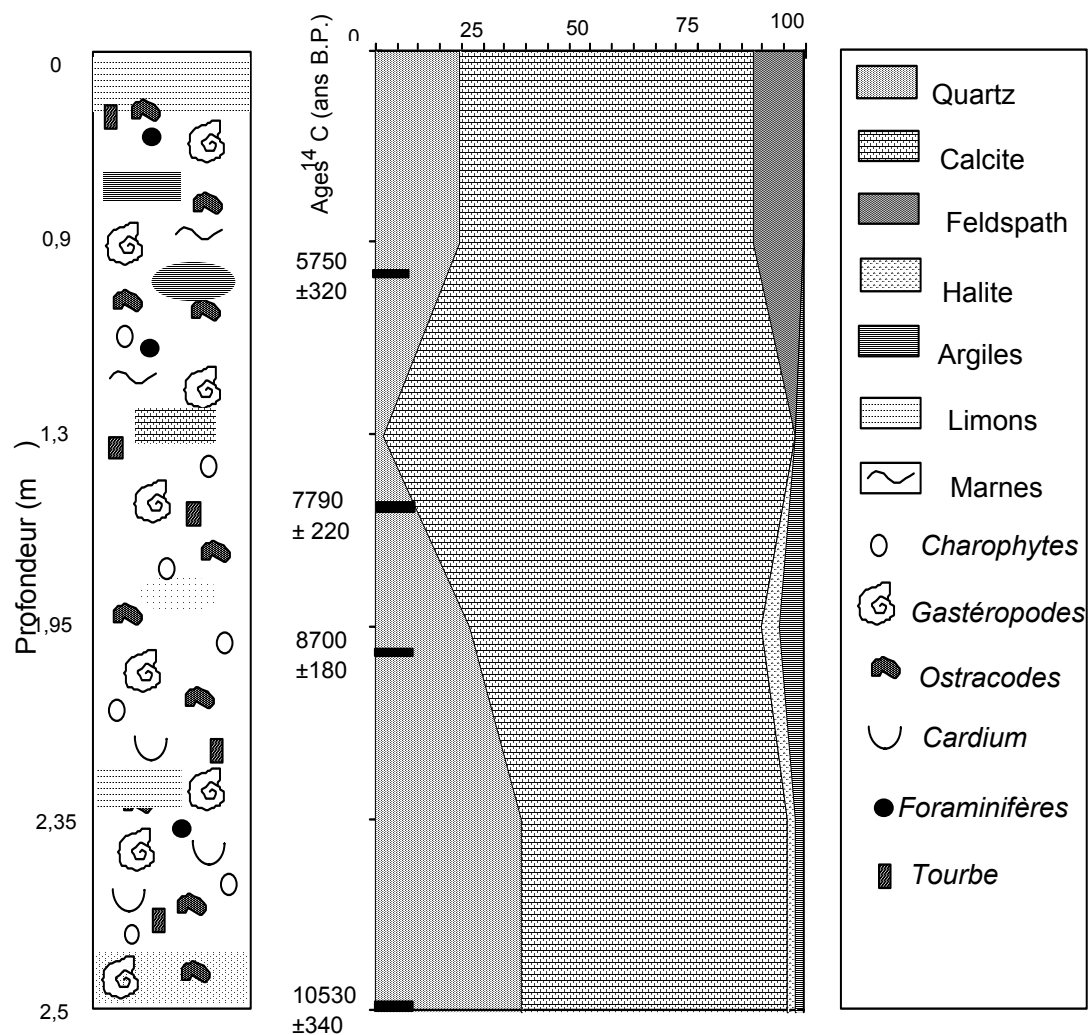


FIG.5. Holocene deposits in Wadi Akarit valley [9].

- Glacial maximum (recent Würm) coincides with an arid episode. Sedimentology analyses show dry climatic conditions characterised by enhanced eolian transport and by sporadic fluvial floods with increased bottom transport of coarse material.
- An episode more humid than present-day may have occurred between 10 500 and 3 000 y. BP. A sudden rise of aquifer is recorded at 10 500 BP. During early and mid Holocene, ecological conditions fluctuated from fresh to eusaline waters, as deduced from biological remains. Relatively low stable isotopes values indicate that salinity increases were due to evaporation of continental waters.

2.8. Aïn Atrous and Toumbar deposits (Site 9)

These two dead springs are situated respectively, on Southern side of Chott Fejej and Chott Jerid. The Southern Tunisian chott are large saline closed depressions. Present day water supply to these Chotts is reduced to local rains and to vertical leakage of aquifers. Quaternary deposits outcropping along paleoshorelines provide evidence of more humid hydrogeological conditions. A last rise of the aquifer occurred during the early Holocene. This is registered by freshwater spring deposits of Aïn Atrous and Toumbar sites. Mollusc shell ¹⁴C dating yields an age of 8 500 y. Bp (Toumbar) and 9 500 y. Bp (Aïn Atrous). This rise of aquifer can be related to humid episode observed on Wadi Akarit deposits.

3. CONCLUSIONS

Data of Maknassy Basin represent a precious element to reconstruct the paleoclimatic evolution of Central Tunisia during recent Quaternary. The two highest terraces were developed during two Holocene humid phases: the first one between 7 and 10 ka BP, the second from 2 to 4 ka BP. These humid episodes have been highlighted on several sites from northern to southern Tunisia: 2.7 ka BP and 11.2 ka BP on the river bank of Wadi Medjerdha (North) [10]; ~10 ka BP on Wadi Siliana sediments (North-West) [11]; 3.5-5.6 ka BP on Wadi Galet and 2.7 ka BP in Sebkhath Kelbia deposits (Sahel region-East) [13] and between 6 ka BP and 11 ka BP in Wadi Akarit sediments (South) [9].

Geomorphological structure of almost all wadis in the region is similar: generally nested and occasionally superposed terraces of riverbanks. All radiocarbon data have been presented on a schematic cross section (Figure 4). We suggest three humid periods, not all observed on the same site. These humid periods have probably been separated by arid or semi arid short pulsations [4], [16] and [7]. Humid periods may be related to recharge periods of aquifers. Dead spring deposits of Aïn Atrous and Toumbar (Southern Tunisia) may be related to a rise of aquifer table [6]. Moreover, mean time transit of water dated by ¹⁴C method on several Tunisian aquifers ([4], [6], [8], [17]) seems to be in good agreement with humid periods investigated in this study.

REFERENCES

- [1] ILLY, P., Etude hydrogéologique préliminaire de la région de Gafsa-Maknassy – Projet de planification rurale intégrée de la Tunisie Centrale – F.A.O. (1967) 81 p.
- [2] FARHAT, H., Contribution à l'étude hydrogéologique de la cuvette de Maknassy (Tunisie) – Thèse de Doctorat en Sciences de la Terre – université de Bordeaux (1978) 200 p.

- [3] BEN OUEZDOU, H., La partie méridionale des steppes tunisiennes. Etude géomorphologique, Doctorat d'Etat, Université de Tunis I, 2 vol., (1994) 577 p.
- [4] OUDA, B., Paléohydrologie isotopique du bassin de maknassy (Tunisie centrale) pendant le quaternaire récent - Doctorat en Géologie sous la direction de Prof. Kamel Zouari, Faculté des Sciences de Tunis (2000) 233 p.
- [5] GASSE, F. et al., Biological remains, geochemistry and stable isotopes for the reconstruction of environmental and hydrological changes in the Holocene lakes from north Sahara, *Pal. Pal. Pal.* **60** (1987) 1-46.
- [6] ZOUARI, K., Géochimie et sédimentologie des dépôts continentaux d'origine aquatique du Quaternaire supérieur du sud tunisien: Interprétations paléohydrologiques et paléoclimatiques, Thèse de Doctorat d'Etat, Université de Paris XI-Orsay (1988) 216 p.
- [7] SCHULZ, E., Holocene environments in Central Sahara, *Hydrobiologia* **214**: (1991) 359-365.
- [8] FONTES, J.-Ch., GASSES, F., PALHYDAF (PALeoHYDrology in AFrica) program: objectives, methods, major results, *Pal. Pal. Pal.* **84** (1991) 191-215.
- [9] ZOUARI, K., Reprise des conditions humides vers 11 000 BP dans le Sud Tunisien – IAEA-SM-336/137P, *Isotopes in Water Resources management* (1995).
- [10] FAUST, D., ZIELHOFER, C., DIAZ DEL OLMO, F., Holocene morphodynamic changes in the central valley of the wadi Medjerda (Northern Tunisia) Report of DFG-Projekt Holozän in Nord tunisien 1999-2000 (2000).
- [11] JENDOUBI, Le bassin versant de l'wadi siliana (Haut Tell – Tunisie) – Etude du molelé quaternaire, Thèse en Géographie physique - Université de Tunis 1 – Faculté des sciences humaines et sociales (2000) 331p.
- [12] KAMOUN, Y., ZOUARI, K., ZOUARI, H., JAMOSSI, F., BEDIR, M. and BEN JEMAA H., Accumulations éoliennes d'âge pléistocène-holocène en bordure de Sebkhia Sidi El Heni (Tunisie Orientale), Submitted to African Earth Sciences, Septembre 2000, JAES Ref 00-09-0058 (2000).
- [13] BRAHIM, F., Le Sahel Central et Meridional – Géomorphologie et dynamique récente du milieu naturel, Thèse de Géographie physique – Université de Tunis 1 – Faculté des sciences humaines et sociales (2001) 435p.
- [14] FONTES, J.-Ch., COQUE, R., DEVER, L., FILLY, A. et MAMOU, A., Paléohydrologie isotopique de l'wadi el Akarit (sud tunisien) au Pléistocène et à l'Holocène, *Pal. Pal. Pal.* **43** (1983) 41-61.
- [15] BEN OUEZDO, H., CAMPS, G., GRAGUEB, A., MAHJOUB, K. and ZOUARI, K., Sur les dépôts du Pléistocène supérieur et de l'Holocène de la région des chotts et de la plaine côtière du golfe de Gabès (Tunisie) et leur place dans la stratigraphie du Quaternaire, *CRAS*, **302** (1986) 659-664.
- [16] BEN KHELIFA, L., Diatomées continentales et paléomilieus du sud-tunisien (PALHYDAF site 1) au quaternaire supérieur. Approche statistique basée sur les diatomées et les milieux actuels, Thèse de l'université de Paris-Sud- Orsay (1989) 340p.
- [17] GRIES, S., Etude géochimique et isotopique des nappes profondes au Sahara-Sahel; implications pour la gestion des ressources en eau et les reconstructions paléoclimatiques - Thèse de l'université de Paris-Sud- Orsay (2000) 299p.

**ISOTOPE TRACERS FOR
OCEAN-ATMOSPHERE INTERACTIONS**

(Session 3)

Chairpersons

K. FRÖHLICH
Germany

B.L.K. SOMAYAJULU
India

DOES CARBON ISOTOPE DATA HELP EXPLAIN ATMOSPHERIC CO₂ CONCENTRATIONS DURING GLACIAL PERIODS?

K. ALVERSON*

PAGES International Project Office, Bern, Switzerland

P. LE GRAND

University of Western Brittany, Brest, France

Abstract. An inverse ocean box modeling approach is used to address the question of what may have caused decreased atmospheric CO₂ concentration during glacial periods. The inverse procedure seeks solutions that are consistent, within prescribed uncertainties, with both available paleodata constraints and box model conservation equations while relaxing traditional assumptions such as exact steady state and precise prescription of uncertain model parameters. Decreased ventilation of Southern Ocean deep water, decreased Southern Ocean air-sea gas exchange, and enhanced high latitude biological pumping are all shown to be individually capable of explaining available paleodata constraints provided that significant calcium carbonate compensation is allowed. None of the scenarios require more than a very minor (order 1 °C) glacial reduction in low to mid latitude sea surface temperature although scenarios with larger changes are equally plausible. One explanation for the fairly wide range of plausible solutions is that most paleo-data directly constrain the inventory of paleo-tracers but only indirectly constrain their fluxes. Because the various scenarios that have been proposed to explain pCO₂ levels during the last glacial maximum are distinguished primarily by different fluxes, the data, including ocean ¹³C concentrations, do not allow one to confidently choose between them. Oceanic ¹⁴C data for the last glacial maximum, which can constrain water mass fluxes, present an excellent potential solution to this problem if their reliability is demonstrated in the future.

1. INTRODUCTION

During the last four glacial maxima, atmospheric carbon dioxide concentrations were depressed roughly 80 ppm relative to interglacial values [1]. Furthermore, ice core data show a remarkable correlation between rapidly increasing inferred temperature and atmospheric CO₂ concentrations during deglaciations, suggesting some kind of causal link. Several oceanographic mechanisms have been proposed, either individually or in concert, to explain the decrease in atmospheric CO₂ associated with glacial states. These include: increased efficiency of the “biological pump,” in which net carbon uptake, especially by the high latitude marine biosphere, is increased relative to upwelling fluxes [2,3], changes in the rate of ventilation of deep water in the Southern Ocean [4,5], decreased global thermohaline circulation [2,6], enhanced air-sea exchange in the northern Atlantic [7], decreased air-sea exchange in the Southern ocean due to enhanced sea ice cover [8,9], increased solubility of CO₂ in colder seawater [10], and a mid-depth chemical divide separating water masses with low and high CO₂ concentrations [5]. Some studies claim to elucidate simple mechanisms which explain decreased CO₂ during glacial times [5,9], while others claim that all simple mechanisms can be eliminated from consideration [11,12].

A common set of tools used to study the marine carbon cycle and its role in controlling atmospheric CO₂ concentrations are meridional box models of varying levels of complexity [2,5,6,7,9]. These models generally consist of a series of conservation equations for tracers such as total carbon, carbon isotopes, oxygen and nutrients. Parameters, such as the strength of the global meridional overturning circulation, air-sea gas exchange coefficients for various

* Email : alverson@pages.unibe.ch.

surface boxes, the rate of particle sinking out of various surface boxes, and rates of mechanical mixing between various boxes are set to specified values or sometimes varied over a range of potential values to examine parameter sensitivities. Exact, or arbitrarily close to exact, solutions are found, either algebraically, if the box model is simple enough, or by a numerical iterative procedure. If a given set of parameter values allows the model equations to be satisfied, while at the same time satisfying the paleodata constraints, the model is said to explain the decrease in atmospheric CO₂ associated with glacial states.

In this paper we use the recently published 7-box model of Togweiler (1999) [5], referred to hereafter as T99, and explain low glacial atmospheric CO₂ concentrations with several different mechanisms by invoking a new method of solution. The philosophy behind this method of solution can be summarized as follows:

- **Paleo-data are not exact.** Thus, the model parameters and solutions are required only to lie within specified lower and upper bounds based on available data constraints.
- **Paleo-box models are not exact.** Thus, the model equations are required to balance only to within an allowed residual misfit. This criterion can be thought of either as an explicit statement that the model is not believed to be perfect, a rejection of strictly steady state dynamics in favor of a ‘quasi-steady’ state, or some combination of the two.

We argue that previous methods of solution have been struggling to satisfy very stringent constraints, some of which are actually not justified in view of the simplifying assumptions inherent to any box modeling approach. Principal among these are assumptions of model perfection and/or exact steady state dynamics as well as prescription of poorly known model parameters, notably the sea surface temperatures (SSTs) and coefficients of CO₂ gas exchange at the air-sea interface.

These assumptions are often required in order ensure that the number of equations match the number of unknowns. The glacial CO₂ problem is, however, a fundamentally underdetermined problem in which the state of the climate system must be inferred from a limited amount of data and imperfect models. One way to handle underdeterminacy without making unjustified assumptions is to use inverse methods [13]. These methods combine observational and modeling constraints to estimate “to the best of our knowledge” the state of the climate system. They deal with imperfect data and imperfect models by explicitly specifying the uncertainties.

The objective of the present work is to show that a wide (presumably infinite) range of solutions to the LGM CO₂ problem can be found if the assumption of exact steady state is relaxed and parameters, such as piston velocities, are treated as adjustable variables in the model. Inverse methods yield a much wider range of solutions consistent with available constraints than do simple methods based on the resolution of a set of equations with matching number of unknowns because they do not require arbitrary assumptions about missing data or model parameters. Moreover, these methods can be designed to automatically search for optimal solutions consistent with available constraints within their range of uncertainties instead of requiring the modeler to employ a painstaking “manual” search through parameter space. The present study relies on an inverse method specifically designed to solve the last glacial maximum (LGM) CO₂ problem in its box modeling form. An estimate of the state of the climate system during the LGM is searched for, with the requirement that it is consistent with the box model conservation equations and the set of observational constraints presented in T99. Imbalances in the model equations are tolerated as long as they do not exceed small values chosen to represent a reasonable degree of non-steadiness. When

these imbalances are tolerated, various solutions are found spanning a wide range of mechanisms that could have caused the low CO₂ levels during the LGM. In other words, the available paleodata, including decreased atmospheric CO₂, oxygenated deep water, and carbon isotope distributions are consistent with various scenarios, including scenarios that would probably be rejected if exact model constraints were imposed.

The paper is organized as follows. In section 2 we present the numerical machinery that we have used to enable Toggweiler's nonlinear seven box model to incorporate uncertainties in both the paleodata constraints and the box model dynamics. In section 3 we present several model solutions to the reduced glacial CO₂ problem and, in section 4, our conclusions.

2. A NONLINEAR, INVERSE SEVEN BOX OCEAN BIOGEOCHEMICAL MODEL

This study is based on the seven-box model developed by Toggweiler and shown in Figure 1. This model is one of the most complete box models of the oceanic CO₂ system and has shown significant skill in reproducing the paleogeochemical observations available for the LGM. It can be downloaded from the ftp site kosmos.agu.org and, because it is written in FORTRAN, can be incorporated in an inverse procedure based on standard optimization freeware. Our choice to use a published box model makes the impact of the inverse method more salient as our results can be directly compared to those of T99. The basic equations of the seven box model have not been changed, only the method of solution is new. Several model parameters have been recast as additional variables, however, since the inverse approach can handle underdetermined problems. These new variables include volume fluxes in the ocean boxes of the model, particle fluxes sinking from the surface of the ocean, temperatures in the upper ocean boxes, salinity, piston velocities and the amount of total CO₂ added to the carbon system by calcium carbonate compensation. These variables were treated as fixed parameters in T99, although the effects of convection in the polar box and particle flux sinking from the low latitude box were explored in a systematic manner.

The objective of the present study is to show that a wide range of solutions exists which is consistent with the glacial paleo-data and the conservation constraints contained in the 7-box model. We cannot claim to have included all the observational and model constraints available for the LGM, but rather investigate the LGM CO₂ problem as posed in T99.

The procedure used to ensure that the inverse solution fits the data is to constrain every variable of the box model to lie within predefined lower and upper bounds. These bounds are chosen to represent uncertainties in the observations, pCO₂ for instance is required to lie between 180 and 200 μatm for all our LGM experiments. In the absence of direct observations, the bounds can be chosen to represent prior knowledge of the tracer distribution. Oxygen concentrations in the deep ocean, for instance, are constrained to be larger than 25 $\mu\text{moles kg}^{-1}$. Another characteristic of the inverse procedure is that it allows imbalances in the tracer conservation equations while keeping these imbalances small compared to the individual flux terms that comprise the equations. This result is achieved by using an optimization procedure that minimizes the residuals of the conservation equations. The procedure chosen here is an iterative one that belongs to the group of 'minimax' algorithms [14]. At each step, the routine selects the maximum equation residual as the objective function and then minimizes it, whence its name. In mathematical terms, the objective function, which is a scalar, can be written at each iteration:

$$J = \max (|f_i(\mathbf{x})|), i=1,M$$

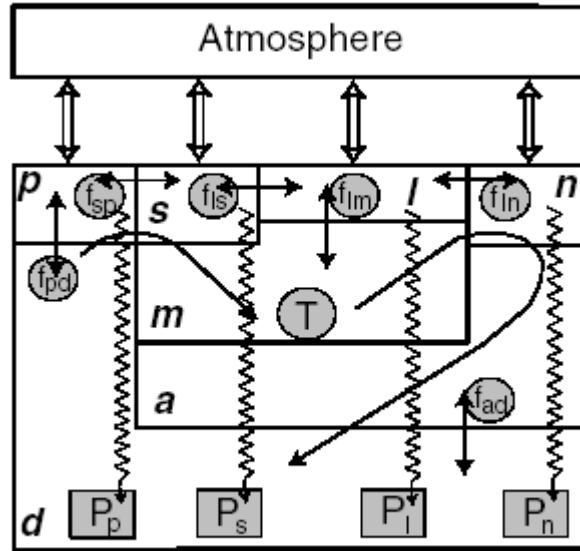


FIG. 1. Schematic representation of the seven box non-linear carbon model adapted from the forward carbon model of Toggweiler (1999) [5].

where M is the number of equations that constitute the box model, f_i is the equation residual number i , \mathbf{x} is a vector that contains all the variables (the ‘state’ vector), and \max is the operator that finds the maximum number among a series of reals. With this notation, the optimization problem can be written:

$$\text{Find } \mathbf{x} \text{ that minimize } J \text{ subject to } \mathbf{lb} \leq \mathbf{x} \leq \mathbf{ub}$$

where \mathbf{lb} and \mathbf{ub} are vectors containing the lower bounds and the upper bounds of the model variables. Using the same mathematical formulation, the box model, as used in T99, would be written:

$$\text{Find } \mathbf{x} \text{ such that } f_i(\mathbf{x}) = 0, i = 1, M$$

In the latter case, the number of equations, M , must be equal to the number of variables in order to have a well-posed mathematical problem. In the inverse formulation, the number of equations is smaller than the number of variables, but this does not present a problem since the state vector is constrained to lie within lower bounds and upper bounds, preventing unreasonable solutions. The equations used in the inverse problem are basically those of T99, namely temperature conservation in the deep ocean boxes, phosphate and alkalinity conservation in all the ocean boxes, oxygen conservation in all the ocean boxes except the low latitude box (where it is simply set to its saturation value), together with CO_2 , ^{13}C , and ^{14}C conservation equations in all the ocean boxes and in the atmosphere box. Conservation of the inventory of phosphate, alkalinity, total CO_2 , total ^{13}C and total ^{14}C is also imposed. Two additional equations link the pH in the mid-depth box and the concentration of the carbonate ion in the deep box to a function of Alkalinity and total CO_2 . These 54 equations, or more precisely these 54 equation residuals, are expressed as functions of the 70 elements of the state vector. These are volume fluxes between the ocean boxes, particles fluxes sinking from the surface boxes, temperature, salinity, phosphate, alkalinity, oxygen and CO_2 concentrations in the ocean boxes, partial pressure of CO_2 in the atmosphere box, $\delta^{13}\text{C}$ and $\Delta^{14}\text{C}$ ratios in the

ocean and atmosphere boxes, piston velocities controlling air-sea gas exchange in each ocean surface box, and the amount of CO₂ added to the ocean/atmosphere carbon system through dissolution of calcium carbonate. The equations that link pH in the mid-depth ocean box and carbonate concentration in the deep ocean box are different from the other equations in the sense that they are not conservation equations, but they are nonetheless treated in the same way as the other equations.

One important issue in the inverse formulation of the box model, and in most inverse methods [13], is the normalization of the residuals $f_i(\mathbf{x})$ of the tracer conservation equations. The residuals must be weighted so that the minimization procedure does not minimize some of them down to infinitesimal levels while leaving others at unrealistically large levels. This problem can arise for instance because residuals are expressed in different units for different tracers, as is the case when temperature residuals are compared with alkalinity or CO₂ residuals. In the present calculation, all the equations were systematically normalized by reference fluxes in order to ensure that the minimization procedure treats all the constraints equally. Details regarding the normalization procedure can be found in [15].

These normalization factors can be thought of as representing non-steady state terms in the tracer conservation equations. The amplitudes of these terms then correspond to the conservative assumption that the non-steady state terms would take 10,000 years to cause changes of the order of those observed during the glacial-interglacial transitions. In reality, the climate system is known to have been subject to much more rapid temporal fluctuations during glacial periods, such as Dansgaard-Oeschger and Heinrich events [16]. An example of how small the allowed residuals are is provided by the fact that the residual carbon fluxes going into and out of box d are of the order of 0.02 GtC/year. However small they are, these residuals are nonetheless fundamental to the results presented in this study. They provide the model enough freedom to find a wide range of solutions that would otherwise be likely to be rejected if exact tracer conservation were imposed. Viewed in this way, the residuals in our model play the same role as the time-dependent terms in the open modeling approach of [17] in which small imbalances between riverine input and sediment burial are sufficient to radically change the solution to which their model converges. Interestingly, the order of magnitude of the rate of change in the inventory of PO₄ tolerated in our study (about 3×10^{12} moles in 10,000 years) is of the same order of magnitude as the rate of change obtained by [17] for a doubling of the thermohaline cell (about 10^{15} g in 50,000 years, or 2×10^{12} moles in 10,000 years).

An alternative interpretation of the equation residuals is that they constitute an explicit allowance for the limitations of the box model. In this interpretation, much larger residuals could be tolerated because the 7-box ocean model is a very crude representation of the real global carbon system. In this case, the small amplitude of the tolerated residuals shows that the assumptions made in the present study are rather conservative.

The minimization of the cost function is carried out using a simulated annealing algorithm. For a reference in an oceanographic context, see [18]. The minimization package employed here, is a freeware initially developed by researchers in econometrics [19]. This particular algorithm was chosen because it ensures that no individual residual is too large and because it requires very few assumptions regarding the form of the function to be optimized. Further information about the minimization procedure can be found in [15].

3. SOLUTIONS

The modern, preindustrial (or interglacial) high atmospheric CO_2 solution, shown in Figure 2, is within numerical precision the same as in T99. Note that this solution is also similar to the modern, pre-industrial solution presented by [9], referred to hereafter as SK00, using a 6-box model. Starting with such an interglacial/modern preindustrial solution, several mechanisms have been suggested for how the ocean model should be perturbed in order to produce the ~ 80 ppm decrease in atmospheric CO_2 associated with glacial conditions. Here we present four different model experiments, three of which are consistent with both model dynamics and the observational constraints associated with glacial periods plus one unsuccessful attempt. All these experiments involve significant CaCO_3 dissolution, which is parameterized in the model by the addition of a uniform amount of CO_2 in all the ocean boxes and the addition of twice this amount of alkalinity equivalents. These experiments are:

- A. Reduced ventilation of Southern Ocean deep water
- B. Reduced air-sea gas exchange at high southern latitudes
- C. Enhanced high latitude biological pumping
- D. Decreased global SST

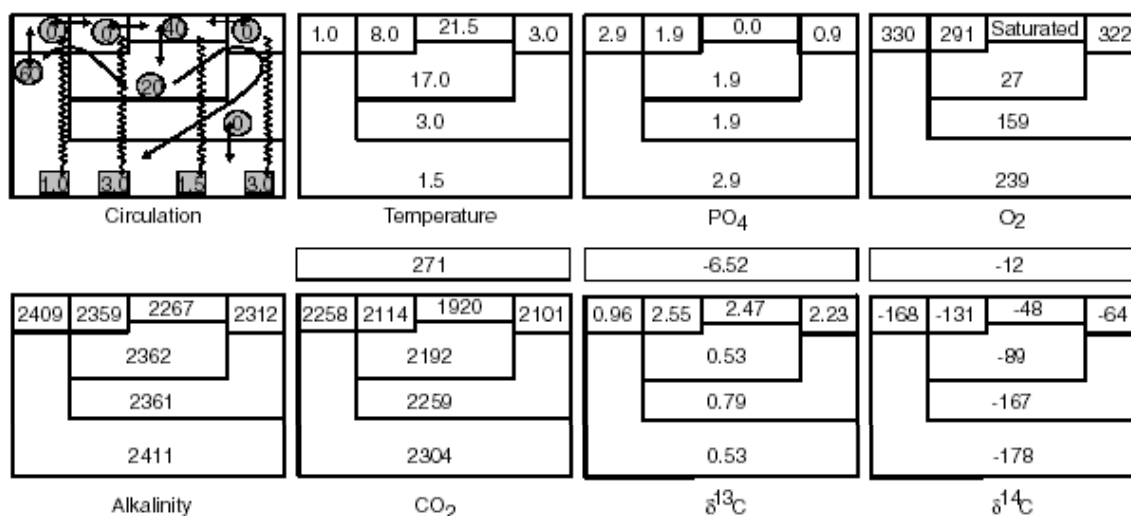


FIG. 2. Modern, preindustrial reference solution (M) found using the inverse model.

Each of these solutions is obtained with a significant, imposed change in the control variables that characterize the individual scenario, small, automated changes to the other ocean model parameters and minimal allowed equation residuals. Although changes in parameters other than the control variables are individually small, they are often required in order to achieve consistency with the principal change imposed in each scenario. In the reduced ventilation scenario for instance, failing to allow small changes in transport variables other than southern ocean ventilation would lead to an artificial reduction in the range of possible solutions. In that case, one would not be searching for a general reduced ventilation solution for the LGM, but a very specific LGM solution in which, T is exactly 20 Sv, f_{lm} is exactly 40 Sv, etc. If such

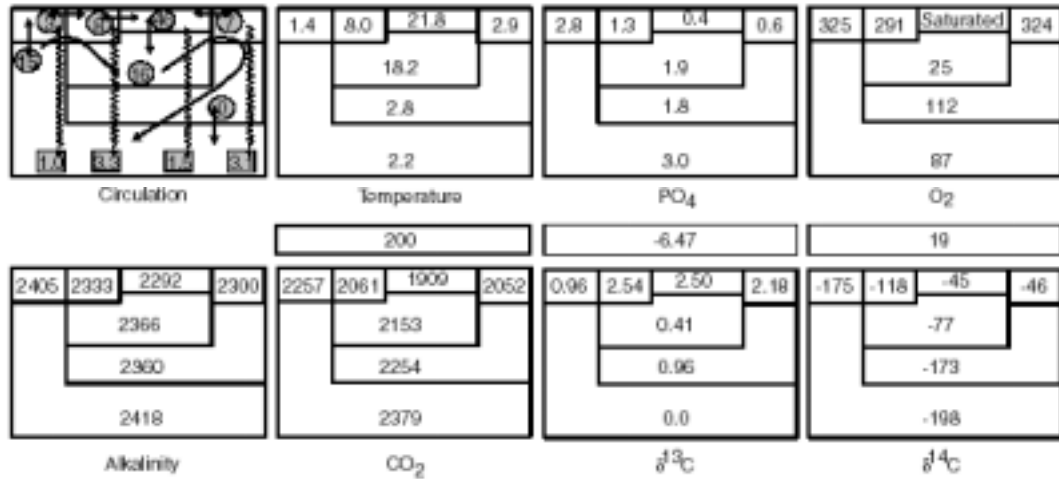


FIG. 3. An LGM solution (A) with reduced ventilation of Southern Ocean deep water found using the inverse model. The solution is similar to that of (Toggweiler 1999) [5], but does not require as large a surface temperature decrease. The CO_2 and alkalinity values shown do not take into account the addition of $60 \mu\text{mol kg}^{-1}$ and $120 \mu\text{mol kg}^{-1}$ respectively by CaCO_3 dissolution.

a solution could not be found to be consistent with the low pCO_2 levels of the LGM, one might wrongly conclude that the reduced ventilation scenario is not consistent with paleo-data. Below, we briefly present each of the LGM solutions in turn.

A. Reduced ventilation of Southern Ocean deep water

In this solution, shown in Figure 3, reduced mixing between the surface and deep ocean in high southern latitudes, combined with a dissolution of CaCO_3 that raises the mean total CO_2 of the ocean by $60 \mu\text{moles/kg}$ and otherwise very limited changes, is able to explain low glacial period atmospheric CO_2 . This solution was found using the modern solution as an initial state and, unless otherwise specified, allowing the inverse model to vary model parameters within a 10% range. Ocean transports were allowed to vary between 0 and 60 Sv. Deep ocean $\delta^{13}\text{C}$ was initialized to resemble the reconstruction of [20], however the low mid-depth $\delta^{13}\text{C}$ values in his reconstruction were found to be inconsistent with the total inventory of ^{13}C in the reservoirs of the model. The value-of $\delta^{13}\text{C}$ in box a was therefore allowed to increase up to 1‰. An alternative, more rigorous, approach would have been to recompute the modern ocean solution in order to make it consistent with the inventory implied by the Boyle reconstruction [20], but the present approach was preferred because it allows direct comparisons of our solutions to the solutions found by T99. This choice has no impact on our conclusions. Surface $\delta^{13}\text{C}$ was constrained to be $2.7 \pm 0.3\text{‰}$ in the low latitude box (l). Note that all of our solutions are presented without the ‘terrestrial biosphere effect’, which is expected to reduce $\delta^{13}\text{C}$ values by approximately 0.35‰ [5]. Therefore, as in T99, no CO_2 of biospheric origin was added to the ocean/atmosphere inventory. Finally, in order to satisfy the constraint of higher pH at mid depths during the LGM [21], the mid-depth (box a) pH is constrained to be consistent with alkalinity and total CO_2 with a value of 8.3 ± 0.1 . The paleodata constraints applied to this, and all other, LGM solutions presented in this paper are summarized in Table I.

Table I. Paleodata constraints imposed on all LGM experiments

Atmospheric Carbon (ppm)	Atmospheric partial pressure of CO ₂ must be order 80 ppm lower than preindustrial values. [1]	$180 \leq p\text{CO}_2 \leq 200$
Oceanic Oxygen ($\mu\text{mol Kg}^{-1}$)	The deep water must remain oxygenated (T99)	$O \geq 25$ in all ocean boxes
$\delta^{13}\text{C}$ (‰)	The mid latitude vertical $\delta^{13}\text{C}$ gradient must be order 50% higher than for the modern control. The enhanced gradient must be driven by a decrease in the deep ocean. [20]	$-6.47 \leq \delta^{13}\text{C}_{\text{atm}} \leq -6.87$ $-0.2 \leq \delta^{13}\text{C}_{\text{d}} \leq 0.0$ $-0.1 \leq \delta^{13}\text{C}_{\text{a}} \leq 1$ $0.35 \leq \delta^{13}\text{C}_{\text{m}} \leq 0.77$ $-1.0 \leq \delta^{13}\text{C}_{\text{p,s,n}} \leq 4.0$ $2.9 \leq \delta^{13}\text{C}_{\text{l}} \leq 3.2$
Mid-depth pH (box a)	Mid depth pH must be relatively high [21]	$8.2 \leq \text{pH}_{\text{a}} \leq 8.4$
Salinity	The expected ~1 ‰ glacial salinity increase has not been included in order to keep our results consistent with T99. This does not effect our conclusions.	$34.6 \leq S \leq 34.8$
Deep CO ₃ ⁼ (box d)	This uncertainty range is extrapolated from T99, Table 6. Values actually remain between 87.2 and 90.1 in all LGM scenarios.	$83 \leq \text{CO}_3^= \leq 93$
Phosphate	Low latitude surface concentrations must remain low (T99)	$0 \leq P_{\text{l}} \leq 0.4$
All other parameters (unless specified otherwise in text)	Must remain within 10% of their prescribed initial values. Exceptionally, parameters with initial values at or near zero are given small absolute limits. For example mixing between surface boxes must remain between 0 and 2 Sv and $\Delta^{14}\text{C}$ within 50‰ of its initial values.	$0.9X_{\text{init}} \leq X \leq 1.1X_{\text{init}}$

Solution A is not markedly different from the reduced ventilation LGM solution presented in T99, except that it does satisfy the paleo-constraints without requiring a large change in the surface ocean temperatures. Whereas T99 required reduction of low to mid latitude SST's by 4°C at LGM, our solution has no significant change (Table II). Of course this does not mean that we cannot find a solution with a larger drop in SST. Indeed, the inverse model does find a solution with a strong reduction in temperature in the low-latitude surface box (not shown). We conclude only that a large temperature decrease is not required. The concentration in total CO₂ goes up by 75 $\mu\text{mol kg}^{-1}$ in the deep ocean box because of the reduced ventilation of this box. This value does not include the rise of approximately 60 $\mu\text{mol kg}^{-1}$ associated with the dissolution of CaCO₃. Because the inventories of tracers are not exactly conserved, the ratio of the input of alkalinity over the input of total CO₂ turns out to be 2.13:1 instead of the generally employed 2:1 ratio. This small deviation from the theoretical ratio is associated with a decrease in CO₃⁼ of only 0.9 $\mu\text{mol kg}^{-1}$ in the deep box and thus does not significantly affect the depth of the lysocline.

Table II. Modern – LGM temperature changes (°C) employed in previous studies and scenarios A, B, C. The mid to low latitude values are shaded

	SK00	T99	A**	B**	C**
Polar southern box (p)	~3*	~2*	-0.4	1.0	0.9
Southern box (s)	5	2	0	1.0	0.9
Low latitude box (l)	5	4	-0.3	1.0	1.0
Northern box (n)	~4*	2	0.1	0.7	1.0

* Temperature was not allowed to drop below the freezing point of surface sea water.

** Temperature was not constrained. Solutions were also consistent with larger temperature anomalies. Note that attempts to find an LGM solution driven only by SST decreases were unsuccessful.

Solutions that would be consistent with the low PCO_2 values of the LGM atmosphere without CaCO_3 dissolution were also searched for but with no success. This does not mean that such a solution does not exist, but that the search algorithm failed to find one. However, in view of the number of trials that we carried out, our intuition is that such a solution is unlikely to exist. This suggests that CaCO_3 dissolution plays a key role in lowering atmospheric pCO_2 . Note that the small departures from the modern reference solution required for variables other than the transport variables, such as the 0.4°C temperature difference in box (p), would be very difficult to detect using paleo-data. In fact, they would even be difficult to detect if the modern ocean were to be represented by a crude inverse 7-box model. We conclude that a reduction in ventilation of the deep ocean at high southern latitudes is one possible scenario consistent with all of the paleo-constraints we employed. However, such a scenario is not required by either the data or the model, as demonstrated by our other solutions.

B. Reduced air-sea gas exchange at high southern latitudes

Solution B, shown in Figure 4, is similar to the solution of SK00 in which extensive Antarctic sea ice during the LGM is postulated to have drastically restricted air sea fluxes of CO_2 in high southern latitudes. In order to mimic this effect, rather than changing the actual area of gas exchange, which would require that the topology of the model itself be changed, we have instead allowed the model to adjust the local exchange coefficient (piston velocity). An overview of piston velocities employed in our scenarios, alongside those from T99 and SK00, is shown in Table III. Since the exchange coefficient is always multiplied by the surface area in the model, this has exactly the same effect as reducing the surface area available for exchange. The model was started from the modern solution M as an initial condition and the gas exchange rates were allowed to vary within 0.5 to 10 m/day. Except for the dissolution of CaCO_3 , which increases average total CO_2 by $54 \mu\text{mol.kg}^{-1}$ and total alkalinity by $108 \mu\text{eq.kg}^{-1}$, the most significant change found by the model with respect to the modern solution is the reduction of the piston velocity at the surface of the southern polar box from 3 m/day to 0.5 m/day. This gas exchange value of 0.5, the lowest we have allowed the model to adjust to, is a decrease by a factor of 6 relative to our modern value. By comparison, the change in sea-ice extent proposed by SK00 corresponds to a reduction in gas exchange at high southern latitudes in their LGM solution by a factor of 100 relative to the modern value. In our experiment, the flux of CO_2 from the surface polar box to the atmosphere is reduced by only a factor of 2 relative to the modern solution, the five-fold reduction in piston velocity being partly compensated by an increase in the air-sea gradient of pCO_2 these regions.

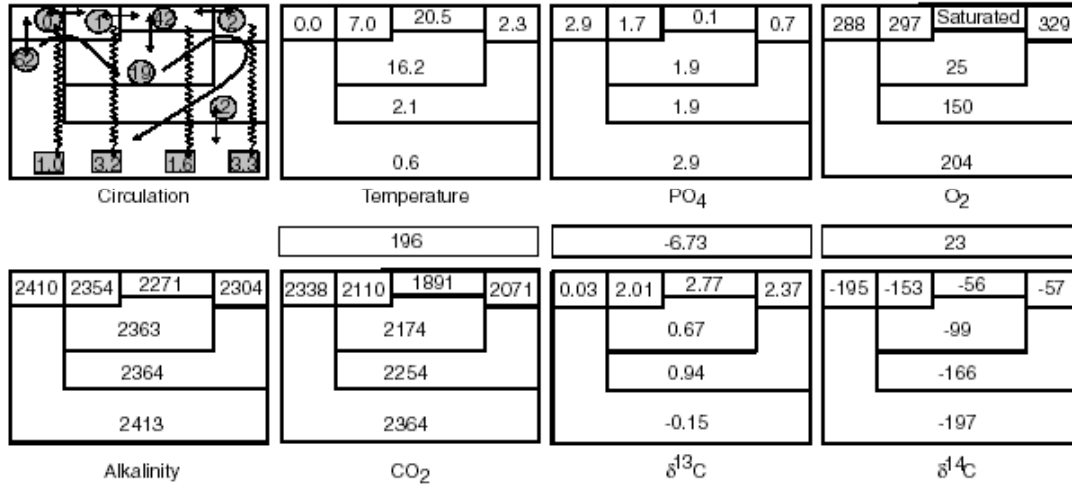


FIG. 4. An LGM solution (B) with reduced air-sea flux in the Southern Ocean found using the inverse model. The solution is similar to that of Stephens and Keeling(2000) [9], but involves a smaller gas exchange perturbation relative to the modern and a smaller surface temperature decrease. The CO₂ and alkalinity values shown do not take into account the addition of 54 $\mu\text{mol kg}^{-1}$ and 108 $\mu\text{mol kg}^{-1}$ respectively by CaCO₃ dissolution.

Table III. Piston velocities (m day⁻¹) in previous studies and scenarios A, B, C

	SK00**	M & T99*	A	B	C
Polar southern box (p)	6.6 (5.9) 0.066 (0.059)	3.00	2.72	0.50	2.72
Southern box (s)	7.8 (6.5)	3.00	3.16	3.15	2.71
Low latitude box (l)	4.1 (3.6)	3.00	3.19	2.58	2.92
Northern box (n)	6.9 (5.9)	3.00	3.29	4.31	2.70

* T99 employs a uniform value of 3 m/day in all boxes for both modern and LGM experiments.

** SK00 report their air sea flux parameterization as a CO₂ “invasion rate” of 0.15 and 0.05 moles m⁻² yr⁻¹ μatm^{-1} at high and low latitudes respectively. In order to convert to m day⁻¹, as expressed here, requires dividing by the solubility of seawater, which is a function of temperature and salinity. The values presented here have been calculated using solubility calculated from the surface water properties employed by SK00 for their modern control solution. The values in brackets include the temperature reductions they impose for LGM, namely a uniform 5 °C cooling not to exceed the freezing point of seawater. The value in bold, represents the factor of 100 degrees in ice-free area which distinguishes the SK00 ‘possible glacial’ state.

It is interesting to note, that the coefficient of air sea exchange is a parameter to which the model is quite sensitive, yet it is at the same time extremely poorly known, both for the modern ocean and especially for the LGM. T99 employs a uniform value of 3 m/day while SK00 use quite different values (Table III). The difference between these two published high latitude gas exchange flux coefficients is more than a factor of two. It is known that the coefficient has a strong dependence on wind speed, and a rather weaker dependence on SST. Calibrations against these physical parameters are summarized by Wanninkhof [22], who suggests a first order wind speed dependence, for long term, climatological winds, of $k = 0.39u^2$ with an uncertainty in the coefficient 0.39 of about 25%. The temperature dependence

is smaller than that for wind, partly due to counteracting temperature effects on gas diffusion coefficients (the Schmidt number dependence) and the chemical enhancement factor [22]. Nonetheless, the temperature dependence represents roughly an additional 10% uncertainty in piston velocity. Thus, for the modern ocean, the piston velocity can only reasonably be prescribed to within about 35% uncertainty. The generally accepted uncertainty in modern air-sea CO₂ fluxes, which includes uncertainties in both piston velocity and the air-sea CO₂ partial pressure difference, is of order 100% [23].

For the LGM, when wind speeds were likely to have been significantly higher the situation is even more undetermined. For example, if, for a given region, modern average wind speed is 5 m s⁻¹, and the LGM average was 7 m s⁻¹, the piston velocity at LGM in this region, as a result of the necessity of squaring these values, would be approximately double its modern value, based on wind speed change alone. Of course regional wind speeds may have been less during the LGM, meaning that for any one surface box at LGM, piston velocity probably cannot be prescribed with an uncertainty of less than 100%. This range of uncertainty, combined with the possibility of large temporal and regional variations, suggest that the range of piston velocities tolerated in this study is plausible, and that studies which prescribe piston velocity values exactly possibly miss a large range of relevant parameter space.

Allowing for the uncertainty in piston velocities at LGM, together with some CaCO₃ dissolution, is thus sufficient to enable the inverse model to find a LGM solution consistent with the paleodata and model which we have employed. In contrast to the SK00 solution, which incorporates a 5°C decrease in low to mid latitude SSTs, our solution contains only a 1°C decrease (Table II), although solutions consistent with larger SST certainly cannot be ruled out.

C. Enhanced high latitude biological pumping

The possibility of an enhanced LGM biological pump in which net carbon uptake by the marine biosphere is increased relative to upwelling fluxes and subsequently sequestered in the deep ocean via particle fluxes is well known [2,3,24,25]. Our Enhanced biological pump solution, C, is shown in Figure 5. The experiment was initialized with the modern solution M with the exception of the $\delta^{13}\text{C}$ values, which were constrained, as in previous runs, to match the LGM values. In addition, the biological particle fluxes out of the surface ocean boxes (p,s,n and l) were provided allowable ranges of 0.5 to 10 molesCm⁻²yr⁻¹. The principal difference between this solution and the modern solution, apart from higher values of total CO₂ and alkalinity of respectively 53 μmolkg^{-1} and 106 μeqkg^{-1} due to CaCO₃ dissolution, is an enhanced particle flux in the high northern and southern latitude boxes. The particle flux found by the inverse model in polar ocean box, p, is 6.7 molesCm⁻²yr⁻¹ compared to the modern value of 1 moleCm⁻²yr⁻¹ and in the northern ocean box, n, 5.7 molesCm⁻²yr⁻¹ instead of 3 molesCm⁻²yr⁻¹, about double that in the modern value. Relative to modern conditions temperature in all the surface ocean boxes decreases by 1°C or less (Table II), although solutions with larger temperature drops are equally acceptable. Note that this enhanced biological pumping solution does not cause anoxia in the deep ocean and does satisfy the imposed LGM $\delta^{13}\text{C}$ constraints, including increased $\delta^{13}\text{C}$ vertical gradients driven by lighter values in the deep ocean. Thus, when one allows for reasonable uncertainty in model parameters and small imbalances in model equations, an increase in biological activity in the Southern Ocean, combined with reasonable CaCO₃ dissolution, is sufficient to produce an LGM solution consistent with the prescribed paleodata constraints.

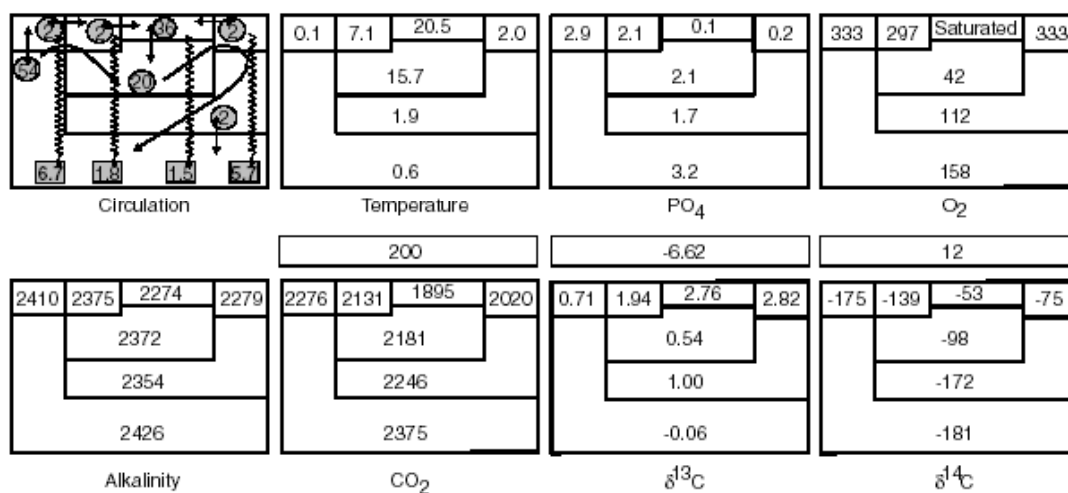


FIG. 5. An LGM solution (C) with enhanced biological carbon pumping at high latitudes found using the inverse model. This solution satisfies observational constraints on the distribution of $\delta^{13}\text{C}$ and allows for oxygenated deep water. The CO_2 and alkalinity values shown do not take into account the addition of $53 \mu\text{mol kg}^{-1}$ and $106 \mu\text{mol kg}^{-1}$ respectively by CaCO_3 dissolution.

D. Reduced SST

It is well known based on the temperature dependence of the equilibrium partial pressure of CO_2 in surface seawater that cooling the ocean surface alone can account for a significant fraction of the decrease in atmospheric CO_2 during glacial times. We therefore sought a solution consistent with the paleo-constraints, including the low $p\text{CO}_2$ in the atmosphere, which would not differ much from the modern solution, except that much lower temperatures would be tolerated in the ocean boxes, together with reasonable amounts of CaCO_3 dissolution. No such solution was found by the model. Although this does not constitute proof that such a solution does not exist, it does suggest that other mechanisms are probably required to satisfy all the constraints. The problem with this scenario seems to be not so much a difficulty lowering $p\text{CO}_2$ in the atmosphere, which can easily be done by combined lower ocean temperatures and CaCO_3 dissolution, but the difficulty in doing so while keeping carbonate close to modern levels. Apparently, lower temperatures do not allow a sufficient increase in CO_2 in the deep ocean to compensate for the large rise in alkalinity produced by CaCO_3 dissolution. Because of this, the difference between alkalinity and total CO_2 is too high in the deep ocean and results in unreasonably high $\text{CO}_3^{=}$ levels. One conclusion to be drawn from this attempt is that, even within the context of the wide range of solutions available to the inverse model, it seems unlikely that a solution forced by ocean temperature changes alone exists. It is interesting to note that we have also sought a solution with minimal change from modern parameters, i.e. with CaCO_3 dissolution providing the only mechanism for CO_2 drawdown. No such solution was found to be consistent with all the paleo-constraints, apparently for similar reasons as in the low temperature experiment.

4. CONCLUSIONS

We present our conclusions in two parts. First with respect to the use of inverse modeling techniques and, second with respect to the cause of glacial-interglacial changes in atmospheric $p\text{CO}_2$.

The T99 box model is not the only model amenable to solution with inverse techniques. The model was chosen because it is one of the most complete box models of the oceanic CO₂ system, because it has shown significant skill in reproducing the paleogeochemical observations available for the LGM, and because the author has generously made it publicly available by ftp. There are some aspects of the model which, from the point of view of inverse modeling, could be improved. In theory, solutions would be found with greater ease if mixing terms between every box were retained, whereas the T99 model sets several inter-box mixing terms (between boxes m and a, n and a, and m and d) identically to zero. Allowing small amounts of mixing to occur is both more reasonable physically, and would also allow the inverse procedure to more easily find solutions.

The curious reader may wish to insert one of our solutions into the T99 model as an initial condition and check if the model converges. The model does converge, but to a solution different from the one we produce (usually the main differences are in the ¹³C values). At first this may seem to invalidate our solutions. We argue that this is not the case. In fact, it highlights the importance of the inverse method. A researcher employing a trial and error or parameter space mapping approach with the forward model would not find these solutions because the model cannot deviate from exact steady state. In the forward modeling approach, relaxing the steady state assumption requires that the time-dependant terms are modeled explicitly as in the open ocean approach of [17]. Note that the inverse modeling methodology can also be applied to time-dependent problems using data assimilation techniques developed in meteorology and physical oceanography. The difficulty involved in such a task is merely a technical one and is the subject of ongoing research. One obvious advantage of using a time dependent model would be that non-steady state terms would be explicitly modeled rather than incorporated in the equation residuals. In this case the equation residuals would likely be decreased relative to those that we have tolerated, though they should not be expected to vanish completely since no model is perfect. Even the most sophisticated time-dependent general circulation models have errors.

One obvious question to ask is whether our solutions are dependent on having used a simple box model. We believe that more sophisticated models, such as 3 dimensional box models, or even general circulation models, will produce similar results, and possibly even widen the range of potential solutions. This is because for each box added, the model will be provided additional degrees of freedom. That is, the system will contain more unknowns, while the number of data constraints may remain unchanged or be only slightly increased. For instance, if one were to add a box to represent the terrestrial biosphere, rough estimates of the terrestrial carbon input to the ocean during LGM that have been published in the literature would provide one additional weak constraint. However, the very stringent constraint that the oceanic inventories of total CO₂ and alkalinity can vary only through CaCO₃ dissolution would then be released. The system would thus become more underdetermined despite the increase in complexity of the model, making solutions easier to find, not more difficult.

Finally, there are probably data constraints for the LGM that we have not taken into account in the current study. As the field of paleoceanography grows, the appearance of new, and tighter constraints is inevitable. New data constraints which may conflict with the solutions presented in this paper, will only require that the model be rerun incorporating the additional constraints. Only if the model proves incapable of finding a new solution satisfying such hypothetical new constraint, would any of the three scenarios we have explored need to be rejected.

In conclusion, the paleo CO₂ problem is not fully determined by available paleo-data or paleo-box models. Several plausible solutions exist, including increased ventilation, increased biological pumping or decreased gas exchange in the Southern Ocean. Our model scenarios satisfy all the paleo-constraints considered in T99, including carbon isotope distributions, oxygenated deep water, and mid-depth pH reconstructions. The model reconciles the reduced polar air-sea flux scenario proposed by SK00 with atmospheric levels of $\delta^{13}\text{C}$ during the LGM and the biological pump scenario proposed by many researchers with the distribution of $\delta^{13}\text{C}$ in the glacial ocean. It also finds solutions similar to those proposed by T99 and SK00 without requiring the large low to mid latitude SST changes (4 and 5 °C respectively) employed in those studies. All the parameters modified by the inverse procedure, other than the parameters central to each experiment, are so slightly changed that they are unlikely to be detectable in the glacial ocean or, arguably, in the present day ocean. The available paleo-constraints does not discriminate between these three scenarios, all are equally acceptable.

One explanation for the fairly wide range of plausible solutions is that most paleo-data constrain the inventory of paleo-tracers rather than their fluxes. ^{13}C data, for instance, tell us what the inventory of this isotope was during the LGM in the various basins of the ocean, but they do not directly tell us the rate at which this tracer was exchanged between the reservoirs. This point is particularly obvious if one releases the constraints on conservation of total inventories of phosphate, alkalinity, and CO₂ isotopes, and the constraint on carbonate ion concentration in the deep ocean box (in some sense, the constraint on $\text{CO}_3^{=}$ in the deep ocean is also a constraint on the inventories because it constrains the depth of the lysocline). We began the present study without these constraints and found that almost any scenario, including the modern solution, was consistent with the paleo-data provided that very minor changes in the circulation were tolerated. This is because all that is required to lower pCO₂ in the atmosphere is either a decrease in total oceanic CO₂ levels, or an increase in alkalinity. In such solutions, the glacial $\delta^{13}\text{C}$ profiles can easily be reproduced by small adjustments to the ocean circulation [26]. Of course, constraints on global inventories cannot be released, but this example does show that the fluxes of volume and tracers are, for the most part, not directly constrained by the paleo-data. The data constraints that we have employed, primarily constrain inventories, yet the model solutions are best distinguished from one another by differences in fluxes.

The only robust feature in all the inverse calculations presented here is the dissolution of CaCO₃, which is presumably caused by the transfer of CO₂ from the atmosphere box to the deep ocean box. Adjustments in carbon fluxes between the various reservoirs are then required to keep glacial $\text{CO}_3^{=}$ levels close to their interglacial values. The details of these adjustments cannot be determined from the constraints used in the model. Thus, discriminating between the various plausible scenarios may require new observations that directly constrain oceanic fluxes. Oceanic ^{14}C data, which can constrain water mass fluxes, or Barium data, which may constrain particle fluxes, could be the answer if their reliability is demonstrated in the future. These data have the potential to determine which scenario, or which combination of the scenarios, can maintain constant carbonate levels in the deep ocean despite calcium carbonate dissolution. Whether such a scenario would also provide a definitive explanation as to how the transfer of CO₂ from the atmosphere to the deep ocean occurred in the first place is still unclear.

REFERENCES

- [1] PETIT, J.R., J. JOUZEL, D. RAYNAUD, N.I. BARKOV, J.M. BARNOLA, I. BASILE, M. BENDER, J. CHAPPELLAZ, M. DAVIS, G. DELAYGUE, M. DELMOTTE, V.M. KOTLYAKOV, M. LEGRAND, V.Y. LIPENKOV, C. LORIUS, L. PEPIN, C. RITZ, E. SALTZMAN, M. STIEVENARD, "Climate and atmospheric history of the past 420,000 years from the Vostok ice core, Antarctica." *Nature* **399** (1999) 429-436.
- [2] SARMIENTO, J. L., R. TOGGWEILER, "A new model for the role of the oceans in determining atmospheric pCO₂." *Nature* **308** (1984) 621-624.
- [3] SIGMAN, D. M., E. A. BOYLE, "Glacial/interglacial variations in atmospheric carbon dioxide." *Nature* **407** (2000) 859-869.
- [4] FRANCOIS, R., M. ALTABET, E.-F. YU, D.M. SIGMAN, M.P. BACON, M. FRANKL, G. BOHRMANN, G. BAREILLE, L.D. LABEYRIE, "Contribution of Southern Ocean surface-water stratification to low atmospheric CO₂ concentrations during the last glacial period." *Nature* **389** (1997) 929-935.
- [5] TOGGWEILER, J.R., "Variation of atmospheric CO₂ by ventilation of the ocean's deepest water." *Paleoceanography* **14**(5) (1999) 571-588.
- [6] SIEGENTHALER, U., T. WENK, "Rapid atmospheric CO₂ variations and ocean circulation." *Nature* **308** (1984) 624-626.
- [7] KEIR, R. S., "Cold Surface Ocean Ventilation and Its Effect on Atmospheric CO₂." *Journal of Geophysical Research* **98**(C1) (1993) 849-856.
- [8] ELDERFIELD, H., R. E. M. RICKABY, "Oceanic Cd/P ratio and nutrient utilization in the glacial Southern Ocean." *Nature* **405** (2000) 305-310.
- [9] STEPHENS, B.B., R.F. KEELING, "The influence of Antarctic sea ice on glacial-interglacial CO₂ variations." *Nature* **404** (2000) 171-174.
- [10] BACASTOW, R.B., "The effect of temperature change of the warm surface waters of the oceans on atmospheric CO₂." *Global Biogeochemical Cycles* **10**(2) (1996) 319-333.
- [11] ARCHER, D., A. WINGUTH, D. LEA, N. MAHOWALD, "What caused the glacial/interglacial atmospheric pCO₂ cycles?" *Reviews of Geophysics* **38** (2) (2000) 159-189.
- [12] PEDERSEN, T.F., P. BERTRAND, "Influences of oceanic rheostats and amplifiers on atmospheric CO₂ content during the Late Quaternary." *Quaternary Science Reviews* **19** (2000) 273-283.
- [13] WUNSCH, C., *The Ocean Circulation Inverse Problem*, Cambridge University Press (1996).
- [14] GILL, P. E., M. H. MURRAY, M. H. WRIGHT, *Practical Optimization*, Academic Press (1981).
- [15] LEGRAND, P., K. ALVERSON (submitted). "Variations in Atmospheric CO₂ During Glacial Cycles from an Inverse Ocean Modeling Perspective." *Paleoceanography*.
- [16] ALVERSON, K., F. OLDFIELD, R. BRADLEY, Eds., *Past Global Changes and Their Significance for the Future*. Quaternary Science Reviews, Elsevier Science Ltd. (2000).
- [17] HOTINSKI, R. M., L. R. KUMP, R. G. NAJJAR, "Opening Pandora's Box: The impact of open system modeling on interpretation of anoxia." *Paleoceanography* **15** (2000) 267-279.
- [18] BENNETT, A. F., *Inverse Methods in Physical Oceanography*, Cambridge University Press (1992).
- [19] GOFFE, B., FERRIER, ROGERS, "Global Optimization of Statistical Functions with Simulated Annealing." *Journal of Econometrics* **60**(1/2)(1994) 65-100.

- [20] BOYLE, E.A., "Cadmium and $\delta^{13}\text{C}$ Paleochemical Ocean Distributions During the Stage 2 Glacial Maximum." *Annual reviews of Earth and Planetary Science* **20** (1992) 245-87.
- [21] SANYAL, A., N.G. HEMMING, G.N. HANSON, W.S. BROECKER, "Evidence for a higher pH in the glacial ocean from boron isotopes in foraminifera." *Nature* **373** (1995) 234-236.
- [22] WANNINKHOF, R., "Relationship Between Wind Speed and Gas Exchange Over the Ocean." *Journal of Geophysical Research* **97**(C5) (1992) 7373-7382.
- [23] DONEY, S.C., D.W.R. WALLACE, H.W. DUCKLOW, *The North Atlantic Carbon Cycle: New Perspectives from JGOFS and WOCE. The Changing Ocean Carbon Cycle.* R. B. Hanson, H. W. Ducklow and J. G. Field, Cambridge University Press. **5** (2000) 375-391.
- [24] KUMAR, N., R.F. ANDERSON, R.A. MORTLOCK, P.N. FROELICH, P. KUBIK, B. DITTRICH-HANNEN, M. SUTER, "Increased biological productivity and export production in the glacial Southern Ocean." *Nature* **378** (1995) 675-680.
- [25] WATSON, A.J., D.C.E. BAKKER, A.J. RIDGEWELL, P.W. BOYD, C.S. LAW, "Effect of iron supply on Southern Ocean CO₂ uptake and implications for glacial atmospheric CO₂." *Nature* **407** (2000) 730-733.
- [26] LEGRAND, P., C. WUNSCH, "Constraints from paleotracer data on the North Atlantic circulation during the last glacial maximum." *Paleoceanography* **10**(6) (1995) 1011-1045.

**ISOTOPES AS TRACERS OF THE OCEANIC CIRCULATION:
RESULTS FROM THE WORLD OCEAN CIRCULATION EXPERIMENT
(Abstract)**

P. SCHLOSSER, W.J. JENKINS, R. KEY, J. LUPTON

Lamont-Doherty Earth Observatory, Palisades, New York, United States of America

During the past decades, natural and anthropogenic isotopes such as tritium (^3H), radiocarbon (^{14}C), ^3He , or the stable isotopes of water have been used in studies of the dynamics of natural systems. Early applications of tracers to studies of the ocean were directed at determination of circulation patterns and mean residence times of specific water masses, as well as estimates of mixing coefficients. These exploratory studies suggested that tracers can add significantly to our understanding of the oceanic circulation. In order to fully exploit this potential, the first global tracer study, the GEochemical Ocean SECTIONS Study (GEOSECS), was launched. From the GEOSECS results it was immediately apparent that very close coordination of tracer programs with physical oceanography studies is required for full utilization of tracer data.

During the 1980s plans for the World Ocean Experiment (WOCE) were developed. As part of its Hydrographic Program (WHP), especially during the one-time survey, a set of tracers were measured on a global scale with unprecedented spatial resolution (both lateral and vertical). The original plan included a larger number of tracers (CFCs, $^3\text{H}/^3\text{He}$, ^{14}C , ^{39}Ar , stable isotopes of water, helium isotopes, ^{228}Ra , ^{90}Sr , ^{137}Cs , ^{85}Kr) than could actually be measured systematically (CFCs, $^3\text{H}/^3\text{He}$, ^{14}C , $\text{H}_2^{18}\text{O}/\text{H}_2^{16}\text{O}$, helium isotopes). Nevertheless, the resulting data set, which presently is under evaluation, exceeds those obtained from pre-WOCE tracer studies by a wide margin.

In this contribution, we describe the existing WOCE data set and demonstrate the type of results that can be expected from its interpretation on the basis of a few selected examples. These examples include: (1) the application of tritium and ^3He to studies of the ventilation of the upper waters in the Pacific Ocean, (2) the spreading of intermediate water in the Pacific and Indian oceans as derived from the distribution of ^3He , and (3) the evaluation of global ^{14}C maps with respect to the bottom water circulation in the Pacific Ocean. Although most of the presented results are preliminary, they demonstrate the potential of the WOCE tracer data set for obtaining insights into the oceanic circulation that were not possible on the basis of pre-WOCE data sets.

BIOGEOCHEMICAL PROXIES IN SCLERACTINIAN CORALS USED TO RECONSTRUCT OCEAN CIRCULATION

T.P. GUILDERSON*, M. KASHGARIAN

Center for Accelerator Mass Spectrometry,
Livermore, California, United States of America

D.P. SCHRAG

Laboratory for Geochemical Oceanography, Department of Earth and Planetary Sciences,
Harvard University,
Cambridge, Massachusetts, United States of America

Abstract. We utilize monthly ^{14}C data derived from coral archives in conjunction with ocean circulation models to address two questions: 1) how does the shallow circulation of the tropical Pacific vary on seasonal to decadal time scales and 2) which dynamic processes determine the mean vertical structure of the equatorial Pacific thermocline. Our results directly impact the understanding of global climate events such as the El Nino-Southern Oscillation (ENSO). To study changes in ocean circulation and water mass distribution involved in the genesis and evolution of ENSO and decadal climate variability, it is necessary to have records of climate variables several decades in length. Continuous instrumental records are limited because technology for continuous monitoring of ocean currents has only recently been available, and ships of opportunity archives such as COADS contain large spatial and temporal biases. In addition, temperature and salinity in surface waters are not conservative and thus can not be independently relied upon to trace water masses, reducing the utility of historical observations. Radiocarbon (^{14}C) in sea water is a quasi-conservative water mass tracer and is incorporated into coral skeletal material, thus coral ^{14}C records can be used to reconstruct changes in shallow circulation that would be difficult to characterize using instrumental data. High resolution $\Delta^{14}\text{C}$ time-series such as these, provide a powerful constraint on the rate of surface ocean mixing and hold great promise to augment onetime surveys such as GEOSECS and WOCE. These data not only provide fundamental information about the shallow circulation of the Pacific, but can be used as a benchmark for the next generation of high resolution ocean models used in prognosticating climate change.

1. OVERVIEW

Instrumental and climate proxy records document an increase in surface temperatures over the last ~125 years [1] as well as a recent change in the frequency and intensity of El Nino - Southern Oscillation (ENSO) events [2,3]. A fundamental question is whether or not the observed variation in climate characteristics such as temperature or El Nino frequency is a consequence of human activities or natural variability. To study changes in ocean circulation and water mass distribution involved in the genesis and evolution of ENSO and decadal climate variability, it is necessary to have records of climate variables such as sea surface temperature or precipitation several decades in length. Such records do not currently exist because technology for continuous monitoring of ocean currents (eg. satellites and buoy arrays) have only recently been available and historical observations (ships of opportunity) have large spatial and temporal gaps.

* Also at Institute of Marine Sciences and Dept. of Ocean Sciences, University of California-Santa Cruz, 1156 High Street, Santa Cruz, CA 95064, USA.

We have focussed our research toward two primary goals: the first is a better quantification and documentation of the redistribution of surface waters in the tropical and sub-tropical Pacific and the second is a better understanding of the sources of the water which upwells in the equatorial Pacific. In a zonally averaged and simplified sense, there exists an upper oceanic Hadley Cell in the Pacific: subduction occurs in the sub-tropics during the winter season and this water ventilates the tropical thermocline where it upwells and returns to the subducting regions through surface flow [4]. These questions are important because modeling studies have shown that changes in the thermal structure of the equatorial thermocline can influence decadal variability of ENSO. In fact, of all the parameter sensitivity studies which have been conducted with the coupled Zebiak and Cane model, changing the temperature structure of the thermocline has the strongest influence on model behavior [5]. Building on observational evidence of Deser et al., [6] it has been hypothesized that temperature anomalies originating at the sea-surface in the northern hemisphere subtropics can be propagated via this sub-surface pathway and interact with the equatorial thermocline, changing the character and sensitivity of ENSO [7,8]. Tritium and ^3He tracer data indicate that the ventilation time-scale of the tropical thermocline is on the order of decades [9]. It is a logical extension to hypothesize that the intergyre exchange between the subtropical subduction zones and the tropical thermocline could determine the decadal-scale climate character of the tropical Pacific.

1.1. Oceanographic setting

The tropical ocean-atmosphere system exhibits a systematic and relatively irregular interannual variability, the dominant mode of which is the atmosphere's Southern Oscillation and its ocean companion, El Niño [10]. The tropical ocean and atmosphere are intimately coupled through the interaction of the surface winds and the underlying SST field. The mean southeasterly trade winds combined with surface heating results in a buildup of warm surface water in the western tropical Pacific, the Pacific "warm pool." The accumulation of warm water at the western margin of the Pacific Ocean drives tropospheric circulation by creating deep convection aloft. In the east, the trade winds induce shoaling of the thermocline and outcropping of colder isotherms, primarily of the Equatorial Under Current. This east-west sea surface temperature (SST) gradient is accompanied by a concomitant sea-height slope of several 10s of centimeters and a basin-wide slope to the thermocline: deeper in the west and shallower in the east. When the trade winds relax or even fail, the warm water normally constrained to the western margin migrates back down the geopotential slope. At such time the normally cold eastern equatorial Pacific is warmer than normal due to a reduction or even cessation of upwelling and a deepening of the thermocline. Indonesia (and Australia) experiences drought whereas the normally arid central equatorial Pacific may receive several meters of rain (Figure 1). Corresponding changes also occur under the South Pacific Convergence Zone and the inter-tropical convergence zone in the eastern Pacific.

Contemporary research has determined relationships or patterns associated with the displacement of the major convective centers such as the Indonesian Low. Variations in the location and intensity of the Indonesian Low impacts the redistribution of sensible and latent heat as well as potential precipitable water within the atmosphere. This "wholesale" redistribution affects the structure of the planetary waves and thus is able to orchestrate far-field temperature and precipitation responses. In this fashion, the tropical Indo-Pacific is linked to the extra-tropics in both hemispheres via teleconnections.

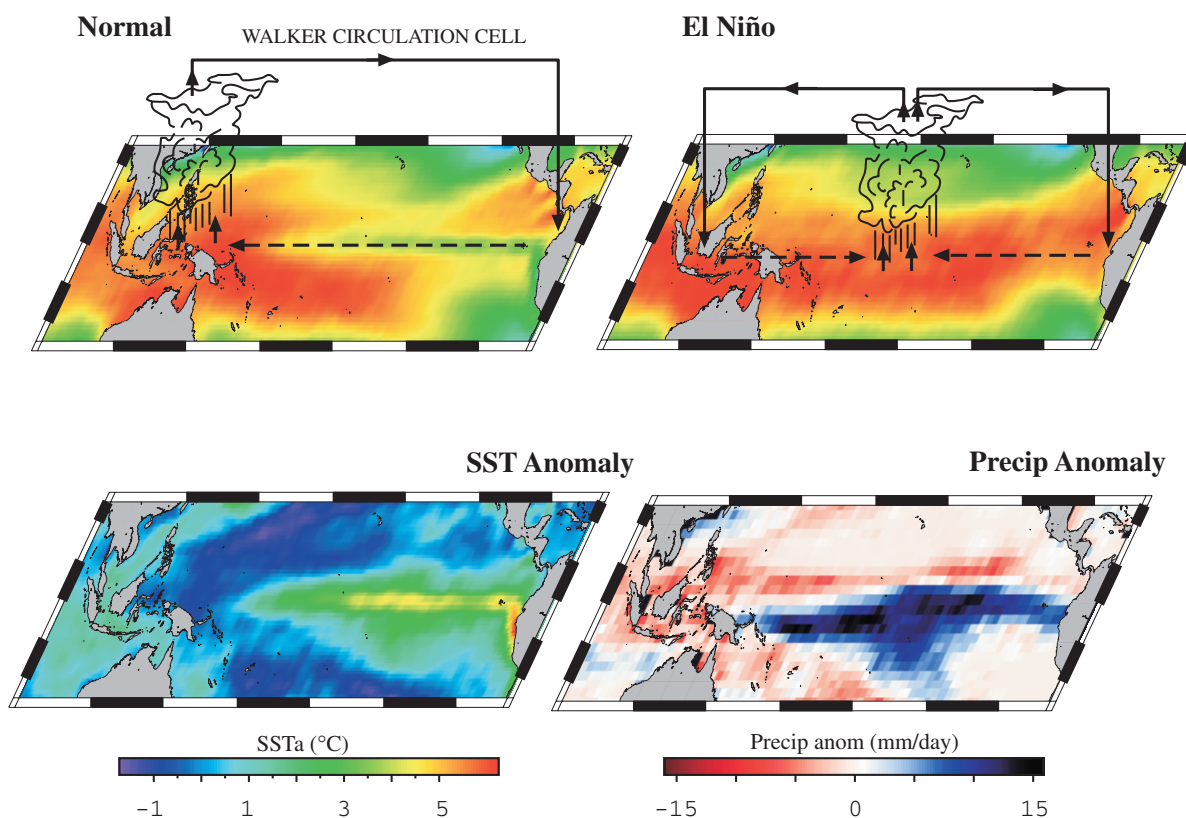


FIG. 1. A schematic of the nature of the coupled tropical ocean-atmosphere system. Upper panels depict non-El Nino (“normal” or La Nina) precipitation and sea surface temperatures (left) and El Nino conditions (right). Warm water in the western equatorial Pacific localizes deep convection which exports latent and sensible heat to both hemispheres. The corresponding winds have both a meridional (Hadley Cell) and zonal (Walker Circulation) component, which includes the surface trade winds. Middle panels are the respective SST and precipitation anomalies observed during the 1982/1983 ENSO. Lower panel is equatorial subsurface data from the TOGA/TAO array (courtesy of PMEL, NOAA) and exemplifies the shift in thermocline tilt and depth during an ENSO cycle that conspires to suppress upwelling in the eastern equatorial Pacific.

1.2. Radiocarbon in the ocean

The distribution of radiocarbon (^{14}C) in the surface ocean is a sensitive indicator of ocean circulation. Radiocarbon is produced in the stratosphere by the collision of nitrogen atoms with thermal neutrons produced naturally by cosmic rays or artificially by atmospheric nuclear bomb testing. Atomic ^{14}C is rapidly oxidized to $^{14}\text{CO}_2$ in the atmosphere and is introduced into the surface ocean via gas exchange. The flux of radiocarbon to the deep ocean is accomplished by convective processes, and by settling of particulate matter. Because the residence time of water in the deep ocean is long enough to allow for significant radioactive decay (^{14}C half-life = 5730 y), the deep ocean is depleted in ^{14}C relative to the surface ocean. This contrast makes the distribution of radiocarbon in the surface ocean particularly sensitive to vertical mixing and subsequent lateral exchange.

Since the 1950s, excess production of ^{14}C from nuclear weapons testing and its subsequent invasion into the surface ocean has augmented the difference between the surface and the deep ocean. Over this time frame radioactive decay and biological processes have minimal

impact on surface water $\Delta^{14}\text{C}$, and as a consequence $\Delta^{14}\text{C}$ is a quasi-conservative tracer which effectively “tags” water masses. The use of ^{14}C as a global ocean circulation tracer was a primary objective of the study of the distribution of natural and bomb-produced ^{14}C in the Geochemical Ocean Sections Study (GEOSECS) of the 1970s [11] and of the present day World Ocean Circulation Experiment (WOCE [12]). Radiocarbon measurements of coral skeletal material which accurately records $\Delta^{14}\text{C}$ of ΣCO_2 ^[13,14] have added important information to water sampling programs. The ^{14}C in the coral aragonite skeleton reflects seawater radiocarbon content at the time of deposition and as such measurements in corals make it possible to reconstruct the radiocarbon content of the surface ocean back to pre-bomb and pre-industrial values[13,14]. High-resolution coral-based time-series have clearly identified a time-varying surface water gradient of post-bomb ^{14}C from the equator toward the temperate latitudes with a total dynamic range in excess of 220‰. The distribution represents upwelling of low ^{14}C water from the lower thermocline in equatorial regions, with migration of the ^{14}C rich surface water toward higher latitudes. Using coral time-series we have demonstrated that for the surface ocean, where radiocarbon gradients are highest and transport is rapid that temporal variability is of the same order as spatial variability a fact lost in discrete analyses like GEOSECS or WOCE.

2. ANALYTICAL METHODS

After identifying both in terms of an oceanographically significant context, and potential quality (eg. length, continuity) of the potential coral record, the coral is cored with an underwater drilling apparatus. Coral cores (nominally 8mm diameter) are cut into ~1cm slabs, cleaned in distilled water, and air-dried. Visual inspection is performed to identify regions infilled or disturbed by boring organisms. X-radiographs are taken in order to clarify the skeletal architecture and to document density variations. After identifying the major vertical growth axis, the coral is sequentially sampled at 1-mm (or 2-mm) increments with a low-speed drill. Splits (~1 mg) are reacted in vacuo in a modified common acid-bath autocarbonate device at 90°C and the purified CO_2 analyzed on a gas source stable isotope ratio mass spectrometer ($\pm 0.05\text{‰}$ 1- σ). Strontium to calcium ratios are also determined on ~1mg splits using an inductively coupled plasma atomic emission mass spectrometer (ICP-AES) following the methodology of Schrag [15]. Analytical precision based on an in-house homogenized coral standard is $\pm 0.2\%$ equivalent to $\sim 0.3^\circ\text{C}$.

For the data that we have generated, the remaining sample splits (nominally 8-10 mg) are placed in individual reaction chambers, evacuated, heated, and then acidified with orthophosphoric acid at 90°C. The evolved CO_2 is purified, trapped, and converted to graphite in the presence of cobalt catalyst in individual reactors [16]. Graphite targets were measured at the Center for Accelerator Mass Spectrometry, LLNL [17]. Radiocarbon results are reported as age-corrected $\Delta^{14}\text{C}$ (‰) as defined by Stuiver and Polach [18].

Coral chronology has historically relied upon the presence of annual high- and low-density band couplets[19] or the seasonal variability in coral $\delta^{13}\text{C}$ which has been interpreted to reflect surface irradiance[20]. Independent chronologies based on these two methods on the same coral specimen tend to agree within a few to 6 months [21]. Such an age-model is not adequate for high-resolution $\Delta^{14}\text{C}$ records where one of the ultimate goals is to compare the observed time-series and those simulated in high-resolution ocean models. We create a preliminary age-model using sclerochronology (ie. banding) and $\delta^{13}\text{C}$ variations, but in order to obtain the best timescale and because we are not interested in the coral $\delta^{18}\text{O}$ and $[\text{Sr}/\text{Ca}]$ as

an independent measure of temperature[15], we refine our age-models by correcting the preliminary age-model through $\delta^{18}\text{O}$ and $[\text{Sr}/\text{Ca}]$ comparisons with instrumental records of SST and or precipitation (Figure 2). Because the oxygen isotopic composition of the coral responds to not only temperature but salinity, or more accurately $\delta^{18}\text{O}_w$ variations, it is necessary to use both the $\delta^{18}\text{O}_{\text{coral}}$ and $[\text{Sr}/\text{Ca}]_{\text{coral}}$ data to derive an accurate age-model depending on the phasing of the local SST and salinity (precipitation) seasonal cycle. In fast growing corals where there is strong seasonality in either precipitation and or temperature, the corresponding age-model can have an error on the order of ± 1 month.

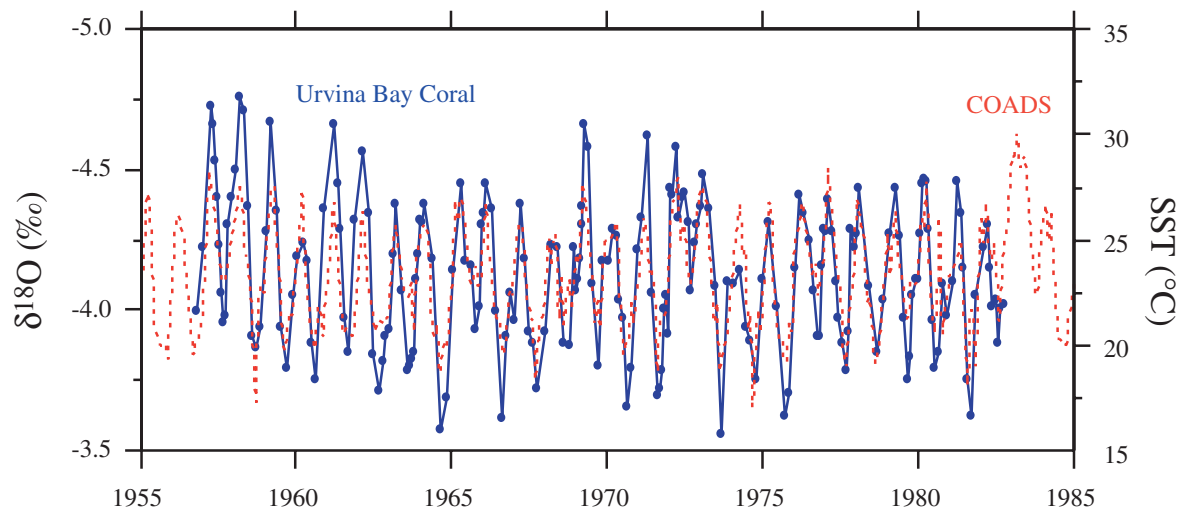


FIG. 2. Refined coral chronology through the use of $\delta^{18}\text{O}$ and available instrumental data. A preliminary $\delta^{13}\text{C}$ - sclerochronology model was created and then optimized by matching peaks and troughs in $\delta^{18}\text{O}$ corresponding to SST, and to some extent salinity variations [15].

3. CORAL TIME-SERIES RESULTS AND DISCUSSION

Corals act like strip-recorders continuously recording the radiocarbon content of the waters in which they live and thus it is possible to use records derived from these biogenic archives to study lateral mixing [22] and vertical exchange processes [23,24]. Although the idea of using corals as recorders of the ^{14}C content of waters is not new, our application of sub-annual multi-decadal studies is novel. Previous coral-based studies tended to be based on annual and bi-annual sampling [13,14], or a few-years of sub-annual samples [25]. This difference in part due to the advantages afforded by accelerator mass spectrometry (throughput, and sample size) and the foreknowledge that in order to study seasonal dynamic processes (eg. upwelling or winter-time Ekman pumping) that coarse sampling could bias or miss the desired signal. We use sub-annually resolved records to gain a window into subsurface processes when our site is chosen for this purpose.

Our work in the Pacific has focussed on sites within the equatorial wave-guide, the extra-tropics, and most recently the Indonesian region (Figure 3). In a general sense, one can think of the sea-surface temperature as reflecting $\Delta^{14}\text{C}$. The upwelling in the eastern tropical Pacific exposes water from the equatorial undercurrent, a subsurface water mass that flows west to east bounded approximately by the 24 and 26 potential density surfaces (isopycnals, $\text{kg}\cdot\text{m}^{-3}$). This water is derived from subduction of surface water in the sub-tropics and water entrained from greater depths in the tropical thermocline. The sub-tropics water brings higher bomb-

produced ^{14}C levels from the sea surface down into the undercurrent. The entrained component mixes colder, low- ^{14}C water into the undercurrent, and augments the contrast in $\Delta^{14}\text{C}$ between the undercurrent and the sea surface. This water is then advected to the warm pool where it mixes with high ^{14}C water from the subtropics.

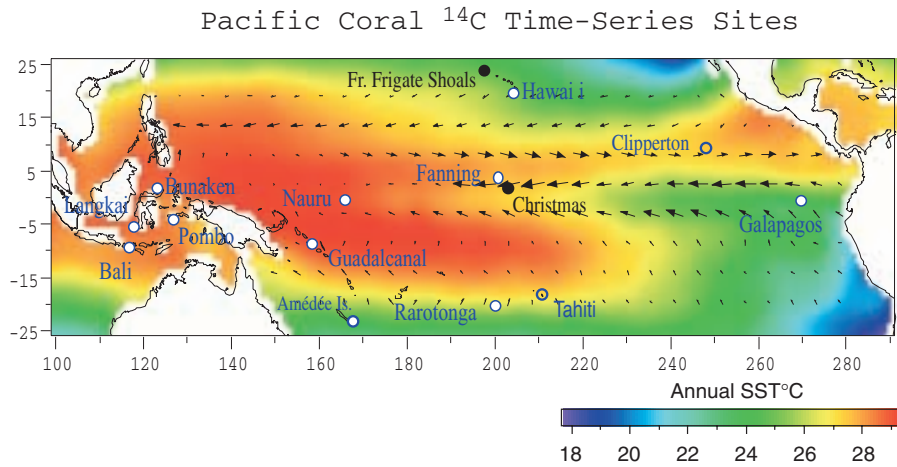


FIG.3. Location of coral sites where we or others are actively working on developing ^{14}C time-series. Mean annual sea surface temperature and general surface current pattern is also shown.

High resolution coral $\Delta^{14}\text{C}$ studies by Moore et al. [26], and Guilderson et al. [22], demonstrate the utility of ^{14}C time series in corals to study the dynamics of ocean circulation over multi-decadal time scales. Our continued objective is to document ^{14}C variability in the surface ocean in the Pacific by making measurements on additional coral samples, and to determine how that variability relates to shallow circulation and mean vertical structure of the tropical Pacific. We have completed post-bomb (~1950 to present) time series from Nauru (166°E 0.5°S) and Guadalcanal (167°E, 7°S) in the western tropical Pacific; Rarotonga (21°S, 160°W) and the Big Island of Hawai'i (20°N, 156°W) in the subtropics; and a multi-decadal record from Galapagos (90°W, 0°) in the eastern equatorial Pacific (Figure 4). In general, the subtropics (Rarotonga, Hawai'i) have higher $\Delta^{14}\text{C}$ reflecting longer mean residence time of surface water in the gyres and higher air-sea exchange. $\Delta^{14}\text{C}$ in eastern equatorial Pacific surface waters (Galapagos) are lower and due to the subsurface pathway of the Equatorial Undercurrent and entrainment of deeper thermocline waters which feed the upwelling in this region. Radiocarbon values in the warm pool region (Nauru, Guadalcanal) are intermediate between the higher subtropics and those in the east.

Our data show both the long-term increases in $\Delta^{14}\text{C}$ reflecting oceanic uptake of bomb derived ^{14}C and high amplitude seasonal to interannual variations associated with changes in circulation. The post-bomb $\Delta^{14}\text{C}$ maxima in the subtropics occurs in the early 1970s whereas at Nauru, Guadalcanal, and Galapagos it is delayed by 10 years. The delay is a consequence of the subsurface history of waters upwelling in the east and the subsequent advection and mixing of this water in the west. Superimposed upon these long-term trends is seasonal to interannual variability, which reflects ocean dynamic processes. At Nauru and Guadalcanal these high amplitude variations reflect the cross-basin advection of surface waters in the tropical Pacific in conjunction with ENSO whereas the Galapagos $\Delta^{14}\text{C}$ record reflects variations in upwelling intensity. Variability in the subtropics primarily reflects vertical exchange concomitant with winter-time Ekman pumping.

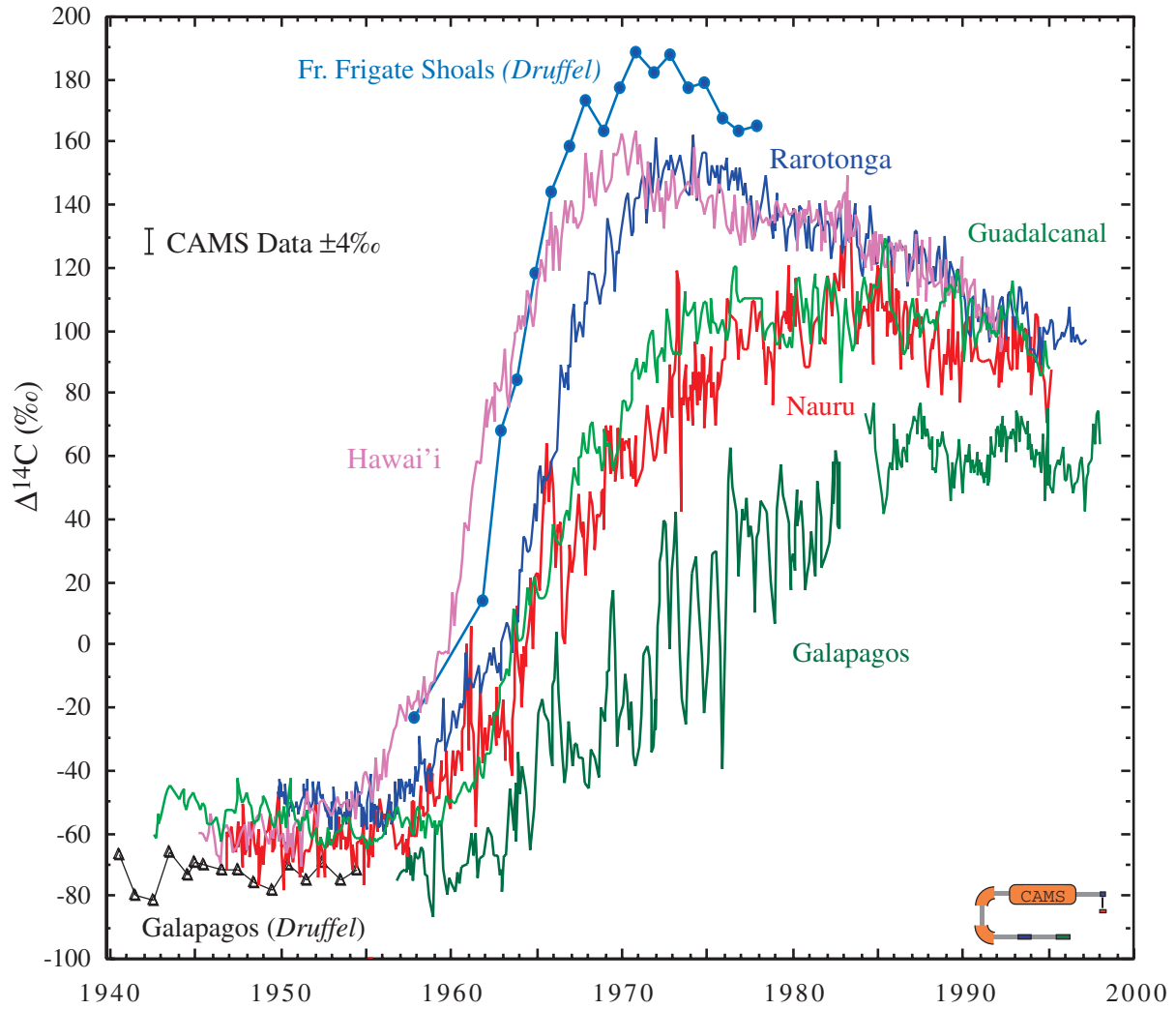


FIG. 4. High-resolution coral-based $\Delta^{14}\text{C}$ timeseries in the Pacific reflect the invasion of bomb- $^{14}\text{CO}_2$ (slow trend) and ocean dynamic processes (higher frequency variations).

Our own work on corals from the tropical Pacific is best illustrated using a coral record from Nauru Island. The temporal variability in the coral from Nauru is comparable to the spatial variability from tropics to mid-latitudes described by WOCE and GEOSECS. The temporal variability at Nauru is not a local or coastal signal due to upwelling around the island as it does not correlate with seasonal changes in wind stress that might drive coastal or island-induced upwelling. If upwelling near coastlines were an important effect, this would require that large volumes of water enter the mixed layer from great depths (i.e. lower thermocline), as vertical gradients in radiocarbon are relatively small above the thermocline. Since air-sea isotopic equilibration (gas exchange) occurs too slowly to account for large variability over time scales shorter than one year (it is roughly an order of magnitude slower than the seasonal cycle), a dynamical process internal to the ocean must be responsible.

The general pattern of interannual radiocarbon variability is strongly associated with ENSO, as seen in the comparison with the Nino-3 index (Figure 5). During ENSO warm events (including during the pre-bomb period), the $\Delta^{14}\text{C}$ value at Nauru increases, and continues to rise for several months this is followed by a large and rapid decrease, and then a return to mean values. In a simple sense, this pattern can be understood from a conceptual model of ENSO. As a warm event begins, the upwelling of deep, radiocarbon-poor water from the

upper thermocline is diminished, causing an increase in $\Delta^{14}\text{C}$ in the eastern Pacific. Amplifying this factor, the transport time of eastern Pacific water to the Nauru site is longer as tradewinds decrease in strength, allowing for more invasion of bomb-radiocarbon from the atmosphere. If westerlies develop along the equator at the western margin, this will mix in off-equatorial waters with much higher radiocarbon content, also causing an increase in $\Delta^{14}\text{C}$ values at Nauru. The large drops in $\Delta^{14}\text{C}$ following the ENSO warm events are consistent with the re-establishment of the tropical waveguide following an El Nino event. In this situation one expects an increase in upwelling, and an increase in the strength of westward-flowing currents, basically bringing more water with lower radiocarbon into the eastern Pacific sea surface, and then transporting that water more rapidly to the west with less time to exchange with the atmosphere.

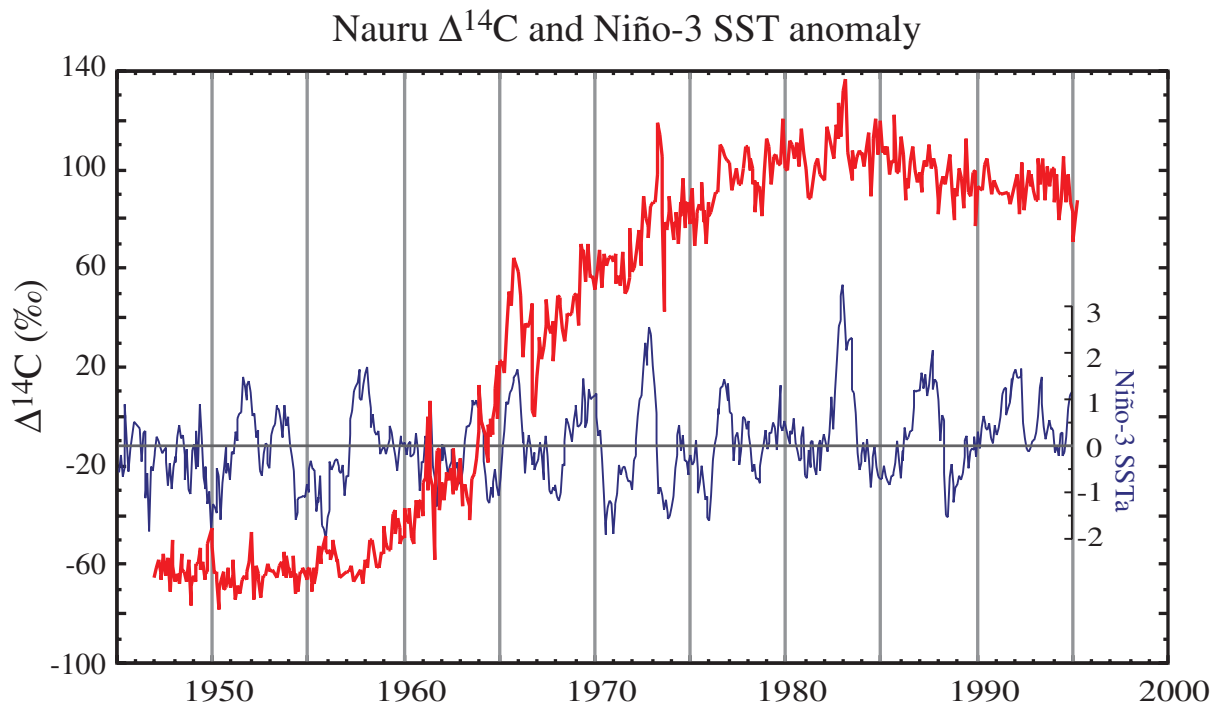


FIG. 5. $\Delta^{14}\text{C}$ time-history from Nauru Island in the Western Equatorial Pacific and the Nino-3 SST anomaly index. Interannual variability at Nauru reflects a redistribution of surface waters in concert with ENSO. During an El Nino event, equatorial tradewinds slacken which reduced the amount of low- ^{14}C eastern equatorial Pacific water advected into the warm pool region. In addition the reduction in sea surface height affords increased infiltration by higher- ^{14}C northern subtropic surface waters.

4. FUTURE DIRECTIONS AND IMPACT

The tracer data that we generate can identify specific changes in the shallow circulation that occurred prior to the implementation of moored arrays instituted in the mid 1980s, and would be difficult to characterize with existing instrumental data. An obvious extension of studies such as those briefly documented here is to constrain fractions of water-masses mixing in a particular region, or with into particular water-mass.

In addition, comparison of model results with observations of radiocarbon and other tracers is an effective way to identify problems or deficiencies in models, and ultimately leads to improved modeling skill [27,28] particularly with respect to vertical exchange processes which are relatively poorly represented in most ocean models. Thus although the data

provides fundamental information on the shallow circulation in and by itself, the true strength is a combined approach which is greater than the individual parts; the data helps uncover deficiencies in ocean circulation models and the model results place long $\Delta^{14}\text{C}$ time series in a dynamic framework which helps to identify those locations where additional observations are most needed. The time history of $\Delta^{14}\text{C}$ is a direct record of the invasion of fossil fuel CO_2 and bomb ^{14}C into the oceans. Therefore the $\Delta^{14}\text{C}$ data that are produced in studies such as ours can be used to study the ocean uptake of fossil fuel CO_2 in coupled ocean-atmosphere models [28,29].

ACKNOWLEDGEMENTS

This work was supported by a CAMS minigrant, and grants to M. Kashgarian and T. Guilderson (LLNL 98-ERI-002) and to D. Schrag from NSF's program in Physical Oceanography (OCE-9796253). Radiocarbon analyses were performed under the auspices of the U.S. Department of Energy by the University of California Lawrence Livermore National Laboratory (contract W-7405-Eng-48).

REFERENCES

- [1] MANN, M. E., BRADLEY, R.S., HUGHES, M.K., Global-scale temperature patterns and climate forcing over the past six centuries, *Nature* **392** (1998) 779-787.
- [2] TRENBERTH, K.E., HOAR, T.J., The 1990-1995 El Niño- Southern Oscillation event: Longest on record. *Geophysical Research Letters* **23** (1996) 57-60.
- [3] RAJAGOPALAN, B., LALL, U., CANE, M.A., Anomalous ENSO occurrences: an alternate view. *Journal of Climate* **10** (1997) 2351-2357.
- [4] WYRTKI, K., KILONSKY, B., Mean water and current structure during the Hawaii to Tahiti shuttle experiments. *Journal of Physical Oceanography* **14** (1984) 242-254.
- [5] ZEBIAK, S.E., CANE, M.A., Natural climate variability in a coupled model, pp. 457-470, Elsevier, New York, (1991).
- [6] DESER, C., ALEXANDER, M.A., TIMLIN, M.S. Upper-ocean thermal variations in the North Pacific during 1970-1991, *J. Climate* **9** (1996) 1840-1855.
- [7] GU, D., PHILANDER, S. G. H., Interdecadal climate fluctuations that depend on exchanges between the tropics and extratropics. *Science* **275** (1997) 805-807, (1997).
- [8] ZHANG, R.H., ROTHSTEIN, L.M., A.J. BUSALACCHI, A.J., Origin of upper-ocean warming and El-Nino changes in the tropical Pacific Ocean, *Nature*, **391** (1998) 879-883.
- [9] JENKINS, W.J., Studying thermocline ventilation and circulation using Tritium and ^3He , paper presented at Maurice Ewing Symposium "Application of Trace Substance Measurements to Oceanographic Problems," AGU, Washington, D.C., (1996).
- [10] PHILANDER, S. G. H., El Niño, La Niña, and the Southern Oscillation, Academic San Deigo, Calif. (1990) 293 pp.
- [11] ÖSTLUND, H. G., H. CRAIG, W. S. BROECKER, SPENCER, D., GEOSECS Atlantic, Pacific, and Indian Ocean Expeditions, vol, 7, Natl. Sci. Found., Washington, D.C. (1987) 200pp.
- [12] KEY, R. M., et al., WOCE AMS radiocarbon I: Pacific Ocean results (P6, P16, and P17). *Radiocarbon*, **38** (1996) 425-518.
- [13] DRUFFEL, E. M., Radiocarbon in annual coral rings from the eastern tropical Pacific Ocean, *Geophys. Res. Lett.* **8** (1981) 59-62.
- [14] TOGGWEILER, J. R., DIXON, K., BROECKER, W.S., The Peru upwelling and the ventilation of the South Pacific thermocline, *J. Geophys. Res.*, **96** (1991) 20467-20497.

- [15] SCHRAG, D. P., Rapid analysis of high-precision Sr/Ca ratios in corals and other marine carbonates. *Paleoceanography*, **14**, 97-102, (1999).
- [16] VOGEL, J. S., SOUTHON, J.R., NELSON, D.E., Catalyst and binder effects in the use of filamentous graphite for AMS. *Nuclear Instruments and Methods in Physics Research, Sect.B*, **29**, 50-56, (1987).
- [17] DAVIS, J. C., et al., LLNL/UC AMS facility and research program. *Nuclear Instruments and Methods in Physics Research, Sect. B* **52** (1990) 269-272.
- [18] STUIVER, M., POLACH, H.A., Discussion and reporting of ^{14}C data. *Radiocarbon*, **19** (1977) 355-363.
- [19] DODGE, R. E., VAISNYS, J.R., Skeletal growth chronologies of recent and fossil corals, in *Skeletal Growth of Aquatic Organisms*, Top. Geobiology vol. 1, edited by D. C. Rhoads and R. A. Lutz, Plenum, New York (1980) 493-517.
- [20] FAIRBANKS, R.G., DODGE, D., Annual periodicity of the $^{18}\text{O}/^{16}\text{O}$ and $^{13}\text{C}/^{12}\text{C}$ ratios in the coral *Montastrea annularis*, *Geochim. Cosmochim. Acta* **43** (1979) 1009-1020.
- [21] GUILDERTSON, T.P., SCHRAG, D.P., Reliability of Coral Records from the Western Pacific Warm Pool: A Comparison Using Age-Optimized Records. *Paleoceanography*, **14** (1999) 457-464.
- [22] GUILDERTSON, T.P., SCHRAG, D.P., KASHGARIAN, M., SOUTHON, J., Radiocarbon Variability in the Western Equatorial Pacific Inferred from a High-Resolution Coral Record from Nauru Island. *J. Geophys. Res.* **103** (1998) 24641-24650.
- [23] GUILDERTSON, T.P., SCHRAG, D.P., Abrupt shift in subsurface temperatures in the Eastern Tropical Pacific associated with recent changes in El Niño. *Science* **281** (1998) 240-243.
- [24] GUILDERTSON, T.P., et al., Southwest subtropical Pacific surface radiocarbon in a high-resolution coral record. *Radiocarbon*, **42** (2000) 249-256.
- [25] BROWN, T. A., FARWELL, G.W., GROOTES, P.M., SCHMIDT, F.H., STUIVER, M., Intra-annual variability of the radiocarbon content of corals from the Galapagos Islands, *Radiocarbon* **35** (1993) 245-251.
- [26] MOORE, M. D., SCHRAG, D.P., KASHGARIAN, M., Coral radiocarbon constraints on the source of the Indonesian throughflow, *J. Geophys. Res.* **102** (1997) 12,359-12,365.
- [27] RODGERS, K.B., SCHRAG, D.P., CANE, M.A., NAIK, N.H., The bomb C-14 transient in the Pacific Ocean, *J. Geophys. Res.* **105** (2000) 8489-8512.
- [28] GUILDERTSON, T.P., CALDEIRA, K., DUFFY, P.B., Radiocarbon as a diagnostic tracer in ocean and carbon cycle modeling. *Global Biogeochem. Cycles* **14** (2000) 887-902.
- [29] ENGLAND, M.H., RAHMSTORF, S., Sensitivity of ventilation rates and radiocarbon uptake to subgrid-scale mixing in ocean models, *J. Phys. Oc.* **11** (1999) 2802-2827.

ENVIRONMENTAL CHANGE STUDIES IN THE CASPIAN SEA AND THE NORTH-EAST ATLANTIC OCEAN

P. POVINEC, B. OREGIONI, J. GASTAUD

International Atomic Energy Agency,
Marine Environment Laboratory, Monaco

Abstract. Caspian Sea and NE Atlantic water profiles were investigated for radionuclide content. Radionuclide data on the water samples collected in 1995 and 1996 in the Caspian Sea show a rapid exchange of water masses in the two deep basins (the Central and Southern Basins). The main source of radionuclides is global fallout. In the NE Atlantic Ocean elevated concentrations of ^3H and ^{14}C were observed at medium depths (2000–3000 m) which could be explained by high latitude injection processes.

1. INTRODUCTION

Isotopic tracers have proved to be useful tools for the investigation of changes with time in the marine environment. Isotopic investigations could help the development of suitable models to explain past environmental observations and help to protect marine ecosystems against anthropogenic impacts.

IAEA-MEL in the framework of marine radioactivity studies has participated in several expeditions to the Atlantic, Arctic, Indian and Pacific Oceans to sample seawater, sediment and biota. The expeditions covered a wide range of marine radioactivity surveys to study the distribution of key radionuclides (^3H , ^{14}C , ^{90}Sr , ^{129}I , ^{137}Cs , U, Pu and Am isotopes) in the world oceans, changes in their concentrations with time and to investigate marine environmental change using isotopic signals in the marine environment.

Environmental change studies carried out by IAEA-MEL will be illustrated by two examples: the Caspian Sea and the North-East Atlantic Ocean.

2. THE CASPIAN SEA

To explore the potential of isotope techniques in the study of water balance and water dynamics in the Caspian Sea and the aspects related to changes in the sea level, two research/training cruises were carried out in 1995 and 1996 under an IAEA technical co-operation project [1]. During these cruises, oceanographic parameters (such as salinity, seawater, temperature) were measured and seawater samples were collected for laboratory analysis of ^{90}Sr , ^{137}Cs and $^{239,240}\text{Pu}$.

In the two principal basins, the Central and Southern Caspian Basins, the behaviour of $^{239,240}\text{Pu}$, ^{90}Sr and ^{137}Cs appeared quite different (Fig. 1). $^{239,240}\text{Pu}$ delivered by fallout in surface water decreased from the Northern Basin to the Southern Basin and penetrated to deeper water, as expected for this particle reactive element. The concentrations in the intermediate layers of the Central Basin are higher than in the Southern Basin, which is reflected by their inventories. The observed concentrations and transport of water masses between the two main basins may be explained by these data.

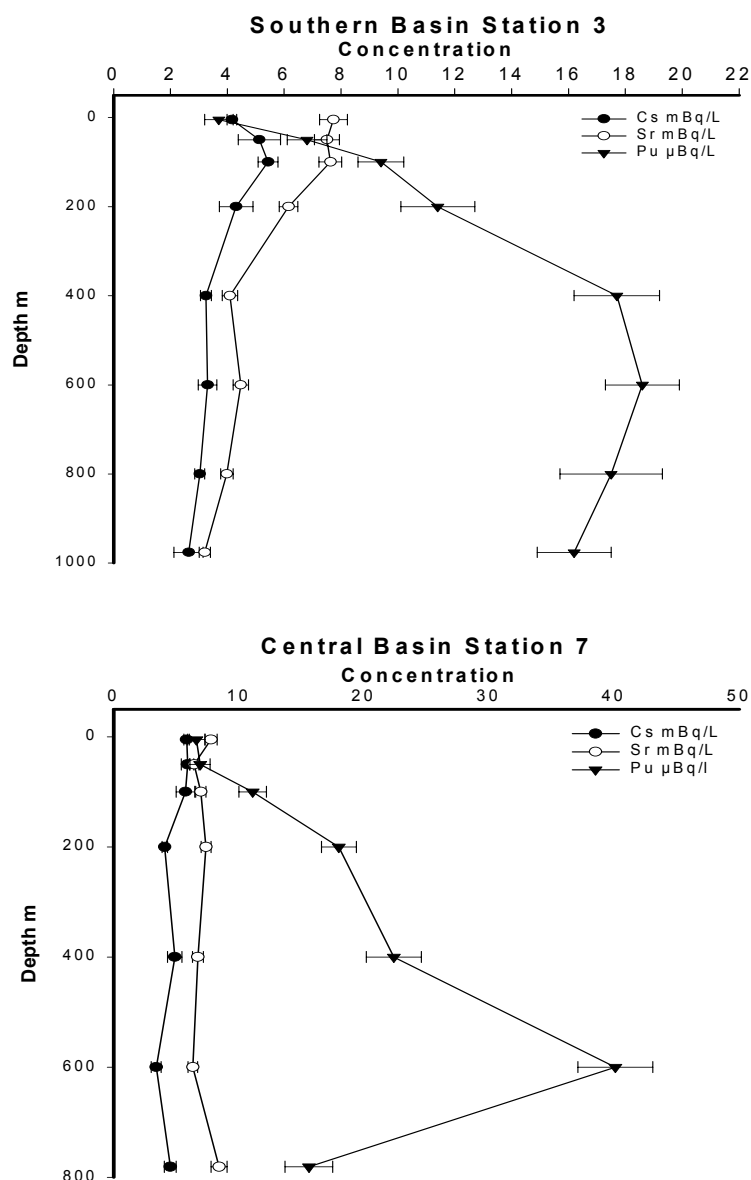


FIG 1. ^{90}Sr , ^{137}Cs and $^{239,240}\text{Pu}$ profiles in the Central and Southern Basins (1996).

The concentration level of strontium in the water mass which appeared to be higher than expected from global fallout could be a result of a significant contribution from soil remobilization and river run-off. The excess of strontium was shown by the lower ratios of $^{239,240}\text{Pu}/^{90}\text{Sr}$ and $^{137}\text{Cs}/^{90}\text{Sr}$. In the Central basin, the similar vertical distribution of ^{90}Sr in the water column is probably due to transport of surface water to greater depths. This gave a higher inventory compared to the Southern Basin where the concentration decreased with depth.

The caesium concentrations were in agreement with the level expected from global fallout. In the Southern Basin, the activities clearly show a decrease with depth. Similar trends at the same depths for strontium and caesium demonstrate the typical behaviour for these conservative fallout radionuclides which move essentially in true solution.

Although the turnover time of water in the Caspian Sea is of the order of 200 years, both deep basins appear to be rapidly ventilated, as was shown by a small decrease in radionuclide concentrations with depth. The main source of radioactivity in the Caspian Sea is global

fallout and subsequent river run-off from catchment areas. At the stations visited, there were no signs of dumping of radioactive wastes. However, more detailed studies are necessary to better understand deep water formation in the basins which is expected to occur during the winter season. As well as the development of an appropriate model for the radiological assessment of the Caspian Sea which would require further sampling of seawater and also sediment and biota.

3. THE NE ATLANTIC OCEAN

In the North-East Atlantic Ocean, a $\Delta^{14}\text{C}$ profile in the water column of samples taken at $46^\circ 05'\text{N}$; $17^\circ 10'\text{W}$ has shown a remarkable peak at medium depths between 2000 and 3000 m. A similar profile was obtained for ^3H as can be seen from Fig. 2. The persistence of a minimum in $\Delta^{14}\text{C}$ and ^3H data for North-West Atlantic waters at around 1000 m depth were also visible in GEOSECS data as well, although the present maxima (between 2000 and 3000 m depth) are much higher and comparable to surface levels [2]. However, such clear medium depth maxima were not observed in TTO data for the North-East Atlantic (there were no GEOSECS stations in the NE Atlantic Ocean).

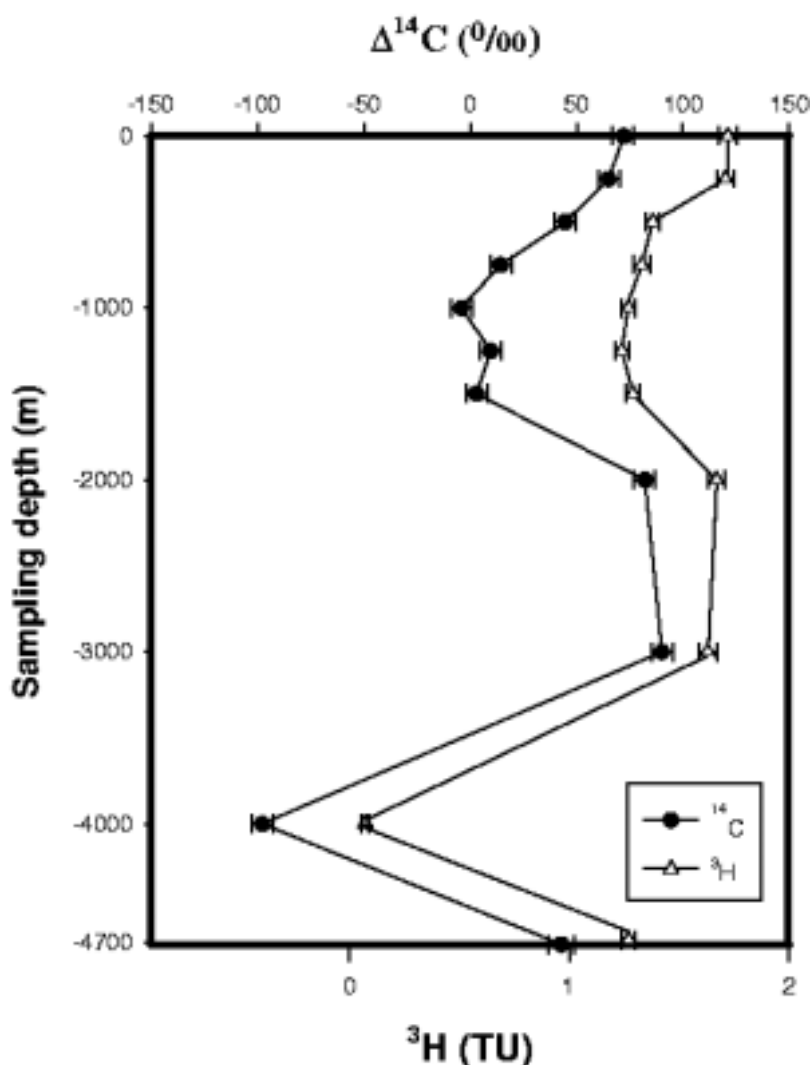


FIG. 2. ^3H and ^{14}C profiles in the NE Atlantic Ocean.

It is a known fact that the high latitude North Atlantic areas (north of 42°) which coincide with the water mass formation areas of the North Atlantic Deep Waters (NADW) are an important sink for atmospheric CO₂ [3]. High latitude injection processes could therefore be responsible for the observed evolution of $\Delta^{14}\text{C}$ and ^3H concentrations below 1000 m, downwelling high surface radionuclide concentrations to medium depths. This subduction mode water regime, when water masses labelled by global fallout are transported from the surface to medium depths has also been observed for ^{90}Sr and ^{137}Cs radionuclides. Surface waters may be directly transported into the deep interior of the Atlantic via conveyor circulation, also known as thermohaline circulation [4].

ACKNOWLEDGEMENTS

The collaboration of the IAEA's Isotope Hydrology Section (Dr. K. Froehlich) during the sampling missions to the Caspian Sea, is highly acknowledged. IAEA-MEL operates under a bilateral agreement between the IAEA and the Government of the Principality of Monaco.

REFERENCES

- [1] FROEHLICH, K., ROZANSKI, K., POVINEC, P.P., OREGIONI, B., GASTAUD, J., Isotope studies in the Caspian Sea. *Sci. Total Environ.* **237/238** (1999) 419-427.
- [2] POVINEC, P.P., JULL, A.J.T., BURR, G.S., Radiocarbon in Seawater at Radioactive Waste Dumping Sites in the Northeast Atlantic and Northwest Pacific. *Radiocarbon* (in print).
- [3] TAKAHASHI, T., TAKAHASHI, T.T., SUTHERLAND, S.C., An assessment of the role of the North Atlantic as a CO₂ sink, *Phil. Trans. Royal Soc. London*.
- [4] BROECKER, W.S., The great ocean conveyor, *Oceanography* **4** (1991) 79-89.

THE KARA BOGAZ GOL BAY, LAKE ISSYK KUL AND ARAL SEA SEDIMENTS AS ARCHIVES OF CLIMATE CHANGE IN THE ARAL-CASPIAN CATCHMENT BASIN

V.I. FERRONSKY, V.S. BREZGUNOV, L.S. VLASOVA, Y.A. KARPICHEV

Water Problems Institute of the Russian Academy of Sciences, Moscow, Russian Federation

V.A. POLYAKOV, A.F. BOBKOV

Research Institute of Hydrogeology and Engineering Geology,

Zeleny, Moscow Region, Russian Federation

V.V. ROMANOVSKY

Water and Hydropower Problems Institute of the Kirghiz Academy of Sciences,

Bishkek, Kirghiz Republic

T. JOHNSON, D. RICKETTS, K. RASMUSSEN

Large Lake Observatory, University of Minnesota, United States of America

Abstract. A 5-m long core of bottom sediments from the Kara Bogaz Gol Bay of the Caspian Sea, 4-m and 2-m cores from the Issyk Kul Lake of the Thian Shan Mountains, and a 4-m core from the Aral Sea were examined for evidence of climatic and environmental changes in the catchment basin of the Central Asia Region. The distribution of ^{18}O and ^{13}C in the bulk carbonates, ^2H in the pore water, radiocarbon age, oxygen and hydrogen isotopes in the lake water, abundance of CaCO_3 , MgCO_3 , and the basic salt ions of Na^+ , K^+ , Cl^- , SO_4^{2-} in the cores were measured. The isotope and hydrogeochemical data of the Kara Bogaz Gol Bay sediments prove a historical scenario for the basin which suggests that fresh water has been discharged to the Caspian Sea during the Bay's humid episode across the Central Asia Region (~ 9 Ka BP). Isotope and geochemical evidence indicate that the sedimentation of the upper core segment has taken place during the last ~ 2.2 Ka BP in the environment of sea water recharged from the Central Caspian Basin. The period of between 4.3 and 6 Ka BP, which relates to the core depth interval of between 170 cm and 260 cm, demonstrates the most dramatic change in the sedimentation rate in the Issyk Kul Lake. It means that active melting of the mountain glaciers and warming of climate has happened just in this period. The swamp plant peat layers at depths of 230 cm and 130 cm indicate that during 3.5-3.7 Ka BP and 1.6-1.8 Ka BP the Aral Sea dried and broke up into a number of lakes and swamps. Sediment cores taken from the bottom of the Kara Bogaz Gol Bay, Lake Issyk Kul and Aral Sea show periodic rise and fall in water levels during the last $\sim 10\,000$ years. Two peat layers within the sediment core of the Aral Sea and dated at 1.6-1.8 Ka BP and 3.5-3.7 Ka BP demonstrate that this reservoir also periodically dried.

1. INTRODUCTION

While studying bottom sediments from the central and southern basins of the Caspian Sea, a reversal in main direction of the river runoff to the sea in the past was discovered [1, 2]. Since the beginning of the Holocene, runoff to the Caspian Sea has been mainly derived from the northern Volga-Ural basin. Previously, the Aral Sea catchment basin was the principal drainage area, which was at that time situated in the humid zone. As such, the Aral-Caspian basin can be considered as a single catchment covering both humid and arid zones. By studying bottom sediments from the Aral Sea, Lake Issyk Kul and Kara Bogaz Gol Bay we explore new evidence which proves that past environmental changes occurred in the region due to climatic variations.

The Aral Sea catchment basin is situated within the Turanian Lowlands and is bounded by the inner slopes of the surrounded highlands. The upper water level of the sea is limited by the mount Kugunek sill (+58 m a.s.l.). The sill is the origin of the Uzboy River which discharges excess water from the Aral to the Caspian Sea. The Issyk Kul catchment basin is located in the Thian Shan mountains at altitude of ~1600 m a.s.l. Lake Issyk Kul is also a closed reservoir. It has a volume that is roughly two times larger, and a depth that is roughly ten times larger than that of the Aral Sea. The upper limit of the lake water level is determined by the sill (+15 m) on the right bank of the Chu River that discharges to the Aral Sea basin (Fig.1, Table I).

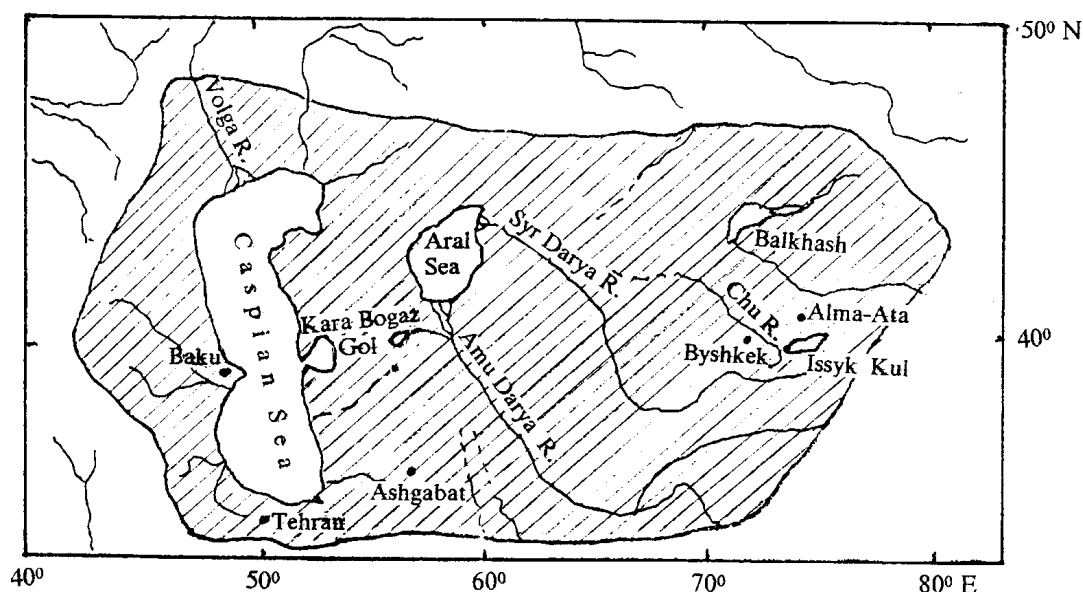


FIG. 1. Aral-Caspian catchment basin and position of the studied closed reservoirs.

Table I. Hydrological characteristics of the studied reservoirs

	Aral Sea	Lake Issyk Kul	Kara Bogaz Gol Bay
Location	45°N, 60°E	42°30'N, 77°45'E	40°10'N, 50°20'E
Surface area [km ²]	64 500	6 330	10 000
Volume [km ³]	1000	1700	200
Catchment area [km ²]	690 000	21 900	50 000 (?)
Mean / max depth [m]	20/67	278/702	1/3,5
Mean annl. tempr.			
surface / bottom [°C]	10/3	8/2	6/4
Salinity [o/oo]	11	5,8	250
River runoff [km ³ /a]	55	3	10
Precipitation [km ³ /a]	6	1,2	1
Evaporation [km ³ /a]	61	4.2	11

2. CORING, SAMPLING AND MEASUREMENTS

Three 4 to 5 m-long cores of bottom sediments taken from the Kara Bogaz Gol Bay, Lake Issyk Kul and Aral Sea at water depths of 0.5 m, 250 m, and 23 m respectively, were analyzed in laboratories of the above authors and interpreted from the point-of-view of establishing relationships between climate change and water balance of the closed reservoirs in the same catchment basin. Distribution of oxygen-18 and carbon-13 in bulk carbonates, deuterium in pore water, radiocarbon dating, oxygen and hydrogen isotopes in lake water, abundance of CaCO_3 and MgCO_3 and the major salt ions Na^+ , K^+ , Cl^- , SO_4^- in sediments were studied.

Oxygen and carbon isotopes were measured by conventional mass-spectrometry and reported with respect to the PDB standard (NBS-17 distributed by the IAEA Analytical Services) with analytical precision of $\pm 0.1\text{‰}$ for $\delta^{18}\text{O}$ and $\pm 0.2\text{‰}$ for $\delta^{13}\text{C}$. Oxygen and hydrogen isotopes in water samples were analysed by mass spectrometry and reported with respect to V-SMOW standard distributed by the IAEA. Radiocarbon age of sediments was determined by conventional methods. Major salt forming ions Na^+ , K^+ , Cl^- , SO_4^- were measured by means of extraction from dried samples. Distilled water was poured over the dried sample at room temperature and at a sample-to-water weight of 1:5. Then the value of Na^+ and K^+ in solution were determined using flaming photometry and Cl^- was measured by titration. For determination of carbonate mineral contents, the samples were processed with hydrochloric acid to transfer the readily soluble carbonate fraction into solution. The concentration of Ca^{++} and Mg^{++} in the solution were determined by titration.

3. RESULTS AND INTERPRETATION

3.1. Kara Bogaz Gol (Black Throat Lake)

Due to limited temporal resolution of our experimental data, we focus here on interpretation of the long-term changes in sedimentary properties. Fig. 2 presents information obtained by isotope and chemical analysis of the sediment samples and by their geological description. The lithology represents alternated layers of silty clay and sandy silt with localized inclusions of salt crystals. Three stages in changing sedimentation environment can be marked within the core section. The data related to its deepest part from 5.2 to 4 m shows that sedimentation occurred in a reservoir which was being actively replenished by fresh river water starting at $\sim 9\text{ Ka}$. In fact, positive values of $\delta^2\text{H} = +6\text{‰}$, characteristic of a nearly dessicated lake, are depleted up to -6‰ at 4-m depth. The values of K^+ , Na^+ , Cl^- , SO_4^- , CaCO_3 and MgCO_3 within that depth interval are typical for river water. Oxygen and carbon isotopes demonstrate their relationship with continental carbonates. Precipitation of carbonates in lake water in equilibrium with atmospheric CO_2 at $\sim +22^\circ\text{C}$ gives $\delta^{13}\text{C} = +3\text{‰}$. The second stage of sedimentation covers the core interval from 4 to 1.7 m. The measured parameters over this interval suggest that sedimentation occurred in a more actively replenished fresh water environment. Here $\delta^2\text{H}$ values in pore water decrease to $\sim -18\text{‰}$. The values of $\delta^{13}\text{C}$, Na^+ , Cl^- , SO_4^- decrease and those of $\delta^{18}\text{O}$, K^+ , CaCO_3 and MgCO_3 increase due to inflow of terrigenous carbonates by freshwater. A narrow variation in the measured values suggests that the lake outflow may have been regulated by discharge to the Central Caspian basin. Precipitation of carbonates in equilibrium with atmospheric CO_2 at $\sim +10^\circ\text{C}$ and $\delta^{13}\text{C}_{\text{organic}} = -20\text{‰}$ gives $\delta^{13}\text{C} = +3.5\text{‰}$. In contrast, the uppermost part of the core from 1.7 to 0 m is characterized by negative values of $\delta^{18}\text{O}$ in carbonates. $\delta^2\text{H}$ values in pore water are close to their modern ma-

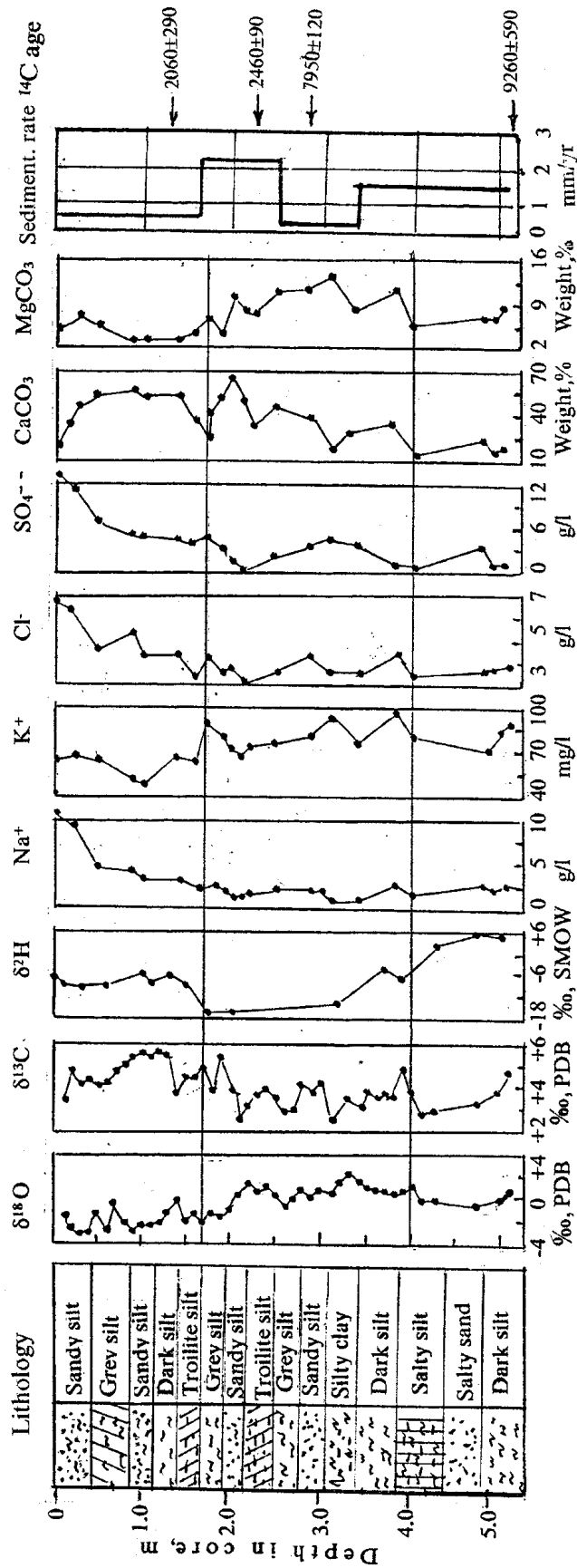


FIG. 2. Oxygen and carbon isotopes of carbonates, deuterium of pore water, major salt ions Na^+ , K^+ , Cl^- , SO_4 , CaCO_3 and MgCO_3 in core sediments from Kara Bogaz Gol Bay.

gnitude and are equal to about -6 ‰ for the Bay. The content of Na^+ , Cl^- , SO_4^{2-} , CaCO_3 rises and the amount of K^+ and MgCO_3 also decreases. Combined, these features indicate that sedimentation of the upper core segment took place during the last ~2.2 Ka in an environment influenced by marine water recharged from the Central Caspian basin.

It appears from the above evidence that the Kara Bogaz Gol Bay was a high-throughflow lake during the middle Holocene. Its name in local Turkmenian dialect, meaning ‘Black Throat Lake’, seems to be more appropriate in this sense than its present name ‘Bay’. Due to its small capacity and 4-m high sill (relative to its present state) located at a distance of 11 km from the shore of the Caspian Sea, the lake becomes open for inflow and outflow of surface water depending on the sea level. Prior to ~2.2 Ka, water levels in the Central basin were lower than in Kara Bogaz Gol and the lake was recharged by its catchment basin. After that, the situation was reversed.

3.2. Lake Issyk Kul (Hot Lake)

Issyk Kul is a typical high-mountain lake of tectonic origin. Its water level is governed by inflow from about 50 rivers and springs mainly of glacial origin. Our previous isotope studies have shown that about 10-20% of total precipitation over the catchment is derived from local lake vapour [3]. Water level of the lake is continuously changing. For instance, the lake level dropped by 130 cm between 1965 and 1985, and since 1985 has been slowly rising. In order to study palaeoclimatic effects in the basin, two sediment cores of roughly 4-m and 2-m in length were extracted and analyzed from waters depths of 250 m and 650 m, respectively.

The results of isotope, chemical and textural analysis of sediments, including radiocarbon dating of adult shells of the ostracode *Candona sp.* are presented for one core in Fig.3. Three specific periods in sedimentation history are distinguished here. The deepest part of the core from 4.3 m to 2.6 m is characterized by rather uniform textures and low values of $\delta^{18}\text{O}$, Sr/Ca, total organic carbon, monohydrocalcite and slightly increasing content of CaCO_3 and MgCO_3 to the upper direction. Such parameters are indicative of steady state sedimentation process, and minor water level fluctuations due to continuous overflow of excess water to the River Chu. The sediment parameters of the second stage of lake evolution between 6 and 4.3 Ka (or from 2.6 to 1.7 m) are consistent with decreasing lake levels, including increase of salinity and decrease of sedimentation rate. Such conditions are further evidenced by an increase of $\delta^{18}\text{O}$, Sr/Ca, CaCO_3 values and decrease of MgCO_3 content. The properties of the uppermost part of the core show that changes in water level caused periodic overflow of the excess water to River Chu. Overall, since about 2.9 Ka, water level of the lake has undergone a notable decrease. The values of sedimentation rate, $\delta^{18}\text{O}$, Sr/Ca and variation of organic carbon content in sediments further support that conclusion. The amplitude of water level rise is limited by the occurrence of a 6-km wide and 12-m high sill (relative to present state) that separates the River Chu from the lake on its western side. During humid episodes of climate, or periods of active melting of the mountain glaciers, the lake capacity was shortly filled in up to the sill level. After that, excess of water discharged to River Chu. The existence of 10-12 m terraces situated around the lake also support this conclusion. Discharge of lake water over the sill is thought to have occurred before ~6 and periodically after ~4.3 Ka BP. A cooling period from 6 to 4.3 Ka is likewise accompanied by reduced glacial melting, decreased runoff, and a reduction in lake sedimentation rates and lake water levels.

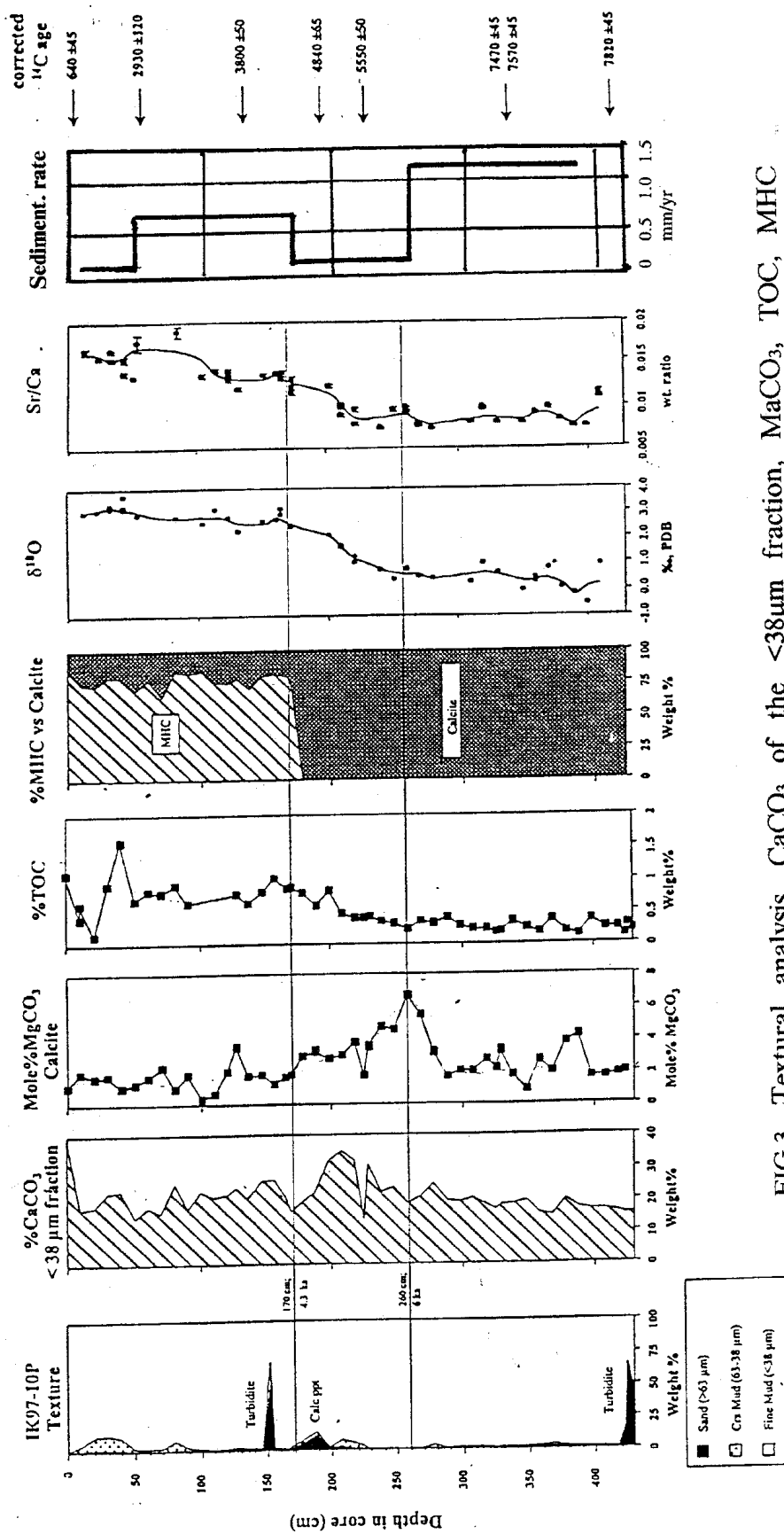


FIG.3. Textural analysis, CaCO₃ of the <38μm fraction, MgCO₃, TOC, MHC (monohydrocalcite) vs calcite, δ¹⁸O contents and Sr/Ca ratio of adult shells of the ostracode *Candona* sp. and corrected ¹⁴C ages of the Issyk Kul core sediments.

3.3. The Aral Sea

From evidence gathered during studies of coastal terraces and bottom sediments, four transgressive and three regressive episodes are distinguished in the Holocene history of the Aral Sea. The rise of the sea level during the transgressions was fixed at elevations of +57, +54.5, +53.5 and +53 m a.s.l. The regression drops were observed at elevations of +44, +43 and +35 m a.s.l. This implies that at least once in the early Holocene the Aral Sea discharged to the Caspian Sea, and twice or three times during this period it became nearly dried up. Evidence of drying episodes include the occurrence of two layers of swamp plant peat and a salt layer within bottom sediments collected in water depths of 20-25 m [3].

During a field expedition organized by Moscow State University in 1980, a 4 m-long core of bottom sediments at 23 m depth in central part of the sea was taken. Lithological descriptions, carbonate content determinations and ^{14}C dating were also carried out. Radiocarbon age of *Cardium* shells, swamp plant and dispersed organic carbon and bulk carbonates in 36 samples of the core were accurately measured at the Water Problems Institute [4] in order to compare radiocarbon ages obtained for different carbon compounds of the same sediments. Table II and Fig.4 demonstrate comparative results of C-14 ages of bulk carbonates, *Cardium* shells and organic carbon for the Aral core. The data show that *Cardium* shells and swamp plant peat ages appears to be in harmony. However, dispersed organic matter deviates slightly from the above values. Considerable dispersion is observed in bulk carbonate ages due to the presence of dead terrigenous carbon.

TABLE II. Radiocarbon ages of bulk carbonates (CaCO_3), carbonates of cardium shells (CaCO_3^*), carbon of total dispersed organic matter (TOC) and carbon of swamp plant peat (TOC*) in the Aral bottom sediments

Depth [cm]	Dating material	Corrected ^{14}C age [yr]	$\pm \sigma$	Depth [cm]	Dating material	Corrected ^{14}C age [yr]	$\pm \sigma$
0-17	CaCO_3	750	120	205-221	TOC*	3450	80
0-17	TOC	460	160	225-238	CaCO_3	7670	180
19-30	CaCO_3	4370	100	242-260	CaCO_3	6390	80
19-40	TOC	1560	100	260-287	CaCO_3	9030	150
34-47	CaCO_3	3050	100	260-287	CaCO_3^*	4810	180
34-47	TOC	720	120	288-300	CaCO_3	8200	220
72-84	CaCO_3	3950	120	288-300	TOC	4990	250
84-98	CaCO_3	3690	100	310-324	CaCO_3	6890	150
84-98	TOC	1830	300	310-324	TOC	5750	250
98-111	CaCO_3	3550	120	310-324	CaCO_3^*	5610	220
98-111	TOC	1270	250	325-341	CaCO_3	8160	100
111-125	TOC	2300	180	325-341	TOC	7960	120
125-130	TOC*	1510	150	342-345	CaCO_3	7590	150
141-150	CaCO_3	2730	100	342-345	CaCO_3^*	6090	150
150-164	CaCO_3	3600	120	367-377	CaCO_3	8030	100
150-164	TOC	1900	250	367-377	TOC	7300	390
164-190	CaCO_3	3970	100	382-400	CaCO_3	7540	100
205-221	CaCO_3	5330	100	382-400	TOC	6650	390

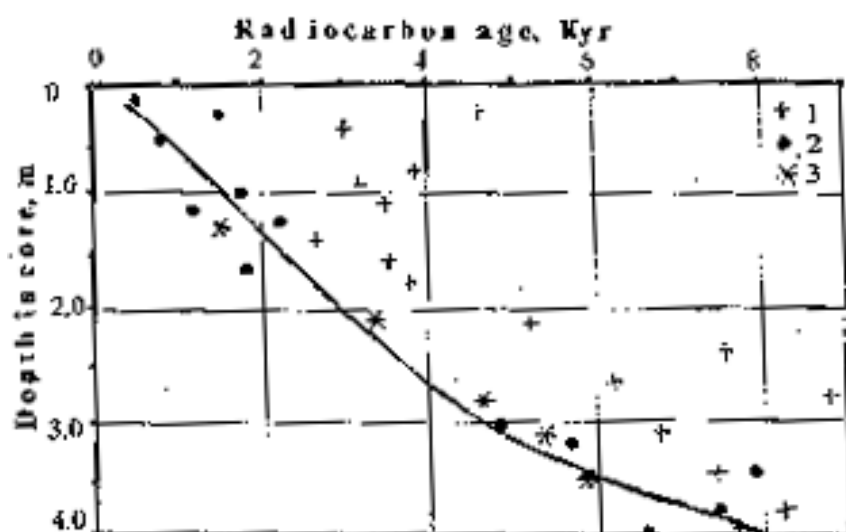


FIG. 4. Radiocarbon ages of bulk carbonates (1), carbon of dispersed organic matter (2) and shell carbonates and carbon of swamp peat (3) in the Aral sediments.

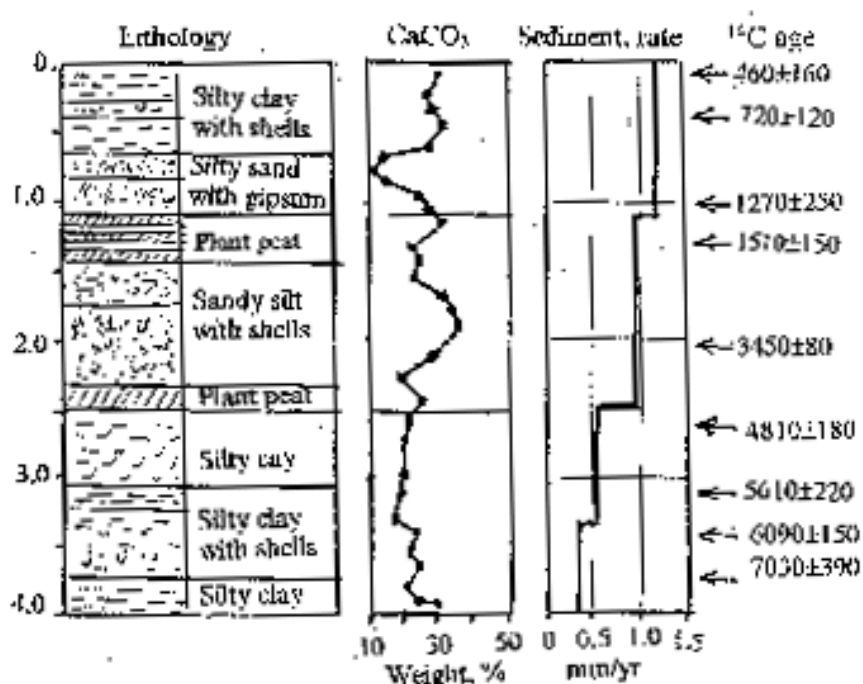


FIG. 5. Lithology, bulk carbonate content and sedimentation rate of the Aral core taken at 23 m depth in the central part of the sea.

Figure 5 demonstrates lithology, bulk carbonate content and sedimentation rate of the Aral core. Three stages of sedimentation regime are divided within the core. The deepest part from 4 to 2.5 m was formed during the early Holocene under low sedimentation rates and decreasing sea water levels. The swamp plant peat layer of 20 cm thickness at 2.3 m depth indicates that the sea dried and broke up into a number of isolated lakes and swamps by about 4.5 Ka BP. The subsequent sea level rise and fall culminated in a second drying event at about 2 Ka. This date was fixed by a series of thin layers of the swamp plant peat identified in the sediment core. Sedimentation of the uppermost part of the core after ~1.3 Ka occurred under a regime of variable runoff, a condition recorded in the alternation of silty clay and sandy silt layers.

A specific feature is noted in the relationship between sedimentation rate and sea water level. The Aral Sea is a shallow reservoir. Its maximum depth in 1960 was 60 m. Until 1990 the sea level dropped by ~15 m during which time the water area decreased from 65 000 to 40 000 km² and sea volume reduced from 1000 to 400 km³. Over that time salinity increased from 10 to 24‰. Increase of the sea level to its maximum value (+58 m a.s.l. or 65 m depth) extends the water area 3- to 4-fold and increases the water volume by 2- to 3-fold. During these high level stands, the source of sediment (Amu Darya, Syr Darya, other rivers and coastal area) becomes more distal. The observations in Fig.5 show a general increase in sedimentation rate from bottom to top in the core which indicates that there has been a tendency towards sea level decrease since about 7 Ka.

4. ARAL - CASPIAN EVENTS

A general picture of hydroclimatic change in the Aral-Caspian catchment during the Late Pleistocene-Early Holocene is presented in Fig. 6. Latitudinal shifts in climatic zones in the region during this time have been discussed previously [1, 2]. The data presented here for Kara Bogaz Gol, Issyk Kul and the Aral Sea bottom sediments appear to provide additional support for interpretation of the paleoclimate and paleohydrology of the region, and support and expand on the interpretations of our previous work.

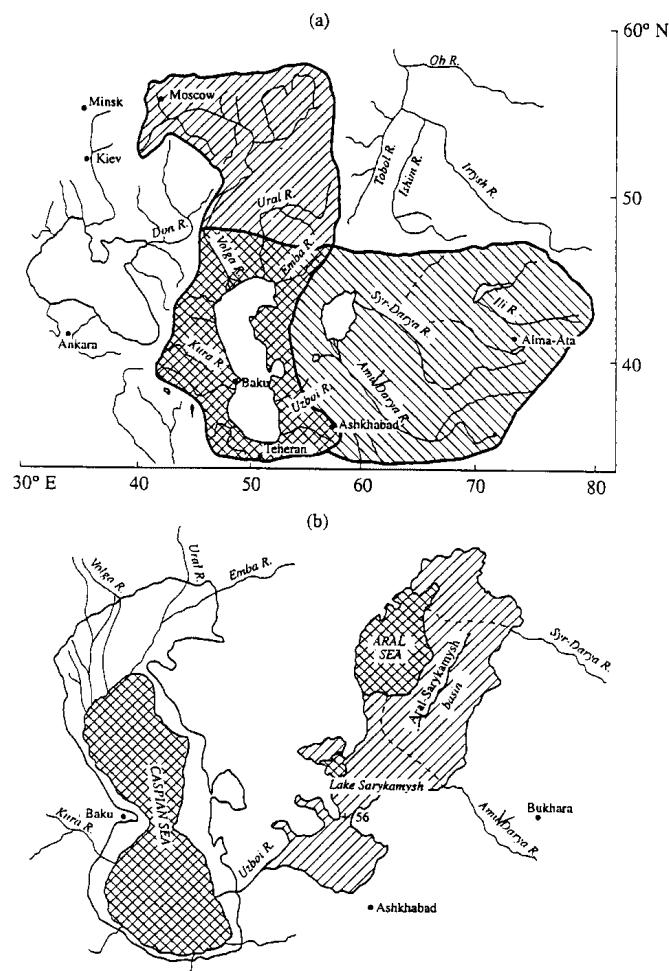


FIG.6. Effect of latitudinal shift of the zone of humid climate in the Aral-Caspian basin: (a) drainage basin change from the Volga-Ural to the Amu Darya-Syr Darya; (b) regression of the Caspian and transgression of the Aral Sea during the transition time.

5. CONCLUSION

The results presented herein demonstrate that climate change in the Aral-Caspian catchment was the main factor governing variations in the hydrological cycle over the region. More detailed studies over longer time-intervals using sedimentary archives from lakes and seas appears to be a promising direction for future water resources research in this and other arid zone basins.

ACKNOWLEDGEMENTS

The research was conducted within the framework of the State regular budget of the Russian Academy of Sciences and supported by EU-INCO-COPERNICUS Project (EU Contract IC-CT96-0112)

REFERENCES

- [1] FERRONSKY V.I., POLYAKOV V.A., LOBOV A.L., BATOV V.I., FROELICH K., GROENING, M. "Sedimentation rate record in the Caspian Sea bottom sediments as indicator of climate changes in the basin", Isotope Techniques in the Study of Past and Current Environmental Changes in the Hydrosphere and the Atmosphere (Proc. Intern. Symp. Vienna, 1999), IAEA, Vienna (1999) Session 3, 1-15 (CD-ROM).
- [2] FERRONSKY V.I., POLYAKOV V.A., KUPRIN P.N., LOBOV A.L. The nature of variations in the level of the Caspian Sea (based on bottom-sediment data). *Water Resources* **26**: (1999) 652-666 (in Russian) **26**: (1999) 583-596 (in English).
- [3] BREZGUNOV, V.S. Application of oxygen isotopes for study of water exchange in the Lake Issyk Kul basin. *Water Resources* **1**: (1980) 108-120.
- [4] NIKOLAEV, S.D. Isotope palaeogeography of inner seas, VNIRO, Moscow (1995).
- [5] MAEV E.G., KARPICHEV Y. A. Radiocarbon dating of the Aral bottom sediments: sediment ages and sea level changes, *Water Resources* **26**: (2000) 212-220.

¹⁴CO₂ MEASUREMENTS IN MARITIME AIR OVER THE NORTHERN INDIAN OCEAN

K. DUTTA*, R. BHUSHAN, B.L.K. SOMAYAJULU

Physical Research Laboratory,
Navrangpura, Ahmedabad, India

Abstract. ¹⁴C in the carbon dioxide of air overlying the Northern Indian Ocean was measured during the spring of 1993 to 1995 and 1997 to 1999. Considerable variations of ¹⁴C over this region have been observed during this period, which reflect both regional and interannual variations. The interannual variations of ¹⁴C of the tropospheric CO₂ over this region is found to correlate with the El Niño/Southern Oscillation (ENSO) events, with positive excursions of ¹⁴C before the onset of warm phase of ENSO.

1. INTRODUCTION

The tropospheric ¹⁴C/¹²C level almost doubled during early 1960s from its natural values, due to injection of ¹⁴C from large-scale testing of thermonuclear bombs. These tests were performed mainly in the northern hemisphere. The tropospheric Δ¹⁴C attained a peak value of 900 to 1000‰ in the northern hemisphere between 1963 and 1964 [1, 2] and 640‰ in the southern hemisphere during 1965 [3, 4]. After the global moratorium of atmospheric nuclear testing following the Test Ban Treaty of 1963, the tropospheric ¹⁴C is decreasing mainly through air-sea exchange of CO₂, transfer to the biosphere and dilution with ¹⁴C free fossil fuel CO₂, with an approximate exponential trend. The bomb ¹⁴C pulse in the atmosphere has been successfully used as a transient tracer for studying the global carbon cycle dynamics, e.g. for studying air-sea gas exchange, tracing transfer of CO₂ from surface to deep layers in oceans, and for monitoring fossil fuel emission [5]. Tropospheric Δ¹⁴C measurements in the maritime air over the Arabian Sea and the Bay of Bengal have been made during early to late springs of 1993 to 1999 (Fig.1), as part of our ongoing studies on air-sea CO₂ exchange over the Northern Indian Ocean using radiocarbon [6, 7, 8, 9]. From our measurements over the Arabian Sea and the Bay of Bengal done during the 1990's it is demonstrated here that the interannual variations of ¹⁴C in the troposphere are also possibly controlled by the complex coupled ocean atmosphere interactions, during strong El Niño/Southern Oscillation events.

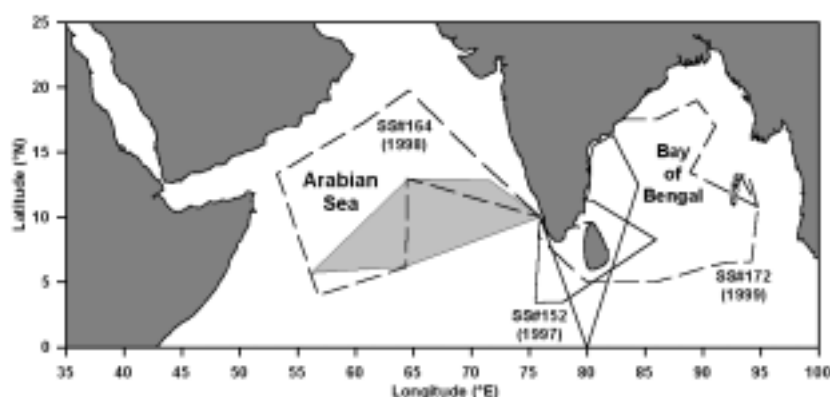


FIG. 1. Cruise tracks for maritime CO₂ sampling over the Arabian Sea and the Bay of Bengal, between 1997 and 1999. Area sampled between 1993 and 1995 over the Arabian Sea is shaded.

* Email: koushik@prl.ernet.in.

2. EXPERIMENTAL

Tropospheric CO₂ was sampled for ¹⁴C measurements onboard research vessels ORV *Sagar Kanya* during 1993 and FORV *Sagar Sampada* during 1994 to 1999 (except 1996). The apparatus used for the sampling is shown in Fig.2. Two of these systems were installed on the front deck of the research vessels and operated simultaneously. Air was sucked in through a greaseless compressor, and allowed to bubble through two plastic bottles kept in series, each containing 250ml of 2N NaOH solution, free from inorganic CO₂. A third bottle containing 250ml of distilled water was fitted at the end, to trap any escaping NaOH aerosols. Air was allowed to bubble through the NaOH solution at 5 lit.min⁻¹, for about 2 to 3 days to collect enough CO₂ (around 5lit), required to prepare adequate amount of benzene for ¹⁴C analysis. Sampling was done only while cruising between stations and when the ship was about 200 km away from the coast. This is to avoid contamination from the ship's emissions and proximity to coastal CO₂ emissions. For a given year, we collected about 3 to 4 samples during 1993 to 1995 and between 8 to 10 samples (which include some duplicates) during 1997 to 1999.

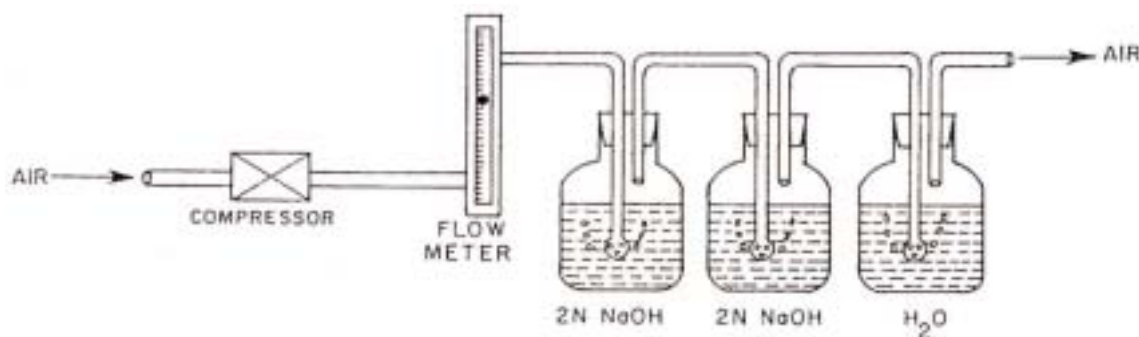


FIG.2. Sampling of tropospheric CO₂ for ¹⁴C analysis, by dynamic pumping of atmospheric air through NaOH solution.

In the laboratory the resultant Na₂CO₃ solution was acidified with dilute H₃PO₄ (30% v/v) in a vacuum system. The liberated CO₂ was purified and converted to benzene for ¹⁴C analysis, through the formation of Li₂C₂ and acetylene, using TASK benzene synthesizer [10]. Considerable isotopic fractionation of carbon in CO₂ is observed during absorption of CO₂ in NaOH solution [11]. However, dynamic pumping of atmospheric air in NaOH solution can minimize this fractionation effect. The extent of this fractionation depends on the sampling rate of CO₂. ¹³C/¹²C ratios were measured in an aliquot of CO₂ used for benzene synthesis, using a PDZ Europa Geo 20-20 stable isotope mass spectrometer. The ¹³C/¹²C ratios are expressed as permil deviation (δ¹³C ‰) from the V-PDB standard. Typical 1σ precision on δ¹³C is ±0.05‰. The δ¹³C values of CO₂ used for benzene synthesis range from -8 to -20‰ (Table I) generally depleted than the normal atmospheric values (-7.7 to -8.0‰) measured over Seychelles (4°40'S, 55°10'E) between 1991 and 1997 [12]. The δ¹³C values have been used only for fractionation correction of ¹⁴C activities. The benzene samples were assayed for ¹⁴C using a Packard 2250CA Liquid Scintillation Counter in low-level count mode. NBS Oxalic Acid-II (SRM 4990C) has been used as standard. The ¹⁴C activities are reported as permil notation (Δ¹⁴C‰) following standard conventions [13], after normalizing to isotopic fractionation of δ¹³C = -25‰ and correcting for decay. Typical 1σ precision on Δ¹⁴C for a single sample is ±5 to 8‰. The results of isotopic measurements and error-weighted means for each year are given in Table 1. Out of 12 duplicate analyses, 9 samples fall within the errors of measurement. Five anomalous Δ¹⁴C values are rejected.

TABLE I

Lab code (PRLCH)	Sample code	Sampling track		$\delta^{13}\text{C}_{\text{PDB}}$ (‰)	$\Delta^{14}\text{C} \pm 1\sigma$ (‰)
		Begin (Lat°N, Long°E)	End (Lat°N, Long°E)		
<i>ORV Sagar Kanya cruise SK-83 (Apr – May, 1993) Arabian Sea</i>					
194	SK-83-A1	15.0, 73.0	12.5, 67.0	-15 [†]	124.0 ± 6.0
196	SK-83-A2	12.5, 67.0	13.0, 68.0	-15.1	119.1 ± 5.2
201	SK-83-A3			-15.3	118.8 ± 4.7
204	SK-83-A4	13.0, 68.0	12.5, 69.5	-15 [†]	121.0 ± 8.0
Mean =				-15.2	120.3 ± 2.8
<i>FORV Sagar Sampada cruise SS-117 (Jan – Feb, 1994) Arabian Sea</i>					
240	SS-117-A1	6.0, 74.0	8.0, 73.0	-15 [†]	104.0 ± 5.0
315	SS-117-A2	8.0, 73.0	13.0, 64.8	-16.4	135.2 ± 5.0
316	SS-117-A3	13.0, 64.8	12.8, 71.6	-14.6	109.5 ± 5.5
Mean =				-15.5	116.6 ± 3.0
<i>FORV Sagar Sampada cruise SS-132 (Apr – May, 1995) Arabian Sea</i>					
326	SS-132-A1	11.0, 75.0	13.0, 64.5	-11.5	101.3 ± 4.7
327	SS-132-A2	13.0, 64.5	5.7, 56.2	-18.0	121.6 ± 5.7
328	SS-132-A3	5.7, 56.2	6.2, 64.4	-8.0	104.2 ± 5.0
329	SS-132-A4	6.2, 64.4	8.0, 75.0	-8.2	91.6 ± 6.7
Mean =				-11.4	105.1 ± 2.7
<i>FORV Sagar Sampada cruise SS-152 (Feb – Mar, 1997) Bay of Bengal</i>					
351	SS-152-1A			-7.7	*75.7 ± 7.0
398	SS-152-1B	7.2, 76.0	3.9, 78.1	-9.3	105.8 ± 7.7
392	SS-152-2A			-9.0	119.9 ± 8.6
399	SS-152-2B	3.9, 78.1	8.5, 86.0	-8.8	120.1 ± 6.5
393	SS-152-3A			-13.6	111.5 ± 7.4
400	SS-152-3B	8.5, 86.0	16.3, 82.3	-15.0	99.8 ± 7.6
394	SS-152-4AB	16.3, 82.3	7.4, 83.8	-13.6	99.8 ± 6.7
395	SS-152-5AB	7.4, 83.8	0.0, 80.0	-7.1	*82.1 ± 6.4
396	SS-152-6AB	0.0, 80.0	0.0, 80.0	-13.8	112.3 ± 8.5
397	SS-152-7AB	2.2, 79.0		-10.8	106.5 ± 7.7
Mean =				-10.9	109.3 ± 2.6
<i>FORV Sagar Sampada cruise SS-164 (Mar – Apr, 1998) Arabian Sea</i>					
424	SS-164-1A			-14.1	95.7 ± 7.7
425	SS-164-1B	12.0, 74.2	16.5, 69.0	-17.1	100.3 ± 6.4
426	SS-164-2A			-13.9	83.4 ± 7.5
427	SS-164-2B	16.5, 69.0	19.8, 64.6	-14.9	*56.3 ± 6.7
428	SS-164-3AB1			-17.0	*119.8 ± 6.8
429	SS-164-3AB2	19.8, 64.6	17.2, 60.7	-17.0	106.5 ± 6.7
430	SS-164-4A			-16.1	104.5 ± 6.3
431	SS-164-4B	17.2, 60.7	14.3, 54.9	-19.6	105.1 ± 6.2
432	SS-164-5AB	13.3, 53.2	3.9, 56.8	-10.7	93.0 ± 6.9
433	SS-164-6A			-16.5	99.0 ± 7.1
434	SS-164-6B	3.9, 56.8	6.2, 64.3	-17.3	93.4 ± 6.0
435	SS-164-7A			-10.2	95.7 ± 6.2
437	SS-164-7B	6.2, 64.3	12.9, 64.5	-17.9	89.1 ± 6.6
Mean =				-15.6	97.3 ± 2.0

TABLE I (cont.

Lab code (PRLCH)	Sample code	Sampling track		$\delta^{13}\text{C}_{\text{PDB}}$ (‰)	$\Delta^{14}\text{C}\pm 1\sigma$ (‰)
		Begin (Lat°N,Long°E)	End (Lat°N,Long°E)		
<i>FORV Sagar Sampada cruise SS-172 (Feb, 1999) Bay of Bengal</i>					
466	SS-172-1A	17.5, 85.9	17.0, 91.1	-12.6	89.3 ± 7.3
467	SS-172-1B			-10.6	94.5 ± 8.3
468	SS-172-2A	16.9, 91.1	13.4, 88.9	-13.1	84.2 ± 5.4
469	SS-172-2B			-8.2	85.2 ± 5.9
470	SS-172-3AB	13.4, 88.9	13.0, 93.0	-14.0	95.1 ± 5.1
471	SS-172-4AB1	10.8, 93.2	6.5, 91.7	-13.2	91.7 ± 5.0
472	SS-172-4AB2			-13.2	88.7 ± 5.4
473	SS-172-5AB	6.5, 91.7	5.0, 86.0	-15.1	80.5 ± 4.8
474	SS-172-6AB	5.0, 86.0	8.0, 76.0	-9.3	*67.5 ± 4.7
Mean =				-12.1	88.1 ± 2.0

*Rejected for mean calculation, due to possible fractionation or contamination.

† $\delta^{13}\text{C}$ not measured, mean value of -15‰ have been used for $\Delta^{14}\text{C}$ calculation.

Data for 1993–1995 are from [9]. A and B are duplicate samples for the same cruise track. AB denotes duplicate samples combined due to insufficient CO_2 trapping. SK and SS represent Sagar Kanya and Sagar Sampada respectively.

3. TRENDS OF $^{14}\text{CO}_2$ OVER THE NORTHERN INDIAN OCEAN

The $\Delta^{14}\text{C}$ values given in Table 1 are the mean obtained along a cruise track. The mean value for a given year represents the springtime $\Delta^{14}\text{C}$, averaged over a wide area of the ocean basin. Amplitudes of seasonal ^{14}C oscillation in tropical maritime atmosphere are $\leq 5\text{‰}$ [14]. Therefore, springtime $\Delta^{14}\text{C}$ values are expected to be close to the annual mean within the limits of uncertainty.

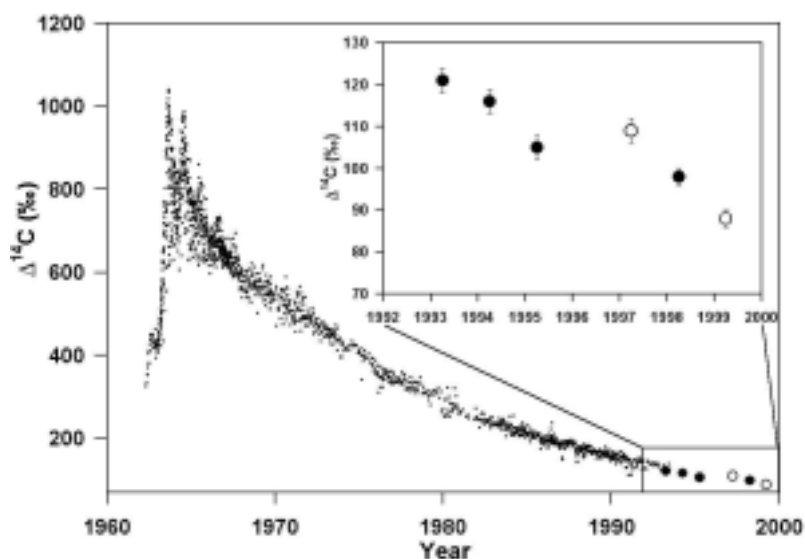


FIG. 3. Tropospheric $\Delta^{14}\text{C}$ measured from the Northern and the Southern Hemisphere sites (dots) [1]. Inset, is the plot of average tropospheric $\Delta^{14}\text{C}$ measured over the Arabian Sea (filled circles) and the Bay of Bengal (open circles).

The $\Delta^{14}\text{C}$ values of tropospheric CO_2 over the Northern Indian Ocean show deviations from the normal exponential decreasing trend. This reflects either regional difference of $^{14}\text{CO}_2$ over this region or interannual tropospheric $^{14}\text{CO}_2$ variations resulting from anomalous ocean-atmosphere CO_2 exchange or terrestrial flux of CO_2 . $\Delta^{14}\text{C}$ measured in 1997 over the Bay of Bengal is equal to or higher than that over the Arabian Sea in 1995. Rate of $\Delta^{14}\text{C}$ decrease over the Arabian Sea was slower between 1995 and 1998, than that between 1993 and 1995. To resolve the interannual ^{14}C variations over the Northern Indian Ocean, we have compared the time scale of atmospheric ^{14}C decrease and its relative deviation from a smooth trend, determined for each year as described below.

The exponential decreasing trend of the tropospheric $^{14}\text{CO}_2$ at any given location can be characterized by its decay (or e-folding) time constant τ . The average e-folding time is about 16 years in the northern hemisphere [15] and about 17 years in the southern hemisphere [3]. The e-folding times were calculated for different years by choosing 1980 as the base year from the relation,

$$\Delta^{14}\text{C}_t = \Delta^{14}\text{C}_{1980} e^{-\Delta t / \tau}$$

where $\Delta^{14}\text{C}_t$ is the measured value in a given year (t) and Δt is time since 1980. Here $\Delta^{14}\text{C}_{1980}$ is taken as 265‰, from the tropical maritime tropospheric ^{14}C measurements at Izaña, Canary Islands, Spain (28°N, 16°W, 2376m asl) [1]. This value agrees well with $\Delta^{14}\text{C}$ value of 260 ± 5 ‰ for 1980, measured in dendro-dated tree rings of teak grown at Thane (19°14'N, 73°24'E) near the Arabian Sea coast [16]. The e-folding times over the Northern Indian Ocean range from 16.0 to 18.8 (± 0.5) years (Table 2), with a mean of 17.0 ± 0.2 years. This compares well with the e-folding time of 16.6 years reported earlier for this region [9], obtained relative to the base year 1970 with $\Delta^{14}\text{C}_{1970} = 550$ ‰ and applying Suess effect correction of -0.68 ‰.yr⁻¹. To resolve the interannual variations, the ^{14}C data have been detrended by removing an exponentially decaying trend. The residual of $\Delta^{14}\text{C}$ obtained after detrending is given by,

$$\Delta^{14}\text{C}_{\text{residual}} = \Delta^{14}\text{C}_t - \Delta^{14}\text{C}_{1980} e^{-\Delta t / 17.0}$$

The residual $\Delta^{14}\text{C}$ values (with 1σ errors) are summarized in Table 2. Apparently, the $\Delta^{14}\text{C}$ values of the Arabian Sea are less than over the Bay of Bengal. A part of this regional variation can be explained from the contrasting upwelling characteristics of the Arabian Sea and the Bay of Bengal. Arabian Sea being a perennial source of CO_2 from upwelling of CO_2 rich deep water [17], the regional atmospheric $\Delta^{14}\text{C}$ will be lower due to evasion of ^{14}C -depleted CO_2 . The Bay of Bengal being a sink of atmospheric CO_2 [18], such regional depletion of tropospheric ^{14}C will be lower. Regional upwelling induced ^{14}C depletion was documented from tree ring $\Delta^{14}\text{C}$ measurements from northwestern Thailand [4] and from coastal South Africa [19].

TABLE II

Year (t) / Region	$\Delta^{14}\text{C}_t$ (‰)	τ (year)	$\Delta^{14}\text{C}_{\text{residual}}$ (‰)
1993 / Arabian Sea	120.3 ± 2.8	16.2 ± 0.5	-4.5 ± 3.0
1994 / Arabian Sea	116.6 ± 3.0	16.6 ± 0.5	-2.7 ± 3.0
1995 / Arabian Sea	105.1 ± 2.7	16.0 ± 0.5	-5.9 ± 3.0
1997 / Bay of Bengal	109.3 ± 2.6	18.8 ± 0.5	9.4 ± 3.0
1998 / Arabian Sea	97.3 ± 2.0	17.7 ± 0.4	3.7 ± 2.0
1999 / Bay of Bengal	88.1 ± 2.0	16.9 ± 0.4	-0.7 ± 2.0

However, considering the close proximity of the Arabian Sea and the Bay of Bengal, rapid zonal mixing is expected to quickly smooth out any such variation. More data are needed to verify the presence of any zonal gradient of tropospheric $\Delta^{14}\text{C}$ across these two basins. This regional depletion can be confirmed by simultaneous $\Delta^{14}\text{C}$ measurements over the two basins.

The $\Delta^{14}\text{C}_{\text{residual}}$ for the Arabian Sea during 1998 is nearly 10‰ higher than that during 1995, similar to the $\Delta^{14}\text{C}_{\text{residual}}$ difference for the Bay of Bengal between 1997 and 1999. The anomalous high values of residual $\Delta^{14}\text{C}$ during 1997 and 1998 coincide with the very strong El Niño/Southern Oscillation (ENSO) event of 1997–‘98. The ENSO events are characterized by anomalously warm sea surface temperature in the equatorial Pacific. These events cause significant perturbation in the global carbon cycle, through changes in the ocean-atmosphere CO_2 exchange and terrestrial CO_2 fluxes [20, 21]. A reduction in the depth of the thermocline in the equatorial Pacific which causes significant reduction in the upwelling of CO_2 rich deep waters during the El Niño events, reducing the sea-air efflux of CO_2 to 30–80% of a normal year [22], resulting in negative CO_2 anomaly in the atmosphere. Reduction in rainfall over tropical rainforests result in increase of net respiration of the terrestrial biosphere, enhancing the biospheric CO_2 flux [23], which offsets the ocean induced negative CO_2 anomaly. For the last three decades, such arid conditions would favor release of CO_2 from oxidation of ^{14}C rich fast cycling soil organic matter [24]. The El Niño events are accompanied by anomalous atmospheric circulation patterns, with higher tropopause height and higher stratosphere-troposphere exchange [25], which can favor enhanced transport of stratospheric air with higher $\Delta^{14}\text{C}$ [26] to the troposphere. All these phenomena, e.g. reduction of ^{14}C depleted CO_2 from oceans, biospheric release of ^{14}C enriched CO_2 , and enhanced mixing with stratospheric air, are conducive to an enhanced level of $^{14}\text{CO}_2$ in the troposphere during the El Niño events. In Fig. 4, the ^{14}C anomalies over the Northern Indian Ocean are compared with the Tahiti–Darwin Southern Oscillation Index (SOI) [27] and the Multi-variate ENSO index (MEI) [28].

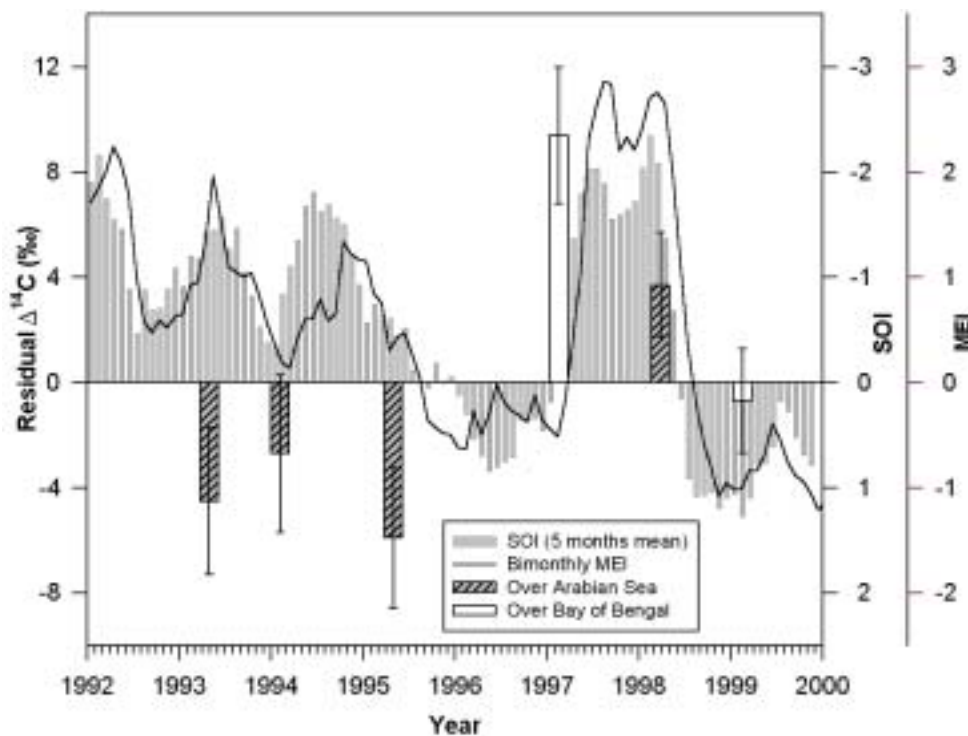


FIG. 4. Anomalies of ^{14}C over the Arabian Sea (hatched bars) and the Bay of Bengal (open bars). The gray bars are SOI averaged over 5 months and the solid curved line is the bimonthly multi-variate ENSO index (MEI). Negative SOI or positive MEI values represent the El Niño condition.

It is important to note in Fig.4 that the highest positive $\Delta^{14}\text{C}$ anomaly of 1997 was observed about 8 months prior to the development of peak El Niño condition during November 1997. From the inversion of atmospheric concentration and stable isotopic composition, it has been shown that interannual variability of the tropical CO_2 fluxes are significantly correlated with southern oscillation index, with flux anomalies leading the SOI anomaly by 4 to 9 months [29]. The negative CO_2 flux anomalies from oceans are synchronous or lead early months of the El Niño events by few months and positive anomalies from lands occur toward the end of these events. Thus it is possible to explain the early occurrence of the positive $\Delta^{14}\text{C}$ anomaly by the onset of the reduction of ^{14}C -depleted oceanic CO_2 fluxes. If the El Niño induced atmospheric ^{14}C excursion is confirmed from other tropical sites, it will be of considerable interest to compare these ^{14}C anomalies with the tropical CO_2 flux anomalies.

4. EVIDENCES OF POSSIBLE MODULATION OF TROPOSPHERIC $^{14}\text{CO}_2$ BY ENSO

There are some reports on possible ENSO modulation of tropospheric $^{14}\text{CO}_2$ both during the pre-nuclear and the post-nuclear era. It has been demonstrated that ENSO influences regional differences in tree ring ^{14}C from Washington State and Arizona, USA, during 1930 to 1955 [30]. Periodicities in the 2–6.4 year range observed in the spectrum of annual high precision tree ring ^{14}C data (1511 to 1954 AD) from Pacific northwest, Washington, USA have been associated with ENSO related thermohaline circulation change [31]. In the post nuclear period, modulation of $^{14}\text{CO}_2$ on regional scale by ENSO events was observed in atmospheric CO_2 samples collected in the equatorial Pacific region between 1991 and 1993 [32]. A very regular quasi-biannual variation has been observed in the recent data of $^{14}\text{CO}_2$ from the southern hemisphere, which has a possible association with the El Niño phenomenon [33]. At the high latitudes of the northern hemisphere, slower decrease of tropospheric $^{14}\text{CO}_2$ was observed over Abisko, Sweden ($68^\circ 20.5' \text{N}$) and Svalbard, Spitsbergen ($78^\circ 04' \text{N}$) during the ENSO years between 1982 and 1987 [34].

5. CONCLUSIONS

The spatial and temporal variations of tropospheric $\Delta^{14}\text{C}$ values observed over the Northern Indian Ocean between 1993 and 1999 show:

- (a) During the 1990's $\Delta^{14}\text{C}$ has been decreasing at the rate of $5\text{‰}.\text{yr}^{-1}$ on an average. The decrease corresponds to average e-folding time of about 17 years for the removal of tropospheric ^{14}C over this region, assuming $\Delta^{14}\text{C}_{1980}$ to be 265‰.
- (b) The rate of this decrease is not uniform. The observed $\Delta^{14}\text{C}$ over this region was about 7‰ higher than the expected trend, during the very strong El Niño event of 1997–'98.
- (c) $\Delta^{14}\text{C}$ in air overlying the Arabian Sea appears to be lower than that over the Bay of Bengal (by about 5‰, comparing the $\Delta^{14}\text{C}$ values of non-ENSO years 1995 and 1999). This is due to the fact that the Arabian Sea is a perennial source of CO_2 , from the upwelling of ^{14}C -depleted CO_2 rich water. More measurements are needed to confirm this regional depletion of ^{14}C in the air overlying the Arabian Sea.

ACKNOWLEDGEMENTS

This study was partly funded by the Department of Ocean Development (DOD) and Department of Space (DOS), Government of India. We thank director, DOD Cell Cochin and his associates and the captain and crew of FORV *Sagar Sampada* and ORV *Sagar Kanya*. We

also thank Dr. Klaus Wolter for the MEI data and Prof. S. Krishnaswami for discussion. BLKS is Honorary Professor and CSIR Emeritus Scientist during this study.

REFERENCES

- [1] NYDAL, R., LÖVSETH, K., Carbon-14 measurements in atmospheric CO₂ from Northern and Southern Hemisphere sites, 1962–1993. NDP-057, CDIAC, Oak Ridge National Laboratory, Oak Ridge, Tennessee, USA (1996).
URL: <http://cdiac.esd.ornl.gov/epubs/ndp/ndp057/ndp057.htm>
- [2] LEVIN, I., KROMER, B., SCHOCH-FISCHER, H., BRUNS, M., MÜNICH, M., BERADU, B., VOGEL, J.C., MÜNICH, K.O., 25 years of tropospheric ¹⁴C observations in central Europe. Radiocarbon **27**: (1985) 1–19.
- [3] MANNING, M.R., LOWE, D.C., MELHUISE, W.H., SPARKS, R.J., WALLACE, G., BRENNINKMEIJER, C.A.M., MCGILL, R.C., The use of radiocarbon measurements in atmospheric studies. Radiocarbon **32**: (1990) 37–58.
- [4] HUA, Q., BARBETTI, M., JACOBSEN, G.E., ZOPPI, U., LAWSON, E.M., Bomb radiocarbon in annual tree rings from Thailand and Australia. Proceedings of 8th AMS Conference, Nuclear Instruments and Methods in Physics Research B **172**: (2000) 359–365.
- [5] LEVIN, I., HESSHAIMER, V., Radiocarbon – A unique tracer of global carbon cycle dynamics. Radiocarbon **42**: (2000) 69–80.
- [6] DUTTA, K., BHUSHAN, R., SOMAYAJULU, B.L.K., Anthropogenic radiocarbon in Bay of Bengal: Two decades after GEOSECS. Abstracts, 17th International Radiocarbon Conference, June 18–23 2000, Judean Hills, Israel, (2000) 97.
- [7] DUTTA, K., Study of marine processes in the Bay of Bengal using Radiocarbon. Ph.D.-Thesis in preparation (2001).
- [8] BHUSHAN, R., SOMAYAJULU, B.L.K., CHAKRABORTY S., KRISHNASWAMI, S., Radiocarbon in the Arabian Sea water column: Temporal variations in bomb ¹⁴C inventory since the GEOSECS and CO₂ air–sea exchange rates. Journal of Geophysical Research **105**: (2000) 14279–14282.
- [9] BHUSHAN, R., KRISHNASWAMI, S., SOMAYAJULU, B.L.K., ¹⁴C in air over the Arabian Sea. Current Science **73**: (1997) 273–276.
- [10] BHUSHAN, R., CHAKRABORTY, S., KRISHNASWAMI, S., Physical Research Laboratory (Chemistry) radiocarbon date list I. Radiocarbon **36**: (1994) 251–256.
- [11] NYDAL, R., Variation of ¹⁴C concentration in the atmosphere during the last several years. Tellus (1966) 271–279.
- [12] MASARIE, K.A., WHITE, J., VAUGHN, B., TANS, P., Stable isotopic composition of atmospheric carbon dioxide (¹³C and ¹⁸O). INSTAAR, University of Colorado and NOAA Climate Monitoring and Diagnostic Laboratory (CMDL), Carbon Cycle Group (1999).
URL: <http://www.cmdl.noaa.gov/ccgg>
- [13] STUIVER, M., POLACH, H.A., Reporting of ¹⁴C data. Radiocarbon **19**: (1977) 355–363.
- [14] MEIJER, H.A.J., VAN DER PLICHT, J., GISLEFOSS, J.S., NYDAL, R., Comparing long-term atmospheric ¹⁴C and ³He records near Groningen, The Netherlands with Fruholmen, Norway and Izaña, Canary Islands ¹⁴C stations. Radiocarbon **37**: (1995) 39–50.
- [15] LEVIN, I., KROMER, B., Twenty years of atmospheric ¹⁴CO₂ observations at Schauinsland station, Germany. Radiocarbon **39**: (1997) 205–218.

- [16] CHAKRABORTY, S., RAMESH, R., KRISHNASWAMI, S., Air–sea exchange of CO₂ in the Gulf of Kutch, northern Arabian Sea based on bomb–carbon in corals and tree rings. *Proceedings of the Indian Academy of Sciences* **103**(2): (1994) 231–42.
- [17] SARMA, V.V.S.S., KUMAR, M.D., GEORGE, M.D., The central and the eastern Arabian Sea as a perennial source of atmospheric carbon dioxide. *Tellus B* **50**: (1998) 179–184.
- [18] KUMAR, M.D., NAQVI, S.W.A., GEORGE, M.D., JAYAKUMAR, D.A., A sink for atmospheric carbon dioxide in the northeast Indian Ocean. *Journal of Geophysical Research* **101**: (1996) 18121–18125.
- [19] DAMON, P.E., BURR, G.S., PERISTYKH, A., $\Delta^{14}\text{C}$ and Ekman transport, spiral and west coast upwelling. Abstracts, 8th International Conference on Accelerator Mass Spectrometry, 6–10 September 1999, Vienna, Austria, (1999) 101.
- [20] KEELING, C.D., REVELLE, R., Effects of El–Niño southern oscillation on the atmospheric content of carbon dioxide. *Meteoritics* **20**: (1985) 437–450.
- [21] KEELING, C.D., WHORF, T.P., WAHLEN, M., VANDERPLICHT, J., Interannual extremes in the rate of rise of atmospheric carbon dioxide since 1980. *Nature* **375**: (1995) 666–670.
- [22] FEELY, R.A., WANNINKHOF, R., TAKAHASHI, T., TANS, P., The influence of El Niño on the equatorial Pacific contribution to atmospheric CO₂ accumulation. *Nature* **398**: (1999) 597–601.
- [23] PRENTICE, I.C., LLOYD, J.C., C–Quest in the Amazon Basin. *Nature* **396**: (1998) 619–620.
- [24] TRUMBORE, S., Potential of soil organic carbon to global environmental change. *Proceedings of the National Academy of Sciences, USA* **94** (1997) 8,284–8,291.
- [25] GAGE, K.S., REID, G.C., The tropical tropopause and the El Niño of 1982–1983. *Journal of Geophysical Research* **91**: (1986) 13,315–13,317.
- [26] NAKAMURA, T., NAKAZAWA, T., NAKAI, N., KITAGAWA, H., HONDA, H., ITOH, T., MACHIDA, T., MATSUMOTO, E., Measurement of ^{14}C concentrations of stratospheric CO₂ by accelerator mass spectrometry. *Radiocarbon* **34**: (1992) 745–752.
- [27] ROPELEWSKI, C.F., JONES, P.D., An extension of the Tahiti–Darwin Southern Oscillation Index, *Monthly Weather Review* **115**: (1987) 2161–2165.
URL: <http://www.cru.uea.ac.uk/cru/data/soi.htm>
- [28] WOLTER, K., TIMLIN, M.S., Measuring the strength of ENSO—how does 1997/98 rank? *Weather* **53**: (1998) 315–324.
URL: <http://www.cdc.noaa.gov/~kew/MEI/mei.html>
- [29] RAYNER, P.J., LAW, R.M., DARGAVILLE, R., The relationship between tropical CO₂ fluxes and the El Niño–Southern Oscillation. *Geophysical Research Letters* **26**: (1998) 493–496.
- [30] JIRICOWIC, J.L., KALIN, R.M., A possible paleoclimatic ENSO indicator in the spatial variation of annual tree–ring ^{14}C . *Geophysical Research Letters* **20**: (1993) 439–442.
- [31] STUIVER, M., BRAZIUNAS, T.F., Sun, ocean, climate and atmospheric $^{14}\text{CO}_2$: an evaluation of causal and spectral relationships. *The Holocene* **3**: (1993) 289–305.
- [32] ROZANSKI, K., LEVIN, I., STOCK, J., GUEVARA FALCON, R.E., Atmospheric $^{14}\text{CO}_2$ variations in the equatorial region. *Radiocarbon* **37**: (1995) 509–516.
- [33] LEVIN, I., HESSHAIMER, V., KROMER, B., Long–term observations of $^{14}\text{CO}_2$ in the global atmosphere. Abstracts, 16th International Radiocarbon Conference, June 16–20 1997, Groningen, The Netherlands, (1997) 115.
- [34] OLSON, I., Recent ^{14}C activity in the atmosphere, clean air and the Chernobyl effect. *Radiocarbon* **31**: (1989) 740–746.

AN UNEXPLORED SEDIMENTARY RECORD FOR THE STUDY OF ENVIRONMENTAL CHANGE IN MEDITERRANEAN COASTAL ENVIRONMENTS: *Posidonia oceanica* (L.) DELILE PEATS

M.-A. MATEO, P. RENOM

Departament d'Ecologia, Universitat de Barcelona,
Barcelona, Spain

R. JULIA

Institute de Ciències de la Terra Jaume Almera,
Barcelona, Spain

J. ROMERO

Departament d'Ecologia, Universitat de Barcelona,
Barcelona, Spain

R. MICHENER

Boston University Stable Isotope Laboratory, Department of Biology,
Boston, Massachusetts, United States of America

Abstract. Information on seagrass paleo-ecology is very scarce because detailed seagrass paleo-records are virtually lacking. The endemic Mediterranean seagrass *Posidonia oceanica* conjugates two unusual features that allow the reconstruction of the past history of the plant at two different time scales. On the one hand, the study of the leaf sheaths that remain attached to the rhizomes after leaf abscission (lepidochronology), allows to differentiate up to 30 yearly cycles. On the other hand, radio-carbon dating of peat-like deposits derived from *Posidonia oceanica* rhizomes and roots ('mattes'), reveals a chronological organic record of the plant spanning several thousands of years. Changes in the isotopic signature ($\delta^{13}\text{C}$) of the sheaths along *Posidonia* rhizomes from a meadow off Medes Islands (NW Mediterranean, Spain), were highly correlated with changes in annual leave production and with water transparency. These relationships and the isotopic analysis of sheath debris from several *Posidonia* peats along the Spanish Mediterranean coast are used to make some preliminary inferences about long-term meadow history. Several phenomena potentially difficulting the interpretation of the information contained in *Posidonia* peats are critically discussed. It is concluded that a detailed study of *P. oceanica* peats will open new vistas in Mediterranean paleo-ecological and paleo-environmental research.

1. INTRODUCTION

Our knowledge of terrestrial and aquatic freshwater angiosperm plant communities of the late-Pleistocene and the Holocene ages is considerable due to the wealth of fossil remains preserved in sedimentary deposits [1]. Paleorecords of the only angiosperms that have invaded the submarine realm, seagrasses, are virtually lacking because the appropriate preservation conditions apparently have been very rarely met and because, with a few exceptions, seagrass pollen lacks exine, the outermost coat of the pollen grain. The endemic Mediterranean seagrass *Posidonia oceanica* (L.) Delile, however, conjugates two unusual features that allow investigation of the past history of the plant at different time scales. In many seagrasses it is possible to distinguish yearly cycles through the observation of various characteristics of the sheaths (lepidochronology; [2]) and sheath scars along the rhizome [3]. Several features of the biology of *Posidonia* such as number of leaves, leaf production, plastochron, seasonality, vertical growth, or rhizome production, can be reconstructed for periods spanning up to 3 decades with a seasonal resolution. Moreover and, exceptionally, *Posidonia oceanica* belowground organs accumulate in the sediment forming organic peat-like deposits, so-called

‘mattes’, several meters in thickness. Previous studies using radio-carbon techniques have revealed that these peats, largely sheath- but also root- derived recalcitrant organic matter, constitute an unique organic record spanning several thousands of years, which stratigraphy accurately reflects its chronology of formation [4,5,6]. The *Posidonia* peats thus offer unprecedented possibilities to perform detailed studies of seagrass-dominated paleo-environments.

In this study such possibilities are explored combining lepidochronology and radio-carbon dating with the analysis of stable carbon isotopes in order to obtain clues about the physical surroundings and the growth history of *Posidonia oceanica* meadows along the spanish coast. To this end, the relationships between the number of leaves produced per year, water transparency, and the stable carbon isotope composition of *P. oceanica* have been studied at a decadal scale in recent sheath material using lepidochronology. With this information, a few preliminar inferences about changes in *Posidonia oceanica* biological and environmental features over a time-scale of thousands of years are made using radio-carbon dating and carbon isotopic analysis in *Posidonia* peats.

2. MATERIALS AND METHODS

For the short-term (decadal) approach, 12 vertically growing rhizomes of *P. oceanica* were collected in the Natural Reserve of the Medes Islands, NW-Mediterranean, Spain, over an area of ca. 250 m². Sheaths were counted and grouped by years using lepidochronology [2]. The rhizomes were divided in separate segments, each bearing the sheaths formed over one-year periods. In this study we have assumed that the number of sheaths produced per year (which equals the number of leaves produced) is positively related with plant aboveground annual production. The possible use of sheath biomass as a proxy for production was discarded because sheath biomass can be affected by erosion and decay processes.

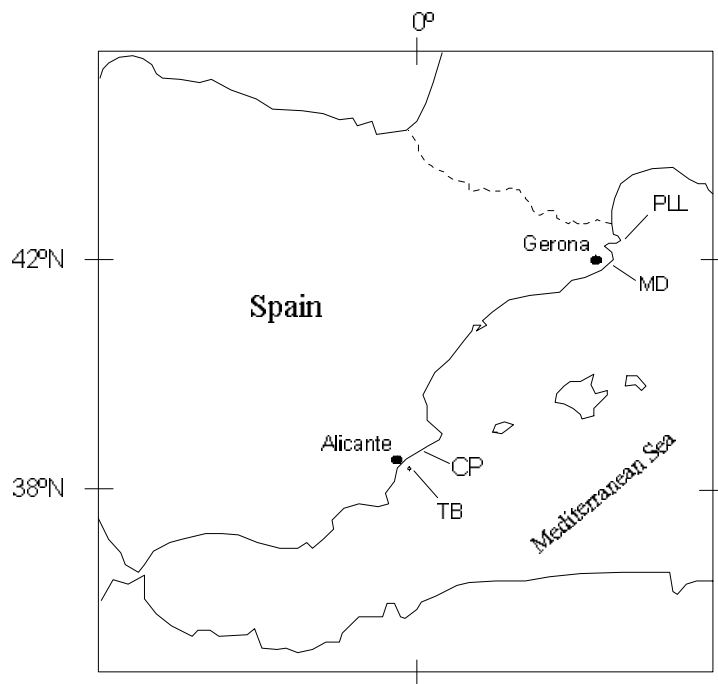


FIG. 1. Geographical location of the sampling sites. *Posidonia oceanica* peats were sampled at 4 locations: Port lligat (PLL), Medes Islands (MD), El Campello (CP), and Tabarca Island (TB). Additionally, *Posidonia* rhizomes were collected in Medes Islands.

Table I. Main features of the various *P. oceanica* peats studied

Site	Age range			Thickness	$\delta^{13}\text{C}$	SEM	<i>N</i>	Max.	Min.	Range
	(years B.P.)			(cm)	(‰)			(‰)	(‰)	(‰)
PLL	710	-	1600	123	-12.7	0.41	5	-11.3	-13.8	2.5
MD	1310	-	3330	200	-13.7	0.69	10	-13.2	-14.2	1.0
CP-A	670	-	1490	200	-15.5	0.77	5	-14.1	-17.4	3.3
CP-B	540	-	1340	200	-14.7	0.45	5	-13.0	-15.5	2.5
CP-C	530	-	1240	200	-14.6	0.39	5	-13.6	-15.8	2.2
TB-A	210	-	1330	170	-13.8	1.22	5	-12.4	-15.1	2.7
TB-B	210	-	1020	140	-16.1	0.28	4	-15.3	-16.6	1.3
TB-C	310	-	1060	140	-16.3	0.20	4	-15.7	-16.6	0.9

SEM: Standard error of the mean
Adapted from [6]

Table II. Average accretion rates and $\delta^{13}\text{C}$ values for the various *P. oceanica* peats studied

Site	Accretion rates (cm year ⁻¹)	$\delta^{13}\text{C}$ (‰)	SEM	N
PLL	0.088	-12.7	0.41	5
MD	0.079	-13.7	0.69	10
CP	0.203	-14.8	0.31	15
TB	0.114	-15.4	0.34	13

SEM: Standard error of the mean
Adapted from [6]

For the pluri-millennarian approach, *Posidonia oceanica* peats were sampled in 4 locations along the Spanish Mediterranean coast (Figure 1; Tables I and II). In Port Lligat, a peat core was obtained by means of a floating drilling platform that combined pneumatic percussion and rotation. A jagged drilling head was specially designed to adequately penetrate into the fibery peat minimizing material compaction. Only the first section (123 cm length) of the ca. 5 m core obtained, was sectioned into 1 cm slices. Five of these slices were selected for radio-carbon dating and isotopic analysis (see further). Data from the rest of the core will not be reported in this work. From each of the selected 1 cm slices, the organic fraction retained by a >1mm mesh sieve (that consisted in 100% *P. oceanica* detritus) was separated and fractionated again into sheath-, root-, and rhizome-derived material. The rest of the peats were sampled by horizontally coring naturally-cut faces of *P. oceanica* peat using a corer operated by SCUBA divers. Details on the sampling sites and sampling procedures are described elsewhere [6]. Only sheath material was selected off the samples for analytical procedures.

Root-derived organic material was discarded because downwards growth of the roots may lead to incoherences between radio-carbon age and stratigraphic position in the peat. All *P. oceanica* samples (recent and old material) were oven-dried at 70 °C until constant weight and ground to a fine powder in a glass mortar prior to elemental and isotopic analysis.

2.1. Isotopic analysis

The carbon stable isotope ratios were determined by mass spectrometry (Finnigan Delta S Isotope RMS – Conflo II interface; total analytical error was 0.13 ‰). Isotopic ratios are expressed in the common notation:

$$\delta^{13}\text{C}\left(o/_{oo}\right)=\frac{R_{sa}-R_{std}}{R_{std}}\cdot 1000$$

where R is the isotopic ratio $^{13}\text{C}/^{12}\text{C}$ of the sample (sa) or of the standard (std) VPDB.

2.2. Age determination

The age of the millenary samples was established by determining the ^{14}C content of the samples using high-precision accelerator mass spectrometry (National Ocean Sciences AMS Facility, Woods Hole Oceanographic Institution). For each of the 5 samples dated, the carbon dioxide from the combustion of ca. 1 mg of powdered *P. oceanica* sheath material was reacted to graphite using a Fe/H_2 catalytic-reduction. Graphite was analyzed on the accelerator along with the NBS Oxalic Acid I (NIST-SRM-4990) standard and with a process blank sample (graphite powder, Johnson-Mathey 99.9999%). Ages are calculated using the internationally accepted modern value of $1.176 \pm 0.010 \times 10^{-12}$ [7] and a final ^{13}C -correction was made to normalize to a $\delta^{13}\text{C}_{\text{VPDB}}$ value of -25 ‰. Ages are reported as radio-carbon ages (years before present; 1950) following the convention outlined in [8, 9].

2.3. Water transparency data series

Annual mean water transparency (Secchi depth) was calculated by averaging daily measurements available for the same period in the proximity of Medes Islands (J. Pascual, unpublished data).

2.4. Numerical procedures

Relationships between the studies variables were explored using simple regression procedures [10] and time series analysis (STATISTICA Kernel release 5.5, '99 Edition, STATSOFT, Inc, OK, USA).

3. RESULTS AND DISCUSSION

3.1. Recent archives

Lepidochronological dating of the *Posidonia oceanica* vertical rhizomes allowed the identification of 14 complete years (from 1979 to 1992). The effect of light intensity on the stable carbon isotope composition of seagrasses has been repeatedly demonstrated either by field sampling along a bathymetrical gradient [11], in situ shading experiments [12], or mesocosms experiments [13, 14]. The pattern found in the mentioned experiments (i.e. lower $\delta^{13}\text{C}$ values at lower irradiances) is corroborated in the present study by the good correlation between the annual average carbon isotopic composition of the sheaths and the corresponding average Secchi depths ($\delta^{13}\text{C} = -17.40 + 0.24 \times \text{Secchi}$; , $R = 0.78$, $P = 0.003$, $N = 14$; Fig. 2). This pattern is a consequence of a differential enzymatic discrimination against ^{13}C during photosynthesis of the individuals growing at different light intensities (lower discrimination at higher irradiances; see review by [15]. Coherently, a good correlation between $\delta^{13}\text{C}$ values and the annual leaf production of the plant was found (number of leaves = $-16.44 + 0.40 \times \delta^{13}\text{C}$, $R = 0.75$, $P = 0.002$, $N = 14$; Fig. 3).

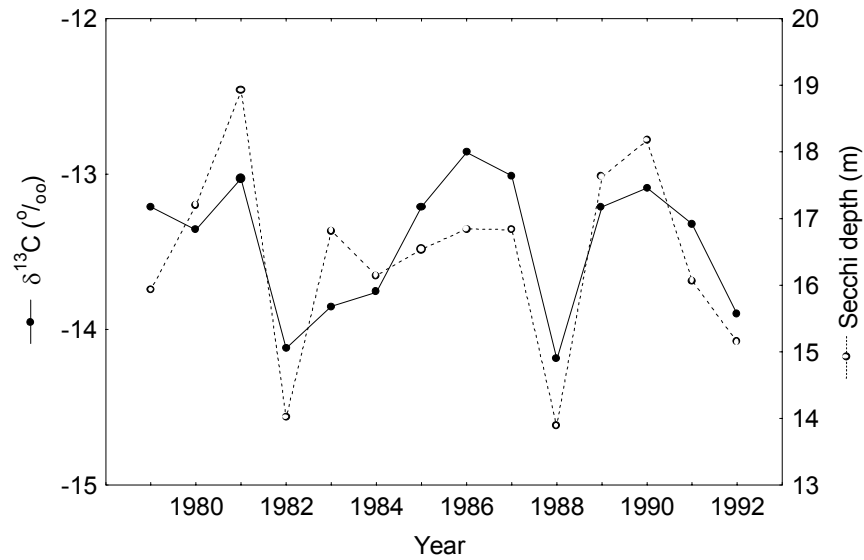


FIG. 2. Relationship between annual average water transparency (Secchi depth) and the carbon stable isotope composition of *Posidonia oceanica* sheaths. Sheat age was determined using lepidochronology.

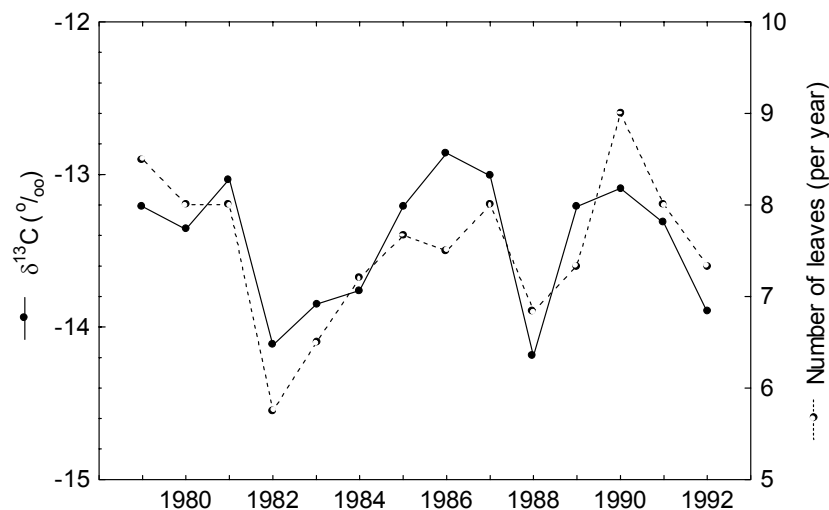


FIG. 3. Relationship between annual average leaf production (number of sheaths) and the carbon stable isotope composition of *Posidonia oceanica* sheaths. Sheat age was determined using lepidochronology.

3.2. Millenary archives

A departure point for determining the potential of *P. oceanica* for paleo-reconstruction purposes, is the assessment of the maximum period of time that can be expected to be spanned by continuous *Posidonia* peats. In this study the oldest sample was that in the base of a 2 m-thick peat wall in Medes Islands, revealing a ca. 3400 yr BP organic record (Table I).

That peat wall in Medes Islands continued 2 more meters downwards, potentially duplicating the actual age observed. Direct observations reported in early works on *Posidonia* meadows describe natural cut faces of *Posidonia* peats as thick as 6 m, probably continuing deeper down the sediment [16]. Assuming a constant accretion rate of the organic material, a 6 m-thick peat could be as old as 10 000 years. Accretion rates, however, have been found to be

highly variable within the same peat wall (A, B, C, replicates where separated only 50 cm from each other) or between peat walls of different sampling sites ([6] and present work, Table II, Fig. 4). It has been suggested that the most ancient *Posidonia* continuous peats cannot be older than ca. 11 000 yr BP [17]. In that time, the last glacio-eustatic regression of the Mediterranean Sea took place, hypothetically enabling the present *Posidonia oceanica* meadows to initiate the last colonization and, therefore, the buildup of the peats.

The isotopic composition in the different peats studied showed a considerable geographical variability, the average value being -14.2 ‰ and the range 6.1 ‰, (Tab. I). Significant differences between the sites located around the parallel 42.5°N (PLL and MD) and those around the parallel 38.5°N (CP and TB) were found (-13.2 ‰ and -15.1 ‰, respectively; $P < 0.01$). A significant latitudinal gradient has been observed in the isotopic composition of seagrasses [15]. However, the pattern observed here, i.e. higher isotopic discrimination in the southernmost sites, is in contradiction with that latitudinal gradient and with most of studies relating latitude, irradiance, and $\delta^{13}\text{C}$ ([15] and references therein). Local variability is likely to account for this contradiction. This hypothesis is supported by the lack of correlation found across the studied sites for peat accretion rate, suggesting that within certain geographical limits, the effects of local factors on seagrass biology can override those of environmental changes at a larger geographical scale [6].

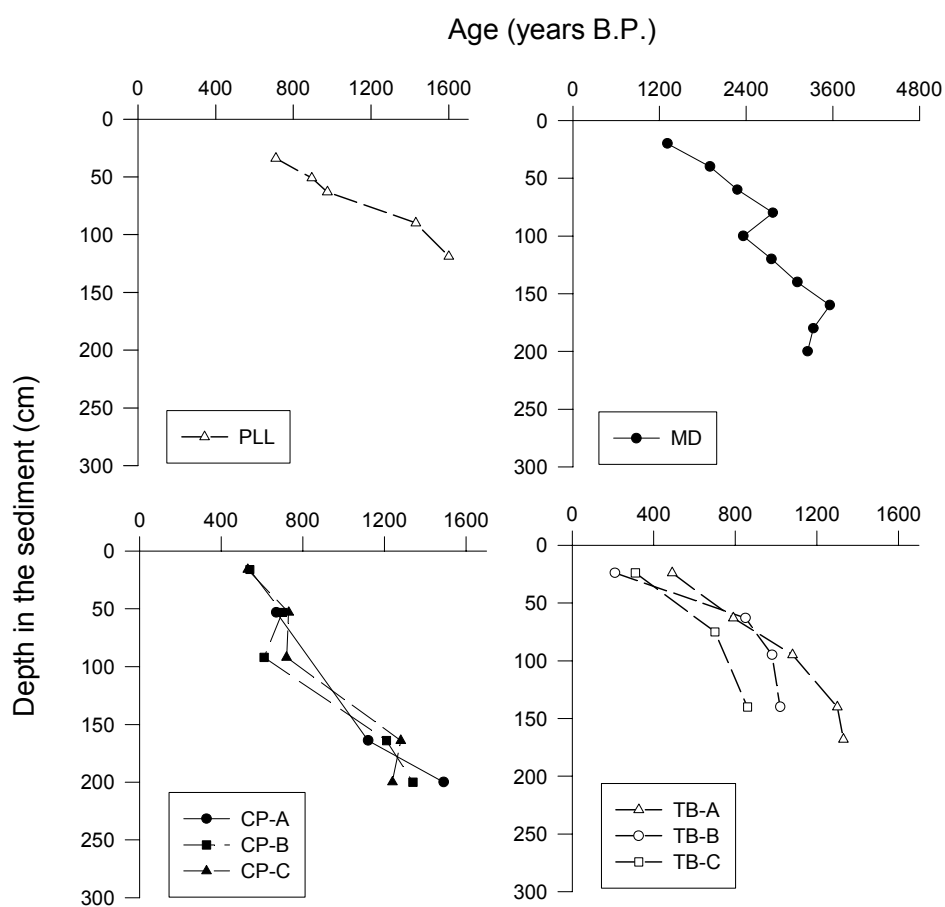


FIG. 4. Radiocarbon-age distribution along the various *Posidonia oceanica* peats studied. A, B, and C are replicates separated ca. 50 cm from each other. Present time is referred to 1950.

One typically local factor that is critical for seagrass growth is water transparency [18]. Taking into account the relationship found between *Posidonia* sheaths $\delta^{13}\text{C}$ and Secchi depths (Fig. 2), the present carbon isotopic compositions of the studied peats suggest that water transparency has been, in the average, higher in the northern areas than in the southern areas of the Spanish Mediterranean coast (3 or more meters clearer). *Posidonia oceanica* reacts to decreasing water transparency (and/or to increasing sedimentation) by increasing the vertical elongation rates of its rhizomes [18, 19, 20].

This results in potentially higher peat accretion rates. This fact can be one of the reasons explaining the higher peat accretion rates observed in the peats from the south (CP, TB) respect to those in the peats from the north (PLL, MD). Also, as derived from the positive relationship between sheaths carbon isotopic composition and annual leaf production, it can be hypothesized that such an effort in increasing the vertical elongation of the rhizomes, may lead to a reduction in the investment in total leaf productivity as reported elsewhere.

The robustness of the inferences made in paleo-reconstruction studies using *P. oceanica* peats, can be compromised by various phenomena. Below, we critically consider the several phenomena potentially hindering a correct interpretation of the $\delta^{13}\text{C}$ profiles along the peat wall.

3.2.1. Changes in the carbon isotope signature of the carbon source

Seagrass meadows grow in shallow coastal areas. The input of terrestrially-derived debris into the meadows can be highly variable depending on the local meteorological and hydrological characteristics (e.g. precipitation and sea current pattern). The CO_2 released during the decomposition of terrestrial organic matter is relatively depleted in ^{13}C respect to the marine autochthonous CO_2 . This is due to a higher discrimination against ^{13}C during photosynthesis of most terrestrial (C_3) vegetation. It follows that terrestrial organic inputs may lead to changes in the isotopic signature of the carbon source for seagrass photosynthesis. This may be regarded as an advantage when the aim pursued is the reconstruction of the periodicity in terrestrial runoff. To discriminate between changes in this isotopic ‘background level’ and the changes accounted for by plant physiological processes, the isotopic signature of the dissolved inorganic carbon (DIC), needs to be known. This can be done with the aid of the carbonate parts of e.g. calcareous benthic algae, foraminifera, sponges, bryozoans, bivalves or gastropods associated with seagrass meadows. Although isotopic disequilibrium exists during carbonate precipitation from the surrounding DIC, $\delta^{13}\text{C}$ values of organogenic carbonates serve to extract accurate information on DIC- $\delta^{13}\text{C}$ values at the time deposition took place [21].

3.2.2. Erosion and redeposition

Alterations of the accretion or depositional chronology of *Posidonia oceanica* peats by erosion and redeposition of peat layers or by changes in the sedimentary regime of the area, may result in abrupt or incoherent changes in sample ages and isotopic values, hampering reconstruction tasks.

3.2.3. Diagenetic effects

To which extent the carbon isotopic signature of *P. oceanica* tissues remains constant long after plant death, is another major question to be addressed. Diagenetic processes possibly

may produce changes in detrital $^{13}\text{C}/^{12}\text{C}$ ratios. During the early stages of the decomposition process, the relative proportion of the various carbon compounds of the plant debris changes due to differences in decomposition susceptibility. In *spartina alterniflora* a slight $\delta^{13}\text{C}$ decrease in bulk plant material has been observed as a consequence of the preferential loss of isotopically heavier polysaccharides remaining the relatively ^{13}C -depleted lignin-derived carbon [22, 23]. In the case of decomposing seagrass detritus, however, no significant changes were observed [24]. Studies on long-term diagenetic effects conclude that in typical marine sediments, a diagenetic ^{13}C -depletion in organic matter up to 2.8 ‰ may take place [25, 26]. Other workers, however, consider that diagenesis effect on $\delta^{13}\text{C}$ values of organic matter below the bioturbation zone may be negligible [27, 28]. In general, none of the works cited above have observed any systematic difference between the isotopic composition of the sedimentary organic matter and its natural precursor (phytoplankton). Moreover, a diagenetic effect would be expected to result in an gradual change of the isotopic signature, and, so far, this has not been observed neither in those works or in the present one. A possible solution to overcome potential problems derived from diagenetic effects, could be the use of seagrass-specific recalcitrant compounds for isotopic analyses (e.g. seagrass sheaths lignin; [29, 30]). This will minimize early diagenetic effects and avoid 'isotopic noise' from non-seagrass material (e.g. micro-decomposers associated with seagrass detritus).

3.2.4. Paleo-meadow depth

The depth limit for seagrass distribution strongly depends on the light arriving to the canopy. *Posidonia oceanica* meadows extend from nearly the water surface to depths of 35-40 meters, where the photosynthetic compensation point is attained. As discussed before, the most obvious cause of changes in light availability (at least in the Medes Islands) is the change in the turbidity of the water surrounding the meadow. Such changes would result in cyclic or random changes in plant productivity.

Changes in paleo-meadow relative depth due to eustatic sea level changes, however, would lead to recognizable trends in light availability, as a consequence of changes in the length of the water column acting on light extinction. Several phenomena may account for long-term changes in meadow depth, mainly: (1) organic accretion, (2) compaction, (3) subsidence, and (4) sea-level changes. (1) The growth of *P. oceanica* results in the elevation of the meadow bottom as the organic material derived from rhizomes and roots accumulates together with sediment. The elevation rate has been estimated to be around 0.1 cm yr^{-1} ($0.061\text{-}0.414 \text{ cm yr}^{-1}$; [4, 5, 6, 31]). This estimate is substantially lower than very early ones suggesting a rate of 1 meter per century [16]. The latter estimate may be closer to the potential elevation rate of the peat, as it does not consider long-term perturbations affecting meadow growth or survival. (2) The compaction of the peat, as expected from all sedimentary formations, may be enhanced by decay of the organic matter in the peat. It has been shown that the organic material of the peats undergoes a very slowly decay process (decay rate from 0.00008 to 0.00036 yr^{-1} ; [6]). In time, the lower layers may gradually collapse as a consequence of the weakening of the structure and of the weight of the overlying layers, concurring with typical compaction. Such a process has been described for peats [32]. Although in the seagrass peat the proportion of sediment is much higher, a certain degree of compaction can be expected. This would be evidenced by a negative exponential relationship between strata age and relative position within the peat. Such a relationship is not found, however, in the various peats studied. The high proportion of sediment forming the matrix of the peat, the hard nature of the organic material and the low susceptibility to be affected by gravity forces, will probably keep compaction in *Posidonia oceanica* peats at an almost negligible level. (3) Subsidence is a relatively local phenomenon resulting from the interplay of a complex set of geological

processes. A local geological study would be required to assess the magnitude of these processes in the study site. (4) Since the end of the last glacioeustatic sea level rise (ca. 5000 yr BP), the level of the Mediterranean Sea seems to have experienced only very small fluctuations, in the order of a few centimeters [33, 34]. Depth gradients of 40 m have been shown to be needed to result in a ca. 5 ‰ change in the seagrass isotopic signature [11]. So the relative depth changes associated to sea level fluctuations are not likely to have been a potential source of changes in production or in $\delta^{13}\text{C}$ values for the time period considered.

3.2.5. Sampling procedures

Using the corer diameter (15 cm) and the accretion rates estimated for the sampled peats (0.079-0.414 cm yr⁻¹; [6]), it can be roughly calculated that every sample was pooling the material of ca. 35-190 years. The result is the smoothing of changes in the isotopic signal preventing the identification of phenomena occurring with a frequency higher than 35-190 years. That was the case for the present peats studied except for the case of PLL, where a drilling platform was used.

4. CONCLUDING REMARKS

In conclusion, as is true for other palaeo-reconstruction studies based on the analyses of chronologically-deposited materials, the interpretation of the information recorded in *Posidonia oceanica* peats must be tackled with caution. *Posidonia oceanica* peats, however, have a clear advantage to pure sediment cores. Bioturbation, erosion and re-deposition phenomena, are unlikely to have serious effect on the chronology of the strata due to the firm nature of these peats. In addition, its abundant presence along the Mediterranean sea offers the possibility of making comprehensive and comparative studies on Mediterranean coastal environments. Much longer *Posidonia oceanica* organic records may be obtained by means of vertical deep vibro-coring as has been done for mangrove millenary deposits [35]. The detailed analysis of the *Posidonia* cores may provide the necessary chronological resolution to study local and global changes in key environmental and biological variables during the Holocene. Moreover, it will give the unprecedented opportunity to assess the persistence of seagrass-dominated communities during several thousands of years. We conclude that the combined analyses of various isotopic signatures of the plant material (e.g. $\delta^{13}\text{C}$, $\delta^{18}\text{O}$ and $\delta^{15}\text{N}$) and associated fossil fauna (e.g. foraminiferans, ostracods, and molluscs) in *Posidonia oceanica* peats, will open new vistas in Mediterranean paleo-ecological and paleo-environmental research.

ACKNOWLEDGEMENTS

The authors are grateful to Dr. John Hayes (NOSAMS) for speeding up radiocarbon dating of the samples and to Antonio Baños for his assistance in various technical aspects of sampling and sample preparation. The authors thank the biologists Irene Martínez, Sergio García, Carles Guallar and Marc Gilabert for their help in laboratory tasks. This work has been partially financed by the Spanish 'Comisión Interministerial de Ciencia y Tecnología' (CICYT), project MAR98-0356.

REFERENCES

- [1] RITCHIE, J. C., Current trends in studies of long-term plant community dynamics. *New Phytol.* **130**: (1995) 469-494.
- [2] PERGENT, G., BOUDOURESQUE, C.-F., CROUZET, A., MEINESZ, A., Cyclic changes along *Posidonia oceanica* rhizomes (lepidochronology): present state and perspectives. *PSZNI: Marine Ecology* **10**: (1989) 221-230.
- [3] DUARTE, C. M., MARBA, N., AGAWIN, N., CEBRIAN, J., ENRIQUEZ, S., FORTES, M.D., GALLEGOS, M.E., MERINO, M., OLESEN, D., SAND-JENSEN, K., URI, J., VERMAAT, J., Reconstruction of seagrass dynamics: age determinations and associated tools for the seagrass ecologist. *Mar. Ecol. Prog. Ser.* **107**: (1994) 195-209.
- [4] BOUDOURESQUE, C.-F., GIRAUD, G., THOMMERET, J., THOMMERET, Y., First attempt at dating by ^{14}C the undersea beds of dead *Posidonia oceanica* in the bay of Port-Man (Port-Cros, Var, France). *Tav. Sci. Parc. Nation. Port-Cros, France.* **6**: (1980) 239-242.
- [5] ROMERO, J., PEREZ, M., MATEO, M.A., SALA, E., The belowground organs of the Mediterranean seagrass *Posidonia oceanica* as a biogeochemical sink. *Aquatic Botany* **47**: (1994) 13-19.
- [6] MATEO, M. A., ROMERO, J., PEREZ, M., LITTLER, M., LITTLER, D., Dynamics of millenary organic deposits resulting from the growth of the Mediterranean seagrass *Posidonia oceanica*. *Estuarine Coastal and Shelf Science* **44**: (1997) 103-110.
- [7] KARLEN, I., OLSSON, I.U., KALLBURG, P., KILICI, S., Absolute determination of the activity of two ^{14}C dating standards. *Arkiv Geofysik*, **4**: (1968) 456-471.
- [8] STUIVER, M., POLACH, H.A., Discussion: Reporting ^{14}C data. *Radiocarbon*, **19**: (1977) 355-363.
- [9] STUIVER, M., Workshop on ^{14}C data reporting. *Radiocarbon* **22**: (1980) 964-966.
- [10] SOKAL, R.R., ROHLF, F.J., Introducción a la bioestadística. Editorial Reverté, Barcelona. (1980) 362pp.
- [11] COOPER, L. W., DENIRO, M. J., Stable carbon isotope variability in the seagrass *Posidonia oceanica*: evidence for light intensity effects. *Mar. Ecol. Prog. Ser.* **50**: (1989) 225-229.
- [12] DURAKO, M.J., HALL, M.O., Effects of light on the stable carbon isotope composition of the seagrass *Thalassia testudinum*. *Mar. Ecol. Prog. Ser.* **86**: (1992) 99-101.
- [13] GRICE, A. M., LONERAGAN, N.R., DENNISON, W. C., Light intensity and the interactions between physiology, morphology and stable isotope ratios in five species of seagrass. *J. Exp. Mar. Biol. Ecol.* **195**: (1996) 91-110.
- [14] MATEO, M.A., HEMMINGA, M.A., VAN SOELEN, J., SINKE, B., Interactions between light, water motion, growth, and carbon isotopic composition in the seagrass *Zostera marina* (in prep.).
- [15] HEMMINGA, M.A., MATEO, M.A., Stable carbon isotopes in seagrasses: variability in ratios and use in ecological studies. *Mar. Ecol. Prog. Ser.* **140**: (1996) 285-298.
- [16] MOLINIER R., PICARD, J., Recherches sur les herbiers de phanérogames marines du littoral méditerranéen français. *Ann. Inst. Océanogr.* **27**: (1952) 157-234.
- [17] PERES, J.M., La regression des herbiers a *Posidonia oceanica*, In: C.F. Boudouresque, A. Jeudy De Grissac, and J. Olivier [eds.], *International Workshop on Posidonia beds.*, Vol. 1. (1984) 445-454.
- [18] DUARTE, C.M., Seagrass depth limits. *Aquatic Botany* **40**: (1991) 363-377.
- [19] MARBA, N., DUARTE, C. M., Growth response of the seagrass *Cymodocea nodosa* to experimental burial and erosion. *Mar. Ecol. Prog. Ser.* **107**: (1994) 307-311.

- [20] BACH, S.S., BORUM, J., FORTES, M.D., DUARTE, C.M., Species composition and plant performance of mixed seagrass beds along a siltation gradient at Cape Bolinao, The Philippines. *Mar. Ecol. Prog. Ser.* **174**: (1998) 247-256.
- [21] WEFER, G., BERGER, W. H., Isotope paleontology: growth and composition of extant calcareous species. *Mar. Geol.* **100**: (1991) 207-248.
- [22] BENNER, R., FOGEL, M. L., SPRAGUE, E. K., HODSON, R. E., Depletion of ^{13}C in lignin and its implications for stable carbon isotope studies. *Nature* **329**: (1987) 708-710.
- [23] BENNER, R., FOGEL, M.L., SPRAGUE, E.K., Diagenesis of belowground biomass of *Spartina alterniflora* in salt-marsh sediments. *Limnol. Oceanogr.* **36**: (1991) 1358-1374.
- [24] ZIEMAN, J.C., MACKO, S.A., MILLS, A.L. 1984. Role of seagrasses and mangroves in estuarine food webs: temporal and spatial changes in stable isotope composition and amino acid content during decomposition. *Bull. Mar. Sci.* **35**: (1984) 380-392.
- [25] DEAN, W.D., ARTHUR, M.A., CLAYPOOL, G.E., Depletion of ^{13}C in Cretaceous marine organic matter: source, diagenetic, or environmental signal? *Mar. Geol.* **70**: (1986) 119-157.
- [26] FONTUGNE, M.R., CALVERT, S.E., Late Pleistocene variability of the carbon isotopic composition of organic matter in the Eastern Mediterranean: Monitor of changes in carbon sources and atmospheric CO_2 concentrations. *Paleoceanog.* **7**: (1992) 1-20.
- [27] SACKETT, W. M., Delta ^{13}C signatures of organic carbon in southern high latitude deep sea sediments; paleotemperature implications. *Org. Geochem.* **9**: (1986) 63-68.
- [28] CALVERT, S.E., NIELSEN, B., FONTUGNE, M.R., Evidence from nitrogen isotope ratios for enhanced productivity during formation of eastern Mediterranean sapropels. *Nature* **359**: (1992) 223-225.
- [29] KLAP, V.A., Biogeochemical aspects of salt-marsh exchange processes in the SW Netherlands. Ph.D. Thesis, University of Amsterdam, (1997) 171 pp..
- [30] KLAP, V.A., HEMMINGA, M.A., BOON, J.J., The retention of lignin in seagrasses, angiosperms that returned to the sea. *Limnol. and Oceanogr.* (submitted).
- [31] BOUDOURESQUE, C.F., JEUDY DE GRISSAC, A., MEINESZ, A., Relations entre la sédimentation et l'allongement des rhizomes orthotropes de *Posidonia oceanica* dans la Baie d'Elbu (Corse). In: Boudouresque, C.F., Jeudy de Grissac, A., and Olivier, O. (eds.) *International Workshop on Posidonia oceanica beds*, G.I.S. Posidonie Publ., Marseilles (1984) 185-191.
- [32] CLYMO, R.S., The limits to peat bog growth. *Phil. Trans. R. Soc. Lond.* **303**: (1984) 605-604.
- [33] FLEMMING, N.C., Archaeological evidence for eustatic change of sea level and earth movements in the Western Mediterranean in the last 2000 years. Special Paper of the Geological Society of America **109**: (1969) 1-125.
- [34] FLEMMING, N. C., Holocene eustatic changes and coastal tectonics in the north east Mediterranean: implications for models of crustal consumption. *Philosophical Transactions of the Royal Society of London, Series A.* **289**: (1978) 405-458.
- [35] MACINTYRE, I.G., LITTLER, M.M., LITTLER, D.S., Holocene history of Tobacco Range, Belize, Central America. *Atoll Research Bulletin* **430**: (1995) 1-18.

EXCESS AIR IN GROUNDWATER AS A POTENTIAL INDICATOR OF PAST ENVIRONMENTAL CHANGES

W. AESCHBACH-HERTIG¹, U. BEYERLE², J. HOLOCHER, F. PEETERS, R. KIPFER³
Water Resources and Drinking Water,
Swiss Federal Institute of Environmental Science and Technology (EAWAG),
Dübendorf, Switzerland

Also affiliated with:

¹Environmental Physics, Swiss Federal Institute of Technology (ETH), Zürich, Switzerland

²Physics Institute, University of Berne, Berne, Switzerland

³Isotope Geology, Swiss Federal Institute of Technology (ETH), Zürich, Switzerland

Abstract. Dissolved noble gases in groundwater are used to reconstruct paleotemperature, but also yield information about "excess air", a component of dissolved gases in excess of solubility equilibrium, derived from dissolution of trapped air in the ground. A good characterization of the excess air component is necessary not only to obtain reliable noble gas temperatures, but also to investigate the potential of excess air as a proxy for past environmental conditions. Two excess air related quantities can be derived from groundwater noble gas data sets: The initial air/water ratio and the pressure exerted on the entrapped air. Under recharge conditions typical for many aquifers, the excess of dissolved gases, expressed by the relative Ne excess ΔNe , is mainly determined by the hydrostatic pressure on the entrapped air. Thus, we suggest that ΔNe is essentially a measure of the amplitude of water table fluctuations in the recharge area. Comparing data sets from three aquifers in temperate, humid latitudes and three aquifers in tropical, semi-arid regions, we find that ΔNe is generally higher in the tropical aquifers, possibly related to larger water table fluctuations in these aquifers characterized by deep unsaturated zones. Whereas ΔNe shows little temporal variation in the mid-latitude aquifers, there is a strong signal of higher ΔNe in the paleowaters of the tropical aquifers as compared to water recharged under modern climate conditions. This finding may indicate a higher variability of recharge in the past at the studied tropical sites.

1. INTRODUCTION

The temperature dependence of noble gas solubilities in water has successfully been used to reconstruct ground temperatures during the last glacial maximum (LGM) from noble gas concentrations in groundwaters (see [1, 2] for reviews). In comparison to other paleoclimate proxies, the noble gas paleothermometer has the advantage of providing absolute temperature estimates, but the disadvantage of low temporal resolution which is inherent to the groundwater archive. The importance of the method thus lies in the quantification of the temperature shift between the LGM and the Holocene. However, the calculation of the noble gas temperature (NGT) is complicated by the empirical finding of an excess of dissolved gases relative to solubility equilibrium with the atmosphere in virtually all groundwaters. Traditionally, correction for this "excess air" [3] component has been accomplished by iterative subtraction of atmospheric air from the measured noble gas concentrations [4, 5]. In certain aquifers, this procedure does not yield satisfactory results [6, 7]. In order to derive paleotemperatures from such records, a model of elemental fractionation of the excess air by partial diffusive re-equilibration has been proposed [6].

Yet, rigorous inverse modeling has shown that even the refined model does not provide an adequate description of the data [8]. As a solution to this problem, we have proposed a model explaining excess air as the result of closed-system equilibration of groundwater with persistent entrapped air [9]. Also using an inverse modeling technique [10], we could show that the new model performed best in fitting several noble gas data sets, that it has physically

meaningful parameters, and that fits to the data yield plausible values for these parameters. These results provide a new basis for the interpretation of noble gas data, in particular with respect to the excess air component, which is increasingly being viewed as a potentially useful paleoenvironmental proxy rather than a disturbing effect in the calculation of NGTs. Relationships between the amount of excess air and the lithology of the recharge area as well as the precipitation rate have been observed [11]. A peak of excess air in an aquifer in Namibia has been attributed to the water table rise during a transition to a wetter climate [12]. Here, we first discuss the closed-system equilibration model for excess air and the physical meaning of its parameters. We then apply the model to several published and new noble gas data sets from paleogroundwaters, look for systematic patterns of the excess air parameters, and try to relate the observed patterns to plausible environmental factors.

2. THE MODEL

The traditional assumption that excess air is formed by complete dissolution of small air bubbles trapped in soil pores [1, 3] can be expressed by the following model equations for the concentrations of dissolved atmospheric gases i [10]:

$$C_i(T, S, P, A_d) = C_i^*(T, S, P) + A_d \cdot z_i \quad (1)$$

where A_d is the concentration of dissolved dry air, and z_i are the volume fractions of the individual gases in dry air. The moist air solubility equilibrium concentrations C_i^* are functions of temperature T , salinity S , and atmospheric pressure P , given by Henry's law:

$$C_i^*(T, S, P) = \frac{p_i^{atm}}{H_i(T, S)} = \frac{(P - e(T))f_i}{H_i(T, S)} \quad (2)$$

where $H_i(T, S)$ are the Henry coefficients and $e(T)$ is the saturation water vapor pressure.

The conceptual idea of our model for the formation of excess air [9] is that during a rise of the water table bubbles of soil air are trapped in some pores and pressurized by hydrostatic overload and surface tension. However, this entrapped air does not completely dissolve, but instead reaches solubility equilibrium with the surrounding water under the enhanced pressure. The water eventually reaches the fully saturated zone, whereas the gas bubbles remain trapped in their pores. During fluctuations of the water table, the gas phase is periodically replaced by soil air, which is assumed to be identical to atmospheric air.

In the initial situation we have a water volume V_w with gas concentrations $C_i^*(T, S, P)$, i.e., in atmospheric solubility equilibrium at the conditions in the recharge area. The finite trapped gas volume V_g^0 contains moist air under a total pressure $P_g > P$. The STP-volume of dry air in the trapped gas per unit mass of water is given by:

$$A = \frac{V_g^0}{\rho(T, S)V_w} \cdot \frac{P_g - e(T)}{P_0} \quad (3)$$

where P_0 is the standard pressure (1 atm). In summary, the initial state of the system is completely described by five parameters: T , S , P , P_g , and V_g^0/V_w . Note that only the ratio V_g^0/V_w is relevant, not the absolute volumes.

Complete dissolution of the entrapped air A would lead to an unfractionated excess air component corresponding to A_d in eq. 1. However, if the trapped air is only partly dissolved, a

final state is reached in which a gas volume V_g remains, which is in solubility equilibrium with the constant water volume V_w under the constant total pressure P_g . Thus, in the final state the partial pressures p_i of all gases in V_g are related to the dissolved gas concentrations C_i in V_w by Henry's law:

$$p_i = H_i(T, S) \cdot C_i \quad (4)$$

Since we describe a finite, closed system ($V_w + V_g$), the total number of moles n_i of all gases within the system must be the same in the initial and the final state:

$$n_{i,w}^0 + n_{i,g}^0 = n_{i,w} + n_{i,g} \quad (5)$$

In order to derive an equation for the dissolved gas concentrations in the final state from this condition of mass conservation, it is useful to introduce the following definitions:

$$v \equiv \frac{V_g}{V_g^0}, \quad q \equiv \frac{P_g - e}{P - e}, \quad \text{and} \quad F \equiv \frac{v}{q}, \quad (6)$$

where v is the ratio of the gas volumes in the final and initial state, q is the ratio of the dry gas pressure in the trapped gas to that in the free atmosphere, and F describes the reduction of the volume of entrapped air (A) due to partial dissolution (v) and compression ($1/q$). By spelling out eq. 5, using eqs. 2, 3, 4, and 6 as well as the ideal gas law, we obtain the model equations that describe the final gas concentrations in the water phase:

$$C_i(T, S, P, A, F) = C_i^*(T, S, P) \cdot \frac{1 + A z_i / C_i^*}{1 + F A z_i / C_i^*} = C_i^* + \frac{(1 - F) A z_i}{1 + F A z_i / C_i^*} \quad (7)$$

Note that only the combined parameter $F = v/q$ is needed to define the excess air component, not v and q individually. From the physical requirement that the sum of the partial pressures of all gases in the trapped volume equals the total pressure, we can derive (by using eqs. 2, 4, 6, and 7) an implicit equation that couples the parameters q , v , and A :

$$q = \sum_i z_i \frac{1 + A \frac{z_i}{C_i^*}}{1 + \frac{v}{q} A \frac{z_i}{C_i^*}} \quad (8)$$

Once F is determined from fitting eq. 7 to the data, both q and v can be calculated from eq. 8. Any pair of the parameters A , F , q , and v fully determines the amount and composition of excess air, the most intuitive choice being A (\approx volume of entrapped air) and q (\approx pressure exerted on the entrapped air).

The decomposition of F into v and q is of interest for the physical interpretation of the excess air parameters. To illustrate this, it is useful to examine some limiting cases. A trivial case is $F = 1$, when eq. 8 implies also $q = v = 1$. This means that there is no pressure excess and no dissolution, thus, no excess air at all. Another simple case is $F = 0$, when eq. 7 reduces to eq. 1, i.e., complete dissolution. The important point to note is that for any given concentration of entrapped air (any value of A), eq. 8 prescribes the pressure q that is needed to achieve

complete dissolution ($v = F = 0$). This limiting pressure is essentially the pressure needed to hold all nitrogen contained in V_g^0 in solution in the water volume V_w .

Another, not so obvious but very interesting, limiting case is that A approaches infinity (very large reservoir of entrapped air). In this case, we find from eq. 8 that v approaches 1, i.e., the gas volume remains constant independent of the pressure q . Eq. 7 reduces to:

$$C_i = C_i^* \frac{1}{F} = q C_i^* = \frac{P_g - e}{P - e} C_i^* = C_i^*(T, S, P_g) \quad (9)$$

This means that all concentrations are enlarged by the constant factor q , corresponding to atmospheric equilibrium at the increased pressure P_g . Thus, eq. 9 describes a pressure effect, or equilibration with an infinite air reservoir (e.g., the free atmosphere) at increased pressure. Apparently, eq. 7 is a very general description of the concentrations of dissolved gases in groundwater, describing all possible cases between no excess air ($F = v = q = 1$), pure excess air ($F = v = 0$, A and q linked by eq. 8), and a pure pressure effect ($A = \infty$, $v = 1$).

Interestingly, noble gas data from groundwater samples can often be described quite well by a pressure effect, i.e., using only T and P as free parameters. However, the solutions obtained from a pure pressure model tend to yield unrealistically high values for T and P . In contrast, the closed-system equilibration model (eq. 7) with T , A , and F as free parameters usually yields realistic values for all parameters. Sometimes, however, the fitting procedure converges to the "pressure effect" solution with large A . Fits with large A tend to behave numerically unstable, because any large value of A produces a similarly good fit (measured by χ^2), and because of a strong correlation of the parameters A and T . Empirically we find these problems for solutions with $A > 0.1 \text{ cm}^3\text{STP/g}$ (corresponding to an air/water volume ratio $> 1:10$ at STP). Although such solutions provide the best fit to the data, they appear to be rather accidental, because usually slightly worse but still acceptable fits with lower and more realistic A -values exist. Care should therefore be taken in interpreting results with large values of A . In the literature, the excess air component is often expressed by the relative Ne excess, $\Delta\text{Ne} (\%) = (C_{\text{Ne}}/C_{\text{Ne}}^* - 1) \cdot 100$. In the case of complete dissolution of entrapped air (eq. 1), ΔNe is directly related to the excess air parameter A_d . In general, however, the relationship between ΔNe and A is not straightforward. Nevertheless, ΔNe is a very useful measure of the size of the excess air component. In particular, it is practically an observable quantity, nearly independent of the choice of the correct model for excess air and the exact calculation of T , because the equilibrium concentration C_{Ne}^* does not strongly depend on temperature.

3. RESULTS AND DISCUSSION

In order to investigate systematic patterns of the excess air parameters, we applied the closed-system equilibration model to six groundwater noble gas data sets, three of them representing temperate northern latitudes, and three representing semi-arid tropical locations. These paleorecords originate from: 1) Belgium, Ledo-Paniselian aquifer, about 51°N , 4°E ; 2) France, Miocene aquifer in the Valreas Basin, about 44°N , 5°E [13]; 3) USA, Maryland, Aquia aquifer, about 39°N , 77°W [14, 15]; 4) Niger, Continental Terminal aquifers in the Basin of Iullemeden, about 13°N , 3°E ; 5) Brazil, Piaui Province, Serra Grande and Cabeças aquifers, about 7°S , 41°W [6]; 6) South Australia, J-K aquifer in the southwestern Great Artesian Basin, about 27°S , 134°E [16]. With the exception of the classical data set from Brazil, taken from [6], these are unpublished data. Full accounts of the paleoclimatic implica-

tions of these data sets will be given elsewhere. Here, we focus on the excess air component and its possible relationship to environmental conditions.

The six data sets comprise a total of 188 samples from 164 wells. 18 of these samples could not well be fitted by eq. 7 ($p < 0.01$ in the χ^2 -test), apparently mostly due to degassing during sampling. The remaining data were checked for outliers of A , F , v , q , or ΔNe . Samples for which one of these quantities deviated by more than three standard deviations from the mean of the respective data set were excluded. This step eliminated 7 samples with very high ΔNe ($\approx 200\%$ and higher) that are likely the result of air contamination, and 4 samples with high values of A ($\approx 0.2\text{ cm}^3\text{STP/g}$ and higher) that may be artefacts of the fitting procedure. Yet, still 9 samples with $A > 0.1\text{ cm}^3\text{STP/g}$ remained, that exhibited the problems described above (large correlation and uncertainty for A and T). We also excluded these samples in order to avoid a possibly artificial bias.

Thus, we are finally left with 150 samples from six different sites as a basis for our analysis of the excess air systematics. The results are summarized in Table I and visualized in Figs. 1 and 2. An intriguing pattern is revealed by Fig. 1, showing ΔNe as a function of A . The samples from the semi-arid tropical sites align close to the line for unfractionated excess air ($F = 0$) and are characterized by low values of A and F , but high values of ΔNe . In contrast, the samples from aquifers in temperate regions tend towards high A and F but low ΔNe . This pattern is also evident in the mean values of the parameters for the different sites (Table I).

Table I. Mean values of excess air parameters for the studied aquifers

Data set	N	A	F	q	v	ΔNe
Belgium	23	0.042 ± 0.030	0.65 ± 0.28	1.15 ± 0.08	0.76 ± 0.32	19 ± 10
France	22	0.018 ± 0.008	0.57 ± 0.16	1.23 ± 0.09	0.69 ± 0.17	35 ± 14
USA	26	0.035 ± 0.017	0.76 ± 0.05	1.16 ± 0.04	0.87 ± 0.06	21 ± 4
Niger	34	0.017 ± 0.008	0.41 ± 0.13	1.48 ± 0.24	0.57 ± 0.13	64 ± 33
Brazil	19	0.016 ± 0.005	0.37 ± 0.16	1.51 ± 0.22	0.53 ± 0.17	71 ± 34
Australia	26	0.018 ± 0.013	0.34 ± 0.23	1.41 ± 0.20	0.48 ± 0.29	57 ± 26

Mean values and standard deviations of the results for the individual samples are listed.

N is the number of accepted samples.

A is given in $\text{cm}^3\text{STP/g}$, ΔNe in %, the other parameters are dimensionless.

The results for Belgium, USA, and Brazil slightly differ from those listed in [9], because a more rigorous data selection has been applied here.

Figure 1 clearly shows that there is no simple relationship between ΔNe and A . In contrast, Fig. 2 reveals a strong linear link between ΔNe and q . The explanation for these observations is that the effective excess of dissolved gases (e.g., ΔNe) is not limited by the available reservoir of entrapped air (A), but by the pressure exerted on this reservoir (q). In most cases, the pressure appears to be too low to induce complete dissolution ($F = 0$ line in Fig. 1). In fact, if entrapped air occupies 1 % of the pore space ($A \approx 0.01\text{ cm}^3\text{STP/g}$), an excess pressure of about 0.5 atm ($q = 1.5$) is needed to induce complete dissolution (at 12°C). The data of Table I show that typical values of A range between 0.02 and $0.04\text{ cm}^3\text{STP/g}$. Thus, excess pressures up to 2 atm would be needed to completely dissolve this entrapped air. Surface tension can produce such pressures only for bubble sizes $< 1\text{ }\mu\text{m}$. For a typical sandy aquifer, capillary forces are of minor importance, and the pressure excess can be interpreted as due to hydrostatic overload. Thus, water level rises of up to 20 m would be needed for complete dissolution, which are obviously impossible in many recharge zones where water tables are only a few meters below the surface.

Hence, if the A -values found in this study are typical, we have to conclude that partial dissolution is the rule rather than the exception compared to complete dissolution or even the model of diffusive re-equilibration, which often implies very large initial excesses of dissolved gases. The literature on air entrapment in soils [17-20] suggests that entrapped air typically occupies several percent of the pore space, with some values ranging as high as 50%. The perhaps most reliable data from careful experiments suggest that only a few percent of the pore space contain immobile air that can persistently be trapped [20]. This result is consistent with the A -values found here.

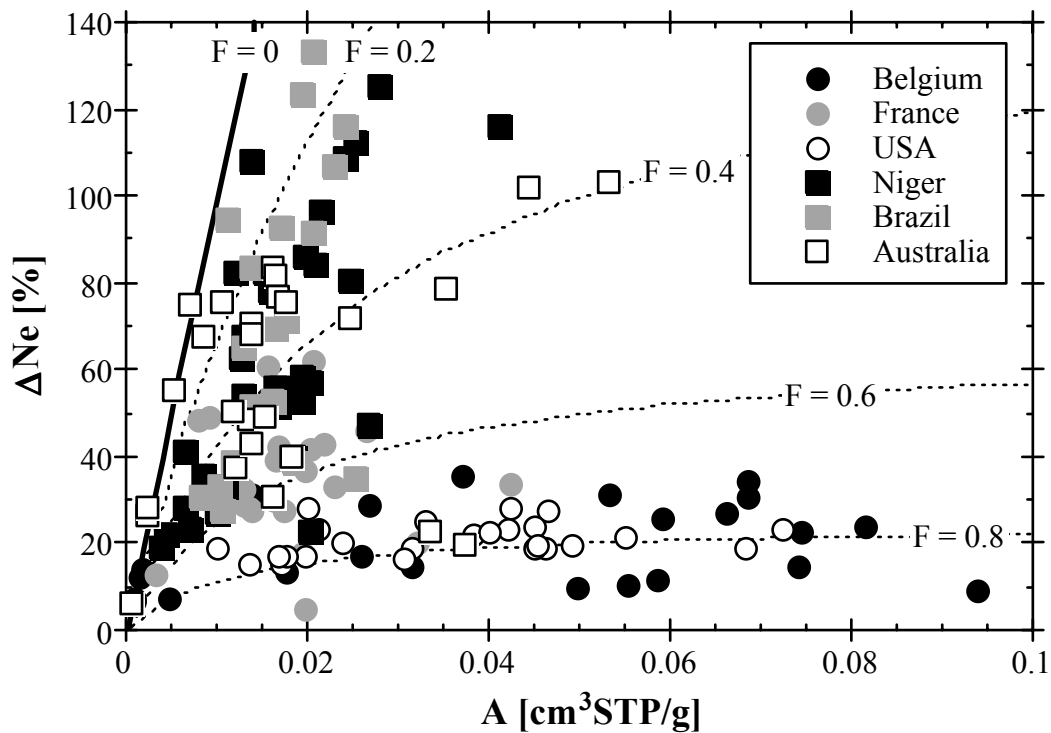


FIG. 1. The relative Ne excess ΔNe versus the initial concentration of entrapped air (A). The (dashed) lines represent solutions of eq. 7 for the indicated values of F , and $T = 20^\circ\text{C}$, $P = 1 \text{ atm}$, $S = 0\%$. Most samples have $F > 0$, indicating only partial dissolution of the entrapped air. Samples from aquifers at temperate latitudes are indicated by circles, samples from tropical aquifers by squares.

The most important conclusion from Fig. 2 is that the observable quantity ΔNe obtains a direct physical interpretation: it is essentially a measure of the pressure in the entrapped air. This pressure is always larger than the atmospheric pressure ($q > 1$), and if the overpressure is ascribed to the hydrostatic load of infiltrating water, then ΔNe should be a measure of the amplitude of water table fluctuations. This interpretation sheds new light on the observed differences between tropical and temperate sites. Typical q -values are ≈ 1.2 for the aquifers from temperate, humid regions, and ≈ 1.5 for the aquifers from semi-arid, tropical sites (Table I). Explaining these values by hydrostatic pressure due to water table rises implies typical fluctuations of 2 and 5 m, respectively. Although we have no records of the water levels at our study sites, there are arguments for larger fluctuations in the semi-arid aquifers. On the one hand, recharge in such climates is episodic, on the other hand, the unsaturated zone tends to be much deeper than in humid regions, offering a higher potential for large water table rises. An open question is whether ΔNe might be especially sensitive to water table fluctuations of a particular periodicity (e.g., seasonal or interannual).

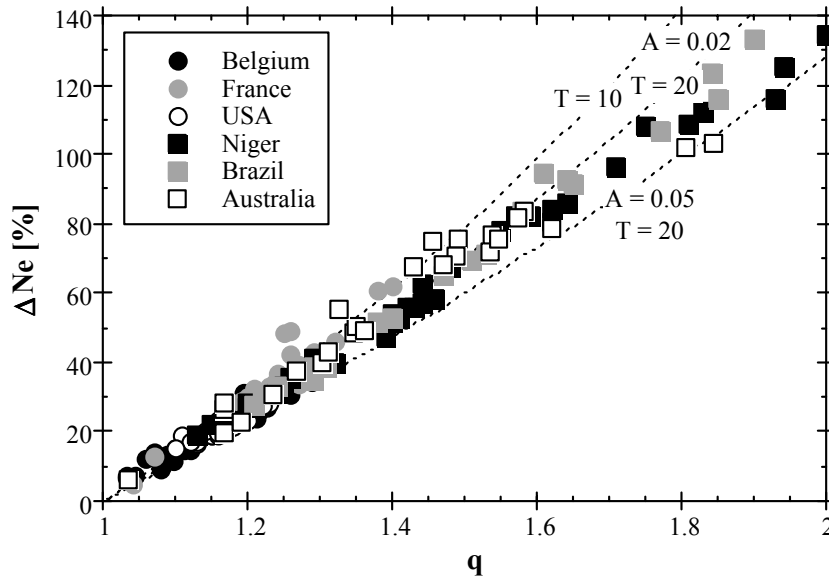


FIG. 2. The relative Ne excess ΔNe versus the pressure on the entrapped air relative to the atmospheric pressure (q). The dashed lines represent solutions of eq. 7 for the indicated values of A (in $\text{cm}^3\text{STP/g}$) and T (in $^\circ\text{C}$), as well as $P = 1 \text{ atm}$, $S = 0 \text{ ‰}$. ΔNe depends mainly on q , and only to a much lesser extent on A and T .

If ΔNe is related to water table fluctuations, it may be a proxy for the variability of recharge, and hence of precipitation, in the past. This interpretation provides a theoretical foundation for the attribution of a peak in the record of ΔNe in an aquifer in Namibia to the water table rise during a transition to a wetter climate [12]. In our data sets, we also find some systematic variations of ΔNe with groundwater age. As an example, Fig. 3 shows NGT and ΔNe as functions of the concentration of radiogenic He for the study site in France. A strong correlation between He and ^{14}C -ages [13] shows that He is a good proxy for age in this system. The samples with radiogenic He concentrations above about $4 \cdot 10^{-8} \text{ cm}^3\text{STP/g}$ are of Pleistocene age, as indicated also by a colder NGTs. The Holocene samples have ΔNe -values varying between 5 and 40 %, whereas the range for the Pleistocene samples is 30 to 65 %. Although the variability in both groups is quite high and the two ranges overlap, it is possible that the difference reflects actual changes of the recharge conditions, such as higher variability during the late Pleistocene. An interesting detail is that the highest ΔNe -values seem to form a peak, reminiscent of the stronger peak observed in Namibia [12]. Although not exactly at the same time, the peaks occur close to the time of the climatic transition in both records. However, similar features were not found in the other records studied here.

Although a detailed discussion of each record is not possible here, a general indication of climatic effects on the excess air may be obtained from correlations between NGT and ΔNe (Fig. 4). It is not expected that NGT directly influences ΔNe , but it can serve as a proxy for overall climatic conditions and to discern between Holocene and Pleistocene samples. In general, within each record high NGTs correspond to Holocene samples and low NGTs to Pleistocene samples, although there are some exceptions (e.g., the record from Australia may span several glacial-interglacial cycles [16]). Figure 4 shows that for the records from temperate regions, the correlations between NGT and ΔNe are rather weak and have different signs. In contrast, all three tropical sites show strong and very similar decreases of ΔNe with NGT, presumably reflecting climate-related changes in recharge conditions, such as higher and/or more variable precipitation during cooler climate periods in the past.

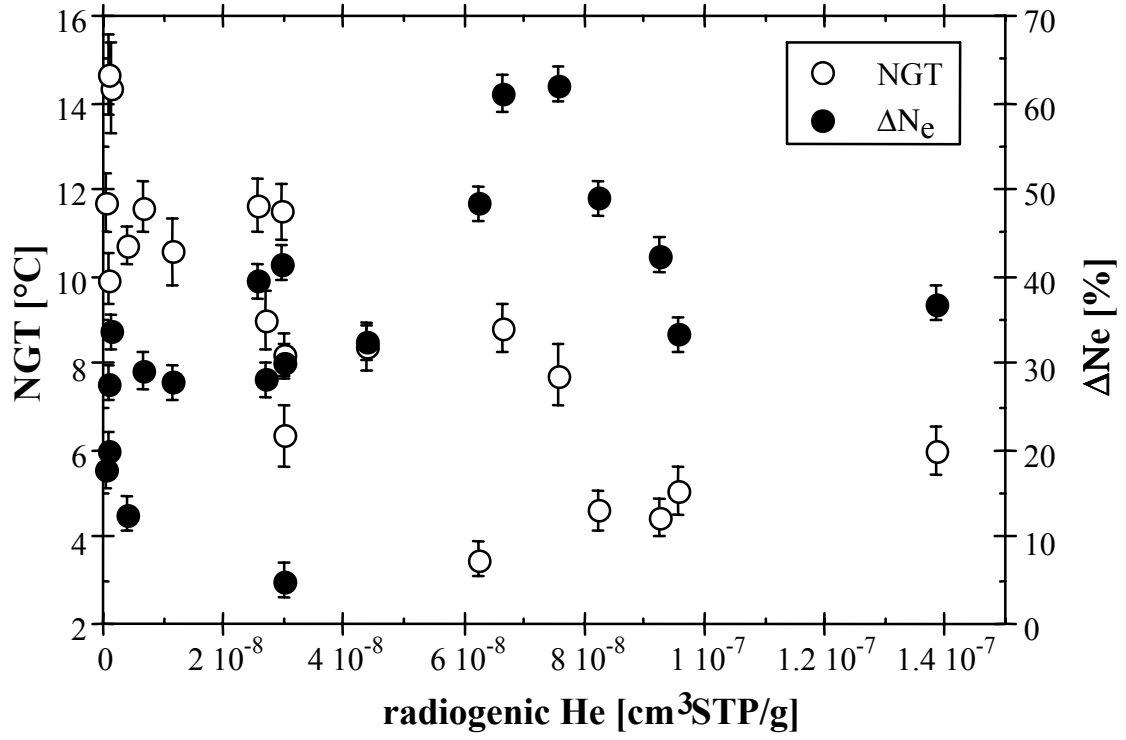


FIG. 3. Noble gas temperature (NGT) and Ne excess (ΔNe) in the aquifer from France (Valreas Basin) as functions of radiogenic He (a proxy for groundwater age). The transition between Holocene and Pleistocene samples occurs around $4 \cdot 10^{-8} \text{ cm}^3\text{STP/g}$ [13].

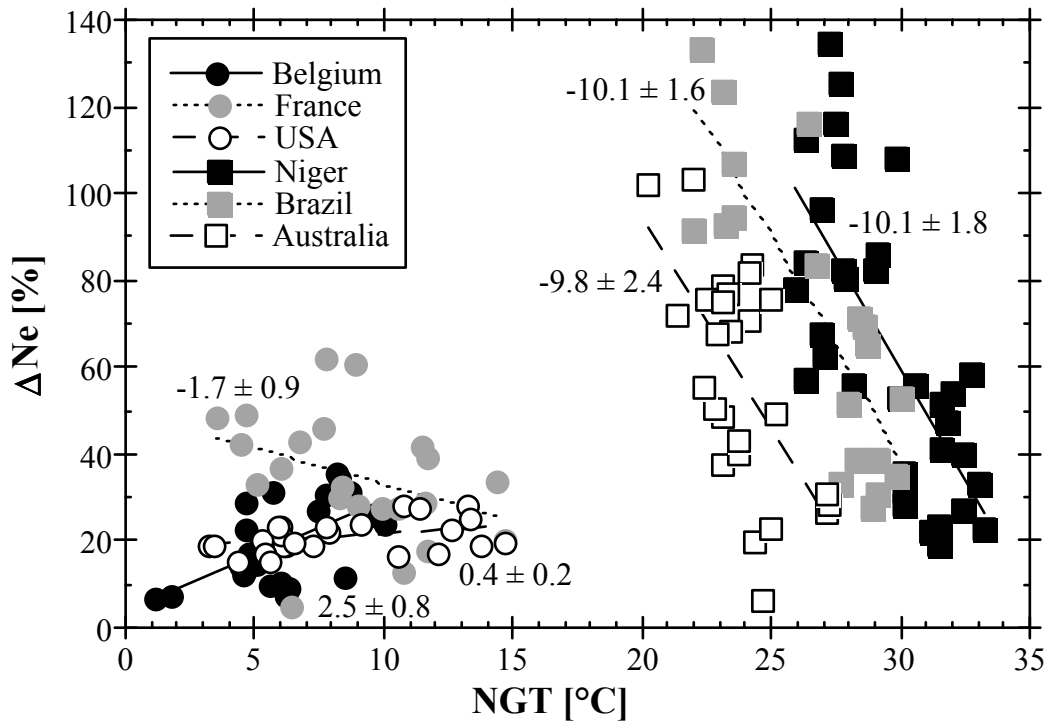


FIG. 4. Correlation between ΔNe and NGT for the different aquifers. Regression lines and their slopes (in $\% \text{ } ^\circ\text{C}^{-1}$) are indicated. All three tropical aquifers show strong correlations.

The results of Fig. 4 are in excellent agreement with the only previous study comparing excess air in different aquifers [11], which found no relationship between NGT and ΔNe for limestone aquifers of the UK, a certain decrease of ΔNe with NGT for a sandstone aquifer in the UK, and a strong decrease of ΔNe with NGT for a sandstone aquifer in Niger. Thus, in particular the strong relationship between ΔNe and some climatic factor in tropical, arid to semi-arid regions appears to be a consistent feature. The data are not conclusive as to whether this factor could be precipitation. Wilson and McNeill [11] found an increase of ΔNe with mean annual precipitation when comparing different aquifers, but ascribed this effect to different lithologies and inferred a decrease of ΔNe with precipitation when comparing data from the same lithologies. We think that lithology should not have a major influence on ΔNe , because it may control A , but not q . Although the aquifers discussed in our study all have similar lithologies (sands and sandstones), they cover a large range in ΔNe . Moreover, we expect ΔNe to depend on water table fluctuations and thus on the variability of precipitation rather than on its mean value. However, in semi-arid climates with a distinct rainy season, higher variability of precipitation may be equivalent to higher mean precipitation.

4. CONCLUSIONS

The parameters of the model of excess air formation by equilibration of groundwater with a finite reservoir of entrapped air under increased pressure and closed conditions have a clear physical interpretation. The parameter A describes the volume of entrapped air per unit mass of water, and q describes the increase of pressure relative to the atmospheric pressure. Moreover, the widely used measure of the size of the excess air component, ΔNe , is strongly related to q and thus is mainly a measure of pressure on the entrapped air bubbles. This leads us to the assumption that ΔNe might reflect fluctuations of the water table and hence the variability of recharge and precipitation.

Although both A and q are quite variable in all investigated data sets, there are systematic differences between aquifers from tropical and temperate latitudes. The data from tropical aquifers yield relatively low values of A and high values of q , whereas those from temperate latitudes give high A and low q . In some data sets there are indications for differences in q between Pleistocene and Holocene samples, most prominently all aquifers from semi-arid tropical sites indicate a strong decrease of ΔNe with NGT. A more detailed discussion of the tropical records is needed to substantiate the conjecture that the changes of ΔNe indicate climatic changes such as a higher variability of precipitation during cooler periods in the past.

In summary, it appears that the excess air component does carry valuable information about past environmental conditions, which is however difficult to read due to natural variability and incomplete understanding of the controlling processes. Further detailed investigations both on the laboratory and field scale are needed to firmly establish relationships between excess air parameters and environmental conditions.

ACKNOWLEDGEMENTS

We thank all the people who were involved in the projects from which noble gas data were used, in particular: R. Reuter, M. Stute, and P. Schlosser (for the study in Maryland, USA), F. Huneau and B. Blavoux (for France), J. Lermytte and K. Walraevens (for Belgium), A. Dodo and J. Rüedi (for Niger), A. Love, R. Purtschert, and B. Lehmann (for Australia).

REFERENCES

- [1] STUTE, M., SCHLOSSER, P., "Principles and applications of the noble gas paleothermometer", *Climate Change in Continental Isotopic Records* (SWART, P. K. et al., Eds.), Geophysical Monograph **78**, Am. Geophys. Union, Washington, DC (1993) 89-100.
- [2] STUTE, M., SCHLOSSER, P., "Atmospheric noble gases", *Environmental tracers in subsurface hydrology* (COOK, P., HERCZEG, A. L., Eds.), Kluwer Academic Publishers, Boston (2000) 349-377.
- [3] HEATON, T. H. E., VOGEL, J. C., "Excess air" in groundwater, *J. Hydrol.* **50** (1981) 201-216.
- [4] RUDOLPH, J., *Edelgastemperaturen und Heliumalter ^{14}C -datierter Paläowässer*, PhD thesis, Universität Heidelberg (1981).
- [5] STUTE, M., *Edelgase im Grundwasser - Bestimmung von Paläotemperaturen und Untersuchung der Dynamik von Grundwasserfließsystemen*, PhD thesis, Universität Heidelberg (1989).
- [6] STUTE, M., FORSTER, M., FRISCHKORN, H., SEREJO, A., CLARK, J. F., SCHLOSSER, P., BROECKER, W. S., BONANI, G., Cooling of tropical Brazil (5°C) during the Last Glacial Maximum, *Science* **269** (1995) 379-383.
- [7] CLARK, J. F., STUTE, M., SCHLOSSER, P., DRENKARD, S., BONANI, G., A tracer study of the Floridan aquifer in southeastern Georgia: Implications for groundwater flow and paleoclimate, *Water Resour. Res.* **33** (1997) 281-289.
- [8] BALLENTINE, C. J., HALL, C. M., Determining paleotemperature and other variables by using an error-weighted, nonlinear inversion of noble gas concentrations in water, *Geochim. Cosmochim. Acta* **63** (1999) 2315-2336.
- [9] AESCHBACH-HERTIG, W., PEETERS, F., BEYERLE, U., KIPFER, R., Palaeotemperature reconstruction from noble gases in ground water taking into account equilibration with entrapped air, *Nature* **405** (2000) 1040-1044.
- [10] AESCHBACH-HERTIG, W., PEETERS, F., BEYERLE, U., KIPFER, R., Interpretation of dissolved atmospheric noble gases in natural waters, *Water Resour. Res.* **35** (1999) 2779-2792.
- [11] WILSON, G. B., MCNEILL, G. W., Noble gas recharge temperatures and the excess air component, *Appl. Geochem.* **12** (1997) 747-762.
- [12] STUTE, M., TALMA, A. S., "Glacial temperatures and moisture transport regimes reconstructed from noble gases and delta ^{18}O , Stampriet aquifer, Namibia", *Isotope techniques in the study of environmental change* (Proc. Symp. Vienna, 1997), IAEA, Vienna (1998) 307-318.
- [13] HUNEAU, F., *Fonctionnement hydrogéologique et archives paléoclimatiques d'un aquifère profond méditerranéen*, PhD thesis, Université d'Avignon (2000).
- [14] AESCHBACH-HERTIG, W., STUTE, M., SCHLOSSER, P., CLARK, J., REUTER, R., "Large (9°C) glacial-interglacial temperature difference derived from an aquifer in Maryland", *Proc. Am. Geophys. Union Spring Meeting*, Baltimore, 1996, EOS (1996) S157.
- [15] AESCHBACH-HERTIG, W., STUTE, M., CLARK, J., REUTER, R., SCHLOSSER, P., A paleotemperature record derived from dissolved noble gases in groundwater of the Aquia Aquifer (Maryland, USA), *Geochim. Cosmochim. Acta* (submitted).
- [16] BEYERLE, U., AESCHBACH-HERTIG, W., PEETERS, F., KIPFER, R., PURTSCHERT, R., LEHMANN, B., LOOSLI, H. H., LOVE, A., "Noble gas data from the Great Artesian Basin provide a temperature record of Australia on time scales of 10^5 years", *Isotope techniques in water resources development and management* (Proc. Symp. Vienna, 1999), IAEA-CSP-2/C (CD), IAEA, Vienna (1999) 97-103.
- [17] CHRISTIANSEN, J. E., Effect of entrapped air upon the permeability of soils, *Soil Sci.* **58** (1944) 355-365.
- [18] FAYER, M. J., HILLEL, D., Air encapsulation: 1. Measurement in a field soil, *Soil Sci. Soc. Am. J.* **50** (1986) 568-572.
- [19] STONESTROM, D. A., RUBIN, J., Water content dependence of trapped air in two soils, *Water Resour. Res.* **25** (1989) 1947-1958.
- [20] FAYBISHENKO, B. A., Hydraulic behavior of quasi-saturated soils in the presence of entrapped air: Laboratory experiments, *Water Resour. Res.* **31** (1995) 2421-2435.

**PALAEOCLIMATE ARCHIVES II
LAKES AND TERRESTRIAL ENVIRONMENTS**

(Session 4)

Chairpersons

T.W.D. EDWARDS

Canada

L.C.R. PESSEDA

Brazil

ISOTOPE TRACERS IN GLOBAL WATER AND CLIMATE STUDIES OF THE PAST AND PRESENT

T.W.D. EDWARDS, S.J. BIRKS, J.J. GIBSON*

Department of Earth Sciences,
University of Waterloo,
Waterloo, Ontario, Canada

Abstract. To date the global distribution of isotopes in modern precipitation has been characterized almost exclusively from the IAEA/WMO GNIP database, although patchiness of GNIP station records in both time and space has limited the potential of isotope hydrology and climate applications in some areas. Herein, we discuss the prospect of utilizing GCMs for simulating global isotope distributions as a supplementary tool for modern and paleoclimate isotope studies to bridge this gap. Such models currently generate reliable zonal isotope fields, and it is anticipated that future enhancements in fine-scale resolution of GCMs, and incorporation of land-surface feedbacks and topography will allow for future development of a global reanalysis data set ground-truthed by GNIP. Compilation of time-slice maps of past isotope distribution in precipitation from archival records of meteoric waters also offers significant potential to ground-truth paleoclimate simulations extending back tens to hundreds of thousands of years.

1. INTRODUCTION

Water isotope data provide key information about past and present global climate and the global water cycle. The oxygen-isotope records obtained from carbonates in sediment cores from the world oceans, for example, yielded the first indisputable evidence of repeated Quaternary glacial-interglacial cycling, as well as shorter-term climate variability, as expressed by the interplay between the changing isotopic composition of ocean water and its temperature. Even more compelling quantitative evidence for past changes in global water balance and climate at temporal scales relevant to humanity is found in the stable isotope chronologies preserved in non-marine archives, ranging from detailed time-series of paleo-precipitation stored in glaciers, to the variably-resolved records of meteoric waters preserved in ground water, speleothems, lake sediments, tree rings and other materials.

Crucial isotopic records of very recent and ongoing hydrologic and climatic change also exist in the form of contemporary observational data, derived from sampling and isotopic analysis of meteoric waters over the past few decades. These data provide fundamental information about the global water budget that is not directly accessible or testable using other means. Foremost among such observational records, and a primary international resource, is the data base of the Global Network for Isotopes in Precipitation (GNIP), a long-running joint venture of the International Atomic Energy Agency and the World Meteorological Organization, dedicated to the documentation of the distribution of isotopes in global precipitation (e.g., see [1]). The GNIP database has long been used for calibrating isotopic indicators of paleoclimate from various natural archives. Moreover, and perhaps more importantly, it constitutes the only comprehensive source of data for evaluating the modern global isotope field generated by atmospheric general circulation models (GCMs) equipped with water isotope diagnostics. Although simulations of the distribution of global precipitation and bulk water fluxes can be readily evaluated using more conventional data, the incorporation of isotope tracers provides an inherently more critical evaluation of a GCM's water cycle because of the need to account

*Isotope Hydrology Section, International Atomic Energy Agency, P.O. Box 100, Vienna, Austria.

for the differing behaviours and abundances of three water isotopomers ($^1\text{H}^1\text{H}^{16}\text{O}$, $^1\text{H}^2\text{H}^{16}\text{O}$, $^1\text{H}^1\text{H}^{18}\text{O}$), that is, to balance simultaneously both mass and isotopes.

Prompted by the growing ability and potential of isotopic GCMs and the increasing availability of data, studies of isotopes in the hydrologic cycle are turning increasingly from identification of classical isotope effects and climatological norms to mapping and modelling of actual isotope climate (and paleoclimate). This shift in focus reflects growing appreciation of the unique information that water isotope data contribute to the analysis and understanding of global climate dynamics.

This article briefly reviews some of the key issues relevant to the evolving field of isotope climatology, focussing on consideration of the fidelity with which isotopic GCMs can simulate the global isotope field, the current state of observational data with which to evaluate such simulations of contemporary global isotope climate, and the opportunities for using paleo isotope data to assess simulations of the global isotope field under differing climates of the past.

2. MODELLING GLOBAL ISOTOPE CLIMATE

Isotopic GCMs first appeared in the 1980s as coarsely-resolved versions of the Laboratoire de Météorologie Dynamique and the Goddard Institute for Space Sciences models [2,3]. Subsequent developments have included sensitivity studies and simulations using the LMD and GISS models at finer spatial resolutions, as well as the introduction of isotope diagnostics into the ECHAM (Max-Planck Institute, Hamburg) atmospheric GCM in various simulations of present global isotope climate [4-13].

As shown in Fig. 1, control simulations of the “equilibrium” mean annual global $\delta^{18}\text{O}$ field produced by the GISS and ECHAM models both capture the expected major features of the contemporary global precipitation $\delta^{18}\text{O}$ field, notably the progressive depletion in heavy-isotope content inland and poleward (*i.e.*, classical continental and latitudinal or temperature effects) and in the subtropics (amount effects). Convincing evidence that these two models can realistically simulate the poleward transport and distillation of moisture at global scale is also provided by comparison of zonally averaged means in comparison with GNIP-derived data (Fig. 2), although acceptance of these promising results must be tempered by recognition of the limitations in the actual coverage provided by observational data (see below).

Closer examination of the maps shown in Fig. 1 reveals significant differences in the models’ abilities to reproduce the finer-scale structure of the isotope field. This is especially obvious, for example, in the greater skill of the ECHAM model to resolve the anticipated altitude effects (*i.e.*, $\delta^{18}\text{O}$ lows) associated with the Rockies and Andes mountain chains. Some of this apparent superiority would certainly disappear if both maps shared the coarser spatial resolution of the GISS simulation, yet this difference also reflects more fundamental limitations on the accurate portrayal of orographic effects, imposed by grid-based representation of Earth’s surface. As illustrated in Figs 3 and 4, the simulated distillation of moisture traversing a topographic barrier is strongly influenced by the fidelity with which that barrier can be represented, and the results naturally propagate downstream and hence, to some extent, throughout the simulated global isotope field. Improvement in coupling of GCMs and land surface schemes to account for moisture recycling is also expected to enhance the reality of the model simulations.

The skill of isotopic GCMs can also be probed using transient-state simulations, providing additional insight into how well a model's water cycle performs when forced by changing boundary conditions, such as the use of observed sea surface temperatures (SST) over a given period, rather than fixed average climatological SST fields. Although only sparse observational time-series exist for direct comparison, promising representations of variability at daily to interannual time-scales have been generated (*e.g.* [8, 9, 12]).

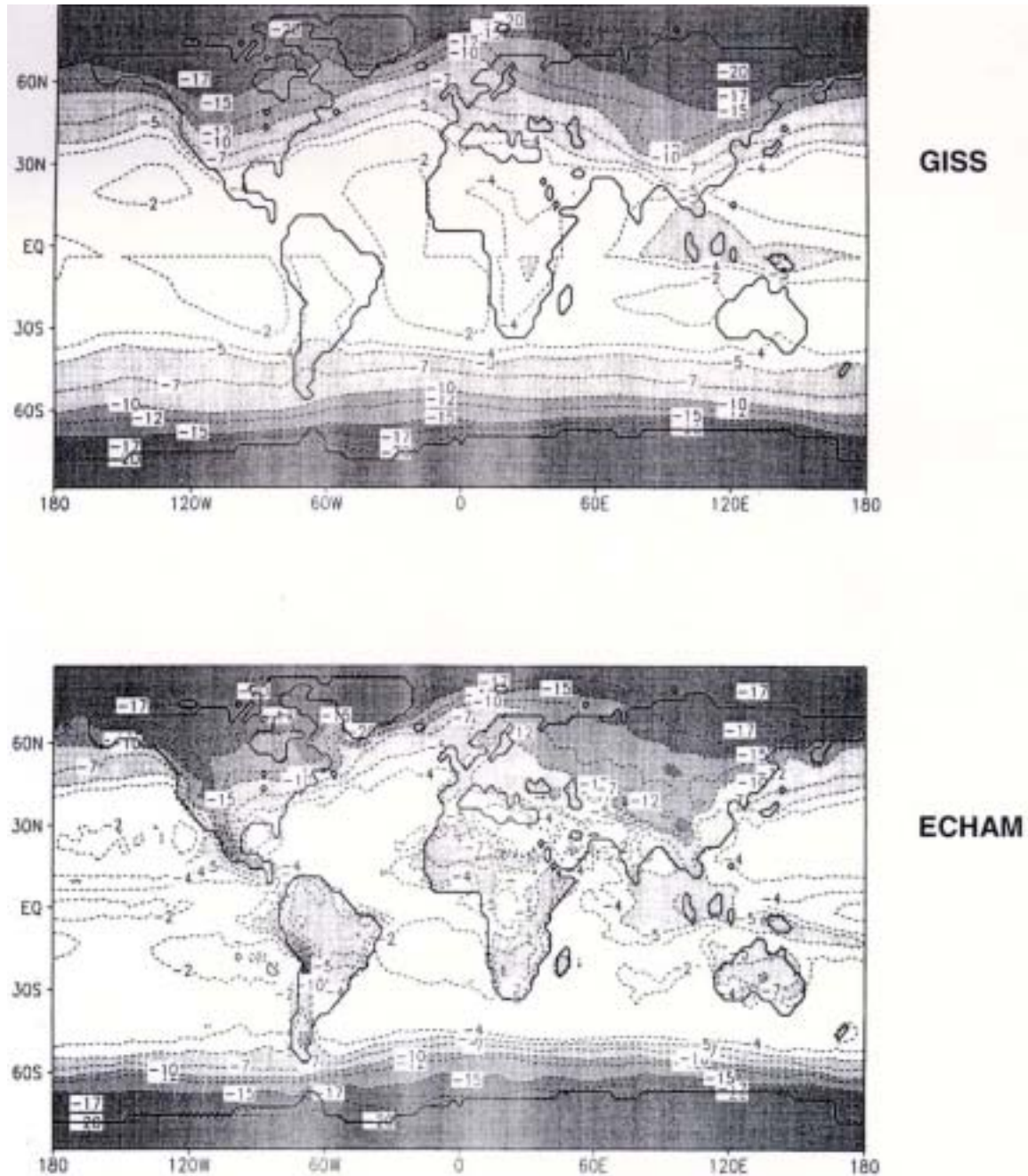


FIG. 1. Comparison of the long-term average global weighted mean annual precipitation $\delta^{18}\text{O}$ field as derived from "equilibrium" simulations using the GISS and ECHAM isotopic GCMs (after [13; Fig. 2]). The GISS map is contoured from 8° latitude \times 10° longitude gridded output, whereas the ECHAM map is based on a $2.8^\circ \times 2.8^\circ$ grid. Note the significantly better representation of altitude and continental effects in the ECHAM simulation, especially at low to mid latitudes, in part attributable to more realistic representation of orography permitted by the finer spatial resolution.

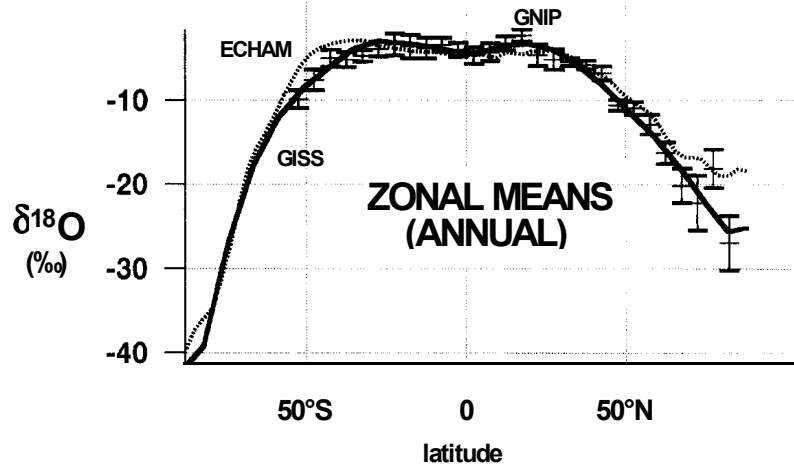


FIG. 2. Zonally averaged $\delta^{18}\text{O}$ of weighted mean annual precipitation, as depicted in the GISS and ECHAM simulations shown in Fig. 1, compared to zonal means over 5° latitudinal intervals based on GNIP data (after [13; Fig. 3]). Both isotopic GCM simulations provide a remarkably good fit, including the steeper latitudinal gradients in the southern high latitudes versus the more shallow gradients observed in the northern hemisphere.

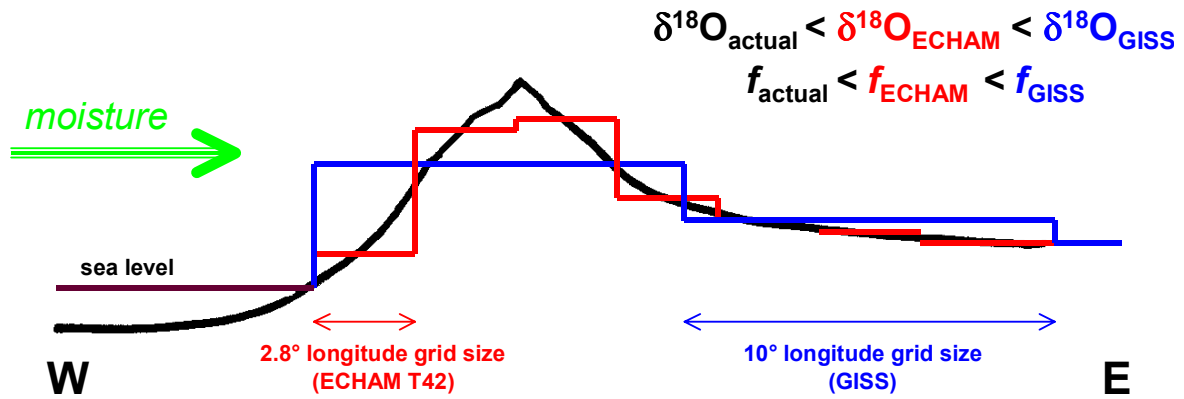


FIG. 3. Schematic representation of variations in the distillation of atmospheric moisture crossing a topographic barrier as simulated for differing GCM grid sizes. The progressive smoothing and lowering of the topography with increasing GCM grid size leads to increased heavy-isotope and mass transfer downstream, as shown also in Fig. 4.

3. PRESENT GLOBAL ISOTOPE CLIMATE AND DATA-MODEL COMPARISON

As noted above, knowledge about the actual distribution of isotopes in contemporary global precipitation derives almost exclusively from the IAEA/WMO GNIP database. In spite of the patchiness of GNIP station records in both time and space, they provide the fundamental observational data for evaluating isotope-climate linkages and, ultimately, the only set of convincing benchmarks for ground-truthing isotopic GCM simulations. Consideration of the global $\delta^{18}\text{O}$ field as mapped from GNIP data (Fig. 5) in relation to the two aforementioned GCM control simulations (Fig. 1), however, provides a strikingly less favourable impression of the potential for direct data-model comparison than that suggested by zonally averaged results (Fig. 2). A predominant feature of the observational data field is the presence of significant gaps over the oceans, as well as some continental areas, such as northeastern Eurasia (due to lack of stations) and northern Africa (due to lack of precipitation). Although

Open-System Rayleigh Distillation

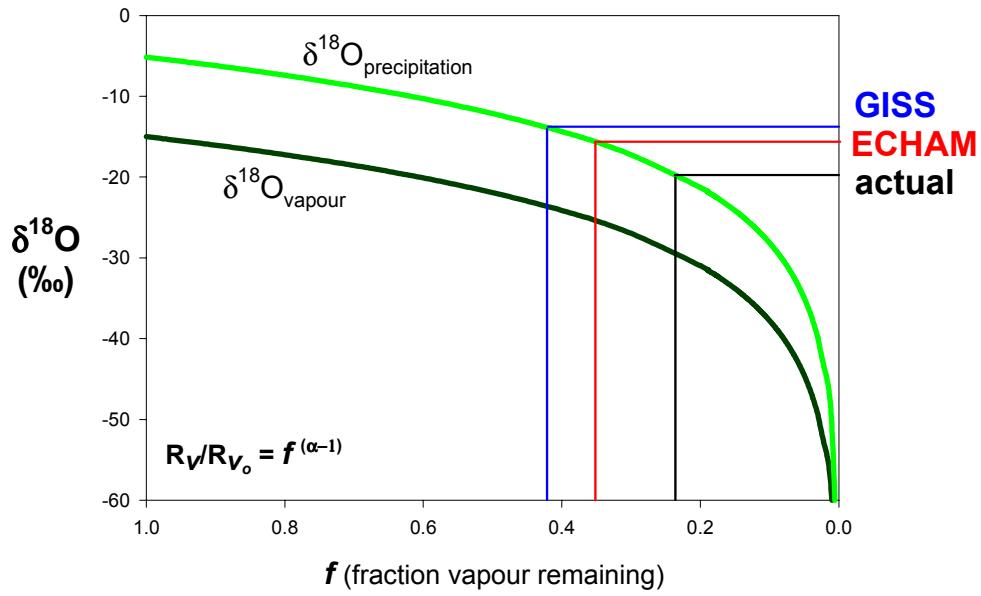


FIG. 4. Variations in Rayleigh-type distillation of atmospheric moisture corresponding to the situations depicted in Fig. 3. Increasingly coarse GCM grid size has the effect of suppressing both heavy-isotope and mass losses downstream, leading to reductions in both isotope- and rain-shadow effects.

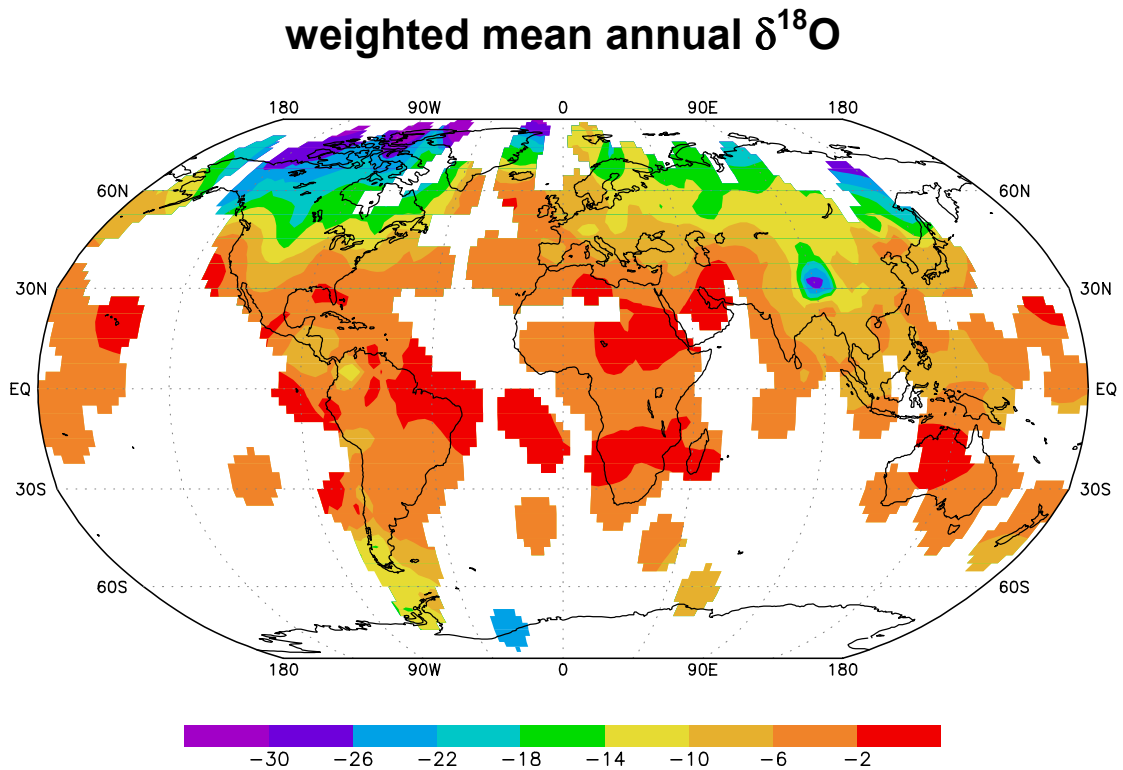


FIG. 5 Contour map of amount-weighted mean annual $\delta^{18}\text{O}$ in precipitation derived from the GNIP database, for stations reporting as of 1997 (see [1]).

data do exist to fill in some areas (like the polar ice caps), much of this could only be filled by unreasonably extreme interpolation between existing GNIP station data. Recognizing the practical impossibility of fully mapping the entire global isotope field in sufficient detail, this comparison clearly suggests that direct ground-truthing of isotopic GCM output through point-for-point data-model comparison is not a realistic goal.

Nevertheless, more thoughtful consideration of the mapped and modelled results does lead to the alternative concept that models constrained by GNIP “benchmarks” and the prescribed need to conserve mass and isotopes, could be used to fill in the gaps in the observational data field. Informed interpolation of the global isotope field in this way could, in theory, lead to the creation of a harmonized reanalysis data set, including both annual and monthly means, as well as actual monthly time-series, analogous to those generated for various other climatological parameters. This would enhance the value of the GNIP data base significantly as a source of hydrologic input functions for water resource studies (one of its initial purposes) and as a primary training set for calibration of isotope indicators of paleoclimate, as well as providing new scope for testing and refinement of the isotopic GCM(s) used to undertake the reanalysis. Moreover, and perhaps even more importantly, the availability of a long time-series (potentially on the order of 40 years) of monthly maps of the global isotope field would offer tremendous opportunity for detailed synoptic analysis of isotope climate, including investigation of the expression of characteristic modes of climate variability on interannual to decadal time scales like the El Niño-Southern Oscillation and the North Atlantic Oscillation.

4. PAST GLOBAL ISOTOPE CLIMATE

Documentation of past global isotope climate is highly fragmentary and relatively little data-model comparison has been undertaken to evaluate isotopic GCM paleoscenarios, largely because of the paucity of well-constrained estimates of the isotopic composition of paleoprecipitation during appropriate time-slices. The Last Glacial Maximum (LGM) has been targeted frequently because of the pervasive difference from contemporary conditions, as well as the availability of a global paleo-SST field, but robust LGM paleo-isotope data are mainly limited to the polar ice caps and the best records at mid- and low latitudes originate primarily from glaciers at elevations too high to be adequately represented by GCMs. Conversely, efforts to simulate the mid-Holocene warm period (*c.* 6000 yr BP), for which more relevant paleo-isotope benchmarks exist, has been hindered by the lack of an appropriate SST field [7,13].

Although compilation of comprehensive global paleo-isotope maps remains a challenging long-term task (and a goal of the International Geosphere-Biosphere Programme, Past Global Changes project), significant opportunities already exist to selectively map smaller areas in greater detail. A prime example is the northern circumpolar region, where the highly detailed records from Greenland ice-cores can be used to anchor time-slices incorporating relatively abundant data from high-latitude glaciers, lake sediments and other archives from northern Eurasia and North America. Evidence for pronounced spatial and temporal fluctuations in apparent isotope-temperature relations (so-called “non-Dansgaard effects”) in some sectors during the Holocene, speculatively linked to changes in the prevailing strength of zonal atmospheric circulation, affords particularly intriguing potential for probing isotopic GCM ability (see Fig. 6).

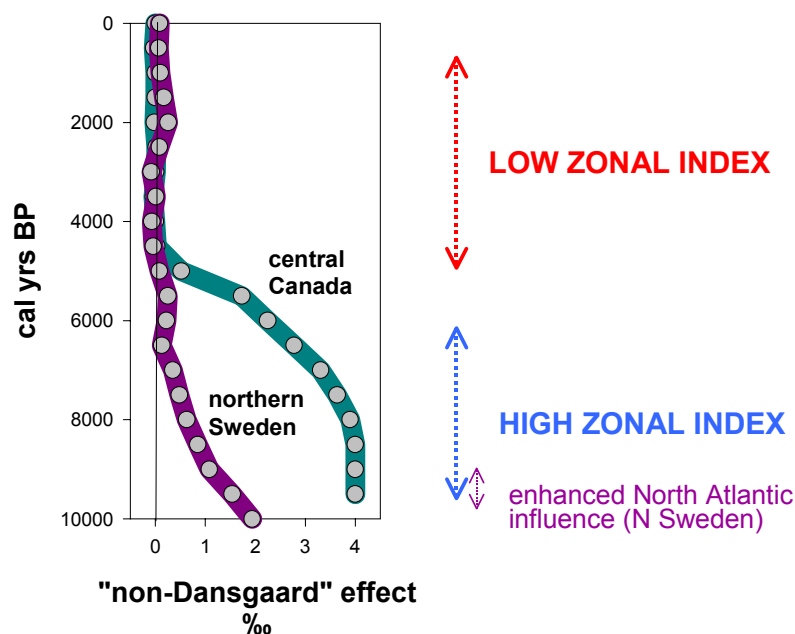


FIG. 6. Apparent deviations from present-day (i.e., “Dansgaard”) isotope-temperature relations for two areas in the northern circumpolar region, based on independent assessments of local mean annual precipitation $\delta^8\text{O}$ and temperature. The major “non-Dansgaard” signals in both areas are consistent with reduced distillation of atmospheric moisture under conditions of higher zonal index, conceptually analogous to the effect of lowering topography depicted in Fig. 3 and 4 (data from [14,15]).

5. CONCLUDING COMMENTS

The science of isotope climatology is developing rapidly, fueled in part by the accumulation and accessibility of global isotope data, especially as provided by the IAEA/WMO GNIP programme. The growing promise of isotopic GCMs is also a factor, fostering the need to critically assess and ultimately improve understanding of global climate dynamics. Particularly exciting potential exists to actively integrate mapping and modelling, with the aim of creating an actual time-series global isotope reanalysis data set. Isotope paleodata also have a role to play in these endeavours by offering access to global climate states lying well beyond the limited range captured by contemporary observations.

REFERENCES

- [1] IAEA. GNIP Maps and Animations. International Atomic Energy Agency, Vienna (2001). (Accessible at <http://isohis.iaea.org>)
- [2] JOUSSAUME, S., SADOURNY, R., JOUZEL, J. A general circulation model of water isotope cycles in the atmosphere. *Nature* **311** (1984) 24-29.
- [3] JOUZEL, J., RUSSELL, G.L., SUOZZO, R.J., KOSTER, R.D., WHITE, J.W.C., BROECKER, W.S. Simulations of the HDO and H_2^{18}O atmospheric cycles using the NASA GISS General Circulation Model: The seasonal cycle for present-day conditions. *Journal of Geophysical Research* **92** (1987) 14,739-14,760.
- [4] JOUZEL, J., KOSTER, R.D., SUOZZO, R.J., RUSSELL, G.L., WHITE, J.W.C., BROECKER, W.S. Simulations of the HDO and H_2^{18}O atmospheric cycles using the NASA GISS General Circulation Model: Sensitivity experiments for present-day conditions. *Journal of Geophysical Research* **96** (1991) 7495-7507.

- [5] JOUZEL, J., KOSTER, R., JOUSSAUME, S. Climate reconstruction from water isotopes: What do we learn from climate models? *In* *Climate Variations and Forcing Mechanisms of the Last 2000 Years*. Edited by R.S. Bradley, J. Jouzel, and P.D. Jones. Springer-Verlag, Berlin (1996) 213-241.
- [6] JOUZEL, J., FRÖHLICH, K., SCHOTTERER, U. Deuterium and oxygen-18 in present-day precipitation: data and modelling, *Hydrological Sciences Journal* **42** (1997) 747-764.
- [7] JOUZEL, J., HOFFMANN, G., KOSTER, R.D., MASSON, V. Water isotopes in precipitation: Data/model comparison for present-day and past climates. *Quaternary Science Reviews* **19** (2000) 363-379.
- [8] COLE, J.E., RIND, D., FAIRBANKS, R.G. Isotopic responses to interannual variability simulated by the GISS GCM. *Quaternary Science Reviews* **12** (1993) 387-406.
- [9] COLE, J.E., RIND, D., WEBB, R.S., JOUZEL, J., HEALY, R. Climatic control on interannual variability of precipitation $\delta^{18}\text{O}$: The simulated influence of temperature, precipitation amount and vapour source region, *Journal of Geophysical Research* **104** (1999) 14,223-14,235.
- [10] HOFFMANN, G., HEIMANN, M. Water tracers in the ECHAM general circulation model. *Proceedings, Symposium on Isotope Techniques in the Study of Past and Current Environmental Changes in the Hydrosphere and the Atmosphere*, IAEA, Vienna, 19-23 April 1993, IAEA-SM-329/7 (1993) 3-14.
- [11] CHARLES, C., RIND, D., JOUZEL, J., KOSTER, R., FAIRBANKS, R. Seasonal precipitation timing and ice core records. *Science* **269** (1995) 247-248.
- [12] HOFFMANN, G., WERNER, M., HEIMANN, M. Water isotope module of the ECHAM atmospheric general circulation model: A study on timescales from days to several years. *Journal of Geophysical Research* **103** (1998) 16,871-16,896.
- [13] HOFFMANN, G., JOUZEL, J., MASSON, V. Stable water isotopes in Atmospheric General Circulation Models, *Hydrological Processes* **14** (2000) 1385-1406.
- [14] EDWARDS, T.W.D., WOLFE, B.B., MACDONALD, G.M. Influence of changing atmospheric circulation on precipitation $\delta^{18}\text{O}$ -temperature relations in Canada during the Holocene. *Quaternary Research* **46** (1996) 211-218.
- [15] HAMMARLUND, D., BUCHARDT, B., EDWARDS, T.W.D., BARNEKOW, L., BIRKS, H.J.B. Holocene changes in atmospheric circulation recorded in the oxygen-isotope stratigraphy of lacustrine carbonates from northern Scandinavia. *The Holocene* **12** (2002) 355-367.

PALAEOVEGETATION DYNAMICS OF AN ECOTONE FOREST-SAVANNA IN THE SOUTHERN BRAZILIAN AMAZON DURING THE LATE PLEISTOCENE AND HOLOCENE BASED ON CARBON ISOTOPES OF SOIL ORGANIC MATTER

L.C.R. PESSENDA, S.E.M. GOUVEIA, H.A. DE FREITAS

Centre for Nuclear Energy in Agriculture,
University of São Paulo,
Piracicaba, São Paulo, Brazil

B.M. GOMES

University of Rondônia,
Rondônia, Brazil

R. ARAVENA

University of Waterloo
Waterloo, Ontario, Canada

A.S. RIBEIRO

University of Sergipe,
Aracaju, Sergipe, Brazil

R. BOULET

IRD–France
University of São Paulo,
São Paulo, São Paulo, Brazil

J.A. BENDASSOLI

Centre for Nuclear Energy in Agriculture,
University of São Paulo,
Piracicaba, São Paulo, Brazil

Abstract. This study was carried out in the Brazilian southern Amazon region (Rondônia state and Humaitá, southern Amazon state). Carbon isotope data on soil organic matter have been collected along an ecosystem transect of about 750 km that includes a savanna, a wooded savanna (cerrado), a tropical semideciduous forest (cerradão), a forest transition type and a tropical forest. The main objective is to evaluate the expansion-regression dynamics of these vegetation units in relation to climate changes during the Late Pleistocene (Late Glacial) and Holocene. Large ranges in $\delta^{13}\text{C}$ values were observed in soil organic matter collected from profiles in the savanna (-27 to -14‰) and forest regions (-26 to -19‰) reflecting changing distribution of ^{13}C -depleted C_3 forest and ^{13}C -enriched C_4 savanna vegetation in response to climate change. ^{14}C data of humin fraction and buried charcoal indicate that the organic matter in these soils is at least 17,000 years BP at 300-cm depth. In this period, the entire ecosystem transect are characterized by $\delta^{13}\text{C}$ soil depth profiles, generated typically by C_3 plants (forest), inferring a humid climate in the southern Amazon region after the end of last glaciation. ^{13}C data also indicate that C_4 plants (grasses) have influenced significantly the vegetation at the transitional forest and the cerrado sites of southern Rondônia state and two distinct points in the forest ecosystem in the southern Amazon state. These typical C_4 type isotopic signatures probably reflect a drier climate during about 9000-8000 yr BP to 3000 yr BP and the savanna and wooded savanna expansion in distinct points of the transect. The ^{13}C records representing the 3000 yr show an expansion of the forest, due to a climatic improvement, in areas previously occupied by savanna vegetation. This study adds to the mounting evidence that extensive forested areas existed in the Amazon during the last glacial and that savanna vegetation expanded in response to warm and dry conditions during the early to middle Holocene.

1. INTRODUCTION

The Amazon region is one of the key ecosystems that are being investigated as part of the Global Change Research Program. Most of the research efforts have focused on the understanding of the link between climate changes and past vegetation in the Amazon region during the Quaternary [1, 2]. Palaeoenvironmental studies done on peat, lake sediments and soil organic matter [3, 4] associate with pollen records [5, 6] and paleofauna [7] shows several periods of expansion/regression between forest and savanna vegetation during the late Quaternary.

It has been proposed that during cold and dry climatic periods, extensive humid forests (natural refuges) probably existed in fairly large regions of the Amazonian lowlands, where sufficient surface relief was present to create rainfall gradients [8, 9]. Open forests and gallery forests probably existed in the regions between the postulated forest refugia, where variously extensive wooded savannas may, at times, have dominated the landscape [9].

Stable carbon isotope composition of SOM (soil organic matter) profiles has been instrumental in identifying the changing distribution of C₃ and C₄ plant communities in the Amazon Basin (i.e. forest vs. savanna vegetation, respectively) and elsewhere [10, 11]. The typical carbon isotope values of C₃ photosynthetic-pathway plants range from -20‰ to -35‰ whereas values of C₄ photosynthetic-pathway plants range from -9‰ to -16‰. Thus, C₃ and C₄ plant species have distinct, non-overlapping carbon isotope signatures [10].

This paper presents data collected along a transect covering four different types of vegetation communities, representative of the ecosystem's diversity that presently exists in the Amazon region. These include a wooded savanna (Cerrado), a tropical semideciduous forest (Cerradão), a forest transition type and a tropical forest. Recent carbon isotope studies on SOM of several sites in the Amazon region [4, 5] suggest that vegetation communities in the Cerrado and Cerradão ecosystems should be more sensitive to climate changes. This study is part of a major research program carried out at the Center for Nuclear Energy in Agriculture (CENA) whose aim is to evaluate vegetation dynamics during the last 20,000 years in Brazil using carbon isotopes [12, 13, 14].

2. MATERIAL AND METHODS

2.1. Study sites

The study area is located in the Rondônia state and in the Humaitá region, southern Amazon state (Fig. 1), northwestern part of Brazil. The sampling sites in Rondônia, a transect of about 500 km (Fig. 2), are located close to the city of Vilhena (12°42' S and 66°07' W), representative of the Cerrado, a wooded savanna. Grass species including *Trystachia* sp, *Panicum* sp, *Eleusine* sp, *Bulbostylis* sp are interspersed with trees, mainly *Curatella americana*, *Miconia* sp, and *Cassia* sp. The other sites are near Pimenta Bueno (transition site) under vegetation of Cerradão (11°49' S and 61°10' W), a transitional state between the dense evergreen forest and the savanna denominated tropical semideciduous forest [15] and natural forest (11°46' S and 61°15' W), and in Ariquemes (10°10' S and 62°49' W) under vegetation of natural forest (Fig. 1). Some of the dominant C₃ plants in these forested sites are *Miconia* sp, *Piper* sp, *Cecronia* sp, *Protium* sp, *Andira* sp, *Inga* sp and *Euterpe precatoria*. The soils in Vilhena (Cerrado site) and in Pimenta Bueno (Cerradão and forest transition sites) are Oxisols according with the Soil Taxonomy (USDA) classification. In Ariquemes is an Ultisol. The distance between Vilhena and Pimenta Bueno is about 200 km and from Pimenta Bueno to Ariquemes about 400 km. In the transition Cerradão-forest, the distance between the study sites is about 40 km.

In the Humaitá region the eight sampling sites are located on a 250-km transect along BR 319 in sites of savanna and tropical forest vegetation (Fig. 3). The study transect is located between the coordinates 8°43' S/63°58' W (km 5) and 7°31' S/63°02' W (km 250) where natural forest/savanna vegetation boundaries are well defined. The savanna vegetation, called "Campos de Humaitá" [16], is composed mainly of grasses (*Eryamtus* sp, *Panicum* cf *laxum* SWARTZ, *Paspalum* cf *multicaule* POIR) and few short (< 8 m) trees (*Miconia* sp, *Piper* sp, *Byrsonima* sp). This ecosystem changes in some places gradually and in others abruptly to a Tropical Mesophitic opened-canopy forest (known as *floresta de terra firme*) with palms. These forests surround the savannas whose areas range from about ten to a hundred square kilometers.



FIG. 1. Map of Brazil showing the study sites.

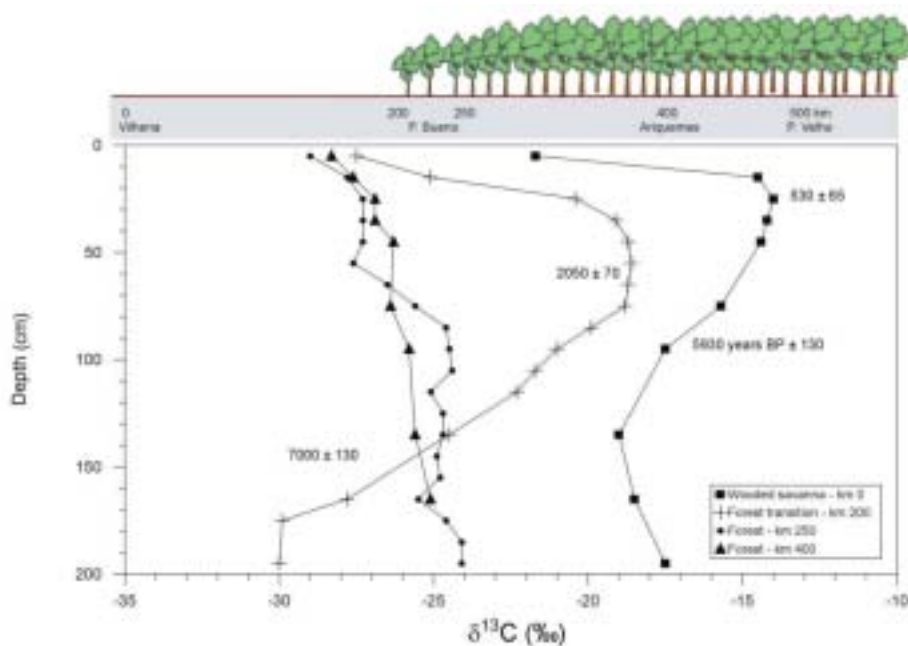


FIG. 2. Variation of $\delta^{13}\text{C}$ of SOM with depth of the forest-savanna ecotone in Rondônia state. The ^{14}C datings were obtained from charcoal samples.

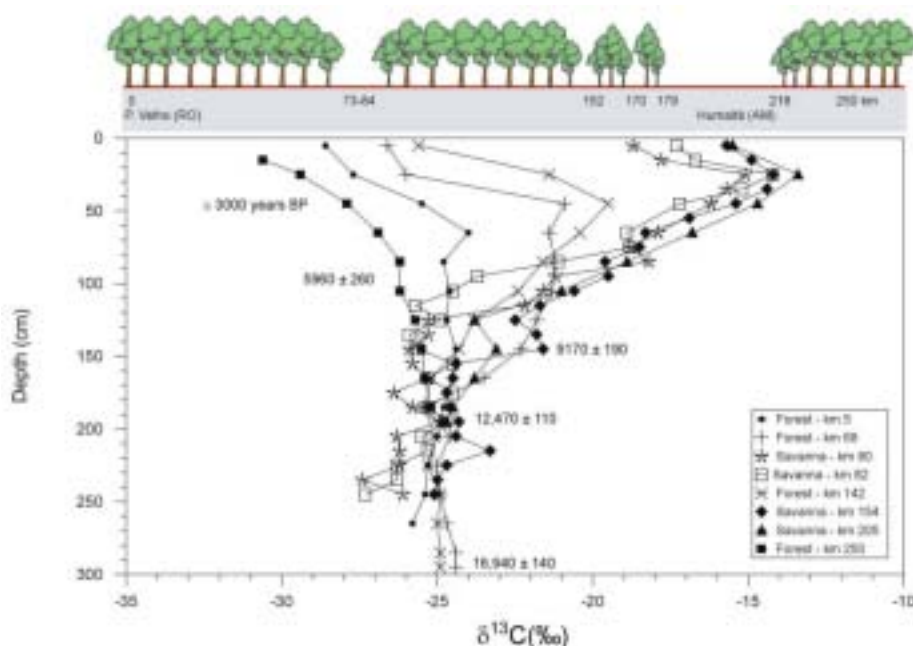


FIG. 3. The variation of $\delta^{13}\text{C}$ of SOM with depth of the forest-savanna ecotone in the Humaitá region (southern Amazon state). The ^{14}C datings were obtained from humin samples.

The soils were classified as Plintic Gley (km 80, 82 and 154), Ferralitic Cambisol (km 5, 142), Oxisol (km 68, 250), Troporthent (km 205), according to American soil taxonomy. Soil samples were collected from trenches or using a hand-auger.

The climate of the region is characterized by a mean annual temperature of 26°C (the mean temperature during the cooler month is higher than 18°C) and irregular rainfall (1800 to 3500 mm/yr), with a dry season from June to September when precipitation is less than 50 mm per month [16]. The altitude lies between 80 and 150 m above sea level.

2.2. Sampling and analytical aspects

From trenches, up to 5 kg of material were collected in 10-cm increments to a maximum depth of 300 cm. For $\delta^{13}\text{C}$ analysis, about 0.5 kg of soil or about 0.2 kg of hand-auger samples was sieved (5 mm) and dried at 50°C to a constant weight. Root fragments were discarded by hand picking. The dry samples were sieved again (210 μm) and any remaining debris was removed by flotation in 0.01 M hydrochloric acid and wet-sieved (210 μm). For ^{14}C analysis, the humin fraction was isolated using an acid-alkaline-acid treatment [11], dried to a constant weight and sieved (210 μm). Charcoal samples were also collected for carbon isotope analysis. A detailed description of the chemical treatment for soil and charcoal samples was previously described [11].

The ^{14}C analyses on humin fraction and charcoal samples were carried out at the Radiocarbon Laboratory, Centro de Energia Nuclear na Agricultura (CENA), following the standard procedure for liquid scintillation counting [17]. The ^{14}C on small samples of charcoal were carried out at the Isotrace laboratory of the University of Toronto, employing the AMS technique. Radiocarbon ages are reported as years BP.

Grain size analyzes were carried out at the Soil Science Department of the Escola Superior de Agricultura "Luiz de Queiroz", Piracicaba, Brazil. The results are expressed in percentage (%).

Plants representative of the modern vegetation were also collected at each study site in an area equivalent to 1000 m². For ¹³C analysis, the leaves were washed, dried and grounded to < 0.100 mm. The ¹³C analysis on soil and plants samples were carried out at the Environmental Isotopes Laboratory, University of Waterloo using a Carlo Erba Analyzer attached to an Optima mass spectrometer. Stable isotope results are expressed as δ¹³C with respect to the PDB standard using the conventional δ (‰) notation:

$$\delta^{13}\text{C} (\text{‰}) = \left(\frac{R_{\text{sample}}}{R_{\text{standard}}} - 1 \right) \times 1000$$

where, R_{sample} and R_{standard} are the ¹³C/¹²C ratio of the sample and standard, respectively. Analytical precision is ± 0.2‰.

3. RESULTS AND DISCUSSION

3.1. Soil properties

The grain size analysis indicated that clays comprise between 20 and 34% of the shallow soil horizons and increase to 57% in the deeper part of the soils representative of the forest, forest-transition and Cerrado. The site representative of the Cerradão show higher clay content, ranging from 53% to 78% at the shallow and deeper part of the soil, respectively [12]. In the Humaitá region the analyses show that the clay content in the shallow parts of the soils are lower (20-30%) than in the deeper strata (32-56%). No clear difference was observed between the vegetation type and the soil clay content. The soils were classified as clayey or medium-clayey [18].

The carbon contents show the typical soil profiles of decreasing carbon content with depth, similar to results obtained from most Amazonian soils. In Rondônia they range between 1.9 to 5% in the shallow soil horizons decreasing to a carbon content as low as 0.30% in the deeper soil horizons [5]. Higher carbon content, between 5% at the surface and 0.8% in the deeper part of the soil, is observed at the Cerrado site. This pattern may be related to the presence of small charcoal remains observed along most of the soil profile at this site. In a forest-savanna ecotone on medium-texture Oxisols in Roraima, northern part of the Amazon region, it was found significant differences in the total C content between both vegetation types [3]. The lower C content of savanna compared to the forest soil was related to its lower clay content and smaller litter input. The carbon content data in soils of Humaitá region also show a general decrease. Values range from 3.39% in the shallow part of the soil to 0.05% in the deeper strata. Soils of three profiles under savanna (km 80, 82 and 154) contain notably high carbon content in the upper 10 cm (2.5 to 3.9%), probably due to the transport of organic material from forested sites that surround the savannas located in depressions. Below 30 cm, similar carbon concentration was found both in savanna and forest profiles [18].

3.2. Carbon isotope data

3.2.1. Radiocarbon data

The radiocarbon data presented in Fig. 2 correspond to charcoal samples at the Cerrado and the Cerradão sites and provide a reliable estimate of the time represented in the soil profiles. These data show radiocarbon ages of 540 years and 5930 years at the sampling intervals 20-30 cm and 90-100 cm, respectively at the Cerrado site, and 2050 years and 7000 years was obtained at 60 cm and 150 cm in the Cerradão soil. This suggests that the ^{13}C record in the 200-cm soil profiles presented in this paper represent changes in the vegetation communities perhaps as much as 8000 years. Soil age-depth profiles obtained on humin and charcoal samples in other study sites in Brazil (including two sites in the Amazon Basin) yield an age of about 9000 to 12,000 yr BP for the 200 cm soil horizon [12, 19], broadly consistent with our estimates. The radiocarbon data for the humin fraction in the Humaitá region (Fig. 3), also indicate increasing age with depth. Similar soil age profiles have been reported in others parts of the Amazon Basin and sites in Brazil [11, 20]. The radiocarbon data indicate that the soil profiles represent at least the last 17,000 ^{14}C yr BP, approaching the last glacial maximum (LGM). This is the longest ^{14}C record for soils reported in the Amazon Basin. Most of the reported soil profiles span the last 10,000 ^{14}C yr [11, 20], although older records describing vegetation changes during the last 40,000 ^{14}C yr in the Amazon Basin have been reported from lake sediments [2, 21] and marine core [22].

3.2.2. ^{13}C Results

The $\delta^{13}\text{C}$ values for SOM on the forest and forest transition regions in Rondônia range from -28.3‰ to -25.1‰ and -29.0‰ to -24.1‰, respectively (FIG. 2). The ^{13}C enrichment with depth is probably due to decomposition of SOM [23, 24] and is typical for soil organic matter generated by C_3 vegetation type [25]. These results indicate that the C_3 vegetation type has been predominant in the regions represented by the forest transition site, Pimenta Bueno (central-southern region of Rondônia state) and the forest site, Ariquemes (northern region of Rondônia state), during the time represented by this record.

A wider range of $\delta^{13}\text{C}$ values between -30‰ and -14‰ are observed at the soil sites representative of Cerradão and Cerrado vegetation communities (FIG. 2). The $\delta^{13}\text{C}$ depth profile for the Cerradão site show a ^{13}C trend ranging from -30‰ and -25‰ in the deepest part of the profile (150-200 cm), increasing to about -18.8‰ between 30-90 cm and then reversing towards more ^{13}C -depleted values (-27.5‰ and -25.1‰) at the surface (0-20 cm). This trend suggests a predominance of C_3 vegetation in the lower part of the record that should represent the early Holocene, changing to a vegetation community consisting predominantly of C_4 plants, recorded in the interval between 120 and 30 cm (middle and late Holocene), then returning to a predominance of C_3 plants in the interval 30 cm at the surface (recent). Similar $\delta^{13}\text{C}$ profiles have been reported in Brazil [3, 4], implying a change from a C_3 to C_4 to C_3 vegetation type. A detailed study of the composition of modern vegetation at the Cerradão site and $\delta^{13}\text{C}$ data show that about 96% of the identified vegetation are C_3 plants and one CAM (orchid) species [12].

The $\delta^{13}\text{C}$ record at the Cerrado site seems to show a similar pattern, but much more ^{13}C -enriched values than at the Cerradão site (FIG. 2). The $\delta^{13}\text{C}$ values range from -17.5 and to -19.0‰, in the depth interval 90-200 cm, increasing to more positive values (-14.8 to -15.7‰) at 10-80 cm and reversing toward more negative $\delta^{13}\text{C}$ values (-21.7‰) at the surface layer (0-

10 cm). This site clearly shows the influence of C_4 plants during most of the time represented at this site. Palynological and paleolimnological studies in central Brazil and eastern Amazon have shown that savannas appeared with the development of a drier climate, beginning 8000 yr BP and reaching a maximum at 6000-5000 yr BP [2, 26]. The existence of charcoal samples dated between 7000 and 6000 yr BP in the Cerradão and Cerrado soils, probably derived from paleofires that occurred during the dry period, supports the interpretation that the present savanna appeared during the mid-Holocene. A survey of modern vegetation and $\delta^{13}C$ data indicated that about 80% of the identified vegetation of the Cerrado communities are C_3 plants, and 20% are composed of C_4 plants [12].

The $\delta^{13}C$ pattern in soil organic matter and inferred vegetation changes reported in this study have also been reported in other transitional regions between forest and savanna of the Amazon region [3, 4] suggesting regional scale changes in vegetation communities occurred in the Amazon Basin during the Holocene. The regional dimension represented by the Cerrado and the Cerradão sites separated by 200 km also support the hypothesis that large areas of the Amazon region have been affected by vegetation changes.

In Humaitá region, the savanna soils show a wide range in isotopic composition that varies between -27 and -14‰ (Fig. 3). The lower parts of the profiles (300-cm to 150-cm depth) show the most ^{13}C depleted values ranging from -27.3‰ (at 250-cm depth; km 82) to -23.3‰ (at 220-cm depth; km 154). A trend towards ^{13}C -enriched values occurs between 150-cm and 30-cm depth in the savanna profiles reaching values as high as -14.2‰ (km 154). This trend is reversed in the shallow part of the savanna profiles toward slightly more ^{13}C -depleted values.

The soils at the forest sites also show large isotopic variations (-26 to -19‰). The deepest interval (300-190 cm) show $\delta^{13}C$ values between -25 and -24‰. Similar to the savanna profiles, a trend towards ^{13}C -enriched values occurs between 190-cm and 40-cm depth in the forest profiles. This trend is more pronounced at sites km 68 and km 142, whereas no isotopic change is observed at site km 5 within this depth interval. The shallow parts of the forest profiles show a shift towards ^{13}C -depleted values.

Thus, the low $\delta^{13}C$ values of -27.3 to -23.3‰ observed between 300 cm and 150 cm at the savanna sites are presumed to reflect SOM formed under forest vegetation. Similarly, the lower interval from 300-cm to 190-cm depth in the soils of forest sites show $\delta^{13}C$ values typical of SOM formed under forest [3, 11].

Substantial isotopic enrichment observed in the 150 to 30-cm depth interval in the savanna soils, and from about 190 to 70 cm in most of the forest sections, is likely related to an increase in the contribution of C_4 plant biomass due to savanna expansion. In the southern part of the transect, ^{13}C -enrichment is most pronounced in soil profiles presently located in savanna (km 80 and 82), reaching values as high as -14.2‰ and becomes less evident in forested sections to the south and north, where the highest value is -19.3‰. The trend towards ^{13}C -depleted values in the upper 70 cm in the forest soil profiles probably reflects a shift towards increasing influence of C_3 plants at the expense of declining savanna vegetation.

The forest SOM in the lower strata of the soil profiles was probably formed between 17,000 and 9000 ^{14}C yr BP based on radiocarbon dating of the Fig. 3. Dominance of forest vegetation, during the last part of the last glacial to the early Holocene, is consistent with other vegetation reconstructions [6, 22]. In our study region, widespread savanna expansion does not appear to have been initiated until around 9000-8000 ^{14}C yr BP and lasting until

about 3000 ^{14}C yr BP. This interpretation is similar to other documented forest to savanna vegetation changes in the Amazon Basin during the early and middle Holocene [12, 20, 24]. However, some regions in the Amazon Basin remained forested during the middle Holocene [6, 13] possibly reinforcing the Refugia Hypothesis. Some authors argue that savanna expansion was not on a regional scale but much more localized [19].

Our results show forest expansion at the expense of savanna since about 3000 ^{14}C yr BP. This vegetation pattern has also been documented near Humaitá-AM [4, 20]. A similar study showed the advance of forest over savanna in Roraima, northern Amazon region [3].

Therefore, according to our study the period 17,000-9000 ^{14}C yr BP appears to have been wetter and probably cooler. The expansion of the savanna between 9000-8000 ^{14}C yr BP and 3000 ^{14}C yr BP, suggests drier and probably warmer conditions than the previous period, during early and middle Holocene. Similar climate pattern has been suggested for this region around the Late Pleistocene [27]. After 3000 ^{14}C yr BP to the present, expansion of C_3 vegetation (forest) suggests that suitable wetter conditions have favoured this change in the region.

4. CONCLUSIONS

This study presents the first long Late Quaternary record of vegetation dynamic inferred from carbon isotope composition of SOM in southern Amazon. Significant carbon isotope variations reflecting changes in vegetation were observed in 12 soil profiles collected along a 750-km transect that included forest and savanna sites in Rondônia state and Humaitá region, Amazonas state. Three major vegetation phases were identified. These include: 1) a forest phase between 17,000 and 9000 ^{14}C yr BP; 2) savanna expansion between 9000-8000 and 3000 ^{14}C yr BP; and 3) forest expansion after 3000 ^{14}C yr BP. Our study suggests that forest vegetation was not replaced by regional savanna expansion during the last part of the last glacial in the region, as has been suggested by others studies, and brings into question the relationship between climate change and non-uniform vegetation response in the Amazon. Similarly, savanna expansion appears to have occurred during the dry and warm early and middle Holocene, although the regional significance of this vegetation change also remains uncertain in light of other studies that indicate forest vegetation was widespread during this interval. Further studies utilizing carbon isotope profiles in SOM at other forest-savanna ecotonal boundary regions, may contribute to a more effective characterization of local versus regional vegetation response to past climate change in the Amazonia.

ACKNOWLEDGEMENTS

Financial support for this study has been provided by São Paulo Foundation for Research (FAPESP), grant n° 97/11733-4, PRONEX grant n° 41.96.0938.00 and by National Council of Research and Development (CNPq), grant n° 522923/96-8. FAPESP and CNPq provided the fellowship to Susy Eli Marques Gouveia and Hermes Augusto de Freitas, respectively.

REFERENCES

- [1] LIU, K.B., COLINVAUX, P., Forest changes in the Amazon basin during the last glacial maximum, *Nature* **138**: (1985) 556-557.

- [2] ABSY, M.L., CLEEF, A., FOURNIER, M., MARTIN, L., SERVANT, M., SIFFEDINE A., SILVA, M.F., SOUBIÈS, F., SUGUIO, K., TURCQ, B., VAN DER HAMMEN, T., Mise en évidence de quatre phases d'ouverture de la forêt dense dans le sud-est de l'Amazonie au cours des 60.000 dernières années. Première comparaison avec d'autres régions tropicales, *C. R. Acad. Sci., Ser. 2* **312**: (1991) 673-678.
- [3] DESJARDINS, T., CARNEIRO FILHO, A., MARIOTTI, A., CHAUVEL, A., GIRARDIN, C., Changes of the forest-savanna boundary in Brazilian Amazonia during the Holocene revealed by isotope ratios of organic carbon, *Oecologia* **108**: (1996) 749-756.
- [4] PESSENDA, L.C.R., GOUVEIA, S.E.M., ARAVENA, R., GOMES, B.M., BOULET, R., RIBEIRO, A.S., ^{14}C dating and stable carbon isotopes of soil organic matter in forest-savanna boundary areas in Southern Brazilian Amazon Region, *Radiocarbon* **40**: (1998), 1013-1022.
- [5] VAN DER HAMMEN, T., Changes in vegetation and climate in the Amazon Basin and surrounding areas during the Pleistocene, *Géologie en Mijnbouw* **51**: (1972) 641-643.
- [6] COLINVAUX, P.A., OLIVEIRA, P.E., MORENO, J.E., MILLER, M.C., BUSH, M.B., A long pollen record from lowland Amazonia: forest and cooling in glacial times, *Science* **274**: (1996) 85-88.
- [7] RANCY, A., A paleofauna da Amazônia indica áreas de pastagem com pouca cobertura vegetal, *Ciência Hoje* **16**: (1993) 48-51.
- [8] VAN DER HAMMEN, T., ABSY, M.L., Amazonia during the last glacial, *Science* **109**: (1994) 247-261.
- [9] HAFFER, J., Alternative models of vertebrate speciation in Amazonia: an overview, *Biodiversity and Conservation* **6**: (1997) 451-476.
- [10] BOUTTON, T.W., Stable carbon isotope ratios of soil organic matter and their use as indicators of vegetation and climate change. In "Mass spectrometry of soils" (T.W. Boutton, S. Yamasaki, Eds.), New York, Marcel Dekker (1996) 47-82.
- [11] PESSENDA, L.C.R., ARAVENA, R., MELFI, A.J., TELLES, E.C.C., BOULET, R., VALENCIA, E.P.E., TOMAZELLO, M., The use of carbon isotopes (^{12}C , ^{13}C , ^{14}C) in soil to evaluate vegetation changes during the Holocene in central Brazil, *Radiocarbon* **38**: (1996) 191-201.
- [12] PESSENDA, L.C.R., GOMES, B.M.; ARAVENA, R.; RIBEIRO, A.S; BOULET, R., GOUVEIA, S.E.M. The carbon isotope record in soils along a forest-cerrado ecosystem transect: implication for vegetation changes in Rondônia State, southwestern Brazilian Amazon region, *The Holocene* **8**: (1998) 631-635.
- [13] PESSENDA, L.C.R., VALENCIA, R., ARAVENA, R., TELLES, E.C.C., BOULET, R., Palaeoclimate studies in Brazil using carbon isotopes in soils. In "Environmental geochemistry in the tropics" (J.C. Wasserman, E.V. Silva-Filho and R. Villas-Boas Eds.), pp.7-16. Springer-Verlag (Lecture Notes in Earth Sciences, 72) (1998).
- [14] GOUVEIA, S.E.M., PESSENDA, L.C.R., BOULET, R., ARAVENA, R., SCHEEL-YBERT, R., Isótopos do carbono dos carvões e da matéria orgânica do solo em estudos de mudança de vegetação e clima no Quaternário e da taxa de formação de solos do estado de São Paulo, *An. Acad. Bras. Ci.* **71**: (4-II) (1999) 969-980.
- [15] GOODLAND, R., POLARD, R., The Brazilian cerrado vegetation a fertility gradient, *Ecology* **61**: (1973) 219-224.
- [16] BRASIL. Ministério das Minas e Energia. Projeto RADAMBRASIL. Folha SB.20 - Purus. Rio de Janeiro, 1978. (Levantamento de Recursos Naturais, 17).
- [17] PESSENDA, L.C.R., CAMARGO, P.B., Datação radiocarbônica de amostras de interesse arqueológico e geológico por espectrometria de cintilação líquida de baixa radiação de fundo, *Química Nova* **14** 2: (1991) 98-103.

- [18]FREITAS, H.A., PESSENDA, L.C.R., ARAVENA, R., GOUVEIA, S.E.M., RIBEIRO, A.S., BOULET, R., Late Quaternary vegetation dynamics in the southern Amazon Basin inferred from carbon isotopes in soil organic matter, *Quaternary Research* **55**: (2001) 39-46.
- [19] MARTINELLI L.A., PESSENDA L.C.R., ESPINOZA E., CAMARGO P.B., TELLES E.C., CERRI C.C., VICTORIA R.L., ARAVENA R., RICHEY J., TRUMBORE S., Carbon-13 variation with depth in soils of Brazil and climate change during the Quaternary, *Oecologia* **106**: (1996) 376-381.
- [20]GOUVEIA, S.E.M., PESSENDA, L.C.R., ARAVENA, R., BOULET, R., ROVERATTI, R., GOMES, B.M., Dinâmica de vegetações durante o Quaternário recente no sul do Amazonas indicada pelos isótopos do carbono (^{12}C , ^{13}C e ^{14}C), *Geochim. Brasil.* **11** 3: (1997) 355-367.
- [21]SIFEDDINE, A., FRÖHLICH, F., FOURNIER, M., MARTIN, L., SERVANT, M., SOUBIÈS, F., TURCQ, B., SUGUIO, K., AND VOLKMER-RIBEIRO, C., La sédimentation lacustre indicateur de changements des paléoenvironnements au cours des 30,000 dernières années (Carajás, Amazonie, Brésil), *C. R. Acad. Sci., Ser. 2* **318**: (1994) 1645-1652.
- [22]HABERLE, S.G., AND MASLIN, M.A., Late Quaternary vegetation and climate change in the Amazon Basin based on a 50,000 year pollen record from the Amazon Fan, ODP Site 932, *Quaternary Research* **51**: (1999) 27-38.
- [23]NADELHOFER, K.F., FRY, B., Controls on natural nitrogen-15 and carbon -13 abundances in forest soil organic matter, *Soil Sci. Soc. Am. J.* **52**: (1988) 1633-1640.
- [24]BECKER-HEIDMANN, P.B., SCHARPENSEEL, H.W., The use of natural ^{14}C and ^{13}C in soils for studies on global climate change, *Radiocarbon* **34** 3: (1992) 535-540.
- [25]CERRI, C.C., FELLER, C., BALESDENT, J., VICTORIA, R., PLENECASSAGNE, A., Application du traçage isotopique naturel en ^{13}C , à l'étude de la dynamique de la matière organique dans les sols, *C. R. Acad. Sci. Paris, Ser. 2* **300**: (1985) 423-426.
- [26]LEDRU, M.P., Late quaternary environmental and climatic changes in central Brazil, *Quaternary Research* **39**: (1993) 90-98.
- [27]MARTIN, L., BERTAUX, J., CORRÈGE, T., LEDRU, M.P., MOURGUIART, P., SIFEDDINE, A., SOUBIÈS, F., WIRRMANN, D., SUGUIO, K., TURCQ, B., Astronomical forcing of contrasting rainfall changes in tropical South America between 12,400 and 8800 cal yr B.P., *Quaternary Research* **47**: (1997) 117-122.

**TEMPORAL VARIATION IN ORGANIC CARBON STABLE ISOTOPE
COMPOSITIONS OF LACUSTRINE SEDIMENTS FROM
SUB-ARID NORTHERN TANZANIA***
(Abstract)

A.N.N. MUZUKA, N. NYANDWI

Institute of Marine Sciences, University of Dar es Salaam, Zanzibar, Tanzania

The stable isotope compositions for four sediment cores recovered from three shallow lakes located in the Ngorongoro crater (Lake Magat) and head of the Olduvai Gorge (Lakes Ndutu and Messak) are used to document climatic changes in sub-arid northern Tanzania during the late Pleistocene-Holocene period. The two lakes, which are located on the head of the Olduvai Gorge about 1 km apart and 100 km from the Ngorongoro Crater, were probably once one lake during periods of high precipitation. All four cores were collected using a flow-through type of corer, and sub-sampled every 10 cm with each sample representing a homogenate of 1 cm.

Two cores (40 cm and 500 cm long) were collected from Lake Magat, and AMS ^{14}C age on total organic matter (OM) for a nearby core collected about 1 m apart indicate that the sedimentation rate at these sites is approximately 17 cm/ka. Assuming that these sites have a constant rate of sedimentation, the analysed long core represents sediments that were deposited during the late Pleistocene-Holocene period.

The $\delta^{13}\text{C}$ for 40 cm long core shows a downcore increase, with δ -values ranging from -21‰ to -12.5‰ . A similar downcore increase in ^{13}C values is observable for the 500 cm long core. Apart from this general trend, this core also shows three peaks of low δ -values centred at 200 cm, 380 cm and 490 cm. A general downcore increase in the ^{13}C for the two cores from the Ngorongoro crater suggests changes in the relative proportion of C_3 and C_4 , probably indicating changes in precipitation and lake levels in the area. High precipitation and lake levels being associated with deposition of OM depleted in ^{13}C . Although, diagenetic changes might have contributed to the observed trend, but a change of up to 7‰ cannot solely be attributed to diagenetic changes. High content of organic carbon and nitrogen in sections enriched in ^{13}C excludes the possibility of diagenetic effects.

Although record from Lake Ndutu is not a continuous one (gaps in between), the $\delta^{13}\text{C}$ values shows a general downcore decrease contrary to the Ngorongoro crater record. This general trend is punctuated by periods of above normal enrichment in ^{13}C , and $\delta^{13}\text{C}$ values are as high as -6‰ . Peaks enriched in ^{13}C probably indicate periods of reduced precipitation, where phytoplankton used dissolved bicarbonate rather than dissolved atmospheric CO_2 . A general downcore decrease may probably indicate either an increase in precipitation over time or diagenetic effects. It has been shown that diagenetic effect is significant in sediments poor in OM [1]. A downcore decrease in $\delta^{13}\text{C}$ values associated with a low contents of organic carbon and nitrogen that shows a downcore decrease, probably is an indication of diagenetic changes. A core from Lake Messak shows near constant $\delta^{13}\text{C}$ values around -19‰ , with exception of two peaks depleted in ^{13}C at about 120 cm and 240 cm. Moreover, the contents of organic carbon and nitrogen for this lake are low relative to other sites. Sections depleted in ^{13}C were

* Only an abstract is given here as the full paper was not available.

probably deposited when lake levels were high as a result of increase in precipitation. ^{210}Pb activity for the upper 50 cm shows that the sediments from Lake Ndutu have been recently deposited while that of Lake Messak are older. Owing to the lack of good chronology, inter-core correlation is not possible. However, all three long cores point to a significant change in paleoclimatic conditions that were most likely associated with changes in the vegetation cover.

REFERENCE

- [1] ALTABET, M.A., MURRAY, D.W., and PRELL, W.L., Climatically linked oscillations in Arabian Sea denitrification over the past 1 m.y.: Implications for the marine N cycle. *Paleoceanography* (1999) **14** 732-743.

STABLE ISOTOPE COMPOSITION OF INORGANIC CARBONATES FROM LAKE ABIYATA (ETHIOPIA): ATTEMPT OF RECONSTRUCTING $\delta^{18}\text{O}$ OF LAKE SURFACE WATER AND IMPLICATIONS FOR PALAEOHYDROLOGICAL CHANGES DURING THE HOLOCENE

E. GIBERT

Equipe «Hydrologie, Paléohydrologie, Paléoenvironnement,
Université Paris-Sud, Orsay, France

Y. TRAVI

Laboratoire d'Hydrogéologie, Faculté des Sciences d'Avignon,
Avignon, France

M. MASSAULT

Equipe Hydrologie, Paléohydrologie, Paléoenvironnement,
Université Paris-Sud, Orsay, France

T. CHERNET

Addis-Ababa, Ethiopia

Abstract. Due to the sensitivity of its regional climate to the African monsoon seasonal shifting, Ethiopia has been designated as a key site for palaeoenvironmental reconstructions mainly within the IGBP-PAGES-PEPIII programme. Under the French-Ethiopian ERICA project, we focused on Lake Abiyata located in the Ziway-Shala basin (Central Ethiopia) which has experienced several lacustrine highstands during the Late Pleistocene and Holocene. At present, Lake Abiyata is a closed lake with a very flat catchment area, and corresponds to a half, deep graben infilled by 600-m of sedimentary deposits. In 1995, a 12.6-m-long sequence ABII was cored in Lake Abiyata. A reliable ^{14}C -AMS chronology was defined on both organic matter and inorganic carbonates. Both the modern hydrogeological and geochemical balances of the “groundwater-lake” system indicate that (i) carbonate crystallization mainly occurs at the water-sediment interface via the mixing of lake water and ^{14}C -depleted groundwaters, and that (ii) modern algae form in equilibrium with the atmospheric reservoir. Phytoplankton is thus considered as an authigenic material, and Core ABII has registered 13,500 cal. yr B.P. of environmental history. The evidence of calcite precipitation at the water-sediment interface calls into question the direct palaeoclimatic reconstruction based on inorganic carbonates. Since the evolution of isotopic contents of carbonates might be linked to the variable proportion of the “lake/groundwater” end-members in the mixing, calculations based on isotopic mass balance models may allow for the reconstruction of $\delta^{18}\text{O}$ composition of the lake water. Two major changes can be highlighted: (i) the ~12,000-5500 cal. yr B.P. period is associated to low ^{18}O contents of lake water, and corresponds to an open hydrological system, with a high lacustrine phytoplanktonic productivity, and (ii) from ~5500 cal. yr B.P. to Present, regressive conditions are suggested by the $\delta^{18}\text{O}$ enrichment of the lake water, indicating more arid conditions and the closure of the lake.

1. INTRODUCTION

Despite complex meteorological features [1-3], and specific hydrological and geochemical processes and evolutions in lakes linked to intense volcano-tectonic activity, East Africa remains a key site for palaeoenvironmental reconstructions mainly under the IGBP-PAGES programme/PEP III transect (see for previous works: e.g. [4-8]) since (i) it is influenced by the present-day monsoonal circulation and (ii) long-term rainfall variations can be related to global climatic fluctuations, with major changes in atmospheric circulation and/or moisture balance [9-10].

Pluridisciplinary studies already conducted on the four Ziway-Langano-Abiyata-Shala lakes (*i.e.* Ziway-Shala basin, East Ethiopian Rift) have highlighted several lacustrine transgressive/regressive phases during the Late Pleistocene-Holocene period [4-6].

Under the French-Ethiopian Project ERICA ("Environmental Research for Intertropical Climate in Africa"), a coring campaign was initiated in 1995 on Lake Abiyata deposits. Both hydrological and hydrochemical balances of the lake were firstly defined [11]. Then, 12.5-m-long sedimentary sequence (*i.e.* Core ABII) was sampled and firstly investigated for the establishment of ^{14}C datings performed on both carbonated deposits and organic materials. Both hydrological and hydrochemical balances of the lake were defined, and the comparison of carbonates- and organic-inferred ^{14}C chronologies highlighted a constant discrepancy between the 2 chronologies, the ^{14}C time-scale on carbonates being always older by 200 to 600 yr than the one on organic matter [12]. Once this anomaly explained by calcite precipitation at the lake-sediment interface where a mixing between the lake water and ^{14}C -depleted groundwater occurs, we focused on the interpretation of stable isotopes contents of inorganic calcite in terms of palaeohydrological changes, since the main problem encountered in palaeoclimatic reconstructions remains the establishment of quantified data to be integrated in regional and global climatic models.

We thus present here:

1. the stable isotopes profiles of inorganic carbonates from Core ABII, and
2. the step-by-step carbon and water mass balance models established in order to define the stable isotope characteristics of the mixed water (*i.e.* lake-sediment interface),

with the aim of reconstructing the isotopic composition of Lake Abiyata surface water.

2. GEOLOGICAL AND CLIMATOLOGICAL SETTINGS

The four lakes Ziway, Langano, Abiyata, and Shala belong to a 100-km-long and 40-km-wide, NNE-SSW-trending faulted and caldera-bearing system located in the axial zone of the Main Ethiopian Rift between 7° and 8°30' Latitude N (Figure 1). This complex basin is bounded to the East by the Sountheastern Plateau including the Arussi-Bale Massif, and in the West, by the Ethiopian Shewan Plateau.

Lake Abiyata (7°40'N, 38°40'E ; 1500 masl ; Figure 1) corresponds to a half, deep graben. Its catchment area is limited to the east by the NNE-SSW faults of the Katlo horst, and to the West by the volcanic systems linked to the Shala volcano. Its northern shore opens on the Bulbula alluvial plain where the thickness of lacustrine and alluvial deposits can reach 600 m [13]. The western and southwestern margins of Lake Abiyata have shown volcanic activities at 0.18 Ma. Since then, only very slight tectonic movements from the NNE fault system during the Holocene are suspected [13], in agreement with the eastward migration of tectonic activity of the East African Rift. Despite the fact that intense geothermal activity is observed at the Corbetti and Aluto volcanic centers, geothermal springs do not influence Lake Abiyata basin.

The regional climate is of tropical monsoonal type, and the pluviometric regime is driven by the yearly oscillation of the intertropical convergence zone (ITCZ), which determines a warm-wet summer (maximum rainfall from June to September) and a dry, cold and windy winter. The mean annual precipitation amount varies between 1050 and 750 mm from the

plateau to the plain, while the mean annual temperature evolves from 20 to 22°C at the lakes level [14]. Lake Abiyata is presently situated at the limit between the unimodal (e.g. Addis-Ababa station; [10, 15], and bimodal rainfall cycles, the latter system inducing a second, short rainfall season in March-April [14].

3. MODERN HYDROLOGICAL SYSTEM

3.1. Surface water

Mainly developed upstream, a simple surface network connects the 3 northern lakes of the basin via the Horakelo River from Lake Ziway to Lake Abiyata, and the Bulbula River from Lake Ziway to Lake Langeno (Figure 1). Lake Abiyata thus represents the terminal lake of the Ziway-Langeno-Abiyata sub-system since no present-day surface connection exists between Lake Abiyata and Lake Shala.

At present, strong evaporative conditions prevail, and Lake Abiyata surface waters are of alkaline- to highly alkaline-type chemical facies, due to the unbalanced initial stage between HCO_3^- and concentrations in earth alkali elements [11].

3.2. Groundwater

The lacustrine sedimentary basement of Lake Abiyata basin is characterized by a multilayered aquifer, in which 2 main levels are exploited: (i) the shallow aquifer of the Bulbula Plain connected to the lake and supporting most of the village water-supply wells, and (ii) a deeper system exploited by the Soda Ash Plant borehole. Despite some clayey lens which can cause the deeper aquifer to be locally confined, these 2 producing levels can be considered as hydraulically connected at the basin scale. Groundwater flowpaths move towards Lake Shala, which has the lowest elevation (1550 m) [14].

At sampling time, the *in-situ* parameters of the deep aquifer connected to the lake *via* the lake bottom in the 600-m infill of Lake Abiyata basin were as follows: pH = 8.69; TC = Total Carbon content = $1.03 \cdot 10^{-2}$ mole.L⁻¹.

3.3. Modern geochemical and stable isotope data

1. At sampling time (11/1995), *in-situ* geochemical parameters of Lake Abiyata surface water were as follows: T=Temperature = 22°C; Electrical Conductivity = EC = 25.5 mS.cm⁻¹; pH = 10.1 and TC = $1.85 \cdot 10^{-1}$ mole.L⁻¹. The corresponding long-term $\delta^{13}\text{C}_{\text{TDIC}}$ and $\delta^{18}\text{O}$ values are +3.5‰ vs PDB, and comprised between +7.5 and +9.0‰ vs SMOW respectively (Y. Travi, pers. Comm.) [16]. Since the ^{18}O contents fluctuate according (1) the geography (distance to the shore, sampling depth, distance to river mouths), and (2) the meteorology (yearly rainfall amount, evaporation), a mean $\delta^{18}\text{O}$ value of +8‰ vs SMOW is considered as representative of the lake water at the core site [11, 14].
2. Knowing that precipitation isotopic signature is homogeneous when entering the Rift Valley, the comparison with data from nearby meteorological stations, mainly Awasa station [15] indicates that present-day yearly rainfalls have a modern mean composition of about -2‰ vs SMOW.
3. For the deep aquifer, the buffered values obtained from the Kertefa borehole drilled in the central part of the Bulbula plain were chosen for the calculation: TC = $1.03 \cdot 10^{-2}$ mole.L⁻¹; $\delta^{13}\text{C}_{\text{TDIC}}$ = -2.5‰ vs PDB; $\delta^{18}\text{O}$ = -2.0‰ vs SMOW; A^{14}C = 62.2 pMC.

4. MATERIALS AND METHODS

4.1. Materials

The 12.6-m piston-cored sequence ABII was cored under a well-mixed 7-m water column in 1995 from the southeastern part of Lake Abiyata (core ABII), and as far as possible from former and modern rivers to avoid detrital inputs (Figures 1 and 2a). The core consists mainly of shell-free, homogeneous clayey and organic muds, alternating with sandy marls, either finely or coarsely laminated (Figure 1). Organic matter and carbonates, under calcite or Mg-calcite form, are present along the whole core, and the increase in the number of tephra layers downwards correlates to increasing numbers of coarse sandy layers.

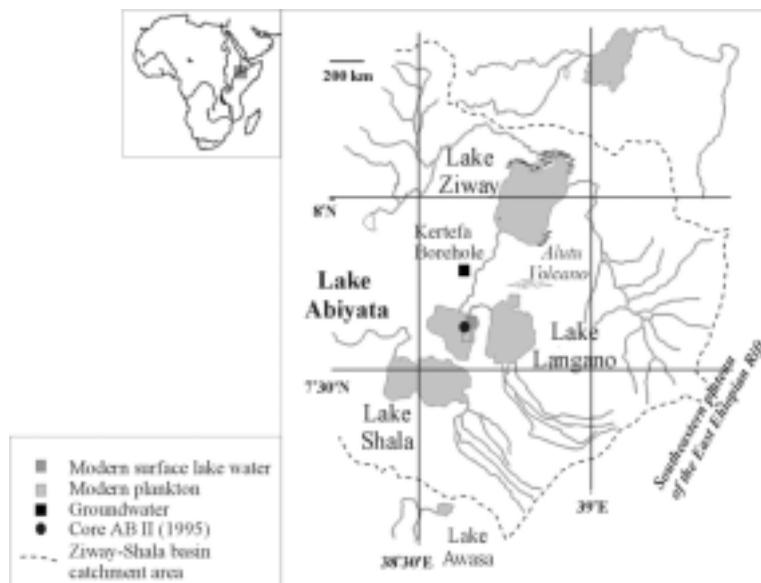


FIG. 1. Location of Lake Abiyata (Ziway-Shala basin, Central Ethiopia), of water samples and of lacustrine Core ABII (1995).

The modern sedimentation of Lake Abiyata is dominated by lacustrine organic matter in relation to an intense primary productivity. Its reduced catchment area and the lack of inflowing rivers preclude inputs of important detrital vegetation debris, and reduce the sedimentation of pedogenetic organic matter. Palynofacies analyses of organic compounds show that sediments mainly consists on phytoplanktonic organic matter (almost 90% of plankton at the core top), while ligno-cellulosic debris are almost absent from the samples (<1%), showing the lack of input from emergent plants or local vegetation growing around the lake. Moreover, radiocarbon activities of modern lake waters (^{14}C Activity=111.6 pMC; $\delta^{13}\text{C}_{\text{TDIC}}=+3.5\text{‰}$ vs PDB) and plankton (^{14}C Activity=111.4 pMC; $\delta^{13}\text{C}=-21.5\text{‰}$ vs PDB), at sampling time demonstrate the equilibrium of the Total Dissolved Inorganic Carbon (TDIC) with both the atmospheric reservoir and the organic matter. This allows for the phytoplankton to be considered as an authigenic material.

Modern inorganic carbonates crystallize at the lake water/sediment interface, where a mixing occurs between the sodi-carbonated lake water and the ^{14}C -depleted, but relatively Mg-Ca-enriched groundwater [12, 17]. The participation of this groundwater remains the only possible source of 1) enough ^{14}C -low dissolved calcium to allow for calcite precipitation, and 2) enough ^{14}C -low activity carbon *via* the calco-carbonic system to account for the ageing of the inorganic carbonated fraction.

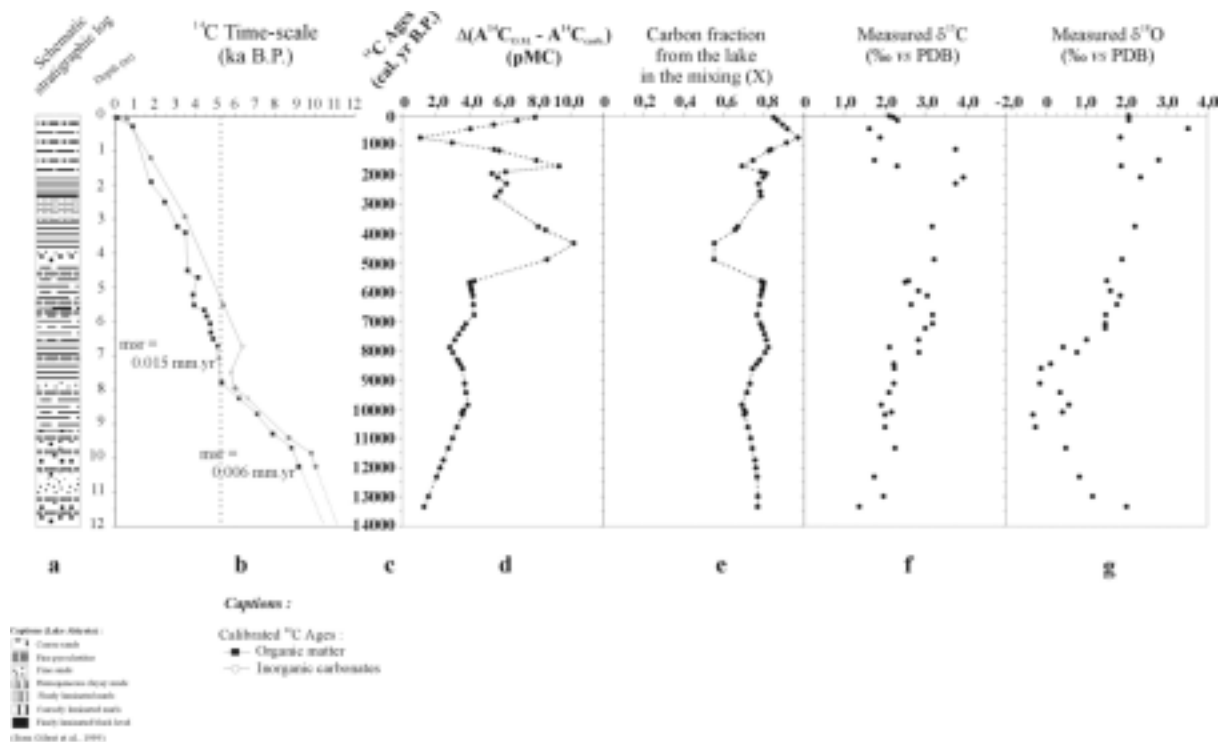


FIG. 2. Lake Abiyata, a.) Schematic stratigraphic log; b.) Calibrated ^{14}C datings on organic matter (black squares) and inorganic carbonates (empty circles), plotted against Core ABII depth; c.) Calibrated ^{14}C time-scale as defined on organic matter; d.) Discrepancy between ^{14}C activities on organic matter and carbonates respectively; e.) Calculation of the carbon fraction from the lake water in the mixing at the water-sediment interface; f) Measured $\delta^{13}\text{C}$ on inorganic carbonates (‰ vs PDB); g.) Measured $\delta^{18}\text{O}$ on inorganic carbonates (‰ vs PDB).

The AMS- ^{14}C the time-scale defined on organic matter samples on the upper 11-m of Core ABII is thus considered as the “reference” time-scale, showing that the whole Holocene period (ca. 13,500 cal yr B.P. to Present; Figures 2b and 2c) is registered in Core ABII with a mean sedimentation rate of about 1.1 m/ka [12].

4.2. Methods- analysis and mass balance calculations

Both $^{13}\text{C}/^{12}\text{C}$ and $^{18}\text{O}/^{16}\text{O}$ ratios were determined on inorganic carbonates at specific levels (Figures 2f and 2g), the removal of the low organic content having been achieved through a weak H_2O_2 -leaching. Carbonated samples were then transfer to CO_2 gas by acid attack (concentrated H_3PO_4 acid). Isotopic results are expressed in δ values (‰ deviation of $^{13}\text{C}/^{12}\text{C}$ and $^{18}\text{O}/^{16}\text{O}$ ratios with reference to the PDB standard). Uncertainties are of 0.1 ‰ vs PDB for both isotopic ratios.

The choice of samples as well as the laboratory treatment for ^{13}C contents and AMS- ^{14}C analyses for both inorganic carbonates and organic matter had been already described [12]. Graphite sources were prepared in the Laboratory of Hydrology and Isotope Geochemistry in Orsay (France), and counted with the accelerator mass spectrometer (Tandem facility) of Gif-sur-Yvette (France). Analytical errors on measured ^{14}C activities, including laboratory errors, are comprised between 0.5 and 0.8 pMC.

4.2.1. Carbon-14 – Definition of X, carbon contribution of the lake water in the mixed water

The calculation of the initial ^{14}C activity of inorganic carbonates is reached *via* the ^{14}C activity of organic samples considered as true activities [12] (Figure 2d).

$$^{14}\text{C } A_{\text{mixed water}} = ^{14}\text{C } A_{\text{measured on carbonates}} / e^{-\lambda \cdot t \text{ (O.M.)}} \quad (1)$$

$$\text{and } N_{\text{mixed water}} = (1/\lambda) * (A_{\text{mixed water}}/100) * 13.56 \text{ for 1 g of carbon} \quad (2)$$

$$\text{then } N_{\text{mixed water}} = (1/\lambda) * ([^{14}\text{C } A_{\text{measured on carbonates}} / e^{-\lambda \cdot t \text{ (O.M.)}}] / 100) * 13.56 \quad (3)$$

Then, a simple mass balance equation can be formulated to extract X, carbon contribution of the lake in the mixing :

$$N_{\text{mixed water}} = X * N_{\text{lake water}} + (1-X) * N_{\text{groundwater}} \quad (4)$$

Knowing that :

$$N_{\text{lake water}} = (1/\lambda) * (A_{\text{lake water}}/100) * 13.56 \text{ for 1 g of carbon}$$

$$\text{And } N_{\text{groundwater}} = (1/\lambda) * (A_{\text{groundwater}}/100) * 13.56 \text{ for 1 g of carbon}$$

$$N_{\text{mixed water}} = X * [(1/\lambda) * (A_{\text{lake water}}/100) * 13.56] + (1-X) * [(1/\lambda) * (A_{\text{groundwater}}/100) * 13.56] \quad (5)$$

Combining equations (4) and (5) gives:

$$^{14}\text{C } A_{\text{mixed water}} = X * ^{14}\text{C } A_{\text{lake water}} + (1-X) * ^{14}\text{C } A_{\text{groundwater}} \quad (6)$$

Integrating equation (1) in equation (6) gives:

$$^{14}\text{C } A_{\text{meas. on carbonates}} / e^{-\lambda \cdot t \text{ (O.M.)}} = X * ^{14}\text{C } A_{\text{lake water}} + (1-X) * ^{14}\text{C } A_{\text{groundwater}} \quad (7)$$

Then (Figure 2e) :

$$X = [^{14}\text{C } A_{\text{meas. on carbonates}} / e^{-\lambda \cdot t \text{ (O.M.)}}] / [^{14}\text{C } A_{\text{lake water}} - ^{14}\text{C } A_{\text{groundwater}}] \quad (8)$$

At that step of the calculations, all the above-mentioned equations are independent from pH and temperature.

4.2.2. Oxygen-18– $\delta^{18}\text{O}_{\text{lake water}}$ reconstruction

The use of measured $\delta^{18}\text{O}$ values of inorganic carbonates for the reconstruction of the ^{18}O content of the lake water requires to transfer X (carbon contribution of the lake in the mixed water) to X' (water fraction of the lake water in the mixed water; Figure 3).

Considering that the equilibrium between the TDIC (Total Dissolved Inorganic Carbon) content of the lake surface water and the atmospheric CO_2 remained constant through time, the respective water fractions of lake and of groundwater in the mixing, weighted by their respective carbon contributions *via* their TC expressed in mole.L^{-1} , can be stated as follows:

$$\text{TC}_{\text{lake water}} * X' = X * \text{TC}_{\text{mixed water}}$$

$$\text{TC}_{\text{groundwater}} * (1-X') = (1-X) * \text{TC}_{\text{mixed water}}$$

Considering all the modern geochemical data sets available for the Ziway-Shala basin [11, 14], Figure 3 gathers isotopic profiles plotted against the calibrated AMS- ^{14}C O.M.-time-scale, and calculated with the following parameters entering the model at equations (4), (13), (15) and (16) respectively: $A^{14}\text{C}_{\text{Groundwater}} = 62.2 \text{ pMC}$; $\text{TC}_{\text{Groundwater}} = 1.03 \times 10^{-2} \text{ mole.L}^{-1}$ and $\text{TC}_{\text{LakeWater}} = 500 \text{ mg.L}^{-1}$; $T = 22^\circ\text{C}$ (mean annual temperature of the area), and $\delta^{18}\text{O}_{\text{Groundwater}} = -2\text{‰}$ vs SMOW.

The interpretation of the profiles are complex. Nevertheless, the results show that:

- a. From the core base to 1115 cm (13,500~ 12,700 cal. yr B.P.), the values are enriched and almost equals to that of the present-day Lake Abiyata, and seems to indicate a *Closed Lake System* status.
- b. The lowest isotopic contents of Lake Abiyata surface water (mean value of +1‰ vs SMOW) are observed from 1115 to 870 cm (~12,000~5500 yr B.P.), although interrupted by a short-term ^{18}O -enriched phase at around 10,000 cal. yr B.P. These low ^{18}O contents likely indicate more humid conditions. Lake Abiyata reconstructed ^{18}O contents are comprised between the ^{18}O contents of modern rainfall (i.e. -2 ‰ SMOW) and that of modern Lake Ziway (~+4‰ SMOW). Although we are far to directly reconstruct the “Precipitation-Evaporation” ratio at that step of the study, this suggests that during this phase, Lake Abiyata was reacting as the modern shallow Lake Ziway, i.e. an open lake probably more extensive and less influenced by evaporation processes.
- c. The highest values of $\delta^{18}\text{O}_{\text{Lake Water}}$ are situated from 870 cm to the core top (~5000 cal. yr B.P. to Present), with clear, sharp fluctuations at the core top (~2000 cal. yr B.P. to Present.), suggesting strong evaporative processes, and a higher residence time of the lake water, indicating likely a progressive evolution to a smaller lake alternatively open and closed. This hypothesis is in agreement with previous studies of the lake shorelines having evidenced a negative hydrological balance and regressive climatic conditions at that time [4-5]. This also agrees with on-going works on stable isotope contents of the fossil organic matter, showing very high $\delta^{15}\text{N}$ values attributed to the hyper-alkalinisation of the surface water after the closure of the lake, and the use of DIN instead of air nitrogen by the phytoplanktonic O.M. [19].

6. UNCERTAINTIES

As already mentioned, the reconstructed stable isotope contents of the mixed water, and consequently results on the calculated ^{18}O content of the lake water, refer to the following conditions:

* For carbon-14 equations (i.e. carbon fraction reconstruction):

- i. taking into account constant values of ^{14}C activities for both lake surface water and groundwater (^{14}C activity could be higher at the time of lacustrine highstand, distance and transit time being reduced on the catchment);
- ii. considering no Suess effect [20], which means a constant atmosphere activity (and then a constant ^{14}C $A_{\text{lake water}}$) during the pre-bomb period (100 pMC; pre-bomb year = 1950);

* In addition, for the ^{18}O mass balance model :

- i. taking into account constant Total Carbon contents through time (assumption *Open Lake System/Closed Lake System*) ; considering the data already gathered for recent periods (Chernet, 1982), this Total Carbon content could be 10 times lower than that of a smaller lake ;
- ii. Assuming a constant $\delta^{18}\text{O}$ value for groundwater through time, although the rainfall signal could have been slightly varying with respect to climatic changes;
- iii. estimating that calcite precipitation occurs in equilibrium with the mixed water at the lake-sediment interface ;
- iv. considering the fractionation factor definition between inorganic calcite and HCO_3^- for temperature between 0 and 35°C [18] ;
- v. taking into account any pH fluctuations through time (*i.e.* the whole lake water carbon content being assumed to be under HCO_3^- form) ; this last assumption is generally true except for highly concentrated water.

The main uncertainties remain the Total Carbon content and the $\delta^{18}\text{O}$ values for both lake and groundwater. Although we cannot constrain the model all the hypothesis at that step of the reconstruction, some experiments can be made on the two above-mentioned parameters, and also with varying temperatures.

1. The first calculation refers to the temperature, evolving from 15 to 25°C , with $\delta^{18}\text{O}_{\text{Groundwater}}$ as constant (*i.e.* -2.0‰ vs SMOW). The minimum and maximum δ -standard deviation are 2.3 and 3.9 ‰ vs SMOW respectively, with respect to the profile defined with present-day of temperature (20°C) and isotopic values of groundwater (-2‰ vs SMOW) (cf. Figure 3d).
2. The second calculation refers to $\delta^{18}\text{O}_{\text{Groundwater}}$ (constant temperature = 20°C) which varies between 0 and -4‰ vs SMOW, these values having been chosen with reference to present-day precipitation (uncertainties of $\pm 2\text{‰}$ vs SMOW). Resulting calculations give minimum and maximum standard deviation of 0.1 and 2.8 vs SMOW respectively, again with respect to the profile defined with present-day of temperature (20°C) and isotopic values of groundwater (-2‰ vs SMOW) (cf. Figure 3d).
3. More importantly, and according previous studies [11-12, 14], two cases can be envisaged in relation with the two extreme values of $\text{TC}_{\text{lake water}}$ deduced from the modern hydrological behaviour of the basin, and which can be introduced in the ^{14}C model: (i) the modern geochemical evolution of Lake Ziway ($\text{TC}=500 \text{ mg.L}^{-1}$) which can be considered as representing an *Open Lake System* status (Figures 3c and 3d), and (ii) the present-day parameters measured for Lake Abiyata ($\text{TC}=7000 \text{ mg.L}^{-1}$) likely representing the *Closed Lake System* end-member (Figures 3e and 3f). These two poles are considered as reflecting the evolution of Lake Abiyata through time, and are of high importance when calculating the water fraction X' of the lake in the mixing.
 - **Case 500 mg.L^{-1} :** Despite the few data available so far, the way of reconstructing the ^{18}O contents of the lake surface water with a corresponding TC of 500 mg.L^{-1} seems to be correct since our simple model which takes into account the participation of the groundwater makes

the top-most $\delta^{18}\text{O}$ values to range from +7.5 to 8.7 ‰ vs SMOW, and to be similar to that of modern Lake Abiyata (Figure 3d).

- **Case of 7000 mg.L⁻¹:** On the opposite, the values found for the reconstruction with a TC of 7000 mg.L⁻¹ for the lake water do not correspond to already natural observed value, except for Lake Chad [21] where the super-evaporation of the lake can conduct to enriched $\delta^{18}\text{O}$ values up to 35 ‰ (Figure 3f). This could envisaged only if the lake was completely confined without groundwater input. The values up to 35‰ could be reached if groundwater level was strongly decreasing. However, this does not correspond to the present-day hydrogeological situation. Nevertheless, other hypothesis can be envisaged to explain these discrepancies: (i) the increase in primary productivity, this increase biasing the lake water proportion in the mixing and its TC content ; (ii) the mixing of chemically very different water, this phenomenon implying reversal chemical evolution and a different remaining solution at one given time “+1” ; (iii) the hypothesis of the assimilation of concentration (*i.e.*[C]) and ionic activity in an *Open Lake Status* cannot be taken into account in a *Closed Lake System* since [C] is then completely different from the ionic concentration.

7. CONCLUSION

As a conclusion, the reconstruction of the stable isotope contents of the mixed water, and consequently results of the calculated ^{18}O content of Lake Abiyata surface water allow for a new description of the lake evolution, which takes into account the groundwater influence. The results based on several assumptions could be improved by using, for simulations, specific values at different levels of the core, considering the regional evolution of precipitation, and the related hydrogeological behavior of the Ziway-Shala basin. (better definition of the $\delta^{18}\text{O}_{\text{Groundwater}}$). This will be possible as these investigations enter in a multidisciplinary study of Lake Abiyata, and in the next future, they will be compared to other proxies, both bio-indicators or geochemical parameters, such as the diatom-inferred pH and salinity [22], and the stable isotope contents of organic deposits [19].

REFERENCES

- [1] NICHOLSON, S.E., “A Review of Climate Dynamics and Climate Variability in Eastern Africa”, Johnson TC, Odada E, (Eds), The Limnology, Climatology and Paleoclimatology of the East African Lakes, The Netherlands, Gordon and Breach Publishers (1996) 25-56.
- [2] BERGONZINI, L., “Bilans hydriques de lacs (Kivu, Tanganyika, Rukwa et Nyassa) du Rift Est-Africain“ Musée Royal de l’Afrique Centrale, Tervuren, Belgique, Geological Sciences **103** (1999) 183 p.
- [3] BERGONZINI, L., et al., “Bilans hydrologiques et isotopiques (^{18}O et ^2H) du lac Massoko, Tanzanie. Quantification des échanges lac-eaux souterraines“, Comptes Rendus de l’Académie des Sciences de Paris (2001, in press).
- [4] GASSE F., STREET, F.A., “Late Quaternary lake-level fluctuations and environments of the northern Rift Valley and Afar region (Ethiopia and Djibouti)”, Palaeogeography, Palaeoclimatology, Palaeoecology **25** (1978) 145-150.

- [5] STREET, F.A., "Chronology of Late Pleistocene and Holocene lake-level fluctuations, Ziway-Shala Basin, Ethiopia", Leakey RE, Ogot BA", (Eds), Proceedings of the 8th Panafrican Congress of Prehistory and Quaternary Studies, Nairobi, September 5-10 (1981) 143-146.
- [6] GILLESPIE R., et al., "Post-glacial arid episodes in Ethiopia have implications for climate prediction", Nature **306** (1983) 680-683.
- [7] BONNEFILLE. R., et al., "Palaeoenvironment of Lake Abijata, Ethiopia during the past 2000 years" In Forstick L.E. *et al.* (Eds), Sedimentation in the African Rifts, London, Geol. Soc., Spec. Paper, **25** (1986) 253-265.
- [8] JOHNSON, T. C., "Sedimentary processes and signals of past climatic change in the large lakes of the East African Rift Valley", Johnson TC, Odada E, (Eds), The Limnology, Climatology and Paleoclimatology of the East African Lakes, The Netherlands, Gordon and Breach Publishers (1989) 367-412.
- [9] WEBB T. III, et al., "Climate changes during the past 18,000 years: regional syntheses, mechanisms, and causes", Wright HE Jr, editors, Global Climate since the Last Glacial Maximum, USA, University of Minnesota Press (1993) 569p.
- [10] ROZANSKI, K., et al., "Isotope patterns of Precipitation in the East African Region", Johnson T.C. and Odada E., (Eds.), The Limnology, Climatology and Paleoclimatology of the East African Lakes, Gordon and Breach, Amsterdam (1996) 79-93.
- [11] TRAVI, Y., et al., "Study of hydrological behaviour of the Lake Region in the Ethiopian Rift, using hydrological, hydrochemical and isotopic data : palaeohydrological implications", Meeting on Volcanisme, Rifting et Paléoclimats dans le Rift Ethiopien et la Dépression de l'Afar, Addis-Ababa, Ethiopia, 3-16/02/1997 (1997) 36.
- [12] GIBERT E., et al., "Comparison between carbonate and organic AMS ¹⁴C ages in Lake Abiyata sediments (Ethiopia): hydrochemistry and palaeoenvironmental implications", Radiocarbon **41**(3) (2000) 251-266.
- [13] LE TURDU C., et al., "The Ziway-Shala basin system, Main Ethiopian Rift, East Africa. Mechanisms of basin formation and sediment accumulation. Implications for a lake drilling project", Palaeogeography, Palaeoclimatology, Palaeoecology **150**(1999) 135-177.
- [14] CHERNET, T., "Etude des mécanismes de minéralisation en fluorure et éléments associés de la région des lacs du Rift Ethiopien », PhD Thesis, Université d'Avignon (1998) 203 pp.
- [15] WMO/IAEA/GNIP NETWORK, "Statistical Treatment of Data on Environmental Isotopes in Precipitation", IAEA (Vienna, Austria)/WMO (Eds.), World Survey of Global Network for Isotopes In Precipitation, Nr 311 (2001).
- [16] CHERNET, T., "Hydrogeology of the Lakes Region, Ethiopia" Ministry of Mines and Energy, Ethiopian Institute of Geological Surveys, Mem. **7** (1982) 97p.
- [17] TALBOT, M.R., "A review of the palaeohydrological interpretation of carbon and oxygen isotopic ratios in primary lacustrine carbonates", Chemical Geology (Isotope Geoscience Section) **80** (1990) 261-279.
- [18] MOOK, W., "Carbon-14 in hydrogeological studies", Hanbook of Environmental Isotope Geochemistry, P. Fritz & J.-Ch. Fontes (Eds), The Terrestrial Environment, Elsevier, The Netherlands (1980) 49-71.
- [19] GIBERT, E., et al., "Stable isotope composition of fossil organic matter and inorganic carbonates from Lake Abiyata (Ethiopia). Comparison and implications for palaeoenvironmental changes during the Holocene", in prep.
- [20] SUESS, H.E., "Radiocarbon concentration in modern wood", Science **122** (1955) 415-417.

- [21] CLARK, I., FRITZ, P., "Environmental Isotopes in Hydrogeology", Clark, I. & Fritz, P. (Eds), Lewis Publishers, New York (1997) 327p.
- [22] CHALIE, F., GASSE, F., "A ~13,000 year diatom record of water chemistry and lake level change from the tropical East African rift Lake Abiyata (Ethiopia)", *Palaeogeography, Palaeoclimatology, Palaeoecology* (International Congress on Palaeolimnology, Special Issue), submitted (2001).

$\delta^{15}\text{N}$, $\delta^{13}\text{C}$ AND RADIOCARBON IN DISSOLVED ORGANIC CARBON AS INDICATORS OF ENVIRONMENTAL CHANGE

S. GEYER*

UFZ-Centre for Environmental Research Leipzig-Halle,
Department for Hydrogeology, Halle, Germany

K. KALBITZ

University of Bayreuth, Bayreuth Institute for Terrestrial Ecosystem Research (BITOEK),
Department of Soil Ecology,
Bayreuth, Germany

Abstract. Decomposition, humification, and stabilization of soil organic matter are closely related to the dynamics of dissolved organic matter. Enhanced peat decomposition results in increasing aromatic structures and polycondensation of dissolved organic molecules. Although recent studies support the concept that DOM can serve as an indicator for processes driven by changing environmental processes in soils affecting the C and N cycle (like decomposition and humification) and also permit insight in former conditions some 1000 years ago, it is unknown whether dissolved organic carbon (DOC) and nitrogen (DON) have an equal response to these processes.

1. INTRODUCTION

The main objective of this paper is the question if a change in the degree of humification of DOM caused by different environmental conditions in a recent fen area is linked with different dynamics of DOC and DON as a basis for interpretation of carbon and nitrogen isotopes of DOM in older groundwater [1].

As a first step we tested this hypothesis by analyzing DOC and DON concentrations of topsoils, groundwater and surface water of six differently used sites in a fen area. Furthermore, the degree of humification of DOM as deduced from synchronous fluorescence spectra were related to the natural variation of carbon (^{13}C , ^{14}C) and nitrogen (^{15}N) isotopes of DOM [5].

2. RESULTS AND DISCUSSION

We detected differences in the isotope signature between carbon and nitrogen at different stages of humification (Fig. 1). The degree of humification of soil organic matter was found to be not crucial for both DOC and DON release. Intact peatlands (low degree of decomposition and humification) favour the release of DOC whereas degraded peatlands (high degree of decomposition and humification) favour the release of DON.

DOC concentration in topsoil, groundwater and surface water depends on soil organic carbon content and therefore on the degree of peat decomposition. Whereas the inorganic N pool is more important for DON release than the whole organic N pool.

* Email: geyer@hdg.ufz.de.

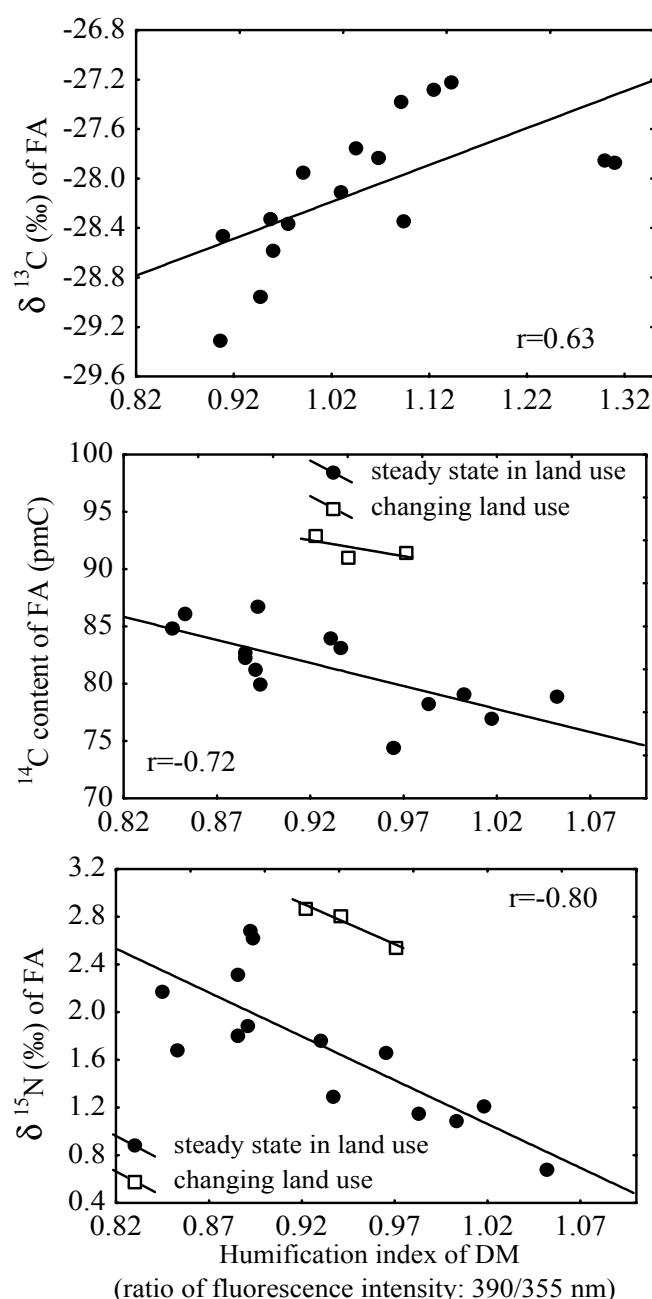


FIG. 1. Dependence of $\delta^{13}\text{C}$ ratio (topsoil water-soluble FA), ^{14}C content (groundwater FA) and $\delta^{15}\text{N}$ ratio (groundwater FA) on the humification index of DOM.

DOC and DON showed a similar dynamic after a short-term land-use change from crop production to an unimproved grassland as indicated by unchanged concentrations and humification of DOM and increased ^{14}C and ^{15}N values. A high humification of DOM is linked with a high C turnover and an increased microbial modification and age of DOC but with low $\delta^{15}\text{N}$ ratios. If one considers the promoting effect of inorganic N on DON release we assume that an addition of mineral fertilizer N increases the microbial mobilization of amino acids. These amino acids could be responsible for the low $\delta^{15}\text{N}$ ratios. Furthermore, the condensation of amino acids with carbohydrates to humic substances is accompanied by a high humification of DOM at these sites which got inorganic N fertilizers. However, an incorporation of fertilizer N into the DON fraction can not be excluded. At all, we have to

conclude opposite patterns of DOC and DON at different stages of humification of DOM. Therefore, both DOC and DON have to be considered in studies concerning the dynamic of DOM, especially the humification of DOM.

The degree of humification of soil organic matter is not crucial for both DOC and DON release. The amount of SOM which is, however, dependent on the degree of decomposition determines the release of DOC whereas the inorganic N pool affects the release of DON. Therefore, intact peatlands (low degree of decomposition and humification) favour the release of DOC whereas degraded peatlands favour the release of DON. Humification of DOM did not change after a short-term land-use from crop production to an unimproved grassland. Increased ^{14}C and ^{15}N values showed an equal response of DOC and DON to this land-use impact. A high humification of DOM is linked with a high C turnover and an increased microbial modification and age of DOC but with low $\delta^{15}\text{N}$ ratios. An incorporation of fertilizer N into the DON fraction is not proven but can also not be excluded. It is more likely that an addition of mineral fertilizer N increases the microbial mobilization of amino acids followed by a condensation with carbohydrates to humic substances. At all, we have to conclude opposite patterns of DOC and DON at different stages of humification of DOM. Therefore, both DOC and DON have to be considered in studies concerning the dynamic of DOM, especially the humification of DOM.

REFERENCES

- [1] BUCKAU, G., ARTINGER, R., KIM, J. I., GEYER, S., FRITZ, P., WOLF, M., AND FRENZEL, B. Development of climatic and vegetation conditions and the geochemical and isotopic composition in the Franconian Albvorland aquifer system. *Appl. Geochemistry* **15** (8) (2000) 1191-1201.
- [2] GEYER S, WOLF M, WASSENAAR LI, FRITZ P, BUCKAU G, KIM JI. Isotope investigations on dissolved organic carbon (DOC) for ^{14}C -groundwater dating. Vienna: IAEA-SM-329 (1993) 359-380.
- [3] GEYER S, KALBITZ K, GEYER W. The influence of changing land use (intensive to extensive) on the isotopic (^{14}C) and chemical signature of DOC - conclusions for the initial ^{14}C content of DOC for groundwater dating. Vienna: IAEA-SM-349 (1998) 780-785.
- [4] KALBITZ K, GEYER S., GEHRE M. Land use impacts on the isotopic signature (C-13, C-14, N-15) of water-soluble fulvic acids in a German fen area. *Soil Science*, **165**(9) (2000) 728-736.
- [5] KALBITZ K, GEYER S, GEHRE M, GEYER W. Correlation between ^{14}C , ^{15}N , ^{13}C and spectroscopic properties of dissolved humic substances. Vienna: IAEA-SM-361 (1999) 270-271.
- [6] SCHIFF SL, ARAVENA R, TRUMBORE SE, HINTON MJ, ELGOOD R, DILLON PJ. Export of DOC from forested catchments on the Precambrian Shield of Central Ontario: Clues from C-13 and C-14. *Biogeochem.* **36** (1999) 43-65.

NEW ESTIMATES OF OXYGEN ISOTOPE FRACTIONATION BY PLANTS AND SOILS — IMPLICATIONS FOR THE ISOTOPIC COMPOSITION OF THE ATMOSPHERE

A. ANGERT*, B. LUZ

The Institute of Earth Sciences, The Hebrew University of Jerusalem,
Jerusalem, Israel

Abstract. Oxygen concentration and $\delta^{18}\text{O}$ of O_2 have been monitored in light and heavy soils. Steep oxygen gradients were present at the heavy soil site (minimal O_2 concentration was 1% at 150cm depth) and $\delta^{18}\text{O}$ values typically ranged from 0‰ to -1.6‰ relative to air O_2 . In the light-soil site, the O_2 concentration was 20.38% to 20.53% and $\delta^{18}\text{O}$ values ranged from -0.06 ± 0.015 ‰ to 0.06 ± 0.015 ‰ relative to atmospheric O_2 . The fractionation in soil respiration was estimated from the observed $[\text{O}_2]$ and $\delta^{18}\text{O}$ profiles and their change with time by a five-box numerical model. Diffusion due to concentration and temperature gradients was taken into account. Good agreement was found between the model results and the measured values. The average discrimination against ^{18}O in the two study sites was 12 ± 1 ‰. The current understanding of the composition of air O_2 attributes the magnitude of the fractionation in soil respiration to biochemical mechanisms alone. Thus the discrimination against ^{18}O is assumed to be 18‰ in cyanide-sensitive dark respiration and 25‰ to 30‰ in cyanide-resistant respiration. The discrimination we report is significantly less than in dark respiration. This overall low discrimination is explained by slow diffusion in soil aggregates, and in root tissues that results in low O_2 concentration in the consumption site. Since about half of the terrestrial respiration occurs in soils, our new discrimination estimate lowers significantly the discrimination value for terrestrial uptake. Higher than currently assumed discrimination was found in experiments with illuminated plants. This high discrimination might compensate for the low discrimination found in soils.

1. INTRODUCTION

Soil-respiration is a major component of the global carbon cycle and contributes about one third of the global O_2 uptake. Since the uptake rates of various stable oxygen isotopes are different, soil respiration significantly affects the isotopic composition of atmospheric O_2 . The ^{18}O enrichment of air O_2 with respect to ocean water is known as the “Dole effect”. Changes in the Dole effect have been used to infer past variations in the ratio of marine to terrestrial biospheric production, related to past climatic changes [1, 2]. However, in order to derive quantitative estimates, it is necessary to gain better understanding of the basic mechanisms affecting the isotopic composition of O_2 during its photosynthetic production and respiratory consumption.

In recent treatments of past variations in the Dole effect, it was assumed that global terrestrial respiration preferentially discriminates against ^{18}O by 18‰ with respect to ^{16}O [1-3]. This value is based on measurements in isolated plant organs [4, 5]. However, it has been noted [5] that when O_2 diffusion to the consumption site is slow, the discrimination of a system would depend not only on the discrimination in the consumption process but also on the discrimination in diffusion, and on the relative rates of consumption and diffusion. In an extreme case where diffusion is very slow in comparison to respiration, oxygen level in the consumption site is near zero, and any O_2 entering is immediately respired. The discrimination in this case is the discrimination in diffusion since no discrimination in respiration takes place.

Bender et al. [1] recognized the role of diffusion limitation on oxygen isotope discrimination in their treatment of the Dole effect. They suggested that in the ocean the role of diffusion

* Email: alon_a@mail.com.

limitation is negligible, because most of the respiration takes place by small organisms in which the ratio of surface area to volume is large. However, this limitation cannot be neglected in soils in which the O₂ supply to the consumption site is slowed down by low diffusivity of root tissues and soil aggregates. Hence, we expect the overall discrimination against ¹⁸O in soil respiration to be lower than in dark respiration alone (18‰ in cyanide-sensitive respiration [5]). This expectation is strengthened by incubation experiment we conducted with intact roots in which low discrimination were measured [6].

To the best of our knowledge, there is only one previous study in which the $\delta^{18}\text{O}$ of O₂ in soil air was measured [7]. In the present study, the discrimination against ¹⁸O in soil respiration has been evaluated by monitoring [O₂] and $\delta^{18}\text{O}$ in two sites with heavy and light soils. To this end the soil air was sampled in the upper 1.5m of the soil, where most of the biological activity and respiration take place.

2. METHODS

2.1. The study sites

Two model study-sites were chosen in the coastal plane of Israel. The first was a citrus orchard near Alexander stream. At this site, the soil changes gradually from clay in the top layers to sandy clay loam in the deeper ones, and therefore this site will be referred to as the “heavy-soil site”. In the summer months this orchard is irrigated every second week.

The second site was an avocado orchard located near Caesarea, about 20 km north of the first one. The soil in this site is sandy and it will be referred to as the “light-soil site”. In the summer months this orchard is irrigated every morning.

2.2. Monitoring of soil air

To sample soil air at the heavy-soil site, we have inserted five Nalgene™ tubes (1/16” ID, 1/8” OD) at evenly spaced intervals (30 to 150 cm) in a drilled hole. The hole was filled with alternate layers of sand and bentonite clay in such a way that the opening of each tube was centered in a 10-cm layer of sand. The sand layers ensured easy pumping of air from the ground, and the clay layers prevented movement of air from layer to layer during sampling.

In the light-soil site, a stainless steel tube (10mm ID, 12.5mm OD) was inserted into a pilot hole made by hammering a 10mm diameter rod into the soil. The tube end was pointed to ensure easy insertion into the pilot hole, and 2mm diameter holes were drilled above the pointed end for soil air collection. A 7mm-diameter rod inserted inside the tube reduced its dead volume. The soil air was collected from a depth of 90cm.

In the heavy-soil site all samples were measured in duplicate and the average error based on the duplicates was $\pm 0.03\text{‰}$ and $\pm 4\text{‰}$ for $\delta^{18}\text{O}$ and $\delta\text{O}_2/\text{Ar}$ respectively. Due to the very weak signal in the light-soil site, 10 replicates were taken from the sampling depth. The confidence intervals for the light-soil samples were (for 95% confidence level) $\pm 0.015\text{‰}$ for $\delta^{18}\text{O}$ and $\pm 0.8\text{‰}$ for $\delta\text{O}_2/\text{Ar}$.

The diffusivity of the soil (k) was assessed after [8]. The oxygen concentration was evaluated from the ratio of O₂ to Ar, which was determined by mass spectrometric analysis of the same sample used for isotopic analysis. Sample preparation and mass spectrometry was according to [9].

2. RESULTS

Soil air from the heavy-soil site was sampled in two field experiments. In each experiment soil air was sampled over 2-3 days intervals. The first experiment started 10 days after the last irrigation and lasted 3 days. The second experiment started 3 days after a rain event and lasted 8 days. Both experiments ended before the next rain/irrigation event. The results of these experiments are shown in Fig. 1.

Steep O₂ gradients were present at the heavy-soil site. The O₂ concentration in all sampling dates decreased with depth. In both experiments the O₂ concentration increased with time in all depths while the $\delta^{18}\text{O}$ values decreased with time. The $\delta^{18}\text{O}$ profile shows a decreasing trend with depth. In addition to these experiments, soil air was sampled once at 90cm, one day after irrigation and O₂ concentration was very low – less than 3%. The $\delta^{18}\text{O}$ was about 10‰ but due to the very low O₂ concentration, the accuracy of this measured value is less than in the rest of the results.

Two field-experiments were performed in the light-soil site. Soil air was sampled at 90cm depth in a different spot in the orchard for each experiment. In the first experiment soil air was sampled 3, 9 and 21 hours after the irrigation. In the second experiment soil air was sampled 2 and 6 hours after the irrigation. The O₂ concentration in the soil air at all sampling times was 20.38% in the first experiment, and 20.53% in the second. The soil air was enriched in ¹⁸O, on the average, by 0.06‰ relative to atmospheric oxygen in the first experiment and by -0.06‰ in the second, with no significant changes among the different sampling times. The temperature difference between the soil at 90cm depth and the soil surface was 1.4°C to 3.4°C with an average of 2.8°C in the first experiment and 1.6°C to -1.6°C with an average of 0.0°C in the second.

3. DISCUSSION

3.1. Soil air monitoring in the heavy-soil site

In order to evaluate the discrimination in soil respiration, it is first necessary to understand the dynamics of the oxygen in the soil. Two trends in oxygen concentration were observed: 1. A depth-trend of decreasing O₂ concentration with depth due to respiration in the soil and slow replenishment with fresh atmospheric oxygen. 2. A time-trend of increasing O₂ concentration after irrigation that could be explained as follows: irrigation/rain caused a decrease in the air-porosity of the soil, and consequently lowered gas diffusivity. The respiration in the soil combined with very low diffusivity caused lowering of O₂ concentration. As evapotranspiration and drainage removed part of the water, the diffusivity increased and allowed the introduction of fresh oxygen from the atmosphere.

The $\delta^{18}\text{O}$ profile is somewhat surprising because the $\delta^{18}\text{O}$ values decreased with depth. If respiration were the sole important mechanism, an increase in $\delta^{18}\text{O}$ with the decrease in oxygen concentration would be expected. The most probable mechanism that introduced oxygen with an isotopic composition lighter than in air, is diffusion into the soil profile, in which the lighter isotope moves faster (a discrimination of 14.1‰ against ¹⁸O is derived from the theory of binary diffusion of gases [10]). As discussed above, the increase in diffusivity that resulted from drainage of the soil caused a net flux of oxygen from the atmosphere to the soil. This oxygen has light isotopic composition due to the discrimination in diffusion, and hence caused the observed decrease in $\delta^{18}\text{O}$.

The discrimination of the soil can not be evaluated from a simple Raleigh distillation calculation, since the soil air is not a closed system. To estimate the discrimination we used a five box numerical model. In this model the soil profile is divided into five 30cm thick layers. In each layer the balance of ^{16}O and ^{18}O concentrations is calculated, separately for each isotope species, from the diffusion and respiration fluxes by a finite difference approximation. The model time-step was 1/8 hour. In a sensitivity analysis we found that adding more layers to the model, or decreasing the time step, do not significantly change the predicted profile.

To estimate the overall discrimination in the soil, we assumed that the respiration rates, diffusion coefficients, and discrimination in all the layers were constant in the time span between two samplings. By repeated simulation runs we determined the respiration rates (for each layer) that gave the best fit between the observed and the simulated $[\text{O}_2]$ profiles. This rate was then used in similar simulation runs to derive the discrimination value which gave the best fit between the observed and the simulated $\delta^{18}\text{O}$ profiles (Fig. 1).

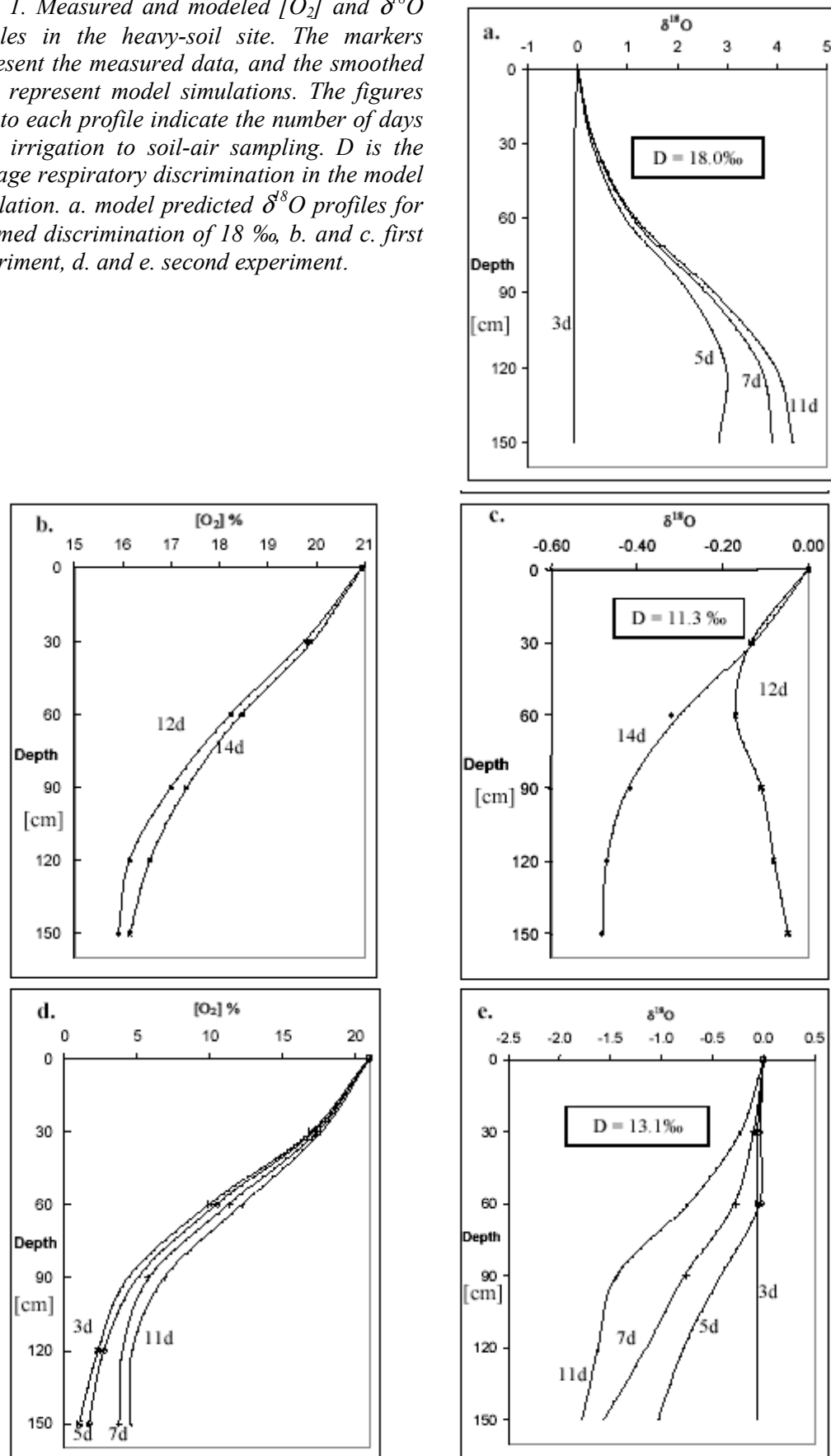
The weighted-average discrimination calculated for all the layers was $11.3 \pm 0.3\%$ for the first experiment, and $13.1 \pm 0.7\%$ for the second (the difference between discriminations found for the different layers was within the error margin). In both cases, the estimated discrimination is much weaker than in dark respiration. The main source of error in calculating the discrimination is the estimated diffusivity of O_2 in the soil. The estimated error is based on assumed relative error in the diffusivity of 50%. In some samples from the second experiment O_2 level was very low, and there was not enough oxygen gas for analysis of $\delta^{18}\text{O}$. However, since the O_2 concentrations were very low, the uncertainty in the initial $\delta^{18}\text{O}$ values did not significantly affect the calculated discrimination.

In the discussion above it was assumed that diffusion and respiration were the only important mechanisms, but three additional mechanisms might affect $[\text{O}_2]$ and $\delta^{18}\text{O}$ in soil: gravitational settling, advection and thermal diffusion. The effect of gravitational settling on $\delta^{18}\text{O}$ is less than 0.01‰ in depth of 1m and can be neglected. Advection can be usually neglected in soils [11] and evidently was not important in our site, otherwise the soil O_2 would not have an isotopic composition lighter than air O_2 . Thermal diffusion will increase $\delta^{18}\text{O}$ at the cold end of a temperature gradient, and in steady state [12]:

$$\Delta\delta^{18}\text{O} = \left(\left(\frac{T_0}{T}\right)^\alpha - 1\right) \cdot 10^3 \quad (1)$$

where α is the thermal diffusion factor (0.0107 after [13]), and T and T_0 are the temperature values at the two ends. A 10°C gradient will generate about 0.4‰ thermal diffusion signal in $\delta^{18}\text{O}$. But, the temperature change in the observed profile, below 20cm, was less than 0.5°C , hence thermal diffusion can be neglected at deeper levels (its effect is about 0.02‰). Steeper gradient was present at the top 20cm ($\sim 4^\circ\text{C}$), but since the direction of the gradient changes between night and the day, and the diffusivity of the soil was low ($\sim 0.1\text{m}^2\text{day}^{-1}$) the effect of thermal diffusion must have been erased (by reversing its direction) before it could be established. Severinghaus et al. [14] described a “water vapor flux fractionation effect” in a sand dune located in an arid area. This effect is driven by water vapor gradients in the dune. In our study site this effect must be negligible because the soil moisture content was high throughout the profile (10%-30% by volume) and the relative humidity of the soil-air was probably 100% at all depths.

FIG. 1. Measured and modeled $[O_2]$ and $\delta^{18}O$ profiles in the heavy-soil site. The markers represent the measured data, and the smoothed lines represent model simulations. The figures next to each profile indicate the number of days from irrigation to soil-air sampling. D is the average respiratory discrimination in the model simulation. a. model predicted $\delta^{18}O$ profiles for assumed discrimination of 18 ‰, b. and c. first experiment, d. and e. second experiment.



3.2. Soil air monitoring in the light-soil site

The small difference in O₂ concentration between the soil air and ambient atmosphere at the light-soil site indicates rapid diffusive mixing between the two reservoirs. The stability of both [O₂] and $\delta^{18}\text{O}$ values in both experiments shows that the soil air was close to diffusion-respiration steady state. However, since the signals in the light soil were so weak, the effect of thermal diffusion on $\delta^{18}\text{O}$ (in the order of 0.1‰) could not be neglected (the effect on $\delta\text{O}_2/\text{Ar}$ is negligible).

As in the case of the heavy soil, we can find the discrimination of the soil by studying the soil air with the 5-layer numeric model. In the light soil site soil-air was sampled from one depth only, because the signals were so small that any difference between the soil-air in distinct layers were expected to be within the measurement error. Hence, the model can be calibrated only by the measurements at one depth (90cm). The respiration was assumed to decrease asymptotically to zero with depth (the model results were insensitive to the rate of decrease), and the discrimination was equal in all depths. Since appreciable temperature gradient occurred only in the upper 20cm of the soil, the top of the soil was assumed to be in thermal-diffusion equilibrium with the atmosphere. As in the analysis of the heavy-soil site, respiration rate and discrimination were adjusted by iteration until the best fit to the observed data was found (Fig. 2).

The discrimination determined in this method was $13.0 \pm 0.4\text{‰}$ for the first experiment and $11.5 \pm 0.4\text{‰}$ for the second. Both values are in close agreement with the results derived from one box analytical model (Angert et al., submitted to Global biogeochemical cycles). The main source of error in calculating the discrimination is the $\delta^{18}\text{O}$ -measurement error, since the estimated diffusivity has small effect on the calculated discrimination when the soil-air is in steady state. Although the changes in $\delta^{18}\text{O}$ during the day were not statistically significant, they behave in the same pattern as predicted by the model and followed (with some lag) the diurnal temperature changes.

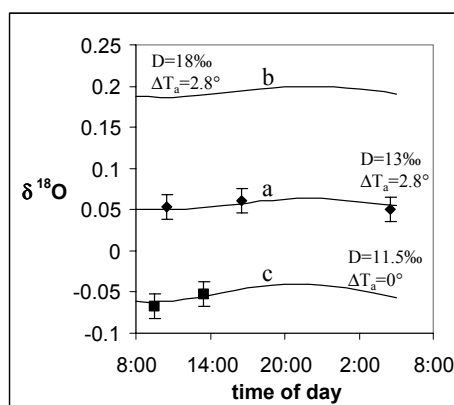


FIG. 2. Measured and modeled $\delta^{18}\text{O}$ versus time in the light-soil site. Markers with error bars represent the measured data, and the lines represent model simulations. The variations of $\delta^{18}\text{O}$ in time are caused by thermal diffusion that is driven by the diurnal temperature changes. ΔT_a is the average temperature difference between 90cm depth and the surface. a. first experiment. b. model predicted $\delta^{18}\text{O}$ changes for assumed discrimination of 18‰ (all other parameters as in a.). c. second experiment. Note that the main cause for the difference in $\delta^{18}\text{O}$ between a and c is not the respiratory discrimination but the temperature gradient.

The average overall discrimination in both the light soil and the heavy soil sites is $12 \pm 1\text{‰}$ and is significantly smaller than the commonly accepted value for dark respiration ($\sim 18\text{‰}$). This low discrimination is probably the result of diffusion limitation of O_2 transfer to the consumption sites in root tissues and in soil aggregates.

3.3. Implications for the Dole effect

The overall discrimination in soil respiration measured in the present study is about 12‰ . This discrimination is markedly lower than the discrimination of dark respiration (18‰) that has been used in interpretations of the Dole effect. Although more research is needed in natural systems, especially forests as well as other globally important ecosystems, the similar discrimination that was found in the present research in two very different study sites, suggests that low discrimination is a general phenomenon in soil respiration. This conclusion is strengthened by the low discriminations found in soil and root incubations.

In a review on the regulating factors of the Dole effect [1] the present-day Dole effect was calculated as 20.8‰ , which is 2.7‰ less than the observed value (23.5‰). In this calculation, it was assumed that the mean global $\delta^{18}\text{O}$ of leaf water, which is the substrate for photosynthesis on land, is about $\sim 4\text{‰}$ higher than the $\delta^{18}\text{O}$ of ocean water. It was suggested that the discrepancy between the observed and calculated Dole effect might be resolved by higher $\delta^{18}\text{O}$ of leaf water ($\sim 8\text{‰}$). However, there is no observational evidence to support this suggestion. Our present finding increases the discrepancy even further. Since about half of the terrestrial respiration occurs in soils, our new discrimination estimate lowers the discrimination value for terrestrial uptake from 18‰ to 15‰ .

This discrepancy may be resolved by higher than currently assumed discrimination in illuminated plants. Indeed, very high discrimination is calculated from published data of terrarium experiments [9]. In these experiments the oxygen in an airtight terrarium containing *Philodendron* plants, soil and natural water reached an photosynthesis-respiration steady state. The difference between the $\delta^{18}\text{O}$ of the terrarium air and the terrarium water is the “terrarium Dole effect” and represent the average discrimination of all the consumption process in the terrarium (since there is no discrimination in photosynthesis). By darkening the terrarium and measuring the change in O_2 concentration (form $\delta\text{O}_2/\text{Ar}$) and the changes in $\delta^{18}\text{O}$ the discrimination in dark respiration in the terrarium can be calculated.

In continues illumination, the average discrimination was 24.6‰ , and at 10/14 hours light/dark cycles it was 20.4‰ . Much lower discrimination (14.8‰), similar to soils, was measured in dark experiments. Calculation of isotopic mass balance, assuming that the rate of light respiration was equal to that of dark respiration when the terrariums were in “normal” 10 hours per day illumination, yields 26‰ for the discrimination of the light processes. This discrimination, as well as the one measured in continues illumination, is much stronger then the value used in modeling of the terrestrial Dole effect (18‰ [1]). Moreover, high discrimination ($\sim 23\text{‰}$) was also found in three years study of Lake Kinneret (Luz et al. MS), and similar discrimination was found in an analysis of O_2 isotopes profiles we measured in the Atlantic Ocean near Bermuda (our unpublished data).

These high discriminations can be the result of high rates of cyanide-resistant respiration (which has high discrimination - 25‰ - 30‰) in the light. We suggest that cyanide-resistant respiration is an important global mechanism, but it is hard to detect because it is chiefly engaged during illumination and is associated with O_2 production. Interestingly, light-enhanced engagement of cyanide-resistant respiration was reported in illuminated plants

([15]; [16]). Since the discrimination in cyanide-resistant respiration is high, including higher rates of this respiration in global budgets will compensate for the low discrimination of soil respiration we report.

4. CONCLUSIONS

1. Discrimination against ^{18}O during O_2 uptake in soil respiration is low and ranges from 11‰ to 14‰, with an averaged value of 12‰.
2. The measured discrimination is significantly lower than the commonly accepted dark-respiration value (~18‰).
3. The low discrimination is the result of diffusion limitation on O_2 transfer to the consumption site. This limitation is present in soil aggregates and roots.
4. Wide engagement of cyanide-resistant respiration in light can balance the low discrimination found in soil respiration.
5. These new experimentally determined discriminations will probably alter the interpretation of past changes in the Dole effect and may help to achieve better understanding of the response of the biosphere to global climate change.

ACKNOWLEDGEMENTS

We thank D. Yakir, D. Ronen and H. Shlomo for their help in the field experimental setup, M. Isaac for providing soil CO_2 flux measurements, and I. Kimchi-Angert for assistance with field sampling. The help of E. Barkan in all aspects related to isotopic measurements is greatly appreciated. This research was supported by grants from the Israel Science Foundation and the USA-Israel Binational Science Foundation.

REFERENCES

- [1] BENDER, M., T. SOWERS, and L. LABEYRIE, The Dole effect and its variations during the last 130,000 years as measured in the Vostok ice core. *Biogeochemical Cycles*, **8**(3) (1994) 363-376.
- [2] MALAIZE, B., D. PAILLARD, J. JOUZEL, and D. RAYNAUD, The Dole effect over the last two glacial-interglacial cycles. *Journal of Geophysical Research Atmospheres*, **104**(D12) (1999) 14199-14208.
- [3] BEERLING, D.J., The influence of vegetation activity on the Dole effect and its implications for changes in biospheric productivity in the mid-Holocene. *Proceedings of the Royal Society of London Series B Biological Sciences* **266** (1999) 627-632.
- [4] GUY, R.D., M.L. FOGEL, and J.A. BERRY, Photosynthetic fractionation of the stable isotopes of oxygen and carbon. *Plant Physiology Rockville*, **101**(1) (1993) 37-47.
- [5] GUY, R.D., J.A. BERRY, M.L. FOGEL, and T.C. HOERING, Differential fractionation of oxygen isotopes by cyanide-resistant and cyanide-sensitive respiration in plants. *Planta* **177**(4) (1989) 483-491.
- [6] ANGERT, A. and B. LUZ, Fractionation of oxygen isotopes by root respiration: Implications for the isotopic composition of atmospheric O_2 . *Geochimica et Cosmochimica Acta*, in press.

- [7] AGGARWAL, P.K. and M.A. DILLON, Stable isotope composition of molecular oxygen in soil gas and groundwater; a potentially robust tracer for diffusion and oxygen consumption processes. *Geochimica et Cosmochimica Acta*,. **62**(4) (1998) 577-584.
- [8] DAVIDSON, E.A. and S.E. TRUMBORE, Gas diffusivity and production of CO₂ in deep soils of the eastern Amazon. *Tellus*,. **47B**(5) (1995) 550-565.
- [9] LUZ, B., E. BARKAN, M.L. BENDER, M.H. THIEMENS, and K.A. BOERING, Triple-isotope composition of atmospheric oxygen as a tracer of biosphere productivity. *Nature*,. **400**(6744) (1999) 547-550.
- [10] MASON, E.A. and T.R. MARRERO, The diffusion of atoms and molecules. *Adv. At. Mol. Phys.*,. **6**(1970) 155-232.
- [11] SEVERINGHAUS, J.P., Studies of the Terrestrial O (sub 2) and Carbon Cycles in Sand Dune Gases and in Biosphere 2, Ph.D. Thesis, Columbia University, New York (1995).
- [12] CHAPMAN, S. and T.G. COWLING, *The Mathematical Theory of Non-Uniform Gases*, Cambridge University Press, (1970)
- [13] GREW, K.E. and T.L. IBBS, *Thermal Diffusion in Gases* Cambridge University Press,(1952).
- [14] SEVERINGHAUS, J.P., M.L. BENDER, R.F. KEELING, and W.S. BROECKER, Fractionation of soil gases by diffusion of water vapor, gravitational settling, and thermal diffusion. *Geochimica et Cosmochimica Acta*,. **60**(6) (1996) 1005-1018.
- [15] LEWITUS, A.J. and T.M. KANA, Light respiration in six estuarine phytoplankton species: Contrasts under photoautotrophic and mixotrophic growth conditions. *Journal of Phycology*,. **31**(5) (1995) 754-761.
- [16] RIBAS-CARBO, M., S.A. ROBINSON, M.A. GONZALEZ-MELER, A.M. LENNON, L. GILES, J.N. SIEDOW, and J.A. BERRY, Effects of light on respiration and oxygen isotope fractionation in soybean cotyledons. *Plant Cell and Environment*,. **23**(9) (2000) 983-989.

HYDROCHEMICAL AND ISOTOPE STUDY OF LAKE TITICACA

R. GONFIANTINI, R. CIONI

Istituto di Geocronologia e Geochimica Isotopica del CNR,
Pisa, Italy

M. PAREDES

Proyecto Especial Binacional Lago Titicaca,
Puno, Peru

J. CAMPOS, M. COLLAS, A. GAITA

Autoridad Autónoma del Lago Titicaca,
La Paz, Bolivia

R. ROJAS

Instituto Peruano de Energía Nuclear,
Lima, Peru

J. QUINTANILLA

Instituto de Investigaciones Químicas, Universidad Mayor de San Andrés,
La Paz, Bolivia

L. GOURCY, M. GRÖNING, L.-F. HAN

International Atomic Energy Agency,
Vienna,

K. ROZANSKI

Faculty of Physics and Nuclear Techniques, AGH-University of Technology,
Krakow, Poland

R. KIPFER

Swiss Federal Institute of Environmental Science and Technology,
Dübendorf, Switzerland

Abstract. The chemical and isotopic compositions of Lake Titicaca and its inflow waters (precipitation, tributaries, groundwater) were determined with the aim of establishing the lake chemical and isotope balance. The three main regions of the lake, i.e. the Lago Mayor, the eastern and the western basins of Lago Menor, connected in cascade, show significant chemical and isotopic differences. Chloride and sodium balance indicates that an average of about 92 % of the inflow water evaporates, and the remaining 8 % is lost through Rio Desaguadero and infiltration. The balance of each basin is also obtained, including the inter-basin fluxes. The stable isotope balance is not possible because no data are available on the mean atmospheric vapour isotopic composition. However, this was tentatively computed using the fluxes obtained from chemistry. The vapour δ -values are slightly more negative than those of rainfall. Tritium, noble gases and chloro-fluoro-carbons in vertical profiles show that the lake is vertically well mixed and there is no water segregation at depth.

1. INTRODUCTION

The climatic conditions, animal life, and vegetation of the Peruvian-Bolivian Altiplano are largely determined by Lake Titicaca, which is also the main water source for about 1,000,000 people living in the region. In view of the lake economic and social importance [1], the Government of Peru established in 1985 the Proyecto Especial del Lago Titicaca (PELT) based in Puno, with the task of carrying out investigations on the lake (water balance, fisheries) and

the region around (agriculture, animal farming). Later, PELT became the executive arm of the Autoridad Autónoma del Lago Titicaca (ALT) based in La Paz, Bolivia, jointly financed by the governments of Bolivia and Peru. The zone of activity was extended to the whole lake basin (144,000 km²).

In 1997, a Regional Technical Co-operation Project (RLA/8/022) for the study of Lake Titicaca was launched by the International Atomic Energy Agency (IAEA) having ALT and PELT as counterparts. The main objective of the project was to improve the current knowledge on (i) the lake-atmosphere interactions, including evaporation and precipitation distribution over the lake, and (ii) the lake dynamics with emphasis on the chemical and isotopic balance and the vertical mixing rate. Stable isotopes (²H/¹H, ¹⁸O/¹⁶O) and chemical composition of water were used to this aim, together with few measurements of tritium, noble gas (including ³He/⁴He ratio), and chloro-fluoro-carbon (CFCs) concentration in the lake. The current status of investigations carried out within the framework of the project is presented in this paper.

2. MAJOR MORPHOMETRIC AND HYDROLOGIC FEATURES OF LAKE TITICACA

Lake Titicaca extends from 15°14'S to 16°36'S and 68°34'W to 69°57'W, at mean altitude of 3810 m a.s.l. The lake surface area is 8500 km² and the volume to 930 km³. The lake consists of three main water bodies, the largest (ca. 6500 km²) and deepest (288 m) being the Lago Mayor in the north, containing about 97 % of the lake water. The Lago Menor (approx. 1450 km², 2 % of water) in the south, with a depth of 10-30 m, is connected to the Lago Mayor through the Tiquina Strait. The third basin is the shallow Puno Bay (approx. 550 km²) on the western Lago Mayor.

The lake catchment area covers ca. 48,000 km² and is drained by five major rivers: Ramis (mean discharge 74 m³s⁻¹), Ilave (38 m³s⁻¹), Coata (47 m³s⁻¹), Huancané (19 m³s⁻¹) and Suches (11 m³s⁻¹), all flowing into the Lago Mayor. Rio Tiawanaku, with a mean discharge of 0.5 m³s⁻¹ only, flows into the Lago Menor from the arid southern region. During the last 80 years, the mean tributary water supply to the lake was 6×10⁹ m³·a⁻¹, i.e. 45 % of the mean annual water inflow (1.35×10¹⁰ m³·a⁻¹), the rest being provided by precipitation. The water mean residence time in the Lago Mayor is about 75 years.

The lake is drained by the Desaguadero river, which works as an overflow and flows out from Lago Menor to the south across the Bolivian Altiplano. However, during the time span of our investigation, the lake level was low and no water was flowing out through the Desaguadero.

The mean temperature of Lake Titicaca is 13°C, i.e. 4-5°C higher than the mean air temperature in the surrounding region, as a consequence of enhanced absorption of solar radiation by the water body [2]. The adsorption is higher from September to November, when the sky is generally clear and precipitation scarce. The thermocline starts to develop in Lago Mayor in late spring, penetrates till 60-80 m, and disappears in May-June. In winter, a complete lake overturn normally takes place [3].

3. SAMPLING AND ISOTOPE AND CHEMICAL ANALYSES

Six sampling campaigns were carried out on the lake from July 1997 to October 1999, during which depth profiles were sampled at 18 stations, thirteen of which in the Lago Mayor, one in the Puno bay, one in the Tiquina Strait, and three in the Lago Menor. The location of the sampling stations is shown in Fig. 1. Successively, the number of lake stations in the Lago

Mayor was reduced, in view of the perfect uniformity and stability of isotopic and chemical values. In June 1999, dissolved rare gases were determined in a depth profile in Lago Mayor, and chloro-fluoro-carbons in several profiles.

For logistic reasons, precipitation and river sampling started later, so that the data available are limited. Springs and wells around the lake were sampled to supplement river and precipitation data.

The stable isotope ratios and CFCs concentrations were measured at the Isotope Hydrology Laboratory of the International Atomic Energy Agency, Vienna. Helium, neon, and $^3\text{He}/^4\text{He}$ ratios were measured at the Swiss Federal Institute of Environmental Science and Technology, Dübendorf. Chemical analyses were carried out by the Instituto de Investigaciones Químicas of the Universidad Mayor de San Andrés, La Paz, and the Société Générale de Surveillance Bolivia, S.A., La Paz. Few control analyses were performed at the Istituto di Geocronologia e Geochimica Isotopica, Pisa.

The $^{18}\text{O}/^{16}\text{O}$ and $^2\text{H}/^1\text{H}$ ratios are expressed in δ ‰, i.e. per mille deviation vs. the reference V-SMOW. The measurement standard uncertainties are 0.06 ‰ for $\delta^{18}\text{O}$ and 0.8 ‰ for $\delta^2\text{H}$. The deuterium excess d ($d = \delta^2\text{H} - 8\delta^{18}\text{O}$, uncertainty 1 ‰) is used as evaporation index. The tritium concentration is expressed in tritium units (1 TU = 1 tritium atom per 10^{18} H atoms). The noble gas content in water is expressed in $\text{cm}^3\text{STP}\cdot\text{g}^{-1}$, and the CFCs concentration in $\text{pmol}\cdot\text{kg}^{-1}$. The mean values of isotopic and chemical composition are reported in Tables I-III. Figure 2 shows the deuterium excess variability as a function of $\delta^{18}\text{O}$ in the lake and major water fluxes associated with the system.

4. THE ISOTOPIC AND CHEMICAL DATA

4.1. Precipitation and groundwater

Forty five monthly precipitation samples were collected for stable isotope analyses in 15 stations during the rainy season from December 1999 to March 2000. The rainfall amount was higher than the average, therefore the mean $\delta^{18}\text{O}$ and $\delta^2\text{H}$ values derived from this data set may be more negative than the long term mean values. The data confirm that the isotopic composition of precipitation obeys a seasonal cycle, with less negative δ -values at the beginning of the rainy season (December) than in subsequent months, in agreement with previous observations in the region [4, 5].

The stations were subdivided in three groups: (i) island stations (Taquile, Soto, Pallalla), (ii) stations in the west and south-west region of the lake (Aguallamaya, Camicachi, Caritamayo, Huacullani, Llachahui, Parco, Pomata, Huapaca Santiago), (iii) stations in the north north-west region (Nuñoa, Pailla, Piata, Yanarico). The three groups were dictated by the dominant wind direction, blowing from north-east to south-west. While no significant difference exists between the three groups in the deuterium excess values (around 15 ‰), the weighted mean δ -values indicate that precipitation on islands and in the west and south-west region is enriched by about 3 ‰ in ^{18}O and 20 ‰ in ^2H with respect to the north and north-west region (Table I). This may be due to the contribution of vapour originated from the lake to rain formation.

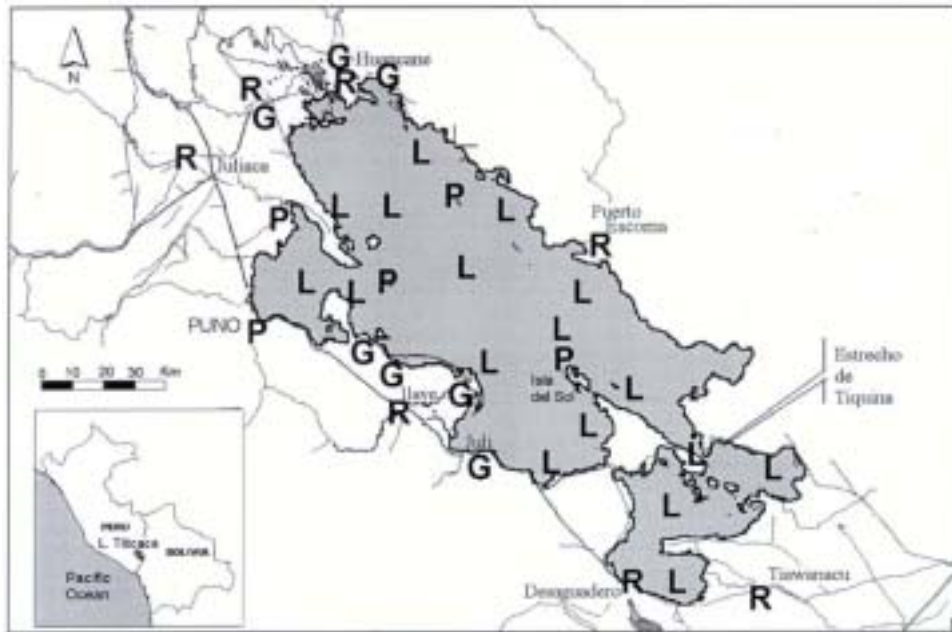


FIG. 1. Lake Titicaca sampling sites. L = lake, P = precipitation, G = groundwater, R = rivers.

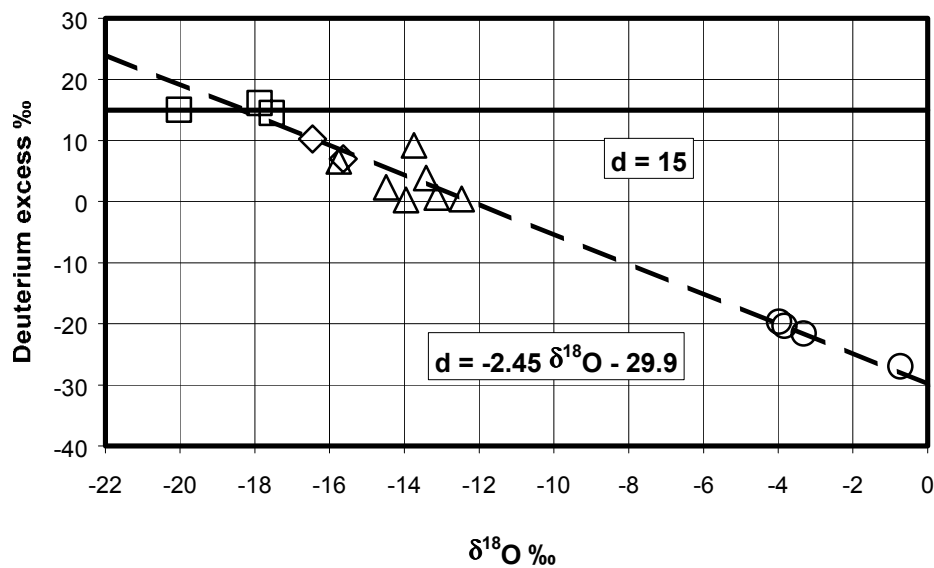


FIG. 2. Deuterium excess vs. $\delta^{18}\text{O}$ as evaporation index. Circles: lake; squares: precipitation; lozenges: groundwater; triangles: rivers.

Another estimate of long term mean δ -values of precipitation can be derived from five springs in areas where recharge from river banks does not occur (Table I). The spring isotopic composition is stable in time, and the geographical variations do not exceed 1.5 ‰ in ^{18}O and 10 ‰ in ^2H . However, the deuterium excess is about 5 ‰ lower than that of precipitation, which may induce the suspicion of evaporation. If true, the original values may be more negative up to about 1.5 ‰ for $\delta^{18}\text{O}$ and 8 ‰ for $\delta^2\text{H}$, becoming similar to those of precipitation over the lake. Shallow wells as well, with δ -values less negative than springs and lower deuterium excess, seem to be affected by evaporation.

Table I. Isotopic and chemical composition of Lake Titicaca and of water components contributing to the lake balance

	$\delta^{18}\text{O} \text{ ‰}$	$\delta^2\text{H} \text{ ‰}$	D excess ‰	$\text{Cl}^- \text{ mg}\cdot\text{L}^{-1}$	$\text{Na}^+ \text{ mg}\cdot\text{L}^{-1}$
<i>Precipitation (Dec 1999 – March 2000)</i>					
Island stations	-17.87	-126.8	16.1		
West and south-west stations	-17.54	-125.8	14.5		
North and north-west stations	-20.02	-145.1	15.1		
<i>Groundwater (1997-1999)</i>					
Springs (5)	-16.46	-121.4	10.3		
Shallow wells (4)	-15.64	-118.1	7.0		
<i>Rivers (1997-1999)</i>					
Rio Achacachi	-13.75	-100.8	9.0	2.6	3.2
Rio Suches (Puerto Escoma)	-12.47	-99.3	0.3	20.3	15.6
Rio Huancané	-13.14	-104.4	0.8	184	155
Rio Ramis	-14.49	-113.6	2.4	47.7	46.1
Rio Coata	-15.76	-119.5	6.6	45.4	35.4
Rio Ilave	-13.96	-111.4	0.3	62.1	47.5
Rio Tiawanaku	-13.42	-103.5	3.9	22.7	25.9
Long term weighted mean	-14.42	-112.5	2.9	60.4	51.5
<i>Lake Titicaca (September 1998)</i>					
Puno Bay ($n = 2$)	-3.83	-51.0	-20.4	257	188
Lago Mayor ($n = 72$)	-3.98	-51.5	-19.6	257	188
Tiquina Strait, surface	-3.69	-50.6	-21.1	262	188
Tiquina Strait, bottom	-2.88	-46.1	-23.0	279	210
Lago Menor, East Basin ($n = 2$)	-3.32	-48.2	-21.6	273	200
Lago Menor, West Basin ($n = 4$)	-0.73	-32.8	-26.9	349	258

Table II. Rare gases in Lake Titicaca (standard uncertainty in brackets)

Lake depth, m	^4He $\text{cm}^3\text{STP}\cdot\text{g}^{-1}\times 10^8$	^3He $\text{cm}^3\text{STP}\cdot\text{g}^{-1}\times 10^{14}$	$(^3\text{He}/^4\text{He}) \times 10^6$	^{20}Ne $\text{cm}^3\text{STP}\cdot\text{g}^{-1}\times 10^7$	$^{20}\text{Ne}/^4\text{He}$
40	2.99 (0.015)	4.10 (0.015)	1.37 (0.005)	1.14 (0.012)	3.81
220	3.02 (0.015)	4.11 (0.015)	1.36 (0.006)	1.15 (0.012)	3.81
equilibrium with air at 14.5°C	2.882	3.917	1.359	1.107	3.842

Table III. Chloro-fluorocarbons in Lake Titicaca
(standard deviation in brackets)

	Mean concentration $\text{pmol}\cdot\text{kg}^{-1}$	Number of samples
CFC-12 (CCl_2F_2)	1.24 (0.12)	40
CFC-11 (CCl_3F)	2.76 (0.32)	45
CFC-113 ($\text{C}_2\text{Cl}_3\text{F}_3$)	0.19 (0.03)	55

Rainfall and groundwater do not contribute significantly to the chemical budget of Lake Titicaca, the first for the low concentration of dissolved compounds, and the second because of the negligible flux.

4.2. The tributaries

The mean isotopic composition of the major Lake Titicaca tributaries is reported in Table I. Although the data available are in principle insufficient to derive the long term weighted mean isotopic composition of rivers, a reasonably good estimate is already possible. Contrary to rainfall, the isotopic composition of rivers does not change drastically with season, because of the damping effect due to groundwater. In fact, the direct contribution of rainwater to runoff is generally smaller than that derived from groundwater and water stored in soil, which are mobilized by rain [6, 7].

Rivers have higher $\delta^{18}\text{O}$ and $\delta^2\text{H}$ values than rainfall and groundwater, and a lower deuterium excess. This indicates evaporation probably occurring in ponds, reservoirs and swamps in the river catchment basin. We do not know whether this effect is a recent one, resulting from current management practices of river water, or it was present in the past as well.

The estimate of the mean chemical composition of lake tributaries is biased by large uncertainty. The ion composition and concentration change drastically in river water as a function of discharge, precipitation versus groundwater fraction, and lithology of catchment regions which contribute to runoff. Even so, preliminary estimates can be made, which are reported in Table I limited to the most conservative ions, chloride and sodium, little affected by sampling technique, transport and storage.

The mean concentrations reported here are significantly different from those of [8], which are based on measurements performed from 1976 to 1979. The difference is attributed to insufficient data for both studies.

4.3. The lake

The lake is considerably enriched in heavy isotopes and dissolved compounds with respect to inflow water as a consequence of evaporation (Table I). The isotopic data well compare with previous measurements [9]. The main basin, Lago Mayor, is isotopically and chemically well mixed, both horizontally and vertically, as the spread of δ -values is comparable with the analytical uncertainty. The size of Lago Mayor is such that the isotopic and chemical variations induced by inflow fluctuations are damped down to undetectable levels.

The isotopic and chemical composition of Puno Bay is very close to that of Lago Mayor, which indicates a good exchange of water between the two basins. However, the Puno Bay water shows small but regular variations, with δ -values slightly more negative after the rainy season, and less negative at the end of the dry season. The variation observed in 1999 was 0.6 ‰ in ^{18}O and 2.2 ‰ in ^2H . The fluctuations are due to Rio Coata, one of the lake major tributaries flowing into the Puno Bay with high discharge from January to April (e.g. $307 \text{ m}^3\text{s}^{-1}$ on 6 April 1999).

The He and Ne concentrations, and the $^3\text{He}/^4\text{He}$ ratio, measured in samples collected at 40 and 220 m depth in Lago Mayor, are close to equilibrium with the atmosphere, with a small saturation excess induced by waves as typical for lakes and ocean (TABLE II). The tritium content at 220 m depth, measured with the $^3\text{H}/^3\text{He}$ method, is 2.99 ± 0.09 TU, which is consistent

with measurements in progress on several samples from other lake locations. This indicates that the lake was vertically well mixed at the time of sampling (June 1999), without any long term water segregation at depth.

This conclusion is further confirmed by the CFCs concentration measured in more than forty samples collected in June 1999 at different depths in seven vertical profiles in the Lago Mayor, Puno Bay, Tiquina Strait and Lago Menor. The results do not show significant variations, the standard deviation being comparable with the analytical precision ($\pm 5\%$), although the water below 5 m depth seems slightly depleted (5-10 %) with respect to saturation at 14.5°C (lake surface temperature). This depletion may be due to mixing with water from the deeper lake regions during the annual turnover [10] or it may reflect the higher temperature occurring in surface water in the time period preceding the sampling, when the thermocline was well developed.

Lago Menor shows heavy isotope and ion concentration higher than Lago Mayor, and reveals distinct spatial inhomogeneities. Lago Menor can be subdivided conveniently in the eastern and western basins, separated by a zone of islands and shallow water (less than 3 m deep). The eastern basin, where the Lago Mayor water flows in through the Tiquina Strait, is deeper (up to 38 m) than the western basin (15 m deep), from where water leaves the lake through the Desaguadero river. The relative surface area of the two basins is approximately 2.5:1 in favour of the western basin. The system Lago Mayor-Eastern Lago Menor-Western Lago Menor can be regarded as a lake cascade. Thus, the Western Lago Menor, whose conditions approach those of a terminal lake, has the highest concentrations of ^{18}O , ^2H and dissolved compounds.

In 1998 to 2000 there was no overflow through Desaguadero river because of the low lake level. Therefore, the western basin of Lago Menor was behaving as a terminal lake, and its heavy isotope concentrations reached the maximum values in September 1998: $\delta^{18}\text{O} = -0.73$ and $\delta^2\text{H} = -32.8$ ‰. The δ -values slightly decreased in June 1999 ($\delta^{18}\text{O} = -1.49$ and $\delta^2\text{H} = -36.4$ ‰) after the rainy season and increased again in the subsequent dry season.

Water stratification was observed in the Tiquina Strait in September 1998. The surface water has the same isotopic and chemical composition of Lago Mayor. The heavy isotope and dissolved compound contents are higher at depth, indicating the occurrence of a deep counter-flux, with the denser water of Lago Menor flowing back to Lago Mayor. The counter-flux may have been promoted by the decreased flux from Lago Mayor and the lack of overflow through Rio Desaguadero. The isotope and chemical stratification was not observed in other sampling campaigns.

5. THE CHEMICAL BALANCE OF LAKE TITICACA

We have now set the stage for computing the chemical balance of Lake Titicaca using chloride (Cl^-) and sodium (Na^+) which are the most conservative and reliable chemical tracers. A conservative tracer is a compound which strictly follows the behaviour of liquid water and is not significantly removed by evaporation, biological processes, chemical precipitation or interaction with bottom rocks and sediments: it can be used, therefore, to study the water balance.

The three lake sub-basins (Lago Mayor, Lago Menor East Basin, Lago Menor West basin) are assumed to be well mixed and in steady state, i.e. with the tracer input rate equal to the re-

moval rate. Effects on tracer concentration due to input rate variations are considered negligible due to the large water volumes involved.

The tracer budget for Lago Mayor is:

$$C_{RM}Q_{RM} + C_PQ_{PM} + C_GQ_{GM} = C_M(Q_{TS} + Q_{IM}) \quad (1)$$

where C_{RM} , C_P , C_G and C_M are the mean concentrations respectively in tributaries, precipitation, groundwater, and Lago Mayor, and Q_{RM} , Q_{PM} and Q_{GM} are the mean water recharge rates by tributaries, precipitation and groundwater. The mean water fraction f_M lost through the Tiquina Strait (Q_{TS}) and infiltration (Q_{IM}), with respect to the recharge rate of the whole lake ($Q_T = Q_R + Q_P + Q_G$), assuming that $C_P \approx 0$ and Q_G (groundwater contribution) be negligible, is:

$$f_M = \frac{Q_{TS} + Q_{IM}}{Q_T} = \frac{C_{RM}Q_{RM}}{C_MQ_T} = \frac{C_{RM}}{C_M}b_Mr \quad (2)$$

where $b_M = Q_{RM}/Q_R$ is the runoff fraction into Lago Mayor versus total runoff, and $r = Q_R/(Q_P + Q_R)$ is the runoff fraction versus the whole lake recharge, typically equal to 0.45. Although yearly runoff and rainfall rate show wild variations, they are well correlated (correlation coefficient = 0.93), so that the variation of r is limited.

The water fraction (with respect to whole lake recharge) lost by evaporation in Lago Mayor is:

$$f_{EM} = \frac{Q_{PM} + Q_{RM}}{Q_T} - f_M = a_M(1-r) + b_Mr \left(1 - \frac{C_{RM}}{C_M}\right) \quad (3)$$

where a_M is the rainfall ratio, i.e. the rainfall fraction falling on Lago Mayor. If the mean precipitation rate is uniform all over lake Titicaca, a_M is equal to the surface ratio between Lago Mayor and the whole lake, as it will be assumed in our computations.

Similar equations can be derived for the other two lake basins. Assuming that water lost by infiltration is negligible, the mean water fraction f_E which flows out from eastern Lago Menor basin into the western basin, with respect to the recharge rate of the whole lake Titicaca, is:

$$f_E = \frac{r}{C_E}(C_{RM}b_M + C_{RE}b_E) \quad (4)$$

The mean evaporation fraction f_{EE} from eastern Lago Menor is:

$$f_{EE} = a_E(1-r) + b_Er + \frac{C_{RM}b_Mr}{C_M} - \frac{r}{C_E}(C_{RM}b_M + C_{RE}b_E) \quad (5)$$

where C_{RE} and C_E are the mean concentrations respectively in tributaries and in eastern Lago Menor, b_E is the runoff fraction, and a_E is the rainfall ratio.

The mean water fraction f_W flowing out from western Lago Menor through Rio Desaguadero is:

$$f_W = \frac{r}{C_W}(C_{RM}b_M + C_{RE}b_E + C_{RW}b_W) \quad (6)$$

The mean evaporation fraction f_{EW} from western Lago Menor is:

$$f_{EW} = a_W(1-r) + b_W r + \frac{r}{C_E}(C_{RM}b_M + C_{RE}b_E) - \frac{r}{C_W}(C_{RM}b_M + C_{RE}b_E + C_{RW}b_W) \quad (7)$$

where C_{RW} and C_W are the mean concentrations respectively in tributaries and western Lago Menor, b_W is the runoff fraction, and a_W the rainfall fraction. The sum of all evaporative terms ($f_{EM} + f_{EE} + f_{EW}$) plus the term for flux through Desaguadero river (f_W) is equal to 1.

Table IV. Mean inter-basin fluxes and evaporation fluxes computed from the chemical budget (uncertainty of parameters in brackets)

	Whole Lake Titicaca	Lago Mayor	Lago Menor East Basin	Lago Menor West Basin
Surface area, m ²	8.50×10 ⁹	7.07×10 ⁹	3.85×10 ⁸	1.045×10 ⁹
Rainfall, m ³ ·a ⁻¹	7.50×10 ⁹	6.24×10 ⁹	3.4×10 ⁸	9.2×10 ⁸
Runoff, m ³ ·a ⁻¹	6.00×10 ⁹	5.88×10 ⁹	3×10 ⁷	9×10 ⁷
Total input, m ³ ·a ⁻¹	13.50×10 ⁹	12.12×10 ⁹		
Runoff/Total input (r)	0.45 (0.03)			
Rainfall fraction (a) ¹⁾	1	0.832 (0.01)	0.045 (0.01)	0.123 (0.01)
Runoff fraction (b)	1	0.98 (0.01)	0.005 (0.005)	0.015 (0.005)
<i>From chloride budget:</i>				
Cl ⁻ in lake, mg·L ⁻¹		257 (3)	273 (10)	349 (10)
Cl ⁻ in rivers, mg·L		60.4 (15)	22.7 (10)	22.7 (10)
Flux out fraction ²⁾	0.076 (0.019)	0.102 (0.026)	0.096 ₅ (0.025)	0.076 (0.019)
Flux out, m ³ ·a ⁻¹ (×10 ⁹)	1.02 (0.26)	1.38 (0.36)	1.30 (0.34)	1.02 (0.26)
Flux out, m ³ ·s ⁻¹	32.5 (8.4)	43.8 (11.4)	41.3 (10.7)	32.5 (8.4)
Evaporated fraction:				
Whole lake ²⁾	0.924 (0.029)	0.795 (0.026)	0.033 (0.007)	0.095 (0.009)
Lake sub-basin ³⁾		0.886 (0.029)	0.256 (0.056)	0.557 (0.053)
Evap. rate, m ³ ·a ⁻¹ (×10 ⁹)	12.47 (0.39)	10.74 (0.36)	0.45 (0.10)	1.29 (0.12)
Evapor. rate, mm·a ⁻¹	1468 (46)	1518 (50)	1164 (252)	1235 (118)
<i>From sodium budget:</i>				
Na ⁺ in lake, mg·L ⁻¹		188 (4)	200 (10)	258 (10)
Na ⁺ in rivers, mg·L		51.5 (15)	25.9 (12)	25.9 (12)
Flux out fraction ²⁾	0.088 (0.026)	0.119 (0.036)	0.112 (0.034)	0.088 (0.026)
Flux out, m ³ ·a ⁻¹ (×10 ⁹)	1.19 (0.35)	1.61 (0.48)	1.52 (0.46)	1.19 (0.35)
Flux out, m ³ ·s ⁻¹	37.6 (11.2)	51.0 (15.2)	48.1 (14.6)	37.6 (11.2)
Evaporated fraction:				
Whole lake ²⁾	0.912 (0.039)	0.779 (0.036)	0.034 (0.09)	0.099 (0.012)
Lake sub-basin ³⁾		0.867 (0.040)	0.234 (0.059)	0.531 (0.062)
Evap. rate, m ³ ·a ⁻¹ (×10 ⁹)	12.31 (0.52)	10.51 (0.48)	0.46 (0.12)	1.34 (0.16)
Evapor. rate, mm·a ⁻¹	1449 (61)	1486 (68)	1201 (303)	1287 (150)

¹⁾ Assumed proportional to surface

²⁾ Expressed with respect to the whole lake water input.

³⁾ Expressed with respect to the water input of each sub-basin.

Typical values of parameters in equations above, with estimated uncertainties, are reported in Table IV. The mean annual water inflow, which is assumed to be reasonably well known, is the main hydrological parameter used in the computations. The values computed for evaporation and inter-basins fluxes, using chloride and sodium concentrations, appear reasonable and consistent each other, taking uncertainties into account. However, the computed evaporation rate from Lago Menor is significantly lower than in Lago Mayor, which may be due to the incorrect estimation of some of the terms, and, for eastern Lago Menor, to some mixing with the Lago Mayor through the Tiquina Strait.

The mean evaporation flux for the whole lake is 1450-1500 mm·a⁻¹, in good agreement with the value obtained by the hydrological balance. The evaporated water fraction, 91.8 (2.6) %, is higher than the 86.5 % reported by Roche et al. [11]. However, these authors report a much larger river input (8.5×10⁹ instead of 6.0×10⁹ m³·a⁻¹) due to higher rainfall rate during their period of observation.

The mean outflow through the Desaguadero river is 1.11×10⁹ (0.22×10⁹) m³·a⁻¹, i.e. 35.0 (7.0) m³·s⁻¹, to be compared with the value of 0.70×10⁹ m³·a⁻¹ (22.1 m³·s⁻¹) obtained by means of the hydrological balance. Although the discrepancy can be explained by the uncertainty associated with the chemical balance, it may also imply that about 3 % of the annual water input is lost by diffuse infiltration and does not flow through Desaguadero river. This figure is much smaller than the infiltration losses of 1.36×10⁹ m³·a⁻¹, i.e. 10 % of the annual input previously estimated on the basis of the chemical balance [12]. Also, using for chloride and sodium mean concentrations in inflowing water the values derived from [8], which are lower by about 10 and 20 % respectively than those adopted here, the mean discharge of Desaguadero river decreases to 0.89×10⁹ (0.22×10⁹) m³·a⁻¹, i.e. 28.2 (6.8) m³·s⁻¹.

The rainfall is higher in the central region of Lago Mayor, possibly as a consequence of lake vapour recycling [1], and in principle the rainfall fractions α 's should be adjusted accordingly. This will be done when the rainfall distribution over the lake will be better known.

Finally, the major contribution to uncertainty of the water fluxes is given by the chloride and sodium concentrations in river water. It is therefore necessary to continue the chemical monitoring of major lake tributaries, in order to refine the mean concentration values and reduce uncertainties.

6. ELEMENTS OF STABLE ISOTOPE BALANCE OF LAKE TITICACA

The stable isotope behaviour in water evaporation [13] can be used to derive the isotope balance of closed or quasi-closed lakes, where evaporation removes most of the input water [14-18]. However, at the current stage of our investigations, a full isotope balance of Lake Titicaca is impracticable, as some basic information is missing or scarce. In particular, no data are available on the isotopic composition of atmospheric vapour above the lake, for which vapour sampling and evaporimeter experiments in islands and on the lake shore are planned for the near future. Also, the isotopic composition of the inflow water is not well known because the data available on precipitation and rivers are insufficient. Nevertheless, it is possible to estimate the isotopic composition of atmospheric vapour above the lake using the information obtained from the chemical budget.

The isotopic composition δ_A of atmospheric vapour above a lake in steady state is related to those of the lake (δ_L) and the input water (δ_I) through the relationship:

$$\delta_A = \frac{(\delta_L - \delta_I)(1 - h + \Delta\epsilon/1000)}{hx} - \frac{\delta_L(1 - h - 1/\alpha + \Delta\epsilon/1000) + \Delta\epsilon + \epsilon/\alpha}{h} \quad (8)$$

where h is the relative humidity normalised at the lake temperature, x is the water fraction lost by evaporation, α is the isotopic equilibrium fractionation factor between liquid water and vapour, $\epsilon = (\alpha - 1) \times 1000$ is the equilibrium enrichment in ‰, and $\Delta\epsilon = k\theta(1 - h)$ is the kinetic contribution to the isotopic fractionation during evaporation, with k equal to 14.2 ‰ for ¹⁸O and 12.5 ‰ for ²H (Vogt, 1978), and θ being a weighing factor which accounts for humidity

build-up over large evaporating surfaces. θ is close to 1 for small water bodies whose evaporation flux does not perturb significantly the ambient moisture [16].

Equation (8) can be written for both ^{18}O and ^2H . A third equation is given by the deuterium excess:

$$d = \delta_A^2\text{H} - 8\delta_A^{18}\text{O} \quad (9)$$

For each lake basin, the chemical budget provides x and the fractions of the various components in inflow water, from which δ_l can be derived. $\Delta\epsilon$ depends on relative humidity and θ , while α and ϵ depend on temperature (assumed equal to 13°C in the three basins). If the deuterium excess is taken equal to 15 ‰ as in precipitation, we are left with the four unknown h , θ , $\delta_A^{18}\text{O}$, and $\delta_A^2\text{H}$ and three equations.

For Lago Mayor, with $\theta = 1$, i.e. the lake vapour contribution to atmospheric vapour is negligible, we obtain $h = 67\%$, which is higher than that observed (about 50-60 % at Copacabana on the Bolivian southern shore [11]), $\delta_A^{18}\text{O} = -19.4$ and $\delta_A^2\text{H} = -140$ ‰. With $h = 55\%$ and $\theta = 0.73$, i.e. about one quarter of vapour derives from the lake, we obtain $\delta_A^{18}\text{O} = -19.6$ and $\delta_A^2\text{H} = -142$ ‰. These values are slightly more negative than those of the mean precipitation, which however largely depend on the December to March rainfall. They are practically unaffected by changing θ .

The isotopic values obtained for the atmospheric vapour above Lago Mayor can now be used to compute the isotopic composition of Western Lago Menor if it would behave as a terminal lake at steady state. With $h = 55\%$ and $\theta = 0.73$, we obtain $\delta_{WT}^{18}\text{O} = 0.0$ and $\delta_{WT}^2\text{H} = -27$ ‰. These values are slightly less negative than those observed in September 1998 ($\delta_W^{18}\text{O} = -0.73$ and $\delta_W^2\text{H} = -32.8$ ‰) indicating that, after about two years of no outflow through Desaguadero river, the isotopic steady state was not reached although it was not far.

The above computations are preliminary. The results will be confirmed or disproved by direct and indirect (through evaporation pan experiments) determination of the isotopic composition of atmospheric vapour above the lake.

REFERENCES

- [1] TABORGA, J., CAMPOS, J., Recursos hídricos en los Andes: Lago Titicaca. Bull. Inst. Français Etudes Andines **24** (1995) 441-448.
- [2] CARMOUZE, J.P., The energy balance. In: Lake Titicaca. A Synthesis of Limnological Knowledge (C. Dejoux & A. Iltis, Editors), Chapter 5, Kluwer, Dordrecht (1992) 131-146.
- [3] RICHERSON, P.J., The thermal stratification regime in Lake Titicaca. In: Lake Titicaca. A Synthesis of Limnological Knowledge (C. Dejoux & A. Iltis, Editors), Chapter 4, Kluwer, Dordrecht (1992) 120-130.
- [4] ROCHE, M-A., GONFIANTINI, R., FONTES, J-CH., ABASTO, N., NORIEGA, L., The isotopic composition of precipitation on the Andes and Amazon of Bolivia. Proc. Int. Symposium Water Resources Development and Management, IAEA, Vienna, May 10-14 (1999).
- [5] GONFIANTINI, R., ROCHE, M-A., OLIVRY, J-CL., FONTES, J-CH., ZUPPI, G.M., The altitude effect on the isotopic composition of tropical rains. Chem. Geology **181** (2001) 147-167.

- [6] CLARK, I., FRITZ, P., Environmental Isotopes in Hydrogeology, Lewis, New York, (1997) 99-104.
- [7] GENEREUX, D.P., HOOPER, R.P., Oxygen and hydrogen isotopes in rainfall-runoff studies. In: Isotope Tracers in Catchment Hydrology (C. Kendall and J.J. McDonnell, editors), Elsevier, Amsterdam (1998) 319-346.
- [8] CARMOUZE, J.P., ARZE, C., QUINTANILLA, J., Hydrochemical regulation of the lake and water chemistry of its inflow rivers. In: Lake Titicaca. A Synthesis of Limnological Knowledge (C. Dejoux & A. Iltis, Editors), Chapter 2, Kluwer, Dordrecht (1992) 98-112.
- [9] FONTES, J-CH., BOULANGE, B., CARMOUZE, J.P., FLORKOWSKI, T., Preliminary oxygen-18 and deuterium study of the dynamics of Lake Titicaca. In: Isotopes in Lake Studies, IAEA, Vienna (1979) 145-150.
- [10] PEETERS, F., KIPFER, R., ACHERMANN, D., HOFER, M., AESCHBACH-HERTIG, W., BEYERLE, U., IMBODEN, D.M., ROZANSKI, K., FROEHLICH, K., Analysis of deep water exchange in the Caspian Sea based on environmental tracers. Deep Sea Res. I **47** (2000) 621-654.
- [11] ROCHE, M-A., BOURGES, J., CORTES, J., MATTOS, R., Climatology and hydrology of the Lake Titicaca basin. Chapter IV.1 of Lake Titicaca. A Synthesis of Limnological Knowledge (C. Dejoux & A. Iltis, Editors), Kluwer, Dordrecht (1992) 63-88.
- [12] CARMOUZE, J.P., AQUIZE JAEN, E., La régulation hydrique du lac Titicaca et l'hydrologie de ses tributaires. Revue d'Hydrobiologie tropicale **14** (1981) 311-328.
- [13] CRAIG, H., GORDON, L.I., Deuterium and oxygen-18 variations in the ocean and the marine atmosphere. In: Stable Isotopes in Oceanographic Studies and Paleotemperatures (E. Tongiorgi, editor). C.N.R.-Laboratorio di Geologia Nucleare, Pisa (1965) 9-130.
- [14] GONFIANTINI, R., Environmental isotopes in lake studies. In: Handbook of Environmental Isotope Geochemistry (P. Fritz and J.Ch. Fontes, editors), Vol. 2, Elsevier, Amsterdam (1986) 113-168.
- [15] KRABBENHOFT, D.P., BOWSER, C.J., ANDERSON, M.P., VALLEY, J.W., Estimating groundwater exchange with lakes. 1. The stable isotope mass balance method. Water Res. Research **26** (1990) 2445-2453.
- [16] GAT, J.R., Stable isotopes of fresh and saline lakes. In: Physics and Chemistry of Lakes (A. Lerman, D. Imboden and J.R. Gat, editors), Springer-Verlag, Berlin (1995) 139-165.
- [17] YEHDEGHO, B., ROZANSKI, K., ZOJER, H., STICHLER, W., Interaction of dredging lakes with the adjacent groundwater field: an isotope study. J. Hydrology, **192** (1997) 247-270.
- [18] FROEHLICH, K., Evaluating the water balance of inland seas using isotopic tracers: the Caspian Sea experience. Hydrol. Processes **14** (2000) 1371-1383.

**CLIMATIC RESPONSE OF STABLE ISOTOPE VARIATIONS
IN WOOD CELLULOSE OF PINE (*PINUS SYLVESTRIS* L.)
AND THEIR TREE-RING WIDTH ON THE
KOLA PENINSULA, NORTH-WESTERN RUSSIA**

T. BOETTGER, A. HILLER, M. GEHRE
UFZ Centre for Environmental Research Leipzig-Halle,
Halle, Germany

M. FRIEDRICH
Institute of Botany, University of Hohenheim,
Stuttgart, Germany

C. KREMENETSKI
Institute of Geography, Russian Academy of Sciences,
Moscow, Russian Federation

Abstract. The Kola Peninsula region of northwestern Russia, adjacent to relatively well studied Scandinavian areas, is climatically affected by not only the Gulf Stream and the North Atlantic but also the Eurasian continent. Living and subfossil pine trees from the Khibiny mountains on the Kola Peninsula were analysed for carbon, oxygen and hydrogen isotope composition and for tree-ring width. Comparisons of local meteorological and tree-ring data revealed significant correlations. $\delta^{13}\text{C}$ and $\delta^{18}\text{O}$ values are particularly sensitive to changes in the temperature in July and August and to precipitation in the winter months of the previous year, respectively. On average, ^{13}C in the cellulose of pine trees between c. 1000 and 1300 AD is enriched by δ values of around 1‰ compared to the modern trees from this region. This indicates a distinctly warmer summer climate at that time (the Medieval Warm epoch in Europe) than recently observed. The $\delta^{18}\text{O}$ values of wood cellulose and the $\delta^2\text{H}$ values of non-exchangeable hydrogen of tree cellulose from both fossil and modern samples cover a wide range between around 22 and 29‰ and between about –80 and –120‰ vs. SMOW, respectively. This suggests variations in the seasonal distribution of precipitation at that time, assuming its source has remained the same as in the past.

1. INTRODUCTION

High latitudinal regions are of great interest for studies of global climate variations because their ecosystems are very sensitive, especially to temperature changes. The Kola Peninsula region in north-western Russia is climatically affected by not only the Gulf Stream and the North Atlantic but also the Eurasian continent. It is located at the dividing line between northern Scandinavia – which has been the subject of dendro-climatological and isotope-geochemical investigations – and the eastern Polar regions of Russia, which have so far only been sporadically studied. Trees from the northern and alpine tree line, are very sensitive to climatic variations because growth is only subject to a few factors. Tree-ring chronologies provide an annual, absolute time frame, which can be rigorously tested by the internal replication of many overlapping sections and cross-checking with independently established chronologies of adjacent regions. The ring width and the wood density record climatic conditions prevailing during the growth season. The results of tree ring measurements have been used to reconstruct the average summer temperatures in Fennoscandia and in the Kola Peninsula, southeast of the port city of Murmansk [1-3].

The ratios of stable isotopes of carbon, hydrogen and oxygen stored in the cellulose in tree-rings provide additional climatic information. In particular late wood cellulose reveals high correlations with the air-temperatures of the vegetation period, as the cells stem exclusively from current photosynthesis, whereas reserve carbohydrates from the previous year are also involved in the development of early wood [4, 5].

The isotope fractionation of carbon in trees is determined by the ratio between the CO₂ concentration in the cell fluid and that in the atmosphere [6]. The regulation of the stomata of the trees or needles greatly influences the photosynthetic discrimination of the heavy isotope ¹³C. Climatic factors such as air temperature and relative humidity, as well as local factors such as light conditions and soil moisture, also affect the fractionation of the isotopes via stomatal resistance. Hot and dry conditions generally lead to a greater ¹³C/¹²C ratio. Moreover, specific locational factors such as the soil's nutrient content, along with species-specific and individual plant characteristics (leaf morphology, the age of the tree, state of health, etc.) and anthropogenic influences (e.g. the increase in the CO₂ concentration and a declining trend in its $\delta^{13}\text{C}$ value owing to the combustion of fossil fuels) exert a major impact on the carboxylation process of photosynthesis – and on the ¹³C level [7-13]. For instance, if the $\delta^{13}\text{C}$ values are corrected to take into account the atmospheric trend since the start of the industrial era, the carbon isotope values in the cellulose of pine tree rings in North Finland closely correlate with the average temperatures for the months of July and August [14, 15].

The $\delta^2\text{H}$ and $\delta^{18}\text{O}$ values in the wood cellulose are determined by the isotope signature of the source water available for tree growth (including groundwater, precipitation, soil water), humidity (via evapotranspiration) and the biochemical fractionation processes during photosynthesis. If the source water is mainly meteoric water, the $\delta^2\text{H}$ - and $\delta^{18}\text{O}$ -values in the tree rings largely depend on regional precipitation. The isotopic effects observed in the precipitation, which are climatically controlled and depend on the location's temperature and relative humidity [16, 17], can also be observed in the cellulose nitrate or cellulose [5,18-21]. Higher temperatures and/or reduced humidity frequently result in the relative enrichment of the heavy isotopes ²H and ¹⁸O in the tree ring cellulose owing to the increasing evaporation fractionation in the source water.

This work reports on the preliminary results of isotope and ring widths measurements in the cellulose of living and subfossil pines from the tree line in the Khibin mountains on the Kola Peninsula. Combining two independent methods provides an excellent method of multi-proxy access to filter out the effects stemming from biological causes and hence obtain reliable information about past climatic and environmental conditions. Once the isotopic time series have been calibrated against instrumental climatological time series, they can be used as proxy indicators of changes in local temperature and moisture, which in turn can be interpreted as changes in the large-scale atmospheric circulation.

2. STUDY AREA AND METHODS

The Khibiny low mountains with a maximum height of 1250 m a.s.l. are located on the Kola Peninsula between ca. 67–68°N and 33–34°E. The climate on Kola is maritime and characterised by relatively mild (for these latitudes) winters and strong winds. The modern annual mean temperature is about –1.1°C (near the city Kirovsk), and heavy rainfall (500–1,000 mm) is characteristic of the area. Dense clouds and high humidity (87–93%) are even greater in the Khibiny region than in the lowlands. The growing season is limited to a period of about 2–2.5 months [22, 23].

Subfossil wood samples were collected from the surface in the mountain tundra above the modern tree line from 8 different sampling sites. Sampling is described in detail in [24]. We investigated subfossil pine wood (*PINUS SYLVESTRIS* L.) and 3 increment wood cores obtained from living pines from the modern tree line. For wood identification, three-dimensional wood cross-sections were examined according to [25, 26]. Cellulose from the approximately 20 external rings of ^{14}C dated and tree rings from the 5-year blocks of dendrochronologically dated tree rings were used for isotope measurements.

To examine the information contained in the ring widths of pines, different collectives of living pines were dendrochronologically studied at various locations on the tree line. The total tree-ring width chronologies were established by standard methods in the Hohenheim laboratory [27].

The annual isotope investigations on increment cores of the living trees were carried out on the cellulose of the late wood. The late wood from tree ring was cut under a microscope. The cellulose was extracted and nitrated using the methods described by [28, 29]. The combustion of the samples was conducted in two ways. In the first, combustion offline in ampoules with CuO (30 hours, 690°C) was followed by the cryogenic separation of CO_2 and H_2O , and the reduction of the H_2O to H_2 in a laboratory vacuum apparatus, before measurement was carried out with a Delta S mass spectrometer. In the second method, samples were pyrolysed and measured online using the Xlplus mass spectrometer (also produced by Finnigan MAT). We obtained almost identical results with both methods, e.g. for the $\delta^2\text{H}$ values (*FIG. 1a*).

The results are shown using the conventional notation¹ with respect to the PDB and SMOW standards. The overall precision of the replicate samples analyses is estimated to be better than 0.02‰ for $\delta^{13}\text{C}$, 0.1‰ for $\delta^{18}\text{O}$ and 1.5‰ for $\delta^2\text{H}$.

3. RESULTS

The present dendrochronological investigations yielded different modern tree-ring chronologies and a floating tree-ring chronology of 594 years spanning the period AD 915–1508. The floating chronology was synchronised with the pine tree-ring chronology from Finnish Lapland of the METLA tree-ring research laboratory in Rovaniemi [30]. Results from previously investigated locations indicate that the tree-ring widths of subfossil and modern pines closely correlate with each other ($r_{\text{Mean}} > 0,7$; percentage of coincidence: >80%).

The curve of the average carbon isotope values of the late wood cellulose from three increment cores of young pine trees is shown in *FIG. 2*. The $\delta^{13}\text{C}$ and $\delta^{18}\text{O}$ values of individual tree rings correlate significantly with each other ($r_{\text{mean}} = 0.46$; $n = 63$). These measuring data were compared with the meteorological data (temperature and precipitation amounts) recorded at the weather station near the study area (67°43'N; 33°15'E; H 134m). A significant correlation was found between the $\delta^{13}\text{C}$ values and i) the average temperatures for July and August ($r_{\text{July/August}} = 0.49$; $n = 44$), ii) the precipitation amounts in July ($r_{\text{July}} = -0.35$), and iii) the levels of precipitation in the previous year ($r_{\text{December}} = 0.42$). The $\delta^{18}\text{O}$ values correlated well with the precipitation amounts in autumn and winter of the previous year (e.g. September: $r = 0.46$; December: $r = 0.36$; $n = 44$).

¹ $\delta = R_{\text{sample}} - R_{\text{Standard}} / R_{\text{Standard}} \times 1000$ [‰]; $R = {}^2\text{H}/{}^1\text{H}$, ${}^{13}\text{C}/{}^{12}\text{C}$, ${}^{18}\text{O}/{}^{16}\text{O}$.

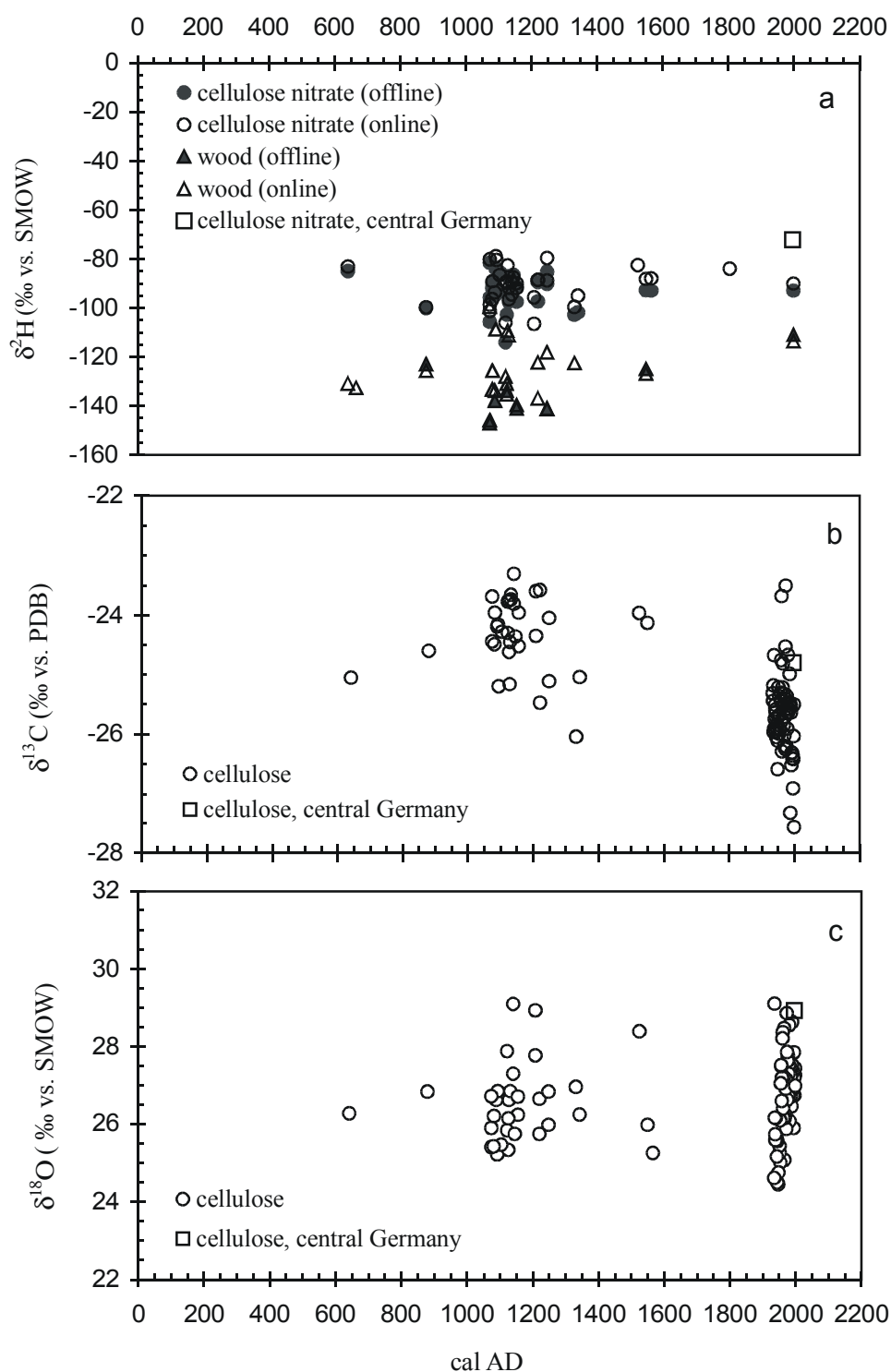


FIG. 1. Original $\delta^2\text{H}$ (a), $\delta^{13}\text{C}$ (b) and $\delta^{18}\text{O}$ (c) values for the cellulose nitrate, whole wood and cellulose of living and dead *Pinus Sylvestris* L. tree samples from Khibiny mountains on the Kola Peninsula

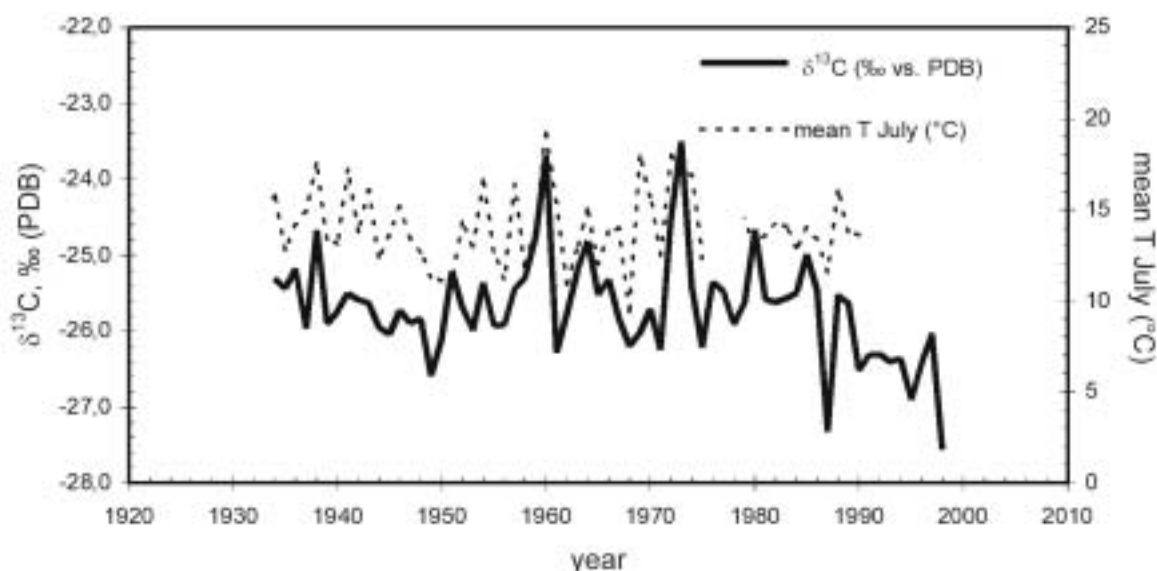


FIG. 2. Time series of mean $\delta^{13}\text{C}$ -values (not corrected via anthropogenic trend in atmospheric $\delta^{13}\text{C}$ values) from late wood cellulose of 3 living pine trees and monthly mean temperatures of July at Khibiny mountains on the Kola Peninsula

The carbon isotope values of the cellulose of all samples from the Khibiny region vary between about -23.5 and -27.5‰ . The $\delta^{13}\text{C}$ values of the samples from the period from c. 1000 to 1300 AD have an average of about -24.4‰ and are clearly more positive (by about 1‰) than the mean $\delta^{13}\text{C}$ value of living pines in this region (FIG. 1b).

The oxygen isotope values of all the fossil samples (FIG. 1c) fluctuate widely between about 22 and 29‰ around an average of 26.14‰ vs. SMOW. The $\delta^2\text{H}$ -values calculated throughout the period investigated (measured on cellulose nitrate) are also scattered widely between about -80 and -120‰ vs. SMOW around an average of -94‰ (FIG. 1a). The living trees from the Khibiny region indicate a similar average $\delta^{18}\text{O}$ value of 26.10‰ (FIG. 1c) and a mean $\delta^2\text{H}$ value of about -89‰ . By comparison, our laboratory-standard, homogenised wood dust from at least 5 living pine trees from the Leipzig district in central Germany had a $\delta^{18}\text{O}$ value of $28.93 \pm 0.07\text{‰}$ and a $\delta^2\text{H}$ value of about $-70 \pm 3\text{‰}$.

We are performing carbon, oxygen and hydrogen isotope measurements on cellulose and cellulose nitrate from this the medieval tree-collection in 5-year blocks of rings. At present we have the results of isotope measurements for 3 complete subfossil pine slices, which cover a period from 1110 to 1310. The isotope curves of various trees correlate well with each other. In this work, the findings are only used as means in FIGS. 1a,b,c and discussed together with the isotope data of the ^{14}C -dated samples.

4. DISCUSSION

Initial results from the tree-ring carbon and oxygen isotope measurements on the cellulose of late wood from increment cores from living pines from the Khibiny region show that, similar to the results found for pines from northern Finland [14, 15], a positive relationship exists between the $\delta^{13}\text{C}$ values and the average temperatures for the summer months of July and

August. We also found a (much less pronounced) negative correlation between the $\delta^{13}\text{C}$ values and the precipitation amounts of the summer months. During this time, a late wood is formed, and the formation of the tree ring is completed. As the temperature (and dryness) increase, the sensitive stomata close. This reduces the availability of CO_2 in the cell liquid, limits the photosynthetic discrimination of the ^{13}C isotope, and causes the $\delta^{13}\text{C}$ values to become heavier.

The carbon and oxygen isotope values correlated positively with each other. The isotope ratios in the period of late wood formation probably depend on varying humidity conditions [8]. The short summer in Khibiny is a season with relatively little humidity, even though this region is generally characterised by high rainfall and the relative humidity owing to the dense cloud is usually very high. Unfortunately, we do not yet have monthly regional humidity data for the calculations; they will only become available at a later date.

According to our results, the $\delta^{18}\text{O}$ values of the late-wood cellulose do not depend on the changes to either the average monthly temperatures or the annual temperatures. We found a positive correlation between the carbon and oxygen isotope values and the precipitation amounts in autumn and winter (September, November and December) of the previous year. At present we are unable to explain this.

In the subfossil tree sections from the medieval period chronology (AD 915–1508), the ring widths of the pines correlate extremely well, and the curves are very homogeneous. The ring widths show clearly long-term (decadal–centennial) fluctuations, indicating climatic fluctuations. The highly homogeneous signals ($r_{\text{mean}} \geq 0.7$) of tree-ring width chronologies from modern and subfossil pines seem to harbour a great potential for climate reconstruction. Although the ring widths of the young living pines correlate positively ($r=0.3$) with the monthly mean temperatures of the summer months, no significant correlations were found with the monthly or annual precipitation. However, the links with the monthly climate data, above all with the summer temperatures, are significantly lower than those found for the pines on the polar tree line in northern Scandinavia, [1, 2], Siberia [1] or the alpine tree line [27]. Therefore further investigations are needed to resolve the links between climate and growth. All in all, our preliminary findings show that the $\delta^{13}\text{C}$ values react better to temperature changes in summer than the ring widths. The latter appear to correlate more closely to the $\delta^{18}\text{O}$ values rather than the $\delta^{13}\text{C}$ values. The extension of the chronologies and the multi-proxy approach with the stable isotopes in the cellulose of the same tree rings will in future enable additional insights.

The majority of the ^{14}C -dated subfossil pines date back to the period between c. 1000–1300 AD (*FIG. 1*). This period corresponds to the medieval climatic optimum [31], a warm phase of the Holocene in many parts of Europe. We can reconstruct a tree line for this period which is at least 100–140 m higher than the current tree line [24], which according to the literature is above all attributed to the higher mean summer temperature in northern Europe [1,34]. The vegetation distribution in the Khibiny region has probably not changed since this time; we only found fossil pine trunks above the present-day pine forest.

The results of the stable isotope investigations show the enrichment of the heavy carbon isotope ^{13}C by about 1‰ in the cellulose of subfossil pines compared to the living trees from this region. Judging by our initial findings from the living tree cores, we can mainly attribute the higher $\delta^{13}\text{C}$ values during that time to the temperature increase in July and August. An additional effect is caused by the reduced water availability in mountainous areas during

warmer periods and the decrease in humidity. By comparison, living pine cellulose from the Leipzig region has an average $\delta^{13}\text{C}$ value of around -25‰ . Irrespective of the movement of the tree line, these data indicate a warmer, dryer summer in the Khibiny region at *c.* 1000 than nowadays – both there and in central Germany.

The oxygen and hydrogen isotope values are subject to wide scattering in the period investigated in both the modern and fossil samples. We found similar findings for the living pine trees, which are lower than for central German pines (*FIGS 1a,c*). The $\delta^{18}\text{O}$ and δD values might reflect the air masses responsible for rainfall as they move across the region. If we assume that the precipitation source remained unchanged during this region (North Atlantic), sharp differences must have occurred in the seasonal distribution of the precipitation during the 2nd millennium and even during the past few decades. Comparing the (not yet available) results of the $\delta^2\text{H}$ measurements in the tree rings of living pines from various sites in the Khibiny region with regional meteorological data series may help solve this issue.

5. SUMMARY AND OUTLOOK

The preliminary findings clearly show the climatically related control of the isotope signatures of the pines in the Khibiny mountains on the Kola Peninsula. The $\delta^{13}\text{C}$ values measured on the cellulose of the late wood and the widths of the tree rings depend mainly on the average temperature of July and August. The $\delta^{18}\text{O}$ values in the wood cellulose of the tree rings probably reflect the movements of air masses (which are not very visible in the tree-ring widths) and the related precipitation formation above the Kola region. Tree-ring data on 200-year-old pines from various locations in the Khibiny region currently being conducted should provide a basis for the interpretation of the isotope data.

Our results show that the medieval climatic optimum was the most pronounced warm phase on the Kola Peninsula in the last 1,500 years or so. Hence this period was not just a climatic phenomenon in central Europe, but has for the first time also been clearly demonstrated to have occurred in northern Europe, too.

The extension of the chronologies and the multi-proxy approach to include the stable isotopes in the cellulose of the same tree rings will enable further insights to be achieved into the climatic variations of the past millennium in north-west Russia.

REFERENCES

- [1] BRIFFA, K.R., JONES, P.D., BARTHOLIN, T.S., ECKSTEIN, D., SCHWEINGRUBER, F.H., KARLÉN, W., ZETTERBERG, P., ERONEN, M., Fennoscandian summers from AD 500: temperature changes on short and long timescales, *Climate Dynamics* **7** (1992) 111-119.
- [2] KALELA-BRUNDIN, M., Climatic information from tree-rings of *Pinus sylvestris* L. and a reconstruction of summer temperatures back to AD 1500 in Femundsmarka, eastern Norway, using partial least squares regression (PLS) analysis, *The Holocene* **9/1** (1999) 59-77.
- [3] GERVAIS, B.R., MACDONALD, G.M., A 403-year Record of July temperatures and treeline dynamics of *Pinus sylvestris* from the Kola Peninsula, Northwest Russia, Arctic, Antarctic, and Alpine Research **32** (2000) 295-302.
- [4] LIPP, J., TRIMBORN, P., FRITZ, P., MOSER, H., BECKER, B., FRENZEL, B., Stable isotopes in tree ring cellulose and climatic change, *Tellus* **43B** (1991) 322-330.

- [5] PENDAL, E., Influence of precipitation seasonality on pinon pine cellulose delta D values, *Global Change Biology* **6/3** (2000) 287-301.
- [6] FARQUHAR, G.D., O'LEARY, M., BERRY, J.A., On the relationship between carbon isotope discrimination and the intercellular carbon dioxide concentration in leaves, *Australian Journal of Plant Physiology* **9** (1982) 121-137.
- [7] SAURER, M., SIEGENTHALER, U., SCHWEINGRUBER, F., The climate-carbon isotope relationship in tree rings and the significance of site conditions, *Tellus* **47B** (1995) 320-330.
- [8] SAURER, M., AELLEN, K., SIEGWOLF, R., Correlating $\delta^{13}\text{C}$ and $\delta^{18}\text{O}$ in cellulose of trees, *Plant, Cell and Environment* **20** (1997) 1543-1550.
- [9] SCHLESER, G.H., Parameters determining carbon isotope ratios in plants, in: B. FRENZEL, B. STAUFER, M.M. WEISS, Eds, Problems of stable isotopes in tree rings, lake sediments and peat-bogs as climatic evidence for the Holocene, *Paläoklimaforschung-Palaeoclimate Research* **15** (1995) 71-96.
- [10] SCHLESER, G.H., HELLE, G., LÜCKE, A., VOS, H., Isotope signals as climate proxies: the role of transfer functions in the study of terrestrial archives, *Quaternary Science Reviews* **18** (1999) 927-943.
- [11] ROBERTSON, I., ROLFE, J., SWITSUR, V.R., CARTER, A.H.C., HALL, M.A., Signal strength and climate relationship in $^{13}\text{C}/^{12}\text{C}$ ratios of tree ring cellulose from oak in southwest Finland, *Geophysical Research Letters* **24** (1997) 1487-1490.
- [12] DUQUESNAY, A., BRÉDA, N., STIEVENARD, M., DUPOUEY, J.L., Changes of tree-ring $\delta^{13}\text{C}$ and water-use efficiency of the beech (*Fagus sylvatica* L.) in north-eastern France during the past century, *Plant. Cell and Environment* **21** (1998) 565-572.
- [13] EDWARDS, T.W.D., GRAF, W., TRIMBORN, P., LIPP, J., PAYER, H.D., $\delta^{13}\text{C}$ response surface resolves humidity and temperature signal in trees, *Geochimica et Cosmochimica Acta* **64/2** (2000) 161-167.
- [14] SONNINEN, E., JUNGNER, H., Stable carbon isotopes in tree rings of a Scot pine (*Pinus Sylvestris* L.) from northern Finland, in: B. FRENZEL, B. STAUFER, M.M. WEISS, Eds, Problems of stable isotopes in tree rings, lake sediments and peat-bogs as climatic evidence for the Holocene, *Paläoklimaforschung-Palaeoclimate Research* **15** (1995) 121-128.
- [15] SONNINEN, E., JUNGNER, H., Carbon isotopes in tree rings of recent and subfossil Scots pines from northern Finland, in: M. KANNINEN, P. HEIKIHEIMO, Eds, The Finnish Research Programme on Climate Change, Final Report, Publications of the Academy of Finland (1996) 19-24.
- [16] DANSGAARD, W., Stable isotopes in precipitation, *Tellus* **16** (1964) 436-468.
- [17] YURTSEVER, Y., GAT, J.R., Atmospheric waters, stable isotope hydrology, Deuterium and Oxygen-18 in the water cycle, Technical Report Series No. 210, IAEA Vienna.
- [18] EDWARDS, T.W.D., FRITZ, P., Assessing meteoric water composition and relative humidity from ^{18}O and ^2H in wood cellulose: Palaeoclimatic implications for southern Ontario, Canada, *Appl. Geochem.* **1** (1986) 715-723.
- [19] LIPP, J., TRIMBORN, P., GRAFF, W., BECKER, B., Climatic significance of ratios in the cellulose of late wood in tree rings from spruce (*Picea abies* L.), Proceedings of an internationales symposium on applications of isotope techniques in the studying past and current environmental changes in the hydrosphere and the atmosphere, IAEA, Vienna, 19.-23.04.1993, (1993) 395-405.
- [20] FENG, X., EPSTEIN, S., Climatic temperature records in D data from tree rings, *Geochimica et Cosmochimica Acta* **59/14** (1995) 3029-3037.

- [21] BUHAY, W.M., EDWARDS, W.D., Climate in southwestern Ontario, Canada, between AD 1610 and 1885 inferred from Oxygen and Hydrogen isotopic measurement of wood cellulose from trees in different hydrologic settings, *Quaternary Research* **44** (1995) 438-446.
- [22] RJABZEVA, K. M., Phisiko-geographicheskij ocherk khibinskich tundr, University of Moscow, Moskva (1969) 83pp.
- [23] ATLAS MURMANSKOY OBLASTI, Glavnoe Upravleniye Geodezii i Kartografii, Moskva, (1971) 33 pp.
- [24] HILLER, A., BOETTGER, T., KREMENETSKI, C., Evidence of the Holocene timberline shift on the Kola Peninsula/Russia Holocene **11** (2001) 491-497.
- [25] WAGENFÜR, R., Anatomie des Holzes, Leipzig VEB Fachbuchverlag (1966) 383 S.
- [26] SCHWEINGRUBER, F.H., Mikroskopische Holzanatomie, Kommissionsverlag F. Flück-Wirth. 2. Aufl. (1982) 226 S.
- [27] FRIEDRICH, M., Dendrochronologische Datierung von Almen des östlichen Dachsteinplateaus, *Mitteilungen der ANISA* **18/1-2** (1998) 71-94.
- [28] GRAY, J., SONG, S.E., Climatic implication of the natural variations of D/H ratios in tree ring cellulose, *Earth and Planetary Science Letters* **70** (1984) 129-138.
- [29] TRIMBORN, P. (personal communication).
- [30] TIMONEN, M., Developing a supra-long ring-width chronology for Northern Finland. Final report on Advance project. In: *Analysis of Dendrochronological Variability and Associated Natural Climates in Eurasia - the Last 10 000 years (ADVANCE-10K)*, ENV4-CT95-0127, Final Report to the Commission of the European Communities Directorate General XII (1999) 36-42.
- [31] LAMB, H.H., The early medieval warm epoch and its sequel. *Palaeogeography, Palaeoclimatology, Palaeoecology* **1** (1965) 13-37.

PALEOCLIMATIC RECONSTRUCTION IN THE BOLIVIAN ANDES FROM OXYGEN ISOTOPE ANALYSIS OF LAKE SEDIMENT CELLULOSE

B.B. WOLFE, R. ARAVENA
Department of Earth Sciences,
University of Waterloo,
Waterloo, Ontario, Canada

M.B. ABBOTT
Department of Geosciences,
Morrill Science Center,
University of Massachusetts,
Amherst, Massachusetts, United States of America

G.O. SELTZER
Department of Earth Sciences,
Heroy Geology Laboratory,
Syracuse University,
Syracuse, New York, United States of America

J.J. GIBSON*
Department of Earth Sciences,
University of Waterloo,
Waterloo, Ontario, Canada

Abstract. Cellulose-inferred lake water $\delta^{18}\text{O}$ ($\delta^{18}\text{O}_{\text{lw}}$) records from Lago Potosi, a seasonally-closed lake in a watershed that is not currently glaciated, and Lago Taypi Chaka Kkota, an overflowing lake in a glaciated watershed, provide the basis for late Pleistocene and Holocene paleoclimatic reconstruction in the Bolivian Andes. Deconvolution of the histories of changing evaporative isotopic enrichment from source water $\delta^{18}\text{O}$ in the lake sediment records is constrained by comparison to the Sajama ice core oxygen isotope profile. At Lago Potosi, the $\delta^{18}\text{O}_{\text{lw}}$ record appears to be dominantly controlled by evaporative ^{18}O -enrichment, reflecting shifts in local effective moisture. Using an isotope-mass balance model, a preliminary quantitative reconstruction of summer relative humidity spanning the past 11,500 cal yr is derived from the Lago Potosi $\delta^{18}\text{O}_{\text{lw}}$ record. Results indicate that the late Pleistocene was moist with summer relative humidity values estimated at 10-20% greater than present. Increasing aridity developed in the early Holocene with maximum prolonged dryness spanning 7500 to 6000 cal yr BP at Lago Potosi, an interval characterized by summer relative humidity values that may have been 20% lower than present. Highly variable but dominantly arid conditions persist in the mid- to late Holocene, with average summer relative humidity values estimated at 15% below present, which then increase to about 10-20% greater than present by 2000 cal yr BP. Slightly more arid conditions characterize the last millennium with summer relative humidity values ranging from 5-10% lower than present. Similar long-term variations are evident in the Lago Taypi Chaka Kkota $\delta^{18}\text{O}_{\text{lw}}$ profile, except during the early Holocene when lake water evaporative ^{18}O -enrichment in response to low relative humidity appears to have been offset by enhanced inflow from ^{18}O -depleted snowmelt or groundwater from the large catchment. Close correspondence occurs between the isotope-inferred paleohumidity reconstruction and other paleohydrological proxies from the region.

* Present address: Isotope Hydrology Section, International Atomic Energy Agency, Wagramer Strasse 5, P.O. Box 100, A-1400, Vienna, Austria.

1. INTRODUCTION

Large moisture fluctuations are dominant features of late Pleistocene and Holocene climate on the Bolivian Altiplano. Wetter conditions compared to the present characterized the late Pleistocene and early Holocene as indicated by pluvial lake high stands spanning from prior to 19,000 to about 14,000 and 10,700 to 9500 cal yr BP [1-2]. Marked aridity, however, is believed to have prevailed during most of the Holocene from about 9500 to 3900 cal yr BP, based mainly on studies of sediment cores from Lake Titicaca [3-7]. New paleo-water level estimates suggest that Lake Titicaca experienced lowest lake levels between 8000 and 5500 cal yr BP [7]. Desiccation may have been widespread at this time in the shallower southern basin of Lake Titicaca and likely in many other ephemeral lakes resulting in discontinuous sedimentary records, which has hampered Holocene paleoclimatic reconstruction in this region. In order to generate a continuous quantitative record of climate change for this region, we have combined a regional lake water sampling survey to assess modern isotope systematics in basins of varying hydrological settings, cellulose-inferred lake water oxygen isotope profiles from two small alpine basins (Lago Taypi Chaka Kkota and Lago Potosi), and an ice core record of precipitation $\delta^{18}\text{O}$ from Sajama [8].

2. CLIMATIC AND HYDROLOGICAL SETTING

Precipitation in the Altiplano region is strongly seasonal with about 75% of the annual total occurring during the austral summer months (December to March) due to convective activity associated with the Bolivian High. Latitudinal gradients in precipitation and relative humidity are evident between Lago Taypi Chaka Kkota (LTCK) and Lago Potosi (LP). At El Alto, La Paz (4105 m asl; 16°30'S; 68°12'W) in the northern Altiplano near LTCK, mean annual precipitation is 564 mm (Dec-Mar: 388 mm) and mean annual relative humidity is 60% (Dec-Mar: 70%). Further south at the town of Potosi (4640 m asl; 19°38'S; 65°41'W) near LP, mean annual precipitation is 301.5 mm (Dec-Mar: 226 mm) and mean annual relative humidity is 38% (Dec-Mar: 50%) [9].

LTCK and LP have significantly different hydrological settings. The LTCK watershed (84 km²) is located at 16°13' S, 68°21' W in the Rio Palcoco Valley on the western slope of the Cordillera Real. Situated at 4300 m asl in elevation, LTCK is 1.3 km² in area and 12 m deep. Through-flow at LTCK is maintained throughout the year by drainage from lakes upstream, which are presently fed by several small alpine glaciers. The LP watershed (3.9 km²) is located at 19°38' S, 65°41' W in the Cordillera Chichas at 4640 m asl and the lake is 0.2 km² in area and 11 m deep. LP is a headwater lake whose watershed does not presently contain glaciers. LP was observed to form a thin ice cover at night and the lake was below its overflow level during June 1997, although outflow channels suggest the water-level reaches the overflowing stage during the summer wet season.

A regional water sampling survey spanning latitudes 13°54' to 19°38' S, conducted during the dry season of 1997, revealed that the $\delta^{18}\text{O}$ and δD composition of lake waters diverge from the Global Meteoric Water Line (GMWL) due to evaporative enrichment (Figure 1). A Regional Evaporation Line can be drawn through these data points ($\delta\text{D} = 5.1\delta^{18}\text{O} - 35.5$; $R^2 = 0.97$) indicating a common atmospheric moisture source for this region. Furthermore, the extent of evaporative enrichment for a given lake was found to vary systematically in relation to the local hydrological setting. Progressively increasing offset from the GMWL was found for lakes directly receiving glacial meltwater, overflowing lakes in glaciated watersheds, overflowing lakes in non-glaciated watersheds, and seasonally-closed lakes. End-members of

the hydrological spectrum in this region are well represented by the depleted isotopic composition of LTCK ($\delta^{18}\text{O} = -14.8\text{‰}$, $\delta\text{D} = -112\text{‰}$), typical for lakes in glaciated watersheds, and the comparatively enriched isotopic composition of LP ($\delta^{18}\text{O} = -5.6\text{‰}$, $\delta\text{D} = -59\text{‰}$), representing the group of lakes that develop hydrological closure during the dry season (Figure 1).

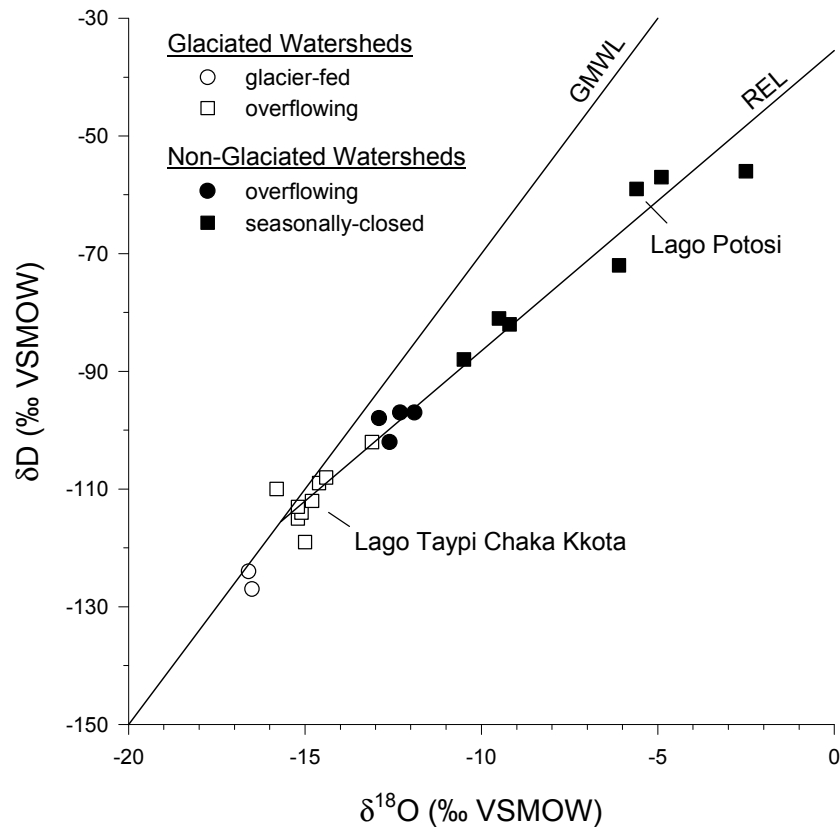


FIG.1. Isotopic composition of lake waters from the Bolivian Andes sampled in June 1997 [10]. Also shown are the Global Meteoric Water Line (GMWL: $\delta\text{D} = 8 \delta^{18}\text{O} + 10$) and the Regional Evaporation Line (REL: $\delta\text{D} = 5.1 \delta^{18}\text{O} - 35.5$).

3. METHODS

Lake sediment sample preparation and analysis for bulk organic elemental (C, N) and cellulose oxygen isotope composition followed methods in [11]. Cellulose oxygen isotope composition was determined using off-line nickel-tube pyrolysis to generate CO_2 for dual inlet isotope ratio mass spectrometry. All elemental and isotopic analyses were conducted at the University of Waterloo - Environmental Isotope Laboratory, Canada. Oxygen isotope results are expressed as “ δ ” values, representing deviations in per mil (‰) from the VSMOW standard for oxygen normalized to $\delta^{18}\text{O}_{\text{SLAP}} = -55.5 \text{‰}$ [12], such that $\delta_{\text{sample}} = [(R_{\text{sample}}/R_{\text{standard}}) - 1] \times 10^3$ where R is the $^{18}\text{O}/^{16}\text{O}$ ratio in the sample and standard. The $\delta^{18}\text{O}_{\text{cell}}$ values have uncertainties of $\pm 0.5\text{‰}$ based on repeated analyses of samples.

Terrestrial macrofossil material was not present in sufficient quantities for AMS ^{14}C measurements from most stratigraphic levels. Therefore, we used *Isoetes* macrofossils at LTCK as well as bulk sediment at LP for AMS ^{14}C measurements. The contemporary

radiocarbon reservoir was assessed in two ways. In LTCK, the ^{14}C activity of live submerged macrophytes was measured and found to be 114% Modern for the year A.D. 1992, indicating that the lake reservoir effect is minimal in the LTCK system today, although it could have been a factor in the past. For LP, the contemporary radiocarbon reservoir was assessed by comparing the ^{14}C activity of paired bulk sediment and macrofossils samples from the same stratigraphic level. Results indicate there is no significant difference between the ages.

4. RESULTS AND DISCUSSION

4.1. Isotope-inferred lake paleohydrology

Cellulose-inferred $\delta^{18}\text{O}_{\text{lw}}$ records for LP and LTCK are shown in Figure 2. Interpretation of $\delta^{18}\text{O}_{\text{lw}}$ records requires identifying signals related to changes in the isotopic composition of source water, reflecting the integrated signature of surface and subsurface inflow and precipitation, from changing hydrological factors (often primarily evaporative enrichment) that may subsequently modify the isotopic content of the lake water. Deconvolution of these isotopic signals in lake sediments from this region benefit from an independent 25,000-year record of precipitation $\delta^{18}\text{O}$ ($\delta^{18}\text{O}_{\text{p}}$) from the Sajama ice core [8]. The ice-core oxygen isotope stratigraphy, which is also shown in Figure 2, illustrates that values at the base of this interval increased to a maximum at about 14,300 cal yr BP, interpreted to reflect climate warming [8]. Subsequent ^{18}O -depletion with low values persisting until 11,500 cal yr BP has been interpreted as a climatic reversal [8] or may be due to dilution of atmospheric precipitation with ^{18}O -depleted vapour derived from pluvial lakes on the Altiplano [10]. Values increase after 11,500 cal yr BP in response to climate warming [8] and/or draw-down of pluvial lakes and reduction in derived vapour [10], and remain at about $-17\pm 1\text{‰}$ throughout the Holocene presumably reflecting constant temperature as well as moisture source and history. Notably, shifting LP and LTCK $\delta^{18}\text{O}_{\text{lw}}$ offsets from the Sajama ice core $\delta^{18}\text{O}_{\text{p}}$ record provides a measure of changing lake water evaporative enrichment [e.g. 16], which appears to be mainly a function of similarly changing moisture regimes at these two locations, as described below.

Although late Pleistocene $\delta^{18}\text{O}_{\text{lw}}$ data at both LP and LTCK are sparse, results are broadly consistent with regional evidence for moisture fluctuations derived from the recently revised chronology of pluvial lake level history on the southern Bolivian Altiplano [2]. Roughly 10‰ offset of LP $\delta^{18}\text{O}_{\text{lw}}$ from Sajama ice core $\delta^{18}\text{O}_{\text{p}}$ between 14,000 and 11,500 cal yr BP may reflect the importance of lake water evaporative enrichment, corresponding to the Ticaña arid phase [2], or may be partly in response to reduced glacial meltwater supply. Reduced LP-Sajama isotopic offset after 11,500 until 9000 cal yr BP correlates with the final, albeit less significant, pluvial lake high stand (the Coipasa high lake phase), which occurred between about 10,500 and 9500 cal yr BP [2]. Similarly, large LTCK-Sajama isotopic offset beginning prior to 12,700 to about 10,500 cal yr BP may be related to the Ticaña arid phase with subsequent reduced isotopic offset until about 9500 cal yr BP due to wetter conditions during the Coipasa event. The lake water shift to more ^{18}O -depleted values, which we presume to indicate the end of the Ticaña arid phase, appears to take place about 1000 years later at LTCK compared to LP perhaps reflecting poor chronological control in these strata, a greater hydrological threshold at LTCK, or reduced significance of this climate change in the northern Bolivian Altiplano. The latter appears to be consistent with the greater prominence of this event in stratigraphic records from the southern Bolivian Altiplano and Chilean Atacama, whereas evidence for this event in Lake Titicaca sediment records is inconclusive [see 2].

Increasing aridity during the early Holocene at LP is indicated by lake water ^{18}O -enrichment beginning after 9000 cal yr BP, broadly consistent with the paleohydrological record of Lake Titicaca, although a brief return to moist conditions is suggested by ^{18}O -depleted values at about 8000 cal yr BP. Based on the LP record, maximum mid-Holocene aridity developed between 7500 and 6000 cal yr BP. The corresponding 9000 to 6000 cal yr BP interval at LTCK, which is dominated by ^{18}O -depleted values, is most likely a result of a local catchment effect, such as input of ^{18}O -depleted water from snowmelt or groundwater and rapid hydrological flushing [10]. Furthermore, abrupt ^{18}O -enrichment at 6000 cal yr BP observed in the LTCK record would appear to be consistent with a rapid change in water balance resulting from cessation of significant snowmelt and/or groundwater supply from the large catchment [10] and very dry conditions.

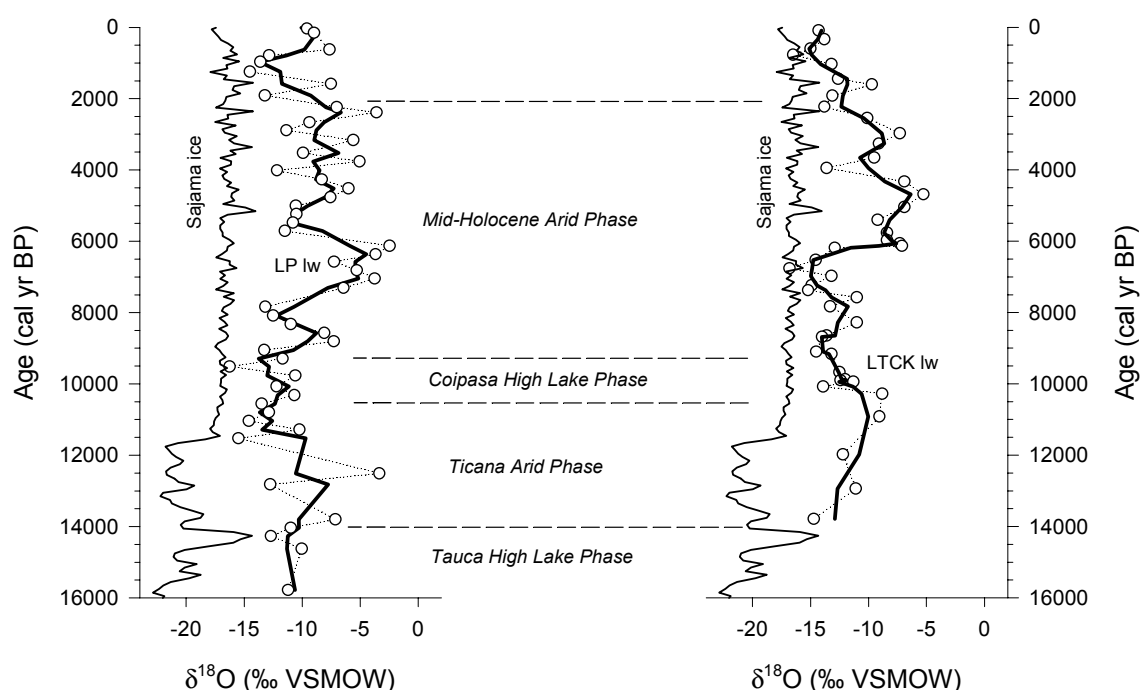


FIG. 2. Lake water $\delta^{18}\text{O}_{\text{lw}}$ records for Lago Potosi and Lago Taypi Chaka Kkota versus cal yr BP, calculated using a cellulose-water oxygen isotope fractionation factor of 1.028 [11,13-14]. Solid lines represent three-point running means. Bulk organic C/N weight ratios range from about 6 to 12 (not shown), which support a dominantly autochthonous origin [15]. Also shown is 16,000 cal yr of the $\delta^{18}\text{O}$ record in the Sajama ice core [8], and stratigraphic zonation of major hydroclimatic intervals based partly on [2].

Analysis of closely-spaced samples has revealed substantial hydrological variability in the 6000 to 2000 cal yr BP $\delta^{18}\text{O}_{\text{lw}}$ record from LP. Highly variable oxygen isotope values have also been obtained on ostracode profiles in lake sediment cores from the Chilean Altiplano during this time interval suggesting predominantly arid conditions were punctuated by short-term climatic shifts [17]. The transition to a more moist climate during the mid- to late Holocene was evidently a step-wise shift characterized by fluctuating moisture conditions on both the Bolivian and Chilean Altiplano [17-19]. Less variability observed in the LTCK $\delta^{18}\text{O}_{\text{lw}}$ during this interval is consistent with this lake's larger size and catchment, and the weak trend to lower $\delta^{18}\text{O}_{\text{lw}}$ values also suggests a gradual shift to more moist conditions overall.

The end of the mid-Holocene arid phase at LP is marked by a decline in $\delta^{18}\text{O}_{\text{lw}}$ values around 2000 cal yr BP, similar to the $\delta^{18}\text{O}_{\text{lw}}$ record from LTCK where glacial meltwater influx returned as a source for the lake [10]. A recent increase in aridity is suggested by ^{18}O -enrichment at both LTCK and LP after 1000 cal yr BP.

4.2. Quantitative reconstruction of paleohumidity

Largely coherent $\delta^{18}\text{O}_{\text{lw}}$ trends between LTCK and LP that conform to the regional paleoclimatic framework can be used to support a more quantitative description of changing paleohumidity by using an isotope-mass balance approach (Figure 3a). At isotopic steady-state, the relationship between the fraction of lake water lost by evaporation and isotopic enrichment by evaporation for a lake with both inflow and outflow can be described by the following equations [20]:

$$(1) \quad E/I = (1-h)/h \times (*_{\text{lw}} - *_{\text{p}}) / (*^* - *_{\text{lw}})$$

where E = vapour flux,

I = inflow,

h = relative humidity at the air-water interface (which may be slightly higher than ambient),

$*^*$ = limiting isotopic enrichment attainable where the water body evaporates to near zero volume

$*_{\text{lw}}$ = lake water isotopic composition,

$*_{\text{p}}$ = precipitation isotopic composition,

and

$$(2) \quad \delta^* = (h\delta_{\text{a}} + \epsilon) / (h - \epsilon)$$

where δ_{a} = vapour isotopic composition,

ϵ = isotopic separation between liquid and vapour including both equilibrium (ϵ^*) and kinetic (ϵ_{K}) effects.

Isotope-mass balance methods can be used to assess contemporary water balance of lakes [21-22], as well as to reconstruct past water balance from lacustrine records of $\delta^{18}\text{O}$ [23]. Here, we use this model to estimate summer relative paleohumidity (SRH) from the LP cellulose-inferred three-point running mean $\delta^{18}\text{O}_{\text{lw}}$ record. The LP $\delta^{18}\text{O}_{\text{lw}}$ record was chosen for SRH reconstruction because the record at this site does not appear to be complicated by additional hydrological effects, as is the case at LTCK during the early Holocene (possible snowmelt and/or groundwater supply) and late Holocene (glacial meltwater influx) [see 10]. The reconstruction is limited to the past 11,500 cal yr where the LP $\delta^{18}\text{O}_{\text{lw}}$ record is more highly resolved and temporally constrained. Model input values include: 1) $\delta_{\text{p}} = -17\text{‰}$ estimated from the Sajama ice core $\delta^{18}\text{O}$ record (Figure 2), which also closely approximates the intersection of the REL and GMWL in Figure 1, 2) $\delta_{\text{a}} = \delta_{\text{p}} - \epsilon^*$ (i.e. isotopic equilibrium between atmospheric vapour and precipitation), 3) $\epsilon^* = 10.66\text{‰}$ from [24] and using an average air temperature of 10°C [9], and 4) $\epsilon_{\text{K}} = 14.2(1-h)$ [25].

SRH is solved iteratively for three water balance scenarios that conservatively span the probable maximum range in natural variability over the past 11,500 cal yr (Figure 3b). 1) $E/I = 1.00$ defines conditions for a terminal basin where evaporation balances inflow so that no liquid outflow occurs. This represents the maximum fraction of lake water lost by evaporation

as long-term hydrological status characterized by $E/I > 1$ is considered unlikely because this would lead to lake desiccation and absence of a stratigraphic record. 2) $E/I = 0.20$ was used to represent the minimum fraction of lake water lost by evaporation. This value is estimated from calculation of modern E/I ratios for overflowing lakes in non-glaciated watersheds and using the most isotopically-enriched lake water sample in our modern data set as a lower limit for δ^* (Figure 1). 3) $E/I = 0.36$ represents an estimate of the average summer water balance at present for LP based on a modern SRH value of 50% [9]. Comparison to modern conditions was used to derive a range in SRH values, bracketing concomitant water balance response to changing effective moisture using the three E/I scenarios. Results are plotted in Figure 3c in terms of minimum, maximum, and mean SRH values.

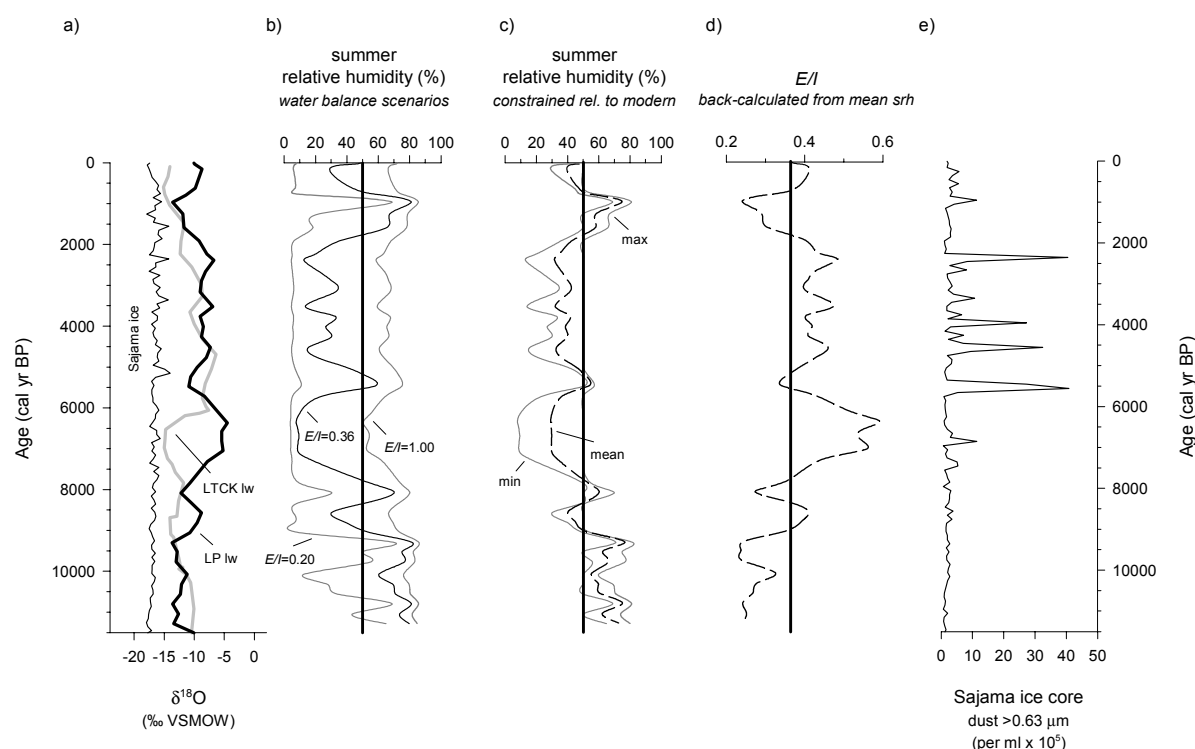


FIG. 3a) Sajama ice core $\delta^{18}O$ (Thompson et al., 1998) and cellulose-inferred three-point running mean $\delta^{18}O_{lw}$ records for Lago Taypi Chaka Kkota and Lago Potosi from Figure 2. b) Summer relative humidity profiles generated by E/I scenarios of 0.20, 0.36, and 1.00 based on the Lago Potosi three-point running mean $\delta^{18}O_{lw}$ profile. c) Summer relative humidity reconstruction representing minimum, maximum, and mean values constrained by values generated by the three E/I scenarios in b) and the modern summer relative humidity value of 50%. d) Estimated average summer water balance conditions (expressed as E/I) derived from back-calculation using mean summer relative humidity values in c). e) The Sajama ice core dust record from [8]. All records are plotted versus cal yr BP.

In general, results from Figure 3c show that SRH values averaged 10-20% higher relative to present at 11,500 cal yr BP with oscillating but generally declining values developing during the early Holocene. This trend culminates in maximum SRH decrease between 7500 and 6000 cal yr BP when reconstructed values average 20% lower than present. SRH values are near present between 6000 and 5000 cal yr BP and then decline to values averaging 15% lower than present until about 2500 cal yr BP. Mean SRH values increase to about 20% greater than present by about 1500 cal yr BP and then decline to around 5-10% less than present over the last 1000 years.

Notably large ranges between minimum and maximum SRH values are evident at low SRH compared to the present value of 50%, which is primarily a function of the large uncertainty in E/I ratios (0.36 to close to 1.00) that bracket these intervals. This extreme sensitivity is somewhat artificial, however, because the actual E/I ratios are relatively high during phases of low SRH, although not as high as 1.00 as values generated by this scenario are nearly always higher than 50%. This indicates that LP may have rarely attained wet-season terminal hydrological status for an extended period even during more arid intervals; a result that is not unexpected, however, as overcoming this threshold would likely have led to rapid volume draw-down, lake desiccation and hiatuses in sedimentation due to the low relative humidity. Indeed, the $\delta^{18}\text{O}_{\text{lw}}$ record is very sensitive to SRH below about 50% and because extreme ^{18}O -enrichment is not observed, SRH values substantially less than 40% are probably not reasonable. Conversely, less uncertainty is evident at high SRH mainly because of the narrower range in E/I ratios (0.20 to 0.36) that were used to delineate these phases (mainly 11,500 to 9000 and 2000 to 1000 cal yr BP). Based on back-calculation using the mean SRH reconstruction, we estimate that the average summer E/I ratio spanned mainly from about 0.25 to 0.60 over the past 11,500 cal yr (Figure 3d).

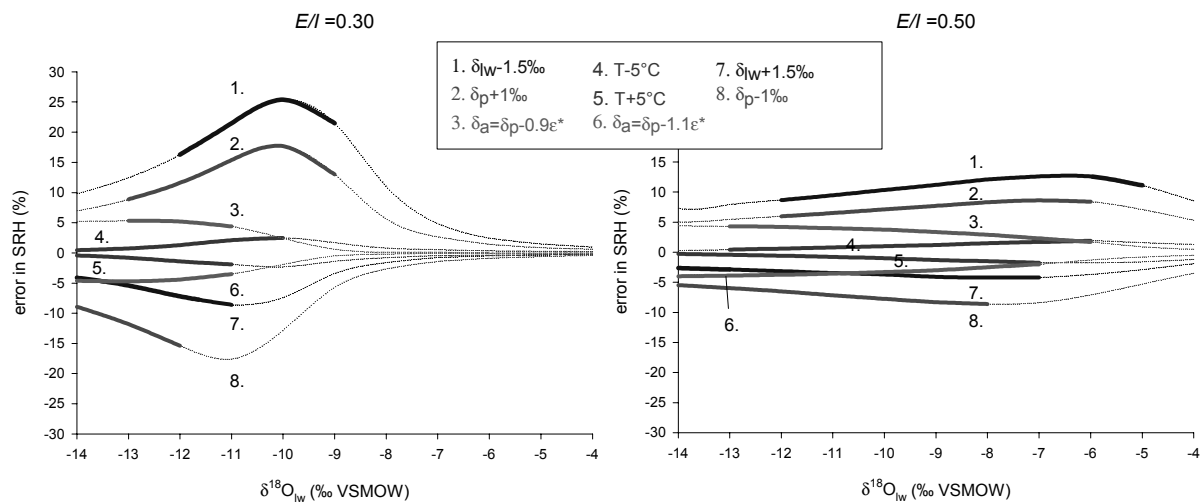


FIG. 4. Sensitivity analysis illustrating potential errors in summer relative humidity (SRH) values for variations of $\delta_{\text{lw}} = \pm 1.5\text{‰}$ (incorporating analytical and cellulose-water oxygen isotope fractionation uncertainty), $\delta_{\text{p}} = \pm 1.0\text{‰}$ (comprising most of the variation in the isotopic record from Sajama ice core over the past 11,500 cal yr BP) [8], $T = \pm 5^\circ\text{C}$ (estimated to reflect changes during the late Pleistocene - early Holocene transition and possibly during the interval of maximum aridity), and $\delta_{\text{a}} = \delta_{\text{p}} - \pm 10\text{‰}(\epsilon^*)$ (10 % deviation from isotopic equilibrium between δ_{a} and δ_{p}). Results are shown for the average summer E/I ratio during wet (0.30) and dry intervals (0.50), as estimated from Figure 3d. Note that solid lines define SRH errors that result in absolute values ranging from 30 to 85%, representing an estimate of the natural range potential in SRH.

Supporting evidence for widespread and similarly arid conditions during the mid- to late Holocene is provided by the LTCK $\delta^{18}\text{O}_{\text{lw}}$ profile and other records of past climate change. Between 6000 and 2000 cal yr BP, the $\delta^{18}\text{O}_{\text{lw}}$ values are broadly similar (Figure 3a) and in the range of lakes that presently drop below their overflow level under more moderate conditions (Figure 1). These overlapping trends may reflect similar E/I ratios and SRH during this time interval. Offset in cellulose-inferred $\delta^{18}\text{O}_{\text{lw}}$ over the last 1000 years suggests that the current effective moisture gradient between these two lakes may be a recent development. SRH minima during the mid- to late Holocene interval also shows close correspondence between

dust concentration maxima in the Sajama ice core record, with both records reflecting dominantly arid but highly variable moisture conditions (Figure 3e), in agreement with other records on the Chilean Altiplano as mentioned above [17-19]. Lake Titicaca lowstands at about 6100 and 2400 cal yr BP [5, 26] and lake-level inferred maximum aridity between 8000 and 5500 cal yr BP [7] also compare well with the SRH reconstruction.

4.3 Model uncertainties

A sensitivity analysis was conducted to estimate potential sources of error associated with input parameters to equations (1) and (2) to derive past SRH values, in addition to uncertainties due to shifting E/I . Figure 4 illustrates the effect of $\delta_{lw} = \pm 1.5\text{‰}$, $\delta_p = \pm 1.0\text{‰}$, $T = \pm 5^\circ\text{C}$, and $\delta_a = \delta_p - \pm 10\text{‰}$ (ϵ^*) on reconstructed SRH values for two water balance scenarios: 1) $E/I = 0.30$, which is estimated to reflect average conditions during wet intervals, and 2) $E/I = 0.50$ corresponding to estimated average conditions during dry phases (see Figure 3c). Overall, potential error in SRH values is less in the $E/I = 0.50$ scenario, with δ_{lw} and δ_p input variations resulting in mostly $<10\%$ error, and T and δ_a input variations producing $<5\%$ error.

Potential SRH errors are greater in the $E/I = 0.30$ scenario, although only $\delta_{lw} - 1.5\text{‰}$ and $\delta_p + 1\text{‰}$ variations over a narrow range of $\delta^{18}\text{O}_{lw}$ values result in errors in excess of $(+)\text{15\%}$.

5. CONCLUSION

Comparison of cellulose-inferred lake water oxygen isotope profiles from two lakes in the Bolivian Andes provides a record of late Pleistocene and Holocene paleohydrological history that is largely in agreement with the regional framework based mainly on pluvial lake history, water level changes in Lake Titicaca, and the Sajama ice core record. Overall, the isotopic records indicate dominantly moist conditions during the late Pleistocene - early Holocene transition (roughly 10,500 to 9000 cal yr BP) and between 2000 and 1000 cal yr BP, whereas more arid conditions prevailed during the mid-late Holocene (mainly 8000 to 2000 cal yr BP) and over the past millennium. At LP, sustained maximum mid-Holocene aridity occurred between 7500 and 6000 cal yr BP and quantitative reconstruction of SRH, based on an isotope-mass balance model, indicates a decline of perhaps as much as 20% during this time. SRH values averaged 15% less than present but was highly variable during the later part of the mid-Holocene arid interval (*ca.* 5000-2000 cal yr BP), in agreement with other paleoclimatic records from the region [17-19, 26] including the Sajama ice core record where close correspondence occurs between several elevated dust particle concentrations [8] and SRH minima. Sensitivity analyses suggests potential errors in reconstructed SRH values are mainly related to uncertainty in the E/I ratio during arid intervals and cellulose-inferred $\delta^{18}\text{O}_{lw}$ and ice-inferred $\delta^{18}\text{O}_p$ values during wet intervals.

Notably, the SRH reconstruction sets the stage for comparison with new proxy records currently being obtained from similar lakes north of the equator in the Venezuelan Andes. In addition, these results reveal the potential for quantitative paleoclimatic reconstructions based on cellulose-inferred lake water oxygen isotope records. Key factors that have contributed to the viability of this approach include an independent detailed record of $\delta^{18}\text{O}_p$ and analysis of lake sediment records in contrasting settings, the latter having effectively allowed differentiation of local hydrological variations from regional climatic changes.

ACKNOWLEDGEMENTS

Comments by A. Longinelli, an anonymous reviewer, and T. Edwards helped to clarify several aspects the manuscript. We also thank L. Thompson for providing data from the Sajama ice core and A. Wolfe for assistance in obtaining the lake sediment cores. Assistance with sample preparation and analysis by R. Elgood and the UW-EIL is greatly appreciated. This research was funded by NSF grant ATM-9632267 to M.B. Abbott and ATM-9613991 to G.O. Seltzer. Additional financial support was provided by an NSERC postdoctoral fellowship to B.B. Wolfe.

REFERENCES

- [1] CLAYTON, J.D., CLAPPERTON, C.M., Broad synchrony of a late-glacial glacier advance and the highstand of paleolake Tauca in the Bolivian Altiplano. *J. Quat. Sci.* **12** (1997) 169-182.
- [2] SYLVESTRE, F., SERVANT, M., SERVANT-VILDARY, S., CAUSSE, C., FOURNIER, M., YBERT, J.P., Lake-level chronology on the southern Bolivian Altiplano (18°-23° S) during late-glacial time and the early Holocene. *Quat. Res.* **51** (1999) 54-66.
- [3] WIRRMANN, D., DE OLIVIERA ALMEIDA, L.F., Low Holocene level (7700 to 3650 years ago) of Lake Titicaca (Bolivia). *Palaeogeogr., Palaeoclimatol., Palaeoecol.* **59** (1987) 315-323.
- [4] WIRRMANN, D., MOURGUIART, P., Late Quaternary spatio-temporal limnological variations in the Altiplano of Bolivia and Peru. *Quat. Res.* **43** (1995) 344-354.
- [5] MOURGUIART, PH., CORRÈGE, T., WIRRMANN, D., ARGOLLO, J., MONTENEGRO, M.E., POURCHET, M., CARBONEL, P., Holocene palaeohydrology of Lake Titicaca estimated from an ostracod-based transfer function. *Palaeogeogr., Palaeoclimatol., Palaeoecol.* **143** (1998) 51-72.
- [6] CROSS, S.L., BAKER, P.A., SELTZER, G.O., FRITZ, S.C., DUNBAR, R.B., A new estimate of the Holocene lowstand level of Lake Titicaca, central Andes, and implications for Tropical palaeohydrology. *The Holocene* **10** (2000) 21-32.
- [7] BAKER, P.A., SELTZER, G.O., FRITZ, S.C., DUNBAR, R.B., GROVE, M.J., TAPIA, P.M., CROSS, S.L., ROWE, H.D., BRODA, J.P., The history of South American tropical precipitation for the past 25,000 years. *Science* **291** (2001) 640-643.
- [8] THOMPSON, L.G., DAVIS, M.E., MOSLEY-THOMPSON, E., SOWERS, T.A., HENDERSON, K.A., ZAGORODNOV, V.S., LIN, P.-N., MIKHALENKO, V.N., CAMPEN, R.K., BOLZAN, J.F., COLE-DAI, J., FRANCOU, B., A 25,000-year tropical climate history from Bolivian ice cores. *Science* **282** (1998) 1858-1864.
- [9] BOLETIN METEOROLOGICO DEL DEPARTAMENTO DE POTOSI, Servicio Nacional De Meteorologia E Hidrologia (SENAMHI). Potosi, Bolivia (1996).
- [10] ABBOTT, M.B., WOLFE, B.B., ARAVENA, R., WOLFE, A.P., SELTZER, G.O., Reconstructing hydrological conditions during the Holocene in an alpine Andean lake from stable isotopes and palaeolimnology, Cordillera Real, Bolivia. *Quat Sci. Rev.* **19** (2000) 1801-1820.
- [11] WOLFE, B.B., EDWARDS, T.W.D., BEUNING, K.R.M., ELGOOD, R.J. Carbon and oxygen isotope analysis of lake sediment cellulose: methods and applications. In: Last, W.M., Smol, J.P. (Eds.), *Tracking Environmental Change Using Lake Sediments: Volume 2: Physical and Chemical Techniques*. Kluwer, Academic Publishers, Dordrecht. (2001 in press).
- [12] Coplen, T.B., 1996. New guidelines for reporting stable hydrogen, carbon, and oxygen isotope-ratio data. *Geoch. Cosmoch. Acta* **60** (1996) 3359-3360.

- [13] STERNBERG, L.S.L., Oxygen and hydrogen isotope ratios in plant cellulose: mechanisms and applications. In: Rundel, P.W., Ehleringer, J.R., Nagy, K.A. (Eds.), *Stable Isotopes in Ecological Research*. Springer-Verlag, New York (1989) 124-141.
- [14] YAKIR, D., Variations in the natural abundance of oxygen-18 and deuterium in plant carbohydrates. *Pl. Cell Environ.* **15** (1992) 1005-1020.
- [15] MEYERS, P.A., LALLIER-VERGÈS, E., Lacustrine sedimentary organic matter records of late Quaternary paleoclimates. *J. Paleolim.* **21** (1999) 345-372.
- [16] SELTZER, G.O., RODBELL, D., BURNS, S., Isotopic evidence for late Quaternary climatic change in tropical South America. *Geology* **28** (2000) 35-38.
- [17] SCHWALB, A., BURNS, S.J., KELTS, K., Holocene environments from stable isotope stratigraphy of ostracods and authigenic carbonate in Chilean Altiplano lakes. *Palaeogeogr., Palaeoclimatol., Palaeoecol.* **148** (1999) 153-168.
- [18] VALERO-GARCÉS, B.L., GROSJEAN, M., SCHWALB, A., GEYH, M., MESSERLI, B., KELTS, K., Limnogeology of Laguna Miscanti: evidence for mid to late Holocene moisture changes in the Atacama Altiplano (northern Chile). *J. Paleolim.* **16** (1996) 1-21.
- [19] GROSJEAN, M., VALERO-GARCÉS, B., GEYH, M.A., MESSERLI, B., SCHREIER, H., KELTS, K., Mid and late Holocene limnogeology of Laguna del Negro Francisco (South-Central Andes, North Chile) and paleoclimatic implications. *The Holocene* **7** (1997) 151-159.
- [20] GAT, J.R., Lakes. In Gat, J.R., Gonfiantini, R. (Eds.), *Stable Isotope Hydrology - Deuterium and Oxygen-18 in the Water Cycle*. Technical Report Series No. 210, IAEA, Vienna (1981) 203-221.
- [21] GAT, J.R., LEVY, Y., Isotope hydrology of inland sabkhas in the Bardawil area, Sinai. *Limnol. Oceanogr.* **23** (1978) 841-850.
- [22] GIBSON, J.J., EDWARDS, T.W.D., BURSEY, G.G., PROWSE, T.D., Estimating evaporation using stable isotopes: quantitative results and sensitivity analysis for two catchments in northern Canada. *Nord. Hydrol.* **24** (1993) 79-94.
- [23] EDWARDS, T.W.D., WOLFE, B.B., MACDONALD, G.M., Influence of changing atmospheric circulation on precipitation $\delta^{18}\text{O}$ - temperature relations in Canada during the Holocene. *Quat. Res.* **46** (1996) 211-218.
- [24] Majoube, M., 1971. Fractionnement en oxygène et en deutérium entre l'eau et sa vapeur. *J. Chim. Phys.* **197** (1971) 1423-1436.
- [25] GONFIANTINI, R., Environmental isotopes in lake studies. In Fritz, P., Fontes, F. Ch. (Eds.), *Handbook of Environmental Isotope Geochemistry 2*. Elsevier, New York (1986) 113-168.
- [26] ABBOTT, M.B., BINFORD, M.W., BRENNER, M., KELTS, K.R., A 3500 ^{14}C yr high-resolution record of lake level changes in Lake Titicaca, Bolivia/Peru. *Quat. Res.* **47** (1997) 169-180.

**PALAEOCLIMATE ARCHIVES III
ICE CORES AND RELATED ENVIRONMENTS**

(Session 5)

Chairpersons

A. HENDERSON-SELLERS
Australia

L.G. THOMPSON
United States of America

PAST CLIMATE CHANGES DERIVED FROM ISOTOPE MEASUREMENTS IN POLAR ICE CORES

J. BEER, R. MUSCHELER, G. WAGNER

Swiss Federal Institute of Environmental Science and Technology (EAWAG),
Dübendorf, Switzerland

P.K. KUBIK

Paul Scherrer Institute, Zürich, Switzerland

Abstract. Measurements of stable and radioactive isotopes in polar ice cores provide a wealth of information on the climate conditions of the past. Stable isotopes ($\delta^{18}\text{O}$, δD) reflect mainly the temperature, whereas $\delta^{18}\text{O}$ of oxygen in air bubbles reveals predominantly the global ice volume and the biospheric activity. Cosmic ray produced radioisotopes (cosmogenic nuclides) such as ^{10}Be and ^{36}Cl record information on the solar variability and possibly also on the solar irradiance. If the flux of a cosmogenic nuclide into the ice is known the accumulation rate can be derived from the measured concentration. The comparison of ^{10}Be from ice with ^{14}C from tree rings allows deciding whether observed ^{14}C variations are caused by production or system effects. Finally, isotope measurements are very useful for establishing and improving time scales. The $^{10}\text{Be}/^{36}\text{Cl}$ ratio changes with an apparent half-life of 376,000 years and is therefore well suited to date old ice. Significant abrupt changes in the records of ^{10}Be , ^{36}Cl from ice and of $\delta^{18}\text{O}$ from atmospheric oxygen representing global signals can be used to synchronize ice and sediment cores.

1. INTRODUCTION

Stable and radioactive isotopes are useful tools to study present and past environmental changes. Due to progress in analytical techniques, very small samples can now be analyzed with high precision. This opens up the possibility of reconstructing past environmental changes with high temporal resolution in natural archives and of obtaining a comprehensive picture of the spatial and temporal variability of our climate system. For several reasons, ice cores merit special attention. They are the only archive, which stores not only all particular constituents removed from the atmosphere but also air samples. This unique property allows for instance to reconstruct the history of greenhouse gas concentrations as well as isotopic changes in atmospheric oxygen, a proxy for the global ice volume. During the last few decades, several ice cores were successfully retrieved from Greenland and Antarctica containing complete and continuous ice records of the last 100,000 or more years. Recently, the information derived from polar ice cores has been complemented by new data from an increasing number of low-latitude ice cores drilled into high-altitude ice sheets. The latter are crucial to the understanding of the regional patterns of climate changes. In this short overview, we will concentrate mainly on isotopes from polar ice cores.

1.1 Stable isotopes

Usually, an ice core is first analyzed for $\delta^{18}\text{O}$ and/or δD . The isotopic fractionation that takes place in the inversion layer during the condensation of water vapor to raindrops or snowflakes is strongly temperature dependent. The calibration of the relationship between $\delta^{18}\text{O}$ and temperature is usually made by applying linear regression to a set of annual data from different sites, where $\delta^{18}\text{O}$ and/or δD and temperature have been measured. In Fig. 1a, the δD record from Vostok, Antarctica is shown [1]. It covers more than 4 glacial cycles. Spectral analysis of the Vostok record reveals the Milankovich cycles caused by changes in the orbital

parameters of the Earth. Periodicities around 100 kyrs (eccentricity), 40 kyrs (obliquity), and 20 kyrs (precession) were found. A detailed view of climate changes during the younger part of the last glacial is depicted in Fig. 2 showing the GRIP $\delta^{18}\text{O}$ record from Greenland [2]. Being representative for the North Atlantic temperature the GRIP $\delta^{18}\text{O}$ record is dominated by a series of very rapid fluctuations, the so-called Dansgaard-Oeschger events (DOE). Typically, $\delta^{18}\text{O}$ increases by about 5‰ within decades, then begins to decline slowly and subsequently drops rapidly to the low value it had at the beginning. The general explanation for this behavior is the switching on and off of the deep-water formation in the North Atlantic [3]. Melt water from the Laurentide ice sheet surging into the North Atlantic leads to a drop in the density of the surface water and shuts down the thermohaline circulation. As a consequence, the heat transport from low latitudes to Greenland is interrupted and the temperature decreases dramatically. After some time, the thermohaline circulation sets in again and the temperature rises. As we will see below, this process can be studied on a global scale using radioisotopes.

However, one should bear in mind that the simple linear relationships between $\delta^{18}\text{O}$ or δD and the temperature have been established based on a spatial network of climatically different stations. These relationships depend also on other parameters such as the source area and the transport of water vapor and the seasonal distribution of precipitation. In fact, using these simple relationships leads to a temperature change of approx. 10°C for central Greenland between the Holocene and the last glacial maximum. The analyses of borhole temperatures on the other hand points to a much larger change (20°C) [5] indicating that besides temperature changes other changes were involved as well.

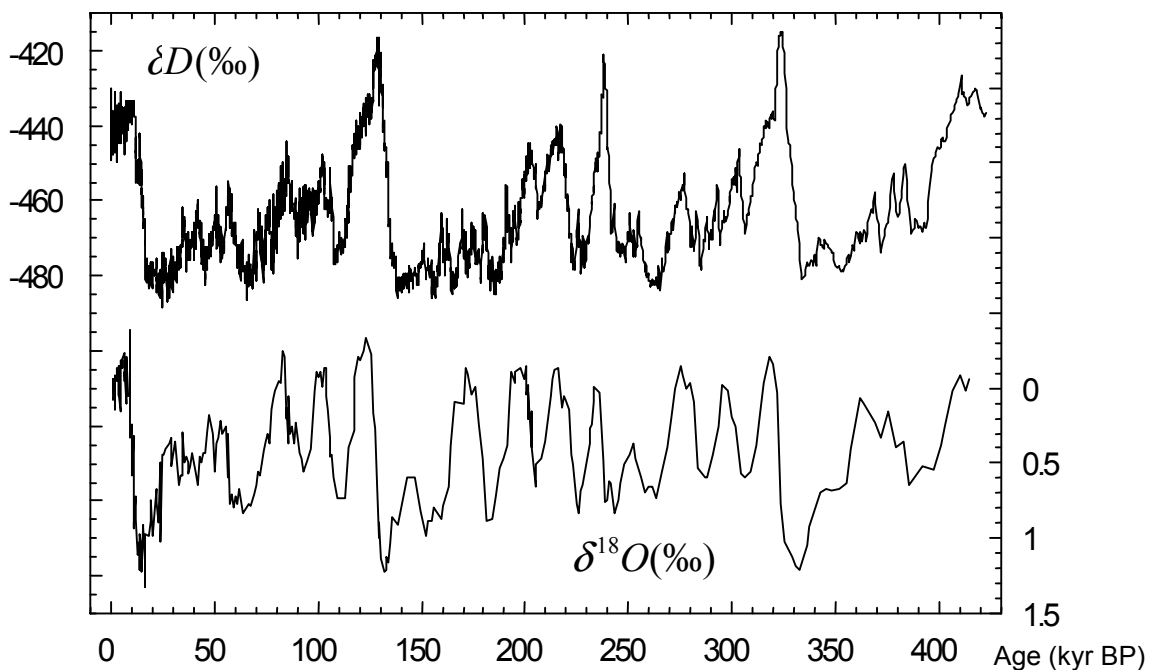


FIG. 1. Records of stable isotopes from the Vostok ice core over the last 440 kyrs, a) δD measured in the ice reflects the temperature [1], (b) $\delta^{18}\text{O}$ measured in air bubbles provides information on the global ice volume and the biospheric activity [4].

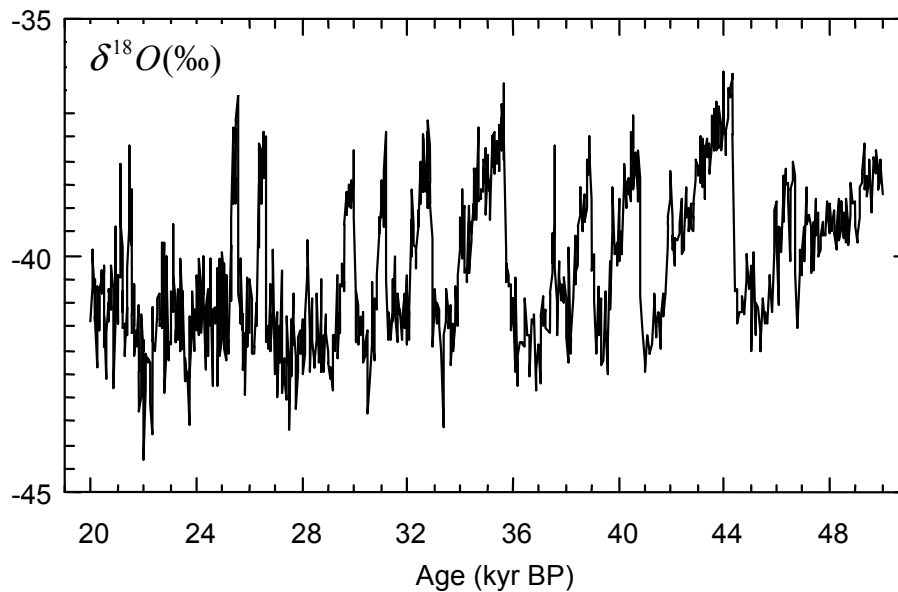


FIG. 2. Section of the $\delta^{18}\text{O}$ record from that section of the GRIP ice core, which is characterized by abrupt climate changes, the so-called Dansgaard-Oeschger events [2].

Ice cores offer the unique opportunity to measure $\delta^{18}\text{O}$ not only in solid precipitation (snow and ice) but also in gaseous O_2 trapped in air bubbles. $\delta^{18}\text{O}$ of atmospheric oxygen reflects the $\delta^{18}\text{O}$ signal of sea water after modification by hydrological (transpiration, evapotranspiration) and biochemical (photosynthesis, respiration) processes. [6]. The $\delta^{18}\text{O}$ difference between sea water and atmospheric oxygen (Dole effect) is mainly due to fractionation during respiration. Hence $\delta^{18}\text{O}$ in an ice core provides information about the local temperature and the global ice volume and the biospheric activity at the same time. As shown in Fig. 1 the overall agreement between the δD of ice and the $\delta^{18}\text{O}$ in air bubbles in the Vostok core is good [4]. However, small differences indicate that some of the involved processes were not constant.

1.2. Radioisotopes

Ice sheets and glaciers are ideal archives for all radioisotopes, which are transported through the atmosphere and removed by wet or dry deposition processes. In the following discussion, we consider only so-called cosmogenic radionuclides. Galactic cosmic ray particles interact in high-energy nuclear reactions with atmospheric nitrogen, oxygen and argon. As a result, a cascade of secondary particles develops until all the energy of the primary particle is dissipated. Among the secondary particles, mainly neutrons and protons are responsible for the reactions leading to cosmogenic nuclides. For some of them the main properties such as half-life, main target elements and mean global production rate are given in Table I. The flux of the galactic cosmic rays is modulated by magnetic fields, which deflect mainly the low-energetic particles. The Earth's magnetic dipole field prevents particles of a rigidity below a geomagnetic-latitude dependent cut-off energy from penetrating into the atmosphere. The second magnetic modulation effect originates from the sun. Solar wind carrying frozen-in magnetic fields fills the vicinity of the solar system and also acts as a magnetic shield. During periods of high solar activity, the solar wind intensity increases enhancing the shielding effect and therefore reducing the production rate of cosmogenic nuclides and vice-versa. After production, the fate of cosmogenic nuclides depends strongly on their geochemical properties. Some of them, such as ^{10}Be , become attached to aerosols and follow their pathways. After a mean residence time of 1 to 2 years, they are removed from the atmosphere mainly by wet

precipitation. ^{14}C , on the other hand, becomes oxidized to $^{14}\text{CO}_2$ and exchanges between the carbon reservoirs atmosphere, biosphere and ocean. The production rate of cosmogenic nuclides can be calculated as a function of solar and geomagnetic modulation [7]. In the following, we will discuss some of the most important applications of cosmogenic nuclides for climate change research of the past.

Table I. Some properties of cosmogenic nuclides

Nuclide	$T_{1/2}$ (y)	Target	Production rate (atoms $\text{cm}^{-2} \text{s}^{-1}$)
^{10}Be	$1.5 \cdot 10^6$	N, O	0.018
^{14}C	5730	N, O	2.02
^{36}Cl	$3.01 \cdot 10^5$	Ar	0.0019

2. SOLAR VARIABILITY

The sun is the fundamental source of energy that drives the climate system. Changes in solar radiation inevitably lead to adjustments in the radiation balance of the earth and to modifications of the complex climate system. Direct measurements of solar irradiance (solar constant) with satellite-based radiometers revealed variations in phase with the 11-year Schwabe cycle over the last two decades [8]. The yearly averaged amplitude of this cycle is too small (0.1%) and the changes are too fast to induce relevant climate changes. However, this does not mean that over longer time scales, the solar irradiance did not undergo much larger changes, which may have significantly affect the climate [9]. In fact, there are clear indications that solar irradiance has increased since the Maunder minimum (1645-1715 AD) by about 0.24% [10]. The Maunder minimum period is famous for its almost complete lack of sunspots pointing to a different mode of the solar magnetic dynamo. At the same time, this period is known for much cooler temperatures (Little Ice Age). Evidence for a much larger potential of solar variability than observed in our sun so far comes from other solar type stars [11]. A long-term study of many such stars suggests that changes in radiation of up to 1% can occur. To investigate, whether the sun ever made use of this potential it becomes necessary to learn more about the solar activity of the past. Direct, detailed and reliable observations of solar variability are limited to the telescopic era, which goes back to about 1600 AD. To extend this period, one has to rely on indirect solar parameters such as cosmogenic nuclides. The analyses of ^{14}C records in tree rings and ^{10}Be data from polar ice cores [12] reveals periodicities around 11 years (Schwabe cycle) and 90 years (Gleissberg cycle), as expected from the sunspot records. The 205 De Vries cycle could be found during the Holocene and between 25 and 50 kyrs B.P. [13]. This suggests that the solar dynamo is characterized by several periodicities which appear to be active and rather constant averaged over long times, although the amplitudes may change with time.

Special features attributed to reduced solar activity are the so-called “grand minimum” periods like the Maunder minimum. Such minima occur irregularly with different durations throughout the Holocene. In Fig. 3, the $\Delta^{14}\text{C}$ (of the atmospheric $^{14}\text{C}/^{12}\text{C}$ ratio from a standard in permil) derived from tree rings [14] is shown for the last 7 kyrs after subtraction of the long-term trend. The solar minimum periods, which correspond to production maxima, are indicated with arrows. It is interesting to note that several of these minima in solar activity can be related to deteriorations in the climate [15] underlining that cosmogenic nuclides play a key role in establishing a causal relationship between solar variability and climate change [16].

3. ACCUMULATION RATE

Probably the most fundamental parameter of climate change is the precipitation rate. In theory, an ice core represents a complete collection of all the past precipitation and measuring annual layer thicknesses can therefore be used to reconstruct the history of precipitation. However, in practice, there are two problems that complicate the situation considerably. Firstly, ice flows and this leads to a thinning of the annual layer thickness with increasing depth. To correct for this effect one has to apply ice flow models. Secondly, the discrimination between annual layers becomes impossible at larger depths. Again, cosmogenic nuclides provide a solution. It is based on the following two assumptions: 1. Averaged over a large area, the flux of e.g. ^{10}Be from the atmosphere into the ice is proportional to the production rate in the atmosphere: $F = \alpha \cdot P$. 2. Averaged over millennia the production rate is mainly determined by the geomagnetic field intensity.

F can also be expressed by:

$$F = \rho \cdot c \cdot \text{acc},$$

the product of ice density ρ , radionuclide concentration c and accumulation rate acc which leads to

$$\text{acc} = \alpha \cdot P / (\rho \cdot c).$$

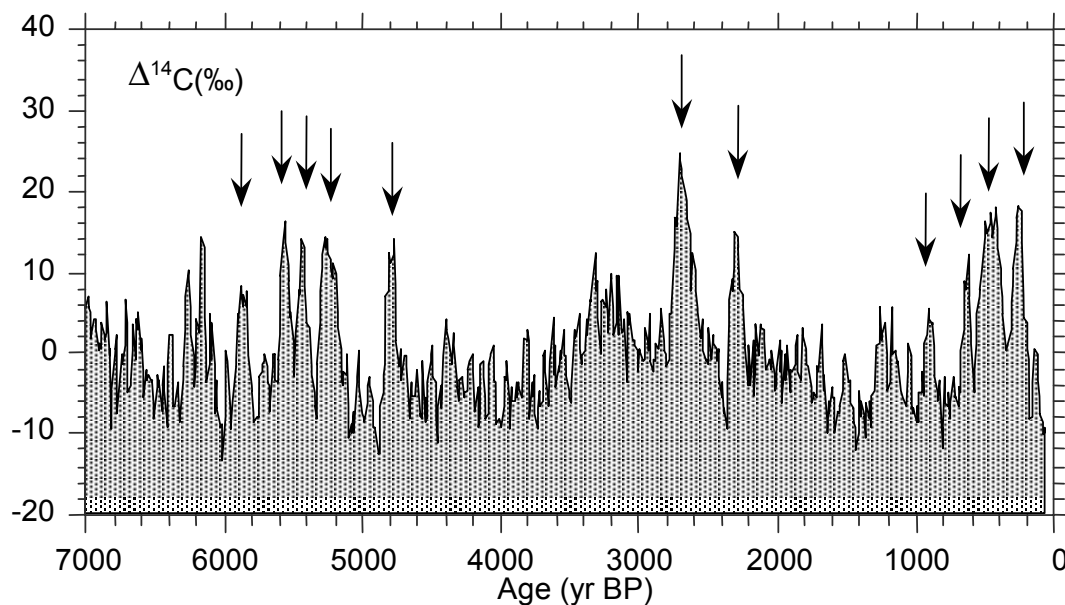


FIG. 3. $\Delta^{14}\text{C}$ record derived from tree rings [14] after subtraction of the long-term trend. Periods of increased ^{14}C production, which are generally thought to coincide with periods of a quiet sun are indicated by arrows.

Since ρ is virtually constant (0.92 g/cm^3), α can be determined for modern times and P can be derived from paleomagnetic measurements [17] the accumulation rate can be calculated. The results of this approach when using ^{10}Be in the GRIP ice core confirm Johnson's reconstruction which is based on an empirical relationship between $\delta^{18}\text{O}$ from ice and the annual layer thickness corrected for the thinning [18]. Fig. 4 shows that, in Greenland, the precipitation or accumulation rate changed dramatically during the last glacial in phase with the temperature.

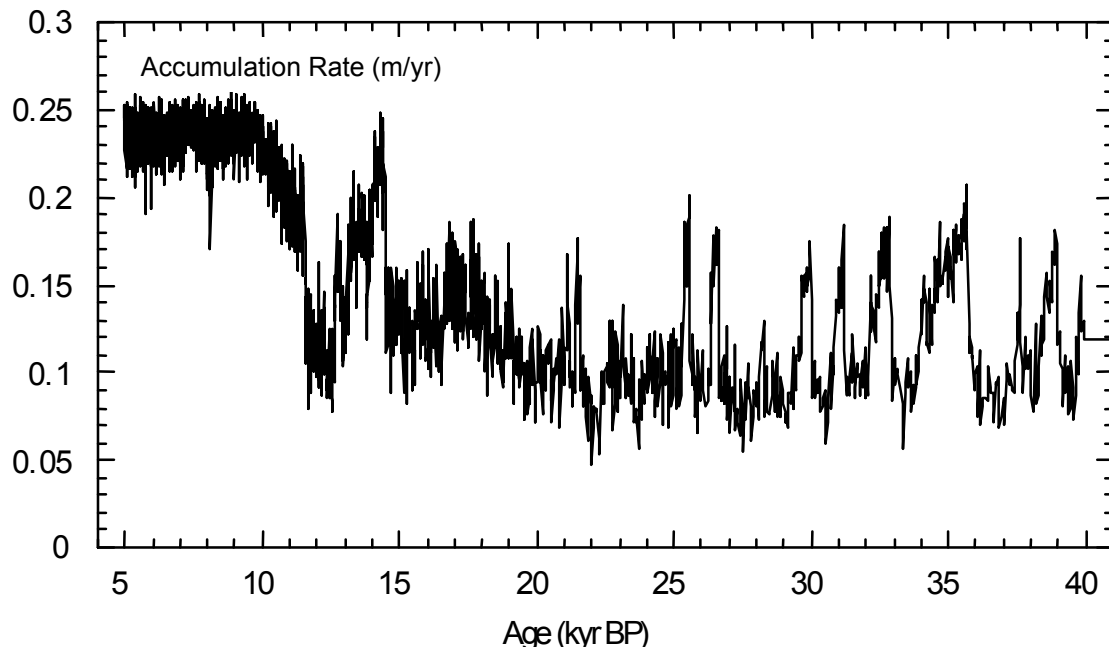


FIG. 4. Accumulation rate at Summit (Central Greenland) based on an empirical relationship between $\delta^{18}\text{O}$ [18] and the accumulation rate determined by layer counting and extrapolated to older ages (see text). This accumulation rate is confirmed by the accumulation rate derived from ^{10}Be measurements in the GRIP ice core.

4. THERMOHALINE CIRCULATION

The thermohaline circulation is a basic process for the oceanic heat transport from equatorial to polar regions. Since most of the deepwater formation takes place in the North Atlantic, Greenland's climate is especially sensitive to modifications in thermohaline circulation. In fact, it is generally believed that the rapid climate fluctuations during glacial times (DOE) (Fig. 2) are due to changes in this transport system. Since the ocean is the main reservoir of atmospheric CO_2 , and the mean oceanic residence time of CO_2 is about 1,000 years, the thermohaline circulation affects the atmospheric $^{14}\text{C}/^{12}\text{C}$ ratio. A slowdown of the thermohaline circulation leads to a reduction in the removal rate of ^{14}C from the atmosphere and therefore to an increase in atmospheric $\Delta^{14}\text{C}$. But an increase could also be caused by a higher ^{14}C production rate due to a reduction in solar activity or geomagnetic field intensity. To distinguish between these two possibilities (thermohaline circulation or production), additional information is necessary. This is provided by ^{10}Be , which is produced in a very similar way as ^{14}C but differs considerably in its geochemical behavior. As a consequence, production changes affect both nuclides, while changes in the global deep-water formation only affect ^{14}C . This new approach has been successfully applied to the $\Delta^{14}\text{C}$ peak during the Younger Dryas cold event (Fig. 5) [19]. By comparing the $\Delta^{14}\text{C}$ record with the ^{10}Be record from GISP 2 [20] it has been shown that only the combination of a production change and a reduction of the global deep-water formation is consistent with both the ^{14}C and ^{10}Be measurements. Should a high quality, detailed $\Delta^{14}\text{C}$ record become available for the glacial time period from 15,000 to 50,000 years, this technique can be applied to study the DOE events.

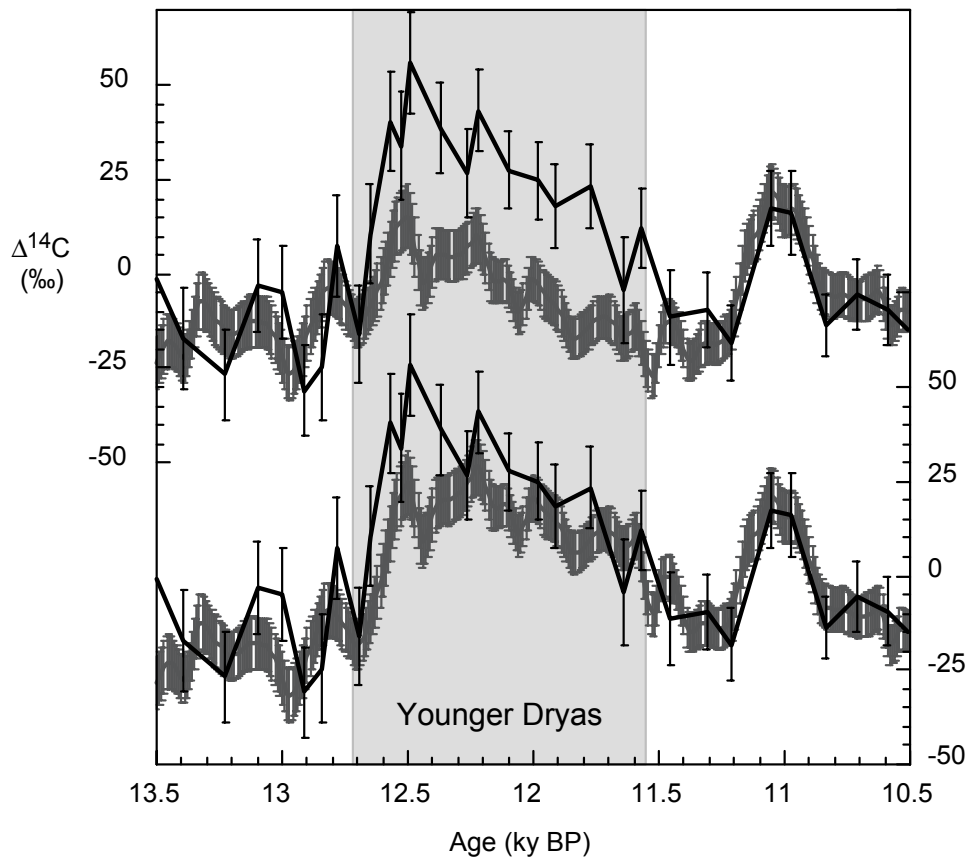


FIG. 5. Comparison of measured $\Delta^{14}\text{C}$ with $\Delta^{14}\text{C}$ calculated using the ^{10}Be data from the GISP ice core [20]. The discrepancy between the two curves during the Younger Dryas period indicates that the peak of the measured $\Delta^{14}\text{C}$ is not only due to a production change (upper panel). In fact, assuming in addition to the production increase a reduction of the global deep-water formation leads to a much better agreement (lower panel) [19].

5. DATING

A classical but still very important application of cosmogenic nuclides is dating. Precise time information is crucial to a comparison of hemispheric or regional climate changes and to determine rates of changes. In the case of polar ice cores, there are two major problems using cosmogenic nuclides for dating. Firstly, the concentration of radionuclides such as ^{14}C is very low. Even when using accelerator mass spectrometry (AMS), the extraction and processing of the tiny amounts of CO_2 occluded in air bubbles is extremely difficult. In addition, there is still no reliable ^{14}C calibration curve available for the glacial part, where the uncertainties of other dating techniques are larger and ^{14}C would be useful. Secondly, in most cases the initial concentration of a radionuclide is not well enough known to calculate an age with a precision of a few percent. One way of circumventing this problem is to use isotopic ratios. Since the production rates of both nuclides fluctuate in phase, the production rate ratio is constant at first order and can be determined experimentally on modern samples. One example is the $^{10}\text{Be}/^{36}\text{Cl}$ ratio, which is ideal for dating very old ice. It has an apparent half-life of 376,000 years and is therefore well suited to date the older parts of deep-drilling ice cores. Unfortunately, the situation is complicated by processes such as changes in transport or loss of chlorine from the ice. The latter process mostly occurs in low accumulation areas with low dust content (Antarctica) [21]. In Greenland, however, this dating technique looks promising, as shown by work in progress.

The accumulation rate derived from measurements of the cosmogenic nuclides as described above can then be used in ice flow models to establish a time scale.

Significant abrupt changes in the production rate of cosmogenic nuclides provide global markers that can be used to synchronize time scales of different ice and sediment cores [22]. An example of such a marker is the Laschamp event around 40 kyrs BP when the magnetic field intensity almost vanished [23].

In a similar way, $\delta^{18}\text{O}$ derived from oxygen in air bubbles can be used to synchronize ice and sediment cores [6].

6. CONCLUSIONS

Stable and radioactive isotopes are extremely versatile tools to study various processes and to deepen our understanding of the complex environmental system and the couplings between its components. In natural archives such as ice cores, they allow us to reconstruct past climate conditions and to analyze the dynamics of processes on time scales from decades to millennia. A look back into the past is therefore crucial for the development of realistic models that may help to shed light on the future of the earth.

ACKNOWLEDGEMENTS

This work was supported by the Swiss National Science Foundation

REFERENCES

- [1] PETIT, J. R., JOUZEL, J., RAYNAUD, D., BARKOV, N. I., BARNOLA, J.-M., BASILE, I., BENDER, M., CHAPPELLAZ, J., DAVIS, M., DELAYGUE, G., DELMOTTE, M., V. KOTLYAKOV, M., LEGRAND, M., LIPENKOV, V. Y., LORIUS, C., PEPIN, L., RITZ, C., SALTZMAN, E., STIEVENARD, M. "Climate and atmospheric history of the past 420,000 years from the Vostok ice core, Antarctica," *Nature* **399** (1999) 429-436.
- [2] DANSGAARD, W., JOHNSEN, S. J., CLAUSEN, H. B., DAHL-JENSEN, D., GUNDESTRUP, N. S., HAMMER, C. U., HVIDBERG, C. S., STEFFENSEN, J. P., SVEINBJOERNSDOTTIR, A. E., JOUZEL, J., BOND, G., "Evidence for general instability of past climate from a 250-kyr ice-core record," *Nature* **364** (1993) 218-220.
- [3] BROECKER, W. S., BOND, G., KLAS, M., BONANI, G., WOELFLI, W., "A Salt Oscillator in the Glacial Atlantic? 1. The Concept," *Paleoceanography* **5** (1990) 469-477.
- [4] SOWERS, T., BENDER, M., RAYNAUD, D., KOROTKEVICH, Y. S., and ORCHARDO, J., "The $\delta^{18}\text{O}$ of atmospheric O_2 from air inclusions in the Vostok ice core: timing of CO_2 and ice volume changes during the penultimate deglaciation," *Paleoceanography* **6** (1991) 679-696.
- [5] DAHL-JENSEN, D., MOSEGAARD, K., GUNDESTRUP, N., CLOW, G. D., JOHNSEN, S. J., HANSEN, A. W., BALLING, N., "Past temperatures directly from the Greenland ice sheet," *Science* **282** (1998) 268-271.
- [6] LEUENBERGER, M., "Modeling the signal transfer of seawater $\delta^{18}\text{O}$ to the $\delta^{18}\text{O}$ of atmospheric oxygen using a diagnostic box model for the terrestrial and marine biosphere," *J. Geophys. Res. Lett.* **102** (1997) 26841-26850.

- [7] MASARIK, J. BEER, J., "Simulation of particle fluxes and cosmogenic nuclide production in the Earth's atmosphere," *J. Geophys. Res.* **104** (1999) 12,099 - 13,012.
- [8] FROELICH, C., "Observations of irradiance variations," *Space Science Reviews* **94** (2000) 15-24.
- [9] BEER, J., MENDE, W., STELLMACHER, R., "The role of the Sun in climate forcing," *Quat. Sci. Rev.* **19** (2000) 403-415.
- [10] LEAN, J., BEER, J., BRADLEY, R., "Reconstruction of solar irradiance since 1610: implications for climate change," *Geophysical Research Letters* **22** (1995) 3195-3198.
- [11] RADICK, R. R., LOCKWOOD, G. W., BALIUNAS, S. L., "Stellar activity and brightness variations: a glimpse at the sun's history," *Science* **247** (1990) 239-247.
- [12] BEER, J., JOOS, C. F., LUKASCZYK, C., MENDE, W., SIEGENTHALER, U., STELLMACHER, R., SUTER, M., "¹⁰Be as an indicator of solar variability and climate," in *The solar engine and its influence on terrestrial atmosphere and climate*, vol. I. 25, NATO ASI, E. Nesme-Ribes, Ed. Berlin: Springer-Verlag (1994) 221-233.
- [13] WAGNER, G., BEER, J., KIBIK, P. W., LAJ, C., MASARIK, J., MENDE, W., MUSCHELER, R., RAISBECK, G. M., YIOU, F., "Presence of the solar de Vries cycle (205 years) during the last ice age," *Geophys. Res. Lett.* (2000 in press).
- [14] STUIVER, M., REIMER, P. J., BARD, E., BECK, J. W., BURR, G. S., HUGHEN, K. A., KROMER, B., McCORMAC, G., VAN DER PLICHT, J., SPURK, M., "INTCAL98 Radiocarbon age calibration, 24,000-0 cal BP," *Radiocarbon* **40** (1998) 1041-1083.
- [15] VAN GEEL, B., RASPOPOV, O. M., V. d. P. J., and RENUSSEN, H., "Solar forcing of abrupt climate change around 850 calendar years BC," in *Natural catastrophes during the Bronze Age civilisations*, BAR International Series 728, B. J. Peiser, T. Palmer, and M. E. Bailey, Eds. (1998) 162-168.
- [16] BEER, J., "Long-term indirect indices of solar variability," *Space Science Reviews*. Nov **94** (2000) 53-66.
- [17] MASARIK, J., BEER, J., "Monte Carlo simulation of particle fluxes and cosmogenic nuclide production in Earth's atmosphere," presented at ICRC 25, Durban (1997).
- [18] JOHNSEN, S. J., DAHL-JENSEN, D., DANSGAARD, W., GUNDESTRUP, N., "Greenland palaeotemperatures derived from GRIP bore hole temperature and ice core isotope profiles," *Tellus* **47B** (1995) 624-629.
- [19] MUSCHELER, R., BEER, J., WAGNER, G., FINKEL, R. C., "Changes in deep-water formation during the Younger Dryas cold period inferred from a comparison of ¹⁰Be and ¹⁴C records," *Nature* **408** (2000) 567-570.
- [20] FINKEL, R. C., NISHIZUMI, K., "Beryllium-10 concentrations in the Greenland ice sheet project 2 ice core from 3-40 ka," *J. Geophys. Res.* **102** (1997) 26699-26706.
- [21] WAGNON, P., DELMAS, R. J., and LEGRAND, M., "Loss of volatile acid species from upper firn layers at Vostok. Antarctica," *J. Geophys. Res.* **104** (1999) 3423-3431.
- [22] BEER, J., JOHNSEN, S. J., BONANI, G., FINKEL, R. C., LANGWAY, C. C., OESCHGER, H., STAUFFER, B., SUTER, M., WOELFLI, W., "¹⁰Be peaks as time markers in polar ice cores," presented at Proc. Erice Nato Workshop. The last delegation: absolute and radiocarbon chronologies (1992).
- [23] WAGNER, G., MASARIK, J., BEER, J., BAUMGARTNER, S., IMBODEN, D., KUBIK, P. W., SYNAL, H.-A., SUTER, M., "Reconstruction of the geomagnetic field between 20 and 60 ka BP from cosmogenic radionuclides in the GRIP ice core," *Nucl. Instr. Meth.* **172B** (2000) 597-604.

STABLE ISOTOPES AND THEIR RELATIONSHIP TO TEMPERATURE AND PRECIPITATION AS RECORDED IN LOW LATITUDE ICE CORES

L.G. THOMPSON

Department of Geological Sciences, The Ohio State University,
Columbus, Ohio, United States of America

M.E. DAVIS, PIN-NAN LIN

Byrd Polar Research Center, The Ohio State University,
Columbus, Ohio United States of America

Abstract. The potential of stable isotopic ratios ($^{18}\text{O}/^{16}\text{O}$ and $^2\text{H}/^1\text{H}$) in mid to low latitude glaciers as modern tools for paleoclimate reconstruction is reviewed. The isotopic composition of precipitation should be viewed not only as a powerful proxy indicator of climate, but also as an additional parameter for understanding climate-induced changes in the water cycle, on both regional and global scales. To interpret quantitatively the ice core isotopic records, the response of the isotopic composition of precipitation to long-term fluctuations of key climatic parameters (temperature, precipitation amount, relative humidity) over a given area should be known. Furthermore, it is important to establish the transfer functions that relate the climate-induced changes of the isotopic composition of precipitation to the isotope record preserved in the glacier. The factors that govern the values of stable isotopes in snowfall are enigmatic and as yet no satisfactory model has been developed to link them directly with any one meteorological or oceanographic factor. This is particularly problematic in the high altitude glaciers in the tropics, where complications are present due not only to continental effects, but also to altitude effects and convective air mass instability, particularly in the monsoon climates of the tropics. This paper presents long and short-term perspectives of isotopic composition variations in ice cores spanning the last 25,000 years from the mid- to low-latitude glaciers. The isotopic records will also be examined as a function of the altitude of the individual coring sites which ranges from 5325 meters to 7200 meters. On the short, term isotopic records from ice cores from the Andes of South America, the Tibetan Plateau and Kilimanjaro in Africa through the year 2000 will be presented. All the tropical glaciers for which data exist are disappearing, and these sites show isotopic enrichment in the 20th century that suggests that large scale low latitude warming is taking place. In general this warming appears to be amplified at higher elevation sites. The evidence for recent and rapid warming in the low latitudes is presented and possible reasons for this warming are examined.

1. INTRODUCTION

An overview is presented of the oxygen isotopic ($\delta^{18}\text{O}$) records from seven low latitude, high altitude glaciers around the world. This paper will address the question of how well these data record temperature through time and then will examine the perspective provided by over 25,000 years of documented climatic history. Finally an overview of the disappearance of these tropical archives over the last 30 years is presented along with evaluation of recent changes in mean stable isotopic composition.

Ice core records are available from selected high altitude, low and mid-latitude ice caps (Figure 1). Comparisons are made between three from the Tibetan Plateau: Dunde, (38°N, 5325 m asl), Guliya, (35°N; 6200 m asl) and Dasuopu in the Chinese Himalayas (28°N, 7200 m asl). These Tibetan records are compared with three tropical ice core records from the Andes of South America, Huascarán, Peru (9°S, 6050 m asl) Quelccaya, Peru (14°S, 5670 m asl) and Sajama (Bolivia, 18°S, 6550 m asl). Finally, we introduce our most recent site at Kilimanjaro, Tanzania (3°S, 5895 m asl). Some of these sites contain ice deposited during the Last Glacial Stage (LGS)

and the $\delta^{18}\text{O}$ of this ice suggests significant cooling ($\sim 5^\circ\text{C}$) in the tropics. These records contribute to a growing body of evidence that tropical climate was cooler and more variable during the LGS [1,2] and to renewed interest in the low latitude water vapor cycle. Ice core evidence for past changes in this hydrological cycle, as well as evidence for recent warming at high elevations in the tropics, suggest that changes in water vapor inventories are a significant component of climate variability.

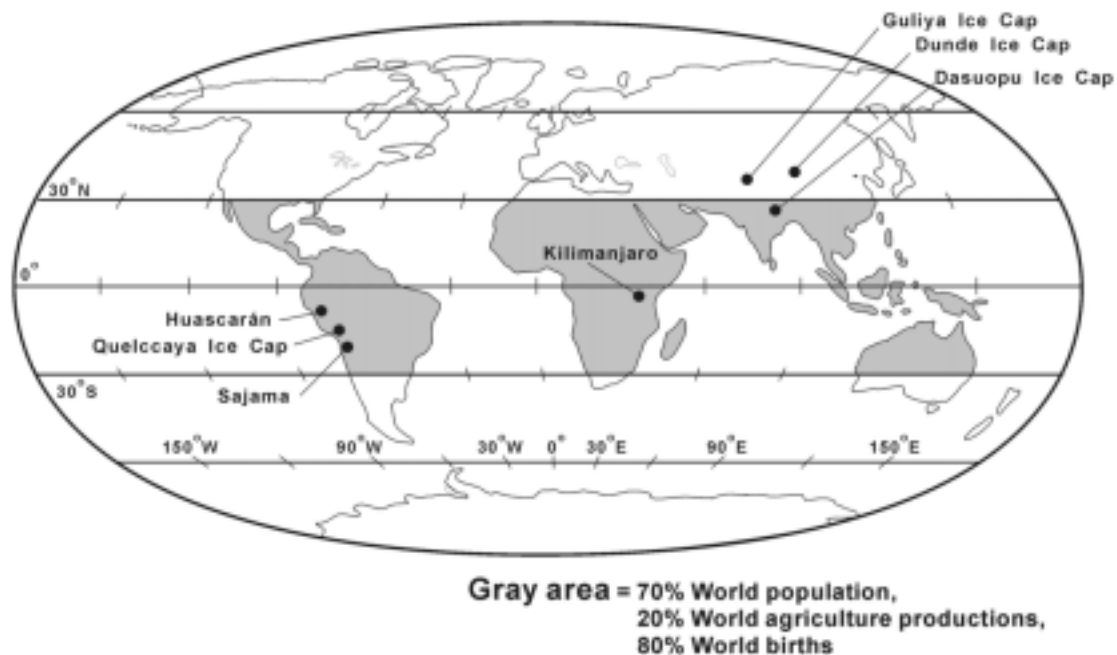


FIG. 1. Map illustrating the seven sites from which ice cores have been recovered. The shaded area between 30°N and 30°S represents the tropical regions that contain 50% of the world's surface area, 75% of its population and 80% of the new births, but only produces 20% of the agricultural products.

2. $\delta^{18}\text{O}$ AS A TEMPERATURE RECORDER IN LGS/EARLY HOLOCENE ICE CORES FROM TROPICAL SOUTH AMERICA

The controversy over whether oxygen isotopic ratios are more influenced by temperature or by precipitation is addressed by the examination of the climatic and environmental history from Sajama, which is one of the best dated of the all the tropical ice core records. The profiles of $\delta^{18}\text{O}$, dust and anion concentrations were transferred to a ^{14}C -constrained time scale (Figure 2) according to techniques discussed in [2]. The increases in dust and anions, particularly in chloride (Cl^-) are linked to the desiccation of the Altiplano lakes, and when the lakes are dry aerosols are entrained by winds over the salt flats and deposited on the ice cap. In general, the LGS is much wetter, colder and less dusty than the dryer Holocene climate on the Altiplano.

Recently, Baker *et al.* [3] asserted that since the Sajama $\delta^{18}\text{O}$ record shows a similar structure to the nearby Salar de Uyuni γ -radiation record, then the $\delta^{18}\text{O}_{\text{ice}}$ is inversely correlated with precipitation amount (or runoff fraction). However, this is disputed by the ice core record itself. A closer examination of the termination of the deglaciation cold reversal between 11.8 and 11.5 ka (Figure 3a) shows an isotopic enrichment of 5.2‰ at a time when the Cl^- and dust concentrations changed very little. This indicates that during a time of rapid and dramatic warming, the lake

levels remained relatively stable, suggesting that regional precipitation rates did not vary. Another example of the disconnect between temperature and effective moisture is seen in Figure 3b, the transition into the Last Glacial Maximum (LGM) between 22 ka and 21.7 ka. Here, the lake levels were clearly decreasing, as reflected by a five-fold increase in Cl^- , but there was no change in the $\delta^{18}\text{O}$ of the precipitation on the ice cap. Thus, as in polar cores, temperature is the more dominant control on the mean oxygen isotopic values of tropical snow than precipitation amounts.

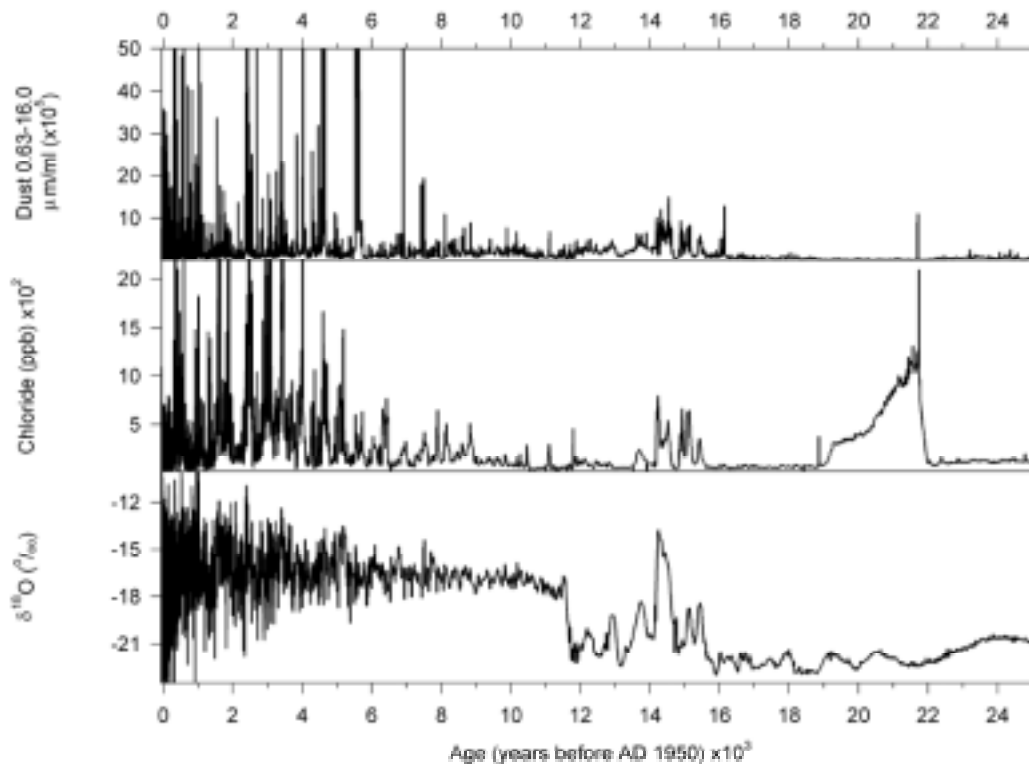


FIG. 2. High-resolution plots of $\delta^{18}\text{O}_{\text{ice}}$ and dust and chloride (Cl) concentrations from Sajama for the past 25 ka.

Additional arguments for this case are taken from the comparison of the climate reconstruction from Sajama with that from Huascarán at 9°S of the equator [4]. The record from the latter illustrates that the LGS in northern Peru was cold and dry, but that the Early Holocene was warm and wet. Conversely, the Sajama record [2] clearly shows that the climate history on the Altiplano was of a cold and wet LGS and a warm and dry Early Holocene. However, the LGS isotopic mean on Huascarán of -22.9‰ is very close to the Sajama mean of -22.1‰, and the Early Holocene Huascarán average of -16.6‰ is almost identical to -16.7‰ for Sajama. This strongly argues that the long-term $\delta^{18}\text{O}$ is not inversely correlated to precipitation amount as argued by Baker *et al.* [3], since almost equal isotopic values occur under quite different effective precipitation conditions.

In a global array of ice core records, the $\delta^{18}\text{O}$ shift from Early Holocene to LGM is similar (Figure 4, Table I), and includes 5.4‰ in Sajama [2], 6.3‰ in Huascarán [4], 5.4‰ to 5.1‰ in central Greenland [5], 6.6‰ in Byrd Station, Antarctica [6] and 5.4‰ in Vostok, Antarctica [7]. These ice core records join with other proxy data to provide a picture of significant global cooling during the LGM. These other data originate from such diverse archives as corals [8,9], noble gases from groundwater [10]; marine sediment pore fluids, [11], snowline depression [12-17], and pollen studies [18].

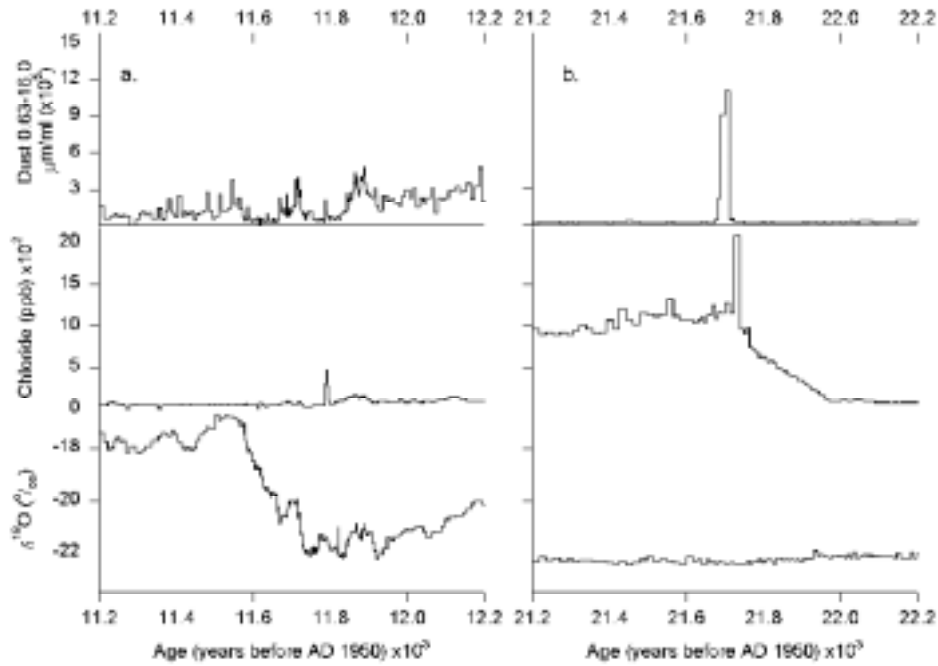


FIG. 3. (a) Detailed plots of $\delta^{18}\text{O}_{\text{ice}}$, and dust and CT concentration variations during the transition from the deglaciation climatic reversal (DCR) into the Holocene in the Sajama record. (b) The same parameters from the Sajama record during the Last Glacial Maximum.

TABLE I. Comparison of averages of $\delta^{18}\text{O}_{\text{ice}}$ for the Modern period (0 to 1 ka), the early Holocene (EH, 6.8 to 10 ka) and the Last Glacial Maximum (LGM, 18.0-21.2 ka) and the differences between the LGM and the Modern and the LGM and the EH for the cores shown in Figure 4.

Core:	Modern (0-1 ka)	Early Holocene (EH) (6.8 - 10.0 ka)	Last Glacial Maximum (LGM) (18.0-21.2 ka)	LGM- Modern (‰)	LGM-EH (‰)
Sajama (Bolivia)	-16.8	-16.7	-22.1	5.4	5.4
Huascarán (Peru)	-18.5	-16.6	-22.9	4.4	6.3
GISP2 (Greenland)	-35.0	-34.6	-39.7	4.7	5.1
Guliya (W. China)	-14.4	-13.1	-18.5	4.1	5.4
Byrd (Antarctica)	-32.8	-33.9	-40.5	7.6	6.6
Vostok (Antarctica)	-441(-56.4)	-436(-55.7)	-472(-60.2)	3.9	4.5
Vostok (21.0 - 24.2 ka)	-441(-56.4)	-436(-55.7)	-479(-61.1)	4.8	5.4

These cooler tropical temperatures during the LGM would likely weaken the Hadley circulation and lower the water vapor budget of the Earth's atmosphere. Such changes have the potential for very large impacts on adiabatic lapse rates, particularly in the tropics. As the Earth is a thermodynamically non-linear planet, tropical glaciers are particularly sensitive to climate change. Lapse rates will undergo a greater change with height in a moister atmosphere than in a

drier atmosphere. If sea surface temperatures (SST) warm uniformly around the globe, tropical lapse rates will decrease, conversely a global-scale cooling would lead to increased rates. In both cases the changes would be greater at high elevations in the tropics. Thus, according to the Clausius-Clapeyron relationship, under a warming Earth scenario tropical glaciers would be expected to retreat rapidly, but under colder conditions such as those of the LGS, with 5° to 6°C cooling suggested by the ice cores and other records mentioned above, tropical glaciers would be expected to expand rapidly. Therefore, such changes between dry and moist adiabatic lapse rates should lead to tropical amplification of either a warming or a cooling.

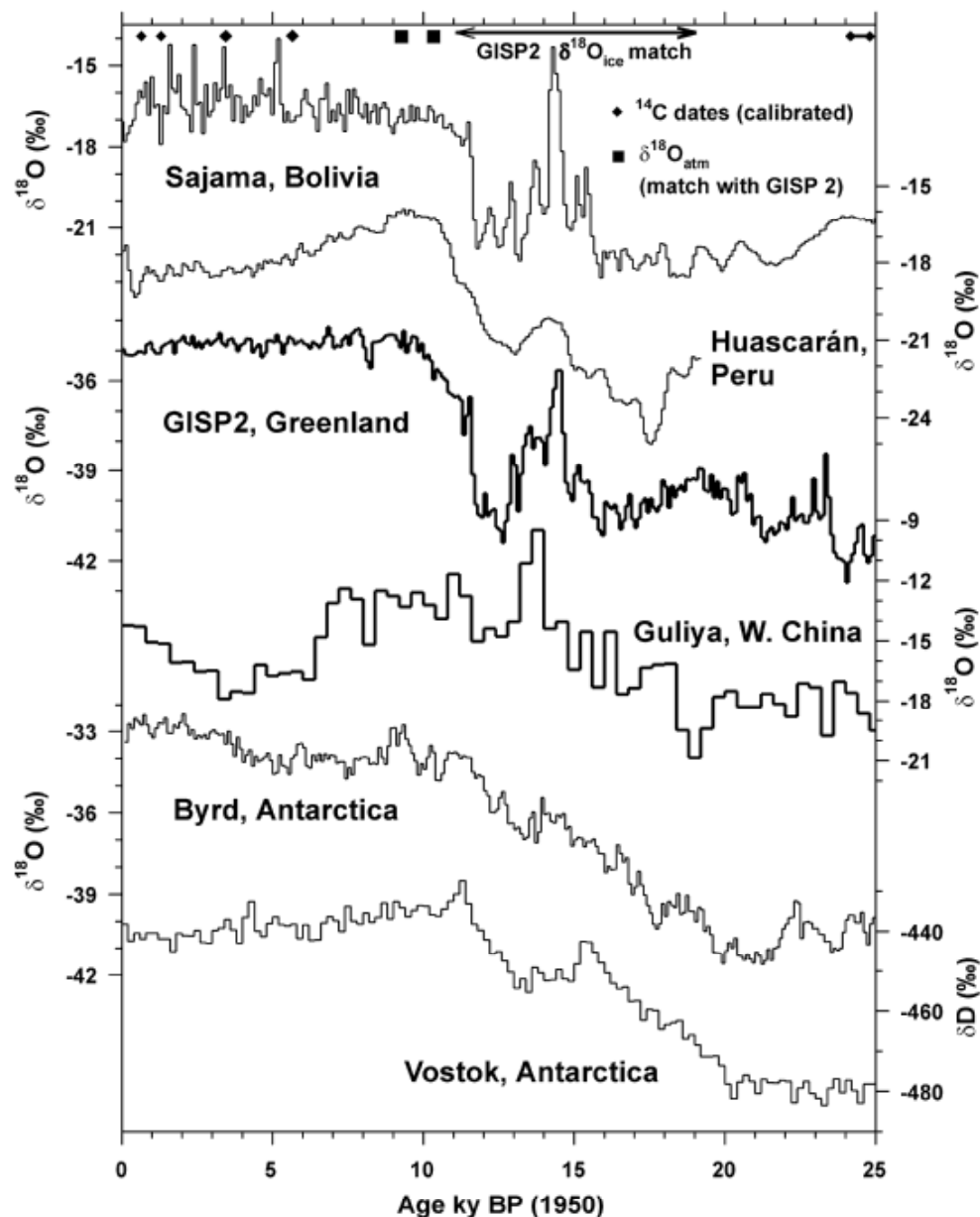


FIG. 4. Global extent of the Late Glacial Stage and a climatic reversal (cooling) during deglaciation is illustrated by the stable isotope records from two tropical sites (Sajama and Huascarán), two Northern Hemisphere sites (Guliya and GISP 2) and two Southern Hemisphere sites (Byrd Station and Vostok). All records shown are 100-year averages, except the records for Vostok (200-year averages) and Guliya (400-year averages).

3. STABLE ISOTOPES OVER THE LAST MILLENNIUM

3.1. The Tibetan Plateau

Long ice core records are available from three sites on the Tibetan Plateau. The Dunde ice cap, the Guliya ice cap, and the Dasuopu glacier form a regional triangular pattern with summit elevations decreasing from south to north (Fig.1). Dasuopu, the highest site, has the most depleted average $\delta^{18}\text{O}$ (-20.32‰ for the last millennium) while the lowest elevation site, Dunde has the least isotopically depleted millennial average (-10.81‰). The elevation of Guliya is between the other sites, and has a medium isotopic value of -14.23 ‰ for the last millennium (Figure 5). As the precipitation at all these sites is dominated by the advection of moisture from the Indian Ocean with possible contributions from the Arabian Sea during the summer monsoon, these data provide qualitative support for the hypothesis that temperature, not the amount effect, is the dominant process controlling $\delta^{18}\text{O}$ over the Tibetan Plateau. This is further supported by the much stronger statistical relationship between $\delta^{18}\text{O}$ and NH temperatures ($r^2 = 0.37$), and the much weaker relationship between $\delta^{18}\text{O}$ and accumulation ($r^2 = 0.19$) [19].

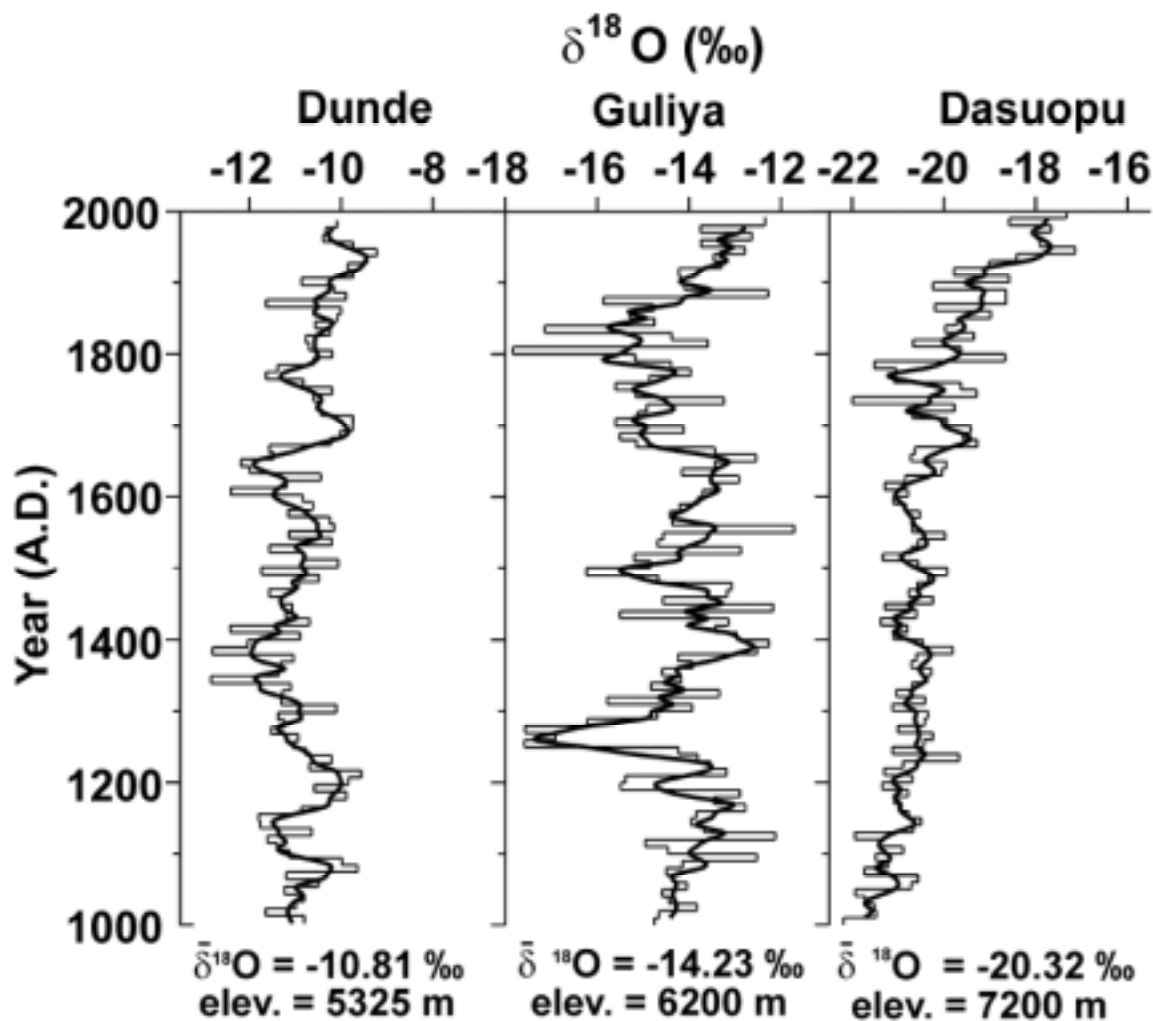


FIG. 5. Decadal averages of $\delta^{18}\text{O}_{\text{ice}}$ for the last millennium from Dunde, Guliya and Dasuopu, Tibetan Plateau.

The question of whether stable isotopes are proxy indicators of temperature for the lower troposphere was qualitatively addressed above in the discussion of long-term climate records from Andean cores. However, in order to quantify that relationship, real-time field observations and measurements are required. We have collaborated with our Chinese colleagues at the Lanzhou Institute of Glaciology and Geocryology (LIGG), who collected precipitation samples and measured temperatures at six meteorological stations across the Tibetan Plateau. At the Delingha station, which is the closest to the Dunde ice cap (150 km to the southeast), the r^2 between the $\delta^{18}\text{O}$ of the precipitation collected and the atmospheric temperature measured at the time of collection is 0.86 [20]. These data suggest, at least for the period of measurement, that $\delta^{18}\text{O}$ is a faithful recorder of temperature in this section of the Plateau.

Figure 5 compares the decadal averages of $\delta^{18}\text{O}$ over the last 1000 years for the three Tibetan Plateau ice cores. These profiles display major differences through the past millennium, possibly due to their different precipitation sources and post-depositional processes. Over most of the millennium, the $\delta^{18}\text{O}$ -inferred temperature variations recorded on Guliya have been generally out of phase with those on Dunde [19]. Dasuopu and Dunde show broadly more similar trends, although the Dunde profile contains more higher amplitude variations before 1250 AD.. Over the last 200 years, however, all three clearly show strong isotopic enrichment taking place, suggesting a recent warming across the entire Tibetan Plateau. This warming is particularly notable in the 20th century (although the recent isotopic enrichment is more pronounced on Dasuopu) and is the most regionally consistent climate signal of the last 1000 years.

Meteorological observations on the Plateau are relatively few and of short duration. A recent study [21] utilizes monthly surface air temperature data from most meteorological stations on the Plateau since their installation in the 1950's. Not only do they report a linearly increasing annual temperature trend of $\sim 0.16^\circ\text{C}$ per decade from 1955 to 1996 and an increasing winter trend of $\sim 0.32^\circ\text{C}$ per decade, they also report evidence that the rate of warming has increased with elevation. The 1960 to 1990 records from 178 stations across the Plateau reveal that the greatest rate of warming ($\sim 0.35^\circ\text{C}$ per decade) has occurred at the highest elevation sites. Consistent with these recent meteorological data, the $\delta^{18}\text{O}$ records from the three Plateau ice cores reveal the same trend of increasing isotopic enrichment with increasing elevation. Specifically, the average $\delta^{18}\text{O}$ in Dunde since 1950 is 0.99‰ higher than the millennial mean while on Guliya it is 1.05‰ and on Dasuopu it is 1.84‰ (Figure 6). The isotopically inferred 20th century temperatures on both Dunde and Dasuopu are the warmest of the millennium and the recent warming is most pronounced at the highest elevation site, Dasuopu, along the southern edge of the Tibetan Plateau (Figure 5).

3.2. The Andes of South America

The map in Figure 1 illustrates the three sites in the tropical Andes from which ice cores have been recovered. The sites lie in a southeast-northwest trend from 18°S to 9°S . Huascarán, the most equatorial of the three and the world's highest tropical mountain, provided in 1993 two records of climate variability that extend the LGS. Cores recovered from the Quelccaya ice cap (14°S) in 1983 yielded an annually resolved record back to A.D. 470 [22-24]. Further to the south, Sajama, Bolivia (18°S) is a 6550 m asl extinct volcano on which two cores were drilled to bedrock in 1997 [2]. The ice cores from this site are very unusual in that they contain both insects and plant remains in large enough supply to allow AMS ^{14}C dating to be made in two separate laboratories. Thus, unusually good absolute time control is possible for these records.

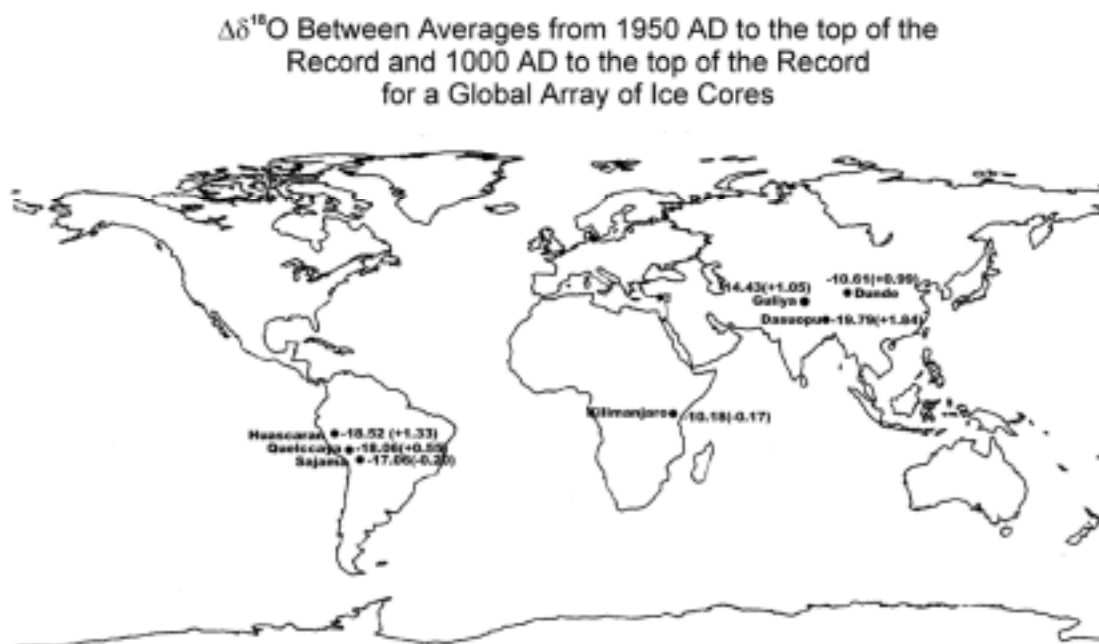


FIG. 6. Global map showing mean $\delta^{18}\text{O}_{ice}$ from 1000 AD to the top of each record for the seven high-altitude ice core sites, with the differences between those means and the means from 1950 AD to the top of each record in parentheses.

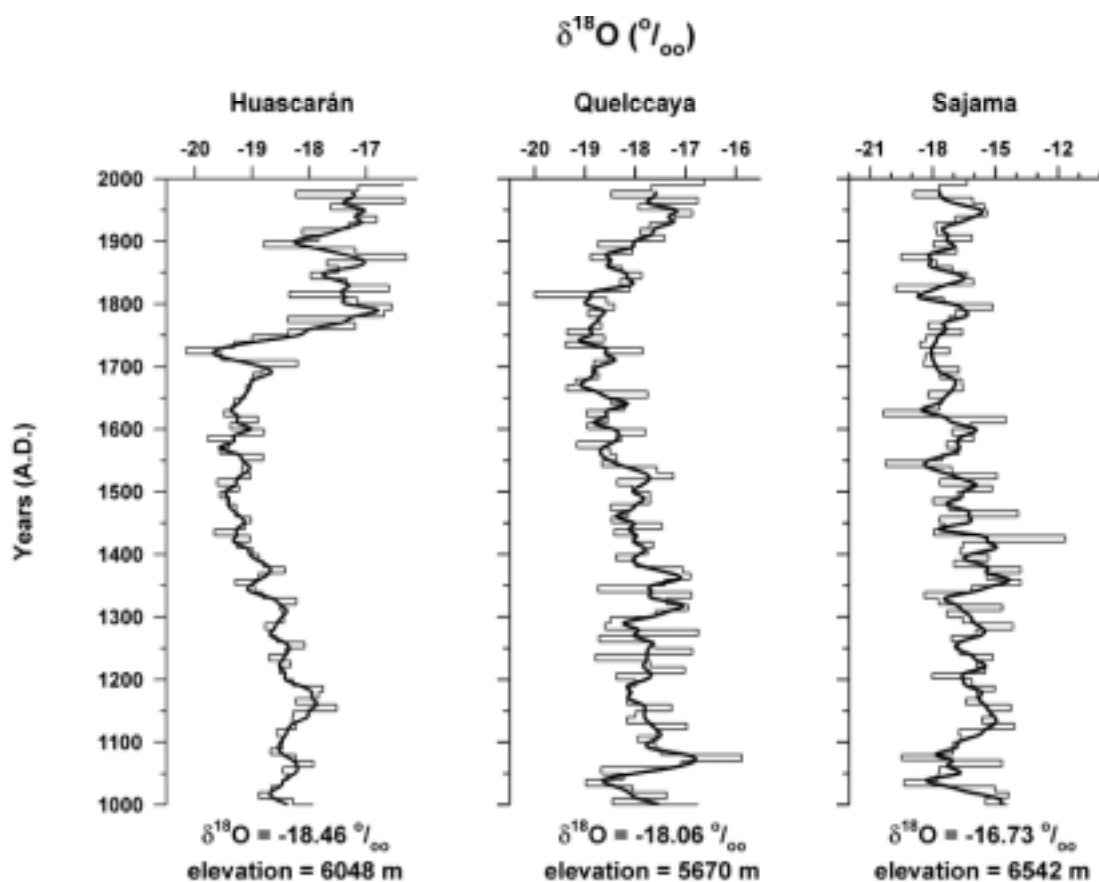


FIG. 7. Decadal averages of $\delta^{18}\text{O}_{ice}$ for the last millennium from the three tropical Andes sites, Huascarán, Quelccaya and Sajama.

Figure 7 compares the decadal oxygen isotopic values from these three tropical Andean sites for the last 1000 years. Earlier than 1700 AD the profiles show similar trends, but Sajama does not record the isotopic enrichment of the last 200 years that is quite obvious in Huascarán, Quelccaya and all three of the Tibetan Plateau sites. Moreover, unlike the Tibetan cores there is no clear relationship between elevation and mean isotopic value over the last millennium. Sajama at 6542 m asl is the highest of the three glaciers, but it contains the most enriched average $\delta^{18}\text{O}$ (-16.73‰). The inconsistencies presented by this ice core may be related to the extreme aridity of the Altiplano region and the potential role of post-deposition sublimation.

For all the Andean sites the moisture source is the tropical Atlantic Ocean by way of the Amazon Basin, and this source has remained consistent since the LGM as shown by the tilt of the mountain snowlines toward the Amazon Basin both at 20 ka and today [14]. The seasonality of the $\delta^{18}\text{O}$ in the South American records is opposite that of the polar regions, i.e. the most depleted values occur in wet season (summer) snowfall and the most enriched in the dry season (winter) layers. Currently there are at least two models which explain the $\delta^{18}\text{O}$ composition of ice cores in the tropical Andes. The first, developed by Grootes *et al.* [25], is a hydrological model of moisture transport. The isotopic values are initially determined by the composition of oceanic water, and as the vapor moves across the Amazon Basin it is recycled in thunderstorms. Each time condensation takes place the heavier isotopes are preferentially removed. The condensate falls from clouds and is transported out of the Amazon Basin by the river system in the wet season. In the dry season most of the water that falls in the Amazon is re-evaporated, and thus very little isotopic fractionation takes place. However, by the time the moisture reaches the base of the Andes in the wet season, it has a mean isotopic value of -20‰ . When the air masses are forced to rise over the Andes (above 5000 meters) an additional 10‰ depletion takes place.

There is a major factor to take into account when considering the interpretation of stable isotopes in the tropics, and how they differ from those in the higher latitudes. In the Andes, the snowfall comes from thunderstorms that contain convective cells with very high vertical extent, therefore the mean level of condensation is higher than in the polar regions. More importantly, this condensation level changes in location and height from wet to dry season. In the wet season, Huascarán is located in the center of the region affected by maximum deep convection, but in the dry season this activity moves to the north. The condensation level during the height of the wet season is about two km higher, where the temperatures are cooler, and in the dry season condensation forms at a lower, warmer elevation in the atmosphere. The isotopic composition of precipitation may well reflect these changes [26].

Meteorological observations in the tropical Andes, as in Tibet, are scarce and cover relatively little time. In a recent study, Vuille and Bradley [27] determined that the mean annual temperature trends in the tropical Andes over the last six decades (1939-1998) have increased by 0.10°C - $0.11^{\circ}\text{C}/\text{decade}$. Furthermore, they found that the rate of warming has more than tripled over the last 25 years (0.32°C - $0.34^{\circ}\text{C}/\text{decade}$) and that the last two years of the series, associated with the 1997/98 El Niño, were the warmest of the last six decades. However, the Andes temperature trends vary conversely with altitude and show a generally reduced warming with increasing elevation. This trend is generally consistent with the mean millennial isotopic values from the Andean ice cores. The mean $\delta^{18}\text{O}$ since 1950 AD compared to the 1000th year mean shows which is enrichment toward the equator (Figure 6). The greatest enrichment since 1950 AD of 1.33‰ occurs in the most tropical site Huascarán, a lesser enrichment of 0.51‰ occurs at Quelccaya, while Sajama actually shows a -0.20‰ depletion since 1950.

4. 20TH CENTURY GLACIER RETREAT

Evidence is accumulating for a strong warming in the tropics during in the second half of the 20th century that is causing the rapid retreat and, in some cases, the disappearance, of ice caps and glaciers at high elevations. These ice masses are particularly sensitive to small changes in ambient temperatures as they exist very close to the melting point. This warming and the concomitant retreat of the Quelccaya ice cap (Peru) are well documented. Since 1976 Quelccaya has been visited repeatedly for extensive monitoring and sampling. In addition to the deep drilling in 1983, shallow cores were taken from the summit of the ice cap in 1976, 1979, 1991, 1995 and 2000. Comparison of the $\delta^{18}\text{O}$ records extracted at these six different times reveals (1) the mean isotopic values have continued to become more enriched and (2) the seasonally resolved paleoclimatic record, preserved in the cores drilled in 1983 as $\delta^{18}\text{O}$ variations, is no longer being retained within the currently accumulating snow [1,26]. The percolation of meltwater throughout the accumulating snowpack is homogenizing the stratigraphic record of $\delta^{18}\text{O}$.

The retreat of the margins of Quelccaya has also been monitored. The extent and volume of the largest outlet glacier, Qori Kalis, was measured eight times between 1963 and 2000. These observations have documented a rapid retreat that has accelerated during this 37-year period. The rate of retreat from 1983 to 1991 was three times that from 1963 to 1983, and was five times faster in period from 1993 to 1995, eight times faster in the period 1995 to 1998 and thirty-two times faster in the most recent observational period (1998 to 2000). The latest observations made in 2000 confirm the continued acceleration of Qori Kalis' retreat, as well as further retreat of the other margins of the Quelccaya ice cap.

Additional glaciological evidence for tropical warming exists. Hastenrath and Kruss [28] report that the total ice cover on Mount Kenya has decreased by 40% between 1963 and 1987 and today it continues to diminish. The Speke glacier in the Ruwenzori Range of Uganda has retreated substantially since it was first observed in 1958 [29]. The ice fields on Kilimanjaro have lost 75% of their area between 1912 and 1989 [30]. The shrinking of these ice masses in the high mountains of Africa and South America is consistent with other tropical observations.

Tropical and subtropical ice core records have the potential to provide annual to millennial-scale records of climate, El Niño-Southern Oscillation events and monsoon variability and will provide further insight into the magnitude and frequency of these large-scale events. These data also provide unique perspectives for viewing both regional and global scale events ranging from the so-called "Little Ice Age" to the Younger Dryas cold phase to the Late Glacial Stage. There is unambiguous evidence that some, if not all of these archives are in imminent danger of being lost if the current warming persists.

ACKNOWLEDGEMENTS

The authors would like to thank the outstanding members of the paleoclimate ice core group at the Byrd Polar Research Center who have worked on the issue of stable isotopes in ice cores: Keith Henderson, Ellen Mosley-Thompson, and Victor Zagorodnov. Special thanks are given to Yao Tandong, Lanzhou Institute of Glaciology and Geocryology (LIGG), Vladimir Mikhaleenko, Institute of Geography (IG), Bruce Koci, University of Wisconsin (our drilling engineer on these projects) and Henry Brecher for producing the maps of the retreat of the Qori Kalis glacier. We thank the many scientists, technicians, graduate students and support personnel from The Ohio State University, LIGG and IG and the mountain guides of the Casa de Guías, Huaraz, Peru and

the Sherpas of Nepal. This work has been supported by the National Science Foundation and the National Oceanic and Atmospheric Administration. This is contribution number 1244 of the Byrd Polar Research Center.

REFERENCES

- [1] THOMPSON, L. G., et al. "Recent warming": ice core evidence from tropical ice cores with emphasis upon Central Asia, *Global and Planetary Change* **7** (1993) 145-156.
- [2] THOMPSON, L. G., et al., A 25,000 Year Tropical Climate History from Bolivian Ice Cores, *Science* **282** (1998) 1858-1864.
- [3] BAKER, P. A., RIGSBY, C. A., SLETZER, G. O., FRITZ, S. C., LOWENSTEIN, T. K., BACHER, N. P., VELIZ, C., Tropical climate changes at millennial and orbital timescales on the Bolivian Altiplano, *Nature* **409** (2001) 698-701.
- [4] THOMPSON, L. G., et al., Late Glacial Stage and Holocene Tropical Ice Core Records from Huascarán, Peru. *Science* **269** (1995) 47-50.
- [5] GROOTES, P. M., STUIVER, M., WHITE, J. W. C., JOHNSEN, S., and JOUZEL, J., 1993: Comparison of oxygen isotope records from the GISP2 and GRIP Greenland ice cores, *Nature* **366** (1993) 552-554.
- [6] JOHNSEN, S. J., DANSGAARD, W., CLAUSEN, H. B., LANGWAY JR., C. C., Oxygen isotope profiles through the Antarctic and Greenland ice sheets, *Nature* **235** (1972) 429-433.
- [7] JOUZEL, J. et al., Vostok ice core: a continuous isotope temperature record over the last climatic cycle (160,000 years), *Nature* **329** (1987) 403-408.
- [8] GUILDERSON, T. P., FAIRBANKS, R. G., RUBENSTEIN, J. L., Tropical temperature variations since 20,000 years ago; modulating interhemispheric climate change, *Science* **263** (1994) 663-665.
- [9] BECK, J. W., RECY, TAYLOR, F., EDWARDS, R. L., CABIOCH, G., Abrupt changes in early Holocene tropical sea surface temperature derived from coral records, *Nature* **385** (1997) 705-707.
- [10] STUTE, M. et al., Cooling of tropical Brazil (5°C) during the last glacial maximum, *Science* **269** (1995) 379-383.
- [11] SCHRAG, D. P., HAMPT, G., MURRAY, D. W., Pore fluid constraints on the temperature and oxygen isotopic composition of the glacial ocean. *Science* **272** (1996) 1930-1932.
- [12] BROECKER, W. S., DENTON, G. H., Implications of global snowline lowering during glacial time to glacial theory, *Quat. Sci. Rev.* **9** (1990) 305-341.
- [13] HERD, D. G., NAESER, C. W., Mountain snowline lowering in the tropical Andes, *Geology* **2** (1974) 603-604.
- [14] KLEIN, A. G., ISACKS, B. L., BLOOM, A. L., Modern and Last Glacial Maximum Snowline in Peru and Bolivia: Implications for Regional Climatic Change, *Bulletin de l'Institut Français d'Études Andines* **24** (1995) 607-617.
- [15] OSMASTON, H. A., Snowline lowering on the mountains of tropical Africa, Ph.D. thesis, Oxford University, Worcester College (1965).
- [16] PORTER, S. C., Glacial snowline lowering in Hawaii, *Geol. Soc. Am. Bull.* **90** (1979) 980-1093.
- [17] RODBELL, D. T., Snowline lowering in the Peruvian Andes, *Boreas* **21** (1992) 43-52.
- [18] COLINVAUX, P. A., De OLIVEIRA, P. E., MORENO, J. E., MILLER, M. C., BUSH, M. B., A long pollen record from lowland Amazonia; forest and cooling in glacial times, *Science* **274** (1996) 85-88.

- [19] THOMPSON, L. G., et al. A high-resolution millennial record of the South Asian Monsoon from Himalayan ice cores. *Science* **289** (2000) 1916-1919.
- [20] YAO, T., THOMPSON, L. G., MOSLEY-THOMPSON, E., ZHIHONG, Y., XINGPING, Z., LIM, P-N., Climatological significance of $\delta^{18}\text{O}$ in north Tibetan ice cores. *J. Geophys. Res.* **101**(D23) (1996) 29,531-29,537.
- [21] LIU, X., CHEN, B., Climatic warming in the Tibetan Plateau during recent decades, *Int. J. Climatol.* **20** (2000) 1729-1742.
- [22] THOMPSON, L. G., MOSLEY-THOMPSON, E., BOLZAN, J. K., KOCI, B. R., A-1500 year record of tropical precipitation recorded in ice cores from the Quelccaya Ice Cap, Peru. *Science* **229** (1985) 971-973.
- [23] THOMPSON, L. G., MOSLEY-THOMPSON, E., DANSGAARD, W., GROOTES, P.M., The "Little Ice Age" as recorded in the stratigraphy of the tropical Quelccaya ice cap. *Science* **234** (1986) 361-364.
- [24] THOMPSON, L. G., et al. Holocene-Late Pleistocene climatic ice core records from Qinghai-Tibetan Plateau. *Science* **246** (1989) 474-477.
- [25] GROOTES, P. M., STUIVER, M., THOMPSON, L. G., MOSLEY-THOMPSON, E., Oxygen isotope changes in tropical ice, Quelccaya, Peru. *J. of Geophys. Res.* **94**, (1989) 1187-1194.
- [26] THOMPSON, L. G., MOSLEY-THOMPSON, E., THOMPSON, HENDERSON, K. A., Ice-core palaeoclimate records in tropical South America since the Last Glacial Maximum, *J. of Quat. Science* **15** (2000) 377-394.
- [27] VUILLE, M., BRADLEY, R. S., Mean annual temperature trends and their vertical structure in the tropical Andes. *Geophys. Res. Lett.* **27** (2000) 3885-3888.
- [28] HASTENRATH, S., KRUSS, P. D., The dramatic retreat of Mount Kenya's glaciers between 1963 and 1987: Greenhouse forcing, *Ann. Glaciol.* **16** (1992) 127-133.
- [29] KASER, G., NOGGLER, B., Observations on Speke Glacier, Ruwenzori Range, Uganda. *J. Glaciol.* **37** (1991) 315-318.
- [30] HASTENRATH, S., GREISCHAR L., Glacier recession on Kilimanjaro, East Africa, 1912-1989. *J. Glaciol.* **43** (1997) 455-459.

STABLE ISOTOPES IN SPELEOTHEMS AS PROXIES OF PAST ENVIRONMENTAL CHANGES IN THE ALPS

C. SPÖTL

Institut für Geologie und Paläontologie, Universität Innsbruck, Innsbruck, Austria

S.J. BURNS

Department of Geosciences, Morrill Science Center, University of Massachusetts, Amherst, Massachusetts, United States of America

A. MANGINI

Institut für Umweltphysik, Heidelberger Akademie der Wissenschaften, Heidelberg, Germany

Abstract. This short communication presents preliminary results and interpretations from an ongoing research project in the Obir Cave of southeast Austria. This cave system hosts abundant calcite dripstones many of which are actively forming today. The stable isotopic composition of a Holocene stalagmite dated by U-series TIMS techniques shows rather stable values throughout most of the last eight millennia, except for the last few hundred years when both C and O isotope values strongly increase (probably due to changes in the cave air circulation as a result of mining activity).

1. INTRODUCTION

Data of environmental change in the Alps are confined largely to the Late Glacial and Postglacial, because glaciations effectively obliterated older sedimentary records. Cave calcites (speleothems) hold a high promise of providing critically needed paleoenvironmental information complementing the surface sedimentary record and extending it back in time up to several hundreds of thousands of years. We are currently using the stable isotopic composition of alpine speleothems dated by U-series thermal ionization mass spectrometry (TIMS) techniques to infer paleo-environmental changes in the recharge area of the karst systems and in particular in high-mountain sites where existing surface paleodata are rare.

2. SAMPLING SITE AND STRATEGY

Based on a reconnaissance study of caves in Austria we selected four caves for further study placing particular emphasis on sites with modern dripstone formation. In addition to sampling dripwaters at regular intervals we also take milligram samples of wet stalagmite tops for stable isotope analysis. Cave air pCO₂ and relative humidity are being measured using portable instruments and the air temperature is automatically logged. Here we present preliminary data from one of these sites, Obir Caves.

The Obir massif is located in the northern segment of the Karawanken, a mountain range stretching E-W along the Austrian-Slovenian border. The caves developed in Middle and Upper Triassic platform carbonates and were only discovered during mining activities [1-3], mostly during the 18th century (the mines were finally closed in 1913 – [4-6]). No known natural entrances to the caves exist. Parts of the Obir caves have recently been adapted as a show cave [7], but other parts of the extensive system are virtually untouched by tourist activities. We selected a neighboring cave (Rassl system, approximately 1100 m a.s.l.) which

can only be accessed through an abandoned mining adit [8]. This cave is characterized by vadose shafts, narrow subhorizontal passages and chambers with abundant active speleothem deposition. Climatic conditions in the cave are virtually constant throughout the year (air temperature 5.4°C, relative humidity in excess of 97%). The partial pressure of CO₂ varies seasonally with low values during winter and spring (500-600 ppmv) and high values during summer and late fall (up to 1800 ppmv). Active speleothem deposition encompasses flowstones, stalagmites, stalactites and soda straws and pool deposits.

3. METHODS

Speleothem samples, both inactive and active were examined using a combination of thin-section petrography, Th-U dating and stable isotope analysis. Thin sections were examined both using standard transmitted light microscopy and uv-and blue light epifluorescence microscopy. The mineralogical composition of individual samples was checked using powder X-ray diffractometry. Age dating was performed by TIMS measurements of ²³⁸U, ²³⁴U, ²³²Th, and ²³⁰Th using 0.5-1 g of sample. Measurements were performed on a multi-collector Finnigan MAT 262 RPQ utilizing the double filament technique (for analytical details see [9]).

Samples for stable carbon and oxygen isotope analyses were microdrilled and measured with an on-line, automated, carbonate preparation system linked to a triple-collector gas-source mass spectrometer. Results are reported in the usual per mil notation relative to the VPDB standard. Standard deviations (1-sigma) of replicate analyses of standard materials are less than 0.10‰ for both C and O.

A variety of seepage waters were collected in the cave and analyzed for temperature, pH, electrical conductivity, and major cations and anions. Chemical speciation and saturation states are calculated using PHREEQC. The O isotopic compositions are reported on the VSMOW scale.

4. RESULTS AND DISCUSSION

Sample OBI 12 is a 32 cm high stalagmite which was actively forming at the time of sampling. The stalagmite was dated by seven TIMS dates starting at 8.2 ± 0.29 ka and the youngest date was obtained 10 mm below the top (0.32 ± 0.04 ka). All dates are in stratigraphical order and indicate a mean growth rate of 39 mm per thousand years. We obtained a medium-resolution stable isotope record from this sample (approximately 50-year resolution – Fig. 1). Macroscopic and thin-section microscopic inspection showed no evidence of growth discontinuities suggesting continuous growth since 8.2 ka BP. During most of the past 8.2 ka C isotopes vary only within 1.5‰ (Fig. 1). Superimposed are smaller-scale trends, e.g. low C isotope values during a few centuries from about 5.6 to 5.3 ka BP and during an even shorter episode from 4.3 to 4.2 ka BP. We suggest that these periods of low $\delta^{13}\text{C}$ values correspond to times of dense forest vegetation and high soil bioproductivity (and probably also high soil moisture) above the cave, giving rise to a high proportion of pedogenically-derived, isotopically light C in the cave seepage waters. This interpretation of a warmer and probably also more humid climate during periods of low $\delta^{13}\text{C}$ values is consistent with recent data from east-alpine glaciers showing evidence of strong recession during these time periods (e.g., [10]). Our preliminary data also suggest that the warm phase during the 6th millennium BP — whose end coincided with the death of the famous iceman found in the Tyrolian Alps (cf. [11] – Fig. 2) — was probably the warmest during the past 8 ka (with the possibly exception of the late 20th century).

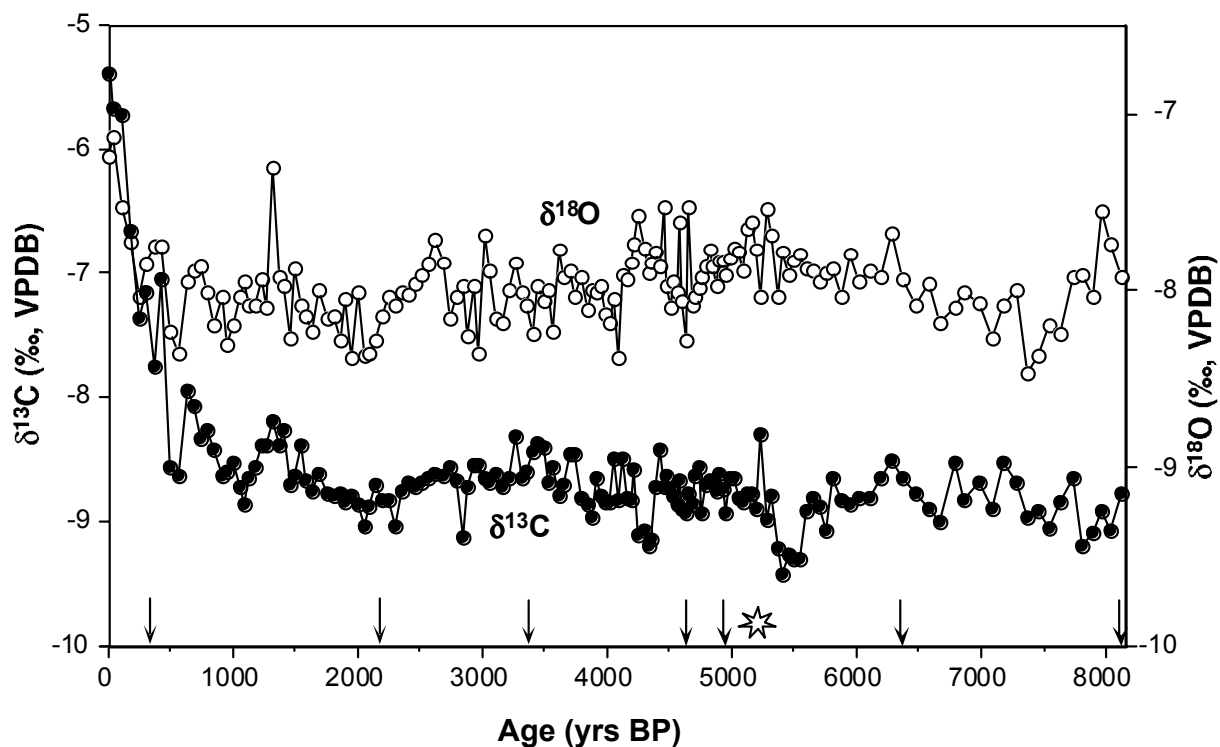


FIG. 1. C and O isotope variation along the extension axis of a Holocene stalagmite (sample OBI 12). Vertical arrows are TIMS Th-U dates and the asterisk indicates the calibrated ^{14}C age of the iceman [11].

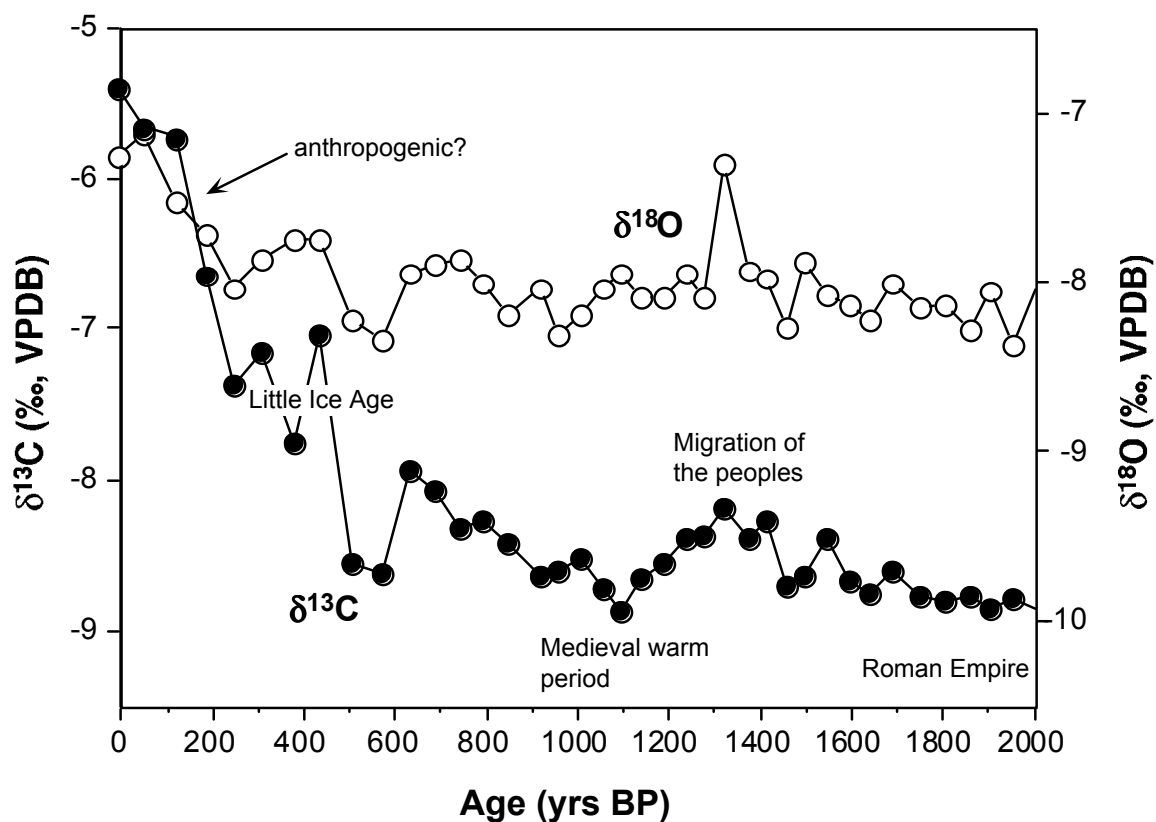


FIG 2. Enlarged view of the most recent part of the speleothem record shown in Fig.1 and possible correlation with historical events.

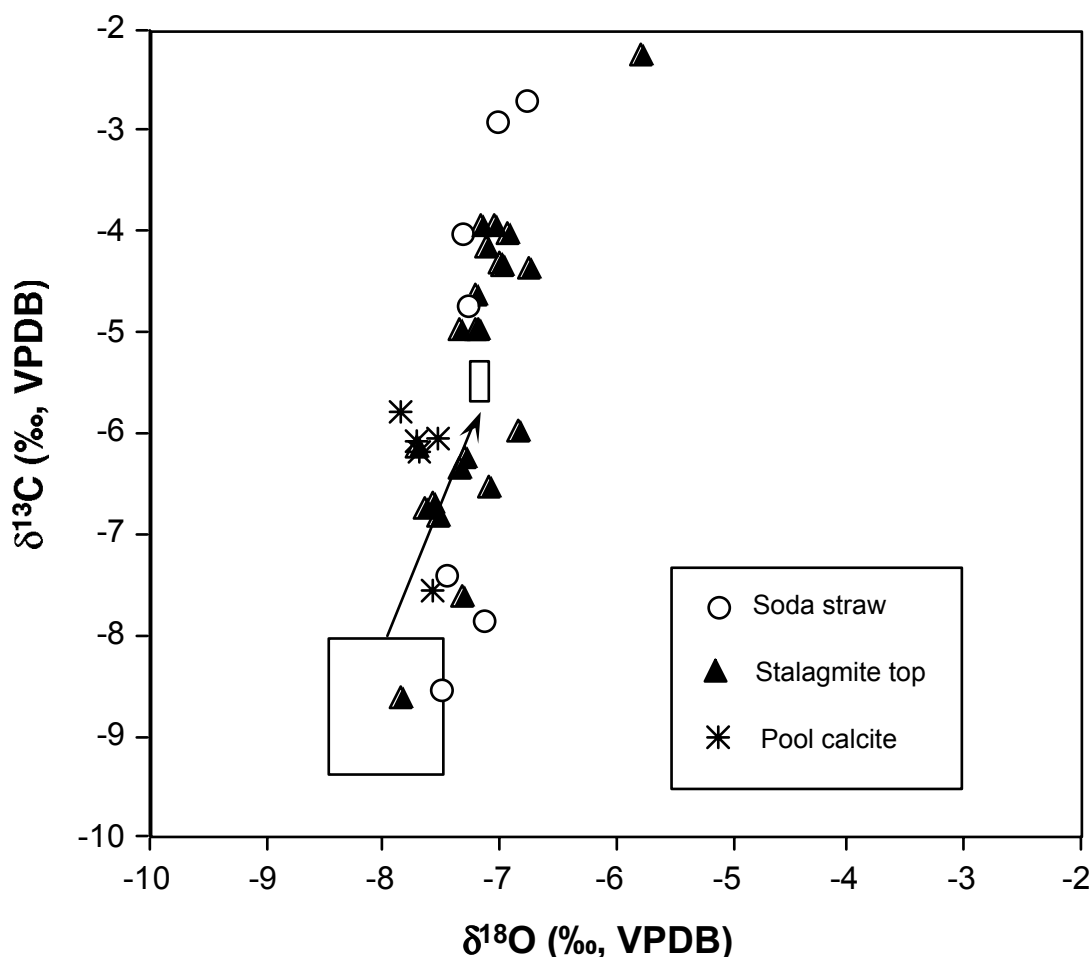


FIG. 3. Stable isotopic composition of modern calcite precipitates in Obir cave. The lower rectangular box indicates the stable isotopic composition of the Holocene stalagmite OBI 12, except for its youngest part, indicated by the smaller box.

The O isotope values vary only by about 1‰ during most of the Holocene, again suggesting fairly stable climatic and hydrologic conditions. Periods of low $\delta^{13}\text{C}$ values do not clearly correlate with relatively high $\delta^{18}\text{O}$ values, probably suggesting that the O isotopes are effectively rock-buffered. This interpretation is consistent with the relatively thick rock overburden of 80-100 m at the sampling site.

The most recent segment of the stable isotope curves shows an interesting and well known pattern reflected mostly in the C isotope data starting with the generally warm climate during Roman times up to the Little Ice Age (Fig. 2). This correlation between the $\delta^{13}\text{C}$ values and the well known cultural trends, though striking, warrants further high-resolution dating and stable isotope analyses and should be regarded as preliminary only. Since the Little Ice Age the C isotopic composition increased to values significantly higher than at any time during the past 8.2 ka. Although less well pronounced, the O isotope values also increased during the last few hundred years (Fig. 2). In order to better constrain the significance of this dramatic increase in the C isotopic composition we analyzed tips of soda straws, modern pool deposits and tops of stalagmites in this cave (Fig. 3). The C isotope values vary from -8.5 to as high as -2.3‰ and delineate an evolutionary trend toward high values. The O isotopic compositions increase only slightly by about 1‰. A possible explanation for this covariance is kinetic isotope fractionation [12], i.e. a slight decrease in relative humidity in the cave interior

causing enhanced degassing of carbon dioxide and mild evaporation. This hypothesis is difficult to test in the modern cave environment, but available instrumental data suggest that the cave interior (where the samples were taken) is close to condensation all year round.

Frisia et al. [13] studied a Holocene stalagmite record from the south-alpine Grotta di Ernesto (Trento) and observed a similar increase in the C isotopic composition during the last few hundred years which they tentatively attributed to extensive wood-cutting above the cave. Anthropogenic changes of the vegetation above Obir cave is a possibility, although we found no historical reports of extensive deforestation in this area. We speculate, however, that the onset of the mining activity may have had a strong impact on the overall air circulation in these caves (which lack natural entrances large enough to be surveyed by man) giving rise to either a lower pCO₂ in the interior cave air and/or a slight decrease in the water vapor saturation. Evaporation, however, is considered to be insignificant in the present-day cave environment. This is supported by the observation that most actively precipitating calcite is in near isotopic equilibrium with the parent dripwater.

ACKNOWLEDGEMENTS

We would like to express our gratitude to F. Orsini-Rosenberg for permission to work in the Obir cave, to Harald and Andreas Langer and Otto Jamelnik and other members of the Fachgruppe für Karst- und Höhlenkunde in Carinthia for their generous support in the cave, to Rene Eichstätter for excellent TIMS work and to the Austrian Science Fonds (Y122-GEO) for funding this research.

REFERENCES

- [1] LEX, F., Die Tropfsteinhöhlen in der Unterschäffleralpe, Carinthia II **112/113** (1923) 5-8.
- [2] LEX, F., Die Tropfsteinhöhlen in der Unterschäffleralpe, Carinthia II **114/115** (1925) 14-17.
- [3] TRIMMEL, H., Beobachtungen aus den Tropfsteinhöhlen bei der Unterschäffleralpe im Hochobir (Kärnten) Die Höhle **10** (1959) 25-33.
- [4] WIESSNER, H., Geschichte des Kärntner Bergbaues, 2. Teil, Archiv vaterl. Geschichte Topogr. **35/36** (1951) 1-298.
- [5] HOLLER, H., Ergebnisse der zweiten Aufschlußperiode (1938-1941) beim Blei-Zink-Erzbergbau Eisenkappel in Kärnten (Hochobir, östliche Karawanken), Carinthia II **167/87** (1977) 31-52
- [6] KÖSTLER, H.J., "Zur Geschichte des Berg- und Hüttenwesens im Hochobir-Gebiet mit besonderer Berücksichtigung des Bleierzbergbaues", Der Hochobir (GOLOB, B., Ed.), Naturwiss. Verein Kärnten, Klagenfurt (1999) 63-82.
- [7] HADERLAPP, P., Obir-Tropfsteinhöhlen, Carinthia II **181/101** (1991) 181-190.
- [8] JAMELNIK, O., Neue Höhlen im Obirgebiet, Carinthia II **184/104** (1994) 77-92.
- [9] FRANK, N., et al., Warm period growth of travertine during the Last Interglaciation in southern Germany, Quat. Res. **54** (2000) 38-48.
- [10] MAISCH, M., The longterm signal of climate change in the Swiss Alps: glacier retreat since the end of the Little Ice Age and future ice decay scenarios, Geogr. Fisica Din. Quat. **23** (2000) 139-151.
- [11] ROM, W., et al., AMS 14C dating of equipment from the iceman and of spruce logs from the prehistoric salt mines of Hallstatt, Radiocarbon **41** (1999) 183-197.

- [12] HENDY, C.H., The isotopic geochemistry of speleothems — I. The calculation of the effects of different modes of formation on the isotopic composition of speleothems and their applicability as palaeoclimatic indicators, *Geochim. Cosmochim. Acta* **35** (1971) 801-824.
- [13] FRISIA, S., “Holocene palaeoclimatic fluctuations recorded by stalagmites: Grotta di Ernesto (northeastern Italy)“, *Proceedings of the 12th International Congress of Speleology*, Vol. **1** (JEANNIN, P.Y., Ed.), La Chaux-de-Fonds (1997) 77-80.

STABLE ISOTOPES IN ALPINE ICE CORES: DO THEY RECORD CLIMATE VARIABILITY?

U. SCHOTTERER

Physics Institute and Department of Chemistry, University of Bern, Switzerland

W. STICHLER, W. GRAF

GSF – Institute for Hydrology, Neuherberg, Germany

H-U. BÜRKI

Physics Institute, University of Bern, Switzerland

L. GOURCY

Isotope Hydrology Section, International Atomic Energy Agency, Vienna

P. GINOT, T. HUBER

Department of Chemistry, University of Bern, Switzerland

Abstract. Data from the national networks of stable isotopes in precipitation in Switzerland, Germany and Austria reveal distinct structures of climate variability within the Alpine region during the past three decades. To investigate the possibility of linking on longer time scales water isotopes and climate anomalies like the North Atlantic Oscillation (NAO), a high-resolution stable isotope record of an ice core from the Bernese Alps is examined with respect to the isotope information obtained from the precipitation data. Dating of the ice core is performed by annual layer counting of water isotopes, controlled by well known discrete time markers like reference horizons from nuclear weapon tests, the Chernobyl fall out, extreme events of Saharan dust falls and additionally compared to the seasonal behaviour of chemical constituents. After checking for post-depositional effects, the defined year-to-year isotope data sets are sub-divided into monthly composites according to the precipitation distribution of a high altitude precipitation station from the Swiss isotope network. For the last thirty years, the normalised data sets of the stable isotopes in the ice core show close similarities to the regional isotope distribution and the NAO index. Although the method has to be refined, an extension of the existing isotope record several centuries back in time to study climate variability seems to be feasible and reasonable.

1. INTRODUCTION

Stable isotopes in precipitation contain composite information on evaporation site conditions, air moisture transport and rainout history. Their climate signal in natural archives like ice cores, tree rings or lake sediments is not only used to reconstruct past conditions of the water cycle but also to validate model experiments of past and present atmospheric circulation [1, 2]. A critical review of the Global Network for Isotopes in Precipitation (GNIP) underlined the importance of long-term data series for climate studies [3] and a recent workshop in Hamburg “*In Memoriam Hans Oeschger: Towards an Isotope Climatology*” proved the close connection of water isotopes in European precipitation to NAO indices [4].

Great parts of Europe have experienced pronounced changes in climatic conditions during the last decades. This stimulated interest towards an extension of climate variability indices beyond the instrumental era to discriminate natural variability against anthropogenic perturbations on longer time scales. Although water isotopes could serve such needs, the

limited time series of the GNIP data have to be extended back in time for such purpose. A few cold glaciers, principally in the European Alps, offer such a possibility since they store, at selected sites, the history of precipitation of several hundred years with sufficient time resolution. However, in most cases, post-depositional processes alter the originally accumulated isotopic (or chemical) information to an extent, which may completely mask any climate-induced variability [5]. It is necessary to look for summit regions over 4000m in order to retrieve ice cores from glaciers cold enough throughout the year to avoid melting and percolating and refreezing melt water in deeper layers. Unfortunately, these sites are often exposed to strong winds that preferentially erode light winter snow containing the most depleted isotope values. Although in sheltered places at lower altitudes winter precipitation may stick better to the surface, increased summer melting disturbs the seasonal distribution at such places. Since seasonal differences in the isotope content of precipitation are much larger than those expected to trace a climate anomaly, any post-depositional change limits the possibilities for detecting climate and environmental variability from the layers left. Examples are shown in Fig.1. At the cold Colle Gnifetti glacier, the isotopic variability is reduced due to the loss of winter snow and at the temperate Jungfrauoch Saddle additional melting further reduces it.

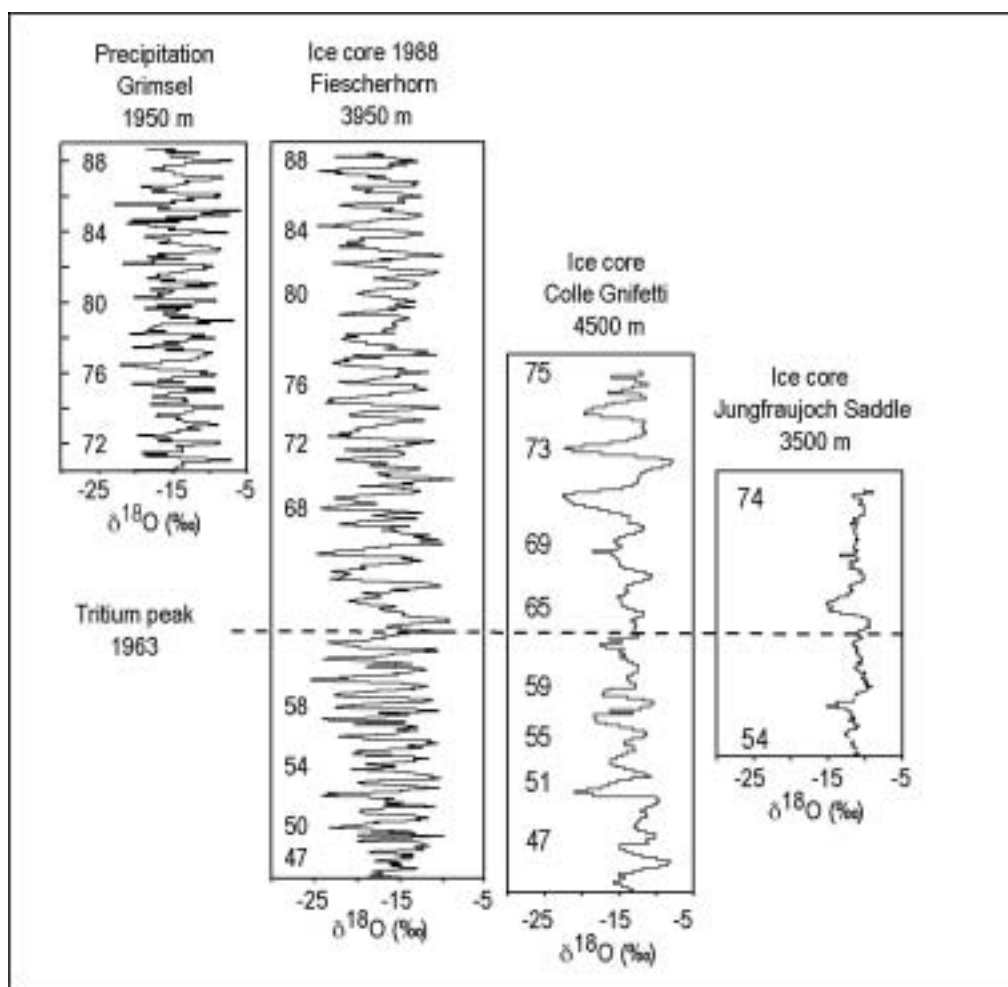


FIG. 1. Variability of stable isotopes in monthly composites of precipitation and well dated ice core records from the Swiss Alps.

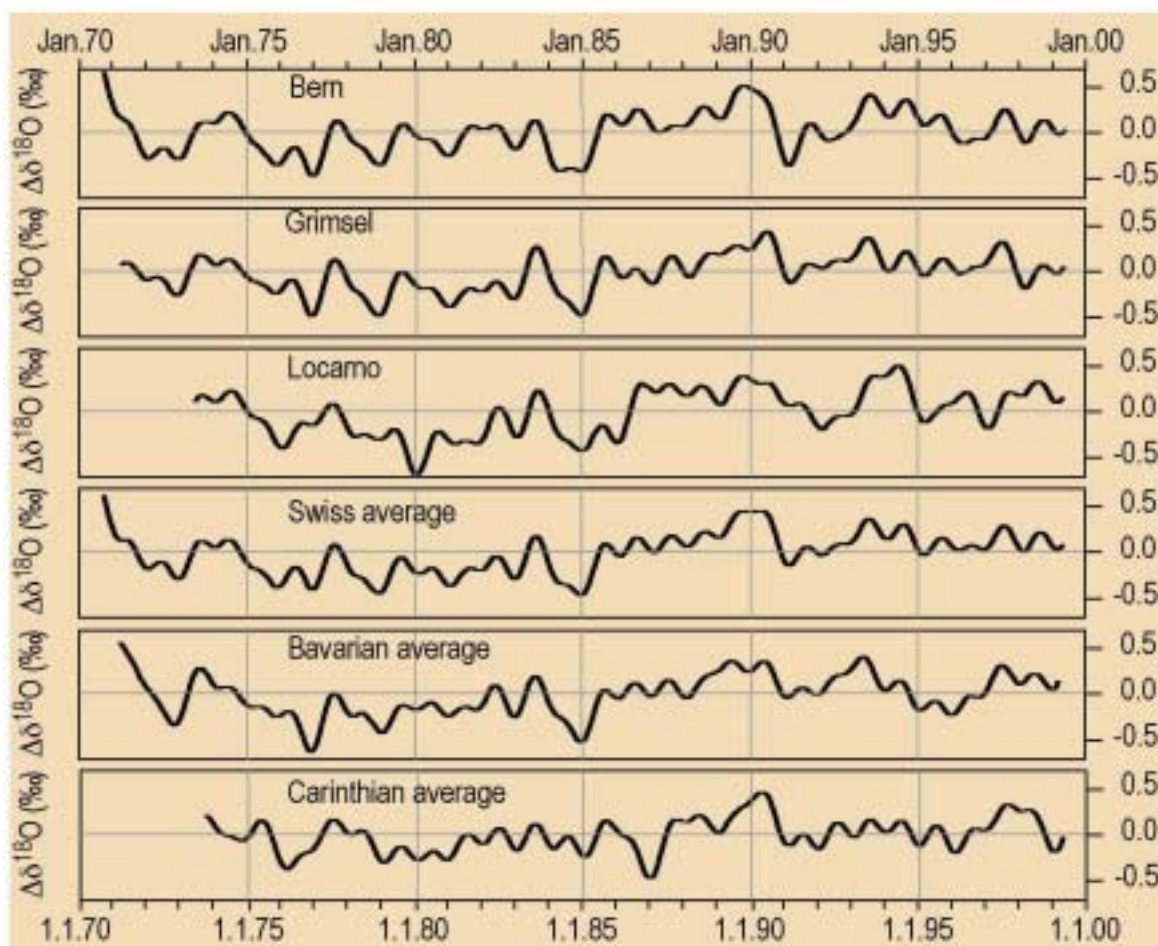


FIG. 2. Distribution of precipitation stations and the ice core drilling sites (top) together with smoothed (25-fold Gaussian filter) and normalised $\delta^{18}\text{O}$ signals (down) on local to regional scales north and south of the Alps.

Only ice cores at Fiescherhorn Plateau, drilled between 1986 and 1989, store the isotopic variability throughout the seasons. Extensive studies of isotopes and chemical constituents proved the good conservation of the signal [6, 7, 8]. The longest core from that site reached a depth of 78m that corresponds to the year 1946. Fiescherhorn Plateau was re-drilled in May 2000 to continue investigations on the distribution of chemical constituents [9]. On this occasion a high-resolution stable isotope record was performed too. In our contribution we combine the data sets from the cores 1988 and core 2000 and compare the obtained composite record with that of the long-term Swiss isotope network in order to examine the possibility to reconstruct NAO indices.

2. LOCAL AND REGIONAL ISOTOPE DISTRIBUTION

Ice core drilling locations and sampling sites from the network stations used in this study are shown in Figure 2 together with their respective smoothed and normalised time series of $\delta^{18}\text{O}$. The available stations – five from the Swiss, the Bavarian and the Austrian network respectively - were chosen to cover with isotope data the past 30 years and the specific climatic regions north of the Alps, south of the Alps, and within the Alps (upper part of Figure 2). Data for Swiss stations are plotted for Bern (north), Grimsel (intermediate) and Locarno (south) to illustrate the influence of the Alpine division on circulation pattern and therefore on the local isotope distribution. The values for the regional isotope distribution in Bavaria, Switzerland and Carinthia are the weighted means of five individual stations (upper part of Figure 2).

From an individual station, the comparison of stable isotope time series with the regional average allows to assess the ability and robustness of the local signal to transmitting climate induced changes regarding conditions in the source region and circulation modes of atmospheric moisture. Similarities and differences in $\delta^{18}\text{O}$ between the northern and the southern part of the Alps are clearly visible for a single station and the regions as well. Pronounced negative deviations from the mean starting in 1970, 1984, and 1990 are recorded in all stations and regions. In Carinthia, the first two events started later one and two years respectively. The same holds for the period with an increase in $\delta^{18}\text{O}$ between 1985 and 1990. In general, the South behaves somewhat different from the North; the similarities between Switzerland and Bavaria are obvious.

The distribution is understandable from the geographic distribution of the precipitation stations and their vicinity to oceanic moisture sources, the Atlantic and the Mediterranean. It confirms also that the inter-annual stable isotope imprint from the source region and the circulation pattern is not modified by the local micro-climatic situation. However, to what extent the glacier at Fiescherhorn Plateau records these patterns (despite minor but likely post-depositional effects) has to be clarified prior to climate variability considerations.

Since 1983, monthly composites of precipitation (daily removed from the sampler to avoid evaporation effects) are collected at Junfrauoch research station, only a few kilometres apart from the Fiescherhorn drilling site. Although no official data are published for the amount of precipitation because of uncertainties regarding wind drift at nearly 3600m in altitude, the net weight of accumulated precipitation is reported. The isotopic signature of these monthly samples is very similar to that of the official network stations Bern, Meiringen, Guttannen and Grimsel. We use this record to control how much of the isotope signal is stored on the glacier

area around. For this purpose, a test core was drilled in about 1 km distance on a sheltered (but sun exposed) place at the temperate Jungfraujoch firn at 3500m. The results are plotted in Figure 3.

When precipitation occurs as snow and melting is minor, the agreement between precipitation and ice core data is nearly perfect (left). Information from rain and melt water is not stored in the core. It does not re-freeze in deeper layers to an amount that changes seriously the isotopic composition remaining in the core, at least to a depth of about 10m. In addition, the δD - $\delta^{18}O$ relation seems not to be disturbed by fractionation processes caused by evaporation or melting (right). Although melting plays a minor role at the drilling site on Fiescherhorn Plateau [6], the precipitation data set from Jungfraujoch research station was also used too for controlling post-depositional effects and to date the surface layers.

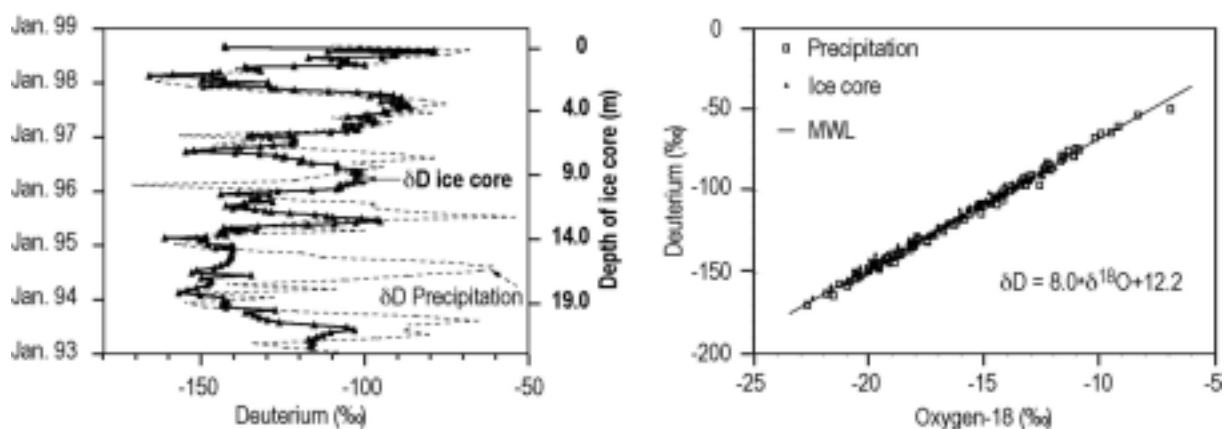


FIG.3. δD and $\delta^{18}O$ in monthly precipitation and the ice core at Jungfraujoch Firn. This coring site keeps more isotopic information than the wind exposed Jungfraujoch Saddle in Fig. 1.

3. THE HIGH RESOLUTION TIME SCALE AT FIESCHERHORN PLATEAU

The first drilling at Fiescherhorn started in 1986 with the purpose to reconstruct fall out from the Chernobyl event. Because of frequent unfavourable weather conditions, the drilling had to be interrupted several times. For this reason, the upper part (containing the period May 1986 to February 1989) is a composite of several drilling attempts. The whole core (in the following named FH 88) of 79m covers the period back to 1946. Dating was mainly based on stable isotope layer counting and controlled by a complete tritium fall out reconstruction from the beginning of the nuclear weapon tests to the year 1983 [7]. The specific seasonality of numerous chemical constituents could be applied for a dating control [8, 9]. This technique was also applied for the core 2000 (FH 00) and the refinement of the combined data set FH 88 and FH 00. The two important steps are 1) the time control of the surface layers with low firn density and 2) the perfect link between the data sets of the two cores. Any shift in dating would seriously disturb a correlation with the calendar based time scale of the isotope-in-precipitation data. These two steps are illustrated in Figure 4.

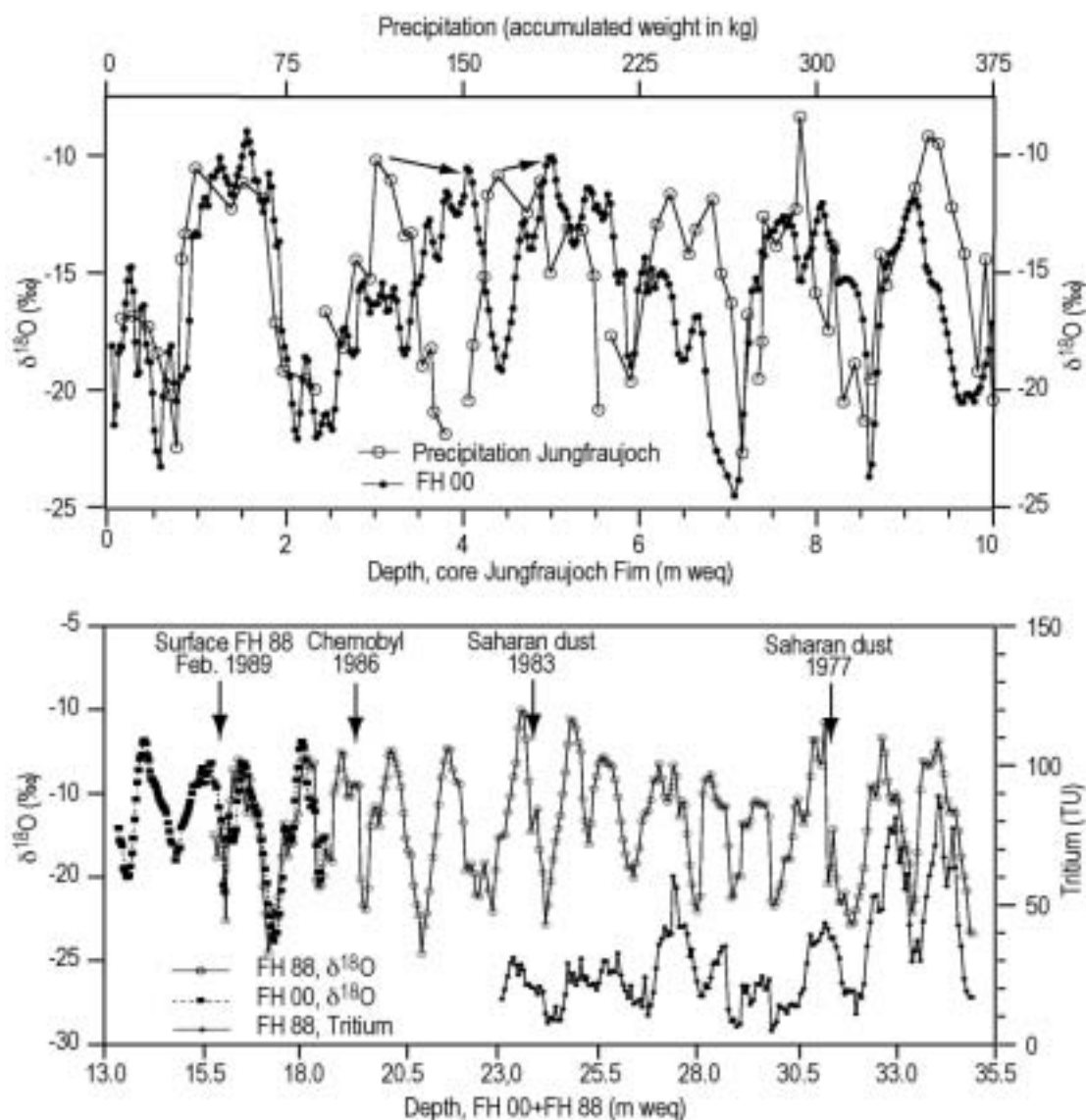


FIG. 4. Linking and year-by-year dating of the Fiescherhorn ice cores FH 00 and FH 88.

The direct comparison of the stable isotope seasonality in the core with the monthly precipitation data from Jungfrauoch research station is convincing. The accumulation distribution at the glacier is not a one to one picture of the research station one and for matching some features have to be stretched or compressed as illustrated by arrows in the upper part of the figure. It is important that the seasonal structure of δD and $\delta^{18}O$ remains comparable, which indicates that post-depositional processes have not removed any important parts of the accumulation. The individual amounts of seasonal partitions variation are expected as natural variability. This amount of precipitation variability may influence weighted means of isotope data sets. The linking of FH 00 and FH 88 is shown in the lower part. Time control in both cores matches perfectly the overlapping two years. Although the two drilling sites were chosen approximately 100m distant to avoid disturbances from the drilling surface of 1986 to 1989, the isotopic fine structure with a resolution of more than 20 samples per year does not show differences in the overlapping period. However, the most crucial part in comparing more quantitatively the ice core record and the precipitation data sets is the composition of monthly means from the high-resolution ice core samples. This is

necessary because all interesting climate data sets (including the isotope-in-precipitation data) have at least monthly resolution. The sensibility of NAO indices to express climate variability is also highest during specific winter month. To establish monthly composites in an ice core is thus necessary but also the main restriction. Namely, the assumption that the distribution in amount of monthly precipitation as recorded at high altitudes (in our case the station Grimsel at 1950m, approximately 30km apart) is similar to that of the Fiescherhorn Plateau. We selected the following procedure: the winter season - as usual - is defined as the part with the most depleted stable isotope values and January of a specific year is then placed near a meteorological anomaly; the Christmas thaw is often recorded as precipitation event with distinct enriched stable isotopes. Furthermore, the starting point of a year should be also close to the beginning of the seasonal tritium increase beginning February. The number of ice core samples within these January-to-January defined years is then combined to monthly averages according to the monthly precipitation sums at Grimsel and the respective water equivalent in the core. Figure 5 illustrates this on a well-dated three years interval between 1975 and 1978.

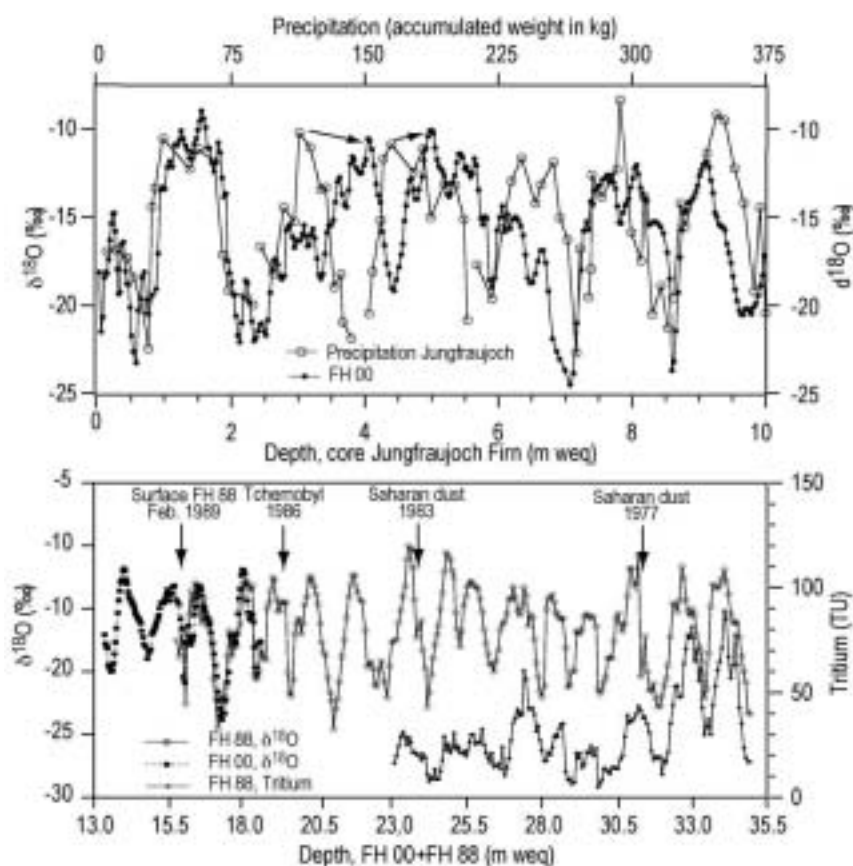


FIG. 5. $\delta^{18}\text{O}$ values in a section of FH 88 normalised to the monthly precipitation distribution at Grimsel for the years 1975 to 1978 (left) and the correlation of seasonal averages with the respective values from Grimsel and Locarno for the years 1973 to 1986 (right).

Although the number of matching years increase when data is normalised it still remains sections in the core where the data differ remarkably. This is not astonishing since the accumulated yearly mean at Fieschehorn Plateau varies by more than a factor of 2 during the last decades and the amount at Grimsel only in the order of 20-30%. Nevertheless, a

correlation of composite seasonal averages (right) with Grimsel (central-north of the Alps) and Locarno (south of the Alps) reveals some interesting features.

The correlation of the normalised Fiescherhorn and precipitation stations seasons is remarkably good especially with Grimsel. Winter values with Locarno do not correlate, nor do the winter values between the two precipitation stations. This may be already a hint that winter NAO is differently influencing the isotope-in-precipitation regimes represented by Locarno, Grimsel, and Fiescherhorn respectively.

4. THE FIESCHERHORN ICE CORE AND NAO: A PRELIMINARY CONCLUSION

We treated the constructed monthly composites from both Fiescherhorn ice cores in the same way as the precipitation data in Figure 2 between the years 1970 and 2000 for the comparison with the regional stable isotope distribution. In this comparison, all regional data is combined. The same data treatment is applied to the NAO index. Since the summer months have minor influence on the associated climate variability, we do not select specific winter month for this attempt but rather use the whole year. Figure 6 presents the result.

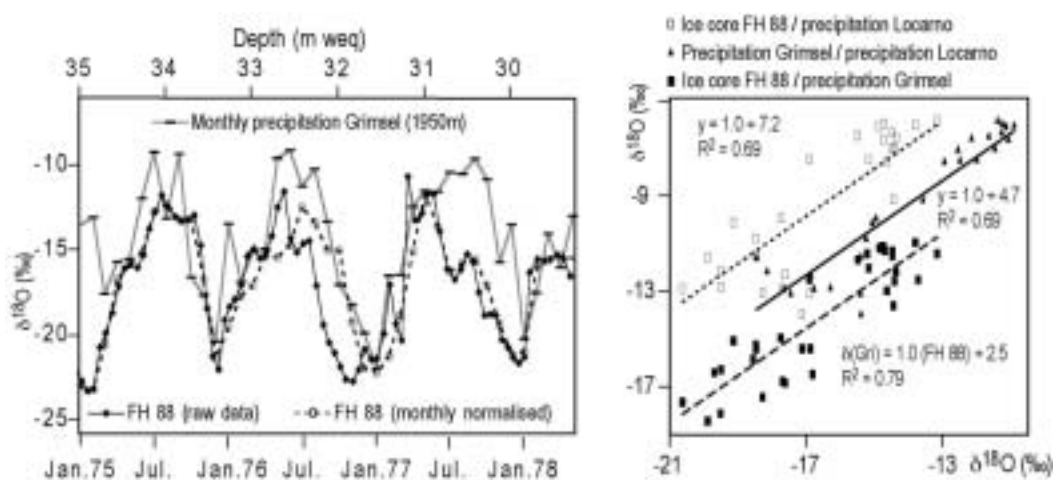


FIG. 6. Normalised $\delta^{18}\text{O}$ variability in Alpine precipitation together with the NAO-index. All monthly data are smoothed with a 25 fold Gaussian filter. The regional $\delta^{18}\text{O}$ average is based on five Swiss, five Bavarian, and five Carinthian stations respectively.

The similarities between the data, although the treatment is still preliminary, are convincing. Small peak differences may be also a result of dating. The $\delta^{18}\text{O}$ signal from Fiescherhorn Plateau is linked to the varying NAO index and periods with strong positive and negative correlation change with time. As already seen from the precipitation records, this is not surprising, since the Alpine division separates the pathways of atmospheric circulation. During negative NAO indices the southern parts of the Alps get more precipitation with a stronger influence of the Mediterranean. During a positive NAO the Westerlies dominate with a more direct influence from the Atlantic.

Tracing atmospheric moisture from the source region to the place of precipitation is an established domain of water isotopes. The potential of tracing NAO with the GNIP data sets has also been demonstrated in this volume. The potential of selected glacier sites in the Alps to extend the physical behaviour of this climate anomaly back in time for several centuries may offer new possibilities for ocean – atmosphere model experiments in the Atlantic region that consider balance equations for stable isotopes too.

ACKNOWLEDGEMENTS

The work was supported by the Swiss National Science Foundation and the Swiss Geological Survey (Federal Office for Water and Geology, FOWG), who operates the Swiss Network for Isotopes in the Hydrological Cycle.

REFERENCES

- [1] JOHNSEN, S.J., DANSGAARD, W., WHITE, J.W.C., The origin of Arctic precipitation under present and glacial conditions, *Tellus Ser.B*, **41** (1989) 452-468.
- [2] JOUZEL, J., HOFFMANN, G., KOSTER, R.D., MASSON, V., Water isotopes in precipitation: data/model comparison for present-day and past climates, *Quaternary Science Reviews* **19** (2000) 363-379.
- [3] ROZANSKI, K., ARAGUAS-ARAGUAS, L., GONFIANTINI, R., Isotope patterns in modern global precipitation, in *Climate Change in Continental Isotopic Records*, AGU, Washington DC (1993) 1-37.
- [4] GRASSL, H., LATIF, M., SCHOTTERER, U., GOURCY, L., Climate Variability from Isotope records in Precipitation, this volume.
- [5] STICHLER, W. SCHOTTERER, U., From accumulation to discharge; Modification of stable isotopes during glacial and post-glacial processes. *Hydrol. Process.* **14** (2000) 1423-1438.
- [6] SCHOTTERER, U., FROEHLICH, K., GÄGGELER, H.W., SANDJORDJ, S., STICHLER, W., Isotope records from Mongolian and Alpine ice cores as climate indicators. *Climatic Change* **36** 3-4, (1997) 519-530.
- [7] SCHOTTERER, U., SCHWARZ, P., RAJNER V., From pre-bomb levels to industrial times: A complete tritium record from an alpine ice core and its relevance for environmental studies. *Proc. Conf. on Isotope Techniques in the Study of Environmental Change*, IAEA Vienna (1998) 581-590.
- [8] SCHWIKOWSKI, M., BRÜTSCH, M.S., GÄGGELER, H.W., SCHOTTERER, U., A high resolution air chemistry record from an Alpine ice core (Fiescherhorn glacier, Swiss Alps), *J. Geophys. Res.* **104** (1999) 13709-13720.
- [9] HUBER, T., Bestimmung historischer Spurenstoffverläufe in alpinem Firn mittels kontinuierlicher ionen-chromatographischer Analyse, Thesis, Dept. of Chemistry, Univ. Bern Switzerland (2001).

CLIMATE HISTORY OF THE TIBETAN PLATEAU FOR THE LAST 1500 YEARS AS INFERRED FROM STABLE CARBON ISOTOPES IN TREE-RINGS

G. HELLE, G.H. SCHLESER

Forschungszentrum Jülich, Jülich, Germany

A. BRÄUNING

Institut für Geographie, Universität Stuttgart, Stuttgart, Germany

Abstract. For the south-eastern part of Tibet, i.e. Qamdo, a carbon isotope chronology from spruce and juniper trees, covering the last 400 and 1600 years, respectively, has been developed. Juniper tree-rings were sampled in pentad blocks, whereas the spruce chronology is annually resolved in order enable appropriate calibration of isotope data with the short instrumental temperature record available. The chronology shows a number of different climatic phases which have their analogues in Europe and North America. A short warm phase between 1200 and 1300AD appears to correspond to the Mediaeval Warm Period and a larger cool phase from about 1450 to 1600AD appears to correspond to the Little Ice Age with a short recurring episode around 1850. The current results suggest that the observed events may have occurred over the entire Northern Hemisphere, though they do not seem to have been contemporaneous with Europe and North America.

1. INTRODUCTION

The Tibetan Plateau is of great importance for the climate system of Asia due to its large area and average altitude of over 4000 m a.s.l.. This is especially true in view of the atmospheric monsoonal circulation. The Tibetan Plateau is characterized by high insolation and low albedo during northern hemispheric summer months leading to a large stable low pressure system sucking moist air masses inland from the southeastern direction [1]. In the northern hemispheric winter, low insolation and high albedo change the air pressure system resulting in westerly cyclonic activity over the plateau.

For a better understanding and prediction of changes in the South Asian monsoonal intensity, detailed investigations of the past climatic variations on the Tibetan Plateau are most useful. The necessary informations can indeed only be drawn from the past, since all the meteorological time series available are much too short for appropriate model investigations. Unfortunately, very few historical climate recordings do exist of the Tibetan region [2, 3] and the multiple historical data sets from Eastern China are difficult to interpret. They are not always relevant for the area, as well as discontinuous and partly restricted to extreme events of climatic or phenological provenance [4, 5, 6, 7, 8, 9, 10].

Therefore, long proxy records of high time resolution have to be investigated. In this respect, ice cores [11, 12] and tree rings are highly promising archives containing isotope proxies, by which variations in the natural climate system of the Tibetan Plateau can most likely be assessed.

The present results are part of an ongoing extensive tree-ring study based on stable carbon and oxygen isotope studies, as well as ring width and x-ray density measurements to pursue temperature and humidity changes at several sites in High Asia.

2. STABLE CARBON ISOTOPES AS CLIMATE PROXIES

Current models for the fractionation of stable carbon isotopes during photosynthetic uptake of CO₂ indicate that besides genetic properties and type of photosynthesis, environmental factors such as temperature, precipitation or relative humidity, photosynthetic active radiation and concentration of atmospheric CO₂ influence the isotopic composition of plant organic matter.

Because of its importance for plant growth temperature has been and is one of the important quantities which is being looked for in climate reconstructions. Therefore, numerous studies have dealt with and still deal with the problem of transferring carbon isotope data of plant organic matter into temperature values, least translating carbon isotope variations into relative temperature changes.

Depending on the location at which plants grow, plant growth is dominated by just one or two variables. These variables are then primarily responsible for the carbon isotope composition of the corresponding plant organic matter. Carbon isotopes are, therefore, suited as climate proxies for palaeoclimate research, if appropriate sites are chosen. At upper treeline sites temperature is generally known to be the primary growth limiting ecological factor.

An expression for the photosynthetically determined carbon isotope composition in C₃ plants has first been given by [13] which reads in its most elementary form:

$$\delta^{13}C_{om} = \delta^{13}C_a + \epsilon_D(1 - c_i/c_a) + \epsilon_C(c_i/c_a)$$

ϵ_D is the fractionation for diffusion (-4.4‰), ϵ_C is the fractionation at the CO₂ fixing enzyme, RuBisCO (-30‰), including the equilibrium effect for CO₂ dissolution) and c_i and c_a are the leaf intercellular and ambient atmospheric CO₂ concentrations.

In principle, the isotope variations have to be given relative to the source value, i. e. the $\delta^{13}C$ value of atmospheric CO₂, because any changes in the source value will otherwise be interpreted as a false environmental or climatic signal. Therefore, isotope shifts should be given as deviations from the source value, characterising the fractionation of the whole process in question. Generally, this discrimination is expressed by Δ , giving the shift between air ($\delta^{13}C_a$) and plant organic matter ($\delta^{13}C_{om}$). To a good approximation Δ is given by:

$$\Delta \equiv \delta^{13}C_a - \delta^{13}C_{om} = -\epsilon_D(1 - c_i/c_a) - \epsilon_C(c_i/c_a)$$

As long as $\delta^{13}C_a$ is constant or known, $\delta^{13}C_{om}$ variations are independent of the source or can be corrected and $\delta^{13}C_{om}$ can be used just as well as Δ .

Obviously, Δ is not merely the sum of the individual fractionations. The contribution from each step depends basically on the ratio of c_i/c_a . In case of reduced stomata aperture, e. g. when dry and/or high temperature conditions prevail, the uptake rate of CO₂ is restricted, resulting in low internal CO₂ concentrations. Under these conditions the corresponding enzyme (RuBisCO) converts almost all leaf internal CO₂, thus, suppressing the carboxylation fractionation. Δ is then primarily determined by ϵ_D which leads to low values ($\Delta = 4.4\text{‰}$ and $\delta^{13}C_{om} = -8 - 4.4 = -12.4\text{‰}$). If the concentration of leaf internal CO₂ increases, e. g. when humid and/or low temperature conditions prevail, due to wide stomata apertures, the fractionation for the step of carboxylation ϵ_C becomes important, while the contribution from

diffusional fractionation can be ignored. Δ is then basically determined by ϵ_c which results in high values ($\Delta=30\text{‰}$ and $\delta^{13}\text{C}_{\text{om}} = -8-30 = -38\text{‰}$). It should, however, be emphasized that c_i/c_a is not merely a function of meteorological quantities. For example, leaf morphology and anatomy also influence the ratio of c_i/c_a [14, 15]. Furthermore, under certain conditions carboxylation efficiency can change c_i/c_a independent of changes of stomatal aperture. In nature, leaf internal CO_2 does not approach the two extremes discussed above. Therefore, Δ and $\delta^{13}\text{C}$ will generally be intermediate between the two extreme values.

From the expression of Δ follows that atmospheric $\delta^{13}\text{C}_a$ and $p\text{CO}_2$ which constitute the input level of the system, affect the carbon isotope composition of organic matter, either directly ($\delta^{13}\text{C}_a$) or indirectly (c_i/c_a - with regard to stomata index or stomatal density). Since $\delta^{13}\text{C}_a$ is currently decreasing and $p\text{CO}_2$ is increasing due to burning of fossil fuels and deforestation [16], $\delta^{13}\text{C}_{\text{om}}$ values originating from the last 200 years have to be corrected accordingly, in order to compare them with values from previous centuries.

Since the effect of increasing $p\text{CO}_2$ on different C_3 -plants is under debate and still not known in detail [17] three different kinds of corrections will be given in this paper. At present, this uncertainty makes it indeed difficult to interpret carbon isotope variations from tree-rings reliably.

3. MATERIALS AND METHODS

Samples of 10 Juniper (*Juniperus cf. tibetica*) and 5 spruce (*Picea balfouriana*) trees were collected during the summers 1992 and 1994 by joint Chinese-German expeditions. The investigated sites ($31^\circ05.3'\text{N}/ 96^\circ58'\text{E}$ (juniper); $31^\circ05'\text{N}/ 96^\circ57.5'\text{E}$ (spruce)) are located near Qamdo ($31^\circ08'\text{N}/ 96^\circ59'\text{E}$) on the southeastern part of the Tibetan Plateau. Samples were taken from dominant trees of open forest stands near or at the alpine timberline at an elevation of 4400 to 4600m a.s.l..

In a number of cases two or three increment cores per tree were drawn. But wherever feasible, the sampling of tree-discs was favoured. To extend the chronology as far back in time as possible, standing trunks from dead trees were included. The maximum number of tree-rings collected from a single tree was 1260. Increment cores from spruce trees were analysed in order to compare the juniper data with those from another species of that area. The core material contained up to 589 tree-rings but the exact age of the tree could not be deduced because the pith was not hit by the increment corer. Corresponding tree-ring material was dated and cross-dated by dendrochronological methods which have been described elsewhere e.g. [18, 19].

Since the juniper tree-rings were in most cases extremely narrow (often less than 0.1mm), several rings had to be combined for one isotope sample. The cross-dated cores and prisms were carefully cut and radially separated into successive tree-ring pentads using a razor blade. The wood material from each tree was separately processed, ground and carefully homogenized. Contrary to the juniper trees the ring widths of the spruce trees proved to be rather wide. Therefore, it was no problem to separate samples on a yearly basis. After tree-ring preparation cellulose was extracted from the woody material by using sodium hydroxide and sodium chlorite [20]. Details of the procedure are given elsewhere [21].

Subsequently sample material (200-250 μg) was packed in tin foil boats and combusted in an excess of oxygen at 1020°C with an elemental analyser (Carlo Erba NA 1500). Carbon

isotope ratios of the generated CO₂ were analysed by an isotope ratio mass spectrometer (Optima, Micromass Ltd.) interfaced to an elemental analyser. Carbon isotope results are given in the international δ notation as [‰] versus VPDB. Analytical reproducibility, taking into account sample preparation and mass spectrometry, was generally better than 0.1‰.

Each tree has a different $\delta^{13}\text{C}$ mean value. To enable a comparison of these trees, especially with regard to the set-up of an isotope chronology, it is necessary to normalize the $\delta^{13}\text{C}$ values to the same average for the overlapping sequences by subtracting the mean of each individual series from raw data. All dates mentioned in this article are given in AD.

Unfortunately, the pentad blocks of tree-rings from different juniper trees could not always be taken from synchronous time periods. Therefore, averaging the single $\delta^{13}\text{C}$ records has resulted in a smoothed data series of yearly values (yearly averaged pentad blocks).

4. RESULTS AND DISCUSSION

Climate influences tree growth and plant isotopic fractionation, but tree growth is governed by numerous plant physiological processes and generally does not react directly to changes of one or more meteorological quantities. In addition, the mechanisms which transfer an environmental signal such as temperature or any other quantity or a combination thereof into a biological sequence of proxies do not translate linearly. The capability to optimise growth in a given environment is a characteristic of biological systems. Consequently, trees show an optimal response for a certain signal strength, while stronger or weaker signals provoke a decline in the biological response.

In this respect, site conditions are highly important and site selection is imperative to minimize the number of environmental parameters affecting tree growth and, thus, isotopic fractionation. The Tibetan juniper and spruce trees investigated originate from one of the highest sites for tree growth in the world. In these regions temperature is known to be the dominant growth limiting factor. Thus, $\delta^{13}\text{C}$ values should in the first place record temperatures of the growing season from the corresponding years.

For calibration of the carbon isotope proxies with instrumental records the meteorological data set from Qamdo weather station (3241 m a.s.l) was used, as well as calculated regional means of surface temperatures [22] (see Tab. 1 and Fig. 1).

Unfortunately, the calibration of isotope values with recent meteorological data, causes a number of problems. Firstly, most meteorological stations on the Tibetan Plateau were established in the early 1950's and, therefore, only data for the last 40 years are available. Secondly, the weather station of Qamdo is situated in a valley more than 1000m below the site of the trees investigated. The large altitudinal gradients in this area are producing local circulation patterns which are most important for the trees and, therefore, the precipitation record measured at this station is not representative for the stand and must not be taken up for calibration. At least, annually resolved isotope measurements of spruce tree-ring series from the time period between 1950 and 1994 were compared with the corresponding surface temperature data series. According to the mechanisms of carbon isotope fractionation during photosynthetic uptake of atmospheric CO₂, the massive impact of increasing atmospheric CO₂ partial pressure in conjunction with decreasing $\delta^{13}\text{CO}_2$ values is producing a declining $\delta^{13}\text{C}$ trend and aggravates a reliable calibration. In order to overcome this problem year to year changes (first differences) of tree-ring $\delta^{13}\text{C}$ and temperature values were correlated.

Table I. Correlation coefficients between mean tree-ring $\delta^{13}\text{C}$ differences ($D\delta^{13}\text{C}_{\text{Spruce}}$) and temperature differences (DT_{Qa}) of various time intervals measured at Qamdo and mean surface temperature differences of the Tibetan Plateau (DT_{TP}) [22]. (*Significance level 5% ; ** Significance level 1% ; *** Significance level 0.1% ; Spring = March to May; Veg. period = May to September; Summer = June to August).

correlation r	$D\delta^{13}\text{C}_{\text{Spruce}}$ mean	DT_{TP} (Summer)
DT_{Qa} (annual)	0.36*	
DT_{Qa} (Veg. period)	0.59***	
DT_{Qa} (Summer)	0.67***	0.74***
DT_{Qa} (June)	0.40*	
DT_{Qa} (July)	0.45**	
DT_{Qa} (August)	0.50***	
DT_{TP} (Summer)	0.56***	

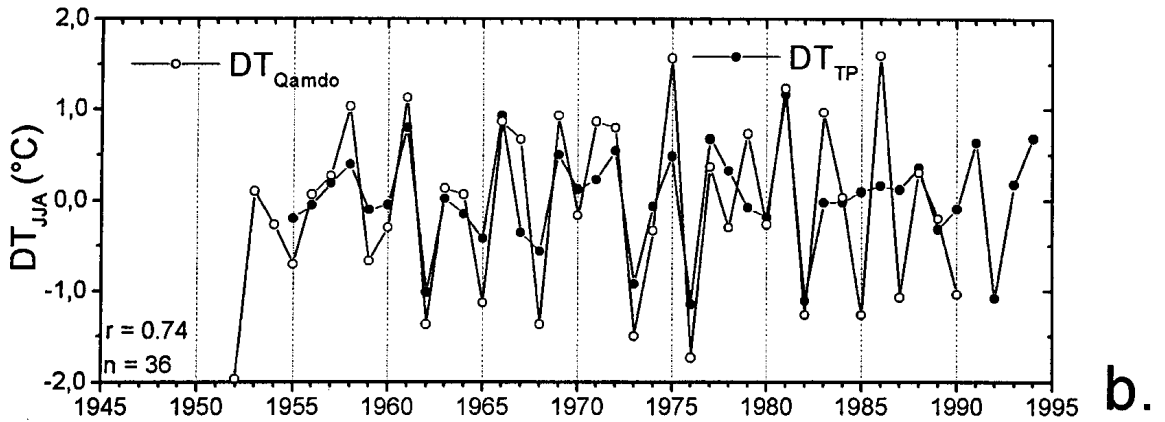
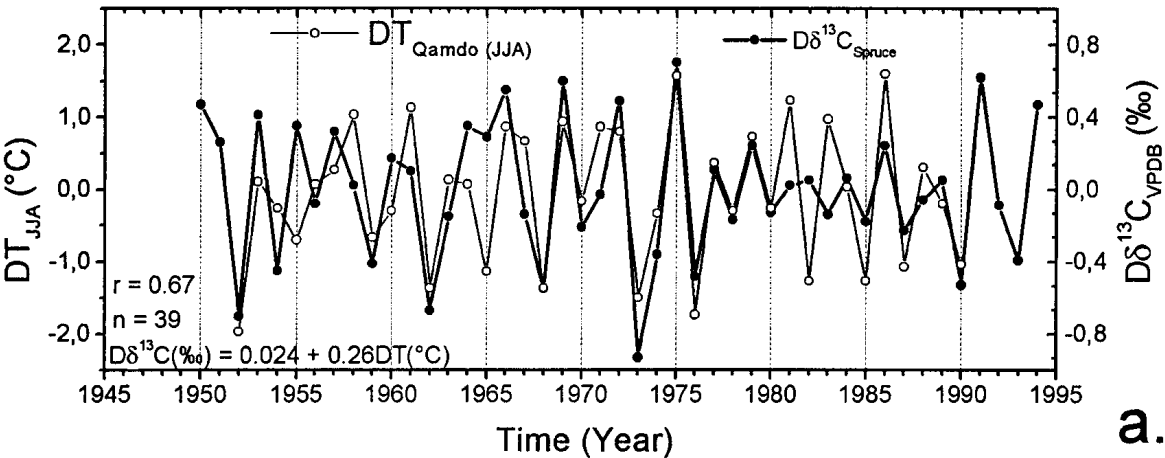


FIG. 1. Comparison of year to year $\delta^{13}\text{C}$ ($D\delta^{13}\text{C}$) changes as deduced from tree-ring series of spruce with the summer temperature changes (JJA) at Qamdo, covering the period from 1950 to 1994 (a.). Comparison of year to year summer temperature changes at Qamdo with the corresponding averaged summer temperature changes of the Tibetan Plateau (TP) [after 22] (b.).

Numerous investigations show that sites in which one climatic factor is the main growth limiting quantity exhibit a positive correlation with the corresponding carbon isotopes. Spruce $\delta^{13}\text{C}$ variations do likewise show a significant positive correlation with different monthly mean and seasonally averaged temperatures of the vegetation period as measured at Qamdo (Table I, Fig. 1). The highest correlations between $\delta^{13}\text{C}$ and temperature changes do exist with averaged monthly mean summer temperatures (June – August) and whole vegetation period temperatures (May – September).

Regional climate is frequently reconstructed as an average of several instrumental data series. The recent study mentioned above [22] uses monthly surface air temperature data from 78 meteorological stations on the Tibetan Plateau since their installation in the 1950s.

Although it is difficult to carry over site specific data to other locations, because the ecological settings are rarely the same, tree-ring carbon isotopes of the Qamdo site have a significant relationship with the regional summer temperature data set. Trees respond to climate conditions particular to their site and not to grid point data, but in the present case, differences of mean summer surface temperature at Qamdo are closely correlated with the regional means of the Tibetan Plateau (Table I).

At Qamdo, the temperature coefficient τ derived from least-square linear regression with year to year mean summer surface temperature is $0.26\text{‰}/^\circ\text{C}$. At this station summer temperature changes of 1.5 to 2.0°C from one year to another are frequently observed (Fig. 1). The summer temperature changes of the regional mean is somewhat lower which results in a higher τ of $0.38\text{‰}/^\circ\text{C}$ for the Tibetan Plateau.

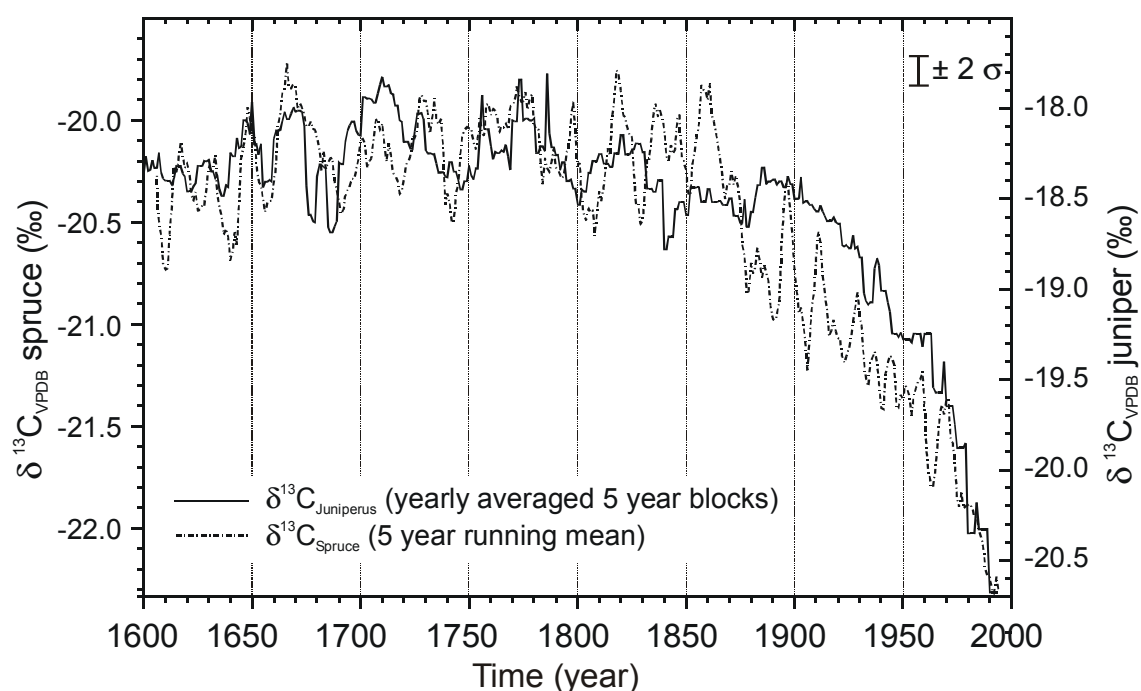


FIG. 2. The $\delta^{13}\text{C}$ -records of tree-ring cellulose from juniper and spruce chronologies covering the period from 1600 till 1994. Sites are located on the Tibetan Plateau near Qamdo at 4400 to 4600 m a.s.l. Juniper tree-rings show higher $\delta^{13}\text{C}$ -values than spruce tree-rings, but the trends of both curves are rather similar. The two species show a remarkable decline of more than 2.3‰ during the last 200 years. This decline documents the changes in atmospheric CO_2 induced by fossil fuel burning and deforestation.

Figure 1 indicates, that the sensitivity of tree-ring $\delta^{13}\text{C}$ to temperature variation is not constant. During 1977 to 1989 $\delta^{13}\text{C}$ changes are rather low. This indicates, that the trees are additionally influenced by other environmental quantities resulting in a compensation of the predominant temperature regime. The temperature calibration of spruce $\delta^{13}\text{C}$ should enable a better climatic interpretation of the long juniper $\delta^{13}\text{C}$ pentad record. This could only be possible if both species have similar isotope variations.

Figure 2 displays the smoothed $\delta^{13}\text{C}$ -records of tree-ring cellulose of both tree-species, juniper and spruce, from 1600 to 1994. Juniper tree-rings show rather high $\delta^{13}\text{C}$ -values varying around -18.5‰ , which is in line with observations of high mountain plants. On the other hand, spruce tree-ring $\delta^{13}\text{C}$ varies around -20.4‰ . However, the trends of both curves are rather similar, especially during the time period before 1800.

Positive excursions prevail 1645–1650, 1660–1670, 1700–1720 and 1760–1785, while more negative $\delta^{13}\text{C}$ values occur during 1675–1695, 1735–1755 and 1793–1815. From about 1800 onwards the isotope values decrease steadily, leading to the lowest isotope values of the whole record. From 1825 to 1990 the record decreases by almost 2.5‰ .

Generally, carbon isotope records of trees from other regions also show a decline, though the gradients are rather different ranging from 0.7 to 4‰ (given the period since 1800) [23]. However, these differences are by no means indicating a contradiction because the environmental conditions of various locations are generally not comparable. It has nicely been demonstrated that trees from a dry and a moist location situated close to each other exhibited a decrease of 0.7 and 1.4‰ , respectively, considering the period from 1935 to 1989 [24]. The tree-ring $\delta^{13}\text{C}$ decline documents the changes in atmospheric CO_2 induced by fossil fuel burning and deforestation [16]. According to the steadily increasing CO_2 concentration of the atmosphere, releasing ^{13}C depleted CO_2 , the $\delta^{13}\text{C}$ values of the last 150 years cannot be compared with the previous, pre-industrial data unless corrected accordingly. The corrections applied are based on measurements of atmospheric CO_2 concentration and its $\delta^{13}\text{CO}_2$ derived from ice cores [25] and direct measurements [26, 27, 28, 29]. A correction of the changing $\delta^{13}\text{CO}_2$ source value is commonly accepted, whereas the question to what extent changing $p\text{CO}_2$ influences plant isotopic discrimination is under discussion.

Figure 3 exhibits the possible shifts between a mere $\delta^{13}\text{CO}_2$ source correction and an extreme additional $p\text{CO}_2$ effect of $0.2\text{‰}/10\text{ppm}$. This coefficient is derived from linear regression of the difference between $\delta^{13}\text{C}$ of tree-rings and $\delta^{13}\text{C}_{\text{atm}}$ as a function of $p\text{CO}_2$ during 1740 to 1988 [30]. The dashed-dotted curve in-between the grey shaded area represents a possible $p\text{CO}_2$ correction of $0.073\text{‰}/10\text{ppm}$, an effect derived from greenhouse experiments with oak trees [31]. The question of correcting $\delta^{13}\text{C}$ in tree-ring records due to the atmospheric changes of $p\text{CO}_2$ and $\delta^{13}\text{C}_{\text{atm}}$ will be discussed in detail elsewhere [17].

The moderate corrections for the changing atmospheric CO_2 concentration with its $^{13}\text{CO}_2/^{12}\text{CO}_2$ shift would not lead to the warming trend, i.e. increasing $\delta^{13}\text{C}$ -values observed in several archives for the last decades of this century. A decrease of roughly 0.7‰ persists. Only the extreme correction leads to an increasing $\delta^{13}\text{C}$ trend.

If, as assumed, trees of this area and that altitude are mainly temperature limited, the declining $\delta^{13}\text{C}$ trend should indicate a slight decrease in the temperature regime of the site in question. However, it has to be emphasized that such a temperature decline does not comprise the whole year.

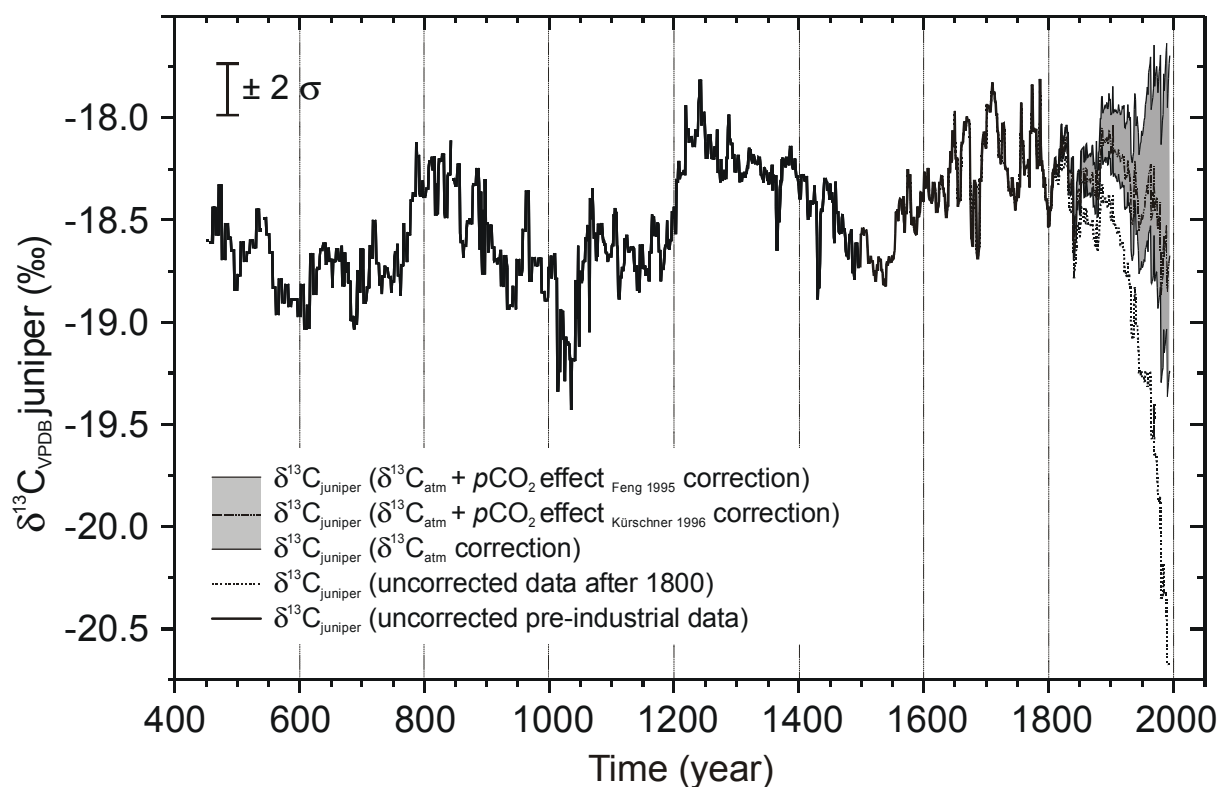


FIG. 3. The $\delta^{13}\text{C}$ time series of the *Qamdo juniper* trees from 450 to 1992. For the last 200 years different corrections have been applied to eliminate the effects of declining atmospheric $\delta^{13}\text{CO}_2$ and increasing $p\text{CO}_2$ on tree-ring carbon isotope ratios. A correction of the changing atmospheric $\delta^{13}\text{CO}_2$ source value is commonly accepted, whereas the question to what extent changing $p\text{CO}_2$ conditions influence plant isotopic discrimination is still under discussion. The grey shaded area marks the possible shifts between a mere $\delta^{13}\text{CO}_2$ source correction and an additional $p\text{CO}_2$ effect of $0.2\text{‰}/10\text{ppm}$ [30]. The dashed-dotted curve in between the grey shaded area represents a $p\text{CO}_2$ correction of $0.073\text{‰}/10\text{ppm}$, as deduced from greenhouse experiments with oak trees [31].

It is, thus, tacitly assumed that the signal of the isotope values is primarily expressing the vegetation period, i.e. the summer months. The Tibetan Plateau mean temperature record reveals a large linearly increasing temperature trends of $\sim 0.32^\circ\text{C}$ per decade for winter, and a small trend of $\sim 0.09^\circ\text{C}$ per decade for summer during 1955 to 1996 [22]. This does, however, not contradict the finding of slightly decreasing summer temperatures as inferred from tree-rings at Qamdo. The corresponding summer temperature observed at the nearest meteorological station shows a slight linear decrease if the whole record from 1951 to 1990 is considered.

On the other hand, the $\delta^{18}\text{O}$ records from three Plateau ice cores reveal increasing isotopic enrichment (e.g. warming) for the 20th century and the temperatures inferred from these Himalayan ice cores are the warmest of the millennium [11, 12]. The recent warming is most pronounced at the Dasuopu glacier ($28^\circ 23'\text{N}$, $85^\circ 43'\text{E}$), the highest elevation ice core site [11, 12] and nearest to the Qamdo tree site. Presumably the oxygen isotope record from tree-rings will help to improve the interpretation because different relationships $\delta^{13}\text{C}$ and $\delta^{18}\text{O}$ indicate different environmental impacts affecting the trees.

The whole Tibetan isotope record from juniper trees as given in figure 3 is an extension to the already published record [32], and currently covers a period of almost 1600 years. Note, however, that the averaged isotope curve does not represent an equally weighted sequence

over the whole record. The earliest phase (450 to 611) is currently represented by one tree and only from 900 onwards three or more trees were available for analysis. The period from 1370 to 1670 is even based on seven or eight trees.

As indicated earlier, it is difficult to carry over site specific correlations to other locations, because the ecological settings are rarely the same. The southerly exposed juniper trees encountered at the sites of investigation are sometimes covered with epiphytic beard lichens (*Lethariella zahlbruckneri*) which indicate more humid environmental conditions [33] as compared to the easterly exposed spruce trees. In this respect it has to be mentioned that dry sites do normally show a higher correlation of $\delta^{13}\text{C}$ with precipitation as compared to humid sites [34] which makes it difficult to carry over the temperature coefficient τ of 0.26‰/°C derived from spruce to the relationship of juniper $\delta^{13}\text{C}$ with temperature.

Indeed, temperature coefficients determined at various places show a wide variety of values [35]. However, if a mean value τ is adopted, similar to values $\sim 0.33\text{‰}/^\circ\text{C}$ [36, 37, 38], several periods (780–860; 1225–1380; 1640–1670; 1700–1715; 1770–1780; 1810–1830) can be given in which temperatures may have been by at least 0.75°C higher than the average of –18.45‰ as deduced for the period from 611 to 1800. The most prominent deviations, i.e. positive temperature excursions are found for the periods from 788 to 850 and from 1204 to 1360 respectively. Similarly a number of negative temperature excursions can be given, the most prominent extending from 1012 to 1049 and 1475 to 1554. Extreme $\delta^{13}\text{C}$ maxima are observed at about 800, 1250 and 1700 to 1715, while two strong minima are given at 1040 and 1550, respectively. It is interesting to note that the shift from a minimum to the subsequent maximum is generally proceeding faster than the corresponding decline from high isotope levels to low levels. The periods of transition from cold to warm phases appear to have been always rapid, while the transitional periods from warm to cold seem to have been sluggish.

In conclusion, a number of different climatic phases can be established which have their analogues in Europe and North America. A short warm phase between 1200 and 1300 appears to correspond to the 'Medieval Warm Period' and a longer cool phase from about 1450 to 1600 appears to correspond to the 'Little Ice Age' with a short recurring episode around 1850. The current results suggest that the observed events may have occurred over the entire Northern Hemisphere, though they do not seem to have been contemporaneous with Europe and North America.

ACKNOWLEDGEMENT

The authors wish to thank Prof. Dr. B. Frenzel, University of Hohenheim for initiating these tree-ring stable isotope investigations. We also acknowledge Dr. Xiadong Liu for conceding his calculated climate data of the Tibetan Plateau.

REFERENCES

- [1] MURAKAMI, T., Effects of the Tibetan Plateau. (CHANG, G.P., KRISHNAMURTI, T.N., Eds.), Monsoon Meteorology. Oxford Monographs on Geology and Geophysics 7 (1987) 235-270
- [2] LIN Z., WU, X., Some features of climatic fluctuation over the Qinghai-Xizang plateau. (YE D., FU, C., CHAO J., YOSHINO, M., Eds.), The climate of China and global climate. China Ocean Press, Beijing (1984) 116-123.

- [3] WU, X., Dendroclimatic studies in China. (BRADLEY, R. S. & JONES, P. D. Eds.), Climate since A.D. 1500. Routledge, London and New York (1992) 432-445.
- [4] CHU, K.-C., A preliminary study on the climatic fluctuations during the last 5,000 years in China. *Scientia Sinica XIV* **2** (1973) 226-256.
- [5] WANG, R., WANG, S., Reconstruction of winter temperature in China for the last 500 years. *Acta Meteorologica Sinica* **33** (1989) 279-289.
- [6] ZHANG, J., CROWLEY, T.J., Historical climate records in China and reconstruction of past climates. *J. Climate* **2** (1989) 833-849.
- [7] WANG, S., Reconstruction of palaeo-temperature series in China from the 1380s to the 1980s. *Würzburger Geogr. Arb.* **80** (1991) 1-19.
- [8] WANG, R., WANG, S., FRAEDRICH, K. An approach to reconstruction of temperature on a seasonal basis using historical documents from China. *Int. J. Climatology* **11** (1991) 1-12.
- [9] ZHANG, D., Historical records of climate change in China. *Quat. Sci. Rev.* **10** (1991) 551-554.
- [10] ZHANG, D., Paleoclimate and environmental records available from Chinese historical documents. (MIKAMI, T., MATSUMOTO, E., OHTA, S., SWEDA, T. Eds.), Paleoclimate and Environmental Variability in Austral-Asian Transect during the Past 2000 Years. Proc. Nagoya IGBP-PAGES/PEP-II Symposium (1996) 20-26.
- [11] THOMPSON, L.G., YAO, T., DAVIS, M.E., HENDERSON, K.A., MOSLEY-THOMPSON, E., LIN, P.-N., Beer, J., Synal, H.-A., Cole-Dai, J., Bolzan, J.F., Tropical climate instability: The last glacial cycle from a Qinhai-Tibetan ice core. *Science* **276** (1997) 1821-1825
- [12] THOMPSON, L.G., YAO, T., MOSLEY-THOMPSON, E., DAVIS, M.E., HENDERSON, K.A., LIN, P.-N., A high-resolution millennial record of the south Asian monsoon from Himalayan ice cores, *Science* **289** (2000) 1916-1919.
- [13] FARQUHAR, G.D., O'LEARY, M.H., BERRY, J.A., On the relationship between carbon isotope discrimination and the intercellular carbon dioxide concentration in leaves. *Austr. J. Plant Physiol.* **9** (1982) 121-137.
- [14] SCHLESER, G.H., BERNHARDT, K.-G., HURKA, H., Climatic adaptability of populations of *Diplotaxis eruroides* D.C. (Brassicaceae) from Sicily, based on leaf morphology, leaf anatomy and $\delta^{13}\text{C}$ studies, *Int. J. Biometeorol.* **33** (1989) 109-118.
- [15] KÖRNER, C., FARQUHAR, G.D., WONG, S.C., Carbon isotope discrimination by plants follows latitudinal and altitudinal trends, *Oecologia* **88** (1991) 30-40.
- [16] MOOK, W. G.; KOOPMANS, M.; CARTER, A. F. & KEELING, C. D. (1983) Seasonal, latitudinal and secular variations in the abundance and isotopic ratios of atmospheric carbon dioxide. 1. Results from land stations. *J. Geophys. Res.* **88** 10915-10933.
- [17] TREYDTE, K., HELLE, G., SCHLESER, G.H., On the question of correcting $\delta^{13}\text{C}$ in tree-ring records due to the atmospheric changes of $p\text{CO}_2$ and $\delta^{13}\text{C}_{\text{atm}}$, in Prep.
- [18] FRITTS, H.C., Tree-rings and climate, Academic Press, London (1976) 567pp.
- [19] BRÄUNING, A., Dendrochronology for the last 1400 years in Eastern Tibet. *GeoJournal* **34** (1994) 75-95.
- [20] SOHN, A.W., REIF, F., Natriumchlorit als Aufschlußmittel. *Der Papierfabrikant* **40** (1942) 1-7.
- [21] WIESBERG, L., Die ^{13}C Abnahme in Holz von Baumjahresringen, eine Untersuchung zur anthropogenen Beeinflussung des CO_2 Haushalts der Atmosphäre. PhD thesis, RWTH Aachen (1974) 121.
- [22] LIU, X., CHEN, B., Climatic warming in the Tibetan Plateau during recent decades, *Int. J. Climatol.* **20** (2000) 1729-1742.

- [23] FENG, X., Trends in intrinsic water-use efficiency of natural trees for the past 100-200 years: A response to atmospheric CO₂ concentration. *Geochim. Cosmochim. Acta* **63** 13/14 (1999) 1891-1903.
- [24] SAURER, M., SIEGENTHALER, U., SCHWEINGRUBER, F.H., The climate-carbon isotope relationship in tree rings and the significance of site conditions, *Tellus* **47B** (1995) 320-330.
- [25] FRIEDLI, H., LÖTSCHER, H., OESCHGER, H., SIEGENTHALER, U., STAUFFER, B., Ice core record of the ¹³C/¹²C ratio of atmospheric carbon dioxide in the past two centuries. *Nature* **124** (1986) 237-238.
- [26] KEELING, C.D. MOOK, W.G., TANS, P.P., Recent trends in the ¹³C/¹²C ratio of atmospheric carbon dioxide. *Nature* **217** (1979) 121-123.
- [27] KEELING, C.D., BACASTOW, R.B., TANS, P.P., Predicted shift in the ¹³C/¹²C ratio of atmospheric carbon dioxide. *Geophys. Res. Let.* **7** (1980) 505-508.
- [28] FRANCEY, R.J., ALLISON, C.E., ETHERIDGE, D.M., TRUDINGER, C.M., ENTING, I.G., LEUENBERGER, M.C., LANGENFELDS, R.L., MICHEL, E., STEELE, L.P., A 1000-year high precision record of δ¹³C in atmospheric CO₂. *Tellus* **51B** (1999) 170-193.
- [29] FRANCEY, R.J., ALLISON, C.E., In situ ¹³CO₂ from Cape Grim, Tasmania, Australia: 1982-1993. (TRENDS: A Compendium of Data on Global Change. CDIAC, Oak Ridge National Laboratory, U.S. Department of Energy, Oak Ridge, Tenn., U.S.A (1998).
- [30] FENG, X., EPSTEIN, S., Carbon isotopes of trees from arid environments and implications for reconstructing atmospheric CO₂ concentration, *Geochim. Cosmochim. Acta* **59** 12 (1995) 2599-2608.
- [31] KÜRSCHNER, W.M., Leaf Stomata as biosensors of palaeoatmospheric CO₂ levels. LPP Contribution Series 5 (1996) pp. 152
- [32] ZIMMERMANN, B., SCHLESER, G.H. AND BRÄUNING, A., Preliminary results of a Tibetan stable C-isotope chronology dating from 1200 to 1994, *Isotopes Environ. Health Stud.* **33** (1997) 157-165
- [33] OBERMAYER, W., Graz, pers. comm..
- [34] SAURER, M., BORELLA, S., SCHWEINGRUBER, F.H., SIEGWOLF, R., Stable carbon isotopes in tree-rings of beech: Climatic versus site-related influences. *Trees* **11** (1997) 291-297.
- [35] SCHLESER, G. H., HELLE, G., LÜCKE, A., VOS, H., Isotope signals as climate proxies: the role of transfer functions in the study of terrestrial archives, *Quat. Sci. Rev.* **18** (1999) 927-943.
- [36] TANS, P. P., MOOK, W.G., Past atmospheric CO₂ levels and ¹³C/¹²C levels in tree-rings. *Tellus* **32** (1980) 268-283.
- [37] STUIVER, M., BRAZIUNAS, T.F., Tree cellulose ¹³C/¹²C isotope ratios and climate change. *Nature* **327** (1987) 58-60.
- [38] LIPP, J., TRIMBORN, P., FRITZ, P., MOSER, H., BECKER, B., FRENZEL, B., Stable isotopes in tree ring cellulose and climatic change, *Tellus* **43B** (1991) 322-330.

STUDY OF RECENT CHANGES IN SEDIMENTATION REGIME INSIDE CIENFUEGOS BAY, CUBA USING ^{210}Pb AND ^{137}Cs AS TRACERS

C. ALONSO-HERNANDEZ*

Centro de Estudios Ambientales de Cienfuegos, Cienfuegos, Cuba

R. DELFANTI

Centro Ricerche Ambiente Marino ENEA,
La Spezia, Italy

M. DIAZ-ASENCIO

Centro de Estudios Ambientales de Cienfuegos, Cienfuegos, Cuba

C. PAPUCCI

Centro Ricerche Ambiente Marino ENEA,
La Spezia, Italy

A. MUNOZ-CARAVACA

Centro de Estudios Ambientales de Cienfuegos, Cienfuegos, Cuba

Abstract. Sedimentation dynamics in the Cienfuegos Bay was investigated based on profiles and inventories of $^{210}\text{Pb}_{\text{ex}}$ and ^{137}Cs in cores collected at two sites. The age of sediment layers was determined using the CRS model. Both cores show changes in sedimentation regime in the last 40 years. Since 1960-1965 sediment accumulation rates have doubled in both cells of the bay, from 0.2 to 0.4 g.cm⁻².y⁻¹. This change was probably one of the factors that influenced the important environmental modifications observed in the area.

1. INTRODUCTION

Cienfuegos Bay is a semiclosed bay with a surface area of 90 km² and an average depth of 14 m, connected to the Caribbean Sea by a narrow channel about 3 km long (Fig. 1). The bay is divided in two well-defined hydrographic cells, due to the presence of a submerged ridge about 1 m below the water surface. The northern cell receives most of the anthropic impact from the outfall of Cienfuegos City, industrial pole in the country, and the fluvial supply of Damuji and Salado rivers, draining agricultural areas. The southern cell receives a lower anthropic impact from the Caonao and Arimao river inputs. Part of this southern cell is a natural protected park, which represents a niche of migratory birds and marine species in conservation status.

The bay represents the most important natural resource in the province, due to fishing activities, maritime transport, tourism industry, and natural parks. In the last three decades, deleterious ecological signes in the area have been observed. Declining of biodiversity in the ecosystem, benthonic communities' movement, reduction of size and capture levels of commercial marine species, erosion of coastline, could be associated with changes of the sedimentation regime in the bay.

The natural radionuclide ^{210}Pb and the anthropogenic ^{137}Cs have been widely used as tools studies of sedimentation regime on a time scale less than 100 years [1,2,3].

*Email: carlos@ceac.perla.inf.cu ; Fax: +53 43 28912 .

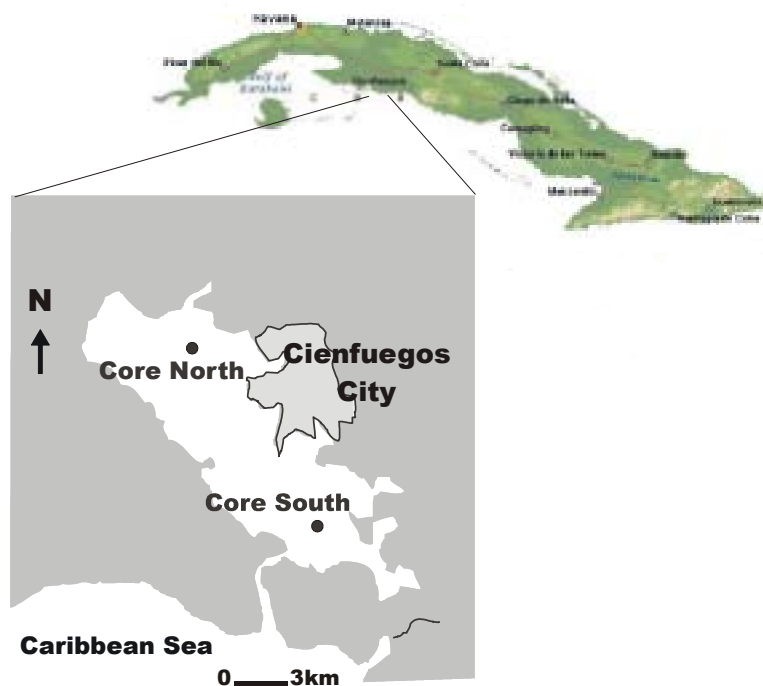


FIG. 1. Location of Cienfuegos Bay and the sampling sites.

In the present study, $^{210}\text{Pb}_{\text{ex}}$ and ^{137}Cs dating techniques were employed to estimate the recent sedimentation rates in the Cienfuegos Bay.

2. METHODS

Two sediment cores, (South and North, Fig. 1) have been collected in 1999 using a gravity corer. The core South was collected at a water depth of 19 m, and the core North at a water depth of 9 m. The length of the cores was 0.93 m. The cores were extruded and sliced immediately in 1.5 cm intervals. Aliquots of 5g of each core sections were used for complementary analyses like water content, porosity, calcium carbonate, granulometric and mineralogic compositions. The remaining parts were dried at 60 °C prior to radiometric assay.

Subsamples of dried sediment from each section were sent to the *Centro Ricerche Ambiente Marino, ENEA*, Italy, where they were analysed for ^{210}Pb [4], ^{226}Ra , and ^{137}Cs contents, by gamma spectrometry using low background intrinsic germanium coaxial detector coupled with multichannel analyser. The samples were placed in sealed containers and left for three weeks before counting to ensure the stabilishment of $^{222}\text{Rn}/^{226}\text{Ra}$ equilibrium. ^{210}Pb was determined via its gamma emissions at 46.5 keV, and ^{226}Ra by the 295 keV, 352 keV and 609 keV gamma rays emitted by its daughters ^{214}Pb and ^{214}Bi . ^{137}Cs was measured by its emissions at 662 keV. Efficiency calibration was performed using a Standard U-Ore (CANMET) and QCY44 Certificated Solution (Amersham). NBS and IAEA Reference Material were used to check the accuracy of the results. The reported uncertainty in the measured activity was calculated from the random counting error at the one standard deviation level.

Of the two simple models that can be used for calculating ^{210}Pb dates, CIC (Constant Initial Concentration) and the CRS (Constant Rate Supply), we have selected the second one, which is more accurate, when the ^{210}Pb vertical profile is irregular, as in our case [5].

^{210}Pb inventories were calculated by integrating from the surface to the deepest detectable activity. Concentrations in missing intervals were linearly interpolated from adjacent measured values.

3. RESULTS AND DISCUSSION

In Table I and II the concentration of unsupported ^{210}Pb and ^{137}Cs for the core South and core North are presented, respectively.

The complementary analyses indicate that there is no evidence of significant variations in the characteristics of the fluvial supply. The vertical distributions show homogeneous grain-size and mineralogic composition.

Figure 2 shows the vertical profile of $^{210}\text{Pb}_{\text{ex}}$ and ^{137}Cs in core South.

$^{210}\text{Pb}_{\text{ex}}$ profile is irregular with non-monotonic variations in activity with depth. These fluctuations indicate that the activity of the sediment reaching the seabed has varied with time. This core shows two different trends: below about 30 cm depth the profile is quite regular, with ^{210}Pb activity declining monotonically. Above 30 cm strong irregularities are observed. In this case, the CRS model is recommended for calculating ^{210}Pb dates [5,6]. The CRS model indicated two layers with different sediment accumulation rates. The deeper part of the core is characterised by a sediment accumulation rate of $0.26 \text{ g cm}^{-2} \text{ y}^{-1}$, while, around 30 cm depth and towards the surface, the rate increases to $0.42 \text{ g cm}^{-2} \text{ y}^{-1}$.

The vertical profile of ^{137}Cs shows maximum values around 28 cm, corresponding to a CRS date 1969 and to the discontinuity of the ^{210}Pb profile.

The major irregularities observed in the layers 10 - 15 cm and 22 - 27 cm might be related to extreme meteorological events in the area: intense rainfall in June 1988 (1000 mm in 7 days), that enhanced particle supply from the rivers, and the increased frequency of hurricanes in 1963-1966, that might have led to intense sediment re-suspension. Figure 3 shows the vertical profile of $^{210}\text{Pb}_{\text{ex}}$ and ^{137}Cs in core North.

As for core South, there is a discontinuity in the ^{210}Pb vertical profile at a depth of about 40 cm. Also in this case the CRS model indicated two layers with different sediment accumulation rates: $0.20 \text{ g cm}^{-2} \text{ y}^{-1}$ in the deep layer (up to the late fifties) and $0.46 \text{ g cm}^{-2} \text{ y}^{-1}$ in the upper layer. In this case the vertical profile of ^{137}Cs shows a smeared peak corresponding to CRS dates between 1945-1965.

The irregularities in the radionuclide profiles in the upper layer and the changes in sedimentation regime in this area may be related to a combination of anthropic factors and the

above mentioned natural events. In fact, in the late fifties, the catchment area of the rivers flowing into this part of the bay have been interested by intense de-forestation for agricultural development.

An increase in sedimentation rates is visible in the two cores, documenting changes in the sedimentation regime in the last four decade in the whole bay.

Table I. Cumulative sediment mass, water content (%), concentrations of $^{210}\text{Pb}_{\text{ex}}$ and ^{137}Cs in sediment core South.

Depth interval (cm)	Cumulative Sediment mass (g.cm ⁻²)	H ₂ O (%)	$^{210}\text{Pb}_{\text{ex}}$ (Bq.kg ⁻¹)	^{137}Cs (Bq.kg ⁻¹)
0 – 1.5	0.16	79	99 ± 6.1	
1.5 - 3	0.49	76	97 ± 9.0	
3 – 4.5	0.87	74	95 ± 6.2	9.9 ± 0.5
4.5 - 6	1.28	73	92 ± 7.1	9.9 ± 0.5
6 – 7.5	1.81	70	101 ± 8.1	12.7 ± 0.6
7.5 - 9	2.21	69	89 ± 7.8	7.9 ± 0.4
9 – 10.5	2.74	68	67 ± 6.3	7.8 ± 0.4
10.5 - 12	3.28	65	68 ± 4.8	11.3 ± 0.6
12 – 12.5	3.87	64	67 ± 6.0	12.0 ± 0.6
12.5 - 15	4.5	62	68 ± 5.4	11.5 ± 0.6
15 – 16.5	5.18	59	70 ± 6.4	10.7 ± 0.5
16.5 - 18	5.87	59	63 ± 4.8	11.9 ± 0.6
18 – 19.5	6.58	59	61 ± 3.8	10.7 ± 0.5
19.5 - 21	7.28	58	59 ± 5.7	13.6 ± 0.7
21 - 22.5	7.99	59	74 ± 5.1	12.1 ± 0.6
23.5 - 24.5	8.81	61	65 ± 3.9	10.7 ± 0.5
24.5 - 25.5	9.25	59	71 ± 4.9	11.5 ± 0.6
25.5 - 26.5	9.7	57	66 ± 5.4	14.0 ± 0.7
26.5 - 27.5	10.13	58	64 ± 5.1	12.3 ± 0.6
27.5 - 28.5	10.59	58	61 ± 3.5	11.4 ± 0.6
29.5 - 30.5	11.48	58	56 ± 3.4	9.2 ± 0.5
31.5 - 32.5	12.4	56	54 ± 4.1	9.4 ± 0.5
32.5 - 33.5	12.89	55		8.6 ± 0.4
34.5 - 36.5	14.02	57		7.3 ± 0.4
36.5 - 37.5	14.52	55		6.7 ± 0.3
47 - 48.5	20.55	59	23 ± 2.3	2.2 ± 0.2
53 - 54.5	24.22	58	15 ± 1.6	
56 - 57.3	25.93	64	14 ± 1.2	
57.3 - 59	26.78	60		0.3 ± 0.0
62 - 63.5	29.37	58	8 ± 0.8	0.1 ± 0.0
65 - 66.5	31.11	58		NM
66.5 - 68	31.99	59	7 ± 0.7	NM
72.5 - 74	35.42	60	6 ± 0.5	NM
81.5 - 83	40.81	58	3 ± 0.6	NM

Table II. Cumulative sediment mass, water content (%), concentrations of $^{210}\text{Pb}_{\text{ex}}$ and ^{137}Cs in sediment core North.

Depth (cm)	Cumulative Sediment mass ($\text{g}\cdot\text{cm}^{-2}$)	H ₂ O (%)	$^{210}\text{Pb}_{\text{ex}}$ ($\text{Bq}\cdot\text{kg}^{-1}$)	^{137}Cs ($\text{Bq}\cdot\text{kg}^{-1}$)
0 - 1	0.25	86	30 ± 4.0	3.7 ± 0.5
4 - 5.5	0.87	79	33 ± 4.0	4 ± 0.5
5.5 - 7	1.59	78	38 ± 5.0	3.4 ± 0.5
10 - 11.5	3.02	78	39 ± 7.0	3 ± 0.5
13 - 14.5	4.18	76	37 ± 4.5	3.9 ± 0.6
14.5 - 16	4.92	78	36 ± 4.3	5.8 ± 0.7
16 - 17.5	5.55	73	36 ± 4.3	6.6 ± 0.8
17.5 - 19	6.5	73	25 ± 3.0	4.4 ± 0.7
19 - 20.5	7.22	72		4.1 ± 0.6
20.5 - 22	7.87	73	29 ± 3.5	3 ± 0.5
22 - 23.5	8.61	73		1.6 ± 0.3
23.5 - 25	9.23	75	22 ± 2.7	1.1 ± 0.1
28 - 29.5	11.14	76	22 ± 2.7	0.5 ± 0.1
29.5 - 31	11.71	75	22 ± 2.6	2.1 ± 0.2
32.4 - 34	12.89	73	22 ± 2.6	7.3 ± 0.9
34 - 35.5	13.78	74	27 ± 3.3	9.4 ± 1.1
37 - 38.5	15.24	76		14.9 ± 0.9
41.5 - 42.5	17.03	77	33 ± 4.0	9.4 ± 1.1
45.5 - 47	19.1	73	9.7 ± 1.2	15.7 ± 1.9
50 - 51.5	21.47	76	13 ± 1.5	15.3 ± 1.8
54.5 - 56	23.79	74	8.6 ± 1.0	4.7 ± 0.6
57.5 - 59	25.3	73	7.8 ± 1.0	3.1 ± 0.4
65 - 66.5	28.86	76	2.4 ± 0.3	0.6 ± 0.1
72 - 73.5	31.58	75	0.82 ± 0.1	0.5 ± 0.1
85.5 - 87.5	37.78	76	0.38 ± 0.1	NM

4. CONCLUSIONS

A clear signal of change in sedimentation regime in the last 40 years has been identified from the vertical radionuclide profiles in the two sediments cores.

Although the two cells of the bay are separated by a shoal and receive different particles inputs from different sources, the change in sediment accumulation rates are strongly correlated, and correspond to the same date (1960 - 1965).

The recent sediment accumulation rates ($0.40 - 0.45 \text{ g}\cdot\text{cm}^{-2}\cdot\text{y}^{-1}$) is almost double that estimated for the period before 1960 (0.26 to $0.42 \text{ g}\cdot\text{cm}^{-2}\cdot\text{y}^{-1}$). These changes in the sedimentation processes are probably connected with concomitant changes in the land uses.

The increases in sediment accumulation rates might be one of the factors influencing the observed important changes in biodiversity of the bay and the spatial migration of benthic communities.

This work constitutes the first example of application in Cuba of the techniques that uses $^{210}\text{Pb}_{\text{ex}}$ and ^{137}Cs as “*clocks for dating*” the sedimentation processes.

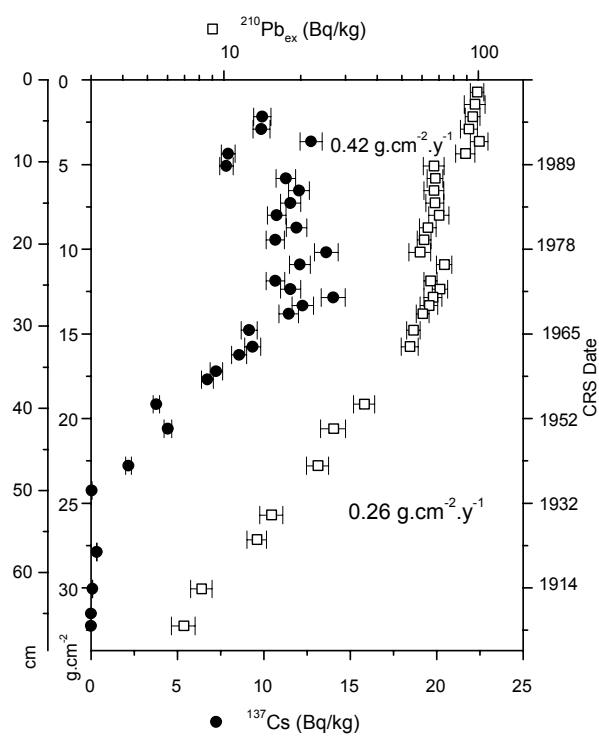


FIG. 2. Profiles of $^{210}\text{Pb}_{\text{ex}}$ and ^{137}Cs in core South.

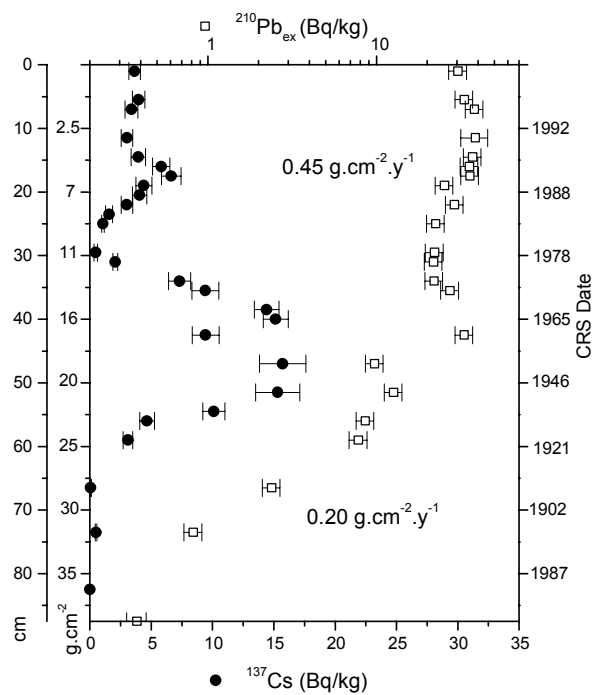


FIG. 3. Profiles of $^{210}\text{Pb}_{\text{ex}}$ and ^{137}Cs in core North.

ACKNOWLEDGEMENTS

The major funding for this research comes from Cuban Nuclear Energy Agency. One of the authors (Alonso-Hernandez C.M.) undertook this work with support of the “ICTP Programme for Training and Research in Italian Laboratories, Trieste, Italy”.

REFERENCES

- [1] GOLDBERG, E.D., Geochronology with ^{210}Pb In Radioactive Dating. IAEA (1963) 121-131.
- [2] KRISHNASWAMI, S., LAL, D., MARTIN, J.M., MEYBECK, M., Geochronology of lake sediments. *Earth Plan Sci. Lett.* **11** (1971) 407-414.
- [3] ROBBINS, J.A., EDGINGTON, D.N., Determination of recent sedimentation rates in lake Michigan using ^{210}Pb and ^{137}Cs . *Geochim. Cosmochim. Acta.* **39** (1975) 285-304.
- [4] CUTSHALL, N.H., LARSEN, I.L., OLSON, C.R., Direct analysis of ^{210}Pb in sediment sample; self-absorption correction. *Nuclear Instruments and Methods* **206** (1983) 309-312.
- [5] APPLEBY, P.G., OLDFIELD, F., The calculation of lead-210 dates assuming a constant rate of supply of unsupported ^{210}Pb to the sediment. *Catena* **5** (1978) 1-8.
- [6] APPLEBY, P.G., FLOWER, R.J., MACKAY, A.W., ROSE, N.L., Paleolimnological assessment of recent environmental change in Lake Baikal: sediment chronology. *Journal of Paleolimnology* **20** (1998) 119-133.

NEW INSIGHTS IN POSTGLACIAL PALEOCLIMATIC AND PALEOENVIRONMENTAL CHANGES IN CENTRAL EUROPE DERIVED FROM ISOTOPE ANALYSES OF LAMINATED LAKE SEDIMENTS AND PEAT DEPOSITS

B. MAYER

University of Calgary, Departments of Physics & Astronomy and Geology & Geophysics,
Calgary, Alberta, Canada

L. SCHWARK, K.G. ZINK

University of Cologne, Geological Institute,
Cologne, Germany

W.M. BUHAY

Department of Geography, University of Winnipeg,
Winnipeg, Manitoba, Canada

J. LECHTERBECK

University of Tübingen, Geological Institute, Tübingen, Germany

Abstract. Isotope ratio determinations in concert with geochemical and palynological analyses performed on material from German continental archives (lake sediments, peat cores) provided information about paleoclimatic and paleoenvironmental changes in Central Europe throughout the last 15,000 years. Oxygen isotope ratio variations of (i) bulk carbonates from lake sediments (Lake Steisslingen) and of (ii) cellulose extracted from peat cores suggest the following climatic trends: an early postglacial climate optimum in the Bølling; a distinct cooling phase during the Younger Dryas; an early Holocene warming period in the Preboreal; another warming phase in the Boreal leading into the mid-Holocene warm period; a gradual decrease of mean annual air temperatures since the mid-Holocene warm period. Evaluation of other isotopic proxy data in concert with geochemical and palynological information revealed that the above-described climatic variations in Central Europe triggered marked paleoenvironmental changes in the study region between the Bølling and the onset of the mid-Holocene warm period. Elevated organic carbon contents in lake sediments and increasing $\delta^{13}\text{C}$ values of organic carbon were typically associated with climatic warm phases and seem to indicate enhanced in-lake productivity. Pollen counts and biomarker data suggest a predominance of *Betula* during climatic warm phases and a predominance of *Pinus* during colder periods. The Mid Younger Dryas event was observable in pollen and biomarker data, but oxygen isotope ratios of bulk carbonates from Lake Steisslingen did not record temperature variations at that time. The data presented for the chronozones Bølling through Boreal provide evidence that the elucidation of paleoclimatic and paleoenvironmental variations on our continents can benefit greatly from a joint interpretation of isotope analyses, palynological evidence, and inorganic and organic geochemistry data derived from continental archives.

1. INTRODUCTION

Within the framework of a multidisciplinary research initiative funded by the German Science Foundation (DFG), continental archives including laminated lake sediments and peat deposits were sampled at numerous locations throughout the Federal Republic of Germany. Geochemical, palynological, and isotopic tools were combined to derive information about paleoclimatic and paleoenvironmental changes in Central Europe throughout the last 15,000 years. Here we report on results from the study of two laminated lake sediment records (Lake Steisslingen, Hämelsee) and two peat cores from the Weser-Ems region in northern Germany.

For all continental archives, the goal was to use the oxygen isotope ratios of (i) lake carbonates or (ii) peat cellulose to assess paleoclimatic changes by reconstructing the isotopic composition of paleo-precipitation and by assessing changes in the water balances of the study areas. Interpretation of other isotopic proxy data ($\delta^{13}\text{C}_{\text{carb}}$, $\delta^{13}\text{C}_{\text{org}}$) in concert with geochemical (e.g. total inorganic or organic carbon, biomarker) and palynological information were subsequently used to assess the extent to which paleoclimatic variations triggered paleoenvironmental changes in the study area.

2. MATERIALS

Sediment cores obtained from Lake Steisslingen (SW Germany) provided an almost continuous postglacial sedimentary record spanning from the Oldest Dryas to the Subatlantic period. A well-defined chronostratigraphy was established based on sediment type successions with characteristic organic matter and carbonate contents [1], pollen associations [2], volcanic ash layers such as the Laacher See Tephra (LST) and the Vasset Kilian Tephra (VKT) [3] and $^{14}\text{C}_{\text{AMS}}$ dating, as summarized in [4]. Laminated lake sediments from Hämelsee (Central Germany) were deposited between the end of the Younger Dryas and the Boreal and provided a high-resolution record for the early Holocene. Additionally, two peat cores obtained from raised bogs in the Weser-Ems region (NW Germany) were analyzed chemically and isotopically. $^{14}\text{C}_{\text{AMS}}$ dating revealed that the peat cores represented paleoclimatic and paleoenvironmental records for the second half of the Holocene (6,245 years BP to present).

3. METHODS

Sediments from Lake Steisslingen (SW Germany) were dried at a maximum temperature of 40°C prior to chemical and isotopic analyses. Pollen counts, contents and isotopic compositions of total organic carbon and bulk carbonate were determined by standard techniques. Lipids were extracted by ultrasonication with dichloromethane/methanol 9:1 v/v and purified over SPE cartridge with aminopropyl-phase. N-alkane identification was achieved by GC separation via known retention times and mass spectrometric identification.

Lake sediments from Hämelsee were characterized by a high siderite content. CO_2 for carbon and oxygen isotope ratio measurements was obtained by reacting siderites from 84 laminated sediment layers with 100% phosphoric acid at 90°C for several hours in a Gilson-type sampler and isotope measurements were subsequently performed by continuous flow isotope ratio mass spectrometry (CF-IRMS).

Peat cores from the Weser-Ems region were subdivided at different intervals. A core from site ‘Lengener Moor’ was sampled at 1 cm intervals, while peat representing 20 cm intervals was homogenized for the ‘Marcardsmoor’ core (code B211). After the samples were air-dried, cellulose was extracted by standard techniques [5]. $\delta^{18}\text{O}$ values of the peat cellulose were determined by pyrolysis CF-IRMS using a Finnigan MAT TC/EA reactor coupled to a delta plus XL via a Conflow II interface.

The obtained isotopic compositions are reported as δ values, representing deviation in per mil (‰) from the internationally accepted standards (PDB, V-SMOW), such that

$$\delta = [(R_{\text{sample}}/R_{\text{standard}})-1]*1000,$$

where R is the $^{13}\text{C}/^{12}\text{C}$ or $^{18}\text{O}/^{16}\text{O}$ ratio of sample and standard, respectively. Analytical uncertainties including extraction, gas preparation, and mass spectrometric measurements were $<\pm 0.2$ ‰ for $\delta^{13}\text{C}_{\text{organic}}$, $<\pm 0.15$ ‰ for $\delta^{13}\text{C}$ and $\delta^{18}\text{O}$ of bulk carbonates, and ± 0.4 ‰ for $\delta^{18}\text{O}_{\text{peat cellulose}}$.

4. RESULTS AND DISCUSSION

Figure 1 summarizes total organic (TOC) and total inorganic carbon (TIC) contents and isotope ratios of total organic carbon ($\delta^{13}\text{C}_{\text{organic}}$) and bulk carbonate ($\delta^{13}\text{C}_{\text{carb}}$, $\delta^{18}\text{O}_{\text{carb}}$). The $\delta^{18}\text{O}$ values of bulk carbonate varied between -8.1 and -1.9 ‰ throughout the observation period. During the Oldest Dryas and the Bølling, $\delta^{18}\text{O}_{\text{carbonate}}$ values around -4 ‰ were observed. Throughout the Allerød, the $\delta^{18}\text{O}_{\text{carbonate}}$ values decreased to approximately -6 ‰. In the Younger Dryas, a further decrease of 2 ‰ was found, resulting in $\delta^{18}\text{O}_{\text{carbonate}}$ values as low as -8.1 ‰. At the beginning of the Holocene, a sharp increase of the oxygen isotope ratios to values of up to -3.5 ‰ was observed. After a decrease of the $\delta^{18}\text{O}_{\text{carbonate}}$ values in the early Boreal (-5 ‰), a further sharp increase occurred at the beginning of the Atlantic, with $\delta^{18}\text{O}_{\text{carbonate}}$ values as high as -1.9 ‰. Variations of oxygen isotope ratios of bulk carbonate in Lake Steisslingen suggest an early climate optimum in the Bølling and clearly recorded the cooling event of the Younger Dryas. An early Holocene warming event in the Preboreal and a second warming phase in the Boreal leading into the mid-Holocene warm period are also documented.

Evaluation of other isotopic proxy data in concert with geochemical and palynological information revealed that the above described climatic variations in Central Europe triggered marked paleoenvironmental changes in the study area throughout the last 15,000 years. Figure 2 displays the pollen distribution and long-chain n-alkane content ratios for sediments from Lake Steisslingen for the time period between the Oldest Dryas and the Boreal chronozones.

During the early climatic optimum in the Bølling, a transition from tundra to open forest vegetation is documented by the onset of *Betula* pollen after previous dominance of *Artemisia*. Palynologically observed vegetational shifts are also documented by the compositions of plant wax-derived long chain n-alkanes (biomarkers). Whereas epicuticular wax from *Betula* species is dominated by the nC_{27} -alkane, most grasses and *Artemisia* show a clear preference for nC_{31} . The ratio $\text{nC}_{27}/(\text{nC}_{27}+\text{nC}_{29}+\text{nC}_{31})$, therefore, reflects wax alkane input from different plant groups/species. Evidently, the strong appearance of *Betula* during the Bølling is mirrored by an increasing $\text{nC}_{27}/(\text{nC}_{27}+\text{nC}_{29}+\text{nC}_{31})$ ratio (Fig. 2). High TOC and TIC contents in the lake sediments (Fig. 1) are possibly also a consequence of the moderate climate resulting in high in-lake productivity. The appearance of *Juniperus* pollen (Fig. 2) is another indicator of climatic amelioration. A decrease in the $\delta^{13}\text{C}$ values of organic matter from -26 ‰ to less than -32 ‰ in the sediments of Lake Steisslingen during the Bølling indicates that the change from tundra to open forest vegetation was possibly accompanied by an increase in lacustrine (pytoplanktonik) organic matter production.

Continuously decreasing $\delta^{18}\text{O}_{\text{carbonate}}$ values throughout the Allerød (Fig. 1) are believed to indicate decreasing mean annual temperatures. This climatic shift was accompanied by decreasing sedimentary TOC contents (Fig. 1), a steady decline in *Betula* pollen, and a simultaneous increase in *Pinus* pollen (Fig. 2). This trend was mirrored by a decreasing $\text{nC}_{27}/(\text{nC}_{27}+\text{nC}_{29}+\text{nC}_{31})$ ratio.

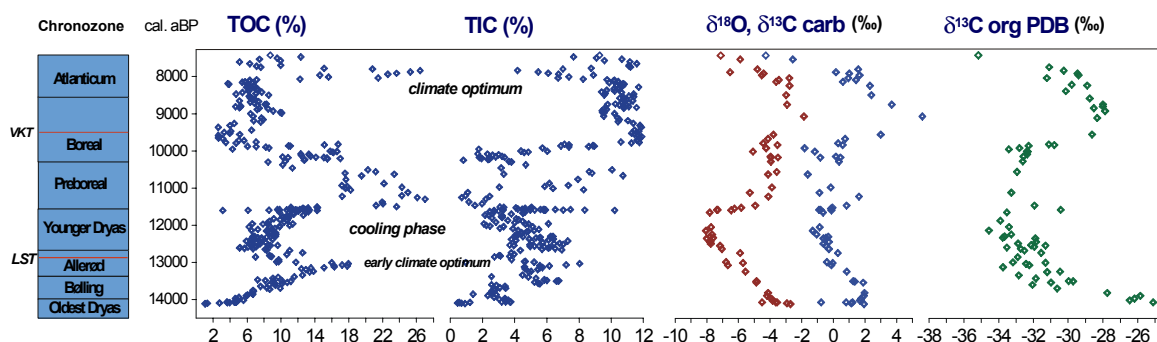


FIG. 1. Total organic carbon (TOC) and total inorganic carbon (TIC) contents, $\delta^{18}\text{O}$ and $\delta^{13}\text{C}$ values of bulk carbonate, and $\delta^{13}\text{C}$ values of bulk organic matter for sediments from Lake Steisslingen for the time period between the Oldest Dryas and Atlantikum chronozones.

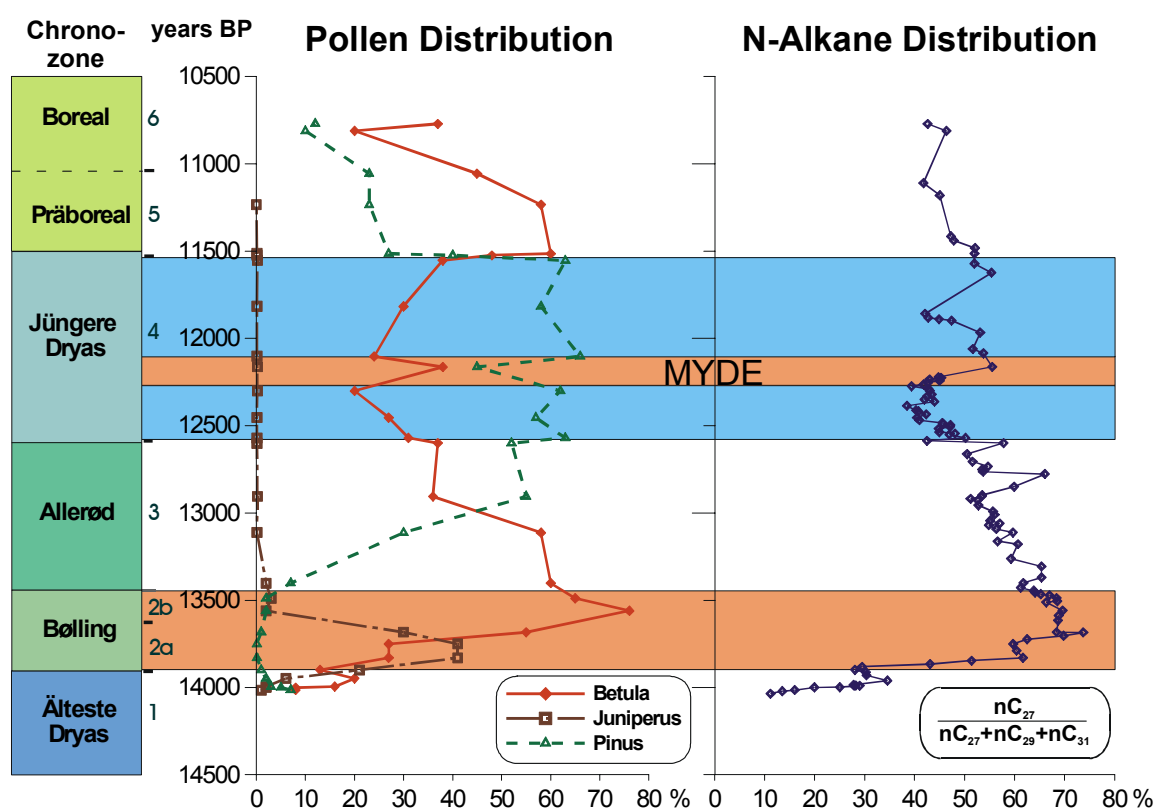


FIG. 2. Pollen distribution and the long-chain *n*-alkane ratio $n\text{C}_{27}/(n\text{C}_{27}+n\text{C}_{29}+n\text{C}_{31})$ for sediments from Lake Steisslingen for the time period between the Oldest Dryas and the Boreal chronozones.

The cooling event of the Younger Dryas coincides with a low abundance of *Betula* pollen and a high abundance of *Pinus* pollen, initially accompanied by a low $n\text{C}_{27}/(n\text{C}_{27}+n\text{C}_{29}+n\text{C}_{31})$ ratio (Fig. 2). A brief (<50 years) increase of *Betula* pollen and of the $n\text{C}_{27}/(n\text{C}_{27}+n\text{C}_{29}+n\text{C}_{31})$ ratio might indicate the Mid Younger Dryas Event (MYDE), although $\delta^{18}\text{O}_{\text{carbonate}}$ values do not reveal significant temperature variations during that period (Fig. 1).

Sediments deposited during a first Holocene climate optimum in the Preboreal were again characterized by a high abundance of *Betula* pollen and by sharply increasing $\delta^{13}\text{C}_{\text{org}}$ and

$\delta^{13}\text{C}_{\text{carb}}$ values (Fig. 1), suggesting enhanced in-lake productivity. This interpretation is supported by high total organic carbon contents in the sediments (Fig. 1). Similar observations made for early Holocene sediments from the Hämelsee indicate that the proposed Preboreal warming event had at least regional significance in Central Europe.

After a slight decrease in the isotope ratios of organic and carbonate carbon of Lake Steisslingen sediments in the early Boreal, both $\delta^{13}\text{C}_{\text{org}}$ and $\delta^{13}\text{C}_{\text{carb}}$ values increased again sharply in the later stages of the Boreal and at the beginning of the Atlanticum (Fig. 1). This event marks the beginning of the mid-Holocene warm period, which presumably resulted in increased productivity and eutrophication in Lake Steisslingen.

Since the oxygen isotope ratios of bulk carbonate from Lake Steisslingen did not constitute reliable paleoclimatic proxy data for the second half of the Holocene [4], $\delta^{18}\text{O}$ values of cellulose extracted from the two peat cores (Fig. 3) were interpreted as an alternate record. A gradual decrease in the $\delta^{18}\text{O}_{\text{cellulose}}$ values of 3 ‰ was apparent between the mid-Holocene climate optimum (+24 ‰) and present (+21 ‰). The high resolution oxygen isotope data for the ‘Lengener Moor’ core coincide with $\delta^{18}\text{O}_{\text{cellulose}}$ values of the low resolution ‘Marcardsmoor’ core (code B211) at several segments. In other intervals, a marked deviation of the $\delta^{18}\text{O}_{\text{cellulose}}$ values was observed, with the ‘Lengener Moor’ core displaying generally the higher values.

The organic components of peat, derived from a variety of plants occupying Weser-Ems wetland areas, provide an archive of the isotopic response of various plants to changes in atmospheric temperature and moisture. Oxygen isotope ratios of cellulose from plants supplying organic matter to these wetlands should dominantly respond to changes in the isotopic composition of atmospheric moisture, which is in turn related to atmospheric temperature and/or airmass circulation variations. However, differences in hydrologic settings for the wetland plants would likely manifest as variable isotopic responses to changes in atmospheric moisture content. Homogenization of peat cellulose over longer intervals (as for the ‘Marcardsmoor’ core) would reduce or even erase individual plant responses to atmospheric moisture content in favour of the more dominating precipitation isotopic composition signal. Subtracting 28 ‰ from the ‘Marcardsmoor’ core $\delta^{18}\text{O}_{\text{cellulose}}$ values to account for the biochemical fractionation between leaf chloroplast water and plant cellulose [6] results in an inferred reconstruction of $\delta^{18}\text{O}_{\text{precipitation}}$ since the mid-Holocene climate optimum (see Figure 3).

The observed trends in the $\delta^{18}\text{O}_{\text{cellulose}}$ values of both peat cores are interpreted as a gradual decrease in the oxygen isotope ratios of precipitation in the study region since the mid-Holocene. This is attributed to the combined effects of a decrease in the regional mean annual air temperature and a potential change in airmass dynamics. Intervals of coincidental $\delta^{18}\text{O}_{\text{cellulose}}$ values in both cores probably represent periods of higher atmospheric moisture that are separated by drier intervals. The latter are indicated by the markedly higher $\delta^{18}\text{O}_{\text{cellulose}}$ values of the ‘Lengener Moor’ core compared to those of the ‘Marcardsmoor core’ (code B211).

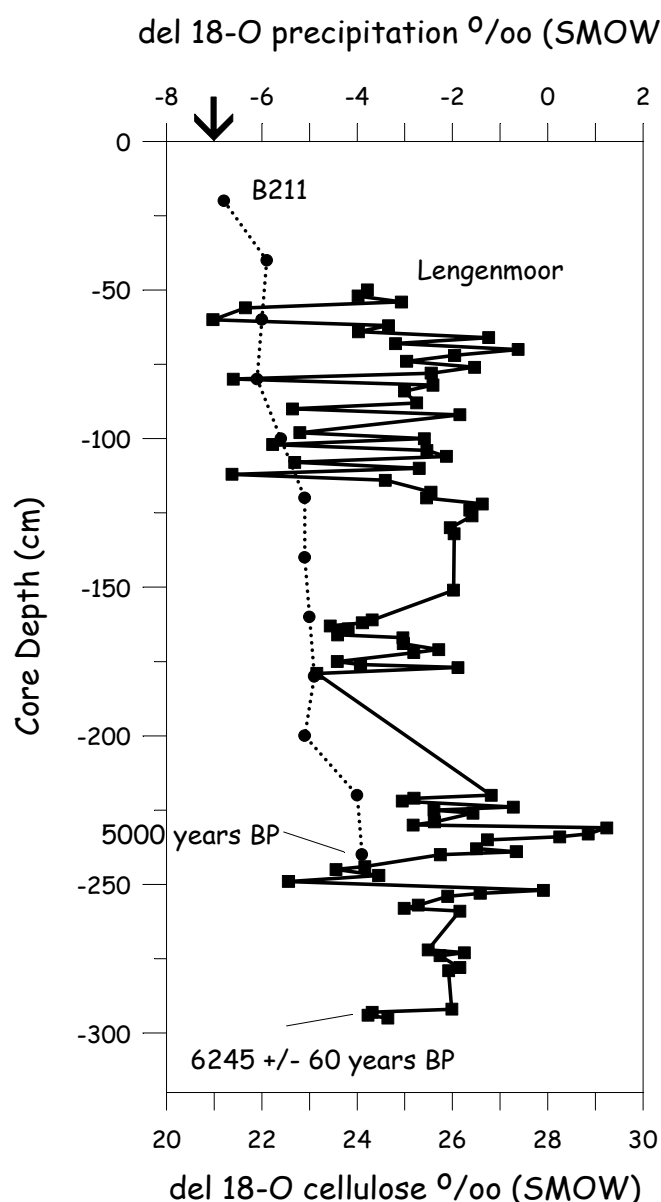


FIG. 3. $\delta^{18}\text{O}$ values for cellulose (lower x-axis) extracted from two peat cores from the 'Lengener Moor' and the 'Marcardsmoor' (code B211) in the Weser-Ems region in NW Germany and inferred $\delta^{18}\text{O}$ values of paleowater on the upper x-axis. The mean annual $\delta^{18}\text{O}$ value of modern precipitation in the study area is -7‰ (see arrow on upper x-axis).

5. CONCLUSION

In the study of sedimentary material from continental records, isotope data alone do not always provide the basis for unequivocal interpretations of paleoclimatic or paleoenvironmental change. The here presented data for the chronozones Bølling through Boreal provide evidence that the elucidation of paleoclimatic and paleoenvironmental variations on our continents can benefit greatly from a joint interpretation of isotope analyses, palynological evidence, and inorganic and organic geochemistry data. A similar data base for material from continental archives representing the second half of the Holocene is currently not available.

ACKNOWLEDGEMENTS

We are grateful to J. Schneider (University of Göttingen, Germany) for providing sedimentary material from Lake Steisslingen, to J. Merkt and A. Kleinmann (NLfB Hannover, Germany) for supplying sediments from the Hämelsee, and to K.-E. Behre and B. Petzelberger (Institute for Historical Coastal Research, Wilhelmshaven, Germany) for providing peat core samples from the Weser-Ems region. Financial support from the Deutsche Forschungsgemeinschaft (DFG grants MA 1815/2, SCHW 545/3, SCHW 554/8, LE 469/3) is also acknowledged. This contribution is a product of the DFG-Schwerpunktprogramm “Wandel der Geo-Biosphäre während der letzten 15,000 Jahre”.

REFERENCES

- [1] WOLF, U., Nähr- und Schadstoffbelastung kleiner Seen in Baden-Württemberg unter Berücksichtigung der Sedimentationsgeschichte. Cuvillier Verlag, Göttingen (1994).
- [2] LECHTERBECK, J., Vegetationsgeschichtliche Untersuchungen im Spätglazial und Holozän des Steisslinger Sees (Hegau, Südwestdeutschland). M.Sc. Thesis, University Tübingen, Germany (1996).
- [3] WOLF, U., SCHNEIDER, J., The Steisslinger See: changing climate and environmental conditions over the last 15,000 years in Southern Germany. – *Terra Nostra* **2** (1994) 299.
- [4] MAYER, B., SCHWARK, L., A 15,000 year stable isotope record from sediments of Lake Steisslingen, Southwest Germany. *Chem. Geol.* **161** (1999) 315-337.
- [5] GREEN, J. W., Wood cellulose. In: *Methods in Carbohydrate Chemistry*, Vol. III (ed. R. L. Whistler) Academic Press (1963) 9-20.
- [6] BUHAY, W. M, PENDALL, E., ANDERSON, W., EDWARDS, T. W. D. Terrestrial organic archives of the isotopic composition of paleo-precipitation (in prep.).

ADVANCES IN ISOTOPE AND ANALYTICAL TECHNIQUES I

(Session 6)

Chairpersons

C. TUNIZ
Australia

W. KUTSCHERA
Austria

ACCELERATOR MASS SPECTROMETRY: AN IMPORTANT TOOL FOR THE GEOCHRONOLOGY OF PAST CLIMATIC EVENTS*

(Abstract)

A.J.T. JULL, G.S. BURR, J.W. BECK, D.J. DONAHUE
NSF Arizona AMS Laboratory, University of Arizona,
Tucson, Arizona, United States of America

The development of a good chronology is very important to the understanding of past climatic changes and their relationship to other events. The correlation of distinct climatic features requires a precise chronology. More important also is the need to be able to correlate phenomena which are dated independently. For example, several authors have tried to cross-correlate climatic events observed in Greenland ice cores with climatic events identified in other terrestrial and marine records.

The improvement in the radiocarbon calibration curve over the last 25,000 yr and the ability to cross-correlate fluctuations in the ^{14}C curve directly with those in the ice-core records has improved the situation. This extension of the calibration curve uses tree rings to about 11,900 calibrated years and beyond, using corals and varved marine sediments [1]. Other records take us back to the limits of radiocarbon dating, using lake sediments and speleothems.

Another important problem in geochronology of past climate change is that events may be manifest differently in different parts of the world. For example, the uniformly "cold" younger Dryas in northern Europe can be correlated with oscillatory cold and wet behavior in other parts of the world. Chinese loess deposits show an oscillatory pattern during this time period, and the deserts of the American southwest show a drought followed by a period of increased precipitation. Hence, we must identify local and regional variations as well as global events.

Many megafauna became extinct close to the end of the late Pleistocene and the exact time of these extinctions, and whether they are caused by climate alone, or by other pressures such as the expansion of humans into previously unoccupied areas.

The exact timing of climatic change is also of importance in understanding the expansion of early man in the New World. The exact time of arrival of early man in the western hemisphere is usually thought to be close to the end of the last glacial, via a Bering land bridge. The rapid expansion of early man into central north America does not appear to have occurred until about 12,000 radiocarbon years BP. This is still consistent with the established idea of an ice barrier east of the Rockies which ceased to exist about this time. The Bering land bridge would have remained intact until ~10,000 radiocarbon years BP. We can understand this. However, recent evidence of some possible older occupations raises some questions about this model and there may also have been other modes of settlement.

During the Holocene, we also observe climatic fluctuations. An excellent example is the periodicity of forest fires in western North America. Meyer et al. [2] showed these can be correlated with periods of aridity. Other periodicities in the Holocene climatic record can often be related to solar fluctuations, the most obvious are the medieval warm period and the Maunder minimum, a time also associated with colder weather in Europe.

* Only an abstract is given here as the full paper was not available.

In this paper, we will highlight paleoclimate studies which can be well dated using AMS radiocarbon. These signals manifest themselves not only in the climate record but affect the extinction of megafauna and archeological events. There are also climatic effects in such varied reservoirs as Chinese loess deposits, forest fire recurrence, meteorite weathering rates and other phenomena will be discussed, as well as the more familiar ice cores and oceanic sediments. We will also focus on hiatuses in the radiocarbon calibration curve which appear to be related to some major climatic events.

REFERENCES

- [1] STUIVER, M. et al., Radiocarbon **40** (1998) 1041-1084.
- [2] MEYER, G. et al., Geol. Soc. Amer. Bull **101** (1995) 1211-1230.

CLIMATIC CHANGES AT HIGH ALTITUDES FROM C-14 DATING AT THE DISCOVERY SITE OF THE ICEMAN OETZI*

(Abstract)

W. KUTSCHERA, B. JETTMAR, R. GOLSER, A. PRILLER,
S. PUCHEGGER, P. STEIER, E.M. WILD
Vienna Environmental Research Accelerator (VERA),
Institute for Isotope Research and Nuclear Physics,
University of Vienna, Vienna, Austria

S. BORTENSCHLAGER, K. OEGGL
Institute for Botany, University of Innsbruck, Austria

W. ROM
AMS C-14 Dating Laboratory, Institute for Physics and Astronomy,
Aarhus University, Aarhus, Denmark

An extraordinary archaeological discovery was made in 1991 at a high-altitude mountain pass (Tisenjoch, 3120 m) of the Ötztal Alps near the Austrian-Italian Border. Two mountain hikers accidentally found the body of a man sticking half-way out from a shallow ice-filled depression. Unusual climatic conditions had partly freed the body from his icy grave, where he apparently had rested for thousands of years. Radiocarbon dating of bone and tissue of the Iceman "Ötzi" - as he was quickly nicknamed - revealed that he had lived some 5200 years ago [1,2]. This established Ötzi as the oldest well-preserved body from the Neolithic period. In addition to the body, a variety of equipment was found at the site, most of it dating to the same time period [3]. A collection of this and other measurements with emphasis on the environment of the Iceman can be found in [4]. The Iceman story with emphasis on ^{14}C dating is summarized in [5].

Recently, we dated a variety of materials found at the discovery site of the Iceman with ^{14}C AMS at the Vienna Environmental Research Accelerator (VERA) [6]. Among these materials there are plant remains which grow at high altitudes when the conditions are favorable. They thus serve as sensitive indicators of climatic conditions. The ^{14}C dates cover a time range from approximately 6000 to 4000 years ago, and give first hints on how the climatic conditions may have changed at the Iceman discovery site during this period of time. Combining this with materials found at the site which must have been brought there by animals and/or humans, the ^{14}C dates support the general hypothesis that in ancient times people in this region first populated high-altitude areas of the Alps above the timber line, since there they found natural pastures for domesticated animals. It is likely that these first settlers approached the Alps from the south, which also seems to be the direction from which the Iceman came to the Tisenjoch..

In this paper we will summarize our current ideas of the climatic conditions in the Ötztal Alps around the period of the Iceman. In order to get a more general picture also other climatic and environmental indicators (e.g. pollen analysis) of this region will be considered. At present, we are engaged in additional ^{14}C measurements of plant remains from the Ötzi site, which should help to establish a more detailed picture about temperature variations in this time period.

* Only an abstract is given here as the full paper was not available.

REFERENCES

- [1] BONANI, G., IVY, S., HAJDAS, I., NIKLAUS, T.R., SUTER, M., “AMS ^{14}C age determinations of tissue, bone and grass samples from the Ötztal Ice Man”, Radiocarbon 36/2 (1994) 247-50.
- [2] HEDGES, R.E.M., HOUSLEY, R.A., BRONK, C.R., VAN KLINKEN, G.J., “Radiocarbon dates from the Oxford AMS system: Archaeometry datelist 15”, Archaeometry 34/2 (1992) 337-357.
- [3] ROM, W., GOLSER, G., KUTSCHERA, W., PRILLER, A., STEIER, P., WILD, E.M., “AMS ^{14}C dating of equipment from the Iceman and of spruce logs from the prehistoric salt mines of Hallstatt”, Radiocarbon 41/2 (1999) 183-197.
- [4] BORTENSCHLAGER, S., OEGGL, K., eds., “The Iceman and his natural environment”, The Man in the Ice, Vol. 4, Springer-Verlag Wien (2000), pp. 166.
- [5] KUTSCHERA, W., ROM, W., “Ötzi, the prehistoric Iceman”, Nucl. Instrum. and Meth. B 164-165 (2000) 12-22.
- [6] JETTMAR, B., GOLSER, G., KUTSCHERA, W., PRILLER, A., ROM, W., STEIER, P., WILD, E.M., BORTENSCHLAGER, S., OEGGL, K., “The finding place of the Iceman “Ötzi”: implications from new ^{14}C dates”, to be published in Radiocarbon.

CLOCKS FOR QUATERNARY ENVIRONMENTS IN AUSTRALIA*

(Abstract)

C. TUNIZ**

Australian Nuclear Science and Technology Organisation,
Menai, New South Wales, Australia

The Australian continent offers a variety of natural systems where records of the Earth's past environment have been stored, including sediment cores, tree rings, rock surfaces and corals. Rock varnish, mud-wasp nests and pack-rat middens provide alternative archives for vegetation and environmental change in arid areas, where continuous sedimentary sequences or trees are not available. Each of these media contain specific information on past climatic conditions but we must determine their chronology and decipher the relevant environmental parameters. Cosmogenic radionuclides, such as ^{14}C , ^{10}Be , ^{26}Al and ^{36}Cl , analysed by accelerator mass spectrometry, provide valuable radiometric clocks to establish an absolute time scale for the environmental events of the Quaternary. U-series, potassium-argon, argon-argon and optically stimulated luminescence are other dating methods used in palaeoenvironmental studies. ANSTO supports the Quaternary science community in Australia providing the analysis of long-lived radionuclides: some significant projects from this program will be illustrated.

* Only an abstract is given here as the full paper was not available.

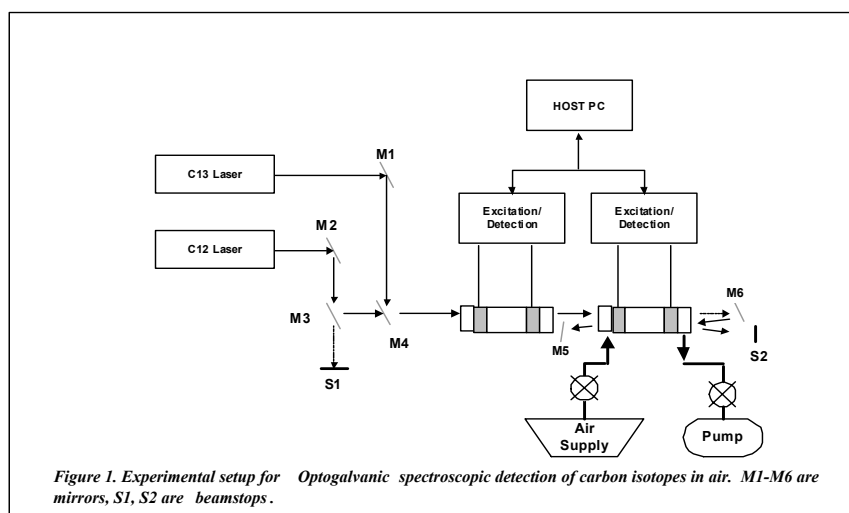
** Present address: Permanent Australian Mission to the United Nations, Mattiellistrasse, 2-4/111, A-1040 Vienna, Austria.

REAL TIME MONITORING OF ISOTOPIC CO₂ IN THE ATMOSPHERE***(Abstract)**

J. OKIL, T.J. McCARTHY, D.E. MURNICK
 Department of Physics, Rutgers University,
 Newark New Jersey, United States of America

A system suitable for real time analysis of atmospheric carbon dioxide concentration and isotopic ratios is under development. The system is based on laser assisted isotope ratio analysis [1] (LARA) and should be suitable for unattended use at field stations.

A schematic of laboratory version of the system is shown in Figure 1. Two sealed lasers, one resonant only with ¹³CO₂ and the second resonant only with ¹²CO₂ compare optogalvanic responses from air slowly flowed through a low pressure electrical discharge cell to signals from a similar sealed cell containing a known CO₂ gas mixture. For system development, standard air [2] is flowed at 0.4 SCCM through one cell. The entire system, which is run under PC control, can be left unattended for long periods.



The LARA technology has previously been successfully applied for isotopic CO₂ measurements in human breath [3] which is approximately 5% CO₂. In order to obtain adequate signal levels at the two order of magnitude lower concentrations in the atmosphere, several enhancements are required, including multipass of the laser beam through the air discharge and improved detection and analysis algorithms. Preliminary results indicate that concentration variations at the 0.1ppm level and ¹³C/¹²C ratio variations at the 0.5 δ level can be obtained with a few minutes averaging times.

For field operation, relative humidity and temperature in the flow system will have to be controlled. Extension to ¹⁸O/¹⁶O ratios using a third laser is possible. CO and CH₄ measurements will also be possible with the development of a pre-concentration gas separation module for the flow stream.

* Only an abstract is given here as the full paper was not available.

ACKNOWLEDGEMENTS

This work is supported by the NSF Atmospheric Chemistry Division under Grant 0082415.

REFERENCES

- [1] MURNICK, D.E., PEER, B.J., "Laser-Based Analysis of Carbon Isotope Ratios", *Science* **263** (1994) 945-947.
- [2] UN1002 natural air, calibrated by the Climate Monitoring and Diagnostics Laboratory of the National Oceanic and Atmospheric Administration, USA.
- [3] MURNICK, D.E., COLGAN, M.J., STONEBACK, D.N., "Laser Optogalvanic Effect Isotope Ratio Analysis in Carbon Dioxide", in *Synthesis and Applications of Isotopes and Isotopically Labeled Compounds* 1997 ed. by J.R. Heys and D.G. Melillo, John Wiley and Sons, Chichester (1998) 111-115.

IODINE-129 AS A LONG-LIVED TRACER IN THE ENVIRONMENT

R. MICHEL, T. ERNST, S. SZIDAT*

Centre for Radiation Protection and Radioecology, University Hannover,
Hannover, Germany

C. SCHNABEL

Institute for Particle Physics, ETH Hoenggerberg,
Zürich, Switzerland

H.-A. SYNAL

Paul Scherrer Institute, c/o Institute for Particle Physics, ETH Hoenggerberg,
Zürich, Switzerland

Abstract. ^{129}I is an important tracer of human activities as well of environmental processes. However, its potential can only be exploited if the ^{129}I abundances in and the pathways between the different environmental compartments are known. Until today, our knowledge of the radioecology of ^{129}I is still insufficient. Results are presented from a long-term project which shall improve this situation. ^{129}I and ^{127}I abundances were investigated in precipitation, surface and ground waters from Lower Saxony, Germany, and in soil samples from various European locations. From the analysis of ^{129}I in rain, ^{129}I annual deposition densities were determined for the time period from 1997- 1999. We conclude that ^{129}I deposition rates in Switzerland and Germany increased by three orders of magnitude since 1950 and changed just little after 1987. The different $^{129}\text{I}/^{127}\text{I}$ ratios in precipitation, surface and ground waters allow to estimate mean residence times of iodine in surface soil zones. From the analysis of soils, ^{129}I deposition densities at various places of Europe were determined. Thereby, the ^{129}I natural equilibrium deposition density as well as that of the fall-out from atmospheric weapon tests was estimated. Elevated ^{129}I abundances in Ukrainian soils contaminated by Chernobyl fall-out provide a basis for retrospective dosimetry of the radiation exposure due to ^{131}I . Soil profiles from Germany exhibit the influence of ongoing emissions from European reprocessing plants and demonstrate the complexity of iodine migration. Biospheric $^{129}\text{I}/^{127}\text{I}$ ratios in Germany are an order of magnitude lower than in precipitation. Because of the disequilibrium of iodine isotopes in the different compartments further detailed investigations of the pathways of ^{129}I through the environment to man are considered necessary.

1. INTRODUCTION

The long-lived radionuclide ^{129}I ($T_{1/2} = 15,7 \text{ Ma}$) is produced in nature by cosmic-ray induced spallation of Xenon in the atmosphere and by spontaneous fission in the geosphere. The natural abundances of ^{129}I have been globally and sustainably changed by anthropogenic ^{129}I released due to atmospheric explosions of nuclear weapons, nuclear accidents and most importantly due to releases from reprocessing plants. Though these changes are of radiological relevance only in the closest proximity of reprocessing plants, they should be carefully monitored and the potential of ^{129}I as a man-made tracer for environmental processes should be exploited. This requires a detailed understanding of the pre-nuclear baseline values, of the anthropogenic changes, of the radioecology of ^{129}I , and of the environmental chemistry of iodine. However, due to analytical and methodological problems the radioecology of ^{129}I is still insufficiently known and further investigations of the pre-nuclear abundances and of anthropogenic changes are needed [1]. We therefore started systematic investigations to establish reliable analytical protocols for ^{129}I and ^{127}I analyses in various environmental materials [1-5], to improve our knowledge about the environmental abundances and behaviour of ^{129}I , and to provide the baseline data for some tracer applications, in particular with respect to retrospective dosimetry [5, 6].

* Present address: Department of Chemistry and Biochemistry, University Bern.

This paper deals with the development with time of atmospheric ^{129}I fall-out and ^{129}I deposition densities in Europe and shortly addresses the potential of ^{129}I for retrospective dosimetry of the exposure to ^{131}I from the Chernobyl accident. Exemplary data on the migration of ^{129}I in soils and on the ^{129}I transport from surface to ground waters are presented. Finally, the biospheric response to the environmental ^{129}I contamination is discussed.

2. MATERIALS AND METHODS

Since 1997, precipitation, surface waters and ground water samples from Lower Saxony, Germany, were collected at various stations of the Deposition Measurement System. Moreover, surface and shallow ground water samples were taken at stations of the Information System of Surveillance of Environmental Radioactivity (IMIS) (Fig. 1). In order to establish a spatial separation, Lower Saxony was divided into four regions with sampling sites of every sample type each. In addition to open field precipitation sampled in each region, through-fall precipitation was collected in two regions; through-fall here means rain that falls down on forests and interacts with the canopy of the trees on its way down. The four regions were chosen to represent the close proximity to the North Sea (region I), northern German lowlands distant from the North Sea (region II), the fringe of the Harz mountains (region III) and the area of the Elbe river in Lower Saxony in the vicinity of Gorleben (region IV). Up to 10 L of precipitation were made available to us as three-months composite samples. 2 L of surface water were collected as spot samples once a quarter and 10 L of ground water once half a year. Two 1 L North Sea water samples were taken singularly near the shore in 1999 at Spieka-Neufeld. Samples were made alkaline and stored in the dark in polyethylene containers until analysis.

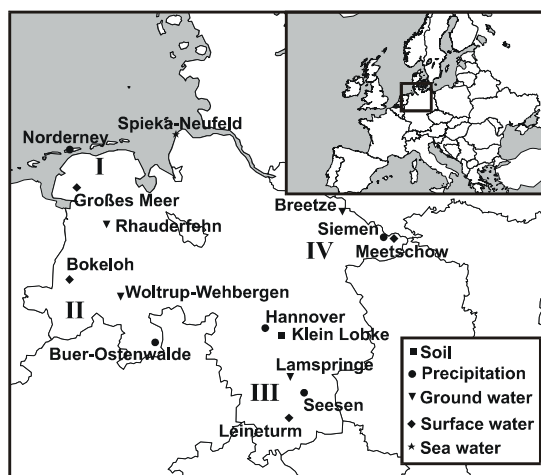


FIG. 1. Sampling sites of natural waters and soil in Lower Saxony, Germany.

Soil samples were obtained from different sources. A total of 48 soil profiles was taken between 1995 and 1997 at Moscow and in the Northern Ukraine and analyzed for ^{129}I and ^{127}I using RNAA and AMS [7]. In 1999, seven well characterized soil profiles were taken at seven locations in Lower Saxony down to a maximum depth of 250 cm. For three of the latter profiles the analyses of ^{129}I and ^{127}I were finished up to now. A pre-nuclear soil profile from 1939 was obtained from the Timiryazev Agricultural Academy, Moscow, courtesy of Prof. Dr. A. Fokin.

For matrix separation and enrichment of iodine two different methods were used. All the solid environmental samples were combusted under an excess of oxygen with adsorption of the iodine in the exhaust gas as iodide in an aqueous alkaline NaHSO_3 solution. The chemical yield of the iodine extraction was determined using ^{125}I as tracer. For liquid samples only an enrichment of iodine is necessary for the analysis of ^{129}I . For this preparation a solid phase extraction (SPE) on an anion exchange resin is carried out after carrier addition. Before the SPE, all iodine species must be converted into iodide. The concentrations of ^{127}I in the filtered aqueous samples and in the NaHSO_3 solution were analyzed by ion chromatography (IC) and/or inductively coupled plasma mass spectrometry (ICP-MS). The concentration of ^{129}I was determined by measuring the ratio $^{129}\text{I}/^{127}\text{I}$ via accelerator mass spectrometry (AMS). Further details of sample preparation, AMS techniques and measurements, and quality control measures are given elsewhere [1-6, 8].

3. ATMOSPHERIC FALL-OUT OF ^{129}I IN GERMANY AND SWITZERLAND

The geometric means and standard deviations of ^{129}I , ^{127}I and of $^{129}\text{I}/^{127}\text{I}$ ratios in precipitation and in surface and ground waters from Lower Saxony, Germany, are given in Table I for the three years period from 1997 to 1999. The detailed results are presented elsewhere [4, 6]. We will focus first on the discussion of the $^{129}\text{I}/^{127}\text{I}$ ratios. According to model calculations, e.g. [9], iodine pathways through the environment are recognizable via these $^{129}\text{I}/^{127}\text{I}$ ratios. The North Sea and the North Atlantic act as buffer reservoirs for both, stable iodine and ^{129}I , the latter being mainly emitted by the European reprocessing plants Sellafield and La Hague [10, 11]. The subsequent transfer through marine and land atmospheres to precipitation takes place with only a short time scale of about two weeks [9]. In the atmosphere, mixing with iodine from other natural sources occurs and also a direct influence of atmospheric releases from reprocessing plants to ^{129}I in precipitation is possible. After iodine is deposited on the ground by wet or dry precipitation, the iodine isotopes are slowly transported into surface and ground waters. These compartments have distinctly lower $^{129}\text{I}/^{127}\text{I}$ ratios, which makes it possible to estimate residence times of iodine in catchments via the time dependence of ^{129}I abundances. As iodine is biophilic, these residence times may provide evidence regarding the biological condition of a catchment when compared to tritium residence times.

Table I. $^{129}\text{I}/^{127}\text{I}$ in several Lower Saxonian natural waters from 1997-1999 as geometric means with standard deviations

Sample	Region	<i>n</i>	^{129}I in $\mu\text{Bq/kg}$		^{127}I in $\mu\text{g/kg}$		$^{129}\text{I}/^{127}\text{I}$ in 10^{-10}	
Precipitation (open-field)	I	10	17.0	$\cdot 1.34^{\pm 1}$	3.10	$\cdot 1.39^{\pm 1}$	8250	$\cdot 1.20^{\pm 1}$
	II	9	6.07	$\cdot 1.41^{\pm 1}$	1.48	$\cdot 1.31^{\pm 1}$	6190	$\cdot 1.34^{\pm 1}$
	III	9	4.09	$\cdot 1.87^{\pm 1}$	1.33	$\cdot 2.05^{\pm 1}$	4650	$\cdot 1.82^{\pm 1}$
	IV	9	3.57	$\cdot 1.61^{\pm 1}$	1.31	$\cdot 1.45^{\pm 1}$	3740	$\cdot 1.59^{\pm 1}$
Precipitation (through-fall)	II	9	24.1	$\cdot 1.40^{\pm 1}$	6.92	$\cdot 1.31^{\pm 1}$	5260	$\cdot 1.13^{\pm 1}$
	III	9	14.2	$\cdot 1.33^{\pm 1}$	5.08	$\cdot 1.23^{\pm 1}$	4220	$\cdot 1.29^{\pm 1}$
Surface water	I	12	7.20	$\cdot 2.25^{\pm 1}$	23.6	$\cdot 1.48^{\pm 1}$	460	$\cdot 2.07^{\pm 1}$
	II	12	0.94	$\cdot 1.67^{\pm 1}$	6.52	$\cdot 1.25^{\pm 1}$	219	$\cdot 1.61^{\pm 1}$
	III	11	0.24	$\cdot 1.58^{\pm 1}$	5.74	$\cdot 1.43^{\pm 1}$	62.8	$\cdot 1.68^{\pm 1}$
	IV	12	0.67	$\cdot 2.00^{\pm 1}$	8.56	$\cdot 1.61^{\pm 1}$	118	$\cdot 2.04^{\pm 1}$
Ground water	I	3	0.283	$\cdot 1.39^{\pm 1}$	4.24	$\cdot 1.30^{\pm 1}$	99.2	$\cdot 1.51^{\pm 1}$
	II	4	0.560	$\cdot 1.23^{\pm 1}$	3.90	$\cdot 1.26^{\pm 1}$	222	$\cdot 1.56^{\pm 1}$
	III	4	0.0367	$\cdot 2.37^{\pm 1}$	1.83	$\cdot 4.24^{\pm 1}$	30.3	$\cdot 1.93^{\pm 1}$
	IV	5	0.0065	$\cdot 5.76^{\pm 1}$	4.98	$\cdot 1.21^{\pm 1}$	2.0	$\cdot 5.80^{\pm 1}$

In 1950, atmospheric $^{129}\text{I}/^{127}\text{I}$ ratios in background regions of the northern hemisphere exceeded 10^{-9} [1,3]. ^{129}I deposition does not show a prominent bomb peak in an alpine ice-core [12] as for instance observed for ^{14}C , ^{36}Cl and ^{137}Cs . Isotopic ratios and deposition densities continued to increase in Europe until the end of the 1980s (Fig. 2). Since then, ratios of nearly 10^{-6} were observed in Germany and Switzerland and remained constant until today. The fall-out of the Chernobyl accident by wet deposition was just a short-term episode with a highest measured $^{129}\text{I}/^{127}\text{I}$ ratio of nearly 10^{-5} .

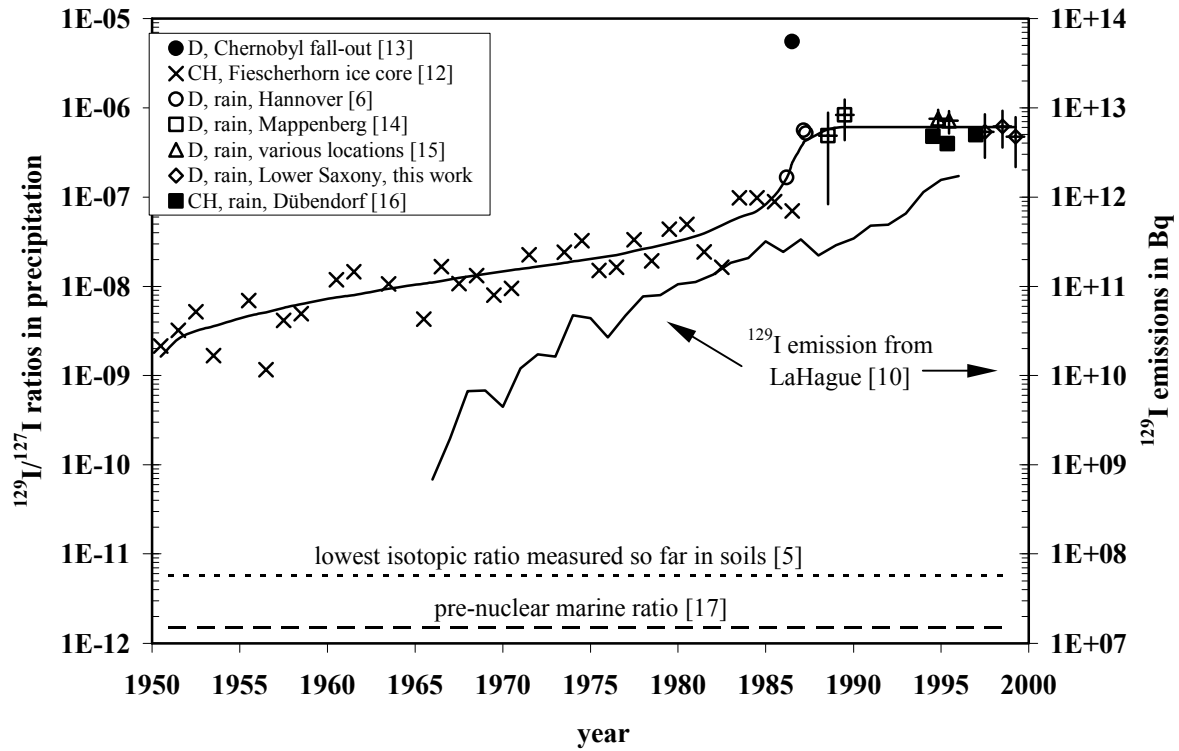


FIG. 2. Development of $^{129}\text{I}/^{127}\text{I}$ isotopic ratios in precipitation as revealed by analyses of precipitation from Switzerland and Germany. The solid line is an eye-guide only. Data of refs. [12], [13], and [16] are calculated under the assumption of an ^{127}I content of $1.4 \mu\text{g/kg}$. For comparison, the development of ^{129}I emissions from the La Hague reprocessing plant, which is the dominant source in Europe, is given.

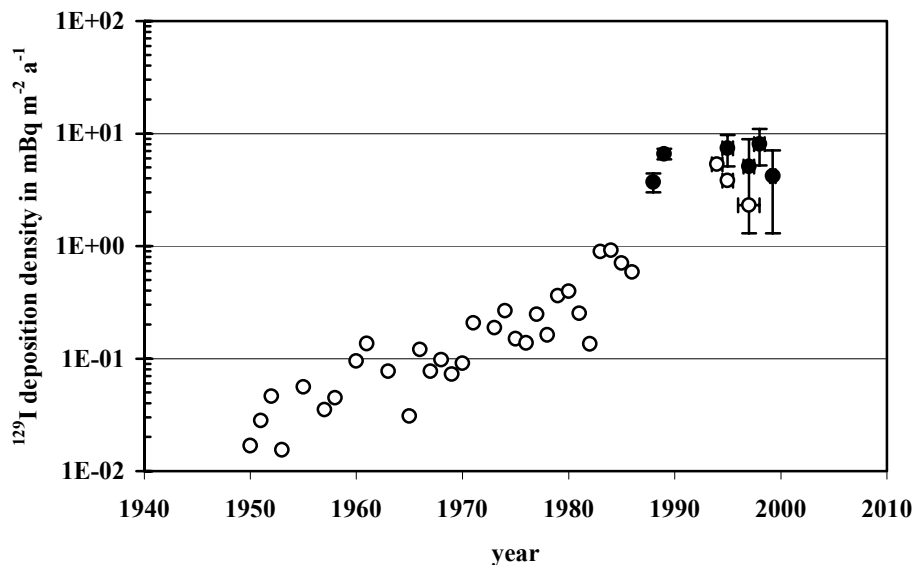


FIG. 3. Development with time of annual deposition densities of ^{129}I in Germany (full circles) [14, 15, and this work] and Switzerland (open circles) [12, 16].

The annual ^{129}I deposition rates as calculated from the measured ^{129}I concentrations in precipitation and annual precipitation rates rose during the last five decades from $0.01 \text{ mBq m}^{-2} \text{ a}^{-1}$ in 1950 in Switzerland by nearly three orders of magnitude to a geometric mean of $6.4 \times 2.1^{\pm 1} \text{ mBq m}^{-2} \text{ a}^{-1}$ for all four regions of Lower Saxony, Germany, during 1997-1999 (Fig. 3). The present deposition in Lower Saxony is inhomogeneous with time and place and shows even some seasonal dependence [4]. The fact, that ^{129}I emissions of the La Hague reprocessing plant, which is the dominating European source, also increased by about three orders of magnitude (Fig. 2) does not yet give conclusive evidence about the pathways of ^{129}I from the emittents to Germany and Switzerland. Though the majority of the emissions occurs into the sea, it is not yet clear whether the present fall-out is dominated by the marine or the atmospheric emissions [16].

4. ^{129}I IN SOILS

From the ^{129}I activity concentrations in the samples of the soil profiles, deposition densities $D(d)$ are calculated according to:

$$D(d) = \int_d^{\infty} A_s(d') \cdot \rho(d') dd' \quad (1)$$

with

$D(d)$	deposition density as function of depth d in Bq m^{-2}
$A_s(d)$	activity per unit mass in the depth interval $[d, d + \Delta d]$ in Bq kg^{-1}
$\rho(d)$	soil density in the depth interval $[d, d + \Delta d]$ in g cm^{-3}
$D(d=0)$	integral deposition density in Bq m^{-2}

For stable iodine, deposition densities were defined analogously by replacing $A_s(d)$ by the ^{127}I concentrations in the soil, $C_{127}(d)$ in g g^{-1} . Illustratively, we show in Fig. 4 the depth dependence of ^{129}I and ^{127}I deposition densities and of the $^{129}\text{I}/^{127}\text{I}$ ratios in a soil profile from Klein Lobke, Lower Saxony, Germany. More than 99 % of ^{129}I is still observed in the upper 60 cm of the profile. But the $^{129}\text{I}/^{127}\text{I}$ ratios below this depth still are of the order of 10^{-10} , i.e. about two orders of magnitude higher than the natural equilibrium ratio in the marine hydrosphere.

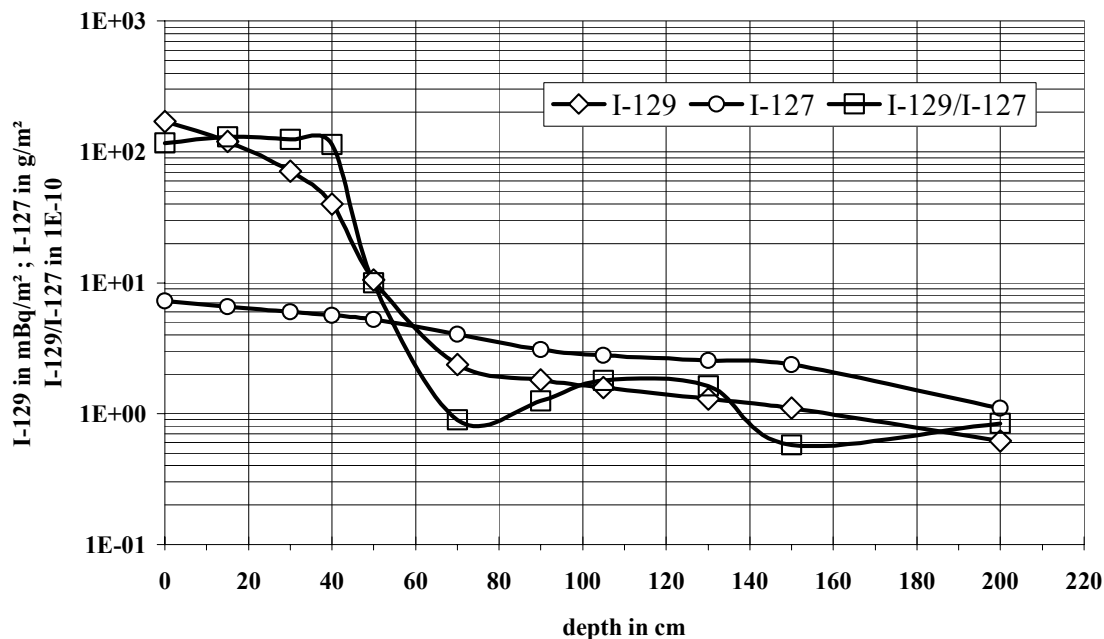


FIG. 4. Deposition densities of stable iodine and of iodine-129 in a soil profile from Klein Lobke, Lower Saxony, Germany.

Integral deposition densities, $D(d=0)$, of ^{129}I were determined from the analysis of soil profiles (Table II). The up to now lowest deposition density was found in a soil profile taken in 1939 in Lutovinovo, Russia, which also showed the lowest isotopic ratio in soils of $(0.057 \pm 0.011) \times 10^{-10}$ [5]. However, this ratio is a factor of four higher than the pre-nuclear marine $^{129}\text{I}/^{127}\text{I}$ equilibrium ratio of $\sim 1.5 \times 10^{-12}$ [17]. Due to the danger of modern contamination during long-term storage, pre-nuclear soil profiles can give only upper limits of the natural equilibrium deposition densities. Contamination during sample preparation and analysis is not a problem here since the complete analytical blanks in our work typically yield $^{129}\text{I}/^{127}\text{I}$ ratios below 2×10^{-13} .

Table II. Integral ^{129}I deposition densities as derived from the analysis of soil profiles from differently contaminated areas

location	number of profiles	depth in cm	date of sampling	integral ^{129}I deposition densities in $\text{mBq} \cdot \text{m}^{-2}$
Lutovinovo, Russia	1	35	1939	0.084 ± 0.017
Moscow, Russia	2	40	1996	$49 \cdot 1.5^{\pm 1}$
Zhytomir, Ukraine	12	40	1997	$38 \cdot 1.7^{\pm 1}$
Lower Saxony, Germany	3	250	1999	$139 \cdot 1.2^{\pm 1}$
Zone III, Ukraine	24	40	1995	$130 \cdot 1.5^{\pm 1}$
Zone II, Ukraine	7	40	1995	$848 \cdot 1.5^{\pm 1}$

Integral deposition densities in Lower Saxony, Germany, are more than three orders of magnitude higher than the pre-nuclear value derived for Lutovinovo, Russia. They are also higher than in Moscow, Russia [5], or Zhytomir, Ukraine, both regions being not significantly contaminated by fall-out from the Chernobyl accident. Only in areas of Ukraine which are seriously contaminated by this accident, we observed higher integral deposition densities than in Germany [7]. Table II gives geometric means and standard deviations of integral deposition densities in contamination zones II (^{137}Cs deposition density 555-1480 kBq/m^2) and III (^{137}Cs deposition density 185 – 555 kBq/m^2) of northern Ukraine. There, ^{129}I can be used for estimates of the fall-out of ^{131}I from the Chernobyl accident. In the highly contaminated areas of Ukraine, the majority of ^{129}I deposition occurred instantaneously. Thus, the depth profiles allow to investigate the migration of ^{129}I in detail. In Ukraine, more than 99 % of the Chernobyl fall-out still resides in the top 30 cm of the soils. Generally, the ^{129}I deposition densities in the soil profiles from Ukraine and from Moscow show a roughly exponential decrease with depth [7]. In Lower Saxony, Germany, the situation is much more complicated due to the complex fall-out pattern with a continuous, but strongly time-dependent deposition (Fig. 2, 3).

5. ^{129}I IN SURFACE AND GROUND WATERS IN LOWER SAXONY, GERMANY

The deposition of atmospheric ^{129}I is the most important source in the upper terrestrial environment in central Europe. When using the precipitation values of Fig. 2 as an input function in a simple exponential model [18] for the transfer of iodine in the surface of a catchment [4], one can estimate mean iodine residence times in the surface soil zone and compare these values with tritium data (Table III). In this model, mean transition times τ are calculated according to

$$\tau = - \frac{t}{\ln(1-H(t))} \quad (2)$$

with the time t of constant input and the fraction $H(t)$ of the input signal that is observed in the investigated compartment. t characterizes the time span between the sampling time of the respective sample and 1986, the interpolated beginning of the constant input; $H(t)$ is given as the ratio of $^{129}\text{I}/^{127}\text{I}$ in the examined sample and the mean precipitation value of 6.5×10^{-7} . τ is calculated for each individual sample and geometric means are given in Table III with standard uncertainties of the mean. This modelling suggests a horizontal and vertical iodine transport delayed by one to three orders of magnitude compared to water movements. Surface and ground waters show similar values except for region IV, where an impermeable zone at the ground water sampling site is supposed.

Table III. Mean residence times of iodine in surface soil zones based on a simple exponential model and characteristic time constants of water transfer into groundwater deduced from ^3H in ground water with standard uncertainties

Sample	Region	τ_{iodine} in a			τ_{tritium} in a		
Surface water	I	biased by sea water			—		
	II	364	·	$1.14^{\pm 1}$	—		
	III	1290	·	$1.16^{\pm 1}$	—		
	IV	670	·	$1.24^{\pm 1}$	—		
Ground water	I	828	·	$1.25^{\pm 1}$	7	±	5
	II	359	·	$1.23^{\pm 1}$	12	±	1
	III	2670	·	$1.36^{\pm 1}$	9	±	4
	IV	40200	·	$2.15^{\pm 1}$	19	±	2

^{129}I IN THE BIOSPHERE

Also the present biospheric iodine isotopic composition has been drastically changed compared to pre-nuclear values. The up-to-now lowest isotopic ratio has been measured in a pig thyroid gland powder prepared by Parke-Davis in 1943 in the USA. The mean of the two analyses of $(0.058 \pm 0.012) \times 10^{-10}$ [1, 5] is still higher than the measured pre-nuclear ratios in ocean sediments. The thyroid glands sampled in 1947 in the USA turned out to have $^{129}\text{I}/^{127}\text{I}$ ratios 10 to 60 times higher than the pre-nuclear marine equilibrium ratio and thus are suspected to be affected already by ^{129}I releases during the Manhattan project and the onset of the nuclear age.

Present days' isotopic ratios in human and animal thyroid glands from Lower Saxony in Germany, which is well away from nuclear installations emitting ^{129}I , show much higher ratios [19]. In bovine thyroid glands, $^{129}\text{I}/^{127}\text{I}$ ratios of $(110 \pm 10) \times 10^{-10}$, $(47 \pm 5) \times 10^{-10}$, and $(400 \pm 196) \times 10^{-10}$ were observed in 1978 ($n = 25$), 1981 ($n = 22$), and 1992/93 ($n = 9$), respectively [19, 20]. The fall-out caused by the Chernobyl accident in Western Europe just appeared as a short-term peak in the isotopic ratios as revealed by analyses of animal thyroids from Austria and Germany [21]. Pre- and post-Chernobyl human thyroid glands from Germany analyzed at ZSR showed $^{129}\text{I}/^{127}\text{I}$ ratios of $(216 \pm 114) \times 10^{-10}$ ($n = 13$) and $(320 \pm 156) \times 10^{-10}$ ($n = 26$), respectively. $^{129}\text{I}/^{127}\text{I}$ ratios are about one order of magnitude lower in thyroid glands from the southern hemisphere as revealed by analyses of human and animal thyroid

glands from Chile [19]. This is well in line with the general differences between global weapons fall-out in the southern and northern hemispheres, on the one hand, and the fact that the emissions from reprocessing plants mainly take place on the northern hemisphere, on the other.

With respect to the radiological significance of these $^{129}\text{I}/^{127}\text{I}$ ratios, one can estimate the associated radiation exposure on the basis of a specific activity model [1]. Assuming the data of ICRP reference man for human iodine content and uptake [22] and a dose factor for a child in its first year of 2.2×10^{-7} Sv/Bq [23], an equilibrium $^{129}\text{I}/^{127}\text{I}$ ratio of 100×10^{-10} corresponds to an annual effective equivalent dose due to intake of ^{129}I of $H_{\text{eff}} \approx 5$ nSv/a. Thus, it can be concluded that the present situation is radiologically not significant. It is to note, however, that this is just a coarse estimate which takes not into account the existing disequilibrium of ^{129}I and ^{127}I in the environment.

The $^{129}\text{I}/^{127}\text{I}$ ratios observed up to now in human and animal thyroid glands in Europe do not yet reach the ratios in precipitation. Given the continuous input of ^{129}I , a further increase of biospheric $^{129}\text{I}/^{127}\text{I}$ ratios is to be expected. In the data obtained over 20 years there appeared an average increase by about an order of magnitude, though there is a considerable scatter of the data [6]. Since there is a strong disequilibrium of iodine isotopes in the different environmental compartments, the exposure of man and animal to ^{129}I , in principle, cannot be estimated on the basis of a specific activity model and the above estimate is just a zero order approximation. For a realistic assessment of the exposure to ^{129}I the radioecological pathways of ^{129}I to man and animal have to be investigated in more detail.

CONCLUSIONS

In Europe, as all over the world, the natural abundance of ^{129}I have been sustainably changed. But, in Western Europe these changes are going on. $^{129}\text{I}/^{127}\text{I}$ ratios in precipitation stabilized after a decades-long increase at a level of nearly 10^{-6} . These ratios are more than one order of magnitude higher than recent ratios of biosphere iodine measured in Germany. The different environmental compartments in Europe show extreme disequilibrium between ^{129}I and stable iodine with the expected consequence of a further rise of biospheric $^{129}\text{I}/^{127}\text{I}$ ratios. In spite of the fact that the present global biospheric ^{129}I abundance does not give rise to a significant radiation exposure, the future development should be carefully surveyed. ^{129}I turns out to be an outstanding quantitative indicator of the long-term human impact onto the environment. It has the potential of a powerful tracer of environmental processes and offers a possibility of retrospective dosimetry after accidental and routine fall-out situations.

ACKNOWLEDGEMENT

This work was funded by the Deutsche Forschungsgemeinschaft (DFG).

REFERENCES

- [1] SCHMIDT, A., SCHNABEL, CH., HANDL, J., JAKOB, D., MICHEL, R., SYNAL H-A., LOPEZ, J.M., SUTER, M., On the analysis of iodine-129 and iodine-127 in environmental materials by accelerator mass spectrometry and ion chromatography. *Sci. Total Environ.* 223 (1998) 131-156.
- [2] SZIDAT, S., SCHMIDT, A., HANDL, J., JAKOB, D., MICHEL, SYNAL H-A., LOPEZ, J.M., SUTER Analysis of iodine-129 in environmental materials: quality assurance and applications. *J. Radioanal. Chem.* 244 (1999) 45-50.

- [3] SCHMIDT, A., SCHNABEL, CH., HANDL, J., JAKOB, D., MICHEL, R., SYNAL H-A., LOPEZ, J.M., SUTER, RNAA and AMS of Iodine-129 in Environmental Materials-Comparison of Analytical Methods and Quality Assurance -. *Kerntechnik* 65 (2000) 160-167.
- [4] SZIDAT, S, Iod-129: Probenvorbereitung, Qualitätssicherung und Analyse von Umweltmaterialien (in German). Ph.D. thesis, Univ. of Hannover (2000). Available at: <http://edok01.tib.uni-hannover.de/edoks/e002/32217211X.pdf>.
- [5] SZIDAT, S, SCHMIDT, A., HANDL, J., JAKOB, D., BOTSCH, R., MICHEL, SYNAL H-A., SCHNABEL, C., SUTER, M., LOPEZ-GUTIERREZ, J.M., STAEDE, W., Iodine-129: Sample preparation, quality control and analyses of pre-nuclear materials and of natural waters from Lower Saxony, Germany. *Nucl. Instr. Meth. Phys. Res. B172* (2000) 699-710.
- [6] MICHEL R.,SZIDAT, S., HANDL, J., JAKOB, D., SYNAL, H-A., SUTER, M., Status and Trends of Iodine-129 Abundances in the European Environment. *Proceedings IRPA10, Hiroshima, May 14 – 19, 2000, CD (2000) P-4a-229*.
- [7] J. Handl, Th. Ernst, W. Botsch, S. Szidat, A. Schmidt, D. Jakob, D. Beltz, R. Michel, L.D. Romantschuk, H.-A. Synal, C. Schnabel, M. Suter, Fallout and migration of ^{129}I in contaminated areas in Ukraine. In preparation (2001).
- [8] SYNAL H.-A., BONANI, G., DOEBILI, M., ENDER, R., GARTENMANN, P., KUBIK, SCHNABEL, C., SUTER, M., Status report of the PSI/ETH AMS facility. *Nucl. Instr. Meth. Phys. Res. B123* (1997) 62-68
- [9] FABRYKA-MARTIN, J., BENTLEY, D., ELMORE, D., AIRLEY, P.L., Natural iodine-129 as an environmental tracer, *Geochim. Cosmochim. Acta* 49 (1985) 337-347.
- [10] Inventaire des rejets radioactifs des installations nucléaires, Volume 1: Historique des rejets (in French), Groupe Radioécologie Nord-Cotentin, c/o Institut de Protection et de Sécurité Nucléaire, Fontenay-aux-Roses (1999).
- [11] RAISBECK, G.M., YIOU, F., ZHOU, Z.Q., KILIUS, L.R., ^{129}I from nuclear fuel re-processing facilities at Sellafield (U.K.) and La Hague (France); potential as an oceanographic tracer. *J. Mar. Sys.* 6 (1995) 561-570.
- [12] WAGNER, M.J.M., DITTRICH-HANNEN, B., SYNAL, H.-A., SUTER, M., SCHOTTERER, U., Increase of iodine-129 in the environment. *Nucl. Instr. Meth. Phys. Res. B113* (1996) 490-494.
- [13] PAUL, M., FINK, D., HOLLOS, G., KAUFMANN, S.A., KUTSCHERA, W., MARGARITZ, M., Measurement of ^{129}I concentrations in the environment after the Chernobyl reactor accident. *Nucl. Instr. Meth. Phys. Res. B29* (1987) 341-345.
- [14] BACHHUBER, K., BUNZL, K., Background levels of atmospheric deposition to ground and temporal variation of ^{129}I , ^{127}I , ^{137}Cs and ^7Be in a rural area of Germany. *J. Environ. Radioactivity* 16 (1992) 77-89.
- [15] KRUPP, G., AUMANN, D.C., Iodine-129 in rainfall over Germany. *J. Environ. Radioactivity* 46 (1999) 287-299.
- [16] SCHNABEL, C., J.M. López-Gutiérrez, S. Szidat, J. Beer, H.A. Synal, ^{129}I in rain water near Zurich. *Extended Abstracts 5th Int. Conf. on Nuclear and Radiochemistry*, Sept. 3-8, 2000, Pontresina, pp. 585-588, submitted to *Radiochimica Acta* (2001).
- [17] FEHN, U., HOLDREN, G.R., ELMORE, D., RUNELLE, T., TENG, R., KUBIK, P.W., Determination of natural and anthropogenic ^{129}I in marine sediments. *Geophys. Res. Lett.* 13 (1986) 137-139.
- [18] ZUBER, A., Mathematical models for the interpretation of environmental radioisotopes in groundwater systems, in: P. Fritz, J.C. Fontes, *Handbook of environmental isotope geochemistry*, Vol. 2B, Elsevier, Amsterdam (1986) pp. 1-59.
- [19] HANDL, J, Concentrations of ^{129}I in the biosphere. *Radiochim. Acta* 72 (1996) 33-38.

- [20] HANDL, J, PFAU, A., and HUTH, F.W., Measurements of ^{129}I in human and bovine thyroids in Europe - transfer of ^{129}I into the food chain. Health Phys. 58 (1990) 609-618.
- [21] VAN MIDDLESWORTH, L., and HANDL, J. ^{129}I , ^{131}I and ^{127}I in animal thyroids after the Chernobyl nuclear accident. Health Physics 73 (1997) 647-650.
- [22] ICRP, Report of the Task Group on Reference Man. ICRP Report No. 23, Pergamon Press, Oxford, 1981, 1st print 1971.
- [23] European Commission (1996) 96/29/EURATOM Council Directive of 13 May 1996 laying down basic safety standards for the health protection of the general public and workers against the dangers of ionizing radiation, OJ L-159 of 29/06/96 page 1.

PORTFOLIO OF RECENT CLIMATE CHANGE STUDIES UTILISING AMS AT ANTARES, ANSTO*

(Abstract)

D. CHILD, A. SMITH, D. FINK, Q. HUA, G. ELLIOT, A. WILLIAMS, G. JACOBSEN
ANSTO, Lucas Heights, New South Wales, Australia

The application of Accelerator Mass Spectrometry (AMS) to the measurement of the radionuclides ^{14}C , ^{10}Be , ^{26}Al and ^{36}Cl has dramatically increased our understanding of factors that affect climate and has led to a greater understanding of natural processes. Using the ANTARES AMS facility at ANSTO we are able to analyse samples containing as few as 10^5 atoms of these radionuclides.

Cosmogenic radionuclides produced by the interaction of cosmic rays with the upper atmosphere and exposed surface rocks are stored in natural archives. By measuring small variations in the concentrations of these isotopes over time, information can be inferred about the systems governing these changes.

Over the last four years we have undertaken a broad range of climate change and environmental studies, based on the ultra-sensitive technique of accelerator mass spectrometry (AMS). Some specific examples of projects investigating the ice sheet at Law Dome, Antarctica and minerals extracted from geological surface formations will be given.

To support this research program, ANSTO operates a suite of geochemistry laboratories specifically for the processing of ice, sediment and rock samples into AMS targets, in addition to pre-treatment and preparation laboratories for radiocarbon sample processing.

Cosmogenic Isotopes as Palaeo-archives in Air from Polar Ice: Accumulating ice sheets consist of a porous, compacting layer of snow (the firn) overlying the compacted, impervious ice.

Due to diffusive and gravitational mixing of the air in the firn (age spreading) and the air bubble formation process in the ice which further convolutes the atmospheric signal, there have been difficulties establishing the chronology of palaeo-atmosphere archives within the ice. By measuring the CO_2 ^{14}C bomb pulse it has been possible to improve the numerical modelling of these processes, resulting in direct improvements in the chronology and resolution of important long term Southern Hemisphere atmospheric records.

In addition, CH_4 was extracted from the firn air samples to examine the anthropogenic contribution from fossil fuel use to the global atmospheric methane budget.

Methods of gas extraction, target preparation and AMS measurement were developed to treat samples containing as little as $12\mu\text{g}$ of carbon. Aspects of these methods and applications will be discussed.

^{10}Be in Antarctic Ice: ^{10}Be concentration in ice is often assumed to be dependent on the snow accumulation rate. We decided to test the validity of this approach in recent times by measuring the ^{10}Be concentration in 3 cores from Law Dome, Antarctica, with known chronology and from sites with widely varying accumulation rates [1]. These sites receive snowfall from the same air mass as it moves from east to west across the dome.

* Only an abstract is given here as the full paper was not available.

The known chronology permitted sampling from mid year to mid year, with an annual sample having an approximate volume of 1L.

Sample handling and preparation techniques were devised to limit contamination of the ice by terrestrial dust and to maximise retention of the $\sim 10^6$ ^{10}Be atoms present. A combination of clean room procedures, filter arrays and ion exchange chromatography were used.

This investigation determined that ^{10}Be had been primarily deposited by wet deposition in recent times, and consequently the measured ^{10}Be concentration contained no information about the accumulation rate. Several pilot studies have been conceived by this work, for example examination of the transport processes involved in incorporating ^{10}Be into the ice by utilising the large disparity between half-lives for ^7Be and ^{10}Be . Aspects of these studies and the methodology used will be discussed.

In situ cosmogenic radionuclides: By measuring *in situ* produced cosmogenic radionuclides accumulated in minerals, the history or evolution of geomorphic formations, where previously buried mineral material has been exposed to cosmic ray irradiation, can be elucidated [2].

This technique is generally applicable to the time period between 5ka to 5Ma, and where erosion rates are within 0.1 to 10 mm/ka.

Due to the many factors affecting *in situ* accumulation rates (eg altitude, latitude, burial of the surface, shielding from cosmic radiation and carry over of cosmogenic isotopes from previous exposures) an intimate knowledge of the geomorphology and geology of the sampling environment are imperative.

The ANTARES AMS facility, ANSTO, has been used to collaboratively examine a number of geological events. Some examples of such projects are:

- Study of ^{10}Be depth profiles from sand regolith escarpments to determine their formation history.
- To determine the extent and history of Pleistocene glacial advances in key Tasmanian and Antarctic glaciation sites.
- A search for evidence of the Southern Hemisphere younger Dryas in New Zealand and Tasmania.

It has been critical to these projects to provide sample processing abilities of high precision [3]. Young samples (<15ka) such as those required for a younger Dryas search contain less target material (^{10}Be , ^{26}Al and ^{36}Cl) and therefore require more careful handling. Also, to simplify calculation of sample ages from measurement results, a single mineral matrix (generally quartz) is isolated from the sampled rock types and processed. Aspects of these applications for exposure age dating and the sample processing required for these projects will be discussed.

REFERENCES

- [1] SMITH, A., FINK, D., CHILD, D., LEVCHENKO, V.A., V. MORGAN, I.V.I., CURRAN, M., ETHERIDGE, D.M., ELLIOT, G., Nuc. Instr. and Meth. B **172** (2000) 847-855.
- [2] FINK, D., MCKELVEY, B., HANNAN, D., NEWSOME D., Nucl. Instr. and Meth. B **172** (2000) 838
- [3] CHILD, D., ELLIOT, G., MIFSUD, C., SMITH, A.M., FINK, D., Nucl. Instr. and Meth. B **172** (2000) 856-860.

ADVANCES IN ISOTOPE AND ANALYTICAL TECHNIQUES II

(Session 7)

Chairpersons

M.H. THIEMENS

United States of America

N. YOSHIDA

Japan

MITIGATION OF GLOBAL WARMING AND THE ROLE OF IDENTIFICATION OF GREENHOUSE GAS SOURCES

Y. KAYA

CREST program, Japan Science and Technology Corporation,
Tokyo, JAPAN

Abstract. Japan Science and Technology Corporation (JST) is an organization supporting R&D of frontier science and technologies under the full sponsorship of the government of Japan. Under the umbrella of JST the author is in charge of a program called "Environment friendly social systems" which includes more than 20 research projects for better environment (with as an average of 1 million US dollars per project per year). One of the projects in this program is on development of isotopomer technology and its use in identifying greenhouse gas (GHG) sources headed by Prof. N.Yoshida. JST earnestly hopes that it can contribute as much as possible to mitigation of global warming through the support of important research projects such as Yoshida's.

1. DIFFICULTIES IN GREENHOUSE GAS (GHG) REDUCTION

Needless to say that global warming is one of the most serious environmental threats mankind has experienced in its history. The framework convention of climate change (FCCC) declares that the ultimate aim of the convention is to stabilize greenhouse gas (GHG) concentration in the air. Taking into account that the concentrations of various GHG's in the air such as CO₂, CH₄ and N₂O increased significantly at least last hundred years probably due to expansion of human activities on the earth, realization of the FCCC's ultimate aim seems not to be an easy task. Particularly anthropogenic emission of CO₂ which occupies more than half of GHG radiative forcing has increased substantially mainly due to increase in fossil fuel consumption which has expanded roughly proportional to expansion of economic activities of the world.

According to IPCC [1] stabilization of CO₂ concentration in the air requires long term continuous efforts for reducing CO₂ emission, as shown in Fig.1. Although it is still uncertain what level of CO₂ concentration in the air is appropriate as the target, 550 ppmv has been very often used in many scenario analyses of global warming. Fig.1 indicates that to realize 550 ppmv target CO₂ emission be limited to the present level by the end of this century and reduced to almost 1/4 of the present level in the long run. What efforts in energy sector are needed to satisfy this requirement?

Many global modellers tried to answer this question, and a typical answer can be found in the analysis conducted in the government of Japan under the name of "New Earth 21" which aims at envisaging long term global scenarios of stabilizing climate change in the long run [2]. Fig. 2 breaks down efforts necessary to limit global CO₂ emission to 550 ppmv by the end of 21st century. The basic criterion of choosing this scenario is the cost: in other words the scenario in Fig. 2 is the least cost scenario of realizing 550 ppmv level of CO₂ concentration. If without global warming the world CO₂ emission will be the top line reflecting the world preference on coal as the cheapest and the most abundant fossil fuel source. However, limiting CO₂ concentration to 550 ppmv requires introduction of a lot of measures reducing CO₂ emission.

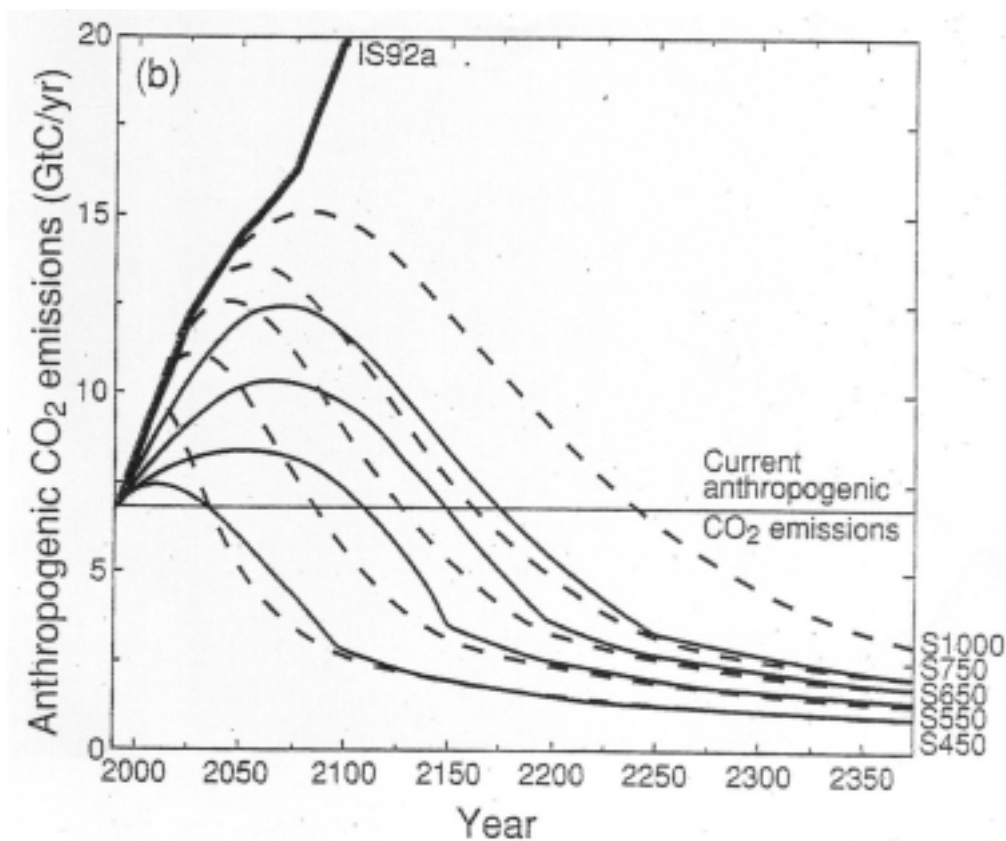


FIG. 1. CO₂ emissions leading to stabilization at concentrations in the air.

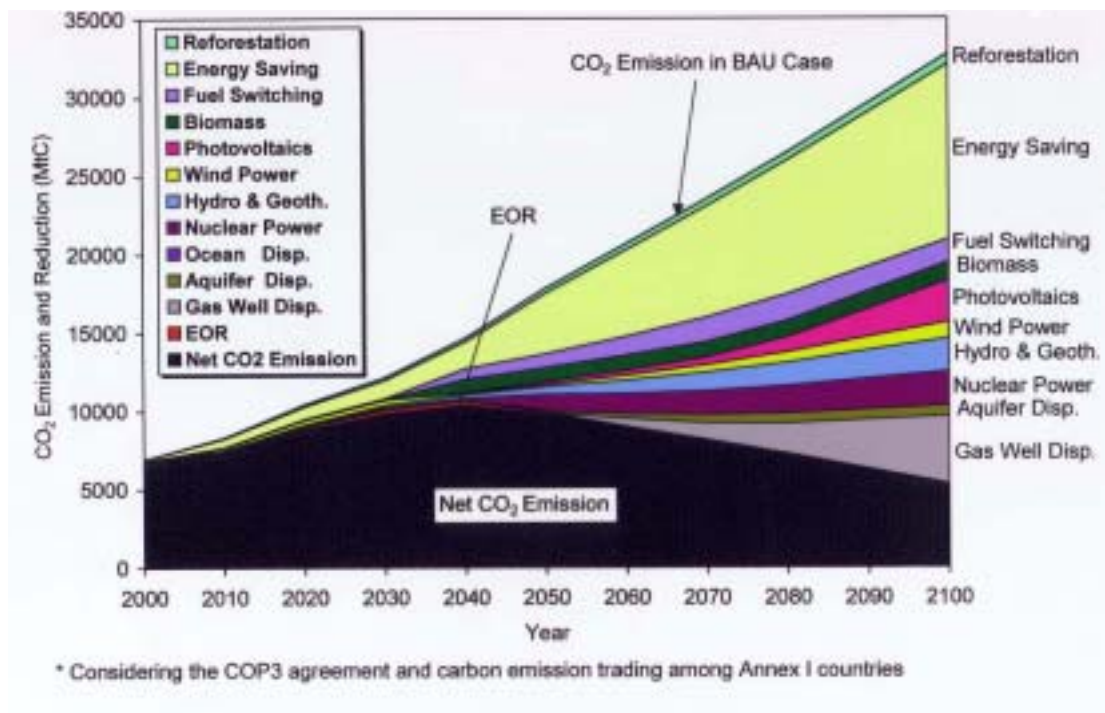


FIG. 2. CO₂ emission reduction effects of technological options under a 550 ppmv limit.

Not only substitution of coal by natural gas and other less carbon dependent fossil fuels than coal, but also various new measures such as introduction of renewable energy as photovoltaics, wind power and biomass and of CO₂ removal and disposal should be expanded. Nevertheless these measures are still in their infancy and vast, extraordinary efforts are called for to satisfy the above requirements well in time.

When we look at short term future envisaged by the Kyoto protocol, the situation may be more serious despite that it aims only at reducing GHG's to a certain degree as the first step toward the realization of the ultimate target of stabilizing GHG concentrations in air. Let us take the case of Japan as an example. The government of Japan agreed in Kyoto to reduce GHG emission by 6 % by around 2010 when compared to the level in 1990. According to the government plans GHG emission should be stabilized by efforts of energy conservation and fuel switching, and furthermore be reduced by 6 % by other efforts such as utilization of emission trading. However we also foresee a number of difficulties in putting these measures into effects. To realize this let us look at recent macroscopic figures of economy and energy in Japan . We see that about 95% of radiative forcing of GHG's from Japan comes from CO₂. So focussing our attention only on CO₂, the author introduces a simple analytical tool, i.e. disaggregation of CO₂ emission in the following factors [3].

$$\text{CO}_2 = (\text{CO}_2 / \text{Energy}) (\text{Energy} / \text{GDP}) \text{GDP} \quad (1)$$

where CO₂/Energy (or C/E) is the carbon intensity of primary energy, Energy/GDP (or E/G) is the energy intensity and GDP is the gross domestic product.

Table I Rates of Change of 3 factors(%/year)

	Carbon intensity C/E	Energy Intensity E/G	Gross Domestic Product GDP	CO2 emission
1980-89	- 0.7	- 1.8	+ 3.5	+ 0.7
1990-99	- 0.6	+ 0.4	+ 1.1	+ 0.9
2000-2010 (scenario)	- 0.6	- 2.2	+ 2.0	- 0.8
20 th century, world average	- 0.3	- 0.9	+ 3.0	+ 1.8

Equation (1) means that the average rate of change of CO₂ emission is simply a sum of those of three factors, i.e. C/E, E/G and GDP. Table I exhibits recent trends of these figures together with those for the government plan for next 10 years. It is seen that we are required to reverse the trends of energy conservation of last ten years and also to keep the level of fuel switching despite of worsening public acceptance of nuclear power.

2. IMPORTANCE OF IDENTIFYING GHG SOURCES AND THE ROLE OF JST

In the previous section the author has stressed how difficult it is to reduce GHG's. Nevertheless, possible serious outcomes of global warming such as sea level rise compels us to doing all kinds of efforts for mitigating global warming. We should also notice the

importance of scientific efforts to reduce uncertainties about GHG emission and sink sources and also their quantities.

In case of CO₂ its anthropogenic emission sources are mainly in energy and industry sectors and the total amount of its emission can be evaluated from economic and industrial statistics of fossil fuel consumption. However we have only limited knowledge about CO₂ absorption by geosphere and ocean: the word "missing sink" symbolizes this situation.

More uncertain are emissions and absorptions of other GHG's such as CH₄ and N₂O. Unlike CO₂ any data of anthropogenic emissions of these gases are not available in ordinary statistics. CH₄ emission sources include natural gas fields, gas pipelines, rice fields, landfills and cows and N₂O comes from agriculture, industry and energy consumption. There are estimates of these emissions but with much lower accuracy than that those of CO₂. At non CO₂ GHG session of GHGT-5 held in Cairns, Australia in August 2000 a question raised from the floor to the authors of the session about the accuracy of their estimates of emissions, and the reply indicated the accuracy of estimates of CH₄ and N₂O to be around 50-100 %.

Taking into account that not only CO₂ but also CH₄ and N₂O are "official" GHG's registered in Kyoto protocol we are required to make efforts for identifying emissions of these gases with as high accuracy as possible. The first step to do this is to identify where these gases come from and then how much they are. The author is convinced that the technology of isotopes and isotopomers helps very much this process and appreciates in this sense the efforts by NOAA CMDL GHG group to expand global networks of measuring GHG's.

REFERENCES

- [1] HOUGHTON, J.T (Ed.), Climate Change 1995, The Science of Climate Change, Cambridge University Press, (1995) 25.
- [2] KAYA, Y. (Ed.), The strategy for reducing CO₂, Nikkan-Kogyo Newspaper Co. (2000) 77 (in Japanese).
- [3] BRUCE J.P. ET AL (Ed.), Climate Change 1995, Economic and Social Dimensions of Climate Change, Cambridge University Press (1995) 27.

ISOTOPOMER FRACTIONATION DURING PHOTOLYSIS OF NITROUS OXIDE BY ULTRAVIOLET OF 206 TO 210 nm

S. TOYODA*

Department of Environmental Chemistry and Engineering,
Tokyo Institute of Technology,
Yokohama, Japan

N. YOSHIDA*, T. SUZUKI

Department of Environmental Science and Technology,
Tokyo Institute of Technology,
Yokohama, Japan

K. TSUJI, K. SHIBUYA

Department of Chemistry,
Tokyo Institute of Technology,
Tokyo, Japan

Abstract. Nitrous oxide (N_2O) is an important trace gas in the stratospheric chemistry as well as in the tropospheric radiative balance. Although there have been observations on the distribution of N_2O in the atmosphere and its flux from individual sources, the global N_2O budget is not fully understood. The isotopic information of N_2O has been useful for constraining the N_2O cycle since each source and sink has its own isotopic signature and isotope fractionation that is unique to the process. We have recently developed a method to determine isotopomers of N_2O and showed that intramolecular distribution of ^{15}N is a parameter that has more fundamental and sensitive information than bulk ^{15}N abundance for constraining the atmospheric N_2O budget. Here, we report the fractionation of isotopomers during ultraviolet photolysis of N_2O in a 206 to 210 nm region. The fractionation factors are different among isotopomers and the site preference between two nitrogen isotopomers becomes larger along with the photolysis. The isotopomer fractionation factors of this representative wavelength are close to the apparent fractionation factors observed in the stratosphere indicating ultraviolet photolysis in the stratosphere is the dominant sink of N_2O . Sources of atmospheric N_2O including terrestrial and oceanic biological processes, agricultural activities, industrial formation and fossil fuel combustion are expected to be characterized to better constrain the global budget of N_2O .

1. INTRODUCTION

Nitrous oxide is an important trace gas in the atmosphere. Although its abundance in the troposphere is about 316 ppb, it has a global warming potential as well as carbon dioxide and methane and is increasing by about $0.3\% \text{yr}^{-1}$ [1]. In the stratosphere, N_2O is decomposed by ultraviolet photolysis and photo-oxidation with an excited oxygen atom, and the reactive decomposition products are incorporated into ozone depleting reactions [2]. Sources of atmospheric N_2O exist in the troposphere and include terrestrial and oceanic biological processes such as nitrification and denitrification, industrial formation as a byproduct in nylon production, fossil fuel combustion, and so on [1]. However, the global N_2O budget is not fully understood.

Natural isotope abundance in N_2O can be used to constrain the N_2O cycle [3,4], as similar manner that applied to carbon dioxide, methane, and so on. Previous studies revealed that N_2O in the stratosphere is enriched in ^{15}N and ^{18}O [4,5], and the back flux of such heavy N_2O

* With CREST project, Japan Science and Technology Corporation.

from the stratosphere into the troposphere is considered an important key to estimate the magnitude of surface natural and industrial source of N₂O. We have developed a mass-spectroscopic method to determine isotopomers of nitrous oxide [6] and found that the enrichment in ¹⁵N at the center position of the asymmetric NNO molecule is larger than at the end position for the tropospheric N₂O, and that the difference increases in the stratosphere [7]. Almost concurrently, other researchers have also reported similar site-specific enrichment in ¹⁵N of N₂O in the stratosphere by similar manner as ours [8] or infrared absorption spectroscopy [9].

The mechanism of the heavy-isotope enrichment of N₂O was first supplied by the theoretical calculation in Ref. [10], which showed that the shift of N₂O absorption spectrum due to the difference in zero-point energy of each isotopomers causes the fractionation. They predicted the difference of the ¹⁵N enrichment at the two intra-molecular sites and wavelength dependence of the enrichment, which turned to be generally in accordance with recent laboratory experiments [11-13] and stratospheric observations [9,14].

However, recent laboratory photolysis experiments showed disagreement with the theoretical calculation in the magnitude of the enrichment. In addition, apparent enrichment factors obtained from stratospheric observations are variable with altitude [14] presumably because the actual photolysis occurs by variable spectrum of the sun instead of monochromatic light.

In this paper, we intend to estimate the fractionation factors of isotopomers of N₂O in the stratospheric sink processes by simulating the photolysis, to discuss about wavelength dependence of the fractionation factor and compare the results with other simulation experiments and theoretical calculations, and to compare the results with stratospheric observations and discuss about N₂O behavior in the stratosphere.

2. NOMENCLATURE

We define an isotopomer as one of the set of molecules that are isotopically substituted. Since N₂O has an asymmetric structure, and nitrogen and oxygen have two and three stable isotopes, respectively, following five isotopomers are significant at natural abundance level: ¹⁴N¹⁴N¹⁶O, ¹⁴N¹⁵N¹⁶O, ¹⁵N¹⁴N¹⁶O, ¹⁴N¹⁴N¹⁷O and ¹⁴N¹⁴N¹⁸O. If we name the center and end positions of the nitrogen atom α and β , respectively, we can define isotopomer ratio for each position, and express it as a permil deviation from the reference material [6]:

$$\delta^{15}\text{N}^{\alpha} = \{^{15}R^{\alpha} / ^{15}R(\text{std}) - 1\} \times 1000 \quad (1)$$

$$\delta^{15}\text{N}^{\beta} = \{^{15}R^{\beta} / ^{15}R(\text{std}) - 1\} \times 1000 \quad (2)$$

where ¹⁵R denotes the ratio of ¹⁵N to ¹⁴N and ¹⁵R(std) is the ratio for atmospheric N₂, the standard material for nitrogen isotope ratio.

Conventional “nitrogen isotope ratio in N₂O” equals the average of two isotopomer ratios since it does not distinguish these two isotopomers:

$$\begin{aligned} \delta^{15}\text{N}^{\text{bulk}} &= \{^{15}R^{\text{bulk}} / ^{15}R^{\text{bulk}}(\text{std}) - 1\} \times 1000 \\ &= (\delta^{15}\text{N}^{\alpha} + \delta^{15}\text{N}^{\beta}) / 2. \end{aligned} \quad (3)$$

Oxygen isotope ratios are expressed by conventional notation:

$$\delta^{17}\text{O} = \{^{17}R / ^{17}R(\text{std}) - 1\} \times 1000 \quad (4)$$

$$\delta^{18}\text{O} = \{^{18}R / ^{18}R(\text{std}) - 1\} \times 1000 \quad (5)$$

where ^{17}R and ^{18}R are the ratio of ^{17}O and ^{18}O to ^{16}O , respectively, and standard material is standard mean ocean water (SMOW).

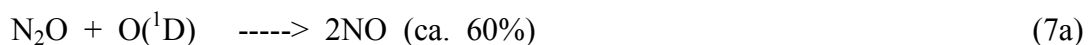
3. EXPERIMENTAL

3.1. Photolysis experiments

Since nitrous oxide has an absorption band in a 170 to 230 nm region that overlaps with the so-called “atmospheric window” ranging between 200-210 nm in the stratosphere, it is photolyzed to molecular nitrogen and excited oxygen atom [15]:



One more reaction known as N_2O sink is oxidation by $\text{O}(^1\text{D})$ produced mainly by the photolysis of ozone [15]:



When integrated over the whole stratosphere, relative contributions of these reactions are 90 and 10%, respectively [16], so we first concentrated on the photolysis in this study. To avoid the possible side reaction with $\text{O}(^1\text{D})$ produced by the photolysis of N_2O , we quenched the excited oxygen by nitrogen gas [17, 18] and checked its effectiveness by changing mixing ratio of N_2 and N_2O .

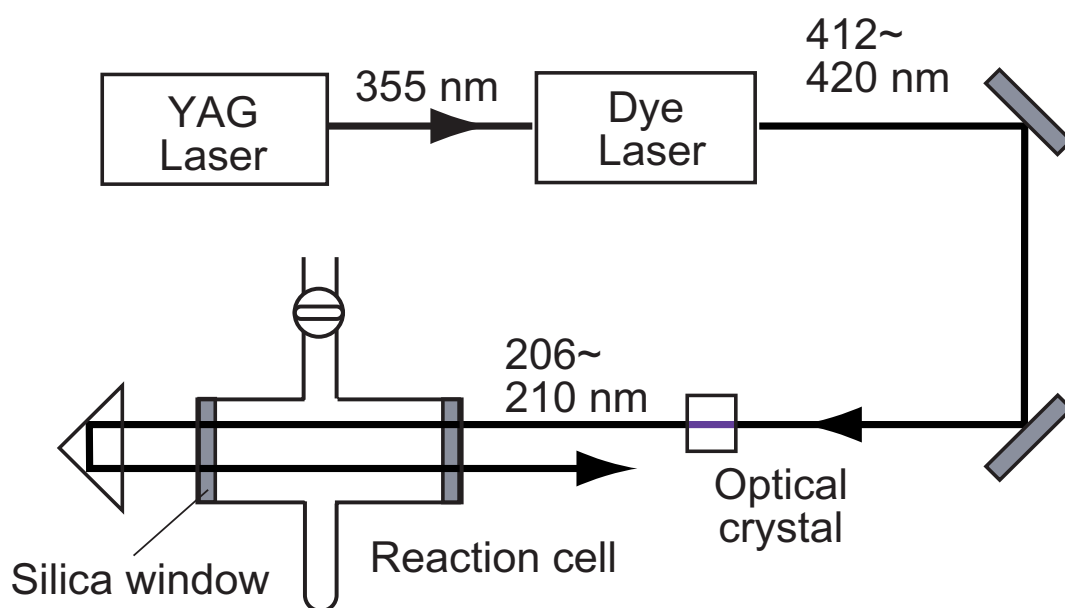


FIG. 1. Apparatus used for photolysis of N_2O .

Figure 1 shows a schematic diagram of our experimental setup for photolysis. We used a dye laser (Lambda Physik, SCANMATE2) pumped by the third harmonic of a Nd:YAG laser (Continuum, Powerlite 8000) to generate the light of between 412 and 420 nm, and obtained the second harmonics of 206.1, 207.1, 209.1 and 210.1 nm through a BBO-A crystal. The light source operates at a repetition rate of 10 Hz with a 206-210 nm pulse energy of ~ 0.4 mJ, pulse duration of 10 ns and resolution of 0.2 cm^{-1} . The wavelengths of 412 and 414 nm were obtained through Exalite 411 (Exciton, INC., dissolved in p-dioxane, approximately 7×10^{-4} mol/l), and those of 418 and 420 nm were obtained through Exalite 416. Calibration of the wavelength was carried out by measuring opto-galvanic spectra of Ne.

An aliquot ($\sim 2.5 \text{ cm}^3 \text{STP}$) of N_2O ($\delta^{15}\text{N}^{\text{bulk}} = -1.59\text{‰}$, $\delta^{15}\text{N}^{\alpha} = -3.61\text{‰}$, $\delta^{15}\text{N}^{\beta} = 0.42\text{‰}$ and $\delta^{18}\text{O} = 21.70\text{‰}$, determined by our N_2O isotopomer standard that were calibrated against atmospheric N_2 and SMOW [6]) was introduced to a Pyrex glass cell of 4 cm inside diameter and 24 cm length (approximately 300 cm^3 volume). The cell was equipped with UV-transparent silica windows of 2 mm thickness at both ends, and optically illuminated area was estimated at about 0.2 cm^2 .

For the quenching of $\text{O}(^1\text{D})$, ultra pure N_2 ($>99.9998\%$, Nippon Sanso Co., Ltd.) was added. Mixing ratio of N_2 to N_2O was typically set to be 150 after the similar photolysis experiment of Ref. [18], but in the experiment at 207 nm, the ratio of 50, 100, and 200 was also tested. Total pressure of the sample mixture was $4.3 \times 10^4 \sim 1.3 \times 10^5 \text{ Pa}$ (320 \sim 1000 Torr).

After the sample mixture was irradiated at room temperature for 3 to 10 hours, residual N_2O was collected at 77 K and purified through cold bath at $\sim 200 \text{ K}$ (for drying) and Ascarite (Thomas Scientific, for removing trace CO_2). Amount of the N_2O was measured manometrically.

3.2. Mass spectrometric analysis

Isotopomer ratios of the photolyzed samples are measured relative to non-photolyzed N_2O on a modified Finnigan MAT 252 mass spectrometer (Thermoquest K.K.) using a conventional dual inlet. Experimental details are given elsewhere [6]. Briefly, intramolecular distribution of ^{15}N was determined by analyzing molecular and fragment ions of N_2O produced by electron impact ionization. NO^+ contains α nitrogen only, while N_2O^+ contains both α and β nitrogen, so that we can deduce the isotope ratio in nitrogen for both α and β site. When converting measured ratios to isotopomer ratios, we applied experimentally determined correction factor for scrambling of nitrogen atom during ionization, and assumed the mass-dependent relationship between abundance of ^{17}O and ^{18}O [17].

4. RESULTS AND DISCUSSION

To analyze the isotopomer data, we assume that the photolysis is irreversible reaction and that isotope fractionation factor is constant during the reaction. Then, the isotopomer ratios should satisfy Rayleigh equation and we can obtain the enrichment factor ϵ from relationship between isotopomer ratios and residual fraction of N_2O [18].

$$\delta - \delta_0 = \epsilon \ln f \quad (8)$$

where

δ is isotopomer ratio (‰),

ϵ is the enrichment factor (‰),

f is the remaining fraction of N_2O ($=[\text{N}_2\text{O}]/[\text{N}_2\text{O}]_0$),

and parameters with subscript zero correspond to the values before photolysis.

Figure 2 shows Rayleigh plots obtained at 207.1 nm. It is clear that all isotopomer ratios are getting higher with the progress of the photolysis, and enrichment in ^{15}N is higher at α site than at β site.

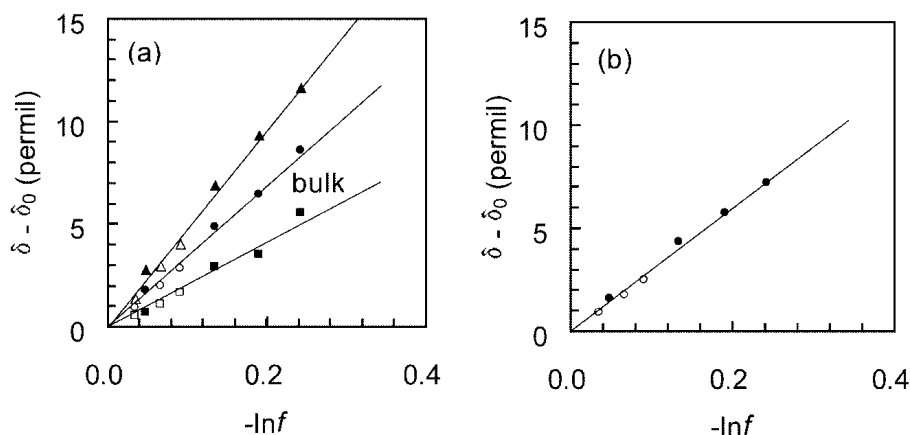


FIG. 2. Rayleigh plots for photolysis of N_2O at 207.1 nm for ^{15}N -containing isotopomers (a) and ^{18}O -containing isotopomers (b).

Three open symbols in each plot in Fig. 2 were obtained when the mixing ratio of N_2 and N_2O were 200, 50, and 100, although irradiation time is also different. We can see that the quenching of excited oxygen atom was effective and hence contribution of photo-oxidation was negligible.

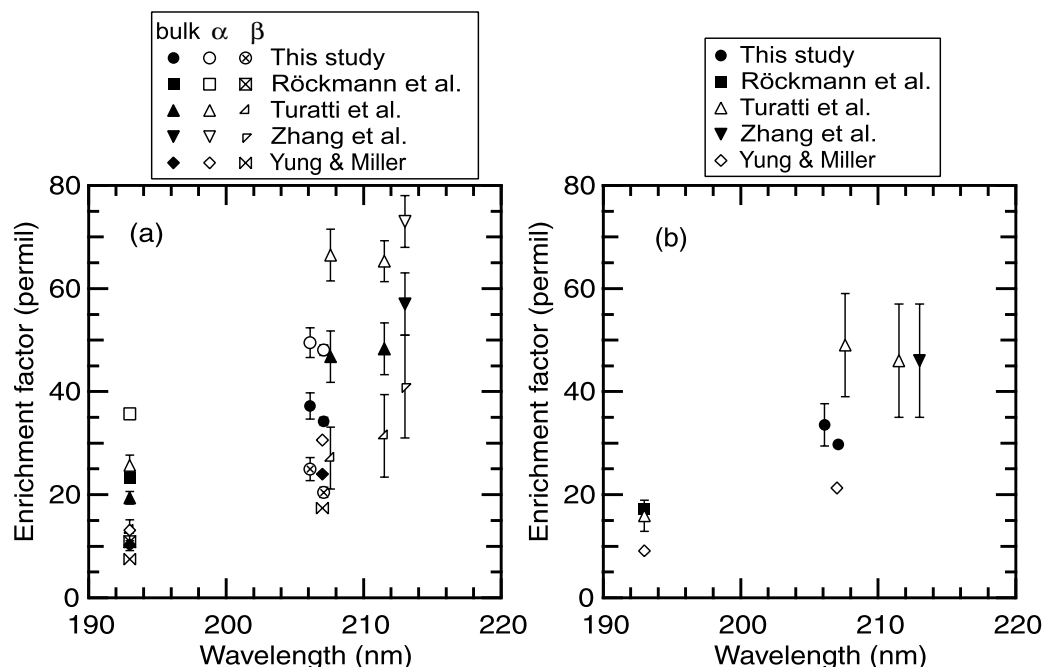


FIG. 3. Enrichment factors during photolysis at various wavelengths experimentally obtained in this study and others [11,12,13], and theoretically calculated value of Ref. [10,19]. For the convenience for comparison, enrichment factors are shown by positive value, although they are negative in our definition using Eq (8) in text. Error bars show the standard deviations of the regression slopes.

In Fig. 3 shown are the enrichment factors obtained at 206.1 and 207.1 nm together with the similar experimental data reported in Ref. [11-13] and theoretical calculation in Ref. [19]. The photolysis at 209 and 210 nm was not successful because the BBO crystal was gradually degraded during the experiments at shorter wavelengths. Nitrous oxide was decomposed only by 8% after 15-hour irradiation and we were able to obtain only three and two data points at 209 and 210 nm, respectively. Thus, the data at 209 and 210 nm were found to give larger errors or offsets when we fit the data by linear regression and calculate the slope (not shown).

Our results at 206.1 and 207.1 nm show smaller values than the experimental data in Ref. [12] at 207.6 nm for each isotopomers. The difference seems to have been caused by some difference of experimental details including analysis of the isotopomers (FTIR absorption spectroscopy was used in Ref. [12]) and/or the dependency of enrichment factor on wavelength though we cannot resolve the effect of these factors at present. However, it is clear that the enrichment factors increase with wavelength when we compare the existing data at 193 nm [11,12] and at 211 [12] and 213 nm [13]. This is in accordance with the prediction in Ref. [10] and we can confirm that their theoretical treatment is generally appropriate. However, a closer look at the experimental and theoretical enrichment factors reveals that the former is higher than the latter for the whole wavelength range and for the all isotopomers. An explanation of this discrepancy has been recently proposed by Ref. [13] that the simple approximation of the model does not consider the dissociation of initially excited N₂O molecule. Our results support such suggestion that further revision should be needed in theoretical calculation.

Next, we compared the enrichment factors of simulation experiments with those of stratospheric observations. We have observed the vertical profiles of N₂O isotopomers over Japan using a balloon-borne cryogenic air sampler [14]. Although the apparent enrichment factor obtained by applying Rayleigh model was not constant throughout the stratosphere, we found it constant if we divide the stratosphere into the higher and lower region at the altitude of about 24 km. The shaded area in Fig. 4 indicates the apparent enrichment factor with estimated error in regression analysis.

In Fig. 4, the slope of the wavelength dependence of the photolysis enrichment factor shows a positive correlation with the difference of stratospheric apparent enrichment factors between higher and lower region, so that the wavelength at the crossing point of the regression line and shaded area is almost same for all isotopomers. If we assume the fractionation of N₂O is solely caused by photolysis, this may indicate that in the higher region, the contribution of longer wavelength is larger than in the lower region.

In fact, the stratospheric *in situ* enrichment factor during photolysis ($\epsilon_{\text{photo}}^*$) is weighted mean of enrichment factors in photolysis at wavelength λ ($\epsilon_{\text{photo}}(\lambda)$) over the whole wavelength range, where the product of actinic flux (I) and absorption cross section (σ) is taken as a weight. Therefore, if we define effective wavelength (λ_{eff}) at which ϵ_{photo} equals the $\epsilon_{\text{photo}}^*$, it is possibly dependent on altitude, latitude, seasons, and so on [14]:

$$\begin{aligned}\epsilon_{\text{photo}}^* &= \int \epsilon_{\text{photo}}(\lambda) I(\lambda) \sigma(\lambda) d\lambda / \int I(\lambda) \sigma(\lambda) d\lambda \\ &= \epsilon_{\text{photo}}(\lambda_{\text{eff}}).\end{aligned}\tag{9}$$

This may explain the difference of stratospheric enrichment factor between higher and lower region and suggests that there would be variation in $\epsilon_{\text{photo}}^*$ with respect to time and space.

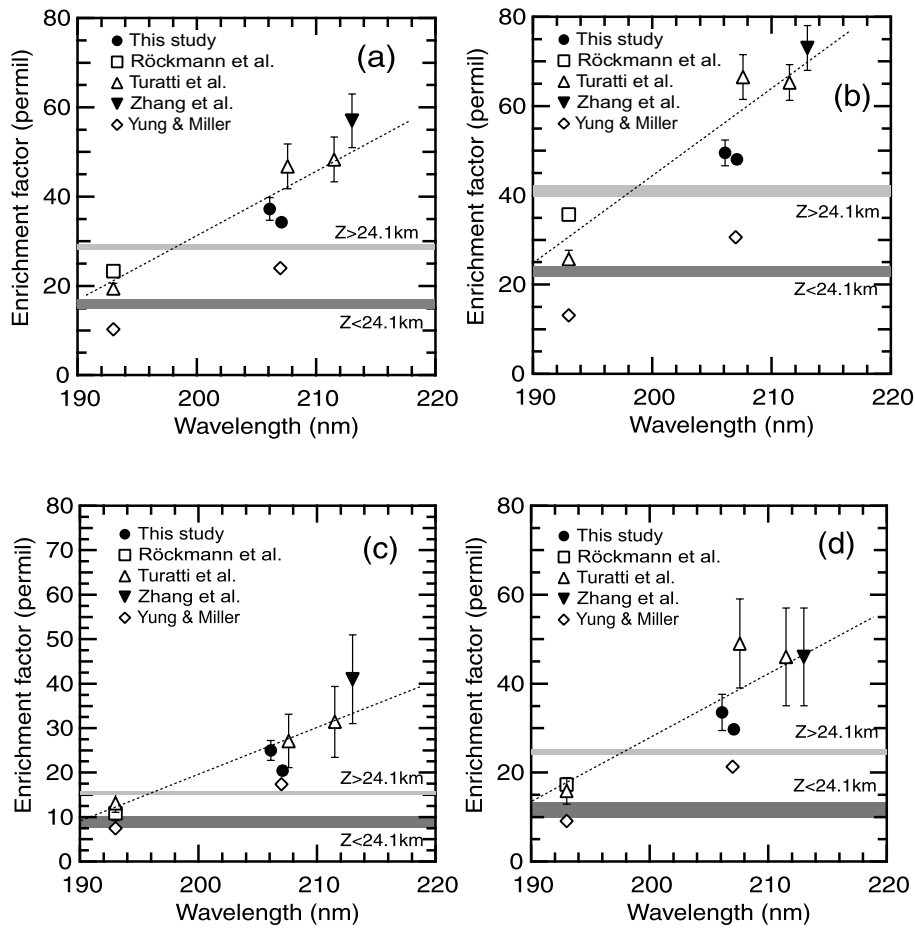


FIG. 4. Comparison of apparent enrichment factors observed in the stratosphere over Japan [14, shaded area] and photolysis enrichment factors obtained in laboratory experiments for (a), bulk nitrogen; (b), α nitrogen; (c), β nitrogen; (d) oxygen. Dotted lines are regression lines for the photolysis data.

Another factor that can affect the apparent enrichment is mixing of N_2O that has been decomposed in different extent. This can occur during transportation of N_2O in the stratosphere. Authors of Ref. [18] showed that a simple one-dimensional diffusion model gives the apparent enrichment factor reduced by about 50% and it can explain the difference of enrichment factors between Ref. [10] and their observations for bulk N and O in the lower stratosphere [5].

One more possible factor is contribution of photo-oxidation, Eqs (7a) and (7b). According to Ref. [17], enrichment in oxygen isotope of N_2O is less in photo-oxidation than in photolysis. Although there are no data respect to bulk and site-specific nitrogen isotope ratio, contribution of this sink reaction may decrease the apparent enrichment factor. From the higher to the lower altitudes, actinic flux contributing photolysis of N_2O becomes weaker exponentially because of the absorption by ozone, while the production rate of $\text{O}(^1\text{D})$ does not decrease as rapidly [15]. Therefore, the lower enrichment in the lower region of the stratosphere may indicate that in the lower stratosphere contribution of photo-oxidation to N_2O destruction is larger than 10%, that is currently estimated value for whole stratosphere based on a two-dimensional photochemical model [16]. Our estimation based on observations and available data of laboratory experiments indicated that the contribution of photo-oxidation could be up to 60% in the lower stratosphere [14].

5. CONCLUDING REMARKS

Enrichment of heavy isotopomers of N₂O during photolysis at 206 and 207 nm was different between each isotopomers, which is in accordance with other simulation experiments, theoretical calculation, and stratospheric observations. Magnitude of the enrichment is higher than that of the theoretical calculation, suggesting that the simple model of the latter should be revised. Comparison with other experiments conducted at different wavelength ascertains that the enrichment factor depends on the wavelength. *In situ* enrichment factors obtained from stratospheric observations suggest that the effective wavelength in photolysis would be variable between 190 and 200 nm when compared to those of photolysis experiments, but factors other than photolysis should also be investigated.

REFERENCES

- [1] PRATHER, M.J., et al., Other trace gases and atmospheric chemistry, in *Climate Change 1994: Radiative Forcing of Climate Change and an Evaluation of the IPCC IS92 Emission Scenarios*, Houghton J. T. et al. (Ed.), Cambridge Univ. Press, New York (1994) 73-126.
- [2] CRUTZEN, P.J., The influence of nitrogen oxides on the atmospheric ozone content, *Quart. J. R. Met. Soc.* **96** (1970) 320-325.
- [3] YOSHIDA, N., MATSUO, S., Nitrogen isotope ratio of atmospheric N₂O as a key to the global cycle of N₂O, *Geochemical Journal* **17** (1983) 231-239.
- [4] KIM, K.-R., CRAIG, H., Nitrogen-15 and oxygen-18 characteristics of nitrous oxide: A global perspective, *Science* **262** (1993) 1855-1857.
- [5] RAHN, T., WAHLEN, M., Stable isotope enrichment in stratospheric nitrous oxide, *Science* **278** (1997) 1776-1778.
- [6] TOYODA, S., YOSHIDA, N., Determination of nitrogen isotopomers of nitrous oxide on a modified isotope ratio mass spectrometer, *Anal. Chem.* **71** (1999) 4711-4718.
- [7] YOSHIDA, N., TOYODA, S., Constraining the atmospheric N₂O budget from intramolecular site preference in N₂O isotopomers, *Nature* **405** (2000) 330-334.
- [8] BRENNINKMEIJER, C.A.M., RÖCKMANN, T., Mass spectrometry of the intramolecular nitrogen isotope distribution of environmental nitrous oxide using fragment-ion analysis, *Rapid Commun. Mass Spectrom.* **13** (1999) 2028-2033.
- [9] GRIFFITH, D.W.T., et al., Vertical profiles of nitrous oxide isotopomer fractionation measured in the stratosphere, *Geophys. Res. Lett.* **27** (2000) 2485-2488.
- [10] YUNG, Y.L., MILLER, C.E., Isotopic fractionation of stratospheric nitrous oxide, *Science* **278** (1997) 1778-1780.
- [11] RÖCKMANN, T., et al., Measurement of the isotope fractionation of ¹⁵N¹⁴N¹⁶O, ¹⁴N¹⁵N¹⁶O and ¹⁴N¹⁴N¹⁸O in the UV photolysis of nitrous oxide, *Geophys. Res. Lett.* **27** (2000) 1399-1402.
- [12] TURATTI, F., et al., Positionally dependent ¹⁵N fractionation factors in the UV photolysis of N₂O determined by high resolution FTIR spectroscopy, *Geophys. Res. Lett.* **27** (2000) 2489-2492.
- [13] ZHANG, H., et al., Fractionation of ¹⁴N¹⁵N¹⁶O and ¹⁵N¹⁴N¹⁶O during photolysis at 213 nm, *Geophys. Res. Lett.* **27** (2000) 2481-2484.
- [14] TOYODA, S., et al., Fractionation of N₂O isotopomers in the stratosphere, *J. Geophys. Res.* **106** (2001) 7515-7522.
- [15] DEMORE, W.B., et al., Chemical kinetics and photochemical data for use in stratospheric modeling, Eval. 12, JPL Publ. 97-4, Pasadena (1997).
- [16] MINSCHWANER, K., et al., Absorption of solar radiation by O₂: Implications for O₃ and lifetimes of N₂O, CFCl₃, and CF₂Cl₂, *J. Geophys. Res.* **98** (1993) 10543-10561.

- [17] JOHNSTON, J.C., et al., Measurement of multioxygen isotopic ($\delta^{18}\text{O}$ and $\delta^{17}\text{O}$) fractionation factors in the stratospheric sink reactions of nitrous oxide, J. Geophys. Res. **100** (1995) 16801-16804.
- [18] RAHN, T., et al., Stable isotope fractionation during ultraviolet photolysis of N_2O , Geophys. Res. Lett. **25** (1998) 4489-4492.
- [19] MILLER, C.E., YUNG, Y.L., Photo-induced isotopic fractionation of stratospheric N_2O , Chemosphere-Global Change Science **2** (2000) 255-266.

DETERMINATION OF ISOTOPOMERS IN POOLS OF MOLECULES WITH POLYISOTOPIC ELEMENTS

A.M. ZYAKUN

Skryabin Institute of Biochemistry and Physiology of Microorganisms,
Russian Academy of Sciences, Pushchino, Moscow Region, Russian Federation

C.A.M. BRENNINKMEIJER

Max Planck Institute for Chemistry, Mainz, Germany

Abstract. Polyisotopic element atoms that are present in a molecule form a pool of isotopomer molecules. Mono- and polyisotopomers are distinguished depending on the quantity of atoms of polyisotopic elements. Methodical approaches have been considered for the quantitative determination of the isotope composition of an element included in mono- and polyisotopic molecules. A possibility of the equally probable (homogeneous) and non-equally probable (non-homogeneous) distribution of isotopes of a polyisotopic element, the atoms of which have different positions in the molecule of polyisotopomer, has been shown. Factors disturbing the homogeneous distribution of isotopes of the element in the polyisotopomer pool have been revealed. When a polyisotopomer is involved in a mass-dependent process or reaction, the homogeneity of isotope distribution of the element is disturbed both in the residual and newly formed pools of polyisotopomer. By the example of CO₂ (polyisotopomer by oxygen) it has been shown that one can judge of the history of the analyzed pool formation by distribution of oxygen isotopes within this pool. The isotope content in the oxygen sites of polyisotopomer is a diagnostic feature of CO₂ involvement in the efflux from a reservoir or influx to the analyzed reservoir from an external source.

1. INTRODUCTION

In the course of their study of radioactive elements, Soddy [1] and Fajans [2] first revealed compounds (isotopes) which contained atoms of an element different in weight but having the same nuclear electric charge and close chemical properties. By the example of neon, Thomson [3] demonstrated the existence of isotopes in light elements using a mass spectrograph. Also Aston [4] and Dempster [5] detected and measured isotope abundances of many other elements with the use of a mass spectrograph. Thus, it was shown that there are natural pools of molecules, which contain isotopic atoms of the corresponding polyisotopic element, i.e., *isotopomers*. Mono- and polyisotopomers are distinguished depending on the quantity of atoms of this element in the molecule structure.

Monoisotopomers are molecules with only one atom of polyisotopic element in their structure. *Polyisotopomers* are molecules with two and more atoms of polyisotopic element. If polyisotopomer by element A contains another element B, then this polyisotopomer may be *symmetrical* or *asymmetrical* relative to element B. In its turn, element B may be a mono- or polyisotopic element. If it is monoisotopic, then there is only one cluster of molecules isotopically different by element A (a *monocluster* pool of polyisotopomer). If element B is a polyisotopic element, then each of its isotopes will have a corresponding cluster of molecules isotopically different by element A (i.e., a *polycluster* pool of polyisotopomer). Carbon dioxide (CO₂), for example, as a polyisotopomer by oxygen, will be a symmetrical isotopomer relative to carbon and consist of ¹²C- and ¹³C-clusters. Polyisotopomer by nitrogen N₂O will be an asymmetrical isotopomer relative to oxygen and consist of three clusters (¹⁶O-, ¹⁷O-, and ¹⁸O-clusters). Polyisotopomer tetrafluoroethylene (F₂CCF₂) will be a symmetrical and monocluster polyisotopomer by carbon. It should be noted that, according to

the established practice, the isotopic composition of element A is measured by the quantitative analysis of molecules isotopically different by this element, using the cluster of the most widespread isotope of element B. The abundances of isotopic atoms for mono- and polyisotopomers are measured by different methodical approaches. The current report was aimed to analyze the known methods of measuring the abundances of stable isotopes of elements occurring in the pool of mono- and polyisotopomers.

2. THEORY

2.1. Monoisotopomers

Precision mass spectrometric measurements of the ratios of abundances of stable isotopes in monoisotopomers were initially developed in [6-10]. The analysis of isotope abundances of the polyisotopic element A occurring in a monoisotopomer consists in the quantitative determination of the ratio of isotopically different molecules with the element A in the monoisotopomer pool, i.e.,

$$R = [{}^pA]/[{}^qA] \quad (1)$$

where $[{}^pA]$, $[{}^qA]$ are quantities of molecules containing pA and qA isotopes of the analyzed element A ($q > p$). The equation describing the isotope distribution in the molecule pool of the monoisotopomer can be written as

$$R - R_0 = 0 \quad (2)$$

where R is a variable, R_0 is the ratio of abundances of isotopically distinctive molecules pA and qA in the pool of the tested monoisotopomer.

Modeling the efflux of the monoisotopomer from a reservoir as a first order reaction would give us the ratios of isotopic abundances (r_f) in a residual part $(1-f)$ of the monoisotopomer pool to the initial isotopic ratio (r_0) as

$$r_f = r_0(1-f)^{1/\alpha-1} \quad (3)$$

where α is the discrimination (fractionation) coefficient of the qA isotope containing monoisotopomer relative to the pA isotope containing monoisotopomer; f is the fraction of monoisotopomer which has left the reservoir; and $r = 1/R = [{}^qA]/[{}^pA]$.

Analogous to the monoisotopomer efflux, the ratios of the element A isotopic abundances (p_f) in the isotopomer pool transferred from a donor reservoir can be expressed as

$$p_f = r_0(1-(1-f)^{1/\alpha})/f \quad (4)$$

If the monoisotopomer containing the element A has three or more isotopic atoms (for instance, oxygen has three isotopes: ${}^{16}\text{O}$, ${}^{17}\text{O}$ and ${}^{18}\text{O}$), there are three or more isotopically distinctive species of molecules. In this case, the abundances of these molecules make up a set of the isotope abundance ratios of the element A. Using one isotopic molecule species as a reference, the quantities of other two or more isotopically distinct molecules can be compared with the above quantity of molecules. Mass dependent or mass independent fractionation may occur only in the molecule pool of the monoisotopomer bearing the element with more than two isotopes.

2.2. Polyisotopomers

The isotope abundances of polyisotopic element in the pool of polyisotopomer were first measured by the analysis of the corresponding monoisotopomers obtained from polyisotopomers. For example, the $^{13}\text{C}/^{12}\text{C}$ ratios in organic substances (polyisotopomers by the carbon element) were determined using CO_2 (monoisotopomer by carbon), which was obtained by quantitative oxidation of these substances. It is obvious that the differences in the carbon isotope content of different carbon positions in the polyisotopomer molecule are leveled by this operation. Isotopic variations of the element constituent of polyisotopomer were revealed by specific chemical reactions isolating structures with the analyzed element. For example, in case of amino acids and organic acids it was possible to isolate and measure the carbon isotopic composition of the carboxyl group and the rest part of the molecule separately, using the reactions of decarboxylation [11]. It was shown that amino acids produced by photoautotrophs were characterized by the lower content of isotope ^{13}C in the alkyl portion of the amino acids as compared with their carboxyl group. On the other hand, amino acids synthesized by heterotrophic organisms have in their carboxyl groups the carbon atoms with the lower content of ^{13}C isotope relative to the rest part of the amino acids.

Thus, the isotope distribution of the polyisotopic element A in the polyisotopomer pool may be intramolecularly heterogeneous, i.e., the ratio of abundances of isotopic atoms of the element A may be distinguished in different sites in the molecule.

Possible finding of isotopic heterogeneity (non-homogeneity) in a polyisotopomer by the quantitative mass spectrometric analysis of the ratios of its isotopically distinctive molecule ions was first proposed in 1974 [12]. Later, this approach was further developed by the examples of analysis of the oxygen isotope composition of CO_2 as an oxygen diisotopomer [13, 14]. The idea of calculation of isotope distribution of the element A in the polyisotopomer pool using a set of isotopically distinctive molecules will be considered in details in the next part.

For simplicity of reasoning, let us consider the distribution of isotopes pA and qA of the element A in the diisotopomer pool. Abundances of these isotopes are equal to a and b , respectively (where $a + b = 1$ by definition) and their isotopic composition is represented by value $R = a/b$. If the element A has the same isotope abundances by positions 1 and 2 in the molecule (i.e., $R_1 = R_2 = R_0 = a/b$), then the equation characterizing the distribution of isotopes in the pool of this isotopomer can be formulated as

$$(R - a/b)^2 = 0, \quad (5)$$

where a and b are abundances of isotopes pA and qA of the analyzed element A.

If $b \neq 0$, then the equation (5) will be written as

$$b^2 R^2 - 2abR + a^2 = 0 \quad (6)$$

Since $a + b = 1$, the values a^2 and b^2 reflect the probabilities of finding one of the isotopes pA or qA by two positions of the element A in the molecule, and $2ab$ is the probability of their simultaneous finding by these positions. Previously Zyakun and Schidlowski [13] discussed that the values b^2 , $2ab$, and a^2 have to be proportional to peak intensities in the mass spectrum of diisotopomer: $I_2 = k b^2$ is the peak intensity determined by the quantity of molecules having in two sites only isotope qA ; $I_1 = k 2ab$ is the peak intensity corresponding to the quantity of molecules having pA and qA isotopes simultaneously by two positions; $I_0 = k a^2$ is the peak

intensity corresponding to the quantity of molecules having only isotope pA by two positions in the molecule of diisotopomer (k is the coefficient of proportionality). Normalizing the intensities of the peaks I_2, I_1, I_0 by I_2 , we obtain a set of values in Eq. (6): 1, I_1/I_2 and I_0/I_2 , or 1, $2a/b$, and a^2/b^2 . It is quite obvious that the solution of the equation (6) with the values 1, I_1/I_2 and I_0/I_2 will be $R_0 = a/b$, i.e., the ratio of abundances of isotopic atoms pA and qA of the element A in diisotopomer.

In case of non-homogeneous isotope distribution in two-site molecules with a different probability of finding isotopes pA and qA by each of the two positions in the pool of diisotopomer (i.e., $R_1 \neq R_2$), Eq. (6) can be presented as

$$(R - R_1)(R - R_2) = 0 \quad (7)$$

or

$$R_2 - (R_1 + R_2) R + R_1 R_2 = 0 \quad (8)$$

The values 1, $(R_1 + R_2)$ and $R_1 R_2$ are normalized intensities of the peaks of molecular ions in the mass spectrum of diisotopomer with different ratios of isotopic atoms pA and qA of the element A in each of its positions in diisotopomer. Therefrom it follows that the quantity of isotopically distinct molecules in the isotopomer pool is determined by the ratios of abundances of isotopes pA and qA of the element A by its individual sites in the molecule. One should remember that the data obtained from solution of the corresponding mathematical Eqs. (5) and (7) may evidence only the existence of sites of the element A in the molecule, which enable the finding of isotope atoms in the analyzed pool with the same or different probability but not identification of their sites in the molecule directly.

The proposed approach to the assessment of the isotope composition of the element A in polyisotopomers allows their classification by distribution of isotopes of the element A within the molecules. If the probability of finding an isotope atom of the element A by all its sites in the molecule is the same (i.e., $R_1 = R_2 = R_3 = \dots = R_n = R_0$), then such a distribution of isotopes of the element A in the polyisotopomer pool is called *homogeneous*. The equation presenting the homogeneous distribution of the element A isotopes will be as

$$(R - R_0)^n = 0 \quad (9)$$

where $R = R_0$ is the solution of this equation.

Non-homogeneous distribution of isotopes of the element A in the pool of polyisotopomer is distribution of isotope atoms that can be found by each of n -sites of the element A with different probabilities (i.e., $R_1 \neq R_2 \neq R_3 \neq \dots \neq R_n$). The equation reflecting the non-homogeneous distribution of isotopes of the element A in the polyisotopomer pool will be written as

$$(R - R_1) (R - R_2) \dots (R - R_n) = 0 \quad (10)$$

where R_1, R_2, \dots, R_n are the solutions of Eq.(10).

It should be noted that the values R_i ($i = 1, 2, \dots, n$) may be both real and complex numbers. If polyisotopic element A contains a mixture of isotope atoms, one of which is predominant in abundance while the rest are in minor quantities, then the isotope composition of the element A in the polyisotopomer pool can be determined by the following three known methods:

1. The *conventional practice* determination of the isotope atom abundance ratios of the element A represented as a measurement of quantities of two isotopically distinct molecule species, one of which contains atoms of only predominant isotope and the other has one atom of the minor isotope along with the major isotope of the element A .
2. The *atomic isotope abundance ratios* of the element A in the pool of the analyzed polyisotopomer calculated as a ratio of the quantity of sums of molecules bearing the light (pA) and heavy (qA) isotopes, respectively.
3. The *average value* of isotope abundance ratios calculated as an average of values R_i ($i=1,2, \dots n$) for all sites of the element A in the polyisotopomer.

Let us compare the data on the isotope composition of the element A in the polyisotopomer pool obtained by the above approaches by the example of a diisotopomer using the Eq. (8). In case of *homogeneous* distribution of isotopes of the element A in diisotopomer, its isotope composition is characterized by values $R_1=R_2=R_{av}$, where R_1 and R_2 are isotope abundance ratios of the element A for site 1 and site 2 in the diisotopomer, respectively; R_{av} is an average of values R_1 and R_2 . The equation describing the isotope distribution of the homogeneous two-site molecule pool can be written as

$$R^2 - 2R_{av}R + (R_{av})^2 = 0 \quad (11)$$

Peak intensities I_2 , I_1 , and I_0 in the mass spectrum of the diisotopomer are proportional to the values 1, $2R_{av}$ and $(R_{av})^2$ (see Eq. 11). The *conventional* practice of the pA and qA isotopic analysis of the element A in diisotopomer relies on the two most intensive peaks of the diisotopomer mass spectrum as:

$$R_c = I_0/I_1 \quad (12)$$

or

$$R_c = (R_{av})^2 / (2R_{av}) = R_{av}/2 \quad (13)$$

Using the peak intensities I_2 , I_1 , and I_0 in the mass spectrum of diisotopomer, the *atomic* isotope ratio can be calculated as

$$R_a = (2I_0 + I_1)/(I_1 + 2I_2) \quad (14)$$

or

$$R_a = (2(R_{av})^2 + 2R_{av}) / (2R_{av} + 2) = R_{av} \quad (15)$$

Consequently, in case of homogeneous distribution of isotopic atoms of the element A in diisotopomer the *atomic* and *conventional* values R_a and R_c are equal or proportional to the *average* isotopic value R_{av} .

In case of *non-homogeneous* isotope distribution of the element A , the two-site diisotopomer pool has two values of isotopic ratios $R_1 \neq R_2$ for the element A in site 1 and site 2, respectively. The equation describing the isotope distribution of the non-homogeneous two-sited diisotopomer pool would be presented as

$$(R - R_1)(R - R_2) = 0 \quad (16)$$

or

$$R^2 - (R_1 + R_2)R + R_1R_2 = 0 \quad (17)$$

where R_1 and R_2 are the solutions of Eq. (17).

Peak intensities I_2 , I_1 , and I_0 in the mass spectrum of the diisotopomer are proportional to the values I , $(R_1 + R_2)$ and R_1R_2 (see Eq. 17), respectively. If $R_{av} = (R_1 + R_2)/2$, then $R_1 = R_{av} + \Delta R$ and $R_2 = R_{av} - \Delta R$. Eq. (17) may be rearranged to

$$R^2 - 2R_{av}R + (R_{av})^2 - (\Delta R)^2 = 0 \quad (18)$$

Determination of the $^pA/^qA$ isotopic ratios for diisotopomer pool with non-homogeneous isotope distribution by *conventional* practice would be calculated as

$$R_c = [(R_{av})^2 - (\Delta R)^2] / 2R_{av} = [R_{av} - (\Delta R)^2 / R_{av}] / 2 \quad (19)$$

The *atomic* isotope ratios for non-homogeneous isotope distribution in the two-sited molecule pool are determined as

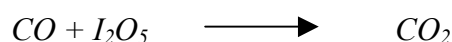
$$R_a = [2((R_{av})^2 - (\Delta R)^2) + 2R_{av}] / (2R_{av} + 2) = R_{av} - (\Delta R)^2 / (R_{av} + 1) \quad (20)$$

The value ΔR reflects deviations of the abundances of isotope atoms of the element A by its individual sites in the diisotopomer molecule from R_{av} . From Exps. (19) and (20) it follows that if the value ΔR is presented by real numbers then the ratios of R_c and R_a will have the lower values than R_{av} , (i.e., $R_a < 2R_c < R_{av}$) and if the value ΔR will be presented by imaginary numbers then the R_c and R_a values will be higher than R_{av} (i.e., $2R_c > R_a > R_{av}$).

3. FACTORS CAUSING THE DISTURBANCE OF HOMOGENEOUS DISTRIBUTION OF THE ELEMENT ISOTOPES IN DIISOTOPOMER POOL

3.1 Different sources of element A in diisotopomer

One of the factors, which may be the reason of disturbed homogeneity of isotope distribution in the polyisotopomer pool, is different sources of the element A for its different sites in the molecule. An example may be carbon dioxide obtained at low-temperature oxidation of CO using I_2O_5 in the reaction [15]:



In this case, one oxygen atom in CO_2 comes from CO (R_1) and the other one – from I_2O_5 —oxidant (R_2). If $R_1 \neq R_2$, then the CO_2 pool will be non-homogeneous by oxygen isotopes. It is essential to note that R_1 and R_2 have to be real numbers and $R_a < 2R_c < R_{av}$.

3.2 Kinetic isotope effects

The second factor disturbing the homogeneity of distribution of isotope atoms in the polyisotopomer pool is a difference in reaction rates for isotopically distinct molecules (the kinetic isotope effect during the diffusion efflux/influx of molecules from/to reservoir, consumption of diisotopomer molecules in chemical and biochemical processes, etc.) With

incomplete utilization of the molecule pool in reactions or processes, its remaining part will show a change in relations between isotopically distinct molecules relative to their initial quantity. This will result in a change of the values in Eq. 18 relative to their initial values.

Let us consider the changes in the isotope abundance ratios of the element A in the diisotopomer pool. In this case, the kinetics of the element A isotope fractionation should deal with two sets of the pA and qA isotopically different molecules, i.e. a) pA_2M and $^pA^qAM$; b) pA_2M and qA_2M . A mathematical expression describing the fractionation of the element A isotopes during the efflux, which involves the molecules A_2M isotopically distinct by the element A (variants a, and b), may be presented as:

$$r_{f(1,2)} = r_{0(1,2)}(1-F)^{(1-\alpha_{1,2})/\alpha_{1,2}} \quad (21)$$

where index 1 or 2 shows the presence of one or two qA atoms, respectively; α_1 and α_2 are the fractionation coefficients of $^pA^qAM$ and qA_2M molecules relative to pA_2M .

A change in the quantities of $^pA^qAM$ and qA_2M isotopically different molecules relative to pA_2M , depending on the share (F) of A_2M consumed, may be expressed in δ units as

$$\delta(^pA^qAM) = [(1-F)^{(1-\alpha_1)/\alpha_1} - 1] \cdot 1000 \text{ ‰} \quad (22)$$

and

$$\delta(^qA_2M) = [(1-F)^{(1-\alpha_2)/\alpha_2} - 1] \cdot 1000 \text{ ‰} \quad (23)$$

In case of mass-dependent fractionation of the molecules of A_2M , the isotopically different by the element A, the coefficients α_1 and α_2 are known to be proportional to the square root of a ratio of masses of the respective molecules, i.e.

$$\alpha_1 \sim ([^pA^qAM]/[^pA_2M])^{1/2} \quad (24)$$

and

$$\alpha_2 \sim ([^qA_2M]/[^pA_2M])^{1/2} \quad (25)$$

By dividing Exp. (22) by (23), we find that the mass-dependent fractionation of A_2M isotopically different by the element A can be expressed as:

$$k = \delta(^pA^qAM)/\delta(^qA_2M) \approx \alpha_2(1-\alpha_1)/\alpha_1(1-\alpha_2) \quad (26)$$

Let a certain reservoir contains a pool of diisotopomer with homogeneous distribution of isotopes of element A (R_0). In the course of a certain reaction, diisotopomer molecules bearing predominantly an isotopically light element A are released from the reservoir. As a result, the share of isotopically heavy molecules will be increasing in the portion of diisotopomer remaining in the reservoir as diisotopomer will efflux, while the other reservoir where some part of molecules enters will contain, respectively, isotopically light molecules of diisotopomer as compared with the initial reservoir. In both cases (efflux and influx), the isotopic composition of the element A in diisotopomer molecules will be characterized by the equation (18).

If homogeneity in distribution of the isotopes of element A is not disturbed in the remaining pool of diisotopomer under its efflux, then $\Delta R = 0$ and $R_{av} > R_0$. We will name such fractionation of the isotopes of the element A as a *collinear* (proportional) fractionation. If each of the isotopic forms of diisotopomer under efflux and influx is characterized by different constants of reaction rates, then the value $\Delta R \neq 0$ (*non-collinear* fractionation of isotopes). It can be easily seen that in case of efflux the free member in the equation (18) will be less than that observed under homogeneous distribution of the isotopes of the element A in the diisotopomer pool. This implies that $(R_{av})^2 - (\Delta R)^2 < (R_{av})^2$, or $(\Delta R)^2 > 0$. In case of influx of isotopically different molecules into the reservoir, the quantity of isotopically light molecules of diisotopomer will be higher than under homogeneous distribution of the element A isotopes in this reservoir, i.e., $(R_{av})^2 - (\Delta R)^2 > (R_{av})^2$, or $(\Delta R)^2 < 0$. From the latter inequality it follows that the value ΔR will be an imaginary number, while R_1 and R_2 are represented by complex numbers. It is obvious that at non-collinear fractionation of isotopes the value ΔR may depend both on the weight of isotopically different molecules of diisotopomer (mass-dependent fractionation) and on other factors (e.g., the secondary isotopic effects determined by the influence of neighboring isotopic atoms during the dissociation or formation of bonds in a molecule). Thus, the above analysis has offered the main parameters determining the isotopic composition of polyisotopomer. Table I shows isotopic characteristics of polyisotopic element A, which follow from the analysis of the polyisotopomer pool.

Table I. Isotopic characteristics of the diisotopomer pool bearing polyisotopic element A

Isotopic characteristics	Remarks
1. <i>Symmetrical</i> distribution of A	In addition to element A, molecule contains other elements
2. <i>Asymmetrical</i> distribution of A	
3. <i>Monocluster</i> isotope pool of A	Molecule has monoisotopic B
4. <i>Polychuster</i> isotope pool of A	Molecule has polyisotopic B
5. <i>Homogenous</i> distribution of isotopes	$R_1 = R_2 = R_{av}; \Delta R = 0$
6. <i>Non-homogenous</i> distribution of isotopes	$R_1 = R_{av} + \Delta R; R_2 = R_{av} - \Delta R; \Delta R \neq 0$
7. Fractionation of isotopes: <i>Efflux</i> of isotopically different molecules <i>Influx</i> of isotopically different molecules	$R_1 \neq R_2; (\Delta R)^2 > 0$ $R_1 \neq R_2; (\Delta R)^2 < 0$
8. <i>Collinear</i> efflux/influx	$R_1 = R_2; R_1 \neq R_2; \Delta R = 0$ $R_1 \neq R_2; \Delta R \neq 0$
9. <i>Non-collinear</i> efflux/influx	
10. <i>Mass-dependent</i> fractionation	$k \approx \alpha_2(1-\alpha_1)/\alpha_1(1-\alpha_2)$
11. <i>Mass-independent</i> fractionation	$k \neq \alpha_2(1-\alpha_1)/\alpha_1(1-\alpha_2)$

4. APPLICATIONS

Let us consider the change in the oxygen isotope characteristics of the carbon dioxide pool during the molecule efflux from reservoir and influx to a certain reservoir. The analysis will use a ^{12}C -cluster of CO_2 molecules isotopically different by ^{16}O and ^{18}O , i.e., C^{16}O_2 , $\text{C}^{16}\text{O}^{18}\text{O}$,

and $C^{18}O_2$. An equation reflecting the distribution of oxygen atoms in this case can be written as

$$^{48}I R^2 - ^{46}I R + ^{44}I = 0 \quad (27)$$

where ^{44}I , ^{46}I and ^{48}I are quantitative characteristics of isotope molecules in the CO_2 pool, respectively.

At a non-collinear and mass-dependent efflux of CO_2 from the reservoir, the quantity of molecules containing ^{16}O will decrease along with CO_2 run-off. Depending on the share of carbon dioxide efflux (f), the contents of $C^{16}O^{18}O$ and $C^{18}O_2$ relative to $C^{16}O_2$ (i.e. $^{44}I_{fe}=1.0$, $^{46}I_{fe}$ and $^{48}I_{fe}$) will be found by expressions

$$^{46}I_{fe} = ^{46}I_0 (1-f)^{1/\alpha_1 - \alpha_1} \quad (28)$$

$$^{48}I_{fe} = ^{48}I_0 (1-f)^{1/\alpha_2 - \alpha_2} \quad (29)$$

In case of CO_2 influx into the reservoir, the quantities of $C^{16}O^{18}O$ and $C^{18}O_2$ relative to $C^{16}O_2$ (i.e. $^{44}I_{fi}=1.0$, $^{46}I_{fi}$ and $^{48}I_{fi}$) will be calculated as

$$^{46}I_{fi} = ^{46}I_0 (1-(1-f)^{1/\alpha_1})/f \quad (30)$$

$$^{48}I_{fi} = ^{48}I_0 (1-(1-f)^{1/\alpha_2})/f \quad (31)$$

where $\alpha_1 = ([C^{16}O^{18}O]/[C^{16}O_2])^{1/2}$ and $\alpha_2 = ([C^{18}O_2]/[C^{16}O_2])^{1/2}$ are coefficients of fractionation of isotopically different molecules of carbon dioxide.

The average value of oxygen isotope composition by two sites in CO_2 molecule (R_{av}) and the value ΔR during the CO_2 efflux from the reservoir (index e) and the CO_2 influx into the other reservoir (index i) will be determined using expressions

$$R_{av(e,i)} = ^{46}I_{f(e,i)} / 2 ^{48}I_{f(e,i)} \quad (32)$$

$$\Delta R_{(e,i)} = [(^{46}I_{f(e,i)})^2 - 4 ^{48}I_{f(e,i)} ^{44}I_{f(e,i)}]^{1/2} / 2 ^{48}I_{f(e,i)} \quad (33)$$

From (32, 33) it follows that with CO_2 efflux/influx from/into reservoir the value R_{av} will decrease, while the absolute value ΔR , on the contrary, will increase.

To be specific, let us consider the change in the isotope composition of carbon dioxide characterized by $\delta^{18}O = -0.73$ ‰ relative to PDB standard, under its efflux from one reservoir and influx into another. In case of homogeneous distribution of ^{18}O in the initial pool of CO_2 , the average value of isotope contents by two sites of oxygen will be $R_{av} = 471.77$, while the corresponding equation will be presented as

$$4.4930 R^2 - 4239.34 R + 10^6 = 0 \quad (34)$$

As mentioned above, the quantitative parameters in the equation (34) will change at the efflux of this CO_2 from one reservoir and its influx into another reservoir. Values R_{av} and ΔR characterizing distribution of oxygen isotopes in CO_2 in the first and second reservoirs will also change.

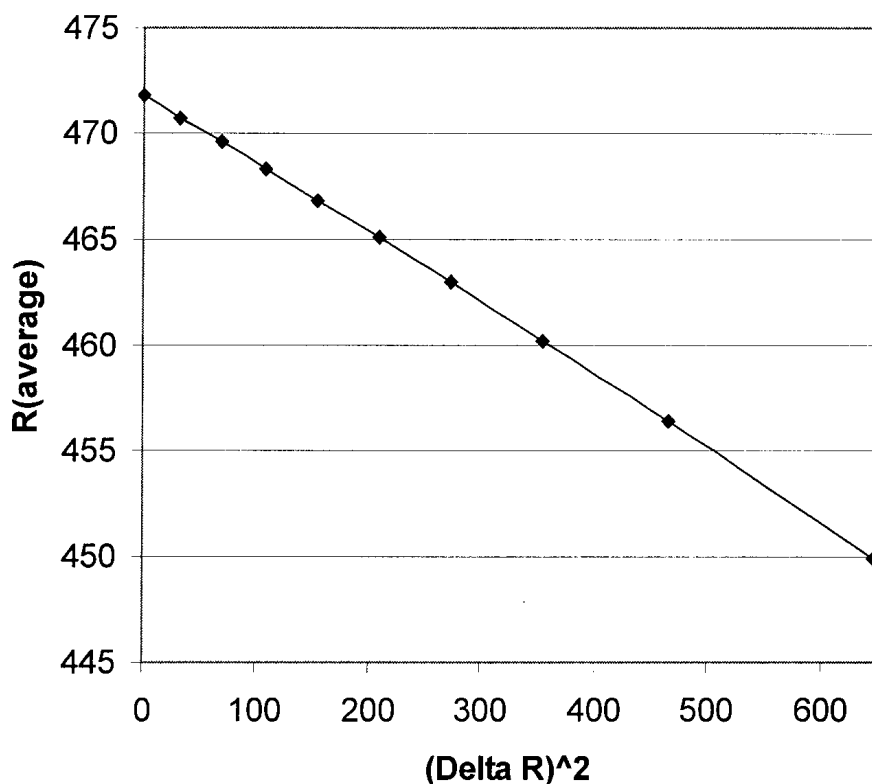


FIG. 1. Relationship between values R_{av} and $(\Delta R)^2$ of carbon dioxide model reservoir for different values f reflecting the increasing portions of reservoir depletion from 0 to 0.9 is represented by $R_{av} = -(0.03368 \pm 0.00014) (\Delta R)^2 + (472.0 \pm 0.08)$. The variation coefficient for the last term of this R_{av} expression is 0.02%. The discrimination coefficients for the functions $^{46}I_{fe}$ (Expr. 28) and $^{48}I_{fe}$ (Expr. 29) are $\alpha_1 = 1.022474$ and $\alpha_2 = 1.0444659$. Values of $^{46}I_0$ and $^{48}I_0$ are borrowed from Expr. 34.

Figure 1 shows a linear dependence between R_{av} and $(\Delta R)^2$ for different values f reflecting the portion of CO_2 efflux from one reservoir:

$$R_{av} = k(\Delta R)^2 + R_0 \quad (35)$$

where R_0 is the characteristic of distribution of isotopes ^{16}O and ^{18}O in the initial reservoir; k is the coefficient of proportionality. From expression (35) it follows that determination of no less than two values of the pair of parameters R_{av} and (ΔR) in the course of efflux and/or influx of CO_2 will allow the calculation of value R_0 characterizing oxygen isotope composition in the initial reservoir.

5. DETERMINATION OF ISOTOPE COMPOSITION OF OXYGEN IN CARBONATE

The basic postulate of determination of isotope distribution was an assumption that the distribution of ^{18}O in carbonate is homogeneous. An object of the analysis was barium carbonate enriched with ^{18}O isotope, whose oxygen isotope composition was strongly different from natural water and orthophosphate acid used as a reagent. Carbonate dissociation by acid results in the formation of CO_2 , whose oxygen isotope composition may be non-homogeneous due to incompleteness of the reaction, its partial exchange with the water present in the acid, etc. Temperature and time of the reaction, as well as the amount of

carbonate participating in the reaction, were used as factors affecting the degree of carbonate dissociation and homogeneity of ^{18}O distribution in CO_2 .

Table II gives the results of analyzing the content of CO_2 molecules, isotopically different by oxygen, which were obtained under acid dissociation of carbonate, and the values R_{av} and ($i\Delta R$) calculated by expressions (32) and (33).

Table II. Isotope characteristics of CO_2 obtained at barium carbonate dissociation by orthophosphoric acid

N	^{44}I	^{46}I	^{48}I	R_{av}	$\pm i\Delta R$	Note
1.	1.000	1.20207	0.53556	1.1223	0.7796	28°, 30 min, 30 mg
2.	1.000	1.17495	0.50846	1.1554	0.7948	25°, 30 min, 30 mg
3.	1.000	1.25270	0.47268	1.1903	0.8359	20°, 30 min, 30 mg
4.	1.000	1.06270	0.43970	1.2084	0.9022	20°, 30 min, 16 mg
5.	1.000	0.95730	0.37670	1.2706	1.0200	100°, 60 min, 30 mg

As follows from Table II, the characteristics of oxygen isotope composition in CO_2 formed indicate a non-homogeneous distribution of ^{18}O in CO_2 , depending on the conditions of carbonate dissociation (temperature and time of reaction, amount of carbonate). At the same time, the values $R_{1,2} = R_{av} \pm i\Delta R$ represented by complex numbers evidence the influx of CO_2 to the analyzed reservoir. Using the values R_{av} and $i\Delta R$ for CO_2 samples obtained at acid dissociation of barium carbonate (Table II), an equation (36) has been defined by the method of least squares, which reflects the dependence between R_{av} and $(i\Delta R)^2$.

$$R_{av} = -(0.2854 \pm 0.0145)(i\Delta R)^2 + (0.9765 \pm 0.0126) \quad (36)$$

The coefficient of variations for the free member in the equation (36) was 2.3%. At $(\Delta R)^2 = 0$ we determine the value R_0 characterizing the oxygen isotope composition in the analyzed barium carbonate. In this case, $R_0 = 0.9765 \pm 0.0126$, which corresponded to the content of ^{18}O in carbonate of $50.6 \pm 0.3\%$.

Thus, the above example demonstrates the possibility to determine the true ratio of oxygen isotopes in carbonate, using several CO_2 samples obtained at partial dissociation of this carbonate.

ACKNOWLEDGMENTS

We thank Naohiro Yoshida for helpful advice to prepare our paper to the International Conference on the Study of Environmental Change Using Isotope Techniques. We thank the Japan Science and Technology Corporation for financial support of our participation in the Conference.

REFERENCES

- [1] SODDY, F. Chem. Soc. Ann. Rep. **7** (1910) 285.
- [2] FAJANS, K. Phys. Z. **14** (1913) 131, 136.
- [3] TOMSON, J.J. Rays of Positive Electricity, New York (1921) 20.
- [4] ASTON, F.N. Phil. Mag. **38** (1919) 707; **39** (1920) 449; **42** (1921) 436.
- [5] DEMSTER, A.J. Phys Rev. **11** (1918) 316; **18** (1921) 415; **20** (1922) 436.

- [6] NIER, A.O., GULBRANSEN, E.A., J. Am. Chem. Soc. **61** (1939) 181.
- [7] TROFIMOV, A.V. Dokl. Akad. Nauk SSSR **66** (1949) 181.
- [8] McKINNEY, C.R., MCCREA J.M., EPSTEIN S., ALLEN H.A., UREY H.G. Rev. Sci. Instr. **21** (1950) 724.
- [9] WANLESS, R.C., THODE H.G. J. Sci. Instr. **30** (1953) 395.
- [10] CRAIG, H. Geochim. Cosmochim. Acta **3** (1953) 53.
- [11] ABELSON, P.H., HOERING T.C., Proc. Nat. Acad. of Sci. **47**, N5 (1961) 623.
- [12] ZYAKUN, A.M., Izv. Akad. Nauk SSSR (Ser. Chim.) **10** (1974) 2226.
- [13] ZYAKUN, A.M., SCHIDLOWSKI M., Int. J. Mass Spectr. and Ion Proces. **161** (1997) 97.
- [14] ZYAKUN, A.M., SCHIDLOWSKI M., Int. J. Mass Spectr. **203** (2000) 83.
- [15] STEVENS, C.M., KROUT, L.L., WALLING, D., VENTERS, A., ENGELMEIR, A. and ROSS, L.E. Earth Planet. Sci. Lett. **16** (1972) 147.

POTENTIAL USE OF THE NON-RANDOM DISTRIBUTION OF N₂ AND N₂O MOLE MASSES IN THE ATMOSPHERE AS A TOOL FOR TRACING ATMOSPHERIC MIXING AND ISOTOPE FRACTIONATION PROCESSES

R. WELL

Institute of Soil Science, University of Göttingen, Germany

R. LANGE, A. REINEKING

Isotope laboratory for biological and medical research, University of Göttingen, Germany

Abstract. The variation in the natural abundance of ¹⁵N in atmospheric gas species is often used to determine the mixing of trace gases from different sources. With conventional budget calculations one unknown quantity can be determined if the remaining quantities are known. From ¹⁵N tracer studies in soils with highly enriched ¹⁵N-nitrate a procedure is known to calculate the mixing of atmospheric and soil derived N₂ based on the measurement of the 30/28 and 29/28 ratios in gas samples collected from soil covers. Because of the non-random distribution of the mole masses ³⁰N₂, ²⁹N₂ and ²⁸N₂ in the mixing gas it is possible to calculate two quantities simultaneously, i.e. the mixing ratio of atmospheric and soil derived N₂, and the isotopic signature of the soil derived N₂. Routine standard measurements of laboratory air had suggested a non-random distribution of N₂-mole masses. The objective of this study was to investigate and explain the existence of non-random distributions of ¹⁵N¹⁵N, ¹⁴N¹⁵N and ¹⁴N¹⁴N in N₂ and N₂O in environmental samples. The calculation of theoretical isotope data resulting from hypothetical mixing of two sources differing in ¹⁵N natural abundance demonstrated, that the deviation from an ideal random distribution of mole masses is not detectable with the current precision of mass spectrometry. ¹⁵N-analysis of N₂ or N₂O was conducted with randomised and non-randomised replicate samples of different origin. ¹⁵N abundance as calculated from 29/28 ratios were generally higher in randomised samples. The differences between the treatments ranged between 0.05 and 0.17 ‰ ¹⁵N. It was concluded that the observed randomisation effect is probably caused by ¹⁵N¹⁵N fractionation during environmental processes.

1. INTRODUCTION

The variation in the natural abundance of ¹⁵N in atmospheric gas species is often used to determine the mixing of atmospheric trace gases from different sources (e.g. Rahn & Wahlen, 2000 [1]). With conventional budget calculations one unknown quantity can be determined if the remaining quantities are known. From ¹⁵N tracer studies in soils with highly enriched ¹⁵N-nitrate a procedure was developed to calculate the mixing of atmospheric and soil derived N₂ based on the measurement of the 30/28 and 29/28 ratios in gas samples collected from soil covers (Hauck et al., 1958 [2]). Because of the non-random distribution of the mole masses ³⁰N₂, ²⁹N₂ and ²⁸N₂ in the mixing gas it is possible to calculate two quantities simultaneously, i.e. the mixing ratio of atmospheric and soil derived N₂, and the isotopic signature of the soil derived N₂. This principle can theoretically be used as a tool to study the mixing of N₂ and N₂O from different sources with distinct differences in natural abundance ¹⁵N. Because maximum differences in ¹⁵N abundance of natural systems is several orders of magnitude lower compared to ¹⁵N tracer experiments a sensitivity analysis is necessary to investigate if non-random distribution of mole masses in natural samples can be detected.

Recently, variations in the intramolecular site preference of ¹⁵N in N₂O isotopomers were discovered in atmospheric samples (Yoshida & Toyoda, 2000 [3]; Röckmann et al., 2000 [4]) and were attributed to differences in site preference among N₂O sources. The possibility of

preferred formation of either $^{14}\text{N}^{15}\text{N}$ or $^{15}\text{N}^{15}\text{N}$ species during the transformation of N_2 or N_2O in geospheric processes has to our knowledge not yet been considered. If such an effect would exist, then it would result in a deviation from random distribution of dinitrogenous mole masses.

Routine standard measurements of laboratory air had suggested a non-random distribution of N_2 -mole masses (Well et al., 1998 [5]). The 29/28 ratio of laboratory air increased by 0.14 ‰ after passing a microwave equilibration unit to randomise mole masses. This finding can be either attributed to the above described processes or to an unknown experimental error during isotope analysis.

The aim of the present study was (1) to conduct a sensitivity analysis on the theory of using non-random distribution of N_2 and N_2O mole masses to identify sources with different isotopic signatures, and (2) to investigate the existence of measurable non-random distribution of N_2 and N_2O mole masses by analysing samples of different origin.

1.1 Isotope effects from the mixing of sources differing in ^{15}N abundance

1.1.1 Principle

Hauck et al. (1958 [2]) proposed a method (referred to as “HAUCK-method” in the remainder of the paper) to study denitrification in soils with the ^{15}N tracer technique. This method uses the distribution of the N_2 mole masses 28, 29 and 30 to calculate the mixing of N_2 evolved by denitrification from highly enriched nitrate with atmospheric N_2 . The calculations are based on the assumption, that the N_2 mole masses from the different pools are randomly distributed, i.e. they follow a binomial distribution, which can be expressed as follows.

$$^{14}\text{a} = 1 - ^{15}\text{a} \quad (1\text{a})$$

$$^{14}\text{a}^2 + 2(^{14}\text{a}^{15}\text{a}) + ^{15}\text{a}^2 = 1 \quad (1\text{b})$$

where ^{14}a and ^{15}a denote the atomic fractions of ^{14}N and ^{15}N , respectively. From Eq. 1b expressions can be derived to calculate the frequencies of masses 28, 29 or 30 at any given ^{15}a :

$$^{28}\text{x} = (1 - ^{15}\text{a})^2 \quad (2\text{a})$$

$$^{29}\text{x} = 2 (1 - ^{15}\text{a}) ^{15}\text{a} \quad (2\text{b})$$

$$^{30}\text{x} = ^{15}\text{a}^2 \quad (2\text{c})$$

If N_2 from two pools (1 and 2) with different ^{15}N enrichment mixes, then the frequency of each of the N_2 mole masses as well as of the ^{15}N frequency can be described with a general mixing formula:

$$^{15}\text{a}_{\text{mix}} = d ^{15}\text{a}_1 + (1 - d) ^{15}\text{a}_2 \quad (3)$$

where d denotes the mixing ratio. The ^{15}N atom fraction of the mixture is defined by the frequency of the three molecular species

$$^{15}\text{a}_{\text{mix}} = (^{29}\text{x}_{\text{mix}} + 2 ^{30}\text{x}_{\text{mix}}) / [2 (^{28}\text{x}_{\text{mix}} + ^{29}\text{x}_{\text{mix}} + ^{30}\text{x}_{\text{mix}})] \quad (4)$$

If the three N₂ mole masses are randomly distributed ³⁰N₂ can be omitted in the calculation:

$$^{15}a_{\text{mix}} = ^{29}x_{\text{mix}} / (2 ^{28}x_{\text{mix}} + ^{29}x_{\text{mix}}) \quad (5)$$

However, N₂ mole masses are non-randomly distributed in a gas mixture as described above. Thus, Eq. 5 would result in a value deviating from the ideal ¹⁵a_{mix}. Consequently, the measurement of masses 29 and 28 is not sufficient. Direct or indirect determination of ³⁰N₂ is necessary for accurate calculation of ¹⁵a_{mix} using Eq. 4. The HAUCK-method uses the relationships of Eqs. 1 – 4 in order to calculate the mixing ratio d and the ¹⁵a of the enriched nitrate pool (¹⁵a_p). Various equations have been developed in order to calculate d and ¹⁵a_p from N₂ or N₂O isotope ratios (Siegel et al., 1982 [6]; Mulvaney, 1984 [7]; Arah 1992 [8]; Well et al., 1998 [5]). Since then, the HAUCK-method has successfully been used in various studies to measure soil denitrification in the field or laboratory.

The natural isotope signatures of many gas species in the environment are subject to multiple fractionation processes and therefore vary considerably in space and time. The natural range of δ ¹⁵N of N₂O for example is approx. 50 ‰ (Rahn & Wahlen, 2000 [1]) with lowest values in N₂O from terrestrial processes and highest values in the oceans. Principally, the HAUCK-method can be used in order to supply additional information for calculating the mixing of gas species with at least two atoms of one element per molecule like e.g. N₂ and N₂O. With conventional mixing models, a mixing ratio of two components can be obtained if their isotopic signatures are defined. In addition to the mixing ratio the HAUCK-method provides the isotopic signature of one of the components, if the distribution of the mole masses of the other component is defined. Thus, the use of the HAUCK-method for analysing natural abundance stable isotopic signatures could theoretically improve the understanding of global budgets of certain gas species.

1.1.2 Sensitivity Analysis

The range of natural isotopic abundances is small compared to the high ¹⁵N enrichment of the tracer experiments where the Hauck-method is used. Therefore, it is necessary to evaluate if instrumental precision of isotope ratio mass spectrometers (IRMS) is sufficient to apply the HAUCK-method to natural abundance levels. A direct proof of the mixing of two sources with distinct differences in ¹⁵N enrichment would be to verify that the distribution of the mole masses in the gas mixture is non-random. In the following it is investigated if this verification is possible with the actual precision of IRMS. The theoretical isotope ratios of hypothetical gas mixtures of two N₂ pools with varying values for ¹⁵a₁, ¹⁵a₂ and d are compared to isotope ratios of samples with equal ¹⁵N abundance but with random distribution of mole masses. Table I gives an example with d = 0.5, ¹⁵a₁ = 6 ‰ and ¹⁵a₂ = -40 ‰. These values were chosen in order to demonstrate the maximum signal that can be expected from the variation in the ¹⁵N natural abundance of N₂O. Eqs. 2 a - c are used to calculate molecular frequencies for each fraction of the mixture. Eq. 3 provides the molecular frequencies and the ¹⁵N abundance of the non-equilibrium gas mixture. Eqs 2 a – c are used again to calculate molecular frequencies of an equilibrium sample with random molecular distribution but with the same ¹⁵N abundance as the non-equilibrium sample. The differences between equilibrium and non-equilibrium values are - 0.002 ‰. These calculations were also conducted for a range of d of 0.5 to 0.0005 and for a range of differences between ¹⁵a₁ and ¹⁵a₂ of 1 to 100000 ‰. The resulting differences between equilibrium and non-equilibrium values in terms of δ ‰ ¹⁵N are plotted in Figure 1. The sensitivity of our IRMS for ¹⁵N gas analysis is typically between 0.03 and 0.1 ‰. Recently, a reproducibility of 0.018 ‰ was achieved for N₂/O₂ ratio meas-

urements with an improved gas inlet system (Leuenberger et al., 2000 [9]). From Table I and Figure 1 it can be seen that the effect from mixing of sources with natural ^{15}N abundance is not detectable with the current sensitivity of IRMS. The positive isotope effect of $0.14 \text{ } \delta \text{ } ^{15}\text{N}$ from randomising as observed earlier (Well et al., 1998 [5]) is two orders of magnitude higher than the maximum N_2O mixing effect calculated in Table I. Because the range of natural abundance ^{15}N is smaller for N_2 than of N_2O the maximum mixing effect of N_2 would be even lower than for N_2O . It can be concluded that the observed isotope effect is either a methodical effect from the equilibration procedure, or must be attributed to an unknown fractionation of the $^{15}\text{N}^{15}\text{N}$ molecule during atmospheric processes.

Table I. Theoretical isotope data of two equilibrium samples with different ^{15}N abundance and of a mixture of the two components ($d = 0.5$). Non-equilibrium values of the mixture are derived from the mixing of the molecular frequencies of the two samples. Equilibrium values are calculated from the ^{15}N atom fraction of the mixture assuming binomial distribution of the mole masses.

	Sample 1	Sample 2	Mixture		
			non-equilibrium	equilibrium	non-equilibrium - equilibrium
$\delta^{15}\text{N}$	6	-40	-170,039	-170,019	-0,0019
^{15}a	$3,6844 \cdot 10^{-3}$	$3,5166 \cdot 10^{-3}$	$3,6005 \cdot 10^{-3}$	$3,6005 \cdot 10^{-3}$	0
^{28}x	0.99264	0.99291	0.99281	0.99281	$7,1 \cdot 10^{-9}$
^{29}x	$7,3417 \cdot 10^{-3}$	$7,0084 \cdot 10^{-3}$	$7,1750 \cdot 10^{-3}$	$7,1751 \cdot 10^{-3}$	$-1,41\text{E} \cdot 10^{-8}$
^{30}x	$1,3575 \cdot 10^{-5}$	$1,2366 \cdot 10^{-5}$	$1,2971 \cdot 10^{-5}$	$1,2964 \cdot 10^{-5}$	$7,1 \cdot 10^{-9}$
29/28-ratio	$7,3961 \cdot 10^{-3}$	$7,0579 \cdot 10^{-3}$	$7,2270 \cdot 10^{-3}$	$7,2270 \cdot 10^{-3}$	$-1,42 \cdot 10^{-8}$
30/28-ratio	$1,3676 \cdot 10^{-5}$	$1,2454 \cdot 10^{-5}$	$1,3064 \cdot 10^{-5}$	$1,3057 \cdot 10^{-5}$	$7,1 \cdot 10^{-9}$

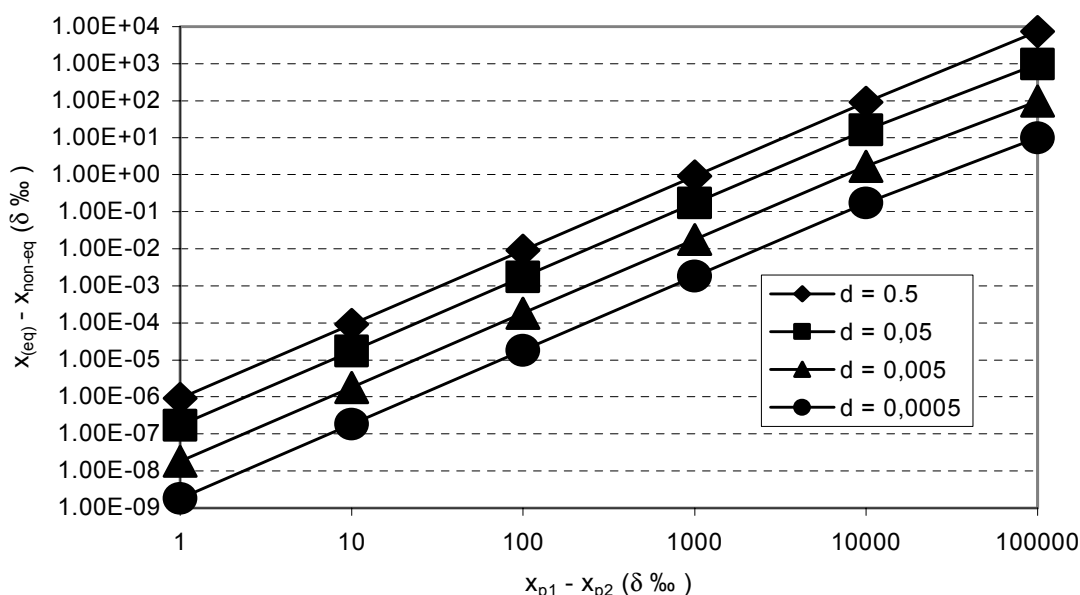


FIG. 1. Theoretical deviation of 29/28-ratios ($\delta \text{ } ^{15}\text{N}$) between equilibrated and non-equilibrated mixtures of two pools with different ^{15}N atom fraction. Differences between pools 1 and 2 = 1 to 100000 $\delta \text{ } ^{15}\text{N}$. Mixing ratio (d) = 0.5 to 0.0005. The detection limit for ^{15}N is between 0.01 and 0.1 $\delta \text{ } ^{15}\text{N}$ (see text).

1.2 Analysis of the distribution of $^{15}\text{N}^{15}\text{N}$, $^{14}\text{N}^{15}\text{N}$ and $^{14}\text{N}^{14}\text{N}$ in N_2 and N_2O

1.2.1 Objectives

The first objective of the measurements was to evaluate if the previously observed randomisation effect reflects the true distribution of N_2 mole masses in the atmosphere or if this was only a methodical effect of the equilibration procedure. In case of a true effect for N_2 , it was intended to investigate also the distribution of N_2O mole masses.

1.2.2 Choice of method

A deviation of the actual distribution of N_2 mole masses from the ideal random distribution can principally be detected in two different ways. If all three molecular species are measured directly, then the measured distribution has to be compared with the calculated random distribution. Direct measurement of mass 30 is complicated by a high background as a result of the formation of $^{30}(\text{NO})^+$ in the ion source of the mass spectrometer (Siegel et al., 1982). To overcome this problem we developed a procedure to measure m/z 30 indirectly by comparing the 29/28 ratio of a sample with non-random distribution of mole masses with the 29/28 ratio of the same sample after randomisation of the mole masses with an electrodeless discharge (Well et al., 1993 [10]; 1998 [5]). Principally, this equilibration procedure is the ideal approach to verify the non-random distribution $^{15}\text{N}^{15}\text{N}$, $^{14}\text{N}^{15}\text{N}$ and $^{14}\text{N}^{14}\text{N}$ in N_2 and N_2O , because the non-randomness is directly proved by any deviation between randomised and non-randomised samples. However, it has to be confirmed that the equilibration procedure yields an ideal random distribution.

1.2.3 Instrumentation

Isotope analysis of N_2 and N_2O was conducted using an instrumentation that was previously described in detail (Well et al., 1998 [5]). Briefly, an elemental analyser (Carlo Erba ANA 1400) was coupled to an isotope ratio mass spectrometer (Finnigan MAT 251). The interface connecting both instruments included a high frequency discharge unit, which enabled online-equilibration of the gas samples prior to isotope analysis. Gas samples of 80 μl were injected with an automated syringe sampler (Combi PAL, CTC Analytics). The injection needle of the sampler was protected with an Ar flow to avoid air contamination. N_2O was reduced to N_2 in the reduction column of the elemental analyser. The purpose of the equilibration procedure was to create a random distribution of mole masses in samples with initially non-random distribution. The result is an increase in the number of $^{14}\text{N}^{15}\text{N}$ molecules while the number of $^{14}\text{N}^{14}\text{N}$ and $^{15}\text{N}^{15}\text{N}$ molecules decreases.

The instrumentation described above was extended to enable removal of N_2 or N_2O prior to isotope analysis. A GC-column (Porapaq QS, 30°C) was connected to the carrier gas circuit of the elemental analyser. Thus, it was possible to separate the N_2 and N_2O fractions of the gas samples before passing the reduction column and to analyse each component separately. The actual configuration of the inlet system requires a sample size of > 50 μg N to obtain maximum precision. For $^{15}\text{N}_2\text{O}$ analysis N_2O concentrations of the gas samples must therefore be relatively large, i.e. > 50%.

1.2.4 Samples

The deviation between equilibrated and non-equilibrated replicates was measured in a variety of samples containing N_2 and/or N_2O . N_2 from combustion of urea, high purity compressed

N₂ and N₂O as well as laboratory and outside air were analysed. Sub-samples were filled into 12 ml vials sealed with butyl stoppers and crimp caps. N₂O produced during the following soil denitrification experiment was also measured.

Anaerobic slurries of an organic soil were prepared in 8 screw-cap bottles (300 ml) sealed with silicone septa. Each bottle was supplemented with 100 g soil and 100 ml nitrate solution (1000 mg N l⁻¹), sealed, flushed with He and incubated at 25°C for 7 days. Subsequently, the bottles were heated to 80°C to degas N₂O from the liquid phase. The headspace gas was then flushed out with a He flow (30 ml min⁻¹), scrubbed for CO₂ and water vapour in Ascarite and MgClO₄, and was frozen in a liquid N₂ cold trap. The gas from the 8 bottles was concentrated into one sample of approx. 20 ml pure N₂O. Finally the trap was heated to transfer the sample into an evacuated 12 ml vial which was cooled with liquid N₂.

2. RESULTS AND DISCUSSION

¹⁵N abundance of the samples ranged between -21.6 ‰ (soil gas) and 1.4 ‰ (N₂ from combustion of urea) (Table II). Equilibration always produced an increase of the ¹⁵N values, i.e. a gain of ¹⁵N¹⁴N molecules, and a loss in ¹⁵N¹⁵N and ¹⁴N¹⁴N molecules. The shifting ranged between 0.05 and 0.17 ‰ ¹⁵N. The differences between the shifting of each sample are close to the detection limit as the standard deviations of the measurements were between 0.02 and 0.11 ‰.

TABLE II. Deviation of 29/28 ratios in equilibrated and non-equilibrated replicate samples expressed as $\delta^{15}\text{N}$ (‰).

Sample	Measured N-species	$\delta^{15}\text{N}$			N
		non-equilibrated	equilibrated	equilibrated – non-equilibrated	
compressed N ₂	N ₂	-14.033 ± 0.019	-13.981 ± 0.073	0.052 ± 0.075	5
laboratory air	N ₂	-0.037 ± 0.057	0.119 ± 0.123	0.156 ± 0.136	5
outside air	N ₂	0.019 ± 0.098	0.116 ± 0.095	0.097 ± 0.138	5
soil gas	N ₂ O	-21.625 ± 0.022	-21.569 ± 0.063	0.056 ± 0.067	3
compressed N ₂ O (1)	N ₂ O	-3.999 ± 0.085	-3.827 ± 0.101	0.173 ± 0.132	6
compressed N ₂ O (2)	N ₂ O	-4.898 ± 0.078	-4.747 ± 0.070	0.152 ± 0.105	13
N ₂ from combustion of urea	N ₂	1.362 ± 0.075	1.446 ± 0.072	0.085 ± 0.104	5

It is notable that the standard deviations varied considerably between the samples. In the samples with lowest standard deviation of the non-equilibrated replicates, the variation was always higher for the equilibrated replicates. This indicates the existence of a methodical effect of the equilibration procedure. Additional factors of variation are the sensitivity of the mass spectrometer, sample dilution with laboratory air during the repeated application of sub-samples from one vial, and the true variation of ¹⁵N abundance between the sub-samples. Sample dilution is insignificant for N₂O analysis because atmospheric N₂O concentration (0.3 ppm) is negligible compared to the pure N₂O of the samples. It is also unimportant for the air samples because these are almost identical with the potentially diluting laboratory air. True variation of ¹⁵N abundance between sub-samples of laboratory air and compressed N₂O was

suspected because some of the sub-samples exhibited consistent deviations from the mean (data not shown).

The shifting in ^{15}N abundance between equilibrated and non-equilibrated samples was lowest in the N_2O sample from soil denitrification ($0.052 \delta \text{‰}$) and in the compressed N_2 ($0.056 \delta \text{‰}$). Highest differences occurred in the compressed N_2O samples (0.152 and $0.173 \delta \text{‰}$) and in laboratory air ($0.156 \delta \text{‰}$). None of the samples was stable during equilibration. This may reflect that all of the samples were in a state of isotopic non-equilibrium. However, we cannot yet exclude the existence of an experimental effect of the equilibration procedure. To evaluate this possibility it would be necessary to measure samples with an ideal random distribution of mole masses. It is difficult to find appropriate samples because each process of N_2 or N_2O formation may include fractionation processes. Because of this uncertainty it is not yet possible to quantify the extent of non-equilibrium of each sample. However, the differences between the samples in the shifting during equilibration are a clear indicator for the existence of non-equilibrium at least in some of the samples.

The observed shifting of 0.052 to $0.173 \delta \text{‰}$ is more than one order of magnitude larger compared to the maximum difference of $0.002 \delta \text{‰}$ that was calculated for the mixing of two sources with difference in ^{15}N natural abundance. It can be concluded that the shifting must be attributed to additional processes. Recently, differences in the fractionation factor of N_2O isotopomers were proved [3,4]. Yung and Miller [11] predicted a maximum fractionation for $^{15}\text{N}^{15}\text{N}^{16}\text{O}$. If isotope fractionation was also different for $^{15}\text{N}^{15}\text{N}$ and $^{15}\text{N}^{14}\text{N}$ during N_2 turn-over processes, then the distribution of N_2 mole masses in the atmosphere would deviate from the ideal random distribution. It is possible that the observed isotope shifting during equilibration of air samples reflects this hypothetical non-equilibrium.

The $^{15}\text{N}^{15}\text{N}^{16}\text{O}$ isotopomer is not measurable with the techniques that have been reported so far [3,4]. The method presented above is principally suitable to measure this molecule. Thus, it is a potential tool to prove $^{15}\text{N}^{15}\text{N}^{16}\text{O}$ fractionation effects and to use this isotopomer as an additional tracer to investigate the global N_2O budget.

Refinements of the methods are necessary to increase its precision. This can be achieved by reducing the factors of variation mentioned above and by modifying the inlet system as described by Leuenberger et al. [9]. To prove the significance of a non-random distribution of $^{15}\text{N}^{15}\text{N}$, $^{14}\text{N}^{15}\text{N}$ and $^{14}\text{N}^{14}\text{N}$ in N_2 and N_2O it is necessary to measure more samples from different environments.

REFERENCES

- [1] RAHN, T., WAHLEN, M., A reassessment of the global isotopic budget of atmospheric nitrous oxide, *Global Biogeochem. Cycles* **14** (2000) 537–543.
- [2] HAUCK, R.D., MELSTED, S.W., YANNKWICH P.E., Use of N - Isotope distribution in nitrogen gas in the study of denitrification, *Soil Science* **86** (1958) 287–291.
- [3] YOSHIDA, N., TOYODA, S., Constraining the atmospheric N_2O budget from intramolecular site preference in N_2O isotopomers, *Nature* **405** (2000) 330–334.
- [4] RÖCKMANN, T., BRENNINKMEIJER, C.A.M., WOLLENHAUPT, M., CROWLEY, J.N., CRUTZEN, P.J., Measurement of isotopic fractionation of $^{15}\text{N}^{14}\text{N}^{16}\text{O}$, $^{14}\text{N}^{15}\text{N}^{16}\text{O}$ and $^{14}\text{N}^{14}\text{N}^{18}\text{O}$ in the UV photolysis of nitrous oxide, *Geophys. Res. Lett.* **27** (2000) 1399–1402.

- [5] WELL, R., BECKER K.W., LANGE R., MEYER B., REINEKING A., Continuous flow equilibration for mass spectrometric analysis of dinitrogen emissions, *Soil Sci. Soc. Am. J.* **62** (1998) 906-910.
- [6] SIEGEL, R.S., HAUCK, R.D., KURTZ, L.T., Determination of $^{30}\text{N}_2$ and application to measurement of N_2 evolution during denitrification, *Soil Sci. Soc. Am. J.* **46** (1982) 68-74.
- [7] MULVANEY, R.L., Determination of ^{15}N -labelled dinitrogen and nitrous oxide with triple collector mass spectrometer, *Soil Sci. Soc. Am. J.* **48** (1984) 690-692.
- [8] ARAH, J.R.M., New formulae for mass spectrometric analysis of nitrous oxide and dinitrogen emissions, *Soil Sci. Soc. Am. J.* **56** (1992) 795-800.
- [9] LEUENBERGER, M., NYFELER, P., MORET, H.P., STURM, P., HUBER, C., A new inlet system for an isotope ratio mass spectrometer improves reproducibility, *Rapid Commun. Mass Spectrom.* **14** (2000) 1543–1551.
- [10] WELL, R, BECKER, KW, MEYER, B, Equilibrating of ^{15}N -gases by electrodeless discharge: a method of indirect mass spectrometric analysis of $^{30}\text{N}_2$ for denitrification studies in soils. *Isotopenpraxis Environ. Health Stud.* **29** (1993) 175-180.
- [11] YUNG, Y.L., MILLER, C.E., Isotopic fractionation of stratospheric nitrous oxide, *Science* **278** (1997) 1778–1780.

USE OF LEAD-210 AS A TRACER TO COMPENSATE CLIMATOLOGICAL EFFECTS OF AIRBORNE SULPHATE TRENDS

J.P. PAATERO, T. RUOHO-AIROLA, J. HATAKKA, Y. VIISANEN

Finnish Meteorological Institute, Air Quality Research,
Helsinki, Finland

Abstract. In Europe the sulphur emissions have decreased from 26 millions of tons in 1980 to less than 8 millions of tons in 1998. The annual atmospheric sulphate concentration in Finland, however, fluctuates, and only after 1988 a clear downward trend in the concentration is evident despite the over 20 percent sulphur emission reduction during the 1980's in Europe. We have used the natural radionuclide ^{210}Pb as a tracer for continental air masses in order to distinguish the causes for the variations in sulphate concentrations in the ground-level air. The observed variability in sulphate concentrations can be due to spatial and temporal changes in sulphur emissions, or due to variations in the prevailing large-scale weather systems transporting continental, maritime or arctic air masses to Finland. The latter factor can be attributed to the North Atlantic Oscillation (NAO), a periodic variation of the temperature and salinity conditions in the North Atlantic Ocean. The results indicate that with the help of ^{210}Pb the impact of climatological factors can be compensated to obtain a more emission-related sulphate concentration time series.

1. INTRODUCTION

The long range transport of acidifying components has been a serious environmental problem in Finland, as well as in the other Nordic countries, for decades. Sulphur has a key role in the acidifying problem. It is mainly emitted as sulphur dioxide from anthropogenic sources: consumption of fossil fuels and industrial processes. The primary compounds undergo transformation in the atmosphere: sulphur dioxide tends to oxidize to sulphate. The sulphur compounds are removed from the atmosphere by wet and dry deposition causing harmful effects on the surface water and fish as well as forest soil properties [1,2]. The geographical distribution of sulphur dioxide emissions affecting the atmospheric particle-bound sulphate concentration in Finland is presented in Fig.1 [3]. They have been discussed in detail in the reports of the EMEP (Co-operative programme for monitoring and evaluation of the long range transmission of air pollutants in Europe) project under the Convention on Long-range Transboundary Air Pollution (LRTAP). The present emission values are based on national emission reports and, in some cases, on estimates made within the framework of the EMEP project [4]. The EMEP emission database is currently probably the most complete and reliable emission survey covering the whole Europe.

Lead-210 (^{210}Pb) is a decay product of ^{222}Rn . The source of atmospheric ^{222}Rn is the continental areas of the Earth. Oceans and anthropogenic activities are a negligible source. This facilitates its use as a tracer for continental air masses. Lead-210 is also a tracer for secondary aerosols, e.g. particle-bound sulphate, as it is also formed in the atmosphere from gaseous precursors. ^{210}Pb has a radioactive half-life of 22 years, but in the atmosphere its concentration is determined by the residence time of the aerosol particles carrying it. Observed atmospheric residence times have varied from a few days to a few weeks [5,6].

Emission of Sulphur dioxide in 1998
(50km x 50km EMEP grid)

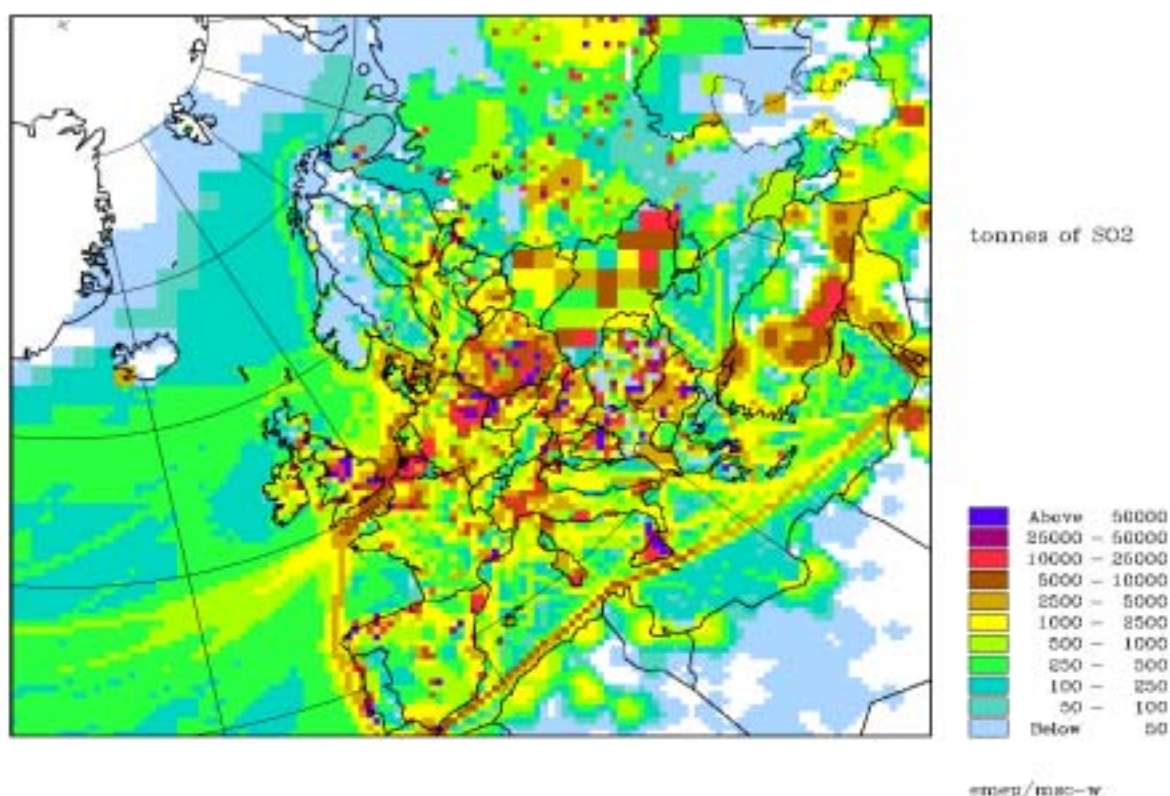


FIG. 1. Sulphur emissions (as tons of sulphur dioxide) in Europe in 1998 [3].

2. MATERIALS AND METHODS

Finnish Meteorological Institute (FMI) has analyzed daily aerosol samples (3500 m³ of air per day) at Nurmijärvi, southern Finland (60°30'N, 24°39'E) for ²¹⁰Pb since 1965 [5]. The measurements have been carried out by alpha counting of the in-grown ²¹⁰Po six months after the sampling.

Daily concentration of sulphur dioxide and particulate sulphate have been measured at the background monitoring station of Ähtäri (62°35'N, 24°12'E) since 1973. The station is situated in an agricultural area surrounded by fields and forests. The measurements were not affected by local sources until late 90's when the increased traffic on a road 100 m south to the measuring station caused relocation of the measurement site. A new station was established 5 km to the north-west from the previous one in June 1997.

The particulate sulphate has been measured from Whatman paper filters. The air volume flow was about 2 l/min during the time period 1973-1998, and about 17 l/min after that. The samples were analyzed first with X-ray fluorescence method, and since 1987 by ion chromatography. The methods for sampling and analysis have been kept as comparable as possible by parallel measurements during the changes in order to create long time series.

The quality of the results have been ensured by a quality assurance programme, which included e.g. intercalibrations and field intercomparisons organised by the ECE/EMEP-programme. The sampling and analysis methods, the station, as well as the quality assurance procedure have been discussed in detail in the FMI's annual report series "Air Quality Measurements" [7].

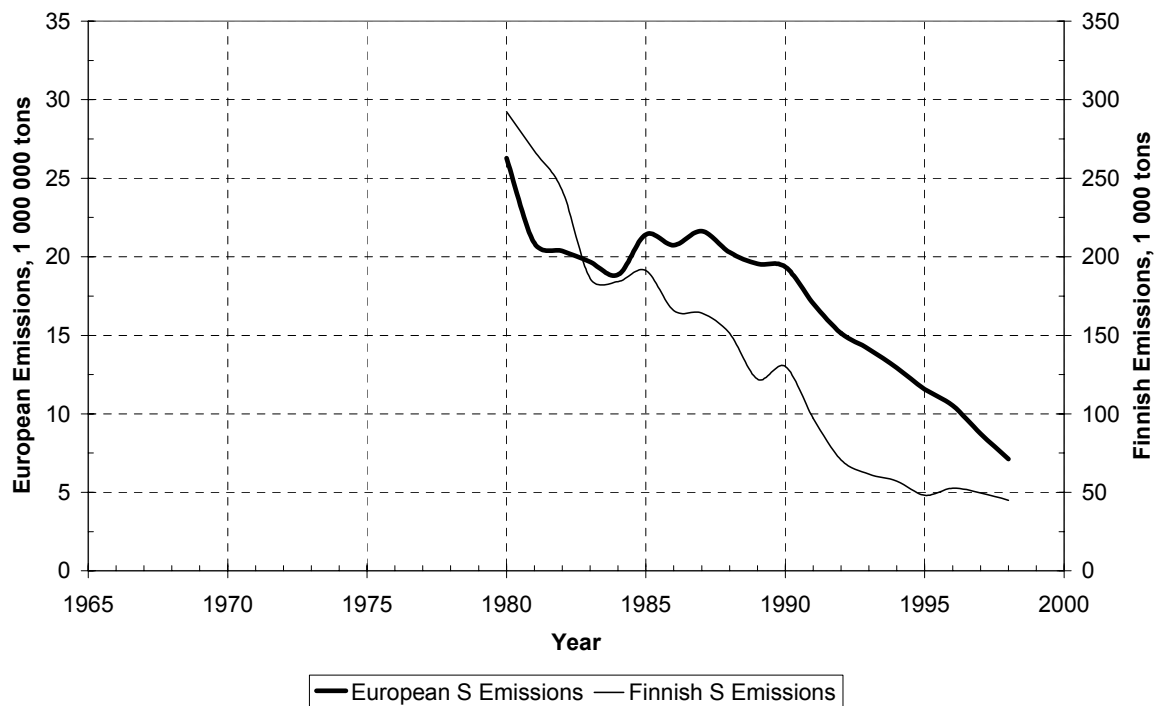


FIG. 2. Annual sulphur emissions in Europe (1000 000 tons) and in Finland (1000 tons) in 1980-1998 [3].

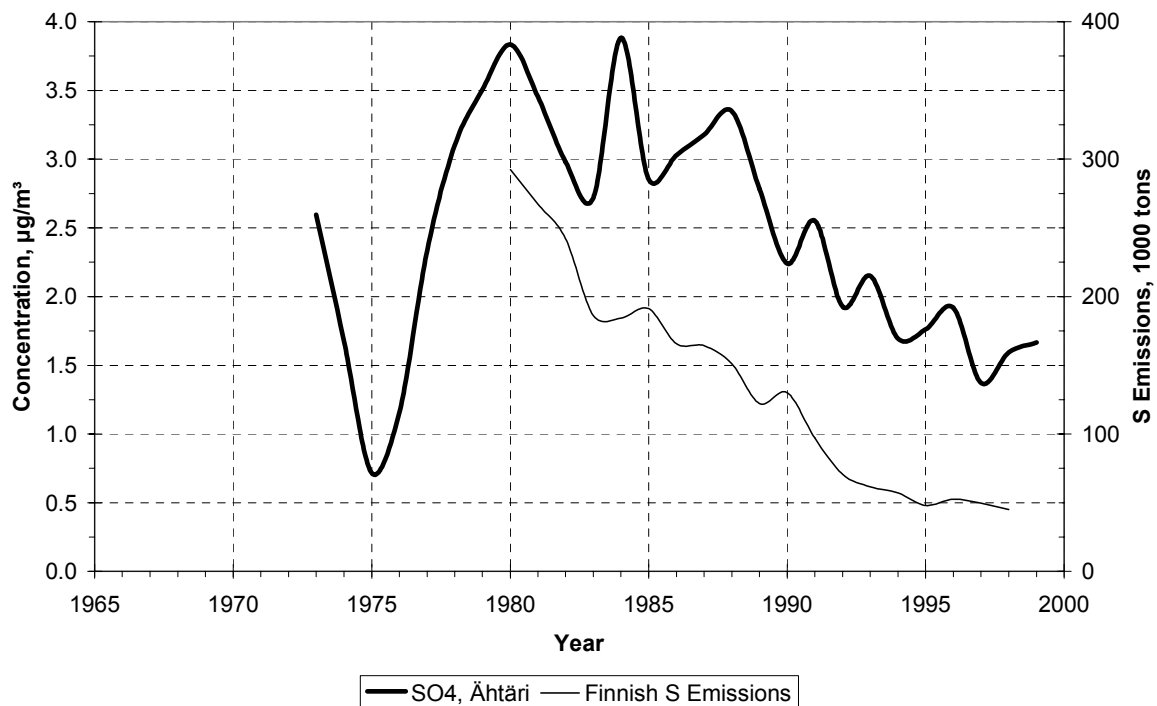


FIG. 3. Annual average sulphate concentration ($\mu\text{g}/\text{m}^3$) at Ähtäri, Finland and annual sulphur emissions (1000 tons) in Finland. [3].

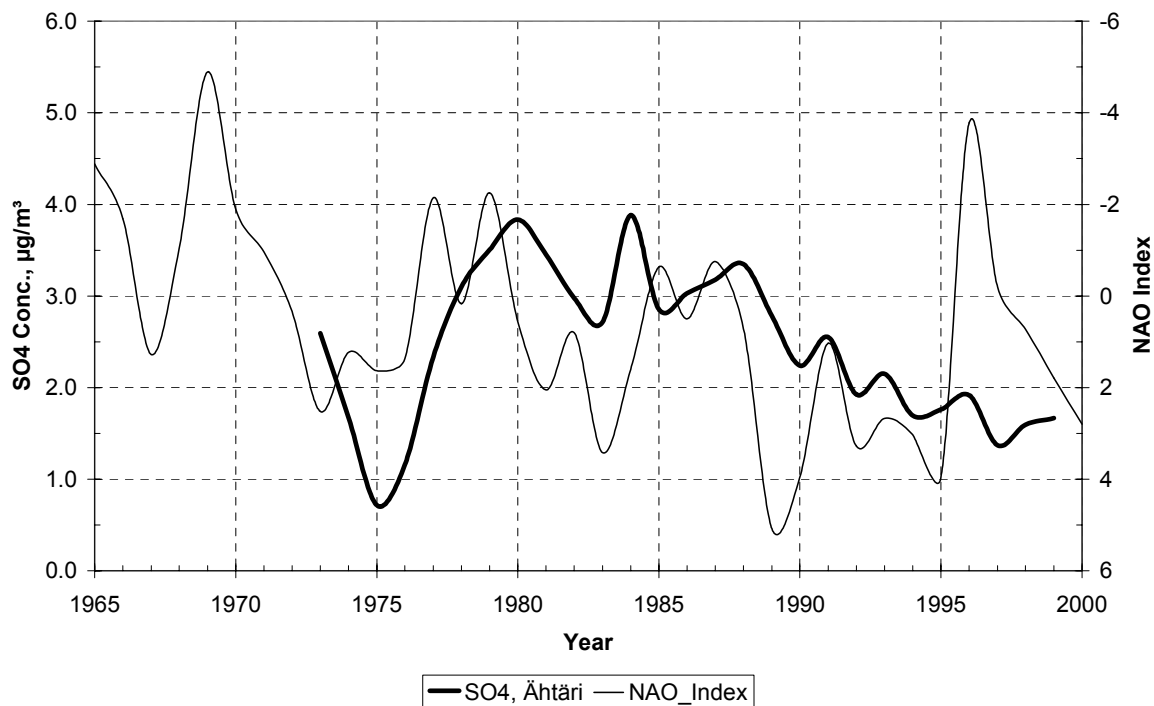


FIG. 4. Annual average sulphate concentration ($\mu\text{g}/\text{m}^3$) at Ähtäri, Finland and the wintertime NAO index [12]. Note the inverted righthand vertical scale.

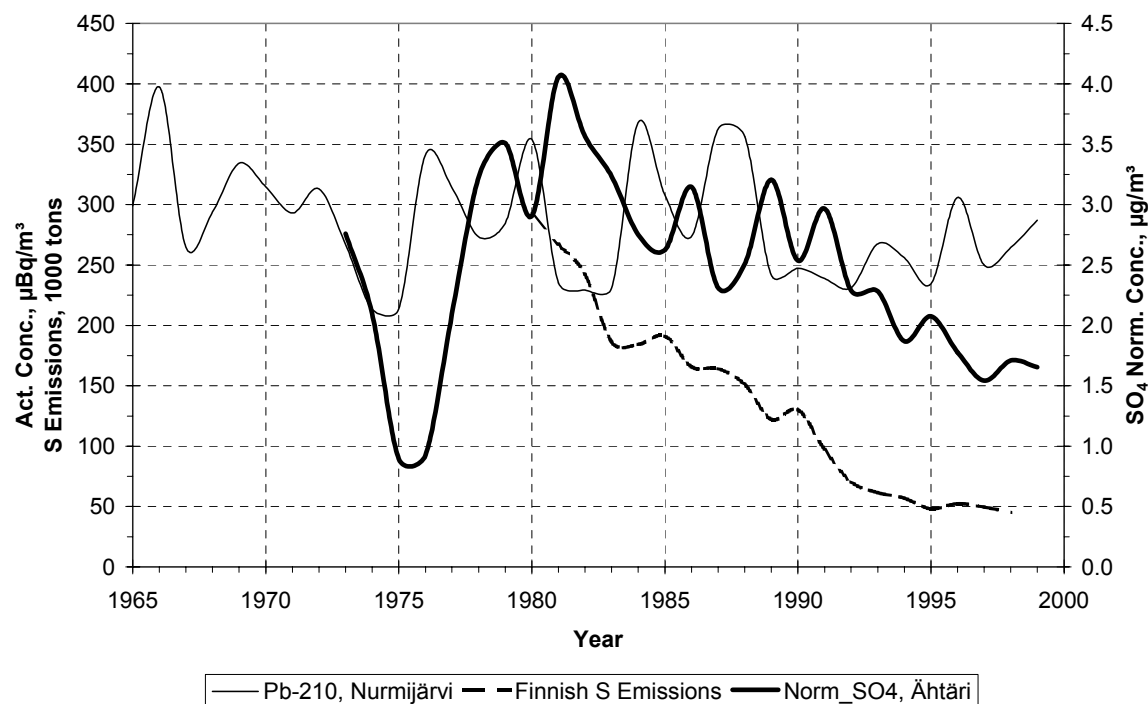


FIG. 5. Annual average ^{210}Pb activity concentration ($\mu\text{Bq}/\text{m}^3$) at Nurmijärvi, sulphur emissions (1000 tons) in Finland, and average normalized sulphate concentration ($\mu\text{g}/\text{m}^3$) at Ähtäri.

The distance between the monitoring sites at Ähtäri and Nurmijärvi is about 220 km but the activity concentration of ^{210}Pb is practically the same at both sites. The reason for this is that the ^{210}Pb concentration depends on large-scale weather phenomena and especially the origin of the air mass. Local effects, such as nocturnal surface inversion layers, have only a marginal effect to ^{210}Pb activity concentrations [8].

3. RESULTS AND DISCUSSION

In Europe the sulphur emissions have decreased from 26 millions of tons in 1980 to less than 8 millions of tons in 1998 [3]. During the same time the sulphur emissions in Finland have decreased from almost 300 000 tons to less than 50 000 tons (Fig. 2). The annual atmospheric sulphate concentration, however, fluctuates, and only after 1988 a clear downward trend in the concentration is evident despite the over 20 percent sulphur emission reduction during the 80's (Fig. 3). A significant ($p < 0.01$) downward trend has been calculated for particulate sulphate at Ähtäri for the time period 1987-1996. The annual Sen's slope estimate was -0.05 and the relative total change for the period -50%. For the longer period 1981-1996 the trend was also significant ($p < 0.001$), but the annual slope more gentle (-0.04). The seasonal Kendall slope estimate was used to calculate difference in trend between summer and winter seasons. At Ähtäri the downward trend ($p < 0.01$) was somewhat steeper (-0.05) during the winter months than during the summer months (-0.04) [9].

The explanation to this apparent discrepancy between emissions and concentrations is the prevailing weather patterns bringing frequently continental air masses to Finland. This, in turn, is related to the North Atlantic Oscillation (NAO), a periodic variation of the temperature and salinity conditions in the North Atlantic Ocean [10]. The NAO variations cause periodic climatic variations in e.g. wind direction and speed distributions and, therefore, also in ^{210}Pb concentrations [11]. This effect can be seen also in sulphate concentrations, although the effect is obscured by the changes in the anthropogenic sulphur emissions (Fig. 4). For example, the low sulphate concentration in the air in 1983 can be explained by the simultaneous high NAO index. This wintertime NAO index is determined as the December...March sea-level barometric pressure difference between Portugal and Iceland. When the NAO index is high, the westerly winds become more dominant bringing maritime air masses with low sulphate concentrations in Finland. When the NAO index is low the continental air masses with a high sulphate content become more frequent. In the 1990's the anticorrelation between the atmospheric sulphate concentration and the NAO index becomes more evident. This can be related to the gradual changes in source areas of atmospheric sulphur compounds. The relative contribution of long-range transported sulphur increases as the nearby emissions in northern Europe have decreased. The long-range transport is more affected by the variations in large-scale weather systems than short-range transport. Thus the changes in large-scale weather patterns is more easily reflected to the sulphate concentrations. The observed sulphate concentrations [$SO_{4 \text{ obs.}}$] can be normalized, however, in respect to simultaneous ^{210}Pb concentrations [^{210}Pb] with:

$$[SO_{4 \text{ norm.}}] = [SO_{4 \text{ obs.}}] - \frac{[^{210}\text{Pb}] - AVG}{AVG} \times [SO_{4 \text{ obs.}}] ,$$

where [$SO_{4 \text{ norm.}}$] is the normalized sulphate concentration and AVG the average ^{210}Pb activity concentration in 1965-1999 ($= 285 \mu\text{Bq/m}^3$). This way we can reduce the effect of purely climatological factors to the sulphate concentration observations (Fig. 5). The result is a temporal sulphate concentration behaviour, which resembles more the annual sulphur emissions.

4. SUMMARY AND CONCLUSIONS

We have used ^{210}Pb as a tracer for continental air masses in order to distinguish the causes for the variations in sulphate concentrations in the ground-level air. The observed variability in atmospheric sulphate concentrations can be due to spatial and temporal changes in sulphur emissions, or due to climatological effects, in other words the prevailing large-scale weather systems transporting continental, maritime or arctic air masses to Finland. The results indicate that with the help of ^{210}Pb the impact of climatological factors can be compensated to obtain a more emission-related sulphate concentration time series.

ACKNOWLEDGEMENTS

The financial support of The Finnish Society of Sciences and Letters and Magnus Ehrnrooth Foundation is gratefully acknowledged.

REFERENCES

- [1] TARRASON, L., SCHAUG, J. (Eds.), Transboundary Acid Deposition in Europe. EMEP/ MSC-W Report 1/99, Oslo (1999).
- [2] RUOHO-AIROLA, T., SYRI, S., NORDLUND, G., Acid deposition trends at the Finnish Integrated Monitoring catchments in relation to emission reductions. *Boreal Env. Res.* **3**: (1998) 205-219.
- [3] <http://www.emep.int> (2001).
- [4] BERGE, E. (Ed.), Transboundary Air Pollution in Europe. MSC-W Status Report 1997. Part 1; Emission dispersion and trends of acidifying and eutrophying agents. EMEP MSC-W Report 1/97, Oslo, (1997).
- [5] MATTSSON, R., Measurements of ^{210}Pb , ^{210}Bi and ^{210}Po in Urban and Rural Air in Finland. Contributions No. 81. Finnish Meteorological Institute, Helsinki (1975).
- [6] PAPASTEFANOU, C., BONDIETTI, E.A., Mean Residence Times of Atmospheric Aerosols in the Boundary Layer as Determined from $^{210}\text{Bi}/^{210}\text{Pb}$ Activity Ratios. *J. Aerosol Sci.* **22**: (1991) 927-931.
- [7] LEINONEN, L. (Ed.), Air Quality Measurements 1999. Finnish Meteorol. Inst., Helsinki (2000).
- [8] PAATERO, J., MATTSSON, R., HATAKKA, J., Measurements of Airborne Radioactivity in Finland, 1983-1990, and Applications to Air Quality Studies. Publications on Air Quality No. 17, Finnish Meteorological Institute, Helsinki (1994).
- [9] KULMALA, A., LEINONEN, L., RUOHO-AIROLA, T., SALMI, T., WALDÉN, J., Air quality trends in Finland. Finnish Meteorological Institute, Helsinki (1998).
- [10] RODWELL, M.J., ROWELL, D.P., FOLLAND, C.K., Oceanic forcing of the wintertime North Atlantic Oscillation and European Climate. *Nature* **398**: (1999) 320-323.
- [11] PAATERO, J., HATAKKA, J., MATTSSON, R., AALTONEN, V., VIISANEN, Y., Long-term Variations of Lead-210 Concentrations in Ground-level Air in Finland. Effects of the North Atlantic Oscillation. Proceedings from the EUROTRAC Symposium 2000. Springer Verlag Berlin, Heidelberg (in press).
- [12] http://www.cgd.ucar.edu/cas/climind/nao_winter.html (2001).

STABLE ISOTOPE ANALYSIS OF POLLEN AS A PALAEOINDICATOR – METHODOLOGICAL CONSIDERATIONS AND FUTURE CHALLENGES

N.J. LOADER

Environmental Change Research Group, Department of Geography,
University of Wales Swansea, Swansea, United Kingdom

D.L. HEMMING

Laboratory of Tree Ring Research,
University of Arizona, Tucson, Arizona, United States of America

Abstract. Samples of modern pollen were analysed for their stable carbon isotope composition and compared with environmental variables to assess the potential of this method as a new quantitative terrestrial palaeoindicator. Results demonstrate a strong positive correlation ($r^2=0.68$) between the temperature during a development period (approximately 4 weeks) prior to efflorescence and $\delta^{13}\text{C}_{\text{pollen}}$. Owing to variations in the chemical composition of the pollen grains and associated post depositional diagenesis we favour the isolation of the sporopollenin exina for isotopic analysis. A broad similarity in isotopic response was observed between three European tree genera, however significant absolute differences in $\delta^{13}\text{C}_{\text{pollen}}$ preclude any meaningful interpretation or palaeoenvironmental inference based solely upon a potentially variable bulk pollen sample. Consequently, we propose the isolation and analysis of a single genus when examining samples from antiquity. Preliminary extraction methods indicate that this approach is feasible using manual separation/hand picking methods and standard combustion continuous-flow isotope ratio mass spectrometry. If these initial results are representative of wider plant response, $\delta^{13}\text{C}_{\text{pollen}}$ may be used to reconstruct environmental change during pollen development and provide an indication of variations in mean annual temperature.

1. INTRODUCTION

Pollen stratigraphy is one of the most widely used and powerful tools in palaeoclimatic research [1-4]. Whilst interpretations of conventional pollen records have shown a remarkable degree of consistency, it is recognised that there are several possible sources of error that require careful consideration. These include spatial and temporal variations in the source of pollen production, its development, dispersal, deposition and preservation, as well as changes in the climatic relationship of modern and palaeo-pollen assemblages and time lags between an environmental event and its manifestation in the palaeo-record. This latter factor is particularly significant in situations where the environmental forcing is either too short in duration or too low in magnitude to overcome local vegetative inertia [5].

The physiological and environmental factors influencing carbon isotope fractionation during photosynthesis are directly linked to the carbon stable isotope composition ($\delta^{13}\text{C}$) of the resulting photosynthate [6-8]. This relationship has been successfully exploited to include $\delta^{13}\text{C}$ analysis of a range of bulk and organ specific plant material as palaeoenvironmental proxies [9-11]. The theoretical basis for this association was modelled by Farquhar [12] who was able to demonstrate environmental control on $\delta^{13}\text{C}$ through modification of stomatal conductance and/or assimilation rate. Since the dominant source of carbon is the same, the fundamental principles linking $\delta^{13}\text{C}$, climate and plant response should also apply to $\delta^{13}\text{C}_{\text{pollen}}$.

Pollen, like wood, comprises a variety of distinct chemical components [13], a cellulose intine, polysaccharide outer layer, a central nucleus and a sporopollenin exine. The relative proportions of these components vary between both species and degree of diagenesis [14-16].

Amundson and co-workers [17] were able to demonstrate that the $\delta^{13}\text{C}$ of raw pollen could be linked to the host plant material. As it is likely that these components have differing isotopic values resulting from the different processes occurring during their formation or through preferential diagenesis, it may therefore be necessary to isolate a single component of the pollen grain for isotopic analysis. From these initial investigations we have developed this work to demonstrate that this signal is also preserved in a single component of the pollen grain, the sporopollenin exine [18]. The pollen exine is particularly resistant to diagenesis [19] and also carries the morphological information essential to the correct identification of the parent plant genus/species. It was therefore decided that isolation and analysis of the sporopollenin exine would provide the most reliable signal for the meaningful interpretation of a palaeosequence.

The term sporopollenin was first used by Zetzsche [20] to describe the resistant component remaining after digestion of spores and pollen grains, (“sporonin” and “pollenin”). Although the exact structure of sporopollenin is not fully known it has been suggested, based upon infra-red spectroscopy, that it most likely comprises β -carotenoid esters of approximate formula $\text{C}_{90}\text{H}_{142}\text{O}_{27}$. [13] Potential therefore exists for the measurement of three isotopic species from this material. This paper describes some of our initial investigations methodological refinements and results from a study to assess the potential for stable isotope analysis of pollen as a quantitative terrestrial palaeoindicator.

2. METHODOLOGY

In conventional palynology the cellulose intine is removed during sample preparation through the acetolysis (acetylation) process [21]. Amundson *et al.* [17] have shown that this process, can lead to the contamination of the sample material by the reagents used for acetylation or by the incomplete removal of cellulose acetate (a by-product of the acetolysis reaction). For this reason we developed a carbon free alternative to acetylation that could be used to prepare pollen grains for stable carbon isotope analysis in which the cellulose is removed from the pollen grain through the addition of concentrated sulphuric acid [18]. We recommend such steps that isolate a single component for palaeoapplications, although the accompanying methodology and protocol may require significant variation depending upon the sample and its surrounding sediments.

In addition to the isolation of a single component, we investigated also the necessity for the isolation and analysis of a single genus/species over the hypothetical measurement of a bulk pollen sample. Samples of *Pinus sylvestris*, *Picea abies* and *Betula pendula* pollen were collected from mixed plant communities along an altitudinal transect in Switzerland. Both raw and extracted pollen grains were analysed to establish the nature or presence of a species effect through differences in bulk pollen chemistry or similarity in response between sites. A significant difference in $\delta^{13}\text{C}_{\text{pollen}}$ between genera would necessitate the isolation of a pure, single genus sample for isotopic analysis.

To investigate the nature of the pollen isotope signal samples of modern *Pinus sylvestris* pollen were collected across a network of 13 European sites (Table I). *Pinus sylvestris* has one of the widest distributions of any tree species. It is also a significant pollen producer and can be easily recognized and sampled in the field by relative non-experts. The trees sampled originated principally from botanical gardens and arboreta. Sampling across such a wide network was only made possible through the invaluable support and collaboration of many colleagues (Table I). Ideally sampling should be standardized to limit collection to natural or semi-natural communities, however this was not always possible. The strategy adopted did,

however, facilitate location and comparison of the resulting pollen isotope data with existing climatic datasets.

Samples were collected during or shortly after florescence, sieved to remove any remnant flower heads or similar large impurities, vacuum dried and stored in a freezer to prevent mould growth. Relatively little is known about isotopic variation during pollen development, however, since significant shifts are known to occur within individual trees, leaves and branches, samplers were instructed to collect pollen from a number of flower heads around a number of trees where possible in an attempt to accommodate such variation until a more accurate quantification of these effects can be made.

Table I. Sample location, approximate timing of pollen development, $\delta^{13}\text{C}_{\text{pollen}}$ and meteorological data used in this study.

Location	Latitude (°N)	Longitude (°E)	$\delta^{13}\text{C}_{\text{pollen}}$ PDB (‰)	Development Period (Month)	Development Period Temperature (°C)	Sample Collection
Murmansk	68.57	33.02	-28.84	June/July	10.60	Botanical Garden Murmansk
Rovaniemi	66.33	25.50	-28.48	June	11.03	R. Jalkanen
Helsinki	60.18	24.57	-26.48	May/June	12.40	M.Kotilainen
Uppsala	59.90	17.60	-27.99	May/June	11.14	K. Bremer
Tallin	59.25	24.47	-26.30	May/June	12.28	J. Ellia
Dawyck	55.25	-02.50	-26.69	May	11.29	D.Knott
Crowthorne	51.23	-00.49	-26.00	May	13.42	A. Loader
Wroclaw	51.05	16.52	-24.55	May	14.70	B. Bogacz
Halle	51.50	11.90	-27.97	April	10.10	Botanical Gardens, Halle
Freiburg	48.00	07.35	-26.52	May	13.66	Botanical Gardens, Freiburg
Dresden	51.07	13.47	-26.05	May	14.76	Tech. University, Dresden
Kiel	54.18	10.10	-27.38	May	12.43	Botanical Gardens, Kiel
Utrecht	52.06	05.07	-28.48	April	09.40	Botanical Gardens, Utrecht
Meise	50.56	04.20	-27.23	April	09.31	Botanical Gardens, Meise
Thessaloniki						
•	40.30	22.57	-24.09	April	15.07	A Gerasimidis
Nice	43.38	07.12	-25.22	April	12.80	Botanical Garden, Nice
Lyon	45.42	04.57	-27.70	April	10.74	P.Berthet
Bordeaux	44.50	-00.42	-26.99	April	11.05	M.Vautravers
Mulhouse	47.45	07.21	-27.56	April	09.89	Botanical Garden, Mulhouse
Nantes	47.10	-01.35	-28.26	April	09.61	C. Figeneau
Nancy	42.38	07.12	-29.61	April	09.26	P. Romaric
Sofiya	42.38	23.22	-27.00	April	12.61	P. Geber
Zagreb	45.48	15.58	-27.26	April	11.60	M. Jurkovic
Madrid*	40.27	-03.32	-29.04	March/April	11.10	Botanical Garden, Madrid
Zurich	47.13	08.20	-29.11	April	08.57	Botanical Garden, Zurich
Le Chesnay	48.57	2.27	-27.73	April	09.40	D. Lobreau-Callen
Moveto	46.13	08.45	-26.72	April	10.40	N. Loader
Vienna	48.15	16.22	-30.63	April	11.80	F. Toel

*Samples collected after cessation of florescence.

The stable carbon isotope ratios of the archived pollen were determined using a VG-SIRA II isotope ratio mass spectrometer interfaced with a FISIONS NA1600NC (The Godwin Institute for Quaternary Research, Cambridge) and a Europa ANCA-GSL combustion isotope ratio mass spectrometer (Environmental Dynamics Institute, University of Wales, Swansea). Results are expressed as per mil (‰) deviations from the Pee Dee Belemnite standard [22,23]. Repeat analyses of a laboratory standard pollen yield a reproducibility typically less than 0.1 per mil (1 standard deviation).

The $\delta^{13}\text{C}_{\text{pollen}}$ data are compared with temperature from meteorological stations nearest to the collection sites (Table I). Although the pollen initial is formed in the growing season of the previous year, a period of between 4-6 weeks immediately prior to pollen release is believed to represent the period during which the majority of pollen mass is accumulated [24]. The average temperature during this period, hereafter referred to as 'development period temperature' was correlated against $\delta^{13}\text{C}_{\text{pollen}}$. Although development period temperature may be a physiologically relevant and useful indicator for some palaeoclimate analyses the relationship between $\delta^{13}\text{C}_{\text{pollen}}$ and a more stationary climate indicator, mean annual temperature (MAT), was also determined.

3. RESULTS

Carbon isotope analyses of selected pollen samples suggest that when operating under standard conditions *ca.* 500 spruce *exina* approximate to 9 micrograms of carbon. To what extent such samples sizes are representative of the local signal is yet to be determined, however it demonstrates that for carbon isotope analysis relatively small samples are required (Figure 1).

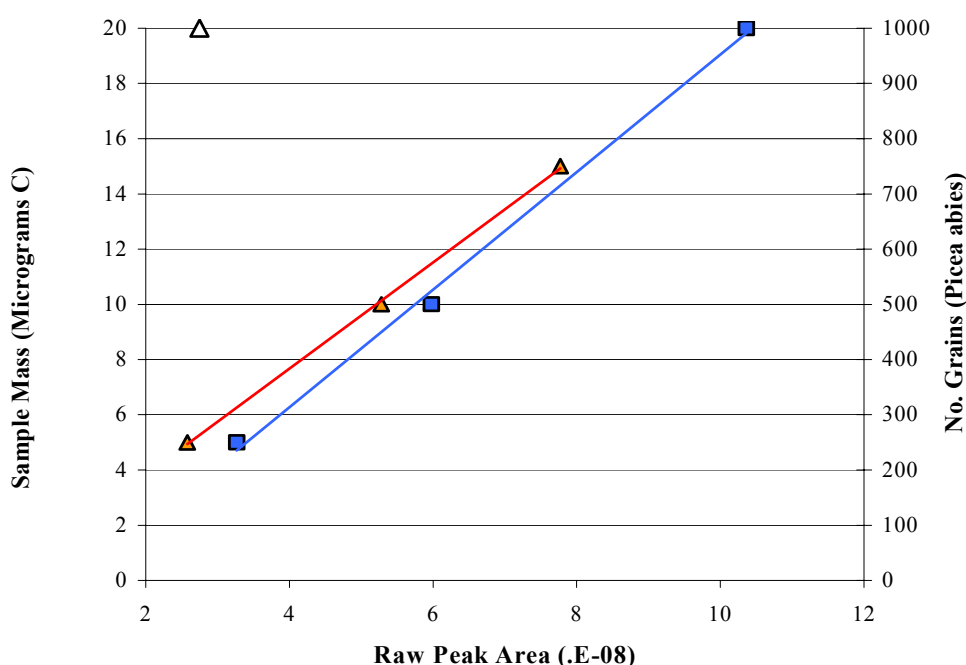


FIG. 1. Relationship between sample sizes (No. *Picea abies* pollen grains (filled triangles) and reference material (filled squares)) and mass spectrometer peak area. Open triangle represents a sample comprising 1,000 *Pinus sylvestris* grains.

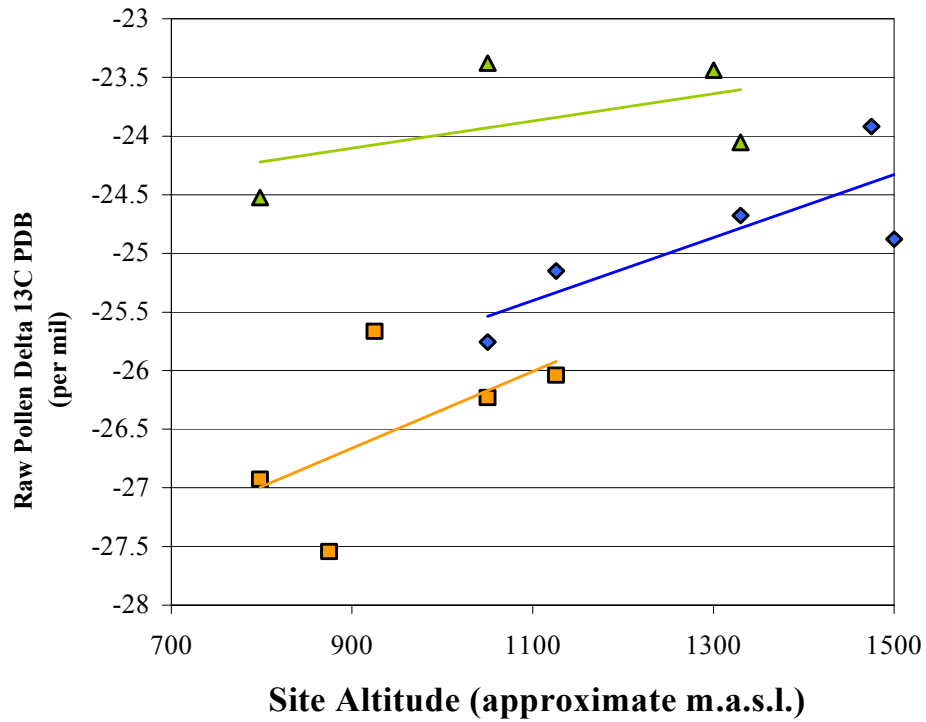


FIG. 2. Relationship between $\delta^{13}C_{\text{pollen}}$ and site altitude for three European tree genera; *Picea abies* (triangles), *Betula pendula* (diamonds) and *Pinus sylvestris* (squares). The significant offset between the three trend lines demonstrate the requirement for analysis of pollen from a single genus.

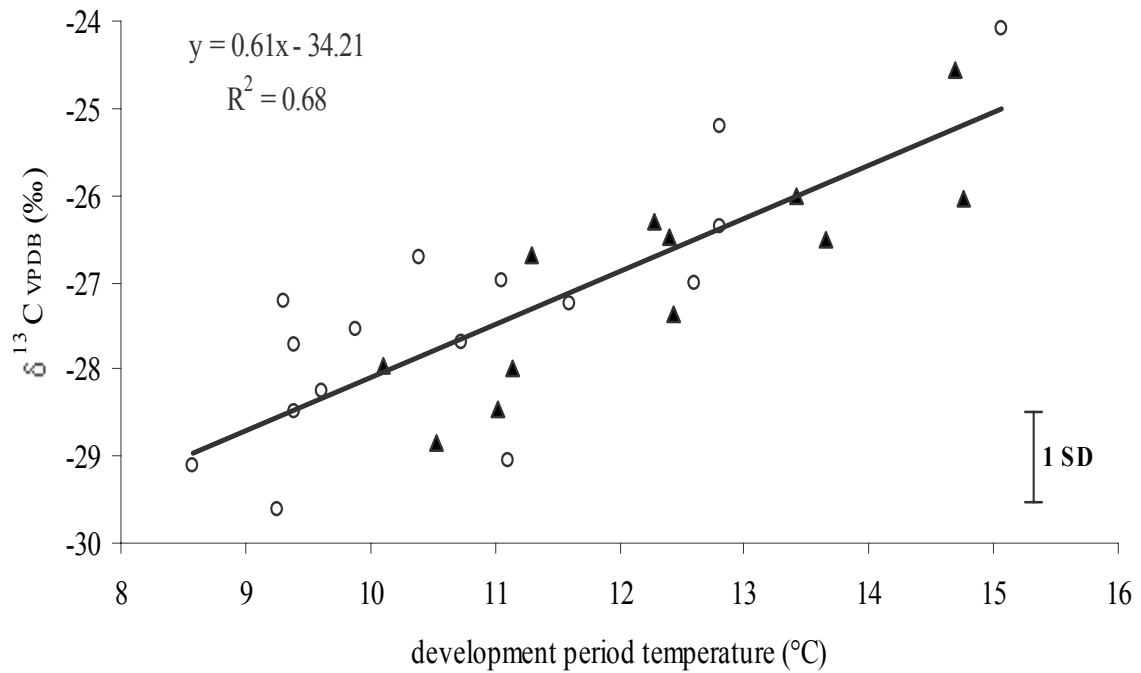


FIG. 3. Relationship between $\delta^{13}C_{\text{pollen}}$ and development period temperature (with 1 standard error confidence interval). Open circles and filled triangles represent the 'southern group' (including Madrid) and 'northern group' respectively.

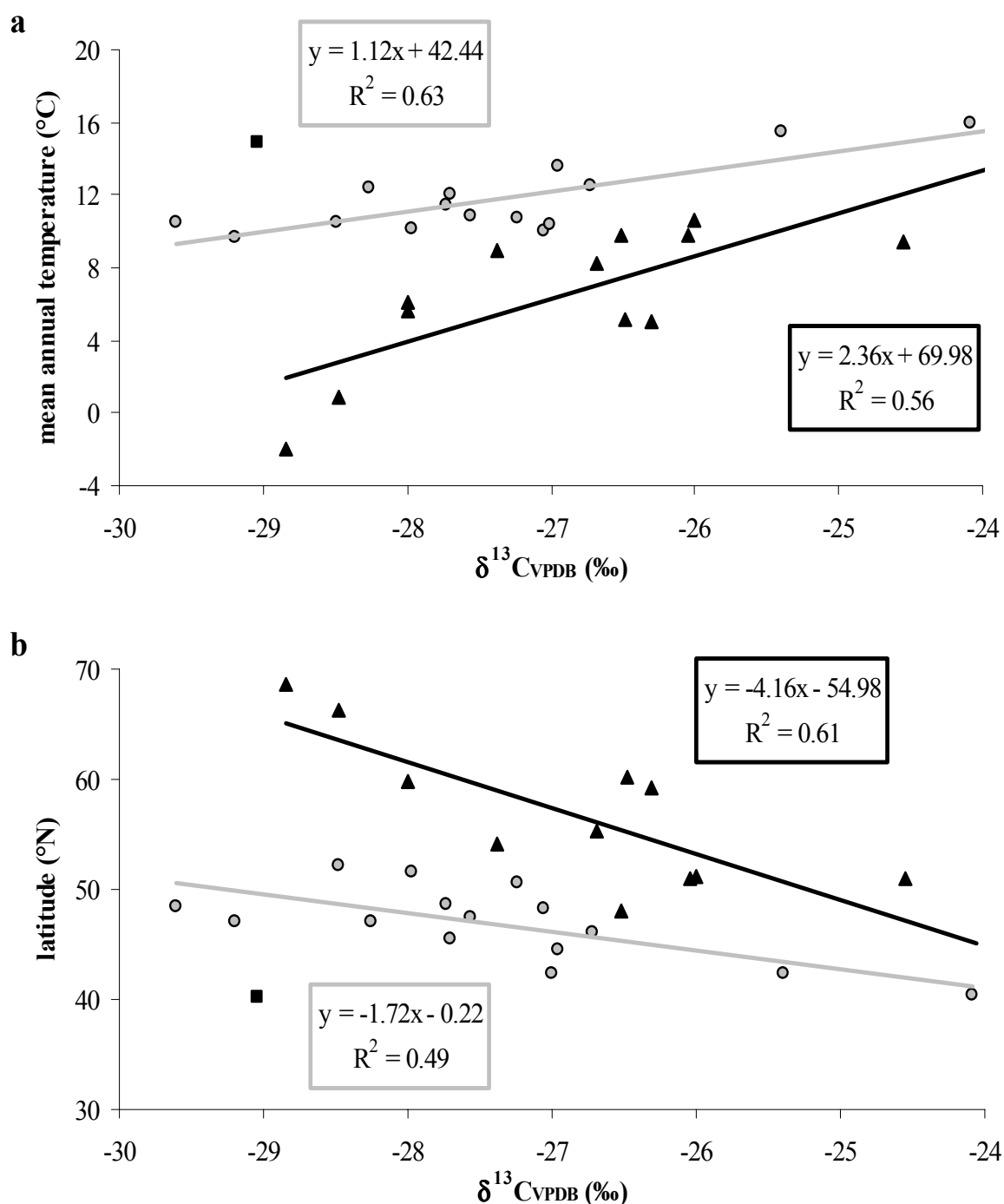


FIG. 4. Relationships between $\delta^{13}C_{pollen}$ and (a) mean annual temperature and (b) latitude for the 'northern' (black triangles) and 'southern' (grey circles) groups. The data for Madrid (black square) may be associated with another, more southern group.

From a comparison of the three European plant genera analyzed it is also apparent that significant differences exist between their raw carbon isotope signals. These off-sets are likely to relate to differences in the processes operating during photosynthesis and the role of stored photosynthate in pollen development. Although significant scatter is apparent from the pollen collected along the transect (some of which could be related to variations in aspect) it is interesting to note that the overall trends are similar. Nevertheless these findings emphasize the importance of a "single genus approach" when analyzing palaeosequences (Figure 2).

A strong positive linear relationship was observed between $\delta^{13}\text{C}_{\text{pollen}}$ and development period temperature (Figure 3). This is in agreement with most temperature related associations found in studies of tree ring $\delta^{13}\text{C}$ [25], and may be explained theoretically through a relative increase in carboxylation fractionation, resulting from a decrease in stomatal conductance and/or an increase in assimilation. The slope of the temperature regression (0.61 ‰/ °C) is steeper than those generally observed with tree ring $\delta^{13}\text{C}$, suggesting greater temperature sensitivity. This may reflect the fact that the majority of pollen formation occurs in a considerably shorter time window than tree rings, and the timing of this formation is highly temperature dependent [26].

Figure 4a describes the relationship between $\delta^{13}\text{C}_{\text{pollen}}$ and MAT. The data cluster around two regression lines that display similar maxima and minima for both temperature and $\delta^{13}\text{C}$. If these data are compared with site latitude (Figure 4b) it is evident that these clusters are associated with geographical location; one being composed of pollen from the relatively cold, northern sites ($>50^\circ\text{N}$) and warmer, southern sites ($<50^\circ\text{N}$). Each group shows an increase in $\delta^{13}\text{C}_{\text{pollen}}$ with increasing temperature and decreasing latitude, but the slope of this relationship is steeper for the northern group, again suggesting greater temperature sensitivity. Enhanced temperature sensitivity with increasing latitude is also observed in tree-ring studies [27,28], and is to be expected given that temperature is typically more limiting at higher latitudes.

Although it is clear that the two linear relationships between $\delta^{13}\text{C}$ and MAT are the result of the close association between latitude, MAT and development period temperature, it is not apparent from these data why there are two groupings and what causes the switch between groups. The reason for this shift (from ~ -30 ‰ to ~ -25 ‰) appears to be related to a change in the timing of the development period from April/May to May/June. During this switch MAT remains approximately equal but development period temperature changes from $\sim 9^\circ\text{C}$ (southern group minimum) to $\sim 15^\circ\text{C}$ (northern group maximum). These temperatures and associated $\delta^{13}\text{C}_{\text{pollen}}$ values may therefore represent temperature thresholds for pollen development. It is also possible that this shift in response might represent the emergence of an additional (as yet undetermined) limiting factor to pollen development within the harsher higher latitude environment. Luomajoki [29] identified early ($<63^\circ\text{N}$) and late ($>63^\circ\text{N}$) flowering populations of *Pinus sylvestris* across Finland. In the more northerly group anthesis occurred later than in the south and required a lower actual threshold, but greater proportion of the annual heat sum. Significant hybridisation and genetic differences in *Pinus sylvestris* are known to occur across Europe [30,31]. It is possible that the observed trends in $\delta^{13}\text{C}_{\text{pollen}}$ response reflect such genetic differences.

4. CONCLUSIONS

This pilot investigation represents an early attempt to determine the nature of the relationship between $\delta^{13}\text{C}_{\text{pollen}}$ and external environmental controls. In doing so it has identified several important questions, methodological issues and areas of further study that must be addressed before a meaningful interpretation of the palaeorecord can proceed.

Through a spatial study we demonstrate a statistically significant relationship between $\delta^{13}\text{C}_{\text{pollen}}$ and development period temperature. Whilst it is likely that temperature is not the only factor influencing $\delta^{13}\text{C}$ in pollen, this preliminary work suggests that a link (direct or indirect) appears to exist which may, in future, be exploited in the palaeo-record. Carbon isotope analysis of pollen from different plant genera show a degree of similarity, however the off-set between each is such that variations in pollen type within bulk samples could result in ambiguous pollen derived isotopic time series. Where possible a single genus is therefore

recommended for stable isotope determination. Analysis of sporopollenin extracts from spruce and pine grains reveal that the absolute quantities of pollen required for measurement of $\delta^{13}\text{C}_{\text{pollen}}$ are within realistic limits for manual selection/hand picking. Variations in the resistance of the pollen components through time emphasizes the need for extraction and analysis of a single component of the pollen grain when applying these methods to the palaeorecord.

Further research is already underway to assess variations in response at species level and to refine the pollen development and statistical models used in this study through incorporation of additional environmental factors including altitude, site hydrology, insolation, photosynthetic relative humidity and cumulative degree-day totals.

ACKNOWLEDGEMENTS

We thank all those who provided pollen for this investigation. We are also grateful to the following for their advice and support: Prof. Sir Nicholas Shackleton, Mike Hall, Roy Switsur, Tony Carter, Zhou Liping (Godwin Institute for Quaternary Research, University of Cambridge), John Waterhouse, Alison Barker (Anglia Polytechnic University), Owen Davis (University of Arizona), Iain Robertson, (CSIR Environmentek), Kath Ficken, Danny McCarroll (Environmental Dynamics Institute, Prifysgol Cymru Abertawe). This work was partially funded by a grant to NJL from the British Ecological Society and the Leverhulme Trust 19990411.

REFERENCES

- [1] BIRKS, H.J.B., GORDON, A.D., Numerical Methods in Quaternary Pollen Analysis. Academic Press Inc. U.S.A (1985).
- [2] HUNTLEY, B., PRENTICE, I.C. 1988: July temperature in Europe from pollen data 6000 years before present. *Science* **241** (1988) 687-689.
- [3] GUIOT, J. PONS, A., BEAULIEU, J-L DE, REILLE, M., A 140,000 year continental climate reconstruction from two European pollen records. *Nature* **338** (1989) 309-313.
- [4] TZEDAKIS, P.C., BENNETT, K.D., Interglacial vegetation succession: a view from Southern Europe. *Quaternary Science Reviews* **14** (1995) 967-982.
- [5] LOWE, J.J., WALKER, M.J.C., 2nd Edition. Reconstructing Quaternary Environments. Longman, Harlow. U.K. (1997).
- [6] FRANCEY, R.J., FARQUHAR, G.D., An explanation of $^{13}\text{C}/^{12}\text{C}$ variations in tree rings. *Nature* **297** (1982) 28-31.
- [7] SCHLESER, G.H., Carbon isotope fractionation during CO_2 fixation by plants. In: Esser & Overdieck (Editors). *Modern Ecology: Basic and Applied Aspects*. Elsevier, The Netherlands (1991).
- [8] PATE, J., ARTHUR, D., Delta ^{13}C analysis of phloem sap carbon: novel means of evaluating seasonal water stress and interpreting isotope signatures of foliage and trunk wood of *Eucalyptus globulus*. *Oecologia* **117** (1998) 301-311.
- [9] HEMMING, D.L., SWITSUR, V.R., WATERHOUSE, J.S., HEATON, T.H.E., CARTER, A.H.C., Climate variation and the stable isotope composition of tree ring cellulose: an intercomparison of *Quercus robur*, *Fagus silvatica* and *Pinus sylvestris*. *Tellus* **50B**(1) (1998) 25-33.
- [10] WHITE, J.W.C., CIAIS, P., FIGGE, R.A., KENNY, R., MARKGRAF, V., A high resolution record of atmospheric CO_2 content from carbon isotopes in peat. *Nature* **367** (1994) 153-156.

- [11] BEERLING, D.J., WOODWARD, F.I., Leaf stable isotope composition records increased water use efficiency of C₃ plants in response to atmospheric CO₂ enrichment. *Functional Ecology* **9** (1995) 394-401.
- [12] FARQUHAR, G. D., O'LEARY, M. H., BERRY, J. H., On the relationship between carbon isotope discrimination and the intercellular carbon dioxide concentration in leaves. *Australian Journal of Plant. Physiology* **9** (1982) 121-137.
- [13] MOORE, P.D., WEBB, J.A., COLLINSON, M.E., *Pollen Analysis*. 2nd Ed. Blackwell Scientific, Oxford. U.K. (1991).
- [14] BENNER, R., FOGEL, M.L., SPRAGUE, E.K., HODSON, R.E., Depletion in ¹³C in lignin and its implications for stable carbon isotope studies. *Nature* **329** (1987) 708-710.
- [15] SCHLESER, G.H., FRIELINGSdorf, J., BLAIR, A., Carbon isotope behaviour in wood and cellulose during artificial aging. *Chemical Geology* **158** (1999) 121-130.
- [16] SHAW, G., YEADON, A., Chemical studies on the constitution of some pollen and spore membranes. *Grana Palynologica* **5**(2) (1964) 247-252.
- [17] AMUNDSON, R., EVETT, R.R., JAHREN, A.H., BARTOLEME, J., Stable Carbon Isotope composition of Poaceae pollen and its potential in palaeovegetational reconstructions. *Review of Palaeobotany and Palynology* **99** (1997) 17-24.
- [18] LOADER, N.J., HEMMING, D.L. 2000: Preparation of pollen for stable carbon isotope analyses. *Chemical Geology* **165** (2000) 339-344.
- [19] BROOKS, J., SHAW, G., Identity of sporopollenin with older kerogen and new evidence for the possible biological source of chemicals in sedimentary rocks. *Nature* **220** (1968) 678-679.
- [20] ZETZSCHE, F., Sporopollenine. In: G. Klein (Editor). *Handbuch der Pflanzen Analyse*. 3rd Edition. Vienna (1932).
- [21] ERDTMAN, G., The acetolysis method. *Svensk Botanisk Tidskrift* **54** (1960) 561-564.
- [22] CRAIG, H., Isotopic standards for carbon and oxygen correction factors for mass spectrometric analysis of carbon dioxide. *Geochimica Cosmochimica Acta* **12** (1957) 133-149.
- [23] COPLEN, T.B., Discontinuance of SMOW and PDB. *Nature* **373** (1995) 285.
- [24] GORDON, A.G., *Seed Manual for Forest Trees*. Forestry Commission Bulletin **83**. HMSO, Great Britain (1992).
- [25] SCHLESER, G.H., Causes of carbon isotope behaviour in tree rings. In: Spiecker, H. and Kahle, P. (Editors). *Modelling of Tree-Ring Development - Cell structure and Environment*. Workshop, Freiburg (1994).
- [26] PESSI, A-M., PULKKINEN, P., Temporal and spatial variation of airborne Scot's Pine (*Pinus sylvestris*) pollen. *Grana* **33** (1994) 151-157.
- [27] FRITTS, H.C., *Tree Rings and Climate*. Academic Press, London. U.K. (1976).
- [28] SCHWEINGRUBER, F.H., *Tree Rings and Environmental Dendroecology*. Haupt, Berne (1996).
- [29] LUOMAJOKI A., Climatic adaptation of Scots pine (*Pinus sylvestris*) in Finland based on male flowering phenology. *Acta Forestalia Fennica* **237** (1993) 27.
- [30] TUTIN, T.G., BURGESS, N.A., CHATER, A.O., EDMONDSON, J.R., HEYWOOD, V.H., MOORE, D.M., VALENTINE, D.H., WALTERS, S.M., WEBB, D.A. (Editors), *Flora Europaeae Volume 1*. 2nd. Edition. Cambridge University Press, Cambridge, U.K. (1993).
- [31] JALAS, J., SUOMINEN, J. (Eds.), *Atlas Florae Europaeae*. Helsinki (1973).

CAN EC AND UK NATIONAL METHANE EMISSION INVENTORIES BE VERIFIED USING HIGH PRECISION STABLE ISOTOPE DATA?

D. LOWRY, C.W. HOLMES, E.G. NISBET, N.D. RATA

Atmospheric Monitoring and Isotope Laboratory,
Department of Geology,
Royal Holloway, University of London,
Egham, United Kingdom

Abstract. The main anthropogenic sources of methane in industrialised countries (landfill/waste treatment, gas storage and distribution, coal) are far easier to reduce than CO₂ sources and the implementation of reduction strategies is potentially profitable. Statistical databases of methane emissions need independent external verification and carbon isotope data provide one way of estimating the expected source mix for each country if the main source types have been characterised isotopically. Using this method each country participating in the CORINAIR 94 database has been assigned an expected isotopic value for its emissions. The averaged $\delta^{13}\text{C}$ of methane emitted from the CORINAIR region of Europe, based on total emissions of each country is -55.4‰ for 1994. This European source mix can be verified using trajectory analysis for air samples collected at background stations. Methane emissions from the UK, and particularly the London region, have undergone more detailed analysis using data collected at the Royal Holloway site on the western fringe of London. If the latest emissions inventory figures are correct then the modelled isotopic change in the UK source mix is from -48.4‰ in 1990 to -50.7‰ in 1997. This represents a reduction in emissions of 25% over a 7-year period, important in meeting proposed UK greenhouse gas reduction targets. These changes can be tested by the isotopic analysis of air samples at carefully selected coastal background and interior sites. Regular sampling and isotopic analysis coupled with back trajectory analysis from a range of sites could provide an important tool for monitoring and verification of EC and UK methane emissions in the run-up to 2010.

1. INTRODUCTION

Global CO₂ emissions are not being reduced at the rates expected to meet Kyoto targets, so more attention is being given to reduction of methane, the greenhouse gas with the second biggest global warming potential (GWP). Statistical inventories suggest that methane emissions are reducing in developed countries, but to verify these findings it is essential to make independent atmospheric measurements. In addition, the carbon isotopic analysis of air samples provides a method of understanding which source emissions are changing.

To date, assessments of methane emission are mostly made by 'bottom-up' methods, using statistical databases multiplied by estimates of emission factors. Typically, 'bottom-up' estimates of emissions are very precise, cited to the nearest source unit and often without errors, but are highly inaccurate, as the emissions factors are poorly known and vary greatly with local conditions, climate, and cultural factors. Moreover, such estimates necessarily depend on government, and cannot easily be verified independently. In contrast, direct 'top-down' atmospheric measurement of emissions are accurate in that there is a known amount of methane in the atmosphere but are imprecise with large error margins when assigning the methane to source regions. Direct atmospheric studies can be independent of national administrations, and indeed can be made from outside national borders. Methane has considerable attraction as a way of complying with Kyoto promises if source fluxes can be quantified accurately. In comparison to the difficult but essential task of social redesign to reduce carbon dioxide emissions, some methane sources can be reduced without major costs or even with profit [1]. In densely populated industrial regions the two major sources of methane are landfills and fossil fuel extraction and distribution and examples of reduction

strategies include reducing gas leaks or utilising landfill gas. Such fluxes should be a major target for efforts to reduce greenhouse gas emissions.

The use of isotopes of methane in correlation with concentration data and regional and national emissions statistics is still in its infancy. The detailed study of methane sources in the Heidelberg region of Germany by *Levin et al.* [2] revealed that calculation of source proportions by isotopic analysis could, when combined with data from background methane measurement stations, be used in the long term to monitor the progress of reduction strategies. *Levin et al.* [2] showed clearly that the official emissions inventory that region of Germany would need substantial revision to be consistent with the atmospheric record.

2. METHANE INVENTORY DATA

Official inventory estimates are calculated for the UK and European Union, as part of the Kyoto process, e.g. *CORINAIR 94* [3]. Such estimates depend largely on statistical calculations that scale up from the ‘per-unit’ results of studies of specific source types to obtain a regional bulk estimate. Wider ranging but less detailed inventories are maintained by the EMEP co-operative programme for monitoring and evaluation of the long range transmission of pollutants in Europe (www.emep.int/), but many countries do not provide methane data and yet more do not provide up to date information. Similar data can be obtained through the United Nations Framework Convention on Climate Change (www.unfccc.de). The data are normally divided by the UNESCO snap categories of sources, which in the case of methane allow each source group to be assigned a $\delta^{13}\text{C}$ value. Even when the data are reported there are some inconsistencies. It is not compulsory to include natural emissions. Wetland emissions are a significant source in some regions of Ireland, Sweden and Finland, with other localised pockets around Europe. Such emissions are highly variable depending on season and annual temperature and so are difficult to quantify, but have a significant influence on the isotopic mix of emissions in the regions where they are present.

3. ISOTOPES OF METHANE

3.1. Isotopic characterization of methane sources

Anthropogenic and natural methane sources in Europe have a wide range of $\delta^{13}\text{C}$ signatures [e.g. 4,5,6,7,8]. Depending on the combination of sources in a particular region, these signatures can be used to estimate the proportion of each source category within a source mix. If the emission from one source is accurately quantified then it is also possible to use the isotopic signature to estimate emissions from the other sources.

Natural sources, mostly from wetlands, are an important source in some peripheral regions of Europe and have widely varying isotopic values from around -58‰ for tropical wetlands, to -63‰ in the boreal wetlands, to -67‰ for those more than 60°N which are only active during the summer months. They are important in regional source isotopic mixes because they are depleted in ^{13}C relative to other sources and the value assigned to this category for the mostly temperate European wetlands is -63‰ .

The isotopic signatures of specific anthropogenic sources vary according to local conditions [e.g. 2,4,9,10]. However, some generalisations can be made. Emissions to atmosphere from landfills have a tightly constrained range of $\delta^{13}\text{C}$ from -56 to -50‰ with averages varying from -55 to -51‰ [4,6,8,11] dependent on the region of the world and the landfill practices in operation. Eructations from ruminants have been measured at $-62\pm 3\text{‰}$ [4]. Organic wastes

from animals typically have $\delta^{13}\text{C}$ values between the landfill gases and the ruminant emissions, probably $-58\pm 3\text{‰}$.

Coal mining activity and domestic coal burning, although in decline in much of Europe, is still a significant contributor to emissions, and has well defined $\delta^{13}\text{C}$ of $-35\pm 3\text{‰}$ [7]. Natural gas, in contrast, has a very wide range of values. The gas from the North Sea fields. is very distinctive: it is thermogenic gas with a range of isotopic values from -37 to -28‰ . To constrain the gas source in the SE of England the $\delta^{13}\text{C}$ of the natural gas supply at Royal Holloway, University of London (RHUL) was measured each month from 1997 to 1999 giving an average of $-34.2\pm 1.4\text{‰}$ ($n=20$) [8]. This source of gas is significantly heavier isotopically than the mix of Siberian gases supplied to most European countries east of the Rhine, and averaging close to -50‰ when used in the Heidelberg system, SW Germany [2]. Our own measurements of gas from St. Petersburg, Russia, are in the range -51.5 to -48.5‰ , and confirmed by Levin (pers. comm. 1998, 2000). This represents mixing of the shallow West Siberian gas which is dominantly biogenic -64 to -58‰) and deeper reserves which are more thermogenic -50 to -38‰ , [12]).

Minor emissions of methane from vehicles are around $-28\pm 3\text{‰}$ based on experiments in Heidelberg [3,4]. These emissions are related to the $\delta^{13}\text{C}$ of the hydrocarbon mix of the fuel used and the distribution and age of vehicle types (probably very similar throughout western Europe); those which have less efficient combustion giving higher methane emissions which are more depleted in ^{13}C [13]. The industrial combustion source of methane, also declining in recent years is dependent on the fuel being combusted, and for the purposes of calculating national $\delta^{13}\text{C}$ mixes, it is taken to be the same as the fossil fuel mix for each country.

3.2. The regional isotopic mix of atmospheric methane

Once background concentration and isotopic records have been established for stations in the European realm of the Northern Hemisphere it is possible to use the excess concentration and isotopic shift to calculate the $\delta^{13}\text{C}$ of the source or source mix responsible for this excess (Table I). The data for background and samples are plotted with $\delta^{13}\text{C}$ on the y-axis and $1/\text{concentration}$ on the x-axis. Lines passing through both background and sample points will intercept the y-axis at the $\delta^{13}\text{C}$ value representing the source or source mix of the excess methane (in simplified terms when $1/\text{concentration}$ approaches 0).

The ideal background stations are maritime sites where during certain wind directions the air is well mixed and has negligible influence of continental emissions during the 4-5 days prior to arrival. The background stations used for Europe are Mace Head, Ireland, and Izaña, Tenerife. Isotopic seasonality is of the order of 0.4‰ at 53°N [see 8,14] for Atlantic air arriving from the western sector. When the wind changes to the east the air mass contains excess methane from European emissions. Most air masses follow trajectories along which there is incorporation of emissions from more than one country (Fig. 1). An isotopic shift from -48 to -53‰ was observed in the source mix for the Heidelberg region between 1990 and 1995 [2], largely due to reduction of coal mining emissions and a change in the source of the gas supply. Monitoring the isotopic shift in central European air arriving at Mace Head shows change from -54.0 to -55.6‰ between 1996 and 2000. Furthermore air from southern Europe shows greater depletion in ^{13}C , down to -57‰ , indicative of more natural and agricultural sources and less fossil fuel and landfill.

Table I. $\delta^{13}\text{C}$ estimations of methane source regions for selected air masses arriving at Mace Head and west London during the period 1995 to 2000. (sampling station indicated in parentheses).

Date	Sample		Background		Calc source	Possible error
	$\delta^{13}\text{C}$ (‰)	CH_4 (ppb)	$\delta^{13}\text{C}$ (‰)	CH_4 (ppb)	$\delta^{13}\text{C}$ (‰)	(‰)
<i>Regional and Remote Sources (Mace Head)</i>						
Canadian Source					$-63 \pm 1\text{‰}$	
31/7/96	-47.29	1780	-47.13	1761	-62.1	+8 / -15
12/2/97	-47.39	1820	-47.23	1802	-63.4	+9 / -17
4/2/98	-47.35	1824	-47.20	1812	-70.0	+14 / -40
7/9/98	-47.45	1849	-47.25	1825	-62.7	+7 / -9
19/8/99	-47.58	1824	-47.41	1805	-63.7	+8 / -16
European Mixed Source - decreasing					-54 to -56‰	
31/1/96	-47.87	1984	-47.20	1795	-54.2	± 0.8
20/3/96	-47.79	1973	-47.15	1790	-54.1	± 0.8
24/9/97	-47.95	1912	-47.50	1795	-54.9	± 1.3
24/9/98	-48.14	2017	-47.35	1805	-55.0	± 0.6
1/4/99	-47.73	1920	-47.20	1795	-55.3	± 1.3
21/10/99	-47.94	1947	-47.45	1815	-55.2	± 1.3
28/6/00	-47.99	1922	-47.38	1780	-55.6	± 1.3
Irish Source (peatbogs / ruminants)					$-66 \pm 1\text{‰}$	
27/4/95	-47.57	1817	-47.15	1775	-65.3	± 5.2
16/8/95	-47.86	1805	-47.45	1765	-65.9	± 5.5
31/10/95	-48.03	1850	-47.60	1805	-65.5	± 4.9
14/8/96	-47.94	1849	-47.12	1765	-65.2	± 2.5
19/12/96	-47.94	1859	-47.28	1795	-66.5	± 3.5
19/11/98	-47.78	1872	-47.30	1825	-66.4	± 4.8
4/8/99	-47.79	1840	-47.31	1795	-66.9	± 5.2
10/11/99	-48.25	1896	-47.45	1815	-66.2	± 2.8
<i>Urban Sources (within 20km of Royal Holloway sampling site)</i>						
a) West London Source Mix						
14/6/96	-47.58	2053	-47.40	1795	-48.8	± 0.5
18/8/96	-48.11	3356	-47.45	1800	-48.8	± 0.2
5/12/96	-47.54	2611	-47.08	1825	-48.6	± 0.2
11/9/97	-47.97	2245	-47.56	1800	-49.6	± 0.4
b) Natural Gas Source (-32.8 to -35.0‰ measured)						
1/4/97	-42.35	2882	-47.10	1820	-34.2	± 0.2
9/7/97	-44.27	2352	-47.15	1800	-34.9	± 0.4
19/3/98	-45.00	2182	-47.20	1820	-33.9	± 0.5
c) Biological Anthropogenic Sources (Landfill -dominated)						
14/6/96	-49.21	2946	-47.40	1795	-52.1	± 0.2
18/8/96	-49.51	3554	-47.45	1800	-51.6	± 0.1
11/9/97	-49.51	2824	-47.50	1840	-53.3	± 0.2

Errors are calculated using $\pm 3\text{ppb}$ for all concentrations and $\pm 0.03\text{‰}$ for all $\delta^{13}\text{CH}_4$ data.

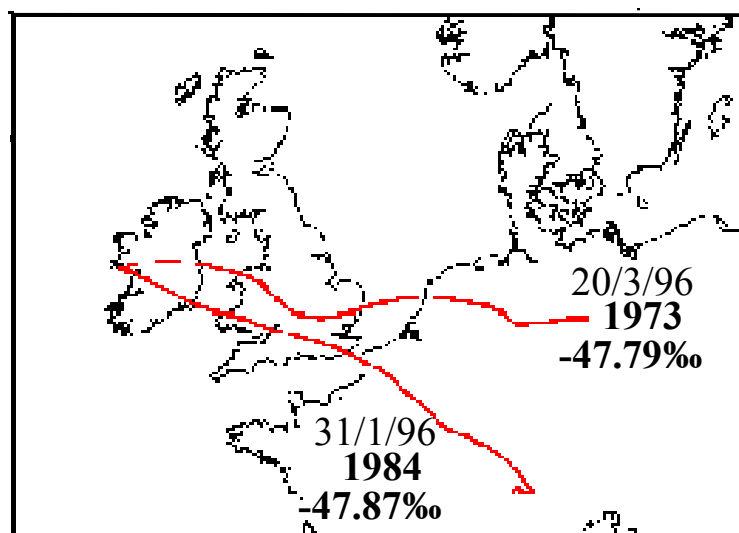


FIG. 1 Examples of 4-day back trajectories for air masses arriving at Mace Head. These examples are shown in Table I and were used to calculate the -54‰ source mix for 1996. These continental air masses normally contain 150-200 ppb methane in excess of the Atlantic background signal.

The isotopic signal of some large regional sources (e.g. western Europe as a whole; Canadian wetlands; Siberian wetlands and gasfields) can be detected at background stations up to 5000 km away [14]. Table I outlines the range of regional and local sources which have been identified by measuring excess methane over background at the Mace Head and London sites. The difference in the main local sources is clearly highlighted. Over central Ireland, close to Mace Head, the emissions to air will be mostly agriculture and wetland with signatures of $\delta^{13}\text{C}$ below -60‰ , whereas in the urban and industrial conurbations such as London the source mix will be mostly fossil fuel or landfill-related with the excess emissions mix being mostly in the range -52 to -48‰ .

4. THE LONDON REGION AND UK EMISSIONS

Diurnal measurement and analysis campaigns at the Royal Holloway site have been used to estimate emissions from the London region. Methane emissions from the London area are dominated by 2 main source groups (Table I), waste treatment (landfill and sewage with $\delta^{13}\text{C}$ calculated as -52.5‰) and fossil fuel extraction and distribution (natural gas, -34‰). Other minor sources are road traffic, due to inefficient engine combustion (-27‰) and agriculture (enteric fermentation and animal waste, -62.4‰).

The distinctive isotopic character of the major methane sources in SE England and the UK as a whole allow emissions estimates for comparison with inventory data. A regional source mix of methane with $\delta^{13}\text{C}$ -49.0 to -48.4‰ for the London area during 1996 and 1997 [8], suggests that the emission for London was 240-312 kt/yr, less than 10% of the UK total, but 38-79% higher than suggested by the latest statistical inventory estimates for those years [15]. The proportion of landfill can be calculated from the isotopic mix, using the isotopic signatures for the main source categories, statistical figures for gas leakage and the number of farm animals within the region. The London source mix consists of 77-81% emissions from

waste processing (mostly landfill), 16-21% from fossil fuels (mostly leakage in the gas distribution network), and about 1% each from transport and animals.

In the case of the London study, isotopic techniques were developed for monitoring methane emissions from a large conurbation by using a peripheral measurement site. The results are significant in that they could be used in devising policies to reduce emissions in the region; more generally, the technique is applicable to devising and monitoring reduction strategies in other large conurbations or regions with high methane emissions.

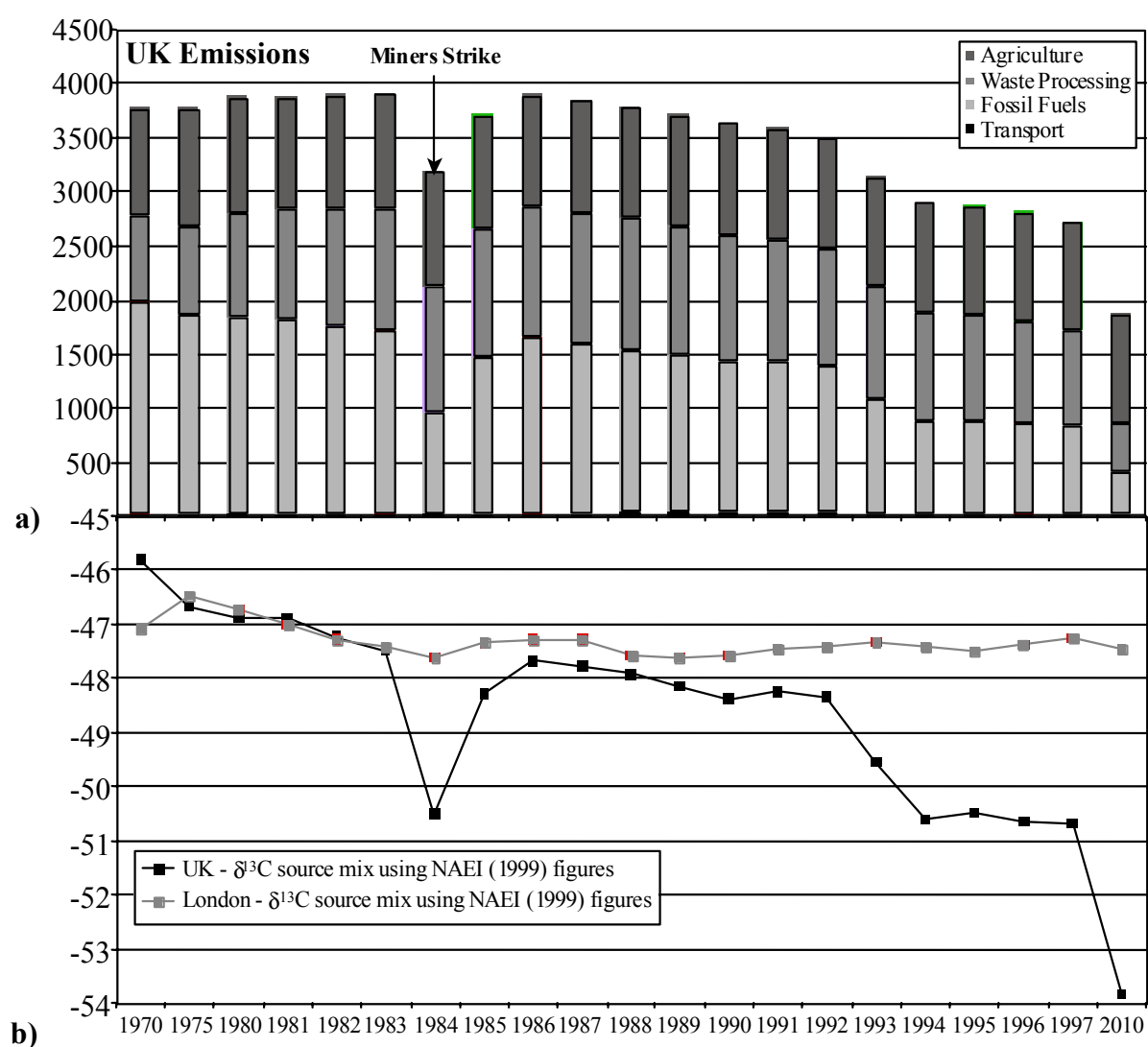


FIG. 2 Graphs derived from the data in NAEI [15]: a) Changing UK emissions 1970-97, and b) Changing isotopic signature of the UK and London source mix. All graphs show a 2010 estimate for a further 50% cut on the 1997 figure for all emissions except agriculture.

For the UK as a whole the agriculture sector is a far more important contributor to emissions, with coal emissions an important, but declining source in the remaining mining regions. The inventory suggests that the UK methane emissions have been reducing annually since 1986 (Fig. 2). Recent adjustments of methane emissions figures from UK sources between the publication of the 1996 and 1997 [15,16] inventories was due to a 'recalculation' of the landfill emissions figures, which were lowered by 40-45%. In terms of the $\delta^{13}\text{C}$ signature, the

lowering of the landfill emissions, should mean that the isotopic mix for the UK is more enriched in ^{13}C by approximately 0.5‰ than previously thought. More importantly this recalculation would result in an enrichment of 2‰ for the London source mix, but this is clearly not seen in the air sample data. The other main changes observed in the UK statistics since 1970 have been attributed to reduction in emissions from coal mining and coal combustion as the industry has declined, and the effects of the strike of 1984 are clear from the inventory (Fig. 2a,2b). This has removed a source with relative ^{13}C enrichment from the emissions mix.

The modelled isotopic change for the UK source mix using recent emissions figures [16] is from -48.4‰ in 1990 to -50.7‰ in 1997. This represents a reduction in emissions of 25% over a 7-year period, important in meeting Kyoto targets. Further reductions in the attempt to reach the 2010 UK targets of 20% cuts in greenhouse gas emissions will be clearly seen in the isotopic record. Fig. 2 shows the effects of a further 50% reduction in fossil fuel, waste and transport emissions between 1997 and 2010, resulting in a shift in the UK $\delta^{13}\text{C}$ mix from -50.7 to -53.8‰. Much will depend on the perceived accuracy of the emissions inventory figures, especially when landfill statistics have errors of $\pm 40\%$.

5. METHANE EMISSIONS FROM EUROPE

5.1. Methane emissions from the European Community

Statistical databases of methane emissions [e.g. 3,16] need independent external verification and carbon isotope data provide one way of estimating the expected source mix for each country if the main source types have been characterised isotopically. The CORINAIR 94 database provides the most detailed statistical database for methane emissions from western Europe to date and this has been used to give a first estimation of what the isotopic mixes for the emissions for each country should look like (Table II, Fig. 3). Those countries with large urban centres and much heavy industry (Germany, United Kingdom) are close to -51‰, those with emissions dominated by agriculture and wetlands (Finland, Sweden, Ireland) are closer to -60‰ (Fig. 3). Although there will be variations from region to region within a country (as with London at -49‰), most air masses crossing countries should be expected to pick up a component which is fairly representative of the emissions from that country. Even for Europe as a whole it seems that this basic premise holds true. The table allows some estimates to be made of what isotopic mix should be expected for air collected at remote sampling sites such as Mace Head, when the trajectory comes from continental Europe. The overall isotopic mix for emissions from the EC 15 is calculated as -55.4‰ for 1994 (Table II), close to the observed values from the continental trajectories arriving at Mace Head for 1995-2000 (-54.0 to -55.6‰), but the ^{13}C for air collected in central Europe in 1994 is approximately 2‰ enriched relative to the estimate from CORINAIR inventory data, based on results from Heidelberg [2]. The isotopic shift from -48 to -53‰ observed in the source mix for the Heidelberg region in the early 1990's [2] was interpreted as being largely due to reduction of coal mining emissions and a change in the source of the gas supply.

The comparison between atmospheric and inventory isotopic calculations suggest reductions in anthropogenic sources have been occurring, the isotopic shift is very clear although the rate of change is now slowing, but the isotopic offsets clearly suggest that there are discrepancies in the source proportions. While this difference could be explained by national statistics underestimating the magnitude of anthropogenic sources, it could also be explained by eastern European emissions to the air masses. Both of these possibilities will be explored below.

TABLE II. 1994 statistical emissions estimates [3] for EC15, Norway and Switzerland. Isotopic emissions mixes for each country based on proportions of emissions from coal (–35‰), gas, waste treatment and disposal (–52.5‰), agriculture, nature (–63‰) and transport (–27‰). Gas $\delta^{13}\text{C}$ depends on source region (e.g. North Sea –35‰, Siberia –50‰), agriculture $\delta^{13}\text{C}$ depends on proportions of enteric fermentation (–63‰) to animal waste (–58‰).

Country	Kt/yr CH ₄	% tot	$\delta^{13}\text{C}$ (‰)	Country	Kt/yr CH ₄	% tot	$\delta^{13}\text{C}$ (‰)
Italy	4853	17.8	–56.4	Denmark	785	2.9	–59.9
Germany	4848	17.8	–51.2	Austria	632	2.3	–59.4
UK	3848	14.2	–51.2	Greece	483	1.8	–57.0
Spain	3164	11.6	–55.1	Norway	467	1.7	–52.6
France	2937	10.8	–55.8	Belgium	434	1.6	–55.5
Sweden	1964	7.2	–62.4	Portugal	383	1.4	–60.4
Holland	1190	4.4	–54.6	Switzerland	374	1.4	–58.6
Ireland	845	3.1	–60.5	Luxembourg	23	0.1	–59.1
Finland	803	3.0	–60.6	Total	27191	100.0	–55.4

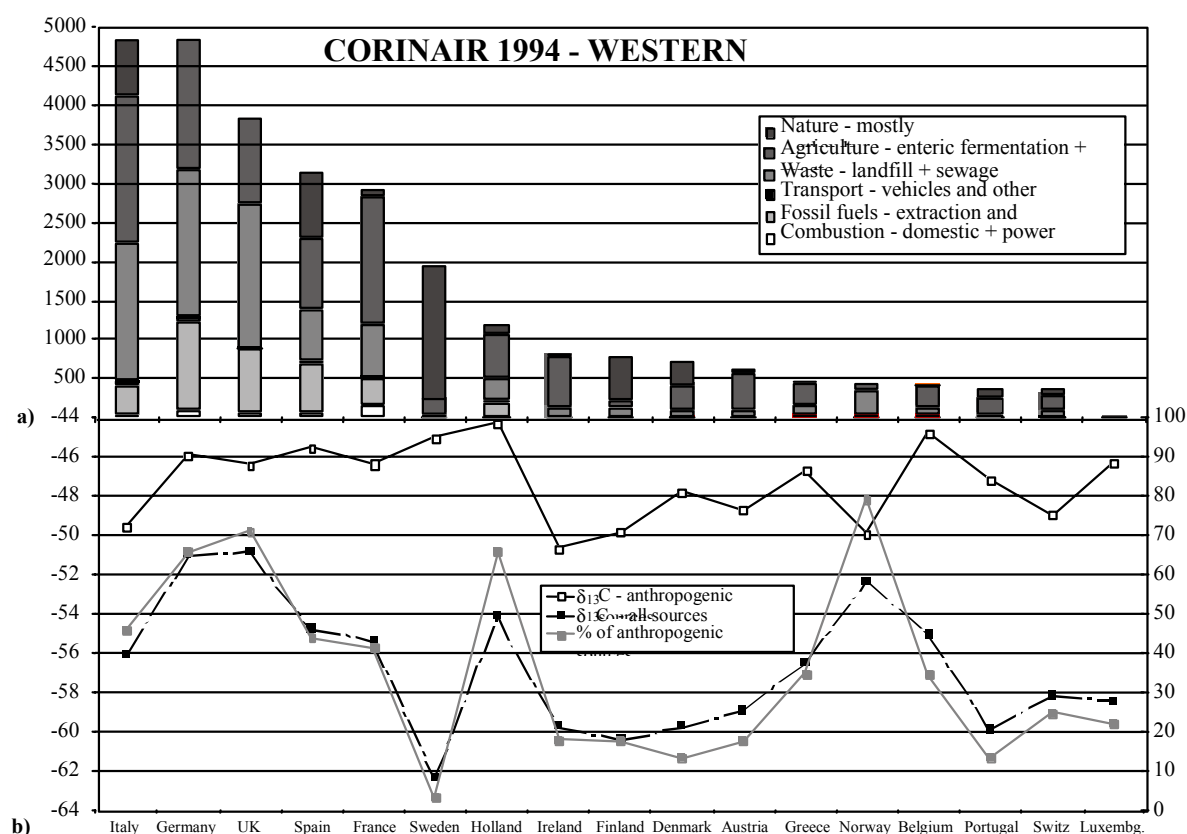


FIG. 3 a) Methane emissions for countries of western Europe from CORINAIR 94 [3] ranked in order from highest to lowest. Note the highly variable reported emissions from nature (mostly wetlands). b) Isotopic signature of anthropogenic compared to all sources and the percentage contribution of anthropogenic sources to the national totals. Note that the anthropogenic sources group here does not include agriculture, only those sources which are potential targets for emissions reduction.

5.2. Changes to emissions inventories from 1994 to 1998

Inventory data is currently available from EMEP up to 1998, but not all countries have reported data since 1996. In addition more countries than for CORINAIR 94 (notably Sweden and Spain) have chosen not to report their natural emissions. This makes an enormous difference in emissions, with the isotopic ratio thereof increasing from -62 to -56‰ and -55 to -51‰ , respectively. Overall the revised estimate for the EC15 for 1996 is -53.8‰ , very close to the -54‰ observed based on trajectory calculations during 1996, but known to be underestimating natural emissions. Since the 1994 inventory most countries have recalculated their methane emissions. The most significant changes have been the cuts in landfill emissions estimates. These reductions were 40-60% by the 3 biggest emitters, Germany, United Kingdom and Italy.

While some of the landfill reduction is down to increased incineration, the main reason is a reduction in the amount of carbon in landfills thought to be converted to methane. Estimated emissions from fossil fuels and agriculture remained relatively constant over the 1994-98 period, except for Italy who also introduced a 40% cut in agricultural emissions. These major cuts in emissions by Italy could have been isotopically verified because the isotopic mix would shift from -56.0 to -54.3‰ . Most other countries changed by less than 1‰ compared to 1994 figures.

5.3. Emissions from eastern Europe – effects on the European isotopic mix

Many of the air masses crossing Europe from the east sample emissions from countries such as Poland, the Czech Republic and Ukraine which still have large coal industries and which produce significant methane emissions (at $\delta^{13}\text{C}$ of -35‰) from these regions. The gas supply comes mostly from Russia, which is taken as -50‰ from our previous studies, otherwise the same isotopic values have been selected for the source categories. The low fossil fuel emissions inventory estimate for the Czech Republic in the EMEP database is difficult to reconcile with the amount of coal being mined, unless coal emissions are 2-3 times lower than Germany, France or the United Kingdom per tonne of coal produced. Making adjustments for this anomaly would put the Czech republic with the most ^{13}C -enriched source mix in Europe at -44‰ . Poland at -50‰ is the only further anomaly compared to the EC15, with the Baltic States giving the most depleted mixes for this region at -58‰ . Overall though, the mix for all the countries of Eastern Europe with currently available data is -51.3‰ , a significant difference to the EC 15. This means that using the 1996 data the European mix would be close to -53‰ , which does not fit with the atmospheric data evidence, further implicating an underestimation of natural emissions in the inventories.

6. CAN ISOTOPES OF METHANE BE USED TO VERIFY INVENTORIES?

The work of Levin et al. [2] and Lowry et al. [8] have shown that national statistical self-assessments of methane emissions can be verified using independent atmospheric measurements. Many more stations are needed across Europe to develop a detailed picture of the changing methane emissions, but already there is a sparse E-W transect of isotopic records through Europe to draw upon, from Mace Head in the west to St. Petersburg in the east. This atmospheric data already distinguishes the urban regions from the rural regions and allows Europe wide estimations of source changes. The shift toward greater depletion in ^{13}C of the European source mix should continue as better landfill practice, reduction in gas leaks and the decline of the coal industry continue but as the proportion of natural and agricultural emissions increases the rate of change of the mix will slow down.

The further development of automated continuous flow techniques for isotopic analysis of greenhouse gases over the coming years (and already capable of precision of $\pm 0.06\text{‰}$) will rapidly increase the number of samples which can be analysed and reduce the amount of sample required by 2 orders of magnitude. While the initial set-up costs will be high the proceeding analytical and sampling costs will be greatly reduced. Analysis of daily back trajectories for a range of background sampling sites will allow the isotopic source mix changes for individual countries to be monitored and compared with statistical data. By careful selection of coastal background and interior sampling sites the isotopic data will provide an important tool for monitoring and verification of EC and UK methane emissions in the run-up to 2010. When urban emissions are better understood, it should also be possible to monitor the progress of reduction strategies in those countries not able, or not willing, to keep track of their emissions.

REFERENCES

- [1] HOGAN, K. (Ed.), Options for reducing methane emissions internationally: vol. 1: Technological options for reducing methane emissions, Report to Congress, US Environment Protection Agency, EPA 430-R-93-006, (1993).
- [2] LEVIN, I., et al., Verification of German methane emission inventories and their recent changes based on atmospheric observations, *J. Geophys. Res.* **104** (1999) 3447-3456.
- [3] CORINAIR 94, European Air Emissions for 1994, European Environment Agency, (1996) www.aeat.co.uk/netcen/corinair/94.
- [4] LEVIN, I., et al., Stable isotopic signature of methane from major sources in Germany *Chemosphere* **26** (1993) 161-177.
- [5] STEVENS, C.M., Isotope abundances in the atmosphere and sources, In: *Atmospheric Methane: Sources, Sinks and Role in Global Change*, NATO ASI Series I, **13** (KHALIL, M.A.K., Ed.), Springer Verlag, New York, (1993) 62-88.
- [6] WHALEN, M. The global methane cycle, *Annual Review of Earth and Planetary Science* **21** (1993) 407-426.
- [7] WHITICAR, M.J., "Stable isotopes and global budgets", In: *Atmospheric Methane: Sources, Sinks and Role in Global Change*, NATO ASI Series I, **13** (KHALIL, M.A.K., Ed.), Springer Verlag, New York, (1993), 139-167.
- [8] LOWRY D., et al., London Methane Emissions: use of Diurnal Changes in Concentration and $\delta^{13}\text{C}$ to Identify Sources and Verify Inventories. *J. Geophys. Res.* **106**, D7 (2001).
- [9] ZONDERVAN, A., MEIJER H.A., Isotopic characterisation of CO_2 sources during regional pollution events using isotopic and radiocarbon analysis, *Tellus* **48B** 601-612 (1996).
- [10] FLORKOWSKI, T., et al., "Isotopic composition of CO_2 and CH_4 in a heavily polluted urban atmosphere and in a remote mountain area (southern Poland)", *Isotope techniques in the study of environmental change*, Proceedings of IAEA Symposium **SM-349** (1998) 37-48.
- [11] BERGAMASCHI, P., et al., Stable isotopic signatures $\delta^{13}\text{C}$ δD) of methane from European landfill sites, *J. Geophys. Res.* **103** (1998) 8251-8265.
- [12] GRACE, J.D., HART G.F., Giant gas fields of Northern West Siberia, *AAPG Bulletin* **70** (1986) 830-852.
- [13] CHANTON, J.P., et al., Factors influencing the stable carbon isotopic signature of methane from combustion and biomass burning, *J. Geophys. Res.* **105** (2000) 1867-1877.

- [14] LOWRY, D., et al., “ $\delta^{13}\text{C}$ of atmospheric methane: an integrated technique for constraining emission sources in urban and background air”, Isotope techniques in the study of environmental change, Proceedings of IAEA Symposium **SM-349** (1998) 57-67.
- [15] NAEI, UK Emissions of Air Pollutants 1970 to 1997, UK National Atmospheric Emissions Inventory Annual Report 1997, UK National Air Quality Information Archive, (1999) www.aeat.co.uk/netcen/airqual/naei/annreport/naei97.html.
- [16] SALWAY, A.G., UK Greenhouse Gas Inventory, 1990-1997, AEA Technology, National Environmental Technology Centre, AEAT-5689 Issue 1 (1999).

POSTER SESSIONS

CLIMATIC CHANGES AND ISOTOPIC CONTENT ALONG THE RIVER NILE VALLEY

A.A. NADA

Sitting and Environmental Dept. NCNSRC,
Atomic Energy Authority, Cairo, Egypt

M.F. HASSEIN

Faculty of Agriculture, Cairo, Egypt

K. FRÖHLICH

International Atomic Energy Agency, Vienna

The stable isotope composition of rain and snow has considerable variation with climatology, with geography and with time at a given location. This variation primarily results from the lower vapour pressure of water molecules which contain heavy isotopes of deuterium and oxygen-18 compared to molecules consisting of only the lightest. Because of vapour pressure differences, heavier isotopes tend to be enriched in liquid phase relative to vapour phase. Subsequent precipitation formed from the depleted vapour will be progressively “lighter” in stable isotope composition. Surface waters became enriched in deuterium and oxygen-18 relative to their initial isotopic composition as losses by evaporation occur. According to the IAEA precipitation sampling at Entebbe, which represent the source region of white Nile, with isotopic composition range (-33 to $+4\%$ in δD and -5.7 to -1.1 in $\delta^{18}O$). The isotopic composition of precipitation station at Addis Ababa which is the main source of Blue Nile ranges from -8.4 to $+7\%$ in δD and from -0.7 to -2.27% in $\delta^{18}O$. Assuming the Central Africa run-off contribution to white Nile downstream of the Sudan represents 20% of natural discharge to Egypt, and the balance 80% is derived from Ethiopia (Blue Nile), we obtain a composite stable isotope composition of $\delta D = -1\%$ and $\delta^{18}O = -1.8\%$, as an order of magnitude estimate on the propable long term stable isotope composition of the River Nile reaching upper Egypt under natural condition (before High Dam construction).

Stable isotopes were used to estimate the evaporation from Naser Lake at the High Aswan Dam. According to isotopic content, the lake can be divided into two sectors; the first sector with pronounced vertical isotope gradients, and the second with subdued isotope gradients.

Isotope content in surface waters varies with time and environmental effects (humidity, wind velocity, temperature, etc.). In order to detect this effect, Nile surface water samples have been collected at Cairo throughout the period 8/11/1994 to 6/7/1996, beginning immediately following a heavy storm event in the beginning of November 1994 which deposited precipitation across Egypt of isotopic composition close to -44% in δD and -6.5 in $\delta^{18}O$. The isotopic content of Nile water samples fluctuated and slightly changing with time. The conventional relation between $\delta^{18}O$ and δD in precipitation for the region is given by $\delta D = 9.978 \delta^{18}O - 4.15$.

The variation of the bomb-tritium response of the Nile has been reconstructed by using a model calibrated using measurements taken in the Nile basin. The results show that pre-bomb tritium content in the Nile was likely close to 5 T.U which peaked in the early 1960s at about 500 T.U. At present, the tritium level content of the Nile is about 9 T.U.

REFERENCES

- [1] SHOHEIB, R.E., Study environmental isotopes and trace elements abundance in Egyptian water. Ph.D Thesis Faculty of Science, Cairo University, Egypt (1980).
- [2] RAMADAN, E.F., Isotope and chemical composition of surface and groundwater in northern Nile valley soils. M.Sc. Thesis Faculty of Agriculture, Cairo University (1998).
- [3] NADA, A.A. et al, Environmental isotopes and over pumping over recharge in Nile valley soils Egypt. IAEA, Vienna (1999) SM-361.

TROPOSPHERIC CO₂ IN ROMANIA: CONCENTRATION AND ISOTOPIC COMPOSITION MEASUREMENTS

A. TENU, F. DAVIDESCU, V. CUCULEANU

National Institute of Meteorology and Hydrology, Bucharest, Romania

Long-term observations on isotopic composition and the first quantitative determinations were carried out for atmospheric CO₂ in Romania, in two locations: Bucharest, as a large city area and Cernavoda, as location of a nuclear power plant. In a previous paper [2] we have presented the first results obtained but only regarding the isotopic composition in Bucharest station.

The isotopic sampling was made by static absorption in NaOH, during the first half of each month. Radiocarbon activity is measured by liquid scintillation technique in benzene while the ¹³C/¹²C ratio is measured by mass spectrometry. The radiocarbon activity is expressed as Δ¹⁴C ‰, corrected by individual δ¹³C values.

For CO₂ concentration, the sampling is made by continuously aspiration; a GFC analyzer was used for measurements, stored as half-hour averages. The values are expressed as ppmv.

In order to determine the carbon isotopes, ¹³C and ¹⁴C, monthly atmospheric CO₂ samples were collected at Bucharest (during the last eight years) and Cernavoda (during the last five years). The Bucharest series include 96 monthly values (February 1992-December 1999) while the Cernavoda series includes only 57 samples (April 1995-December 1999). The values for both locations range generally from -80 to 400 ‰.

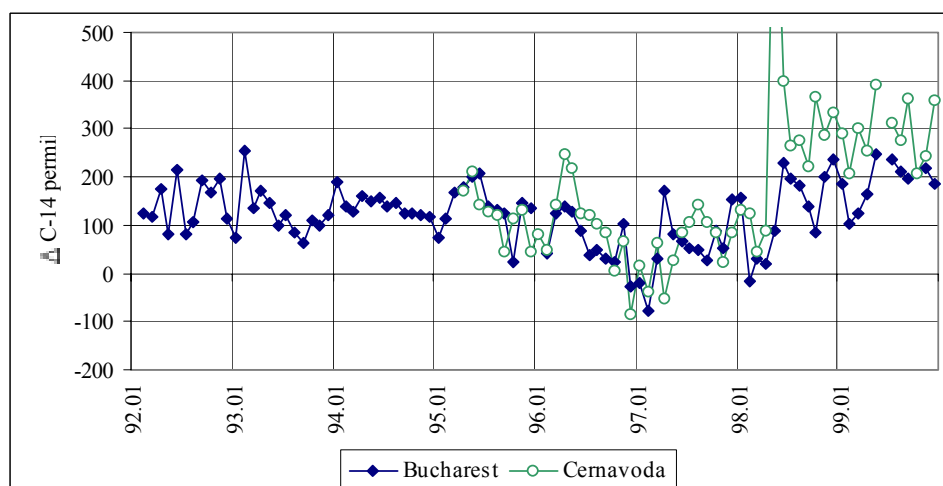


FIG. 1. Δ¹⁴C time-variation in Romania.

As can be seen in FIG. 1., until the spring of 1998 the values in both stations were approximately at the same level, except a short interval (April - May 1996) when, in the plant testing period, some higher values are noticed at Cernavoda. Also, were recorded:

- during 1995 and 1996, a continuous decrease (some values are even negative);
- a significant rise of values in both stations, but much more at Cernavoda, beginning with the spring of 1998.

In order to evaluate our yearly results as trend evolution was used “Europe-clean air”, a synthetic series considered - in our previous paper (Tenu et Davidescu, 1998) - as $\Delta^{14}\text{C}$ background level for Central Europe. The experimental data at Bucharest overlap satisfactorily the extrapolated exponential trendline only for 1992-1997 interval.

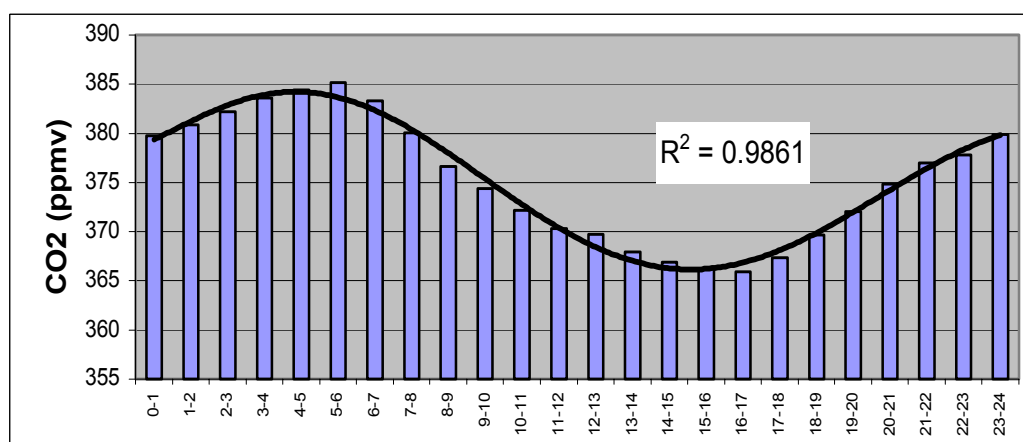


FIG. 2. Global diurnal variation for 1997 CO₂ contents in tropospheric air at Bucharest station.

CO₂ concentration was measured at Bucharest station and refers to 1996 (incomplete) and 1997 years; the annual mean values are of 379 and 375 ppmv, with minimum and maximum hourly values of 328 (July) and 507 (December) ppmv, respectively. It seems that these values are enhanced compared to other European regions (Levin et al., 1995) but are much below those recorded for others region, for example China (Xu and Zhang, 1993). A seasonal and daily variation, very ordered and well marked, were recorded (FIG. 2). The diurnal cycle for characteristic months in the four seasons allow to retrieve useful observations not only for the daily variability cycle but also for natural or anthropic (fossil fuel emission) influences along a year.

REFERENCES

- [1] LEVIN, I., GRAUL, R., TRIVETT, N. B. A., (1995). “Long-term observations of atmospheric CO₂ and carbon isotopes at continental sites in Germany”. *Tellus*, 47 B, pp. 23-34.
- [2] TENU, A., DAVIDESCU, F., (1998). “Carbon isotope composition of atmospheric CO₂ in Romania. Isotope Techniques in the Study of Environmental Change”. *Proc. of International Symposium on Isotope Techniques in the Study of Past and Current Environmental Changes in the Hydrosphere and the Atmosphere*, IAEA, Vienna, pp. 19-26.
- [3] XU, Y., ZHANG, L., (1993). “The character of the concentration and isotopic ratios of the atmospheric CO₂ in the north western China”. *Applications of isotopes techniques in studying past and current environmental changes in the hydrosphere and the atmosphere*, IAEA-SM-329, Extended Synopses, Vienna, 19-23 April, pp. 162.

USE OF $^{15}\text{N}/^{14}\text{N}$ RATIO TO EVALUATE THE ANTHROPOGENIC SOURCE OF NITRATES IN SURFACE AND GROUNDWATERS IN THE UPPER ORONTES BASIN (CENTRAL SYRIA)

Z. KATTAN

Department of Geology, Atomic Energy Commission, Damascus P. O. Box 6091,
Syrian Arab Republic

The $^{15}\text{N}/^{14}\text{N}$ ratio of dissolved nitrogen species has long been used for the identification of the different sources of nitrate contamination of water systems [1-4].

This study, which aims at providing a practical example of the utility of the ^{15}N stable isotope in identifying the natural and anthropogenic sources of nitrate in surface and groundwaters in the upper Orontes Basin, was implemented within the framework of the IAEA Regional technical project entitled "Isotope Hydrology Techniques in Water Resources Management (RAW/8/002)".

The selected area for this work is located in the upper part of the Orontes River Basin, which occupies the central zone of the Syrian territories. This heavily populated region is characterized by intensive agricultural and industrial developments. Hence, the influence of the growing domestic activities is reflected by rapidly deteriorating of the surface and groundwaters qualities in this area.

The relief of the of the study area is dominated by the presence of the coastal Mts in the west, the Palmyrides Mts in the east, the Mts of Lebanon and Anti-Lebanon in the south, and the Homs depression in the central zone. The climate of the basin is of Mediterranean type, with a mean annual precipitation ranging from 150 to 800 mm/a. The Orontes River (Al-Assi), which originates in the Mts of Lebanon and Anti-Lebanon and flows northwards across the Homs plain and Al-Ghab graben, is the most important fluvial axis in this region. This river drains, mainly, massif calcareous rocks and joins the Mediterranean Sea at the Suwaidieh Gulf.

From a hydrogeological point of view the following water-bearing systems can be distinguished in the study area: the Cenomanian-Turonian complex, the basaltic Neogene aquifer, the continental Neogene aquifer and the shallow Quaternary aquifer. The groundwaters of these aquifers are the most potential resources being used for both drinking water supply and irrigation.

Water samples for this particular work were taken from about 20 sites covering selected locations on the Orontes River flow path, the Qattineh Lake, the Rastan Lake as well as some shallow dug wells drilled in the above mentioned aquifer systems. Samples for the determination of $\delta^{15}\text{N}$ analyses of nitrate in water were collected in special glass bottles according to the recommendation and procedures of the protocol DIN 38402, and analyzed for $\delta^{15}\text{N}$ composition in the Radioagricultural Laboratory of Juelich in Germany. In parallel, duplicate water samples were collected and analyzed for $\delta^{18}\text{O}$, $\delta^2\text{H}$, ^3H and major chemical species in other different laboratories in Syria, Jordan and the IAEA.

The interpretation of the chemical and isotopic results shows that surface water in the Orontes River is rather clean before the Qattineh Lake, and progressively becomes more polluted along

its flow path. This spatial evolution is clearly shown by the gradual increase of $\delta^{15}\text{N}$ value, total nitrogen composition as well as the concentrations of some other chemical species (Cl^- , K^+ , NH_4^+ , PO_4^{3-}). This evolution is also accompanied by identical decrease of both dissolved O_2 and pH. The probable source for this contamination is, mainly, due to the domestic waste disposable and sewage discharge into the river.

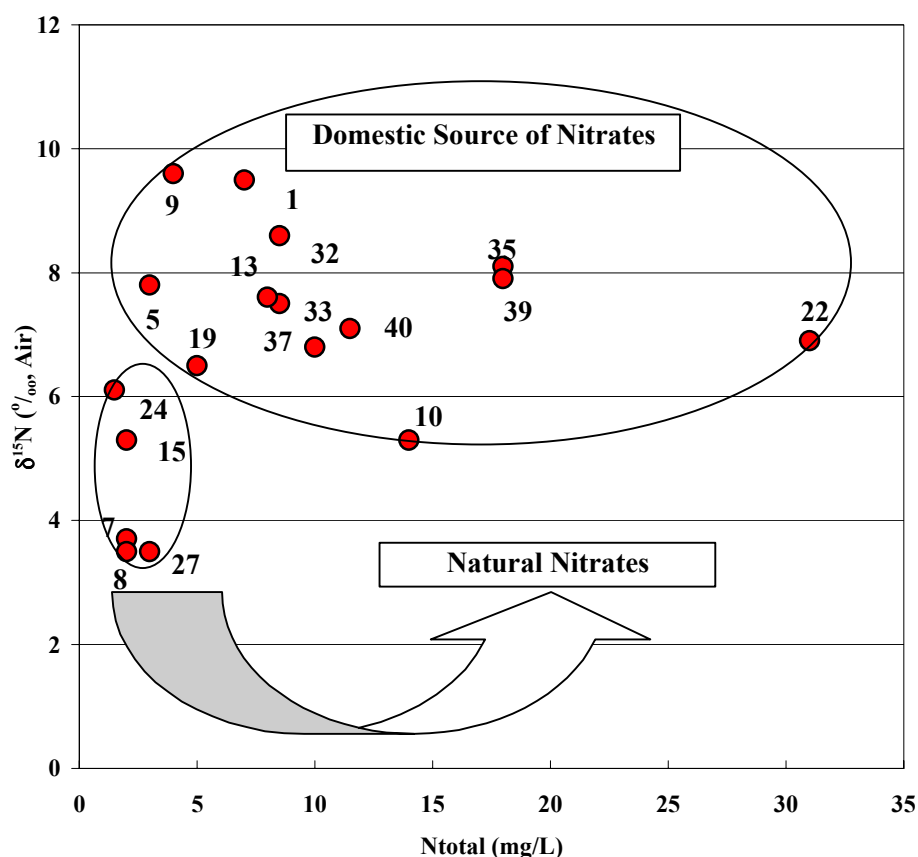


Fig. 1. $\delta^{15}\text{N}$ values versus total nitrogen (N_{total}) concentrations for surface and groundwaters from the upper Orontes Basin.

As it is shown in Fig. 1 the results of ^{15}N had also permit to distinguish between the following:

- The group of rather clean water bodies from the Orontes River (sites nos. 7 & 8), the Qattineh lake (sites nos. 15 & 24) and the groundwater of the well no 27. The water of this group is characterized by a low nitrogen content (less than 4 mg/L) and low $\delta^{15}\text{N}$ values (+3 to +6 ‰). It is concluded that the water of this group could reflect the nitrate originated from the natural source of the carbonate aquifers, from which the Orontes River takes its resources.
- The second group includes the waters from the remaining sites. The waters of this group show higher $\delta^{15}\text{N}$ values (+5.5 ‰ to +10.3 ‰) accompanied with high levels of nitrate or total nitrogen composition (3-31 mg/L). The nitrates of this group are probably

leached from fermentation of ammonium and organic matters originated from domestic sources. The high scatter of the representative water sampling points is related to the different intensity degrees of fermentation of the organic matters as well as the quantity of the waste disposable and sewage discharge into the river. The groundwaters with high concentrations in nitrate and other pollutant elements are found in specific locations near the river valley. These locations prove also the possibility of the interconnection between the river and the considered aquifer systems.

REFERENCES

- [1] KOHL, D. H., SHEARER, G. B., COMMONER, B., Fertilizer nitrogen: contribution to nitrate in surface water in a corn belt watershed, *Science* **174** (1971) 453.
- [2] MARIOTTI, A., 1984. Utilisation des variations naturelles d'abondance isotopique en ^{15}N pour tracer l'origine des pollutions des aquifères par les nitrates. In: *Isotope Hydrology, 1983*, IAEA, Vienna (1984) 605-633.
- [3] EXNER, M. E., SPALDING, R. F., N-15 Identification of nonpoint sources of nitrate contamination beneath cropland in the Nebraska Panhandle: two case studies, *Applied Geochemistry* **9** (1994) 73-81.
- [4] WILSON, G. B.; ANDREWS, J. N.; BATH, A. H., 1994. The nitrogen isotope composition of groundwater nitrates from the East Midlands Triassic Sandstone aquifer, England, *Journal of Hydrology* **157** (1994) 35-46.

USE OF Cs-137 FOR THE CALIBRATION OF THE CIRCULATION MODEL OF LITHUANIAN COASTAL WATERS

L. DAVULIENE, G. TRINKUNAS, V. REMEIKIS, L. VALKUNAS
Institute of Physics, Vilnius, Lithuania

S. DICK
Bundesamt für Seeschifffahrt und Hydrographie, Hamburg, Germany

It is well established that radioactive contamination of waters and sediments in the Lithuanian coastal area of the Baltic Sea is distributed unevenly [1]. To describe the distribution of the radionuclides in waters of the Lithuanian coastal area of the Baltic Sea, the model based on the operational circulation model of the Bundesamt für Seeschifffahrt und Hydrographie (BSH) for the North and Baltic seas [2, 3] was developed. The area under consideration contains both the Lithuanian coast of the Baltic Sea as well as the Curonian Gulf of the fresh water. The interplay between the salt and fresh water flows via the Kaipeda strait has impact on the distribution of radionuclides. For instance, Cs-137 is a typical radionuclide demonstrating this effect. It is experimentally well established that this radionuclide in the salt water is mainly in the dissolved form (about 90%) and just its minor part is concentrated in the suspended matter (about 10%). In fresh water the dissolved/suspended matter ratio for Cs-137 is totally opposite. Therefore, Cs-137 can be considered as the tracer following the fresh and salt water mixing. With samples of the radionuclide concentration in the sea area under consideration at hand, Cs-137 is used to normalize the tracer concentration simulated by the developed circulation model.

The model was based on the grade of 1 nautic mile (nm), while the boundary conditions were taken from the more extended BSH model on the 6 nm grade. In order to understand the sensitivity of this local model to the initial conditions, the artificial conditions taken from the more general and coarse model were used. It has been obtained that the effect of the initial conditions is lost within 2-3 weeks. This result is independent of the coarse grain of the grade as calculations carried out on 1 nm and 0.5 nm grades show.

The model was adopted for the PC Pentium III, and calculations of the salinity distribution depending on the meteorological conditions were carried out. Real-time calculations have been performed for the period of 99.04.01-99.06.01 matching the time of radioactivity measurements at HELCOM stations. It was obtained, for instance, that depending on the wind direction, some local spots of uneven salinity in the sea could be formed. This can qualitatively explain the abrupt increase in the Cs-137 concentration as it was observed experimentally.

In addition, the possible inflow of the pollution from the Nemunas river was also considered. It has been obtained that independently of the meteorological conditions the main pathway of the pollution is directed to the Klaipeda strait and afterwards to the Baltic Sea, while the southern part of the Curonian Gulf is almost not influenced by the pollution inflow (see Fig. 1). This result is also qualitatively supported by experimental observations. Further development of this model has to be focused on studies of i) more detailed model calibration in the Klaipeda strait, ii) shallow water effects in the Curonian Gulf, and iii) comparison with the experimental data.

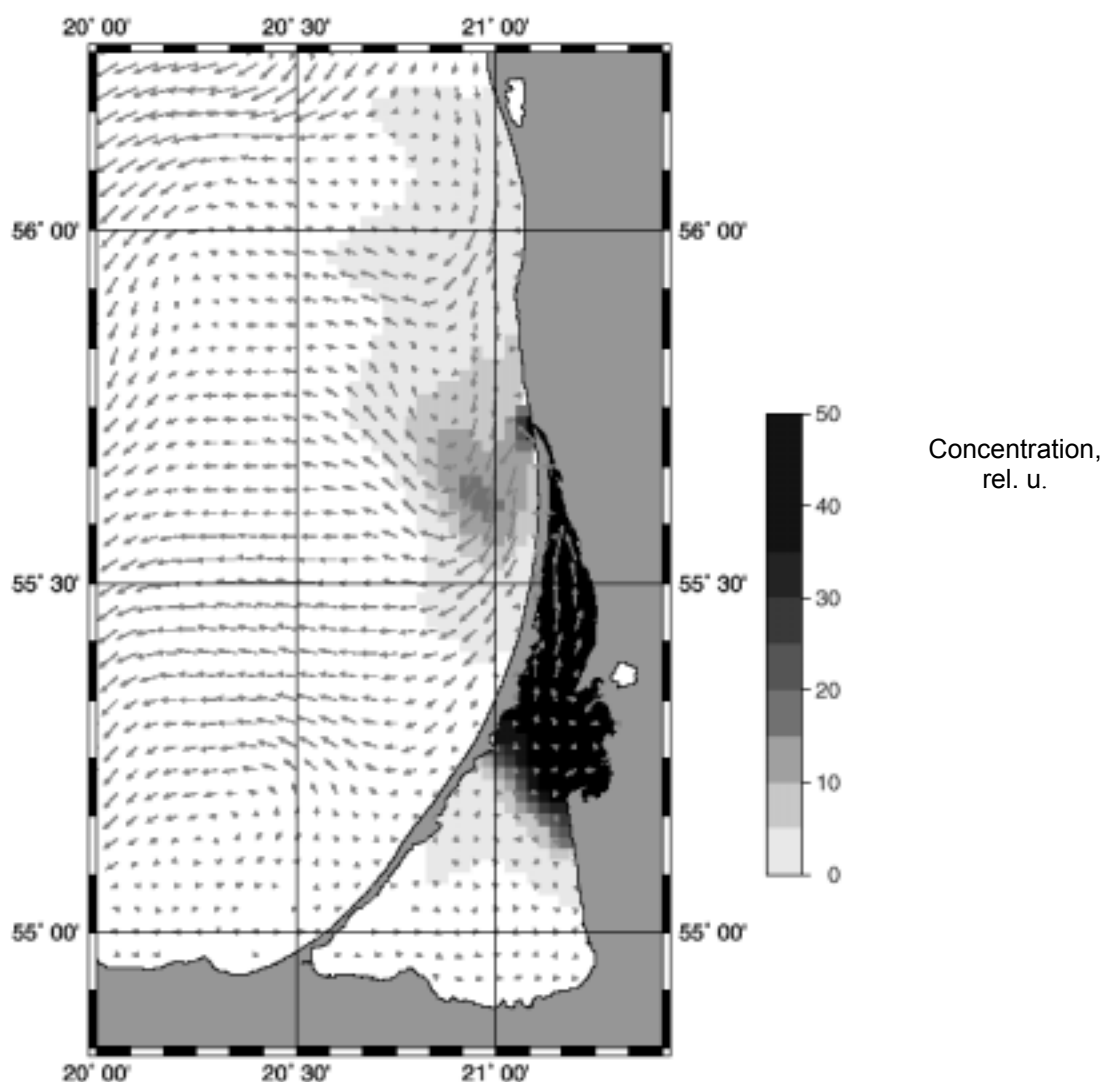


FIG. 1. Uneven tracer concentration distribution on 99.05.13, 12:00 UTC; wind SO 5 m/s. Simulation started on 99.04.01 with the inflow of the pollution from the Nemunas river. Arrows indicate flow directions; the arrow length scales with the flow rate.

REFERENCES

- [1] TARASIUK, N., SPIRKAUSKAITE, N. Radioactive contamination of the coastal zone of the Baltic Sea of Lithuania, *Atmospheric Physics* **18** (1994) 85-89.
- [2] KLEINE, E. Das operationelle Modell des BSH für Nordsee und Ostsee – Konzeption und Übersicht, Unveröffentl. Manuscript (1994) 126 pp.
- [3] DICK, S. SCHOENFELD, W. Water Transport and Mixing in the North Frisian Wadden Sea – Results of Numerical Investigations, *German J. Hydrography* **48** (1996) 27-48.

USING ISOTOPES FOR GLOBAL WARMING OBSERVATION

K. NAMATA

Ministry of Environment, Niger

Abstract. This paper, based on a literature review, discusses the main aspects of using isotopic techniques to obtain information about global warming. The rapid increase concentration of carbon dioxide (CO₂) and methane (CH₄) in the atmosphere will result in global warming by the greenhouse effect, and the isotopic techniques constitute an efficient tool to explain this complex environmental phenomenon.

Isotopic analysis of carbon contributes to a large extent to explain the evolution of atmospheric gases which cause greenhouse effect (CO₂) and (CH₄). Nitrogen and Sulfur isotopes reveal correlations between Oxides produced by industry and acid rains. Oxygen and Hydrogen isotopes in water constitute excellent indicators for climatic parameters such as temperature of air surface, relative humidity and volume of precipitation. The work presents an inventory of atmospheric gases which cause greenhouse effect. The sectors concerned include the following: Energy, Agriculture, Change in land and forest use, waste management. The table below (TABLE I) gives a recapitulation of greenhouse gases (GHG) emission (in Gg) for 1990.

Table I. Modified from [1]

	CO ₂ emis	CO ₂ seques	CH ₄	N ₂ O	CO	NOX	COVNM	SO ₂	E.CO ₂	%
ENERGY Fossil fuel	588.91	0	13.66	0.17	220.62	7.51	27.65	1566.03	928.47	0.862
INDUSTRIAL PROCESSING										
- Ciment	9.26	0	0	0	0	0	0	0.0058	9.26	0.005
- Lime	0.3	0	0	0	0	0	0	0	0.3	0.0
- Beer	0.0	0	0	0	0	0	0.0036	0	0	0.0
AGRICULTURE										
- Enteric fermentation	4.232	0	0	0.0136	0	0	0	0	8.448	0.003
- Rice production	141.17	0	6.722	0	0	0	0	0	282.382	0.435
- Arabe Lands	729.49	0	0	2.353	0	0	0	0	1458.92	0.5636
- Bush burning	40.826	0	1.643	0.02	0.0735	43.149	0	0	81.529	0.043
CHANGE IN LANDS AND FOREST USE										
- Patrimonial Forests	0	3613758	0	0	0	0	0	0	0	92.971
- Disturbed forests and prairies	6082.48	0	0	0	0	0	0	0	6082.48	3.1257
- Forest burning	0	0	1.028	0.00706	0.2554	8.994	0	0	23.7766	0.008
- Abandonel Agricultural Lands	0	6637.5	0	0	0	0	0	0	0	1.707
- Agricultural Lands	0.004436	0	0	0	0	0	0	0	0.004436	0.0
WASTE										
- Municipal Solid Wastes	0	0	0	0	0	0	0	0	0	0
- Domestic Waste Waters	0	0	0.0082	0.0905	0	0	0	0	28.2272	0.007
TOTAL	7596.67	368013.3	2306.12	2.65416	220.949	59.653	27.6536	1566.0358	8903.797	

Source : Document de Synthèse des inventaires de gaz à effet de serre et des études de vulnérabilité et adaptation aux changements climatiques ; Commission Nationale sur les changements et variabilités climatiques - Niger. 1999.

REFERENCE

- [1] Document de synthèse des inventaires de gaz à effet de serre et des études de vulnérabilité et adaptation aux Changements Climatiques-Commission Nationale sur les changements et variabilités climatique, Niger (1999).

CLIMATIC SIGNIFICANCE OF STABLE ISOTOPE CHARACTERISTICS OF AIR-CO₂ AND RAINFALL IN DELHI AREA WATER-PLANT-AIR SYSTEM

P.S. DATTA, S.K. TYAGI

Nuclear Research Laboratory,
Indian Agricultural Research Institute,
New Delhi, India

In recent years, there is a global concern on the role of carbon dioxide in atmosphere in affecting the climate. The present models of global atmospheric circulation suggest that oceans sequester about one-third of the CO₂ released by anthropogenic activities, and biospheric productivity is the primary cause of the interannual fluctuations in the atmospheric CO₂ [1, 2]. However, most of the times, the excess of CO₂ in air is associated with the presence of anthropogenic pollutants from urbanised centres. Therefore, the studies on the pattern of local variations in the isotopic composition of air CO₂ and rainfall in urban areas are expected to provide important information on the atmospheric circulation processes which affect the climate on a regional scale. Internationally, aspects of climate change have been so far demonstrated using isotopic data mainly from temperate climates, and there is limited understanding of the factors controlling stable isotopic composition of air-CO₂ and rainfall in tropical regions. In this context, to assess the magnitude of the above mentioned effects, analysis of the data on the variations in the ¹³C/¹²C and ¹⁸O/¹⁶O signatures of air-CO₂ in Delhi area water-plant-air system is presented here.

In Delhi area, located in the path of the Indian southwest monsoon trough movement, about eighty percent of the annual rainfall occurs during the monsoon period (July to September). This brings a significant change in the weather and increase in the plant biomass productivity. The air-CO₂ concentration during March to September showed a wide range of 330 to 458 ppmv, with an average value of 357.8 ppmv and the $\delta^{13}\text{C}$ value of CO₂ varied from -7.8 ‰ to -11.6 ‰, with an average of -8.9 ‰. While, the pre-monsoon months (March to June) had higher CO₂ levels (mean 366 ppmv), monsoon months July and August had significantly depleted concentration (mean 345 ppmv). An inverse relationship has been observed between CO₂ concentration and $\delta^{13}\text{C}$. Depleted CO₂ concentration associated with enriched $\delta^{13}\text{C}$ value during the monsoon months clearly indicate rapid consumption of ¹²CO₂ by photosynthesis due to increasing biomass productivity [3]. Simple mass balance calculations suggest that before the onset of monsoon in Delhi, CO₂ contribution to the atmosphere from burning of fossil fuel ranged between 10 to 24 % in the investigated area. The $\delta^{18}\text{O}$ value of CO₂ in Delhi ranged from +38.7 ‰ to +50.9 ‰, with an average of +41.2 ‰, close to that of normal atmospheric CO₂ ($\delta^{18}\text{O}$ =+41 ‰). Relative humidity of air during monsoon months being quite high (70-80 %), the depleted $\delta^{18}\text{O}$ in CO₂ during monsoon months can be possibly ascribed to equilibration of CO₂ with relatively less enriched leaf water of the vegetation [3, 4].

Analysis of the variations in the $\delta^{18}\text{O}$ and δD composition of New Delhi rainfall (IAEA Global Network Data 1961-96) showed that although, the monthly mean values range from -15.3 to +8.0 ‰ for $\delta^{18}\text{O}$ and -120 to +55.0 ‰ and agree with the world meteoric line, yet, the isotopic composition of rainfall events of less than 50 mm show deviation from the meteoric line, following different evaporation line for different summer months. Earlier studies, based on IAEA Global Network Data 1961-83 suggested that the long-term mean temperature and mean rainfall together account for about 80-95 % of the long-term average variability of ¹⁸O

composition [5], with temperature alone accounting for 80 % variability. Lack of correlation between the monthly ^{18}O isotopic composition and rainfall reflect that the temporal variability in $\delta^{18}\text{O}$ depends also on the atmospheric water vapour circulation patterns, distribution and intensity of rainfall, composition of the air-mass from which the rainfall derives and the trajectory of the moist air-mass movement [5]. However, months with heavy rainfall is generally associated with depleted $\delta^{18}\text{O}$, and each monsoon months July, August and September shows different pattern of amount effect, i.e., depletion in $\delta^{18}\text{O}$ with increasing amount of rainfall, in the rainfall range of 50-350 mm. Monthly values of $\delta^{18}\text{O}$ in rainfall show maximum enrichment during the summer months May and June, and closely match with the maximum monthly temperature in the corresponding year, and is associated with higher air- CO_2 level in some of the years. The data suggest that as compared to the monthly isotopic composition of rainfall in the normal monsoon years, relatively enriched monthly $\delta^{18}\text{O}$ in rainfall in other years is generally associated with El Nino years and rainfall deficient years. Although, it is difficult to ascertain whether El Nino affects India, as the Indian monsoon is a very complex phenomenon, yet, studies reported earlier found that El Nino years are associated with weak Indian summer monsoon [2]. Since, average monthly atmospheric circulation features in normal monsoon years differ considerably from that in deficient monsoon years, further systematic monitoring and modelling of seasonal variations in isotopic composition of rainfall and air- CO_2 can provide useful information on the environmental changes and distribution of water in the atmosphere, in relation to the atmospheric circulation patterns, as influenced by green house gases.

REFERENCES

- [1] KEELING, C.D., BACASTOW, R.B., CARTER, A.F., PIPER, S.C., WHORF, T.P., HEIMANN, M., MOOK, W.G. AND ROELOFFZEN, H., In: "Aspects of climate variability in the Pacific and the Western Americas", Geophys. Monograph **55** (1989) 165-236.
- [2] SIEGANTHALER, U., "El-Nino and atmospheric CO_2 ", Nature **345** (1990) 295-296.
- [3] DATTA, P.S., BHATTACHARYA, S.K., TYAGI, S.K., JANI, R.A., "Vegetative growth and ecophysiological significance of ^{13}C and ^{18}O composition of air- CO_2 ", Plant Physiol & Biochem. **22** (1) (1995) 64-67.
- [4] BHATTACHARYA S.K., JANI R.A., "Monsoon effect on isotopic composition of atmospheric carbon dioxide", Curr. Sci. **62** (1992) 525-528.
- [5] DATTA, P.S., TYAGI, S.K., CHANDRASEKHARAN, H., "Factors controlling stable isotopic composition of rainfall in New Delhi, India", J. Hydrol. **128** (1991) 223-236.

RECONSTRUCTION OF ^{137}Cs SIGNAL IN CUBA USING ^7Be AS A TRACER OF VERTICAL TRANSPORT PROCESSES IN THE ATMOSPHERE

C.M. ALONSO HERNANDEZ, H. CARTAS-AGUILA,
M. DIAZ-ASENCIO, A. MUNOZ CARAVACA

Centro de Estudios Ambientales de Cienfuegos. Cienfuegos, Cuba

The goal of this study is to estimate the ^{137}Cs signal in Cuba using the relation $^{137}\text{Cs}/^7\text{Be}$ for Miami and Cienfuegos City's obtained for four year and data base of ^{137}Cs concentration in aerosols for Miami since 1957. The temporal behaviour of ^{137}Cs and ^7Be in aerosols in the Central and Southern region of Cuba are shown too.

Sampling of aerosols was carried out in the Environmental Study Centre (22°03'N, 80°29'W) facilities during June/1994 - December/1998 in Cienfuegos Province. Aerosols were collected by an integral method using the facility *Primus I*, with 0.65 m² collection area, 1200 m³h⁻¹ air flux during 7 days collection time. Petrianov filter FPP-15-1.5 was used (efficiency collection of 99% to aerosols 0.3-1.5 µm diameter). After collection, the filters were ashed at 350 °C for 72 hours, put in appropriate geometry and analysed by gamma spectrometry. ^{137}Cs mean concentration in aerosols was 1.09 µBqm⁻³ and the range of variations was 0.18-3.24 µBqm⁻³; while the ^7Be was 4.10 mBqm⁻³ with 0.96-10.46 mBqm⁻³ variation range. Figure 1 shows the monthly behaviour of ^{137}Cs and ^7Be values. From the graphic, it is observed that ^{137}Cs has the same temporal behaviour as ^7Be ; so both radionuclides are affected by the same vertical transportation processes in the stratosphere.

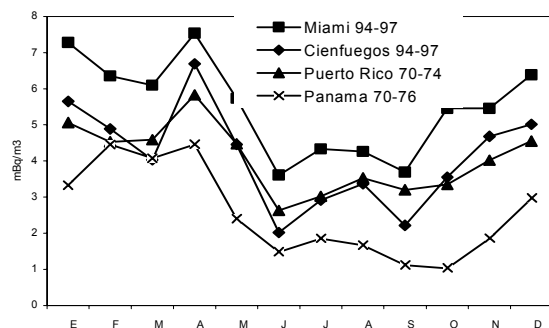


FIG.1. Monthly behaviour of ^{137}Cs and ^7Be in aerosols during the period 1994-1998 in Cienfuegos.

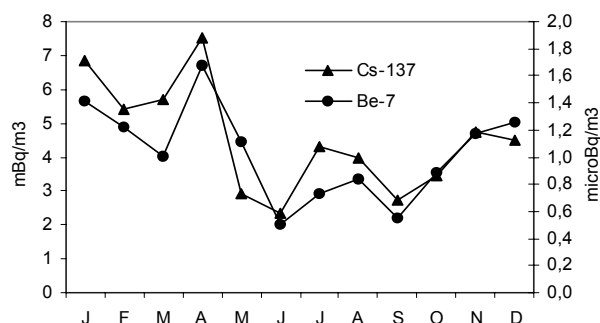


FIG. 2. Monthly behaviour of ^7Be in aerosols from Cienfuegos, Miami, Puerto Rico and Panama.

Figure 2 shows the seasonal behaviour reported by Feely et al [1,2] and Laser et al [3] in Miami (25° 49'N, 80° 17'W) San Juan, Puerto Rico (18° 26' N, 66° 00' W) and Balboa, Panama (8° 58'N, 79° 34'W); they are compared with the values obtained in our monitoring site. The data obtained in Cienfuegos show the same behaviour compared with other zones, where a maximum in concentrations is observed in the first four months of the year matching with the lowest levels of rain reported to this region. The observed increment in all cases in April, has been explained by Feely et al [1]; it is a consequence of the tropopause breaking in the last months of winter when the transport from the stratosphere to the troposphere is greater. The observed variations in ^7Be concentrations are explained principally by the

monthly regime of precipitation in each locality and in lesser degree by the longitudinal variations.

These results allow to establish a relationship between ^{137}Cs concentrations in aerosols from Cienfuegos and Miami in the same period, normalising in both cases with ^7Be values; this normalisation allows to discriminate the variations due to local meteorological conditions and latitudinal position. To do this we use the 42 years series of radionuclides measurements in aerosols sampled in Miami, Florida (25° 49'N, 80° 17'W) which may be found "on line" in http://www.eml.doe.gov/databases/SASP/sasp_data_search.htm. If we represent in a graphic (Figure 3a) the monthly relation $^{137}\text{Cs}/^7\text{Be}$ to Miami and Cienfuegos during the period June/94- March/97, we can observe a good agreement between these variables, reporting 0.93 as correlation coefficient value.

Using the obtained linear equation and systematising to a monthly constant the relation $^7\text{Be}_{\text{Cienf.}}/^7\text{Be}_{\text{Miami}}$, ^{137}Cs concentrations in aerosols from Cienfuegos may be represented as: $^{137}\text{Cs}_{\text{Cienf.}} = 0.729 ^{137}\text{Cs}_{\text{Miami}} \times R$ where R is systematised relation $^7\text{Be}_{\text{Cienf.}}/^7\text{Be}_{\text{Miami}}$ by month. From the equation and ^{137}Cs monthly concentrations determined by aerosols from Miami in the period 1957-1994, ^{137}Cs levels of aerosols in Cienfuegos may be estimated in the same period (Figure 3b).

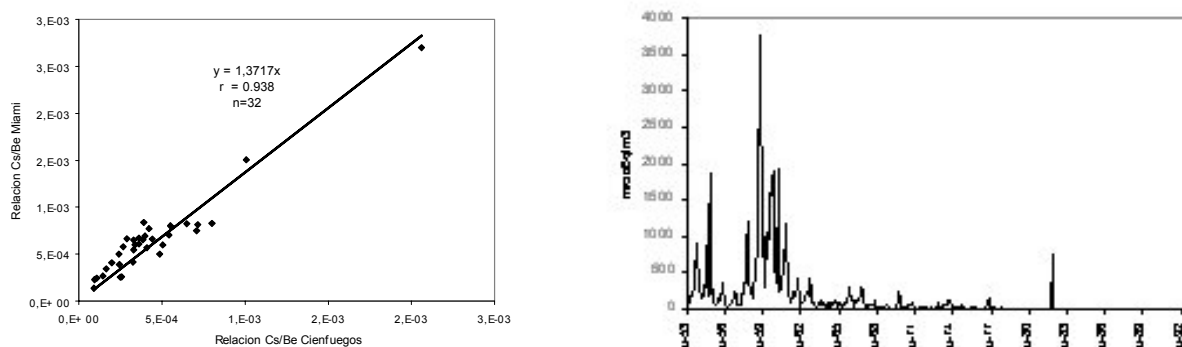


FIG. 3a. Relation $^{137}\text{Cs}/^7\text{Be}$ in Miami and Cienfuegos in the period June/94 - March/97.
3b. Estimated ^{137}Cs signal in Cienfuegos City for the nuclear era.

^{137}Cs calculated values in aerosols are in agreement with those reported to Puerto Rico (1970-1974), Bahamas (1968-1972), Panama (1965-1967) and Hawaii (1970-1994). The highest levels, 3.7 mBq m^{-3} , were calculated in 1963, coinciding with the period of highest number of atmospheric nuclear weapons tests. A significative and relevant fact in this study is the possible observation of the signal of Chernobyl accident in our territory, where in May 1986 it a concentration of 0.74 mBq m^{-3} is estimated, two orders higher than the mean value determined in Cienfuegos region in the sampling period of this memory. This result agrees with Feely's et al [4] and Larsen et al [5] observations in the eastern coast of the EE.UU from Maine (47°N, 68°W) to Miami (26°N, 80°W) during May 1986. The presence in our latitudes of radionuclides produced in Chernobyl accident has been explained where the global transport processes transferred a part of the plume formed at the beginning in the north of Canada, and later a part of it was associated to a quasistationary depression in the Atlantic Northeast, which allowed the fall of contaminated air in all the Eastern North American coast.

REFERENCES

- [1] FEELY H. W., LARSEN R.J., SANDERSON C.G., Factors that cause seasonal variations in beryllium-7 in surface air. J. Environ. Radioactivity **9** (1989) 223-249
- [2] FEELY H. W., LARSEN R.J., SANDERSON C.G., Annual Report of the surface air sampling program. US Department of Energy Rept EML-447, New York (1988).
- [3] LARSEN, R.J., HAAGENSON, P.L., REISS, N.M., EML Surface Air Sampling Programs 1990-1993 Data. USDOE Report EML-572. New York, NY6. CPHR(1999).
- [4] FEELY H. W., HELFER I.K., JUZDAN Z.R. KLUSEK C.S., LARSEN R.J. LEIFER R., SANDERSON, C.G., Fallout in the New York Metropolitan Area Following the Chernobyl Accident. J. Environ. Radioactivity **7** (1988) 177-191.
- [5] LARSEN, R.J., HAAGENSON, P.L., REISS, N.M., Transport Processes Associated with the initial elevated concentrations of Chernobyl Radioactivity in Surface air in the United States. J. Environ. Radioactivity **10**(1) (1989) 1-18.

THE EFFECT OF CLIMATIC CHANGES ON VAN LAKE

A. DİRİCAN

Ankara Nuclear Research and Training Center,
Ankara, Turkey

Lake levels are influenced by climatic changes, greenhouse effects and anthropogenic activities. These effects are reflected in the hydrological cycle features over the lake drainage basins. Among the significant hydrological variables, lake levels are influenced by different atmospheric and environmental conditions. During wet periods, there may be water-level rise that may cause some social and economical losses to agriculture and human activities along the lake shores. Such rises become serious in the case of shore line settlements and low lying agricultural land. Lake Van currently faces such problems due to water-level rises in eastern Turkey. Because of, it is a closed basin with no natural and artificial outlet and its water contain high concentrations of soda which prevent the use of its water as a drinking or agricultural water source, Lake Van unique. Under these circumstances, in addition to discussion of early studies air temperature, $\delta^{18}\text{O}$ of precipitation, temperature profile of lake and $\delta^{18}\text{O}$ variation of water column of lake Van were examined.

Lakes are natural free-surface bodies and they respond to atmospheric, meteorological, geologic, hydrologic influences. To define the behavior of lakes requires knowledge of these events recorded within or around the catchment area of lake. Stream flow depends on various factors effecting the hydraulic balance of a drainage area and similarly, water level variations present the final result of the complex interplay of the various water balance components, which are surface inflow and outflow and streams, direct precipitation on to the lake mirror and ground water exchange and leakage. Meteorological factors, precipitation over the lake and drainage area, evaporation from the lake surface, wind velocity, humidity and temperature in the adjacent lower atmosphere, all play important role in the lake water level fluctuations.

The effect of these factors also can be seen from $\delta^{18}\text{O}$ composition of precipitation, lake water and water temperature. Due to difficulties of simultaneous measurements of all the effective factors on the lake water level fluctuations, complete measurements for the application of hydrological water balance are missing in many large natural lakes of the world. At the surface water body investigations some basic measurements such as water chemistry, temperature, stable isotopes, sediment rates and classical hydrological measurements can be very important tools to understand the water bodies. One of the largest lake in the world is lake Van which is located at an elevation 1648 m above sea level on the high east Anatolian plateau of Turkey as shown in (Figure 1). It is generally accepted that damming of Nemrut volcano on Murat valley forms lake Van. The lake level rise rose rapidly after the fluvial system was dammed and impoundment of the water began [1].

This study proposes that the lake level rises are due to meteorological variations. Change of water level of lake Van is drawn and correlation among runoff and precipitation is made by using traditional meteorological data. The same water level trend could be seen at Caspian sea when the eight year delay is ignored. The relation between water level of Caspian sea and lake Van are obtained. The seasonal variation of isotopic composition of precipitation and air temperature were investigated for 1996 and 1997 years.

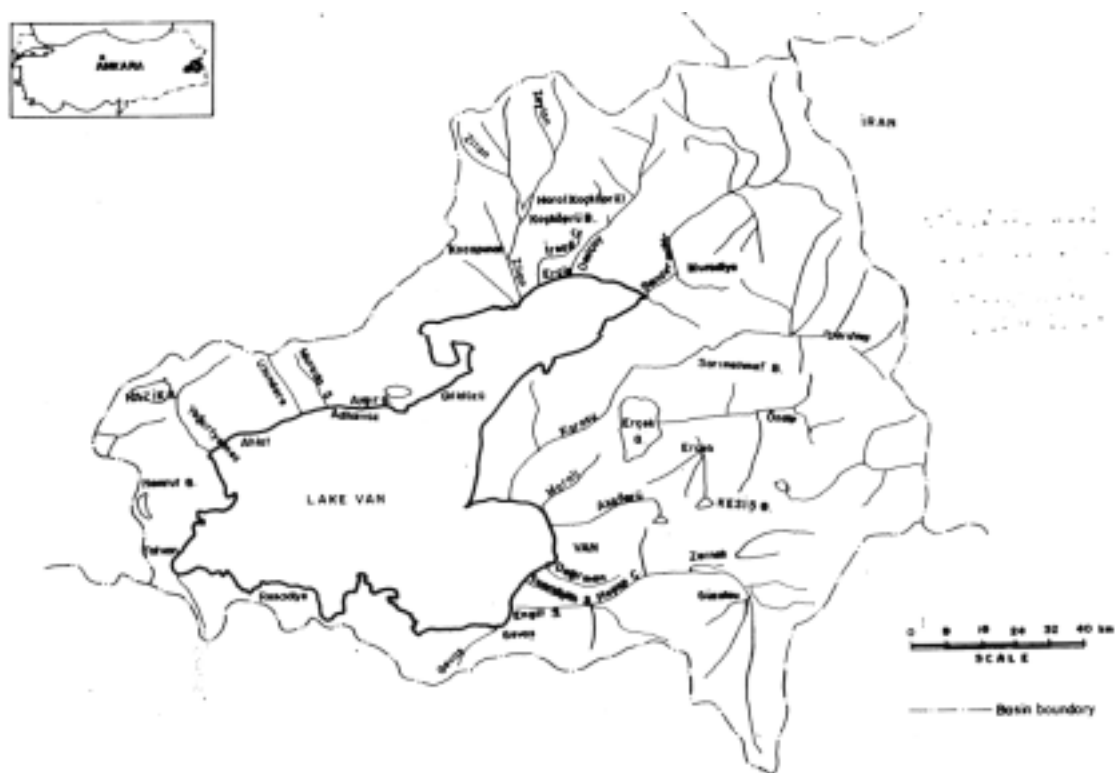


FIG. 1. Map of the study area

REFERENCE

- [1] DEGENS, E. T., KURTMAN F., "The geology of Lake Van", The Mineral Research and Exploration Institute of Turkey, No:169, Ankara, (1978).

RECONSTRUCTION OF TRITIUM TIME SERIES IN PRECIPITATION

H. CELLE-JEANTON

Hydrogeology Department, University of Avignon, Avignon, France

L. GOURCY, P.K. AGGARWAL

Isotope Hydrology Section, International Atomic Energy Agency, Vienna

Tritium is commonly used in groundwaters studies to calculate the recharge rate and to identify the presence of a modern recharge. The knowledge of ^3H precipitation time series is then very important for the study of groundwater recharge. Rozanski & Araguas [1] provided good information on precipitation tritium content in 180 stations of the GNIP network to the end of 1987, but it shows some lacks of measurements either within one chronicle or within one region (the Southern hemisphere for instance). Therefore, it seems to be essential to find a method to recalculate data for a region where no measurement is available.

Different methods can be used to reconstruct ^3H time series. In 1980, Weiss & Roether [2] provided an equation that combines various effects (latitude, precipitation high, vapour exchange rate) but considers, as reference, island, coastal and weathership stations near 50°N and 50°S . Doney et al. [3] published a new approach, derived from the one of Weiss and Roether [2], that integrates spatial and temporal components (seasonal effects, tritium decay). The resulting function can be applied from 1960 to 1986 to marine and continental sites in Northern and Southern hemispheres. The predicted error is of 15-35% for the mean annual tritium concentration, except in Northern Europe, where results have to be improved. It seems that the calculation of the tritium values, based on a graphic determination of 4 factors, could lead to uncertainties.

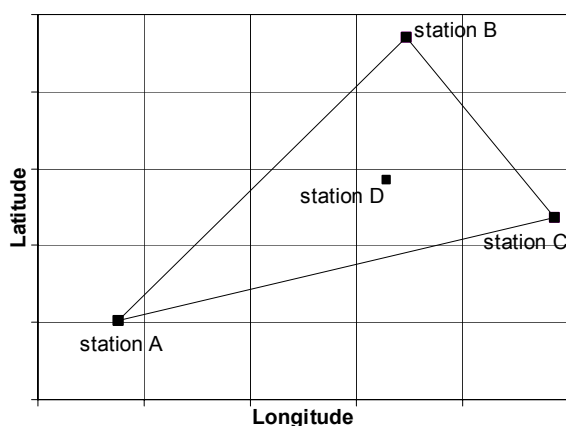


FIG. 1. Triangulation method is based on the knowledge of longitude, latitude and tritium time series for 3 stations (A, B, C) surrounding a 4th one that has no tritium measurements.

To solve this problem, we propose another method which is based on triangulation. It needs the knowledge of ^3H time series of 3 stations (A, B, C) surrounding geographically the 4th station (D) for which tritium input curve has to be reconstructed (Figure 1).

As the source of tritium in precipitation is the upper atmosphere rather than the ocean, tritium has a different distribution than deuterium and presents a reverse continental effect [4]. No altitudinal effect has been quoted in the literature. Knowing the spatial coordinates (L: latitude, l: longitude) of the 4 stations, we can calculate 3 factors f_A , f_B and f_C linking the fourth station to the 3 others:

$$f_A = \frac{(L_C - L_B)(l_B - l_D) - (l_C - l_B)(L_B - L_D)}{(L_C - L_B)(l_B - l_A) - (l_C - l_B)(L_B - L_A)}$$

$$f_B = \frac{(L_C - L_A)(l_A - l_D) - (l_C - l_A)(L_A - L_D)}{(L_C - L_A)(l_A - l_B) - (l_C - l_A)(L_A - L_B)}$$

$$f_C = \frac{(L_B - L_A)(l_A - l_D) - (l_B - l_A)(L_A - L_D)}{(L_B - L_A)(l_B - l_C) - (l_B - l_A)(L_B - L_C)}$$

The modeled tritium values (T_D) for the 4th station can then be calculated through the following equation :

$$T_D = f_A T_A + f_B T_B + f_C T_C$$

We have applied two methods of recalculation (Doney et al.'s model [3] and triangulation) and compared the modeled values with the real ones in 5 cases. The first example concerns the station of Bad Salzuflen (Germany), for which we have made 3 tests in order to verify our comparison between the 2 models. Then 2 other tests have been realized on Bismark (USA) and Valentia (Ireland) with farer surrounding stations.

Figure 2 shows the comparisons between real data, Doney et al.'s model and triangulation model from 1978 to 1995 for the first test we have achieved in Bad Salzuflen. The 6 months moving averages of the 3 curves highlight the fact that modeled values calculated with triangulation method (coarse line) fit better the real values (thick line) than Doney et al.'s model (dashed line). This latter proposes a theoretical approach that explains well the seasonal variations and the global decrease due to the tritium decay since 1963. However, the seasonal cycles shown in Figure 2 are too pronounced. Moreover, as the triangulation model uses real data of 3 stations to calculate Bad Salzuflen values, it provides a better estimation of the small variations. The all period averages confirm the previous conclusions. The average of the triangulation modeled values 27.2 ± 15.7 TU is closed by the one of real values 28.9 ± 16.9 TU. The average of the values issued from Doney et al.'s model is 25.2 ± 18.4 TU.

The 4 other approaches show roughly the same results, with a decreasing quality of the results with the augmentation of the distance between the 4 stations.

Doney et al.'s model [3] provides a good modeling of tritium global decay, seasonal variations and latitude effect. However, local and regional effects are not considered and lead to errors especially for the small values (Figure 2). On the opposite, the triangulation method takes into account this regional effect, but the error between real and modeled data increases with the distance and with the augmentation of the impact of very local effects (movement of air masses, local release of tritium). Moreover, for an overall reconstruction of the tritium time series, we need 3 stations, surrounding the given station, that have rather complete chronicles. These data are most of the time not available in the GNIP database, especially in the Southern

Hemisphere. As a conclusion, we can say that by combining the two methods, we can approach a better definition of the tritium input curve: Doney et al.'s model can be used to reconstruct a long time series since 1960, especially for the values above 50 TU; the triangulation method seems to be the best way to calculate data for a short time series that began in the 1970s, especially in the Northern hemisphere where long chronicles are available.

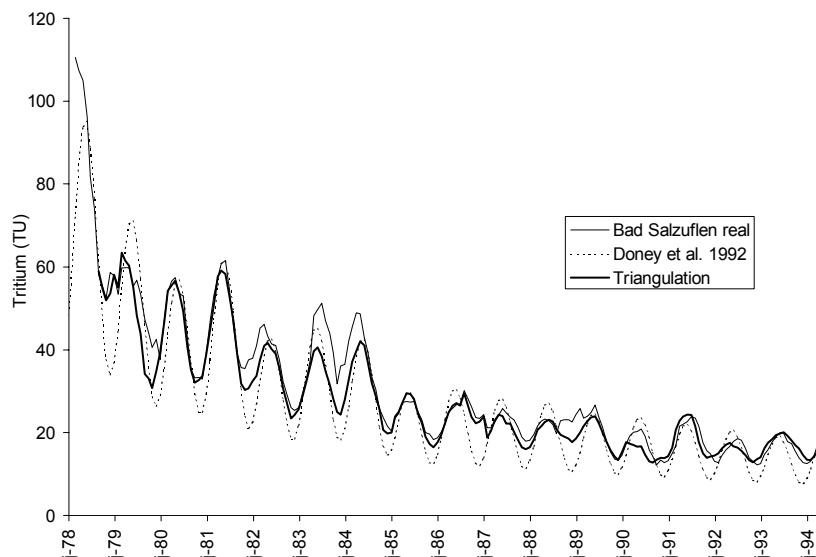


FIG. 2. Comparison between real data (solid line) and modeled values generated by Doney et al.'s model (dashed line) and the triangulation model (thick line).

REFERENCES

- [1] IAEA, «Statistical Treatment of Data on Environmental Isotopes in Precipitation», IAEA-STI/DOC/10/331 (1992) 781pp.
- [2] WEISS W., ROETHER W., «The rates of tritium input to the world ocean», *Earth Planet Sci. Lett.* **49** 435-446, 1980.
- [3] DONEY, S.C., GLOVER, D.M., JENKINS, W.J., «A model function of the global bomb-tritium distribution in precipitation 1960-1986», *Journ. of Geophys. Res.* **97**(C4) (1992) 5481-5492.
- [4] FERRONSKY, V.I., POLYATOV, V.A., «Environmental isotopes in the hydrosphere», Wiley and Sons Publishers (1982).

CARBON ISOTOPES CONFIRM THE COMPETITIVE ADVANTAGES OF *Prosopis* OVER *Acacia erioloba*

I. ROBERTSON, S. WOODBORNE

Quaternary Dating Research Unit, CSIR Environmentek, Pretoria, South Africa

The landscape of the Kalahari Desert is changing as the indigenous *Acacia erioloba* E.Mey. is being replaced by the invasive *Prosopis* spp. Although both species are phreatophytic, the disproportionately large taproot of *Prosopis* enables it to survive extreme moisture stress. $\delta^{13}\text{C}$ values were determined on annually resolved *Prosopis* and *Acacia erioloba* samples to investigate adaptation to changing edaphic conditions. The results confirm that the *Acacia erioloba* sample died during a period of water stress.

Acacia erioloba is extremely well adapted to surviving in arid and semi-arid environments. It is a 'keystone species' upon which a wide variety of plant and animals depend. However, it is being rapidly replaced by *Prosopis*; a species that was originally introduced to South Africa in the late-1880s. *Prosopis* has an extensive lateral root system to obtain water from the unsaturated zone and, depending upon moisture regimes, can develop a large taproot to access ground water.

Ten *Acacia erioloba* and ten *Prosopis* discs were obtained from a bushveld site close to Askham (27°1'S, 20°48'E) in the Northern Cape, South Africa. Precipitation data were obtained from the Police Station at Witdraai, 10 km from the site.

Although *Prosopis* has the potential to be cross-dated [1], asymmetrical growth precluded the establishment of a chronology for *Prosopis* or *Acacia erioloba*. However, marginal parenchyma bands enabled the rings of *Acacia erioloba* to be counted [2] and a high-resolution radiocarbon date (± 1 year) confirmed the *Prosopis* ring count. α -Cellulose was extracted from the annual rings and $\delta^{13}\text{C}$ values were determined using standard techniques.

The $\delta^{13}\text{C}$ values of *Prosopis* (1970-1999) and *Acacia erioloba* (1977-1994) for two samples typical of the site were determined (Fig. 1). The $\delta^{13}\text{C}$ results demonstrate that after a major precipitation event, *Prosopis* and *Acacia erioloba* experience a reduction in water stress. *Acacia erioloba* is almost entirely dependent upon ground water. As a juvenile tree it exhibits water stress (1978-79) as the taproot is extended to reach the water table. In the following relatively dry years, it starts to experience water stress until the major precipitation event in 1987-1988, which replenishes water reserves. The decrease in precipitation and increased extraction of water by *Prosopis* causes eventual death in 1994.

The *Prosopis* $\delta^{13}\text{C}$ values for the period after unusually high precipitation in the mid-1970s indicate that this relief from water stress is short-lived as amount of water in the unsaturated zone is reduced. The increase in water stress is more rapid than *Acacia erioloba* and suggests that *Prosopis* initially uses its lateral roots to extract water from the unsaturated zone until the water reserves are exhausted and it switches to the dormant taproot.

Prosopis is replacing *Acacia erioloba* in arid and semi-arid regions of South Africa. In areas where the limiting factor upon growth is water availability, *Prosopis* appears to maintain a competitive advantage by tracking changes in the level of the water table or extracting deeper ground water. *Acacia erioloba* cannot compete with the increased demand for water. Carbon isotopes confirm mortality of *Acacia erioloba* occurs in times of water stress.

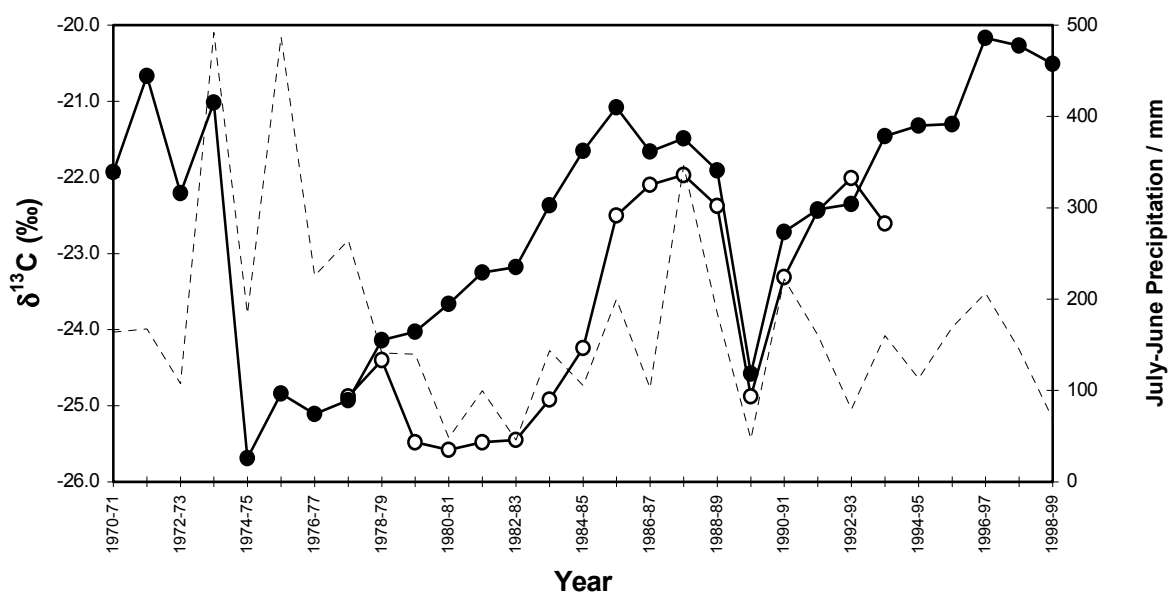


FIG 1. $\delta^{13}\text{C}$ values of *Prosopis* (solid circles) and *Acacia erioloba* (open circles). Annual July-June rainfall is represented by the dotted line. A high resolution radiocarbon date (± 1 year) on the 1974-75 *Prosopis* sample confirmed the ring count.

REFERENCES

- [1] FLINN, R.C., ARCHER, S., BOUTTON, T.W., HARLAN, T., Identification of annual rings in an arid-land woody plant, *Prosopis Glandulosa*, *Ecology* **75**(3) (1994) 850-853.
- [2] GOURLAY, I.D., KANOWSKI, P.J., Marginal parenchyma bands and crystalliferous chains as indicators of age in African *Acacia* species, *IAWA Bulletin* **12**(2) (1991) 187-194.

USE OF K-40 STANDARD SOURCE FOR MEASURING BETA-ACTIVITY IN ENVIRONMENTAL SAMPLES

R.I. MAMATQULOV

State Speciality Inspection of Analytical Control, Tashkent, Uzbekistan

M. Z. ZAKIROV

Sanitary epidemiological station, Tashkent, Uzbekistan

The measurements of beta-activity in ash remainders of environmental samples can be achieved using gas ejection counters. For this purpose we use gas ejection counter -MST-17 with following main characteristics:

max power of the	
start of counting:	1600 V
expansion of plato:	150 V
slope of plato:	5%
max. value of impulses:	10^4 imp/min.

This equipment is initially prepared to operate at a working power of 1650V. The analysis are implemented on samples of air (filtrate), soil, sediments, water (remainder) and bioassay in form of ash remainder with weight range 60-400 mg.

The common formula of determination beta-activity measuring weight has the following equation:

$$A = F \cdot K_T \cdot V \text{ (in Бк/кг)} \quad (1)$$

were: F - correction coefficient of measurement conditions;
 K_T - correction coefficient of self-absorption of beta particles, related with weight of sample;
 V - velocity of counting of signals from sample, measuring by decode - counting system DP-100.

The coefficient K_T could determinate with relations the weight of sample (m) and correction (p) of self-absorption by the equation:

$$K_T = \frac{1,67}{p \cdot m} \cdot 10^4 \frac{\text{Бк}}{\text{кг}} \frac{\text{imp}}{\text{min}} \quad (2)$$

By this formula calculated values of K_T in weight range 60-400 mg and shown by diagram 1. From the mass range more applicable value is 300 mg for which

$$K_T = 89 \frac{\text{Бк}}{\text{кг}} \frac{\text{imp}}{\text{min}}$$

The coefficient F , related of measurement conditions which included corrections to geometry of measurement system, absorptions of beta particles in windows of counter and in air, and back dispersion, could be determinate by using standard source. For this purpose we can use chemical soft salt of kalium chloride - KCl. For preparation of standard source, preliminary should be heat KCl in temperature 130°C during 2 hours, then triturate by the porcelain tool. Then 300 mg KCl, with the proportional density to put in special cuvette.

The source beta-activity of KCl is explained that have radionuclide K-40. In calculation of activity of kalium we knows that half life time of K-40, decay of beta particles 89% and concentration of K-40 in natural kalium is 0,0119% and this dates gives that 1 kg natural K could decay $1,64 \cdot 10^6$ beta impulses per min. From this value we can calculate beta activity concentration which could be $A_0 = 27,37 \cdot 10^3 \text{ Бк/кг}$.

Given the molecular mass of KCl (M) and atomic mass K (m_0) and we can calculate activity concentration (A_s) chloride kalium:

$$A_s = A_0 \cdot \frac{m_0}{M} = 14,32 \cdot 10^3 \text{ Бк/кг} \quad (3)$$

Using equations (1), (3) and value of K_T for 300 mg KCl and measurement value of velocity V we find:

$$F = \frac{A_s}{K_T V} = 4,1 \quad (4)$$

Using this method for determination of beta activity of ash samples it is necessary to choose similar conditions and measured value of velocity V to put in formula (1), which in example of sample $m=300 \text{ g}$ could be: $A = 365 V$.

Such methods are used in laboratories at sanitary epidemiological stations and for State special inspection of analytical control in Uzbekistan.

REFERENCES

- [1] B.V. GOLIKOV et al., "Methods of measurements of nuclide activity", Moskow (1981).
- [2] M.T. MAKSIMOVov, G.O. ODJAGOV "Radiation contamination and their measurements", Moskow (1989).
- [3] B.A. BAJENOV and others "Toxic chemical materials: radioactive materials", Saunt-Peterburg (1990).

MULTI-COLLECTOR ICP-MS FOR HIGH PRECISION ISOTOPE RATIO MEASUREMENTS: APPLICATION TO ISOTOPIC DATING METHODS

H. HERTLE

Micromass GmbH, Augsburg, Germany

S. MEFFAN-MAIN, Z. PALACZ, P. TURNER

Micromass UK, Wythenshawe, Manchester, United Kingdom

Until recently, thermal ionisation mass spectrometry (TIMS) was considered the technique of choice for high precision isotope ratio measurements in the earth sciences when applied to the U/Th-Pb method of dating. However, the evolution of modern Multi-Collector Inductively Coupled Plasma source Mass Spectrometers (MC-ICP-MS) has revolutionised studies in isotope analysis by simplifying sample preparation methodology and allowing the analysis of many new isotope systems. The ability to measure all the isotope ratios of interest simultaneously (with a 17.5% mass spread) removes the measurement instability caused by plasma flicker from the ICP. In addition, the flexibility of sample introduction methods for ICP-MS has resulted in faster and simplified analysis compared with conventional thermal ionisation mass spectrometry. Inductively coupled plasma multi-collector mass spectrometers are extremely versatile isotope ratio analysers. The versatility of the technique owes much to the ICP plasma source as it can be used to ionise material from solutions or from solids. One of the main advantages of the MC-ICP-MS technique is the ability to undertake in-situ measurements of isotope ratios using laser ablation directly coupled to the ICP. Signals from such analysis are transient in nature and so isotopic measurements must involve the static mode of analysis.

The Micromass IsoPro 2™ is a MC-ICP-MS, but is unique in that it uses a modified interface with a RF only Hexapole collision/reaction cell between the sampling interface and the magnetic sector mass analyser (Figure 1). The Hexapole has three key advantages:

1. It is a simple, yet highly efficient, ion-focusing device which leads to very high ion transmission and results in a very sensitive instrument. For example, when using laser ablation as a sample introduction method, 1% ion:atom transmission efficiencies can be achieved when analysing Pb isotope ratios in solids.
2. The introduction of a small volume of an inert gas, such as helium or argon, into the Hexapole collision cell results in inelastic collisions between the ions from the ICP and the collision gas. By repeated collisions the ions from the ICP are thermalised so that they assume the energy of the collision gas. This results in the mean ion energy spread of the ions from the ICP being reduced from >20eV to <1eV. By reducing the mean ion energy spread of the ions from the ICP mass separation becomes far easier in the mass spectrometer. The thermalising of the ion beam also provides the conditions required for producing flat-topped peaks, essential for high precision isotope ratio measurements.
3. Reactive gases, such as hydrogen, can also be introduced into the Hexapole reaction cell to remove argon-based interferences which severely compromise the determination of a number of important elements (e.g. S, Ca and Fe) below m/z 80.

In conjunction with the above technical details from [1], state of the art data will be presented for several isotopic systems in the analysis of solution and solid sample matrices.

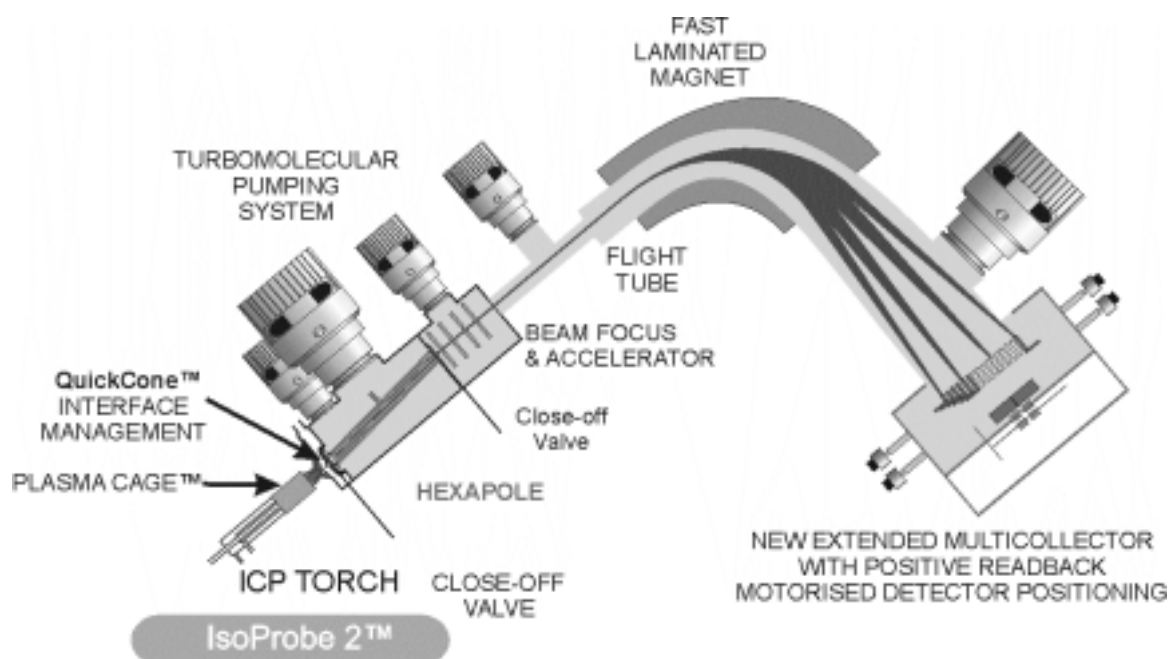


FIG. 1. *The IsoProbe 2™.*

REFERENCE

- [1] P.J. TURNER, T.O. SPEAKMAN, J. SPEAKMAN, R.C. HAINES, Z. PALACZ, S. MEFFAN-MAIN, Ion optics of Multi-collector ICP-MS systems for precise and accurate isotope ratio measurements. Micromass Technical Note 403, Micromass UK, <http://www.micromass.co.uk>

RECONSTRUCTION OF BOMB ^{14}C TIME HISTORY RECORDED IN THE STALAGMITE FROM POSTOJNA CAVE

B. VOKAL

University of Ljubljana, Faculty of Natural Science and Engineering, Department of Geology, Ljubljana, Slovenia,
Jožef Stefan Institute, Department of Environmental Sciences, Ljubljana, Slovenia

D. GENTY

Université de Paris-Sud, Laboratoire d'Hydrologie et de Géochimie Isotopique, Orsay, France

B. OBELIĆ

Ruđer Bošković Institute, ^{14}C and ^3H Laboratory, Zagreb, Croatia

The knowledge of the concentration of natural radioactive isotope ^{14}C in the atmosphere has proved to be a particularly useful tool in the study of the carbon cycle. The carbon cycle plays a dominant role in controlling many of the chemical and biological processes in different ecosystems. A significant increase of the concentration of ^{14}C in the atmospheric CO_2 in the atmosphere and biosphere during the sixties was caused by nuclear bomb tests in the atmosphere [1, 2]. Various nuclear facilities may also contribute to increase of ^{14}C in the atmosphere, while the use of great amounts of fossil fuels causes a dilution of ^{14}C in the atmosphere.

The karstic caves provide valuable resources for reconstruction of environmental conditions on the continent in the past. This is possible due to the great stability of climatic conditions within a cave. Secondary minerals deposited in caves, known as speleothems, preserve records of long-term climatic and environmental changes at the site of their deposition and in the vicinity. The purity of speleothems and their chemical and physical stability make them exceptionally well suited for detailed geochemical and isotopic analysis [3].

Karst areas constitute a large part of Slovenia, with several thousands of caves located in the limestone formations. The Postojna Cave system is composed of 23 km of accessible channels and galleries and is a part of the karst region of the underground Ljubljanica River. The Postojna Karst is located at the northwestern part of the Dinaric Karst ($L=45^\circ46'\text{N}$, $l=14^\circ12'\text{E}$, $Z=529\text{m}$). It is limited to the north by the promontory of the Julian Alps, and to the south by the Adriatic Sea [4]. The karst region has a variable climate under the Mediterranean, Alpine and Pannonian influences. The Postojna Karst is composed of Cretaceous carbonate rocks [5]. The hill under which Postojna Cave is situated is covered by a pine tree forest and grass. Average annual temperature is 8°C and mean annual rainfall is 1500 mm.

The 5 cm high stalagmite was collected in the Biospeleological Gallery, about 200 m from the entrance. There the cave roof consists of 30 meters of upper Cretaceous limestone and the soil thickness is about 4-10 cm. Visible growth laminae are difficult to count. A polished vertical thin section reveals a thin ($<0.1\text{ mm}$) remarkable black layer at 24 mm from the stalagmite top, whose date of deposition was well known (23rd of April 1944).

Between 10-36 mg of CaCO_3 were sampled with a microdriller from a polished stalagmite cross-section. This represents between 1 and 2 years of calcite deposition. Calcite powders were reacted with H_3PO_4 in order to obtain CO_2 . The gas was reduced to graphite on iron with

hydrogen at 650°C for 100 minutes. Carbon atoms were counted with an accelerated mass spectrometer (TANDETRON) at Gif-sur-Yvette.

Radiocarbon activities in the stalagmite are shown in Fig. 1. A sharp peak was expected in the years 1963–1964, due to the nuclear tests in the atmosphere [1]. Based on the two known time markers, the gasoline explosion mark (April 23, 1944) and the top layer (October 24, 1996), the time scale in the speleothem was determined. The maximum ^{14}C activity in the speleothem carbonate occurred in 1974, which was 10 years after the atmospheric peak. The difference of ^{14}C activity between pre- and post-bomb periods is 27.4 pMC between the years 1950 and 1978. Compared with the atmospheric variations of ^{14}C activity from 1950 to 1964 (100 pMC and 190 pMC, respectively), the stalagmite activity variations are small, which means that the ^{14}C signal has been damped. Atmospheric ^{14}C activity shows a well pronounced peak in 1964, and since then decreases exponentially, while radiocarbon activities in the stalagmite only slightly decrease after the year 1974 (from 115.4 pMC in 1974 to 107.2 pMC in 1996). The pronounced ^{14}C peak together with the variation between pre- and post-bomb ^{14}C activities demonstrate that Postojna Cave is sensitive to atmospheric changes. By comparison of the activity curves of the atmosphere and in the speleothem, we can gain information about the processes of carbon transfer from the surface to the cave. Such ^{14}C chronicles can improve our understanding of the soil carbon dynamics, which is of great importance since response of soil carbon reservoirs to climate change and/or human activity is still not well known.

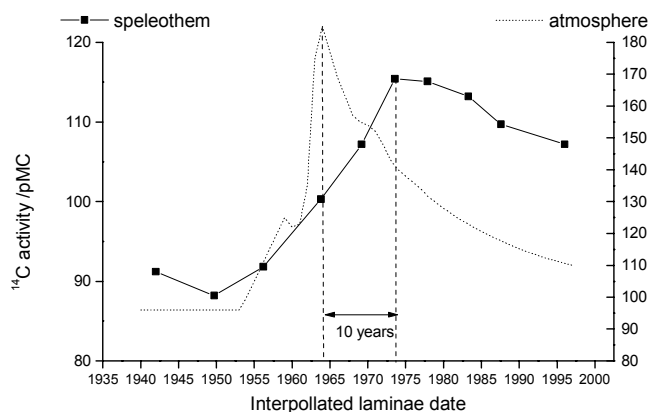


FIG. 1. Radiocarbon activity in the stalagmite and the atmosphere.

REFERENCES

- [1] LEVIN, I., BÖSIGER, R., BONANI, G., FRANCEY, R.J., KROMER, B., MÜNNICH, K.O., SUTER, M., TRIVETT, N.B.A., WÖLFLI, W., Radiocarbon in atmospheric carbon dioxide and methane: Global distributions and trends, In Taylor, R.E., Long A. and Kra R.S., eds, Radiocarbon after four decades, New York, Springer-Verlag (1992) 503-518.
- [2] KRAJCAR BRONIĆ I., HORVATINČIĆ N. and OBELIĆ B. (1998) Two decades of environmental isotope records in Croatia: reconstruction of the past and prediction of future levels, Radiocarbon **40** (1998), 399-416
- [3] RAFTER T.A., FERGUSON, G.J., Atom bomb effect-Recent increase of carbon-14 content of the atmosphere and biosphere, Science **126** (1957) 557-558
- [4] GOSPODARIČ, R., Paleoclimatic record of cave sediments from Postojna Karst, Annales de la Société géologique de Belgique, T.111 (1988) 91-95
- [5] GOSPODARIČ, R., The quaternary cave development between the Pivka Basin and Polje of Planina, Acta Carsologica, **VII/1** (1976) 5-121

TRACE ELEMENT RECORDS IN HIGH MOUNTAIN LAKE SEDIMENTS IN NW SLOVENIA DATED BY ^{210}Pb

P. VREČA, Z. JERAN, S. LOJEN, R. JAČIMOVIĆ, T. DOLENEC
J. Stefan Institute, Ljubljana, Slovenia

A. BRANCELJ, G. MURI
National Institute of Biology, Ljubljana, Slovenia

Abstract. Assessments of trace element concentrations of anthropogenic or natural origin, especially of Cd, Pb and Zn, have been the subject of several studies during the last decade. These metals have been intensively used in industry, especially in the northern hemisphere. Due to worldwide reduction in particulate emission by industry and anti-knock lead in gasoline, their global emission into the atmosphere has been decreasing since 1975 [1, 2].

For many trace elements long-range atmospheric transport is the most important source of contamination and lake sediments can act as archives of atmospheric deposition of those elements. In our study trace element concentrations of As, Cd, Co, Cr, Sb, Pb and Zn were determined in sediments from three small high mountain lakes in northwestern Slovenia. Sediments for trace element analysis were collected in 1999 at Lake Planina pri Jezeru, in 1998 at Lake Krn and in 1996 at Lake Ledvica. Radiometric dating of the sediments was carried out using the Pb-210 method. Ages and sedimentation rates were estimated using constant rate supply (CRS) model using the software package of Shukla [3].

According to Pb-210 dating, the accumulation rates of the sediments range from 0.14cm/year in Lake Ledvica to 0.26 cm/year in Lake Krn (Fig. 1). In Lake Planina pri Jezeru the sedimentation rate was determined to be 0.24cm/year and has greatly increased in the last 15 years.

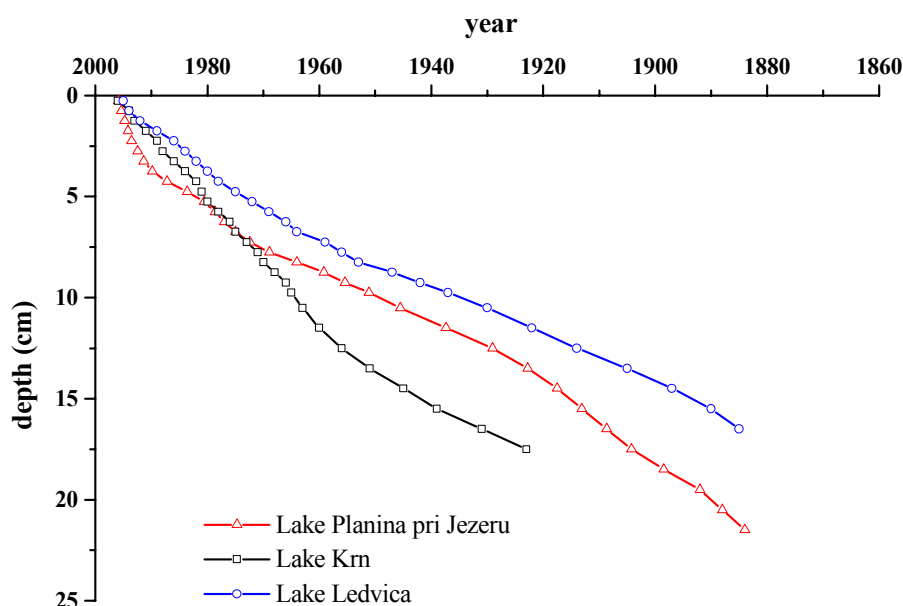


FIG. 1. Results of Pb-210 dating in the studied lakes.

Changes in concentrations with depth are obvious for all determined elements in Lake Planina pri Jezeru and Lake Krn (Fig. 2). In the sediment from Lake Planina pri Jezeru three periods of lake history can be distinguished. Concentrations increase at the depth 0-7cm. The decrease in concentrations, especially of Pb and Cd, in the last 25 years is probably due to use of lead-free gasoline in Western Europe. Concentrations are relatively constant in the segment between 7-19cm and reflect the period of highest industrial emissions in the 20th century. From the depth 19-35cm concentrations decrease rapidly with depth and show the influence of the industrial revolution in the 19th century. Concentrations in the detailed profile from Lake Krn are variable in the upper 8cm and are higher than below this depth. Concentrations are relatively constant in the segment from 8-18cm. In this sediment sequence only the concentration of Sb decreases with depth. Explanation of the concentration changes in Lake Krn is still difficult. The distribution of elements in Lake Ledvica is similar to that in Lake Planina pri Jezeru. Concentrations in the sediment slightly increase to the depth of 3cm, are relatively constant between 3-13cm and decrease to the depth of 16cm. These changes can be explained in the same way as those at lake Planina pri Jezeru.

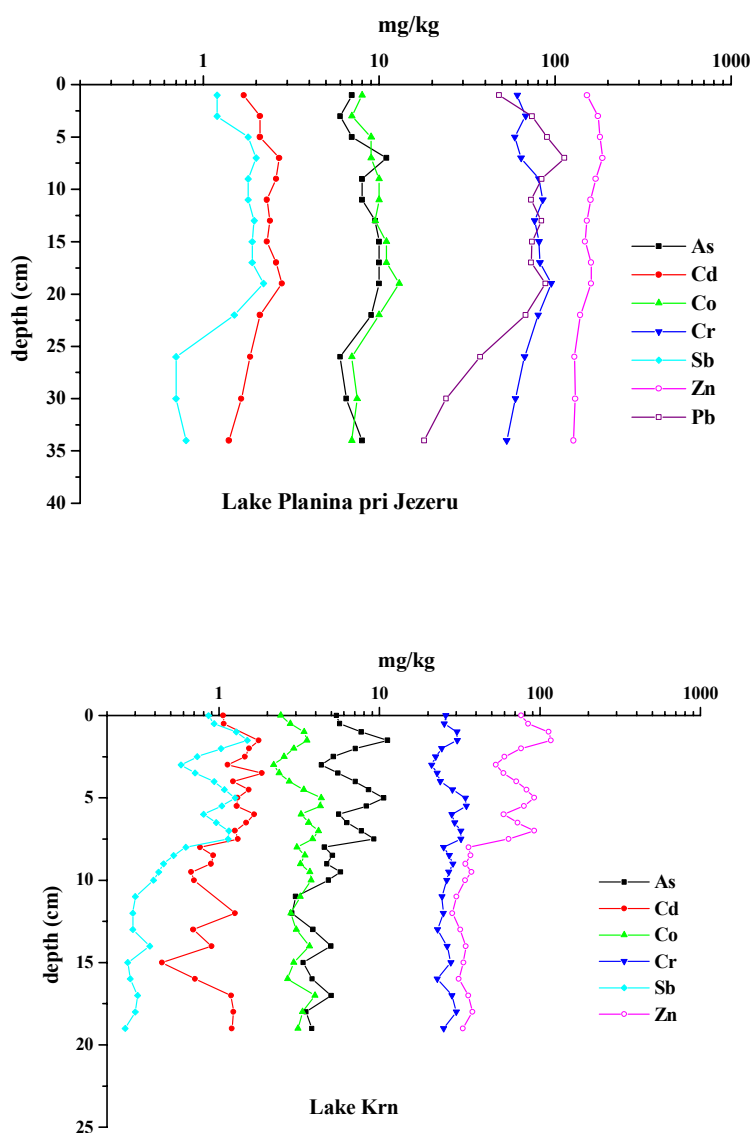


FIG. 2. Distribution of elements in Lake Planina pri Jezeru and Lake Krn.

REFERENCES

- [1] NRIAGU, J.O., “Quantitative assessment of worldwide contamination of air, water and soils by trace metals”, *Nature* **333** (1988) 47-49.
- [2] MONNA, F., CLAUER, N., TOULKERIDIS, T., LANCELOT, J.R. “Influence of anthropogenic activity on the lead isotope signature of Thau Lake sediments (southern France): origin and temporal evolution”, *Applied Geochemistry* **15** (2000) 1291-1305.
- [3] SHUKLA, B.S. “Sedimentation Rate through Environmental Radioactivity”, Software, Part-1, ²¹⁰Pb Dating of Sediments, Environmental Research & Publications Inc., Ontario, Canada (1996).

INFLUENCE OF LOCAL EMISSIONS ON CONCENTRATION AND ISOTOPIC COMPOSITION OF TRACE GASES (CO₂ AND CH₄) UNDER STRONG ANTHROPOPRESSION: A CASE STUDY FROM KRAKÓW, SOUTHERN POLAND

T. FLORKOWSKI, A. KORUS, T. KUC, J. LASA, J.M. NECKI, M. ZIMNOCH

University of Mining and Metallurgy, Faculty of Physics and Nuclear Techniques and Institute of Nuclear Physics, Kraków, Poland

Measurements of the isotopic composition of carbon dioxide and methane together with their concentrations in the atmosphere, yield useful information on the contribution of anthropogenic sources to regional budgets of these gases and their seasonal changes. Observed correlation between isotopic composition and inverse concentration of these gases is used for estimation of mean isotopic composition of the local source.

Monitoring of atmospheric CO₂ has been initiated in Kraków in 1982. The sampling point is located in a polluted urban area with strong contribution of anthropogenic gases originating both from local sources (coal burning, car traffic, leakages from city gas network, landfills) and large distant emitters - industrial district located ca. 80 km to the west from Krakow (Silesia district). Quasi-continuous measurements of CO₂ and CH₄ concentrations in the low atmosphere are performed using gas chromatographic method. For isotope measurements, the atmospheric CO₂ is continuously sampled by sorption on molecular sieve in bi-weekly intervals and radiocarbon concentration is measured by liquid scintillation spectrometer, while $\delta^{13}\text{C}$ is determined by isotope ratio mass spectrometer. Measurement error (1σ for single measurement) is in the order of 0.1 ppm for CO₂ concentration, $\pm 8\%$ for $\delta^{14}\text{C}$, and $\pm 0.1\%$ for $\delta^{13}\text{C}$.

In 1994, a new station for regular observations of greenhouse gases in lower atmosphere was set up in the High Tatra mountains, at Kasprowy Wierch (49°N, 20°E, 1980 m a.s.l., 300 m above the tree line). Kasprowy Wierch, with only small influences from local sources of trace gases can be considered as a reference station for this region of Poland. The record of CO₂ and CH₄ concentration and their isotope composition obtained at Kasprowy Wierch is considered as a background level for Krakow observations.

The presented study was aimed at better characterisation and quantification of the local fossil component coming from anthropogenic emissions of CO₂. A three component mixing model was applied which allows to distinguish biospheric, and anthropogenic sources and their strength. In addition, the radiocarbon data were used. The analysed period extends from 1998 to 2000, presented in the context of the earlier obtained data. The carbon dioxide concentration together with its isotope composition at Kasprowy Wierch sampling point reveals well pronounced daily and seasonal oscillations, superimposed on the long-term trend. Much higher amplitudes are observed at Kraków. The increase of average CO₂ concentration as well as methane mixing ratio is observed since 1998. Linearisation of the radiocarbon record shows steep decrease of ca. 45 % per year for the discussed period. Similar trend is observed for $\delta^{14}\text{C}$ in CO₂ collected in Kraków sampling point located in highly urbanised area. However, measurement values being in the same range for the both records, show fluctuations which are in counterphase.

The average background methane concentration measured at Kraków reveals a systematic shift by a few percent towards higher values, when compared with the Kasprowy Wierch data. This is caused by persistent leakage of methane from the city gas network.

ECOLOGICAL POLICY, ASSESSMENT AND PREDICTION OF THE FATE OF CHERNOBYL RADIONUCLIDES IN SEDIMENTS OF THE BLACK SEA

A.E. KONTAR

P.P. Shirshov Institute of Oceanology,
Russian Academy of Sciences,
Moscow, Russian Federation

The mathematical model has been designed to investigate the fate and distribution of the Chernobyl radionuclides in sediments of the Black Sea. One of the regions of intensive radioactive precipitation during the Chernobyl disaster was the northwestern Black Sea region. There are some canyon systems in this region, where bottom sediments of the shelf zone are removed to the continental slope region and finally to the abyssal part of the sea. The lack of reliable information on the removal intensity of the shelf sediments, which contain different kinds of radioactive precipitation, does not allow changes in the radioactive situation to be predicted reliably enough in the given region. On the other hand, the surface sedimentary layers dated by characteristic Chernobyl precipitation made it possible to obtain information on sediment movement rates and directions, as well as other quantitative and qualitative parameters for the mechanisms of canyon processes. This region was selected for our study. The bottom sediments in this region constitute the permanent repository for material retained by the basin that is derived from the surrounding land mass via the atmosphere, rivers, groundwater discharge and coastal erosion. This includes contaminants, for example heavy metals, organic substances and radionuclides. The results of measurements of the concentrations of ^{137}Cs in the bottom sediments of the northwestern part of the Black Sea indicate the inhomogeneity of their distribution both over the studied area and over the core depth. The intermittency of the layers with different concentration of radionuclides in the cores reflects the active horizontal movements and redistribution of sediments on the shelf and continental slope. The high degree of variability of the radionuclide activities observed on the shelf is probably due to the very heterogeneous nature of the sediment cover due to erosion and sediment redeposition. Some areas close to the shelf edge appear to be devoid of modern sediment. The bottom boundary layer in this region of the Black Sea has not been studied in detail, although it is known that there are local areas of high rates of sediment transfer due to near-bottom currents, turbidity flows and some other dynamic processes on the boundary between the sea water and the sea floor. Present day theory of the bottom boundary layer is based on a model with horizontally homogeneous and statistically stationary turbulent currents. However, a real bottom boundary layer is not stationary. Occasionally there are dramatic velocity increases in the near-bottom current, the so-called "bottom or benthic storms". Different eddies above the area studied are supposed to be the cause of the observed events. In the following it is suggested that additional mechanisms are needed to explain some observations of bottom storms and mixing processes in the Black Sea. The importance of periodic bottom storms springs from the fact that they stir up bottom sediments with radionuclides incorporated, which are then captured and transported over large distances by weaker but stable currents. Some so-called "warm" bottom storms are connected with lutite flows, forming in the upper horizon of the slopes. This is due to bottom erosion, resulting from creeps of sediment, frequently shaken by local submarine earthquakes. There are various approaches for studying the delivery and burial of pollutants in the sea, which were developed in P.P. Shirshov Institute of Oceanology. These approaches were efficiently used for developing the mathematical models. They include determinations of the flux of material from the water column to the sea floor. The materials of the P.P. Shirshov Institute of Oceanology

expedition measurements have been used for the analysis of the current structures, taking into account the internal waves and eddies action on the vertical and longitudinal distribution of the velocity, water density and sediment concentration with incorporated radionuclides. This experimental base allowed approbation of diagnostic methods and above-mentioned mathematical models, which were combined into a general model of the fate of Chernobyl radionuclides in the Black Sea. All the foregoing made it possible to work out a policy and main principles for assessment and prediction of the fate of radionuclides in the Black Sea. The scientifically-based recommendations for assessing and, mainly, minimizing negative pollution effects on the Black Sea environment have been elaborated, and the approaches to prediction of re-contamination of the coastal zone under different scenarios of climate changes and a growing impact of man-induced factors were worked out. The elaboration based on development of the Black Sea-circulation mathematical model tackled by a combined use of radioactive tracers and mathematical modeling of the oceanographic processes. The fluid dynamics mechanisms control the processes of transport and storage of the radionuclides introduced through atmospheric fall-out and river discharge into the Black Sea, including the processes of sedimentation, vertical mixing and geochemical processes in bottom boundary layer (sea water - bottom sediments). We also took into account the processes that could cause a possible backward transport of the pollutants from the deep areas of the Black Sea into the shelf zone. Finally we created a complex mathematical model describing the pollutant behavior from the moment of its input to its output from the ecosystem. This is a step toward the ultimate goal of construction of an ecological model able to give valuable information socio-economic management of the region. Our investigations revealed that the concentration of radionuclides on the Black Sea floor has a patch-like mosaic structure. We used the investigation methods, which include new elements both in the analysis of the natural measurement results and in theoretical interpretations by closure of density currents mathematical models. The density and turbidity current structure theoretical description include four stages: (1) The solution of the hydrodynamic equations for the density current constant in time. This solution gives undisturbed vertical velocity and density distributions. The parameters of these distributions vary in time and along the current very slowly; (2) The solution of the equation system for a model of density or turbidity current. Such a model gives the longitudinal distributions of the velocity and density profiles parameters; (3) The modeling of the vortex-wave distributions field; (4) The description of the current structure as a superposition of the distribution. This superposition includes undisturbed distribution and vortex-wave disturbance profiles in each point and at the corresponding moment of time. The principal possibility and efficiency of such a method has been evaluated during the measurements results analysis. This solution takes into account the simultaneous influence of ambient liquid mobility, turbulent stress profile in stratified medium and the interaction of jet current part with the near-bottom boundary layer. Theoretical distributions describe density and turbidity currents with internal waves in the entire current action field. In the solution of suspended particles diffusion equation, the new turbulent diffusion coefficient distribution - "diffusive triplet" was utilized. On the basis of theoretical solutions and measurements results, the current structure diagnostic method by statistical parameters of suspended particles size spectra was elaborated. As a result of this work scientifically provided recommendations have been elaborated for assessing fate of pollutants in the Black Sea and near-bottom dynamics interaction with the environment in natural and man-induced conditions and also suggestions for monitoring the near-bottom environment, aimed at minimizing negative ecological effects. The results of this work have confirmed once again by research that the Black Sea crisis calls for a concerted international approach and that it is critical for the future of the Black Sea that various programs addressing the Black Sea's environmental problems be coordinated to work together. It promotes sustainable development of efforts towards improved environmental

management in the Black Sea region. The results obtained for the Black Sea can be used in comparable regions of Russia for elaborating a policy, strategy and methodology of predicting the fate of pollution in the sea. Solution of these problems is particularly acute for the new social and economic conditions in Russia.

TREE-RING STABLE OXYGEN ISOTOPE RATIOS INDICATING COOLER AND WETTER CLIMATE CONDITIONS AND HIGH FLOOD FREQUENCY PERIODS IN THE RED RIVER BASIN, MANITOBA, CANADA

W.M. BUHAY

Department of Geography, University of Winnipeg, Winnipeg, Manitoba, Canada

B. MAYER

Departments of Physics and Astronomy, Geology and Geophysics,
The University of Calgary, Calgary, Alberta, Canada

S. St. GEORGE, E. NIELSEN

Manitoba Industry, Trade and Mines,
Winnipeg, Manitoba, Canada

P. HARMS, D. MARCINO

Department of Geography, University of Winnipeg, Winnipeg, Manitoba, Canada

In the Red River region of southern Manitoba, Canada, the frequency of flood events tends to increase during cooler and wetter climate conditions. Predictably, recorded Red River flood stages are primarily a result of meteorological conditions which produce an increase runoff due to excess snowmelt and heavy spring precipitation. Winter skewed precipitation periods corresponding to cooler and wetter conditions in the Red River Basin may provide traceable oxygen isotope signals in hydrologically sensitive trees occupying the basin. To test this hypothesis, three overlapping oak tree-ring chronologies (KPO1: 1990 to 1795; STVO1: 1985 to 1797; STVO2: 1990 to 1845) were annually sampled and processed for their cellulose. It is anticipated that the annual cellulose oxygen isotopic compositions may identify cool and wet climate conditions in the Red River Basin corresponding to other periods of abnormally high runoff years prior to the recorded flood events (post-1880).

Proxy climate data obtained from historical records (Hudson's Bay Archives) suggest that the Red River Basin experienced cooler and wetter conditions during the late Little Ice Age (the early 19th Century). The oxygen isotope and tree-ring width reconstructions for KPO1 support this interpretation. As indicated in Figure 1, progressively decreasing $\delta^{18}\text{O}_{\text{cellulose}}$ values between the early 1800's and 1860 suggest that climate conditions became cooler resulting in lower mean annual $\delta^{18}\text{O}_{\text{precipitation}}$ values. Additionally, the seasonal distribution of precipitation may have been winter skewed during this time providing the trees in the growing season with isotopically depleted meteoric water. The lower annual temperatures and/or the winter skewed seasonal precipitation may have been accompanied by more humid summer growing conditions which would reinforce decreasing $\delta^{18}\text{O}_{\text{cellulose}}$ values. The tree-ring widths generally responded positively to the wetter conditions. KPO1 seems to have responded to the very wet conditions (coupled with possible cooler and winter skewed precipitation) with metabolic vigor between 1850 and 1860, historically a period of frequent Red River flooding events. The minimum in tree-ring widths corresponding to the maximum in $\delta^{18}\text{O}_{\text{cellulose}}$ values in the late 1960's is related to a period of warm and dry conditions.

Further, work currently in progress on the overlapping records provided by the STVO1 and STVO2 isotope and ring-width chronologies should reinforce and add insight into the observations provided by KPO1. Additionally, an extended Red River Basin tree-ring

chronology may eventually be used to identify much earlier cooler and wetter periods and subsequently, periods of increased Red River flood frequency.

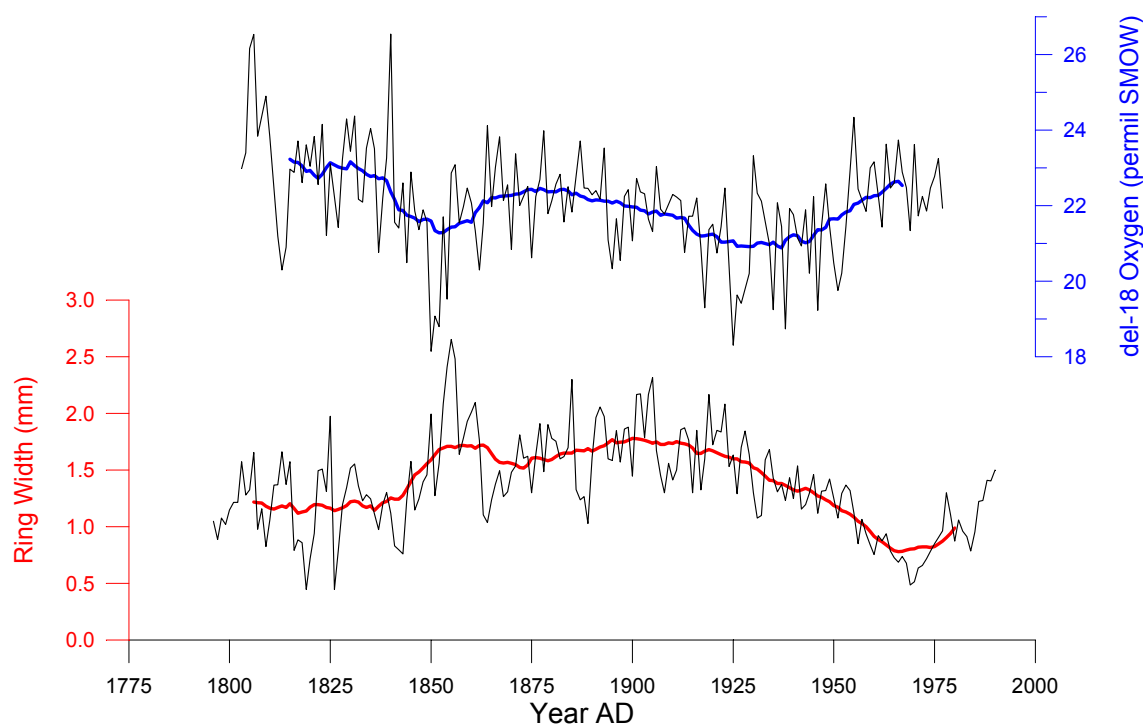


FIG. 1. An annual and 20 year running average comparison of $\delta^{18}\text{O}$ cellulose values and ring widths for KPO1, Winnipeg, Manitoba, Canada.

PRELIMINARY DATA ON DINOSAURS HABITAT DURING THE UPPER MAASTRICHTIAN, HATEG BASIN, ROMANIA

D. GRIGORESCU

University of Bucharest, Faculty of Geology and Geophysics, Romania

A.-V. BOJAR

Department of Geology and Paleontology, Graz, Austria

L. KLARIK

University of Bucharest, Faculty of Geology and Geophysics, Romania

The Hateg basin is located in the south-western part of the Transylvanian Depression and it is filled with sediments that overly the crystalline rocks of the Getic nappe. The basin show multiple stage of Mesozoic evolution. The Latest Cretaceous (Middle and Upper Maastrichtian) with continuous transition to Paleocene is represented by two continental lithostratigraphic units: the Densus-Ciula and the Sinpetru Formations. The Upper Maastrichtian of Densus-Ciula Formation at Tustea Quarry is represented by a pebbly alluvium with massive, matrix supported conglomerates, cross bedded sandstones and mudstones, the last one containing calcretes and dinosaur remains, including eggs and hatchlings of the hadrosaurid *Telmatosaurus transsylvanicus* [1,2].

In order to constrain the paleoenvironment in which dinosaurs lived, calcretes and dinosaur eggshells were analyzed for carbon and oxygen isotopic composition. The standard procedure for carbonate analysis at the Graz laboratory includes CO₂ extraction/measurement with Kiel II/Finnigan MAT MS.

The eggshells reveal $\delta^{18}\text{O}$ values between 29.5 and 30.5‰ (SMOW) and $\delta^{13}\text{C}$ between -13 and -14‰ (PDB). The $\delta^{18}\text{O}$ of eggshells are linear related to the $\delta^{18}\text{O}$ of water ingested by the species [3,4]. According to the empirical relationship between eggshell and water composition, eggshells with values of 29-30‰ indicate that the $\delta^{18}\text{O}$ of water from which the species drunk was around -2‰.

The $\delta^{13}\text{C}$ of the eggshell is controlled by the animal's diet but is also strong modified by metabolic fractionation. For example, the $^{13}\text{C}/^{12}\text{C}$ ratio of carbohydrate feeder eggs is 16‰ heavier than the food material [5]. As the measured $\delta^{13}\text{C}$ range between -13 and -14‰, the isotopic composition of the food source was around -30‰. This indicate that the main food source consisted of plants with C3 photosynthetic pathways as trees, most shrubs and herbs. The calculated food signatures correspond to the most depleted part of the C3 plants showing that these did not grow under stressed water conditions [6].

The carbon isotopic composition of calcretes is controlled by the composition of CO₂ in soils which is further controlled by the proportion of C3 and C4 plants [7,8]. Due to $^{13}\text{CO}_2/^{12}\text{CO}_2$ differential degassing in soil and the isotopic fractionation between CO₂ and carbonate, the total enrichment between carbonates and organic matter vary from 16.5 to 13.5‰ (between 0 and 25°C). As the measured $\delta^{13}\text{C}$ values of calcretes, range between -13 and -14‰ they indicate also a C3 source of food with a composition around -30‰.

The oxygen isotopic composition of calcretes are related to temperature and the isotopic composition of soil water which is further related to local meteoric water [9]. The calcret's $\delta^{18}\text{O}$ range between 24 and 25‰. For a temperature around 25°C, calcretes precipitated from water with $\delta^{18}\text{O}$ around -3‰. Due to processes of evapo-transpirations water from which calcretes precipitated are considered to be enriched relative to rain water. The two source of data (eggshells and calcretes) constrain the source of drinking water to a narrow range probably indicating the limited mobility of the species.

REFERENCES

- [1] GRIGORESCU D., AVRAM, E., POP, G., LUPU, M., ANASTASIU, N., Guide to excursions. International Symposium I.G.C.P. Projects 245/262 (1990).
- [2] WEISHAMPEL, D.B., NORMAN, D.B., GRIGORESCU, D., *Telmatosaurus transsylvanicus* from the Late Cretaceous of Romania: the most basal hadrosaurid dinosaur. *Paleontology* **36** (1993) 361-385.
- [3] SARKAR, A., BHATTACHARY, S.K., Stable-isotope analyses of dinosaur eggshells: Paleoenvironmental implications. *Geology* **19** (1991) 1068-1071.
- [4] TANDON, S.K., SOOD, A., ANDREWS, J.E., DENNIS, P.F., Paleoenvironments of the dinosaur-bearing Lameta Beds (Maastrichtian), Narmada Valley, Central India. *Palaeogeogr., Paleoclimat., Paleoecol.* **117** (1995) 153-184.
- [5] SCHAFFNER, F.C., SWART, P.K., Influence of diet and environmental water on the carbon and oxygen isotopic signatures of seabird eggshell carbonate. *Bulletin of Marine Science* **48** (1991) 23-38.
- [6] EHRLINGER, J.R., Carbon isotope ratios and physiological processes in arid land plants. In *Applications of stable isotopic ratios to ecological research*, Rundel, P.W., EHRLINGER, J.R., NAGY, K.A., eds., Springer Verlag (1988) 41-54.
- [7] SMITH, B.N., EPSTEIN, S., Two categories of $^{13}\text{C}/^{12}\text{C}$ ratios for higher plants. *Plant Physiol.* **47** (1971) 380-384.
- [8] CERLING, T.E., QUADE, J., Stable carbon and oxygen isotopes in soil carbonates. In *Climate change in continental isotopic record*, SWART P.K., LOHMANN, K.C., McKENZIE, J., Savin, eds. (1993) 217-232.
- [9] CERLING, T.E., The stable isotopic composition of modern soil carbonate and its relationship to climate. *EPSL* **71** (1984) 229-240.

**^{13}C ANALYSES ON CO_2 IN AIR USING THE MULTIFLOW:
APPLICATION FOR THE MONITORING OF ATMOSPHERIC $^{13}\text{CO}_2$ OVER
HYDRO-ELECTRIC RESERVOIR IN QUEBEC'S BOREAL REGION – CANADA**

G. BILODEAU, C. HILLAIRES-MARCEL, J.-F. HÉLIE
GEOTOP-Université du Québec à Montréal, Montréal, Canada

F. FOUREL
Micromass UK Limited, Manchester, United Kingdom

L. VARFALVY
Hydro-Québec, Montréal, Canada, and
Chaire de recherche en environnement, Hydro-Québec-CRSNG-UQAM, Canada

The Multiflow™ preparation system (Fig. 1) is a headspace sampling device allowing extraction, purification and introduction of a gas sample into a gas-source Isotopic Ratio Mass Spectrometer for isotopic analysis. The original device was designed for ^{13}C measurements on CO_2 from breath tests. It has been adapted here for $^{13}\text{CO}_2$ analysis in atmospheric low pCO_2 -samples. The sample is stored into special 12 cc-vials known as Exetainers™ which are then loaded into a sample tray. An autosampler equipped with a needle is used to pierce the septum of the vial and to admit some helium above atmospheric pressure in the headspace of the vial.

MultiFlow™ schematic

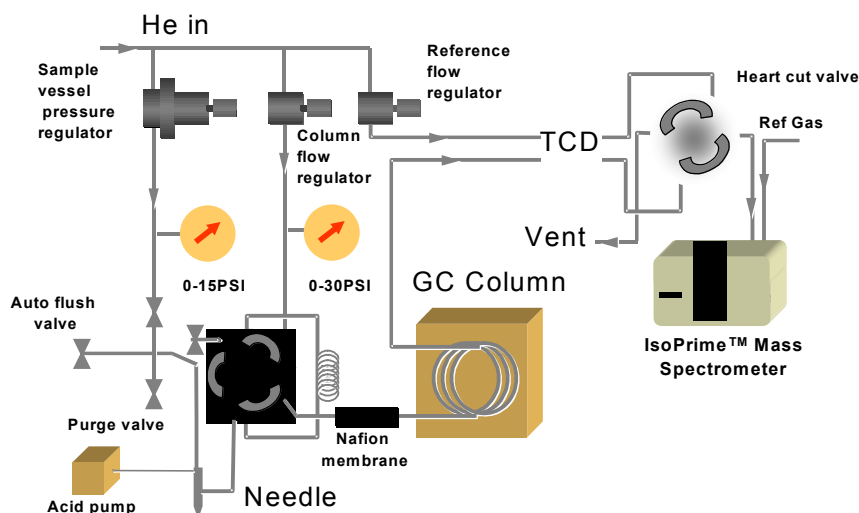


FIG. 1.

A 6-way valve allows then to redirect the excess-helium mixed with the sample gases to flow through a loop. The volume of this loop can be adapted for given types of analyses. The helium carrier and the sampled gases are then directed to a gas chromatography (GC) column that separates the different gas species. A 4-way valve then allow to vent all gases present but the one to analyze. The latter is finally introduced into the source of an isotopic-ratio mass spectrometer. A few adjustments had to be made for the measurement of low- pCO_2 and small

volume atmospheric-air samples for $^{13}\text{C}/^{12}\text{C}$ measurements. A 3 ml-sample loop size is used. The sampling of atmospheric CO_2 is made using pre-evacuated Exetainers™ that are opened and tightly closed on site after sampling. This sample-processing design has been used for a collaborative project with Hydro-Quebec and the GEOTOP research Center (Université du Québec à Montréal). *It aimed at the setting of a rapid, inexpensive and simple technique for ^{13}C measurements in atmospheric- CO_2 over hydro-electric reservoirs of the boreal forest of Quebec.* The scientific rationale was to use stable isotopes for comparative monitoring of CO_2 emissions from reservoirs and natural lakes.

During the summer 2000 sampling campaign, more than 250 samples were collected over the *Robert-Bourassa* hydro-electric reservoir and adjacent lakes (eastern James Bay). Three stations characterized by increasing water depths were selected. Atmospheric gases over each of these stations were sampled during two periods of 24 hours, at approximately 1-hour intervals, 5 cm over above water-surface. The first set of samples was collected following a warm and sunny period of 10 days. The second set of air-samples was collected after a major summer storm event. A most general feature of all CO_2 -samples is their systematic 1 to 3 ‰ depletion in ^{13}C in comparison with the mean atmospheric CO_2 isotopic composition of – 7.8‰. Due to photosynthesis, daily variations in ambient $^{13}\text{CO}_2$, as high as 6 ‰ [1], have been reported in the boreal forest. They are not recorded here over the hydro-electric reservoir. Moreover, a trend towards more steady values is observed from shallow to deep sites, suggesting a decreasing influence of the riverine vegetation on atmospheric $^{13}\text{CO}_2$ contents. Air samples collected at 18 stations of the reservoir before and after the storm indicate enhanced release rates of light $^{13}\text{CO}_2$ by the basin after the storm. It is hypothesized that increased runoff during storm events are responsible for higher supplies of dissolved organic carbon compounds into the reservoir, leading to enhanced bacterial degradation, and thus to higher release rates of isotopically light CO_2 . In the course of this study, we did not observe significant differences of isotopic compositions of the air CO_2 -samples collected above adjacent natural lakes. This leads us to believe that minor differences in CO_2 -fluxes from water bodies are unlikely to be recorded in the ^{13}C - CO_2 signature of the overlying air. However, based on earlier results, they seem clearly recorded in the isotopic composition of dissolved CO_2 .

REFERENCE

- [1] L.B. FLANAGAN, J.E. BROOKS, G.T. VARNEY, S.C. BERRY, J.R. EHLERINGER. Carbon isotope discrimination during photosynthesis and the isotope ratio of respired CO_2 in boreal forest ecosystems. *Global Biogeochemical Cycles* **10** (1996) 629-640.

A RECORD OF ATMOSPHERIC ^{210}Pb FLUX IN SYRIA

M.S. AL-MASRI, H. S. KALIL

Department of Protection and Safety, Atomic Energy Commission of Syria,
Damascus, Syrian Arab Republic

Fallout of ^{210}Pb is of major importance to environmental studies, both for dating lake and marine sediments and as tracer for studying pollutant transport processes [1,2]. Although there is now large data on ^{210}Pb fallout in the world [1,2], but there seems to be no data available on ^{210}Pb flux in the Middle East. In this work, inventories and vertical profiles of ^{210}Pb have been measured in the soils of 51 sites distributed over the Syrian land. Results have shown that ^{210}Pb inventories in the collected cores were relatively uniform with few exceptions where erosion by heavy rain may have occurred in addition to high organic content in some cores. Figure 1 shows some of activity depth profiles of ^{210}Pb ; all ^{210}Pb fallout component was estimated by subtracting the supported component from the measured total ^{210}Pb activity. ^{210}Pb inventories were determined using the method described by Smith [3] and found to vary between 478 Bq.m^{-2} and 13080 Bq m^{-2} , which are relatively high. In addition, ^{210}Pb flux ranged from $15 \text{ Bq m}^{-2}.\text{y}^{-1}$ and $407 \text{ Bq m}^{-2} \text{y}^{-1}$ with a mean value of $128 \text{ Bq m}^{-2} \text{y}^{-1}$ Table 1 which is within the worldwide levels [2] table 2. ^{210}Pb flux was found to depend mainly on the geography of the site and radon air concentration. ^{210}Pb flux was higher in valleys and around the lakes while low fluxes being observed in mountains and flat lands. The highest value observed was in Hama, situated in the middle of Syria, where Al-Ghab faults and high radon concentrations being the main reason for these high levels. Furthermore, high levels of ^{210}Pb were also observed in those cores collected near Palmyra, the phosphate mine sites; high radon concentrations are predominating.

There is no linear relationship found between ^{210}Pb flux and annual rain fall, where high values were observed for low rain fall and vice versa, Table 1. The only two factors affecting ^{210}Pb flux were the geological and climate conditions (especially wind) and in order to obtain a good value for ^{210}Pb flux using the ^{210}Pb inventory in soil, an appropriate number of cores should be collected. In addition, The data obtained in this study can be used as a base value for the Middle East region.

REFERENCES

- [1] EL-DAOUSHY, F., The ^{210}Pb Global Cycle: Dating and Tracing Application. A Paper presented at the first international summer school on low level measurements and their applications to environment radioactivity, La Rabida, Spain, September 27-10, 10/11/1987 (1987).
- [2] IVANOVICH, M., HARMON, R.S., Uranium Series Dis-Equilibrium, Applications to Environmental problems, Clarendon Press, Oxford (1992).
- [3] SMITH, J.T., APPLEBY, P.G., HILTON, J., RICHARDSON, N., Inventories and Fluxes of ^{210}Pb , ^{137}Cs and ^{241}Am Determined from the Soils of Three Small Catchments in Cumbria, UK. J. Environment Radioactivity **37**(2) (1997) 127-142.

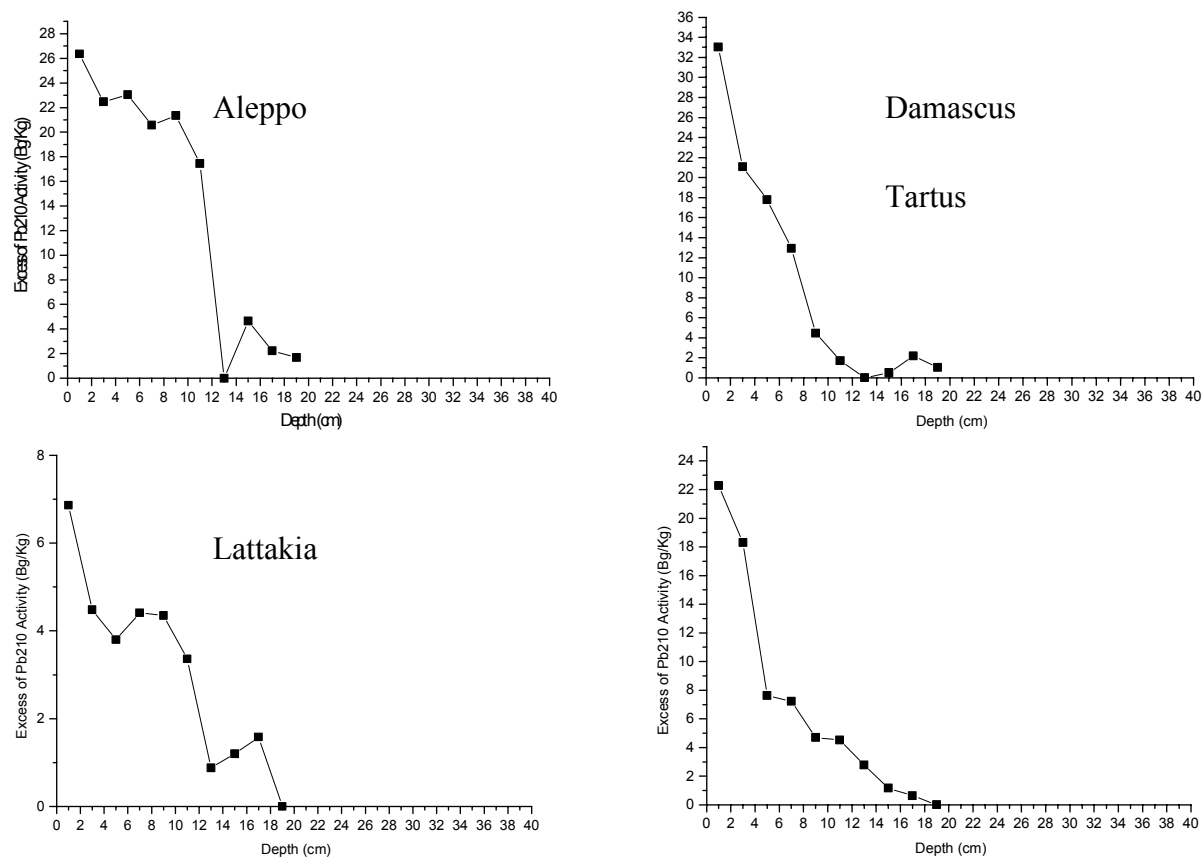


FIG. 1. Activity-depth profiles of ^{210}Pb in some cores.

TABLE I. ^{210}Pb flux values in some Syrian sites.

Site	^{210}Pb ($\text{Bq m}^{-2} \text{y}^{-1}$)	Annual rain fall (mm)
Aleppo	190 ± 85	331
Tartous	118 ± 56	848
Darra	105 ± 38	274
Hamma	171 ± 146	338
Damascus	149 ± 61	212
Palymera	165 ± 99	130
Der Ezzor	64 ± 44	161

TABLE II. ^{210}Pb fluxes in different places in the World.

Site	^{210}Pb ($\text{Bq m}^{-2} \text{y}^{-1}$)
Syria	128
West Europe	99
India	145
Japan	364
New Zealand	51
North America	38
UK	162

SIMPLE ENVIRONMENTAL MODELS FOR TRANSPORT OF NATURAL RADIO-ACTIVITY IN AQUATIC SYSTEMS

A.A. EL-SAYED

Analytical Chem. Dep. Hot Labs, Atomic Energy Authority, Inshas, Egypt

A large number of models exist for describing the dispersal and transportation of radioactivity in aquatic system. The main feature of general model types and choice are base on distribution of naturally occurring trace elements, uranium, thorium and potassium between solid and water. These general model are generic one and requiring few sites specific details.

The basic results of this study are primarily presented in Fig.1 showing distribution of these elements U, Th and K along the chosen sites of surface water studied. Meanwhile, a simplified model of the transportation processes which makes use of the distribution factor, K_d . The results indicated that sediments scavenging the radioactive elements are influenced not only by particulate sedimentation rates but also mainly by distribution of such radionuclides between solid and aqueous phases.

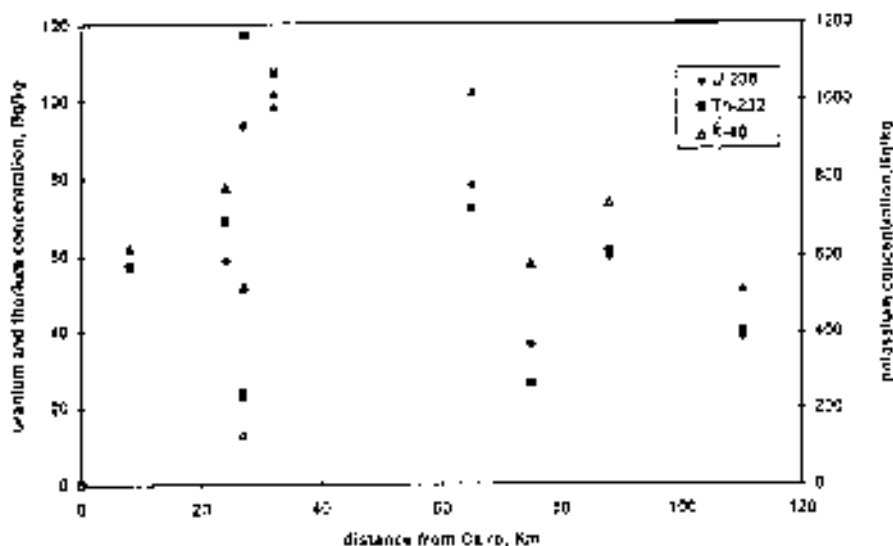


FIG. 1. Distribution of natural radionuclides in sediments collected from different areas along Ismailia canal.

GEOCHEMICAL AND ISOTOPIC CHARACTERIZATION OF GROUNDWATER RESOURCES IN EL HICHA REGION, GABES, SOUTHERN TUNISIA

M.F. BEN HAMOUDA, H. BEN KRAIEM, A. MAHJOUB
Centre National des Sciences et Technologies Nucléaires, Tunisia

B. LABIDI, R.GHOUDI
CRDA – Gabès – Ministère de l'Agriculture, Tunisia

H. HAMROUNI
Direction des Sols – Ministère de l'Agriculture, Tunisia

H. NASR
Institut National de Génie Rural Eaux et Forêts, Tunisia

K. ZOUARI
Ecole Nationale d'Ingénieurs de Sfax, Tunisia

K. FRÖHLICH
International Atomic Energy Agency, Vienna

M.I. SAJJAD
PINSTECH, Islamabad, Pakistan

E. GARCIA-AGUDO
Sao Paulo, Brazil

The groundwater study area is located in the southern part of Tunisia at some kilometers from the Mediterranean Sea, about 35 km north of the town Gabes. It extends over 300 km² and is bounded by the Gulf of Gabes in the East, El Hamma in the West and Skhira in the North. This region is characterized by a semi-arid climate with an average annual rainfall of about 180 mm and a potential evaporation of 2130 mm per year.

The groundwater resources of the region are represented by four hydrogeological units: the Continental Intercalaire, the Sfax Aquifer, the Jeffara Aquifer (north of Gabès) and the shallow aquifer of El Hicha. The dug wells and boreholes used for groundwater abstraction in this region reach depths between a few meters and about 170m. The upper zone of 50m depths is formed by sandy clay and gypsum, and the lower zone of 50 to 70m depths consists of sandy layers.

The salinity measured in groundwater samples from this area is rather high; the values range between 5 and 7g/l. Since the water will be used to grow salt-tolerant plants, it is important to know the origin of the groundwater (to assess its availability) and the source(s) of its salinity. To this end, groundwater samples for isotope and chemical analysis were taken from 6 dug wells, 6 boreholes (one of them is an artesian well), a spring and a drainage canal. Each site was sampled in March, June, July, September and December 1999. During these sampling campaigns, in-situ measurements of temperature and electrolytic conductivity were carried out.

The hydrochemical analysis of the groundwater samples indicates the presence of Cl^- , SO_4^{2-} , Ca^{2+} , Mg^{2+} . The Piper diagram shows the dominance of sodium, chloride and potassium. Observed slight changes of the chemical composition of the water after a rainy period have been attributed to rainwater infiltration into the groundwater.

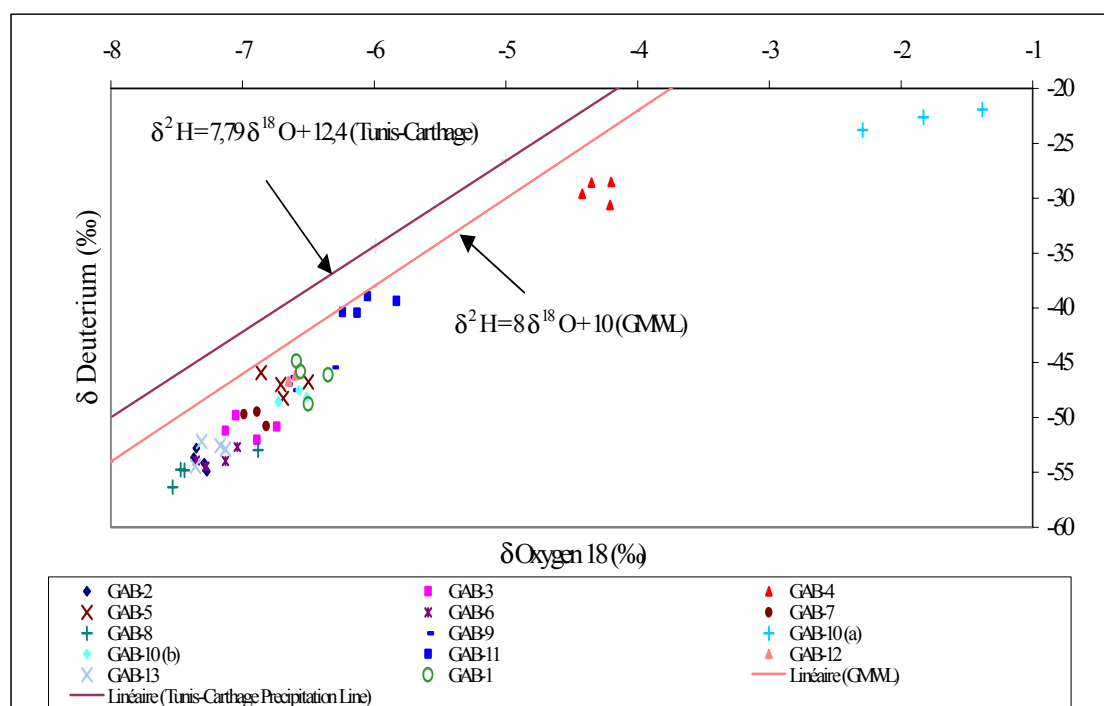


FIG.1. $\delta^{18}\text{O}$ - $\delta^2\text{H}$ Diagram of the groundwater samples from the study area.

The $\delta^{18}\text{O}$ values of the individual water samples vary from -7.53 ‰ to -4.2 ‰ while the $\delta^2\text{H}$ values range from -56.4 ‰ to -28.52 ‰ (Fig. 1). The deuterium excess of the majority of the samples is remarkably constant; the individual values cluster round 5 ‰, the deuterium excess value characteristic for palaeo-groundwater in northern Africa [1]. This finding is also substantiated by the ^{14}C values so far available for some of the collected water samples. The apparent ^{14}C age ranges from about 9000 to 14 000 years B.P. A slightly higher deuterium excess was found for groundwater collected from the dug well GAB-11. The increase of both the deuterium excess and the oxygen-18 value points to an admixture of some rainwater with present-day deuterium excess of about 10 ‰. A small contribution of rainwater is also suggested by the tritium values for this well, which average about 0.4 TU. The water samples taken from dug well GAB-4 appear to contain a higher fraction of recent (rain) water (Fig. 1), as also suggested by the relatively high tritium values (around 1.2 TU). Water from the dug well GAB-10 (a) seems to represent rather young water, because its tritium content is about 1.6 TU. Furthermore, evaporation effects appear to mask the original stable isotope composition, as indicated by the very low deuterium excess and high oxygen-18 values (Fig. 1). Therefore, this water is excluded from the following considerations.

The plot of the average values of electrical conductivity (EC) versus the respective average oxygen-18 values clearly indicates two different types of groundwater: type 1 with an EC around 4.5 mS/cm and $\delta^{18}\text{O}$ between -7.5 and -7 ‰; type 2 with EC around 7.5 mS/cm and $\delta^{18}\text{O}$ around -6.5 ‰. Examining the spatial distribution of the EC and oxygen-18 values, it can clearly be seen that the groundwater south of $37^\circ 90'$ (south of GAB-3) belongs to type 1 while north of this region the groundwater is of type 2.

Taking into account results from earlier isotope investigations in the South of Tunisia [2] – [4], the above findings can be interpreted as follows:

1. The groundwater of type 1 and 2 represents palaeo-groundwater. Type 1 preferentially occurs in the southern part of the study area and can be attributed to the Continental Intercalaire (and/or the Jeffara aquifer), while type 2 seems to belong to the Sfax aquifer.
2. Thus, the salinity of the groundwater is mainly the result of the chemical evolution of the groundwater (water-rock interaction) during the flow through the large confined aquifers. The contribution to the salinity by local infiltration of recent rainfall through the saline soil appears to be comparatively small. Such a contribution is probably manifested in the observed spread of the measured values around the primary salinity and isotopic composition of the palaeo-groundwater (Fig. 2).

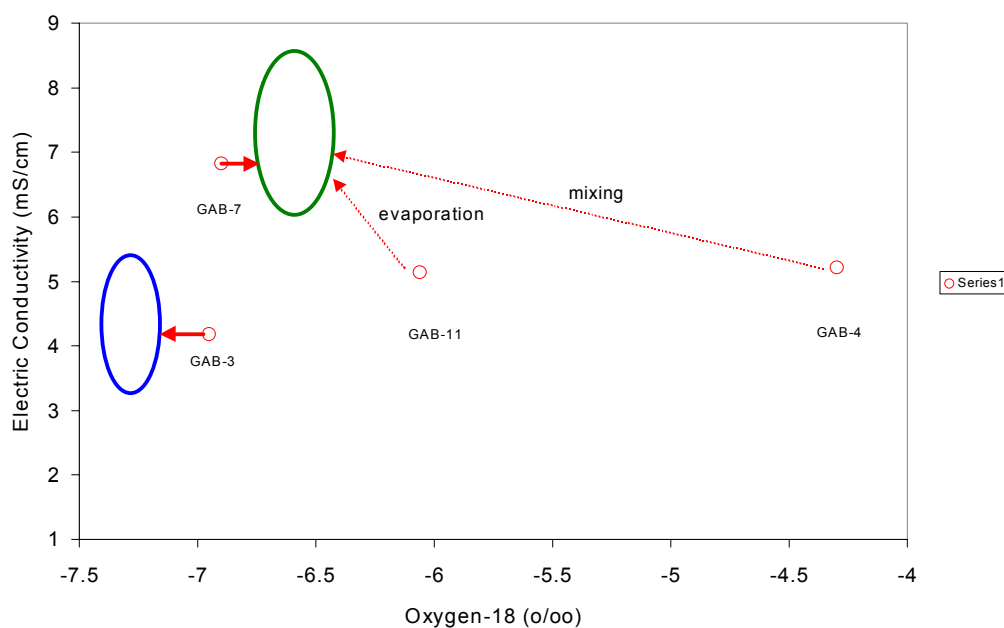


FIG. 2. Plot of the average electric conductivity (EC) and oxygen-18 values of the sampling sites.

REFERENCES

- [1] SONNTAG, C., KLITZSCH, E., LÖHNERT, E.P., EL-SHAZLY, E.M., MÜNNICH, K.O., JUNGHANS, Ch., THORWEIHE, U., WEISTROFFER, K., SWAILEM, F.M., Palaeoclimatic information from deuterium and oxygen-18 in carbon-14 dated North Saharian groundwaters – Groundwater formation in the past. In: Isotope Hydrology 1978, Vol.II, pp. 569–581. Proceedings of a Symposium, held in Neuherberg from 19-23 June 1978. IAEA, Vienna (1979).
- [2] FONTES, J.C., COQUE, R., DEVER, L., FILLY, A., MAMOU, A., Palaeo-hydrologie isotopique de l’oued el Akarit (sud Tunisie) au pleistocène supérieur et à l’holocène, Palaeogeogr., Palaeoclimatol., Palaeoecol. **43** (1983) 41–62.
- [3] UNESCO., Etude des ressources en eau du Sahara Septentrional, Algérie, Tunisie, Rapport sur les résultats du projet conclusions et recommandations (1972).
- [4] ZOUARI K., Etude isotopique et géochimique de l’infiltration naturelle en zone non saturée sous climat semi-aride (sud Tunisie) Thèse troisième cycle, Orsay (1983) 133p.

STUDY OF SOIL EROSION DYNAMICS ON THE ARABLE LANDS OF LUBLIN UPLAND USING ISOTOPE TECHNIQUES (^{137}Cs)

W. ZGŁOBICKI

Department of Geology, UMCS, Lublin, Poland

M. RESZKA

Department of Radiochemistry and Colloid Chemistry, Maria Curie Skłodowska University, Lublin, Poland

One of the consequences of agricultural activity are changes of significant element of the environment, that is terrain relief. Since sixties the radioactive isotope of cesium, ^{137}Cs , is applied in the examination of the dynamics of the erosion processes.

This method is based on the idea that the circulation of this isotope in the environment accompanies to physical transport of soil. Studies proved that cesium is firmly bond by adsorption complex of the soil. Chemical and biochemical processes have limited influence on the transportation of the cesium. By the examination of the horizontal changes of the total cesium activity one can determine a type and intensity of the processes responsible for its migration and thus the migration of the soil particles.

Soil erosion consists on accelerated transportation of soil material from slopes, as results of flowing water, winds and direct human activity. Beside degradation of the soil resources, the erosion also influences accelerated circulation of biogenic substances in the landscape (originated from washed out fertilizers). This process has great influence on the eutrophication of the environment. Extremely high flows, caused by heavy rains, may destroy communication and settlement infrastructures. For this reason learning of the dynamics of the discussed processes and the parameters which influence them is of the great practical meaning.

Our studies were performed in several small catchments of dry valleys located at Northwestern part of Lublin Upland (Southeast Poland). These basins, characterized by varied shape and small areas (20-100 ha), were intensely cultivable. On each area from 20 to 40 sampling points for soil core collection were set. The cores were picked out down to 50 cm in 10 cm layers. These points were localized in various morphology, land use and tillage practices. In soil samples the concentration of ^{137}Cs was measured. The concentration of cesium in the surface layer of the soil ranged from 2.4 to 155.0 Bq/kg although most samples revealed smaller concentrations from 11 to 30 Bq/kg. For each studied profile the total amount of ^{137}Cs was calculated in Bq/m².

The horizontal differentiation of the total activity of ^{137}Cs in a basin was the base for the valuation of the dynamics of the slope processes in examined points and then in morphodynamic zones of the basin. It was assumed that cesium delivery with dry and wet fallout was uniform in the small area of the examined basins. The level of radioactivity (reference level) was estimated in samples taken from mark points such as grasslands interflaves. In such places no erosion or accumulation processes happen. When in examined point the concentration of cesium was lower than in reference point it proved erosion (moving out the soil). The accumulation of the soil was manifested by higher activity of the ^{137}Cs .

A strong connection was noticed between total activity of ^{137}Cs and morphology, coverage and applied cultivation. The lowest activity was observed on the ploughed slopes, especially

when furrows comes along the slope and the slopes were steep. The highest concentration of cesium was at the valley bottoms, regardless the land use.

Presented data confirm that the most intense denudation processes are accompanied with cultivation activity (Table I). The dynamics of slope processes in these areas is connected with the direction of the cultivation, inclination of the slope and micro profile. For the rest of the studied areas the erosion of soils is less intense. Such process was not observed on forests - even though with steep slopes. It was also possible to establish the quantity of the soil which is moved out each year on the interfluvies, valley sides etc. (Table II).

Table I. Relationship between total activity of ^{137}Cs and relief and land use (mean values)

Forms of the relief	Land use	% fallout
interfluvies	arable lands	72
	others	100
slopes of the interfluvies (3-6°)	arable lands	69
valley sides (6-10°)	arable lands	67
	pastures	110
	forests	110
steep valley sides (>10°)	arable lands	58
	pastures	91
	forests	120
bottom of the dry valley	arable lands	148
bottom of the basin-shaped valley	arable lands	105

Table II. Intensity of the denudation processes at cultivated areas (loess areas of Lublin Upland, SE Poland; mean values)

forms of the relief	intensity of the process [t/ha?y]
interfluvies	– 30÷100
slopes of the interfluvies (3-6°)	– 50÷80
valley sides (6-10°)	– 60÷110
steep valley slopes (>10°)	– 100
dry valley bottoms	+ 87

“–” loss of material, “+” delivery of material

Obtained values concerning horizontal changes of the total concentration of the cesium in examined areas demonstrate also the following regularity for denudation processes on loess, cultivated areas.

- a) slope processes demonstrate significant diversity of the direction and the intensity - even on the single slope or its parts.

- b) flat interfluvies also undergo the washing out processes.
- c) in basins the transverse direction prevails: side → bottom of the valley
- d) agriculture erosion is the main factor influencing the soil transportation.

The method for the studies of slope processes with application of ^{137}Cs isotope may give many data difficult to obtain in different way. Despite some limitations and careful interpretation of obtained results it seems to be truthful and allows learn more about the contemporary changes of relief of cultivated areas.

SOME RESULTS ON THE ISOTOPE STUDIES OF WATER EXCHANGE IN BOREAL RAISED BOGS

A.A. SIRIN

Institute of Forest Science, Russian Academy of Sciences, Moscow, Russian Federation

L.S. VLASOVA

Water Problems Institute, Russian Academy of Sciences, Moscow, Russian Federation

V.A. POLYAKOV, A.E. TROFIKOVA

Research Institute of Hydrogeology and Engineering Geology, Ministry of Natural Resources, Moscow, Russian Federation

Raised bogs are rather common and one of the most exciting mire types of the boreal zone. They receive water and nutrients from precipitation and pore water stored in their domes (up to 10 m in height) is spaced above levels of regional ground water or streams draining them. Peatland hydrologists have long assumed (Fig. 1a) that fluid flow occurs mainly in a peat layer near to the surface and water transport is negligible in deeper layers. The «acrotelm/catotelm» paradigm on active and inert horizons for the peat above and below the lowest water level is still widely spread in peatland hydrology. However, recent studies have shown that deep water movement is much more dynamic in raised bogs than was previously thought. Based on geochemical studies and numerical simulations even temporal reverse of the vertical direction of water fluid flow through the peat as connected to climate fluctuations was assumed (Fig. 1b). Relying on isotope studies [1] we consider only the mounded strata of the raised bogs to have relatively active water exchange (Fig. 1c).

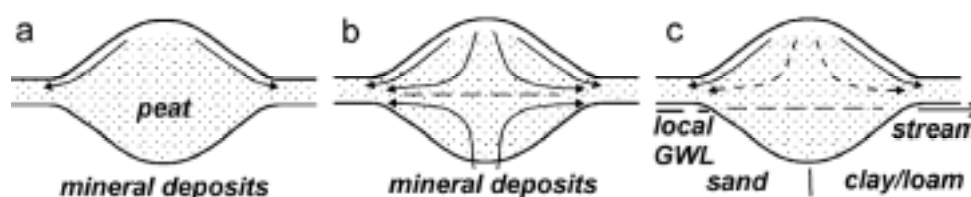


FIG.1. Main hypotheses on water movement in raised bog.

The study included two raised bogs, representing different local hydrological conditions (underlain by outwash sands and moraine clay) at the Zapadnaya Dvina Peatland Field Station of the Forest Research Institute located 400 km west of Moscow (56 N, 32 E). Peatlands, among which raised bogs dominate, constitute >30% of the area, and maximum peat thickness exceeds 7 m.

For water sampling nested piezometers (2.5" PVC pipes) with bottoms closed with wooden plugs and each perforated at the desired depth were used. Before sampling piezometers were pre-pumped and allowed to refill. Started from 1990 pore water sampling was supported by collection of monthly integrated precipitation probes. ^3H was analysed after electrolytic enrichment at Water Problems Institute, ^{18}O and ^2H at Research Institute of Hydrogeology and Engineering Geology. To evaluate water residence time in peat strata specially determined mathematical model which include the equations of water mass and tritium balance, imbedded in a conceptual framework of water dynamics within a raised bog peat body, have been developed and tested [1]. The results from isotope studies were additionally supported by geochemical (pH, Eh, electrical conductivity) data and temperature and dissolved CO_2 and CH_4 monitoring within vertical profiles of the studied raised bogs [2].

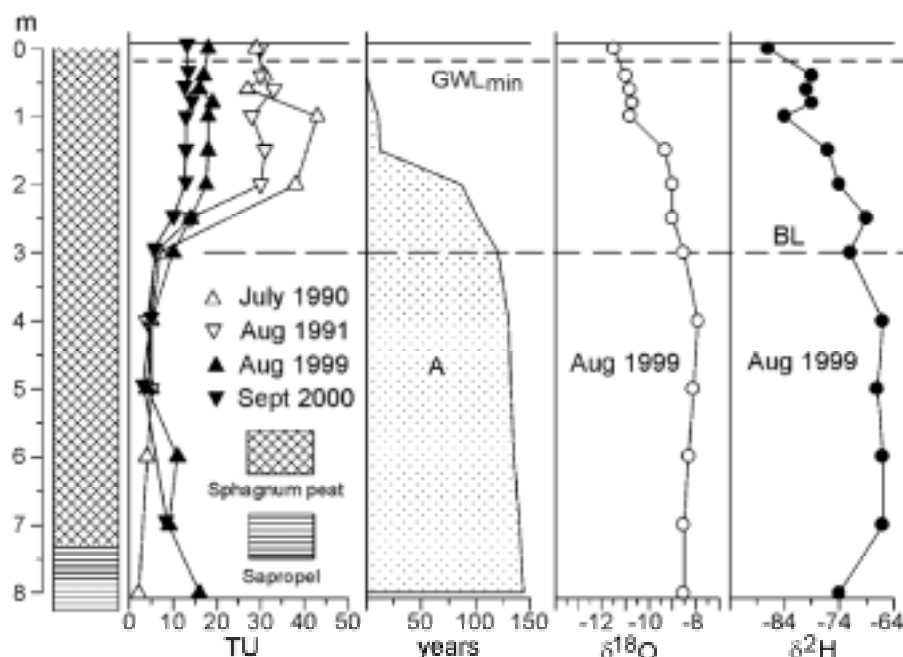


FIG. 2. Isotope data profiles for Petrilovo raised bog underlain by moraine clay at the depth of 10 m. A – peat pore water residence time; BL – base line of the raised bog dome; GWL_{min} – minimum level of the raised bog surface waters.

The water residence time is a useful indicator of water source and flux rate. According to our results the water, in the upper 0,5–0,7 m of both studied raised bogs, was several months to several years old. Data for the raised bog underlain by moraine clay is shown on Fig. 2. The water residence time less then 20 years was typical for 1,5 m stratum, and isotope data indicated existence of water flux within the whole domed strata of the raised bogs. Temperature and dissolved C-gases data also support this conclusion: seasonal temperature shifts in peat pore waters occur up to the bottom of the dome; C-gases concentrations increased with depth, down to the mound base line, and then remained fairly constant [2]. The water residence time in the lower horizons below the base line of the raised bog dome was estimated by 100-150 years [1], which indicates that diffusion processes prevail here.

Having similar 3H and temperature distribution and similar values of water residence time estimates, raised bogs lying on outwash sands and moraine clay had different patterns of ^{18}O and 2H vertical distribution within their vertical profiles. Raised bog on sands had more even distribution of $\delta^{18}O$ (from $-11,3$ to $-10,3$) and δ^2H (from -89 to -71) than the bog on moraine clay (Fig. 2). The depletion of ^{18}O and 2H to the surface of the raised bog on clay indicates larger contribution of evapotranspiration in the output part of its water balance. For the bog on sands much water is lost by lateral flow because of its better draining conditions and smaller size. It is less then 1,5 km in diameter in comparison to more then 3 km of the raised bog on clay.

The results for 1999-2000 year period were obtained within research project No. 10545 supported by IAEA.

REFERENCES

- [1] SIRIN A.A., SHUMOV D.B., VLASOVA L.S. Investigation of bog water circulation using ^3H analysis data. *Water Resources* **24** (1997) 625-633.
- [2] SIRIN A.A., NILSSON M., SHUMOV D.B., GRANBERG G., KOVALEV A.G. Seasonal changes in the distribution of dissolved methane in the vertical profile of mires of the Zapadnaya Dvina Lowland. *Doklady Biological Sciences* **361** (1998) 348-351.

DEVELOPING INSIGHT INTO THE ISOTOPE-CLIMATE OF CANADA AND THE ISOTOPIC EXPRESSION OF THE 1997-98 ENSO

S.J. BIRKS, T.W.D. EDWARDS, J.J. GIBSON*

Department of Earth Sciences, University of Waterloo,
Waterloo, Ontario, Canada

The isotopic composition of precipitation is an integrated climate field reflecting temperature, amount of precipitation, air-mass source and history. Studies are underway to test the sensitivity of the isotope-climate signal in precipitation to changes in these parameters utilizing perturbations in local climate arising from the El Niño/Southern Oscillation (ENSO). Canadian data from IAEA/WMO Global Network for Isotopes in Precipitation (GNIP) and more recent data from the Canadian Network for Isotopes in Precipitation (CNIP) are being combined in a spatial and temporal database to create an isotope overlay compatible with pressure and flux field data from the NCAR/CDAS Re-analysis Project. Comparisons of the isotopic fields ($\delta^{18}\text{O}$, $\delta^2\text{H}$ and d -excess) with climate fields illustrate the complexity and dynamic nature of the isotope-climate not evident in time-series of data from individual stations.

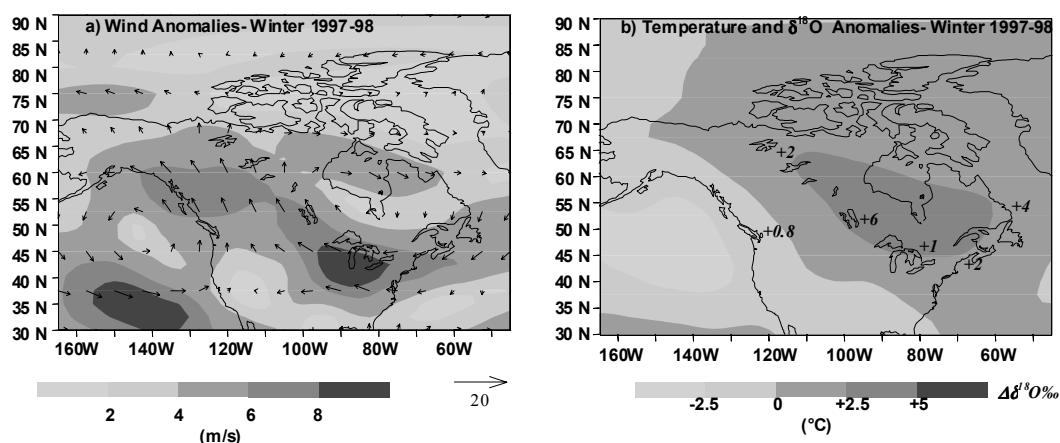


FIG. 1. a) 500 mb wind anomalies for the winter following the 1997 El Niño, obtained by subtracting the climatological (1979-95) seasonal mean streamlines and isotachs (wind speed) from seasonally averaged streamlines and isotachs for Dec 1997-Feb 1998. Vectors show the direction departures and shading shows the magnitude of the wind speed anomaly. b) 500 mb temperature anomalies for the same time period. Differences between the 1997 winter $\delta^{18}\text{O}$ and the weighted mean winter $\delta^{18}\text{O}$ for CNIP station data are shown in italics.

ENSO events are a primary cause of interannual climate variability, affecting conditions not only near their source in the equatorial Pacific Ocean, but also at higher latitudes. In extratropical areas the strength, location and timing of climate variations are less predictable since they are the result of oceanic and atmospheric teleconnections. Intriguing results have been obtained from preliminary analysis of pressure and flux field data for 1997-98 and the newly created CNIP isotope overlay. The strongest climate anomalies were found during the winter following the 1997 El Niño event (Fig. 1), consistent with a strengthening of the Pacific North American pattern expected during this period [1,2,3].

* Also: Isotope Hydrology Section, International Atomic Energy Agency, Vienna.

The temperature anomalies for the 1997-98 ENSO event are similar to those observed in previous events, with air temperatures in the winter following El Niño being warmer over most of Canada and the greatest warming centered over Manitoba and western Ontario [1, 4]. The distribution of isotopic anomalies, on the other hand, is not explained entirely by the temperature anomalies (Fig. 1b), illustrating the potential for decoupling of the isotopic signature of precipitation from temperature when changes in air-mass circulation occur [4, 5].

REFERENCES

- [1] SHABBAR, A., KHANDEKAR, M., "The impact of El Niño-Southern Oscillation on the temperature field over Canada", *Atmosphere-Ocean* **34** (1996) 401-416.
- [2] SHABBAR, A., BONSALE, B., KHANDEKAR, M., "Canadian precipitation patterns associated with the Southern Oscillation", *Journal of Climate* **10** (1997) 3016-3027.
- [3] BONSALE, B.R., LAWFORD, R.G., "Teleconnections between El Niño and La Niña events and summer extended dry spells on the Canadian Prairies", *International Journal of Climatology* **19** (1999) 1445-1458.
- [4] ROPELEWSKI, C.F., HALPERT, M.S., "North American Precipitation and Temperature Patterns Associated with the El Niño/Southern Oscillation", *Monthly Weather Review* **15** (1986) 2352-2362.
- [5] COLE, J.E., RIND, D., FAIRBANKS, R.G., "Isotopic response to interannual climate variability simulated by an atmospheric general circulation model", *Quaternary Science Reviews* **12** (1993) 387-406.
- [6] EDWARDS, T.W.D., WOLFE, B.B., MACDONALD, G.M., "Influence of changing atmospheric circulation on precipitation $\delta^{18}\text{O}$ -temperature relations in Canada during the Holocene", *Quaternary Research* **46** (1996) 211-218.

STABLE ISOTOPE CHARACTERIZATION OF PAN-DERIVED AND DIRECTLY SAMPLED ATMOSPHERIC WATER VAPOUR

R. MARIC, N.A. St. AMOUR, J.J. GIBSON*, T.W.D. EDWARDS

Department of Earth Sciences, University of Waterloo, Waterloo, Ontario, Canada

Isotopic characterization of atmospheric water vapour, δ_A , and its temporal variability are important prerequisites for quantifying water balance of surface reservoirs and partitioning of evaporation and transpiration fluxes using isotope techniques. Here we present results from a detailed comparison of several methods for determining δ_A in field situations, (i) by back-calculation from isotopic and micrometeorological monitoring of a steady-state terminal reservoir (standard Class-A evaporation pan) using boundary-layer mass transfer models [1], (ii) through direct (cryogenic) sampling of ambient atmospheric moisture, and (iii) using the precipitation-equilibrium approximation (i.e., $\delta_A = \delta_p - \varepsilon^*$). The three methods provide differing, but complementary temporal views: Class-A pans can be operated to provide time-averaged information suitable for monitoring of the water balance of a small lake over time periods of days to weeks, for example, whereas direct sampled profiles of atmospheric moisture can be used to develop snapshots of transient isotopic gradients in the boundary layer over lakes or land surfaces at time-scales of minutes to hours. Precipitation equilibrium provides an additional independent method for characterizing atmospheric moisture, though necessarily limited to periods of actual rainfall. As shown below (Fig. 1) data from an experiment run at the University of Waterloo in summer 2000 reveals remarkably consistent agreement between daily pan-derived estimates of δ_A and equivalent "equilibrium" vapour, demonstrating the utility of pan monitoring to span the intervals between precipitation events.

Also evident from the time-series in Fig. 1 is a step-shift in meteorological conditions, with days 145-160 characterized on average by somewhat drier and cooler conditions than the remaining part of the record (days 161-195). This synoptic shift is clearly reflected by a reduction in evaporation rate (not shown), as well as in the respective rates of heavy-isotope enrichment in the pan water and in the pan-derived atmospheric $\delta^{18}\text{O}$ and $\delta^2\text{H}$ values.

Consideration of these isotopic data in $\delta^{18}\text{O}$ - $\delta^2\text{H}$ space (Fig. 2) reveals additional distinction between the two periods. Thus, the day 145-160 period is characterized by a shallower evaporative-enrichment slope than day 161-195 (4.5 versus 5.1), and by more isotopically depleted atmospheric vapour (-21.2‰ versus -16.0‰ and -155‰ versus -123‰ for $\delta^{18}\text{O}$ and $\delta^2\text{H}$, respectively) having a substantially higher *d*-excess (14.3 versus 4.8‰). The differences in $\delta^{18}\text{O}$ and $\delta^2\text{H}$ values, which are larger than expected for typical temperature-related effects, and the large shift in *d*-excess are clear isotopic expressions of the differing synoptic conditions over the two time periods.

We have also made preliminary efforts to incorporate direct sampling of atmospheric moisture in company with evaporation pans at field sites. Initial experiments using cryogenic trapping at a nearby site successfully captured the strongly differing isotopic labelling of atmospheric vapour revealed by the other two methods (see Fig. 2), though with systematic offsets, perhaps related to mixing of locally generated vapour or to isotopic fractionation of the water vapour during collection, similar to isotopic effects predicted during snow formation [2]. On-going experiments will also evaluate non-cryogenic methods of vapour recovery for planned flux-gradient partitioning studies.

* Also: Isotope Hydrology Section, International Atomic Energy Agency, Vienna.

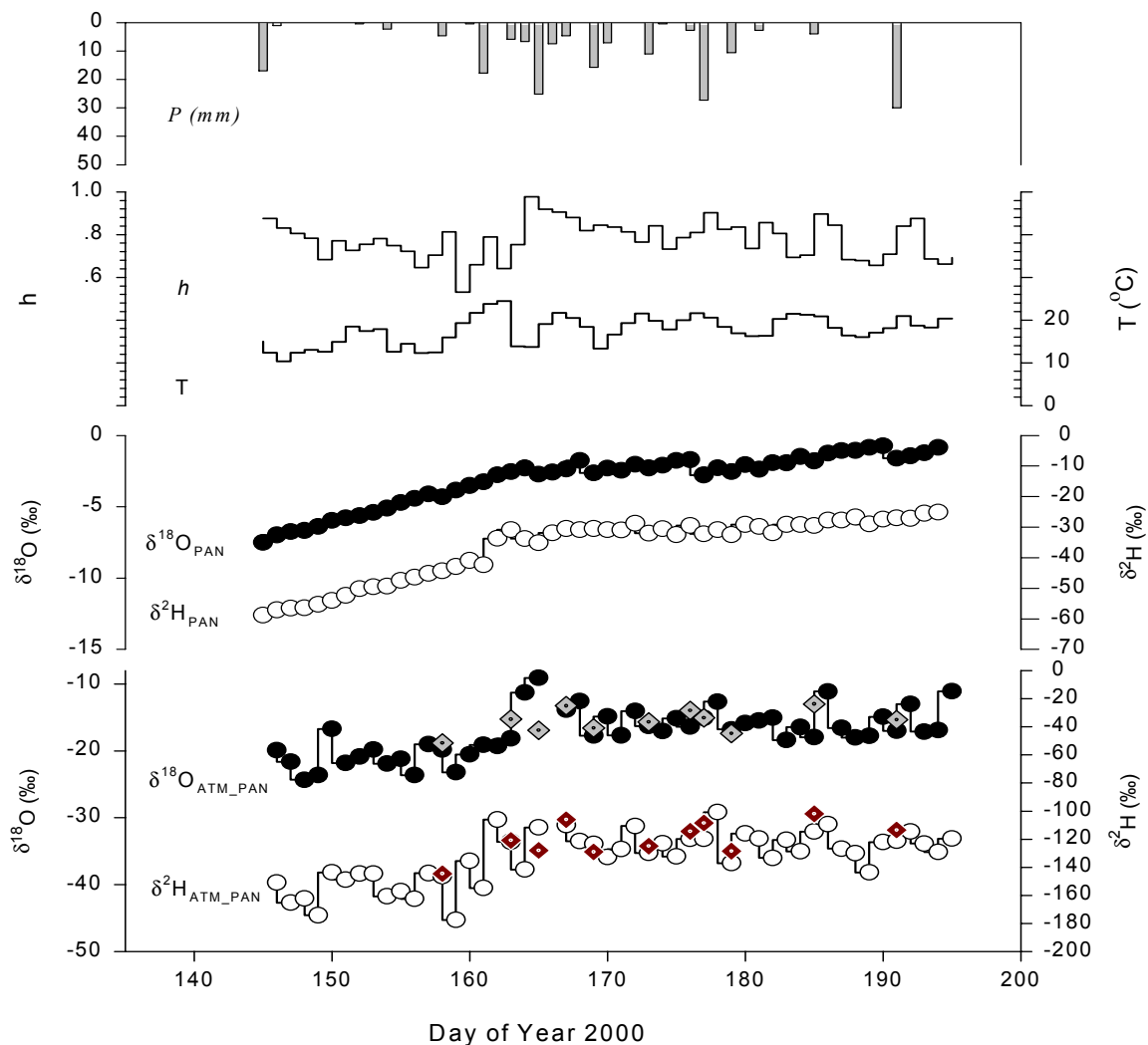


FIG. 1. Daily time-series of precipitation (P), relative humidity (h), temperature (T), $\delta^{18}\text{O}$ and $\delta^2\text{H}$ of pan water, and pan-derived $\delta^{18}\text{O}$ and $\delta^2\text{H}$ of atmospheric vapour during Day 145 to 195 (25 May-14 July) 2000, at the University of Waterloo weather station. The diamonds are $\delta^{18}\text{O}$ and $\delta^2\text{H}$ values for atmospheric vapour in equilibrium with individual precipitation events, revealing good agreement with daily pan-derived estimates.

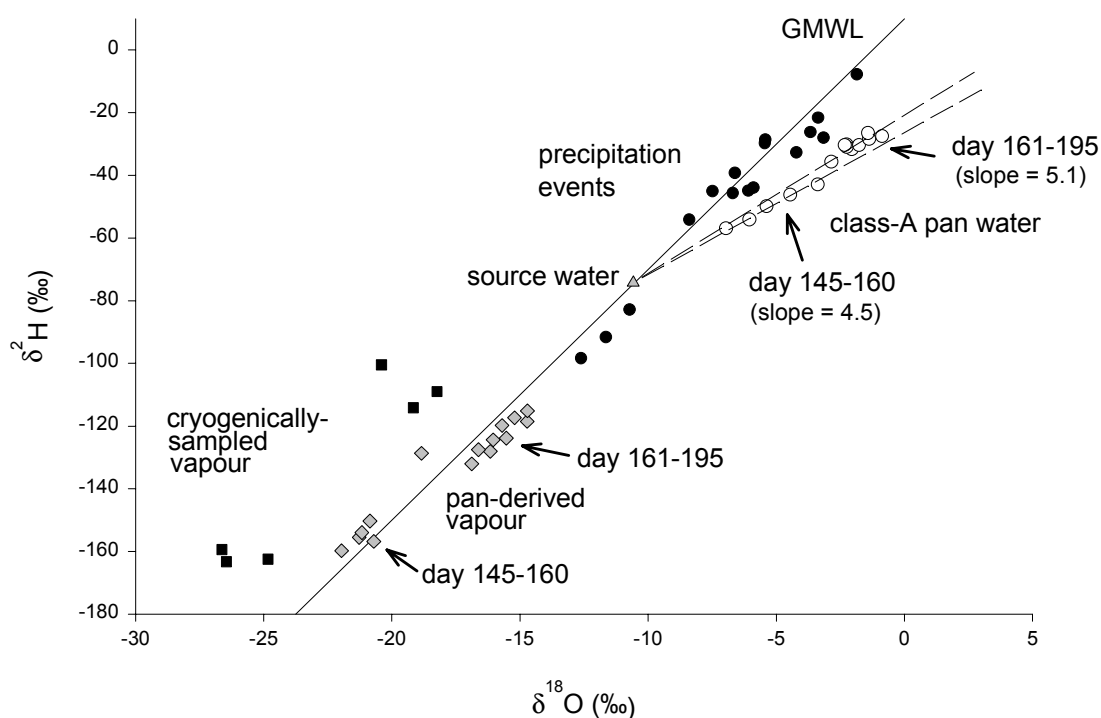


FIG. 2. $\delta^{18}\text{O}$ - $\delta^2\text{H}$ crossplot showing measured and derived isotopic data. For plotting purposes the pan water and pan-derived atmospheric moisture data are expressed as three-day averages, whereas other data points represent individual samples. The Global Meteoric Water Line ($\delta^2\text{H} = 8\delta^{18}\text{O} + 10$) is shown for reference.

REFERENCES

- [1] GIBSON, J.J., EDWARDS, T.W.D., PROWSE, T.D., "Pan-derived isotopic composition of atmospheric water vapour and its variability in Northern Canada", *Journal of Hydrology* **217** (1999) 55-74.
- [2] JOUZEL, J., MERLIVAT, L., "Deuterium and oxygen 18 in precipitation: modelling of the isotopic effect during snow formation", *Journal of Geophysical Research* **89** (1984) 11,749-11,757.

THE QUESTION OF THE RENEWAL OF GROUNDWATER RESOURCES IN SOUTHWESTERN BURKINA FASO

D. DAKOURÉ, G. de MARSILY
Université Paris VI, Paris, France

M. DRAY
CRG, Thonon, France

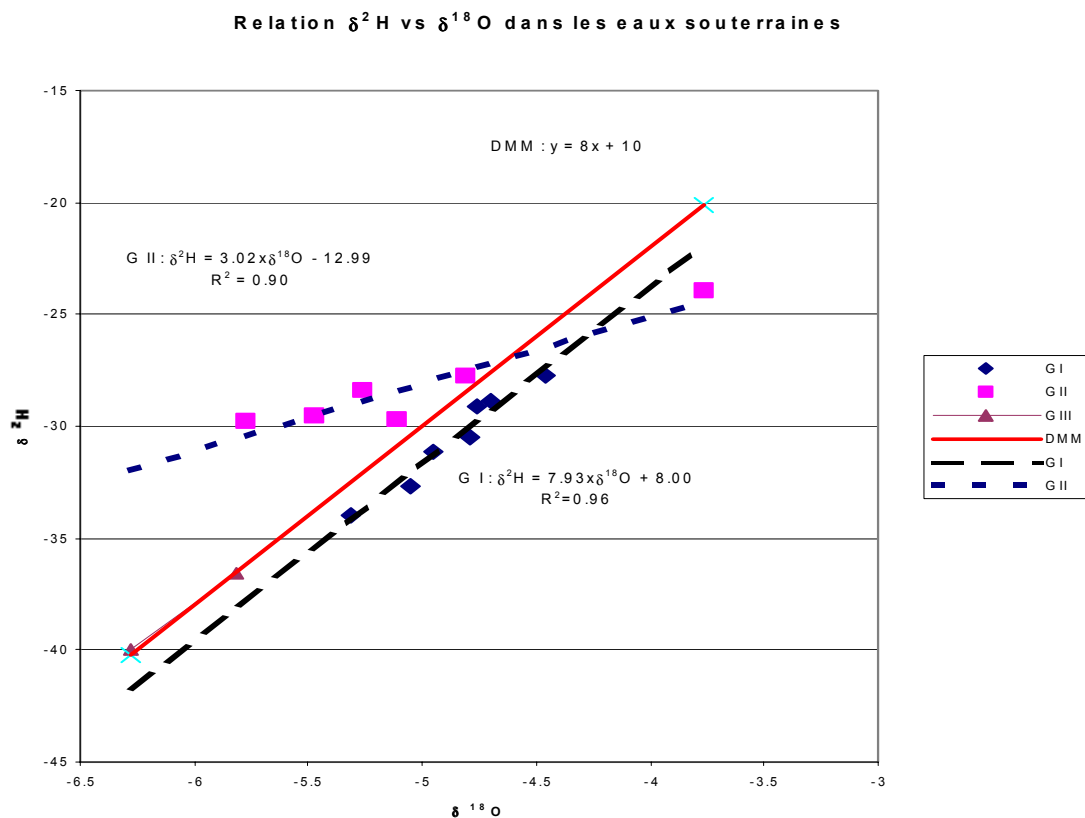
H. SALVAYRE
Millas, France

South-West Burkina Faso (60 000 km²) is located in the upstream parts at the junction of the water basins of the rivers Comoé, Volta and Niger. The mean precipitation value is around 1000 mm in one rainy season (monsoon) starting April and finishing October. More than 80% of precipitation occur between June and August. In our area two great lithological units are encountered: the sedimentary deposits in the West, mainly sandstones of the Upper Precambrian and the crystalline and metamorphic substratum in the East. Our main concern dealt with the sedimentary aquifers within 9 well defined geological formations on the edge of the Taoudeni basin dipping less than 10° NNW. These watersheds have an important hydric potential in surface waters as well as in groundwaters and still embrace nowadays relatively important reclamation lands. The physical context and the water reserve in the southwest present a possibility of expansion and development which has already started being exploited. Since 1970 this region has undertaken an intense activity of mobilization and use of the waters. It has been noted that the managing and exploitation of the important natural potential occurs spontaneously and/or individually without enough critical concern related to the needs and the resources. This situation has already led in some places to shortages, conflicts about the uses and risks of overexploitation of the areas and in an inadequate use of the reclamation lands. This situation implies serious problems as to the qualitative protection of the resource. This inappropriate approach is the consequence of an incomplete knowledge of the water resources. Today new demands arise as to the mobilization the use of the groundwater resources and to the qualitative protection. In order to solve these problems as quickly as possible, from 1997 to 1999 isotopic investigation have been undertaken (¹⁸O enables to identify the recharge areas. ¹⁴C and ³H define the “age” of the water).

These investigations which were meant to understand the behaviour of the different aquifers have led to the following conclusions:

1. The stable isotopes (¹⁸O, ²H) do not allow a large differentiation in the geographical recharge areas. This is due to the low differences in the topography between 300 to 600 m. Most of the values of groundwaters range between –5 and –6 ‰ and the relationship ²H vs ¹⁸O gives leads to the equation $\delta^2\text{H} = 7.93 \delta^{18}\text{O} + 8$ very close to the Craig's line i.e witnessing non evaporated waters.
2. The radioactive isotopes show that the geographical distribution of the tritium contents is more or less random. Nevertheless the tritium content combined with ¹⁴C activity measurements can differentiate three groups of aquifers:

- (i) waters = 2 TU (our background): transit time = 500 years. These are old waters with less than 80% C14 activity. Some of these waters located in the west of our zone are artesian and show ages between 10 to 17 000 years
 - (ii) waters between 3 and 5 TU: mixings between old and recent waters which transit time reach a maximum of few hundreds years.
 - (iii) waters = 5TU: it represents recent waters with tritium content close to rainwater (about 5TU) which correspond to recharge by rivers and/or surface waters.
3. The numerical distribution shows a greater amount of old waters in sedimentary areas and in crystalline substratum as well: almost 80% of the analyzed waters contain less than 5 TU. If this absence of tritium indicates an efficient protection of the aquifers on the other hand it points out the very low rate of renewal of the groundwater resources (from hundreds to thousands years).



The available measurements at this point do not enable a more detailed interpretation of the groundwater behaviour. For a better understanding it is important to take into account the evolution and achieve a chronological follow up of the natural isotope variations (stable and radioactive). The decade to come will be characterized by an intense exploitation of groundwater resources. It is important to show their availability their replenishment and also their spatial distribution which are basic elements of a sustainable economic and social development.

**CHANGES IN THERMAL AND MINERAL WATERS WITHIN THE
“GÖLCÜK–İZMIT AUGUST 17. 1999 EARTHQUAKE AREA”
AS REVEALED BY THE ^{13}C AND ^{36}Cl ISOTOPES**

W. BALDERER

Geological Institute, Engineering Geology, ETH-Hönggerberg, Zürich, Switzerland

H.A. SYNAL

Paul Scherrer Institute, c/o Institute for Particle Physics, ETH-Hönggerberg,
Zürich, Switzerland

T. YALCIN

Technical University of Istanbul, Mining Faculty, Dept. of Geology, Istanbul, Turkey

F. LEUENBERGER

Geological Institute, Engineering Geology, ETH-Hönggerberg, Zürich, Switzerland

The effects of active tectonics as evidenced by geology, geodesy and seismology on groundwater circulation and on the heat flow pattern have been studied in 6 areas along the North Anatolian Fault Zone in the years 1987 to 1996 as part of the joint interdisciplinary project "Marmara" of ETH Zürich and the Istanbul Technical University (ITÜ) [1, 2]. These areas are Tuzla–Çanakkale [3, 4], Kükürtlü and Çekirge–Bursa [5], Kuzuluk–Adapazari [6, 7], Yalova, Gemlik and Armutlu–Yalova [8], Bergama and Dikili–İzmir [9] and Gönen and Ekşidere–Balıkesir [10].

As part of the IAEA Coordinated Research Project on "Isotope response to the dynamic changes in groundwater systems due to long-term exploitation", a new sampling campaign was carried out by W. Balderer and T. Yalcin between the dates of 6.-11 July 1999 in order to investigate the long term changes due to exploitation of thermal waters in the above mentioned areas. Within this same tectonically active area of the Anatolian Fault Zone which was studied before within the "Marmara project" the M 7.4 Gölcük–İzmit epicentered earthquake happened on 17 August 1999 [11].

To investigate possible changes caused by this tectonic event on the thermal and mineral waters of Bursa, Adapazari and Yalova areas, a second sampling campaign was carried between 2-6 October 1999. But again on 12 November 1999 the Düzce earthquake (M7.2) occurred on the North Anatolian Fault Zone in vicinity of the Kuzuluk thermal spa. To investigate the further changes a small sampling was carried out at Kuzuluk–Adapazari areas in November 1999. A last sampling survey including all by the earthquakes potentially affected areas was undertaken on 3–8 October 2000.

From the results of analyses of the corresponding water samples of these 3(4) sampling campaigns especially changes the isotopic composition of ^{13}C and ^{36}Cl with respect to the sampling prior to 1996 [12, 13], respectively to the 17. August 1999 earthquake are recognised. On a preliminary basis the observed changes may be interpreted as related i) to the enhanced up-welling of CO_2 in tectonically induced fractures [14] and ii) to a mobilisation of deep seated brines by the increased seismic-tectonic activity [15].

REFERENCES

- [1] SCHINDLER, C., The Marmara Poly-Project: tectonics and recent crustal movements revealed by space-geodesy and their interaction with the circulation of groundwater, heat flow and seismicity in Northwestern Turkey. *Terra Nova* **5** (1993) 164-173.
- [2] SCHINDLER, C., Geology of NW Turkey: Results of MARMARA Poly-Project. In: Schindler, C. & Pfister, M. eds.: *Active Tectonics of Northwestern Anatolia - The Marmara Poly-Project*, vdf Hochschulverlag Zürich, ISBN 3-7281-2425-7 (1997).
- [3] MUETZENBERG, S., Westliche Biga-Halbinsel: Geologie, Tektonik und Thermalquellen (Canakkale, Türkei). *Mitt. Geol. Inst. der ETH und der Universität Zürich*, Nr. 287 (1991).
- [4] MUETZENBERG, S., Westliche Biga-Halbinsel: Geologie, Tektonik und Thermalquellen (Mützenber, S., Balderer, W. and Rauert, W., 1992, Environmental isotope study of saline geothermal systems in western Anatolia, Çannakkale, Turkey, *Water-Rock Interaction*, edited by: Kharaka and Maest, Balkema, Rotterdam. ISBN 90 5410 075 3, Vol. 2 (1992) 1317-1320.
- [5] IMBACH, Th., Thermalwässer von Bursa. Geologische und hydrogeologische Untersuchungen am Berg Uludag (NW-Türkei), Diss. ETH-Zürich Nr. 9988 (1992).
- [6] GREBER, E., Das Geothermalfeld von Kuzuluk / Adapazari (NW-Türkei), Geologie, aktive Tektonik, Hydrogeologie, Hydrochemie, Gase und Isotope, Diss. ETH-Zürich Nr. 9984 (1992).
- [7] GREBER, E., Deep Circulation of CO₂-rich Paleowaters in a Seismically Active Zone (Kuzuluk/Adapazari, Northwestern Turkey). *Geothermics*, Vol. 23, No. 2 (1994) 151-174.
- [8] EISENLOHR, Th., Die Thermalwässer der Armutlu-Halbinsel (NW-Türkei) und deren Beziehung zu Geologie und aktiver Tektonik, Diss. ETH-Zürich, Nr. 11340 (1995).
- [9] JECKELMANN, Ch., Genese lokaler Thermalwasservorkommen in der Region Bergama/W Türkei, Diss ETH Zürich Nr. 11990 (1996).
- [10] YALCIN, T., Geology and Hydrogeology of the Gönen-Yenice Area. Ph.D. thesis, ITÜ Istanbul, Turkey (1997).
- [11] SIMSEK, S., YILDIRIN, Effects of the 1999 Earthquakes on geothermal fields and manifestations. *IGA News*, No. 40, April-June 2000 (2000).
- [12] BALDERER, W., SYNAL, H.-A., Application of the chlorine-36 method for the characterisation of the groundwater circulation in tectonically active areas: Examples from North Western Anatolia / Turkey. *Terra Nova* **8** (1996) 324-333.
- [13] BALDERER, W., SYNAL, H.-A., Use of Chlorine-36 as Tracer for the Evolution of Waters in Geothermal and Tectonic Active Areas in Western Turkey. *Nuclear Instruments and Methods in Physics Research, B (NIMB)*, Elsevier (1997).
- [14] TSCHUDI, S., Observed pressure variations and their causes in the geothermal field of Kuzuluk/NW Turkey. In: Schindler, C. & Pfister, M. eds.: *Active Tectonics of Northwestern Anatolia - The Marmara Poly-Project*, vdf Hochschulverlag Zürich, 1997, ISBN 3-7281-2425-7 (1997).
- [15] BALDERER, W., Mechanisms and processes of groundwater circulation in tectonically active areas. In: Schindler, C. & Pfister, M. eds.: *Active Tectonics of Northwestern Anatolia - The Marmara Poly-Project*, vdf Hochschulverlag Zürich, 1997, ISBN 3-7281-2425-7 (1997).

STABLE ISOTOPES, $\delta^{18}\text{O}$ AND $\delta^2\text{H}$, IN THE STUDY OF WATER BALANCE OF LAKE MASSOKO, TANZANIA: INVESTIGATION OF THE EXCHANGE BETWEEN LAKE AND UNDERGROUND WATER

L. BERGONZINI, E. GIBERT, A. WINCKEL
Laboratoire d'Hydrologie et de Géochimie Isotopique,
Université Paris-Sud, Orsay, France

The stable oxygen and deuterium isotope compositions of a lake depend upon its water balance. Therefore the balance equations of stable isotopes, which imply calculation of the composition of evaporating moisture δ_E , provide information for assessing the water balance. In most cases, this approach is used to investigate the relationships between lakes and groundwater.

Lake Massoko ($8^{\circ}20'S$, $33^{\circ}45'E$, 870 m.a.s.l.) is a freshwater maar-lake without surface outlet. The lake surface and its runoff area cover 0.38 and 0.55 km² respectively. In contrast with the mean annual rainfall in the other parts of south Tanzania (1000-1200 mm y⁻¹), the presence of Lake Malawi to the South, and the high ranges to the North (Mounts Poroto, Rungwe and Livingstone) imply local climatic features. Air masses overloaded with humidity bypassing Lake Malawi are submitted, especially in April, to ascending currents, producing rainfalls up to 2450 mm y⁻¹ over Massoko area. Because of the evaporation rate from the lake's surface (around 2100 mm y⁻¹) and without taking into account the runoff from the drainage basin, hydrological balance is positive and imply underground lost.

One of most difficult points in the establishment of the isotope balances is the calculation of the composition of the evaporated water (δ_E), which requires an estimation of the isotopic composition of the water vapour in the atmosphere over the lake (δ_{Atm}). Without direct measurements, two ways can be used for the determination of the vapour composition (i) equilibrium with precipitation and reconstitution from them, or (ii) calculation from the balances of a terminal lake of the region. Both approaches are presented and compared, but only the second one allows physical solutions. δ_{Atm} determined from Lake Rukwa hydrological and isotope balances has been used to calculate values for δ_E over Lake Massoko. The estimation of δ_{Atm} obtained from Lake Rukwa budgets presents a deuterium excess higher than the values obtained from precipitation. This fact appears in good agreement with local rivers composition.

However, the hydrological and isotope balances of Lake Massoko gives evidence of important groundwater input and output, overimposed to relationships with groundwater circulation at a regional scale. Water lost by infiltration has been estimated at about 60% of the total lost and inflow from the basin assessed at around 40% of the input. This point indicates that Lake Massoko did not directly amplified the climatic fluctuations, and that its level is maintained by groundwater. In such a scheme, at odds with many lake of East Africa, the sediment preservation is optimised as confirmed by a continuous sedimentary sequence core in the lake in 1996* and having registered more than 35 ky B.P. of environmental history. Sedimentation rate fluctuation over this period are presented and compared with other limnological sequences.

* EC Programme RUKWA: "Investigations of the sediments of Lake Rukwa (Tanzania): a clue for reconstructing the south equatorial climate during the last 130,000 years" (DG XII: Environment, Area I - Global Change).

APPLICATION OF COMPOUND SPECIFIC ^{13}C ISOTOPE INVESTIGATIONS OF CHLORINATED HYDROCARBONS IN CONTAMINATED GROUNDWATERS

K. OSENBRÜCK, M. HEIDINGER, A. VOROPAEV, S. ERTL*, L. EICHINGER
Hydroisotop GmbH, Schweitenkirchen, Germany

Chlorinated hydrocarbons are one of the most common pollutants found in groundwater. Due to complex contamination situations with overlapping contamination plumes the assessment of the organic contaminants requires the installation of expensive observation wells and high analytical effort. Here the determination of the stable isotope ratio $^{13}\text{C}/^{12}\text{C}$ of the organic compounds offers a promising and efficient tool to investigate the origin and the biodegradation characteristics of the chlorinated hydrocarbons in groundwater.

The application of the method is based on characteristic isotope fingerprints, differing in chlorinated solvents. This isotope fingerprint is derived from different production pathways and is not influenced by transport or by retardation processes in the underground. Due to the fact, that two different contaminations can easily be distinguished by isotope ratios, an improved distinction of spatially and temporally different contamination plumes might be possible.

In course of biologically mediated degradation processes a shift of the isotope ratios between the precursor and the product can frequently be observed, such as with denitrification or sulfate reduction processes. The isotope fractionation is due to a preferential reaction of the bonds formed by the lighter isotopes and leads to a progressive enrichment of the heavy isotopes in the precursor while the product becomes depleted in the heavy isotopes. Biological degradation of the highly chlorinated hydrocarbons is due to a co-metabolic dechlorinisation. Tetrachloroethene (PCE) for example degrades under anoxic conditions via trichloroethene (TCE) to *cis*-1,2-dichloroethene (cDCE). Subsequent degradation to vinyl chloride (VC) and ethene may appear under aerobic as well as reducing environments depending on the site specific conditions.

In several laboratory studies [1, 2] it has been shown, that biodegradation of the chlorinated hydrocarbons is accompanied by an isotope fractionation of the stable carbon isotopes. The isotope ratios may be used to assess and quantify the degradation of the organic compounds at the field sites. This application has gained great interest for remediation strategies including monitored natural attenuation of contaminations [2, 3].

In contrast to the laboratory studies, many of the field investigation show no evidence for isotope fractionation although biodegradation of the chlorinated hydrocarbons in the groundwater is significant. Here, we present the results of 21 field studies, where compound specific ^{13}C isotope ratios have been applied. Only in some cases isotope fractionation processes of chlorinated hydrocarbons due to biodegradation have been observed. The measured $\delta^{13}\text{C}$ values agree reasonably with a Rayleigh type isotope fractionation model, where the fractionation factors are used as fitting parameters.

The occurrence and the degree of significant isotope fractionation of chlorinated hydrocarbons is still an open question. Major factors that control the extend of measurable ^{13}C isotope

* Also: Institut für Biogeochemie und Meereschemie, Universität Hamburg, Hamburg, Germany.

fractionation of chlorinated hydrocarbons in groundwater most likely include parameters as activity and type of the microbiological species, availability of cosubstrates as well as hydrochemical and hydrogeological conditions.

REFERENCES

- [1] HUNKELER, D., ARAVENA, R., BUTLER, B.J., Monitoring Microbial Dechlorination of Tetrachloroethene (PCE) in Groundwater Using Compound-Specific Stable Carbon Isotope Ratios: Microcosm and Field Studies. *Environ. Sci. Technol.* **33** (1999) 2733-2738.
- [2] SHERWOOD LOLLAR, B., SLATER G.F., AHAD, J., SLEEP, B., SPIVACK, J., BRENNAN M., MACKENZIE P., Contrasting carbon isotope fractionation during biodegradation of trichloroethylene and toluene: Implications for intrinsic bioremediation. *Organic Geochemistry* **30** (1999) 813-820.
- [3] MECKENSTOCK, R.U., MORASCH, B., SCHINK, B., ANNWEILER, E., MICHAELIS, W., RICJNOW, H.H., In situ Quantifizierung des mikrobiellen Abbaus von aromatischen Kohlenwasserstoffen über $^{13}\text{C}/^{12}\text{C}$ -Isotopenfraktionierung. In: *Proceedings of the DECHEMA-Symposium "Natural Attenuation"*, 27./28.10.1999, **32** (1999).

USE OF ENVIRONMENTAL ISOTOPES FOR STUDYING HUMAN INDUCED CHANGE IN GROUNDWATER ENVIRONMENT IN LAHORE, PAKISTAN

M. AHMAD, W. AKRAM, M.I. SAJJAD, M. RAFIQ, M. AZAM TASNEEM
Pakistan Institute of Nuclear Science and Technology,
Islamabad, Pakistan

Lahore is the second biggest city of Pakistan where groundwater is the only source of drinking water supply for the city. On the other hand, the quality of groundwater is being degraded due to various human activities especially due to waste disposal practices. Untreated domestic and industrial wastes are discharged into open channels, drains, etc. which leads to surface water and groundwater pollution. This study was undertaken to assess the changes in groundwater environment due to such activities.

Water samples were collected on periodical basis from existing handpumps, tube wells and drains and analyzed for isotopic (^2H , ^3H , ^{13}C , ^{18}O) and major dissolved ions. Samples having high nitrate were analyzed for ^{15}N . Selected samples were also analyzed for Coliform bacteria. Results of only selected parameters are discussed here.

The data showed that quality of shallow groundwater has deteriorated at most of the locations and concentrations of several chemical parameters are higher than WHO permissible levels for drinking water. Comparison with a previous study carried out in 1991 [1], indicated a clear increasing trend of total dissolved salts in groundwater.

An outstanding feature of the data is the increasing trend of nitrate concentrations both in shallow and deep groundwater. Results of nitrate analysis indicate that concentrations vary from 10 to 188 mg/l in shallow groundwater and 9 to 41 mg/l in deep groundwater. Frequency histogram of nitrate concentrations is shown in Fig. 1. Nitrates which were generally a few ppm have increased at almost all the surveyed locations and have even crossed the WHO limit of 45 mg/l at several shallow locations. High nitrate waters exist as isolated pockets. Results of tritium analysis indicated that shallow groundwater has generally high tritium values. Presence of more nitrate at shallow depths, occurrence of high nitrate waters as isolated pockets and high tritium in contaminated waters suggest that nitrates are derived from as presently active surface source.

In order to confirm the source of nitrate, samples having nitrate more than 45 mg/l were analyzed for $\delta^{15}\text{N}(\text{NO}_3)$. Values were found ranging from +10.3 to +25.1 ‰. These enriched values show that nitrates are derived from untreated domestic wastes [2] thrown into sewerage drains, open channels, etc. Bacterial contamination of groundwater also proves the penetration from sewerage drains. Penetration of urban recharge was also studied on the basis of $\delta^{13}\text{C}$ data. It was noticed that these values are negatively skewed towards ^{13}C index of sewerage water (Fig. 2) confirming the pollution of shallow aquifer by sewerage drains.

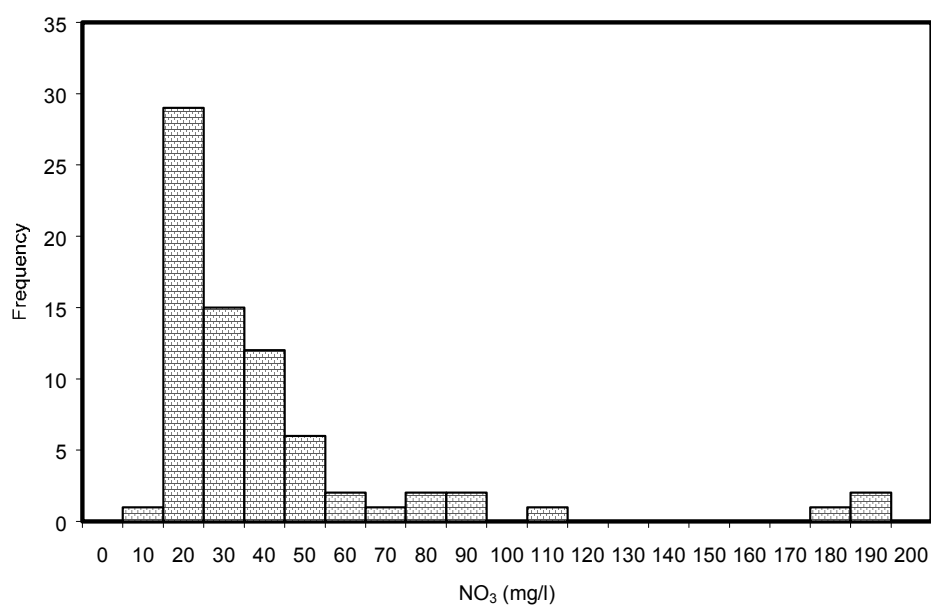


FIG. 1.

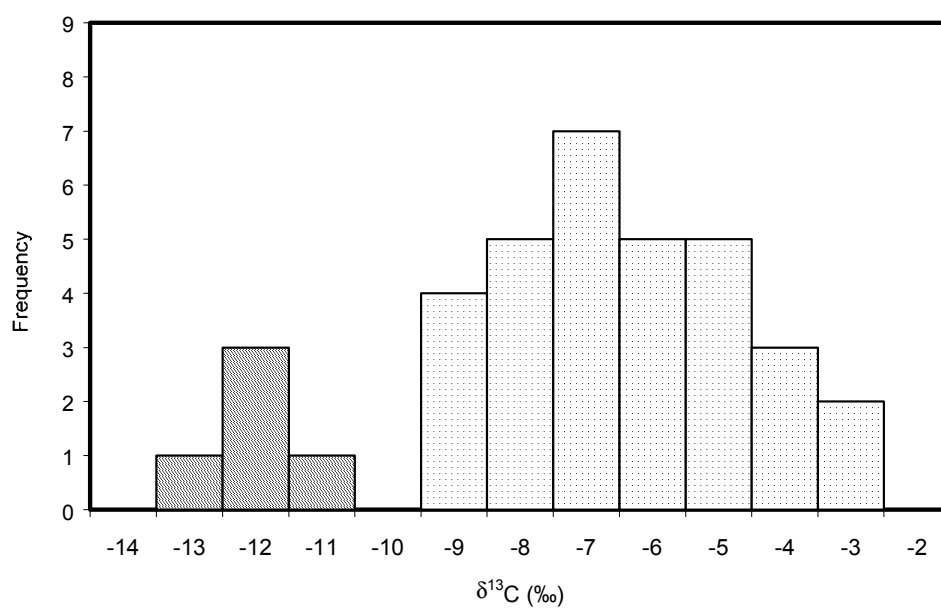


FIG. 2.

REFERENCES

- [1] National Engg. Services of Pakistan Pvt. Ltd. And Binnie & Partners Consulting Engineers, London, UK, Final Report on Groundwater Resources Evaluation and Study of Aquifer Under Lahore, Submitted to Water & Sanitation Agency, Lahore (1991).
- [2] GOPPEL, M., EICHINGER, I., TRAUB, R., LOOSLY, H., Evaluation of hydrological changes and their consequences, Proceedings of a Symposium on Isotope Techniques in the Study of Environmental Change, Vienna, 14 - 18 April, 1997 (1997).

ENVIRONMENTAL RADIOACTIVITY INVESTIGATIONS IN THE GEORGIAN SUBTROPICAL REGION

S. PAGAVA, P. KAKASHVILI, M. AVTANDILASHVILI, G. KHARASHVILI,
Z. ROBAKIDZE, V. RUSETSKI, G. TOGONIDZE
Radiocarbon and Low-Level Counting Section,
I. Javakhishvili Tbilisi State University,
Tbilisi, Georgia

D. BARATASHVILI
Selection and Plants Protection Department,
Batumi Botanical Gardens of Georgian Academy of Sciences,
Batumi, Georgia

Environmental changes in the contamination of the Georgian subtropical region have been investigated by analysing anthropogenic and natural radionuclides in samples of soil and tea leaves for possible chromosome mutations. As the tea industry in Georgia is an important economic activity, such investigations are of great importance. The changes in the morphology of tea leaves, their colour, blossoming, growth inhibition or stimulation, prolongation of the germination period and levels of tanin-katechin complexes have been investigated.

The results of radionuclide measurements in soil and tea leaves (^{40}K , ^{210}Pb and ^{137}Cs) are presented in Table I. Elevated concentrations of ^{137}Cs were observed in soil samples due to fallout from Chernobyl, however, no direct relationship between the concentration of ^{137}Cs in soil and tea leaves has been observed. Cyto-genetic analyses of tea primary roots will be presented and compared for different time periods.

Further, ichthyofauna samples taken from the Georgian subtropical areas were analysed for anthropogenic (^{137}Cs) and natural (^{40}K) radionuclides. The observed concentrations of ^{137}Cs were low, close to the detection limit of the order of 0.4 Bq/kg dry weight (Table II). Some of the investigations were carried out [1] in the framework of the IAEA Technical Co-operation project "Marine Environmental Assessment of the Black Sea Region".

REFERENCE

- [1] AVTANDILASHVILI, M., BURCHULADZE, A., PAGAVA, S., ROBAKIDZE, Z., RUSETSKI, V., TOGONIDZE, G., Radiological Background of the Georgian Part of the Black Sea. Proceedings of the International Symposium on Marine Pollutions, IAEA, Vienna, (1999) 338-339.

TABLE I. Radionuclides in soil and tea samples

Sample ID	Sample type	Activity (Bq/kg)			
		dry weight			
		K-40	¹³⁷ Cs	²¹⁰ Pb	²²⁶ Ra
TB-2229	Soil	205 ± 17	549 ± 11	154 ± 30	101 ± 20
TB-2231	Tea leaves	299 ± 23	23 ± 2	<MDA	<MDA
TB-2247	Soil	255 ± 15	278 ± 6	116 ± 29	70 ± 16
TB-2248	Tea leaves	468 ± 37	20 ± 2	<MDA	<MDA
TB-2249	Soil	180 ± 13	201 ± 5	115 ± 29	50 ± 16
TB-2250	Tea leaves	307 ± 38	15 ± 2	<MDA	,MDA
TB-2234	Soil	246 ± 17	334 ± 7	167 ± 31	126 ± 19
TB-2235	Tea leaves	414 ± 25	8 ± 2	<MDA	<MDA
TB-2232	Soil	201 ± 17	538 ± 11	187 ± 34	101 ± 16
TB-2233	Tea leaves	312 ± 23	12 ± 2	53 ± 21	<MDA

TABLE II. Ichthyofauna

Sample ID	Species	Activity [Bq/kg]	
		⁴⁰ K	¹³⁷ Cs
TB-2213	Mugil cephalus Linne	83 ± 4	0.4 ± 0.2
TB-2215	Odontogadus merlangus euxinus	70 ± 6	0.9 ± 0.3
TB-2211	Mullus barbatus, E	47 ± 6	< MDA
TB-2217	Mullus barbatus, E (spawn)	93 ± 23	< MDA
TB-2212	Platichthys flesus luscus, P	42 ± 6	< MDA
TB-2214	Cottus gobio, Z	63 ± 6	0.6 ± 0.4
TB-2216	Salmo trutta labrax	95 ± 7	< MDA

USING ISOTOPES TO IMPROVE IMPACT AND HYDROLOGICAL PREDICTIONS OF LAND-SURFACE SCHEMES IN GLOBAL CLIMATE MODELS

K. McGUFFIE

Department of Applied Physics, University of Technology,
Sydney, New South Wales, Australia

A. HENDERSON-SELLERS

Environment Division, Australian Nuclear Science and Technology Organisation,
Menai, New South Wales, Australia

Global climate model (GCM) predictions of the impact of large-scale land-use change date back to 1984 [1] as do the earliest isotopic studies of large-basin hydrology [2]. Despite this coincidence in interest and geography, with both papers focussed on the Amazon, there have been few studies that have tried to exploit isotopic information with the goal of improving climate model simulations of the land-surface. In this paper we analyze isotopic results from the IAEA global data base specifically with the goal of identifying signatures of potential value for improving global and regional climate model simulations of the land-surface.

Evaluation of climate model predictions of the impacts of deforestation of the Amazon has been shown to be of significance by recent results which indicate impacts occurring distant from the Amazon i.e. tele-connections causing climate change elsewhere around the globe. It is suggested that these could be similar in magnitude and extent to the global impacts of ENSO events [3]. Validation of GCM predictions associated with Amazonian deforestation are increasingly urgently required because of the additional effects of other aspects of climate change, particularly synergies occurring between forest removal and greenhouse gas increases, especially CO₂.

Here we examine three decades' distributions of deuterium excess across the Amazon and use the results to evaluate the relative importance of the fractionating (partial evaporation) and non-fractionating (transpiration) processes. These results illuminate GCM scenarios of importance to the regional climate and hydrology: (i) the possible impact of increased stomatal resistance in the rainforest caused by higher levels of atmospheric CO₂ [4]; and (ii) the consequences of the combined effects of deforestation and global warming on the region's climate & hydrology [5].

Conventional observational studies in the Amazon have not been able to assist in distinguishing between appropriate and less valuable simulations of this region to date because most are point-based i.e. in one, or at most two, locations. However, the isotopic data available from the IAEA network has the potential to provide clues about the veracity of regional hydrological simulation of the Amazon (e.g. [6]).

Generally, GCMs predict reductions in precipitation and evaporation as a consequence of deforestation. There is less agreement about the sign of the temperature change although most simulations show a temperature rise. There is also disagreement about the sign of the atmospheric moisture convergence change with about a quarter of the GCM simulations undertaken between 1984 and 2000 predicting an increase in moisture convergence while the others anticipate a decrease (Figure 1). These differences in predicted regional moisture convergence change can be examined using $\delta^{18}\text{O}$ and δD data. One widely reported simulation set gives seasonal transpiration and re-evaporated canopy interception budgets different from those derived from isotopic analysis.

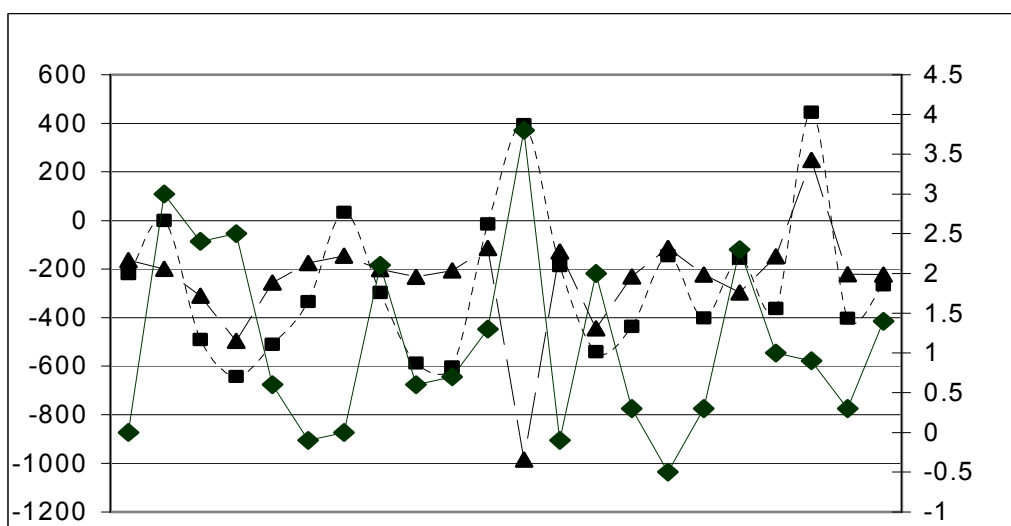


FIG. 1. GCM predicted differences in annual mean Amazonian temperatures (solid with diamonds), precipitation (dotted with squares) and evaporation (dashed with triangles) as a result of simulated deforestation. The right hand scale is in K (temperature) and the left hand scale is in mm (evaporation & precipitation). Points are GCMs from 1984 (left) to 2000 (right). [Note the zero levels are not aligned.]

Our results indicate that the evaporation of moisture intercepted by the canopy is another potential means of evaluating climate model performance. Thus, model estimates of the percentage of intercepted moisture that is evaporated (cf. [7]) can be compared with isotopically-derived fractions. This means that land-surface schemes coupled into modern global climate models and so representing sensitive components of the global hydrological cycle can be evaluated using isotopes.

REFERENCES

- [1] HENDERSON-SELLERS, A., GORNITZ, V., "Possible climatic impacts of land cover transformations, with particular emphasis on tropical deforestation", *Clim. Change*, **6** (1984) 231-258
- [2] SALATI, E., VOSE, P.B., "Amazon Basin: a system in equilibrium", *Science*, **225** (1984) 129-137.
- [3] ZHANG, H., MCGUFFIE, K., HENDERSON-SELLERS, A., "Impacts of tropical deforestation II: the role of large-scale dynamics", *J. Clim.*, **9** (1996) 2498-2521
- [4] HENDERSON-SELLERS, A., MCGUFFIE, K., GROSS, C., "Sensitivity of global climate model simulations to increased stomatal resistance and CO₂ increases", *J. Clim.*, **8**(7) (1995) 1738-1756
- [5] ZHANG, H., HENDERSON-SELLERS, A., MCGUFFIE, K., "The compounding effects of tropical deforestation and greenhouse warming", *Clim. Change* (2001) in the press.
- [6] GAT, J.R., MATSUI, E., "Atmospheric water balance in the Amazon Basin: an isotopic evapotranspiration model", *J. Geophys. Res.*, **96**(D7) (1991) 13,179-13,188
- [7] MCGUFFIE, K., HENDERSON-SELLERS, A., ZHANG, H., "Modelling climatic impacts of future rainforest destruction", in B.K. Maloney (eds), *Human Activities and the Tropical Rainforest*, Kluwer, Netherlands (1998) 169-193.

LONG-TERM POST-CHERNOBYL ^{90}Sr AND ^{137}Cs PROFILES AS THE INDICATORS OF THE LARGE SCALE VERTICAL WATER MIXING IN THE BLACK SEA

V.N. EGOROV, N.A. STOKOZOV, N.Y. MIRZOYEVA

Institute of Biology of the Southern Seas (IBSS),

National Academy of Sciences of the Ukraine, Sevastopol, Ukraine

The radioactive and chemical pollutions, eutrophic elements come to the surface water layer of the Black Sea from the territory of 22 countries. The self-purification of the surface water layer essentially depends from the vertical water mixing.

The atmospheric fallout in the May 1986 after Chernobyl NPP accident were main source of the ^{137}Cs input in the Black Sea. The ^{90}Sr input to the Black Sea was caused by atmospheric fallout as well as the Dnieper River and Danube River runoff during of consequent years.

^{90}Sr and ^{137}Cs are conservative elements in a marine environment and could be used as tracers of the hydrological processes, including vertical water mixing.

The aim of our investigations was an assessment of the large-scale vertical water exchange in the Black Sea on base of analysis time-series ^{90}Sr and ^{137}Cs vertical profiles.

The materials for studies were the published data [1-3] and results of our observations [4-5] in the period 1986 to 1998 which took place in the central part of the Black Sea western cyclonic gyre. The ^{90}Sr and ^{137}Cs vertical profiles are shown on Fig. 1.

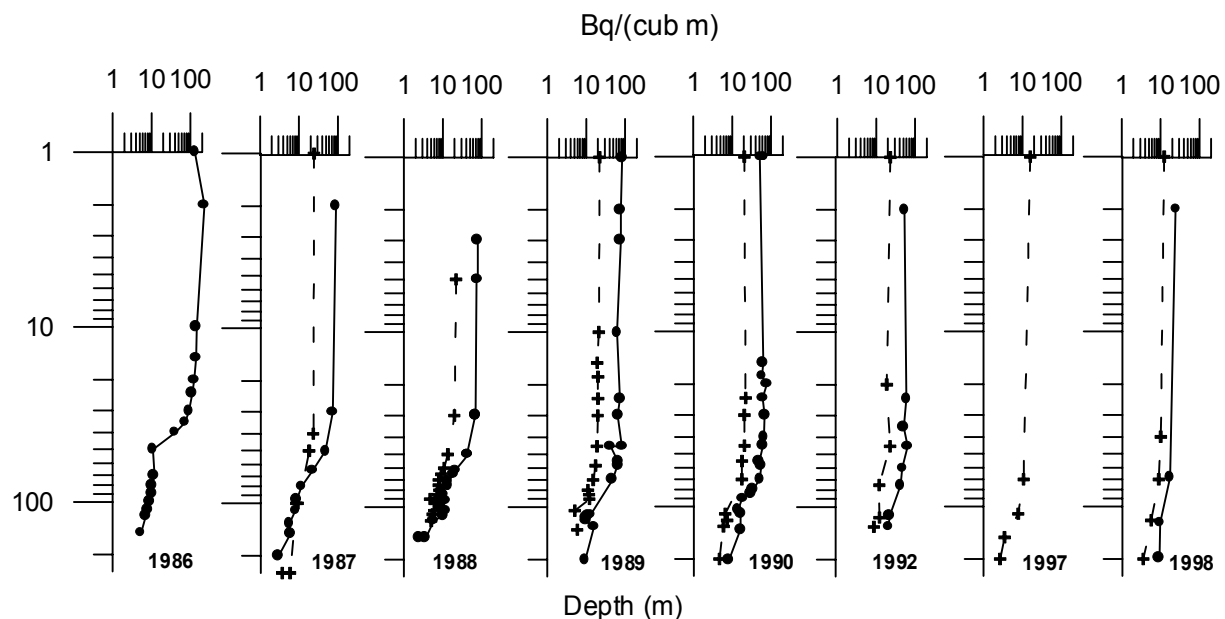


FIG.1. Average ^{90}Sr (+) and ^{137}Cs (•) profile in the Western cyclonic gyre of the Black Sea (Nikitin et al., 1988; Buesseler et al., 1990; Buesseler, Livingston 1997; Egorov et al., 1993, 1999).

After 1986, the decrease of ^{90}Sr and ^{137}Cs concentrations in surface layers was caused by penetrations of these radionuclides into depth. At the same time, the increasing of depth of the gradient layer for ^{90}Sr and ^{137}Cs vertical profiles was observed. For the quantitative assessment of the depth of a gradient layer, the ^{90}Sr and ^{137}Cs vertical profiles were approximated by the function:

$$C_w(h) = C_w(0) + a / (1 + \exp(-(h - h_0)/b)), \quad (1)$$

where: C_w - concentration of the radionuclide (Bq m^{-3}); h - depth (m); $C_w(0)$, a , b , and h_0 - parameters.

The depth of the lower boundary of gradient layer was estimated as depth of lower extremum of the third derivation from the function (1). The calculations were conducted for those profiles only, where the value of gradients exceeded an error of ^{90}Sr and ^{137}Cs determination. The depth of the lower boundary of gradient layer vs time was used as an indicator of vertical water mixing intensity. This dependence is shown on Fig. 2.

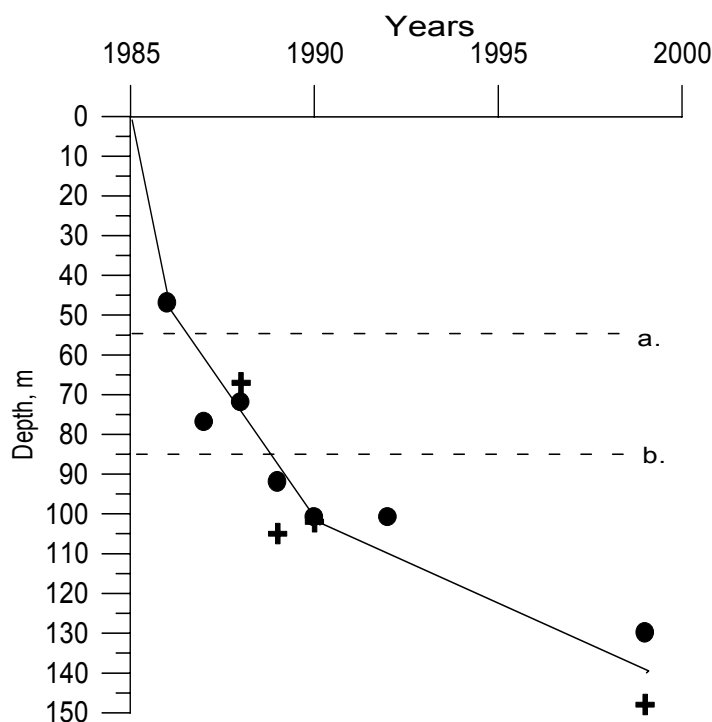


FIG.2. The low boundary of the ^{90}Sr (+) and ^{137}Cs (•) gradient layer vs time at the Western cyclonic gyre of the Black Sea. Notes: summer (a) and winter (b) depths of the maximum salinity gradient in the permanent Black Sea halocline.

These results show that in the course of the first year after Chernobyl NPP accident the lower boundary of gradient layer has reached an upper boundary of the permanent Black Sea halocline. Subsequently the depth of this boundary into the Black Sea halocline increased with velocity about 14.5 m per year or $4.7 \cdot 10^{-5} \text{ cm s}^{-1}$ (Fig. 2).

As it is known, that the Black Sea water circulation consists from the large-scale cyclonic gyres and the rim Main Black Sea Current with small-scale anticyclonic and cyclonic gyres. In these various hydrological structures, the vertical component of velocity of the currents changes in a wide range from $1.0\text{--}1.6 \cdot 10^{-7}$ up to $2.0 \cdot 10^{-2} \text{ cm s}^{-1}$ depending on synoptic and seasonal processes [6].

The above mentioned results testify, that the Black Sea halocline is the main limit factor of vertical water exchange intensity between surface waters and more deep layers of water. Thus, within of central parts of the large-scale Black Sea cyclonic gyres, which square constitute approximately $4 \cdot 10^4 \text{ km}^2$ (10% from total square of the Black Sea surface) [7], the yearly vertical exchange of the surface water with water of the halocline the can be estimated as about 580 km^3 per year.

REFERENCES

- [1] NIKITIN, A.I., MEDINETS, V.I., CHUMICHEV, V.B., KATRICH, V.M., VAKULOVSKY, S.M., KOZLOV, A.I., LEPESHKIN, V.I., Radioactive contamination of the Black Sea in consequence of the Chernobyl NPP accident, as measured in October 1986. *Atomic Energy* **65** (2) (1988) 134-137 (in Russian).
- [2] BUESSELER, K.O., LIVINGSTON, H.D., CASSO, S.A., Mixing between oxic and anoxic waters of the Black Sea as traced by Chernobyl cesium isotopes. *Deep-Sea Research*, **38** (2) (1991) 725-745.
- [3] BUESSELER, K.O., LIVINGSTON, H.D., Time-series profiles of ^{134}Cs , ^{137}Cs and ^{90}Sr in the Black Sea. In *Sensitivity to change: Black Sea, Baltic Sea and North Sea*. Eds. Ozsoy, E. and Mikaelyan A., Dordrecht: Kluwer Academic (1997) 239-251.
- [4] EGOROV, V.N., POLIKARPOV, G.G., KULEBAKINA, L.G., STOKOZOV, N.A., YEVTUSHENKO, D.B., Model of large-scale contamination of the Black Sea with the long-lived radionuclides ^{137}Cs and ^{90}Sr resulting from the Chernobyl NPP accident. *Water Resources* **20** (3) (1993) 326-330 (in Russian).
- [5] EGOROV, V.N., POVINEC, P.P., POLIKARPOV, G.G., STOKOZOV, N.A., GULIN, S.B., KULEBAKINA, L.G., OSVATH, I., ^{90}Sr and ^{137}Cs in the Black Sea after the Chernobyl NPP accident: inventories, balance and tracer applications. *J. of Environ. Radioactivity*. **49**(3) (1999) 137-156.
- [6] OVCHINNIKOV, I.M., POPOV, YU.I., The forming of the cold-intermediate layer of water in the Black Sea. *Okeanologia*. **32**(5) (1987) 739-746 (in Russian).
- [7] VINOGRADOV, M.E., SAPOZSNIKOV, V.V., SHUSHKINA, E.A., *Ecosystem of the Black Sea*. Moscow, Nauka (1992) 111 p. (in Russian).

RIVER UNDER ANTHROPOGENIC STRESS: AN ISOTOPE STUDY OF CARBON CYCLING IN THE VISTULA, POLAND

P. WACHNIEW, K. ROZANSKI

University of Mining and Metallurgy, Faculty of Physics and Nuclear Techniques,
Krakow, Poland

Rivers play an important role in global carbon cycling as they transform and transport substantial amounts of carbon derived from the terrestrial systems to the oceans [1]. Riverine carbon cycling is affected by anthropogenic influences on hydrology, chemistry and biology of the river and its catchment. The Vistula, one of the most mineralized rivers of the world [2], drains industrialized and agriculturally-used areas populated by almost 23 million inhabitants. Moreover, much of the industrial and domestic wastewaters discharged into the Vistula river are untreated or insufficiently treated. High levels of pollution have serious environmental and economical consequences. For example, they limit use of Vistula waters as a source of drinking water and for industrial purposes. Pollutants transported by the Vistula river significantly influence water quality far into the open Baltic Sea [3].

The aim of the paper is to show how stable isotope techniques can be used to assess human impact on sources, fluxes and fate of dissolved inorganic carbon (DIC) and other pollutants in rivers, taking the Vistula river as an example. Vistula waters were sampled over a one-year period at Krakow (upper reaches), where the anthropogenic influences are at the extreme, and at the river mouth. Two campaigns were undertaken to sample the Vistula river along its course in summer and in autumn. Analyses of river water included temperature, pH, alkalinity, conductivity, dissolved oxygen, $\delta^{13}\text{C}$ of dissolved inorganic carbon and stable isotope composition of water ($\delta^{18}\text{O}$ and $\delta^2\text{H}$).

Carbon cycling in the Vistula river is significantly influenced by various anthropogenic factors which modify fluxes of DIC to and from the river system and also influence transformations of inorganic and organic forms of carbon within the river. The $\delta^{13}\text{C}_{\text{DIC}}$ value appeared to be a useful indicator of the overall carbon budget in the system.

There are two anthropogenic sources of DIC into the Vistula river: saline wastewaters from coal mines in the upper Vistula catchment, and highly alkaline (due to the excessive use of fertilizers) tributaries draining agricultural areas. Agriculture and domestic wastewaters are sources of organic carbon whose decomposition in river waters causes the increase of pCO_2 and corresponding lowering of pH and $\delta^{13}\text{C}$ of DIC. On the other hand, nutrients from agricultural and domestic sources support development of phytoplankton communities. Photosynthetic assimilation of dissolved CO_2 results in increase of pH and $\delta^{13}\text{C}$ of DIC. These anthropogenic alterations of carbon cycling result in supersaturation of river waters in CO_2 with respect to the atmosphere. The Vistula, as with many other large rivers, is a net source of CO_2 to the atmosphere.

Fig. 1 shows how photosynthesis and respiration influence the carbon cycle characteristics in a regulated part of river reach. Respiration of organic matter in rivers may cause depletion of dissolved oxygen. This process is intensified in dammed and regulated parts of a river because water velocities are reduced, which in turn allows sedimentation of organic matter. Also the river is not connected with its natural riparian zone, periodically flooded.

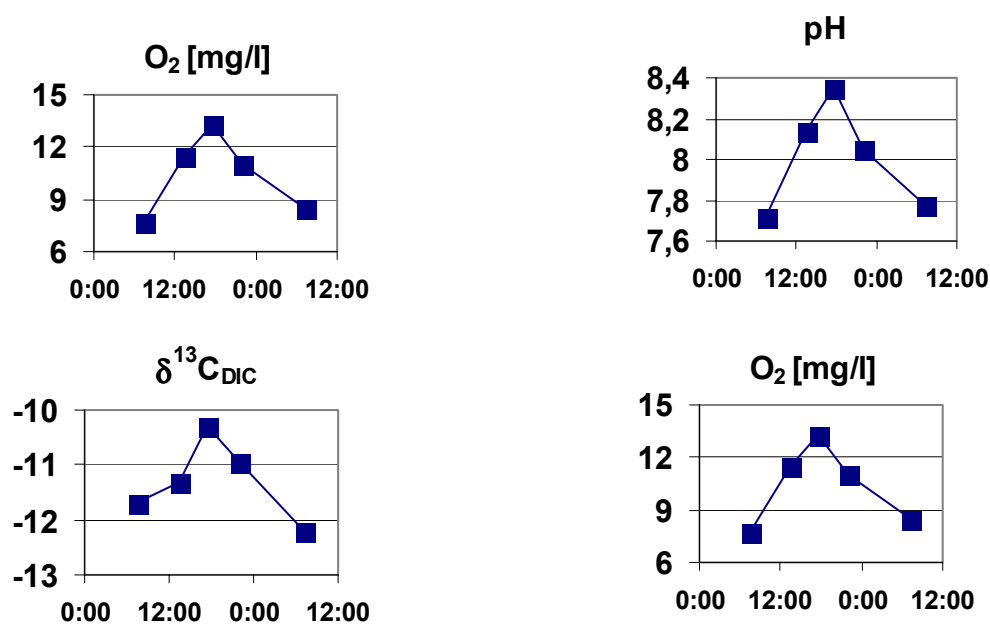


FIG. 1. Biologically induced fluctuations of $p\text{CO}_2$ cause concomitant changes of pH and $\delta^{13}\text{C}_{\text{DIC}}$. Nocturnal respiration consumes significant amounts of oxygen.

The middle Vistula has retained almost a natural character that supports self-purification of river waters. Isotopic composition of DIC reaches values typical for lowland rivers in carbonate terrain. Characteristics of carbon cycling in the less-regulated middle Vistula are not influenced even by untreated domestic sewage from the city of Warsaw (ca. 1.5 million inhabitants). The carbon cycle in the lower Vistula is significantly influenced by an artificial reservoir (Wloclawek). In summer, respiration of organic matter deposited in the reservoir causes severe oxygen depletion and significantly influences pH, $p\text{CO}_2$ and $\delta^{13}\text{C}_{\text{DIC}}$. All these carbon cycle characteristics regain their values only ca. 150 km downstream from the reservoir.

REFERENCES

- [1] BERNER E.K., BERNER, R.A., Global Environment: Water, Air and Geochemical Cycles. Prentice Hall (1996).
- [2] GAILLARDET, J., DUPRE, B., LOUVAT, P., ALLEGRE, C.J., Global silicate weathering and CO_2 consumption rates deduced from the chemistry of large rivers. Chem. Geol. **159** (1999) 3-30.
- [3] WITEK Z., OCHOCKI S., NAKONIECZNY J., PODGÓRSKA B., DRGAS A., Primary production and decomposition of organic matter in the epipelagic zone of the Gulf of Gdańsk, an estuary of the Vistula. ICES Journal of Marine Science **56** Suppl. (1999) 3-14.

RAINFALL-GROUNDWATER ISOTOPIC RELATIONSHIPS IN EASTERN AFRICA: THE ADDIS ABABA ANOMALY

W.G. DARLING

British Geological Survey, Wallingford, United Kingdom

B. GIZAW

University of Munich, Munich, Germany

Rainfall on the eastern side of the African continent is largely derived from Indian Ocean sources. Depending on the amount of rainout promoted by factors such as altitude and distance from the coast, GNIP stations from Khartoum (Sudan) in the north to Harare (Zimbabwe) in the south record different meteoric lines and weighted mean values. It can be demonstrated from hydrological studies in the countries involved that in general the isotopic content of groundwaters is not too different from the weighted mean rainfall (Fig 1).

Addis Ababa appears to be the exception. According to the GNIP database, Addis Ababa has the most isotopically enriched rainfall of the collection stations in eastern Africa. This fact has been noted previously and various explanations have been offered to account for it [1,2,3]. However, the rainfall recorded at Addis Ababa appears to be enriched to an anomalous extent in relation to both local groundwater isotopic values, and therefore it may be debated whether the record adequately reflects the actual rainfall average. It is important not only for water resources work but also for palaeoclimate studies, e.g. [4], that the rainfall-groundwater relationship for Ethiopia should be examined in some detail.

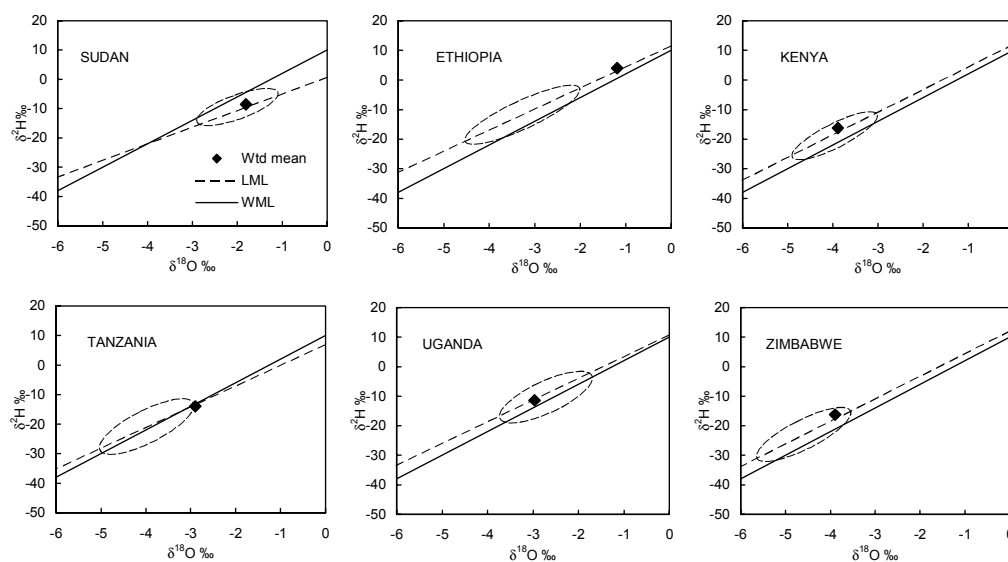


FIG. 1. Weighted means and meteoric lines for GNIP stations in eastern Africa, together with the range of isotopic compositions typically measured in unmodified groundwaters.

The situation of Addis Ababa in the Ethiopian highlands at 2360 m asl (above sea level) makes it the highest altitude GNIP station in Africa, though some other stations adjacent to the East African Rift Valley lie above 2000 m and their records, though brief, appear more 'normal'.

Unmodified, apparently locally-recharged groundwaters from the floor of the Rift Valley in the general latitude of Addis Ababa have isotopic composition typically averaging about -2.0 ‰ $\delta^{18}\text{O}$ [5]. A typical altitude would be 1600 m asl. Addis Ababa is situated some 800 m higher than this, so if the usual altitude-isotope effect is operating then groundwaters in the Addis area should be more depleted than on the rift floor. The existence of typical altitude effects in the general region is indicated by data from the Dessie area on the edge of the highlands to the north, and from the Rift Valley in Kenya. Here, the weighted average of rainfall at the Kericho GNIP station is much closer to groundwater values (Fig 1 - Kenya).

The available data show that the usual altitude-isotope effects seem to apply to groundwater in Ethiopia. Why then is the rainfall weighted average more different from the groundwater average than is the case in the other eastern African examples? Three main options can be considered: the rainfall record is biased, or there is a strong selective recharge mechanism, or the rainfall of recent decades is in some way atypical of the norm. There is no particular reason to suspect the first of these; for example a delta-plot reveals no evidence of significant evaporative modification. The record is admittedly patchy in places, but weighted averages taken from the 1960s, 70s, 80s and 90s are all similar. Mechanisms for selective recharge are also not particularly obvious given that the fissured hard-rock aquifers of the Addis Ababa area are common elsewhere in Africa and do not appear to show strong isotopic selection effects. This leaves the third option, atypical rainfall. In terms of amount, the period 1965-90 saw a reduction of 8 % in wet-season rainfall over the north-central Ethiopian Highlands compared to the previous 25 years [6]. This may conceivably have caused some modification in isotopic content; groundwater tends to be a mixture of components with different residence times and will not necessarily react quickly to secular changes in rainfall isotope composition.

REFERENCES

- [1] SONNTAG, C., ROZANSKI, K., MUNNICH, K.O., JACOB, H., Variations of deuterium and oxygen-18 in continental precipitation and groundwater and their causes, in *Variations in the Global Water Budget*, ed A. Street-Perrot et al. (1983) 107-124.
- [2] ANDREWS, J.N., Isotopic composition of groundwaters and palaeoclimate at aquifer recharge, in *Isotope Techniques in the Study of Past and Current Environmental Changes in the Hydrosphere and the Atmosphere*, IAEA, Vienna (1993) 337-357.
- [3] ROZANSKI, K., ARAGUAS-ARAGUAS, L., GONFIANTINI R., Isotopic patterns in modern global precipitation, in *Climate Change in Continental Isotopic Records*, Geophysical Monograph 78, American Geophysical Union (1993) 1-36.
- [4] LAMB, A.L., LENG, M.J., LAMB, H.F., MOHAMMED UMER MOHAMMED, A 9000-year oxygen and carbon isotope record of hydrological change in a small Ethiopian crater lake, *The Holocene* **10** (2000) 161-171.
- [5] CRAIG, H., LUPTON, J.E., HOROWITZ, R.M., Isotopic geochemistry and hydrology of geothermal waters in the Ethiopian Rift Valley. Rep. of the Scripps Institute of Oceanography (1977) 77-14.
- [6] SELESHI, Y., DEMAREE, G., Identifying the major cause of the prevailing summer rainfall deficit over the north-central Ethiopian Highlands since the mid-60s, in *Tropical Climatology, Meteorology and Hydrology*, Eds G. Demaree et al., Brussels (1998) 516-531.

GAS CHROMATOGRAPHIC ISOLATION TECHNIQUE FOR COMPOUND-SPECIFIC RADIOCARBON ANALYSIS

M. UCHIDA, Y. KUMAMOTO

Japan Marine Science and Technology Center (JAMSTEC), Yokosuka, Japan

Y. SHIBATA, M. YONEDA, M. MORITA

National Institute for Environmental Studies (NIES), Tsukuba, Japan

K. KAWAMURA

Hokkaido University, Sapporo, Japan

We present here a gas chromatographic isolation technique for the compound-specific radiocarbon analysis of biomarkers from the marine sediments. The biomarkers of fatty acids, hydrocarbon and sterols were isolated with enough amount for radiocarbon analysis using a preparative capillary gas chromatograph (PCGC) system. The PCGC systems used here is composed of an HP 6890 GC with FID, a cooled injection system (CIS, Gerstel, Germany), a zero-dead-volume effluent splitter, and a cryogenic preparative collection device (PFC, Gerstel). For AMS analysis, we need to separate and recover sufficient quantity of target individual compounds ($>50 \mu\text{gC}$). Yields of target compounds from C_{14} n-alkanes to C_{40} to C_{30} n-alkanes and approximately that of 80% for higher molecular weights compounds more than C_{30} n-alkanes.

Compound specific radiocarbon analysis of organic compounds, as well as compound-specific stable isotope analysis, provide valuable information on the origins and carbon cycling in marine system. Above PCGC conditions, we applied compound-specific radiocarbon analysis to the marine sediments from western north Pacific, which showed the possibility of a useful chronology tool for estimating the age of sediment using organic matter in paleoceanographic study, in the area where enough amounts of planktonic foraminifera for radiocarbon analysis by accelerator mass spectrometry (AMS) are difficult to obtain due to dissolution of calcium carbonate.

NEW DEVELOPMENTS IN RADIOMETRICS AND MASS SPECTROMETRY METHODS FOR RADIONUCLIDE ANALYSIS OF ENVIRONMENTAL SAMPLES

P.P. POVINEC, J.J. LA ROSA, S.H. LEE, E. WYSE

International Atomic Energy Agency, Marine Environment Laboratory, Monaco

The radionuclide levels observed at present in the environment are very low, therefore high sensitive analytical systems are required for carrying out environmental investigations. One very important recent development in analytical techniques for low-level activity measurements is the production of large volume HPGe detectors (up to 200% relative efficiency to 75 mm diameter \times 75 mm long NaI (TI) crystals). Their high efficiency and excellent energy resolution permit the analyses of various gamma-emitters in composite samples selectively and very often non-destructively (e.g. in sea sediments).

However, this technique is restricted to gamma-emitters only (e.g. for ^7Be , ^{40}K , ^{54}Mn , ^{60}Co , ^{137}Cs , ^{210}Pb , etc.). Other radionuclides frequently found in the marine environment are the pure beta-emitters, like ^3H , ^{14}C , ^{32}Si , ^{32}P , ^{90}Sr , ^{241}Pu , etc., where mainly liquid scintillation counting has made great improvements in recent years. However, for some of these radionuclides mass spectrometry methods represent a real breakthrough in low-level counting, e.g. " ^3He in-growth" mass spectrometry for ^3H , or accelerator mass spectrometry (AMS) for ^{14}C .

Another important group of radionuclides in the marine environment is represented by alpha-emitters, both natural (like Ra, U and Th isotopes) as well as anthropogenic (like Pu and Am isotopes). These radionuclides have traditionally been analysed by semiconductor alpha-spectrometry (SAS). However, there were several limitations, e.g. in sensitivity, resolution and mass of samples used for analysis. Some of them have been partially overcome, e.g. the problems with resolution for analysis of ^{239}Pu and ^{240}Pu using high resolution alpha-spectrometers with suitable deconvolution software. It appears, however, that in the near future, Inductively Coupled Mass Spectrometry (ICPMS), Thermal Ionisation Mass Spectrometry (TIMS) or AMS will be more frequently used for analysis of long-lived alpha-emitters in the marine environment, as these methods eliminate all the above-mentioned problems.

In the present paper we discuss some recent developments in the radiometrics sector for the measurement of low-activity environmental samples and compare them where possible with results obtained by mass spectrometry methods. The presentation will focus on those aspects which are of great relevance for marine environmental change studies.

With the introduction of high resolution and high sensitive ICPMS it has been possible to analyse some of the long-lived radionuclides like ^{99}Tc , ^{129}I , ^{236}U , ^{239}Pu and ^{240}Pu with this technique. This was especially advantageous for reporting separate data for ^{239}Pu and ^{240}Pu and using their ratio for tracing the origin of plutonium in the environment.

Our work until now has concentrated on the analysis of ^{239}Pu , ^{240}Pu and ^{242}Pu in the marine environment. The samples for ICPMS analysis have been prepared either by leaching of electrodeposited plutonium from previously analysed stainless steel disks or by direct preparation of small volume samples using chromatographic resins. This is actually another great advantage of ICPMS that sample volumes can be significantly reduced, e.g. in the case

of seawater from a few hundreds of litres to about a few litres. Both, sample preparation and ICPMS measurements were carried out at IAEA-MEL.

AMS has been widely used as a powerful tool for analysis of long-lived radionuclides (mainly ^{14}C and ^{129}I) in the marine environment. Both radionuclides are important radioactive tracers which have been artificially introduced into the oceans. Small amounts of ^{14}C and ^{129}I can be easily measured by AMS on mg-size samples of carbon and iodine extracted from 500 ml seawater samples. The high analytical sensitivity offered by AMS enables to find even tracer amounts of ^{14}C and ^{129}I which could be released from nuclear installations or stored/dumped radioactive wastes, and to compare the measured levels with the global distribution of these radionuclides. Recently, however, AMS techniques have been developed to analyse other important long-lived radionuclides in the environment like ^{10}Be , ^{36}Cl , ^{99}Tc , uranium and plutonium isotopes. The new techniques open fresh possibilities of their application in marine radioactivity studies as well. It is clear that AMS has become the most powerful technique, although for many laboratories its availability is still a problem. It is believed, however, that in perspective, AMS will be the dominant technique used for the analysis of long-lived radionuclides in the marine environment.

IAEA-MEL in the framework of marine radioactivity studies has participated in several expeditions to the Atlantic, Arctic, Indian and Pacific Oceans to sample seawater, biota and sediment. The expeditions covered a wide range of marine radioactivity surveys to study the distribution of key radionuclides (^3H , ^{14}C , ^{90}Sr , ^{129}I , ^{137}Cs , U, Pu and Am isotopes) in the world oceans and any changes in their concentrations for marine radioactivity assessments and environmental change. We shall discuss in more detail the analysis of ^{239}Pu , ^{240}Pu and ^{242}Pu in marine samples and in IAEA reference materials. The samples for AMS analyses were prepared either by leaching of electrodeposited plutonium from previously analysed stainless disks or by direct preparation of small volume samples using EICHRON resins. The reduction in sample size by a factor of 100 (e.g. in the case of analysis of seawater samples) is another great advantage of AMS over conventional SAS.

A comparison of Pu results obtained by ICPMS, AMS and SAS will be discussed in detail. It will be seen that a reasonably good agreement has been obtained between all three methods. The relative precision of Pu results as obtained until now by SAS, AMS and ICPMS was 5%, 10% and 7%, respectively (for $^{239,240}\text{Pu}$). The evaluations show, however, that from the point of view of sensitivity, ICPMS and AMS have detection limits lower by a factor of 10 than SAS.

A comparison of detection limits for several long-lived radionuclides as obtained by radiometrics (RM), ICPMS, TIMS and AMS techniques will be discussed as well. It will be seen that the most sensitive technique is AMS which gives the lowest detection limits, with the exception of ^3H , three to eight orders of magnitude lower than the RM methods.

CASPIAN SEA WATER BALANCE AND DYNAMICS STUDIES USING ANTHROPOGENIC RADIONUCLIDES: IMPLICATIONS FOR ENVIRONMENTAL CHANGES

B. OREGIONI, J. GASTAUD, M.K. PHAM, P.P. POVINEC

International Atomic Energy Agency, Marine Environment Laboratory, Monaco

Environmental changes in the Caspian Sea have recently become of great interest in connection with fluctuations in sea level changes. Radioactive and stable isotopes have been used as powerful tracers to investigate water balance and dynamics and have contributed significantly to understanding climatically driven environmental changes in the Caspian Sea [1].

The Caspian Sea is the world largest inland water body with a surface area of about 386000 km² and a volume of about 67000 km³, located in a large continental depression about 28 m below sea level. With no surface outlet, the Caspian Sea is particularly sensitive to climatic variations. The drainage area of the Caspian Sea is approximately 3.7 million square kilometers. The Volga, Ural and Terek empty into the North Caspian, with their combined annual flow accounting for 88% of all water entering the sea. The Sulak, Samur, Kura and a number of small rivers contribute about 7% of the inflow, the remainder comes from the rivers of the Iranian shore [2].

The Caspian Sea is divided into three basins with approximately the same surface [3]. The North Caspian Basin, maximum depth 15 m, average depth 5 m, contains 1% of the total water. The Middle Caspian (or Central) Basin has a maximum depth of 800 m and contains 22% of the total water. The South Caspian Basin, maximum depth 1024 m, average depth 330 m, contains 77% of the total Caspian Sea water.

Recently there have been concerns over the environmental conditions of the Caspian Sea, especially over observed sea level changes, which have had a strong impact on the region. Anthropogenic radionuclides like ⁹⁰Sr, ¹³⁷Cs and ^{239,240}Pu are particularly useful tracers for the investigation of water dynamics.

Two research-training cruises were carried out in September 1995 and August-September 1996. At every station, 60-70 liters samples of seawater from different depths were processed for sequential separation of plutonium, cesium and strontium isotopes. This was done by adjusting the acidity of the water and then adding yield determinants (⁸⁵Sr, ²⁴²Pu and ¹³⁴Cs) and chemical carriers. The transuranics were coprecipitated with MnO₂. The pH of the supernatant was adjusted and the cesium was coprecipitated with AMP. In the final step, strontium was precipitated as oxalate. Further purification and radiometric measurements of the samples were completed at IAEA-MEL, Monaco.

For the whole Caspian Sea, the mean ⁹⁰Sr activities found in the 1995 and 1996 cruise surface water samples were respectively 8.0±1.6 mBq/L and 7.5±0.4 mBq/L. No significant trend was observed. Concerning ¹³⁷Cs, the mean activities of 6.3±0.4 mBq/L in 1995 and 5.2±1.0 mBq/L in 1996 did not show any variation over the whole Sea. For ^{239,240}Pu, the activities in 1996 showed a clear tendency to decrease from north to south with average values as follows: North Basin 8.0±0.8 µBq/L, Central Basin 6.8±1.7 µBq/L, Sill 6.8±0.8 µBq/L, and South Basin 4.4±1.3 µBq/L. This trend was not observed in the 1995 cruise data whose mean concentration was 5.0±0.4 µBq/L.

In the two main basins, the Central and South Basins, the behavior of $^{239,240}\text{Pu}$, ^{90}Sr and ^{137}Cs seem quite different. The concentration level of strontium in the water mass which appears to be higher than expected from global fallout could be a result of a significant contribution from land remobilization and river run-off. The excess of strontium is shown by the lower ratios of $^{239,240}\text{Pu}/^{90}\text{Sr}$ and $^{137}\text{Cs}/^{90}\text{Sr}$. In the Central Basin, the similar vertical distribution along the water mass is probably due to the fast transport of surface water to greater depths. Cesium concentrations are in agreement with the level expected from global fallout. The similar trend at same water depths for strontium and cesium demonstrate typical behavior for these conservative fallout radionuclides, which move essentially in true solution. In the central and south Caspian Sea, the leading role in the exchanges between the upper and lower layers of seawater is played by the processes of convective mixing. The intensive cooling and salinisation in the North Caspian Basin during ice formation result in high water density that allows sinking into the deepest part of the Central Caspian depression. $^{239,240}\text{Pu}$ delivered by fallout to surface water decreased from the North Basin to the South Basin and penetrated to deeper water as expected for this particle reactive element. The concentrations at intermediate depths of the Central Basin are higher than in the South Basin. The particulate concentration and the transport of the water mass between the two main basins may be explained by these data: the lower temperature and higher salinity at a given depth in the Central Basin as compared to the South Basin, facilitate the horizontal transport of water from the Central Basin over the sills into the South Basin where this water drops down to approximately 400 m.

REFERENCES

- [1] FROELICH, K., ROZANSKI, K., POVINEC, P., OREGIONI, B., GASTAUD, J., Isotope studies in the Caspian Sea, *The Science of the Total Environment* **237/238** (1999) 419-427.
- [2] RODIONOV, S.N., Global and regional climate interaction: The Caspian Sea experience, *Water Science and Technology Library* (1994) 207 pp.
- [3] VALI-KHODJEINI, A., Hydrology of the Caspian Sea and its problems, *Proceedings of the Vienna Symposium, IAHS publ.* **206** (1994) 45-54.

ARABIAN SEA GEOSECS STATIONS REVISITED: TRACER-DEPTH PROFILES REVEAL TEMPORAL VARIATIONS?

S. MULSOW, P.P. POVINEC

International Atomic Energy Agency, Marine Environment Laboratory, Monaco

B.L.K. SOMAYAJULU

Physical Research Laboratory, Navrangpura, Ahmedabad, India

In March-April 1998, the Physical Research Laboratory and the Regional Research Laboratory (Ahmedabad, India) together with the IAEA Marine Environment Laboratory, Monaco, participated in the research mission to visit GEOSECS (Geochemical Ocean Sections Study) stations in the Arabian Sea. The main objective was to reoccupy these stations which were sampled in the early seventies to observe possible time variations in trace behaviour in this region.

It is generally accepted that both natural (climate variations) and anthropogenic (greenhouse effect) changes can cause modifications of the oceanic characteristics and properties of deep waters on yearly and decadal scales [1]. For long time-scales (100 to 1000 years) one needs to look at the sediments where these changes are subtly recorded. Tracers such as ^{14}C and ^3H (deep waters) and ^{228}Ra surface waters are useful markers of water circulation patterns and changes. Also man-made radiotracers such as ^{90}Sr , ^{137}Cs , ^{99}Tc , ^{238}Pu , $^{239,240}\text{Pu}$ and ^{241}Am , can give information on air-sea exchange as well as penetration (vertical change) rates in the open ocean [2].

We visited GEOSECS stations 415 to 419. In each station, CTD profiles, ^3H , ^{14}C , ^{90}Sr , ^{137}Cs , Pu and Am profiles, nutrients, Be, TOC and oxygen were determined from surface to bottom. Also uranium and trace elements were sampled in function of the oxygen minimum zone. In this paper we report the findings on the physical properties as well as the variations in water circulation patterns and also vertical exchange rates in the Arabian Sea.

PSU profiles collected in this mission compared with those PSU profiles measured in 1974 (GEOSECS) showed marked differences in those stations located in the southeast part of the Arabian Sea (Fig. 1). In contrast, those located more towards the north (415-416) showed little temporal variation. We think these changes may be real given that the PSU values at depth are comparable and reflect the presence of deep Antarctic bottom waters in this region.

After examining vertical variations in the water column in this region, we could compare our ^{137}Cs and ^3H data (Fig. 2) with GEOSECS data. In both cases some changes were discovered over the 15 year interval. We found that at the three stations there appears to be a net outflow of water masses from the Arabian Sea to the Southern Ocean.

This observation is particularly true for surface waters down to 100-200 m and deeper at GEOSECS station 416. We have also found a similar pattern with ^3H vertical profiles (not shown here). Possible temporal variations regarding oceanographic settings due to climate changes and/or anthropogenic changes such as global warming will be further discussed in more detail.

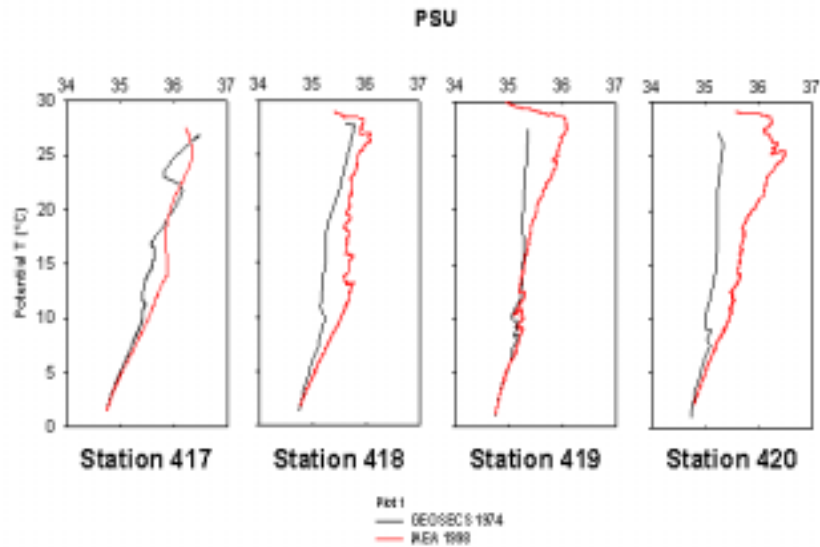


FIG. 1. PSU vertical profiles measured at 4 GEOSEC stations. The profiles are comparable and the differences may reflect temporal variations while sampling during 1974 (GEOSECS) and 1998 (this study).

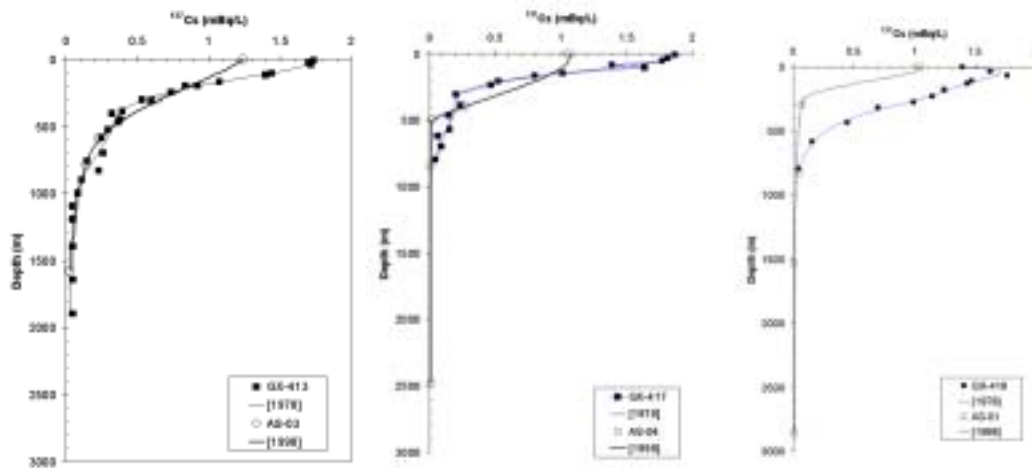


FIG. 2. ^{137}Cs depth profiles of some of the revisited stations. All data have been decay corrected to April 1, 1998. The biggest differences are between 0-200 m. At depth, the values are similar.

REFERENCES

- [1] BACON M.P. Tracers of chemical scavenging in the ocean: boundary effects and large-scale chemical fractionation. Phil. Trans. R. Soc. Lond. (1980) A 325:147-160.
- [2] LIVINGSTON, H.D. The use of Cs and Sr isotopes as tracers in the Arctic Mediterranean Seas. Phil. Trans. R. Soc. Lond. (1980) A 325: 161-176.

TEMPORAL VARIATIONS OF RADIONUCLIDES IN THE PRECIPITATION OVER MONACO

S.H. LEE, M.K. PHAM, P.P. POVINEC

International Atomic Energy Agency, Marine Environment Laboratory, Monaco

Monthly precipitation (total deposition: wet+dry) has been collected to determine the concentration of radionuclides by IAEA-MEL in Monaco. The objectives of this study are to understand radionuclide behaviour in the air according to annual weather conditions as well as to detect any irregularities in the concentration of radionuclides resulting from probable new releases. Higher activities and deposition rates of anthropogenic radionuclides such as $^{239,240}\text{Pu}$, ^{241}Am and ^{137}Cs as well as cosmogenic ^7Be in rain have appeared in the autumn period due to local meteorological conditions and the amount of precipitation rather than in a spring peak by contribution of stratospheric-tropospheric air mixing [1] as documented in previous studies (Fig. 1). Generally, $^{238}\text{Pu}/^{239,240}\text{Pu}$ and $^{241}\text{Am}/^{239,240}\text{Pu}$ ratios agree well with the global fallout ratios of the northern hemisphere, however, a few data on $^{238}\text{Pu}/^{239,240}\text{Pu}$ showed higher ratios. Since the mid 1980's, the annual depositions of $^{239,240}\text{Pu}$ estimated at 35-45° N have not shown any exponential decreasing trend as in previous studies [2]; they are in the range of 6-17 mBq m⁻² year⁻¹. This may suggest that the present Pu fallout originates from resuspension of Pu from soil due to gardening and wind transport. Monthly deposition rates vary throughout the year in a similar way to the precipitation rate (Fig. 2). The estimated average deposition rate of $^{239,240}\text{Pu}$, (16.5 ± 0.4) mBq m⁻² year⁻¹, compensates for about 4% of the mean annual Pu loss in the water column of the Mediterranean Sea as derived from experiments with particle traps [4].

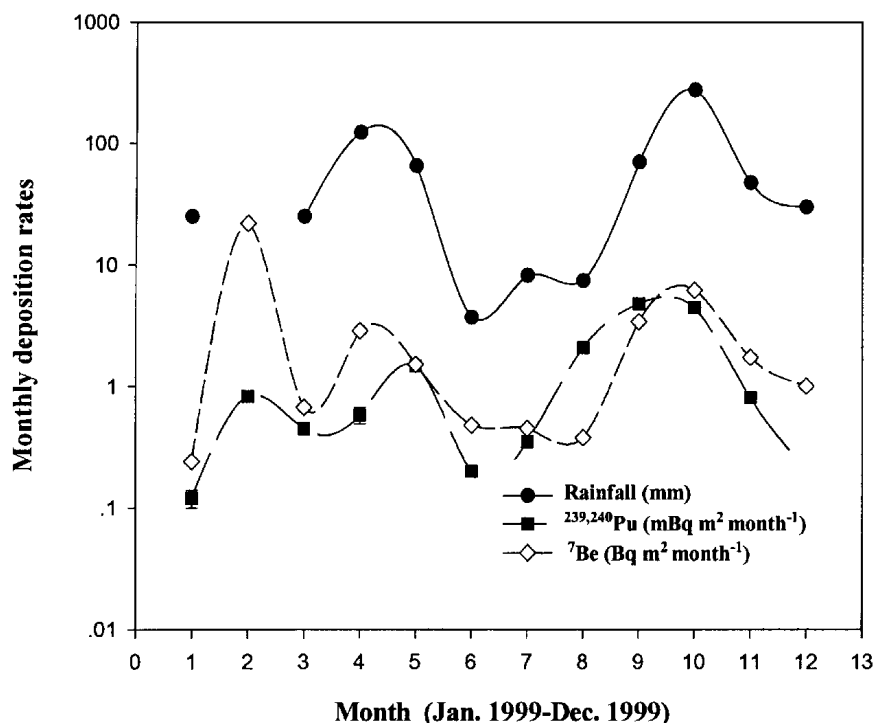


FIG. 1. Monthly deposition of $^{239,240}\text{Pu}$ and ^7Be with rainfall.

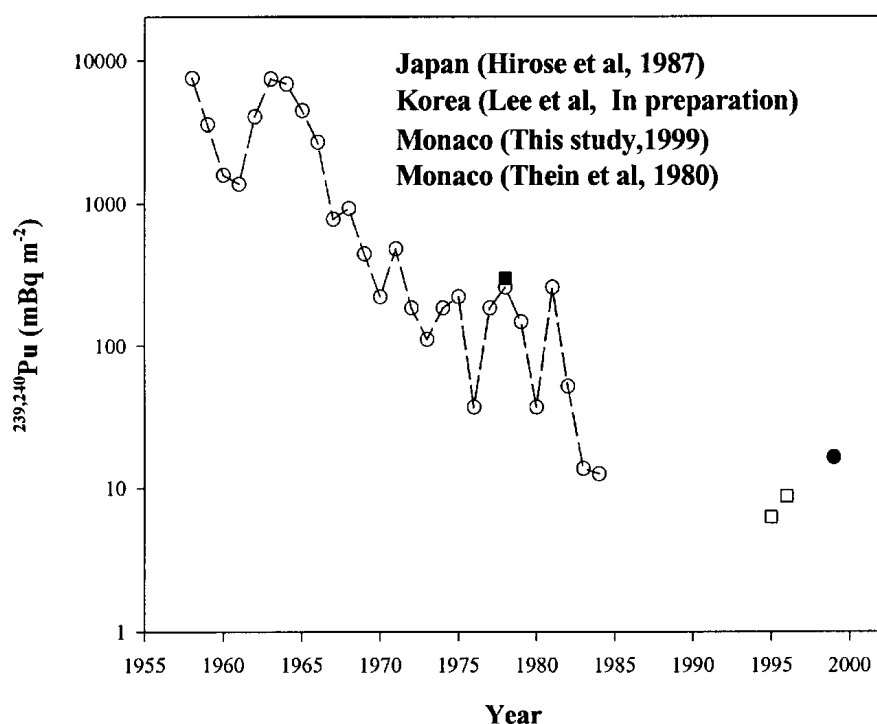


FIG. 2. Annual deposition of fallout $^{239,240}\text{Pu}$ estimated in the 35-45 N.

REFERENCES

- [1] HIROSE K, AOYAMA, M., KATSURAGI, Y. SUGIMURA, Y., Annual deposition of ^{90}Sr , ^{137}Cs and $^{239,240}\text{Pu}$ from the 1961-1980 nuclear explosions: A simple model. J. of Meteor. Soc. Japan (1987) **65** (2), 259-277.
- [2] LEE, S.-H, CHUNG, S., KIM, S.-K., HONG, G.-H., LEE, K.-W., Atmospheric deposition and soil inventory of Pu isotopes in the mid-western part of the Korean Peninsula (in preparation).
- [3] THEN, M., BALLESTRA, S., YAMATO, A., FUKAI, R., Delivery of transuranic elements by rain to the Mediterranean Sea. Geochim et Cosmochimica Acta (1980) Vol.44, 1091-1097.
- [4] FOWLER S.W., NOSHKIN, V.E., LA ROSA, J.J., GASTAUD, J., Temporal variations in plutonium and americium inventories and their relation to vertical transport in the northwestern Mediterranean Sea. Limnol. Oceanogr. (2000) **45** (2), 446-458.

WATER PROFILE TIME SERIES OF ^{90}Sr , ^{137}Cs AND $^{239,240}\text{Pu}$ IN THE NW PACIFIC OCEAN

T. ITO, H.D. LIVINGSTON, P.P. POVINEC

International Atomic Energy Agency, Marine Environment Laboratory, Monaco

The Pacific Ocean is a major repository of anthropogenic radionuclides released from atmospheric tests of nuclear weapons. Both global fallout from radionuclides released to the stratosphere as well as close-in fallout from the troposphere contributed to the present levels of radionuclides in seawater of the Pacific Ocean. On the other hand, these radionuclides are powerful tracer tools providing basic insights into a variety of oceanic processes and environmental change. The changing behaviour of ^{90}Sr , ^{137}Cs and $^{239,240}\text{Pu}$ in the NW Pacific Ocean between 1973 and 1997 (over the last 24 years) has been followed through time-series observations at several locations.

Figure 1 shows profiles of ^{90}Sr , ^{137}Cs and $^{239,240}\text{Pu}$ in water columns of the central NW Pacific Ocean at GEOSECS (1973), Knorr (1978), Hakuho Maru (1982) and IAEA (1997) stations [1, 2]. It is clear that after 24 years, the sub-surface maximum has become smaller; a decrease of 20%, and has moved to deeper water layers, from 500 m to 720 m. In the profiles of ^{90}Sr and ^{137}Cs , it should be noted that, in the upper 1000 m, the decline in the nuclide maxima and inventories is similar to the Pu changes. This would point to the conclusion that at least a major part of the observed $^{239,240}\text{Pu}$ changes over time was in response to physical circulation in the upper water column which brought water masses bearing significantly lower levels of fallout nuclides advectively into the region, although our initial view of these changes was that they were caused by $^{239,240}\text{Pu}$ association with sunken particle fluxes.

On the basis of all available $^{239,240}\text{Pu}$ data for the central NW Pacific Ocean (between 20° - 40° N and 135° - 175° E) in the GLOMARD database, a dependence of the position of the sub-surface maximum in the water column on time has been worked out [3]. The $^{239,240}\text{Pu}$ maximum moves downward in the water column reaching a double depth in about 40 years. A decrease in the maximum $^{239,240}\text{Pu}$ concentration observed at the central NW Pacific stations with time confirms this. The rate of change in the water column to a half value is estimated to be 22 ± 8 years. A change of $^{239,240}\text{Pu}$ inventories in the water column with time has been evaluated for the total water depth between 5000 and 6000 m using data stored in the GLOMARD. The averaged data show that the $^{239,240}\text{Pu}$ inventory in water is slowly decreasing with time from about 130 Bq/m^2 to 100 Bq/m^2 . The rate of decrease of the Pu inventory with time by a factor of two was estimated to be at about 50 years. However it is necessary to keep in mind the physical process changes mentioned earlier [4].

REFERENCES

- [1] BOWEN, V.T., NOSHOKIN, V.E., LIVINGSTON, H.D., VOLCHOK, H.L., Fallout Radionuclides in the Pacific Ocean; Vertical and Horizontal Distributions, Largely from GEOSECS Stations. *Earth Planet Sci. Lett.* **49** (1980) 411-434.
- [2] LIVINGSTON, H. D, Fallout Plutonium in Western North Pacific Sediment. IAEA-TECDOC-368, International Atomic Energy Agency, Vienna (1986).
- [3] INTERNATIONAL ATOMIC ENERGY AGENCY, Global Marine Radioactivity Database (GLOMARD). IAEA-TECDOC-1146, Vienna (2000).
- [4] LIVINGSTON, H.D., POVINEC, P.P., ITO, T., TOGAWA, O., The behaviour of plutonium in the Pacific Ocean. *Environmental Radioactivity* (in press).

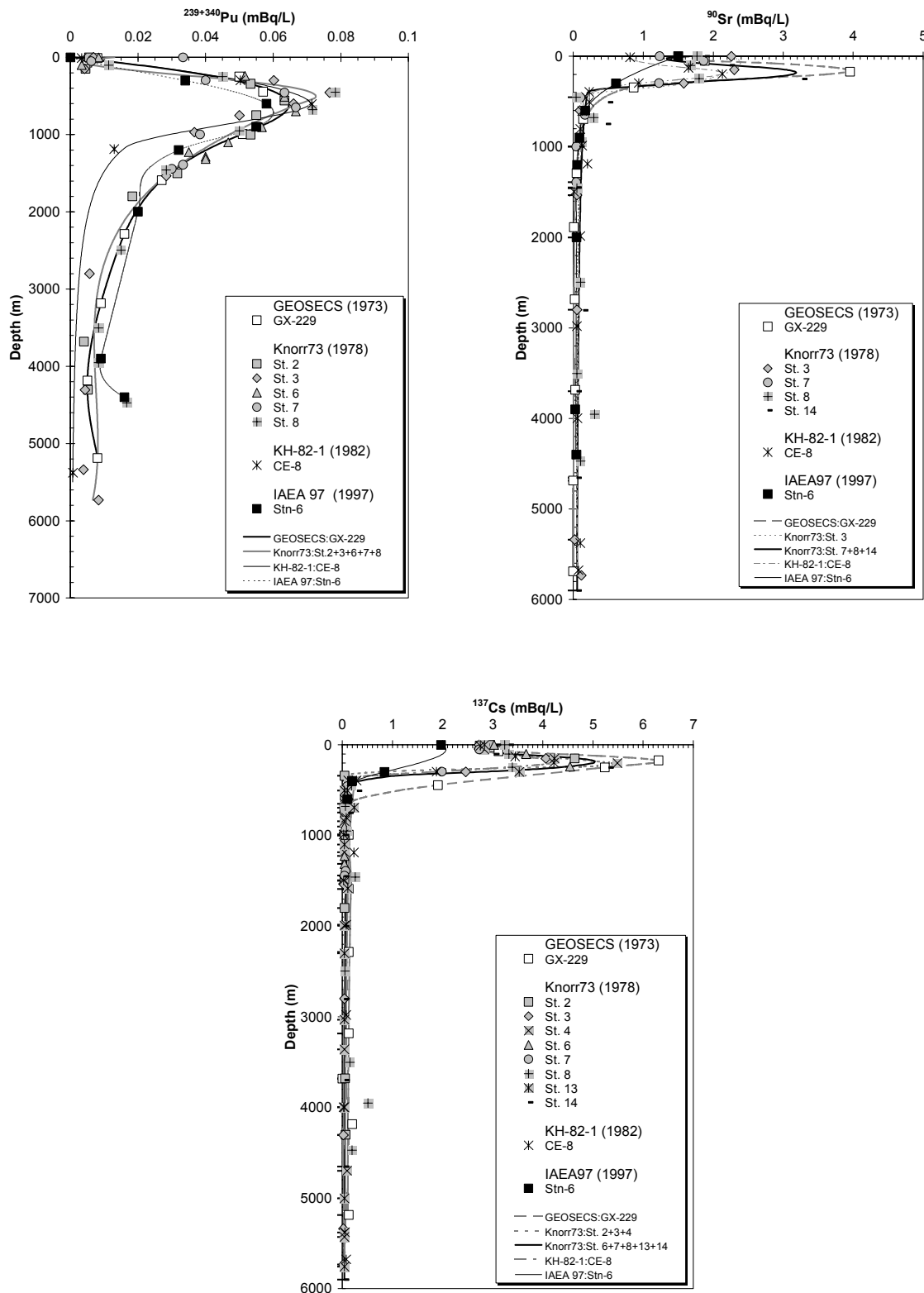


FIG. 1. $^{239,240}\text{Pu}$, ^{90}Sr , and ^{137}Cs profiles in the water column of the GEOSECS, Knorr, Hakuho Maru and IAEA stations in the central NW Pacific Ocean. All ^{90}Sr and ^{137}Cs data have been decay corrected to 1 January 1997.

CORALS – ISOTOPIC ARCHIVES OF MARINE ENVIRONMENTAL CHANGE

P.P. POVINEC, J. GASTAUD

International Atomic Energy Agency, Marine Environment Laboratory, Monaco

A. SIVO

Comenius University, Department of Nuclear Physics, Bratislava, Slovakia

Corals have been used in the past as important indicators for environmental change. It has been documented that, especially for studies of radiocarbon variations in the marine environment, they preserve records of radiocarbon concentrations in seawater during their growth. In the same way as rings on tree trunks are used in terrestrial environmental studies, the bands on corals can be used for detecting the annual concentrations of radiocarbon, stable carbon isotopes, as well as other stable and radioactive isotopes.

In the present work, the results of analysis of carbon isotopes, as well as ^{60}Co , $^{239,240}\text{Pu}$ and ^{241}Am in annual coral samples taken from corals collected in Mururoa and Fangataufa lagoons will be presented. As both atolls have been the sites of nuclear weapons testing, elevated radionuclide concentrations were observed (see Figs 1 and 2). The possible transport of radionuclides between annual coral layers, which could have an important impact on climatological studies using corals, will be discussed in more detail.

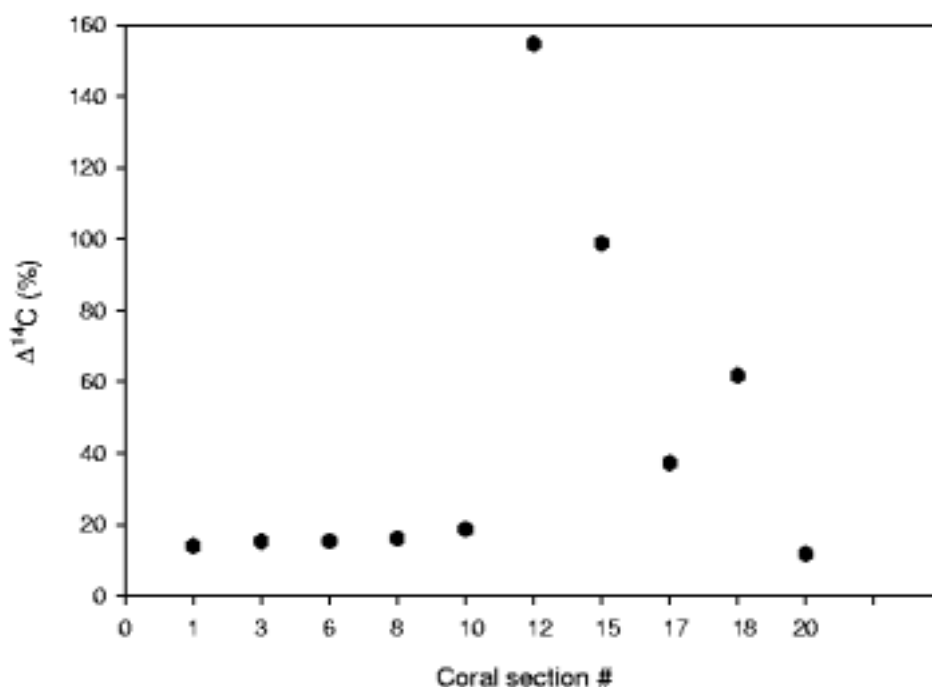


FIG. 1. $\Delta^{14}\text{C}$ in the Fangataufa coral sample.

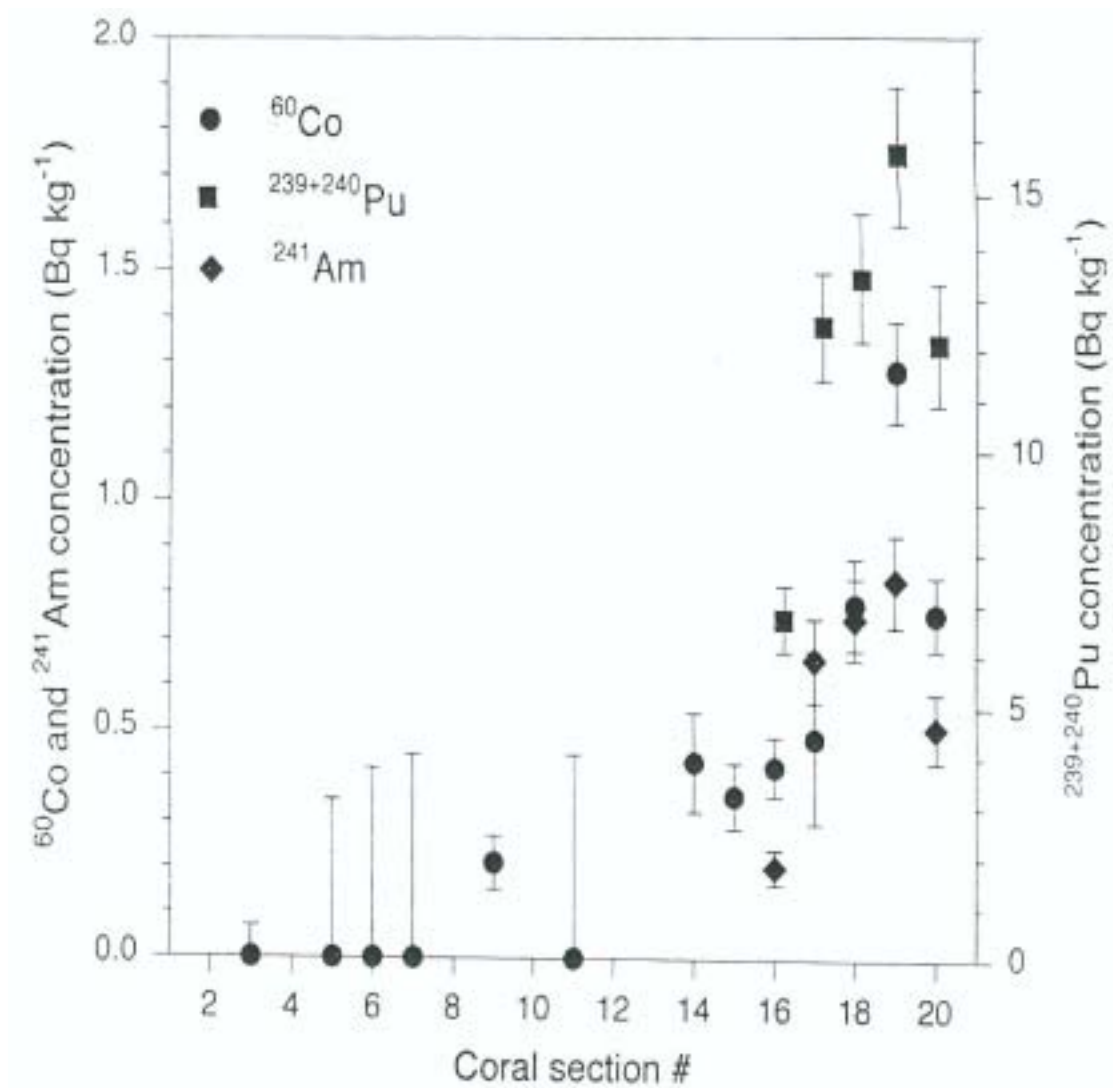


FIG. 2. Concentration of ^{60}Co , $^{239,240}\text{Pu}$ and ^{241}Am in the Fangataufa coral sample.

PALAEOTEMPERATURE CONDITIONS FOR THE SOUTHWEST OF WESTERN AUSTRALIA FROM THE STABLE ISOTOPIC COMPOSITION OF DEEP, CONFINED GROUNDWATER WITHIN THE PERTH BASIN

J.V. TURNER

CSIRO Land and Water, Perth, Western Australia, Australia

P.M. THORPE

Water & Rivers Commission, Perth, Western Australia, Australia

Two major confined aquifers occur within the upper 3000 m of the sedimentary sequence forming the Perth Basin located in the south-west coastal margin of Western Australia. The aquifers comprise multi-layered sequences of interbedded sandstones, shales and siltstones and are an important groundwater resource for metropolitan Perth. Within the context of research into groundwater resource evaluation of the aquifers, undertaken by the Geological Survey of Western Australia [1], ^{14}C , $\delta^2\text{H}$ and $\delta^{18}\text{O}$ data on the deep groundwater were collected. Samples were obtained from nine east-west transects across the coastal plain, four transects in the Northern Perth Basin (A-D in Fig. 1) and five in the Southern Perth Basin. The most northerly transect in the Northern Perth basin is 70 km north of Perth while the most southerly is 50 km south of Perth [1]. The most northerly transect on the Southern Perth Basin is near Bunbury and the most southerly is at Karridale, giving a total north to south range for both basins of 300 km. The purpose of this paper is to investigate palaeoclimatic conditions based on isotopic data within the groundwater archive of the Perth Basin.

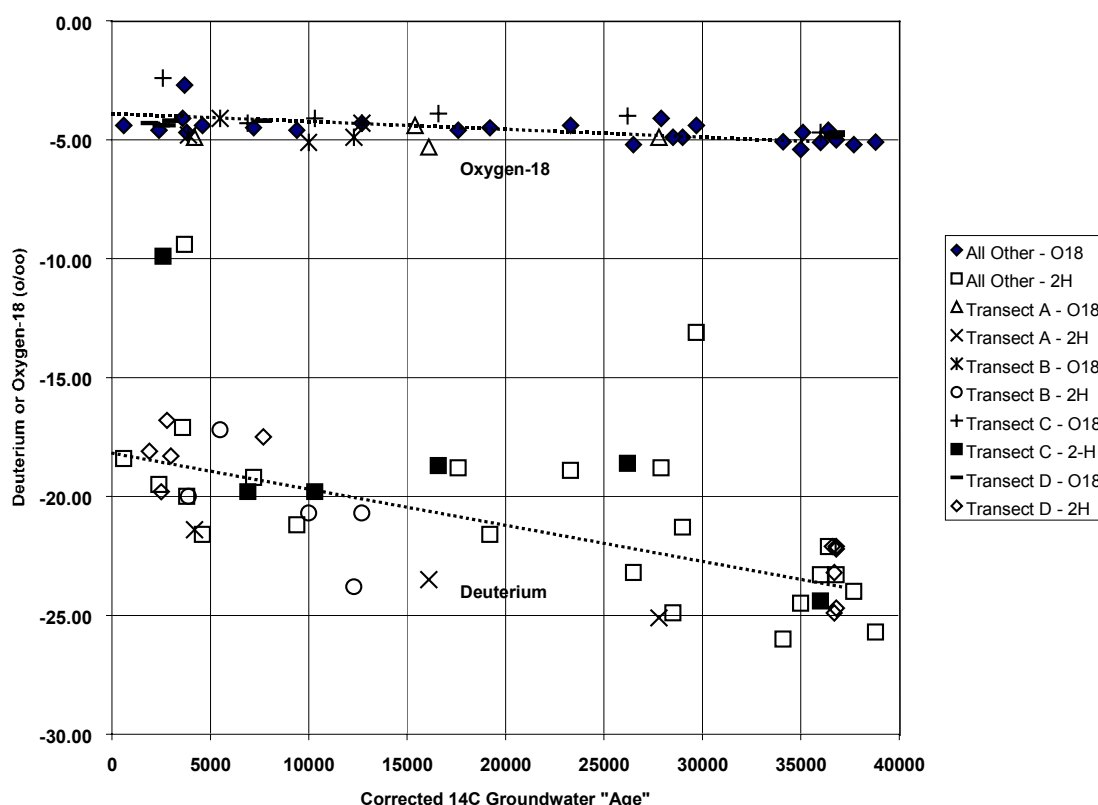


FIG. 1. $\delta^2\text{H}$ and $\delta^{18}\text{O}$ in groundwater from four transects (A, B, C, D) in the Perth Basin plotted against corrected ^{14}C groundwater age.

Results from a total of 151 deep drillholes are reported. The maximum depth from which groundwaters were obtained was 1600 m, with the majority of samples being obtained from depths between 100 and 800 m. The bore network allowed changes in ^{14}C age and stable isotope composition to be measured from the recharge area to discharge along regional east to west groundwater flow paths that range between 30 to 90 km in length [1].

Direct palaeoclimatic evidence for the coastal region of south-west Western Australia is very limited [2,3]. Stable isotope data from the deep confined aquifers provides an important method for obtaining information on palaeotemperature conditions prevailing at the time of recharge. Accordingly, the stable isotope and ^{14}C data are evaluated in terms of the palaeotemperature conditions that prevailed during the period of recharge. Carbon-14 data were used to estimate aquifer parameters and results show a range of ages from modern up to the practical limit of the ^{14}C method, i.e. about 36,000 years. The span of ^{14}C ages is such that some confined aquifer groundwaters would have been recharged during the Holocene and late Pleistocene glacial maximum. This range of groundwater residence times also spans the southern hemisphere temperature minimum considered to have occurred at between 20,000 to 22,000 years BP [4].

Modern data on $\delta^2\text{H}$ and $\delta^{18}\text{O}$ in rainfall collected in Perth provide a comparative reference for the groundwater isotopic compositions. The amount weighted monthly mean $\delta^2\text{H}$ and $\delta^{18}\text{O}$ of rainfall collected between 1962 and 2000 are shown in Table I.

The measurements range between $\delta^{18}\text{O} = -3.85$ to -3.86 ‰ and $\delta^2\text{H} = -14.8$ to -17.4 ‰. The Meteoric Water Line for Perth rainfall is $\delta^2\text{H} = 7.15\delta^{18}\text{O} + 10.6$, determined from the CSIRO data only. Present-day shallow groundwater of the Swan Coastal Plain has an isotopic composition close to the amount weighted mean rainfall data shown in Table I. The $\delta^2\text{H}$ and $\delta^{18}\text{O}$ values of groundwater from the confined aquifers have been divided into four categories on the basis of their groundwater residence times estimated from carbon-14, as shown in Table I.

Table I. Average groundwater and rainfall $\delta^{18}\text{O}$ and $\delta^2\text{H}$ compositions from the Southern Perth Basin and the Perth Metropolitan area

Carbon-14 Age range (x1000 years)	Southern Perth Basin			Northern Perth Basin		
	n	$\delta^{18}\text{O}$	$\delta^2\text{H}$	n	$\delta^{18}\text{O}$	$\delta^2\text{H}$
0 – <10	43	-4.68 ± 0.4	-20.7 ± 1.9	17	-4.22 ± 0.6	-18.1 ± 3.3
10 – <20	16	-4.35 ± 0.4	-18.8 ± 3.3	9	-4.54 ± 0.4	-21.0 ± 1.8
20 – <30	18	-4.86 ± 0.4	-22.2 ± 2.4	7	-4.60 ± 0.4	-20.5 ± 3.8
30+	22	-4.90 ± 0.4	-22.5 ± 1.7	12	-4.92 ± 0.2	-23.8 ± 1.3
<u>Amount Weighted Perth Rainfall</u>						
IAEA (1962-1976)*	99	-3.86	-14.8			
(1973-1975)**	30	–	-17.1			
CSIRO (1983-2000)	165	-3.85	-17.4			

*[5], **[6]

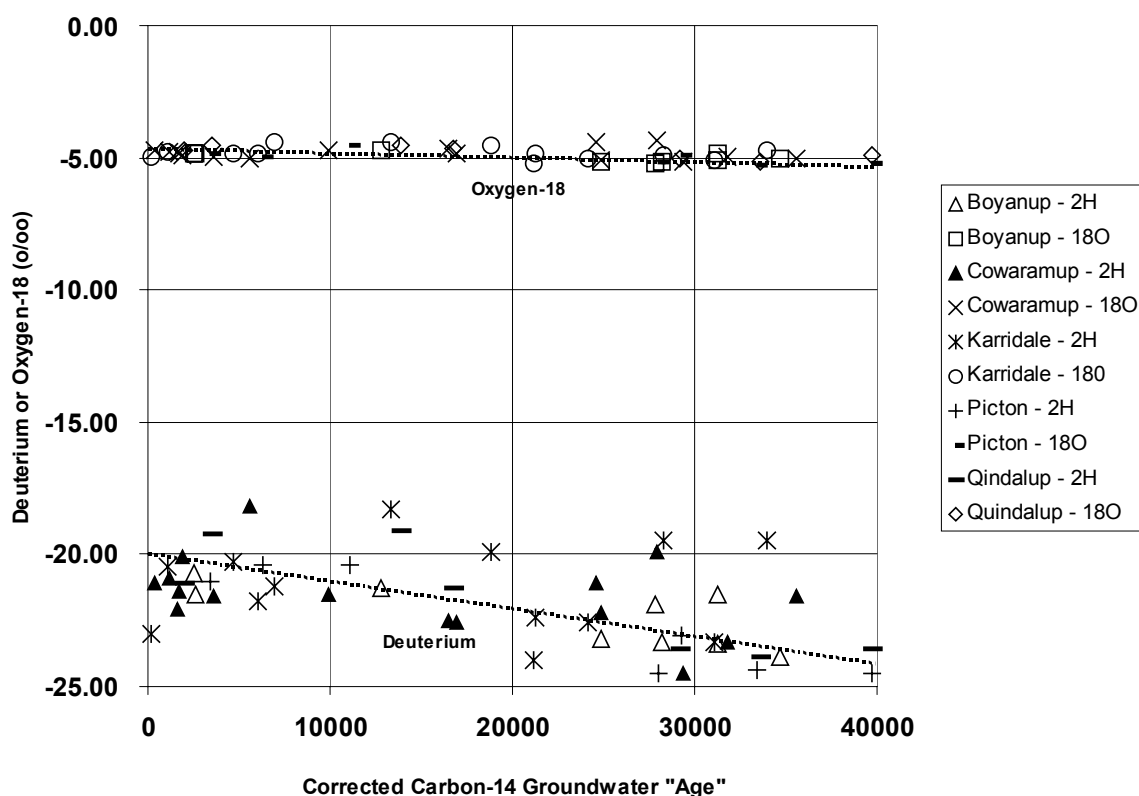


FIG. 2. $\delta^2\text{H}$ and $\delta^{18}\text{O}$ in groundwater from five transects (Boyanup Line, Picton Line, Quindalup Line, Cowaramup Line and the Karridale Line) in the Southern Perth Basin plotted against corrected ^{14}C groundwater age.

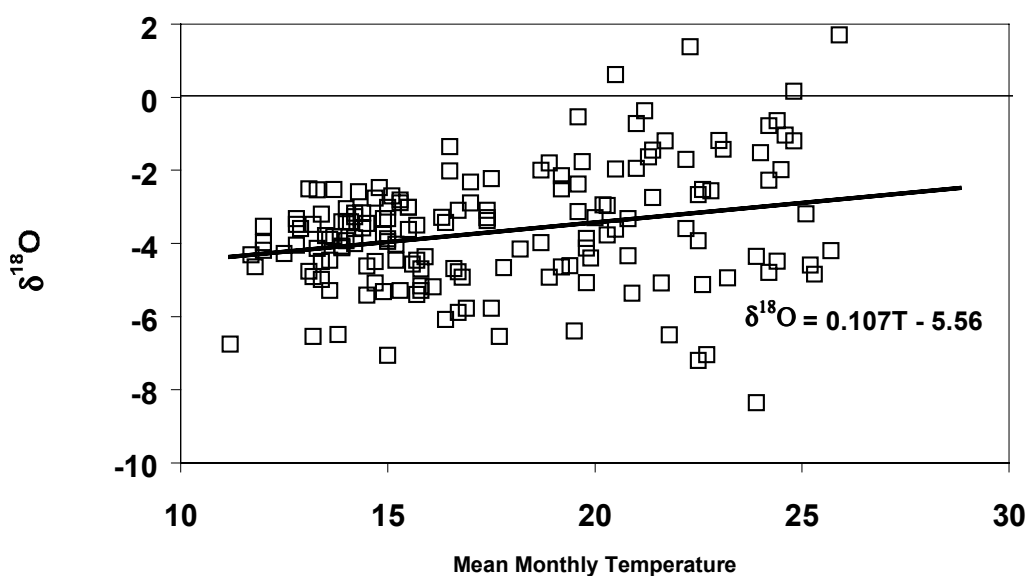


FIG. 3. The amount weighted monthly mean isotopic composition in Perth rainfall against mean monthly temperature.

The $\delta^{18}\text{O}$ of modern rainfall is enriched by a maximum of 1.1 ‰ compared to the measured groundwater values. For $\delta^2\text{H}$, the maximum enrichment is about 7‰. The trend of decreasing $\delta^2\text{H}$ and $\delta^{18}\text{O}$ compositions with increasing ^{14}C age can be seen in Fig. 1 for the Northern Perth basin and in Fig. 2 for the Southern Perth Basin.

In Table I and Figures 1 and 2, the trend of decreasing stable isotope composition is seen in both $\delta^{18}\text{O}$ and $\delta^2\text{H}$ but is most clear in the $\delta^2\text{H}$ data which decreases from about -18‰ to -25‰. On the basis of well-known correlations between the mean isotopic compositions of precipitation and temperature [7, 8] which indicate temperature effects of about 0.5‰/°C for $\delta^{18}\text{O}$ and about 5‰/°C for $\delta^2\text{H}$, we conclude that the groundwater data from the Perth Basin shows evidence for a slight increase in temperature of about 1°C over the past 30,000 years.

The small change in the $\delta^2\text{H}$ and $\delta^{18}\text{O}$ of groundwater may be due in part to moderation of the coastal temperature regime by the ocean in this near-coastal region. In addition, it may also be the result of a small decrease in the isotopic composition of the marine precipitation source which counteracts the temperature fractionation effect.

The principal source of present day precipitation is from water vapour in low pressure frontal systems that originate from the south west over the Indian Ocean. Fig. 3 shows the amount weighted monthly mean isotopic composition of precipitation from 1982 to 2000 in Perth rainfall. A weak trend due to the temperature effect is seen, however the increasing scatter in isotopic composition of rainfall in the warmer summer months indicates a mixed source of water vapour reflecting the influence of water vapour derived from tropical cyclone systems.

Since the stable isotopic composition of precipitation is dependent on the temperature difference between the source area and the location of the precipitation, the close proximity of the marine influence to the recharge location of the confined aquifers could be responsible for the lack of isotopic variation with increasing age. The continental effect is expected to be negligible over the short distances involved. A similar absence of significant change in $\delta^{18}\text{O}$ and $\delta^2\text{H}$ with increasing groundwater age was recorded in the east and central Australia within the Great Artesian Basin where groundwater residence times of up to 2 million years were observed [9,10].

A temperature difference of about 1-2°C from the LGM is estimated for the south west of Western Australia based upon the isotopic composition of the deep groundwater archive within the Northern Perth and Southern Perth Basins. The trend toward depleted stable isotope composition with increasing age is consistent across the nine groundwater transects that range over a north to south distance of 300 km along the Western Australian coastal plain.

The consistent trends found in the extensive isotopic data base shows that the groundwater reservoir contains a true palaeoclimatic signal.

The local on-shore trajectory of rainfall-bearing weather systems on the West Australian coast means that changes in the source of moisture or changes in the isotopic rainout effect are probably negligible and the isotope effects observed are true reflections of a temperature effect.

REFERENCES

- [1] THORPE, P.M., DAVIDSON, W.A., Groundwater age and hydrodynamics of the onfined aquifers, Perth, Western Australia. In Proceedings of the International Conference on Groundwater in Large Sedimentary Basins, Australian Water Resources Council Conference Series **20** (1990) 420-436.

- [2] WASSON, R.J., DONNELLY, T.H., Palaeoclimatic reconstructions for the last 30,000 years in Australia - A contribution to prediction of future climate. CSIRO Division of Water Resources, Technical Memorandum **91** (3) (1991) 48pp.
- [3] PICKETT, E.J., The late Pleistocene and Holocene vegetation history of three lacustrine sequences from the Swan Coastal Plain, southwestern Australia. PhD Thesis, Department of Geography, University of Western Australia, (1997), 266pp.
- [4] HARRISON, S.P., METCALF, S.E., STREET-PERROT, F.A., PITTOCK, A.B., ROBERTS, C.N., SALINGER, M.J., A climatic model of the last glacial/interglacial transition based on palaeotemperature and palaeohydrological evidence. In Proceedings of the SASQA International Symposium (1983) 19-34.
- [5] DANSGAARD, W., Stable isotopes in precipitation. *Tellus* **16** (1964) 438.
- [6] VAN DER STRAATEN, C.M., MOOK, W.G., Stable isotope composition of precipitation and climatic variability. In IAEA Panel Proceedings on Palaeoclimates and Palaeowaters: a collection of environmental isotope studies. (1983) 53-64.
- [7] Statistical treatment of environmental isotope data in precipitation, IAEA Technical Report Series **206** (1981).
- [8] HARTLEY, A.M., Deuterium/hydrogen ratios in Australian rainfall, *J.Hydrol.* **50** (1981) 217-229.
- [9] CALF, G.E., HABERMEHL, M.A., Isotope hydrology and hydrochemistry of the Great Artesian Basin, Australia. In *Isotope Hydrology, 1983*, IAEA Vienna (1984) 397-414.
- [10] RADKE, B.M., FERGUSON, J., CRESSWELL, R.G., RANSLEY, T.R., HABERMEHL, M.A., Hydrochemistry and implied hydrodynamics of the Cadna-owie – Hooray Aquifer, Great Artesian Basin, Australia. Bureau of Rural Sciences, Canberra (2000) 229pp.

A HIGH PRECISION MASS SPECTROMETRY METHOD FOR MEASURING O₂/N₂ RATIOS AND CO₂ CONCENTRATIONS IN AIR

A.D. MARCA, P.F. DENNIS, A. ETCHELLS

School of Environmental Sciences, University of East Anglia,
Norwich, United Kingdom

A full, detailed understanding of the global carbon budget is needed for robust modelling of global climate and environmental change. Since the industrial revolution the carbon cycle has been shifted from a steady state in which removal of CO₂ from the atmosphere through photosynthesis is balanced by its addition through respiration. Currently increased respiration due to deforestation, modern agricultural practises and the burning of fossil fuels dominates photosynthesis resulting in modern atmospheric CO₂ concentrations some 32% higher than the year 1800 levels. However, the CO₂ concentration rises are lower than expected from known fossil fuel combustion inventories. A significant proportion of the excess CO₂ is taken up by the oceans, however a missing carbon sink must still be invoked to account for the difference between measured and expected CO₂ rises. A global greening as a result of increased photosynthesis is required to close the circle.

An important new approach to characterising the global carbon cycle, and the role of photosynthesis in particular, is to accurately measure the changing concentration of oxygen in the atmosphere. Oxygen concentrations are effectively controlled by just two sinks and one source. During photosynthesis (source) and respiration (sink) there is an approximate one to one inverse relationship between oxygen and carbon dioxide. The combustion of the present day mix of fossil fuels (sink) requires the consumption of ca. 15 molecules of O₂ for each 10 molecules of CO₂ produced.

Thus by comparing the measured rate of O₂ decline with CO₂ increase, and that expected from the amount of fossil fuels consumed a direct estimate of global greening can be made. If less O₂ is disappearing than required for fossil fuel burning then the biosphere must be expanding and *vice versa* [1,2].

The long term changes in the oxygen concentration in air, however, are very small and on the order of just 5 ppmv, with larger ranges for the diurnal and seasonal cycles [2-4]. Useful measurements need to be made at a precision of 5 per meg or better, where the oxygen content of an air sample is referenced to a standard air:

$$\delta[O_2]_{per\ meg} = \left(\frac{[O_2]_{sam}}{[O_2]_{ref}} - 1 \right) \times 10^6$$

A precision of 5 per meg corresponds to a measurement of the oxygen concentration to better than 1ppmv. Keeling and Shertz [3] used a refractive index method to measure oxygen concentrations in air to better than 1ppmv. More recently Bender and co-workers [5] have used a modified dual inlet isotope ratio mass spectrometry method to measure the relative oxygen content in air to better than 5 per meg. The method involves measuring the molecular ratio of O₂ (mass 32) to ¹⁵N¹⁴N (mass 29).

Following on from this pioneering work, we present recent improvements in the use of a dual inlet isotope ratio mass spectrometer to allow routine, high precision measurements of the oxygen concentration in air. The analyser is based on a VG 602E, 6cm, 90° sector analyser. The collectors have been replaced with a purpose built triple collector allowing simultaneous collection of masses 28 ($^{14}\text{N}^{14}\text{N}$), 29 ($^{15}\text{N}^{14}\text{N}$) and 32 ($^{16}\text{O}^{16}\text{O}$). With peak jumping simultaneous monitoring of masses 40 (^{40}Ar) and 44 ($^{12}\text{C}^{16}\text{O}^{16}\text{O}$) is also possible. The dual inlet is of an all stainless steel construction using NUPRO diaphragm valves, 40mL variable volume bellows, and 1m long x 15 μm stainless capillaries.

The advantages of using the triple collector geometry is that (a) direct measurement of the 32/28 ratio is made using two high intensity beams thus maximising measurement precision; (b) measurement of the 29/28 ratio allows correction of the 28 signal for CO produced as a result of CO₂ breakdown in the source. Variations in the CO₂ content of samples by 10ppm produces a 1 per meg variation in the measured O₂/N₂ ratio [5]. Finally, by use of peak jumping and simultaneous measurement of the Ar (m/e =40) and CO₂ (m/e = 44) signals, and referencing to standards of known CO₂ concentration the absolute CO₂ levels can be measured to a precision on the order of 1-2 ppm in the same sample.

REFERENCES

- [1] KEELING, R.F., PIPPER, S.C., HEIMANN, M., *Nature* **381** (1996) 218-221.
- [2] BENDER, M. et al, *Global Biogeochemical Cycles* **10** (1996) 9-21.
- [3] KEELING, R.F., SHERTZ, S.R., *Nature* **358** (1992) 723-727.
- [4] KEELING, R.F. et al., *Global Biogeochemical Cycles* **7** (1993) 37-67.
- [5] BENDER, M. et al., *Geochim. Cosmochim. Acta.* **58** (1994) 4751-4768.

CLOSING REMARKS

Jihui Qian

Deputy Director General,
Department of Technical Co-operation,
International Atomic Energy Agency, Vienna

It is a pleasure for me to meet with you at the end of this timely, highly relevant conference on environmental change. In case you have not noticed, some of the environmental change issues that you have been working on, have also been in the headlines this week. Let me quote the cover of this week's edition of Time Magazine: "Global Warming: Climbing temperatures. Melting glaciers. Rising Seas. All over the planet we are feeling the heat. Happy Earth Day!"

While most people now accept that there is climate change both due to natural and human causes, it is often hard to understand the connection of the issue to their personal lives. National leaders and policy-makers, in turn, realize that actions must be taken, but in many cases feel that the scientific basis is not clear enough upon which to base sometimes costly actions.

Understanding the world's climate, its integrated hydrological, marine, climatic and terrestrial systems, is one of the most important issues and challenges of our time. The key knowledge for IAEA Member States is understanding the role that isotopic techniques can play in identifying pieces of the environmental change puzzle.

This makes your efforts to advance understanding and use of isotopic tools to investigate complex interactions of natural systems and the processes of environmental change all the more valuable. For this I commend your efforts. I ask you to continue to show where further work needs to be done; to point the way for taking action; and to develop new tools for monitoring and assessment.

The IAEA has a lead role in facilitating the development and dissemination of appropriate nuclear technologies for peaceful uses. While this has been largely a scientific and research based conference, I want to underline the importance of another important step, translating technology into a suitable framework for use in a development context, and its transfer to developing countries.

In this, I would like to challenge you as scientists, as leaders in the field of global change research, to also keep an important point in mind: how to translate your work to larger audiences and the community of interests in your respective countries and abroad.

Through its Technical Co-operation Programme, the IAEA has long worked to transfer mature technologies to its member states for, in particular, the evaluation, monitoring and assessment of environmental change and natural resources including freshwater, the marine environment and terrestrial ecosystems.

We foresee that the IAEA Member States will place increasing priority on natural resource management issues and seek the support of IAEA for acquiring the necessary tools, and perhaps more importantly, the human and institutional capacities to address pressing national natural resource management and environmental problems.

The IAEA has a special and unique role to play in this field: it has the capacity to facilitate the development, adaptation and validation of new techniques and scientific knowledge; and then transfer the products, to build technical competence in member states. Our current 2001–2002 TC programme, for example, has an increased number of activities to provide tools for freshwater management. We are in the process of identifying the nuclear and isotopic techniques that can help member states address key marine issues like coastal zone management.

In all of this, the IAEA is increasing its efforts to work with good partners, with both international organizations, as well as key national institutions, who can together, more effectively address these problems. You have been good partners this week.

In closing, I would like to thank you again for your excellent contributions. I would also like to ask you to continue your work, as well as to offer our continued partnership in the future for addressing these key issues of global relevance.

CHAIRPERSONS OF SESSIONS

Session 1	D.D. SOOD H.D. LIVINGSTON	IAEA IAEA
Session 2	R. GONFIANTINI W.M. EDMUNDS	Italy United Kingdom
Session 3	K. FRÖHLICH B.L.K. SOMAYAJULU	Germany India
Session 4	T.W.D. EDWARDS L.C.R. PESSEDA	Canada Brazil
Session 5	A. HENDERSON-SELLERS L.G. THOMPSON	Australia United States of America
Session 6	C. TUNIZ W. KUTSCHERA	Australia Austria
Session 7	M.H. THIEMENS N. YOSHIDA	United States of America Japan

SECRETARIAT OF THE CONFERENCE

P. AGGARWAL	Scientific Secretary
T. NIEDERMAYR	Symposium Organizer

LIST OF PARTICIPANTS

Albania

Fuga, P.
Academy of Sciences of Albania,
Fan S. Noli Square,
Tirana, Albania
Fax: +3554227476
EMail: pfuga@akad.edu.al

Australia

Child, D.
ANSTO,
Lucas Heights Sciences and Technology Centre,
New Illawara Road,
Lucas Heights, NSW 2234, Australia
Fax: +61297173257
EMail: david.child@ansto.gov.au

Henderson-Sellers, A.
Environment Division,
Australian Nuclear Science and Technology Organisation,
PMB 1, Menai, NSW 2234, Australia
Fax: +61297173599
EMail: ahssec@ansto.gov.au

McGuffie, K.
Department of Applied Physics,
University of Technology Sydney,
PO Box 123, Broadway NSW 2007, Australia
Fax: +6129514 2219
EMail: kendal.mcguffie@uts.edu.au

Tuniz, C.
The Permanent Mission of Australia to the
International Atomic Energy Agency,
Matiellistrasse 2-4/111, A-1040 Vienna, Austria
Fax: +4315041178
EMail: claudio.tuniz@dfat.gov.au

Austria

Benischke, R.
Joanneum Research,
Elisabethstrasse 16,
A-8010 Graz, Austria
Email: ralf.benischke@joanneum.at

Biasi, C.
Institute of Ecology and Conservation Biology,
University of Vienna,
Althanstrasse 14, A-1090 Vienna, Austria
Fax: +43142779542
EMail: c.biasi@pflaphy.pph.univie.ac.at

Bojar, A.-V.
Department of Geology and Paleontology,
Karl-Franzens University,
Heinrichstrasse 26, A-8010 Graz, Austria
Fax: +433163805580
EMail: ana-voica.bojar@kfunigraz.ac.at

- Hertenberger, G. Institute of Ecology and Conservation Biology,
University of Vienna,
Althanstrasse 14, A-1090 Vienna, Austria
Fax: +43142779542
EMail: ghertenb@pflaphy.pph.univie.ac.at
- Kaiser, A. Central Institute for Meteorology and Geodynamics,
Hohe Warte 38, A-1190 Vienna, Austria
Fax: +43136026
EMail: august.kaiser@zamg.ac.at
- Kralik, M. Umweltbundesamt Wien,
Spittelauer Lände 5, A-1090 Vienna, Austria
Fax: +43131304-3520
EMail: kralik@ubavie.gv.at
- Kutschera, W. Vienna Environmental Research Accelerator (VERA),
Institute for Isotope Research and Nuclear Physics,
University of Vienna,
Währingerstrasse 17, A-1090 Vienna, Austria
Fax: +43142779517
EMail: walter.kutschera@univie.ac.at
- Maringer, S. Institute of Ecology and Conservation Biology,
University of Vienna,
Althanstrasse 14, A-1090 Vienna, Austria
Fax: +43142779542
EMail: smaring@pflaphy.pph.univie.ac.at
- Papesch, W. Österreichisches Forschungs-und Prüfzentrum Arsenal GmbH,
Faradaygasse 3,
Postfach 8, A-1030 Vienna, Austria
Fax: +43505506587
EMail: papesch.w@arsenal.ac.at
- Rank, D. Österreichisches Forschungs-und Prüfzentrum Arsenal GmbH,
Faradaygasse 3,
Postfach 8, A-1030 Vienna, Austria
Fax: +43505506587
EMail: rank.d@arsenal.ac.at
- Richter, A. Institute of Ecology and Conservation Biology,
University of Vienna,
Althanstrasse 14, A-1090 Vienna, Austria
Fax: +43142779542
EMail: andreas.richter@univie.ac.at
- Scheifinger, H. Central Institute for Meteorology and Geodynamics,
Hohe Warte 38, A-1190 Vienna, Austria
Fax: 4313602676
- Spötl, C. Institut Geologie und Paläontologie,
Universität Innsbruck,
Innrain 52, A-6020 Innsbruck, Austria
Fax: +435125072914
EMail: christoph.spoetl@u:bk.ac.at

- Tesch, R. Austrian Research Centers Seibersdorf,
A-2444 Seibersdorf, Austria
Fax: +43105505506587
EMail: tesch.r@arsenal.ac.at
- Wanek, W. Institute of Ecology and Conservation Biology,
University of Vienna,
Althanstrasse 14, A-1090 Vienna, Austria
Fax: +43142779542
EMail: wolfgang.wanek@univie.ac.at
- Zinsberger, Z. SPECTRONEX GmbH,
Bischoffgasse 26, A-1120 Vienna, Austria
Fax: +4318139994
EMail: g.zinsberger@spectronex.co.at
- Brazil**
- Pessenda, L.C.R. Centre for Nuclear Energy in Agriculture,
Av. Centenario, no. 303,
Caixa Postal 96, 13400-970 Piracicaba, SP, Brazil
Fax: +55194294600
EMail: pessenda@cena.usp.br
- Burkina Faso**
- Dakouré, D. Direction Régionale de l'Hydraulique,
Ministère de l'Environnement et de l'Eau,
BP 173, Bobodioulasso, Burkina Faso
Fax: +226980771
EMail: drh.hb@fasonet.bf
- Canada**
- Birks, S.J. Department of Earth Sciences,
University of Waterloo,
Waterloo, Ontario N2L 3G1, Canada
Fax: +15197460183
EMail: sjbirks@scimail.uwaterloo.ca
- Buhay, W.M. Department of Geography,
University of Winnipeg,
515 Portage Avenue,
Winnipeg, Manitoba R3B 2E9, Canada
Fax: +12047744134
EMail: b.buhay@uwinnipeg.ca
- Drimmie, R.J. Environmental Isotope Laboratory,
Department of Earth Sciences,
University of Waterloo,
Waterloo, Ontario N2L 3G1, Canada
Fax: +15197460183
EMail: rdrimmie@sciborg.uwaterloo.ca

Edwards, T.W.D. University of Waterloo,
Waterloo, Ontario N2L 3G1, Canada
Fax: +15197460183
EMail: twdedwar@sciborg.uwaterloo.ca

Maric, R. University of Waterloo,
Waterloo, Ontario N2L 3G1, Canada
Fax: +15197460183
EMail: rmaric@scimail.uwaterloo.ca

Mayer, B. Department of Physics and Astronomy,
University of Calgary,
2500 University Drive NW,
Calgary, Alberta T2N 1N4, Canada
Fax: +14032207773
EMail: bernhard@earth.geo.ucalgary.ca

St. Amour, N. University of Waterloo,
Waterloo, Ontario N2L 3G1, Canada
Fax: +15197460183
EMail: nastamou@sciborg.uwaterloo.ca

Wolfe, B.B. University of Waterloo,
Waterloo, Ontario N2L 3G1, Canada
Fax: +15197460183
EMail: bwolfe@sciborg.uwaterloo.ca

Cuba

Alonso-Hernández, C.M. Centro de Estudios Ambientales de Cienfuegos,
Ap5 Ciudad Nuclear,
CP 59350, Cienfuegos, Cuba
Fax: +534328912
EMail: lvrac@perla.inf.cu

Egypt

Nada, A.-H. Siting and Environmental Department,
Atomic Energy Authority,
P.O. Box 7551, Nasr City 11762, Egypt
Fax: +2274038
EMail: nadaaa51@yahoo.com

Estonia

Vaikmäe, R. Institute of Geology, Tallinn Technical University,
Estonia Avenue 7,
EE-10143 Tallinn, Estonia
Fax: +3726312074
EMail: vaikmae@gi.ee

Finland

Paatero, J. Finnish Meteorological Institute,
Sahaajankatu 20E,
FIN-00810 Helsinki, Finland
Fax: +358919295403
EMail: jussi.paatero@fmi.fi

France

- Celle-Jeanton, H. Hydrogeology Department,
University of Avignon,
33, rue Louis Pasteur,
F-34000 Avignon, France
Fax: +33490144489
EMail: helene.celle@univ.avignon.fr
- Dray, M. Centre de Recherche Geodynamique,
Université Pierre et Marie Curie,
BP 510,
F-74203 Thonon Cedex, France
Fax: +33450704005
EMail: dray@biogeodis.jussieu.fr
- Eckert, S. Permanent Mission of France to the
International Atomic Energy Agency,
Schwarzenbergplatz 16,
A-1010 Vienna, Austria
Fax: +43150182329
EMail: sylvain.eckert@diplomatic.gov.fr
- Gibert, E. Equipe Hydrologie, Paleo-hydrologie, Paeoenvironnement,
CNRS-UMR 8616,
Université Paris-Sud,
Bâtiment 504 F-91405 Orsay, France
Fax: +33169154917
EMail: egibert@geol.u-psud.fr
- Huneau, F. Hydrogeology Department,
University of Avignon,
33, rue Louis Pasteur,
F-34000 Avignon, France
Fax: +33490144489
EMail: frederic.huneau@univ-avignon.fr
- Travi, Y. Laboratoire d'hydrogéologie,
Faculté des sciences,
Université d'Avignon,
33 rue Louis Pasteur,
F-84000 Avignon, France
Fax: +33450704005
EMail: yves.travi@biogeodis.jussieu.fr

Georgia

- Pagava, S. Radiocarbon and Low-Level Counting Section,
Nuclear Research Laboratory,
I. Javakhishvili Tbilisi State University,
I. Chavchavadze Av., 3 Tbilisi 380028, Georgia
Fax: +99532252776
EMail: spagava@access.sanet.ge

Germany

- Boettger, T. UFZ Centre for Environmental Research Leipzig-Halle,
Department of Hydrogeology,
Theodor-Lieser-Strasse 4,
D-06120 Halle, Germany
Fax: +493455585559
EMail: boettger@hdg.ufz.de
- Eichinger, L. Hydroisotop GmbH,
Woelkestrasse 9,
D-85301 Schweitenkirchen, Germany
Fax: +498444928929
EMail: hydroisotop@t.online-de
- Fritz, P. UFZ-Umweltforschungszentrum,
Leipzig-Halle GmbH,
Permoserstrasse 15, Postfach 2,
D-04318 Leipzig, Germany
Fax: +493412352791
EMail: gf@gf.ufz.de
- Fröhlich, K. Viktor Wittner-Gasse 36, RH7,
A-1220 Vienna, Austria
EMail: k.froehlich@aon.at
- Geyer, S. UFZ Centre for Environmental Research Leipzig-Halle,
Department of Hydrogeology,
Theodor-Lieser-Strasse 4,
D-06120 Halle, Germany
Fax: +493455585559
EMail: geyer@hdg.ufz.de
- Grassl, H. Max-Planck-Institut für Meteorologie,
Bundesstrasse 55,
D-20146 Hamburg, Germany
Fax: +494041173350
EMail: zinecker@dkrz.de
- Helle, G. Forschungszentrum Jülich GmbH,
Institut für Chemie und Dynamik der Geosphäre, Institut 4,
Postfach 1913, D-52428 Jülich, Germany
Fax: +492461612484
EMail: h.helle@fz-juelich.de
- Hertle, H. MICROMASS GmbH,
Lorenz-Stötter-Weg 2,
D-86156 Augsburg, Germany
Fax: ++498214443001
EMail: harald.hertle@micromass.net
- Juchelka, D.G. Finnigan MAT GmbH,
Barkhausenstrasse 2,
Postfach 140 162, D-28197 Bremen, Germany
Fax: +494215493396
EMail: juchelka@finnigan.de

- Michel, R. Zentrum für Strahlenschutz und Radioökologie (ZSR),
Universität Hannover,
Herrenhäuser Str. 2,
D-30419 Hannover, Germany
Fax: +495117623319
EMail: michel@mbox.zsr.uni-hannover.de
- Oesselmann, J. Finnigan MAT GmbH,
Barkhausenstrasse 2,
Postfach 140 162,
D-28197 Bremen, Germany
Fax: +494215493396
EMail: 101511,417@compuserve.com
- Osenbrück, K. Hydroisotop GmbH,
Woelkestrasse 9,
D-85301 Schweitenkirchen, Germany
Fax: +498444928929
EMail: osenb@hydroisotop.de
- Schneider, P. Hydroisotop-Piewak GmbH,
Oberfrohnauer Strasse 84,
D-09117 Chemnitz, Germany
Fax: +4937185371
EMail: hydroisotop-piewak@t-online.de
- Stichler, W. GSF Institute of Hydrology,
Ingolstädter Landstrasse 1,
D-85758 Neuherberg, Germany
Fax: +498931873361
EMail: stichler@gsf.de
- Well, R. Institut für Bodenwissenschaften,
Universität Göttingen,
Von-Siebold-Strasse 4,
D-37075 Göttingen, Germany
Fax: +49551394619
EMail: rwell@gwdg.de
- Greece**
- Argiriou, A. National Observatory of Athens,
I. Metaxa and V. Paulou,
Lofos Koufou,
GR-15236 Palea Penteli, Greece
Fax: +3016138343
EMail: thanos@astro.noa.gr
- Leontiadis, I.L. National Center for Scientific Research "Demokritos",
P.O. Box 60228,
GR-153 10 Aghia Paraskevi, Attikis, Greece
Fax: +3016511766
EMail: leontiad@mail.demokritos.gr

Holy See

Ferraris, M.M.

The Permanent Mission of the Holy See to the
International Organizations in Vienna,
Theresianumgasse 33/4,
A-1040 Vienna, Austria
Fax: +431505850175
EMail: holy.see.vienna@aon.at

Hungary

Dobi, B.

Ministry for Environment,
Fö str. 44-50,
H-1011 Budapest, Hungary
Fax: +3612015280
EMail: dobi@mail.ktm.hu

Tetenyi, P.

Institute of Isotopes,
Konkoly-Thege M. u. 29-33,
H-1121 Budapest, Hungary
Fax: +3613922533
EMail: tetenyi@alpha0.iki.kfki.hu

India

Datta, P.S.

Nuclear Research Laboratory,
Indian Agricultural Research Institute,
New Delhi 110 012, India
Fax: +910115711902
EMail: nri@iari.emet.in/dattapsdsd@lycos.com

Somayajulu, B.L.R.

Oceanography and Climate Studies Area,
Physical Research Laboratory,
Ahmedabad 380 009, India
Fax: +91796301501
EMail: soma@prl.ernet.in

Iraq

Al-Janabi, A.H.

Iraqi Atomic Energy Commission,
P.O. Box 765,
Tuwaitha-Baghdad, Iraq
Fax: +964171819201

Hasan, A.M.

Iraqi Atomic Energy Commission,
P.O. Box 765,
Tuwaitha-Baghdad, Iraq
Fax: +96417181929

Israel

Angert, A.

The Institute of Earst Sciences,
The Hebrew University of Jerusalem,
Jerusalem 91904, Israel
Fax: +97225662581
EMail: alto@vms.huji.ac.il

Gat, J.R. Center for Water Science and Technology,
Ben Gurion University of the Negev,
Sde-Boker Campus,
Sde-Boker 84990, Israel
Fax: +97239652191
EMail: jgat@bgumail.bgu.ac.il

Italy

Bono, P. Dipartimento di Scienze della Terra,
Università "La Sapienza",
P. le A. Moro, 5,
I-00136 Rome, Italy
Fax: +390649914925
EMail: bono@uniroma1.it

Gonfiantini, R. Istituto di Geocronologia e Geochimica Isotopica del
Consiglio Nazionale delle Ricerche,
Via Moruzzi 1, I-56100 Pisa, Italy
Fax: +390503152360
EMail: r.gonfiantini@iggi.pi.cnr.it

Zuppi, G.M. Dipartimento Scienze Ambientale,
Università Cà Foscari di Venezia,
Dorsoduro 2137, I-30123 Venezia, Italy
Fax: +390412578565
EMail: zuppi@unive.it

Japan

Kaya, Y. Japan Science and Technology Corporation,
Hiroo Bldg.,
3-12-40 Hiroo 3-chome, Shibuya-ku,
Tokyo 150-0012, Japan
Fax: +81354690503
EMail: y-kaya@st.rim.or.jp

Sahto, S. Japan Science and Technology Corporation,
Hiroo Bldg.,
3-12-40 Hiroo 3-chome, Shibuya-ku ,
Tokyo 150-0012, Japan
Fax: +81354690503
EMail: ssahto@envr.crest.jst.go.jp

Toyoda, S. Department of Environmental Chemistry and Engineering,
Tokyo Institute of Technology,
4259 Nagatsuta, Midori-ku,
Yokohama 226-8502, Japan
Fax: +81459245555
EMail: stoyoda@chemenv.titech.ac.jp

Uchida, M. Japan Marine Science and Technology Center,
2-13 Natsushima,
Yokosuka 237-0061, Japan
Fax: +81298502575
EMail: uchidam@nies.go.jp

Yoshida, N.
Department of Environmental Science and Technology,
Interdisciplinary Graduate,
School of Science and Engineering ,
Tokyo Institute of Technology 4259 Nagatsuta,
Midori-ku Yokohama 226-, Japan
Fax: +81459245519
EMail: naoyoshi@depe.titech.ac.jp

Lithuania

Mazeika, J.
Institute of Geology Sevcenkos 13,
LT-2600 Vilnius, Lithuania
Fax: +3702236710
EMail: jonmaz@geologin.lt

Trinkunas, G.
Institute of Physics,
A. Gostauto 12, LT-2600 Vilnius, Lithuania
Fax: +3702617070
EMail: trinkun@ktl.mii.lt

Pakistan

Akram, W.
Radiation and Isotope Application Division,
Pakistan Institute of Nuclear Science and Technology,
Pinstech, P.O. Nilore,
Islamabad, Pakistan
Fax: +92519290275
EMail: manzoor@pinstech.org.pk

Poland

Florkowski, T.
Faculty of Physics and Nuclear Techniques,
University of Mining and Metallurgy,
Al. Mickiewicza 30,
PL-30-059 Krakow, Poland
Fax: +48126340010
EMail: florkowski@novell.ftj.agh.edu.pl

Rozanski, K.
Faculty of Physics and Nuclear Techniques,
University of Mining and Metallurgy,
al. Mickiewicza 30,
PL-30-059 Krakow, Poland
Fax: +48126340010
EMail: rozanski@novell.ftj.agh.edu.pl

Wachniew, P.
Faculty of Physics and Nuclear Techniques,
University of Mining and Metallurgy,
al. Mickiewicza 30,
PL-30-059 Kraków, Poland
Fax: +48126340010
EMail: wachniew@novell.ftj.agh.edu.pl

Zglobicki, W.J.
Geology Department,
Maria Curie-Skłodowska University,
Akadenicka St. 19,
PL-20-033 Lubin, Poland
EMail: zglobek@biotop.umcs.lubin.pl

Zimnoch, M.

Faculty of Physics and Nuclear Techniques,
University of Mining and Metallurgy,
al. Mickiewicza 30,
PL-30-059 Krakow, Poland
Fax: +48126340010
EMail: zimnoch@novell.ftj.agh.edu.pl

Romania

Tenu, A.

National Institute of Meteorology and Hydrology,
Sos. Bucuresti-Ploiesti, 97,
R-71 552 Bucharest, Romania
Fax: +4012307762
EMail: isotopes@fx.ro/augtenu@hotmail.com

Russian Federation

Ferronsky, V.I.

Water Problems Institute of the
Russian Academy of Sciences,
Gubkin Street 3,
RU-117333 Moscow, Russian Federation
Fax: +70951355415
EMail: ferron@aqua.laser.ru

Kontar, A.E.

P.P. Shirshov Institute of Oceanology,
36, Nakhimovsky prospect,
RU-117851 Moscow, Russian Federation
Fax: +70951245983
EMail: kontar@cityline.ru

Polyakov, V.A.

All Russian Research Institute for
Hydrogeology and Engineering Geology,
RU-142542 Zeleny Village,
Noginsk District, Moscow Region, Russian Federation
Fax: +70959135126
EMail: gvertany@online.ru

Zyakun, A.M.

Institute of Biochemistry and Physiology of Microorganisms,
Russian Academy of Sciences,
Prospekt Nauki 5,
RU-142290 Pushchino, Moscow Region, Russian Federation
Fax: +70959563370
EMail: zyakun@ibpm.serpukhov.su

Jurina, V.

Ministry of Health of the Slovak Republic,
Lazaretska 26, P.O. Box 52,
SK-833 43 Bratislava, Slovakia
Fax: +4217376142
EMail: vladimir.jurina@health.gov.sk

Slovenia

Lojen, S.

Jozef Stefan Institute,
Jamova 39, SI-1000 Ljubljana, Slovenia
Fax: +38612519385
EMail: sonja.lojen@ijs.si

Vokal, B. Department of Geology,
Faculty of Natural Sciences and Engineering,
University of Ljubljana,
Askerceva 12, SI-1000 Ljubljana, Slovenia
Fax: +38615885346
EMail: barbara.vokal@ijs.si

Vreca, P. Jozef Stefan Institute,
Jamova 39, SI-1000 Ljubljana, Slovenia
Fax: +38615885346
EMail: polona.vreca@ijs.si

South Africa

Robertson, I. Quarternary Dating Research Unit,
CSIR Environmentek,
P.O. Box 395,
Pretoria 0001, South Africa
Fax: +27123491170
EMail: irobertson@csir.co.za

Spain

Martínez, I. Universitat de Barcelona,
Diagonal 645,
E-08028 Barcelona, Spain
Fax: +34934111438
EMail: mateo@porthos.bio.ub.es

Mateo, M.A. Universitat de Barcelona,
Diagonal 645,
E-08028 Barcelona, Spain
Fax: +34934111438
EMail: mateo@porthos.bio.ub.es

Renom, P. Universitat de Barcelona,
Diagonal 645,
E-08028 Barcelona, Spain
Fax: +34934111438
EMail: renom@porthos.bio.ub.es

Switzerland

Aeschbach-Hertig, W. Swiss Federal Institute of
Environmental Science and Technology (EAWAG),
Postfach 611,
CH-8600 Dübendorf, Switzerland
Fax: +4118235210
EMail: aeschbach@eawag.ch

Balderer, W.P. Geological Institute, Engineering Geology,
ETH-Hönggerberg,
CH-8993 Zürich, Switzerland
Fax: +4116331108
EMail: balderer@erdw.ethz.ch

- Beer, J. EAWAG,
P.O. Box 611,
CH-8600 Dübendorf, Switzerland
Fax: +4118235210
EMail: beer@eawag.ch
- Leuenberger, F. Geological Institute Engineering Geology,
ETH-Hönggerberg,
CH-8993 Zürich, Switzerland
Fax: +4116331108
EMail: leuenberger@erdw.ethz.ch
- Loosli, H.H. Physikalisches Institut,
Universität Bern,
Sidlerstrasse 5,
CH-3012 Bern, Switzerland
Fax: +41316318742
EMail: loosli@climate.unibe.ch
- Schotterer, U. Physics Institute, Department of Chemistry,
University Bern,
Sidlerstrasse 5,
CH-3012 Bern, Switzerland
Fax: +41316318742
EMail: schotterer@climate.unibe.ch
- Syrian Arab Republic**
- Al-Masri, M.S. Atomic Energy Commission of Syria,
P.O.Box 6091,
Damascus, Syrian Arab Republic
Fax: +963116112289
EMail: aecs@net.sy
- Tunisia**
- Ben Hamouda, M.F. Centre National des Sciences et Technologie Nucléaires,
Bd. 7 Novembre 1987,
Espace Maghrébia Tour A,
2035 Tunis Carthago, Tunisia
Fax: +2161706200
EMail: f.benhamouda@cnsn.rnrt.tn
- Zouari, K. Laboratoire Radio-Analyses et Environnement,
Ecole nationale d'ingénieurs de Sfax (ENIS),
BP "W", 3038 Sfax, Tunisia
Fax: +2164275595
EMail: kamel.zouari@enis.rnu.tn
- Turkey**
- Dirican, A. Ankara Nuclear Research and Training Centre,
Turkish Atomic Energy Authority,
TR-06100 Besevler/Ankara, Turkey
Fax: +903122234439
EMail: abdullah.dirican@taek.gov.tr

Ukraine

Egorov, V.N.

Institute of Biology of Southern Seas,
National Academy of Sciences of Ukraine,
Nakhimov Prospect, 2,
UA-99011 Sevastopol, Ukraine
Fax: +380692452120
EMail: viktor@egorov.sebastopol.ua

United Kingdom

Darling, W.G.

British Geological Survey,
Macleon Building,
Wallingford, Oxon OX10 8BB, United Kingdom
Fax: +441491692345
EMail: g.darling@bgs.ac.uk

Edmunds, W.M.

Hydrogeology Group,
British Geological Survey,
Crowmarsh Gifford,
Wallingford, Oxon OX10 8BB, United Kingdom
Fax: +441491692345
EMail: wme@bgs.ac.uk

Loader, N.J.

University of Wales Swansea,
Singleton Park, Swansea SA2 8PP, United Kingdom
Fax: +441792295955
EMail: n.j.loader@swansea.ac.uk

Lowry, D.

Department of Geology
Royal Holloway University of London,
Egham Hill, Egham, Surrey TW20 OEX, United Kingdom
Fax: +441784471780
EMail: lowry@gl.rhbnc.ac.uk

Marca, A.D.

Stable Isotope Laboratory,
School of Environmental Sciences,
University of East Anglia,
Norwich, Norfolk NR4 7TJ, United Kingdom
EMail: a.marca@uea.ac.uk

United Republic of Tanzania

Muzuka, A.N.N.

Institute of Marine Sciences,
University of Dar-es-Salaam,
P.O.Box 668, Zanzibar, United Republic of Tanzania
Fax: +255242233050
EMail: muzuka@zims.udsm.ac.tz

United States of America

Cheng, S.

Department of Geological Sciences,
Wright State University,
3640 Col. Glenn Hwy,
Dayton, OH 45435, United States of America
Fax: +19377753462
EMail: scheng@wright.edu

Guilderson, T.	Center for Accelerator Mass Spectrometry, UC/LLNL, P.O. Box 808, L-397, 7000 East Avenue, Livermore, CA 94551, United States of America Fax: +19254237884 EMail: guilderson1@popeye.llnl.gov
Jull, A.J.T.	Department of Physics, University of Arizona, 1118 East Fourth Street, Tucson, AZ 85721, United States of America Fax: +15206219619 EMail: jull@u.arizona.edu
Murnick, D.E.	Department of Physics, Rutgers University, Newark, NJ 07102, United States of America Fax: +19733531856 EMail: murnick@newark.rutgers.edu
Schlosser, P.	Lamont-Doherty Earth Observatory of Columbia University, 61 Route 9W, P.O. Box 1000, Palisades, NY 10964, United States of America Fax: +18453658176 EMail: peters@ldeo.columbia.edu
Thiemens, M.H.	Department of Chemistry and Biochemistry, University of California, Gilman Dr., La Jolla, CA 92093-0356, United States of America Fax: +18588220389 EMail: mthiemens@ucsd.edu
Thompson, L.G.	Department of Geological Sciences, Byrd Polar Research Centre, The Ohio State University, Columbus, OH 43210, United States of America Fax: 16142924697 EMail: thompson.3@osu.edu

Uzbekistan

Mamatqulov, R.	State Special Inspection of Analytical Control of the State Committee for Nature, Protection of the Republic of Uzbekistan, 13a, U. Nosir str. 700100 Tashkent, Uzbekistan Fax: +99872552389
----------------	--

European Commission

Bréas, O.	Joint Research Centre, IRMM, Isotope Measurements Unit, Retieseweg, B-2400 Geel, Belgium Fax: +3214571863 EMail: breas@irmm.jrc.be
-----------	--

Chalk, P. Joint FAO/IAEA Division of Nuclear Techniques in Food
and Agriculture,
International Atomic Energy Agency,
P.O. Box 100 A-1400 Vienna, Austria
Fax: ++43126007
EMail: p.m.chalk@iaea.org

Aggarwal, P. Division of Physical and Chemical Sciences,
International Atomic Energy Agency,
P.O. Box 100, A-1400 Vienna, Austria
Fax: +43126007
EMail: p.aggarwal@iaea.org

Gibson, J.J.

Division of Physical and Chemical Sciences,
Internal Atomic Energy Agency,
P.O.Box 100, A-1400 Vienna, Austria
Fax: +43126007
EMail: j.gibson@iaea.org

Gourcy, L. Division of Physical and Chemical Sciences,
International Atomic Energy Agency,
P.O. Box 100, A-1400 Vienna, Austria
Fax: +43126007
EMail: l.gourcy@iaea.org

Groening, M

Division of Physical and Chemical Sciences,
International Atomic Energy Agency,
P.O. Box 100, A-1400 Vienna, Austria
Fax: +43126007
EMail: m.groening@iaea.org

Livingston, H.D. Marine Environment Laboratory,
International Atomic Energy Agency,
B.P. 800, MC-98012 Monaco Cedex, Monaco
Fax: +37797977275
EMail: h.livingston@iaea.org

Pang, Z. Division of Physical and Chemical Sciences,
International Atomic Energy Agency,
P.O.Box 100, A-1400 Vienna, Austria
Fax: +43126007
EMail: z.pang@iaea.org

Povinec, P.P. Marine Environment Laboratory,
International Atomic Energy Agency,
B.P. 800, MC-98012 Monaco Cedex, Monaco
Fax: +37797977273
EMail: p.povinec@iaea.org

Sood, D.D. Division of Physical and Chemical Sciences,
Internal Atomic Energy Agency,
P.O.Box 100, A-1400 Vienna, Austria
Fax: +43126007
EMail: d.d.sood@iaea.org

Turner, J.V. Division of Physical and Chemical Sciences,
Internal Atomic Energy Agency,
P.O.Box 100, A-1400 Vienna, Austria
Fax: +43126007
EMail: j.turner@iaea.org

Wallin, B. Division of Physical and Chemical Sciences,
International Atomic Energy Agency,
P.O.Box 100, A-1400 Vienna, Austria
Fax: +43126007
EMail: b.wallin@iaea.org

International Centre for Theoretical Physics (ICTP)

Molteni, F. The Abdus Salam International Centre for Theoretical Physics,
Strada Costiera 11,
I-34014 Trieste, Italy
Fax: +390402240449
EMail: molteni@ictp.trieste.it

PAGES

Alverson, K. PAGES,
Bärenplatz 2,
CH-3011 Bern, Switzerland
Fax: +41313123168
EMail: alverson@pages.unibe.ch

Preparatory Commission for the Comprehensive Nuclear-Test-Ban Treaty Organization (CTBTO)

Matthews, K.M. Preparatory Commission for the Comprehensive Nuclear-Test-Ban Treaty Organization,
P.O. Box 1250,
A-1400 Vienna, Austria
EMail: murray.matthews@ctbto.org

Saey, P.R.J. Preparatory Commission for the Comprehensive Nuclear-Test-Ban Treaty Organization,
P.O. Box 1250, A-1400 Vienna, Austria
EMail: paul.saey@ctbto.org

United Nations Educational, Scientific and Cultural Organization (UNESCO)

Bonell, M. Hydrological Processes and Climate,
Division of Water Sciences,
United Nations Educational, Scientific and Cultural Organization,
1, rue Miollis, F-75732 Paris, France
Fax: +33145671690
EMail: m.bonell@unesco.org

